HYDROGEOLOGIC FRAMEWORK AND DEVELOPMENT OF A THREE-DIMENSIONAL FINITE DIFFERENCE GROUNDWATER FLOW MODEL OF THE SALT BASIN, NEW MEXICO AND TEXAS

by

André Bleu Ocean Ritchie

Submitted to the Faculty of the

Department of Earth and Environmental Science of the

New Mexico Institute of Mining and Technology

in Partial Fulfillment of the

Requirements for the Degree of

Master of Science in Hydrology

New Mexico Institute of Mining and Technology

Socorro, New Mexico

July 2011

ABSTRACT

The Salt Basin groundwater system was declared by the New Mexico State Engineer during 2000 in an attempt to regulate and control growing interest in the groundwater resources of the basin. By declaring the boundaries of the Salt Basin groundwater system the State Engineer took administrative control of groundwater pumped from the basin, requiring anyone wanting to withdraw groundwater to apply for a permit from the State to do so. In order to help guide long-term management strategies, the goal of the study described in this thesis was to establish a conceptual model of groundwater flow in the Salt Basin, and verify this conceptual model using groundwater chemistry and a numerical groundwater flow model. Development of the conceptual model involved reconstructing the tectonic forcings that have affected the basin during its formation, and identifying the depositional environments that formed and the resultant distribution of facies. The distribution of facies and structural features were then used to evaluate the distribution of permeability within the basin, and conceptualize the groundwater flow system.

A 3-D hydrogeologic framework model of the Salt Basin was constructed by compiling information on the location and characteristics of the structural features within the basin, compiling data from oil-and-gas exploratory wells to constrain the subsurface distribution of the various geologic units, and compiling information on the location of surface exposures of the various geologic units. The 3-D hydrogeologic framework

model was used to develop a 3-D finite difference groundwater flow model of the Salt Basin groundwater system in order to test the conceptual model and quantify the hydraulic properties of the aquifer. The groundwater flow model was constructed using Groundwater Modeling System (GMS) version 6.5, which provides a graphical pre- and post-processor for MODFLOW-2000, the U.S. Geological Survey's modular groundwater flow model. MODPATH, a post-processing program designed to use output from steady-state or transient MODFLOW simulations to compute 3-D flow paths and travel times for imaginary "particles" of water moving through the simulated groundwater system, was used to estimate groundwater residence times for comparison with groundwater ages derived from groundwater chemistry.

Two recharge distributions (water-balance based and elevation-dependent) were tested using MODFLOW-2000 in an attempt to match observed groundwater levels from wells throughout the Salt Basin, and radiocarbon groundwater ages from wells predominantly in the eastern half of the New Mexico portion of the Salt Basin. Total recharge to the groundwater flow model domain using the water-balance based recharge distribution ranged from 160,000 m^3/day (49,000 acre-feet/year) for the minimum recharge scenario to 350,000 m^3/day (110,000 acre-feet/year) for the maximum recharge scenario, with the average recharge scenario producing 270,000 m^3/day (81,000 acre-feet/year). These values for total recharge to the Salt Basin are on the upper end of the range of values reported in previous studies. Total recharge to the groundwater flow model domain using the elevation-dependent recharge distribution ranged from 9,100 m^3/day (2,700 acre-feet/year) for the minimum recharge scenario to 99,000 m^3/day (29,000 acre-feet/year) for the maximum recharge scenario, with the average recharge

scenario producing 50,000 m^3/day (15,000 acre-feet/year). Abundant hydrogeologic evidence suggests that these relatively low recharge values are reasonable.

Both recharge distribution models were calibrated to steady-state groundwater levels in 378 wells throughout the Salt Basin by varying the distribution of horizontal hydraulic conductivity within the groundwater flow model domain. In general, for both recharge distributions, the highest permeability zones within the groundwater flow model domain corresponded to the regions of pervasive faulting and fracturing associated with the Otero Break, the Salt Basin graben, and to a lesser extent the subsurface Pedernal uplift. In contrast, the Otero Mesa and Diablo Plateau regions, which have undergone relatively little faulting and fracturing, were zones of lower permeability within the groundwater flow model.

Both the calibrated water-balance based and elevation-dependent recharge distribution models produced a reasonably good match to observed groundwater levels and regional groundwater flow. However, MODPATH particle ages derived from the average recharge scenario/minimum porosity model and the maximum recharge scenario/minimum and average porosity models of the elevation-dependent recharge distribution resulted in a statistically better match to radiocarbon groundwater ages, as compared to the water-balance based recharge distribution. In general, MODPATH particle ages derived from the water-balance based recharge distribution models ranged from one to three orders of magnitude younger than the radiocarbon groundwater ages.

TABLE OF CONTENTS

<div align="right">**Page**</div>

LIST OF FIGURES

LIST OF TABLES

LIST OF APPENDIX FIGURES

LIST OF APPENDIX TABLES

INTRODUCTION

The Salt Basin is a closed drainage basin which covers an area of approximately 20,000 km^2 (7,700 mi^2) in southeast New Mexico and northwest Texas (Chapman, 1984). The areal extent of the basin is largest in Texas, encompassing parts of Hudspeth, Culberson, Jeff Davis, and Presidio Counties, but also defines an area of approximately 6,200 km^2 (2,400 mi^2) in Otero, Chaves, and Eddy Counties in New Mexico (Chace and Roberts, 2004). The basin owes its current physiographic form to deformation associated with Cenozoic Basin-and-Range extension. This extension is still active today [Goetz, 1980], and some researchers [Dickerson and Muehlberger, 1994; Keller and Cather, 1994] have included the Salt Basin as part of the Rio Grande rift.

The Salt Basin groundwater system was declared by the New Mexico State Engineer during 2000. By declaring the boundaries of the Salt Basin groundwater system the State Engineer took administrative control of groundwater pumped from the basin, requiring anyone wanting to withdraw groundwater to apply for a permit from the State to do so. Interest has arisen in the groundwater resources of the basin as a future source of water supply for El Paso, Texas, Las Cruces, New Mexico, and Ciudad Juárez, Mexico. Thus, long-term management of the water resources is needed. In order to help guide long-term management strategies, the goal of the study described in this thesis was to establish a conceptual model of groundwater flow in the Salt Basin, and verify this

conceptual model using groundwater chemistry and a three-dimensional (3-D) finite difference groundwater flow model.

The development of a conceptual model of groundwater flow in the Salt Basin was accomplished by reconstructing the tectonic forcings that affected the basin during its formation, and identifying the depositional environments and facies distributions that were produced as a result of these forcings. The distribution of facies and structural features were then used to evaluate the distribution of permeability within the basin, and conceptualize the groundwater flow system. A 3-D hydrogeologic framework model of the Salt Basin was constructed by compiling information on the location and characteristics of the structural features within the basin, compiling data from oil-and-gas exploratory wells to constrain the subsurface distribution of the various geologic units, and compiling information on the location of surface exposures of the various geologic units. Five hydrogeologic cross-sections were assembled from this data. Finally, ArcGIS was used to contour the top surface of each hydrogeologic unit using the available subsurface well control and surface exposures, and the location of the structural features.

The rocks within the basin and along the bounding highlands display evidence of a long history of tectonic instability. The tectonic history of the Salt Basin can be divided into four main periods: a) Pennsylvanian-to-Early Permian, b) Mid-to-Late Permian, c) Late Cretaceous, and d) Cenozoic. The collision of the southern margin of North America with South America-Africa during the Pennsylvanian-to-Early Permian Ouachita-Marathon orogeny resulted in the differential uplift and subsidence of the Pedernal landmass, and Diablo and Central Basin Platforms, and the Orogrande, Delaware, and Midland Basins, respectively (Dickerson, 1989). Mid-to-Late Permian structural features

2

outlined the margins of the subsiding Delaware Basin (Black, 1973; Dickerson, 1989; King, 1948). East-west oriented compression during the Late Cretaceous Laramide orogeny produced northwest trending thrust faults and northwest to westerly trending folds in the Otero Mesa region (Black, 1973; Broadhead, 2002). Finally, Cenozoic Basin-and-Range extension overprinted all these former structures with the formation of horst and graben structures bounded by high-angle normal faults (Goetz, 1977).

The primary rocks exposed in the basin are Permian sedimentary rocks (carbonates, such as limestone and dolomite, evaporites, such as gypsum, anhydrite, and halite, sandstones, siltstones, and claystones), which are covered by a thin to locally thick layer of Cenozoic alluvium. These Permian rocks were deposited in a shallow marine shelf to shelf-margin transitional environment adjacent to the subsiding Delaware Basin to the southeast. The rocks in the subsurface display a nearly continuous geologic record from the Precambrian to the Holocene, although rocks of the Mesozoic era are largely absent from the basin (Black, 1973). Permian carbonates are the main water-bearing units in the Salt Basin (Huff and Chace, 2006; Newton et al., 2009). Groundwater flow within these rocks is highly fracture- and solution-controlled (Mayer and Sharp, 1998).

The conceptual and hydrogeologic framework models were then used to aid in the development of a numerical model of groundwater flow in the Salt Basin in order to quantify the hydraulic properties of the aquifer system. A 3-D finite difference groundwater flow model was constructed with MODFLOW-2000 for the northern portion of the Salt Basin in New Mexico and Texas. Two recharge distributions (water-balance based and elevation-dependent) were tested using the groundwater flow model in an attempt to match observed groundwater levels from wells throughout the Salt Basin, and

radiocarbon groundwater ages from wells predominantly in the eastern half of the New Mexico portion of the Salt Basin. The hydraulic properties of the Salt Basin aquifer system were also analyzed using the northward propagation of a periodic pumping signal from Dell City, Texas.

In addition to the conceptual, hydrogeologic framework, and numerical models presented in this thesis, the distribution of environmental groundwater tracers in the Salt Basin was also investigated during this study in order to elucidate sources and amounts of recharge, groundwater flow rates, and controls on the evolution of groundwater chemistry. Although some of the environmental tracers data is presented in this thesis, the bulk of this data was analyzed in a separate thesis: Sigstedt (2010).

CHAPTER 1: PHYSICAL AND GEOLOGICAL SETTING

1.1: Physiographic Features

The Salt Basin watershed is located primarily in the Sacramento section of the Basin and Range physiographic province, but the far southern section (basically that portion south of the city of Van Horn, Texas) is located in the Mexican Highland section of the Basin and Range physiographic province (Fenneman and Johnson, 1946). (Figure 1.1) The Salt Basin is a structural basin that extends in a northwest-southeast direction for approximately 350 km (217 mi) (Goetz, 1977), covering the southeastern portion of Otero County and the extreme southwestern corners of Chaves and Eddy Counties in New Mexico, and the central and eastern portion of Hudspeth County, the western section of Culberson County, and portions of Jeff Davis and Presidio Counties in Texas. (Figure 1.2) Some researchers [Dickerson and Muehlberger, 1994; Keller and Cather, 1994] have included the Salt Basin as part of the Rio Grande rift. (Figure 1.1) The Rio Grande rift is distinguished from the Basin and Range province by deep Miocene grabens, synextensional volcanism, elevated heat flow, Quaternary normal faulting, and evidence for full lithospheric rupture (Dickerson and Muehlberger, 1994).

The Salt Basin can be divided into two groundwater flow systems: a northern and southern system. The northern Salt Basin is essentially that portion of the basin that lies north of the Sierra Diablo (Chapman, 1984). The boundary that separates the Salt Basin into northern and southern portions is a combination of a watershed divide due to the

5

Baylor Mountains, and a groundwater divide associated with the Babb Flexure and Bitterwell Break (Hutchison, 2006). (Figure 1.3)

The northern Salt Basin is bounded on the north by the Sacramento Mountains and the Peñasco Basin, on the west by the Tularosa Basin and the Hueco Mountains, on the southwest by the southeast portion of the Hueco bolson, on the south by the Sierra Diablo and Baylor Mountains, and on the east by the Guadalupe, Brokeoff, and Delaware Mountains. (Figure 1.3) There are several distinct physiographic features within the northern Salt Basin: 1) the Salt Basin graben, 2) the western escarpments of the Guadalupe, Delaware, and Brokeoff Mountains, 3) the Otero Mesa/Diablo Plateau, 4) the Cornudas Mountains, 5) the southern escarpment of the Sacramento Mountains, and 6) the Sierra Diablo. (Figure 1.3)

The Salt Basin graben is an 8 to 32 km (5 to 20 mi) wide, northwest-southeast trending Cenozoic structural feature that marks the easternmost limit of modern Basin and Range tectonism (Goetz, 1980; Veldhuis and Keller, 1980). The graben is asymmetric, composed of four segments, each offset to the west of its adjacent southern segment along Paleozoic transform zones, and extends for approximately 350 km (217 mi) from southern New Mexico to west Texas as an en echelon offset of the Rio Grande rift system (Goetz, 1977, 1980, and 1985). The blocks that form the graben floor dip, in general, to the southwest to west, and are covered by 10 to 700 meters (33 to 2,300 feet) of Cenozoic basin fill (Bjorklund, 1957; Gates et al., 1980; Goetz, 1980; Spirakis et al., 1997). The blocks are being actively down-dropped to the west-southwest, have increasing displacements to the south, and are broken by generally northwest trending, down-to-the-north transverse structural zones which are from north to south: the Otero

6

fault, the Bitterwell Break, and the Babb and Victorio flexures (Goetz, 1980, 1985). (Figure 2.22)

The floor of the Salt Basin graben lies at an elevation of 1,000 to 1,100 meters (3,300 to 3,600 feet) in the far northern segment, and rises gently to the south, where it reaches a maximum elevation of about 1,500 meters (4,900 feet) in the far southern segment (Angle, 2001; Mayer, 1995). The portion of the northern Salt Basin graben in New Mexico is known as Crow Flats, while the portion in Texas is known as Salt Flats (Angle, 2001; Gates et al., 1980; Huff and Chace, 2006). The Crow Flats portion of the graben is underlain by the large Crow Flats syncline (Black, 1976). (Figure 1.6) The Crow Flats syncline may terminate to the north against the "AV" lineament, and narrows to the south where it passes between the Victorio Peak anticline on the west and the Brokeoff Mountains on the east (Black, 1976). (Figure 1.6) The location of the southern termination of the Crow Flats syncline is unknown because it is concealed beneath graben fill (Black, 1976). At the lowest point along the central axis of the graben lie a series of northwest-southeast trending playa lakes or alkali flats, which encompass an area of approximately 150 km^2 (58 mi^2) that serves as the natural discharge region of the northern groundwater system (Bjorklund, 1957). (Figure 1.3) These lakes are normally dry, but can briefly fill with water during intense periods of rainfall (Chapman, 1984).

The northern Salt Basin graben is bounded to the west by the rolling hills and gently eastward sloping surface of the Otero Mesa/Diablo Plateau, and to the east by the steep western escarpments of the Guadalupe, Brokeoff, and Delaware Mountains. (Figure 1.3) The graben floor rises gradually to the west, where it merges with the Otero Mesa/Diablo Plateau at an elevation of 1,250 meters (4,100 feet) (Mayer and Sharp,

1998). Along the western margin of the Salt Basin graben, and just south of the New Mexico-Texas state line lies a broad alluvial outwash plain, known as Dell Valley, which is the site of a large irrigation district associated with the town of Dell City, Texas (Ashworth, 2001). (Figure 1.3) The valley consists of approximately 160 km^2 (62 mi^2) of irrigable land, and rises gently to the west from an elevation of approximately 1,109 meters (3,638 feet) to 1,280 meters (4,198 feet) (Ashworth, 2001).

In the northern two segments of the graben, north of the Sierra Diablo, the high point lies along the eastern side, with the Guadalupe Mountains approximately 1,400 meters (4,600 feet) higher than the Otero Mesa/Diablo Plateau on the western side (Boyd, 1982; Goetz, 1977). However, in the southern two segments, the high point occurs along the western side, with the Sierra Diablo approximately 180 meters (590 feet) higher than the southern Delaware Mountains on the eastern side (Boyd, 1982; Goetz, 1977).

The steep western escarpments of the Guadalupe, Brokeoff, and Delaware Mountains tower over the eastern margin of the Salt Basin graben, rising to a maximum elevation of 2,667 meters (8,748 feet) at Guadalupe Peak, which is also the highest point in Texas, and 2,610 meters (8,561 feet) in Guadalupe Mountains National Park in New Mexico (Boyd and Kreitler, 1986b; Spirakis et al., 1997). (Figure 1.3) The Guadalupe and Delaware Mountains are part of a larger, eastward tilted, largely late Cenozoic Basin and Range fault block that extends from the southern end of the Delaware Mountains north-northwestward towards the northern end of the Guadalupe Mountains in T. 19 S., R. 18 E (Kelley, 1971). Guadalupe Ridge is a northeastward trending spur of the Guadalupe Mountains, which follows the trend of the Early Permian Bone Spring flexure/monocline, and results in part from the presence of the resistant reef rocks that

formed around the margin of the Delaware Basin during the Permian (Hayes, 1964; Kelley, 1971). (Figures 1.15 and 2.22) Guadalupe Ridge consists of several parallel, 40 km (25 mi) long, east-northeastward plunging folds, from north to south: Guadalupe Ridge anticline (whose axial trace is near the crest of the Ridge), Walnut Canyon syncline, and Reef anticline (whose southeast flank is the result of the original sedimentary dip in the reef breccia beds of the Capitan Limestone and a Cenozoic tectonic component of dip (Hayes, 1964; Kelley, 1971). (Figure 2.23)

The Brokeoff Mountains are a down-dropped, and heavily faulted spur of the Guadalupe Mountains, which rise to approximately 1,830 meters (6,000 feet) in New Mexico and trend in a more north-south direction than the Guadalupe or Delaware Mountains (Black, 1973; Spirakis et al., 1997). The floor of the Salt Basin graben and the western escarpments of the Guadalupe, Brokeoff, and Delaware Mountains are separated by a series of gently westward sloping alluvial fans consisting of material derived from the surrounding mountains (Boyd and Kreitler, 1986b). The Guadalupe, Brokeoff, and Delaware Mountains separate the Salt Basin and the associated Basin and Range province from the Permian Delaware Basin, a stable cratonic feature filled with greater than 6,100 meters (20,000 feet) of Paleozoic sediments, and the Pecos Valley section of the Great Plains physiographic province to the east (Fenneman and Johnson, 1946; Sharp, 1989). (Figures 1.1 and 1.15) The Huapache thrust zone/monocline is typically considered the eastern boundary of the Guadalupe Mountains uplift, while the Bone Spring monocline is considered the southern boundary of the uplift (Kelley, 1971). (Figures 2.21 and 2.22)

The Otero Mesa/Diablo Plateau rises gently to the west to an elevation of 1,500 meters (4,900 feet) along the western boundary of the Salt Basin watershed with the

9

Hueco Mountains and Tularosa Basin (Mayer and Sharp, 1998). The Otero Mesa/Diablo Plateau is a continuous feature that encompasses approximately 4,850 km^2 (1,870 mi^2), extends across the New Mexico-Texas state line, and is known as the Otero Mesa in New Mexico and the Diablo Plateau in Texas (Mayer and Sharp, 1998). (Figure 1.3)

In the central portion of the Otero Mesa/Diablo Plateau lie a cluster of Cenozoic intrusive bodies, known as the Cornudas Mountains, which straddle the New Mexico-Texas state line. (Figure 1.3) The Cornudas Mountains rise more than 600 meters (2,000 feet) above the plateau surface to elevations greater than 2,100 meters (6,900 feet), and are composed of Late Eocene to Early Oligocene alkaline intrusive rocks that form the northern portion of the Trans-Pecos magmatic province (Mayer, 1995; McLemore and Guilinger, 1993; Nutt and O'Neill, 1998). The Cornudas Mountains represent the westernmost extent of alkaline magmatism in the Trans-Pecos magmatic province, with intrusive rocks to the west, in the Hueco Mountains for example, being less alkalic to calc-alkalic (McLemore and Guilinger, 1993). (Figure 1.4) This progressive eastward change from calc-alkalic to alkalic igneous rocks is associated with the shallow subduction of the Farallon plate beneath the North American plate during the Late Cretaceous Laramide orogeny. As a result, Trans-Pecos magmatism, including that which formed the Cornudas Mountains, is thought to be related to subduction as opposed to continental rifting that occurred during Basin and Range extension (McLemore and Guilinger, 1993).

Southeast of the Cornudas Mountains, on the Diablo Plateau, Cenozoic alkaline intrusions of the Trans-Pecos magmatic province include, from northwest to southeast: the Sierra Tinaja Pinta group, Cornudas Station, the Antelope Hill intrusives, the Sierra

Prieta sill, and the Marble Canyon intrusives (Barker et al., 1977; Masson, 1956). (Figure 1.4) Cenozoic intrusions are also associated with Dantes dome (centered around the Shiloh Hills) northeast of the Cornudas Mountains on the Otero Mesa, Round Mountain east of Dell City, Texas, and Granite Mountain in the southwest portion of the Diablo Plateau (Ashworth, 2001; Barker et al., 1977; Black, 1973). (Figure 1.4)

The physiographic features of the north and northeast portions of Otero Mesa were discussed extensively by Black (1973). Several distinct features include a) the Chert Plateau, b) the Otero Hills complex, c) Jefferies Peak escarpment, d) the Sacramento River valley, e) the Otero Flats, and f) Manual Mesa. (Figure 1.5)

The Chert Plateau is a heavily drainage-dissected, relatively flat-topped tableland, which rises steeply from the alluvial plains bounding the western margin of Crow Flats and slopes gently eastward from an elevation of approximately 1,460 meters (4,800 feet) in the northwest to approximately 1,250 meters (4,100 feet) in the south (Black, 1973). The northern limit of the Chert Plateau was arbitrarily set by Black (1973) as coinciding with the "AV" lineament. The gently folded surface of the Chert Plateau consists of southeast trending, gently doubly plunging, anticlines and synclines (Black, 1976). The west flank of the western-most anticline, probably the southern extension of the McGregor anticline, forms the east flank of the South Otero syncline of the Otero Flats, while the east flank of the easternmost anticline forms the west flank of the Crow Flats syncline of the Salt Basin graben (Black, 1976). (Figure 1.6) The easternmost anticline may be continuous with the Victorio Peak anticline to the southeast, which plunges to the south beneath valley-fill as it passes to the east of Dell City, Texas (Black, 1976; Sharp et al., 1993). (Figure 1.6)

The Otero Hills, which include the Cornucopia and Collins Hills, extend north and northwest of the Chert Plateau to the town of Piñon, New Mexico, and to the Piñon cross folds, respectively, where they merge to the north with Jefferies Peak escarpment and the Sacramento River valley (Black, 1973). (Figures 1.5 and 1.6) The northwest portion of the Otero Hills is formed by a southeast trending belt of parallel, generally southeast plunging folds 6 to 10 km (4 to 6 mi) wide and 39 km (24 mi) long known as the Otero folds (Black, 1976). (Figure 1.6) Several major anticlines and synclines (Prather anticline and syncline, and McGregor anticline) extend along the entire length of the belt (Black, 1976). (Figure 1.6) The southwest flank of the McGregor anticline, and the associated McGregor fault zone, form the northeast flank of the Otero syncline of the Otero Flats (Black, 1976). (Figure 1.6)

North and east of the Otero folds are a series of small, generally parallel, arcuate, northerly trending, doubly plunging anticlines and synclines known as the Fleming folds (Black, 1976). (Figure 1.6) The Fleming folds are bound on the north by the Piñon Creek valley and the Stevenson fault, and appear to merge to the south with the Prather anticline (Black, 1976). (Figures 1.5 and 1.6) To the east of the Otero and Fleming folds are a 6 to 10 km (4 to 5 mi) wide and 32 km (20 mi) long belt of southwest- to southeast trending folds known as the Cornucopia folds, which include the Cornucopia anticline and the associated Cornucopia fault, and the Jernigan Wash syncline (Black, 1976). (Figure 1.6) The Cornucopia folds are bound on the north by the Stevenson fault, on the east by the Jernigan Wash anticline, and on the south by the "AV" lineament (Black, 1976). (Figure 1.6) The Fleming and Cornucopia folds are on trend with, and are probably the southern continuation of, Kelley's (1971) Dunken uplift and associated folds south of the

12

Stevenson fault (Black, 1976). (Figure 1.6) The Dunken uplift is a 56 km (35 mi) long, 8 to 16 km (5 to 10 mi) wide block bounded on the west by the Elk syncline and on the east by the Dunken syncline (Kelley, 1971).

The gently undulating, northerly trending, 24 km (15 mi) long Jernigan Wash anticline is bound on the east by The Rim of the Guadalupe Mountains, and terminates to the south at the "AV" lineament (Black, 1976). (Figure 1.6) Jefferies Peak escarpment is formed by the large, southeast trending, southeast plunging Sacramento anticline, which is downfaulted to the southwest by the Sacramento Canyon fault (Black, 1973; Black, 1976). (Figures 1.5 and 1.6)

The Sacramento River valley drains an area of approximately 2,100 km^2 (1,300 mi^2) (Scalapino, 1950). The northwest portion of the Sacramento River valley consists of the southeast trending, and southeast plunging Sacramento River syncline, the southeast trending Wild Boy fault (a high-angle reverse fault), and the southeast to east trending, and east plunging Orendorf anticline which subparallels the river (Black, 1973; Black, 1976). (Figure 1.6) The southern portion of the Sacramento River valley consists of the Piñon cross folds and the McGregor folds (Black, 1976). (Figure 1.6) The Piñon cross folds are a 2 to 3 km (1 to 2 mi) wide zone of closely spaced, parallel faults, joints, and tight folds against which the McGregor, Prather, and Orendorf anticlines terminate (Black, 1976). (Figure 1.6) Left shift is suggested by the apparent drag of the axes of these terminated folds as they approach the Piñon cross folds (Black, 1976). The Piñon cross folds are bound on the south by the parallel, but much gentler and open, northeast plunging McGregor folds (Black, 1976). (Figure 1.6) The McGregor folds pass to the south and become lost in the northern portion of Otero Flats (Black, 1976).

The Otero Flats are a series of low-lying (1,269 to 1,307 meters [4,162 to 4,288 feet]) dry lake beds, that were the site of Late Pleistocene lakes, which are bound on the east and northeast by the abrupt rise of the Chert Plateau and Otero Hills, respectively, and on the west by the Manual Mesa (Black, 1973). (Figures 1.5 and 1.6) The Otero dry lake of Black (1973) corresponds to Lake Sacramento of Hawley (1993) and Wilkins and Currey (1997). The topographic low occupied by the Otero dry lake is formed by the large, asymmetric Otero syncline (Black, 1976). (Figure 1.6) To the south, the Otero syncline is bound by the Manual Mesa along the trend of the "AV" lineament (Black, 1976). (Figures 1.5 and 1.6)

The Otero dry lake is connected by a narrow alluviated surface to the South Otero dry lake of Black (1973), which is the site of a large internally-drained basin occupied by Van Winkle Lake. (Figure 1.6) The topographic low occupied by the South Otero dry lake is formed by the South Otero syncline (Black, 1976). (Figure 1.6) The South Otero syncline may be the offset continuation of the Otero syncline south of the "AV" lineament (Black, 1976). (Figure 1.6) The abrupt rise of the Chert Plateau and the Otero Hills on the eastern margin of the Otero Flats is the result of a series of down-to-the-west normal faults and intense fracturing identified by Mayer (1995) as the Otero Break. (Figure 1.5)

Manual Mesa is the western continuation of the Chert Plateau to the east, but lies about 120 to 150 meters (400 to 500 feet) lower than the Chert Plateau due to relative down-dropping along the west side of the Chert Plateau (Black, 1973). (Figure 1.5) Like the Chert Plateau, the Manual Mesa is a relatively flat-topped surface that slopes gently to the southeast, but rises to the southwest as it encounters the intrusive complexes

associated with Dantes dome and the Cornudas Mountains (Black, 1973). (Figure 1.4) Manual anticline is a gently arched, northwest trending anticline that forms a topographic high modified by Dantes dome, and terminates to the north on the "AV" lineament and Otero syncline (Black, 1976). (Figure 1.6) To the southwest, the Cornudas slope rises out of a large southeast trending syncline that flanks the Manual anticline (Black, 1976). (Figures 1.5 and 1.6) The northern boundary of Manual Mesa coincides with the western projection of the "AV" lineament (Black, 1973). (Figure 1.5)

To the north the Otero Mesa merges into the southeastern escarpment of the Sacramento Mountains, a Cenozoic Basin and Range uplift, which rise to an elevation of 2,750 meters (9,020 feet) at Sunspot (Mayer and Sharp, 1998). (Figure 1.3) The Sacramento Mountains uplift is largely the result of displacement along a large fault (Alamogordo fault) at the western base of the uplift, but a broad, gentle anticline defines the uplift east of the fault (Kelley, 1971). (Figure 2.25)

The Sierra Diablo is located in the far southern portion of the northern Salt Basin watershed, and its plateau-like surface rises to greater than 1,830 meters (6,000 feet) (King, 1965). (Figure 1.3) The Sierra Diablo extends in a general north-south direction for approximately 40 km (25 mi), and is bound on the east by the Salt Basin graben and on the west by the Diablo Plateau (King, 1965). (Figure 1.3) The eastern escarpments of the range are steep, dropping almost vertically 910 meters (3,000 feet) to the floor of the Salt Basin graben, although the lower portion of the slope consists of alluvial fans (King, 1965). The western escarpment slopes more gradually downward, about 610 meters (2,000 feet) over 16 km (10 mi), to the Diablo Plateau (King, 1965).

1.2: Climate

The Salt Basin has a semiarid climate typical of the desert Southwest U.S., characterized by long, hot, dry summers, and short, mild winters. Although summer temperatures during the day can be hot, the night-time temperatures can be cool (Chapman, 1984). Temperatures range from -12 to 46ºC (10 to 115ºF) (Boyd, 1982). Based on the Parameter-elevation Regressions on Independent Slopes Model (PRISM) [Daly et al., 1994], average annual temperatures in the northern Salt Basin over the 30 year period from 1971 to 2000 ranged from 6.1 to 17ºC (43 to 63ºF). (Figure 1.7) Using the same model and over the same time period, average minimum annual temperatures ranged from -9 to 1ºC (15 to 33ºF), while average maximum annual temperatures ranged from 21 and 36ºC (69 to 97ºF). (Figures 1.8 and 1.9) Average monthly temperatures range from -1 to 7ºC (30 to 45ºF) in January to 21 to 27ºC (70 to 81ºF) in August (Mayer, 1995).

Precipitation falls mainly during the summer (May through October) due to intense thunderstorms associated with monsoon moisture from the Gulf of Mexico and Pacific Ocean (Black, 1973; Boyd, 1982). Rainfall is controlled by the orographic effect as moisture-laden air rises over the mountain ranges that surround the basin, and therefore is highly elevation-dependent (Mayer and Sharp, 1998). (Figure 1.10) Precipitation averages 20 to 25 cm/year (8 to 10 inches/year) in the valley floors, more than 50 cm/year (20 inches/year) in the Guadalupe Mountains, and more than 90 cm/year (35 inches/year) in the Sacramento Mountains (Boyd, 1982; Mayer and Sharp, 1998). Based on PRISM, from 1971 to 2000 average annual precipitation ranged from 23 cm (9 inches) to 84 cm (33 inches). (Figure 1.11) Weather phenomenon in the form of decadal

droughts every 20 years are also common (Chapman, 1984). Historic periods of drought include: 1887-1898, 1907-1918, 1930-1940, 1950-1956, and Chapman (1984) indicated that the area was in the midst of a drought during the early 1980s.

There is also evidence for a long-term climate shift towards more arid conditions in the region since the Pleistocene (Chapman, 1984). During cold and wet episodes of the Last Glacial Maximum (LGM), annual temperatures in the southwest U.S. were reduced by at least 5ºC (9ºF), and precipitation was 50 to 100% higher than the present (Menking et al., 2004). The vegetation history in the Salt Basin region suggests that summer temperatures were 3.5 to 5ºC (6.3 to 9ºF) lower and precipitation was at least 20% higher than the present (Betancourt et al., 2001). Although the Salt Basin was not directly affected by glaciation, it is likely that it was much wetter during the Pleistocene, as evidenced by the presence of dry lake beds on Otero Mesa and in the Salt Basin graben (Black, 1973; Hawley, 1993; Wilkins and Currey, 1997).

Relative humidity, on average, is low (Black, 1973). Westerly winds are common, and can gust up to 90 km/hour (56 mi/hour) in early spring (Black, 1973; Boyd, 1982). Potential evaporation rates are high, ranging from 190 cm/year (75 inches/year) at high elevations to 250 cm/year (98 inches/year) at low elevations (Mayer and Sharp, 1998). Therefore, while precipitation increases with elevation, temperatures and potential evaporation decrease with increasing elevation (Mayer, 1995).

1.3: Vegetation

Agriculture and cattle ranching are the primary forms of land use in the northern Salt Basin watershed. The Dell City area contains an extensive irrigation district, with up to 160 km^2 (62 mi^2) of irrigable land (Ashworth, 2001). The principal crops, in order of

importance are: alfalfa, onions, wheat, cotton, corn, and sorghum (Goetz, 1977). The primary native plant associations in the basin include the Desert Plains Association (Lower Sonoran zone), which dominates in the southern portion, and the Mixed Grassland Association (Lower portion of the Upper Sonoran zone), which dominates in the higher elevations of the northwest Otero Mesa (Black, 1973). The far northwest portion of the basin includes the Piñon-Juniper Association (upper portion of the Sonoran zone), which shifts into the Yellow Pine Association (Transition zone) at higher elevations (Black, 1973).

Level IV ecoregions compiled by the U.S. Environmental Protection Agency (EPA) indicate that the Otero Mesa and Diablo Plateau primarily fall within the Chihuahuan Desert Grasslands region. (Figure 1.12) At higher elevations in the Sacramento and Guadalupe Mountains, and the Sierra Diablo, the level IV ecoregions include Montane Woodlands, and Rocky Mountain Conifer Forests along the crest of the Sacramento Mountains. These higher elevation ecoregions are separated from the Otero Mesa/Diablo Plateau ecoregion by the Chihuahuan Desert Slopes ecoregion.

1.4: Geologic Setting

The stratigraphy and structure of the Salt Basin, and the physiographic expression of those features, are strongly controlled by the tectonic deformation that has occurred in the region. The rocks exposed at the surface and in subsurface well cores record a long, and complex history of deformation in the Salt Basin region. This deformation controlled the depositional environments that formed, and the resultant distribution of facies throughout the region. The primary aquifer units in the Salt Basin were deposited during the Permian in a shallow marine environment along the shelf and shelf-margin of

subsiding basins to the southeast (Delaware Basin) and west (Orogrande Basin). (Figure 1.15) Basin-and-Range extension during the Cenozoic produced the current physiographic form of the Salt Basin, and resulted in the infilling of the Salt Basin graben with alluvium and lacustrine deposits, which also serve as an aquifer in the Crow Flats, New Mexico and Dell City, Texas regions.

A major rifting event during the Precambrian, about 1.5 Ga, along western and southwestern North America produced a passive continental margin (Shepard and Walper, 1982). Subsequent seafloor subduction beneath this continental margin produced an offshore volcanic arc separated from the North American craton by a marginal basin (Shepard and Walper, 1982). This volcanic arc formed the thick sequence of volcanics that comprise the Carrizo Mountain Group (Shepard and Walper, 1982). (Figure 2.3) About 1.25 Ga the rocks of this volcanic arc, as well as limestones, volcanics, and clastics of the Allamore and Hazel Formations, were metamorphosed and thrust northward into Trans-Pecos Texas to form the Van Horn mobile belt. The Van Horn mobile belt would later form the positive axis of Adams' (1965) Diablo Arch, and the basement of the Diablo Platform, and its southern extension the Coahuila Platform (Shepard and Walper, 1982). (Figures 1.13 and 1.14) The Streeruwitz thrust fault separates the stable Diablo Platform to the north from the unstable Van Horn mobile belt to the south (Goetz, 1977). (Figure 1.13) Subsequent erosion of the Van Horn orogenic belt during the Late Precambrian reduced this area to a hilly, deeply eroded surface over which the Late Precambrian seas advanced and deposited the Van Horn Sandstone (Shepard and Walper, 1982).

In addition to this major collision event during the Grenville orogeny (1.232 to 1.116 Ga), episodic periods of folding and thrusting during the Precambrian are suggested by the presence of various metamorphic terrains, including the 1.6 Ga Torrance metamorphic terrain and Granite Gneiss to the north and west of the region, the 1.34 to 1.41 Ga Granite Rhyolite terrain, which includes the 1.4 Ga and older Chaves Granite gneiss terrain, to the east of the region, and the 1.0 to 1.1 Ga Debaca-Swisher terrain and the 1.0 Ga Franklin Mountains igneous rocks, which underlie most of the study area (Adams et al., 1993; Black, 1973; Denison et al., 1984; Goetz, 1977). (Figure 2.3) Episodic periods of extension also occurred during the Precambrian, as suggested by bimodal igneous intrusions (1.215 to 1.074 Ga) found in the Central Basin Platform, Pajarito Mountain, the Franklin Mountains, and the Van Horn uplift (Adams, 1993; Dickerson, 1989). (Figure 2.3)

Continental rifting again affected the region during the Late Precambrian or Early Cambrian as the North American craton was separated from the proto-Afro-South American plate (Shepard and Walper, 1982). The Tobosa Basin, the precursor to the Permian Basin, formed along the Delaware Aulacogen, one of the failed-rift arms associated with this episode of rifting (Shepard and Walper, 1982). The Tobosa Basin was flanked on the west and east by the Diablo arch and the Texas arch, respectively (Adams, 1965). (Figure 1.14) The Paleozoic (Mid-Cambrian to Devonian) was generally a period of little tectonic activity, with the region occupying the broad, west-northwest trending passive margin of the southwestern North American craton (Dickerson, 1989; Goetz, 1977; Shepard and Walper, 1982). The broad continental shelf that formed along this passive margin consisted of a series of undulating shelf ridges and troughs

(Dickerson, 1989). At the start of the Late Ordovician the proto-Atlantic or Iapetus Ocean began to close as the passive margin of the southwestern North American craton transitioned to an active margin (Shepard and Walper, 1982).

During the Late Paleozoic (Early Pennsylvanian) uplift was renewed due to the collision of the southern margin of North America with South America-Africa during the Ouachita-Marathon orogeny (Dickerson, 1989; Kluth and Coney, 1981). (Figure 1.15) Differential uplift and subsidence in the foreland of the fold and thrust front resulted in the formation of the Diablo and Central Basin Platforms and the adjacent Orogrande (the precursor of the Tularosa Basin), Delaware, and Midland Basins (Dickerson, 1989; Goetz, 1977). (Figure 1.15) The Central Basin Platform was uplifted along reactivated faults of the Delaware Aulacogen, while the Delaware and Midland Basins subsided (Shepard and Walper, 1982). To the north, the Pedernal uplift became a dominant structural feature and acted as a primary source of sedimentary detrital material to the Orogrande Basin to the west and the Delaware Basin to the east during most of the Permian (Black, 1973). The Sierra Diablo region was also uplifted and faulted during the Pennsylvanian (King, 1948).

Uplift of the southern portion of the north-south trending Pedernal landmass was greatest during the Late Pennsylvanian to Early Permian (Wolfcampian Stage), and cut the study area in half (Meyer, 1968). The southeast margin of the Orogrande basin, named the Sacramento shelf, occupied the western portion of the present Otero Mesa as well as the region of the Hueco and Sacramento Mountains (Meyer, 1968). (Figure 1.15) The shelf portion of the Delaware basin, known as the Northwestern shelf, occupied the eastern portion of the study area (Meyer, 1968). (Figure 1.15) This uplift resulted in the

extensive folding and faulting of Precambrian through Early Permian strata, and the localized removal of the thick sequence of Paleozoic rocks overlying the Precambrian basement (Black, 1976; Kottlowski, 1963).

Coarse grained clastic rocks and red beds derived from the Pedernal uplift form most of the Wolfcampian (Abo Formation) near Alamogordo, New Mexico (Kottlowski, 1963). Southward, the coarse-grained clastics are restricted mainly to the lower (Pow Wow Conglomerate) or upper parts (Abo Formation tongues in the Hueco Formation) of the Wolfcampian (Kottlowski, 1963). Uplift of the Diablo Platform also occurred during the Early Wolfcampian, and resulted in the localized deposition of limestone conglomerates and red beds that form the basal part of the Wolfcampian (Pow Wow Conglomerate) in western-most Trans-Pecos Texas (Kottlowski, 1963). By the Late Wolfcampian, the Pedernal uplift was almost completely buried by uppermost red beds of the Abo Formation derived from emergent areas far to the north, and the later Permian units (Leonardian Yeso Formation and Guadalupian San Andres Formation) were deposited over a relatively even surface (Kottlowski, 1963).

During the Permian, down-to-the-northeast faulting propagated along several northwest trends, which include, from north to south, Huapache monocline, the Otero fault, the Babb flexure, and the Victorio flexure (Dickerson, 1989; Goetz, 1977, 1985). (Figures 2.21 and 2.22) The Huapache thrust zone, the Victorio and Babb flexures, as well as the southwest-northeast trending, down-to the-southeast Bone Spring flexure, outlined the northwest margins of the Delaware Basin, and controlled sedimentation in the basin and along the margins of the basin throughout the Late Paleozoic (Black, 1973; Dickerson, 1989; King, 1948). (Figures 2.21 and 2.22) Tectonic activity stopped by the

end of the Permian, and regional uplift through the Late Jurassic resulted in the formation of a broad peneplain, known as the Wichita peneplain (Goetz, 1977; McAnulty, 1976).

During the Mesozoic, extension related to the breakup of Pangea and the opening of the Gulf of Mexico resulted in the development of the northwest trending Chihuahua trough to the southwest of the Diablo and Coahuila Platforms (Goetz, 1977; Keller et al., 1983; Shepard and Walper, 1982). (Figure 1.16) During the Jurassic and Cretaceous approximately 1,830 meters (6,000 feet) of marine sediments accumulated in the Chihuahua trough, and unconformably lapped onto Permian strata along the western edge of the Diablo Platform (Goetz, 1977; McAnulty, 1976; Shepard and Walper, 1982). Towards the close of the Cretaceous Period sedimentation became largely fluvial and deltaic, and finally completely continental (Shepard and Walper, 1982). The beginning of Laramide deformation during the Late Cretaceous brought an end to the extensional regime, and marked a return to compressional tectonics (Black, 1973). The east-west directed compressional stress of the Laramide orogeny thrust and folded the Mesozoic fill of the Chihuahua trough against the stable Diablo-Coahuila Platform, resulting in the formation of the Chihuahua tectonic belt (Goetz, 1977; Keller et al., 1983; McAnulty, 1976). (Figure 1.16) Uplift and folding, associated with Laramide compression, was prominent throughout the Salt Basin region during the Late Cretaceous to Early Cenozoic, resulting in northwest to westerly trending folds (Black, 1973; King and Harder, 1985).

Late Eocene-to-Oligocene igneous activity was widespread throughout Trans-Pecos Texas, overlapping the transition between Laramide compression and Basin and Range extension (McLemore and Guilinger, 1993). (Figure 1.4) These igneous intrusions

form the core of the Cornudas Mountains and Dantes dome (Black, 1973). (Figure 1.4) Cenozoic Basin-and-Range extension produced the current physiographic form of the region, with the uplift of the Sacramento, Hueco, Sierra Diablo, Brokeoff, Guadalupe, Delaware, and Apache Mountains, and the formation of broad intermontane basins (Goetz, 1977). (Figure 1.3) Basin-and-Range extensional structures overprint all the earlier structures, but are strongly influenced by the pre-existing structural grains (Shepard and Walper, 1982). Continued extensional tectonic activity in the Salt Basin graben through the present day is evidenced by the preferential alignment of Quaternary, possibly Holocene, fault scarps, and playa lakes along the western side of the graben (Goetz, 1980).

Goetz (1985) proposed two distinct tectonic episodes related to formation of the Salt Basin graben. First, the Otero Mesa/Diablo Plateau was translated northward and rotated counterclockwise between the left-lateral transtensional Rio Grande rift fault zone and the right-lateral transtensional Salt Basin Fault System. Second, the region experienced a stronger east-west component of Basin-and-Range extension, and the current horst-and-graben structure developed along pre-existing fault zones.

FIGURES – CHAPTER 1
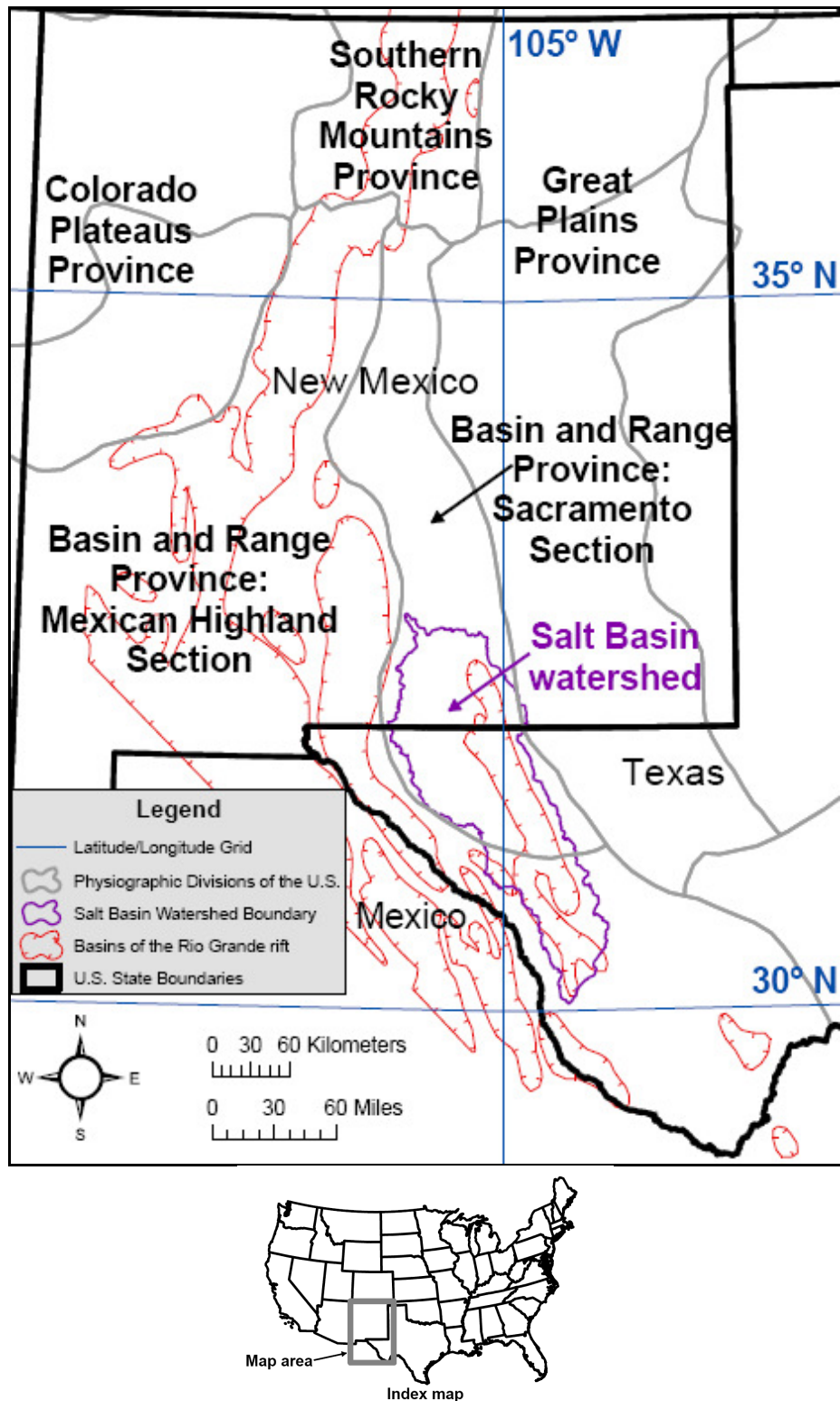
Figure 1.1: Location of Salt Basin watershed with respect to physiographic divisions of the U.S., from Fenneman and Johnson (1946), and basins of the Rio Grande rift, from Keller and Cather (1994).

Salt Basin watershed boundary taken from U.S. Department of Agriculture (USDA). U.S. state boundaries taken from the National Atlas.
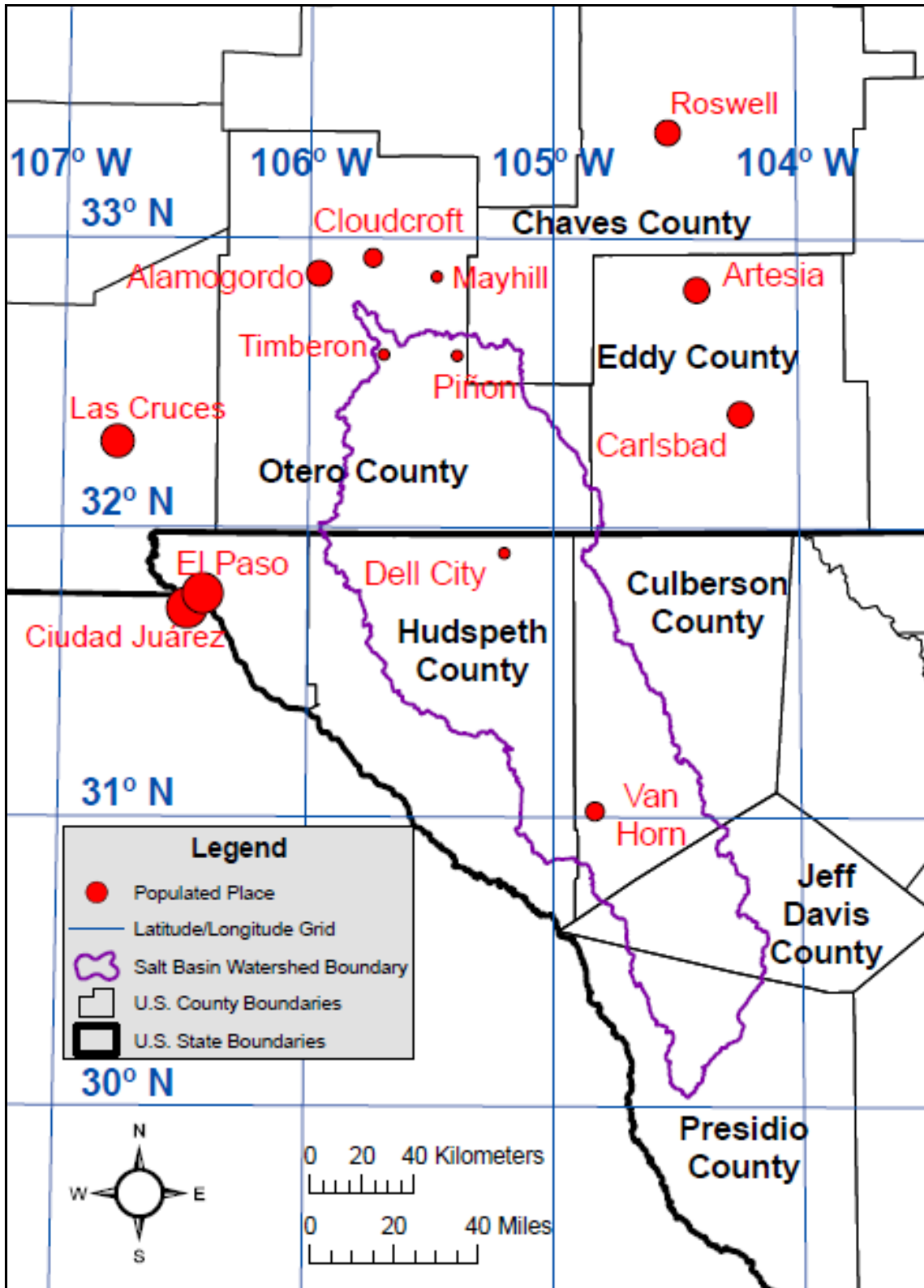
Figure 1.2: Location map of Salt Basin watershed with respect to populated places and U.S. counties of New Mexico and Texas.

Location of populated places, and U.S. county boundaries taken from the National Atlas.
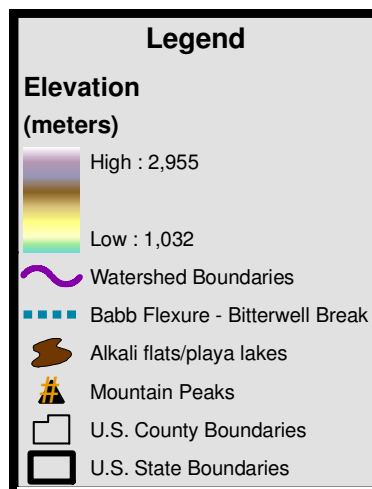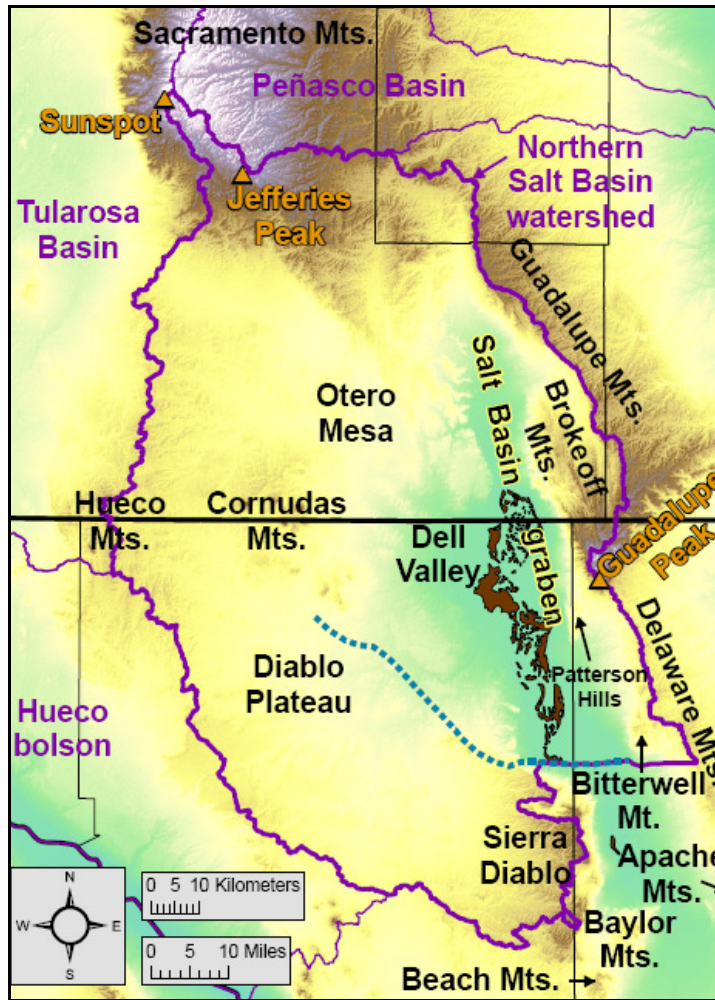
Figure 1.3: Location map of northern Salt Basin watershed, after Hutchison (2006). Elevation taken from the National Elevation Dataset (NED) 1-arc second DEM. Watershed boundaries taken from USDA. Location of Babb Flexure - Bitterwell Break taken from Goetz (1985). Location of alkali flats/playa lakes taken from National Hydrography Dataset (NHD) for New Mexico, and from Stoeser et al. (2005) for Texas.

Figure 1.4: Cenozoic intrusions in the Salt Basin region.
Location of Cenozoic intrusives taken from Stoeser et al. (2005). Alkalic to Calc-Alkalic Line separates calc-alkalic magmatism to the west from alkalic magmatism to the east, from McLemore and Guilinger (1993).
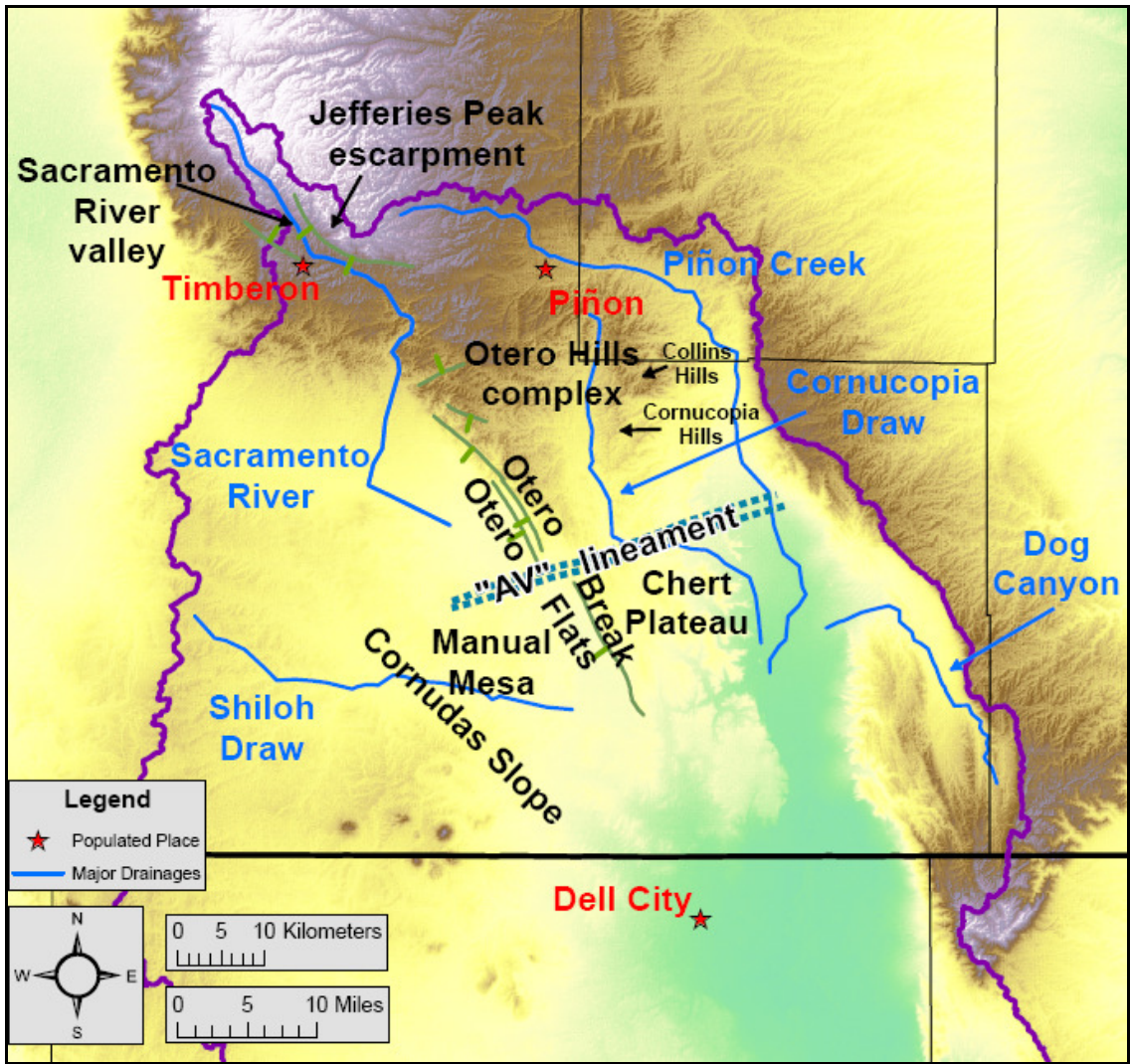
Figure 1.5: Physiographic features of the north and northeast portions of Otero Mesa, from Black (1973).

Bar on downthrown side of normal or high angle faults. Location of major drainages taken from the National Atlas.
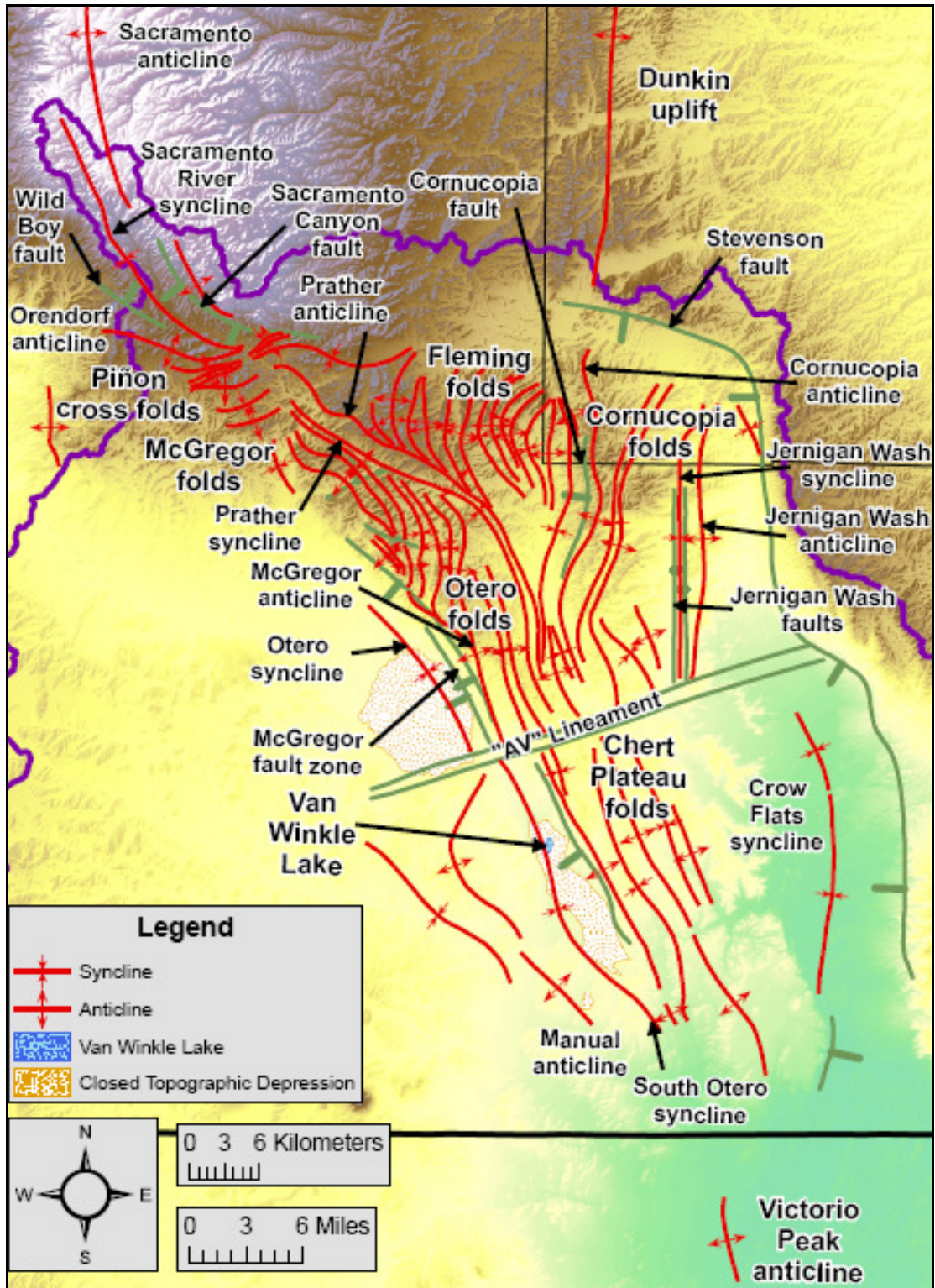
Figure 1.6: Structural features of the north and northeast portions of Otero Mesa, from Black (1973), Broadhead (2002), Goetz (1985), and Kelley (1971). Bar on downthrown side of normal or high angle faults. Location of Van Winkle Lake and closed topographic depressions taken from the U. S. Geological Survey's 1:100,000-scale metric topographic map of Crow Flats, NM-TX.

31
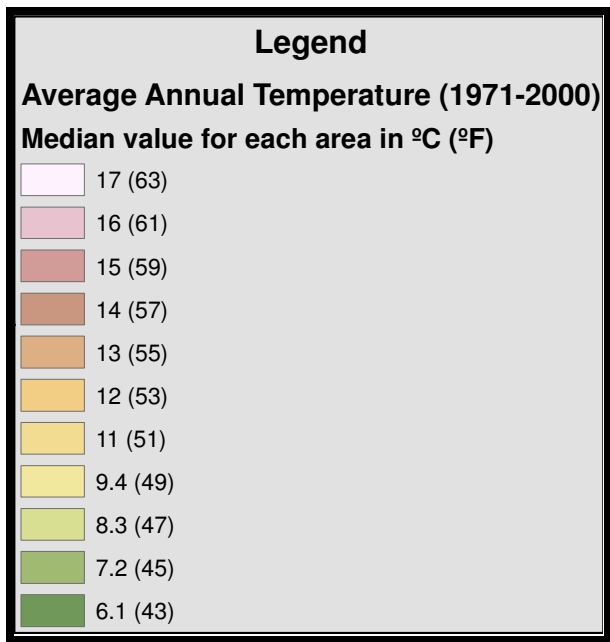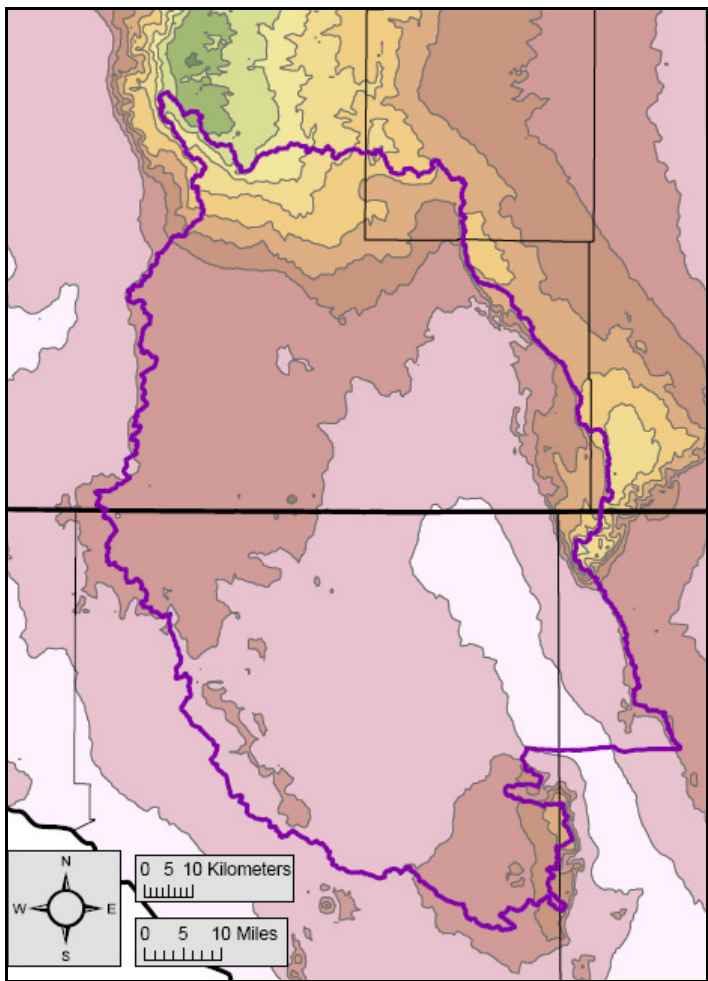
Figure 1.7: Average annual temperature (1971-2000), from USDA.
Source scale: 1:250,000. Horizontal resolution: ~800 meters.
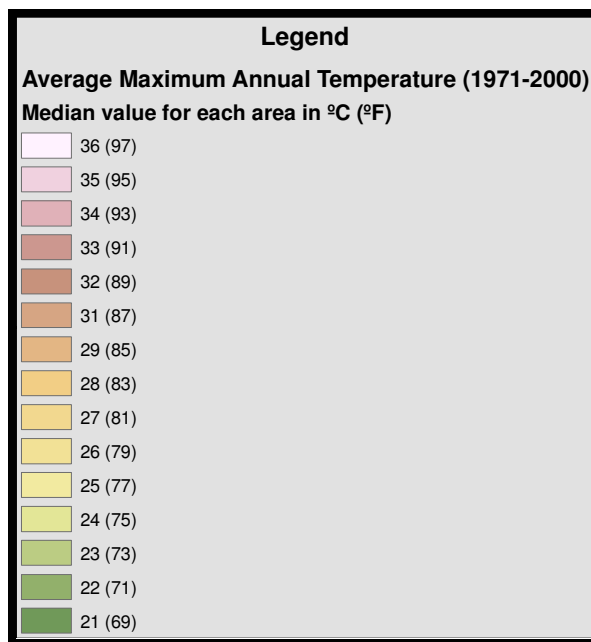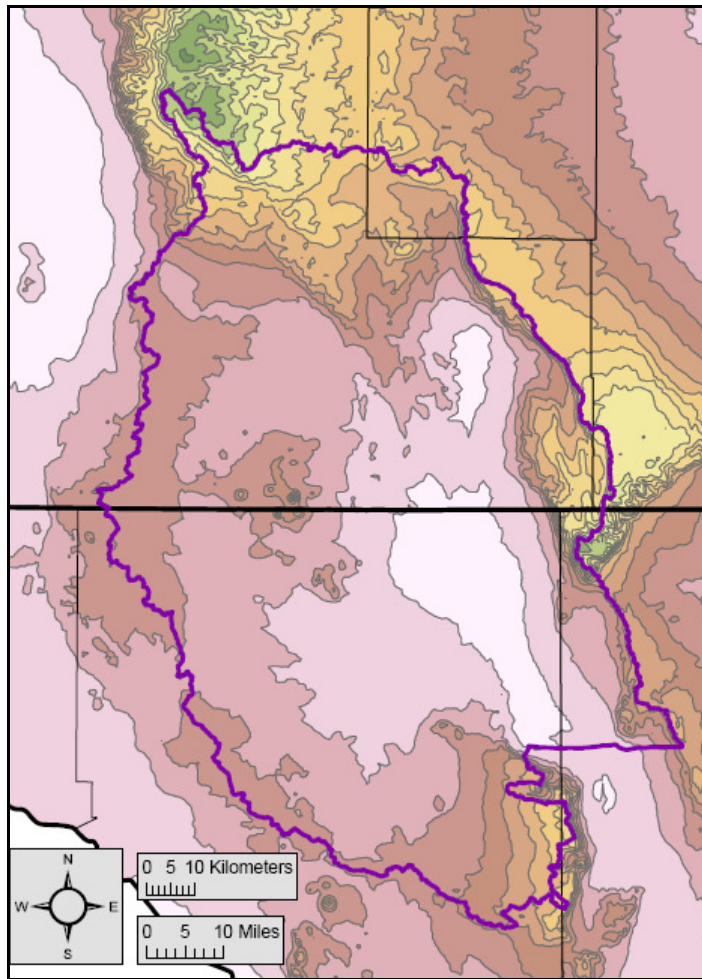
Figure 1.8: Average maximum annual temperature (1971-2000), from USDA.
Source scale: 1:250,000. Horizontal resolution: ~800 meters.
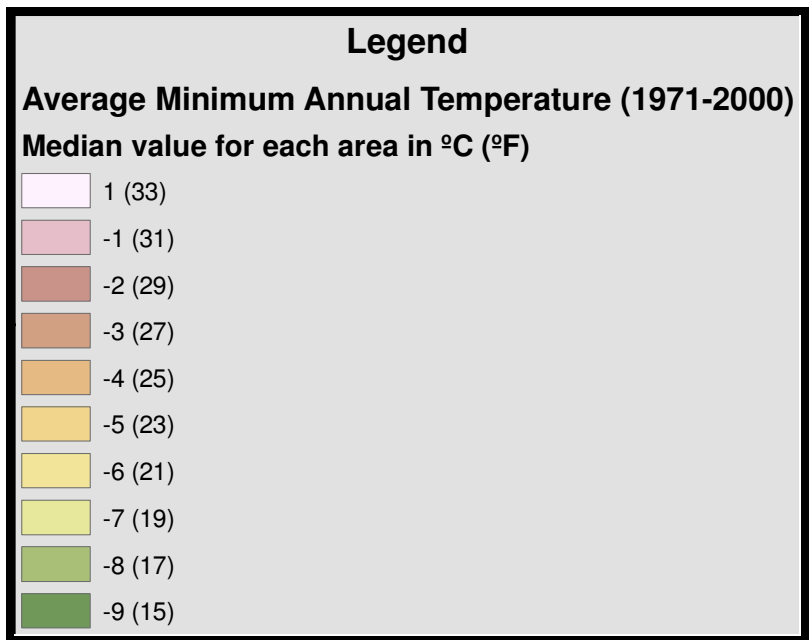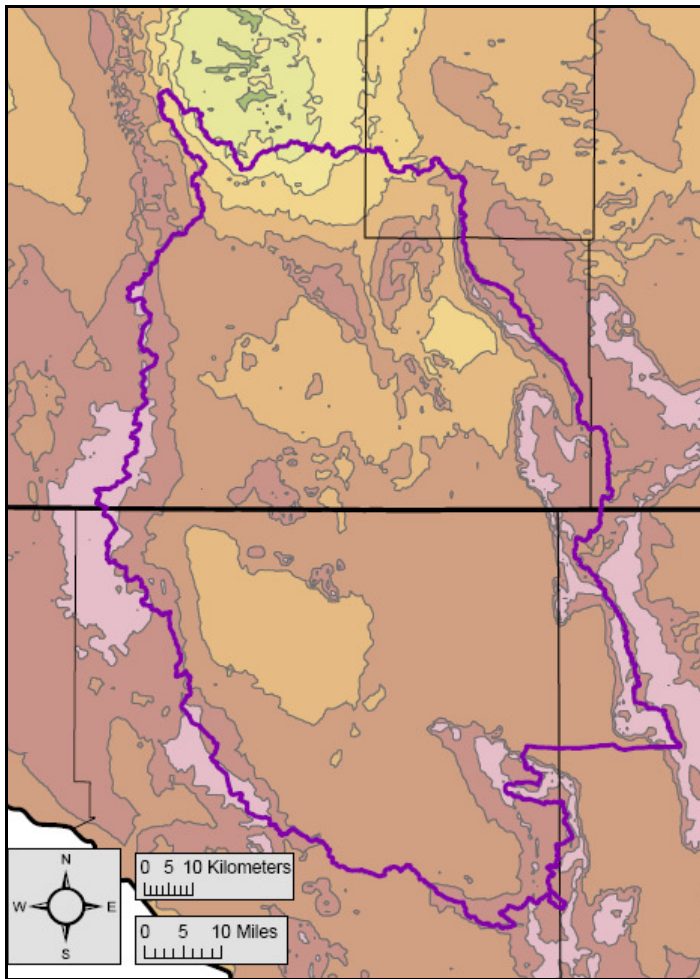
Figure 1.9: Average minimum annual temperature (1971-2000), from USDA.
Source scale: 1:250,000. Horizontal resolution: ~800 meters.
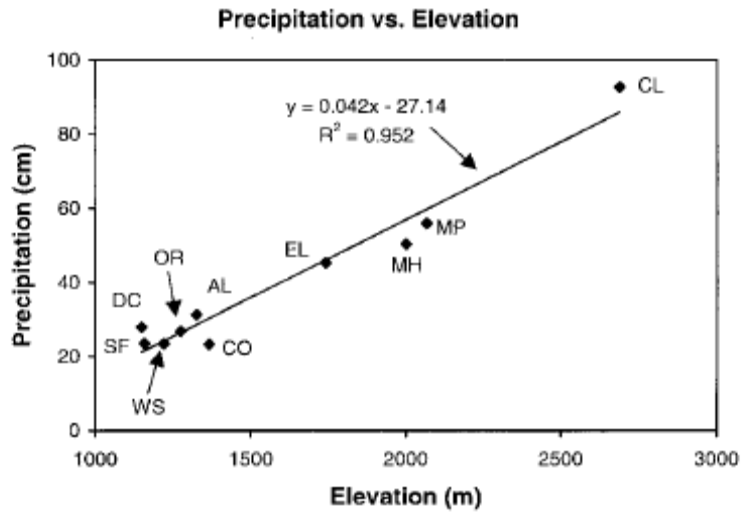
Figure 1.10: Precipitation (cm) as a function of elevation (m) for recording stations in and near the northern Salt Basin watershed, from Mayer and Sharp (1998). Recording stations are: AL – Alamogordo; CL – Cloudcroft; CO – Cornudas; DC – Dell City; EL – Elk; MH – Mayhill; MP – Mountain Park; OR – Orogrande; SF – Salt Flat; WS – White Sands.
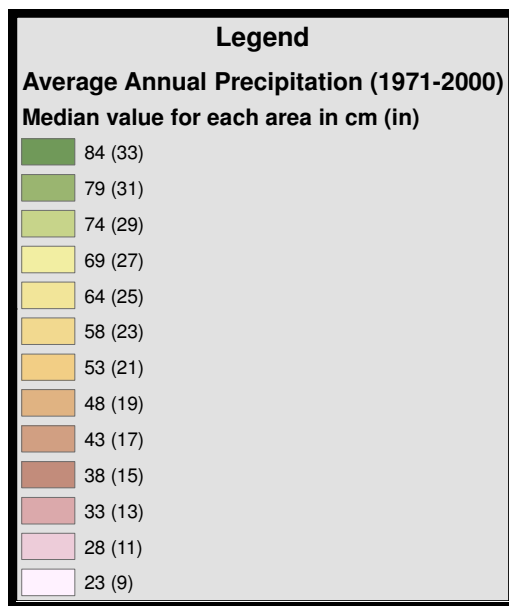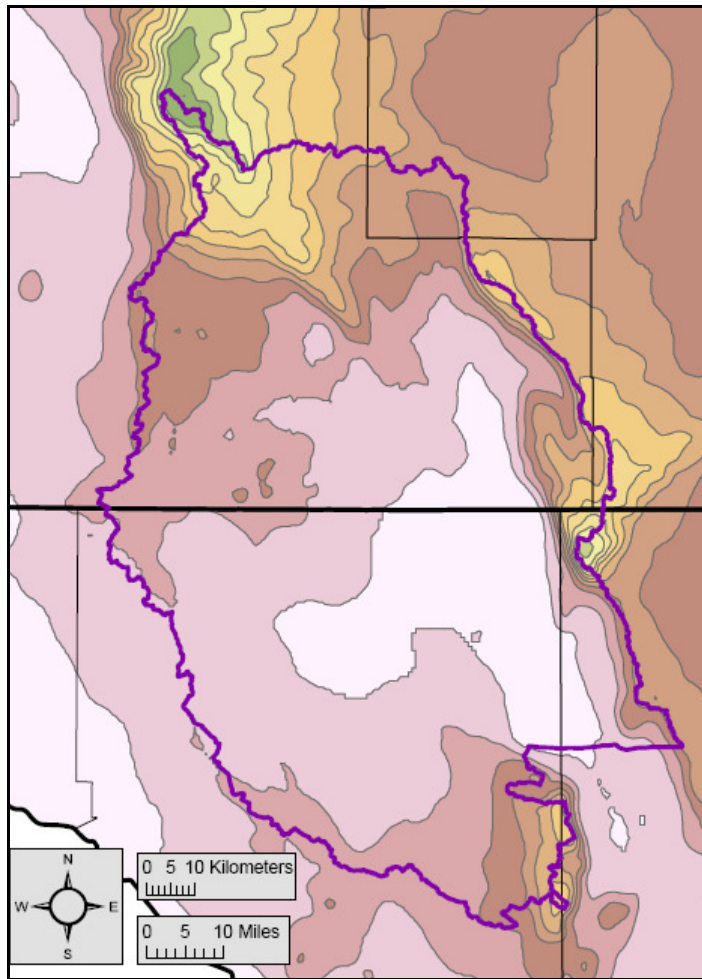
Figure 1.11: Average annual precipitation (1971-2000), from USDA.
Mean monthly precipitation was calculated using PRISM, and then summed to produce
the above map. Source scale: 1:250,000. Horizontal resolution: ~800 meters.
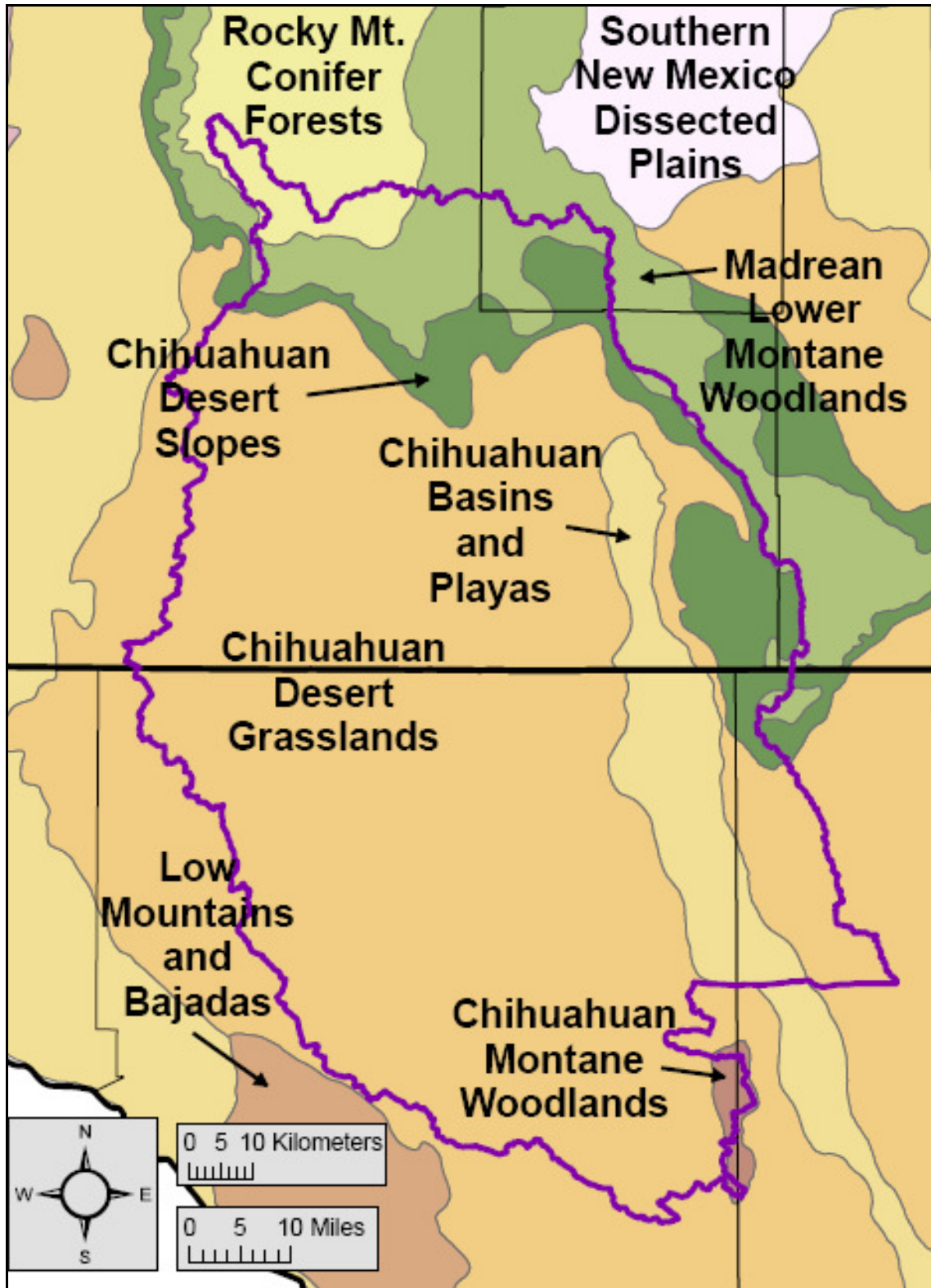
Figure 1.12: Level IV ecoregions within the northern Salt Basin watershed. Ecoregions from the U.S. Environmental Protection Agency (EPA).
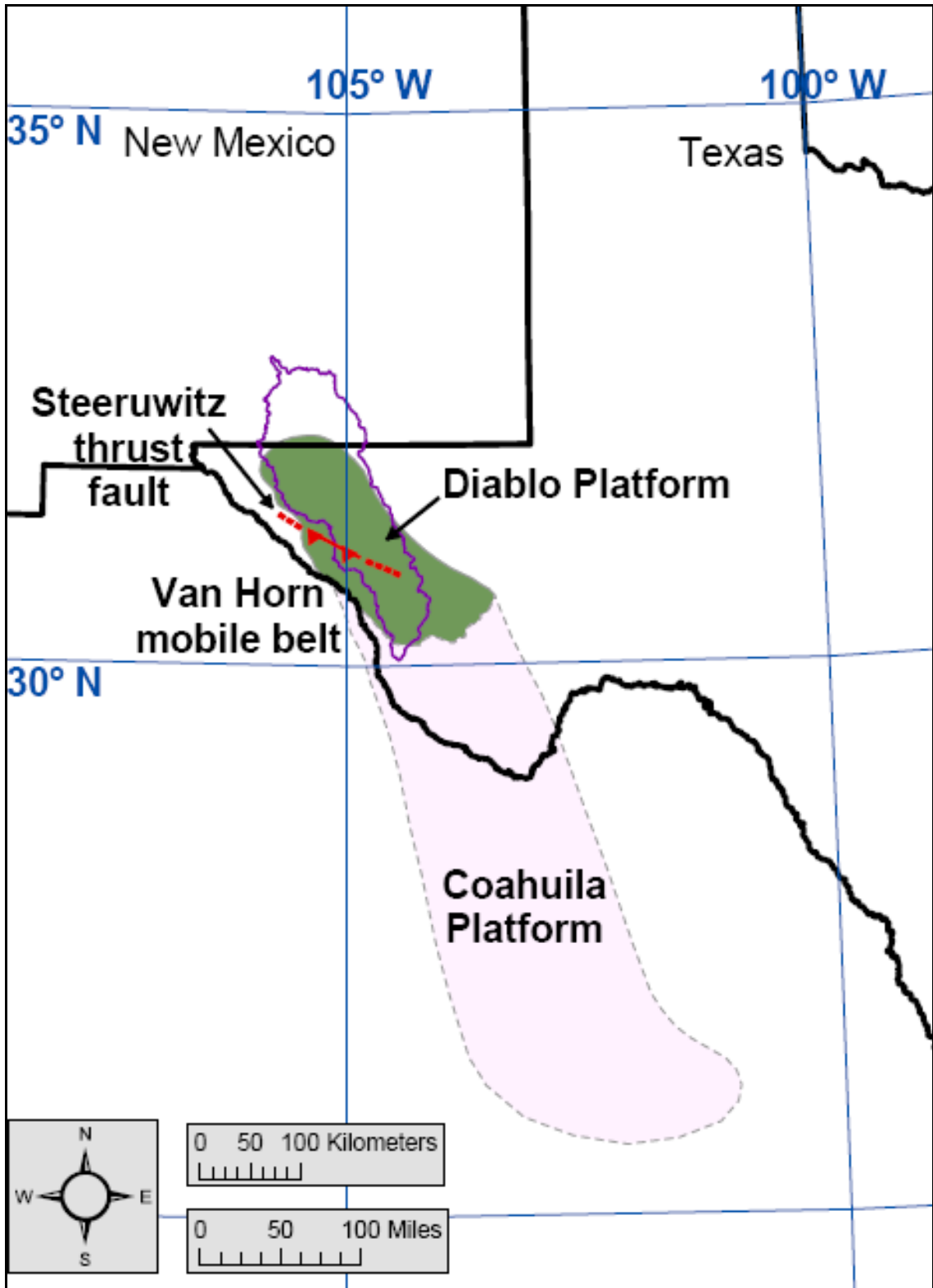
Figure 1.13: Location of the Diablo and Coahuila Platforms, from Shepard and Walper (1982).

Location of Steeruwitz thrust fault taken from Goetz (1977). Features formed about 1.25 Ga.

105° W

100° W

35° N New Mexico

Texas

Diablo arch

Texas arch

Tobosa Basin

30° N

N

W E

S

0 50 100 Kilometers

0 50 100 Miles
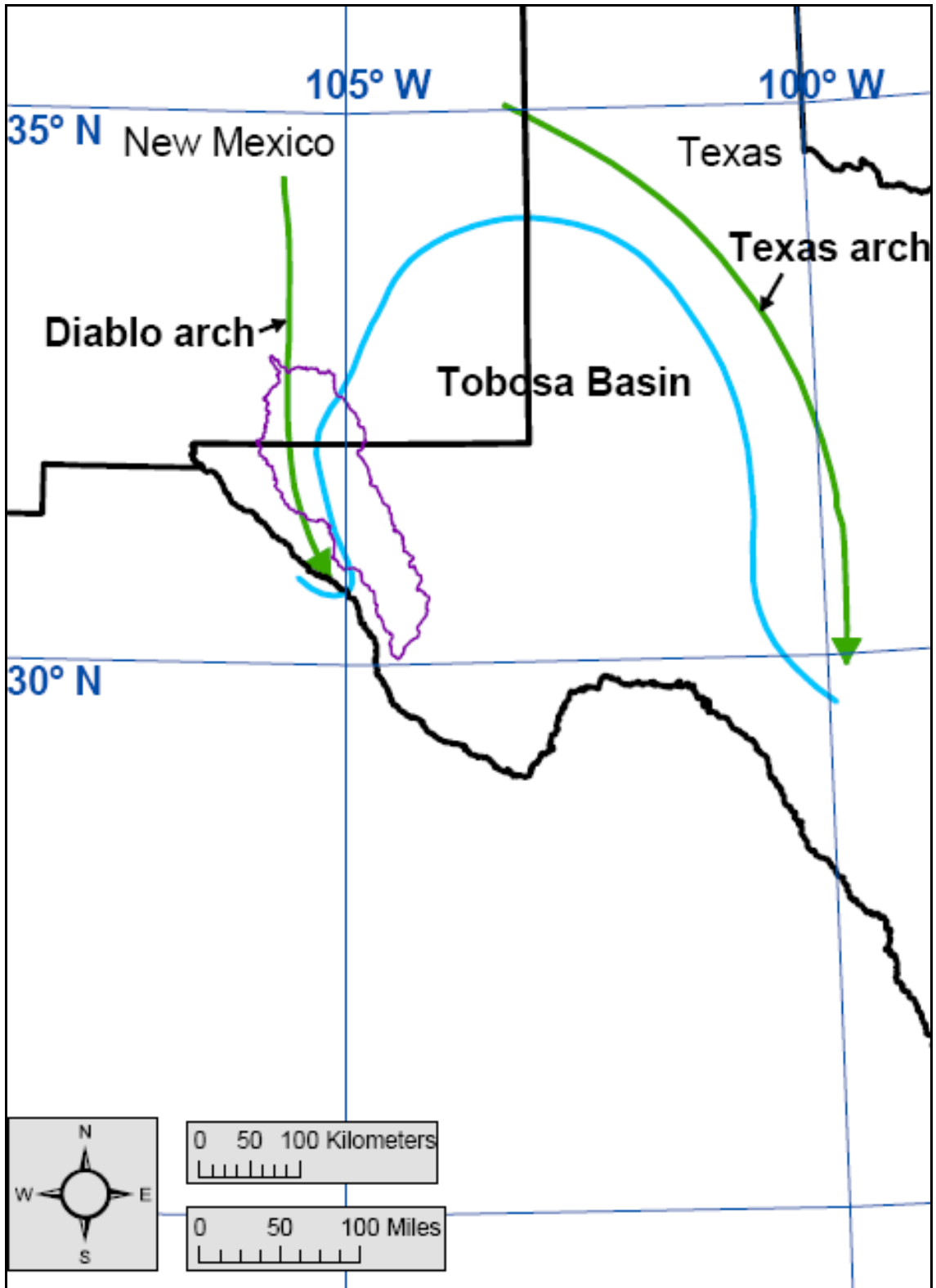
Figure 1.14: Location of the Diablo and Texas Arches, and the Tobosa Basin, from
Adams (1965).
Features formed during the Late Precambrian to Early Cambrian (550 to 510 Ma).
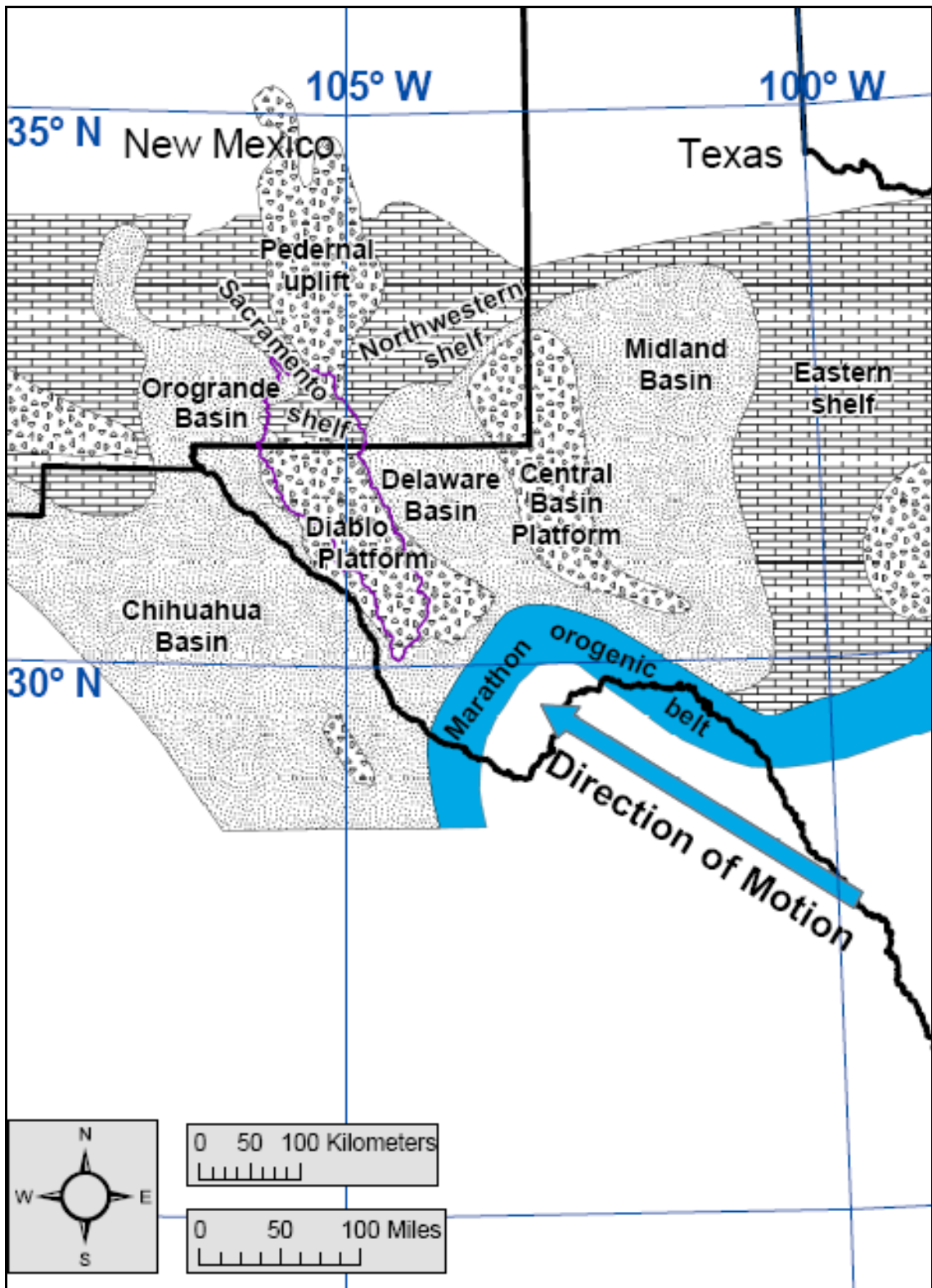
Figure 1.15: Late-Pennsylvanian-to-Early-Permian tectonic features of the Salt Basin region, from Ross and Ross (1985).
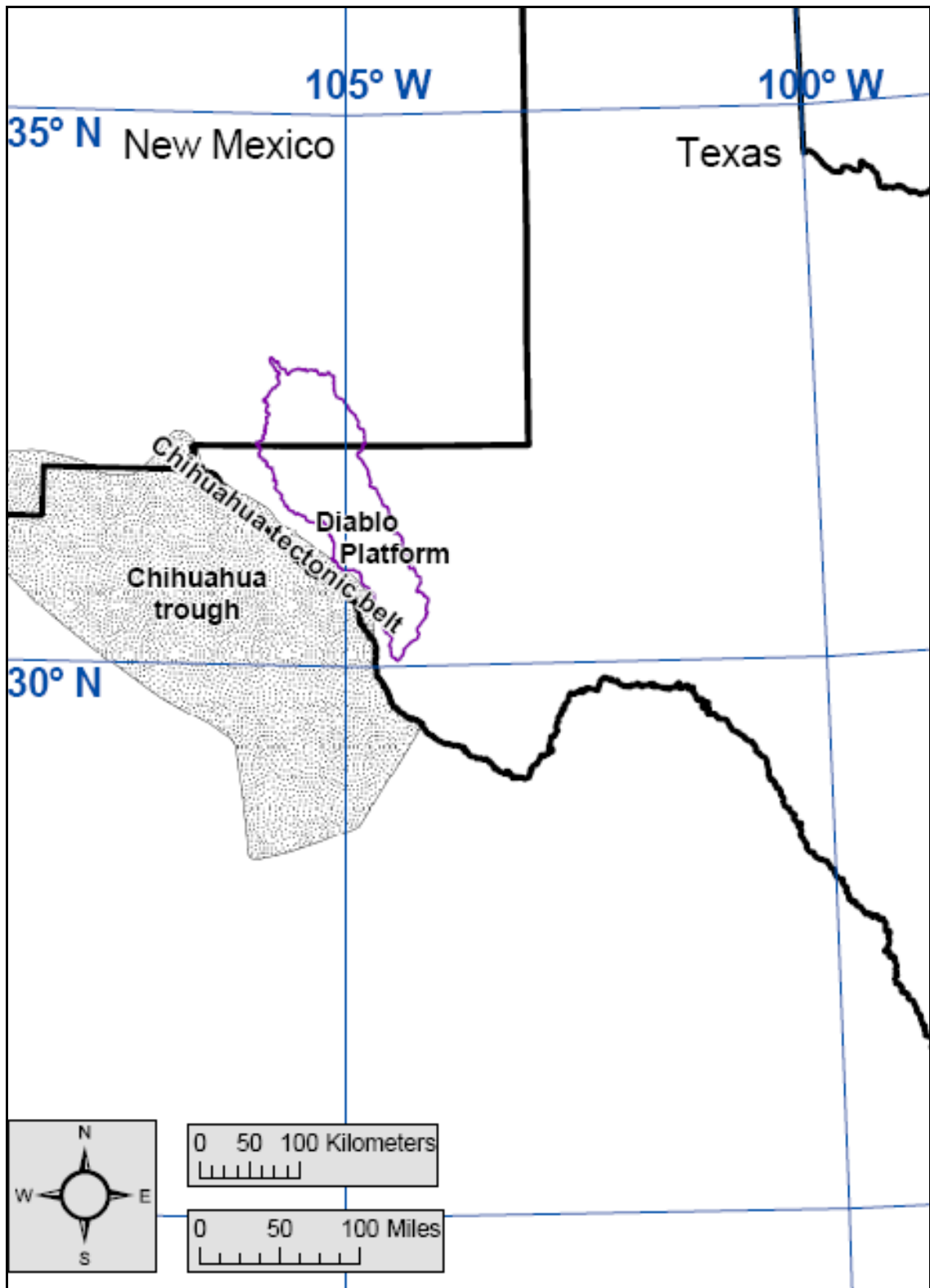
Figure 1.16: Location of the Mesozoic Chihuahua trough and Chihuahua tectonic belt, from Haenggi (2002).

CHAPTER 2: GEOLOGIC FRAMEWORK

2.1: Previous Geologic Studies

Most of the earliest studies in the Salt Basin region were focused on describing the geology of the Guadalupe Mountains (King, 1948). The first observations during the mid-to-late-1800s were associated with the search for a suitable route for a railroad to the Pacific coast (King, 1948). John Pope, G. G. Shumard, and B. F. Shumard were among the most notable of these early explorers (King, 1948). H. S. Tarr of the Texas Geological Survey was the last geologist to visit the Guadalupe Mountains, doing so in 1890, before the turn of the century (King, 1948).

In the early 1900s important studies were conducted in the Guadalupe Mountains by G. H. Girty and G. B. Richardson of the U.S. Geological Survey, and J. W. Beede (Boyd, 1958; King, 1948). In the 1920s the development of oil fields in the region to the northeast and east of the Guadalupe Mountains focused attention on the outcrops exposed in the mountains (Boyd, 1958). A surge of papers were published on the description and interpretation of rocks of the Guadalupe Mountains during this time period, including work by Baker, Blanchard and Davis, Darton and Reeside, Crandall, King and King, Lloyd, and Willis (Boyd, 1958; King, 1948).

P. B. King of U.S. Geological Survey conducted some of the most detailed and important surveys of the stratigraphy and structure of the Salt Basin region in Texas during the mid-1900s. King (1942) described the Permian of West Texas and

Southeastern New Mexico, and developed paleogeographic facies maps of the Permian rocks deposited within the Salt Basin region. King (1948) and King (1965) thoroughly described the stratigraphy and structure of the southern Guadalupe Mountains and the Sierra Diablo, respectively.

Boyd (1958) studied the Permian sedimentary facies and stratigraphic relationships of the central Guadalupe Mountains in New Mexico. Pray (1961) produced a comprehensive account of the stratigraphy and structure of the southern Sacramento Mountains. Kottlowski (1963) provided a regional summary of the Paleozoic and Mesozoic strata of Southwestern and South-Central New Mexico, which included isopach and facies maps. Hayes (1964) described the stratigraphy and structure of the Guadalupe Mountains in New Mexico, which included a detailed description and correlation of the Permian shelf-, shelf-margin-, and basin-facies rocks. Meyer (1968) described the geology of Pennsylvanian and Lower Permian (Wolfcampian) rocks in Southeastern New Mexico, which included isopach and lithofacies maps.

Kelley (1971) investigated the stratigraphy to the north, northeast, and east of the Salt Basin region, as well as the regional structure. Kelley (1971) formally divided the San Andres Formation into three members, in ascending order, the Rio Bonito, Bonney Canyon, and Fourmile Draw Members. Newell et al. (1972) described the stratigraphy and correlation of Permian shelf-, shelf-margin-, and basin-facies rocks of the Guadalupe Mountains in New Mexico and Texas. Black (1973, 1975, and 1976) expanded on the work of Kelley (1971) and produced the first descriptions and interpretations of the stratigraphy and structure of the north-and-northeast portions of Otero Mesa. Foster

(1978) described the stratigraphy and structure of the southern Tularosa Basin, but also included information on the western portion of Otero Mesa.

Goetz (1977, 1980, and 1985) focused on the structure and tectonics of the Salt Basin graben in Texas. Many of the structures displayed on her tectonic sketch map [Goetz, 1985] were incorporated into the structural maps produced for this thesis. King and Harder (1985) studied the oil and gas potential of the Tularosa Basin, Otero Mesa, and Salt Basin graben region in New Mexico and Texas. They described the stratigraphy and depositional environments, produced isopach and lithofacies maps of Paleozoic strata, and discussed the geophysics and structure of the region. Much of the subsurface data presented in their report, in the form of oil-and-gas exploratory well logs and cross-sections, was incorporated into this thesis.

Collins and Raney (1991 and 1997) provided a comprehensive description of the Cenozoic structure of the Hueco bolson and the Salt Basin graben. McLemore and Guilinger (1993), Nutt et al. (1997), and Nutt and O'Neill (1998) studied the geology and mineral resources of the Cenozoic intrusions of the Cornudas Mountains in New Mexico. O'Neill and Nutt (1998) mapped the geology of the Cornudas Mountains region. Their discussion of the stratigraphic relationships around the New Mexico-Texas state line proved invaluable in resolving the differences between the geologic maps of New Mexico and Texas.

More recently, Broadhead (2002) investigated the subsurface structure of the Salt Basin region in New Mexico. He identified numerous Ancestral Rocky Mountain (Pennsylvanian-to-Permian), Laramide (Late Cretaceous-to-Early Cenozoic), and Basin-

and-Range (Cenozoic) structures within the Salt Basin region. His subsurface tectonic map served as a primary reference for the structural maps produced for this thesis.

2.2: Stratigraphy, Depositional Environments, and Facies Distributions

Rocks exposed in the northern Salt Basin range from Precambrian to Quaternary. (Figures 2.1 and 2.2) By far the predominant surface exposures consist of Permian rocks. (Figure 2.1) Figure 2.2 presents a generalized stratigraphic chart of the geologic units in the Salt Basin region, as well as the correlation of these units between different geographic regions and depositional environments. Figures 2.4 through 2.16 present paleogeographic reconstructions of the Salt Basin region from the Late Precambrian, 550 Ma, to the present, and are referenced throughout this section to illustrate the depositional environments associated with the geologic units described herein. Figures 2.17 through 2.19 illustrate the resultant distribution of facies during the Permian, and are also referenced throughout this section.

2.2.a: Proterozoic

There are very few exposures of Precambrian rocks in the Salt Basin, although some do crop out on the Diablo Plateau at Pump Station Hills, in the southern Hueco Mountains, in the southern portion of the Sierra Diablo region, and along the base of the Sacramento Mountains escarpment south of Alamogordo, New Mexico (Denison and Hetherington, 1969; King, 1965; Masson, 1956; Pray, 1961). Pray (1961) described the Precambrian rocks exposed in the Sacramento Mountains as slightly metamorphosed sedimentary rocks (largely shale, siltstone, and fine-grained quartz sandstone) intruded by igneous sills of basic-to-intermediate composition, some of which are porphyritic. In the Hueco Mountains the Precambrian is a red, partly micrographic perthite granite (Denison

and Hetherington, 1969). Masson (1956) extensively described the Precambrian rocks at Pump Station Hills and found the dominant rock type to be a rhyolite porphyry, with some fine micrographic granite porphyry and other rock types also present.

Oil-and-gas exploratory well cores provide the primary source of information on the type and distribution of Precambrian rocks in the region. Precambrian rocks include the 1.4 Ga and older Chaves Granite and Granitic Gneiss, the 1.25 Ga Carrizo Mountain Group metamorphic rocks, the 1.0 to 1.1 Ga DeBaca-Swisher metasedimentary and basaltic rocks, and the 1.0 Ga Franklin Mountains igneous rocks (Denison et al., 1984). (Figure 2.3) Precambrian rocks exposed in the Sacramento Mountains and encountered in the Southern Production Co., Cloudcroft Unit #1 (SPCCLU1) well [Figure 3.1] fall within the DeBaca-Swisher Terrain (Denison and Hetherington, 1969; Pray, 1961). (Figure 2.3) Precambrian rocks exposed in the southern Hueco Mountains and at Pump Station Hills are related to the Franklin Mountains igneous rocks (Denison and Hetherington, 1969). (Figure 2.3) In the southern portion of the Sierra Diablo region the Precambrian is represented by the Carrizo Mountain Group, consisting of quartzite, schist, phyllite, and marble overlain and intruded by metarhyolite and amphibolite, which has been thrust over the thick marbles with interbedded phyllite, chert, and pyroclastic volcanic rocks of the Allamore Formation and the overlying coarse-grained conglomerate and sandstone of the Hazel Formation (Denison and Hetherington, 1969).

Rocks of the Chaves Granitic Terrain were covered by a varied series of later Precambrian sediments (Black, 1973). These later sediments were eventually metamorphosed to form the DeBaca-Swisher Terrain, which were contemporaneously or slightly later intruded by the Franklin Mountains igneous rocks (Black, 1973). These

46

rocks were eventually deeply eroded, and the overlying Lower Paleozoic rocks were deposited over this heavily eroded surface (Black, 1973).

2.2.b: Early Paleozoic

During the Early Paleozoic, the Salt Basin region was situated along the passive margin of the southwestern North American craton (King and Harder, 1985). Seas spread across the region, depositing the Cambrian-Ordovician Bliss Sandstone, Ordovician carbonates of the El Paso and Montoya Groups (LeMone, 1969), and Silurian carbonates of the Fusselman Formation (King and Harder, 1985). (Figures 2.4 and 2.5) In the Salt Basin, all of these Lower Paleozoic units are exposed in the Sacramento and Hueco Mountains, and in the Sierra Diablo region (King, 1965; King et al., 1945; Kottlowski, 1963; Pray, 1961).

The Bliss Sandstone is predominantly a quartz sandstone, partly glauconitic, with thin interbeds and lenses of siliceous hematite, arenaceous shale, and arenaceous limestone that records deposition in a shallow marine environment far from the shoreline (Kottlowski, 1963). (Figures 2.4b, 2.4c, and 2.4d) In general, the Bliss Sandstone thickens southward, but was removed from areas to the north and south due to uplift of the Pedernal landmass and Diablo Platform, respectively, during the Pennsylvanian to Early Permian (Kottlowski, 1963).

The El Paso Group (LeMone, 1969) is equivalent to the Ellenburger Group, which is often indicated in subsurface oil-and-gas wells in the Permian Basin (Hayes, 1964; Kottlowski, 1963). In the Sacramento Mountains the El Paso Group consists of dolomite, minor sandy dolomite, and dolomitic quartz sandstones, which record deposition on a broad open-marine shelf, in shallow, moderately turbulent water (Pray, 1961). (Figures

2.4d and 2.5a) In the Hueco Mountains the El Paso Group consists predominantly of thin-bedded, mottled limestone, with thicker-bedded, dolomitic limestone near the top of the unit (King et al., 1945). In general, the El Paso Group thickens southward due to erosion to the north before deposition of the overlying Montoya Formation (Kottlowski, 1963). Similar to the Bliss Sandstone, the El Paso Group was removed from the areas associated with the uplift of the Pedernal landmass and the Diablo Platform (Kottlowski, 1963).

The Bliss and El Paso are time-transgressive units that are older to the west and become younger to the east, due to the transgression of the Cambrian and Early Ordovician sea from west to east (Hayes, 1964; Kottlowski, 1963; LeMone, 1969). (Figures 2.4b through 2.5a) In actuality this transgression was not a simple, single transgression, but a series of transgressions and regressions (LeMone, 1969).

The Montoya Group was originally deposited as a limestone, but has since been largely irregularly dolomitized (Kottlowski, 1963). (Figure 2.5b) In the Hueco Mountains, however, about 50% of the Montoya is limestone (Kottlowski, 1963). The Montoya Group generally increases in thickness from north to south, the bulk of this increase being depositional (Kottlowski, 1963). Similar to the Bliss and El Paso, the Montoya was removed from the areas associated with the uplift of the Pedernal landmass and the Diablo Platform (Kottlowski, 1963). Valmont Dolomite has been used by Pray (1961) in the Sacramento Mountains to describe the distinctive upper unit of the Montoya Group.

The Fusselman Formation is an aphanitic to coarsely crystalline, grayish brown to dark gray, massive, light brown- to dark yellowish brown-weathering dolomite (Kottlowski, 1963). The Fusselman thickens from north to south, due primarily to Late

Silurian and Early Devonian erosion to the north, but also probably depositional thickening to the south (Kottlowski, 1963). (Figures 2.5d and 2.6a) The Fusselman records deposition on a shallow marine shelf adjacent to the subsiding Tobosa Basin to the southeast (McGlasson, 1969). (Figures 1.14, 2.5c, and 2.5d) The Fusselman is unconformably overlain by Devonian strata, and a Devonian eroded edge is located just north of Alamogordo, New Mexico in the Sacramento Mountains (Kottlowski, 1963). The Fusselman was also removed from the area associated with the uplift of the Diablo Platform during the Early Wolfcampian (Kottlowski, 1963).

Uplift of the Peñasco dome to the north beveled and eroded these older Paleozoic rocks, before shallow seas again spread over the region and deposited the Devonian Oñate and Sly Gap Formations, the Percha and Woodford Shales, and the cherty Canutillo Formation (King and Harder, 1985; Kottlowski, 1969). (Figures 2.6a, 2.6b, and 2.6c) Similar to the Fusselman Formation, the Devonian units record deposition on a shallow marine shelf adjacent to the subsiding Tobosa Basin to the southeast (McGlasson, 1969). (Figures 2.6b and 2.6c) The Devonian Oñate Formation silty facies is found throughout the Sacramento Mountains, but transitions to the gray-black Percha Shale to the south (Kottlowski, 1963; Pray, 1961). The silty Sly Gap facies is largely restricted to the northern and central parts of the Sacramento Mountains (Pray, 1961). The Devonian thickens further to the south in the Hueco Mountains, where it contains an upper shaly zone consisting mostly of soft, calcareous, silty shale and lenses of silty limestone equivalent to the Oñate, Sly Gap and Percha to the north, and a lower zone of cherty limestones of the Canutillo Formation (Kottlowski, 1963). The Devonian is also exposed in the Sierra Diablo region (King, 1965).

The Oñate and Sly Gap Formations record deposition far from a shoreline (Kottlowski, 1963). (Figure 2.6c) The Percha Shale is equivalent to the subsurface Woodford Shale farther to the east (McGlasson, 1969). East of the Hueco Mountains, in the subsurface, the Canutillo Formation becomes argillaceous and eventually grades into the lower part of the Percha/Woodford Shale (McGlasson, 1969). The black, fissile Percha/Woodford Shale and the cherty Canutillo Formation record deposition in restricted, stagnant basins (Kottlowski, 1963). (Figures 2.6b and 2.6c) In general the Devonian units thicken from north to south (Kottlowski, 1963). The Devonian units are also characterized by a similar Late Pennsylvanian and Early Permian eroded edge to the north in the Sacramento Mountains and to the south on the Diablo Platform as the Bliss, El Paso, Montoya, and Fusselman (Kottlowski, 1963).

2.2.c: Late Paleozoic

During the Mississippian and Pennsylvanian, the seas extended even farther into the North American craton, depositing a wide range of carbonates (King and Harder, 1985). (Figures 2.6d through 2.8d) Mississippian and Pennsylvanian rocks are exposed in the Sacramento and Hueco Mountains, and in the Sierra Diablo region (King, 1965; King et al., 1945; Kottlowski, 1963; Pray, 1961). In general, Mississippian strata thicken to the south, due to depositional thickening to the south, and erosional thinning associated with the Pedernal uplift to the north (Kottlowski, 1963). Mississippian strata were also removed from the region of the Diablo Platform due to uplift during the Early Wolfcampian (Kottlowski, 1963). Chesterian strata pinch out to the north of a line approximately along latitude 33º N, which is likely close to the northern shoreline, due to deposition on an inclined surface associated with pre-Chesterian deformation

50

(Kottlowski, 1969; Meyer, 1968). (Figures 2.7a, 2.7b, and 2.7c) Upper Mississippian (Chesterian) strata (Helms Formation of south-central New Mexico and western-most Texas, and its western equivalent the Paradise Formation) consist mainly of massive limestones which grade abruptly southeastward into black shales of the Delaware Basin that are considered to by equivalent to the Barnett Shale of southeast New Mexico and west Texas (Kottlowski, 1969; Meyer, 1968).

North of latitude 33° N Mississippian rocks are Meramecian (Meyer, 1968). Farther to the northwest the strata (Caballero and Lake Valley Formations) are mainly Lower to Middle Mississippian (Kinderhookian to Osagean) (Kottlowski, 1963; Meyer, 1968). Most of these Lower to Middle Mississippian strata are crinoidal limestones that formed biohermal reefs (Kottlowski, 1969). (Figures 2.6d and 2.7a) The Middle Mississippian (Meramec) Rancheria Formation forms an anomalous dark siliceous limestone facies that thins and abruptly grades northward from the Franklin Mountains to near the northern limit of the Helms Formation in the southern Sacramento Mountains (Kottlowski, 1963; Kottlowski, 1969). The Rancheria also occurs locally throughout southeastern New Mexico, and represents deposition in a relatively deep, stagnant basin (Kottlowski, 1969). (Figures 2.7a and 2.7b)

Late Mississippian-to-Early Pennsylvanian uplift to the north in central and northern New Mexico tilted and eroded the older Paleozoic units such that Pennsylvanian strata were deposited on Mississippian to Precambrian rocks from south to north (Kottlowski, 1969; Meyer, 1968). (Figure 2.7c) In the Salt Basin, Lower Pennsylvanian (Morrowan) beds unconformably overlie Mississippian beds with a hiatus that represents the Early Pennsylvanian Springeran (Meyer, 1968). Early movements along the northern

51

portion of the Pedernal uplift during the Late Mississippian-to-Early Pennsylvanian provided a source of sediment to the subsiding Orogrande and Delaware Basins to the west and east, respectively (Kottlowski, 1963; Meyer, 1968). (Figures 2.7b, 2.7c, and 2.7d) The Pennsylvanian was marked by a major transgression that began in the Morrowan and climaxed in the Virgilian at the close of the Pennsylvanian (Meyer, 1968). (Figures 2.7d through 2.8d)

Like the Mississippian, the Pennsylvanian in southeastern New Mexico was a time of carbonate deposition, with the carbonates most commonly being interbedded with shale (Meyer, 1968). Pennsylvanian rocks in southeastern New Mexico represent a marine sequence of two principal facies: 1) black limestones and shales, and 2) light-colored fossiliferous limestones and variegated shales (Meyer, 1968). East of the Pedernal uplift, Pennsylvanian sediments transgress southeast to northwest, onlapping onto the uplift (Meyer, 1968). Upper Mississippian and Pennsylvanian strata were deposited continuously across the southern quarter of the Pedernal uplift (Meyer, 1968). During the Pennsylvanian, the northern three-quarters of the Pedernal uplift was never a high mountain range, but ranged from a slight emergent feature to a shoal area at various times and places (Meyer, 1968).

Subsurface geologists of west Texas often use Bend, Strawn, Canyon, and Cisco for Derryan, Desmoinesian, Missourian, and Virgilian nomenclature, respectively (Meyer, 1968). Also, the Derryan Stage is correlative with the Atokan Stage (Meyer, 1968). In the Sacramento Mountains, Pray (1961) divided the Pennsylvanian into three major rock units in ascending order: the Gobbler, Beeman, and Holder Formations. The Gobbler ranges in age from Morrowan to Middle Missourian, the Beeman ranges in age

from Middle to Upper Missourian, and the Holder is essentially Virgilian (Pray, 1961). Another term, Magdalena (Formation or Group), has been used to refer to all of the Pennsylvanian as well as part of the Permian below the Abo Formation (Pray, 1961). Panther Seep Formation is another term that has been applied to Upper Pennsylvanian (Virgilian) strata in the San Andres Mountains to the west (Kottlowski, 1963; Pray, 1961).

Uplift of the southern portion of the Pedernals during the Late Pennsylvanian provided a large source of sediment to the Orogrande and Delaware Basins, and largely removed the thick sections of Mississippian and Pennsylvanian strata from the region (King and Harder, 1985; Meyer, 1968). (Figures 2.8c and 2.8d) A regression followed during the Wolfcampian, as red beds derived from a major uplift to the northwest of the region spread south over the Pedernal uplift and interfingered with marine deposits of the Northwestern and Sacramento shelves (Meyer, 1968). (Figures 2.9a through 2.9d) By Late Wolfcampian, the Pedernal landmass was almost entirely buried beneath the red-beds of the Abo Formation (King and Harder, 1985). (Figure 2.9d)

2.2.d: Permian

In addition to encompassing the majority of surface exposures in the northern Salt Basin watershed, Permian rocks also form the primary aquifer in the Salt Basin (Huff and Chace, 2006). These Permian units can be divided into 3 distinct facies (shelf, shelf-margin, and basin), similar to those presented by Nielson and Sharp (1985). The margin of the Delaware Basin evolved from a poorly defined boundary during the Wolfcampian to a well defined boundary fringed by the massive reef dolomites and limestones of the Goat Seep and Capitan Formations during the Guadalupian (Hayes, 1964). (Figures 2.9a

through 2.11a) As depicted by Black (1975), the margin of the basin also progressed towards the southeast during the Permian. (Figure 2.20)

Figures 2.9a through 2.11a present the paleogeographic reconstructions for the Permian. Examination of these reconstructions reveals that the Salt Basin region was dominated by a landmass, associated with the Diablo Platform, surrounded by a shallow marine environment. This appears to contradict the predominantly shallow marine environment suggested by the facies distributions displayed in Figures 2.17 through 2.19. However, the facies distribution maps indicate a landmass over a large region of the Texas portion of the Salt Basin during the Early Leonardian [Figure 2.17b], and over a large region of the western portion of the Salt Basin during the Guadalupian [Figures 2.18b through 2.19b]. In addition, the location of the landmass in the paleogeographic reconstructions corresponds closely to the location of the Diablo Platform as presented in Shepard and Walper (1982) [Figure 1.13] and Ross and Ross (1985) [Figure 1.15].

The Early Leonardian of Figure 2.17b corresponds approximately to the Early Permian (280 Ma) and (278 Ma) paleogeographic reconstructions of Figures 2.9d and 2.10a, which indicate a landmass a little farther to the east than is displayed in Figure 2.17b. The Early Permian (275 Ma) paleogeographic reconstruction of Figure 2.10b indicates that the New Mexico portion of the Salt Basin was dominated by a marine environment. This is supported by the Late Leonardian facies distribution displayed in Figure 2.18a. The Guadalupian of Figures 2.18b through 2.19b corresponds approximately to the Early Permian (270 Ma) and (260 Ma) paleogeographic reconstructions of Figures 2.10c and 2.10d, which indicate a landmass a little farther to the east than is displayed in Figures 2.18b through 2.19b.

Despite the apparent agreement between the paleogeographic reconstructions and the facies distributions, it is also possible that the extent and location of the landmass in the paleogeographic reconstructions is incorrect. For example, most of the facies distribution figures suggest that the landmass in the reconstructions should be located a little farther to the west. The paleogeographic reconstructions were obtained from Blakey (2009a), who produced these maps to illustrate the regional paleogeographic evolution of Southwestern North America. Therefore, the extent and location of the landmass within the Salt Basin from these regional reconstructions could be slightly inaccurate, as opposed to what a more localized paleogeographic reconstruction of the Salt Basin region might reveal. Also, the paleogeographic reconstructions from Blakey (2009a) were imported into ArcGIS and georeferenced using the U.S. state boundaries displayed on the reconstructions. The Salt Basin watershed boundary was then overlaid on top of the reconstructions. The georeferencing technique employed probably created some errors in the exact position of the reconstructions relative to the Salt Basin watershed boundary. As a result, all of the paleogeographic reconstructions should be viewed as an indication of the general, rather than exact, distribution of geographic features within the Salt Basin.

-Basin-facies

Rocks of the basin-facies consist of, from oldest to youngest, the Wolfcamp Formation [Figures 2.9a through 2.9d, and Figure 2.17a], the Leonardian Bone Spring Limestone [Figures 2.9d, 2.10a, 2.10b, 2.17b, and 2.18a], the Guadalupian Delaware Mountain Group [Figures 2.10c, 2.10d, 2.18b, 2.19a, and 2.19b], and the Ochoan Castile, Salado, and Rustler Formations [Figures 2.10d and 2.11a] (Hayes, 1964).

Hayes (1964) proposed that the term Hueco Limestone be restricted to those Wolfcampian units of the Northwestern shelf based on a pronounced difference in lithology between the shelf and basin Wolfcampian units. (Figure 2.17a) Thus, he tentatively assigned Wolfcampian rocks of the Delaware Basin to the Wolfcamp Formation. Rocks of the Wolfcamp basin-facies are not exposed in the Guadalupe or Sierra Diablo Mountains, and thus lithologic descriptions are based on subsurface data (Hayes, 1964; King, 1983). In the northern portion of the Delaware Basin the Wolfcamp Series ranges from 450 to 530 meters (1,490 to 1,750 feet) thick, and consists of about equal amounts of gray, black, or brown shale, and fine-crystalline rarely cherty brownish limestone, with a few thin beds of fine-grained gray micaceous and calcareous sandstone (Hayes, 1964). (Figure 2.17a) The Wolfcamp Series lies unconformably on the middle part of the Pennsylvanian sequence, as the upper part is missing (Hayes, 1964).

King (1983) restricted the term Bone Spring Limestone to the black limestone facies deposited in a deep, stagnant water environment. (Figures 2.17b and 2.18a) Outcrops of the Bone Spring Limestone are present in the southern Guadalupe Mountains, and in the Delaware, Baylor, and Sierra Diablo Mountains (King, 1948; King, 1965). The Leonardian Bone Spring Formation consists predominantly of fine-grained, dark-colored, arenaceous limestone in thin (generally < 1 foot thick) even beds, with minor amounts of platy, sandy, black shale and fine-grained, buff quartz sandstone (Newell et al., 1972). The Bone Spring Formation ranges from 600 to 760 meters (2,000 to 2,500 feet) thick near the margin of the Delaware Basin, and becomes somewhat dolomitic as it approaches the basin margin (Newell et al., 1972). The Bone Spring Limestone (King, 1934) has an average calcite-dolomite ratio of 79:21 (Hayes, 1964).

During the first half of Leonard time, the Bone Spring Limestone extended several kilometers farther shelfward across the basin margin, but does not reach the Union Oil Co., Federal White #1 (UNOCFW1) well in the Guadalupe Mountains (Hayes, 1964; King, 1948). (Figures 2.17b and 3.1) Instead, the Bone Spring Limestone grades northwestward into the lower portion of the Victorio Peak Limestone (Hayes, 1964). (Figure 2.17b)

In the Sierra Diablo region the lower part of the Bone Spring Limestone interfingers with tongues of lighter gray, more clastic or dolomitic shelf-margin deposits (King, 1965). (Figures 2.17b and 2.18a) Along the Babb and Victorio flexures the Bone Spring Limestone interfingers with thickening limestone reefs, and wedges out farther to the south (King, 1965). In the Permian Delaware Basin margin region now occupied by the northern portion of the Sierra Diablo Mountains the Bone Spring Limestone thins southwestward from 268 meters (880 feet) to a few hundred feet by overlap on the underlying Hueco Limestone and intergradation with the Victorio Peak Limestone (King, 1965). In the southern portion of the Sierra Diablo the Bone Spring thickens southward towards the Victorio flexure from 295 meters (970 feet) to 320 meters (1,050 feet) as it passes into the marginal facies (King, 1965).

The Guadalupian Delaware Mountain Group attains a maximum thickness of 1,220 meters (4,000 feet) in the Delaware Basin (Newell et al., 1972). The Delaware Mountain Group consists predominantly of gray or black, to weathered buff or tan, flaggy, thin-bedded, fine-grained quartz sandstone with a few thin beds of detrital limestone (Newell et al., 1972). The quartz sandstones of the Delaware Mountain Group wedge out around the margin of the basin, and are replaced by massive dolomites and

limestones of the Goat Seep and Capitan Formations (Newell et al., 1972). (Figures 2.19a and 2.19b) The Delaware Mountain Group consists of three formations, in ascending order: the Brushy Canyon, Cherry Canyon, and Bell Canyon Formations (Newell et al., 1972). (Figures 2.18b through 2.19b)

Limestone beds of the Brushy Canyon Formation have an average calcite-dolomite ratio of 73:27 (Hayes, 1964). The Brushy Canyon Formation wedges out completely over the Bone Spring flexure, and has no equivalent strata on the shelf (Newell et al., 1972). (Figure 2.18b) The Brushy Canyon Formation filled the Delaware Basin level with sand (Newell et al., 1972). (Figure 2.18b) The lowermost sandstone tongue of the Cherry Canyon Formation is unique in that it extends about 24 km (15 miles) shelfward, where it then grades into dolomites of the lower San Andres Formation (Hayes, 1964; Newell et al., 1972). The lowest limestone of the Cherry Canyon Formation, the Getaway Member, is strongly calcitic in the Delaware Basin, with an average calcite-dolomite ratio of 80:20 (Hayes, 1964). It passes across the margin of the basin as thick-bedded dolomite beneath the Goat Seep Formation, before grading into the San Andres Formation on the shelf (Newell et al., 1972). The middle and upper limestone member tongues of the Cherry Canyon Formation (South Wells and Manzanita Members), and the five limestone member tongues of the Bell Canyon Formation (in ascending order, Hegler, Pinery, Rader, McCombs, and Lamar) thicken towards the basin margin where they form massive, inclined beds of reef talus before passing into the Goat Seep and Capitan Formations, respectively (Newell et al., 1972). (Figures 2.19a and 2.19b) In the Delaware Basin the South Wells and Manzanita Members are strongly

dolomitic, while the Bell Canyon Formation limestone members are strongly calcitic (Hayes, 1964).

Ochoan rocks of the Castile, Salado, and Rustler Formations are present only in the Delaware Basin, having been removed by erosion from the margin and shelf regions (Hayes, 1964). None of these rocks fall within the model domain, and thus will not be discussed.

-Shelf-margin-facies

Rocks of the shelf-margin-facies consist of, from oldest to youngest, the Wolfcamp Series [Figures 2.9a through 2.9d, and Figure 2.17a], the Leonardian Victorio Peak Limestone and Cutoff Shale [Figures 2.9d, 2.10a, 2.10b, 2.17b, and 2.18a], and the Guadalupian sandstone tongue of the Cherry Canyon Formation, Goat Seep Dolomite, and Capitan Limestone [Figures 2.10c, 2.10d, 2.19a, and 2.19b] (Hayes, 1964).

The margin of the Delaware Basin was poorly defined during the Wolfcampian, as compared to during the Leonardian and Guadalupian (Hayes, 1964). As a result, a broad transition zone of marginal facies Wolfcamp rocks probably exists, although no outcrops exist in the Guadalupe Mountains to confirm the position of this zone (Hayes, 1964). (Figure 2.17a) In the Guadalupe Mountains, the Union Oil Co., Federal White #1 (UNOCFW1) well [Figure 3.1] apparently penetrates the shelfward portion of this broad transition zone as the Wolfcamp Series consists mostly of fine-crystalline light- to dark-gray dolomite containing minor amounts of gray, brown, green, and black shale (Hayes, 1964). The basal portion of the Wolfcamp Series in the Union Oil Co., Federal White #1 well consists predominantly of light- to dark-gray limestone, suggesting that the transition zone is located farther shelfward in the basal part of the series (Hayes, 1964).

In the central and northern part of the Sierra Diablo region the outcropping Wolfcamp (Hueco Formation) is composed of a thin-bedded dolomitic limestone facies, and further to the northeast includes marl and thin- to thick-bedded limestone (King, 1983). (Figure 2.17a) These facies formed along the margin of the Delaware Basin (King, 1983). Unlike during the Guadalupian, no extensive reefs formed along the margin of the Delaware Basin during the Wolfcampian (King, 1983).

The Victorio Peak Limestone is exposed in the Guadalupe and Sierra Diablo Mountains, and on the Diablo Plateau (King, 1983; Newell et al., 1972). (Figure 2.1) Massive, white and light-buff dolomite and limestone of the Victorio Peak Limestone abruptly replaces black limestones of the Bone Spring Formation around the margin of the Delaware Basin (Newell et al., 1972). (Figures 2.17b and 2.18a) The Victorio Peak Limestone in the Guadalupe Mountains region is restricted to a narrow belt a few kilometers wide around the basin margin (Newell et al., 1972). (Figure 2.17b) Six or eight kilometers (four or five miles) shelfward of the basin rim, the lower and middle portions of the Victorio Peak Limestone and the lower Bone Spring Formation grade into the dolomite and gypsiferous shelf-facies of the Yeso Formation (Newell et al., 1972) (Figure 2.17b) The upper portion of the Victorio Peak Limestone grades northwestward into the basal part of the San Andres Formation (Hayes, 1964). (Figure 2.18a) In the southern portion of the Guadalupe Mountains, King (1948) described the Victorio Peak as a thick-bedded, gray limestone 244 meters (800 feet) thick.

In the Sierra Diablo and on the Diablo Platform the Victorio Peak Limestone ranges from 305 to 457 meters (1,000 to 1,500 feet) thick, and, where the Bone Spring Limestone has wedged out beneath, lies unconformably on the Hueco Limestone (King,

1983). Although the Victorio Peak Limestone is predominantly of the shelf-margin-facies, it does not contain frame-building organic structures similar to those found in the overlying Goat Seep and Capitan Limestones, and is more accurately described as a limestone bank rather than a limestone reef (King, 1948; King, 1983). In the northeast Sierra Diablo the Victorio Peak Limestone consists of a light-gray, thick-bedded calcitic limestone facies, while in the southwest Sierra Diablo the Victorio Peak Limestone consists of a thin-bedded, dolomitic limestone facies (King, 1965). King (1965) interpreted the dolomitic limestone facies to have been deposited on a back-reef platform area behind the low banks formed by the calcitic limestone facies.

At the north end of the Sierra Diablo and north of the Bone Spring flexure in the Guadalupe Mountains, the Cutoff Shale, composed of a few hundred feet (30 to 91 meters [100 to 300 feet] in the Guadalupe Mountains, and 76 to 84 meters [250 to 275 feet] in the Sierra Diablo region) of thin-bedded limestone interbedded with dark siliceous shale, sandy shale, and soft-weathering sandstone, overlies the Victorio Peak Limestone (Hayes, 1964; King, 1965; King, 1983; Newell et al., 1972). In the Guadalupe Mountains, the Cutoff Shale grades to the northwest over a broad transition zone into the San Andres Formation (Hayes, 1964).

As mentioned above, in the Guadalupe Mountains 61 to 91 meters (200 to 300 feet) of the lowermost sandstone tongue of the Cherry Canyon Formation extends across the shelf-margin where it then grades into the lower San Andres Formation of the shelf-facies. In the Sierra Diablo region the Cherry Canyon sandstone tongue is 46 to 58 meters (150 to 190 feet) thick, and unconformably overlies the Cutoff Shale (King, 1965).

In the Guadalupe Mountains the Middle Guadalupian Goat Seep Formation is a narrow reef belt (no more than 1.5 kilometers or 1 mile wide) of predominantly massive dolomite that is equivalent to the Queen and Grayburg Formations of the shelf-facies Artesia Group (Newell et al., 1972). (Figure 2.19a) In the Guadalupe Mountains the Goat Seep ranges in thickness from171 to 366 meters (560 to 1,200 feet) (King, 1948). In the northern part of the Sierra Diablo region the Goat Seep Limestone conformably overlies and intertongues with portions of the Cherry Canyon sandstone tongue (King, 1965). (Figure 2.19a) In the Sierra Diablo region the Goat Seep is 61 meters (200 feet) thick, although its upper contact is missing (King, 1965).

The Capitan Formation of massive white limestones and thin-bedded black limestones and sandstones formed a 4 to 6 km (2.5 to 3.5 mile) wide reef zone for a distance of about 560 to 640 kilometers (350 to 400 miles) around the rim of the Delaware Basin during the Middle to Late Guadalupian (Newell et al., 1972). (Figure 2.19b) About 64 kilometers (40 miles) of the Capitan reef outcrops in the Guadalupe Mountains (Newell et al., 1972). (Figure 2.1) The Capitan Limestone also outcrops in the Patterson Hills (King, 1948). (Figure 2.1) In the southern Guadalupe Mountains the Capitan Limestone ranges in thickness from 305 to 610 meters (1,000 to 2,000 feet) (King, 1948).

-Shelf-facies

Rocks of the shelf-facies consist of, from oldest to youngest, the Wolfcampian Abo Formation and Hueco Limestone, including the Pow Wow Conglomerate Member, [Figures 2.9a through 2.9d, and Figure 2.17a], the Leonardian Yeso Formation [Figures

2.9d, 2.10a, 2.10b, and 2.17b], and the Guadalupian San Andres Formation and Artesia Group [Figures 2.10c, 2.10d, 2.18a, and 2.18b] (Hayes, 1964).

The Wolfcampian was marked by a regression, during which red beds derived from a major uplift to the northwest of the region spread southeast over the Pedernal uplift and interfingered with the marine deposits of the Northwestern shelf (Meyer, 1968). (Figures 2.9a through 2.9d, and Figure 2.17a) The interfingering of red beds with marine shelf limestones and shales also occurred southward in the Orogrande basin and over the Sacramento shelf (Meyer, 1968). (Figure 2.17a) In the Guadalupe Mountains region of the Northwestern shelf, Hayes (1964) identified two distinct members of the Hueco Limestone. The lower member consists of medium-gray, fine-crystalline, locally siliceous limestone interbedded with reddish-brown, greenish-gray, and gray shale and minor amounts of fine-grained sandstone, and reaches a maximum thickness of at least 150 meters (500 feet) (Hayes, 1964). The upper member ranges in thickness from about 270 to 405 meters (880 to 1,330 feet), consists predominantly of medium-gray fine-crystalline dolomite, subordinate greenish-gray shale, and rare grayish-red shale, and grades northwestward into the Abo Formation (Hayes, 1964). The upper member of the Hueco Limestone grades basinward into fine- to coarse-crystalline dolomite beds referred to as "Abo reefs" (Hayes, 1964). Meyer (1968) noted that east of the Pedernal uplift the overlying Yeso Formation is separated from Wolfcampian strata by another Leonardian unit consisting of red beds and brown fine-grained anhydritic dolomite (Abo Formation of the subsurface) that grades to the south and east into a narrow zone of white coarse-grained dolomite (Abo Reef of the subsurface), and then into the black siltstones and black massive limestones of the lower Bone Spring Formation. The upper member of

Hayes (1964) thus probably corresponds to the Abo Formation of the subsurface that Meyer (1968) proposed be designated as the Leonardian Wichita Formation. As Hayes (1964) writes, "Much of the Hueco Limestone is laterally equivalent to rocks of the Wolfcamp Series of the Delaware basin, but the uppermost part is probably equivalent to the basal part of the Bone Spring of Leonard age."

On the Sacramento shelf, Wolfcampian rocks consist of a southward thickening middle tongue of gray shales, limestones, and dolomites designated as the Pendejo tongue of the Hueco Limestone by Pray (1961), surrounded by thick beds of arkose and red shale at the base and at the top, designated as the Danley Ranch and Lee Ranch tongues of the Abo Formation, respectively, by Bachman and Hayes (1958). Pray (1961) described the Abo Formation in the Sacramento Mountains as a sequence of dark, reddish-brown mudstone and arkose. The upper and lower tongues are interpreted by Pray (1961) to represent fresh-water deposits laid down on a broad surface of little relief. (Figures 2.9a through 2.9d) In the Sacramento Mountains the Abo Formation ranges from about 61 to 152 meters (200 to 500 feet) thick, and thickens southward along the escarpment to a maximum of about 168 meters (550 feet) near T. 19 S. (Pray, 1961). The thickness of the tongues of the Abo Formation is structurally controlled, and therefore deformation initiated during the Late Pennsylvanian probably continued into the Early Permian (Pray, 1961).

The Pendejo tongue generally thins from west to east, and pinches out over the axis of the Pedernal landmass (Black, 1973). Eastward across the Pedernal uplift only the upper red shales are present, and the Abo Formation lies unconformably on Missourian (Pennsylvanian) to Precambrian rocks (Kottlowski, 1963; Meyer, 1968). In the Delaware

and Orogrande basins, Wolfcampian rocks are conformable with the underlying Virgilian (Pennsylvanian) (Meyer, 1968). In the southern portion of the Sacramento Mountains, the Abo Formation lies on the Pennsylvanian with an angular unconformity (Pray, 1961). The Abo Formation grades sharply over a short distance into the overlying, conformable Yeso Formation, which Pray (1961) believed represented the sudden invasion of the Yeso marine depositional environment. Black (1973) considered the basal conglomerates in the Danley Ranch tongue to be depositionally equivalent to the Pow Wow Conglomerate Member of the Hueco Formation mapped in the Hueco Mountains by King et al. (1945).

The terms Bursum and Laborcita Formations have been used in the northern portion of the Sacramento Mountains to describe Lower Wolfcampian strata below the Abo Formation (Pray, 1961). Southward from the Sacramento Mountains towards the Hueco Mountains the Abo Formation thins and the upper red bed tongues are replaced by the marine facies of the Hueco Formation (Kottlowski, 1963; Pray, 1961). (Figure 2.17a) The Sun Oil Company, T.J. Pearson #1 (SOCTJP1) well [Figure 3.1] penetrated a Wolfcampian section more than 607 meters (1,990 feet) thick, in which red beds of the Abo Formation occur as a tongue between limestones of the Hueco Formation (Kottlowski, 1963).

In the Hueco Mountains the Wolfcampian is represented by about 488 meters (1,600 feet) of gray to dark-gray, thinly- to thickly-bedded limestones and shaly limestones of the Hueco Formation (Kottlowski, 1963). In the Hueco Mountains and the Diablo Plateau, the basal part of the Wolfcampian (limestone conglomerates and red beds of the Pow Wow Conglomerate) lies with angular and erosional unconformity on older Paleozoic rocks down to the Precambrian basement due to uplift of the Diablo Platform

during the Early Wolfcampian (Kottlowski, 1963; Pray, 1961). Along the west edge of the Diablo Plateau, east of the Hueco Mountains, a dolomite and limestone unit that has been correlated with the Hueco Formation locally contains Leonardian beds in the upper part of the unit (Kottlowski, 1963). Kottlowski (1963) speculated that "either the Hueco grades without appreciable beak up into these Leonardian beds of the Yeso Formation or there is an unconformity between the two units which has not been recognized on the west edge of the Diablo Plateau because of dolomitization, faulting, and burial by alluvium." On the Diablo Plateau and southeastward in the Sierra Diablo Mountains the Hueco Formation thins, and is unconformably overlain by Leonardian (Bone Spring or Victorio Peak) or Cretaceous strata (King, 1983; Kottlowski, 1963).

The thickness of the Hueco Formation in the Sierra Diablo region is highly variable owing to overlap of its unconformable basal surface and erosion of its upper surface before deposition of the Bone Spring Limestone (King, 1965). Along the Sierra Diablo escarpment the Hueco ranges from less than 122 meters (400 feet) to greater than 274 meters (900 feet) thick, averaging 152 meters (500 feet) thick (King, 1965). In the northern Sierra Diablo region the Hueco Formation ranges from more than 335 meters (1,100 feet) at the head of Apache Canyon to a few hundred feet at the lower end of the canyon (King, 1965). In the Baylor Mountains to the southeast the Hueco wedges out in several places (King, 1965). In the southern and southwestern part of the Sierra Diablo region the Hueco Formation is composed of the calcitic limestone facies found to the west in the Hueco Mountains, which formed in an extensive shelf sea (King, 1983). In the Sierra Diablo region, the Pow Wow is more extensive and varied, consisting of

66

varicolored, coarse to fine clastic rocks, and, except for localized wedge outs, everywhere underlies the main body of the Hueco Limestone (King, 1965).

In the shelf area of the Guadalupe Mountains outcrops of the upper portion of the Leonardian Yeso Formation consist predominantly of dark- to light-gray, generally slightly fetid dolomite and dolomitic limestone, interbedded with about equal amounts of massive, white gypsum and thin beds of nonresistant, grayish-yellow, sandy quartzose siltstone (Hayes, 1964). (Figure 2.17b) In outcrop along the lower slopes of the Algerita Escarpment, the percentage of gypsum and siltstone in the Yeso decreases from northwest to southeast (Hayes, 1964). The Yeso Formation is much more gypsiferous in areas to the north (Hayes, 1964). (Figure 2.17b) In the northern portion of the Guadalupe Mountains escarpment a 270 meter (890 feet) measured section of the Yeso Formation consisted of gypsum, gypsiferous siltstone, and dolomite (Kelley, 1971).

In the subsurface of the Guadalupe Mountains, the Yeso Formation ranges in thickness from about 510 to 735 meters (1,685 to 2,410 feet), and is thinnest where the underlying Hueco Limestone is relatively thin, and the Pennsylvanian is thin or absent (Hayes, 1964). In these subsurface wells the Yeso Formation consists predominantly of medium- to light-gray, fine-crystalline dolomite, interbedded with very light gray, coarse quartzose siltstone and very fine grained sandstone, and small amounts of white to very light gray anhydrite in the upper 61 to 76 meters (200 to 250 feet) of the formation (Hayes, 1964). Thus, the Yeso Formation was likely impacted by the continuation of the deformation that affected Pennsylvanian and Wolfcampian sedimentation (Hayes, 1964). (Figures 2.9d through 2.10c) This is supported by Kelley (1971), who postulated that the

Pedernal uplift may have been active during deposition of the Yeso Formation, owing to a lack of carbonate or evaporite beds in an exposure near the top of the axis.

In the Sacramento Mountains Pray (1961) described the Yeso Formation as a heterogeneous unit of carbonate rocks, mostly limestones and some dolomite; red, yellow, and gray shales and siltstones; evaporites, largely anhydrite and minor halite; and yellowish, fine-grained sandstones, that displays rapid vertical and lateral variations in lithology. Carbonate rocks, including some dolomite, become more abundant to the south, especially in the upper part of the formation, while gypsum becomes less abundant (Pray, 1961). "Red beds" and evaporites are most abundant in the lower and middle portions of the formation (Pray, 1961). To the south, these "red beds" and evaporates are confined primarily to the lower and middle portions of the formation, being replaced largely by limestones in the upper part of the formation (Pray, 1961). In a deep groundwater well near the town of Cloudcroft, New Mexico, and the Southern Production Co., Cloudcroft Unit #1 (SPCCLU1) well [Figure 3.1], evaporites (anhydrite, gypsum, and/or halite) were not reported until 283 and 287 meters (930 and 940 feet) below the top of the Yeso, respectively (Newton et al., 2009). In two measured sections, one in the northern and one in the southern part of the escarpment, Pray (1961) noted that limestone increased from 25 to 45%, dolomite increased from 0.1 to 2%, and mixed gypsum and shale and pure gypsum decreased from 47 to 9% from north to south. (Figure 2.17b) Yellow to yellow-brown, silty, very fine- to fine-grained quartz sandstone is a minor constituent of the Yeso Formation (2 to 9%) and occurs mainly in the upper part of the formation as interbeds in limestone (Pray, 1961).

In the Sacramento Mountains escarpment, the Yeso Formation ranges in thickness from about 365 to 550 meters (1,200 to 1,800 feet), based on measured outcrop sections and the Southern Production Co., Cloudcroft Unit #1 (SPCCLU1) well [Figure 3.1] (Pray, 1961). Pray (1961) also suspected that the Yeso Formation underwent similar thickness variations over developing anticlinal and synclinal folds to those observed in the underlying Abo Formation. Black (1973) could not prove these subsurface relationships for the Yeso, and postulated that thickness variations in the Yeso were more likely to be the result of solution and collapse of evaporite beds, and differential compaction of fine-grained clastics.

On the Otero Mesa Black (1973) measured a section of the Yeso Formation in T. 24 S., R. 15 E., secs. 23 and 2 to be 331 meters (1,087 feet) thick. The Yeso Formation records deposition on a broad marine shelf, which experienced periods of restricted circulation and super-saline conditions (Black, 1973; Pray, 1961). (Figures 2.9d through 2.10c) Based on the presence of abundant carbonates in the upper portion of the Yeso in the region of Dantes dome on the Otero Mesa, Black (1973) believed that the Yeso grades from clastics into littoral and lagoonal evaporates, and finally into carbonates towards the south. (Figure 2.17b) Black (1973) also postulated that the light-gray to almost white limestones in the upper portion of the Yeso in the Dantes dome region were the shelf equivalent and correlative with parts of the Victorio Peak Formation to the southeast. (Figure 2.17b) As observed in outcrops in the Sacramento and Guadalupe Mountains, and on the Otero Mesa, the Yeso Formation grades into the conformably overlying San Andres Formation (Black, 1973; Hayes, 1964; Pray, 1961).

The Guadalupian San Andres Formation is exposed over most of the northern and eastern portions of the Otero Mesa, along the crest and most of the eastern slope of the Sacramento Mountains, and in the Guadalupe and Brokeoff Mountains (Black, 1973; Hayes, 1964; Pray, 1961). (Figure 2.1) During the Guadalupian, a relative rise in sea level occurred and the shelf to shelf-margin depositional environment gave way to the deep water carbonates of the San Andres Formation (King and Harder, 1985). (Figures 2.10c and 2.10d)

Hayes (1964) divided the San Andres Formation of the Guadalupe Mountains into two informal units: a lower cherty member and an upper member. In the northwestern part of the Guadalupe Mountains the lower cherty member is predominantly dolomite and dolomitic limestone (average calcite-dolomite ratios of carbonate rock in the member of 16:84) that contains variable amounts of rusty-weathering, light- to medium-gray chert that is most abundant near the top of the member (Hayes, 1964). The upper part of the lower member also tends to be more calcitic (Hayes, 1964). Farther to the southeast towards the basin margin the lower member contains thin beds of grayish-orange-weathering siltstone and silty claystone, and the carbonate rocks are somewhat more calcitic (average calcite-dolomite ratios of 38:62), finer textured, and siltier (Hayes, 1964). The upper dolomitic member is distinguishable from the lower member by a relative lack of chert (Hayes, 1964). Hayes (1964) measured a composite section of the San Andres Formation along the base of the Algerita Escarpment in T. 24 S., R. 20 E., sec. 3 to be a little more than 366 meters (1,200 feet) thick. In the Guadalupe Mountains the upper contact of the San Andres Formation with the Grayburg Formation of the Artesia Group is locally unconformable (Hayes, 1964).

In the Sacramento Mountains the upper contact of the San Andres Formation forms the present erosion surface (Pray, 1961). Pray (1961) described the San Andres Formation in the Sacramento Mountains as a monotonous succession of limestone layers of various shades of mostly dark colored gray and olive gray. Dolomitic beds are present, but dolomite is uncommon in the escarpment area (Pray, 1961). In the Sacramento Mountains the maximum thickness of San Andres noted by Pray (1961) was about 213 meters (700 feet) in the southern part of T. 16 S., R. 11 E., but the top of the formation is missing in the Sacramento Mountains due to erosion.

Kelley (1971) divided the San Andres Formation into three members during the process of field mapping to the north and northeast of the northern Salt Basin watershed, in ascending order: the thick-bedded Rio Bonito, the typically thin-bedded Bonney Canyon, and the typically evaporitic Fourmile Draw Members. The Rio Bonito Member, and the Bonney Canyon and Fourmile Draw Members correspond to the cherty and "noncherty" members, respectively, identified by Hayes (1964) in the Guadalupe Mountains (Kelley, 1971). The Bonney Canyon Member, and maybe a thin lower part of the Fourmile Draw Member, roughly corresponds to the subsurface Slaughter zone of porosity identified to the east near Roswell, New Mexico (Kelley, 1971). In the northern Guadalupe Mountains a pieced together outcrop section of the San Andres Formation measured 368 meters (1,208 feet) thick (Kelley, 1971). Black (1973) projected a total thickness of a composite San Andres section from the Otero Mesa of 258 meters (847 feet).

The Rio Bonito Member thickens to the south of about T. 15 S. at the expense of the overlying Bonney Canyon Member (Kelley, 1971). In the northern portion of the

71

Guadalupe Mountains the Glorieta Sandstone occurs as scattered tongues in the Rio Bonito, which become thinner, and finer grained toward the south (Kelley, 1971). Chert is uncommon in the San Andres Formation, but becomes more abundant in the lower part of the formation in the southern Guadalupe Mountains (Kelley, 1971). The thin-bedded Bonney Canyon Member consists primarily of light- to medium-gray, brownish-gray, fine-grained dolomite and limestone (Kelley, 1971). In the Guadalupe Mountains, the Fourmile Draw Member becomes more evaporitic to the north of T. 21 S., R. 21 E. as gypsum begins to appear (Kelley, 1971). To the south, the lower part of a shelf-margin transition facies of the Fourmile Draw Member grades into the Cherry Canyon sandstone tongue of the Delaware Mountain Group (Kelley, 1971).

On the Otero Mesa, the basal Rio Bonito Member consists predominantly of dark-gray to gray limestone to the north, but becomes more dolomitic and cherty to the south towards the shelf-margin (Black, 1973). Black (1973) believed that this may suggest a more normal, deeper water, and less restricted shelf environment to the north than to the south. In contrast, in areas to the north and northeast of the Salt Basin region, Kelley (1971) found that dolomite decreases from north to south, being replaced by limestone. South of the "AV" lineament the Rio Bonito forms the surface of the Chert Plateau and consists predominantly of cherty dolomites and cherty dolomitic limestones (Black, 1973). Chace and Roberts (2004) report a Rio Bonito thickness of up to 244 meters (800 feet) in the southern portion of Otero Mesa. Along the eastern edge of the northern portion of the Diablo Plateau, the lower cherty limestones of the Rio Bonito Member grade abruptly into the predominantly cherty dolomites of the shelf-margin Victorio Peak Formation (Black, 1973). On the basis of these relationships, Black (1973) inferred that

the upper Victorio Peak is equivalent to the upper portion of the Yeso and the basal portion of the San Andres. (Figures 2.17b and 2.18a) The clean, well rounded and frosted, very fine- to medium-grained orthoquartzites of the Glorieta Sandstone are not found in the Rio Bonito south of the Piñon cross folds, and are replaced by a massive carbonate facies (Black, 1973).

The typically thin- to medium-bedded, light- to medium-gray to black, predominantly limestones or dolomitic limestones of the Bonney Canyon Member form the predominant surface exposures north of the "AV" lineament in the Otero Hills (Black, 1973). Like the Bonney Canyon Member mapped by Kelley (1971) to the north, the Bonney Canyon thins to the south on the Otero Mesa, and cannot be easily identified south of T. 25 S (Black, 1973). The basal portion of the Bonney Canyon also contains scattered oolite beds (Black, 1973). Black (1973) postulated that the occurrence of oolites in the basal Bonney Canyon just to the north of the "AV" lineament and the observed facies change in the Rio Bonito from limestone to dolomite across this feature indicated a possible shelf trough of deeper water partly controlled by the lineament. The Bonney Canyon Member was deposited in a broad, shallow shelf area to the northwest of the shelf-margin (King and Harder, 1985).

The Fourmile Draw Member does not occur in the northern portions of the study area, but an interval that Black (1973) believed may correspond to the carbonate facies of Kelley (1971) does outcrop to the south, near the New Mexico-Texas border. In this area it consists primarily of dark-brown calcareous dolomite, with calcareous sandstones and sandy limestones (Black, 1973). The Fourmile Draw Member was deposited in a restricted shelf environment (King and Harder, 1985).

The Artesia Group consists of five formations, in ascending order: the Grayburg, Queen, Seven Rivers, Yates, and Tansill Formations (Newell et al., 1972). The Artesia Group forms the predominant surface exposures in the southern Guadalupe Mountains and farther to the east, and experiences a rapid facies variation northward from a carbonate facies near the shelf-margin to a clastic and evaporitic facies on the shelf (Kelley, 1971). (Figures 2.1, 2.19a, and 2.19b) The Middle Guadalupian (Goat Seep Formation equivalent) shelf rocks of the Grayburg and Queen Formations outcrop in the southernmost portion of the Guadalupe Mountains, and consist of interbedded dolomite and sandstone (Kelley, 1971; Newell et al., 1972). (Figure 2.19a) The Grayburg Formation is probably 122 meters (400 feet) thick or less in the northern Guadalupe Mountains, and thickens to the southeast towards the basin margin to as much as 183 meters (600 feet) (Hayes, 1964). Measured sections of the Queen Formation range from 64 to 128 meters (210 to 421 feet) thick (Hayes, 1964).

The Upper Guadalupian (Capitan Formation equivalent) shelf rocks of the Seven Rivers, Yates, and Tansill Formations are collectively known as the Carlsbad Group and consist of alternating dolomite and fine-grained quartz sandstone (Newell et al., 1972). (Figure 2.19b) The formations of the Carlsbad Group thicken to the southeast towards the Capitan Formation of the basin margin (Hayes, 1964). In outcrop sections the thickness of the Seven Rivers Formation ranges from 140 meters (460 feet) to possibly 183 meters (600 feet), the Yates Formation ranges from 80 to 114 meters (262 to 375 feet), and the incomplete (due to erosion) Tansill Formation ranges from 38 to 99 meters (123.5 to 325 feet) (Hayes, 1964).

2.2.e: Mesozoic

Rocks of Mesozoic age are largely absent in the Salt Basin region. Post-Wolfcampian strata were removed from the western-most Diablo Plateau during the Early Mesozoic (Kottlowski, 1963). (Figures 2.11b through 2.12d) Here Lower Cretaceous conglomerates unconformably overlie the Wolfcampian Hueco Formation (Kottlowski, 1963). Cretaceous strata have largely been removed from the region by erosion during the Cenozoic (Kottlowski, 1963). (Figures 2.14d through 2.16d) Lower Cretaceous strata where deposited on the western margin of the Diablo Platform as Cretaceous seas overlapped it from the south, and scattered remnants remain on the Otero Mesa and Diablo Plateau (Kottlowski, 1963). (Figures 2.13a, 2.13b, and 2.13c) In the southwestern Diablo Plateau the Cretaceous rocks form a perched, confined to semi-confined aquifer overlying the deeper regional aquifer (Kreitler et al., 1990; Mayer, 1995; Sharp, 1989).

In the Cornudas Mountains, shales, limestones, marls, and basal sandstones of the Washita Group crop out unconformably on the Yeso Formation (Kottlowski, 1963). (Figure 2.13d) In the western-most Diablo Plateau the older Fredericksburg and Trinity Groups are exposed (Kottlowski, 1963). (Figures 2.13b and 2.13c) The oldest units are the calcareous limestone-chert-pebble conglomerate with interbedded red and brown sandy limestone of the Campagrande Conglomerate, which unconformably overlies the Hueco Formation, and is overlain by the coarse-grained cross-bedded sandstone with interbedded fossiliferous limestone of the Cox Sandstone (Kottlowski, 1963). These Trinity Group strata are overlain by the Finlay Limestone of the Fredericksburg Group on the mesa tops (Kottlowski, 1963). To the south these Lower Cretaceous beds thicken

rapidly into the Chihuahua Trough, where they are overlain by younger strata of the Fredericksburg and Washita Groups (Kottlowski, 1963).

It is likely that thick sections of the Upper Cretaceous Dakota, Mancos, and Mesaverde Formations were deposited across the region, and now only occur in scattered locations along the crest of the Sacramento Mountains (Kottlowski, 1963). (Figures 2.14a, 2.14b, and 2.14c) In general, Cretaceous rocks consist of limestone and chert-pebble conglomerate, which are overlain by interbedded limestone and calcareous shale (Mayer, 1995).

2.2.f: Cenozoic

Cenozoic rocks are present in the subsurface as intrusive bodies in the southwestern Otero Mesa and northwestern Diablo Plateau, and are exposed in the Cornudas Mountains, the Sierra Tinaja Pinta group, Cornudas Station, Granite Mountain, the Antelope Hill intrusives, the Sierra Prieta sill, and the Marble Canyon intrusives (Barker et al., 1977; Masson, 1956). (Figure 1.4) These Cenozoic laccoliths, sills, and dikes are predominantly syenite and phonolite in composition, and intrude Precambrian through Cretaceous strata (King and Harder, 1985; McLemore and Guilinger, 1993; Nutt et al., 1997; Nutt and O'Neill, 1998). Also, a small nepheline-bearing trachyte intrusion known as Round Mountain is located east of Dell City, Texas (Ashworth, 2001; Mayer, 1995). A Cenozoic intrusion is also associated with Dantes dome (centered around the Shiloh Hills) northeast of the Cornudas Mountains on the Otero Mesa (Black, 1973).

A veneer of Quaternary bolson sediments, largely consisting of fanglomerates, conglomerates, soft sandstones, caliche, shale, and gypsum, cover the Salt Basin region, and range in thickness from several meters on the plateau surfaces to 700 meters (2,300

feet) within the Salt Basin graben (King and Harder, 1985; Spirakis et al., 1997). Gates et al. (1980) examined electrical resistivity along several electrical-sounding profiles in the Salt Flats region of the Salt Basin graben, and interpreted the data to indicate that the basin-fill underlying the Salt Flats is predominantly low permeability lacustrine clay and sand. Aeolian deposits are common along the eastern margin of the Salt Basin graben, consisting primarily of quartz-based sheet and dune sands (Wilkins and Currey, 1999). These dunes are largely inactive, however gypsum deflated from the playa surface forms active gypsum-sand dunefields between the playa and the inactive dunes (Wilkins and Currey, 1999).

Hussain et al. (1988) identified three major depostional facies in the Salt Flats region: bajada and alluvial fan, sand flat, and sabkha dry mud flat (alkali flat). The bajada consists of coalesced alluvial fans that occupy a 3 to 6 kilometer (2 to 4 mile) wide belt that rises 150 to 500 meters (490 to 1,640 feet) from the floor of the Salt Basin graben to the base of the western escarpments of the Guadalupe and Brokeoff Mountains (Hussain et al., 1988). The bajada facies also extends outward from the escarpments of the Delaware and Sierra Diablo Mountains toward the center of the Salt Basin graben (King, 1965). East of the Beach and Baylor Mountains, the bajada facies extends from the mountains on both sides of the Salt Basin graben to the center of the graben (King, 1965). Debris flow deposits are common in the proximal areas of the alluvial fans, but also are infrequently found throughout the bajada (Hussain et al., 1988). The sand flat facies corresponds to the quartz- and gypsum-sand dunes described above. The sand flat facies forms a belt up to 6 kilometers (4 miles) wide between the bajada and the sabkha

(Hussain et al., 1988). The sabkha mud flat facies consists of a laminated sequence of alternating gypsum and organic-rich micritic sediments (Hussain et al., 1988).

The wetter climate associated with Pleistocene glaciation also resulted in several beach deposits along the shores of lakes in Otero Mesa and the Salt Basin graben (Black, 1973; King, 1948). (Figure 2.16c) These beach ridges consist of very coarse gravel, while the dry lake beds are underlain by lacustrine silt and shale (Black, 1973). During the Pleistocene, lakes occupied the Salt Basin graben region (Lake King) and the region west of the Otero Break near the terminus of the Sacramento River (Lake Sacramento) (Hawley, 1993; Wilkens and Currey, 1997). Lake Sacramento formed in a structural basin and acted as a reservoir for Lake King, transmitting water collected from the Sacramento River through the Permian units of Otero Mesa and into the valley-fill of the Salt Basin graben (Hawley, 1993; Wilkens and Currey, 1997).

2.3: Structure

As discussed above, deformation in the Salt Basin region can be broken into four principal periods: a) Pennsylvanian-to-Early Permian, b) Mid-to-Late Permian, c) Late Cretaceous, and d) Cenozoic. Pennsylvanian-to-Early Permian faulting and folding is associated with the collision of the southern margin of North America with South America-Africa during the Ouachita-Marathon orogeny, and the resulting differential uplift and subsidence of the Pedernal landmass, and Diablo and Central Basin Platforms, and the Orogrande, Delaware, and Midland Basins, respectively (Dickerson, 1989). Mid-to-Late Permian features outlined the margins of the subsiding Delaware Basin (Black, 1973; Dickerson, 1989; King, 1948). Late Cretaceous deformation during the Laramide orogeny produced northwest trending thrust faults and northwest to westerly trending

folds in the Otero Mesa region (Black, 1973; Broadhead, 2002). Cenozoic Basin-and-Range extension produced the current physiographic form of the region, with the formation of horst-and-graben structures bounded by high-angle normal faults (Goetz, 1977).

2.3.a: Pennsylvanian-to-Early Permian Features (Figure 2.21)

-Huapache Thrust Zone and Monocline

The low east-northeastward dipping Huapache monocline defines the eastern boundary of the northern Guadalupe Mountains in New Mexico, and is the surface expression of the Huapache thrust zone (Hayes, 1964). Maximum dips along the generally less than 3 km (2 mile) wide monocline range from 5º to 8º (Hayes, 1964). The Huapache fault zone was intermittently active throughout all or most of the Pennsylvanian, and possibly the Early Permian, and defined the eastern boundary of the rising Pedernal uplift (Hayes, 1964). The age of the fault zone is constrained by the lack of lithologic variation in Mississippian strata on either side of the fault, but the vertical displacement of these units by as much as 1,200 to 1,800 meters (4,000 to 6,000 feet), and the lack of rupture of the Guadalupian Stage San Andres Formation at the surface (Hayes, 1964). The fault zone strikes roughly N 35º W, and the fault planes dip westward at 45º to 85º (Hayes, 1964).

Pennsylvanian rocks show dramatic thickness variation on either side of the fault zone (Hayes, 1964). For example, near the Bone Spring flexure, on the west or upthrown side of the fault zone, the Union Oil Co., Federal White #1 (UNOCFW1) well encountered a Pennsylvanian section about 450 meters (1,500 feet) thick, while on east or downthrown side the Humble Oil & Refining Co., Huapache Oil Unit #2 (HO&RHO2)

well penetrated a Pennsylvanian section about 1,200 meters (3,950 feet) thick. (Figure 2.21) Vertical movement along the thrust zone was even greater to the north as indicated by the absence of the Pennsylvanian in the Continental Oil Co., H.W. Bass #1 (COCHWB1) well, located about 23 km (14 mi) northwest of the Union Oil Co., Federal White #1 well on the west side of the fault (Hayes, 1964). (Figure 2.21) The Tri-Service Drilling Co., Little Dog Federal #1 (TSDLDF1) well and the Standard of Texas, Scarp Unit #1 (SOTSCU1) well, located about 21 km (13 mi) and 30 km (19 mi) west-northwest of the Continental Oil Co., H.W. Bass #1 well, respectively, indicate even greater uplift as no Pennsylvanian or Mississippian rocks are present, and Wolfcampian rocks rest on Silurian rocks (Hayes, 1964). (Figure 2.21)

Wolfcampian (Hueco and Abo Formations) and Leonardian (Yeso Formation) rocks also show thickness variations across the fault zone, which suggests that fault movement continued into the Early Permian (Hayes, 1964). The thrust zone may extend southeast across the Bone Spring flexure into the Delaware Basin [Hayes, 1964], but the hydrogeologic system was not modeled into this region. The Huapache monocline is an east-northeastward dipping, 0.8 to 4 km (0.5 to 2.5 mi) wide fold that resulted from post-Permian (probably Cenozoic) flexing and drape folding over the underlying Huapache thrust zone (Hayes, 1964; Kelley, 1971). The Huapache monocline terminates to the north against the northward trending Lewis buckle, which merges northward with the Y-O buckle, and terminates to the south against the Guadalupe fault zone (Kelley, 1971). The trace of the Huapache monocline was obtained from Broadhead (2002).

-Pedernal Uplift

The northeastern Otero Mesa is dominated structurally by the southern extension of the buried Pedernal uplift, which trends north-south and bisects Otero Mesa (Black, 1975). The location of the main western boundary fault of the Pedernal uplift has been indicated by several researchers to be near the Cornudas Mountains (Black, 1975; Black, 1976; King and Harder, 1985; Nutt, 1997; Broadhead, 2002). In a west-east cross-section through the northern Cornudas Mountains, Black (1975) placed the fault 3.5 km (2 miles) to the east of the Cornudas Mountains. However, King and Harder (1985) positioned the fault beneath the Cornudas Mountains on their Precambrian basement structure contour map of the Otero Mesa-Salt Basin graben area. Nutt (1997) also supported the placement of the fault beneath or just to the west of the Cornudas Mountains based on subsurface oil-and-gas exploratory well data, geologic mapping, and geophysical evidence.

The Hunt Oil Co., McMillan-Turner #1 (HUOCMT1) well drilled 16 km (10 miles) east of the Cornudas Mountains, and the Union Oil Co., McMillan #1 (UNOCMC1) well drilled 8 km (5 miles) northwest of the Cornudas Mountains, encountered 295 m (970 feet) and 210 m (690 feet) thick Yeso sections, respectively, while geologic mapping of the Cornudas Mountains by Nutt (1997) revealed a Yeso thickness of 30 m (100 feet). (Figure 2.21) Audio-magnetoelluric (ATM) soundings conducted across the Cornudas Mountains detected highly resistive rocks (Precambrian crystalline basement) directly east of the Cornudas Mountains, and a layered rock sequence (sedimentary rocks) on the west, which was interpreted to indicate a more elevated Precambrian basement surface east of the Cornudas Mountains (Nutt, 1997). The dramatic thinning of the Yeso Formation in the Cornudas Mountains, and the fact

that the Precambrian basement is 610 m (2,000 feet) deeper to the west than to the east of the Cornudas Mountains suggests that the fault is located west of, or beneath, the Cornudas Mountains (Nutt, 1997).

Nutt and O'Neill (1998) proposed that the alkaline intrusive rocks of the Cornudas Mountains were emplaced along a major fault or fault system along the western margin of the buried Pedernal uplift. Therefore, Nutt and O'Neill (1998) suggested that the cross-section by Black (1975) be altered so that Precambrian basement lie directly beneath the Cornudas Mountains.

Broadhead (2002) presented a subsurface structure and Permian subcrop map of the Otero Mesa-Salt Basin graben region that also places the trace of the fault beneath the Cornudas Mountains. (Figure 2.21) For use in the 3-D hydrogeologic framework model, the trace of this fault presented by Broadhead (2002) was projected to the southwest into Texas. The projection passes to the west of the Magnolia Petr. Co., U-Tex Lease #39881 #1 (MPCUTL1) well, between the Trail Mountain, Inc., University Big Iron "C45" #1 (TMUBIC1) and Trail Mountain, Inc., University Felina "D27" #1 (TMUFD27) wells to the east and the Trail Mountain, Inc., University Sizzler D5 #1 (TMUSD51) well to the west, which indicate down-to-the-west displacement of Precambrian through Pennsylvanian strata, and between the Transocean Oil, Inc., 36-1 MSA Trustee, Inc. (TO36MSA) well to the east and the Pan American Pet. Corp., Phillip F. Hass #1 (PAPPFH1) well to the west, which indicate down-to-the-west displacement of Precambrian through Mississippian strata. (Figures 2.21 and 3.1) This projection is justified because the western fault system of the Pedernal uplift extends southward as the western margin of the Diablo Platform (Ross and Ross, 1985).

-Bug Scuffle Fault

The north-south trending, down-to-the-west fault indicated by Broadhead (2002) just to the east of the Alamogordo fault likely is the Bug Scuffle fault mapped by Pray (1961). (Figure 2.21) Pray (1961) mapped this fault as far south as T. 19 S., R. 11 E., but indicated that it probably extended farther to the south. Pray (1961) described it as a long, high-angle fault that shows evidence of strike-slip and dip-slip displacements associated with pre-Abo Formation deformation. For the hydrogeologic framework model, the trace of the Bug Scuffle fault was obtained from Broadhead (2002), and was projected northward and eventually terminated with the northwest projection of the Sacramento Canyon fault near the headwaters of the Sacramento River. (Figures 2.21, 2.25, and 3.1)

-Unnamed Ancestral Rocky Mountain Faults

Broadhead (2002) studied the subsurface structure beneath the New Mexico portion of the Salt Basin region, and identified numerous Ancestral Rocky Mountain structures (Pennsylvanian to Early Permian) in the form of horst-and-graben blocks bounded by northerly to northwesterly trending high-angle normal faults. Pennsylvanian strata and rocks of the Lower Permian Hueco Formation are present in the grabens, but not on all the horsts (Broadhead, 2002). The Pow Wow Conglomerate unconformably overlies Pennsylvanian and older rocks on the horst blocks, and thickens significantly into the grabens, which suggests either syn-tectonic deposition or post-tectonic deposition into the grabens (Broadhead, 2002). Mississippian strata overlain by Pennsylvanian strata, and post-Wolfcampian strata show no variation in thickness across the fault zones, and therefore are pre- and post-tectonic, respectively (Broadhead, 2002). Ancestral Rocky Mountain structures also include anticlines and synclines in the southern

Sacramento Mountains, in which the Abo Formation unconformably overlies Pennsylvanian strata (Broadhead, 2002).

The traces of the generally north-trending faults associated with the Pedernal uplift were obtained from Broadhead (2002) for incorporation in the hydrogeologic framework model. (Figure 2.21) In his west to east A to A' cross-section, Broadhead (2002) depicted these Ancestral Rocky Mountain structures as displacing Precambrian through Pennsylvanian strata, and cutting through the Lower Permian Pow Wow Conglomerate. Just to the north of the trace of the Otero fault, Broadhead (2002) identified a southeasterly trending Ancestral Rocky Mountain fault that has down-to-the-southwest displacement. This fault was projected to the southeast into Texas, where it passes to the south of the Hunt Oil Co., Dyer #1 (HUOCDY1) well, and eventually terminates against the western boundary fault of the Salt Basin graben. (Figures 2.21, 2.25, and 3.1) This well lacks a Devonian-through-Lower Permian (Wolfcampian) section, which suggests that this region was impacted by the Pedernal uplift.

The locations of the west-northwest trending faults that cut through the southwestern portion of the McGregor Range were obtained from Broadhead (2002). (Figure 2.21) The northernmost west-northwest trending fault in this region corresponds to the trend of the Otero fault of Goetz (1985) and Nutt (1997), and therefore these features were connected. (Figures 2.21, 2.22, and 3.1) The western termination of the Otero fault was chosen at its intersection with the Alamogordo fault of Cather and Harrison (2002). (Figures 2.25 and 3.1) For the hydrogeologic framework model, the southernmost west-northwest trending fault presented by Broadhead (2002) was extended southeastward into Texas based on its southeasterly trend in New Mexico. The fault

projection passes between the Hueco Basin, University #1 (HUBAUN1) well to the north and the California Standard of Texas, Theisen #1 (CASATT1) well to the south based on a sense of down-to-the-north displacement of Pennsylvanian strata between the two wells. (Figures 2.21 and 3.1) The fault then terminates against the southward projection of the main western boundary fault of the Pedernal uplift as defined for New Mexico by Broadhead (2002). (Figures 2.21 and 3.1)

2.3.b: Middle-to-Late Permian Features (Figure 2.22)

-Bone Spring Flexure

The Late Leonardian-to-Early Guadalupian Bone Spring flexure is a broad southeastward dipping monocline that outlined the northwest margin of the subsiding Delaware Basin during the Permian (Hayes, 1964; King, 1948). (Figure 2.22) The gray Victorio Peak Limestone was deposited along the shelfward side of the southwest-northeast trending monocline, with the black Bone Spring Limestone being deposited predominantly south of the flexure (Hayes, 1964; King, 1948). The Bone Spring flexure is overlain by the Guadalupian Goat Seep and Capitan reef limestones (King, 1948). Rocks of the Guadalupian Delaware Mountain Group were derived from the uplifted limestones of the flexure and were deposited along the sloping surface of the monocline as it descended into the Delaware Basin (Hayes, 1964; King, 1948). Beds of the lowermost formation of the Delaware Mountain Group, the Brushy Canyon, are nearly horizontal, but wedge out by transgressive overlap onto the flexure (Newell et al., 1972). The flexure had been almost completely buried by the beginning of deposition of the middle formation of the Delaware Mountain Group, the Cherry Canyon, and had little effect on sedimentation throughout the rest of the Guadalupian (Hayes, 1964). North of

the flexure, the lowermost sandstone tongue of the Cherry Canyon Formation lies unconformably on rocks of the Bone Spring Formation (Newell et al., 1972). For the model, the trace of the Bone Spring flexure was obtained from Goetz (1985). (Figure 2.22)

-Babb and Victorio Flexures

The east-southeast trending Babb and Victorio flexures are northeastward dipping monoclines that also are of Permian age and outlined the northwest margin of the Delaware Basin (King, 1948). (Figure 2.22) Similar to the Bone Spring flexure, these flexures are also ringed by reefs through parts of their courses; however in these cases the reefs are Leonardian (King, 1948). The Leonardian Bone Spring Limestone overlaps the Wolfcampian Hueco Limestone along both of these flexures, and shows evidence of conglomeritic material derived from the Hueco along the Victorio flexure (King, 1948). Exposures on the Victorio flexure indicate that the basement rocks are flexed down to the northeast in the same manner as the overlying younger rocks (King, 1948). Both flexures were major down-to-the-north faults in post-Early Pennsylvanian time, experienced no movement during deposition of the Hueco Formation, and then underwent renewed down-to-the-north movement during the Leonardian (Muehlberger, 1980). Displacement on the Babb and Victorio flexures are 300 m (1,000 feet) and 520 m (1,700 feet), respectively (King, 1965). The Babb flexure and the more easterly trending Victorio flexure cut through the blocks of the Salt Basin graben, and intersect the trend of the Apache Mountains on the east side of the graben (Goetz, 1980). For the hydrogeologic framework model, the trace of the Babb and Victorio flexures was obtained from Goetz (1985). (Figure 2.22)

These flexures were projected northwestward past the end of the traces presented in Goetz (1985), and terminated against the southward projection of the main western boundary fault of the Pedernal uplift as defined for New Mexico by Broadhead (2002). (Figures 2.21, 2.22, and 3.1) The projected western termination of the Babb flexure passes between the Trail Mountain, Inc., University Big Iron "C45" #1 (TMUBIC1) well to the north and the Trail Mountain, Inc., University Felina "D27" #1 (TMUFD27) well to the south based on a sense of down-to-the-north displacement of Pennsylvanian strata between these two wells. (Figures 2.22 and 3.1) The westward projection of the Victorio flexure passes between the Hassle Hunt Trust, Univ. "M-49" #1 (HHUM491) well to the north and the Hassle Hunt Trust, Mosely #1 (HAHUTM1) well to the south based on a sense of down-to-the-north displacement of Ordovician through Silurian strata between these two wells. (Figures 2.22 and 3.1)

-Otero Fault

The Otero fault was first described by Goetz (1985), however King (1965) had hypothesized a northwest striking fault zone terminating at Bitterwell Mountain. (Figure 2.22) Like the Babb and Victorio flexures, the Otero fault strikes about N 60º W and shows displacement down to the northeast (Goetz, 1985). The fault cuts through Otero Mesa and continues southeast towards Dell City along the northeast side of the Cornudas Mountains (Goetz, 1985). The fault passes south of Dell City where it is exposed at the surface before reaching Salt Flat (Goetz, 1985). The fault terminates along a pair of normal faults bounding the eastern side of the Salt Basin graben at Bitterwell Mountain (Goetz, 1985). Total-intensity aeromagnetic and Bouguer gravity anomaly maps presented by Nutt (1997) support the trace of the Otero fault in Goetz (1985) and suggest

it acted as a zone of crustal weakness in the crystalline basement that accommodated the placement of igneous intrusions.

-Bitterwell Break

The Bitterwell Break is a prominent break in the blocks of the Salt Basin graben that trends east-west from the Babb Flexure to the south side of Bitterwell Mountain (Goetz, 1980). (Figure 2.22) The trend of the Bitterwell Break appears to correspond to the trend of the North Sierra Diablo fault zone of Collins and Raney (1997). (Figure 2.25) Like the other Paleozoic transform zones that cut the blocks of the Salt Basin graben (Otero fault, and Babb and Victorio flexures), the Bitterwell Break shows down-to-the-north displacement (Goetz, 1980). The Bitterwell Break is also an important hydrogeologic feature, as it corresponds to a groundwater divide (Nielson and Sharp, 1985). Nielson and Sharp (1985) postulated that the Bitterwell Break may act as a permeability barrier, and noted that the Victorio flexure also corresponds to a groundwater divide. For the hydrogeologic framework model, the trace of the Bitterwell Break was obtained from Goetz (1985), and this trend forms a portion of the southern boundary of the 3-D finite difference (MODFLOW-2000) groundwater flow model.

-Sixmile, Y-O, and Lewis Buckles

The northeast-southwest trending faults northeast of the Salt Basin watershed are from north to south the Sixmile and the Y-O buckles. (Figure 2.22) These features are expressed at the surface in some places as folds and in other places as faults, and also show evidence of right-lateral strike-slip movement (Kelley, 1971). The slightly undulated Sixmile buckle strikes N 41º E (Kelley, 1971). The slightly curved Y-O buckle strikes N 40º E to N 43º E, and shows reversals of the upthrown side along the fault

(Kelley, 1971). The buckle follows a pre-existing grain of deformation which experienced generally down-to-the-southeast displacement during the Paleozoic (Kelley, 1971). The Y-O buckle essentially merges to the south with the Lewis buckle, which eventually terminates against the Guadalupe fault zone (Kelley, 1971). For the hydrogeologic framework model, the traces of these buckles were obtained from Kelley (1971) and Broadhead (2002). (Figure 2.22)

-Artesia-Vacuum Arch, "AV" Lineament, and Piñon Cross Folds

The Artesia-Vacuum arch is a long, easterly-plunging nose that represents the Abo reef trend (Kelley, 1971). (Figures 2.20 and 2.22) The "AV" lineament of Black (1973) trends northeast from the northeast portion of Otero Mesa towards The Rim of the Guadalupe Mountains, and if projected farther to the northeast coincides with the southwest end of the Artesia-Vacuum arch. (Figure 2.22) Structural offsets of the McGregor anticline, The Rim and probably the Guadalupe fault zone, and the Huapache monocline suggest left-lateral movement along this feature (Black, 1973). The offsets of the McGregor anticline, The Rim, and the Guadalupe fault zone indicate that this feature has been active during the Cenozoic. In his C to C' cross-section, Black (1973) depicted the "AV" lineament as two down-to-the-southeast faults that cut Precambrian through Leonardian (Yeso Formation) strata. Early movement along this feature during the Late Paleozoic is suggested by the abrupt facies change in the basal Rio Bonito Member of the San Andres Formation from predominantly limestone north of the lineament to mostly dolomite south of the lineament, and its gross parallelism with the Bone Spring monocline to the south (Black, 1976). It is also possible that the Piñon cross-folds

89

developed as a result of Late Paleozoic deformation, but a similar facies change is not observed across this feature (Black, 1976). (Figure 2.22)

2.3.c: Late Cretaceous Features (Figures 2.23 and 2.24)

-McGregor Fault

The McGregor fault is a northwest trending reverse fault located to the west of the Hueco Mountains in the Tularosa Basin-Hueco bolson that offsets Silurian to Pennsylvanian strata, and is probably a Laramide structure (Broadhead, 2002). (Figure 2.23) U.S. Army Corps of Engineers geothermal test well GDP 51-8 (GDP51-8) constrains the location of this fault as gently-dipping Silurian strata overlie steeply-dipping and overturned Mississippian strata in this well (Finger and Jacobson, 1997). (Figure 2.23) The trace of the fault was also presented in Cather and Harrison (2002). Machette et al. (1998) also described an unnamed structure that forms an east-west trending, down-to-the-south monocline within the Hueco bolson, but then becomes a south-to-southeast trending, down-to-the-west fault along the eastern edge of the bolson. This feature was first mapped by Seager et al. (1987), and corresponds closely to the trace of the McGregor fault presented in Cather and Harrison (2002). The McGregor fault and this unnamed structure are likely the same feature, and are modeled as such. It is likely that this feature extends south into Texas along the boundary between the Hueco bolson and the Hueco Mountains, but its trace has not been defined (Machette et al., 1998). For the hydrogeologic framework model, this fault was projected south-southwestward along the southwestern side of the Hueco Mountains to its intersection with the northernmost down-to-the-west normal fault bounding the Hueco graben mapped by Collins and Raney (1991). (Figures 2.23, 2.25, and 3.1) This "fault zone" continues southeastward along the

90

southernmost down-to-the-west normal fault bounding the Hueco graben of Collins and Raney (1991) to its intersection with the northern end of the Campo Grande fault zone presented by Collins and Raney (1991). (Figures 2.25 and 3.1)

-Otero Mesa and Guadalupe Ridge Folds

Late Cretaceous-to-Early Cenozoic east-west oriented compressional stress associated with the Laramide orogeny also produced northwesterly and northerly trending folds throughout the Otero Mesa region (Black, 1975). (Figures 2.23 and 2.24) These relatively symmetrical, gently dipping and commonly doubly plunging folds affected the carbonate rocks of the San Andres Formation on the surface of the Otero Mesa, and likely also affected the incompetent Yeso Formation in the subsurface (Black, 1975). These structures include the Otero, Fleming, and Cornucopia folds, and possibly the Jernigan Wash anticline and the Chert Plateau folds (Black, 1976). Farther to the north, the Dunkin uplift and associated folds are also probably Laramide structures (Kelley, 1971). Similarly, the Guadalupe Ridge folds are probably the result of Laramide compression, and may be indirectly related to the older Bone Spring monocline (Hayes, 1964).

2.3.d: Cenozoic Features (Figure 2.25)

-Otero Break, and Otero Mesa Folds

The Otero Break, which was named by Mayer (1995), is a northwest trending system of down-to-the-west normal faulting and intense fracturing that extends from the southeastern Sacramento Mountains, where it defines the course of the Sacramento River, to just north of Dell City, Texas. (Figure 2.25) The preferred fracture orientation parallels the trend of normal faults along the Otero Break at N 20º W (Mayer and Sharp, 1998). Mayer (1995) described this fault zone as terminating in the Sacramento Mountains

against the eastern bounding faults of the Tularosa Basin. The Otero Break separates the faulted and fractured Chert Plateau, which is a southeastward structural extension of the Sacramento Mountains, on the east from the relatively unfractured Otero Mesa on the west (Mayer, 1995; Mayer and Sharp, 1998). The Otero Break also separates the predominantly carbonate lithology of the San Andres Formation outcropping on the Chert Plateau from the more heterogeneous transitional marine-terrestrial lithology of the Yeso Formation outcropping on Otero Mesa (Mayer and Sharp, 1998). (Figure 2.1) The lack of fracturing to the west of the Otero Break on Otero Mesa may be due in part to this difference in lithology (Mayer and Sharp, 1998). The Otero Break roughly parallels other major Paleozoic structural features (Huapache monocline, Babb and Victorio flexures, and the Otero fault) and may be a reactivated Paleozoic feature (Mayer, 1995). (Figures 2.21 and 2.22)

The normal faulting and fracturing of the Otero Break are concentrated along the axial crests and steep southwestern flanks of several asymmetrical anticlines mapped by Black (1973). (Figures 1.6 and 2.25) The McGregor anticline extends from the Piñon cross folds southeastward to the "AV" lineament in T. 23 S, R. 16 E, sec. 19 and 20, where the anticline is offset 3.2 km (2 miles) to the east by the lineament (Black, 1973). To the south of the "AV" lineament, the western-most anticline of the Chert Plateau folds likely is the extension of the McGregor anticline (Black, 1973). The McGregor fault zone of Black (1973), which extends along the western flank of the McGregor anticline, consists of numerous high-angle normal faults and associated parallel joints. Black (1973) describes encountering more than a dozen openings along these faults and joints

that could be descended into the subsurface, and were lined with multiple layers of calcite cement.

Cenozoic Basin-and-Range extension produced a series of northwest trending, deep-seated basement fault blocks that are less deformed and uplifted to the south and east, over which the anticlines and synclines that dominate the northeast Otero Mesa formed by drape-folding (Black, 1973; Black, 1976). (Figures 1.6 and 2.25) Large anticlines and synclines outline these tilted fault blocks due to drape folding of the San Andres and underlying Yeso Formations over these structures (Black, 1976). These drape folds include the Sacramento, Orendorf, McGregor, and Prather anticlines, and the Sacramento River, Otero, and Prather synclines (Black, 1976). The Cornucopia and Jernigan Wash anticlines may also be the result of drape folding over eastward-tilted fault blocks (Black, 1976).

Only the southern portion of the Otero Break south of the "AV" lineament is shown by Broadhead (2002), and this trace is used in the hydrogeologic framework model. (Figure 2.21) North of the "AV" lineament the trace of the Otero Break is offset to the west of its southern segment (Black, 1973). For the model, the trace of the Otero Break north of the "AV" lineament was obtained from Black (1976) and Schruben et al. (1994). (Figure 2.25) The trace of this portion of the Break is not mapped by Black (1976) or Schruben et al. (1994) northwest of the point where the Sacramento River takes a dramatic bend from its southeast course to the south-southwest. For the model, the fault was projected to the west along the base of the upland region that is bounded on the south by Cenozoic alluvium, and terminated against the Alamogordo fault of Cather and Harrison (2002). (Figures 2.25 and 3.1) The Otero Break is represented as a single fault

in the model, but is actually a series of en echelon, northwest trending, down-to-the-southwest faults.

John Shomaker & Associates, Inc. [JSAI] (2002) described the structural feature bounded by the Otero Break on the north and east as a "graben." For the hydrogeologic framework model, the southern and western boundary of the "graben" was taken as the down-to-the-north Ancestral Rocky Mountain fault of Broadhead (2002) located just south of the Otero Break. (Figures 2.21 and 3.1) The northwestern trace of this fault was altered from Broadhead (2002) to place the fault farther to the south along the southern edge of the Cenozoic alluvial deposits south of the Otero Break, forming a "graben" filled with alluvium. (Figures 2.21 and 3.1) The projection of this fault also terminates against the Alamogordo fault of Cather and Harrison (2002). (Figures 2.25 and 3.1) The southern portions of this "graben" correspond to the Otero and South Otero synclines of Black (1973), which have steeply-dipping northeastern flanks and more gently-dipping southwestern flanks that rise towards the Otero Mesa. (Figures 1.6, 2.25, and 3.1) Black (1973) noted that the southwestern boundary of the Otero syncline may be fault controlled, and that a large structural depression exits beneath the Otero syncline.

-Sacramento Canyon Fault and Related Faults

Just north of the Otero Break, Broadhead (2002) indicated a northwest trending, down-to-the-southwest fault. (Figure 2.21) This fault trace corresponds to the southern end of a northwest trending fault shown by Schruben et al. (1994) that originates near the headwaters of the Sacramento River and in general trends southeastward along its course until the Sacramento River bends sharply to the south-southwest. (Figures 2.21 and 2.25) The fault trace of Schruben et al. (1994) also corresponds, in general, to portions of the

Sacramento Canyon fault described and mapped by Black (1976). Black (1973) indicated that the Sacramento Canyon fault dips about 80º to the southwest, and displaces the Permian San Andres and Yeso Formations at the surface. In his cross-sections F to F' and G to G' Pray (1961) indicated a series of inferred faults and a single inferred fault, respectively, located between the Sacramento River and the Sacramento anticline that displace the Yeso Formation and older strata. For the hydrogeologic framework model, these faults were combined into one continuous fault that was projected slightly to the northwest and terminated with the northern projection of the Bug Scuffle fault near the headwaters of the Sacramento River. (Figures 2.21, 2.25, and 3.1) The Sacramento Canyon fault, like all the other high-angle normal faults associated with the major anticlines and folds on the Otero Mesa, is the result of Basin-and-Range extensional tectonics (Black, 1973).

-Alamogordo Fault

The uplift of the Sacramento, Hueco, Sierra Diablo, Brokeoff, Guadalupe, Delaware, and Apache Mountains are the result of Cenozoic Basin-and-Range extension and associated normal faulting (Pray, 1961; King, 1965; Kelley, 1971; Black, 1975; Brown et al., 1978). (Figure 1.3) The Sacramento uplift is separated from the Tularosa Basin on the west by a major north to northwest trending boundary fault known as the Alamogordo fault (Cather and Harrison, 2002). (Figure 2.25) The Alamogordo fault is a steep, westerly dipping normal fault that exhibits a minimum offset of 2,100 m (7,000 feet) along the central portions of the escarpment, which decreases to a minimum offset of 1,200 m (4,000 feet) to the north and south (Pray, 1961). The Sacramento uplift also consists of a broad, gentle anticline to the east of the Alamogordo fault, which suggests

that the uplift may be a broken anticline (Kelley, 1971). The Sacramento anticline is asymmetric with a steeply-dipping western flank that approaches 45º, and a gently-dipping eastern flank of generally less than 15º (Black, 1973). For the hydrogeologic framework model, the trace of the Sacramento anticline was obtained from Broadhead (2002). (Figure 2.25) The trace of the Alamogordo fault was obtained from Cather and Harrison (2002). (Figure 2.25) They extended the southern trace of the fault farther to the south-southwest than is indicated in Machette et al. (1998).

-Guadalupe and Dog Canyon Fault Zones

The generally north-south trending Guadalupe fault zone follows along the alluvium-covered base of the Buckhorn Escarpment of The Rim and consists of high-angle, down-to-the-west normal faults (Black, 1973; McKnight, 1986). (Figure 2.25) Apparent throw across the faults ranges from 600 to 1,200 m (2,000 to 4,000 feet) and increases from north to south (Kelley, 1971; Black, 1973). At the intersection of the "AV" lineament with the Guadalupe fault zone, The Rim of the Guadalupe Mountains and the fault zone bend abruptly to the southeast (Black, 1973). (Figure 1.6) From this point south the zone of faulting that continues along the Algerita Escarpment of the Guadalupe Mountains is known as the Dog Canyon fault zone (McKnight, 1986). (Figure 2.25) To the north, the east-west trending Stevenson fault is the possible westward extension of the Guadalupe fault zone, and exhibits high-angle, down-to-the-south normal faulting (Kelley, 1971; Black, 1973; McKnight, 1986). (Figure 2.25) Kelley (1971) found evidence of Quaternary movement in the form of a small Holocene fan scarp on the northern portion of the Guadalupe fault zone in T. 20 S., R. 17 E, and Muehlberger et al. (1978) found a second Quaternary scarp 10 km (6 mi) south. A slight

anticlinal crest parallels the Guadalupe Mountains escarpment just east of The Rim (McKnight, 1986). The trace of the Stevenson fault, the Guadalupe Mountains fault zone, and the Dog Canyon fault zone were obtained from Broadhead (2002).

-Border Fault Zone

The Brokeoff Mountains are an anticlinal horst feature separated like a spur from the Guadalupe Mountains by the synclinal graben of Dog Canyon (McKnight, 1986). (Figure 1.3) The Brokeoff Mountains trend generally north-south, and are bounded on the east and west by down-to-the-east normal faults, and the down-to-the west normal faults of the Border fault zone, respectively (McKnight, 1986). (Figure 2.25) The Border fault zone is a north-south trending zone of down-to-the-west normal faulting that defines the eastern edge of the Salt Basin graben south of the intersection of the "AV" lineament with the Guadalupe fault zone (McKnight, 1986). (Figure 2.25) The Border fault zone shows displacements of 600 to 1,200 m (2,000 to 4,000 feet) (King, 1948). The Border fault zone also shows evidence of Quaternary displacement east of the Patterson Hills in Texas where it strikes N 25º W to N 35º W, and dips 74º to the southwest at the surface (Collins and Raney, 1997). The trace of the Border fault zone was obtained from Broadhead (2002).The trace of the unnamed eastern fault was placed along the northern and eastern base of the Brokeoff Mountains. (Figure 2.25)

-Hueco Mountains Faults

The Hueco Mountains were also uplifted during the Cenozoic. The Hueco Mountains are bounded on the west by the Tularosa Basin-Hueco bolson (Muehlberger et al., 1978). (Figure 1.3) Two major down-to-the-west normal faults separate the Hueco graben from the thin veneer of basin deposits that fill the northeast portion of the Hueco

bolson as it rises towards the Hueco Mountains, and show Quaternary displacement (Muehlberger et al., 1978; Collins and Raney, 1991). (Figure 2.25) These faults have subtle surface traces with northward regional strikes that range from N 40º W – N 20º E to N 20º W – N 10º E, and show displacements at the base of the basin-fill deposits of 1,070 m (3,500 feet) and 870 m (2,850 feet), respectively (Collins and Raney, 1991). The Hueco Mountains are also diced by several northward trending normal faults that show displacement down-to-the-west and east (Collins and Raney, 1991). (Figure 2.25) It is unknown if these faults have experienced Quaternary displacement, but most of the Quaternary fault movement has been focused along the Hueco graben boundaries and within the Hueco bolson (Collins and Raney, 1991). Only the longest down-to-the-west fault shown in Collins and Raney (1991) was included in the hydrogeologic framework model. (Figure 2.25) For the model, the trace of the fault presented in Collins and Raney (1991) was extended to the north along the east side of the Seaboard Oil Co., Trigg-Federal #1 (SEOCTF1) well based on a sense of down-to-the-west displacement of Precambrian strata through the Pow Wow Conglomerate compared to the Harvey E. Yates Co., Bennett Ranch Unit #1 (HEYBRU1) and Bennett Ranch Unit 25 #1 (HEYBR25) wells to the east. (Figures 2.25 and 3.1)

Seager et al. (1987) also mapped an inferred, northerly trending, down-to-the-west fault along the western base of the Hueco Mountains. (Figure 2.25) On their F to F' cross-section and geologic map, Seager et al. (1987) depicted this fault displacing Precambrian through Permian strata, and juxtaposing Pennsylvanian strata and the Permian Hueco Formation of the Hueco Mountains with Cenozoic alluvium at the surface. For the model, this fault was extended southeastward into Texas along the base

of the Hueco Mountains where it passes to the north of the Pan American Pet. Corp.,

Phillip F. Hass #1 (PAPPFH1) well. (Figures 2.25 and 3.1) The fault was placed to the

north of the Phillip F. Hass #1 well based on a sense of down-to-the-south displacement

of Precambrian through Pennsylvanian strata compared to the California Standard of

Texas, Theisen #1 (CASATT1) well to the north. (Figures 2.25 and 3.1) The fault was

then terminated against the southward projection of the main western boundary fault of

the Pedernal uplift as defined for New Mexico by Broadhead (2002). (Figures 2.21, 2.25,

and 3.1) The fault was also extended to the north where it merges with the southern end

of the Alamogordo fault as presented in Cather and Harrison (2002). (Figures 2.25 and

3.1)

-Campo Grande Fault Zone, and Arroyo Diablo Fault

The Diablo Plateau had evolved into a positive area flanking the greater subsiding

Delaware Basin to the northeast by the Early Permian (King, 1965). During the Permian,

the Diablo Plateau was the site of shallow-marine deposition of mainly carbonates, while

the Delaware Basin was the site of deep-marine deposition of black limestone and

siliceous shale (King, 1965). This positive region persisted into the Cretaceous, before

being disturbed by Cenozoic Basin and Range extension that uplifted the Hueco, Sierra

Diablo, Brokeoff, Guadalupe, Delaware, and Apache Mountains, and depressed the

Hueco and Salt Basin grabens (King, 1965; Brown et al., 1978). To the southwest, the

Diablo Plateau is separated from the southeast portion of the Hueco bolson by the Campo

Grande fault zone and the Arroyo Diablo fault, which both show Quaternary

displacement (Collins and Raney, 1997). (Figure 2.25) The Campo Grande fault zone

consists of a series of down-to-the-southwest en-echelon fault strands that strike N 25º W

to N 75º W and dip from 60º to 89º to the southwest (Collins and Raney, 1997). The Campo Grande fault zone separates the thick (> 2,000 m (6,560 feet)) basin-fill deposits of the Hueco graben from the thin (< 175 m (575 feet)) deposits that fill the northeastern margin of the Hueco bolson as it rises towards the Diablo Plateau (Collins and Raney, 1991). From northwest to southeast, three en-echelon subsurface fault sections show displacements on the base of the basin-fill deposits of 1,220 m (4,000 feet), 1,290 m (4,230 feet), and 460 m (1,510 feet) (Collins and Raney, 1991). The Arroyo Diablo fault is en echelon to the southeast segment of the Campo Grande fault zone, striking N 30º W to N 60º W and dipping 60º to 85º to the southwest (Collins and Raney, 1997). Like the Campo Grande fault zone, the Arroyo Diablo fault bounds the Hueco graben on the northeast, and shows down-to-the-southwest displacement of the basin-fill deposits of 240 m (785 feet) (Collins and Raney, 1991).

-North Sierra Diablo Fault Zone, and East Sierra Diablo and East Flat Top Mountains Faults

To the south, the Diablo Plateau is bounded by the Northwest Eagle Flat Basin (Collins and Raney, 1997). No faults cut Cenozoic basin-fill sediments in the Northwest Eagle Flat Basin, but surface bedrock geology, subsurface drill hole data, and seismic reflection data suggest that the underlying Cretaceous and older rocks may be displaced by several faults (Collins and Raney, 1997). To the east and southeast, the Diablo Plateau is bordered by the Salt Basin graben and the Sierra Diablo Mountains, respectively (King, 1965). The Sierra Diablo Mountains and its associated down-dropped southeastern foothills (the Baylor Mountains and Beach Mountain) are bounded on the north and east by major normal faults along the Salt Basin graben (King, 1965). (Figures 1.3 and 2.25)

The North Sierra Diablo fault zone is an east-southeastward trending (N 75º W to N 85º W) zone of primarily down-to-the-north, subparallel, interlacing normal faults that have displacements of 300 m to 520 m (1,000 to 1,500 feet) (King, 1965; Collins and Raney, 1997). (Figure 2.25) To the west, the North Sierra Diablo fault zone coincides with the Babb flexure and is probably the result of renewed movement along this flexure in the Cenozoic (King, 1965). (Figures 2.22 and 2.25) At the west and east ends of the fault zone, north-south trending fault zones continue the displacement to the north (East Flat Top Mountains fault) and south (East Sierra Diablo fault), respectively (King, 1965; Collins and Raney, 1997). (Figure 2.25)

The East Sierra Diablo fault extends southward 37 km (23 mi) along the eastern margin of the Sierra Diablo Mountains, striking N 10º W to N 20º E and dipping to the east (Collins and Raney, 1997). (Figure 2.25) The northern portion of the fault separates the Sierra Diablo uplift from the Salt Basin graben and has the greatest displacement, while the southern portion of the fault separates the Sierra Diablo from the intermediate block of the Baylor Mountains (King, 1965). The fault also shows Quaternary displacement (Collins and Raney, 1997).

The East Flat Top Mountains fault extends northward 23 km (14 mi) from the west end of the North Sierra Diablo fault zone to about the latitude of Salt Flat, Texas (Collins and Raney, 1997). (Figure 2.25) This normal fault strikes N 25º W to N 5º E, dips to the east, forms the western boundary of the Salt Basin graben, and shows Quaternary displacement (Collins and Raney, 1997). Northward, the 19 km (12 mi) long, N 45º W to N 60º W striking, and northeastward dipping Dell City fault of Collins and Raney (1997) may correspond to a southeastern portion of the Otero fault of Goetz

101

(1985). The down-to-the-northeast Dell City fault also bounds the western boundary of the Salt Basin graben, but Quaternary displacement is inconclusive (Collins and Raney, 1997). The traces of the North Sierra Diablo fault zone, and East Sierra Diablo and East Flat Top Mountains faults were obtained from Goetz (1985).

-Southern Sierra Diablo Mountains Faults

The southern Sierra Diablo Mountains are broken by several west-northwest trending, steeply-dipping, down-to-the-south normal faults, which are named, from north to south, the Bat Cave fault, Cox Mountain fault, Sulphur Creek fault, Sheep Peak fault, Circle Ranch fault zone, and South Diablo fault (King, 1965). (Figure 2.25) These faults experienced Cenozoic movement, and are probably reactivated features along a long-persistent, west-northwest structural grain (King, 1965). All of the faults originate near the East Sierra Diablo fault and die out to west, with the Cox Mountain and the South Diablo faults being the longest at 32 km (20 mi) and 48 km (30 mi), respectively (King, 1965). Unlike the other faults, the South Diablo fault does not lose its displacement of >305 m (>1,000 feet) towards the west (King, 1965). Therefore, the South Diablo fault was the only southern Sierra Diablo fault included in the hydrogeologic framework model. (Figures 2.25 and 3.1) For the model, the trace of the South Diablo fault was obtained from Goetz (1985). Similar to the Babb and Victorio flexures, the western end of the South Diablo fault as indicated by Goetz (1985) was projected to the northwest and terminated against the southward projection of the main western boundary fault of the Pedernal uplift as defined for New Mexico by Broadhead (2002). (Figures 2.21, 2.25, and 3.1) The South Diablo fault was projected between the Transocean Oil, Inc., 36-1 MSA Trustee, Inc. (TO36MSA) well to the south and the Lockhart, Roseborough & Benton,

102

Gardner & Mosely #1 (a.k.a. Western States Oil, Gardner & Moseley #1) [LR&BGM1 (WSOG&M1)] well to the northeast based on a sense of down-to-the-south displacement of Silurian strata between the two wells. (Figures 2.25 and 3.1)

-North Baylor Fault, and East Carrizo Mountains-Baylor Mountains Fault

The Baylor Mountains are bounded on the north by the North Baylor fault, which trends eastward and has displacement down-to-the-north (King, 1965). (Figure 2.25) Similar to the North Sierra Diablo fault zone, the trend of the North Baylor fault generally coincides with the east-southeastward trend of the Victorio flexure (King, 1965). (Figures 2.22 and 2.25) The eastern boundary of the Baylor and Beach Mountains with the Wild Horse Flat sub-basin of the Salt Basin graben is formed by a 41 km (25 mi) long, northeastward striking (N 10º E to N 40º E), and southeastward dipping normal fault known as the East Carrizo Mountains-Baylor Mountains fault (King, 1965; Collins and Raney, 1997). (Figure 2.25) This fault also shows Quaternary displacement (Collins and Raney, 1997). For the hydrogeologic framework model, the trace of the North Baylor fault was obtained from Goetz (1985), while the East Carrizo Mountains-Baylor Mountains fault was not included in the model.

-Delaware Mountains Fault Zone

The Delaware Mountains trend generally northwest-southeast along the eastern boundary of the Salt Basin graben. (Figure 1.3) The western flank of the Delaware Mountains is separated from the Salt Basin graben by the N 25º W to N 45º W striking, southwest dipping Delaware Mountains fault zone (Collins and Raney, 1997). (Figure 2.25) This 64 km (40 mi) long fault zone consists of a series of subparallel and en

echelon normal fault strands (Collins and Raney, 1997). The trace of the Delaware Mountains fault zone was obtained from Goetz (1985).

-Unnamed Salt Basin Graben Faults

In their north-south cross-section G to G', King and Harder (1985) indicated that the Salt Basin graben was cut by two additional faults that displace Paleozoic and Cenozoic strata. These faults are located between the E.J. Dunigan, Alpha Federal #1 (EJDALF1), Hunt Petroleum Corp., C.L. Ranch "5" #1 (HPCCL51), and Hunt Petroleum Corp., C.L. Ranch #1 (HPCCLR1) wells (King and Harder, 1985). (Figure 2.25) No information exists on their trends or locations, so for inclusion in the hydrogeologic framework model they were placed half-way between each well, with east-west trends. The eastern boundary faults of the New Mexico portion of the Salt Basin graben include the Guadalupe and Border fault zones, and their traces were obtained from Broadhead (2002). (Figure 2.25) The trace of the unnamed western boundary fault of the Salt Basin graben in New Mexico was also obtained from Broadhead (2002). (Figure 2.25)

FIGURES – CHAPTER 2
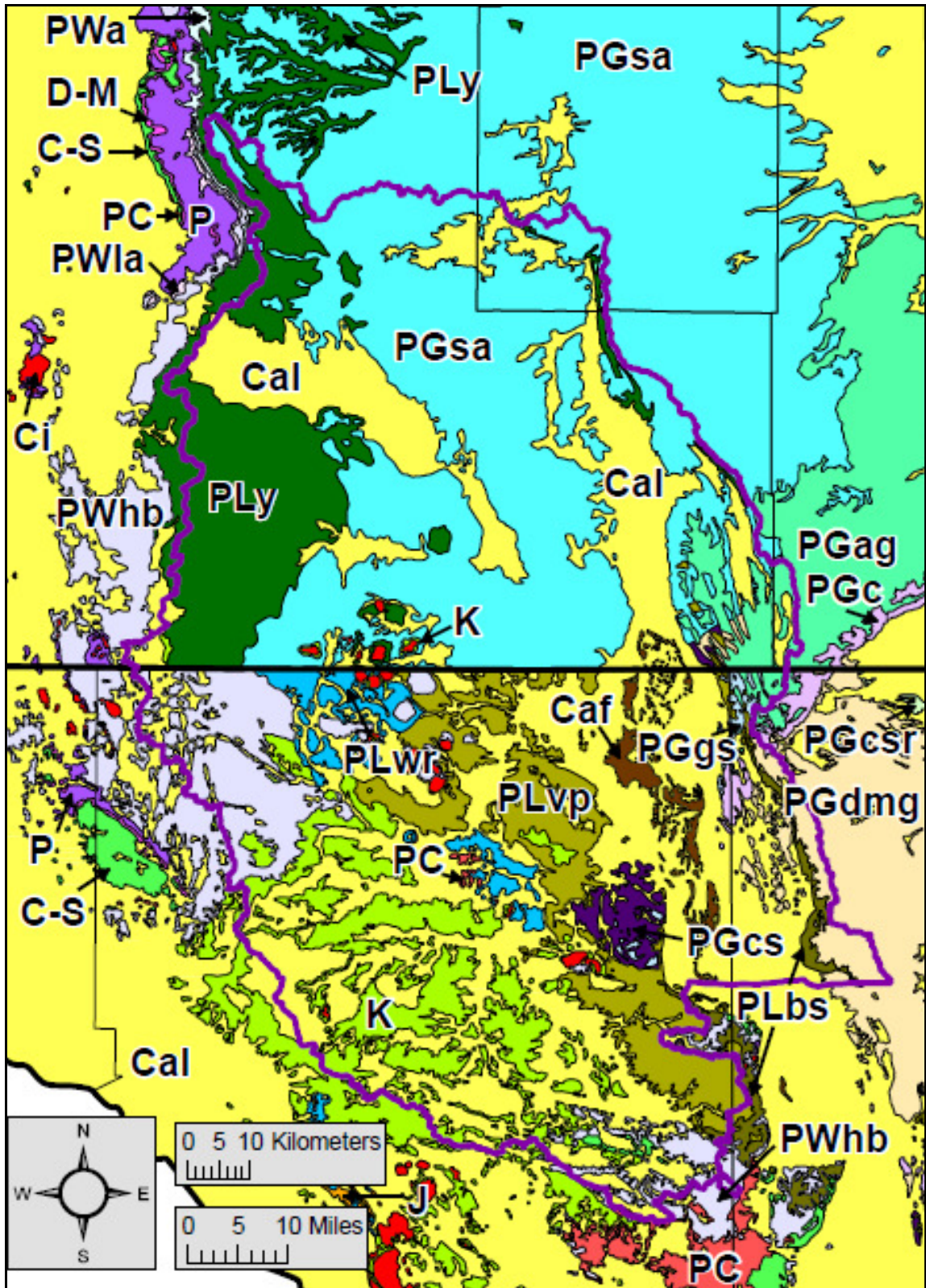
Figure 2.1: Surface geology of the northern Salt Basin watershed. Geology from Stoeser et al. (2005), with location of alkali flats/playa lakes for New Mexico taken from NHD.

Figure 2.1: Legend

Eon   **Era**   **Period**

Cenozoic

Mesozoic

Phanerozoic

Paleozoic   Permian

Proterozoic

Legend

- Alkali Flats/Playa Lakes (Caf)
- Cenozoic Alluvial Deposits (Cal)
- Cenozoic Intrusives (Ci)
- Cretaceous (K)
- Jurassic (J)
- Castile, Salado, and Rustler Formations (POcsr)
- Artesia Group (PGag)
- Capitan Limestone/Formation (PGc)
- Goat Seep Dolomite/Limestone/Formation (PGgs)
- Delaware Mountain Group (PGdmg)
- San Andres Formation (PGsa)
- Cutoff Shale (PLcs)
- Victorio Peak Limestone/Formation (PLvp)
- Wilke Ranch Formation [Leonardian] (PLwr)
- Yeso Formation (PLy)
- Bone Spring Limestone/Formation (PLbs)
- Abo Formation (PWa)
- Hueco Limestone/Formation / Bursum Formation (PWhb)
- Lower Abo / Pow Wow Conglomerate (PWla)
- Pennsylvanian (P)
- Devonian - Mississippian (D-M)
- Cambrian - Silurian (C-S)
- Precambrian (PC)

Ma	System	Series	Stage	Northwestern and Sacramento Shelves (Sacramento Mountains, Otero Mesa/Diablo Plateau, Hueco Mountains)	Shelf Margin (Guadalupe Mountains, Sierra Diablo)	Delaware Basin
2.588 – Present	Quaternary			In mountains and mesas, alluvium, colluvium, terrace gravels, and spring deposits; in grabens, bolson deposits, lacustrine deposits, fanglomerate, and drifted sand.		
65.5 – 2.588	Neogene Paleogene			Intrusive igneous rocks		
99.6 – 65.5	Cretaceous		Gulfian	Mesaverde Fm. / Mancos Fm. / Dakota Fm.		
127 – 99.6	Cretaceous		Comanchean	Washita Group / Fredericksburg Group: Finlay Limestone / Trinity Group: Cox Sandstone, Campagrande Cong.	Also present in the Sierra Diablo	
199.6 – 145.5	Jurassic					
251 – 199.6	Triassic					

108

Age (Ma)	System		Series	Artesia Group / San Andres Fm.		Carlsbad Group		Delaware Mountain Group	
260.4 – 251	Permian		Ochoan	///////	///////	///////	///////	Rustler Fm.	
								Salado Fm.	
								Castile Fm.	
270.6 – 260.4			Guadalupian	Artesia Group	Tansill Fm.	Carlsbad Group	Capitan Lm./Fm.	Bell Canyon Fm.	Delaware Mountain Group
					Yates Fm.				
					Seven Rivers Fm.				
					Queen Fm.		Goat Seep Do./Lm./Fm.	Cherry Canyon Fm.	
					Grayburg Fm.				
				San Andres Fm.	Fourmile Draw		Cherry Canyon		
					Bonney Canyon		///////	Brushy Canyon Fm.	
					Rio Bonito				
					Glorieta		Cutoff Shale		
280 – 270.6			Leonardian	Yeso Fm.			Victorio Peak Lm./Fm.	Bone Spring Lm./Fm.	
							Bone Spring		

299 – 280	Permian		Wolfcampian		Abo Fm. / Lee Ranch tongue / Danley Ranch tongue	Pendejo tongue	Hueco Lm./Fm	Pow Wow Cong.	Wolfcamp Series (Hueco Lm./Fm. and Pow Wow Cong.)	Wolfcamp Fm.
				Magdalena Fm./Group	Bursum / Laborcita Fm.				
305 – 299	Carboniferous	Pennsylvanian	Virgilian		Holder Fm.		Unnamed	Cisco
306.5 – 305			Missourian		Beeman Fm.		Unnamed	Canyon
308 – 306.5			Desmoinesian		Gobbler Fm.		Unnamed	Strawn
311.7 – 308			Atokan/Derryan				Unnamed	Bend
318.1 – 311.7			Morrowan				Unnamed?

110

Age (Ma)	Period	Epoch	Stage	Formation	
333 – 318.1	Carboniferous	Mississippian	Chesterian	Helms Fm.	Barnett Shale
340 – 333			Meramecian	Rancheria Fm.	"Mississippian Limestone"
348 – 340			Osagean	Lake Valley Fm.	
359.2 – 348			Kinderhookian	Caballero Fm.	
385.3 – 359.2	Devonian	Upper		Sly Gap Fm. / Oñate Fm. — Percha Shale / Canutillo Fm.	Percha / Woodford Shale
397.5 – 385.3		Middle			"Devonian"
416 – 397.5		Lower			
438 – 421.3	Silurian		Niagaran	Fusselman Fm.	

				Valmont Dolomite	
451 – 443.7	Ordovician		Cincinnatian	Montoya Group	Montoya Group
488.3 – 471.8			Canadian	El Paso / Ellenburger Group	
501 – 488.3	Cambrian		Croixian	Bliss Sandstone	
	Precambrian				

Figure 2.2: Generalized stratigraphic chart of the Salt Basin region.

Adapted from numerous sources, including Black (1973), Boyd (1958), Foster (1978), Hayes (1964), Kelley (1971), Kottlowski (1963), LeMone (1969), McGlasson (1969), Newell et al. (1972), and Pray (1961).
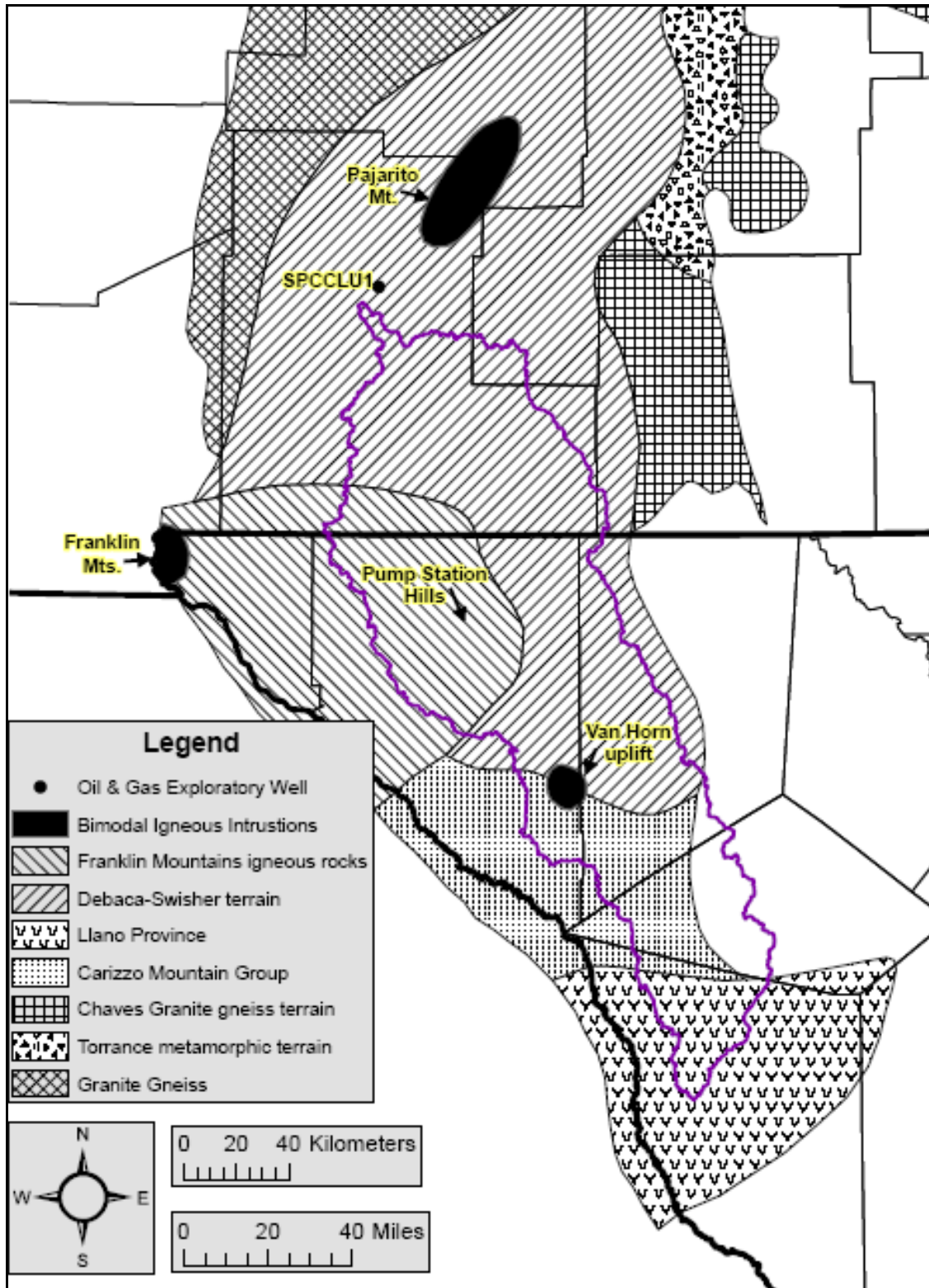
Figure 2.3: Precambrian basement rocks of the Salt Basin region, from Adams et al. (1993) and Denison et al. (1984).
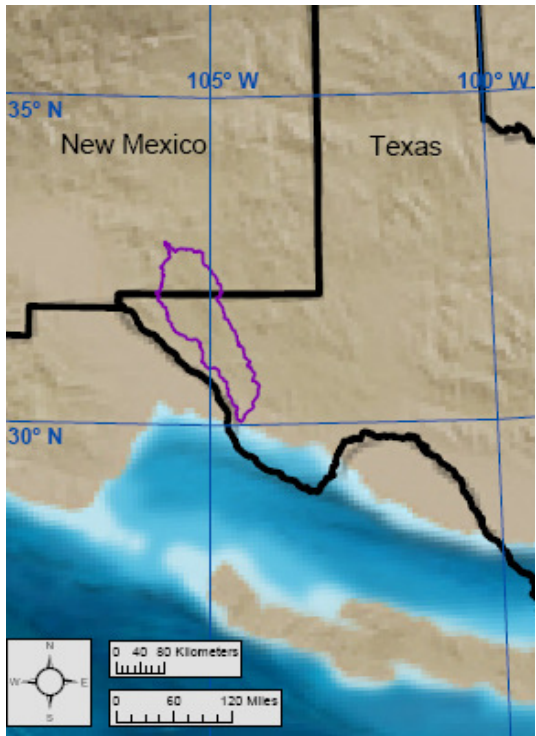
a: Late Precambrian (550 Ma)
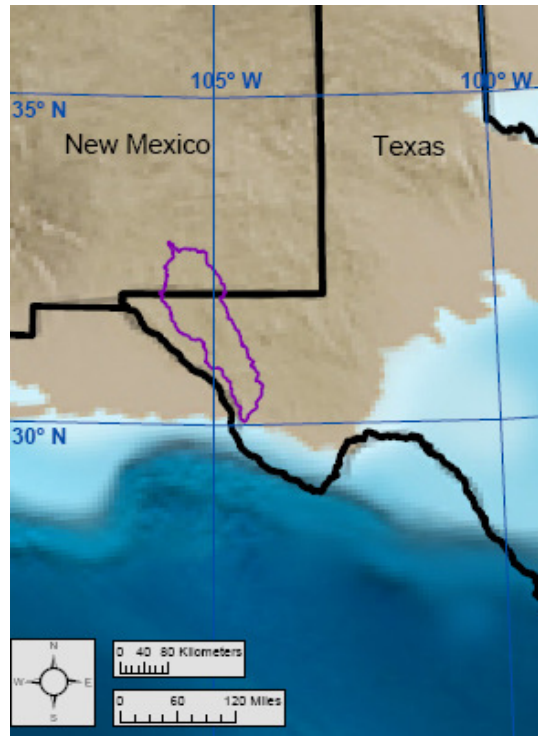
b: Middle Cambrian (510 Ma)
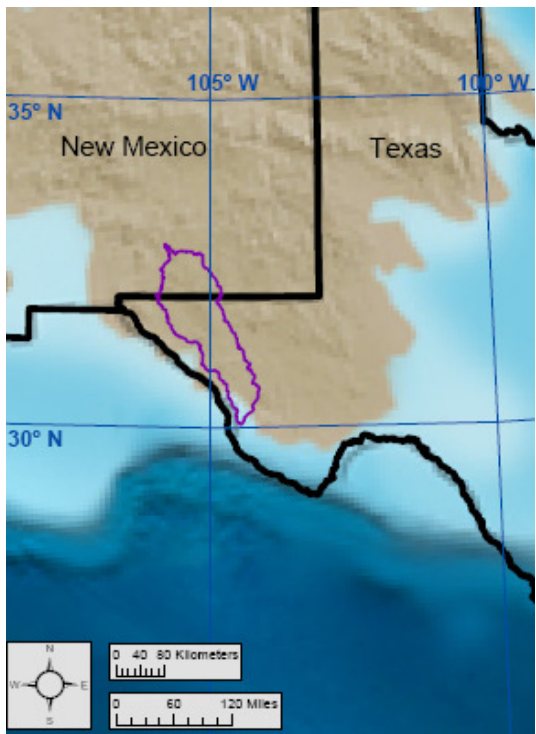
c: Late Cambrian (500 Ma)
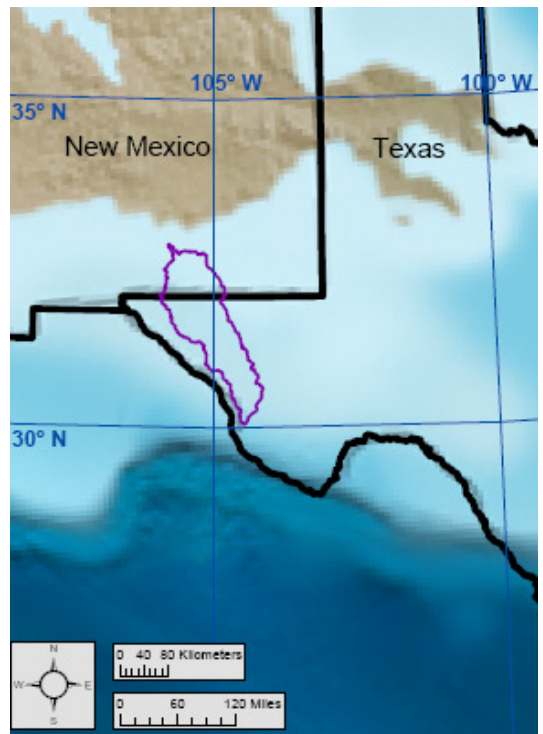
d: Early Ordovician (485 Ma)

Figure 2.4: Late-Precambrian-to-Early-Ordovician paleogeography of the Salt Basin region, from Blakey (2009b).
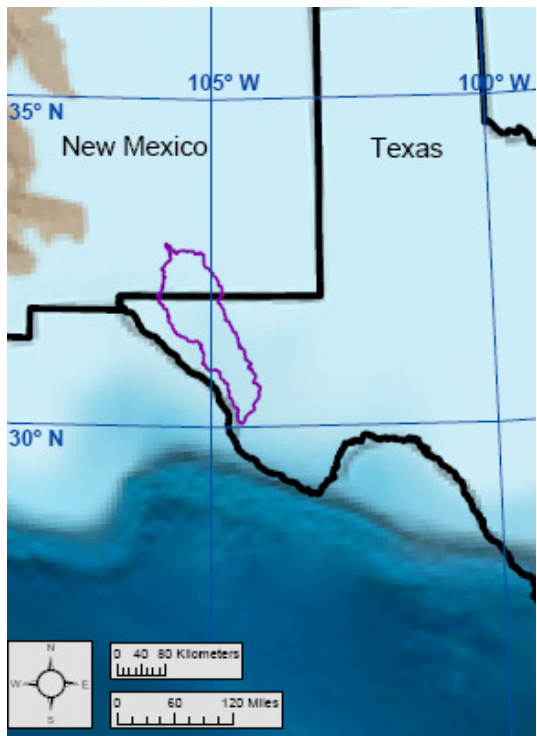
a: Middle Ordovician (470 Ma)
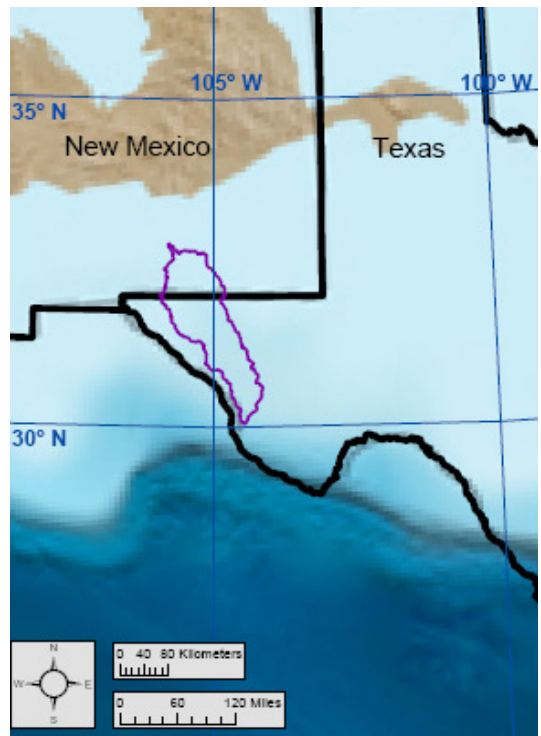
b: Late Ordovician (450 Ma)
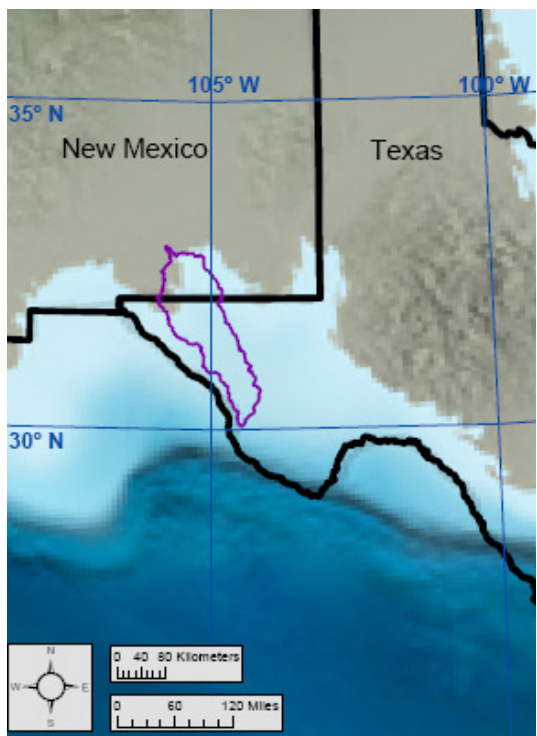
c: Early Silurian (430 Ma)
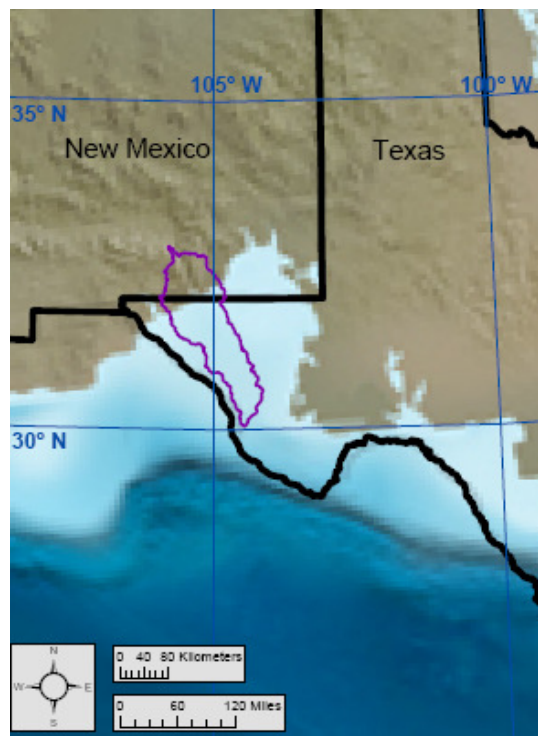
d: Late Silurian (420 Ma)

Figure 2.5: Middle-Ordovician-to-Late-Silurian paleogeography of the Salt Basin region, from Blakey (2009b).

a: Early Devonian (400 Ma)
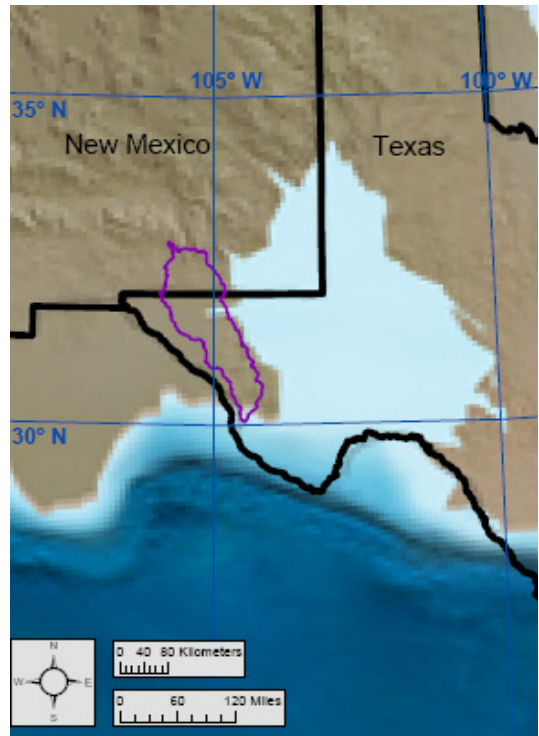
b: Middle Devonian (385 Ma)
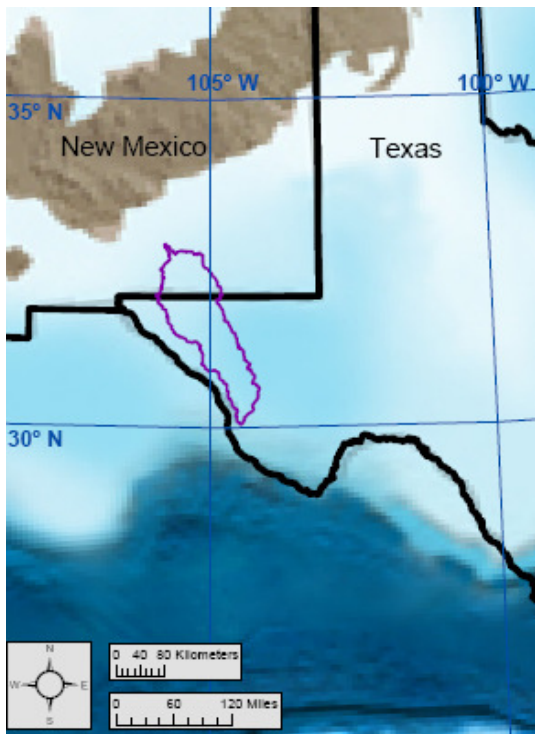
c: Late Devonian (360 Ma)
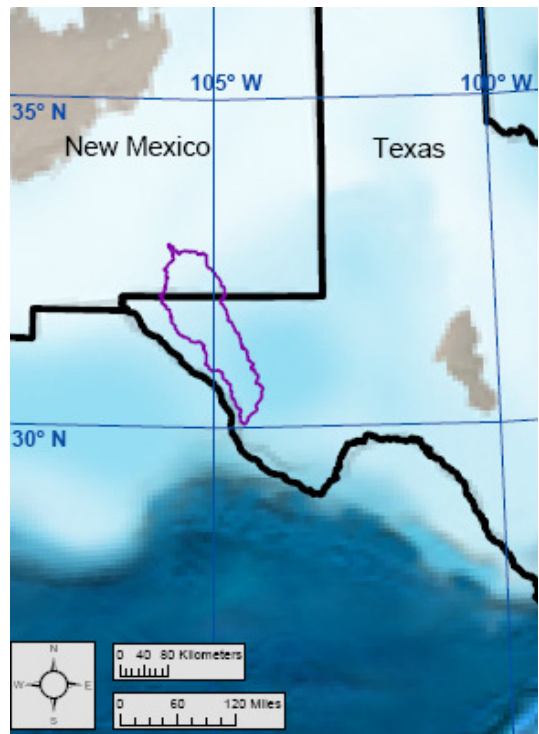
d: Early Mississippian (345 Ma)

Figure 2.6: Early-Devonian-to-Early-Mississippian paleogeography of the Salt Basin region, from Blakey (2009b).
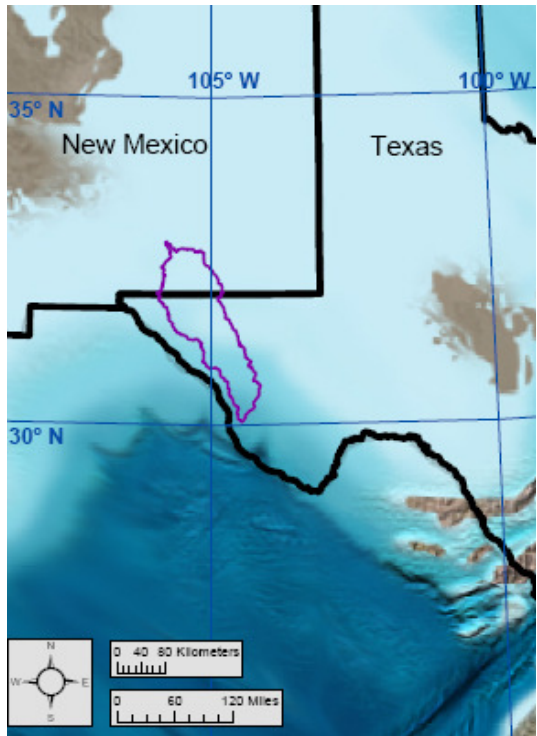
a: Early Mississippian (340 Ma)
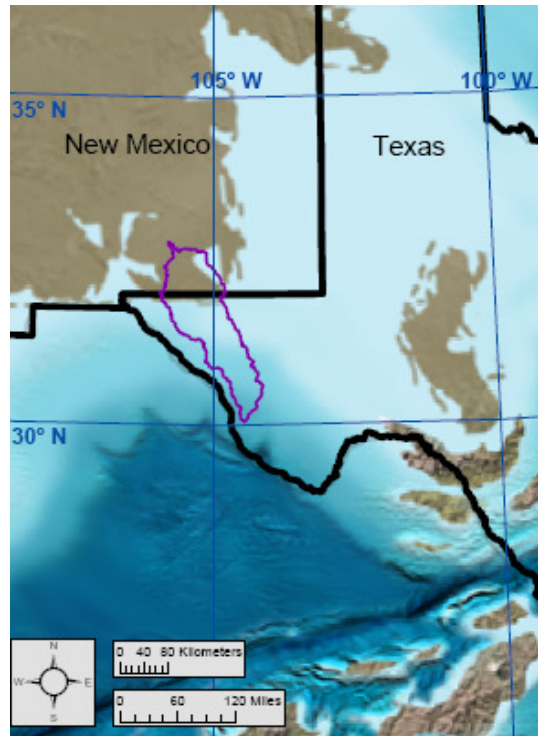
b: Late Mississippian (325 Ma)
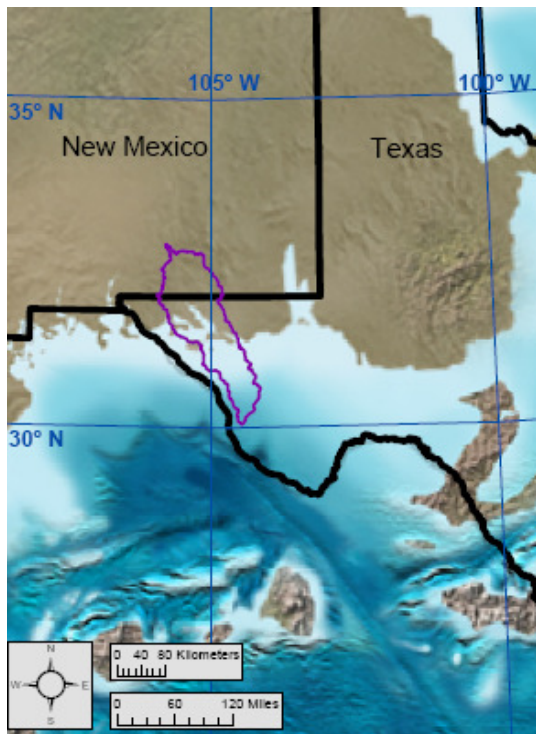
c: Miss.-Penn. lowstand (320 Ma)
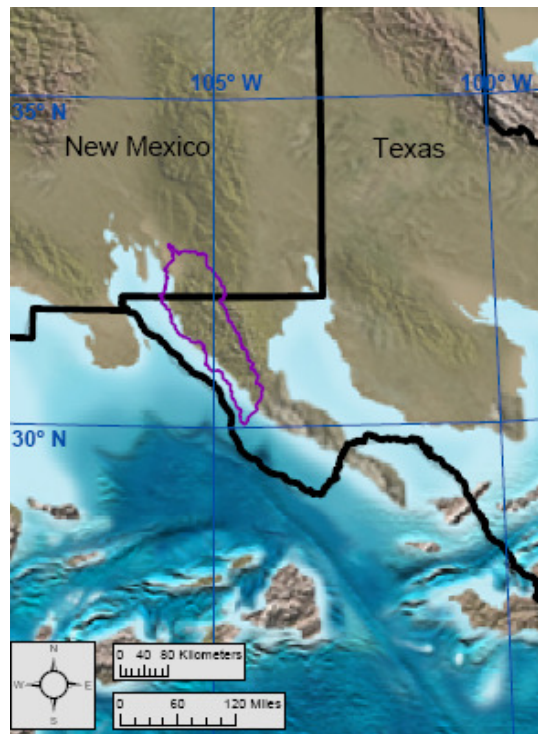
d: Pennsylvanian Morrowan (318 Ma)

Figure 2.7: Early-Mississippian-to-Pennsylvanian-Morrowan paleogeography of the Salt Basin region, from Blakey (2009a).

a: Pennsylvanian Atokan (315 Ma)

b: Pennsylvanian Desmoinian (310 Ma)

c: Pennsylvanian Missourian (300 Ma)

d: Pennsylvanian Virgilian (295 Ma)

Figure 2.8: Pennsylvanian-Atokan-to-Pennsylvanian-Virgilian paleogeography of the Salt Basin region, from Blakey (2009a).
OrB = Orogrande Basin, DeB = Delaware Basin, MiB = Midland Basin.

a: Early Permian (290 Ma)

b: Early Permian (287 Ma)

c: Early Permian (285 Ma)
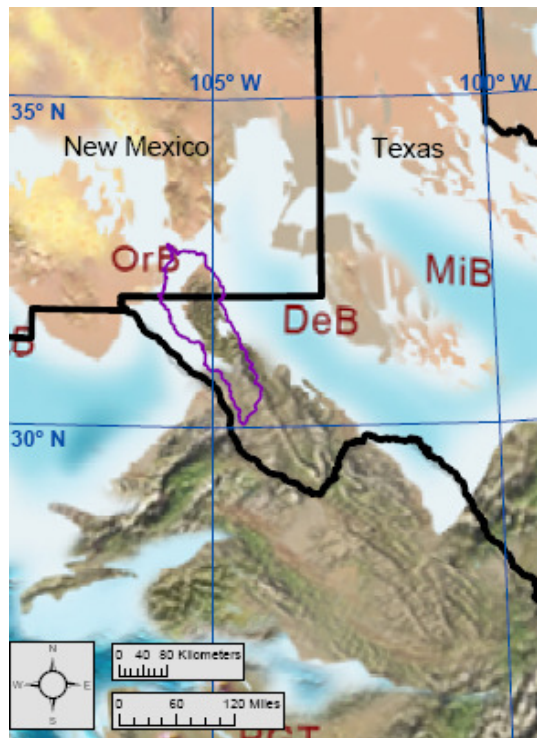
d: Early Permian (280 Ma)

Figure 2.9: Early-Permian paleogeography of the Salt Basin region, from Blakey (2009a).
OrB = Orogrande Basin, DeB = Delaware Basin, MiB = Midland Basin.
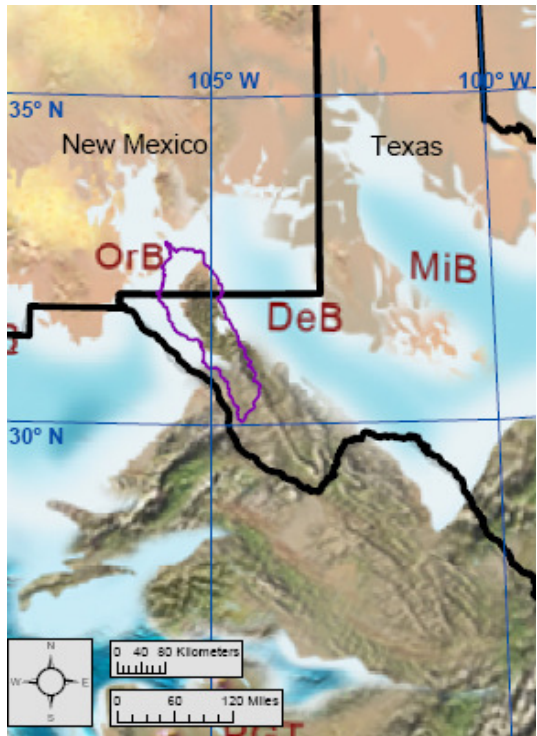
a: Early Permian (278 Ma)
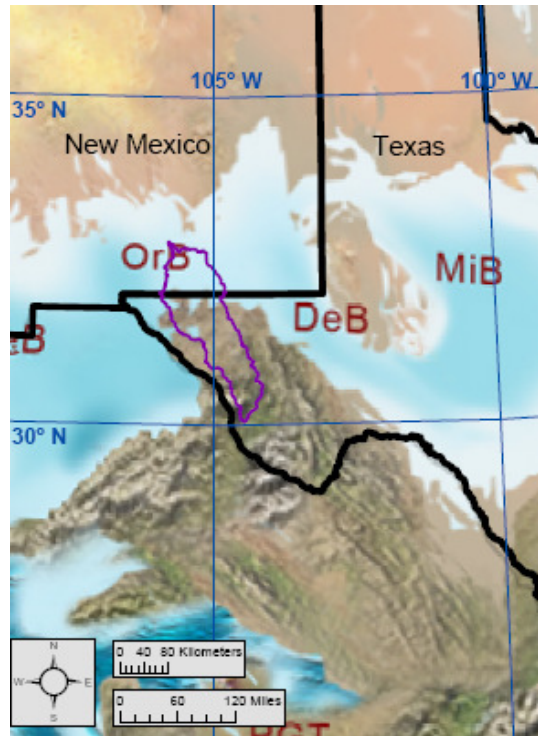
b: Early Permian (275 Ma)
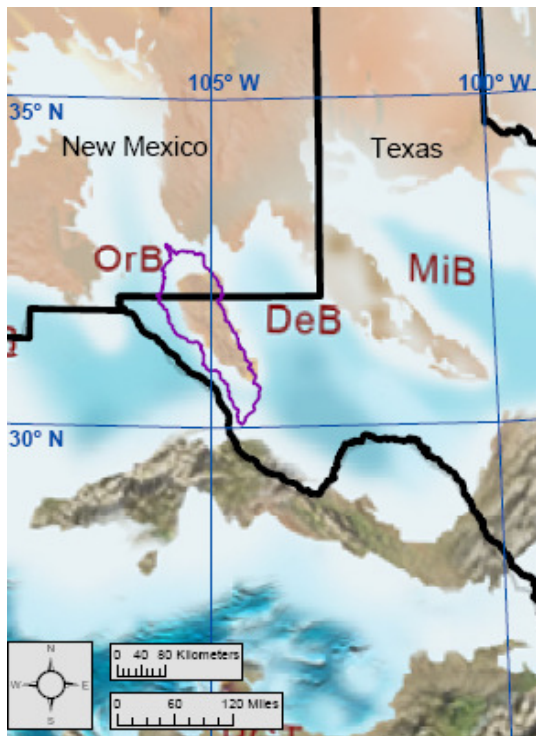
c: Middle Permian (270 Ma)
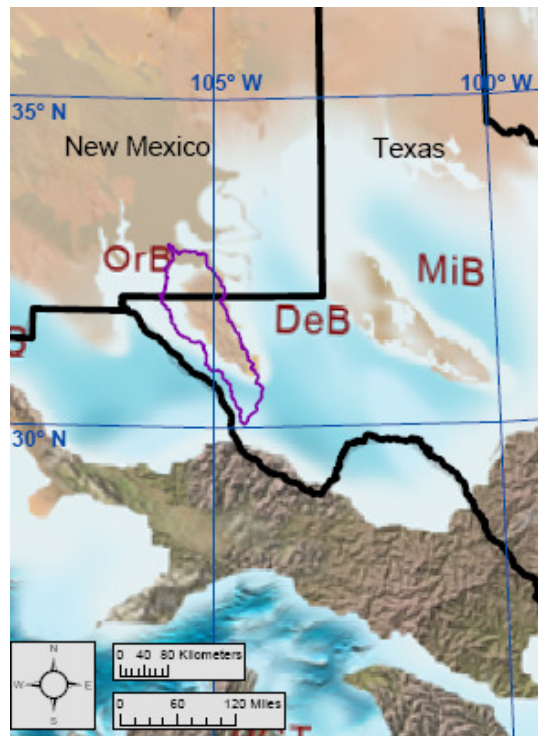
d: Late Permian (260 Ma)

Figure 2.10: Early-Permian-to-Late-Permian paleogeography of the Salt Basin region, from Blakey (2009a).
OrB = Orogrande Basin, DeB = Delaware Basin, MiB = Midland Basin.
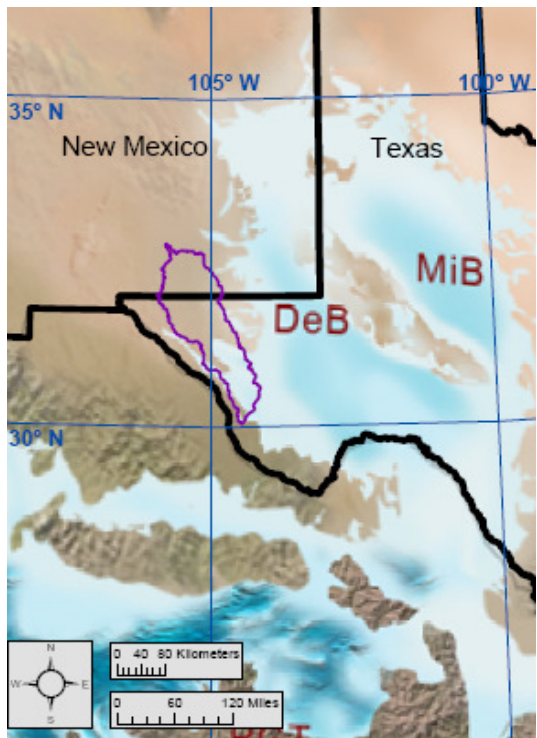
a: Late Permian (255 Ma)

b: Early Triassic (240 Ma)
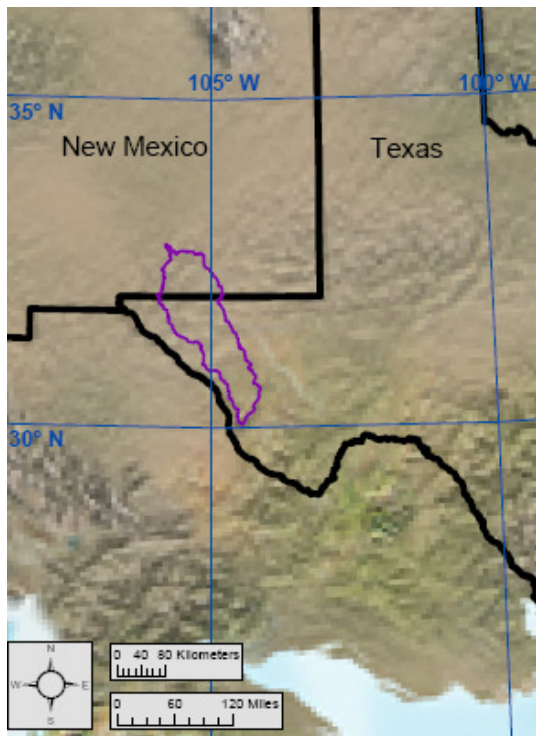
c: Middle Triassic (230 Ma)

d: Late Triassic (210 Ma)

Figure 2.11: Late-Permian-to-Late-Triassic paleogeography of the Salt Basin region, from Blakey (2009a) and Blakey (2009b).
DeB = Delaware Basin, MiB = Midland Basin.

a: Early Jurassic (195 Ma)
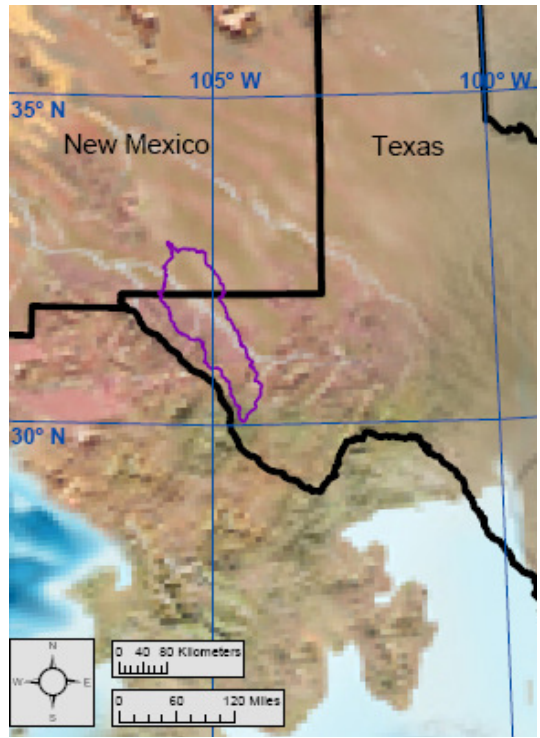
b: Early Jurassic (180 Ma)
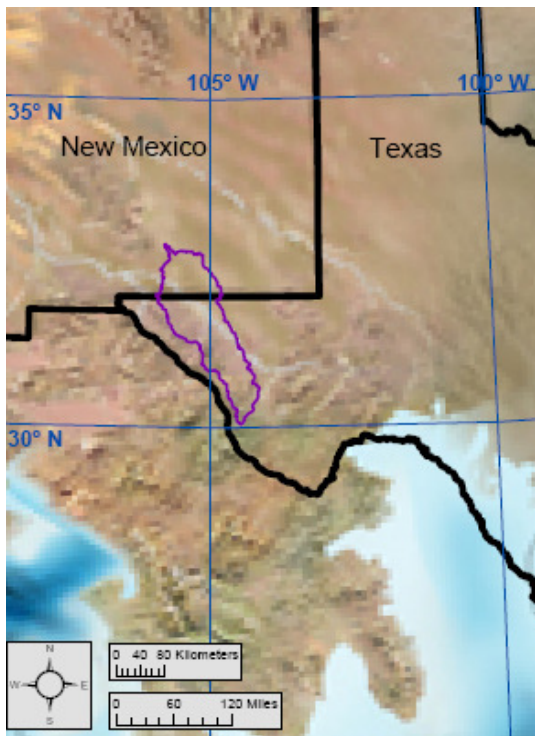
c: Middle Jurassic (170 Ma)

d: Late Jurassic (150 Ma)

Figure 2.12: Early-Jurassic-to-Late-Jurassic paleogeography of the Salt Basin region, from Blakey (2009b).
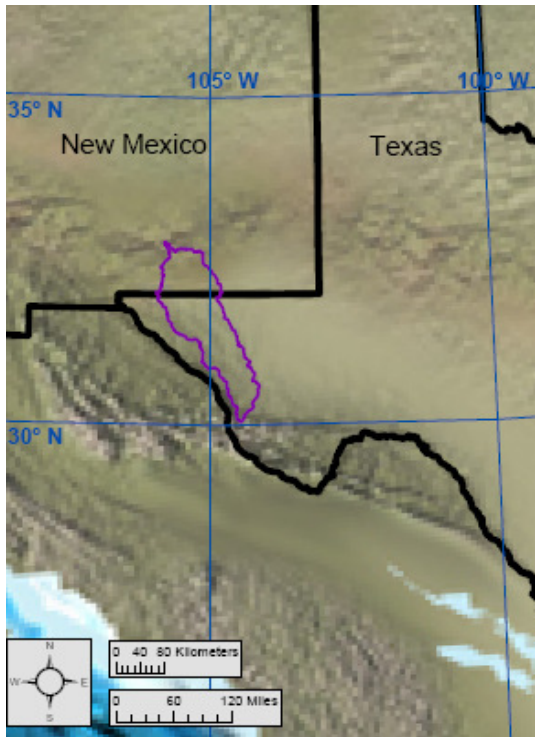
a: Early Cretaceous (140 Ma)
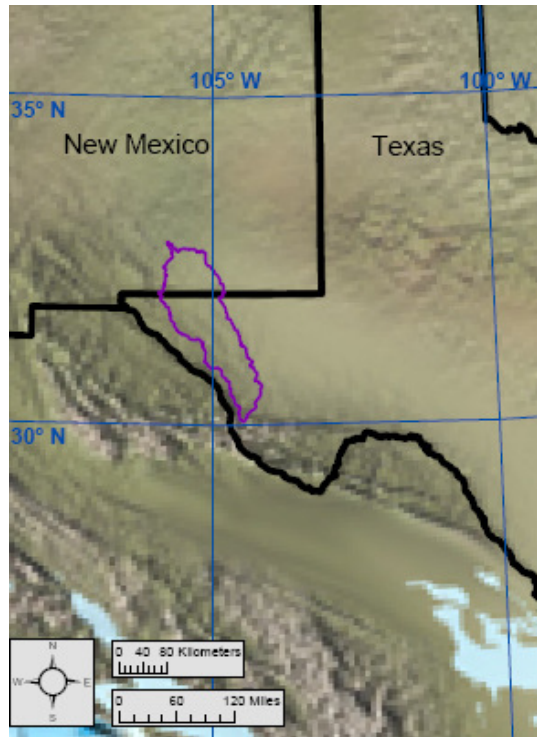
b: Early Cretaceous (130 Ma)

c: Early Cretaceous (115 Ma)

d: Late Cretaceous (100 Ma)

Figure 2.13: Early-Cretaceous-to-Late-Cretaceous paleogeography of the Salt Basin region, from Blakey (2009b).

a: Late Cretaceous (85 Ma)

b: Late Cretaceous (75 Ma)

c: Cretaceous-Paleogene (65 Ma)
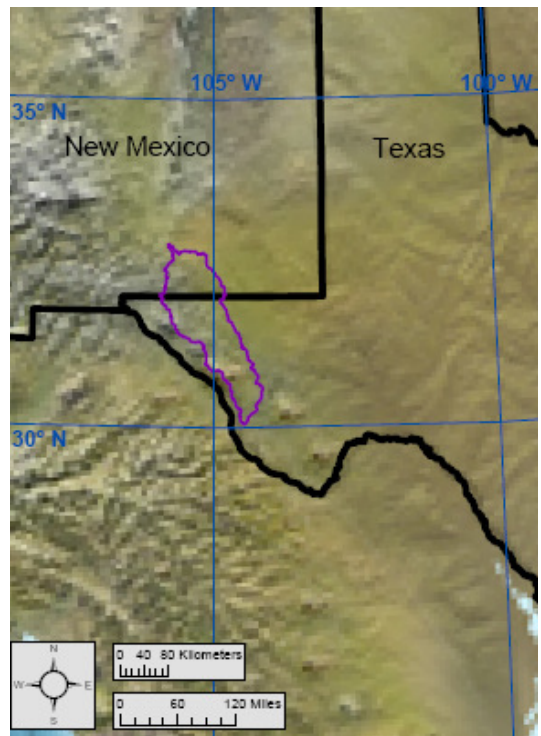
d: Paleogene Paleocene (60 Ma)

Figure 2.14: Late-Cretaceous-to-Paleogene-Paleocene paleogeography of the Salt Basin region, from Blakey (2009b).

a: Paleogene Eocene (50 Ma)
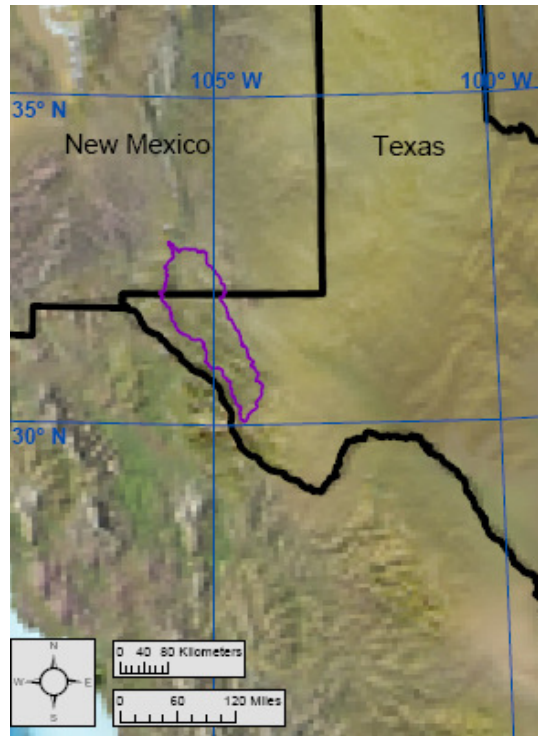
b: Paleogene Eocene (40 Ma)
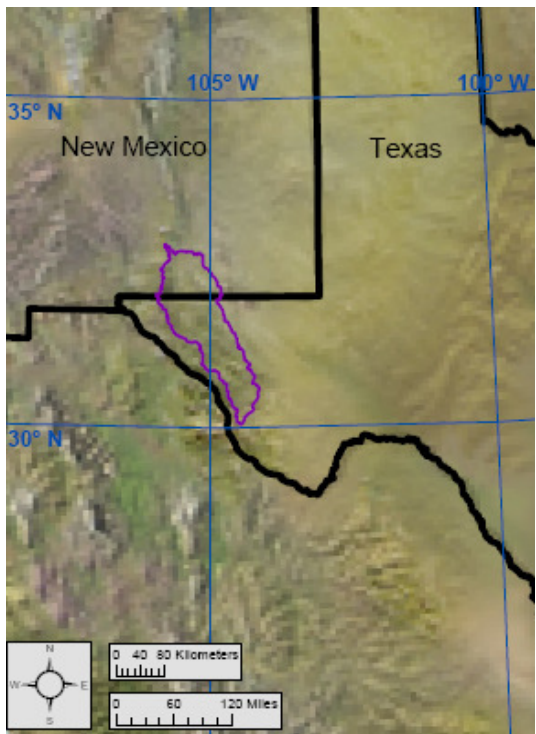
c: Paleogene Oligocene (25 Ma)

d: Neogene Miocene (15 Ma)

Figure 2.15: Paleogene-Eocene-to-Neogene-Miocene paleogeography of the Salt Basin region, from Blakey (2009b).

a: Neogene Miocene (8 Ma)

b: Neogene Pliocene (3 Ma)

c: Quaternary Glacial (0.126 Ma)

d: Present

Figure 2.16: Neogene-Miocene-to-Present paleogeography of the Salt Basin region, from Blakey (2009b).

a: Wolfcampian facies

b: Early Leonardian facies

Legend

Sandstone, fine- to coarse-grained, including some conglomerate		Limestone, thick- to thin-bedded, calcitic or dolomitic	
Anhydrite, generally interbedded with dominant facies		Shale, dark gray to black, and thin-bedded black limestone	
Red beds, in part shaly, in part sandy			
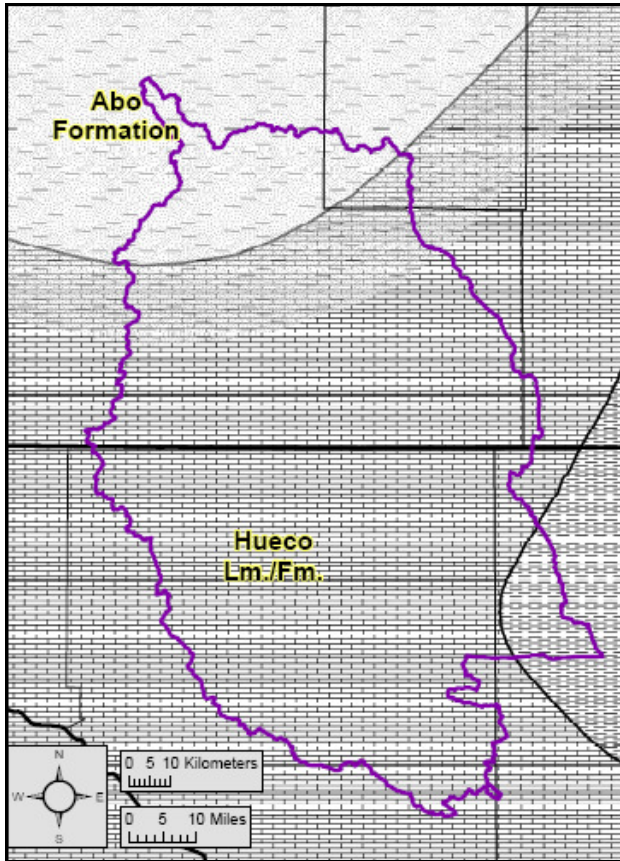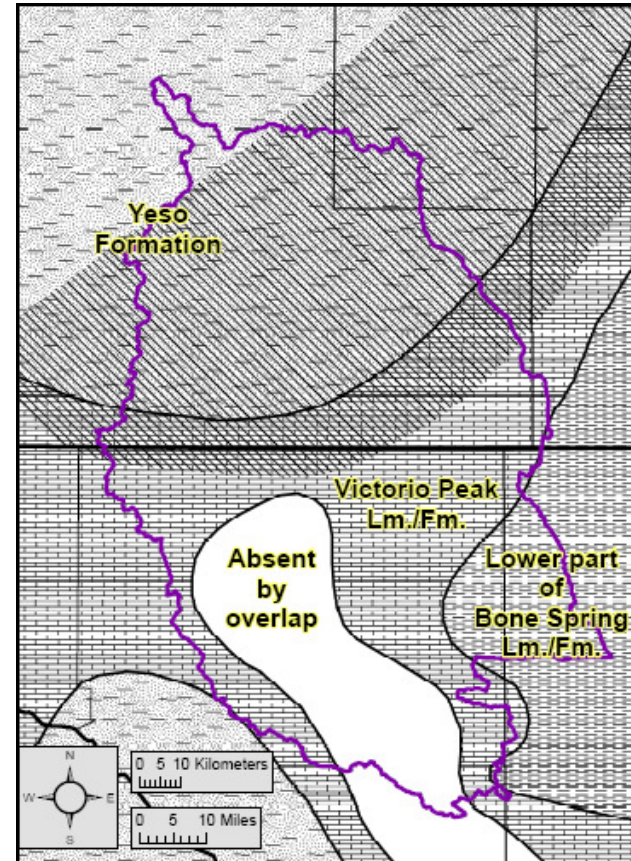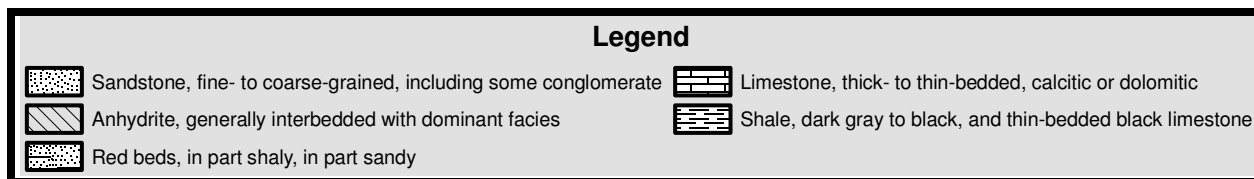
Figure 2.17: Wolfcampian-to-Early-Leonardian facies, from King (1942) and King (1948).

a: Late Leonardian facies

b: Early Guadalupian facies

Legend

Sandstone, fine- to coarse-grained, including some conglomerate	Limestone, thick- to thin-bedded, calcitic or dolomitic
Anhydrite, generally interbedded with dominant facies	Shale, dark gray to black, and thin-bedded black limestone
Red beds, in part shaly, in part sandy	
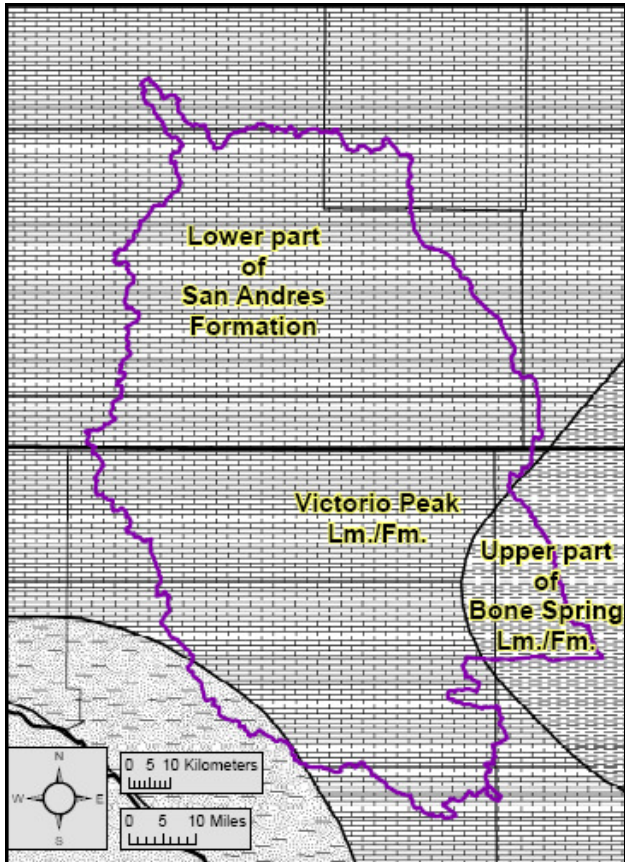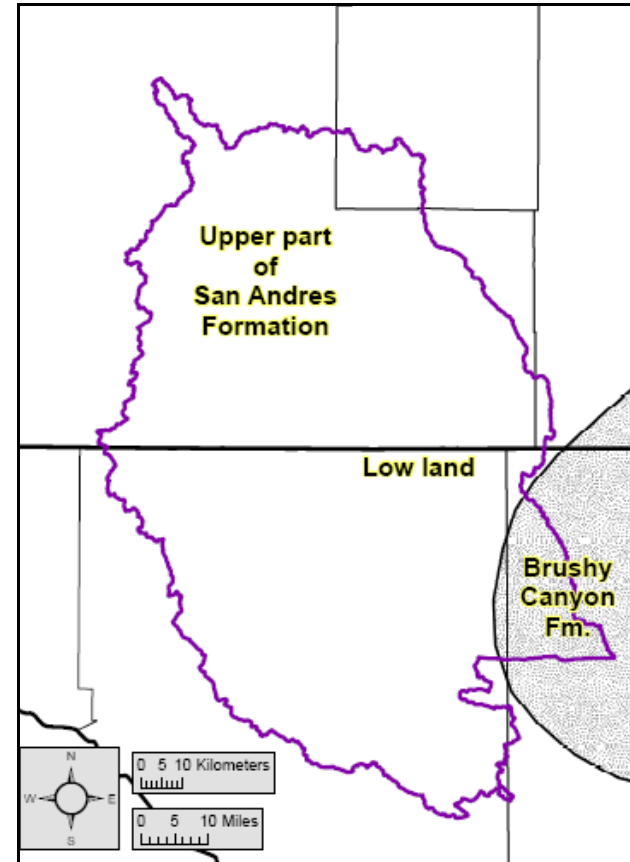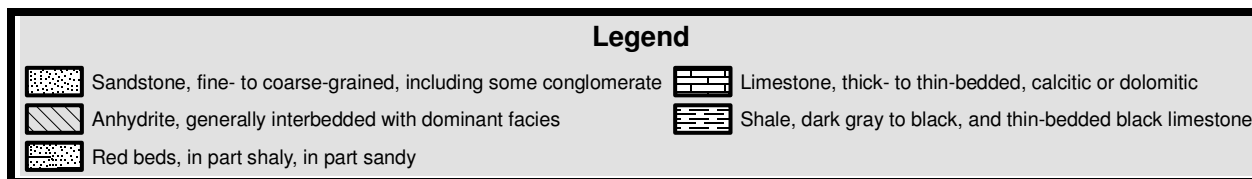
Figure 2.18: Late-Leonardian-to-Early-Guadalupian facies, from King (1942) and King (1948).

a: Middle Guadalupian facies

b: Late Guadalupian facies

Legend

Sandstone, fine- to coarse-grained, including some conglomerate		Limestone, thick- to thin-bedded, calcitic or dolomitic	
Anhydrite, generally interbedded with dominant facies		Shale, dark gray to black, and thin-bedded black limestone	
Red beds, in part shaly, in part sandy			
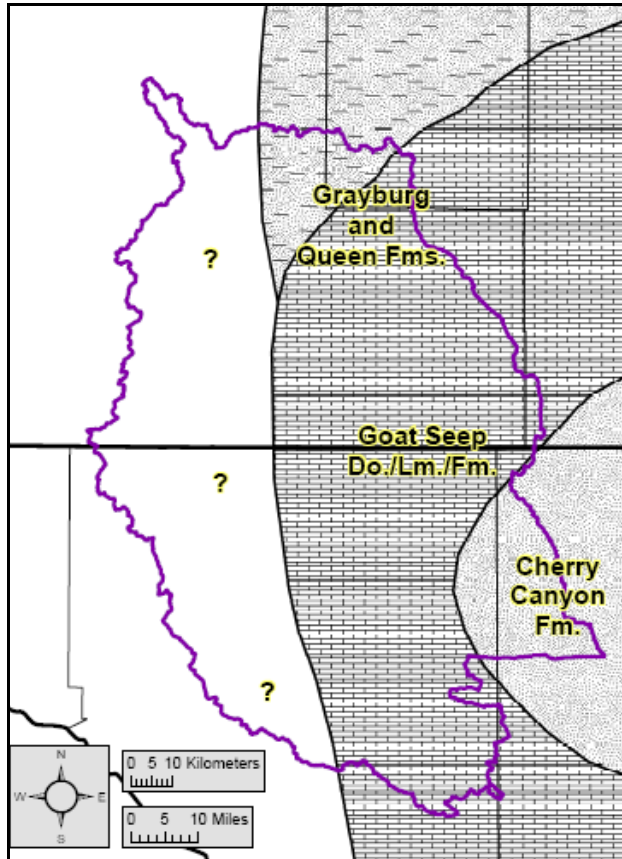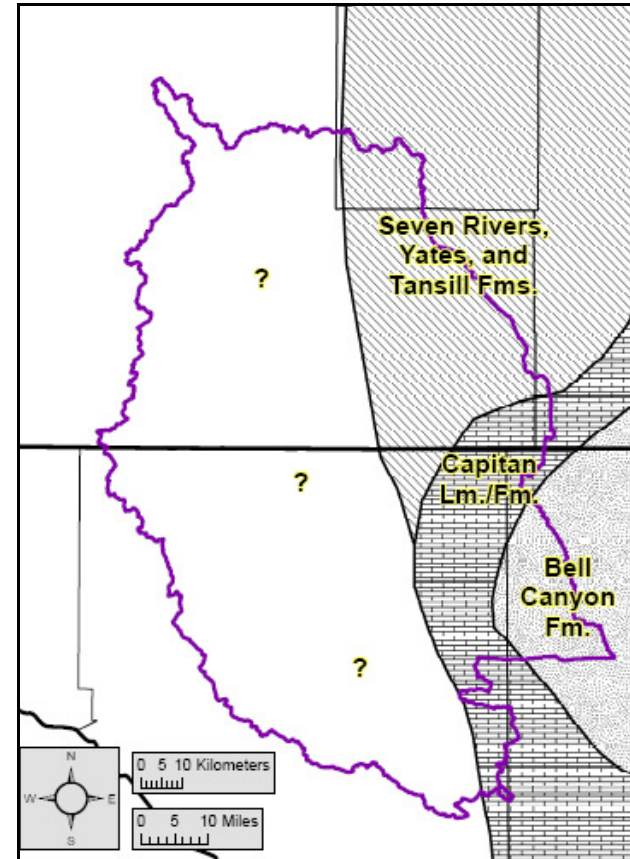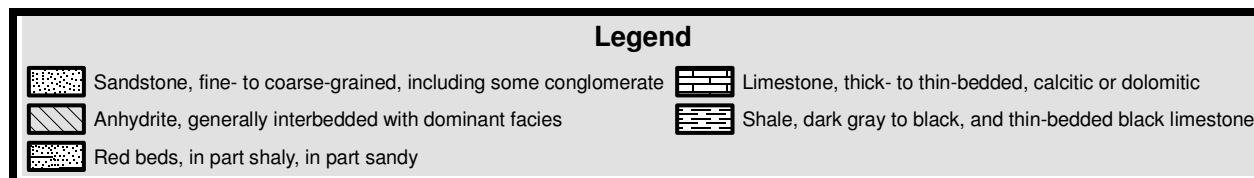
Figure 2.19: Middle-Guadalupian-to-Late-Guadalupian facies, from King (1942) and King (1948).
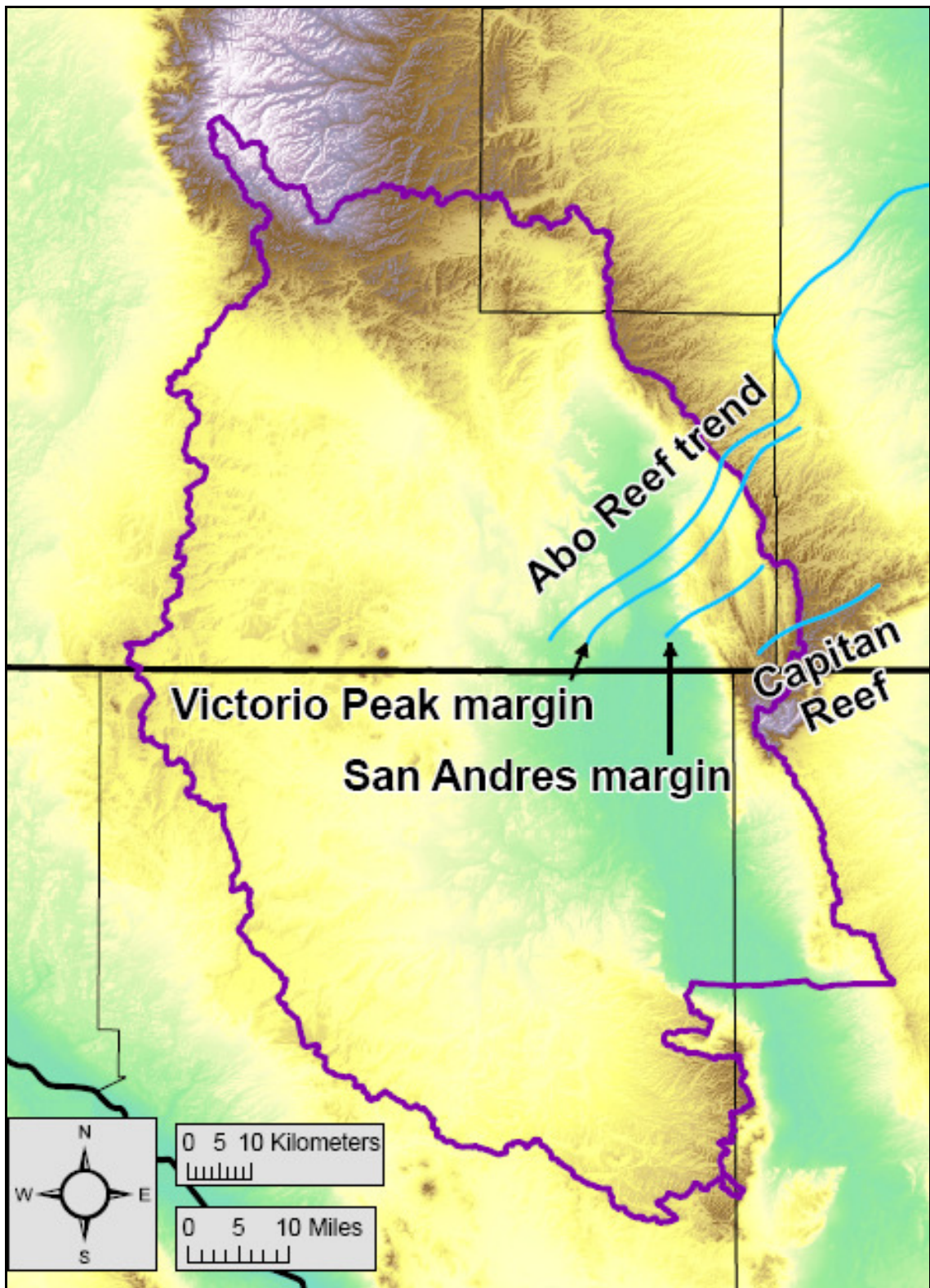
Figure 2.20: Permian shelf-margin trends, from Black (1975).
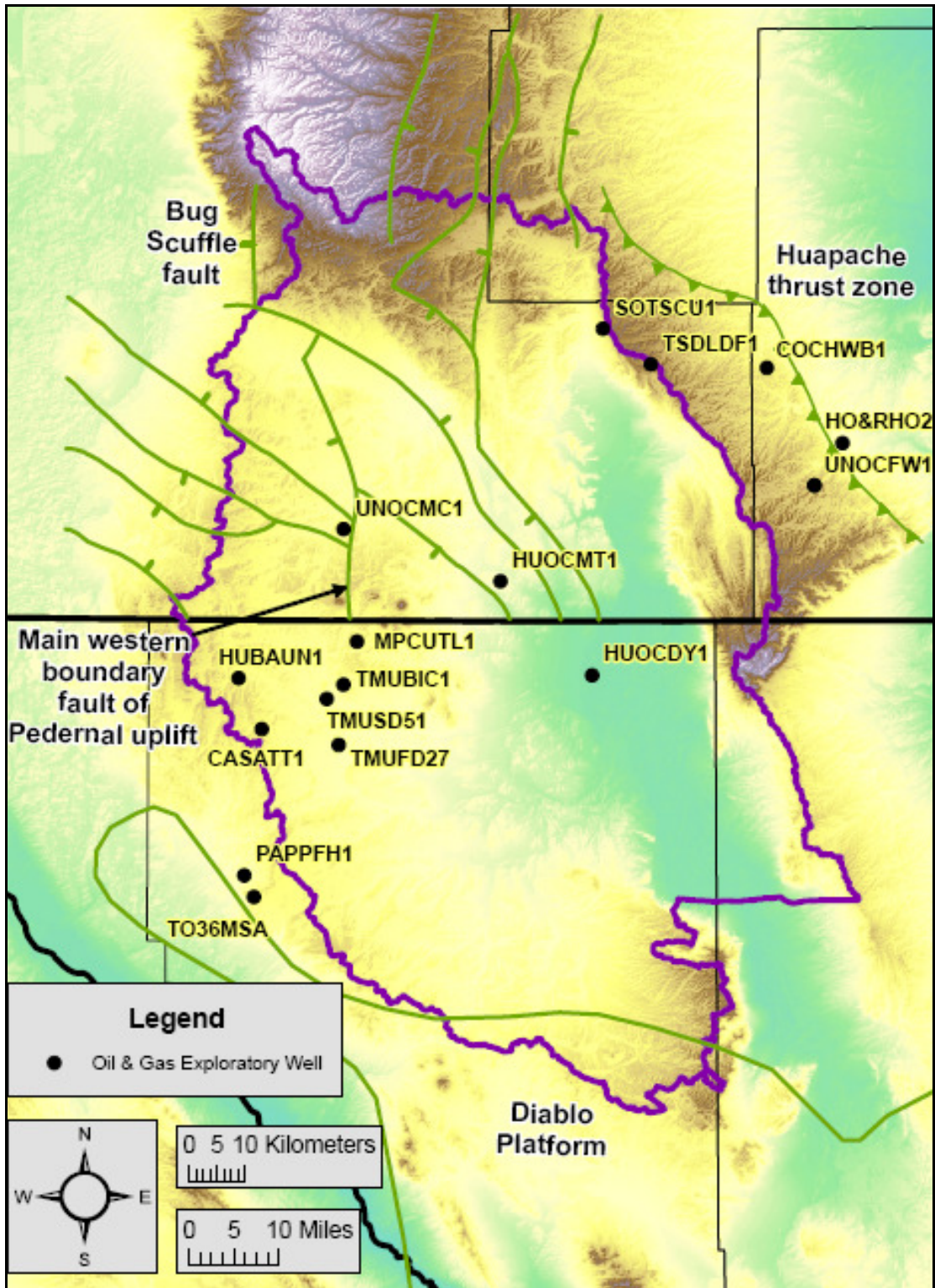
Figure 2.21: Pennsylvanian-to-Early-Permian structural features of the northern Salt Basin watershed.

Bar on downthrown side of normal or high angle faults, triangles on upthrown side of thrust zone. Location of structures in New Mexico taken from Broadhead (2002). Location of Diablo Platform taken from Kottlowski (1969).
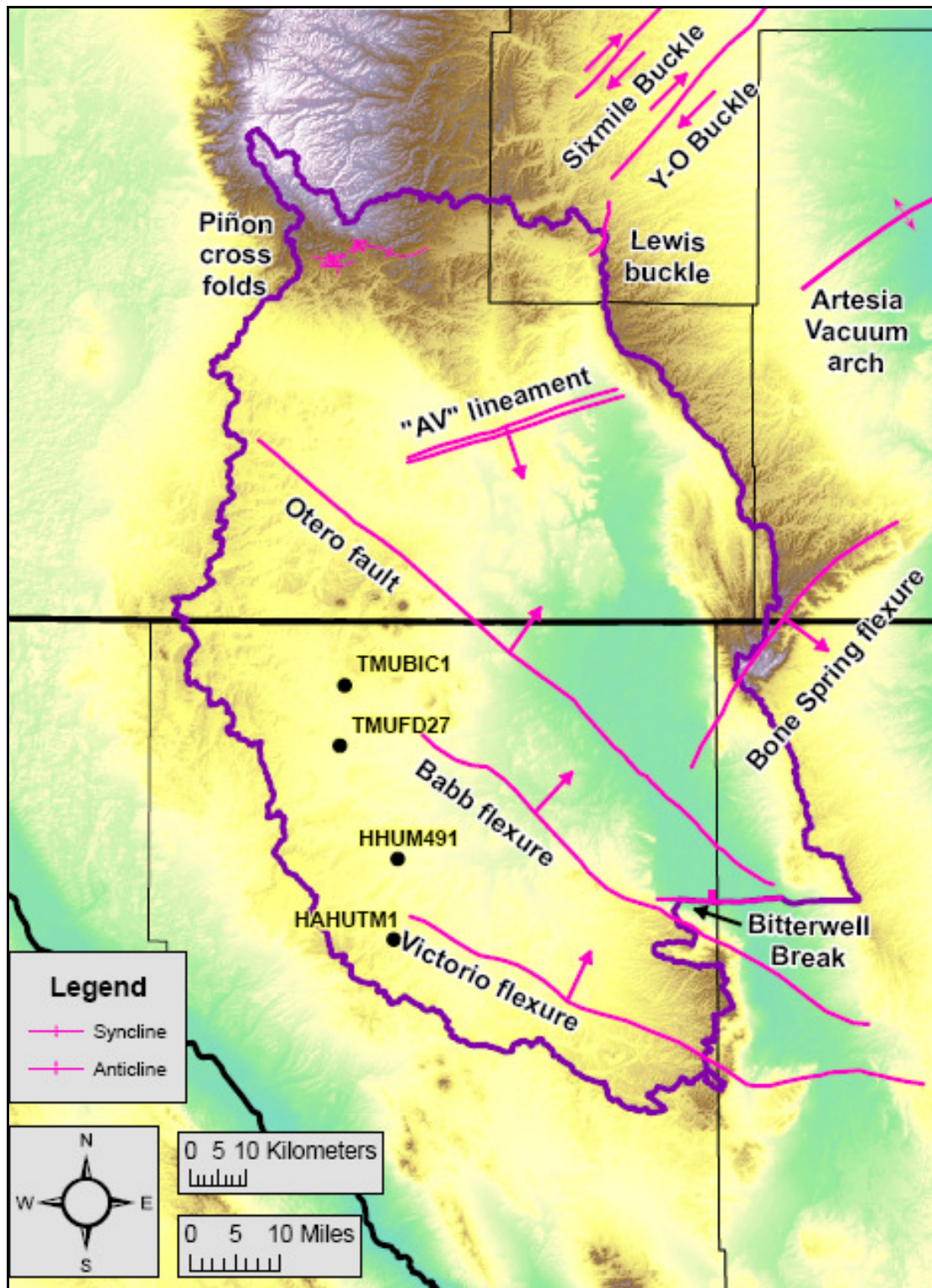
Figure 2.22: Mid-to-Late-Permian structural features of the northern Salt Basin watershed.
Arrows indicate sense of displacement. Bar on downthrown side of Bitterwell Break.
Location of structures taken from Black (1976), Goetz (1985), and Kelley (1971).
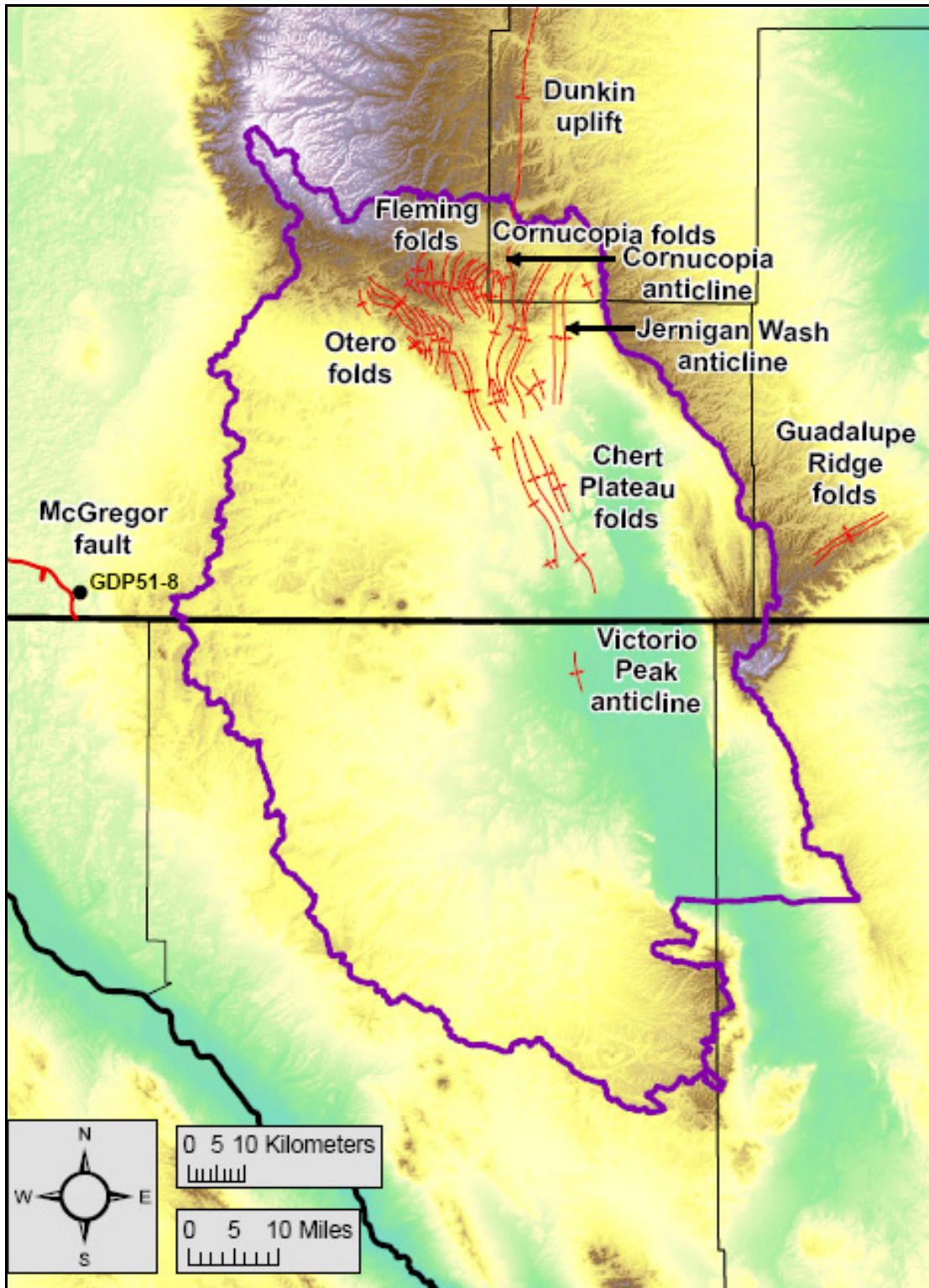
Figure 2.23: Late-Cretaceous (Laramide) structural features of the northern Salt Basin watershed.
Syncline and anticline symbols are the same as those used on Figure 2.22. Bar on downthrown side of McGregor fault. Location of structures taken from Black (1976), Goetz (1985), Kelley (1971), and Seager et al. (1987).
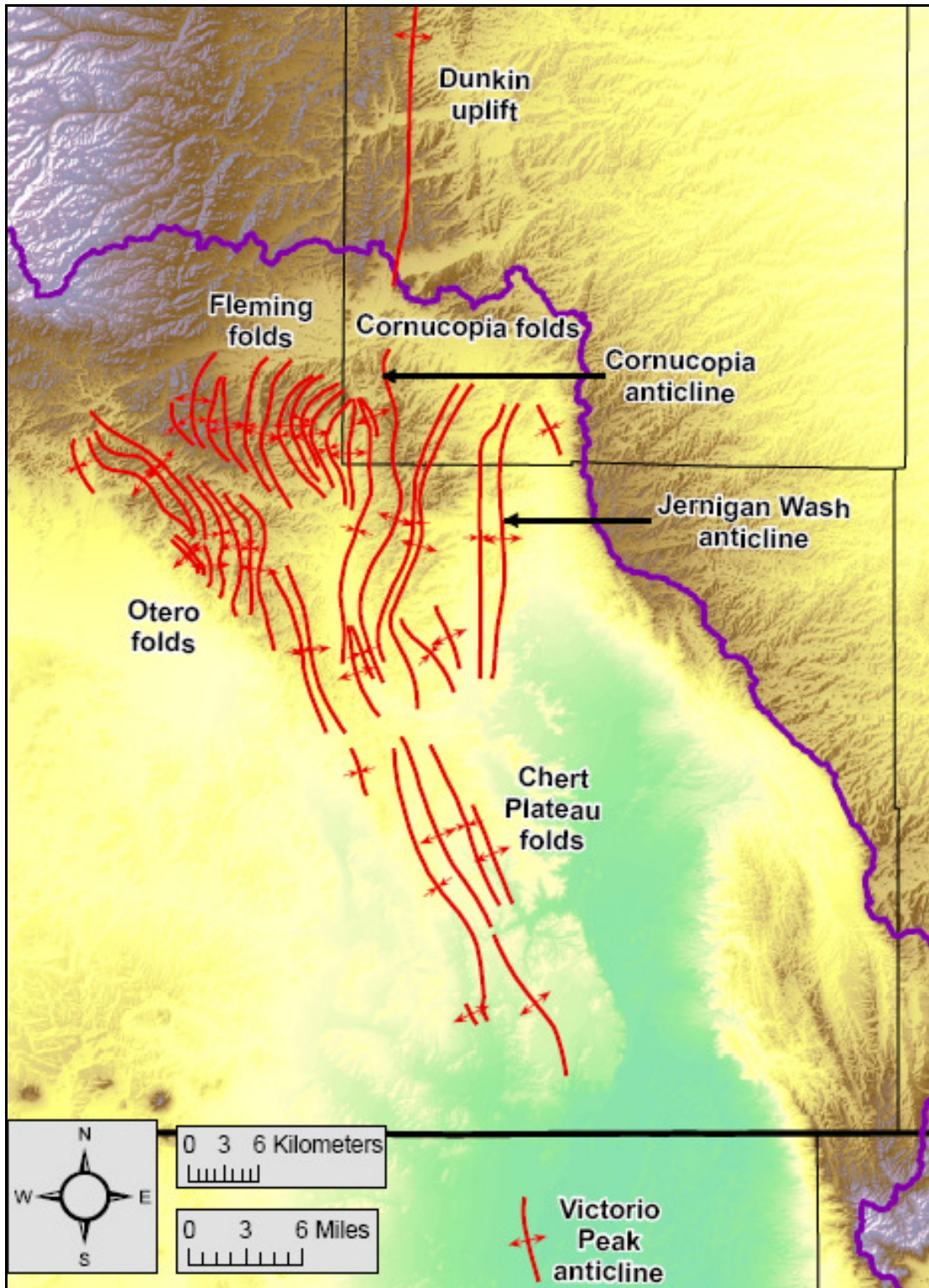
Figure 2.24: Late-Cretaceous (Laramide) structural features of the north and northeast portions of Otero Mesa.
Syncline and anticline symbols are the same as those used on Figure 2.22. Location of structures taken from Black (1976), Goetz (1985), and Kelley (1971).
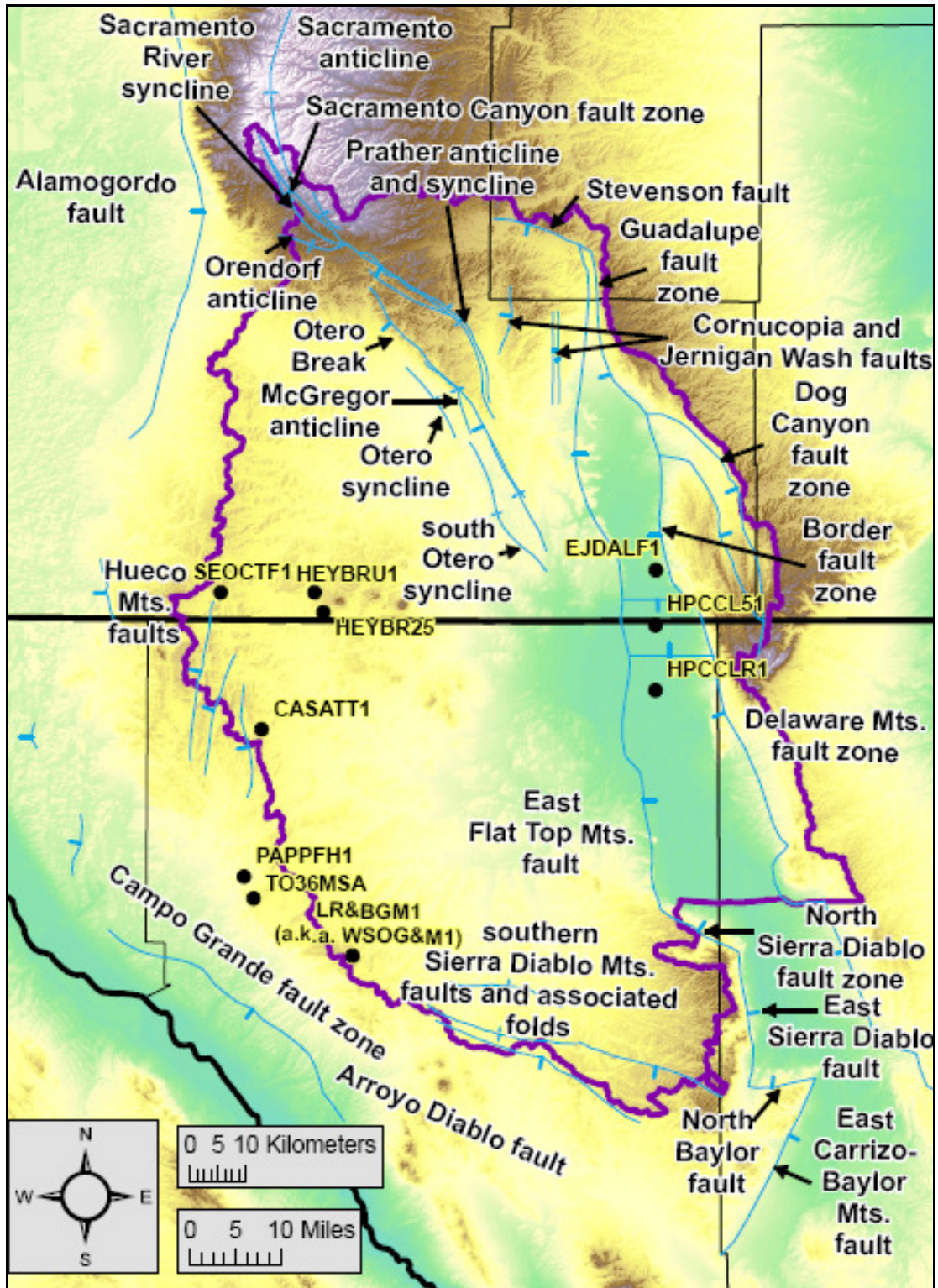
Figure 2.25: Cenozoic structural features of the northern Salt Basin watershed. Syncline and anticline symbols are the same as those used on Figure 2.22. Bar on downthrown side of normal or high angle faults. Location of structures taken from Black (1976), Broadhead (2002), Cather and Harrison (2002), Collins and Raney (1991), Goetz (1985), Pray (1961), Schruben et al. (1994), and Seager et al. (1987).

CHAPTER 3: HYDROGEOLOGIC FRAMEWORK

3.1: Previous Hydrogeologic Studies

The earliest studies of the groundwater system of the Salt Basin region were conducted by Scalapino (1950) and Bjorklund (1957). Scalapino (1950) reported on the direction of movement, quantity, and quality of groundwater in the Dell City area. Scalapino (1950) noted that drilling in the Dell City area indicated that the region is underlain by a limestone with large, solution-enhanced openings along joints and bedding planes, but the distribution of these openings is erratic. Scalapino (1950) also noted that the alluvial material within the Salt Basin graben consisted of interbedded clay and fine-grained sand, and wells completed in this material had small yields. Scalapino (1950) was the first researcher to hypothesize that infiltration of Sacramento River flows was the primary source of recharge to the Dell City region. Scalapino (1950) also identified the Salt Flats region as the primary area of natural discharge from the groundwater system, and reported on the flow of Crow Spring.

Bjorklund (1957) conducted a similar study in the Crow Flats region of New Mexico. Bjorklund (1957) commented on the levelness of the piezometric surface in the southern part of the Crow Flats area, and attributed this to the high permeability of the water-bearing materials, especially the limestone with its many interconnected solution channels. Bjorklund (1957) also identified a zone of perched groundwater in the far northern portion of the Crow Flats region. Bjorklund (1957) hypothesized that recharge is

primarily through infiltration in the beds of ephemeral streams during flash floods. Bjorklund (1957) estimated recharge to the groundwater system as being less than 120,000,000 m^3 (100,000 acre-feet) per year based on the relationship between the quantity of groundwater pumped for irrigation and water level fluctuations between 1948 and 1955. Bjorklund (1957) also noted that Crow Spring had stopped flowing due to groundwater level declines associated with pumping for irrigation.

Gates et al. (1980) conducted a geophysical survey of the Salt Flats region and used this data to estimate the thickness and lithology of the basin-fill within the Salt Basin graben. Based on this data, Gates el al. (1980) interpreted the basin-fill lithology as predominantly low permeability lacustrine clay and sand, saturated with saline water, with a maximum thickness ranging from 244 meters (800 feet) in the north to 610 meters (2,000 feet) in the south. Gates et al. (1980) also identified the lateral extent and thickness of the Goat Seep and Capitan Limestones of the Capitan Reef Complex aquifer in the Salt Flats region, and provided specific capacity data for the Capitan Limestone in the Beacon Hill irrigation area. Gates et al. (1980) noted that recharge to the Capitan and Goat Seep Limestones is concentrated primarily along outcrop areas in the Guadalupe Mountains, Patterson Hills, and Delaware Mountains, and flows generally westward through the Beacon Hill area towards its final discharge region at the Salt Flats.

Nielson and Sharp (1985) discussed the geological controls on the hydrogeology of the Texas portion of the Salt Basin graben. They divided the Permian strata within the Salt Basin graben into three aquifer systems: basin, shelf-margin, and shelf, and provided estimates of transmissivity for each system. Nielson and Sharp (1985) also recognized the

existence of groundwater divides within the Salt Basin graben, and their correspondence to structural features (Bitterwell Break and Victorio flexure).

Kreitler et al. (1990) studied the hydrogeology of the Diablo Plateau. They identified two aquifers in the Diablo Plateau region: a deep regional aquifer, and a shallow, locally perched, confined to semi-confined aquifer in the southwestern portion of the Plateau. Kreitler et al. (1990) produced a potentiometric surface map for the Diablo Plateau and Salt Basin graben regions of Texas, and concluded that groundwater flow on the Diablo Plateau is primarily from southwest to northeast, and the underlying rocks are locally highly transmissive. Based on the presence of tritium in nearly all wells throughout the Plateau, Kreitler et al. (1990) concluded that the entire Plateau area receives recharge. Kreitler et al. (1990) also analyzed soil-water chloride concentrations and interpreted this to indicate that most recharge is concentrated within arroyos during flash flood events.

Ashworth (1995) investigated the groundwater resources in the Dell Valley region. Based on a comparison of irrigation pumpage and water level fluctuations, Ashworth (1995) estimated total annual recharge to the groundwater system, including both lateral inflow and irrigation return flow, to range from 110,000,000 to 120,000,000 m^3 (90,000 to 100,000 acre-feet). Mayer (1995) analyzed the affect that regional fracture systems have on regional groundwater flow within the Salt Basin. Mayer (1995) constructed a two-dimensional, finite element groundwater flow model, and performed several steady-state simulations to investigate the role of fractures in controlling regional transmissivity, and thus regional groundwater flow. Mayer (1995) concluded that the

Otero Break region corresponds to a highly transmissive zone with a transmissivity ranging from 1 to 3 orders of magnitude higher than surrounding regions.

The western and northern boundaries of Mayer's model correspond to the surface water divide defining the Salt Basin watershed. However, Mayer (1995) defined these boundaries as no-flow boundaries, thus neglecting the potential for interbasin groundwater flow from the Peñasco Basin to the north. The eastern boundary of Mayer's model was defined as a no-flow boundary in the north, where westward flow from the Guadalupe Mountains and eastward flow from the Otero Mesa converge, and a constant head boundary in the south, which corresponds to the water table at the Salt Flats. The southern boundary corresponds to a symmetry boundary where regional flow is to the east, parallel to the boundary, and was defined as a no-flow boundary (Mayer, 1995).

Mayer (1995) used the method described by Maxey and Eakin (1949) to estimate the distribution and quantity of recharge above an elevation of approximately 1,675 meters (5,500 feet). The Maxey-Eakin method is an empirical technique based on a water balance analysis of the White River Valley in eastern Nevada (Maxey and Eakin, 1949). Below an elevation of 1,160 meters (3,800 feet) recharge from direct precipitation was assumed to be negligible (Mayer, 1995). For the intermediate regions of the Otero Mesa/Diablo Plateau, a composite recharge rate of 0.018 cm/year (0.0071 inches/year) was calculated based on soil-water chloride data from the Diablo Plateau as cited by Mayer (1995). The above techniques resulted in a total distributed recharge value of 72,000,000 m^3/year (58,370 acre-feet/year).

During each model simulation, Mayer (1995) held recharge and discharge constant and tested three configurations of transmissivity: homogeneous and isotropic,

heterogeneous and isotropic, and heterogeneous and anisotropic. For each configuration, transmissivity was estimated by trial-and-error in order to best match the observed potentiometric surface. Mayer (1995) found that the heterogeneous and isotropic case produced the best match to the observed potentiometric surface, and adding anisotropy did not significantly change the model output because of the coincidental alignment of the hydraulic gradient nearly parallel to the major axis of transmissivity. Mayer (1995) noted that the highest transmissivity zone, corresponding to the Otero Break region, had a transmissivity (860 m^2/day [9,300 ft^2/day]) more than one order of magnitude less than the highest transmissivity values that he cited from the literature for carbonate aquifers in Texas. Based on the modeling approach taken, Mayer (1995) concluded that an equally good match to the observed potentiometric surface could be achieved by either increasing transmissivity and recharge, or lowering transmissivity and recharge.

Angle (2001) described the hydrogeology of the Texas portion of the Salt Basin graben. Angle (2001) presented a basin-fill thickness map for the Salt Basin graben modified from Gates et al. (1980). Angle (2001) also compiled transmissivity values for the aquifers within the Salt Basin graben region. Mullican and Mace (2001) reported on the hydrogeology of the Diablo Plateau region. They noted that the two aquifers in the Diablo Plateau correspond to the geology, with the aquifer on the southwestern portion of the Plateau located in Cretaceous rocks, and the underlying aquifer located in Permian rocks that are exposed on the northern and northeastern portions of the Plateau.

John Shomaker & Associates, Inc. [JSAI] (2002) developed a three-dimensional, finite difference groundwater flow model of the Salt Basin using MODFLOW to help evaluate the potential for developing groundwater from deep wells within the New

Mexico portion of the Salt Basin. The model was calibrated to steady-state and historical-transient conditions, but was based on limited knowledge of the hydrogeologic framework and distribution of recharge (JSAI, 2010). The model domain was defined primarily by the Salt Basin watershed boundary, but also included a portion of the Peñasco Basin to the north (JSAI, 2002). The model consisted of 4 layers, each with a variable thickness (JSAI, 2002).

Recharge was applied along the perimeter of the model domain in the form of fully penetrating wells (JSAI, 2002). Recharge values were determined through model calibration and comparison to known estimates of recharge (JSAI, 2002). Discharge from the Salt Flats was simulated using the MODFLOW Evapotranspiration Package (EVT), with the discharge region delineated by predevelopment depth-to-water less than 15 meters (50 feet) (JSAI, 2002). The steady-state model was calibrated to 1) an estimated recharge of 67,771,000 m^3/year (54,943 acre-feet/year), and 2) predevelopment groundwater contours (JSAI, 2002). Steady-state model calibration involved adjusting hydraulic conductivity values, slightly adjusting the specified recharge up or down for a particular region, and changing the area and rate of evaporation (JSAI, 2002). Steady-state calibrated inflow from the Peñasco Basin was estimated to be 9,811,000 m^3/year (7,954 acre-feet/year) (JSAI, 2002).

The distribution of hydraulic conductivity in each layer was derived from expected values representative of the rock type of each geologic unit, and model calibration (JSAI, 2002). JSAI (2002) estimated the hydraulic conductivity of the Permian units in layers 1 and 2 in the Otero Break, Crow Flats, and Dell City regions to be 30 meters/day (100 feet/day), while the surrounding units had conductivities ranging

141

from 0.02 to 3 meters/day (0.05 to 10 feet/day). In layers 3 and 4 hydraulic conductivities ranged from 0.02 to 1.5 meters/day (0.05 to 5 feet/day), and 0.02 to 0.3 meters/day (0.05 to 1 feet/day), respectively (JSAI, 2002).

George et al. (2005) summarized the current knowledge concerning the hydrogeology of Hudspeth County, Texas. They compiled information concerning geology and hydrostratigraphy, water levels and groundwater flow, recharge, hydraulic properties, discharge, and water quality for the groundwater system in the Dell Valley region, the Diablo Plateau, and the Capitan Reef Complex. In their section on the Diablo Plateau, George et al. (2005) noted that the Cretaceous and Permian aquifers are vertically connected to each other. Huff and Chace (2006) summarized the current knowledge of the hydrogeology of the New Mexico portion of the Salt Basin watershed, and identified future study needs. Huff and Chace (2006) also presented groundwater level changes measured nearly continuously in four wells north of Dell City, Texas over an approximately three and a half year time period from 2003 to the middle of 2006. The data demonstrated that groundwater level declines associated with irrigation pumping at Dell City, Texas can propagate many miles away.

Hutchison (2008) developed three two-dimensional, finite difference groundwater flow models of the Salt Basin using MODFLOW-2000. The purpose of Hutchison's study was to help El Paso Water Utilities assess the groundwater availability in the Dell City and Diablo Farms regions for future City of El Paso water-supply development projects. The three models included a structural geology model, a geochemistry model, and a hybrid model of the two (Hutchison, 2008). The domain of each model was defined by the Salt Basin watershed boundary, except in the far northwestern portion, and along

the western portion (Hutchison, 2008). The far northwestern portion of the Salt Basin watershed was included in initial model simulations, but was later removed because its protruding geometry created numerical problems (Hutchison, 2008). The western edge of each model domain was moved to the east of the watershed boundary in order to correspond more closely to a groundwater divide (Hutchison, 2008).

Hutchison (2008) assumed an aquifer thickness of 300 meters (1,000 feet). The model domain boundary was defined as a no-flow boundary, except in the northwestern, western, and southeastern portions of the domain. The general head boundary package was used to simulate flow into the model domain in the northwestern portion of the domain in the Sacramento Mountains (Hutchison, 2008). Outflow along the western portion of the model domain was simulated using the drain package (Hutchison, 2008). The possibility of outflow along the southeastern portion of the model domain, which corresponds to the groundwater divide associated with the Bitterwell Break, was investigated using the constant head boundary package (Hutchison, 2008). Discharge from the Salt Flats was simulated using the evapotranspiration package (Hutchison, 2008).

The three groundwater flow models were calibrated to steady-state and historical-transient simulations (Hutchison, 2008). Recharge was estimated using a modified Maxey-Eakin approach in which higher elevation areas have a higher recharge rate than lower elevation areas, and higher precipitation years have a higher recharge rate than lower precipitation years (Hutchison, 2008). Average distributed recharge from steady-state calibration of all three models was estimated to be 78,000,000 m^3/year (63,000 acre-feet/year) (Hutchison, 2008). Total steady-state inflow to the model domain, including

inflow from the Sacramento Mountains, ranged from 97,000,000 to 128,000,000 m^3/year (79,000 to 104,000 acre-feet/year) (Hutchison, 2008).

The study described in this thesis was part of a much larger multi-disciplinary study organized by the New Mexico Interstate Stream Commission (NMISC) to obtain a better understanding of Salt Basin groundwater system. Daniel B. Stephens & Associates, Inc. was tasked with estimating groundwater evaporation from playas based on core sampling and developing a watershed model to estimate recharge. John Shomaker & Associates, Inc. was assigned the task of developing a conceptual model and updating the groundwater flow model they developed in 2002. The U.S. Geologic Survey (USGS) was charged with estimating stormwater runoff and potential recharge for major drainages. INTERA was tasked with evaluating groundwater discharge from agricultural pumping and playas using satellite image analysis.

Daniel B. Stephens & Associates, Inc. [DBS&A] (2010a) developed a basin-scale water balance model that evaluated precipitation, evapotranspiration, and resultant percolation through the soil column to estimate the amount and distribution of recharge within the Salt Basin. They conceptualized recharge within the Salt Basin watershed to be the result of four processes: mountain block recharge, mountain front recharge, local recharge, and diffuse recharge (DBS&A, 2010a). Mountain block recharge is concentrated primarily in higher elevation regions where precipitation is greater, the soils are thinner, and the bedrock is exposed and permeable (DBS&A, 2010a). Mountain front recharge is associated with the transition area between mountain block and valley floor, where surface water can flow into thick alluvium and infiltrate into the groundwater system (DBS&A, 2010a). Local recharge is possible along unvegetated sandy drainages

in the interior of the basin or where water may temporarily pond after intense rainfall events (DBS&A, 2010a). The broad lowland areas between drainages can be the site of diffuse recharge when soil water is not evapotranspired and is able to reach the water table (DBS&A, 2010a). They determined water balance components for three years with below-average, average, and above-average precipitation to provide minimum, average, and maximum annual recharge, respectively (DBS&A, 2010a). Recharge originating in the Salt Basin watershed was estimated to range from 46,000,000 to 100,000,000 m^3/year (37,000 to 82,000 acre-feet/year), with an average of 78,000,000 m^3/year (63,000 acre-feet/year) (DBS&A, 2010a).

DBS&A (2010b) also estimated historical playa evaporation rates within the Salt Basin, and these rates were used to infer groundwater recharge rates. They collected core from the Salt Basin playas and used luminescence geochronology to date the evaporative sediments (DBS&A, 2010b). Based on the ages of the cored sediments, the predevelopment annual discharge from the Salt Basin playas was estimated to range from 26,200,000 to 40,300,000 m^3/year (21,250 to 32,700 acre-feet), with an average of 34,900,000 m^3/year (28,300 acre-feet) (DBS&A, 2010b).

JSAI (2010) revised the hydrogeologic framework, and updated the groundwater flow model they developed in 2002. They also developed a conceptual recharge model. Groundwater recharge was conceptualized to be due to direct infiltration of precipitation in the highlands (areal recharge) and infiltration of stormwater runoff into drainage channels and alluvial fans (JSAI, 2010). The distribution of areal recharge was based on the water balance model developed by DBS&A, as well as the delineation of major sub-basins and watershed areas (JSAI, 2010). The amount of areal recharge was based on the

difference between potential recharge and stormwater runoff (JSAI, 2010). Potential recharge was estimated using an empirical relationship, in which potential recharge is some fraction of average annual precipitation, with the fraction increasing with increasing elevation (JSAI, 2010). The amount of stormwater runoff for the Sacramento River, Piñon Creek, Cornucopia Draw, and Big Dog Canyon sub-basins was obtained from the study conducted by the USGS, while the amount of runoff generated in other sub-basins was calculated using the average magnitude and annual frequency of runoff-generating precipitation events based on data obtained from 16 weather stations in and around the Salt Basin (JSAI, 2010). JSAI (2010) assumed that the amount of recharge associated with the infiltration of stormwater runoff was equal to 30 percent of stormwater runoff.

The conceptual recharge model developed by JSAI (2010) resulted in an estimated groundwater inflow from the Peñasco Basin of 7,154,000 m^3/year (5,800 acre-feet/year). Total recharge originating in the Salt Basin watershed was estimated to be 70,550,000 m^3/year (57,196 acre-feet/year), which compared favorably to the amount estimated from the calibrated steady-state groundwater flow model developed by JSAI (2002) (JSAI, 2010). However, the distribution of recharge was different between the two studies, with the conceptual recharge model producing larger recharge contributions from the lower Sacramento River and Otero Mesa, Coffelt Draw, and Shiloh Draw sub-basins, and the watershed areas that drain to Crow Flats, and smaller recharge contributions from the sub-basins that drain the Cornudas and Hueco Mountains, and the Diablo Plateau (JSAI, 2010).

JSAI (2010) used MODFLOW-96 to model groundwater flow in the Salt Basin of New Mexico and Texas. The model was calibrated to steady-state and historical-transient

146

conditions (JSAI, 2010). The model grid was refined from the JSAI (2002) model to consist of 160 rows and 160 columns with an even spacing of 805 meters (2,640 feet) (JSAI, 2010). The model grid consisted of 4 layers, with layer 1 having a variable thickness, layer 2 being 90 meters (300 feet) thick, layer 3 being 150 meters (500 feet) thick, and layer 4 being 900 meters (3,000 feet) thick (JSAI, 2010). The top of layer 1 was defined as the land surface, and the bottom of layer 1 was defined based on initial steady-state model-calibrated heads and saturated thickness based on transmissivity (JSAI, 2010).

The model domain was defined primarily by the Salt Basin watershed boundary, but unlike the JSAI (2002) model the Peñasco Basin was not included in the model domain (JSAI, 2010). Instead, groundwater inflow from the Peñasco Basin was modeled using a series of injection wells located along the northern boundary of the model domain (JSAI, 2010). The remainder of the model domain boundary was defined as a no-flow boundary. The Recharge Package (RCH) was used to apply areal recharge in the basin and mountain-front recharge along arroyos (JSAI, 2010). The Evapotranspiration Package (EVT) was used to model discharge from the Salt Flats, with the discharge region defined by pre-development depth-to-water of 9 meters (30 feet) or less (JSAI, 2010).

The distribution of hydraulic conductivity in each layer was derived from expected values representative of the rock type of each geologic unit (JSAI, 2010). JSAI (2010) assigned a horizontal hydraulic conductivity value of 30 meters/day (100 feet/day), and a vertical to horizontal hydraulic conductivity ratio of 1:100 to the basin fill units in layers 1 through 4. Permian units in layers 1 through 3 in the Otero Break,

Crow Flats, and Dell City regions were assigned higher horizontal hydraulic conductivity values ranging from 15 to 30 meters/day (50 to 100 feet/day), while the surrounding Permian units had conductivities ranging from 0.003 to 2 meters/day (0.01 to 5 feet/day) (JSAI, 2010). Permian rocks in layer 4 were assigned lower horizontal hydraulic conductivity values ranging from 0.003 to 0.03 meters/day (0.01 to 0.1 feet/day) (JSAI, 2010). Permian units with higher horizontal hydraulic conductivities were given a vertical to horizontal hydraulic conductivity ratio of 1:10, while a ratio of 1:100 was used for the lower conductivity Permian units (JSAI, 2010). Cambrian and Precambrian rocks in layers 1 through 4 were assigned horizontal hydraulic conductivity values of 0.02 meters/day (0.05 feet/day) and 0.006 meters/day (0.02 feet/day), respectively, and a vertical to horizontal hydraulic conductivity ratio of 1:500 (JSAI, 2010).

3.2: 3-D Hydrogeologic Framework Model

The development of a 3-D hydrogeologic framework model of the northern Salt Basin was accomplished by:

1)   reconstructing the tectonic forcings that impacted the region and the resulting structural features that formed,

2)   reconstructing the depositional environments and resultant facies distributions during basin formation,

3)   compiling data from oil-and-gas exploratory wells to constrain the subsurface distribution of the various geologic units, and

4)   compiling information on the location of surface exposures of the various geologic units.

Items 1 and 2 were discussed in Chapters 1 and 2. Items 3 and 4 are discussed below.

3.2.a: Subsurface Data

Subsurface data for New Mexico was obtained from the Oil Conservation Division online well files (http://www.emnrd.state.nm.us/OCD/OCDOnline.htm), Foster (1978), King and Harder (1985), Finger and Jacobson (1997), scout cards and well records from the New Mexico Subsurface Data Library at the New Mexico Bureau of Geology and Mineral Resources, and Broadhead (2007). Subsurface data for Texas was obtained from oil/gas well imaged records downloaded from the Railroad Commission of Texas online Public GIS Map Viewer (http://www.rrc.state.tx.us/data/online/index.php#), scout cards and well records obtained from the Bureau of Economic Geology's Austin Core Research Center on the campus of the University of Texas at Austin, King and Harder (1985), and Veldhuis and Keller (1980). Tables 3.1 and 3.2 list all of the subsurface control points for New Mexico and Texas, respectively, used in this study, including the well name, a unique 7 character well I.D. used in this study, the API number (if applicable), the UTM coordinates using the North American Datum 1983 (NAD 83) coordinate system, the well elevation in meters, the reference level for the well elevation and the source (if applicable), the well depth in meters, and the township/section, range/block, and section/survey of each point.

Tops of the various subsurface geologic units were compiled from these resources. In all cases, geologic unit tops were reported as depths, in feet, from some datum, which was not reported. To convert these depths to elevations, relative to mean sea level, the depths were subtracted from the reported well elevations. Often, two or more well elevations were reported from different reference levels, which included the ground surface, kelley bushing, tubing head, derrick floor, and well head. In all cases,

kelley bushing, tubing head, derrick floor, or well head were chosen over the ground surface as the datum if two or more well elevations were available. However, if only one well elevation was reported this elevation was used as the datum, even if it was the ground surface. If no well elevation was reported the elevation was derived from the 1-arc second U.S. Geological Survey (USGS) National Elevation Dataset (NED) discussed below. Tables 3.1 and 3.2 indicate the reference level of the well elevations used to determine the elevation of the top of each geologic unit.

Next, these geologic unit tops were inserted into ArcGIS for analysis. The model region was broken into 33 blocks, bounded by the various structural features described in Chapter 2.2. (Figure 3.1) The top of each geologic unit (in meters above mean sea level) was then contoured by hand separately for each block utilizing the subsurface well control and the known sense of displacement on the bounding structural features. The contours representing the top of the Precambrian basement were modeled after those presented in King and Harder (1985), but were modified slightly to account for additional subsurface data and structural displacement. Some of the subsurface well control for the top of the Precambrian basement was obtained from Foster (1978) and Broadhead (2007), who made projections based on isopach maps and selected geologic unit tops. Additional Precambrian basement control points were compiled from subsurface projections based on the depth-to-basement in neighboring wells. Table A-3.3 lists the subsurface well control for the top of the Precambrian basement.

The tops of the overlying geologic units were then built up from these Precambrian basement contours. Each successive geologic unit was contoured by adding the observed thickness of the unit in the surrounding oil-and-gas wells to the preceding

150

geologic unit contours. In addition to the Precambrian basement, contours were produced

for, from bottom to top, the interval from the Bliss Sandstone to the Fusselman Formation

(the Cambrian through the Silurian), the Devonian, the Mississippian through the

Pennsylvanian, Pow Wow Conglomerate, Hueco Limestone/Formation and Wolfcamp

Formation, Abo Formation, Yeso Formation, Bone Spring Limestone/Formation,

Victorio Peak Limestone/Formation, San Andres Formation, Delaware Mountain Group,

Goat Seep Dolomite/Limestone/Formation and Capitan Limestone/Formation, Artesia

Group, the Cretaceous, and Cenozoic alluvium. These groupings were chosen such that

geologic units with similar lithologies and facies, and thus probably similar hydraulic

properties, were combined. Therefore, the resultant 16 groups represent hydrogeologic

units. The oil-and-gas exploratory wells used as control for the top of each hydrogeologic

unit are listed in Tables A-3.3 through A-3.20.

3.2.b: Surface Data

The land surface geology was modeled based on the USGS digital geologic map

of Stoeser et al. (2005), which consists of a polygon shapefile of the surface geology.

(Figure 2.1) The surface exposures of the various geologic units were modeled by using

the USGS NED at a resolution of 1-arc second downloaded from the National Map

Seamless Server (http://seamless.usgs.gov/index.php). The NED was converted to a

point shapefile in ArcGIS, and this point shapefile was clipped to the various surface

geology polygons in order to represent the elevation, relative to mean sea level, of the

outcropping units.

There are some discrepancies between the surface geologic maps of New Mexico

and Texas, especially around the Cornudas Mountains region. The Yeso and San Andres

Formations are mapped in New Mexico, but are not mapped in Texas. The San Andres Formation as mapped in New Mexico is equivalent to the Victorio Peak Formation and Leonardian limestones and dolomites of the Wilke Ranch Formation as mapped in Texas (O'Neill and Nutt, 1998). According to Stoeser et al. (2005), the Wilke Ranch Formation, as mapped on the Diablo Plateau, is equivalent to the Victorio Peak and Bone Spring Limestones, and contains some beds equivalent to the Hueco Limestone. The Hueco Limestone as mapped in Texas is equivalent to the Hueco Limestone and Yeso Formations as mapped in New Mexico (O'Neill and Nutt, 1998).

The absence of the Yeso and San Andres Formations in Texas may be due to complex stratigraphic relationships between the Permian units, rather than just a difference in nomenclature between New Mexico and Texas geologists. As noted by Black (1973), Hayes (1964), and Newell et al. (1972), the upper Yeso and lower San Andres Formations grade laterally into the shelf-margin-facies Victorio Peak Limestone. The absence of the Yeso Formation in Texas may be due to an abrupt pinch out to the south, and/or an abrupt lateral gradation into the Victorio Peak Limestone (O'Neill and Nutt, 1998). Likewise, the absence of the San Andres Formation in Texas may be due to abrupt lateral gradation into the Victorio Peak Limestone (O'Neill and Nutt, 1998).

The digital geologic map of Stoeser et al. (2005) does not contain all of the geologic units identified in the subsurface oil-and-gas exploratory wells, as it often lumps several geologic units into one group. However, these surface groupings correspond very well to the modeled subsurface hydrogeologic unit groupings discussed above. The surface geologic groups include, from oldest to youngest, the Precambrian, the Cambrian through the Silurian, the Devonian through the Mississippian, the Pennsylvanian, Lower

Abo, Hueco Limestone/Formation (or Bursum Formation), Abo Formation, Yeso Formation, Bone Spring Limestone/Formation, Victorio Peak Limestone/Formation and Cutoff Shale and Wilke Ranch Formation, San Andres Formation, Delaware Mountain Group, Goat Seep Dolomite/Limestone/Formation and Capitan Limestone/Formation, Artesia Group, the Cretaceous, Cenozoic intrusions, and Cenozoic alluvium.

3.2.c: 3-D Hydrogeologic Framework Solid Model Development

The point shapefiles representing the surface geology were combined with the subsurface contours to model the elevation, relative to mean sea level, of the top of each hydrogeologic unit. The Cambrian through the Silurian surface group was combined with the subsurface contour for the interval from the Bliss Sandstone to the Fusselman Formation. The Devonian through the Mississippian surface group was combined with the subsurface contour for the Devonian. The Pennsylvanian surface group was combined with the subsurface contour for the Mississippian through the Pennsylvanian. The Lower Abo surface group was assumed to be equivalent to the Pow Wow Conglomerate contour of the subsurface. The Victorio Peak Limestone/Formation, Cutoff Shale, and Wilke Ranch Formation surface group was combined with the subsurface contour for the Victorio Peak Limestone/Formation. All of the remaining surface groups were combined with their respective subsurface contours, except for the Cenozoic intrusions. Subsurface contours were not produced for this unit. However, the Cenozoic intrusions were incorporated in the 3-D hydrogeologic framework model, as discussed below.

In order to create a 3-D hydrogeologic framework model, the combined surface and subsurface data for each of the 16 hydrogeologic units were converted to raster surfaces using ArcGIS. A raster surface consists of a grid of cells in which each cell

contains a value representing information, such as temperature or elevation. A raster cell size of 500 by 500 meters (1,640 by 1,640 feet) was chosen represent the elevation of the top of each hydrogeologic unit. The combined surface and subsurface data was mapped to the raster surface using a spline with barriers interpolation technique. This interpolation technique allowed the structural features [Figure 3.1] to be designated as barriers that the spline technique would not interpolate across. As a result, the displacement of each hydrogeologic unit across the structural features, as defined by the hand contours of the top of each unit, was maintained during the conversion to a raster surface.

Groundwater modeling system (GMS) version 6.5 was used to graphically display these raster surfaces in 3-D as a solid model of all 16 hydrogeologic units. GMS was also used to construct a 3-D finite difference groundwater flow model of the Salt Basin, which is discussed in Chapter 4.1. A grid of cells with the same cell size and origin as the raster surfaces was created in GMS. The GMS grid was assigned 16 layers to represent the 16 hydrogeologic units. The elevation values from the 16 raster surfaces were used to define the elevation values of the 16 layers in the GMS grid. The land surface expression of the resulting 3-D hydrogeologic framework solid model is displayed in Figure 3.2. The Cenozoic intrusions were modeled as a series of vertical intrusions, extending from their land surface outcrop locations downward, through the other 15 units, to the top of the Precambrian. In total, 17 hydrogeologic units were incorporated into the 3-D framework solid model, from oldest to youngest, the Precambrian, the Cambrian through the Silurian, the Devonian, the Mississippian through the Pennsylvanian, Lower Abo/Pow Wow Conglomerate, Hueco Limestone/Formation (or Bursum Formation) and Wolfcamp

Formation, Abo Formation, Yeso Formation, Bone Spring Limestone/Formation, Victorio Peak Limestone/Formation and Cutoff Shale and Wilke Ranch Formation, San Andres Formation, Delaware Mountain Group, Goat Seep Dolomite/Limestone/Formation and Capitan Limestone/Formation, Artesia Group, the Cretaceous, Cenozoic intrusions, and Cenozoic alluvium.

Figures 3.3 through 3.18 display the elevation, in meters relative to mean sea level, of the top of the 16 hydrogeologic units, excluding the Cenozoic intrusions. Figures 3.19 through 3.33 display the thickness, in meters, of the 15 hydrogeologic units above the Precambrian, excluding the Cenozoic intrusions. Personal computer memory constraints prevented graphical rendering of oblique views of the full extent of the 3-D hydrogeologic framework model displayed in Figure 3.2. However, when the full extent of the 3-D framework model was clipped to the groundwater flow model domain [Figure 3.34], as discussed in Chapter 4, oblique views of the 3-D framework solid model were able to be generated. Figure 3.35 presents several oblique views of the 3-D hydrogeologic framework solid model.

3.3: 2-D Hydrogeologic Cross-sections

3.3.a: Hand-drawn Cross-sections

Before the 3-D hydrogeologic framework model was assembled, the compiled subsurface data and surface geology of Stoeser et al. (2005) were used to construct five hydrogeologic cross-sections through primarily the New Mexico portion of the northern Salt Basin watershed. (Figure 3.36) Two cross-sections trend generally north-south along the eastern portion of the Salt Basin watershed from the Peñasco Basin to the natural discharge region at the Salt Flats (A to A' and B to B'). (Figures 3.37 and 3.38,

respectively) Both of these north-south oriented cross-sections generally follow along a groundwater flow path, and intersect groundwater wells that were sampled for environmental tracers during this study. The remaining three cross-sections trend generally west-east (C to C', D to D', and E to E'). (Figures 3.39, 3.40, and 3.41, respectively) Control on the subsurface geology for each cross-section was provided by the oil-and-gas exploratory wells discussed in Chapter 3.2.a. Tables 3.21 through 3.25 list the oil-and-gas wells used to construct these cross-sections, including the well I.D. used in this study, the distance of the well along the cross-section in meters, the well elevation in meters, and the well depth in meters.

These cross-sections indicate the complex subsurface structure that typifies the Salt Basin region. Ancestral Rocky Mountain structures displace Precambrian through Pennsylvanian-to-Lower Permian strata. The overlying Middle-to-Upper Permian units are gently folded and faulted due to Laramide compression and subsequent Cenozoic extension. Towards the south and east, these Upper Permian units transition into shelf-margin, and eventually basin-facies rocks deposited in the Delaware Basin. Cross-section E to E' indicates the presence of Cenozoic intrusions that cut Precambrian through Permian, and locally Cretaceous, strata in the Cornudas and Hueco Mountains regions. (Figure 3.41) Locally thin to thick deposits of Cenozoic alluvium fill the depressions or grabens bounding uplifts associated with Basin-and-Range extension.

The groundwater surfaces displayed in these cross-sections were contoured by hand using groundwater level data obtained from the New Mexico Office of the State Engineer's (NMOSE) New Mexico Water Rights Reporting System (NMWRRS) online database (http://nmwrrs.ose.state.nm.us/nmwrrs/disclaimer.html), the Texas Water

Development Boards's (TWDB) Groundwater Database (http://www.twdb.state.tx.us/
publications/reports/GroundWaterReports/GWDatabaseReports/GWdatabaserpt.htm),
and from Appendix A of the New Mexico Bureau of Geology & Mineral Resources'
Sacramento Mountains Hydrogeology Study (SMHS) Open File Report – 518
(http://geoinfo.nmt.edu/publications/openfile/details.cfml?Volume=518). Depth-to-water
measurements in these databases were converted to groundwater elevations, relative to
mean sea level, by inserting the location of these groundwater wells into ArcGIS, using
the 1-arc second NED described above in Chapter 3.2.b to define the ground surface
elevation of these wells, and then subtracting the reported depth-to-water from the ground
surface elevation. A subset of the groundwater elevation points from these databases
were used to contour the groundwater surface for the Salt Basin region. (Figure 3.42) The
cross-section lines were then overlaid on top of this groundwater surface [Figure 3.36],
and the intersections of the groundwater surface contours with each cross-section line
were used to define the groundwater surface in each cross-section. Some of the
groundwater elevation data used to construct the groundwater surface was obtained
during this study from personal communication with the owners of the groundwater
wells.

A subset of the groundwater elevation points were also used to hand-contour a
depth-to-groundwater map for the Salt Basin region. (Figure 3.43) The location of
groundwater wells in the NMOSE's NMWRRS database are taken from Water Right
Documents, which often include only township, range, section, and, sometimes, quarter-
section locations using the Public Land Survey System (PLSS). These PLSS locations are
then converted to UTM coordinates using the NAD 83 coordinate system. Therefore,

sometimes several wells occupy the same coordinate location. In such cases, the well with the greatest depth-to-water, or, if no depth-to-water measurements were available, the greatest well depth was chosen as the groundwater elevation control point for that coordinate location.

Groundwater wells in the TWDB's database sometimes have multiple depth-to-water measurements, ranging from the early 1900s to the present. For wells with multiple depth-to-water measurements, the mean of these measurements were used as groundwater elevation control points. In contrast, groundwater wells in the NMOSE's database have only one depth-to-water measurement per well. Researchers for the SMHS have collected multiple depth-to-water measurements per well throughout the Sacramento Mountains, but only the static depth-to-water measurements presented in Appendix A were used as groundwater elevation control points.

Also, all of the groundwater wells in these databases were not used as groundwater elevation control points. If neighboring wells had drastically different depth-to-water measurements, the well with the greatest depth-to-water was chosen as a groundwater elevation control point. The groundwater surface for the Salt Basin region represents the regional groundwater surface, and does not include localized zones of shallow or perched groundwater. (Figure 3.42) However, in the far southwestern portion of the Diablo Plateau, the groundwater surface incorporates a locally perched aquifer in the Cretaceous rocks unconformably overlying the Permian. However, as discussed below in Chapter 3.5.a, the Cretaceous aquifer is hydraulically connected to the underlying Permian aquifer. The depth-to-groundwater map indicates zones of shallower

groundwater than the overall regional trends displayed by the surrounding depth-to groundwater polygons. (Figure 3.43)

Table A-3.26 lists all the groundwater wells used to construct the groundwater surface and depth-to-groundwater maps for the Salt Basin region, including the NMOSE's NMWRRS database point of diversion (POD) number, well ID, or the TWDB's database state well number, the UTM coordinates using the NAD 83 coordinate system, the ground surface elevation in meters, the elevation of the well depth in meters (if available), the groundwater elevation in meters (if available), the aquifer that the well obtains groundwater from (if available), the county the well is located in, whether the well was used as a depth-to-groundwater and/or a groundwater surface control point, and the source of the depth-to-water measurement. Groundwater wells in the TWDB's database contain an aquifer code that indicates the aquifer the well penetrates. The aquifer name associated with each aquifer code is listed under the caption for Table A-3.26.

3.3.b: Cross-sections Through the 3-D Hydrogeologic Framework Solid Model

The same cross-section trends were cut through the 3-D hydrogeologic framework solid model. As discussed above in Chapter 3.2.c, personal computer memory constraints prevented oblique views of the full extent of the 3-D hydrogeologic framework model from being rendered. However, when the 3-D framework model was clipped to the groundwater flow model domain, oblique views of, and cross-sections through the 3-D model were able to be generated. As a result, the beginning of the A to A' and B to B' cross-sections derived from the 3-D hydrogeologic framework solid model are slightly truncated, as compared to the hand-drawn cross-sections presented in Figures 3.37 and

3.38. In addition, both the beginning and the end of the C to C', D to D', and E to E'
cross-sections derived from the 3-D hydrogeologic framework solid model are slightly
truncated, as compared to the hand-drawn cross-sections presented in Figures 3.39, 3.40,
and 3.41.

The locations and an oblique view of the 5 cross-sections within the 3-D
hydrogeologic framework solid model are presented in Figure 3.44. Side views of the 3-
D framework solid model cross-sections are shown in Figures 3.45 through 3.49. In
addition, the hand-drawn cross-sections are displayed alongside the 3-D framework solid
model cross-sections in Figures 3.45 through 3.49. The 3-D hydrogeologic framework
solid model cross-sections compare favorably to the hand-drawn cross-sections, and, in
general, maintain the displacement and juxtaposition of hydrogeologic units across the
structural features.

3.4: Surface Water and Springs

The Sacramento River is the only perennial stream in the Salt Basin watershed.
(Figure 1.5) The USGS measured mean daily discharge in the Sacramento River at
streamgaging station 08492900 near Sunspot, New Mexico from 1984 to 1989, during
which time it ranged from 60 to 370 liters per second (2 to 13 cubic feet per second [cfs])
(JSAI, 2002; Huff and Chace, 2006). All of the other drainages are ephemeral and flow
only during periods of intense rainfall (Hutchison, 2006). It is believed that runoff from
the Sacramento River and Piñon Creek subwatersheds, derived from these intense rainfall
events and melting snowpack, is a major contributor to groundwater recharge in the
northern Salt Basin watershed (JSAI, 2002; Huff and Chace, 2006).

Springs are common in the southern Sacramento Mountains, often near, but below, the contact between the San Andres and the underlying Yeso Formation (Newton et al., 2009). The majority of springs discharge from the Yeso Formation at several different stratigraphic levels, but often from fractured limestone beds immediately overlying low permeability clay or siltstone beds (Newton et al., 2009). During this study, a site was sampled in the upper reaches of the Piñon Creek subwatershed, just east of Piñon, New Mexico, where the land owner had dug down 9 to 11 meters (30 to 35 feet) through yellow rock to a spring discharge above a hard, impermeable layer. Near Timberon, New Mexico, Carissa Spring flows at an average rate of 76 liters per second (1,200 gallons per minute [gpm]) and rapidly infiltrates into the Sacramento Canyon fault (Finch, 2010). (Figures 1.5 and 1.6) Just south of the New Mexico-Texas border, near Dell City, Texas, Crow Spring was reported to be flowing at a rate of 0.2 liters per second (3 gpm) before the development of the Dell City irrigation district, but has since become dry (Bjorklund, 1957; Scalapino, 1950).

3.5: Groundwater

3.5.a: Distribution, Recharge, and Movement

-Permian

Permian rocks can be divided into three hydrogeologic facies, corresponding closely to the geologic facies described above (Sharp, 1989). Permian rocks of the hydrogeologic basin-facies (Guadalupian and Ochoan Series) were deposited in a deep-marine environment within the Delaware Basin, and have low permeability and poor water quality (Nielson and Sharp, 1985; Sharp, 1989). Rocks of the hydrogeologic shelf-margin-facies (Guadalupian) are highly permeable reef limestones (Goat Seep and

Capitan) that were deposited around the margin of the Delaware Basin (Nielson and Sharp, 1985; Sharp, 1989). Rocks of the hydrogeologic shelf-facies (Wolfcampian to Guadalupian) have a highly variable permeability that is strongly dependent on the degree of fracturing in the rocks (Nielson and Sharp, 1985).

-Bone Spring-Victorio Peak Aquifer

As mentioned above, the Victorio Peak Limestone is more accurately described as a limestone bank rather than a limestone reef, and contains strata interpreted to have been deposited in a lagoonal or back-reef environment, separated from the basin by the limestone banks (King, 1948; King, 1983). Also discussed above, during the first half of the Leonardian the Bone Spring Limestone extended several kilometers farther shelfward over the shelf margin (King, 1948). Therefore, based on the hydrogeologic facies characteristics of Nielson and Sharp (1985), the Victorio Peak Limestone and the lower portion of the Bone Spring Limestone fall within the hydrogeologic shelf-facies. The fracture-dependent permeability of the Victorio Peak and Bone Spring Limestones in the Dell City region is indicated by the more-than-one-order-of-magnitude difference in the specific-capacity of wells drilled no more than 30 meters (100 feet) apart, the low success rate (<50%) of wells drilled without the aid of fracture mapping as compared to the high success rate (>90%) of wells drilled with the aid of fracture mapping, and local well drillers reports of lost circulation (Mayer and Sharp, 1998).

The Dell Valley irrigation district is centered around Dell City, Texas just south of the New Mexico-Texas state line in northeastern Hudspeth County (Ashworth, 2001). (Figure 3.50) The irrigated area also extends northward into the Crow Flats region of New Mexico in southeastern Otero County (Ashworth, 2001). (Figure 3.50) The

irrigation area derives groundwater from the hydrogeologic shelf-facies rocks that comprise the Bone Spring-Victorio Peak aquifer (George et al., 2005). (Figure 3.50) Mayer and Sharp (1998) reported a combined thickness of the Bone Spring and Victorio Peak Limestones in the Dell City, Texas area to range from 100 meters (328 feet) to at least 430 meters (1,410 feet). Peckham (1963) reported at least 152 meters (499 feet) of Bone Spring Limestone, and at least 244 meters (800 feet) of Victorio Peak Limestone in the Dell City, Texas area. The Bone Spring-Victorio Peak aquifer is believed to exist under both unconfined and confined conditions (Bjorklund, 1957).

-High Mountain, Pecos Slope, and Salt Basin Aquifers

Groundwater flow converges on the Dell Valley region from the Diablo Plateau to the southwest, and from the Sacramento Mountains and Otero Mesa to the northwest (Kreitler et al., 1990; Mayer and Sharp, 1998). (Figure 3.42) The majority of groundwater in the Dell Valley region originates as recharge in the Sacramento Mountains and along the Sacramento River as it infiltrates into the heavily fractured Permian shelf-facies rocks that constitute the Otero Break (Mayer, 1995; Mayer and Sharp, 1998). In the Sacramento Mountains, snow melt in the high mountains is the primary source of recharge to the groundwater system, although extremely wet monsoon seasons can contribute significantly to groundwater recharge (Newton et al., 2009). Chace and Roberts (2004) report a combined thickness of the San Andres and Yeso Formations of at least 457 meters (1,499 feet) within the northern Salt Basin watershed. Hydraulic gradients in the northern-most portion of the northern Salt Basin watershed also suggest a component of interbasin groundwater flow from the Peñasco Basin to the north (JSAI, 2002; Newton et al., 2009). South Central Mountain RC&D Council, Inc. (2002) estimated the inflow

component from the Peñasco Basin to be 10,000,000 m^3/year (8,000 acre-feet/year). Groundwater flow modeling work by JSAI (2002) and JSAI (2010) resulted in estimates of inflow from the Peñasco Basin of 9,811,000 m^3/year (7,954 acre-feet/year) and 6,724,000 m^3/year (5,451 acre-feet/year), respectively.

In the Sacramento Mountains, west of the town of Mayhill, New Mexico, the regional groundwater system is located primarily in the Yeso Formation (Newton et al., 2009). This high mountain aquifer system consists of several unconfined, perched aquifers connected to each other by regional fracture networks, and probably a deeper, continuous, locally confined, regional aquifer in the eastern portion of the high mountains (Newton et al., 2009). (Figure 3.50) In the high mountains, groundwater is found predominately in fractured limestone, collapse breccias formed by dissolution of gypsum and/or limestone, and less commonly, sandstone beds within the Yeso Formation (80% of groundwater wells with logs) (Newton et al., 2009). Other groundwater zones exist in the underlying Abo Formation along the west face of the mountains, in shallow valley-bottom alluvium, or spring deposits (Newton et al., 2009). East of Mayhill, groundwater occupies a more single, continuous aquifer (Pecos slope aquifer) in both the San Andres and Yeso Formations (Newton et al., 2009). (Figure 3.50)

Groundwater recharge to the high mountain aquifer is focused in the high mountains where the Yeso is exposed at the surface (Newton et al., 2009). The high mountain aquifer recharges both the Pecos slope and Salt Basin aquifers (Newton et al., 2009). (Figure 3.50) As indicated by the discharge of springs from several different stratigraphic levels in the Yeso Formation, groundwater flows at several levels within the Yeso Formation (Newton et al., 2009). Abundant claystone in the upper portion of the

Yeso formation acts as a barrier to vertical groundwater flow (Newton et al., 2009). Hydrogeologic cross-section C to C' suggests that in the higher elevations in the northwestern portion of the Otero Mesa and southeastern Sacramento Mountains groundwater may reside in localized, shallow perched aquifers in the San Andres Formation, which probably overlie the deeper regional aquifer in the Yeso Formation. (Figure 3.39)

Hydraulic gradients also indicate that groundwater generally flows east- to northeastward from the Otero Mesa towards the Dell Valley region (JSAI, 2002; Mayer, 1995). (Figure 3.42) In the western portion of the Otero Mesa shelf-facies rocks of the Hueco and Yeso Formations are exposed (Stoeser et al., 2005). (Figure 2.1) The Hueco Formation also outcrops on the Diablo Plateau to the south, but thins, and is unconformably overlain by Leonardian (Bone Spring or Victorio Peak) or Cretaceous strata southeastward towards the Sierra Diablo Mountains (King, 1983; Kottlowski, 1963; Stoeser et al., 2005). (Figure 2.1) As discussed below, the regional Permian aquifer beneath the Diablo Plateau encompasses rocks of the Hueco Formation. Therefore, the Hueco Formation could be an important aquifer in the New Mexico portion of the Salt Basin (Huff and Chace, 2006). Further, hydrogeologic cross-sections C to C', D to D', and E to E' indicate that groundwater occurs in the Hueco, Abo and Yeso Formations in the western portion of the Otero Mesa. (Figures 3.39, 3.40, and 3.41)

Hydraulic gradients also suggest a component of groundwater flow to the west and southwest from the Guadalupe and Brokeoff Mountains towards the Salt Basin graben. (Figure 3.42) However, the importance of this flow system to the Salt Basin hydrologic system has not been quantified. Depth-to-groundwater in this region ranges

from 230 meters (750 feet) to greater-than 300 meters (1,000 feet). (Figure 3.43) Therefore, it is unlikely that the Guadalupe and Brokeoff Mountains contribute much modern recharge to the Salt Basin hydrologic system.

-Diablo Plateau Aquifer

In the southwestern portion of the Diablo Plateau a regional aquifer is found in the Permian rocks unconformably underlying the Cretaceous rocks, and extends to the northern and northeastern portions of the Plateau where the Permian rocks are exposed at the surface (Kreitler et al., 1990; Mullican and Mace, 2001). (Figure 3.50) The regional Permian aquifer is primarily unconfined, although it is likely confined beneath the Cretaceous rocks (Mullican and Mace, 2001). The regional Permian aquifer (Hueco, Bone Spring, and Victorio Peak Formations) on the Diablo Plateau is hydraulically connected to the Permian rocks (Bone Spring and Victorio Peak Formations) in the Dell City region to the northeast (George et al., 2005). Groundwater flow is predominantly from southwest to northeast (Kreitler et al., 1990).

Depths to water in the regional Permian aquifer are as great as 244 meters (800 feet), and hydraulic gradients are much lower than in the overlying shallow aquifer in the Cretaceous rocks (George et al., 2005; Kreitler et al., 1990). (Figures 3.42 and 3.43) Recharge is distributed over the entire area of the plateau (7,500 km^2 [2,900 mi^2]) based on measurable amounts of tritium in nearly all wells within the regional aquifer (Kreitler et al., 1990). Low chloride concentrations in arroyo soils, compared to high chloride concentration in inter-arroyo soils suggest that most recharge is restricted to flood events through fractures concentrated in the arroyos (Kreitler et al., 1990).

-Capitan Reef Complex Aquifer

In the southern Guadalupe Mountains, and extending southwestward into the Patterson Hills and the Texas portion of the Salt Basin graben is the Capitan Reef Complex aquifer (George et al., 2005). (Figure 3.50) This aquifer consists of the reef rocks of the Goat Seep and Capitan Formations, as well as back-reef (near shelf-edge) rocks of the Artesia Group (Hiss, 1980). This aquifer outcrops in the Guadalupe Mountains and the Patterson Hills, and subcrops south of the Patterson Hills where it supplies water to the Beacon Hill irrigation area (Gates et al., 1980). (Figure 3.50) Recharge to this aquifer is focused where it outcrops in the Guadalupe Mountains, Apache Mountains, and the Patterson Hills, and locally from ephemeral streamflow in and east of the Beacon Hill irrigation area (Gates et al., 1980; George et al., 2005). Gates et al. (1980) reported that the Goat Seep Limestone is as much as 370 meters (1,200 feet) thick in the Salt Flats region, and that the Capitan Limestone is first encountered at depths from 18 to 84 meters (60 to 275 feet) and extends to as much as 514 meters (1,686 feet) in the Beacon Hill area.

The Border fault zone acts as a groundwater divide between two regional groundwater flow systems within the high permeability trend of the Capitan Reef Complex aquifer: one that originates in the southern Guadalupe Mountains and flows to the north and northeast towards Carlsbad, New Mexico, and one that flows south from the recharge zone in the Patterson Hills towards the Apache Mountains (Hiss, 1980; Standen et al., 2009; Uliana, 2001). (Figures 2.25, 3.42, and 3.50) Numerous researchers have presented compelling hydrochemical and structural evidence that supports a regional groundwater flow system from the Wild Horse Flat portion of the Salt Basin

graben eastward through the Capitan Reef Complex in the Apache Mountains to Balmorhea Springs in the Toyah Basin (Nielson and Sharp, 1985; Sharp, 1989; Sharp, 2001; Uliana, 2000; Uliana and Sharp, 2001; Uliana et al., 2007). (Figure 3.50) Using hydrochemical tracers, Chowdhury et al. (2004) concluded that groundwater originating in the Capitan Reef Complex in the area west of the Delaware Mountains and in the Apache Mountains flows southeast to Balmorhea Springs.

-Cretaceous

In the southwestern portion of the Diablo Plateau a shallow, primarily unconfined, locally perched and confined to semi-confined aquifer is located in the Cretaceous rocks unconformably overlying the Permian (Kreitler et al., 1990; Mullican and Mace, 2001). (Figure 3.50) The Cretaceous aquifer is vertically connected to the underlying regional aquifer in the Permian, and is also hydraulically connected to the Hueco bolson aquifer to the west, the aquifer in the Quaternary deposits filling the Salt Basin graben to the east, and the Permian rocks in the Dell City region to the northeast (George et al., 2005). (Figure 3.50) Groundwater flows outward from a groundwater mound in the southwestern part of the Diablo Plateau south of U.S. Highway 62-180 toward the Hueco bolson to the southwest, the Finlay Mountains and northwest Eagle Flats to the southeast, the Salt Basin graben to the northeast, and possibly to the north of Highway 62-180 where it then flows eastward to Dell City, Texas (Mullican and Mace, 2001). (Figure 3.42) Depths to water in the Cretaceous aquifer are generally less than 61 meters (200 feet), and hydraulic gradients are much steeper than in the underlying Permian aquifer (George et al., 2005; Kreitler et al., 1990). (Figures 3.42 and 3.43)

-Cenozoic

Some wells in the Crow Flats and Dell City regions obtain water from the alluvium and lacustrine deposits filling the Salt Basin graben (Bjorklund, 1957). The thickness of valley-fill encountered by most wells drilled in the Crow Flats and Dell City regions range from 7.6 to 91.4 meters (25 to 300 feet) (Bjorklund, 1957). The E.J. Dunigan, Alpha Federal #1 (EJDALF1) well [Figure 3.1] in the Crow Flats region, just west of the Brokeoff Mountains, penetrated 18 meters (60 feet) of basin fill. Farther to the south in the Texas portion of the Salt Basin graben the thickness of valley-fill increases, ranging from 152 to 610 meters (500 to 2,000 feet), with the thickest intervals generally found in the center of the graben (Veldhuis and Keller, 1980). The maximum thickness of the lacustrine clays and sands filling the Texas portion of the graben range from 244 meters (800 feet) in the region north of U.S. Highway 62-180 to 610 meters (2,000 feet) southwest of Bitter Well Mountain in the Delaware Mountains (Gates et al., 1980).

The valley-fill aquifer in the Salt Basin graben is hydraulically connected to the surrounding aquifer in the Dell Valley irrigation area to the west (Bjorklund, 1957). (Figures 3.42 and 3.50) The valley-fill aquifer is unconfined (Bjorklund, 1957). During the late 1940s (1947-1949) in the Dell City region water levels were slightly lower (0.3 to 1.5 meters [1 to 5 feet]) in the valley-fill aquifer than in the surrounding Bone Spring-Victorio Peak aquifer, which suggests that groundwater was flowing from the Bone Spring-Victorio Peak aquifer into the valley-fill aquifer (Bjorklund, 1957). Recharge to the valley-fill aquifer is primarily by flash flood infiltration in the flat-bottomed canyons and bajadas along ephemeral streams draining into the valley floor (Bjorklund, 1957). In

the Salt Flat region the valley-fill aquifer consists predominately of low permeability lacustrine clay and sand saturated with saline water, and is not a good aquifer (Gates et al., 1980).

Farther to the north in T. 21 S., R. 17 E., sec. 12 a perched saturated zone above the regional aquifer is located in the alluvium filling Piñon Creek (Bjorklund, 1957). It is likely that similar shallow, perched groundwater zones exist in the alluvium filling the other ephemeral drainages in the Salt Basin. In the Sacramento Mountains, shallow, perched zones are located in valley-bottom alluvium and spring deposits (Newton et al., 2009).

3.5.b: Discharge

Before the development of the Dell City irrigation district the natural discharge mechanism of the groundwater system in the northern Salt Basin was through evaporation from the playa lakes/alkali flats situated along the center of the Salt Basin graben (Bjorklund, 1957). Groundwater withdrawals due to pumping increased steadily after the installation of irrigation wells in the Dell City region in 1947 and 1948, and in the Crow Flats region in 1949 (Bjorklund, 1957). The amount of groundwater pumped for irrigation purposes temporarily peaked in the late 1970s around 190,000,000 m^3/year (150,000 acre-feet/year) (Ashworth, 2001). Irrigation pumping declined in the 1980s to about 120,000,000 m^3/year (100,000 acre-feet/year) due to economic hardships and government conservation programs, but increased again in the subsequent years to over 250,000,000 m^3/year (200,000 acre-feet/year) in 2000 (Ashworth, 2001). Groundwater withdrawals for irrigation have resulted in a steady decline in regional groundwater levels

170

by as much as 12 meters (40 feet) from the late 1940s to about 2000 (Huff and Chace, 2006).

In the Sacramento Mountains, groundwater discharges to springs and streams (Newton et al., 2009). As mentioned above, prior to development of the Dell City irrigation district, groundwater discharged from Crow Spring just to the east of Dell City (Bjorklund, 1957). Also, as discussed above, groundwater discharges from Carissa Spring near Timberon, New Mexico before rapidly infiltrating into the Sacramento Canyon fault (Finch, 2010).

3.5.c: Structural Controls on Groundwater Flow

Based on hydraulic gradients and hydrochemistry, previous researchers have ascertained that the Otero Break acts as a high permeability conduit for groundwater flow from the Sacramento Mountains to the southeast towards the Dell Valley region (JSAI, 2002; Hutchison, 2006; Mayer, 1995; Mayer and Sharp, 1998). The region surrounding the Otero Break is a heavily fractured zone with a strong preferred fracture orientation of approximately N20W (Mayer and Sharp, 1998). This fracture system may act as an interconnected pathway along which groundwater flow is focused.

Previous researchers [JSAI, 2002; Mayer, 1995; Mayer and Sharp, 1998] have depicted a prominent trough in the groundwater surface that is not centered on the Otero Break, but rather to the west of this feature. (Figure 3.51) The region of the groundwater trough coincides with a plume of fresh water, as indicated by low total dissolved solids (TDS) [$\leq$ 500 milligrams per liter (mg/L)], that extends from the southern Sacramento Mountains toward Dell City (Mayer and Sharp, 1998). John Shomaker & Associates, Inc. (2010) have also measured wells in the region of the groundwater trough with TDS

values that range from 500 to 600 mg/L. Numerous sinkholes that drain significant watershed areas are also located in the region of the groundwater trough parallel to the Otero Break (JSAI, 2010). The groundwater trough is located in a region of karst terrain thought to be characterized by very high transmissivity (JSAI, 2010).

Groundwater elevation contours produced for this study suggest an alternate interpretation of the Otero Break. (Figure 3.42) To the northeast of the Otero Break, the groundwater elevation contours are orthogonal to the trend of the Break, and indicate groundwater flow to the southeast from the southern Sacramento Mountains. (Figure 3.42) Near the Otero Break, the contours bend drastically to the northwest and parallel the trend of the Break. (Figure 3.42) This pattern can also be seen on Figure 3.51. Therefore, an alternate hypothesis is the Otero Break acts as a barrier to groundwater flow perpendicular to this feature, and that most of the groundwater flow in the Salt Basin aquifer from recharge in the southern Sacramento Mountains is restricted to the region along and to the northeast of the Break.

This hypothesis is also supported by the intense faulting and fracturing observed on the Chert Plateau to the northeast of the Otero Break, and the relative lack of fracturing on Otero Mesa to the southwest of the Break (Mayer and Sharp, 1998). The faulting and fracturing on the Chert Plateau parallels the Otero Break, and it is likely that groundwater flow is focused along these features. The prominent trough in the groundwater surface to the west of the Otero Break could be the result of the relatively flat topography in this region, rather than this region acting as a high permeability conduit for groundwater flow. (Figures 3.42 and 3.51)

172

The groundwater elevation contours parallel to the Otero Break could also be interpreted as indicating the direction of groundwater flow from recharge on the fractured Chert Plateau to the highly transmissive karst system. However, as indicated by Mayer and Sharp (1998), the region surrounding the Otero Break has a strong preferred fracture orientation, which parallels the trend of the Otero Break. Therefore, focused groundwater flow orthogonal to these fractures is unlikely.

Around the Cornudas Mountains, closed groundwater elevation contours suggest that this may be a region of recharge. (Figure 3.42) Also, there is a steep gradient in the groundwater elevation contours on the eastern edge of the Cornudas Mountains, along the New Mexico-Texas state line. (Figure 3.42) This steep gradient may be the result of a structural barrier to groundwater flow to the east of the Cornudas Mountains, possibly the Otero fault or an elevated block of Precambrian basement associated with the Pedernal uplift. However, cross-section E to E', which passes through the Cornudas Mountains region, does not indicate any structural features that could act as impediments to groundwater flow in the Permian aquifer units. (Figure 3.41)

An alternate explanation for the groundwater mound and steep gradient associated with the Cornudas Mountains is that the Cenozoic intrusive bodies, which form the core of the Cornudas Mountains, act as a low permeability barrier to vertical groundwater movement in this region. Gravity and aeromagnetic data suggest that the Cornudas Mountains are underlain by a mass, likely syenite, that was emplaced at or just above the level of Precambrian basement (670 meters [2,200 feet] deep) (Nutt et al., 1997). Therefore, it is likely that the relatively impermeable igneous intrusions in the Cornudas Mountains region cause recharge to mound and then spill over to the east towards Dell

City, Texas. (Figure 3.42) This hypothesis is also supported by the fact that the steep gradient zone corresponds to the eastern margin of a broad residual gravity low that is inferred to reflect the subsurface extent of the intrusive mass (Nutt et al., 1997).

As discussed above, a groundwater divide is associated with the Paleozoic transform zone known as the Bitterwell Break (Nielson and Sharp, 1985). Another groundwater divide is associated with the Victorio flexure (Nielson and Sharp, 1985). These groundwater divides are located in the Cenozoic valley-fill aquifer within the Salt Basin graben, and may be the result of permeability barriers formed by these structural features (Nielson and Sharp, 1985). (Figure 3.52) South of the Bitterwell Break, groundwater moves toward and discharges at the alkali flat just to the east of the Sierra Diablo Mountains (Gates et al., 1980). (Figures 1.3 and 3.52) South of the Victorio flexure, groundwater flows toward a groundwater depression associated with irrigation pumping in Wild Horse Flat, and also eastward through the Capitan Reef Complex in the Apache Mountains (Gates et al., 1980). (Figure 3.52) These groundwater divides may not impact the regional groundwater flow system in the Capitan Reef Complex aquifer underlying the valley-fill aquifer in the Salt Basin graben (Standen et al., 2009).

Hydrogeologic cross-section A to A' suggests that the Precambrian bedrock high associated with the Pedernal uplift and later Basin-and-Range tectonism along the Stevenson fault may cause groundwater mounding on the upgradient side of this feature. (Figure 3.37) Groundwater wells in the NMOSE's NMWRRS database indicate that groundwater levels north of the Stevenson fault are about 200 meters (660 feet) higher than groundwater levels south of this feature (see Table A-3.26, and the difference in

water elevation between ST 00005, which is north of the Stevenson fault, and ST 00003, which is south of the Stevenson fault).

Hydrogeologic cross-sections C to C', D to D', and E to E' suggest that the Guadalupe and Dog Canyon fault zones along the eastern edge of the Salt Basin may act as barriers to groundwater flow. (Figures 3.39, 3.40, and 3.41) Groundwater wells in the NMWRRS database indicate that groundwater levels are up to 500 meters (1,640 feet) higher on the eastern side of these structural features. The hydraulic gradient across these features is likely large enough to produce groundwater flow across the mountain front and into the northern Salt Basin watershed. (Figure 3.42) As discussed above, the Border fault zone acts as a groundwater divide between two regional groundwater flow systems within the Capitan Reef Complex aquifer (Standen et al., 2009).

3.6: Hydraulic Properties

3.6.a: Published Values

-Specific-capacity, Hydraulic Conductivity, and Transmissivity

All of the hydraulic conductivity and transmissivity data discussed in this section are presented in Tables A-3.27 and A-3.28, and Figures 3.57 and 3.58. Scalapino (1950) and Bjorklund (1957) presented specific-capacity data for the Dell City, Texas and Crow Flats, New Mexico regions, respectively. These data were analyzed by Hutchison (2006) to estimate transmissivity, and the results are discussed below.

Peckham (1963) reported that specific-capacity values of wells in the Dell City, Texas area completed in the Bone Spring-Victorio Peak aquifer ranged from 1.1 to 13.2 liters per second per meter of drawdown (5.2 to 63.8 gpm per foot of drawdown). In the bolson deposits of the Salt Basin graben, Peckham (1963) reported that specific-capacity

values ranged from 1.9 to 6.89 liters per second per meter of drawdown (9.1 to 33.3 gpm per foot of drawdown) in the Wild Horse Flat region, and from 2.88 to 10.1 liters per second per meter of drawdown (13.9 to 49.0 gpm per foot of drawdown), averaging 5.2 liters per second per meter of drawdown (25 gpm per foot of drawdown), in the Lobo Flat region.

Gates et al. (1980) presented specific-capacity data for the Capitan Limestone in the Beacon Hill area of the Salt Basin watershed. Specific capacities ranged from 1.3 to 12 liters per second per meter of drawdown (6.5 to 58 gpm per foot of drawdown), with a median value of 3.42 liters per second per meter of drawdown (16.5 gpm per foot of drawdown) (Gates et al., 1980). Based on this median value of specific-capacity, Gates et al. (1980) estimated a transmissivity of about 500 m^2/day (5,400 ft^2/day). Gates et al. (1980) also referenced a transmissivity value of 1,500 m^2/day (16,000 ft^2/day) that was calculated from an aquifer test in the Beacon Hill area, but stated that the well had an above-average specific-capacity.

Hiss (1980) did not present any hydraulic property values, but did note that the average hydraulic conductivity of Permian basin-facies strata is generally one to two orders of magnitude less than Permian shelf-margin-facies rocks of the Capitan Reef Complex aquifer.

White et al. (1980) presented specific-capacity data for the Salt Basin region in Texas. Similar to Scalapino (1950) and Bjorklund (1957), these data were analyzed by Hutchison (2006) to estimate transmissivity, and the results are discussed below.

Wasiolek (1991) presented values of transmissivity and hydraulic conductivity calculated from aquifer tests performed on Yeso Formation strata in the Mescalero

Apache Indian Reservation, encompassing parts of the Rio Hondo and Peñasco Basins, to the north of the Salt Basin region. Aquifer tests were run for an average of 48 hours (24 hours of pumping, and 24 hours of recovery), and the water level response was monitored in four deep pumping wells and four associated piezometers. Unfractured siltstones and gypsum beds within the Yeso Formation produced transmissivities that ranged from 0.33 to 1.7 m^2/day (3.5 to 19 ft^2/day). Assuming that water was contributed by the entire screened interval, hydraulic conductivities ranged from 0.0022 to 0.011 m/day (0.0071 to 0.037 ft/day), and averaged 0.0060 m/day (0.020 ft/day). Limestone beds within the Yeso Formation produced transmissivities that ranged from 42 to 86 m^2/day (460 to 930 ft^2/day), and hydraulic conductivities that ranged from 0.18 to 0.45 m/day (0.60 to 1.5 ft/day). Wasiolek (1991) interpreted this data to suggest that the hydraulic conductivity in limestone beds in the Yeso Formation that have fracture and subsequent dissolution-enhanced secondary permeability, is several orders of magnitude higher than the hydraulic conductivity in unfractured siltstone and gypsum beds in the Yeso Formation.

Mayer (1995) referenced two publications that presented transmissivity values for the Otero Mesa/Diablo Plateau aquifer based on aquifer tests. In Kreitler et al. (1987) four data points yielded transmissivities that ranged from 0.0297 to 0.213 m^2/day (0.320 to 230 ft^2/day), with a median value of 0.107 m^2/day (115 ft^2/day) (Mayer, 1995). George et al. (2005) also referenced this data, and indicated that these values came from Permian rocks on the northeast portion of the Diablo Plateau. In Logan (1984) two data points yielded transmissivities that ranged from 4,440 to 4,830 m^2/day (47,800 to 52,000 ft^2/day), with a median value of 4,640 m^2/day (49,900 ft^2/day) (Mayer, 1995).

Angle (2001) presented transmissivity values calculated from aquifer tests and specific capacities for the bolson deposits filling the Salt Basin graben, shelf-margin-facies rocks of the Capitan Reef Complex aquifer, Cretaceous rocks, basin-facies rocks of the Delaware Mountain Group, and Cenozoic volcanics within the Salt Basin graben region in Texas. However, the method used to calculate transmissivity from specific-capacity was not indicated by Angle (2001). The highest transmissivities occur in those wells completed either entirely or partially in the Capitan Reef Complex aquifer (Angle, 2001). Wells completed in Cretaceous rocks beneath the bolson deposits have higher transmissivities than wells completed in the bolson deposits, while wells completed in volcanic rocks have lower transmissivities than wells completed in the overlying bolson deposits (Angle, 2001). Wells completed in basin-facies rocks of the Delaware Mountain Group also tend to have lower transmissivities than wells completed in the overlying bolson deposits.

Mullican and Mace (2001) used the Thomasson et al. (1960) (C = 1.2) method to estimate transmissivity from the specific-capacity range for the Bone Spring-Victorio Peak aquifer in the Dell City, Texas region presented by Peckham (1963). Based on this approach, Mullican and Mace (2001) calculated that transmissivity ranged from 110 to 1,400 m^2/day (1,200 to 15,000 ft^2/day).

Uliana (2001) summarized published values of transmissivity for shelf-margin and shelf-facies Permian rocks in the Texas portion of the Salt Basin watershed. Transmissivities as high as 1,500 m^2/day (16,200 ft^2/day) were reported for the Capitan Reef Complex aquifer by Reed (1965) (Uliana, 2001). Uliana (2001) presented a range of transmissivity values for shelf-facies Permian rocks referenced from Davis and Leggat

(1965), and an average transmissivity value for shelf-facies Permian rocks in the Dell City area referenced from Scalapino (1950). According to Nielson and Sharp (1985), these transmissivity values for shelf-facies Permian rocks were estimated from specific-capacity data, but they do not indicate the method by which transmissivity was calculated. In Davis and Leggat (1965), transmissivity values for shelf-facies Permian rocks ranged from 160 to 1,950 m^2/day (1,720 to 21,000 ft^2/day), while in Scalapino (1950) the average transmissivity for shelf-facies Permian rocks was 3,110 m^2/day (33,500 ft^2/day) (Uliana, 2001).

Some of the data presented in Uliana (2001) is suspect. First, wells 4717202 and 4717204 are listed in the TWDB groundwater database as being completed in the Salt Bolson and Capitan Reef Complex, and the Capitan Reef Complex and Associated Limestones, respectively, whereas in Uliana (2001) they are grouped with Permian shelf-facies wells. Also, well 4717602 is listed in the TWDB groundwater database as being completed in the Salt Bolson and Delaware Mountain Group, while it is grouped with Permian shelf-facies wells in Uliana (2001). The remaining wells listed as Permian shelf-facies wells in Uliana (2001) are completed in the Bone Spring-Victorio Peak according to the TWDB, except for wells 4807605, 4807701, and 4816701, which could not be found in the TWDB database.

George et al. (2005) referenced transmissivity values for the Cretaceous aquifer on the southwest portion of the Diablo Plateau from Kreitler et al. (1987). The transmissivity of the Cretaceous aquifer on the Diablo Plateau ranged from 460 to 620 m^2/day (5,000 to 6,700 ft^2/day) (George et al., 2005). These values are significantly high compared to the range of transmissivity values reported by Kreitler et al. (1987), as

referenced in Mayer (1995) and George et al. (2005), for the Permian aquifer on the northeast portion of the Diablo Plateau.

Hutchison (2006) presented estimates of transmissivity derived from specific-capacity values for the Salt Basin region reported in Scalapino (1950), Bjorklund (1957), and White et al. (1980). Hutchison used eight methods to estimate transmissivity from specific-capacity, six of which are based on empirical relationships between transmissivity and specific-capacity for carbonate aquifers throughout the U.S. as presented in Mace (2001). The other two methods are from Gates et al. (1980); one method is based on the assumption that the aquifer has a storage coefficient of 0.1, the diameter of the well is 30 cm (12 inches), specific-capacity was measured after one day of pumping, and the well is 100 percent efficient, while the other method is based on a comparison of aquifer test and specific-capacity data from individual wells completed in limestone or basin fill in the Salt Basin region.

Some of the wells (4709207, 4717202, 4717204, 4717218, 4717317, 4717321, and 4717602) analyzed by Hutchison (2006) from White et al. (1980) were previously analyzed by Davis and Leggat, as referenced in Uliana (2001), and Angle (2001). However, only one well from Angle (2001) [4717317] had a transmissivity value that was based on an aquifer test, rather than specific-capacity. The average values of transmissivity for wells completed in the Bone Spring-Victorio Peak aquifer in the Dell City region and related Permian shelf-facies rocks in the Crow Flats region ranged from 170 to 26,000 m^2/day (1,900 to 280,000 ft^2/day). Wells associated with the Capitan Reef Complex had average transmissivities that ranged from 140 to 8,200 m^2/day (1,500 to 88,000 ft^2/day).

As discussed above in Chapter 3.1, the distribution of permeability within the Salt Basin has been estimated using both 2-D and 3-D groundwater flow models. Mayer (1995) estimated the transmissivity of the Salt Basin aquifer system to range from 0.86 to 860 m^2/day (9.3 to 9,300 ft^2/day), with the highest transmissivities being assigned to the regions of greatest fracture density. Hutchison (2008) defined numerous hydraulic conductivity zones within the Salt Basin aquifer system on the basis of structure, geochemistry, and a hybrid of the two. Hydraulic conductivities assigned to the zones in the three models ranged from 0.0003 to 61 meters/day (0.001 to 200 feet/day) (Hutchison, 2008). Hutchison (2008) assumed an aquifer thickness of 300 meters (1,000 feet), and thus transmissivities ranged from 0.3 to 61,000 m^2/day (1 to 200,000 ft^2/day). JSAI (2010) developed a 3-D groundwater flow model of the Salt Basin aquifer system. The hydraulic conductivity values incorporated into the model are discussed in Chapter 3.1. Aquifer transmissivity was estimated to range from less than 9.3 to greater than 9,300 m^2/day (less than 100 to greater than 100,000 ft^2/day) (JSAI, 2010).

-Storage Coefficient

Wasiolek (1991) calculated a storage coefficient (S) of 0.00085 from the aquifer test performed on the wells completed in the unfractured siltstones and gypsum beds within the Yeso Formation.

3.6.b: Estimates of Transmissivity Based on ^{14}C Data Along Cross-section A to A'

Cross-section A to A' [Figure 3.37] was chosen to model the geochemical evolution of groundwater in the Salt Basin, because it follows a generalized groundwater flow path along the eastern portion of the northern Salt Basin watershed, and intersects six of the groundwater wells sampled during this study (Beech, Doll Day, Uña, Runyan,

Cauhape, and Harvey Lewis Well) and two wells sampled by the New Mexico Bureau of Geology & Mineral Resources' Sacramento Mountains Hydrogeology Study (SM-0085 and SM-0044). (Figure 3.36) In addition, three other wells sampled during this study (Piñon Well, Evrage House, and Hammock Well) were located near, and projected to this cross-section. (Figure 3.36)

As discussed by Sigstedt (2010) and Newton et al. (2009), data collected from the groundwater wells along this cross-section consist of groundwater temperature, general ion chemistry, including total dissolved solids (TDS), $\delta^{13}C$ (‰ PDB), and ^{14}C (pmC). Sigstedt (2010) analyzed all of the environmental tracers data collected for this project and concluded that the primary process controlling the geochemical evolution of groundwater in the Salt Basin was dedolomitization. Dedolomitization is a process in which dolomite dissolution and the concomitant precipitation of calcite is driven irreversibly by the dissolution of gypsum (or anhydrite) (Back et al., 1983). Miller (1997) also hypothesized that dedolomitization was one of the processes controlling groundwater chemistry in the Cornudas Mountains region.

Morse (2010) also presented evidence that dedolomitization was the primary control on the geochemical evolution of groundwater in the Peñasco Basin. Morse (2010) presented a stoichiometric model of the dedolomitization process that incorporates the change in HCO_3^- and Mg^{2+} concentration along a groundwater flow path to model the change in ^{14}C activity due to dedolomitization alone:

$$^{14}C_f = {}^{14}C_i \frac{\left(mHCO_{3i}\right)}{\left(mHCO_{3f}\right)} \left[1 - \left(\frac{\Delta mHCO_3}{mHCO_{3f} + 2\Delta mMg}\right)\right], \qquad [1]$$

where

$^{14}C_f$ = ^{14}C activity at final well (pmC),

$^{14}C_i$ = ^{14}C activity at initial well (pmC),

ΔmMg = change in $[Mg^{2+}]$ between initial and final wells (mmoles/L),

$\Delta mHCO_3$ = change in $[HCO_3^-]$ between initial and final wells (mmoles/L),

$mHCO_{3i}$ = $[HCO_3^-]$ at initial well (mmoles/L), and

$mHCO_{3f}$ = $[HCO_3^-]$ at final well (mmoles/L).

This equation is first applied to the initial and subsequent wells along a groundwater flow path to calculate the ^{14}C activity at the subsequent well. This calculated ^{14}C activity is then used in the equation as the initial activity to calculate the ^{14}C activity at the next well along the flow path, and so on to the last well along the flow path. The difference between the ^{14}C activity calculated using the stoichiometric dedolomitization model (A_0) and the ^{14}C activity measured in groundwater (A) represents the depletion in ^{14}C activity due to radioactive decay. Using the decay equation (Kalin, 2000):

$$^{14}C \, Age = \left(\frac{-1}{\lambda}\right) \ln\left(\frac{A}{A_0}\right), \qquad [2]$$

where

$^{14}C \, Age$ = ^{14}C groundwater age (years),

λ = ^{14}C decay constant = 0.00012 (years^{-1}),

A = ^{14}C activity measured in the groundwater (pmC), and

A_0 = ^{14}C activity calculated using the stoichiometric dedolomitization model,

a groundwater age can be calculated. Therefore, this stoichiometric dedolomitization model was used to calculate a ^{14}C groundwater age at selected groundwater wells along the A to A' cross-section.

For the purpose of modeling the evolution of Salt Basin groundwater along this cross-section, the Daugherty and Beech wells were not included in this analysis. The groundwater chemistry in these wells appears to be much more evolved than the preceding (SM-0085 and SM-0044) or following (Doll Day) wells along this flow path. The Daugherty and Beech wells may be on a shallower, more local groundwater flow path than the regional flow path modeled with this cross-section. In addition, Piñon Well and Hammock Well were not included in this analysis, because they were projected to the cross-section. However, Evrage House was included as the final well along this flow path, because it has the most evolved groundwater chemistry.

As mentioned above, the calculation of ^{14}C groundwater ages using the stoichiometric dedolomitization model relies on the evolution of HCO_3^- and Mg^{2+} concentration, as well as ^{14}C activity along the groundwater flow path. The groundwater data collected along the line of cross-section displays scatter and does not necessarily continuously evolve from sample point to sample point along the groundwater flow path. When discrete groundwater data are used in the stoichiometric dedolomitization model, the calculated ^{14}C groundwater ages sometimes get younger down the flow path. To yield a more consistent analysis, the evolution of the ^{14}C activity, and the HCO_3^- and Mg^{2+} concentrations measured in the groundwater wells along the cross-section, were modeled as continuous functions versus distance along the cross-section. (Figures 3.53, 3.54, and 3.55) The evolution of the ^{14}C activity was modeled with an exponential function, because ^{14}C decays exponentially, while the evolution of the HCO_3^- and Mg^{2+} concentrations were modeled using functions that produced the highest r^2 values; in this case linear functions.

However, ^{14}C data were not available for the initial wells along the flow path (SM-0085 and SM-0044). A good first approximation for the initial ^{14}C activity of groundwater in both humid and arid climatic regions has been shown to be 85 ± 5 pmC (Vogel, 1970). In addition, ^{14}C data from the Sacramento Mountains, as presented in Newton et al. (2009) and Morse (2010), support this range of initial ^{14}C activity. Therefore, the ^{14}C activity at the beginning of the flow path was set at 85 pmC for the continuous exponential model of the evolution of the ^{14}C activity measured in groundwater. (Figure 3.53)

The values from these continuous functions were then used in the stoichiometric dedolomitization model to calculate the change in ^{14}C activity along the flow path due only to dedolomitization, and finally to calculate the ^{14}C groundwater age. Figure 3.56 presents the continuous exponential model of the ^{14}C activity measured in groundwater (A), and the resultant ^{14}C activity calculated using the stoichiometric dedolomitization model (A_0) versus distance along the cross-section. These ^{14}C activities are also presented in Table 3.29, along with the HCO_3^- and Mg^{2+} concentrations from the linear trends and the calculated ^{14}C ages at each groundwater well along the cross-section. The initial ^{14}C activity ($^{14}C_i$) used in the stoichiometric dedolomitization model for the first groundwater well along the flow path (SM-0085) was taken from the continuous exponential model of the ^{14}C activity measured in groundwater. However, the subsequent initial ^{14}C activities ($^{14}C_i$) used in the stoichiometric dedolomitization model were those final ^{14}C activities ($^{14}C_f$) calculated from the stoichiometric dedolomitization model.

The use of this stoichiometric dedolomitization model to calculate the change in ^{14}C activity along the flow path due only to dedolomitization relies on the assumption

that there are no additional sources or sinks for carbon along the flow path. This assumption is justified, because, as discussed below in Chapter 3.6.c, the Salt Basin groundwater system is tightly confined. Therefore, there is likely very little addition of atmospheric carbon from recharge to the groundwater system along the flow path. Also, as discussed above, this model was applied to groundwater samples along a cross-section that follows a generalized flow path. Thus, there is likely very little convergence of groundwater from different flow paths, or divergence of groundwater to different flow paths along this cross-section. The only region where this assumption may not hold occurs near the Evrage House well, where hydraulic gradients suggest groundwater converges from the Guadalupe and Brokeoff Mountains to the east. (Figure 3.36) However, as mentioned above, the groundwater chemistry of the Evrage House well is the most evolved of any well along the cross-section, and its evolution also appears to be controlled by dedolomitization.

The seepage velocities over the intervals between successive wells along the cross-section were calculated by dividing the distance from well to well along the cross-section by the change in ^{14}C age between wells. The darcy velocity, or specific discharge, can by calculated by multiplying the seepage velocity by the formation porosity (n). Very little information is available on the porosity of the aquifer units in the Salt Basin. However, one oil-and-gas exploratory well (Yates Petroleum Corporation, One Tree Unit #2 [YPCOTU2]) along cross-section A to A' does have some wellsite core analysis porosity (n) and permeability (k) data for the lower portion of the Yeso Formation, the Abo Formation, the El Paso/Ellenburger Group, the Bliss Sandstone, and the Precambrian. (Figures 3.1 and 3.37, and Table 3.30) The Hydraulic conductivity (K)

values in Table 3.30 were calculated from the permeability data. In this well, the porosity of the Permian Yeso and Abo Formations ranges from 0 to 18.3%. Excluding the zero values of porosity for these strata, the porosity ranges from 0.1 to 18.3%, the average porosity is 6.57%, and the median porosity is 6.95%.

The hydraulic gradient for each interval was calculated using the hand-contoured groundwater surface and the distance between successive wells along the cross-section. (Figures 3.36 and 3.42) The hydraulic conductivity (K) for each interval was then calculated by dividing the darcy velocity by the hydraulic gradient. The average saturated thickness of the Permian units was also calculated for each interval along the cross-section using the available oil-and-gas exploratory well subsurface control. The average saturated thickness was then multiplied by the hydraulic conductivity to estimate the transmissivity (T) for each interval along the cross-section. Tables 3.31 and 3.32 present the range of hydraulic conductivity and transmissivity values, respectively, for each interval along the cross-section using the median porosity of 6.95%, the minimum porosity of 0.1%, and the maximum porosity of 18.3% obtained from the YPCOTU2 well. These values of hydraulic conductivity and transmissivity compare favorably to the published values presented in Tables A-3.27, A-3.28, and 3.30 for Permian shelf-facies rocks in the Salt Basin. Figures 3.57 and 3.58 graphically compare the published range of hydraulic conductivity and transmissivity values with the range of values calculated from this analysis.

The large range of hydraulic conductivity and transmissivity values presented in Figures 3.57 and 3.58 are the result of the large range of porosities (0.1 to 18.3%) used to calculate them. A more reasonable estimate of formation-scale porosities would range

from 8 to 15%. The range of hydraulic conductivity and transmissivity values that result from these more reasonable porosity values are highlighted in Figures 3.57 and 3.58.

3.6.c: Estimates of Storage Coefficient Based on the Northward Propagation of a Periodic Pumping Signal from Dell City, Texas

Huff and Chace (2006) presented continuous water level measurements for a three-and-a-half year time period from 2003 to the middle of 2006 from four groundwater wells in the New Mexico portion of the Salt Basin watershed. (Figure 3.59) All four wells show seasonal water level fluctuations that are associated with irrigation pumping near Dell City, Texas during the summer, and an overall decline in water levels from 2003 to the middle of 2006. The data in Huff and Chace (2006) was presented in the form of groundwater level change versus time, and was reproduced for this study [Figure 3.60] using a free computer software known as Plot Digitizer 2.4.1.

The wells range from 8.22 to 47.48 km (5.11 to 29.50 miles) north of Dell City, Texas. The closest well [H&C 1] is 8.22 km (5.11 miles) north of Dell City, the next closest [H&C 2] is 24.59 km (15.28 miles) north-northwest of Dell City, the next closest [H&C 3] is 28.92 km (17.97 miles) north-northeast of Dell City, and the farthest [H&C 4] is 47.48 km (29.50 miles) north of Dell City. The amplitude of the periodic water level fluctuations associated with pumping becomes more attenuated with increasing distance from Dell City. There is also an increasing phase lag in the arrival time of the periodic water level fluctuation signal with increasing distance from Dell City.

The TWDB has one well in the Dell City region with continuous water level measurements for this same time period. State well number 4807516 began daily water level measurements in 2003, and increased to hourly water level measurements in 2006.

When the water level change in 4807516, relative to the first water level measurement made in 2003 on January 15th, versus time is plotted along with the above data [Figure 3.61] it is apparent that the periodic signal at Dell City, Texas is lagged behind the other signals to the north. In theory, the other periodic signals farther away from the periodic forcing at Dell City should be lagged behind the periodic signal at Dell City. There is no hydrologic explanation for the lag of the periodic signal in 4807516 behind the wells to the north. Therefore, well 4807516 was not included in the analysis of the phase lag of the periodic water level fluctuation signal.

The attenuation of the amplitude and the phase lag of the periodic water level fluctuations with increasing distance from Dell City, Texas were analyzed using an analytical solution to a one-dimensional form of the diffusion equation as presented in Ferris (1963):

$$\frac{\partial^2 s}{\partial x^2} = \left(\frac{S}{T}\right)\frac{\partial s}{\partial t}, \qquad [3]$$

where

    s = Water elevation (L),

    x = Distance (L),

    t = Time (t),

    S = Storage coefficient of aquifer (-), and

    T = Transmissivity of aquifer (L^2/t).

Ferris (1963) assumes that the aquifer is homogeneous, has a uniform thickness, and has a great lateral extent in the direction perpendicular to the source of the cyclic water level fluctuations. Further, Ferris (1963) assumes that the change in water storage within the aquifer responds instantaneously with, and at a rate proportional to, the change in

pressure associated with the cyclic water level fluctuations. With the following boundary condition at x = 0:

$$s\,(0,t) = s_0 \sin\left(\omega t_0\right), \quad [4]$$

where

s_0 = Amplitude of fluctuation at x = 0 (L),

ω = Angular frequency = $\dfrac{2\pi}{t_0}$ (t^{-1}), and

t_0 = Period of fluctuation (t),

the solution is:

$$s\,(x,t) = s_0\left[\exp\left(-x\sqrt{\frac{\pi S}{t_0 T}}\right)\right]\sin\left[\left(\frac{2\pi\pi}{t_0}\right) - \left(x\sqrt{\frac{\pi S}{t_0 T}}\right)\right]. \quad [5]$$

The first part of [5] describes the exponential decay of the amplitude of a periodic signal with increasing distance from a periodic forcing, while the second part describes the increasing phase lag in a periodic signal with increasing distance from a periodic forcing. The first part of [5] was used to analyze the attenuation of the amplitude of the periodic water level fluctuations with increasing distance from Dell City:

$$s_T = s_0\left[\exp\left(-x\sqrt{\frac{\pi S}{t_0 T}}\right)\right], \quad [6]$$

where, in terminology adapted to the given problem,

s_T = Amplitude of water level fluctuation at some distance from forcing (L),

s_0 = Amplitude of water level fluctuation of forcing (L),

x = Distance from forcing (L), and

t_0 = Period of water level fluctuation of forcing (t).

Solving for S/T:

$$\frac{S}{T} = \frac{\left[\ln\left(s_T/s_0\right)\right]^2 t_0}{\pi x^2}. \quad [7]$$

In [6] and [7], state well 4807516 was taken as the forcing, because it is the closest well to Dell City. The average annual amplitude of the periodic water level fluctuation was calculated for each well. For wells H&C 1 to 3 and 4807516, the average annual amplitude was calculated directly from Figure 3.61 by picking out the peaks (maximum groundwater level change) and troughs (minimum groundwater level change) of each curve. (Figure 3.62) Well H&C 4 displays a much less distinct seasonal water level fluctuation, but a distinct decreasing trend in groundwater level over its period of record from 2004 to 2006. In order to include this well in the analysis, a linear trend was fit to the data [Figure 3.63], the data was detrended [Figure 3.64], and this detrended data was used to calculate the average annual amplitude of the water level fluctuation in well H&C 4. The locations of the maximum and minimum detrended groundwater level change for well H&C 4 are also displayed in Figure 3.64. These values were then inserted into [7] to calculate S/T for each year using only the data from well 4807516 and one of the Huff and Chace (2006) wells to the north. The results are presented in Tables 3.33, 3.34, and 3.35.

A more robust method was employed which involved calculating s_T/s_0 from the average annual amplitude of the water level fluctuation for each well pair (4807516 and H&C 1 to 4) for each year (2003, 2004, or 2005). The values of s_T/s_0 for each well pair were then plotted versus distance of the Huff and Chace (2006) well from Dell City, Texas for each year. (Figure 3.65) These yearly trends were fit with exponential

functions, and the value inside the exponential was used to calculate S/T using a variation of [6]:

$$\frac{s_T}{s_0} = \exp\left(-x\sqrt{\frac{\pi S}{t_0 T}}\right) . \quad [8]$$

The values of S/T for each year calculated from this method, along with the values of s_T/s_0 for each year, are presented in Table 3.36. This method assumes that the Huff and Chace (2006) wells fall along a single line that projects outward from Dell City, Texas.

The increasing phase lag in the arrival time of the periodic water level fluctuation signal with increasing distance from Dell City, Texas was analyzed using:

$$t_L = x\sqrt{\frac{t_0 S}{4\pi\pi}} , \quad [9]$$

from Ferris (1963), where

t_L = Lag in time of the occurrence of a given maximum or minimum in the water level fluctuation (t).

Solving for S/T:

$$\frac{S}{T} = \frac{t_L^2 4\pi}{x^2 t_0} . \quad [10]$$

The slope of the line defined by plotting values of phase lag versus distance from the periodic forcing can be used to solve [10] for S/T.

The phase lag between the maximum and minimum values of groundwater level change in wells H&C 1, 2, 3, and 4 was calculated using the points indicated in Figure 3.62. As discussed above, state well 4807516 was not included in this analysis. Instead, the phase lag was calculated between well H&C 1 and the other wells farther to the north. The average phase lag between the maximum and minimum values of groundwater level

change in well H&C 1 and wells H&C 2 and 3 was calculated for each year (2003, 2004, and 2005). As mentioned above, no groundwater level change data was available for well H&C 4 for 2003. Therefore, the average phase lag between the maximum and minimum values of groundwater level change in well H&C 1 and well H&C 4 was calculated for 2004 and 2005 only.

The average phase lag between well H&C 1 and wells H&C 2 and 3 in 2003, and well H&C 1 and wells H&C 2, 3, and 4 in 2004 and 2005 was plotted versus the distance of each well from well H&C 1. (Figure 3.66) Values of S/T were calculated from the slope of the best fit line through the phase lag data for each year. The average annual phase lag between each well pair (H&C 1 and H&C 2 to 4) for each year (2003, 2004, or 2005), along with the values of S/T calculated from this method, are presented in Table 3.37.

The values of S/T presented in Tables 3.36 and 3.37 were multiplied by the median, minimum, and maximum values of transmissivity estimated from the stoichiometric dedolomitization model presented in Chapter 3.5.b to calculate a range of S values. The range of S values calculated fall within the typical range reported for confined aquifers (Schwartz and Zhang, 2003). (Figure 3.67) The range of S values also compares favorably to the value of S presented by Wasiolek (1991), and the range of S values reported for confined, predominantly carbonate aquifers in west Texas and southeast Oklahoma (Ryder, 1996), and western South Dakota (Greene, 1993). (Figure 3.67) Tables 3.38 through 3.40 summarize the range of S values calculated from the above analyses and reported in the scientific literature. Figure 3.67 graphically compares the published range of S values with the range of values calculated from these analyses.

The range of S values that were obtained using the range of transmissivities calculated from the more reasonable estimate of formation-scale porosities are highlighted in Figure 3.67.

The propagation of the seasonal pumping signal up to 47.48 km (29.50 miles) away from Dell City, and the above analyses indicates that the basin-floor Salt Basin aquifer system is tightly confined. Hydrogeologic cross-sections compiled for this study indicate that the groundwater surface is primarily within the Yeso Formation, especially in the central portion of the northern Salt Basin watershed. As discussed above in Chapter 3.5.a, in the southern Sacramento Mountains groundwater also is primarily found in the Yeso Formation (Newton et al., 2009). Groundwater flows at several different stratigraphic levels within the Yeso Formation, locally as shallow, unconfined, perched aquifers above a deeper, locally confined, regional aquifer (Newton et al., 2009). It is probable that a similar situation exists in the Salt Basin, as groundwater flows from the high mountain aquifer system in the Sacramento Mountains to the Salt Basin aquifer system. The abundant claystone reported in the upper portion of the Yeso Formation from driller's logs in the Sacramento Mountains may act as confining beds within the Salt Basin aquifer system (Newton et al., 2009; Wasiolek, 1991).

Confined conditions within the Yeso Formation are also suggested by numerous oil-and-gas exploratory well records and groundwater well driller's logs, which note the subsequent rise of the groundwater surface in the hole from the level at which it was first encountered in the Yeso. A total of 17 driller's logs are available for groundwater wells in the Salt Basin from the NMOSE's NMWRRS database, most of which are for wells in and around the town of Timberon, New Mexico. In general, these logs contain very

minimal descriptions of the rocks encountered, often just consisting of a color and a single word descriptor (e.g. limestone, sandstone, siltstone, shale, clay, etc.). These logs indicate the presence of groundwater in primarily fractured carbonate rocks, and to a lesser extent sandstone and siltstone beds, within the Yeso Formation, fractured carbonate rocks of the San Andres Formation, and alluvium filling ephemeral drainages.

FIGURES – CHAPTER 3

Figure 3.1: Structural zones/blocks used in 3-D hydrogeologic framework model. Black circles indicate the location of all oil-and-gas exploratory wells used in this study as control on the subsurface geology. Oil-and-gas exploratory well key on next page.

Figure 3.1: Key

#	Well ID	#	Well ID	#	Well ID	#	Well ID
1	HO&MSL1	48	TO&GFB1	95	GDP61-6	142	COUL462
2	HO&MJL1	49	ARCSAV1	96	GDP45-5	143	JMHCTP1
3	HO&MCL2	50	ZPCF141	97	GDP46-6	144	EOGSR47
4	HO&MFA1	51	SOCTJP1	98	HUOCMT1	145	A&PBOR1
5	LAHTHO1	52	TRBCU1Y	99	HEYBRU1	146	TMUODL1
6	HO&MS31	53	SO&GTU1	100	SEOCTF1	147	PHMTS27
7	MCOCFH1	54	SOTSCU1	101	GDP51-8	148	FMINWW1
8	MCOCGB1	55	LEPCFE1	102	EPCSPF1	149	AQPVCR1
9	HO&RYF1	56	YPCBIOF	103	SO&GGR1	150	HHUM491
10	JCTSA61	57	TSDLDF1	104	HEYBR25	151	EOGWHD7
11	LM&SAR1	58	OTOCMC1	105	HPCCL51	152	PAPPFH1
12	HO&RHY1	59	BRCFEA1	106	TSTFO31	153	COMT105
13	WHBDCS1	60	COCHWB1	107	CODFRS1	154	TO36MSA
14	COCSNN1	61	MOCBCU1	108	MPCUTL1	155	EPCN1MO
15	JCTFA28	62	PIECF91	109	EOGRC24	156	GOCMAG1
16	C&KSLS1	63	SO&GFE1	110	PAPCLA1	157	HAHUTM1
17	SPCCLU1	64	EPCAHU1	111	BONCOPI	158	LR&BGM1/ WSOG&M1
18	YPCDNU1	65	TLISTE1	112	PUOCHU1		
19	YPCDDU2	66	FTUEVE1	113	HUOCDY1	159	COSS701
20	YPCDDU1	67	EPCALI1	114	HUBAUN1	160	SINCLOO
21	SE&PJT1	68	WRWETH1	115	TMUBIC1	161	GOCJBS1
22	C&KLCS1	69	EPCALS1	116	HPCCLR1	162	LOBG&M1
23	LO&GTLW	70	PRIICF1	117	TEXCLF1	163	SOGAL1R
24	MAGHEF2	71	EPCAMF1	118	TOTXLF1	164	H&GJSP1
25	YPCLCU1	72	HO&RHO2	119	PAPCEH1	165	FADWAD1
26	SOCSAV1	73	CO&GCW1	120	TMUSD51		
27	WHIBHU1	74	IOCSBU1	121	TXLCCF1		
28	YPCLCU2	75	CO&GAS1	122	GCOCMV1		
29	MAGBLHI	76	ARCHUU9	123	MPNA1HC		
30	GOCCSU1	77	SOCLCD1	124	EOGKS1H		
31	TEXIFE1	78	UNOCFW1	125	EOGKES2		
32	YPCOTU1	79	HO&RHU5	126	CASATT1		
33	YPCDCF1	80	TDCR21F	127	DJJCHJ2		
34	TO&GFC1	81	FTUJEV1	128	TMUFD27		
35	KOCFMU1	82	EPCAFE1	129	BECHCT1		
36	TEXIFF1	83	FWYDON1	130	TXLCBT1		
37	YPCOTU2	84	FA&FTD1	131	ARJECM1		
38	TEXIFG1	85	UNOCMC1	132	TCST1BS		
39	MOCMVR1	86	UOCV7F1	133	JLCECM1		
40	YPCBAYU	87	WWWWDC1	134	BECJJM1		
41	TO&GFA1	88	TROGJA1	135	TERCMO2		
42	YPCBAVW	89	RHELLC1	136	TSOCCS1		
43	SOCPIU2	90	TDM28F1	137	COIDM3S		
44	SOCPIU1	91	BOCRUS1	138	TMUDWL5		
45	UVILCU1	92	PCS28S1	139	SALSUL2		
46	GOCFMU1	93	FTUJST1	140	HORMCS1		
47	PLOCEV1	94	EJDALF1	141	NARIPO1		

Figure 3.2: Land surface expression of the 3-D hydrogeologic framework solid model. Color-coding of hydrogeologic units corresponds to that used in Figure 2.1. Purple line indicates northern Salt Basin watershed boundary. Red line designates groundwater flow model boundary.

Figure 3.3: Elevation of the top of the Precambrian.
Elevations are in meters relative to mean sea level. Contour interval is 500 meters (1,640 feet). Black circles indicate the oil-and-gas exploratory wells used as control for the unit.

Figure 3.4: Elevation of the top of the Cambrian through the Silurian.
Elevations are in meters relative to mean sea level. Contour interval is 500 meters (1,640 feet). Black circles indicate the oil-and-gas exploratory wells used as control for the unit.
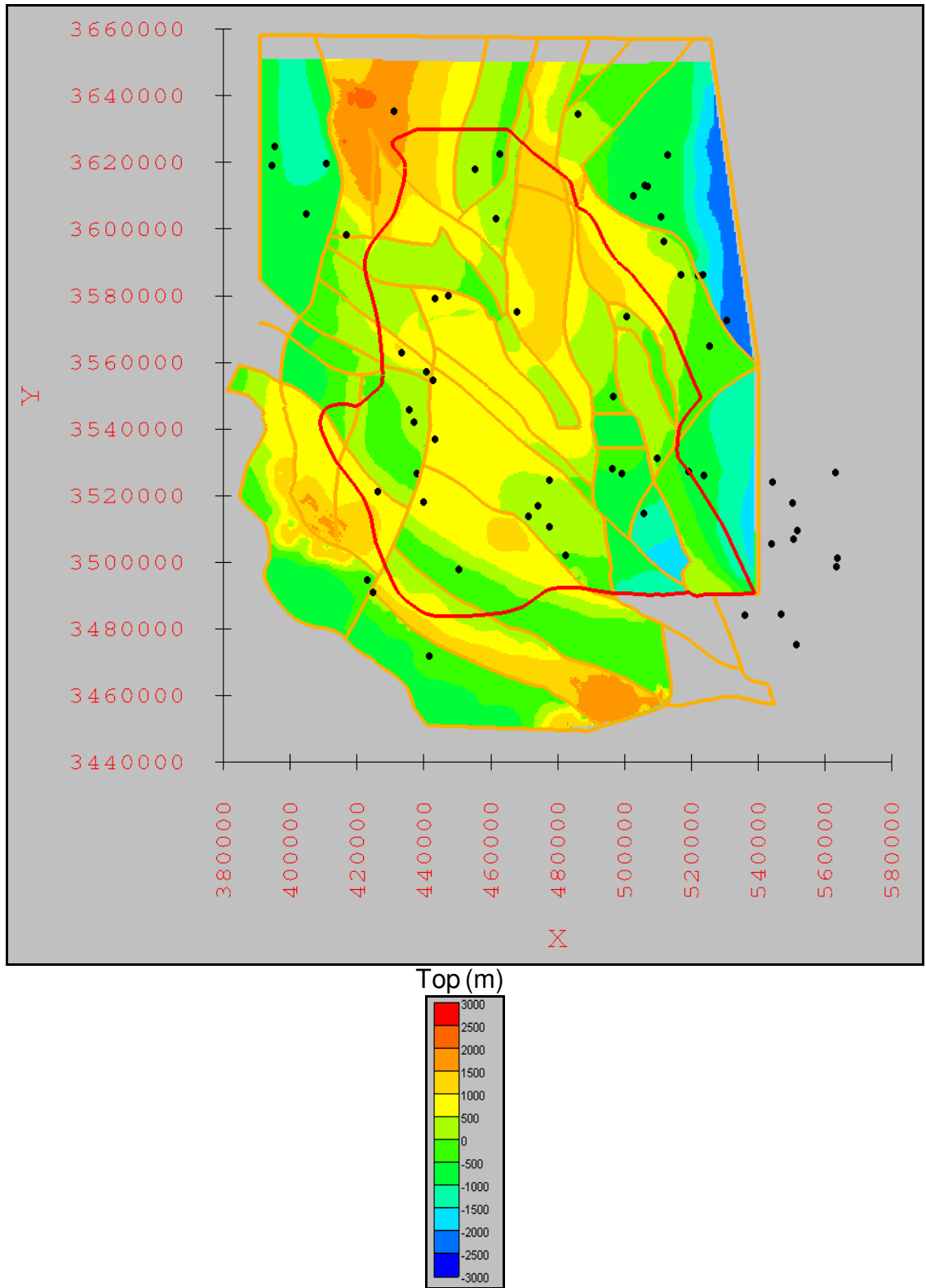
Figure 3.5: Elevation of the top of the Devonian.
Elevations are in meters relative to mean sea level. Contour interval is 500 meters (1,640 feet). Black circles indicate the oil-and-gas exploratory wells used as control for the unit.
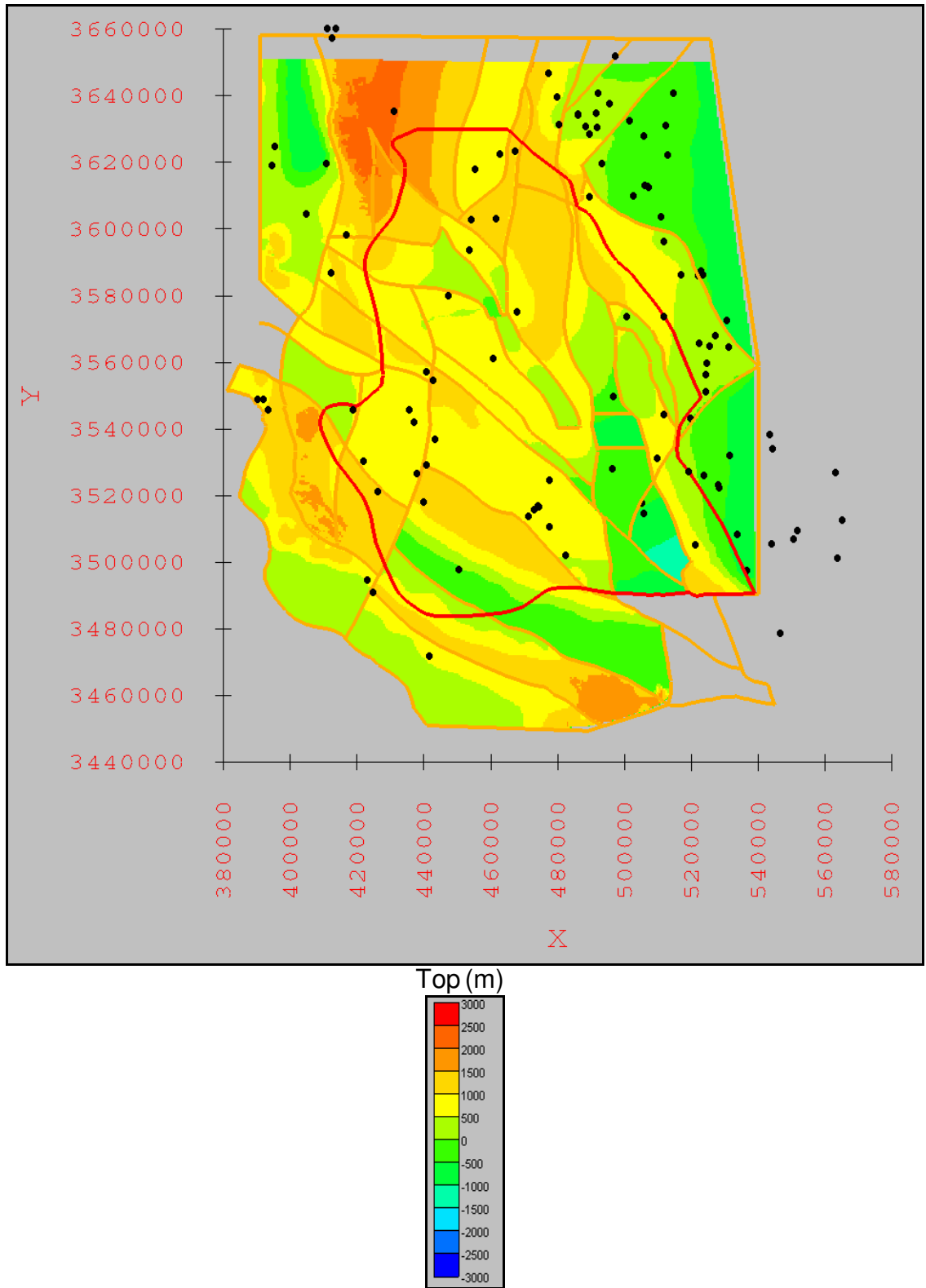
Figure 3.6: Elevation of the top of the Mississippian through the Pennsylvanian. Elevations are in meters relative to mean sea level. Contour interval is 500 meters (1,640 feet). Black circles indicate the oil-and-gas exploratory wells used as control for the unit.
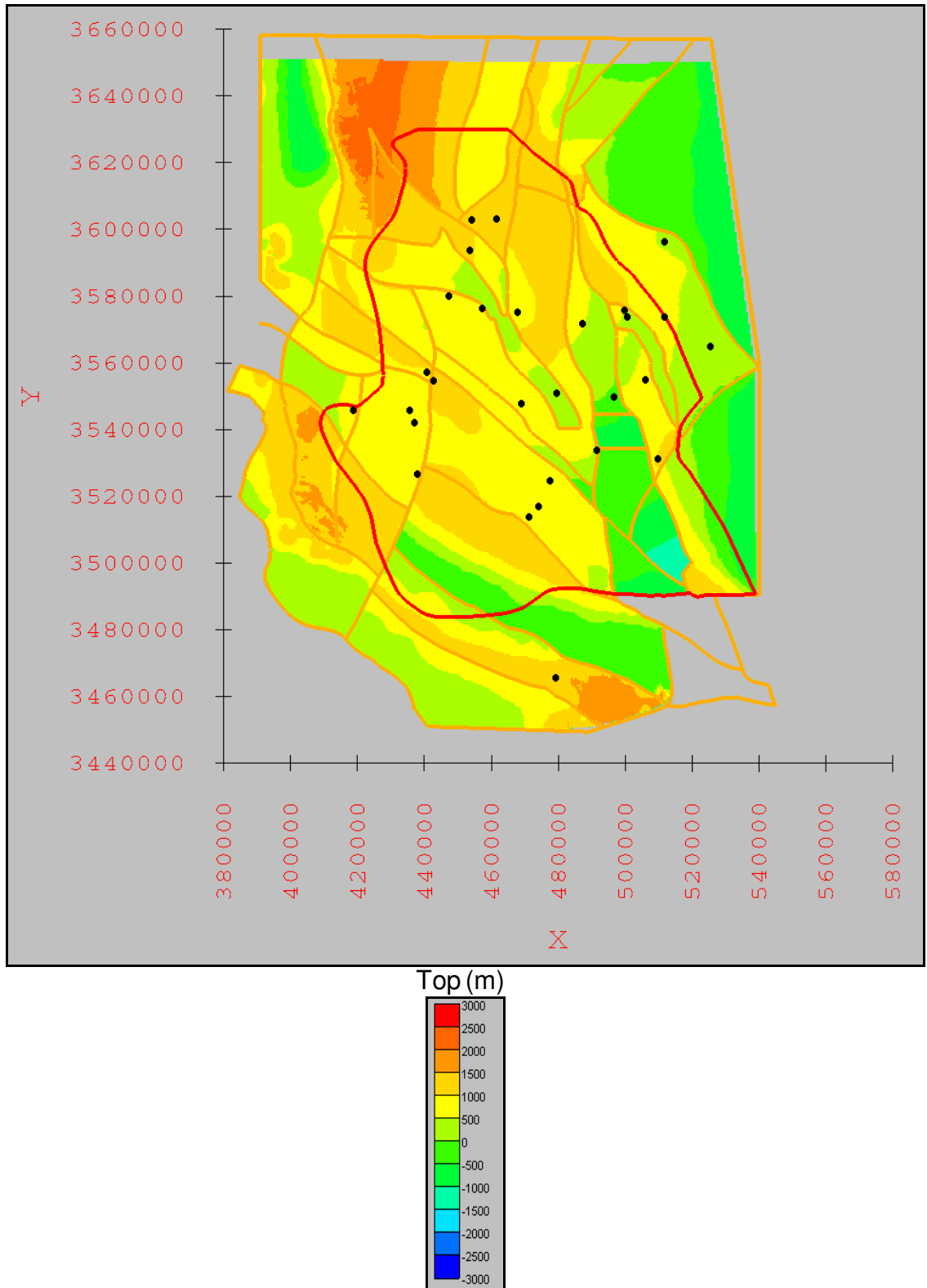
Figure 3.7: Elevation of the top of Lower Abo/Pow Wow Conglomerate. Elevations are in meters relative to mean sea level. Contour interval is 500 meters (1,640 feet). Black circles indicate the oil-and-gas exploratory wells used as control for the unit.
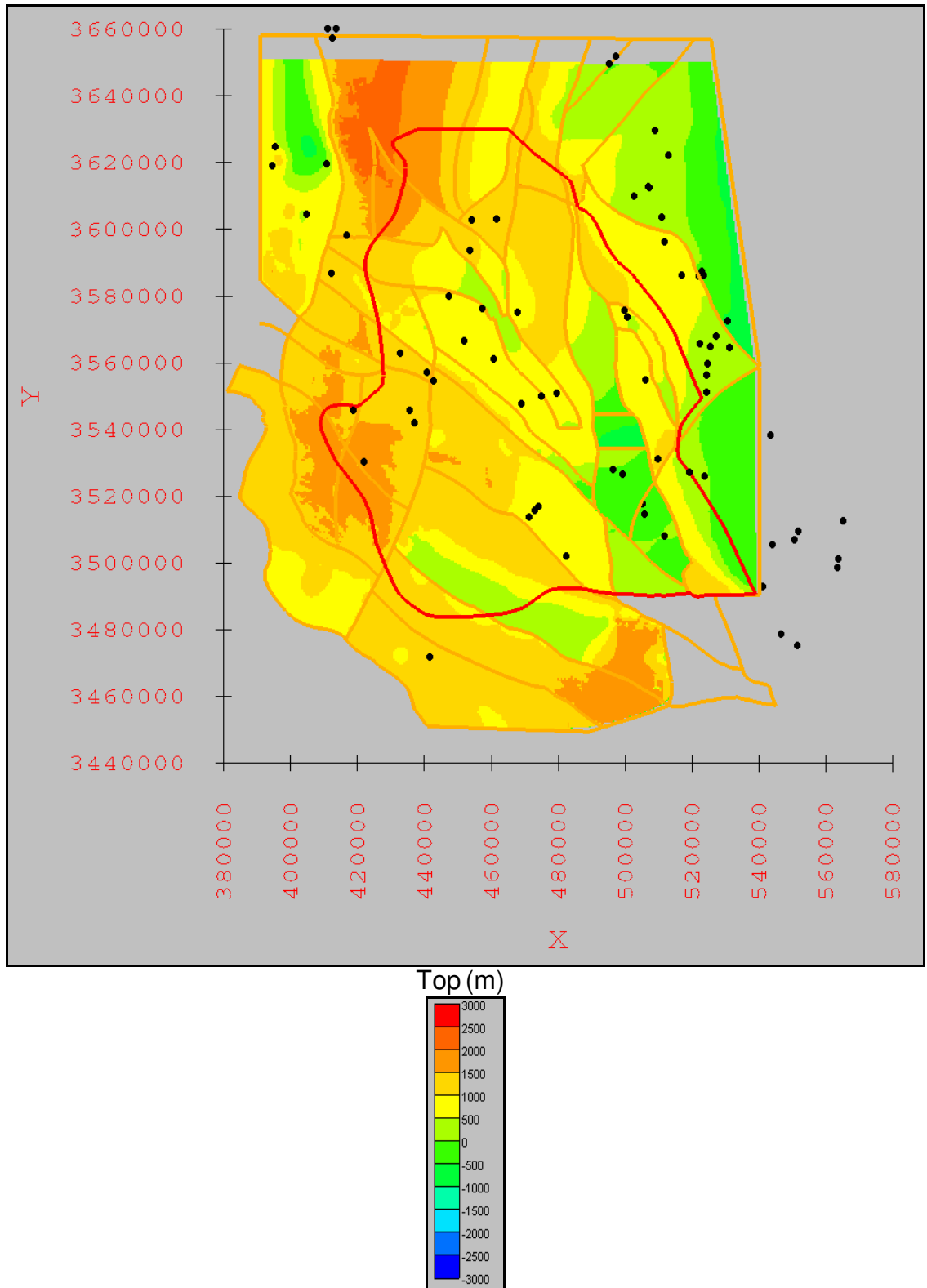
Figure 3.8: Elevation of the top of Hueco Limestone/Formation (or Bursum Formation) and Wolfcamp Formation.
Elevations are in meters relative to mean sea level. Contour interval is 500 meters (1,640 feet). Black circles indicate the oil-and-gas exploratory wells used as control for the unit.
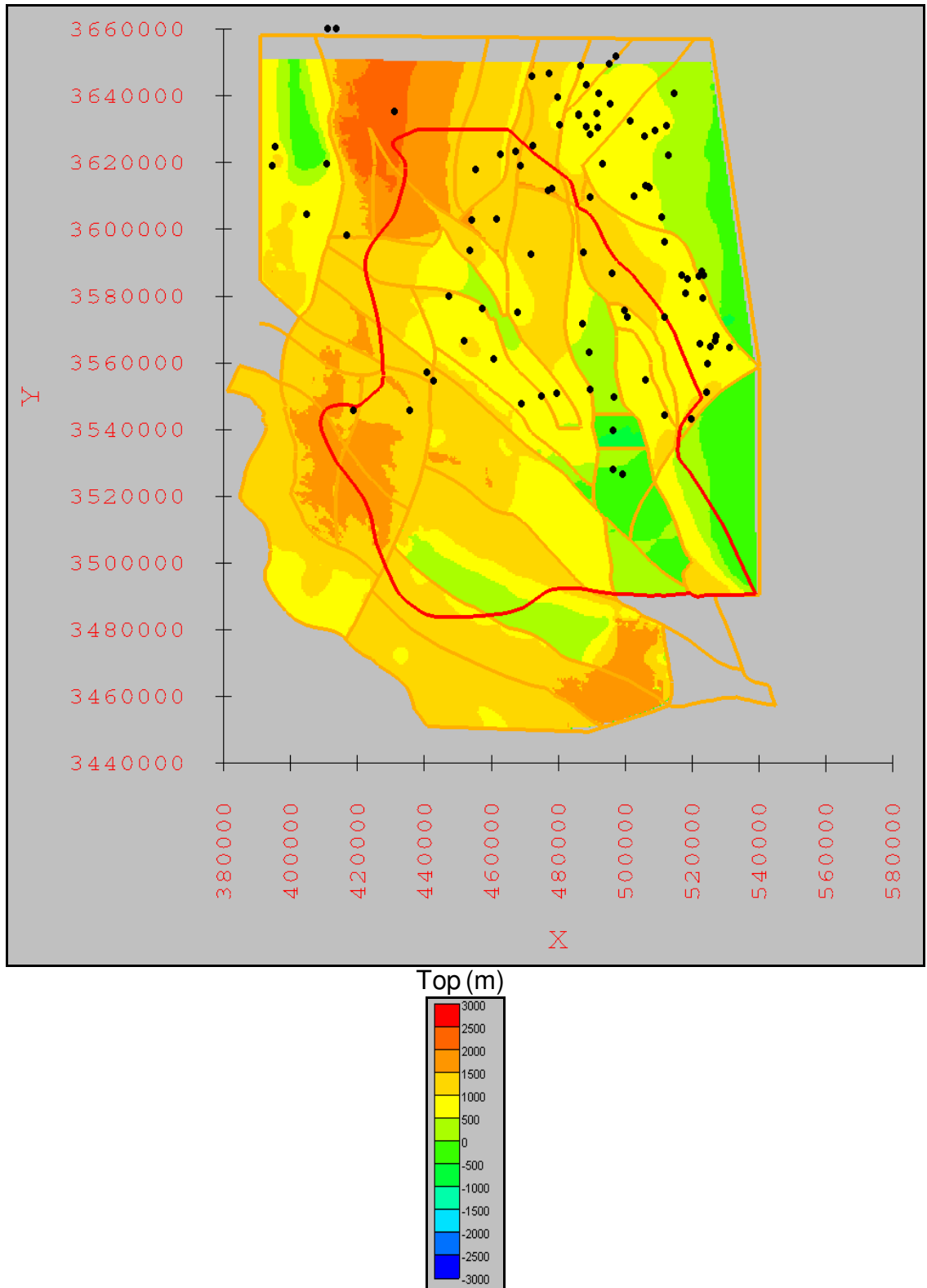
Figure 3.9: Elevation of the top of Abo Formation.
Elevations are in meters relative to mean sea level. Contour interval is 500 meters (1,640 feet). Black circles indicate the oil-and-gas exploratory wells used as control for the unit.
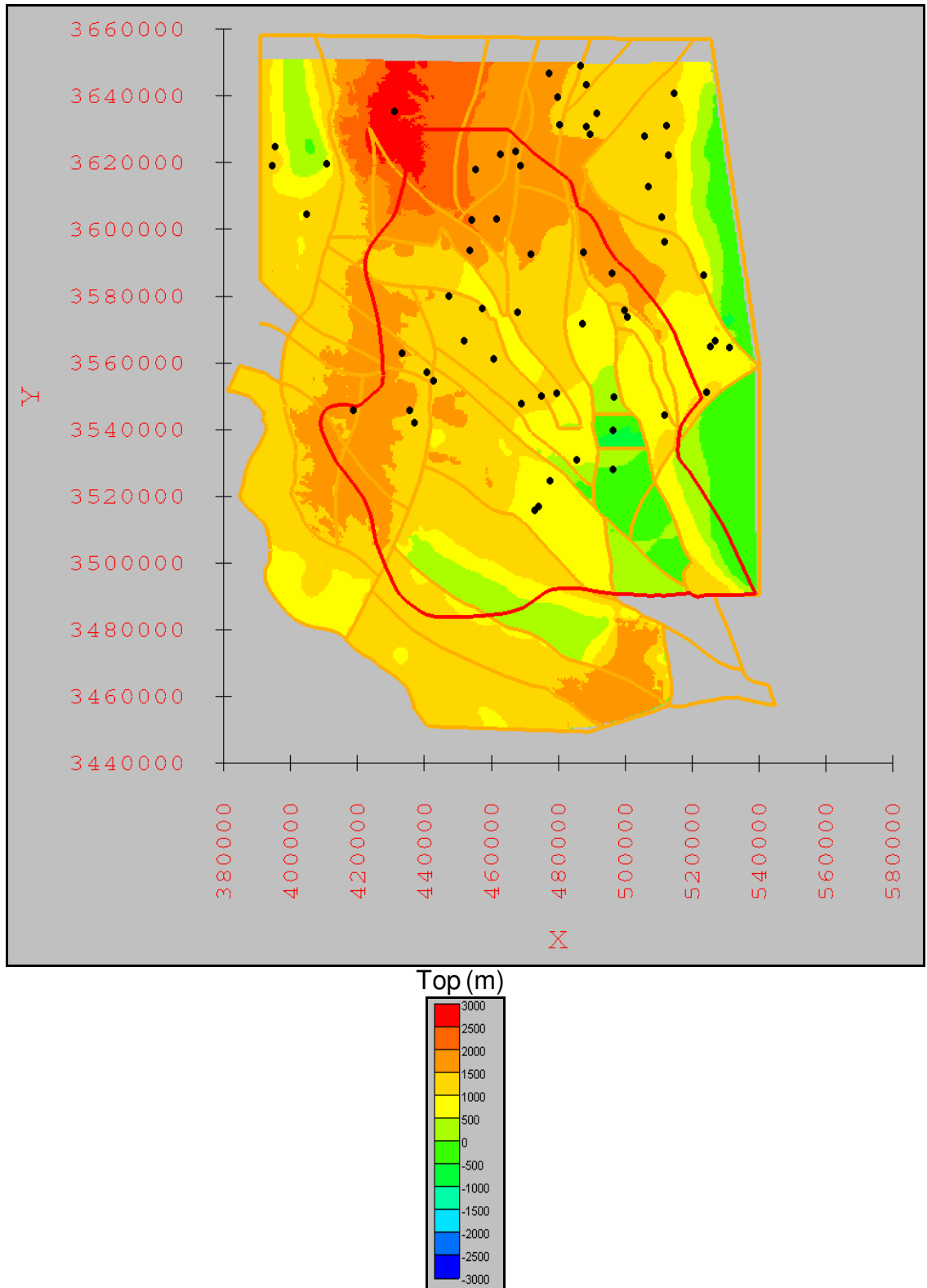
Figure 3.10: Elevation of the top of Yeso Formation.
Elevations are in meters relative to mean sea level. Contour interval is 500 meters (1,640 feet). Black circles indicate the oil-and-gas exploratory wells used as control for the unit.
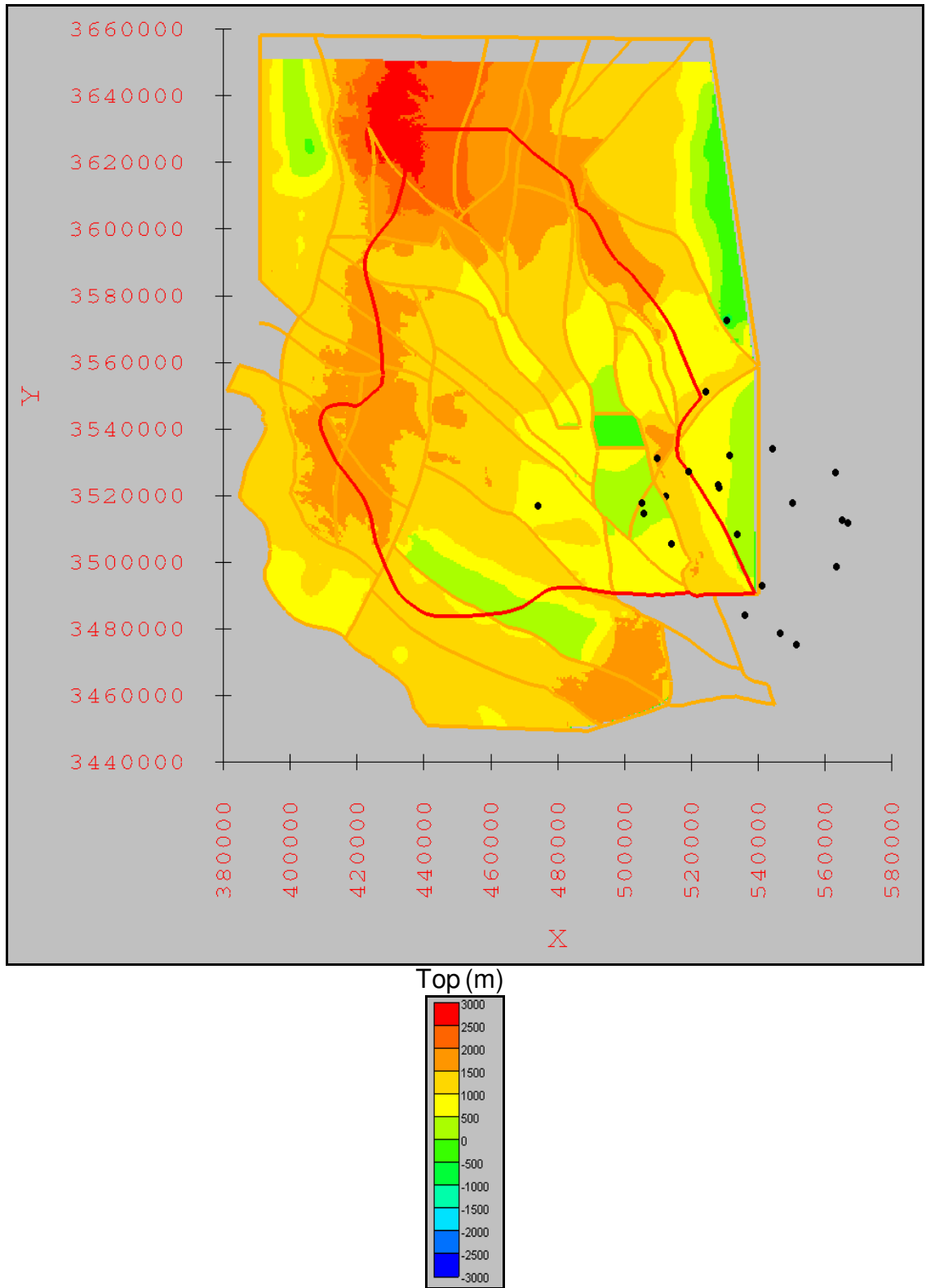
Figure 3.11: Elevation of the top of Bone Spring Limestone/Formation.
Elevations are in meters relative to mean sea level. Contour interval is 500 meters (1,640 feet). Black circles indicate the oil-and-gas exploratory wells used as control for the unit.

Top (m)
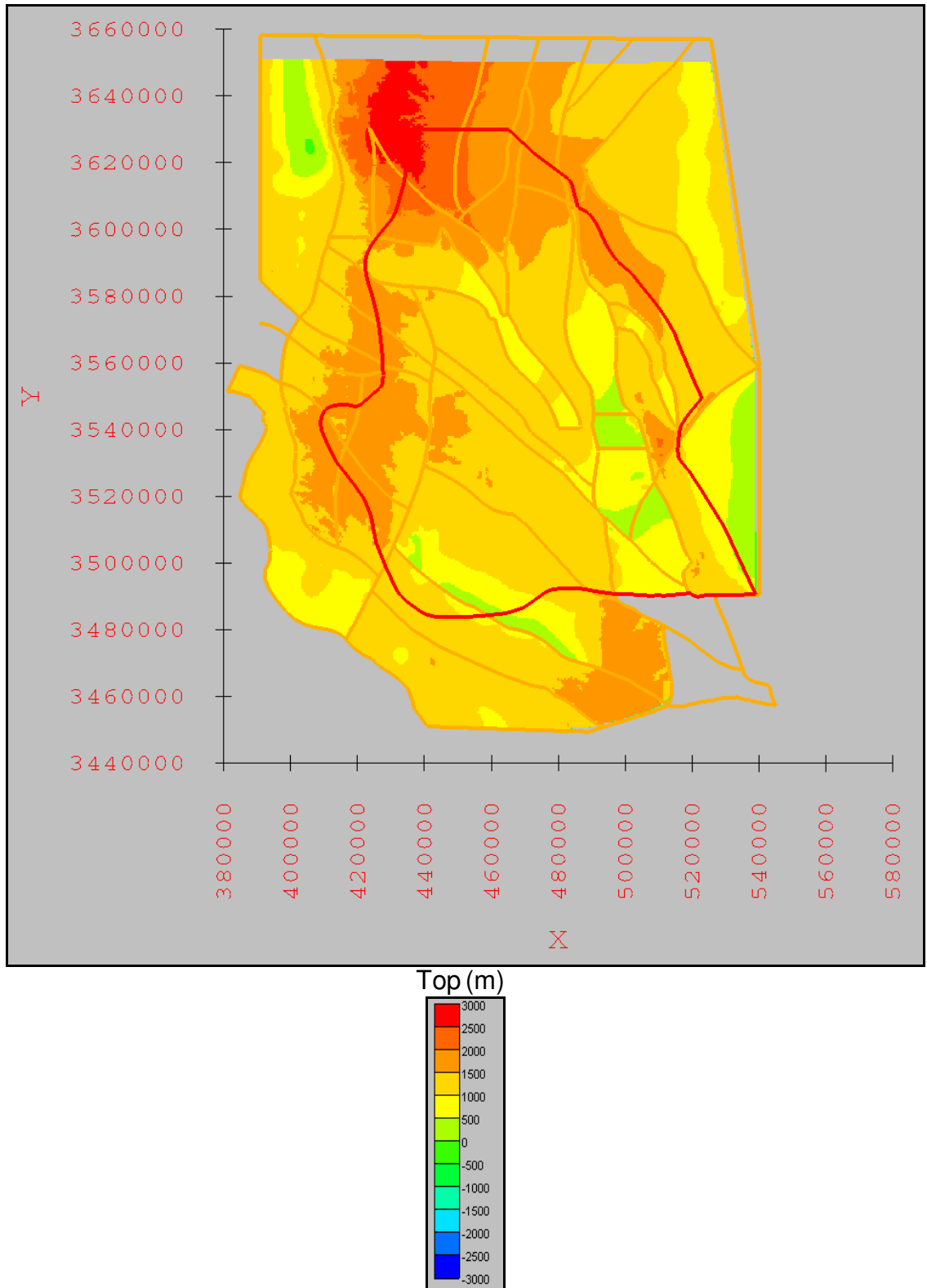
Figure 3.12: Elevation of the top of Victorio Peak Limestone/Formation and Cutoff Shale and Wilke Ranch Formation.
Elevations are in meters relative to mean sea level. Contour interval is 500 meters (1,640 feet). Black circles indicate the oil-and-gas exploratory wells used as control for the unit.
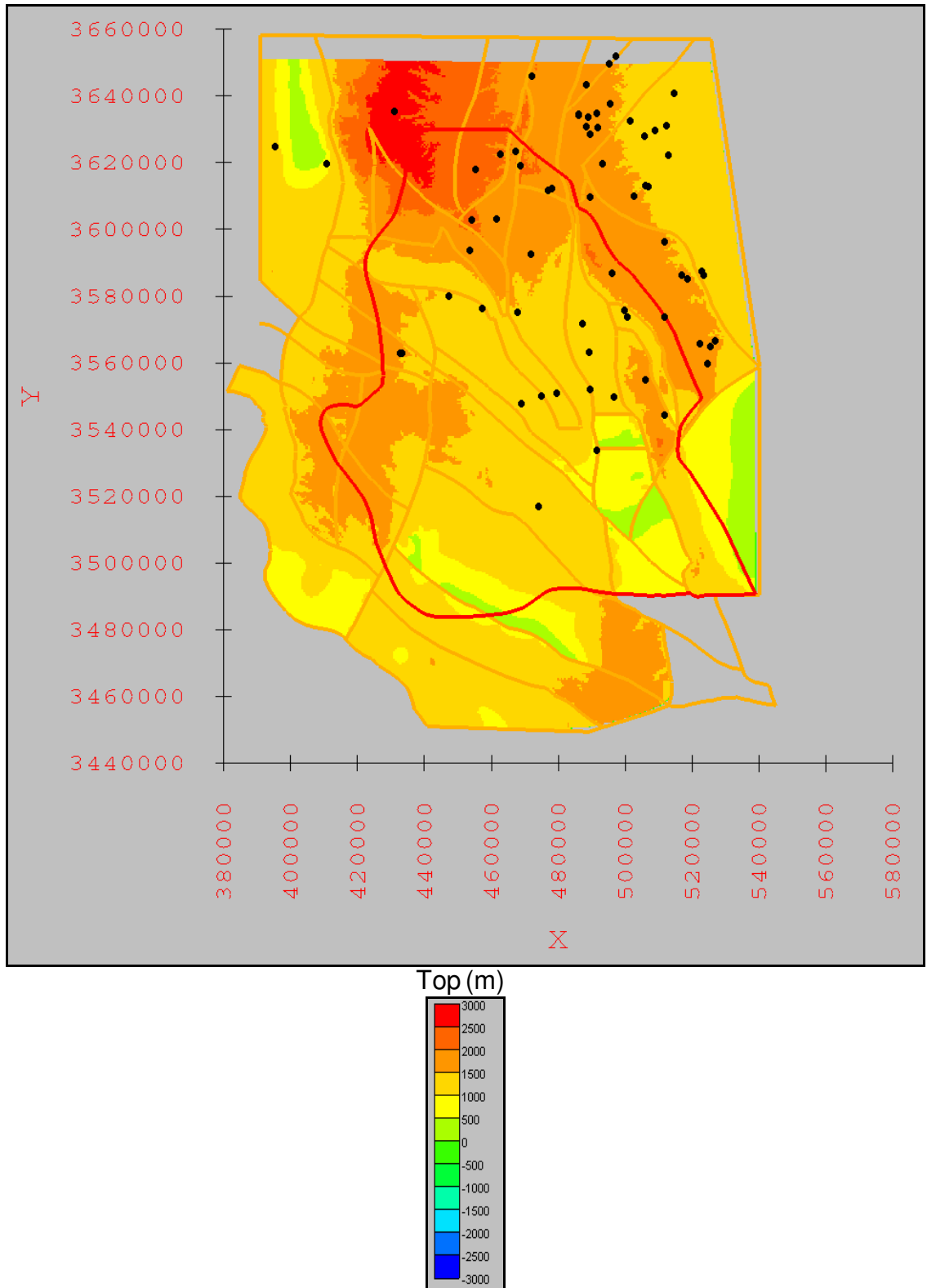
Figure 3.13: Elevation of the top of San Andres Formation.
Elevations are in meters relative to mean sea level. Contour interval is 500 meters (1,640 feet). Black circles indicate the oil-and-gas exploratory wells used as control for the unit.
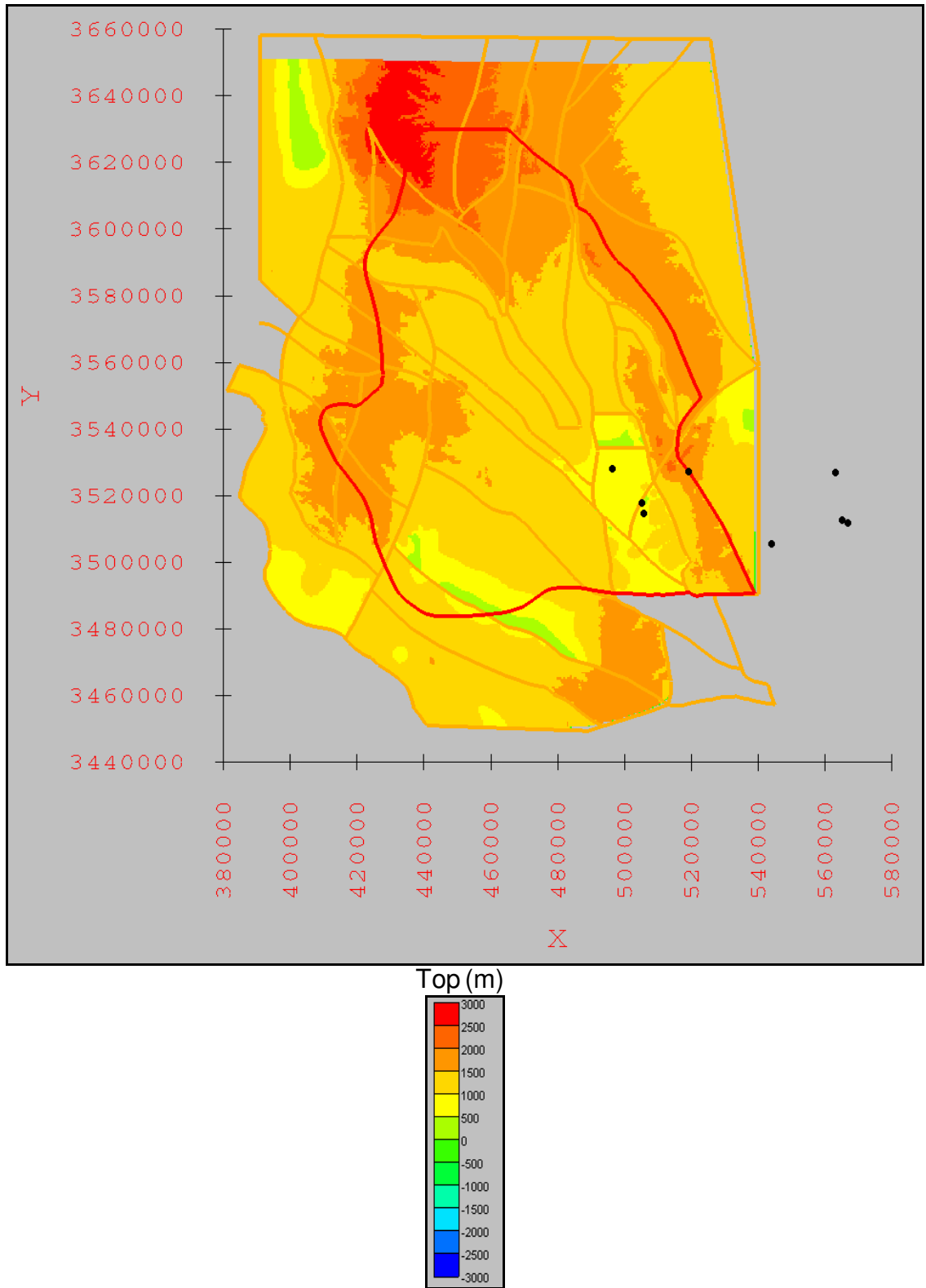
Figure 3.14: Elevation of the top of Delaware Mountain Group.
Elevations are in meters relative to mean sea level. Contour interval is 500 meters (1,640 feet). Black circles indicate the oil-and-gas exploratory wells used as control for the unit.
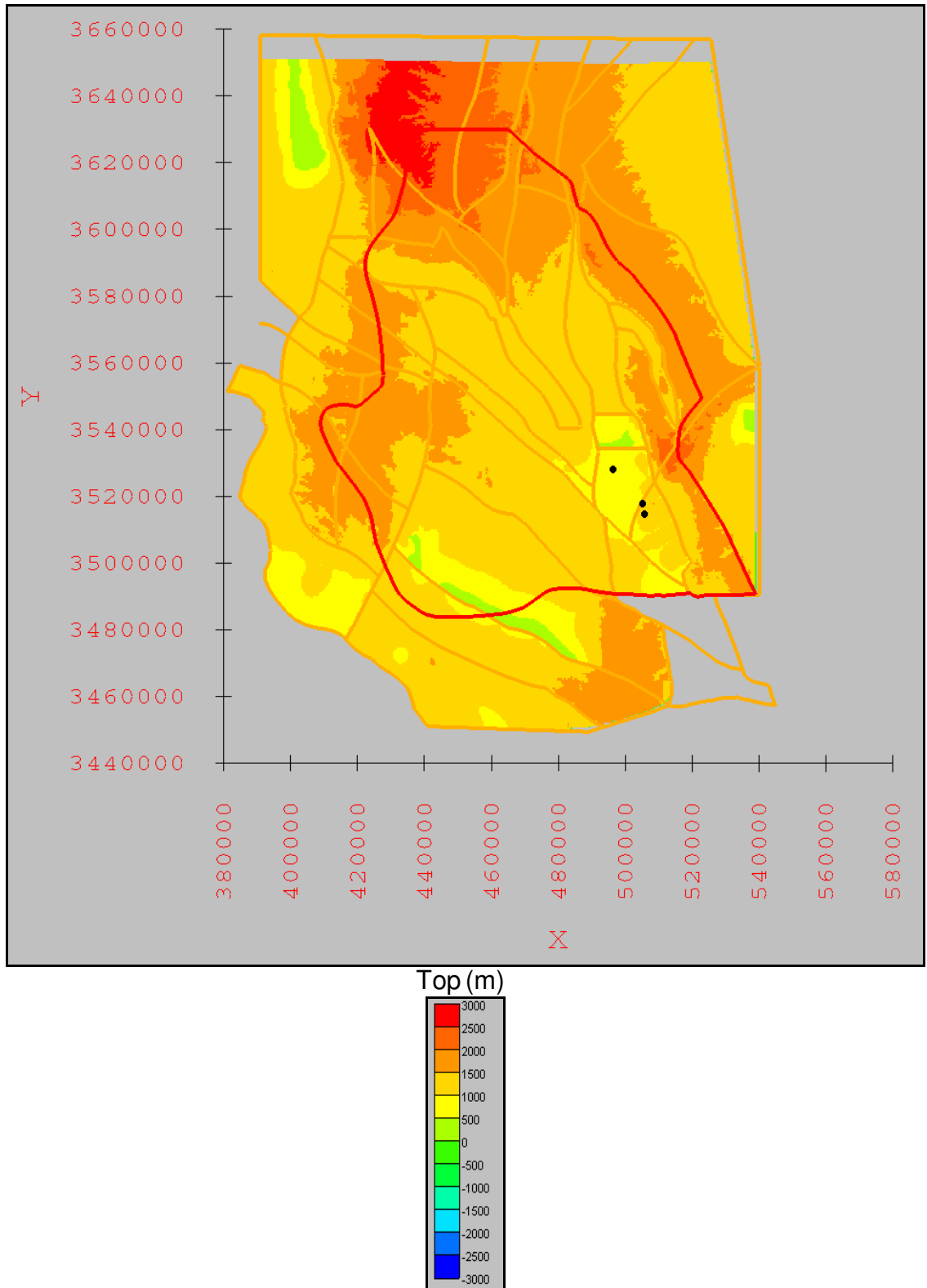
Figure 3.15: Elevation of the top of Goat Seep Dolomite/Limestone/Formation and
Capitan Limestone/Formation.

Elevations are in meters relative to mean sea level. Contour interval is 500 meters (1,640
feet). Black circles indicate the oil-and-gas exploratory wells used as control for the unit.

212
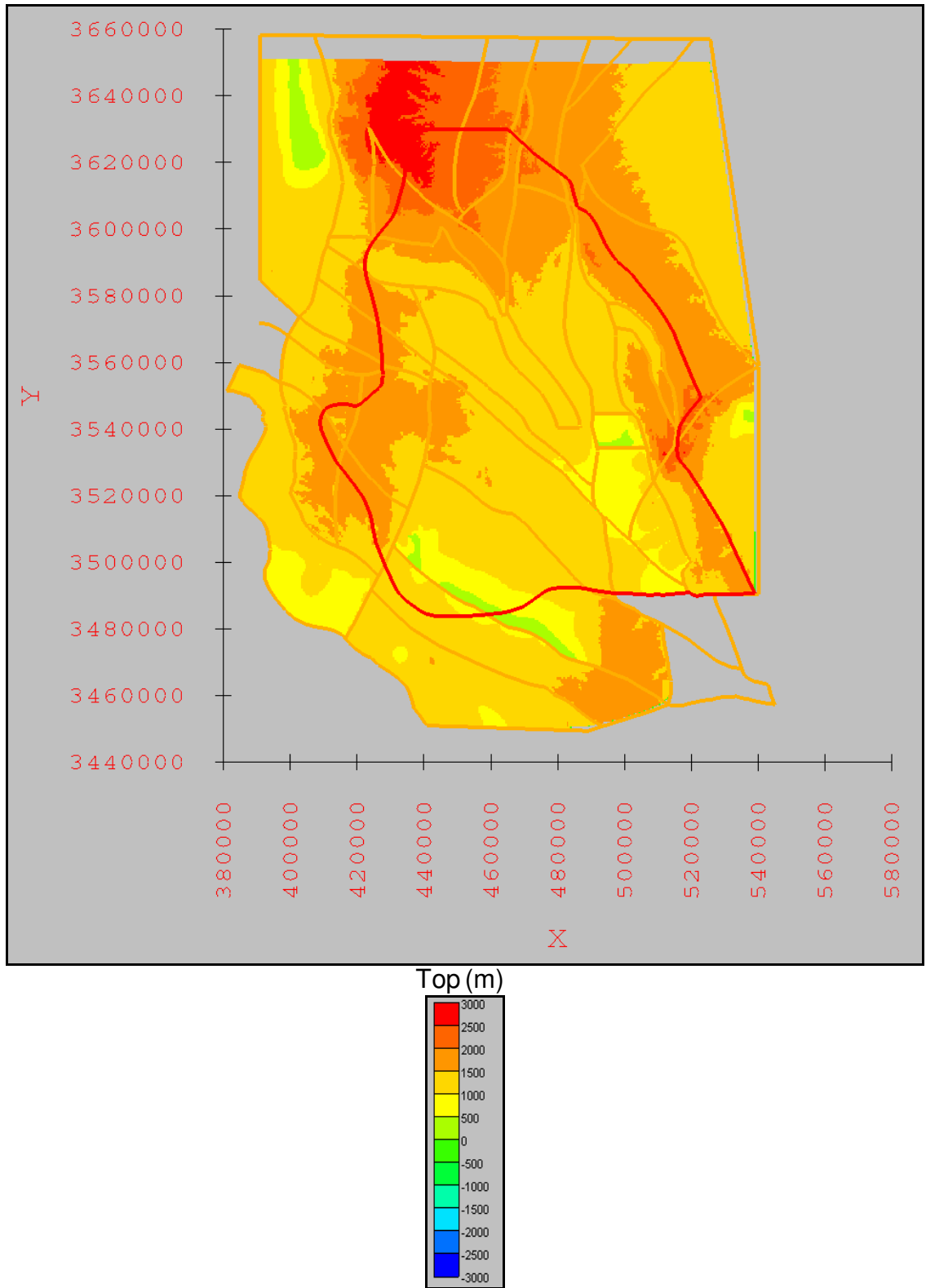
Figure 3.16: Elevation of the top of Artesia Group.
Elevations are in meters relative to mean sea level. Contour interval is 500 meters (1,640 feet). Black circles indicate the oil-and-gas exploratory wells used as control for the unit.
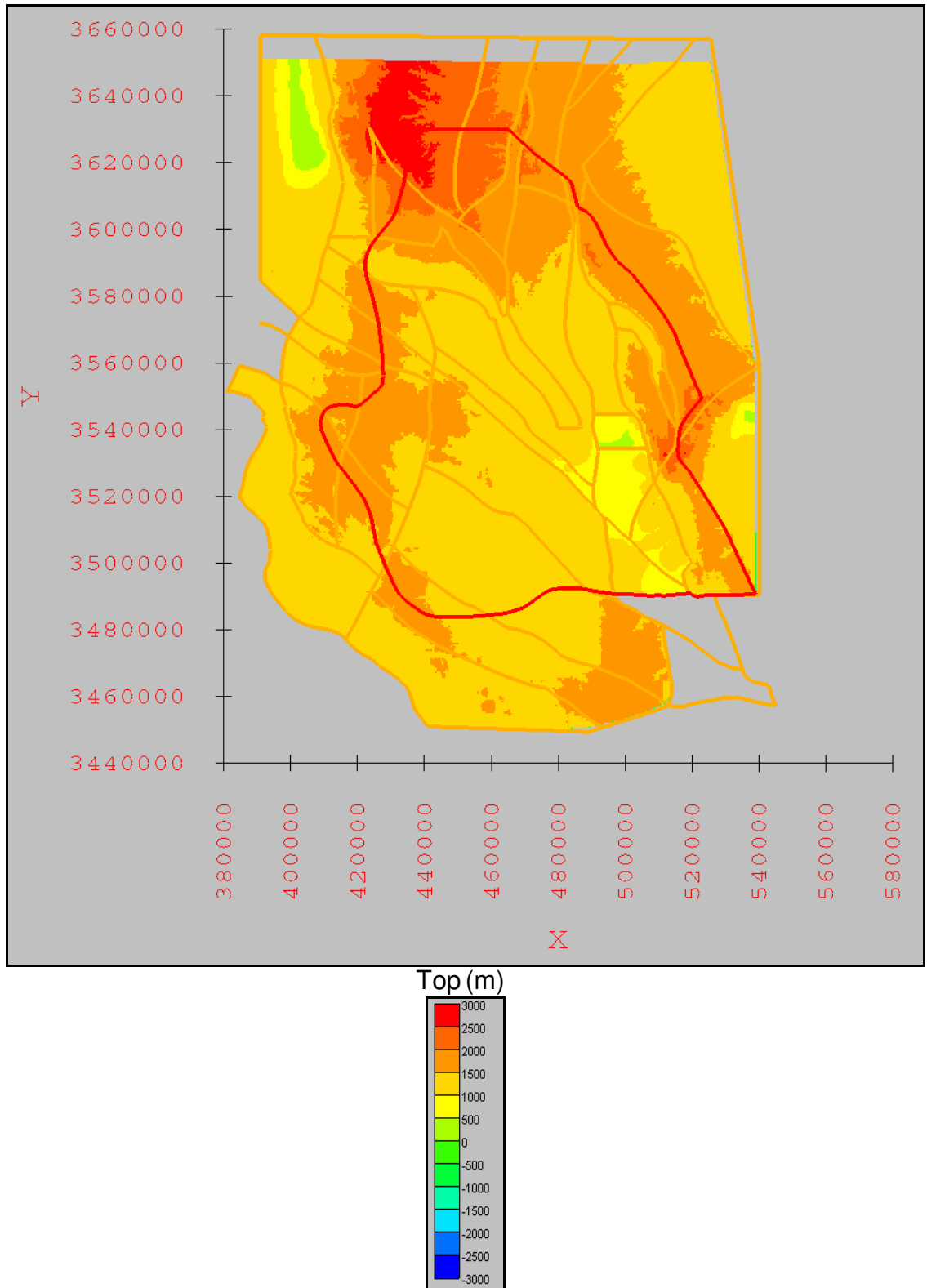
Figure 3.17: Elevation of the top of the Cretaceous.
Elevations are in meters relative to mean sea level. Contour interval is 500 meters (1,640 feet). Black circles indicate the oil-and-gas exploratory wells used as control for the unit.
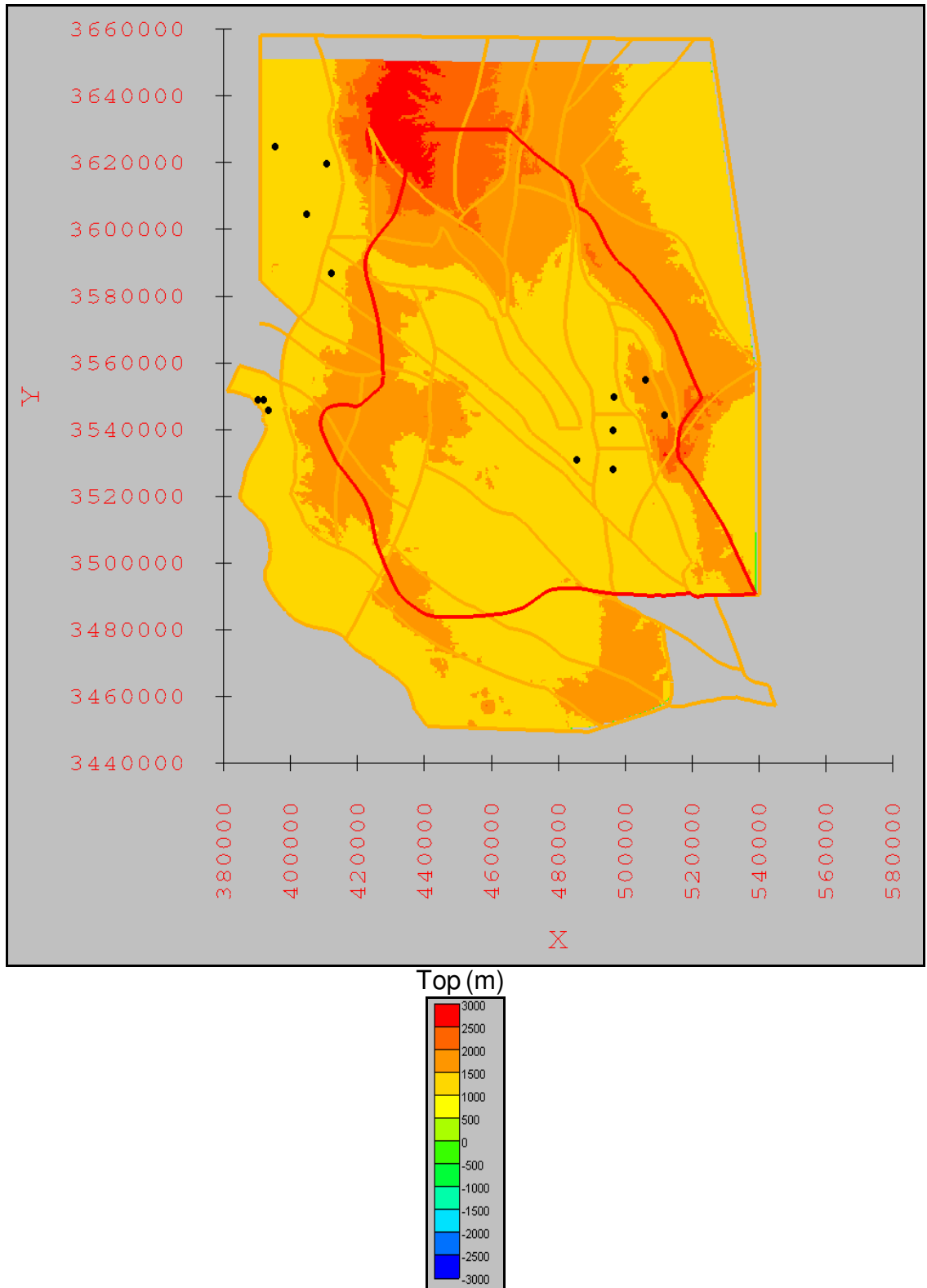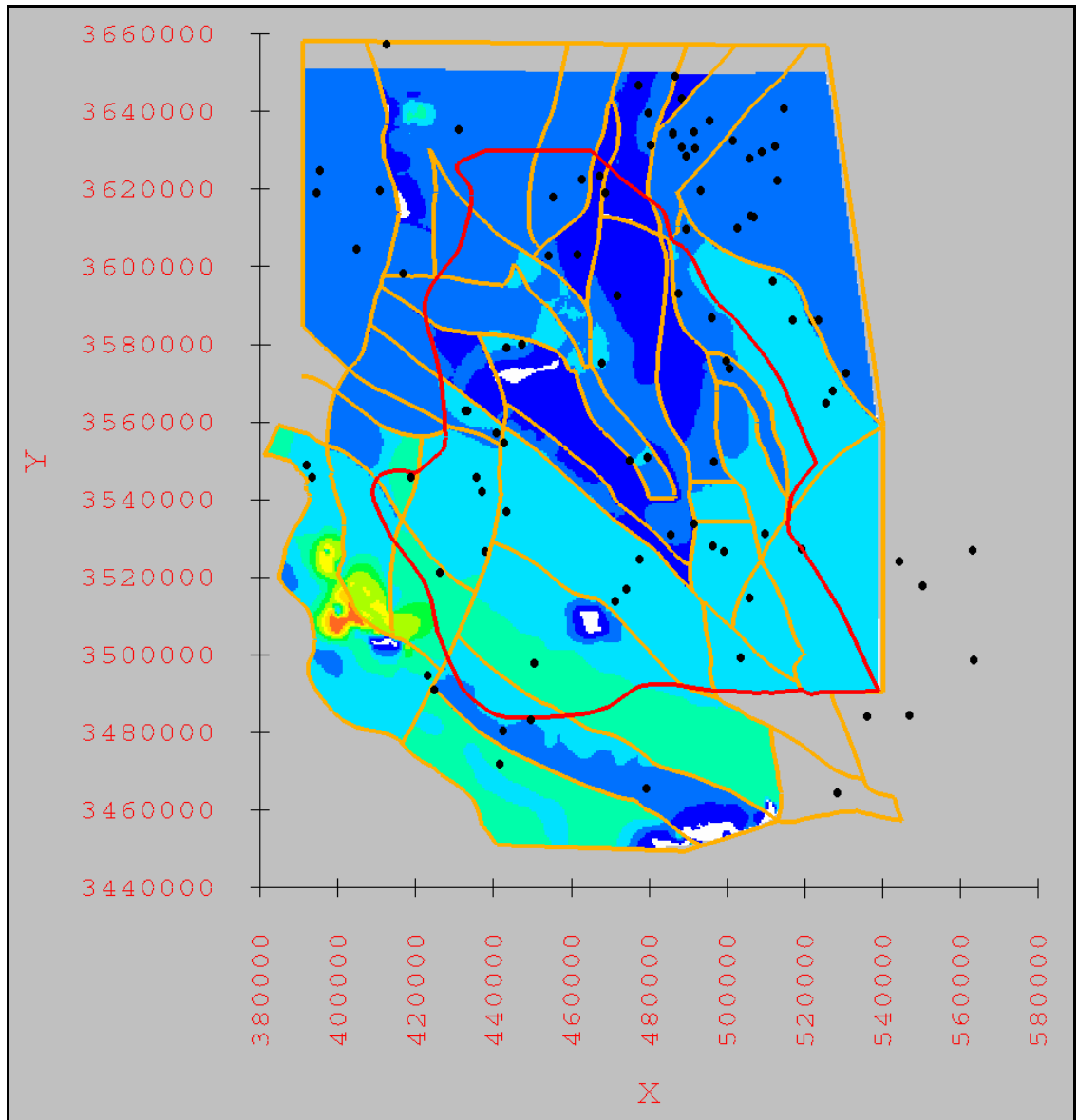
Figure 3.18: Elevation of the top of Cenozoic alluvium.
Elevations are in meters relative to mean sea level. Contour interval is 500 meters (1,640 feet). Black circles indicate the oil-and-gas exploratory wells used as control for the unit.
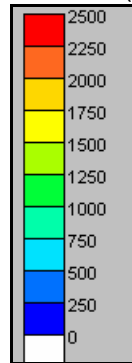
Figure 3.19: Thickness of the Cambrian through the Silurian.
Contour interval is 250 meters (820 feet). White color indicates unit is not present. Black circles indicate the oil-and-gas exploratory wells used as control for the unit.
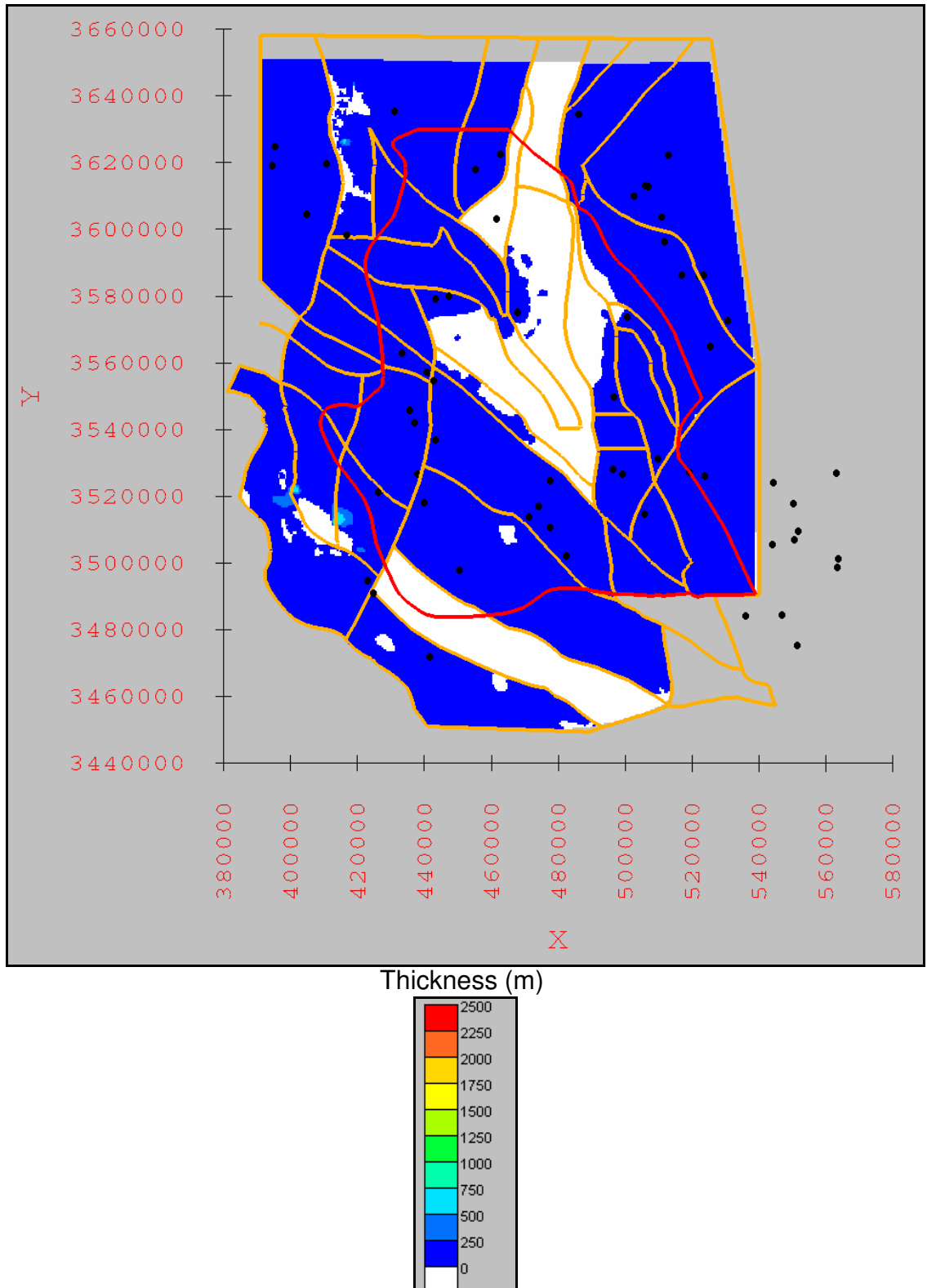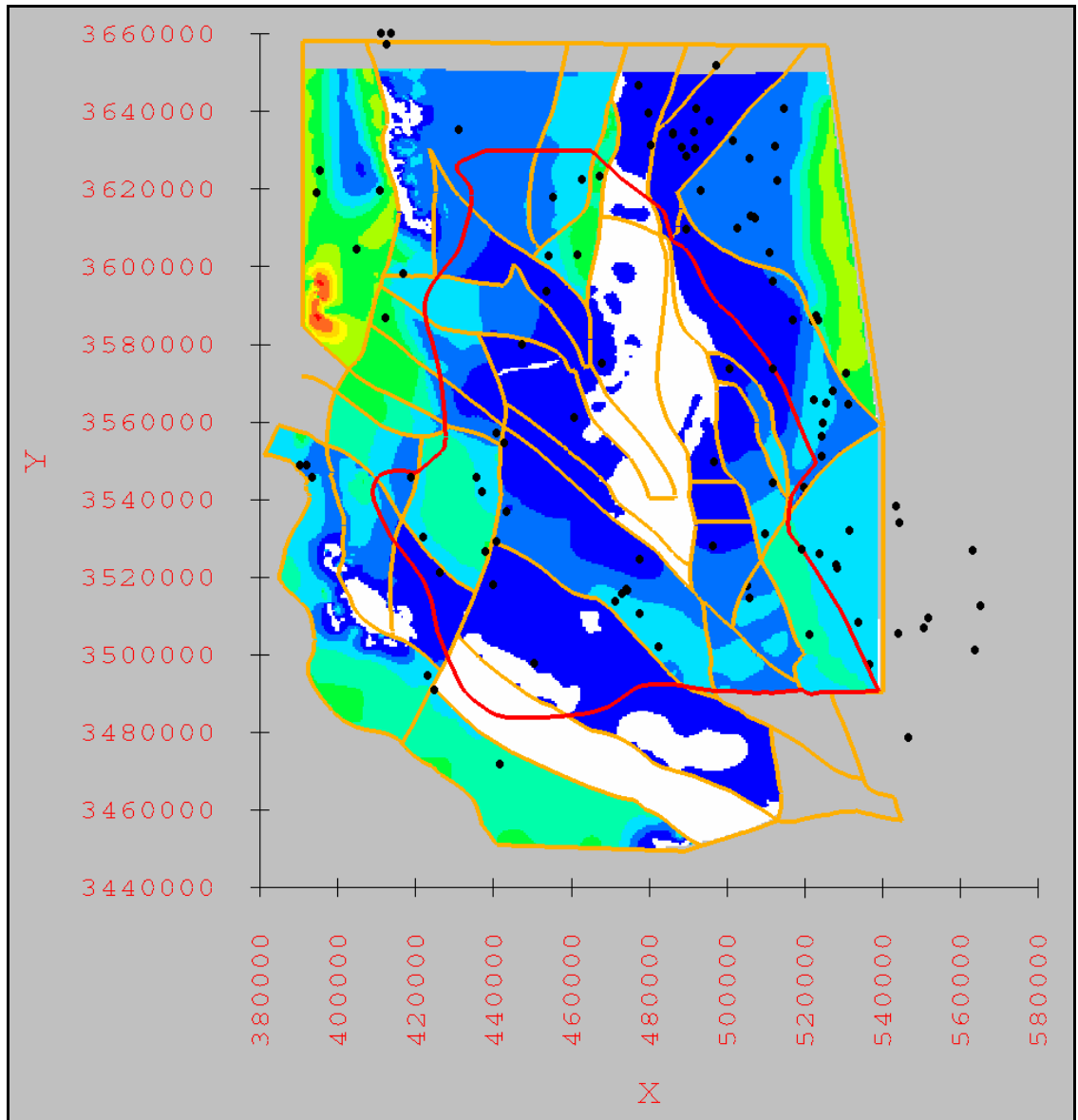
Figure 3.20: Thickness of the Devonian.
Contour interval is 250 meters (820 feet). White color indicates unit is not present. Black circles indicate the oil-and-gas exploratory wells used as control for the unit.
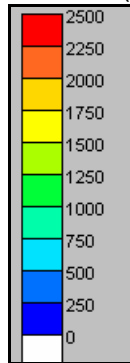
Figure 3.21: Thickness of the Mississippian through the Pennsylvanian.
Contour interval is 250 meters (820 feet). White color indicates unit is not present. Black
circles indicate the oil-and-gas exploratory wells used as control for the unit.
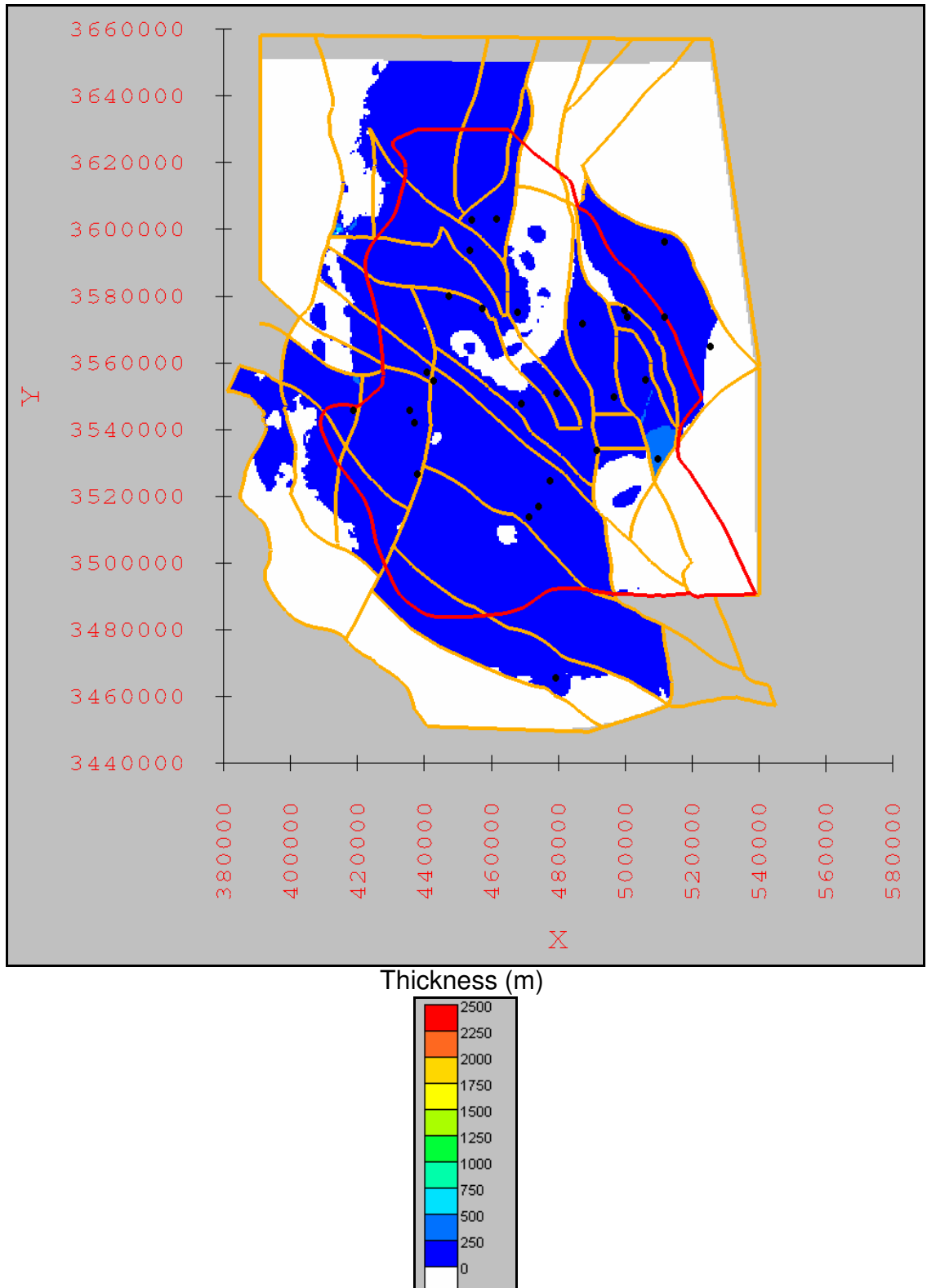
Figure 3.22: Thickness of Lower Abo/Pow Wow Conglomerate.
Contour interval is 250 meters (820 feet). White color indicates unit is not present. Black circles indicate the oil-and-gas exploratory wells used as control for the unit.
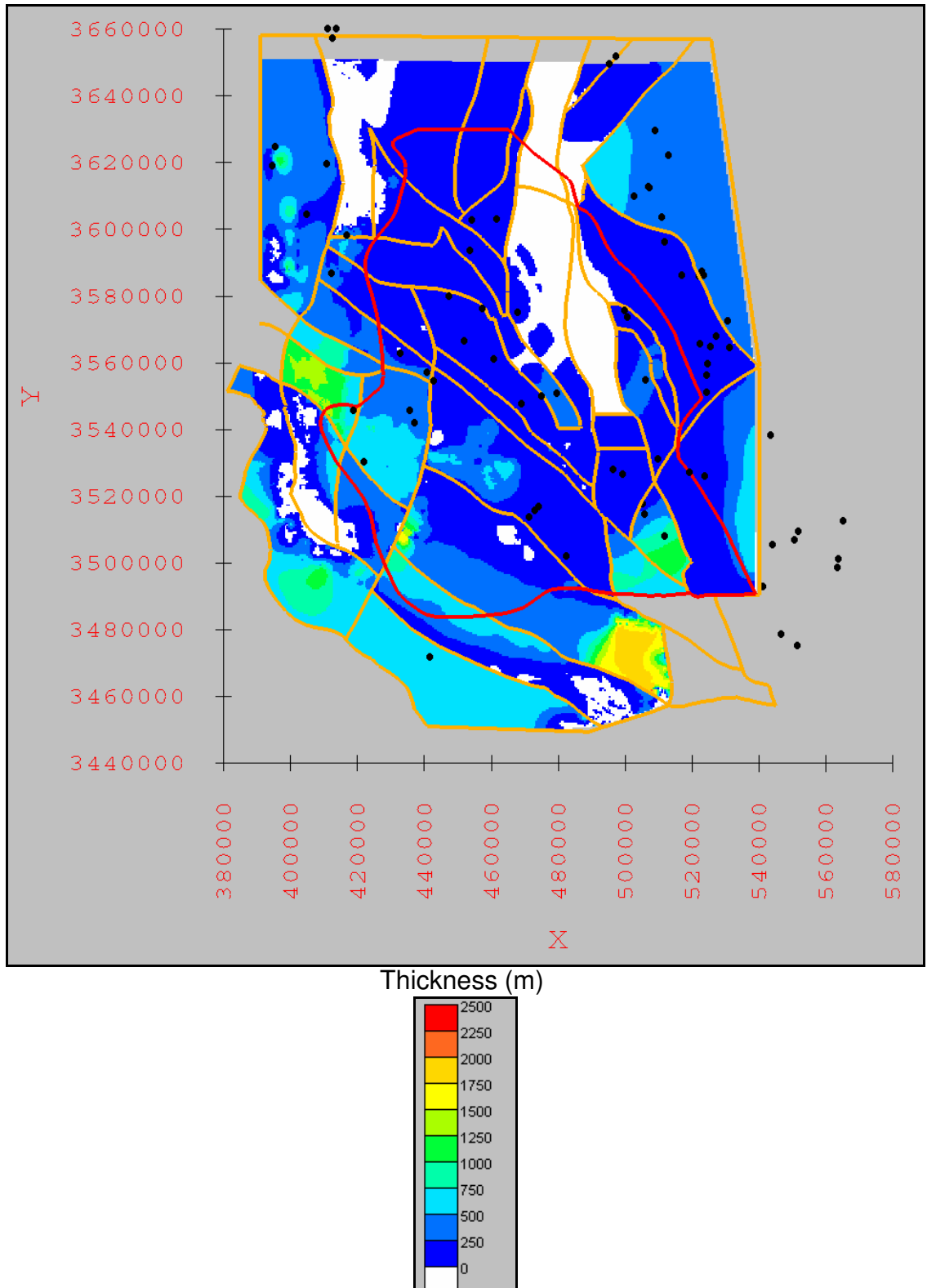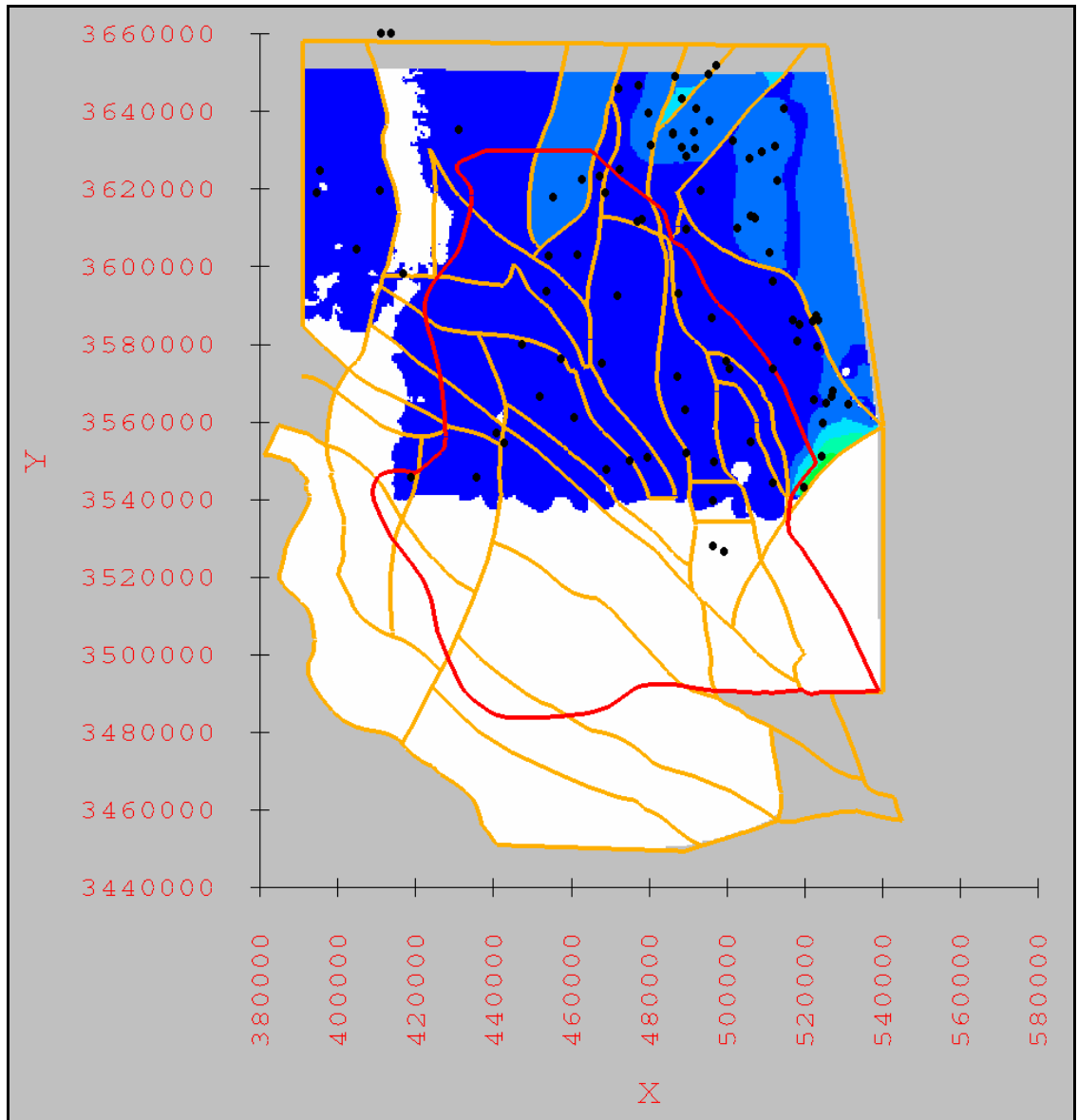
Figure 3.23: Thickness of Hueco Limestone/Formation (or Bursum Formation) and Wolfcamp Formation.

Contour interval is 250 meters (820 feet). White color indicates unit is not present. Black circles indicate the oil-and-gas exploratory wells used as control for the unit.
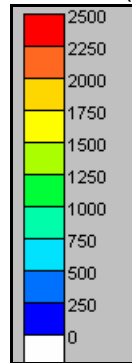
Figure 3.24: Thickness of Abo Formation.
Contour interval is 250 meters (820 feet). White color indicates unit is not present. Black circles indicate the oil-and-gas exploratory wells used as control for the unit.
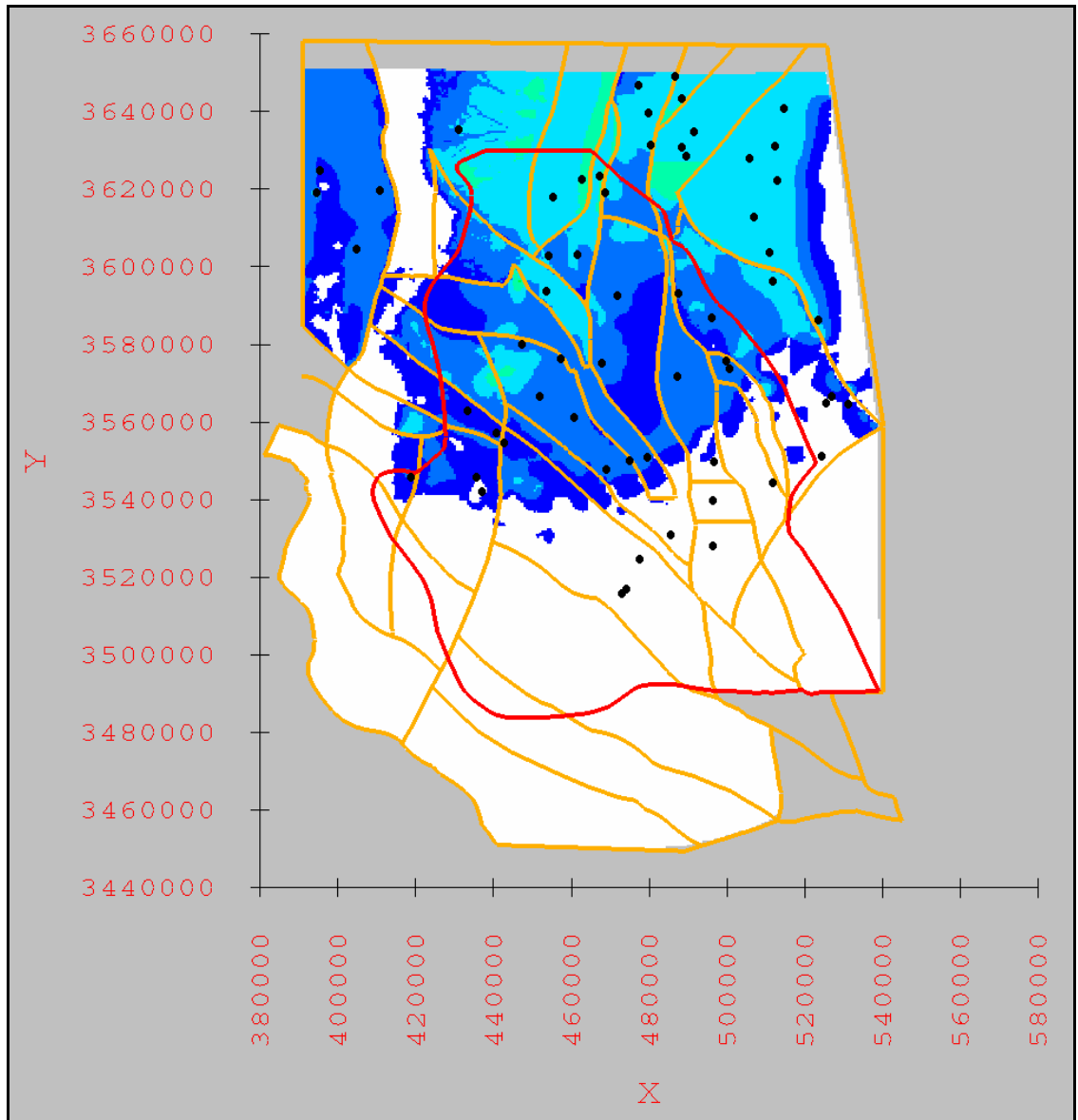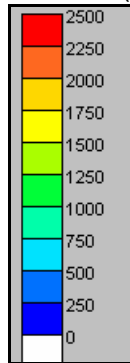
Figure 3.25: Thickness of Yeso Formation.
Contour interval is 250 meters (820 feet). White color indicates unit is not present. Black circles indicate the oil-and-gas exploratory wells used as control for the unit.
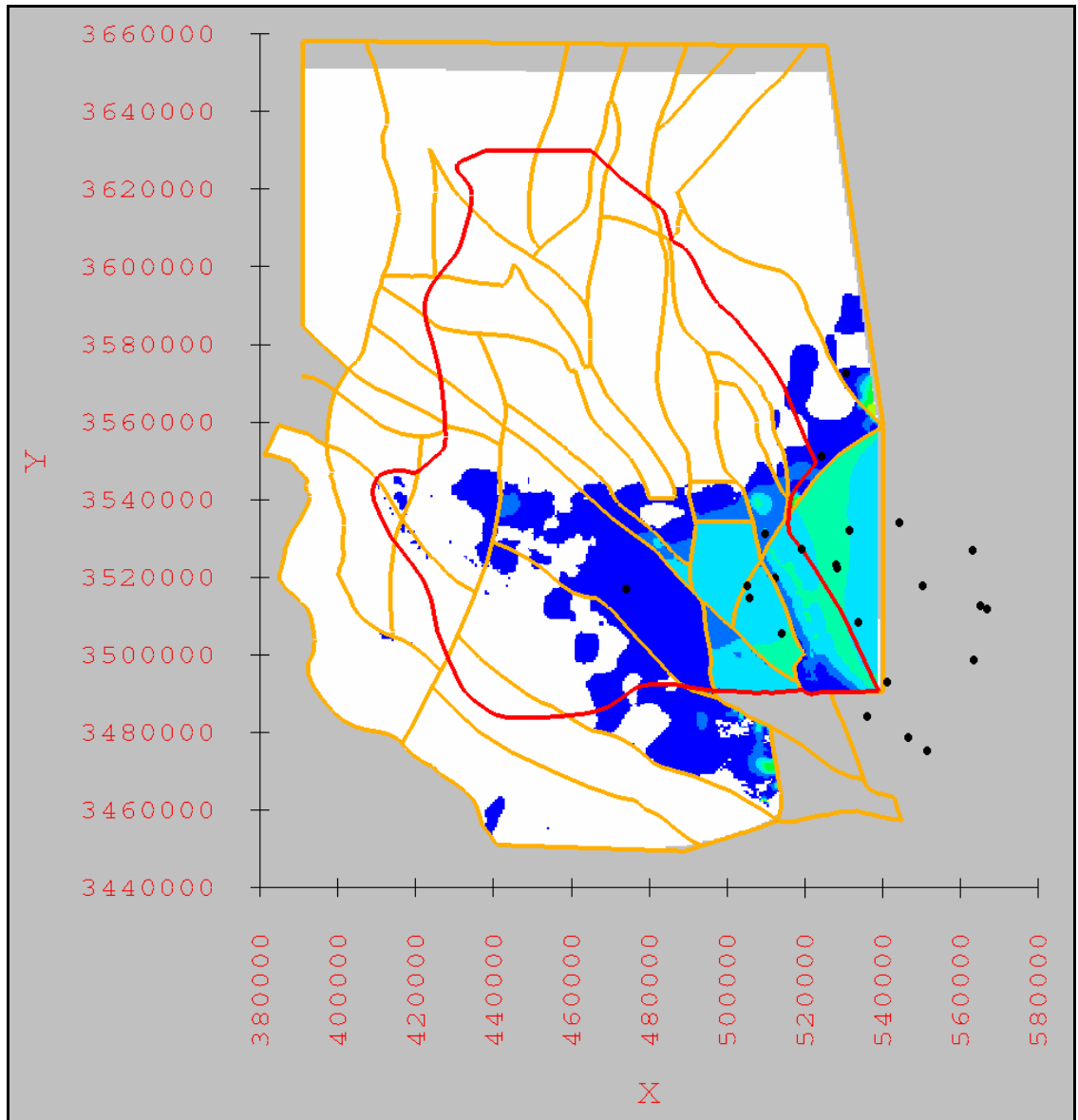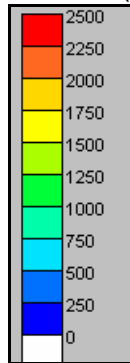
Figure 3.26: Thickness of Bone Spring Limestone/Formation.
Contour interval is 250 meters (820 feet). White color indicates unit is not present. Black circles indicate the oil-and-gas exploratory wells used as control for the unit.
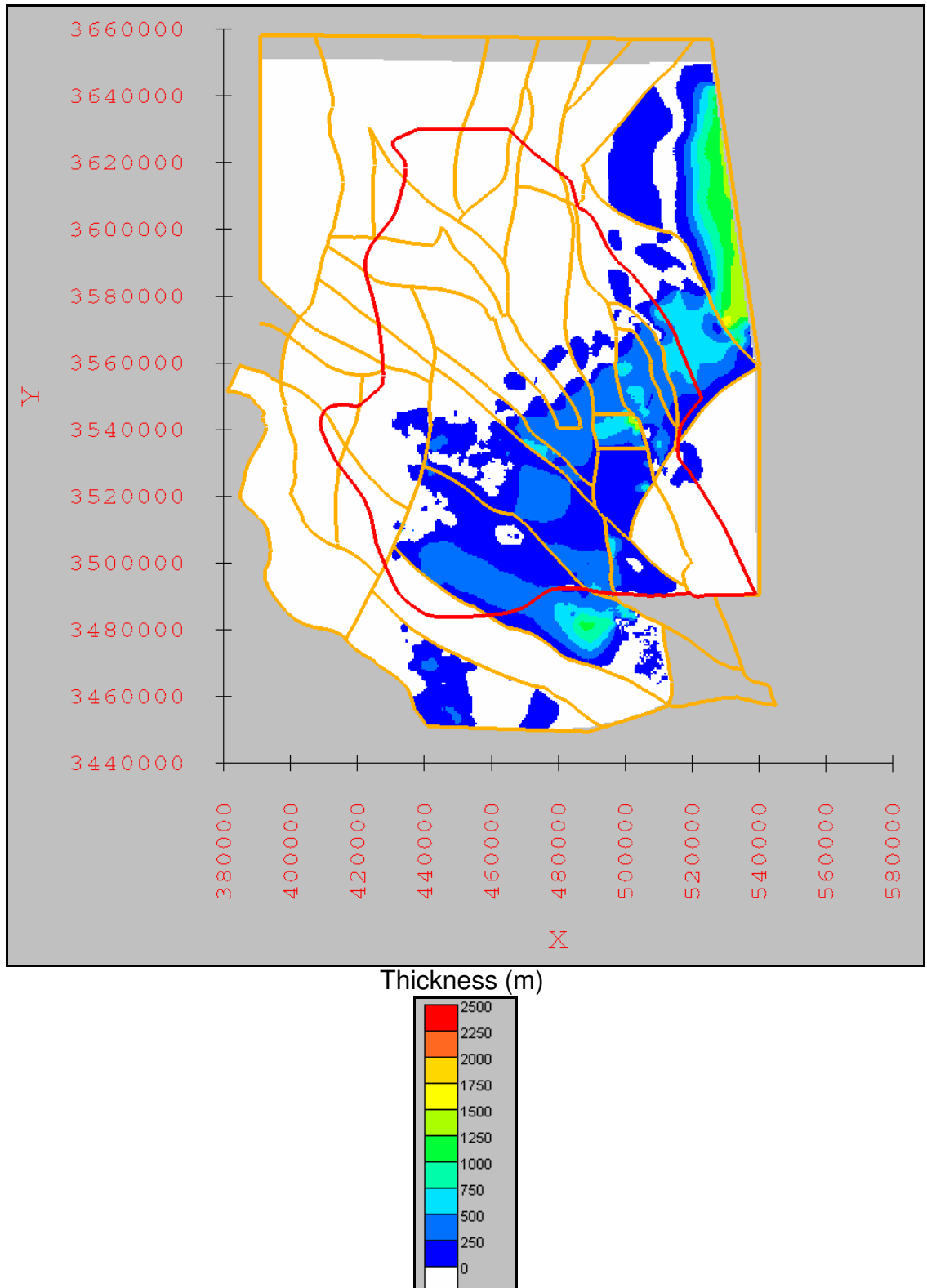
Figure 3.27: Thickness of Victorio Peak Limestone/Formation and Cutoff Shale and Wilke Ranch Formation.

Contour interval is 250 meters (820 feet). White color indicates unit is not present. Black circles indicate the oil-and-gas exploratory wells used as control for the unit.
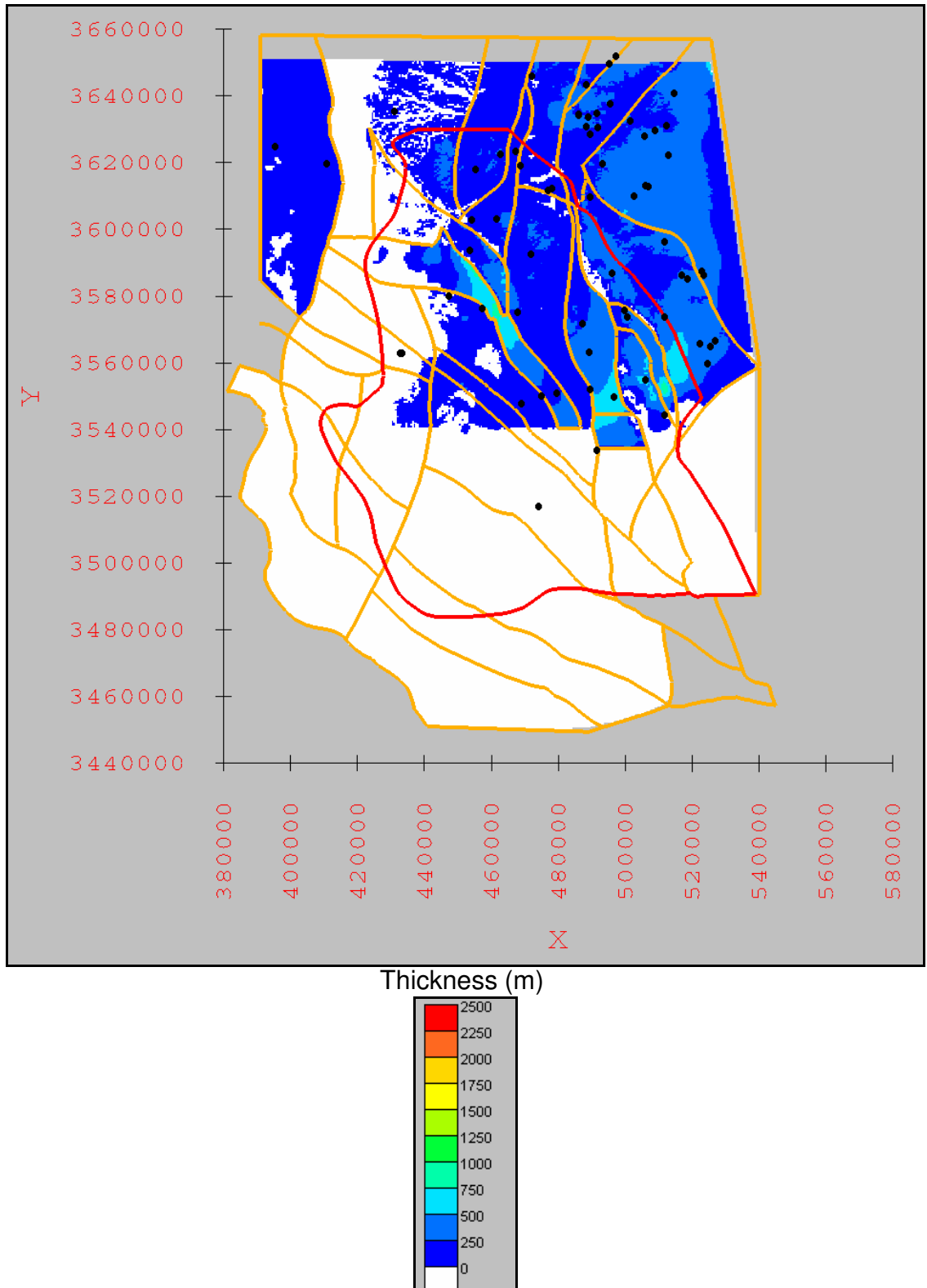
Figure 3.28: Thickness of San Andres Formation.
Contour interval is 250 meters (820 feet). White color indicates unit is not present. Black circles indicate the oil-and-gas exploratory wells used as control for the unit.
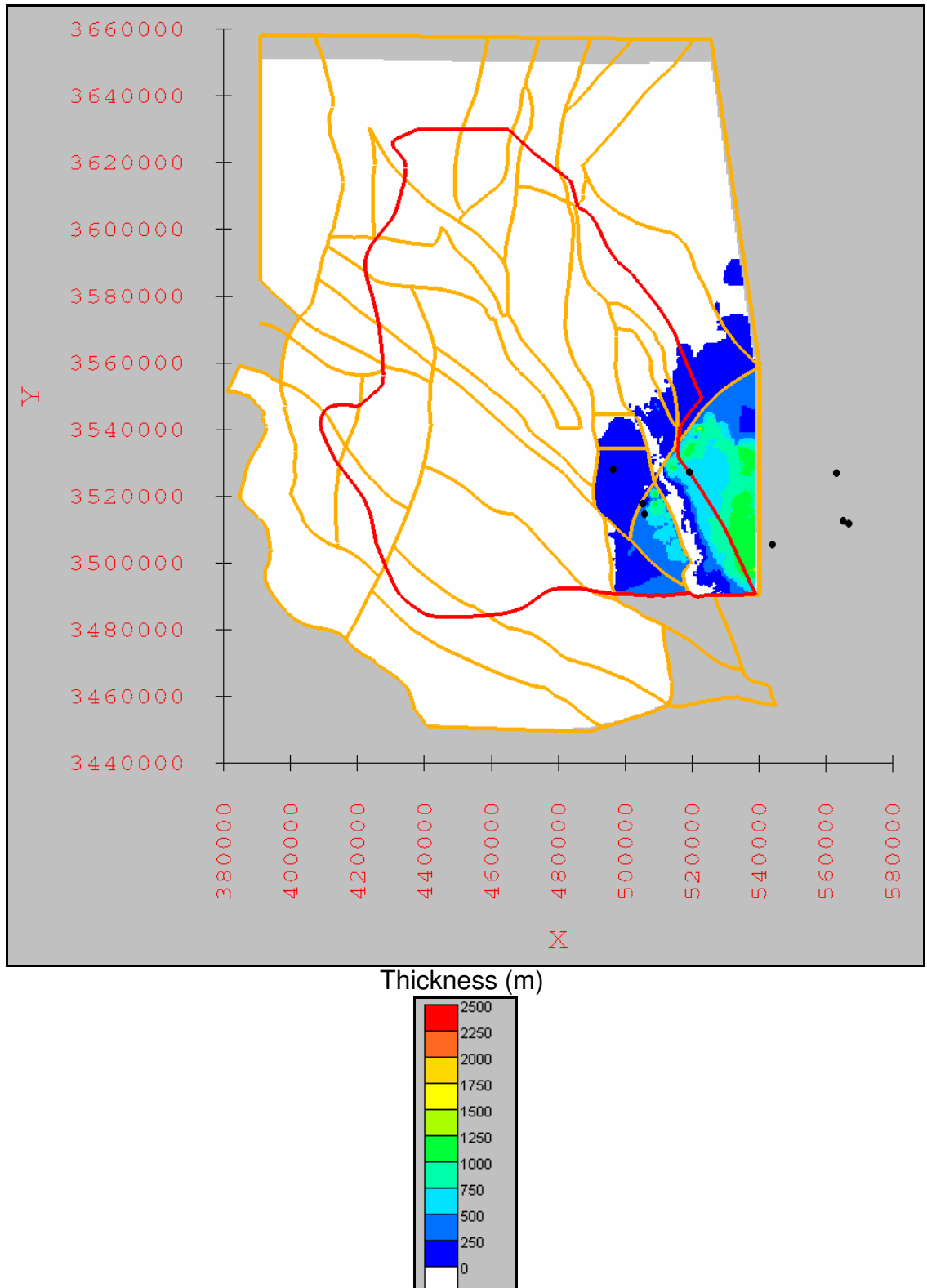
Figure 3.29: Thickness of Delaware Mountain Group.
Contour interval is 250 meters (820 feet). White color indicates unit is not present. Black circles indicate the oil-and-gas exploratory wells used as control for the unit.
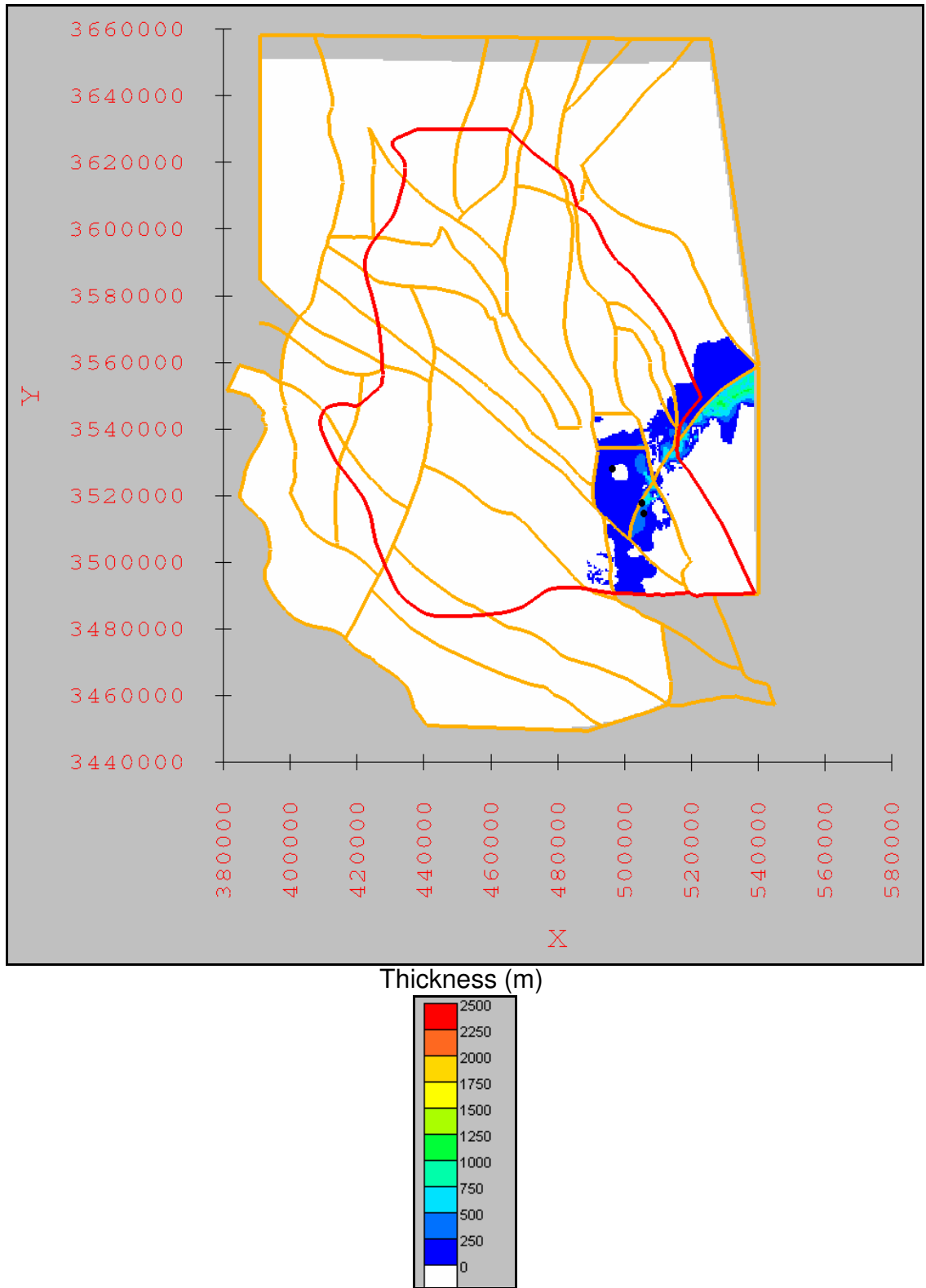
Figure 3.30: Thickness of Goat Seep Dolomite/Limestone/Formation and Capitan Limestone/Formation.

Contour interval is 250 meters (820 feet). White color indicates unit is not present. Black circles indicate the oil-and-gas exploratory wells used as control for the unit.

227
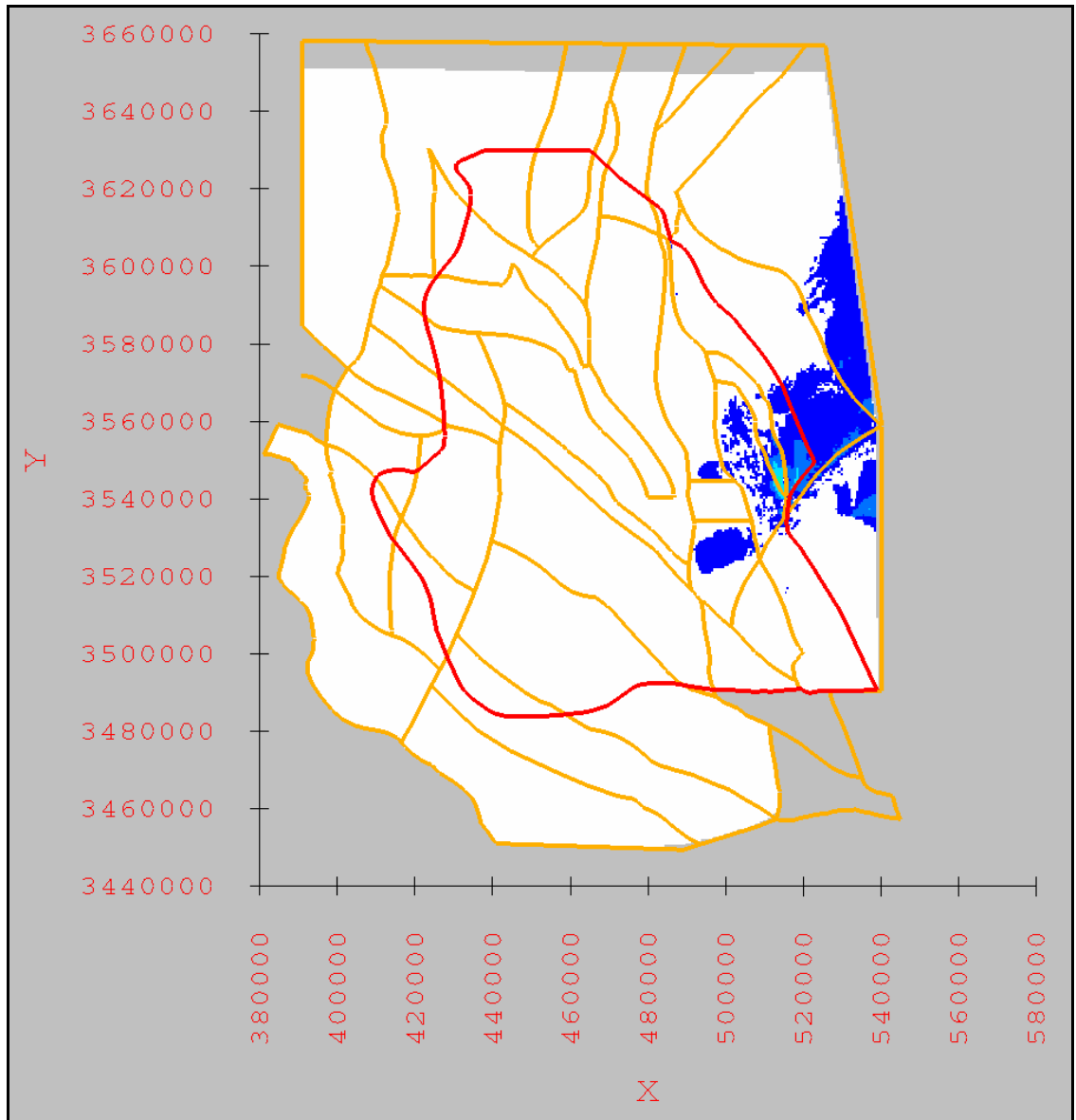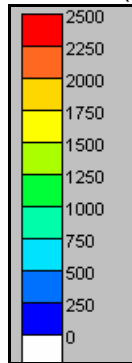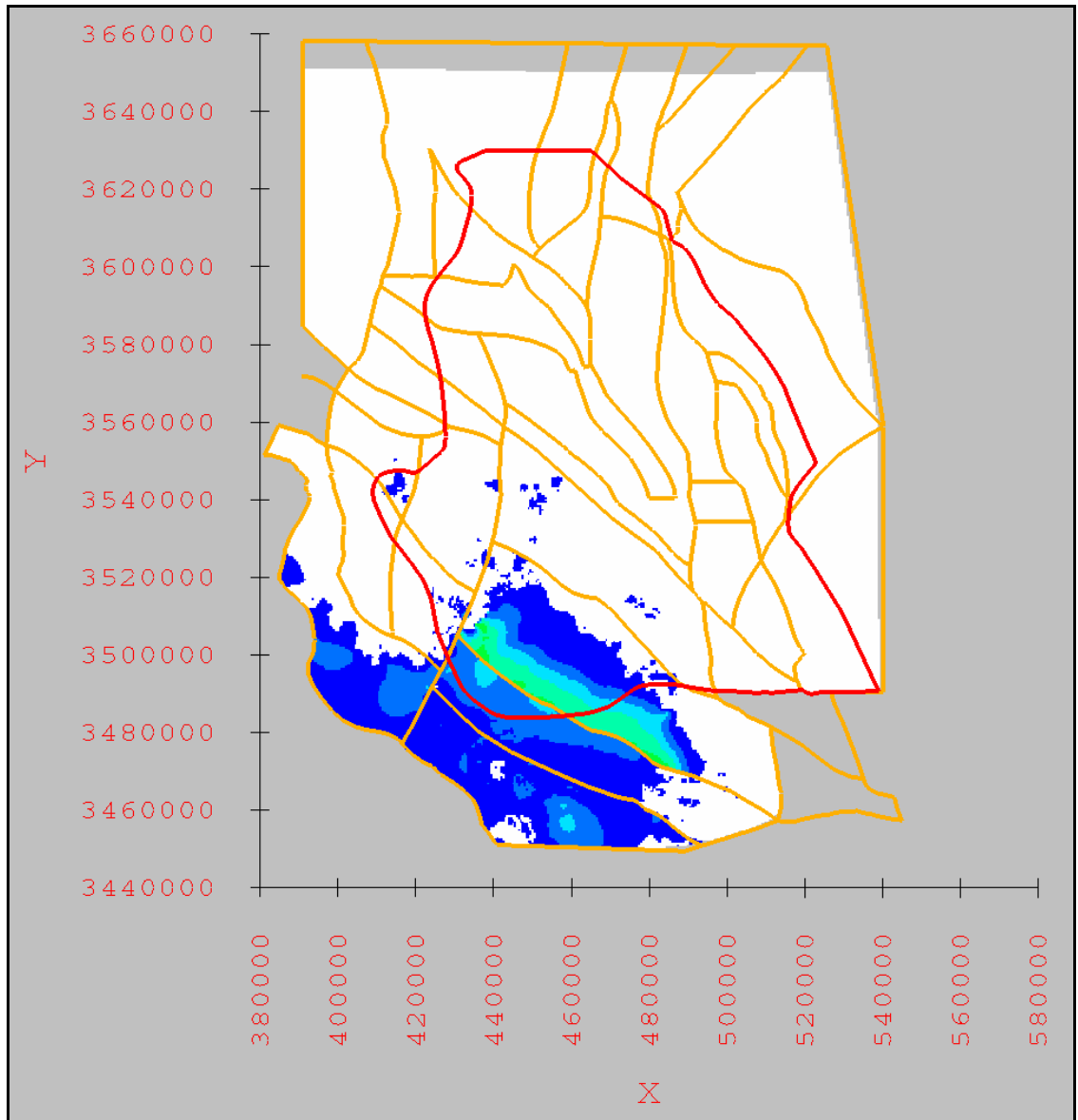
Figure 3.31: Thickness of Artesia Group.
Contour interval is 250 meters (820 feet). White color indicates unit is not present. Black circles indicate the oil-and-gas exploratory wells used as control for the unit.
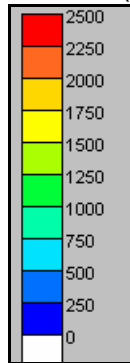
Figure 3.32: Thickness of the Cretaceous.
Contour interval is 250 meters (820 feet). White color indicates unit is not present. Black circles indicate the oil-and-gas exploratory wells used as control for the unit.
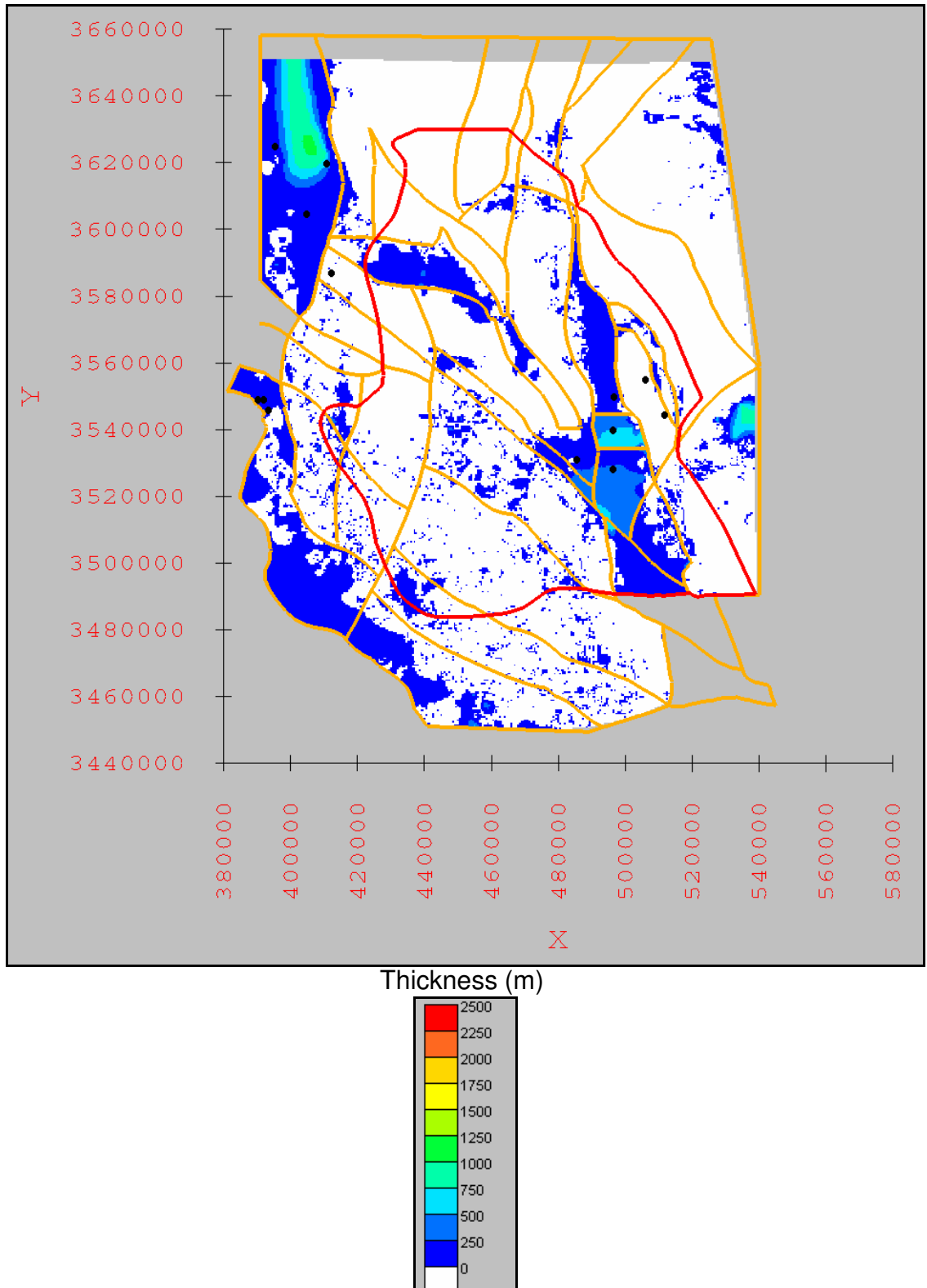
Figure 3.33: Thickness of Cenozoic alluvium.
Contour interval is 250 meters (820 feet). White color indicates unit is not present. Black circles indicate the oil-and-gas exploratory wells used as control for the unit.
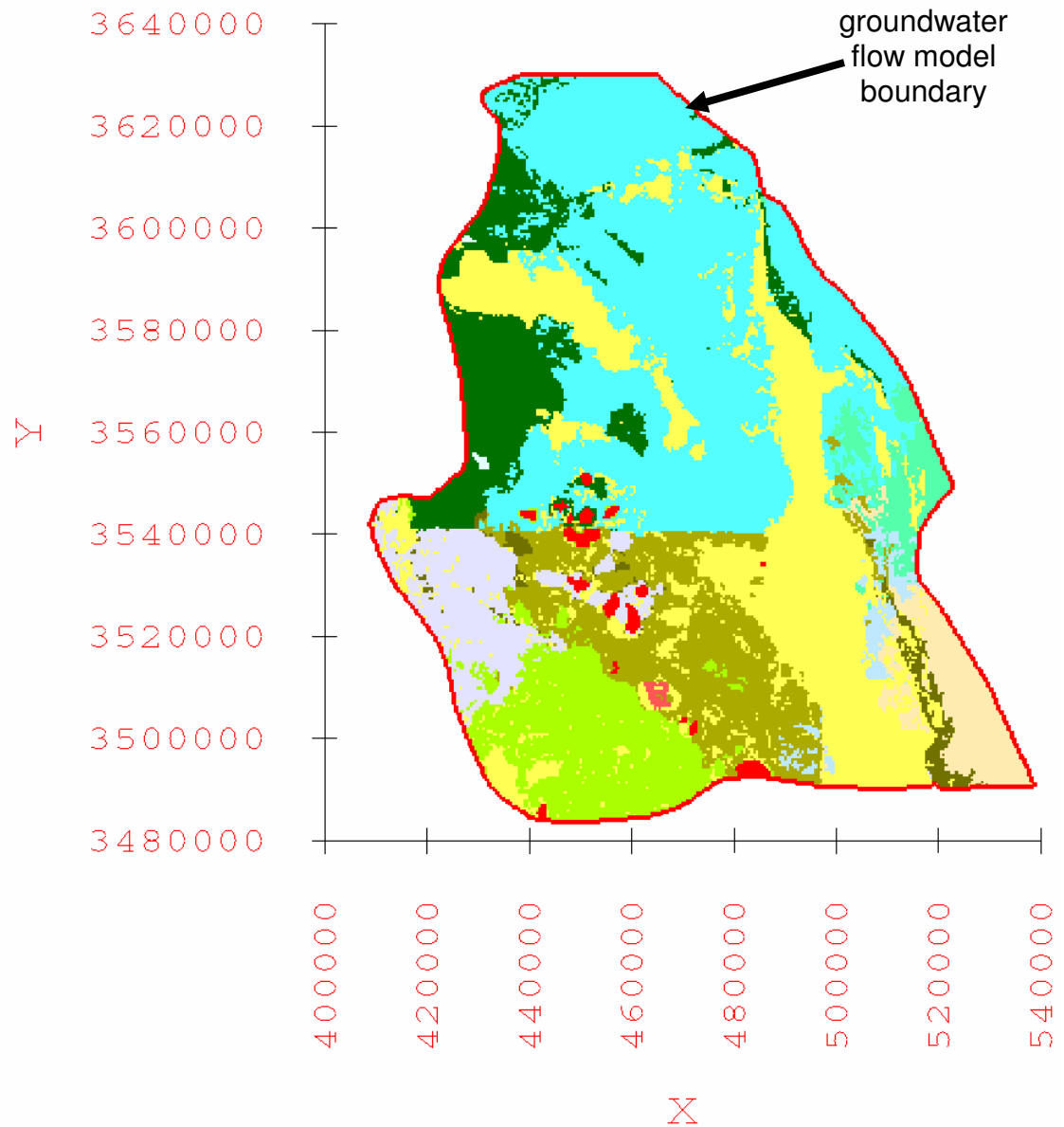
Figure 3.34: Land surface expression of the 3-D hydrogeologic framework solid model clipped to the groundwater flow model boundary.
Color-coding of hydrogeologic units corresponds to that used in Figure 2.1. Red line designates groundwater flow model boundary.
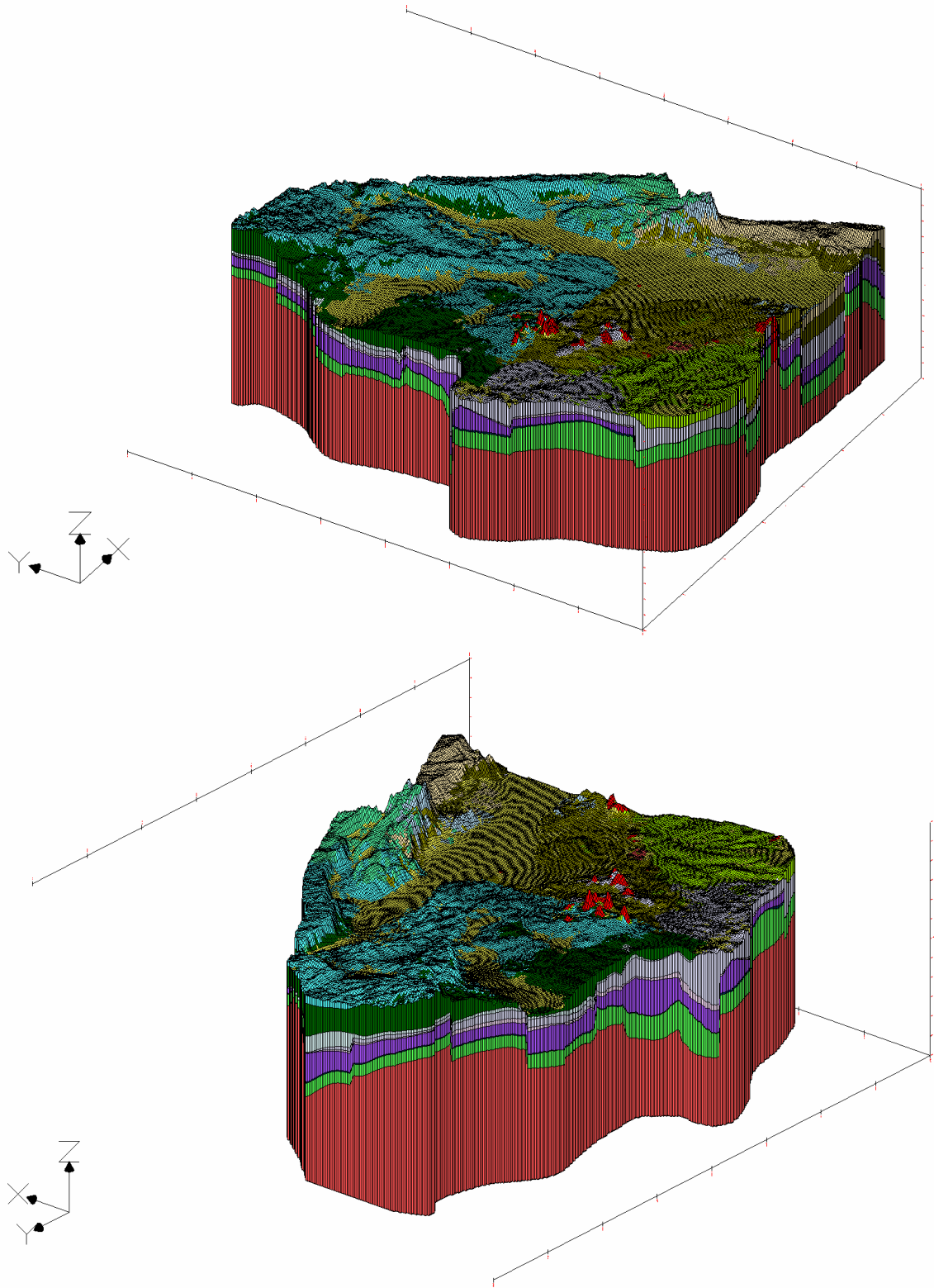
Figure 3.35: Oblique views of the 3-D hydrogeologic framework solid model clipped to the groundwater flow model boundary.
Color-coding of hydrogeologic units corresponds to that used in Figure 2.1. Vertical exaggeration 10×.
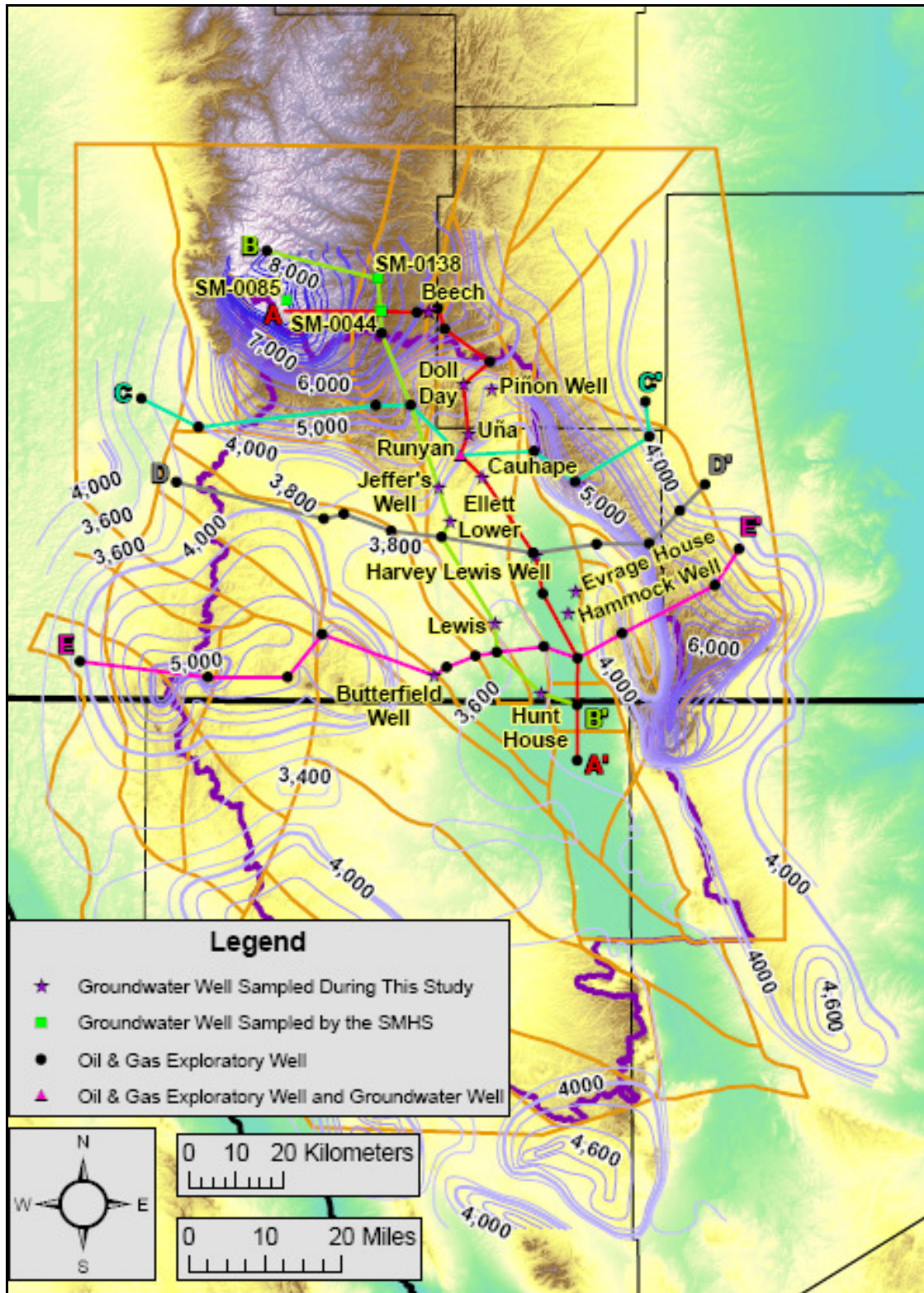
Figure 3.36: Location of the five hydrogeologic cross-sections.
Also includes the location of the groundwater wells sampled during this study along each cross-section, the subsurface geologic control points along each cross-section, and the groundwater surface contours produced for this study.
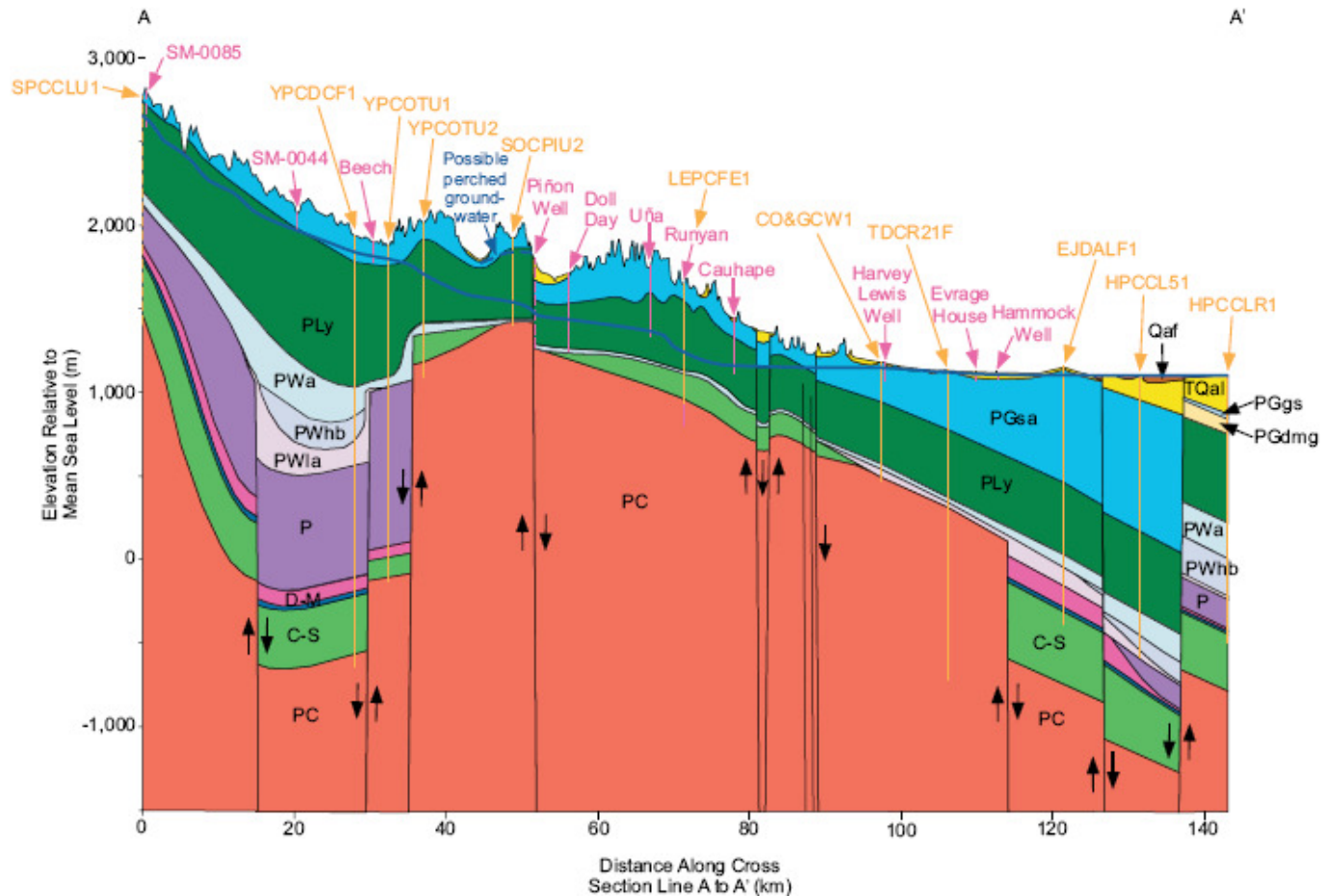
Figure 3.37: North-South cross-section A - A'.

Vertical exaggeration 23×.

On all cross-sections, the light brown vertical lines are oil-and-gas exploratory well subsurface control points, the pink vertical lines are groundwater wells sampled during this study and by the SMHS, and the arrows indicate the sense of displacement on faults. Dashed lines for wells indicate that the well was projected to the line of cross-section. The groundwater surface is represented by the dark blue line. Color-coding of hydrogeologic units and unit labels corresponds to that used in Figure 2.1.
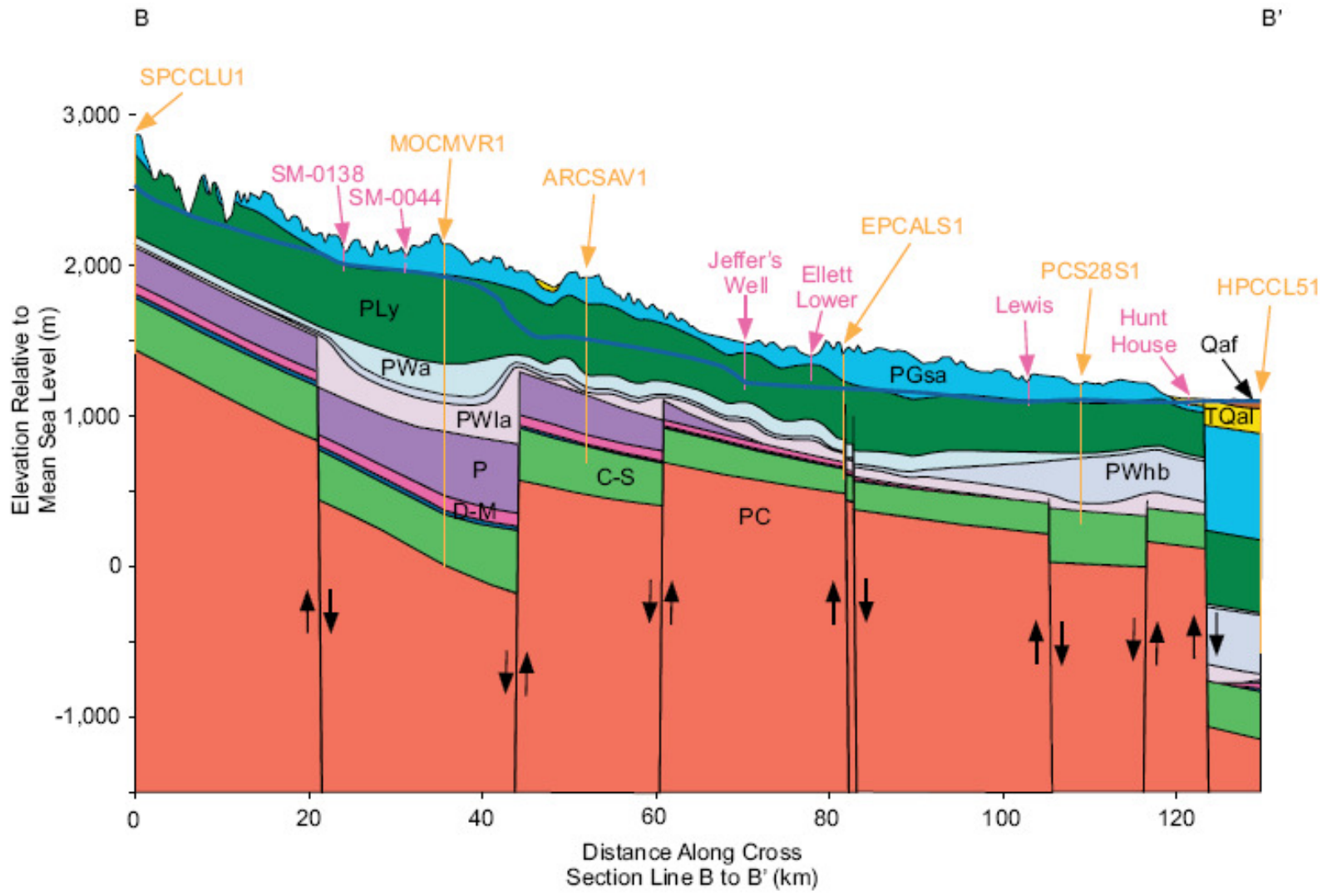
Figure 3.38: North-South cross-section B - B'.

Vertical exaggeration 18×.
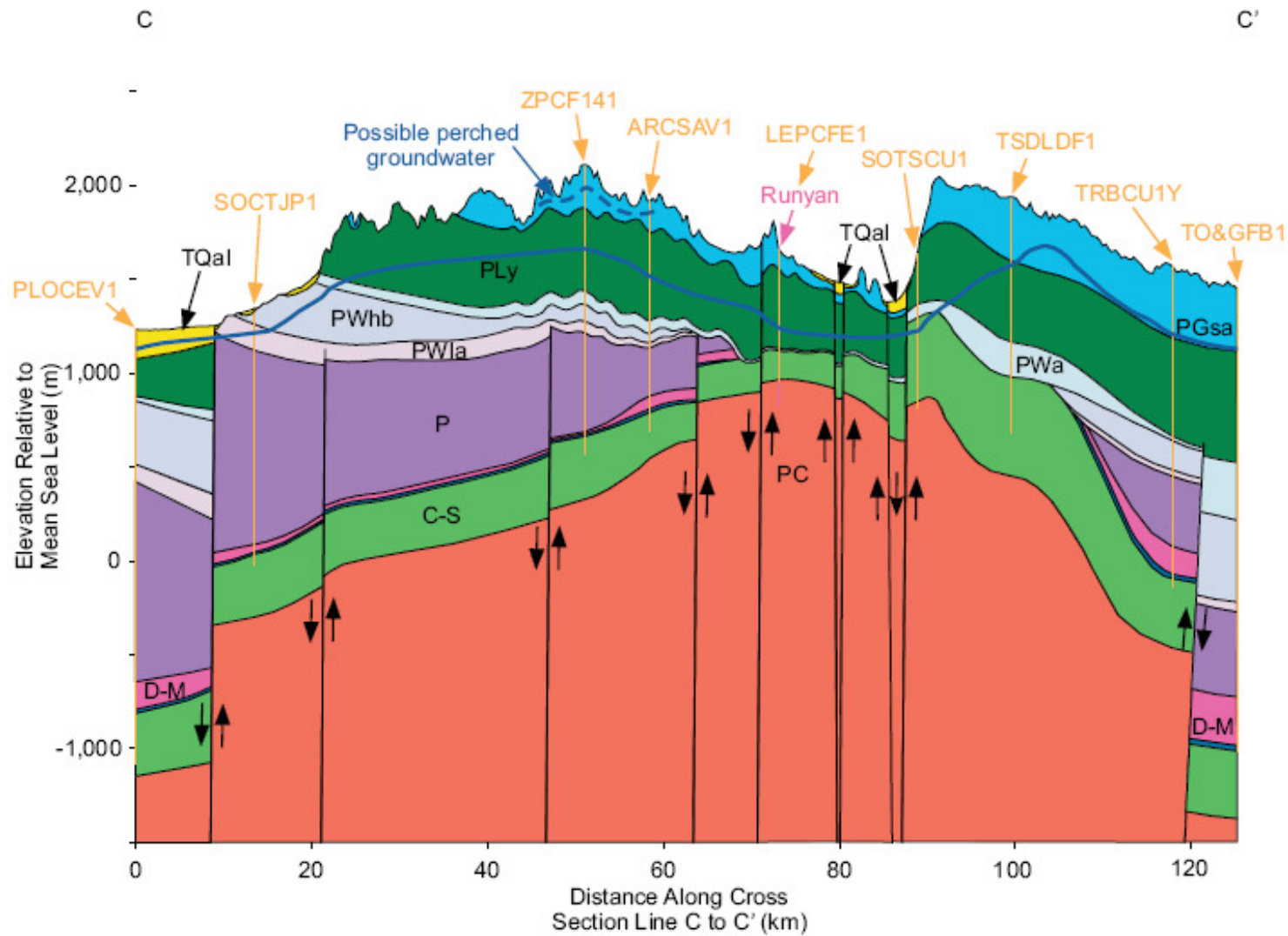
Figure 3.39: West-East cross-section C - C'.

Vertical exaggeration 22×.
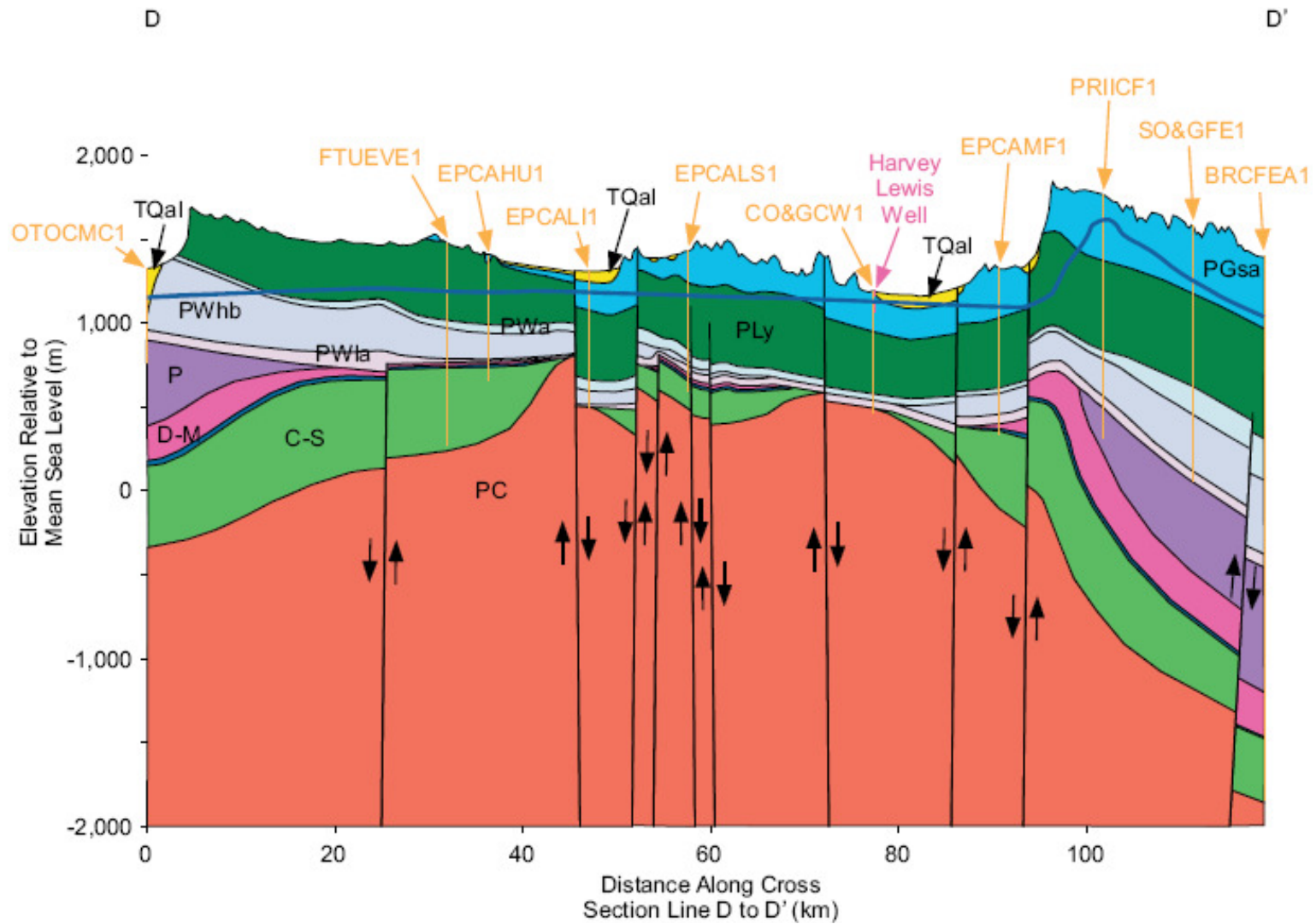
Figure 3.40: West-East cross-section D - D'.

Vertical exaggeration 18×.
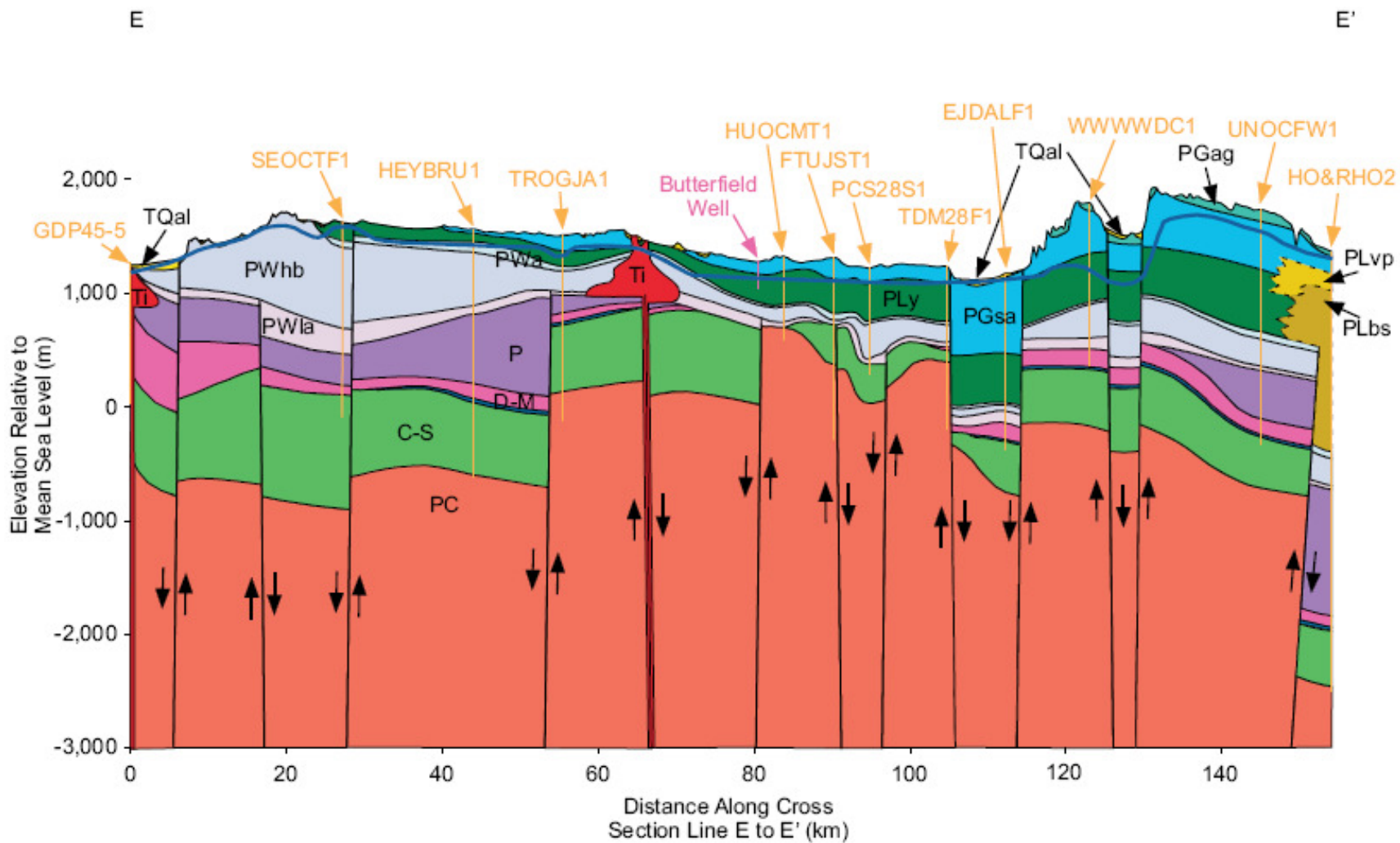
Figure 3.41: West-East cross-section E - E'.

Vertical exaggeration 15×.
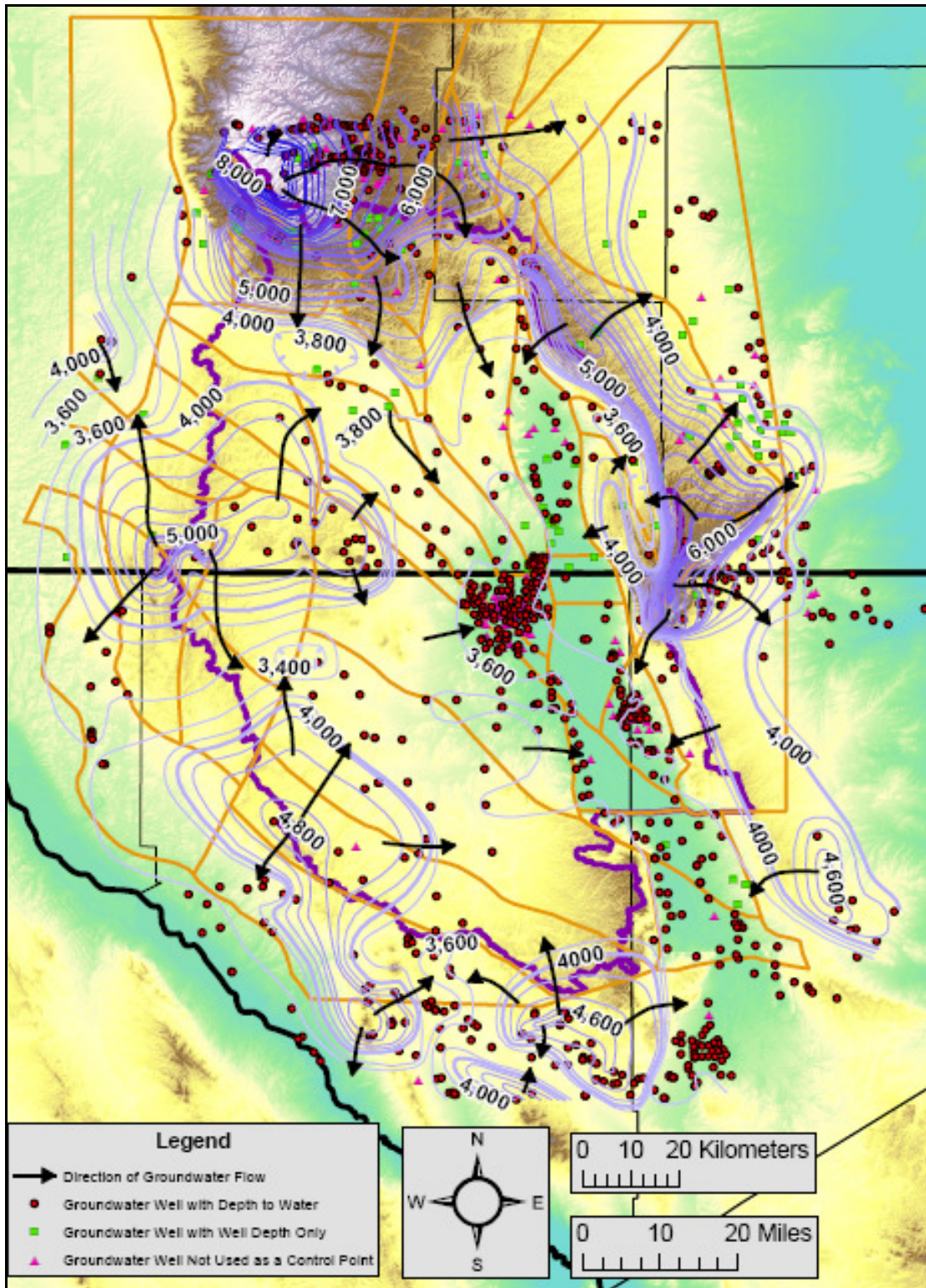
Figure 3.42: Groundwater elevation contours for the Salt Basin region. Elevations are in feet above mean sea level. Contour interval is 200 feet. Hachured contours indicate groundwater depressions. The red circle and green square symbols indicate groundwater wells used as control for the contours, while the pink triangle symbols indicate groundwater wells not used as control points.
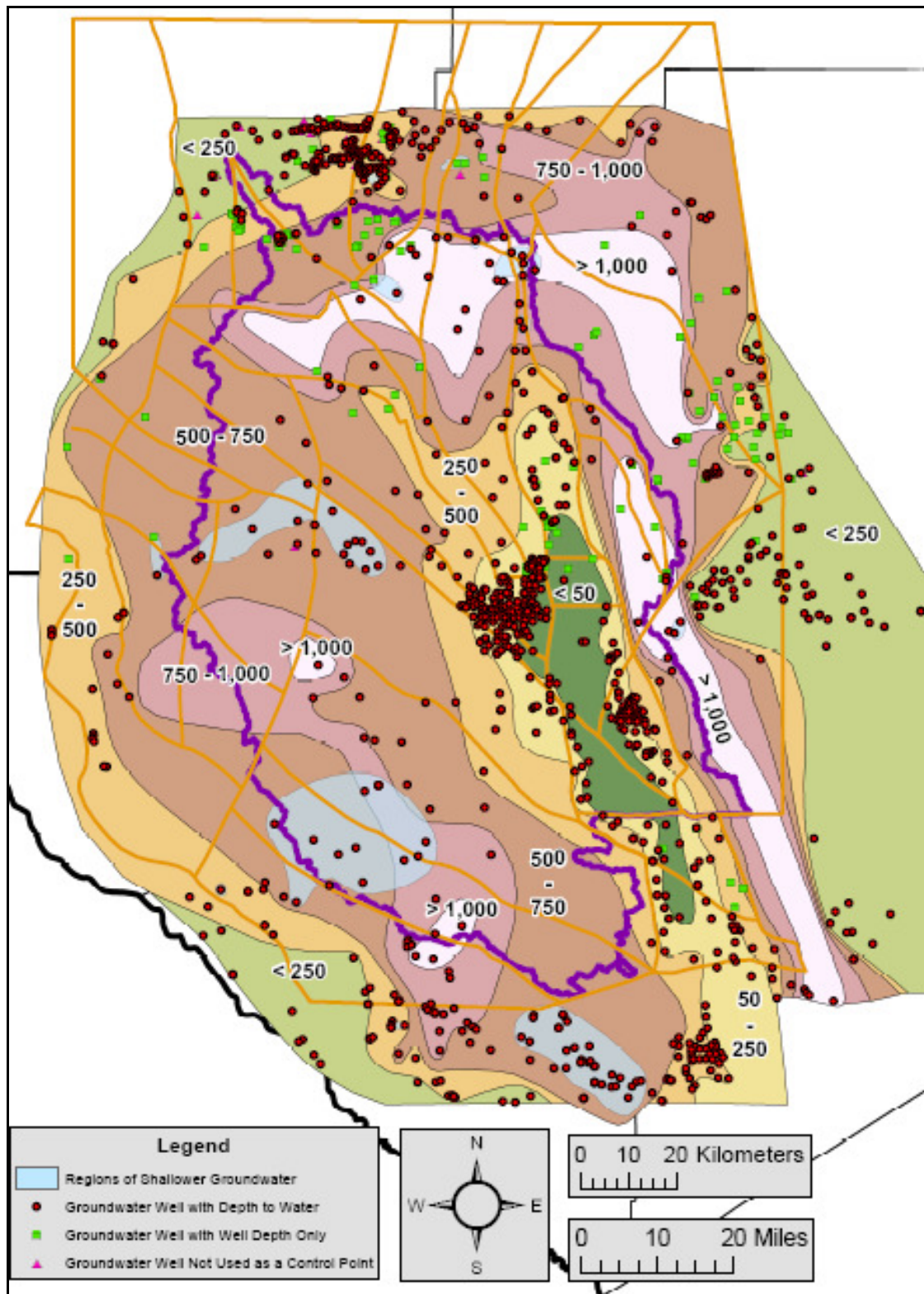
Figure 3.43: Depth-to-groundwater for the Salt Basin region.
Depths are in feet. Groundwater well symbology is the same as Figure 3.42. Light blue regions delineate zones of shallower groundwater than is indicated by the surrounding depth-to-groundwater polygons.
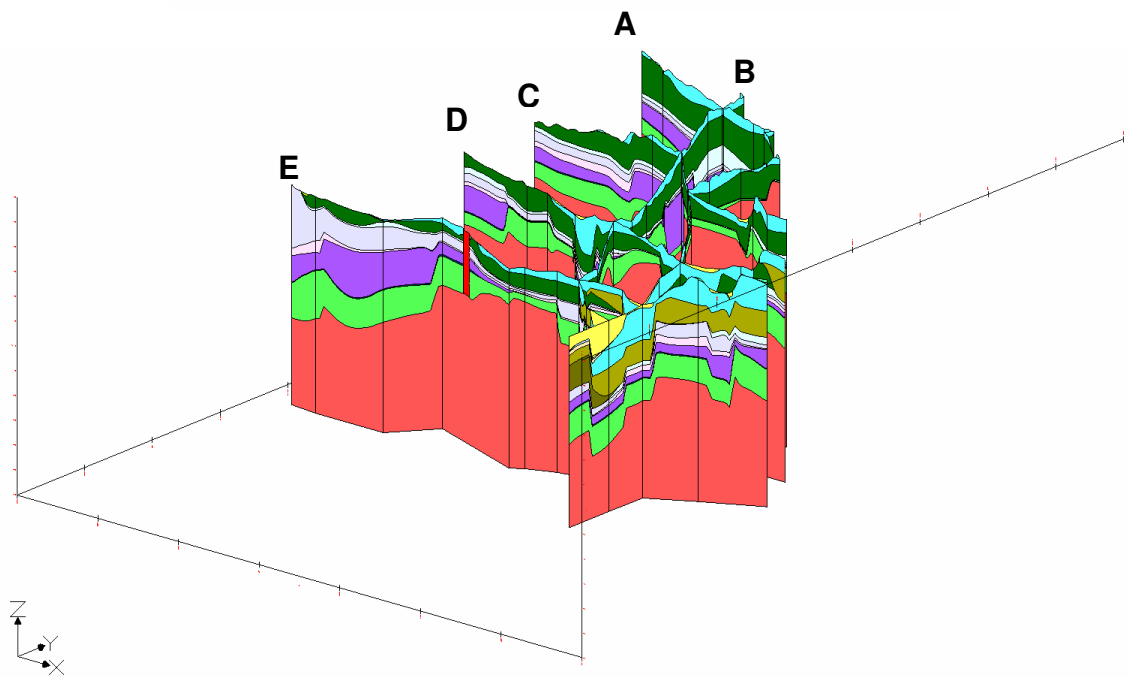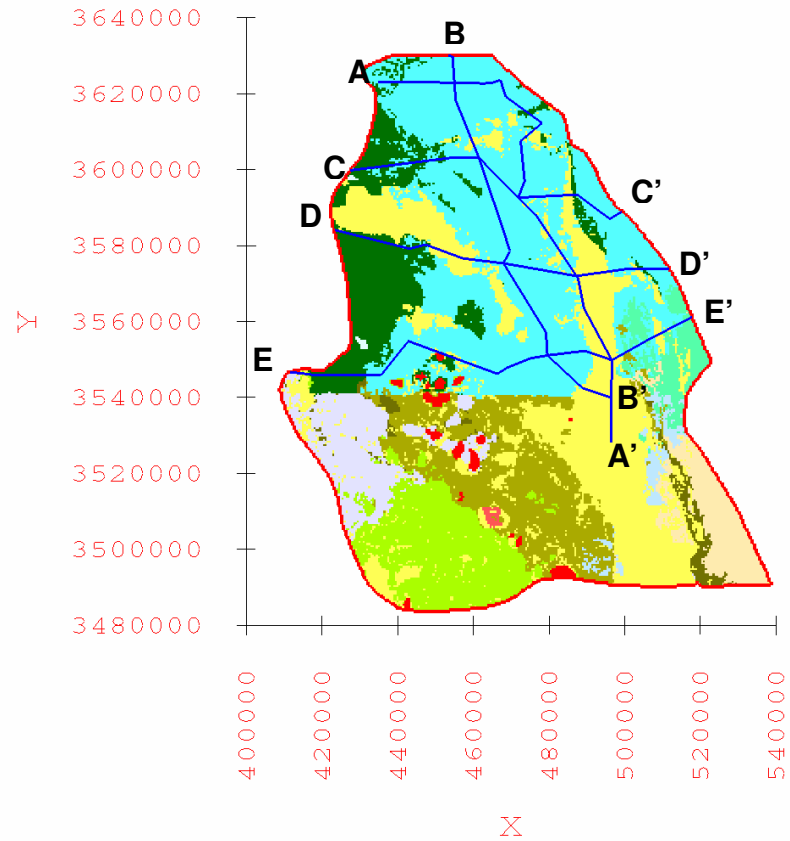
Figure 3.44: Locations and an oblique view of the five cross-sections within the 3-D hydrogeologic framework solid model.
Color-coding of hydrogeologic units corresponds to that used in Figure 2.1, and Figures 3.37 through 3.41. Red line designates groundwater flow model boundary. Blue lines indicate cross-sections. Vertical exaggeration 10×.
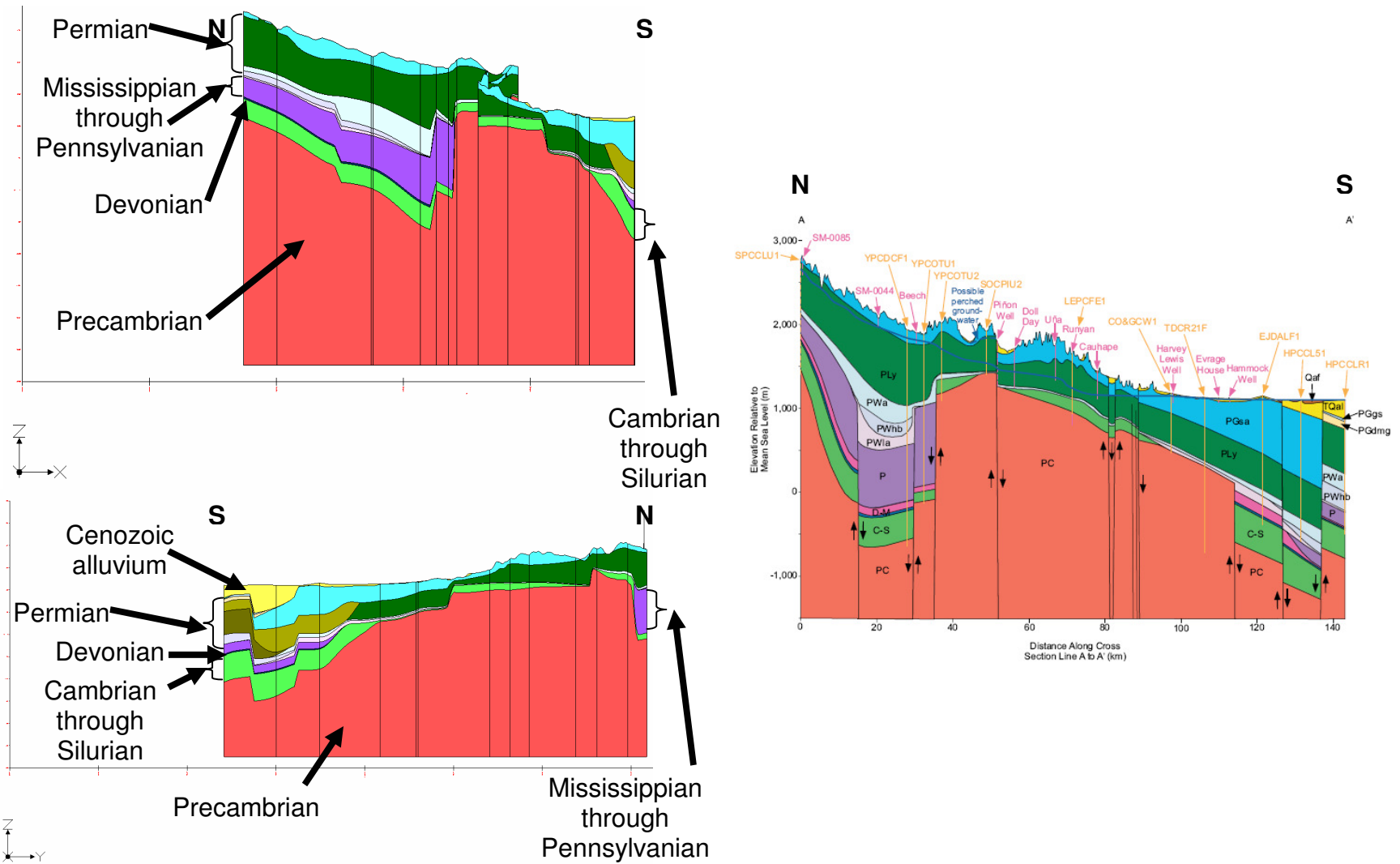
Figure 3.45: Side views along cross-section A - A' of the 3-D framework solid model on left and hand-drawn cross-section on right. Vertical exaggeration 10× on 3-D framework solid model cross-sections. Vertical exaggeration 23× on hand-drawn cross-section.

242
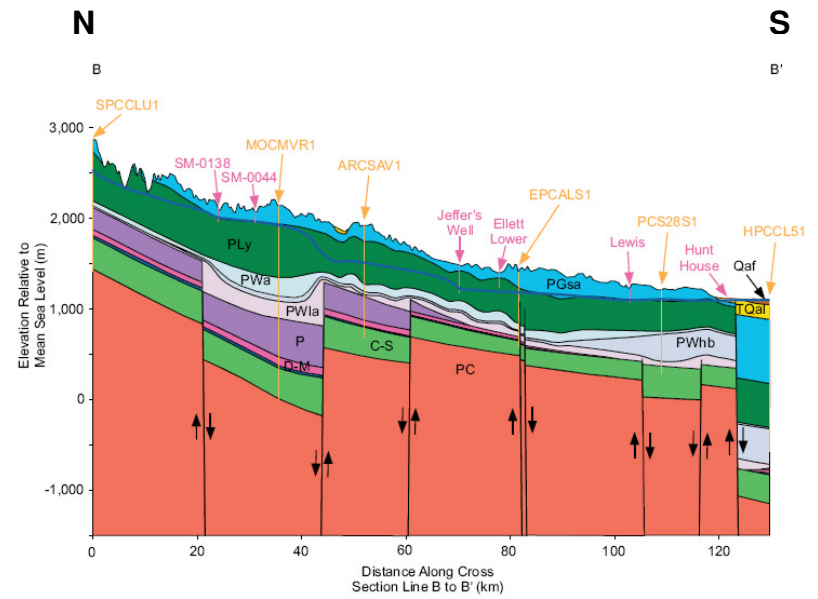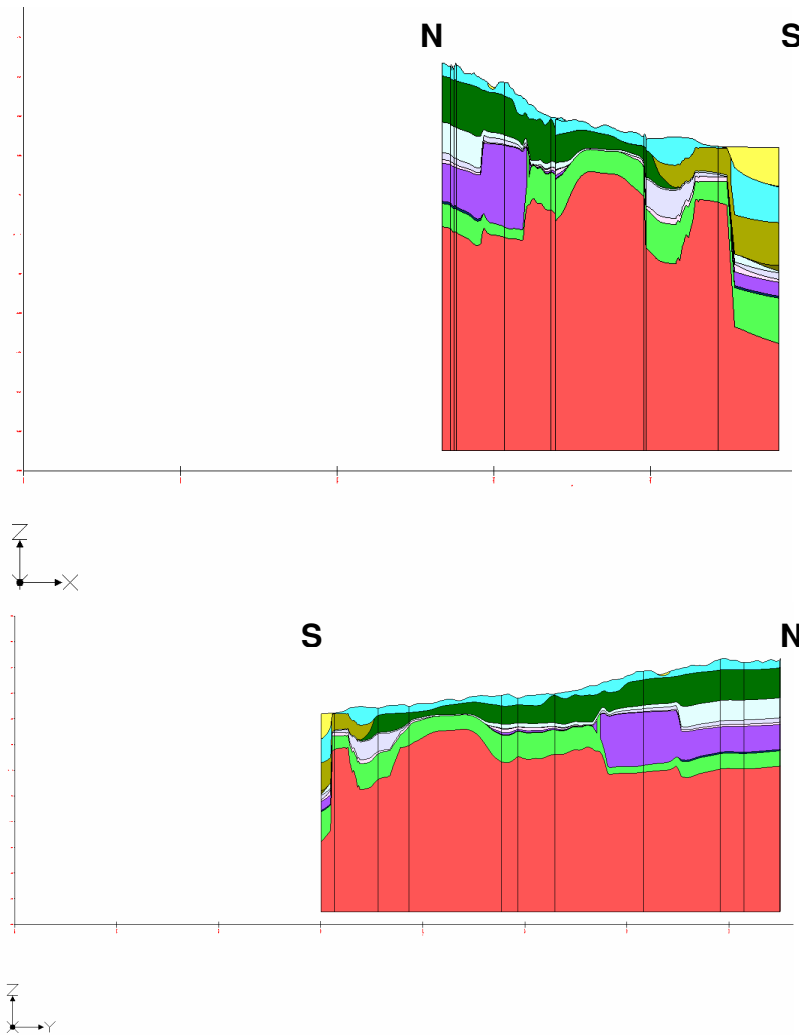
Figure 3.46: Side views along cross-section B - B' of the 3-D framework solid model on left and hand-drawn cross-section on right. Vertical exaggeration 10× on 3-D framework solid model cross-sections. Vertical exaggeration 18× on hand-drawn cross-section.
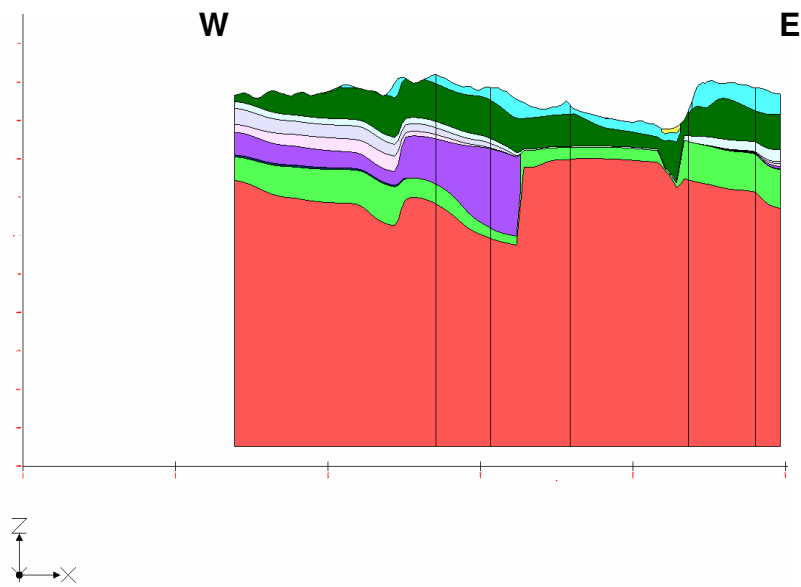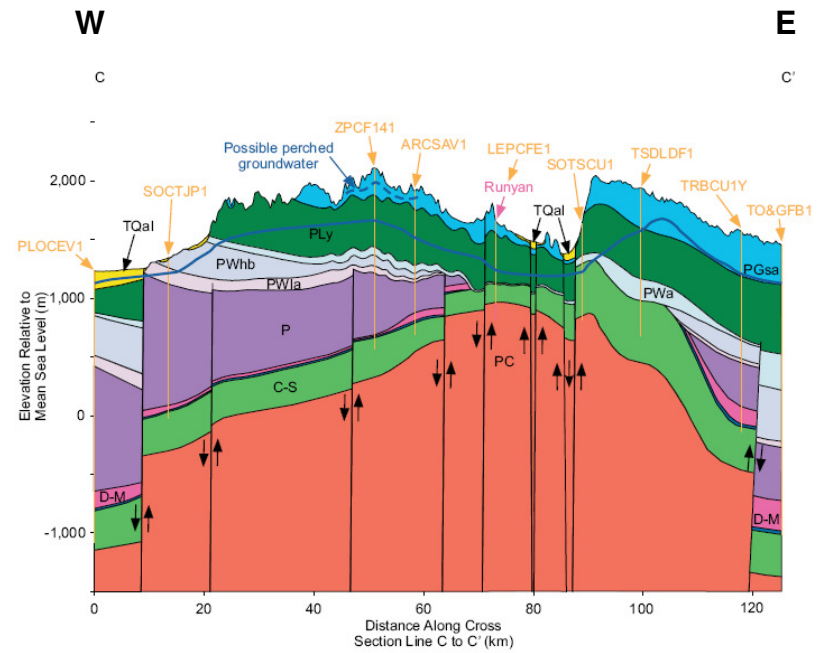
Figure 3.47: Side views along cross-section C - C' of the 3-D framework solid model on left and hand-drawn cross-section on right. Vertical exaggeration 10× on 3-D framework solid model cross-section. Vertical exaggeration 22× on hand-drawn cross-section.
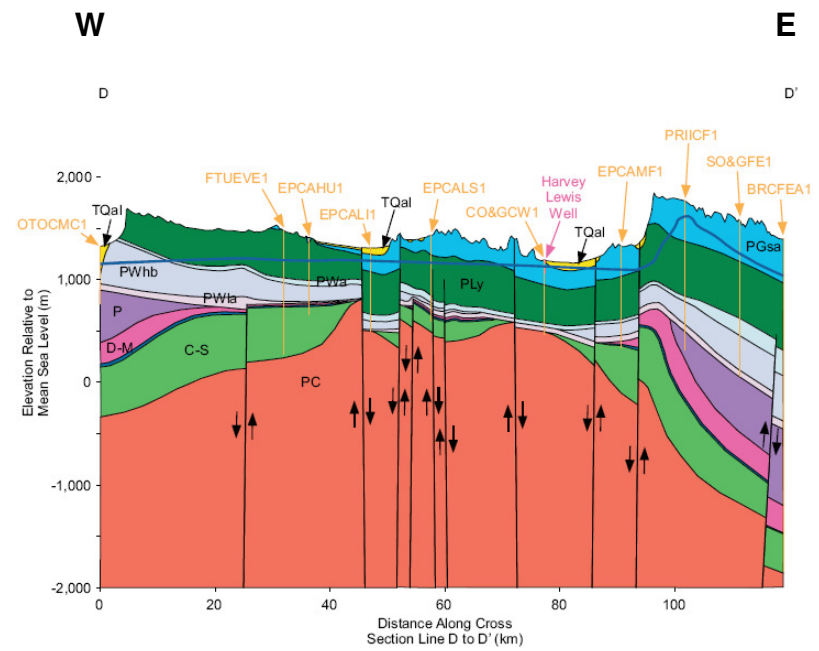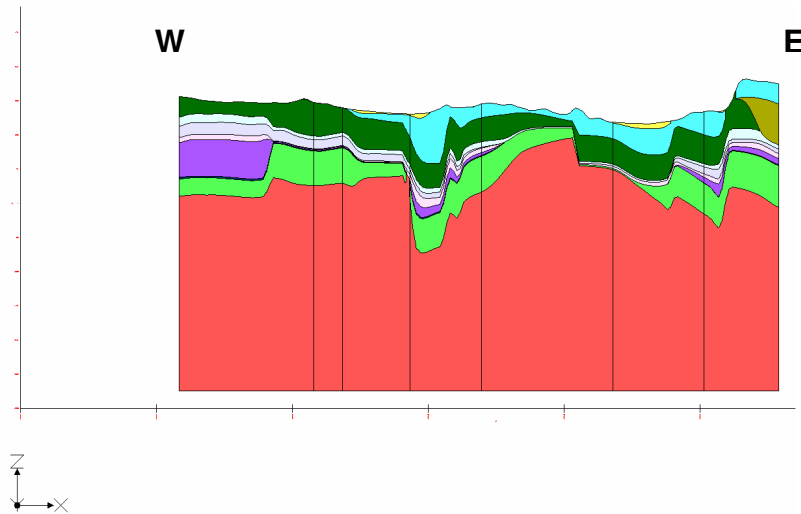
Figure 3.48: Side views along cross-section D - D' of the 3-D framework solid model on left and hand-drawn cross-section on right. Vertical exaggeration 10× on 3-D framework solid model cross-section. Vertical exaggeration 18× on hand-drawn cross-section.
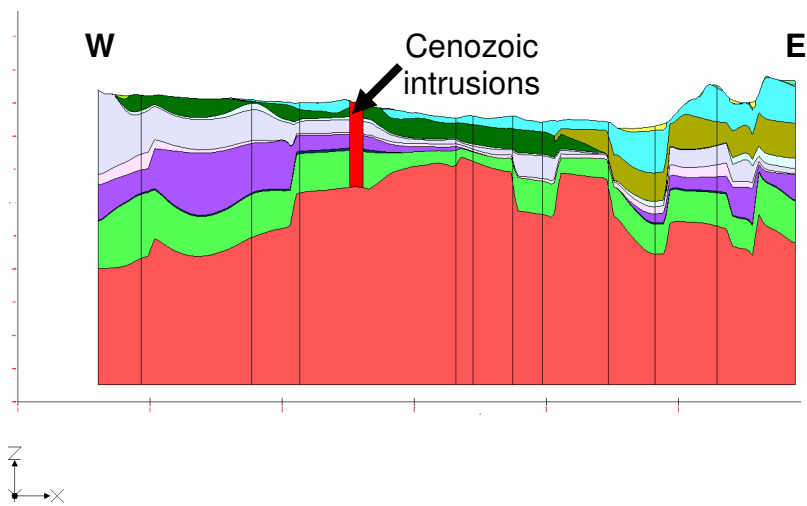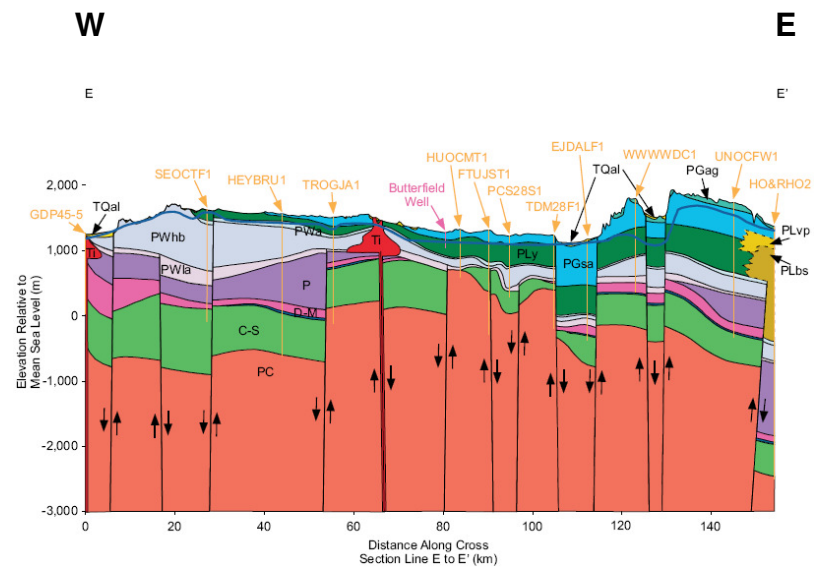
Figure 3.49: Side views along cross-section E - E' of the 3-D framework solid model on left and hand-drawn cross-section on right. Vertical exaggeration 10× on 3-D framework solid model cross-section. Vertical exaggeration 15× on hand-drawn cross-section.
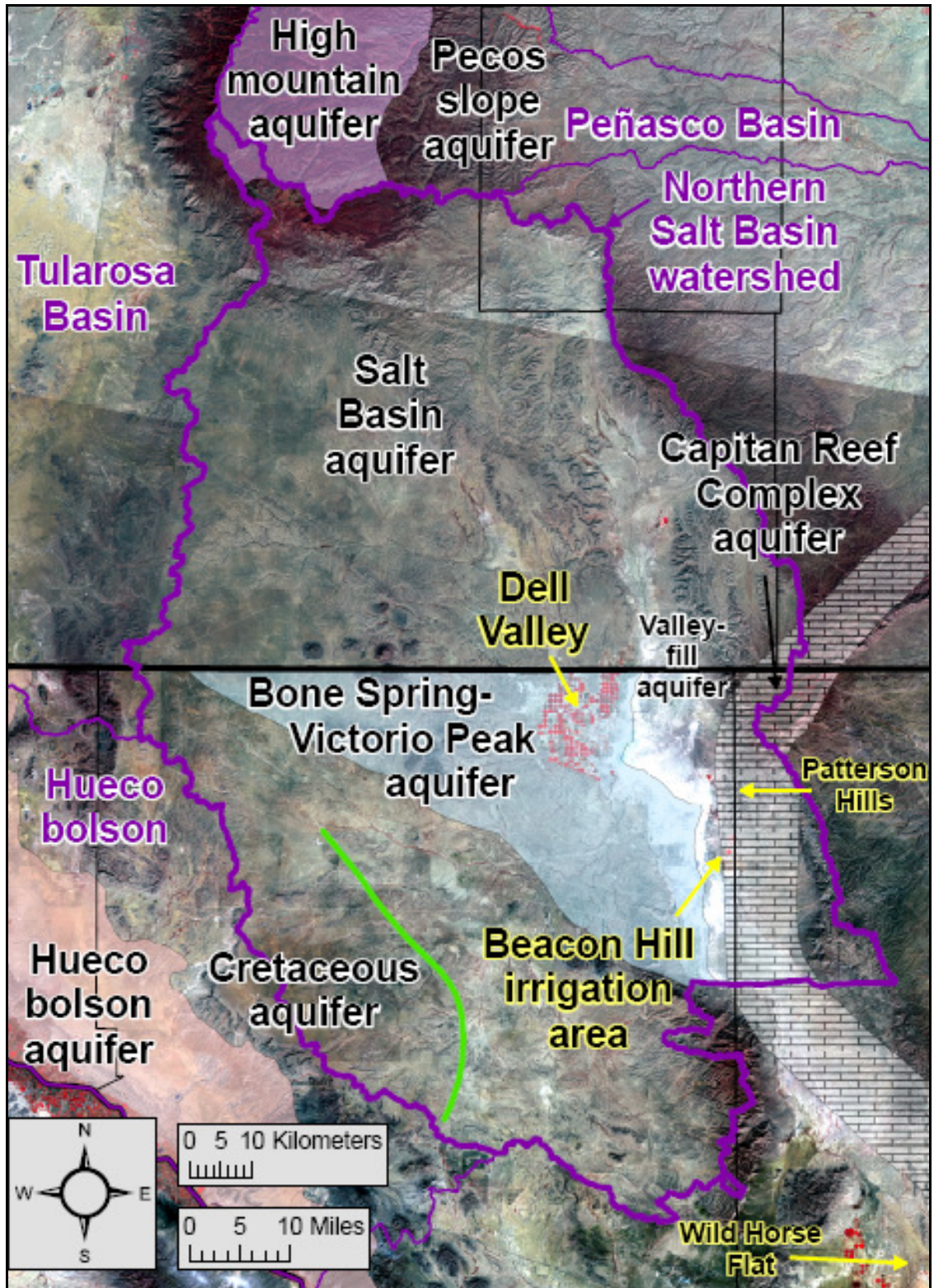
Figure 3.50: Aquifers in the Salt Basin region.
Location of high mountain and Pecos slope aquifers from SMHS. Location of Bone
Spring-Victorio Peak and Hueco bolson aquifers from TWDB. Location of Capitan Reef
Complex aquifer from Uliana (2001). Location of Cretaceous aquifer from Sharp (1989).
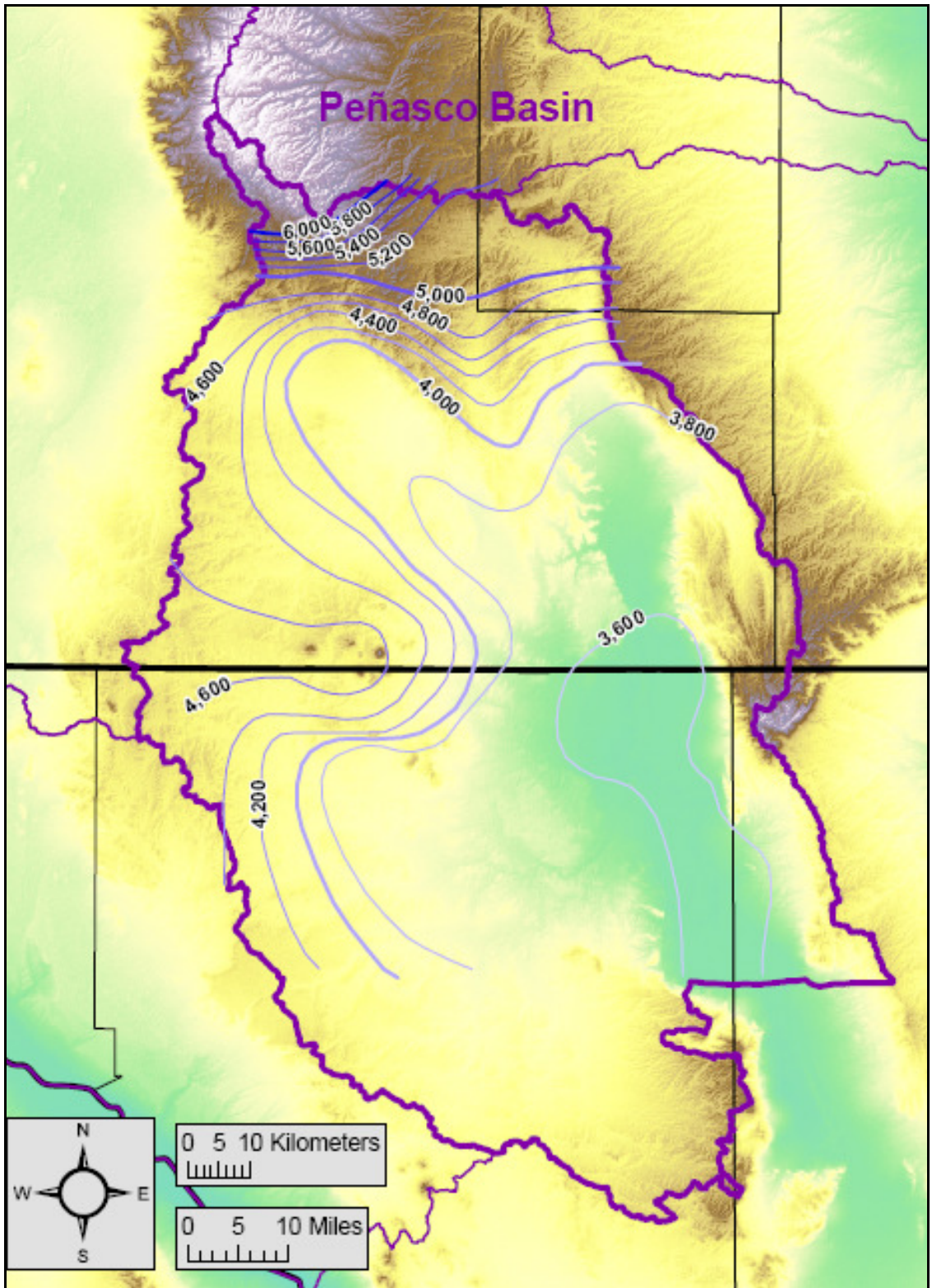
Figure 3.51: Predevelopment groundwater elevation contours, from JSAI (2002). Elevations are in feet above mean sea level. Contour interval is 200 feet.
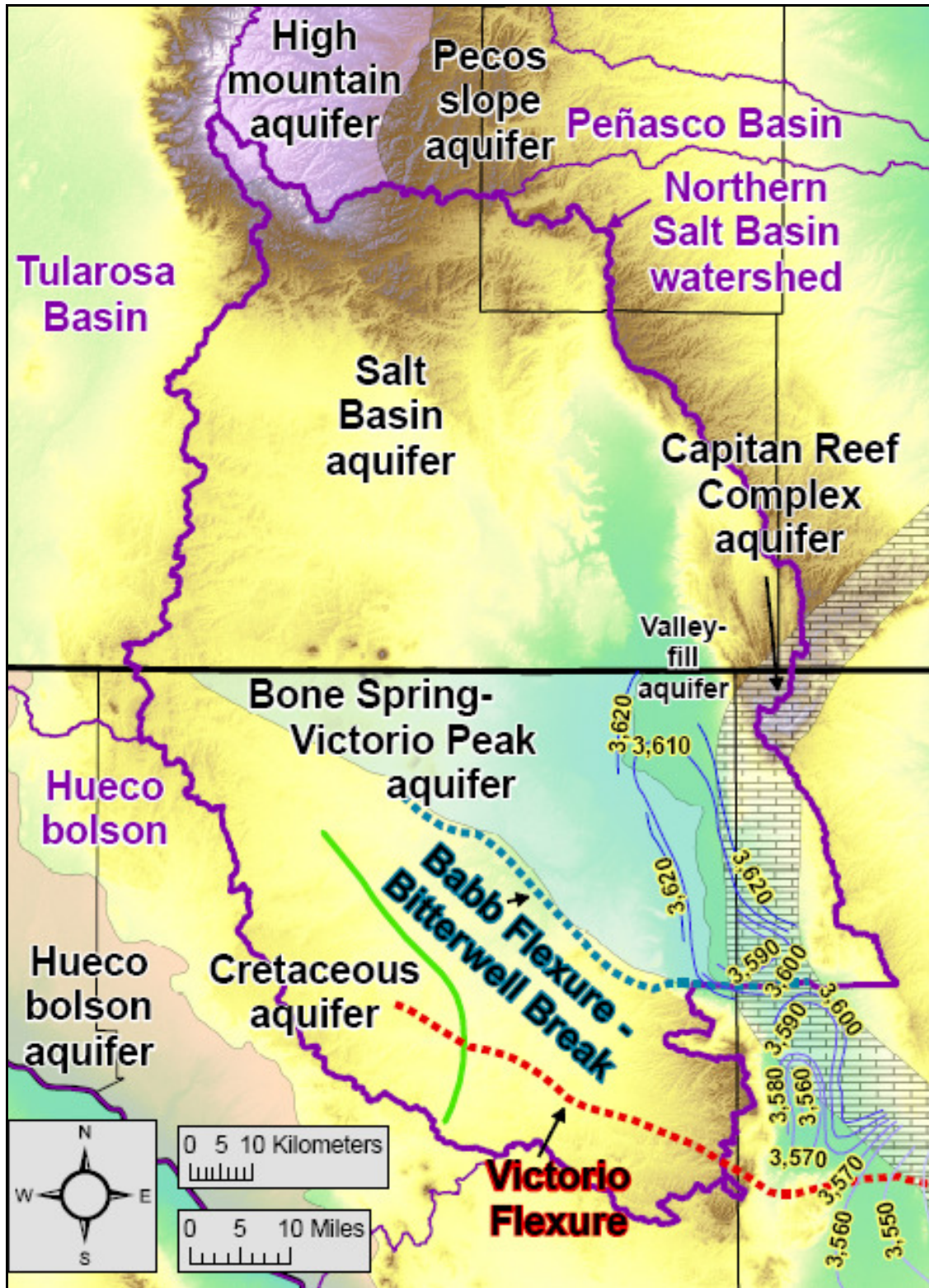
Figure 3.52: Predevelopment groundwater elevation contours for the valley-fill aquifer within the Salt Basin graben, from Sharp (1989).
Elevations are in feet above mean sea level. Contour interval is 10 feet. Also illustrates the structural features associated with groundwater divides in the valley-fill aquifer.
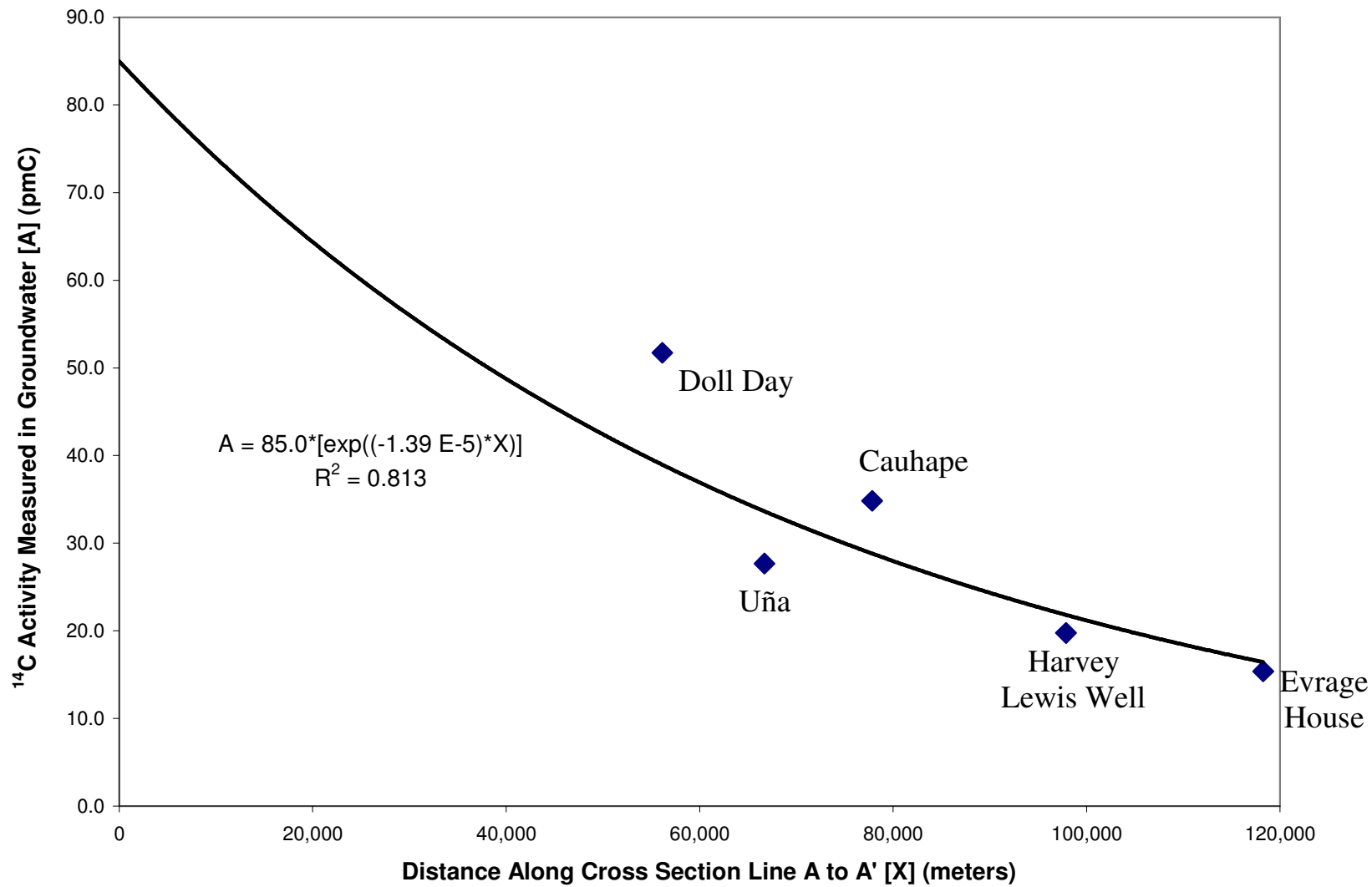
Figure 3.53: ^{14}C activity measured in groundwater versus distance along cross-section line A - A'.
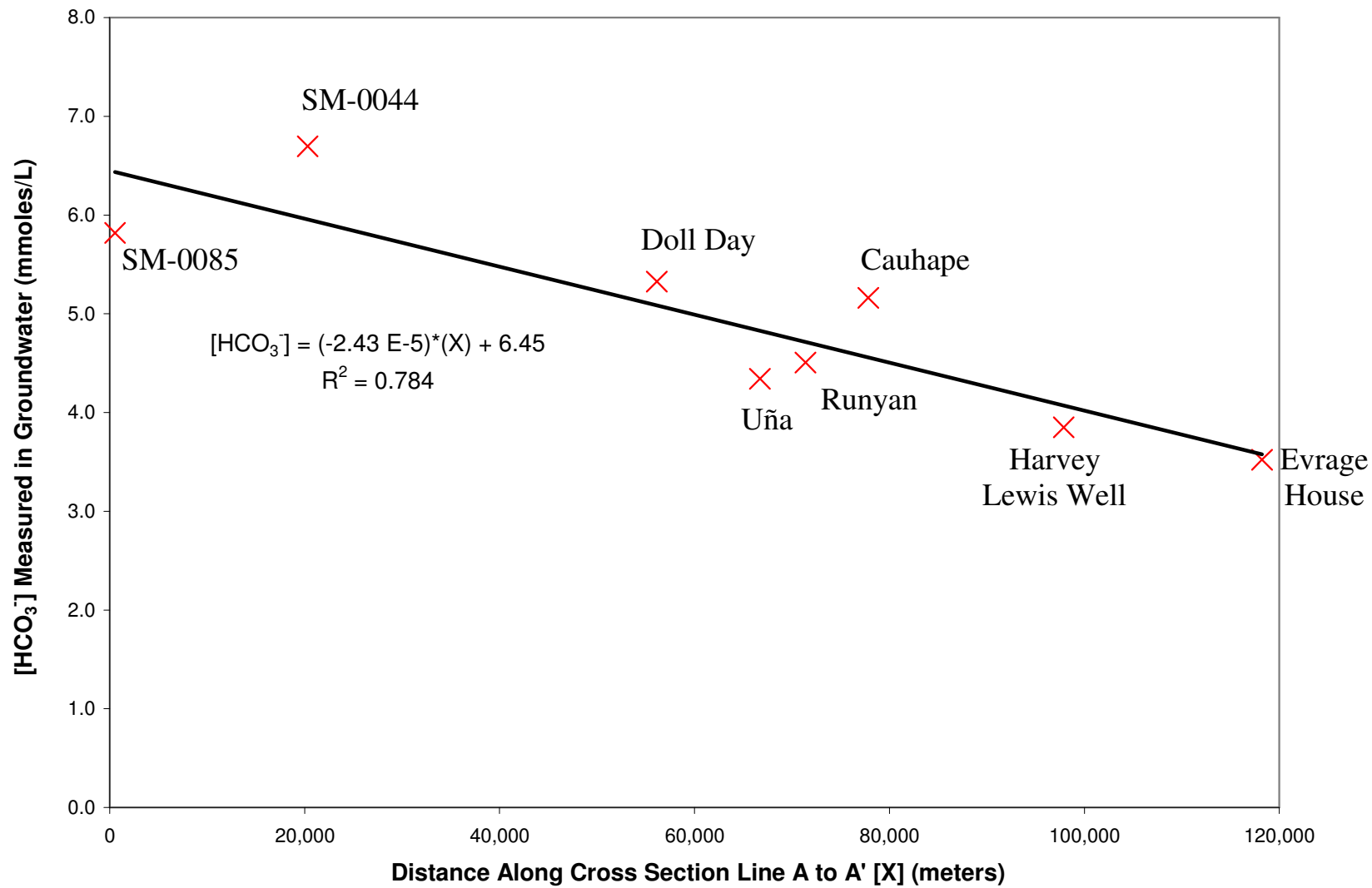
Figure 3.54: [HCO$_3^-$] measured in groundwater versus distance along cross-section line A - A'.

251
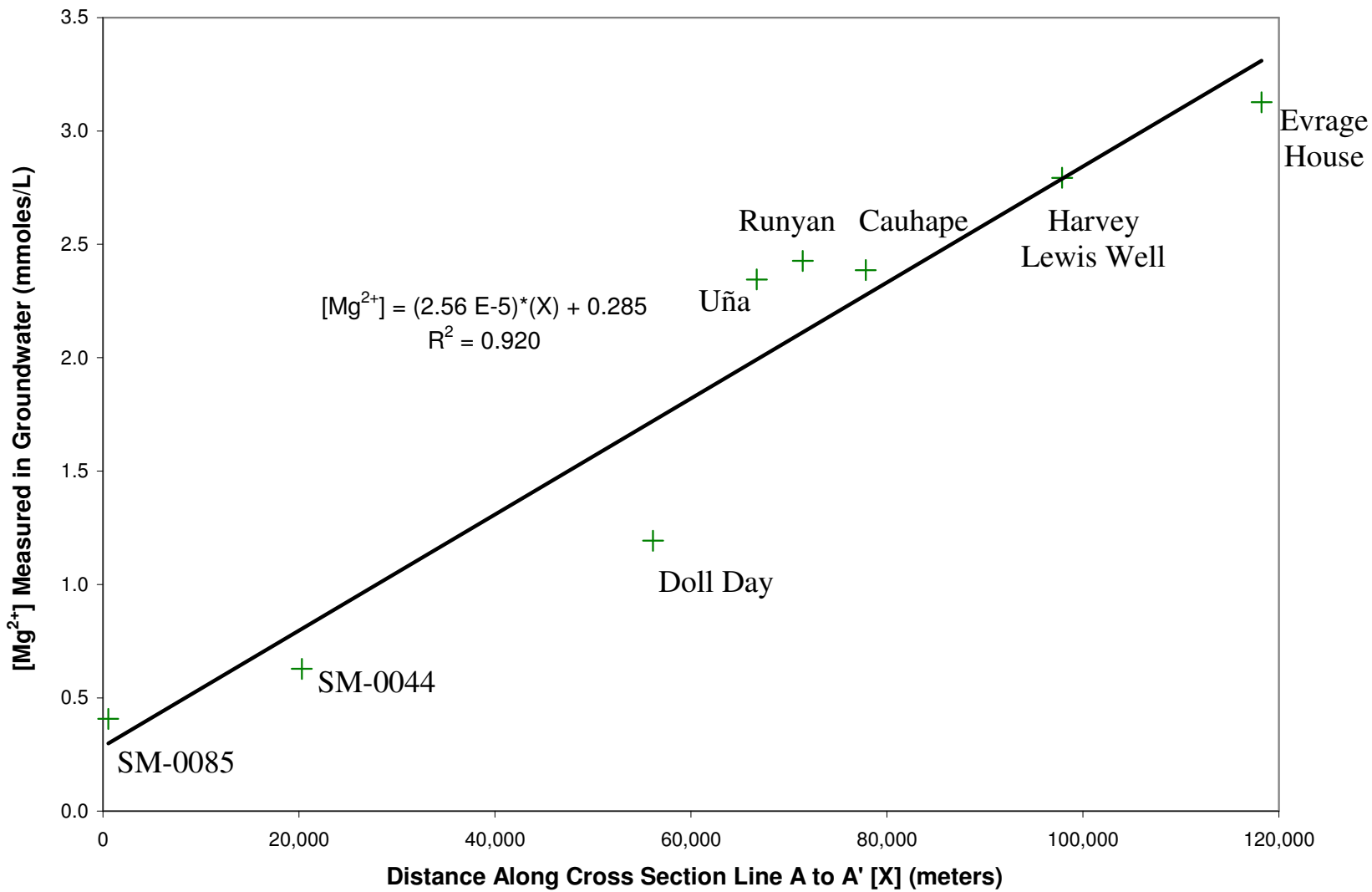
Figure 3.55: [Mg^{2+}] measured in groundwater versus distance along cross-section line A - A'.
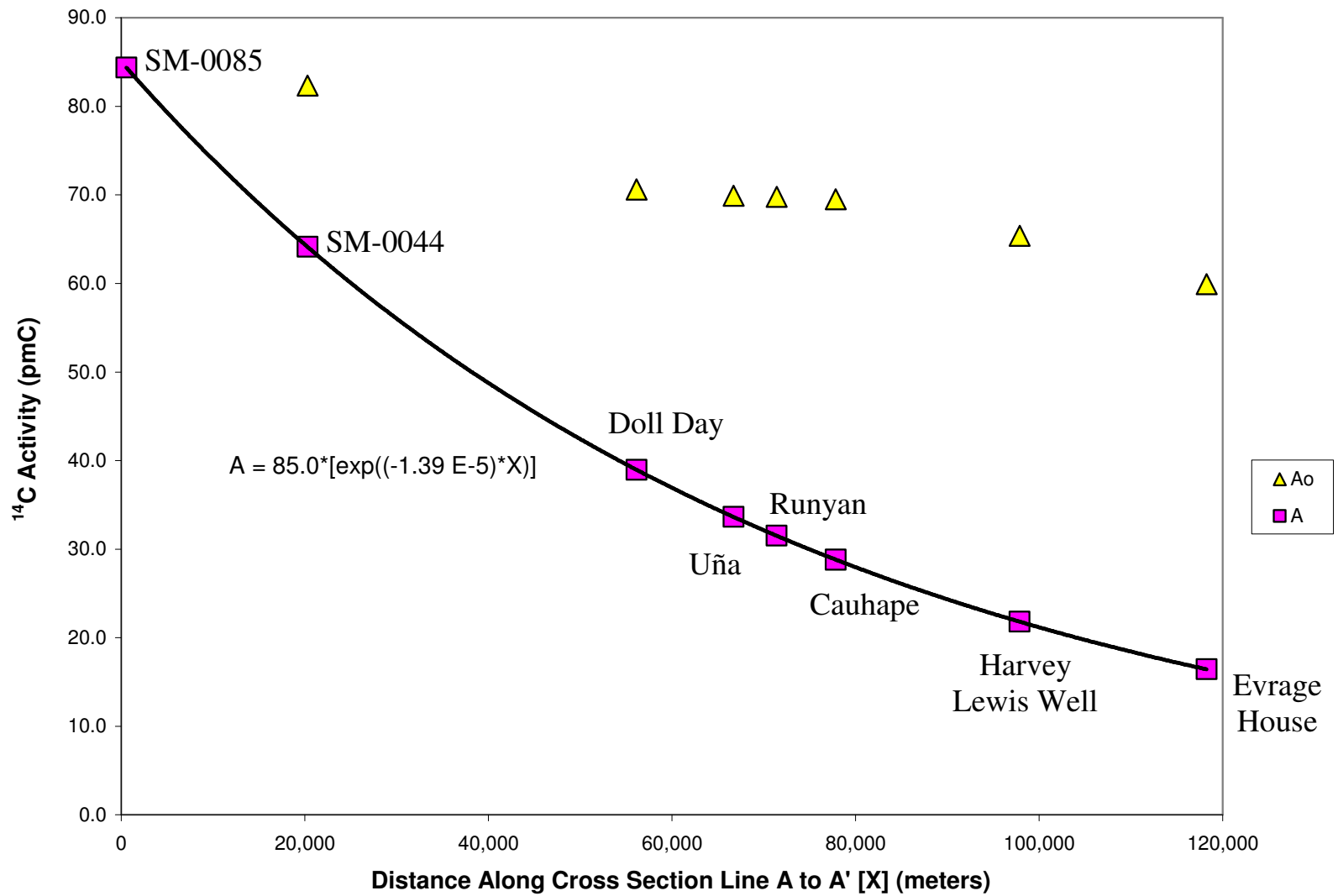
Figure 3.56: ^{14}C activity [A] and [A_0] versus distance along cross-section line A - A'.
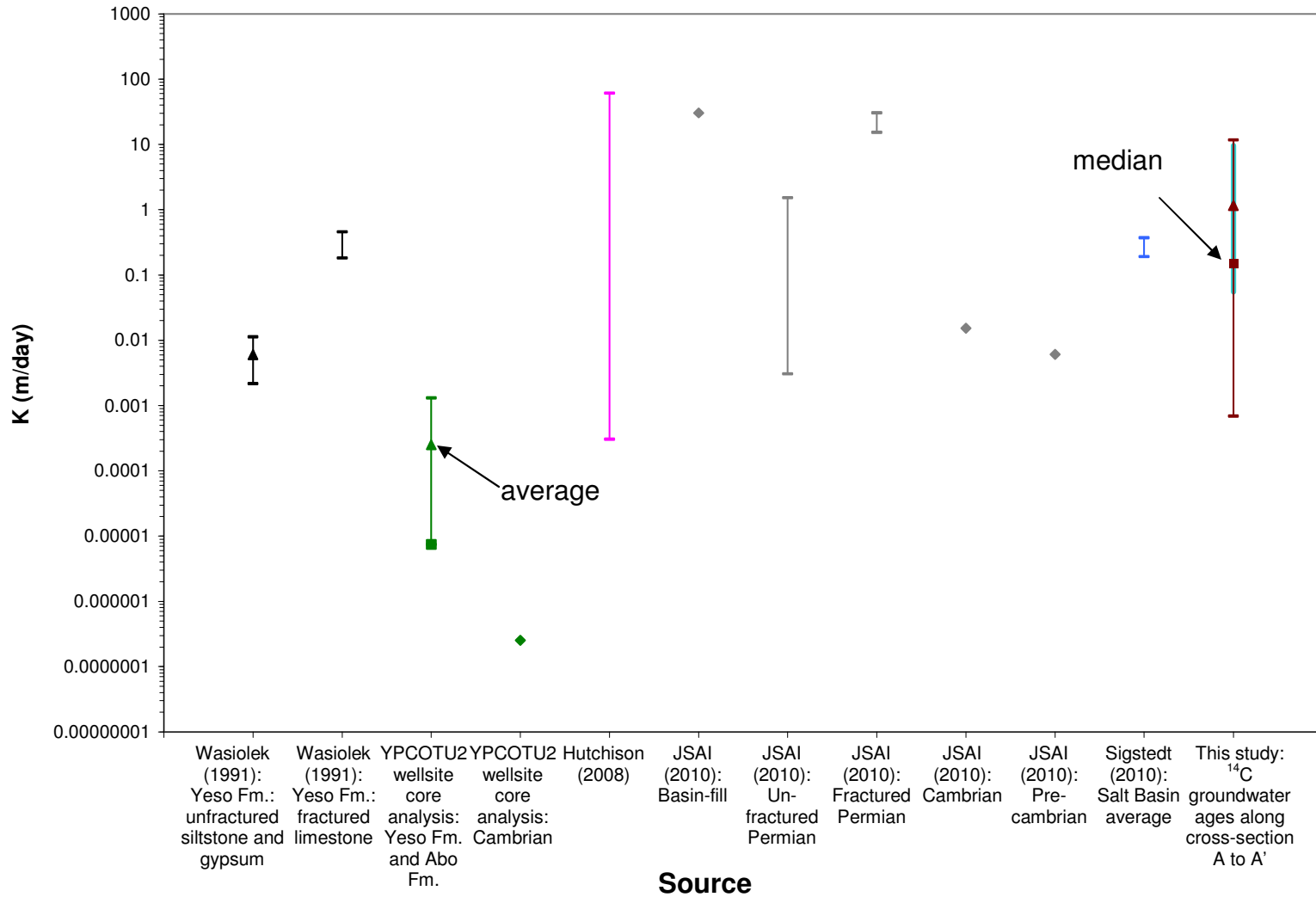
Figure 3.57: Range of hydraulic conductivity [K] values from previous studies and this study.
Vertical axis is logarithmic scale. Squares indicate median values, and triangles indicate average values.
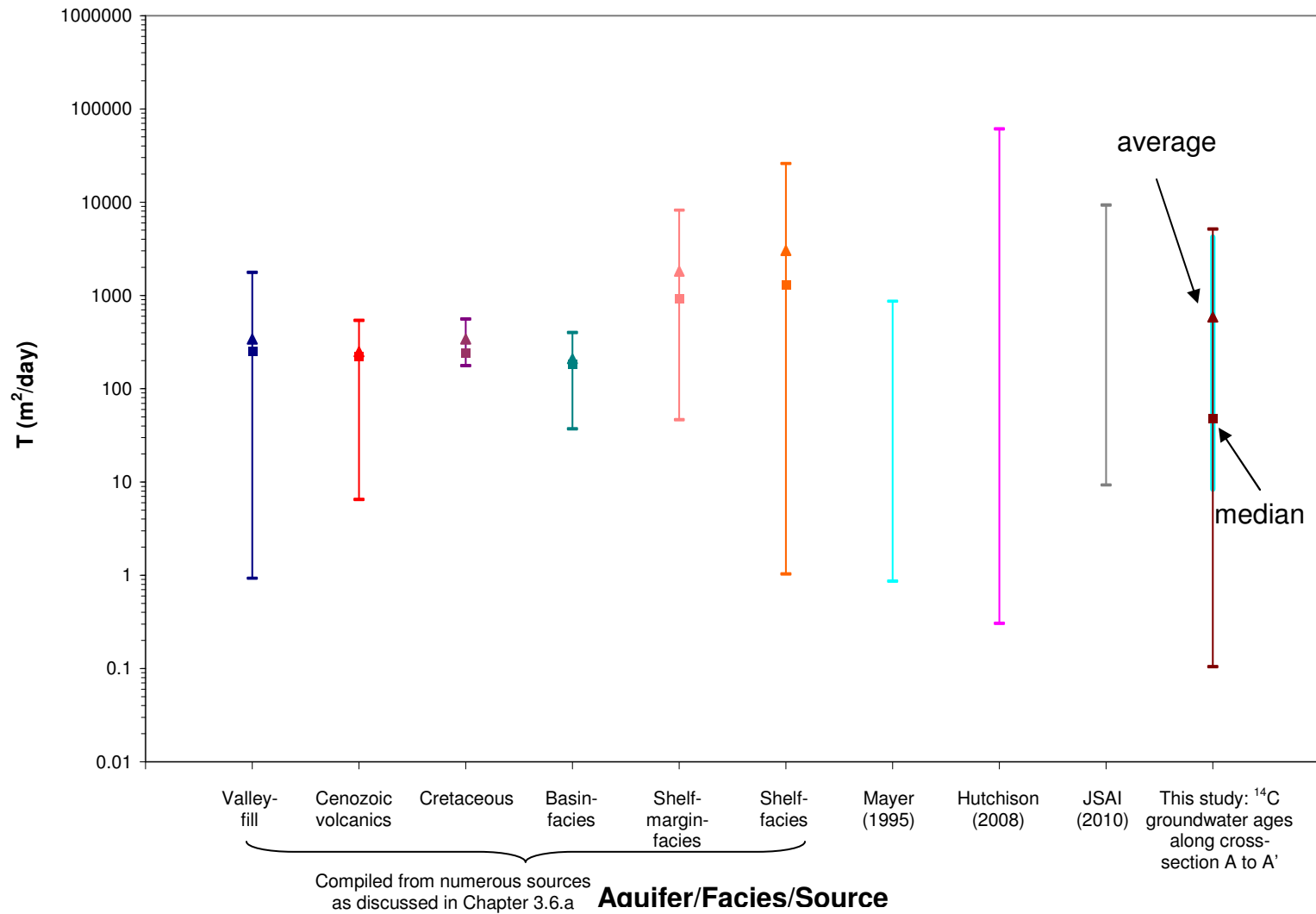
Figure 3.58: Range of transmissivity [T] values from previous studies and this study.
Vertical axis is logarithmic scale. Squares indicate median values, and triangles indicate average values.
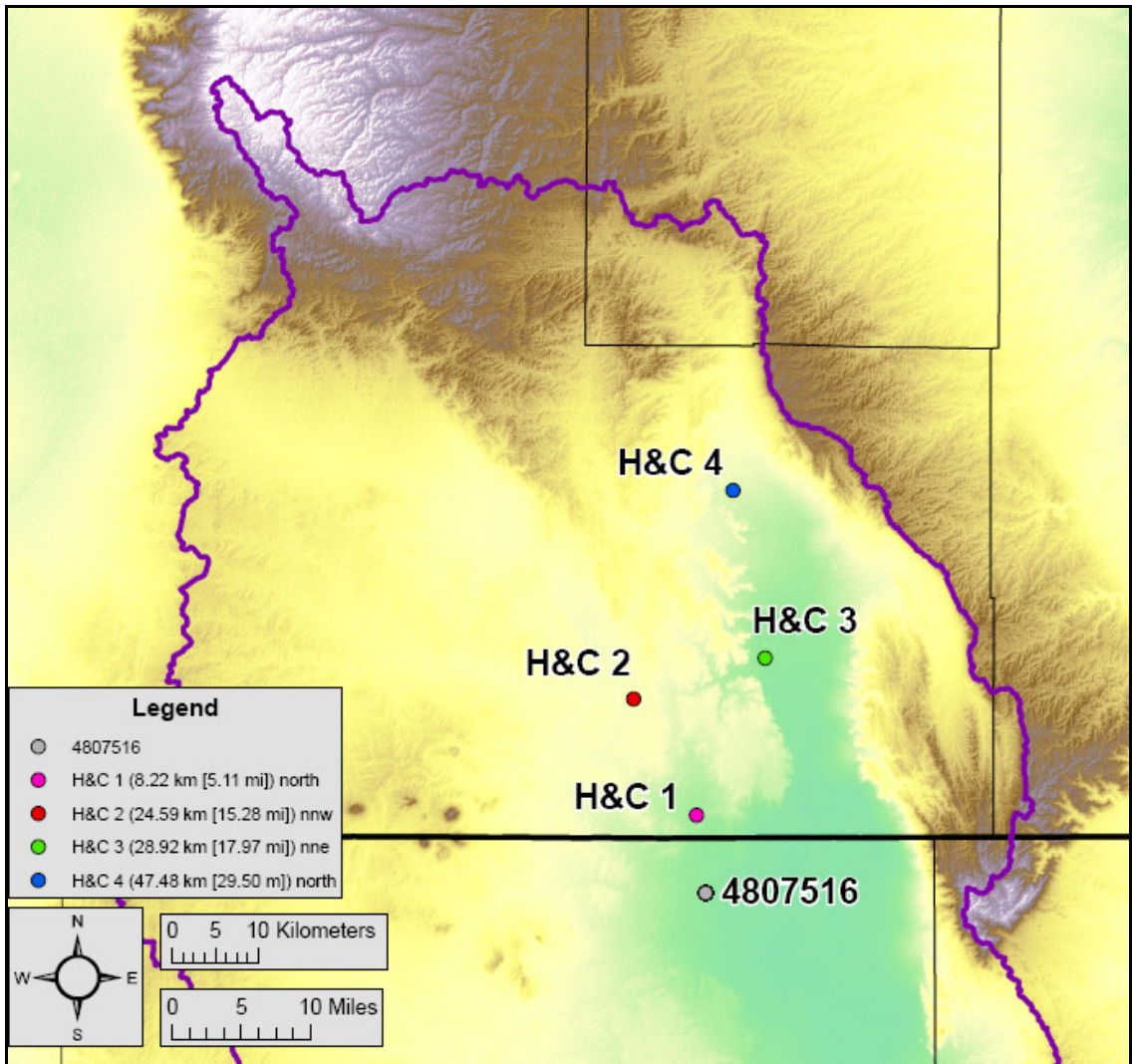
Figure 3.59: Location of the four groundwater wells in the New Mexico portion of the Salt Basin watershed with continuous water level measurements from 2003 to the middle of 2006, as presented in Huff and Chace (2006), and the TWDB's State Well Number 4807516.
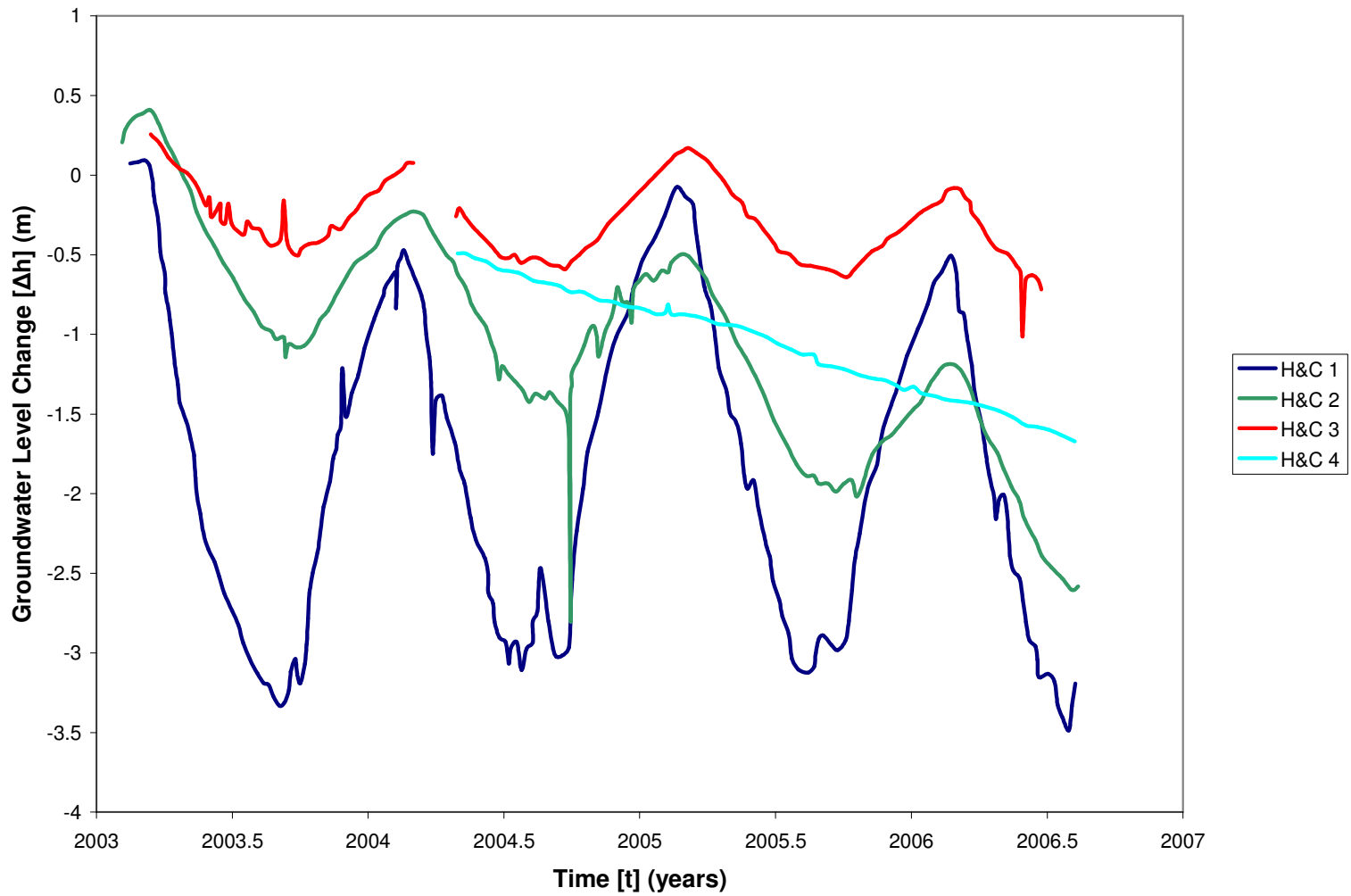
Figure 3.60: Change in groundwater levels versus time for wells H&C 1, H&C 2, H&C 3, and H&C 4.
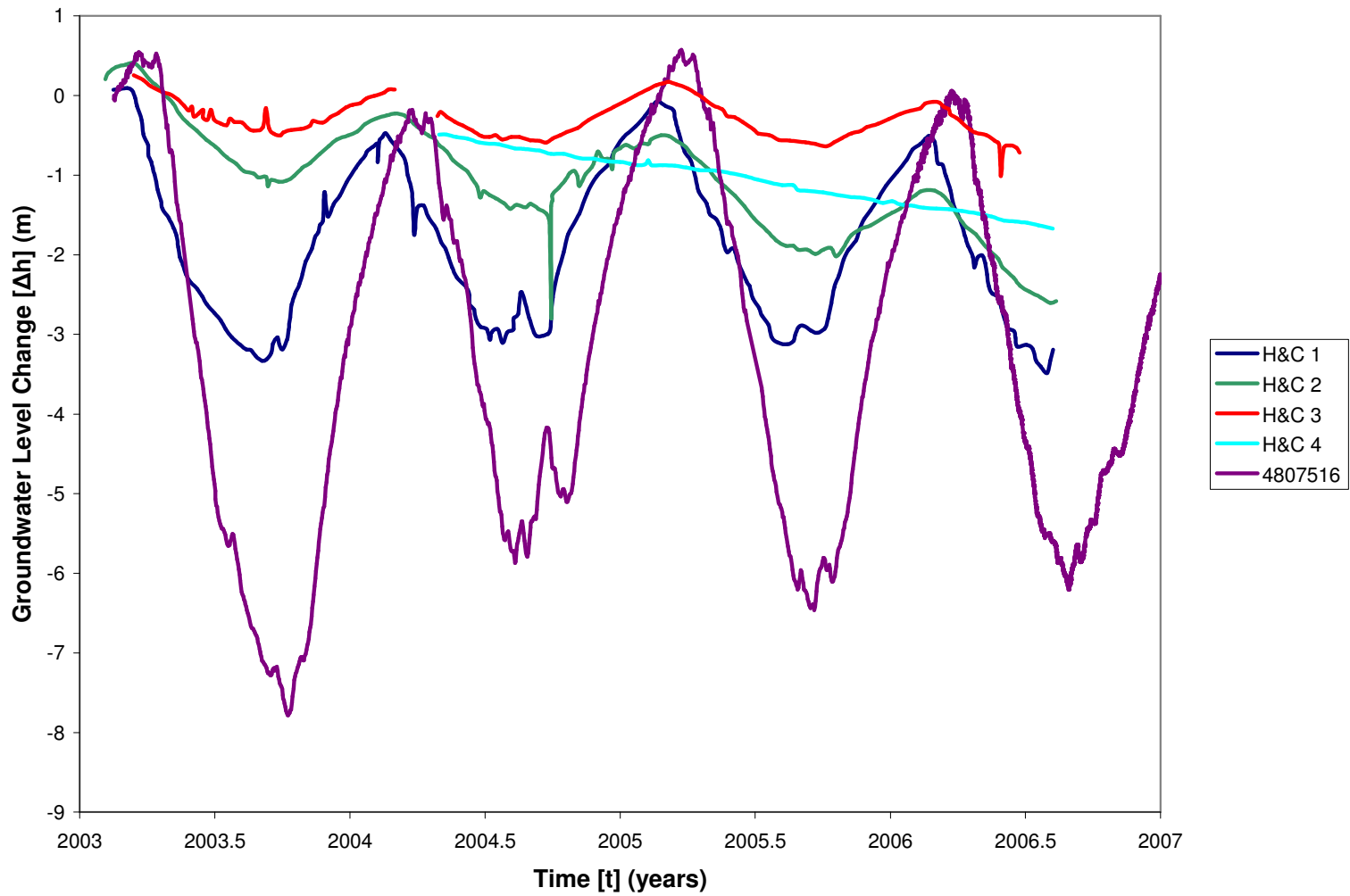
Figure 3.61: Change in groundwater levels versus time for wells H&C 1, H&C 2, H&C 3, H&C 4, and 4807516.
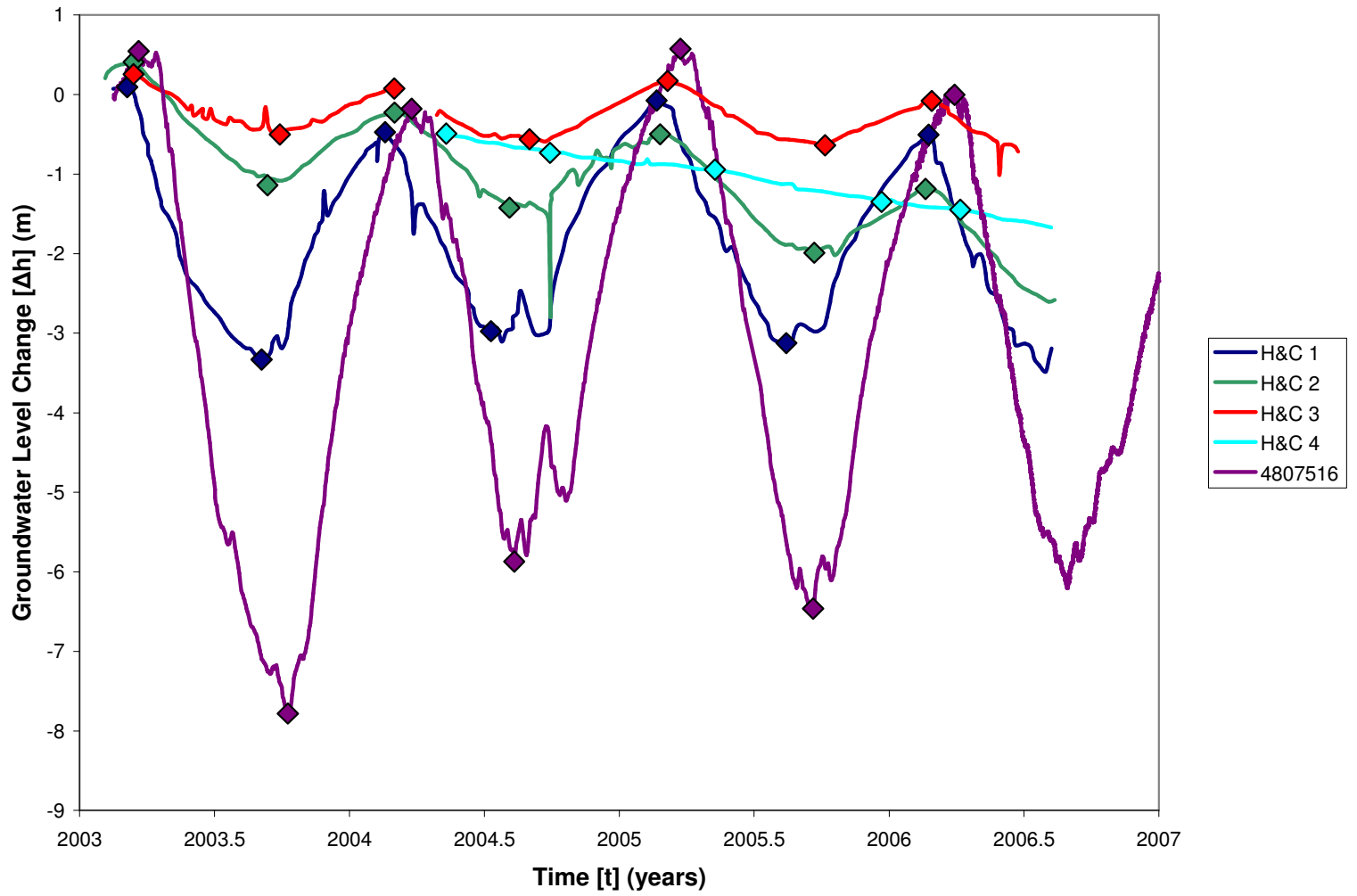
Figure 3.62: Location of maximum and minimum change in groundwater levels used to calculate the average annual amplitude of water level fluctuations in wells H&C 1, 2, 3, and 4, and 4807516.

$\Delta h = -0.507*[t] + 1.02\ E3$

$R^2 = 0.994$
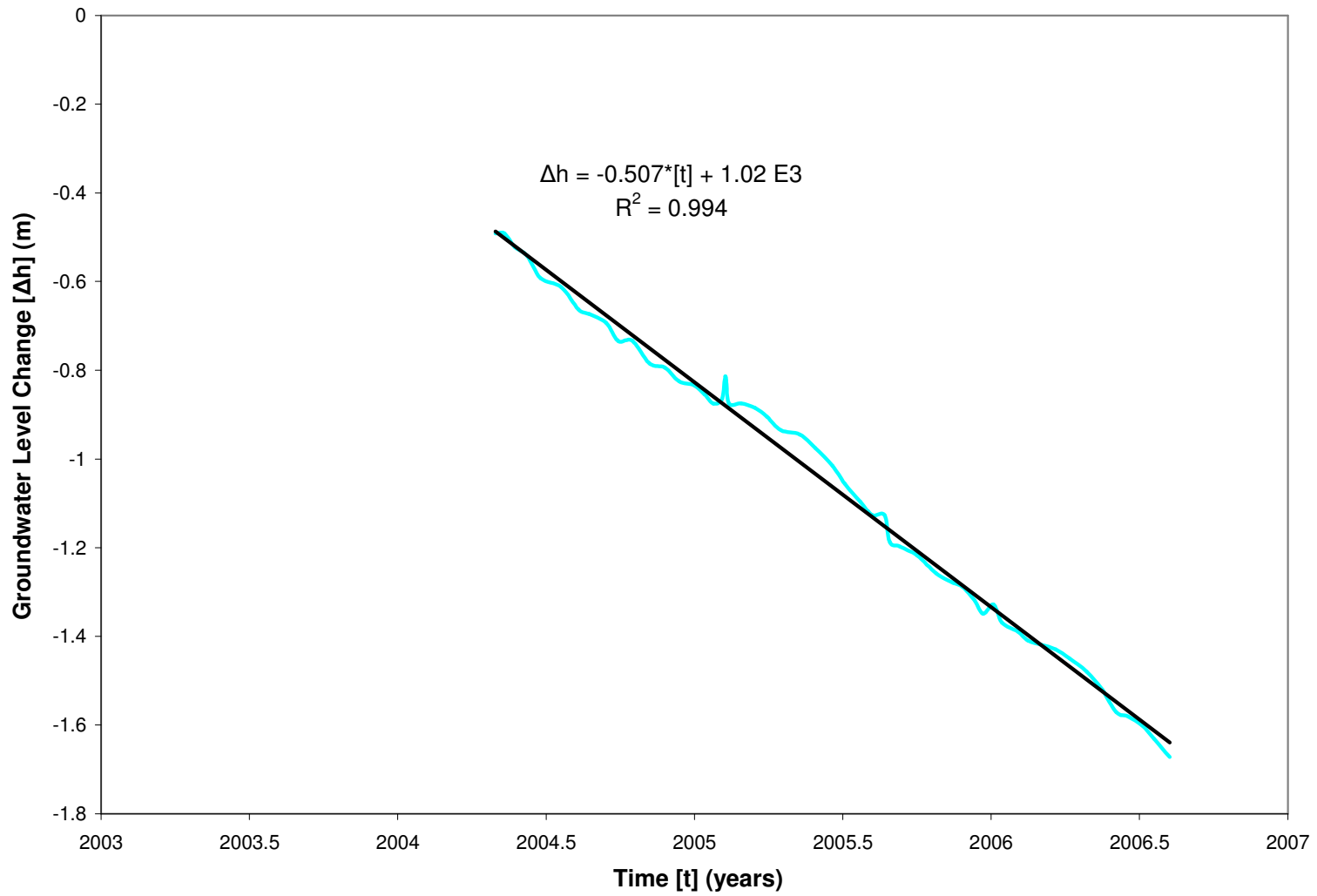
Figure 3.63: Change in groundwater level versus time for well H&C 4.
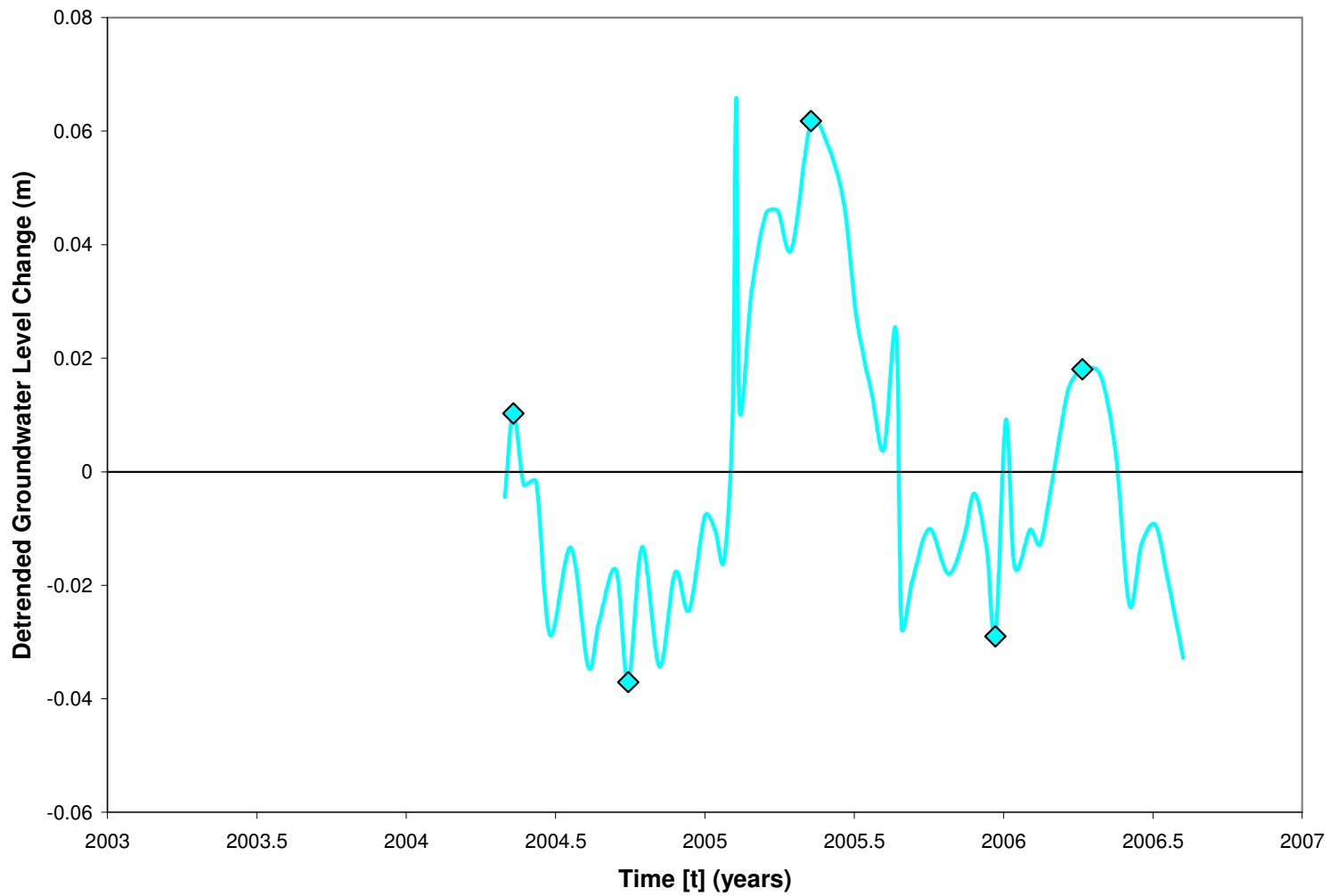
Figure 3.64: Detrended change in groundwater level versus time for well H&C 4.
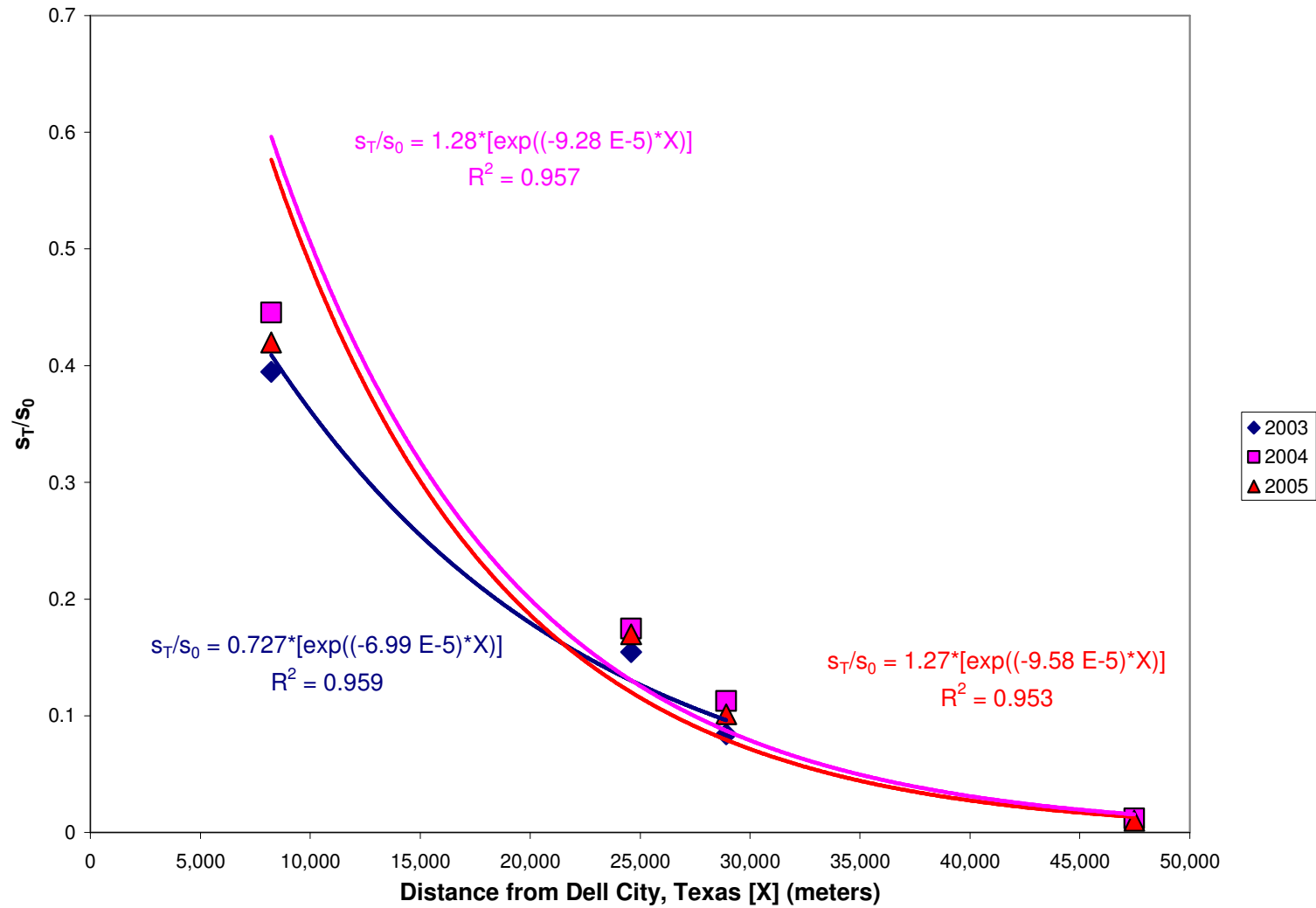
Figure 3.65: s_T/s_0 calculated from water level fluctuations in 2003 at wells H&C 1, 2, and 3, and 4807516, and in 2004 and 2005 at wells H&C 1, 2, 3, and 4, and 4807516 versus distance from Dell City, Texas.
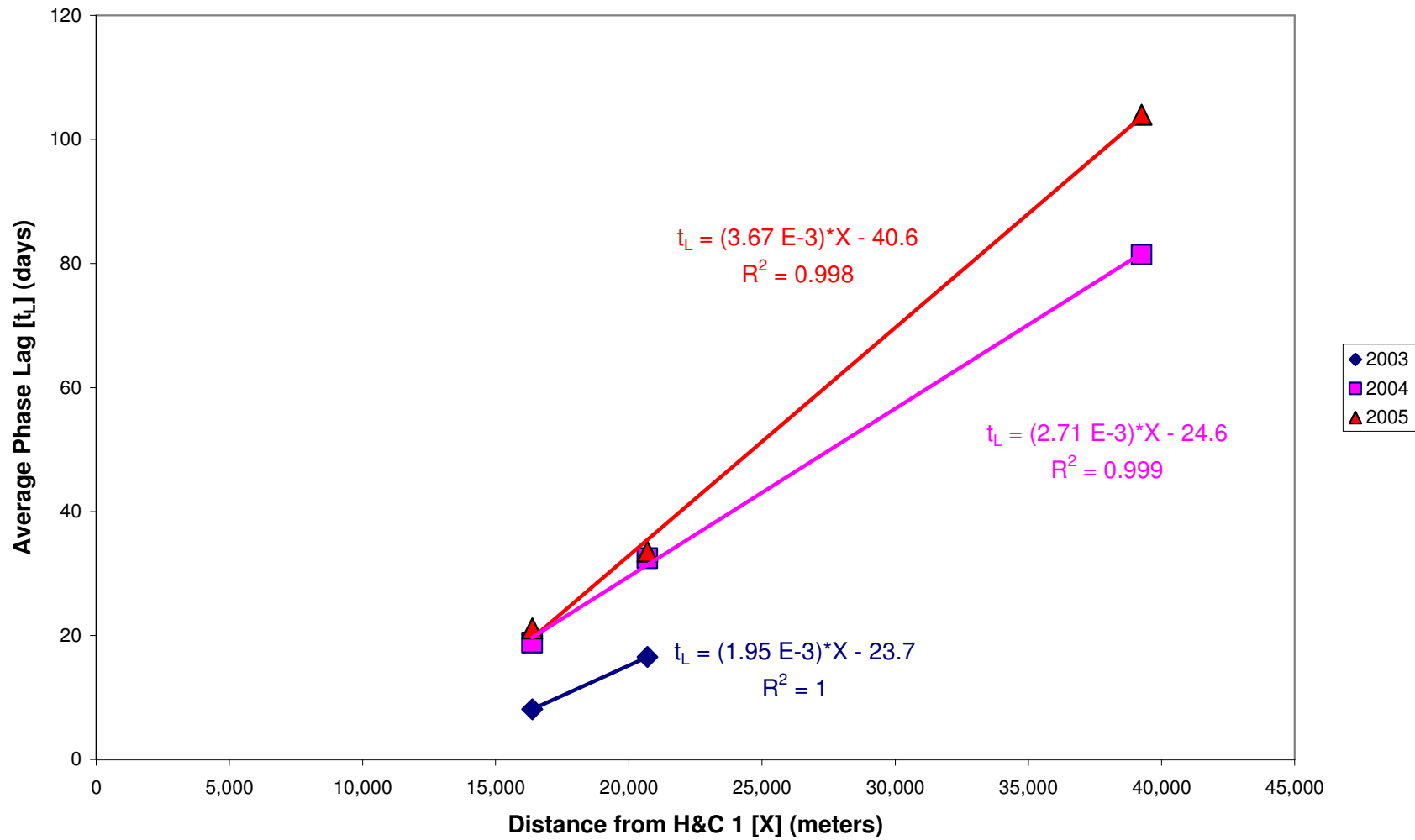
Figure 3.66: Average phase lag between well H&C 1 and wells H&C 2 and 3 in 2003, and well H&C 1 and wells H&C 2, 3, and 4 in 2004 and 2005 versus distance from well H&C 1.

263
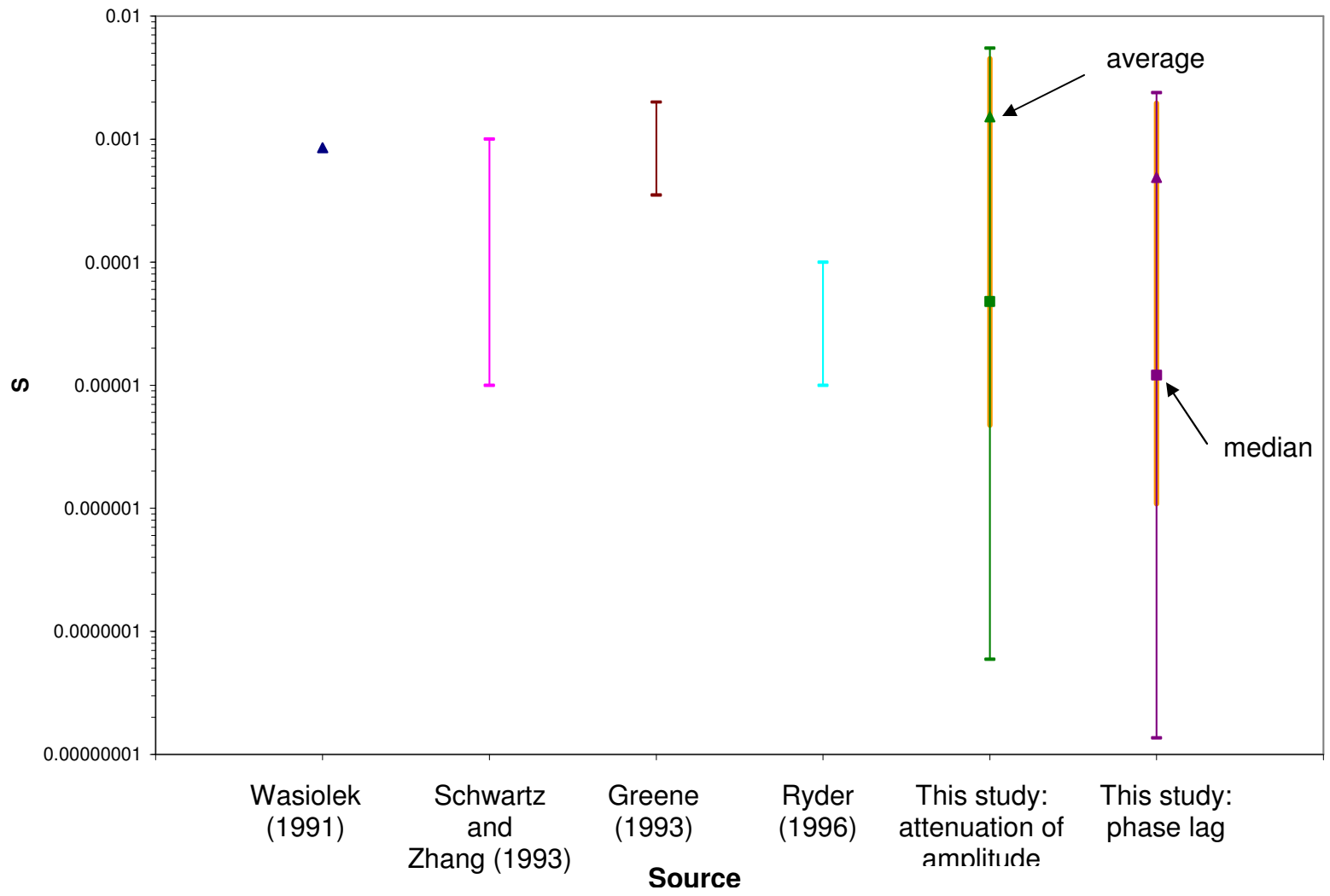
Figure 3.67: Range of storage coefficient [S] values from previous studies and this study.
Vertical axis is logarithmic scale. Squares indicate median values, and triangles indicate average values.

TABLES – CHAPTER 3

Well Name, Lease	Well ID	API Number	Easting	Northing	Well Elevation (m)	Reference Level (Source)	Well Depth (m)	Township (S)	Range (E)	Section
Houston Oil & Minerals Corp., State L.G. "1453" #1	HO&MSL1	3003520013	406876	3685414	1,511	GR	3,003	12	10	5
Houston Oil & Minerals Corp., J.M. Lewelling #1	HO&MJL1	3003520010	402778	3684425	1,440	KB	2,852	12	9	12
Houston Oil & Minerals Corp., Lewelling #2	HO&MCL2	3003520015	399960	3684444	1,373	GR	2,892	12	9	10
Houston Oil & Minerals Corp., Federal "A" #1	HO&MFA1	3003520009	413617	3660369	1,619	GR	1,125	14	10	24
Leland A. Hodges, Trustee, Houston #1	LAHTHO1	3003520005	411157	3660302	1,529	GR	928	14	10	23
Houston Oil & Minerals Corp., State 3724 #1	HO&MS31	3003520011	412512	3657622	1,540	GR	1,396	14	10	36
McClellan Oil Corp., Flying "H" Ranch Unit Tract 3 #1	MCOCFH1	3000562244	497349	3652108	1,554	GR	1,557	15	19	14
McClellan Oil Corp., Gragg B #1	MCOCGB1	3000561993	495371	3649683	1,529	GR	1,407	15	19	27
Humble Oil & Refining Co., Yates Federal #1	HO&RYF1	3000560015	486777	3649300	1,648	GR	1,643	15	18	26
J. Cleo Thompson, State A-6 #1	JCTSA61	3000562988	477111	3646836	1,824	GR	1,203	16	17	6
Lubbook Machine & Supply Co., Inc., Anderson-Randell #1	LM&SAR1	3000500003	472069	3645946	1,767	TH	563	16	16	3
Humble Oil & Refining Co., Humble-Yates N.M. State #1	HO&RHY1	3000510521	488336	3643533	1,574	DF	1,802	16	18	8
W.H. Black Drilling Co., Shildneck #1	WHBDCS1	3000500012	514561	3641046	1,330	?	2,137	16	20	24
Continental Oil Company, State NN #1	COCSNN1	3000560185	492051	3640997	1,538	DF	1,677	16	18	22
J. Cleo Thompson, Federal A-28 #1	JCTFA28	3000562915	479948	3639939	1,649	GR	1,481	16	17	28
C & K Petroleum, Inc., Singer Lake State #1	C&KSLS1	3000560320	495659	3637945	1,545	KB	1,617	16	19	31

Table 3.1: New Mexico oil-and-gas exploratory wells used in this study. Key at bottom of table.

Well Name, Lease	Well ID	API Number	Easting	Northing	Well Elevation (m)	Reference Level (Source)	Well Depth (m)	Township (S)	Range (E)	Section
Southern Production Co., Cloudcroft Unit #1	SPCCLU1	3003500002	431152	3635650	1,511	? (BH)	3,003	17	12	5
Yates Petroleum Corporation, Dunken Nose Unit #1	YPCDNU1	3000560383	491492	3635055	1,440	GR	2,852	17	18	10
Yates Petroleum Corporation, Dunken Dome Unit #2	YPCDDU2	3000560397	485994	3634588	1,373	GR	2,892	17	18	7
Yates Petroleum Corporation, Dunken Dome Unit #1	YPCDDU1	3000560374	486211	3634277	1,619	GR	1,125	17	18	7
Sun Exploration & Production Co., J.T. Jennings #1	SE&PJT1	3000561103	489093	3633855	1,529	GR	928	17	18	9
C & K Petroleum, Inc., Little Cuevo State #1	C&KLCS1	3000560324	501605	3632606	1,540	GR	1,396	17	19	15
Liberty Oil & Gas Corp., T.L. Watts #1	LO&GTLW	3000560766	480341	3631643	1,554	? (BH)	1,557	17	17	21
Magnolia, Headley Federal #2	MAGHEF2	NA	512347	3631229	1,529	?	1,407	17	20	23
Yates Petroleum Corporation, Little Cuevo Unit #1	YPCLCU1	3000561785	488273	3631027	1,648	GR	1,643	17	18	20
Sunray DX Oil Company, N.M. State "AV" #1	SOCSAV1	3000510144	491916	3630614	1,824	GR	1,203	17	18	22
Westcoast Hydrocarbons, Inc., Black Hills Unit #1	WHIBHU1	3000500013	508897	3629768	1,767	?	563	17	20	28
Yates Petroleum Corporation, Little Cuevo Unit #2	YPCLCU2	3000562268	489571	3628557	1,574	GR	1,802	17	18	33
Magnolia, Black Hills	MAGBLHI	NA	505927	3627975	1,330	?	2,137	17	20	31
Gulf Oil Corporation, Chaves State "U" #1	GOCCSU1	3000500002	472386	3625264	1,538	DF	1,677	18	16	10
TEXACO Inc., Federal (USA) "E" #1	TEXIFE1	3003520001	395308	3624999	1,649	GR	1,481	18	8	10
Yates Petroleum Corporation, One Tree Unit #1	YPCOTU1	3000562259	467160	3623529	1,545	KB	1,617	18	16	18

Table 3.1 continued.

Well Name, Lease	Well ID	API Number	Easting	Northing	Well Elevation (m)	Reference Level (Source)	Well Depth (m)	Township (S)	Range (E)	Section
Yates Petroleum Corporation, Dog Canyon "YF" Federal #1	YPCDCF1	3003520024	462754	3622676	1,511	KB	3,003	18	15	15
Texas Oil & Gas Corp., Federal "C" #1	TO&GFC1	3000560017	512954	3622309	1,440	GR	2,852	18	20	23
Kewanee Oil Co., F-M Unit #1	KOCFMU1	3000500009	493140	3619927	1,373	?	2,892	18	18	26
TEXACO Inc., Federal (USA) "F" #1	TEXIFF1	3003520006	410790	3619951	1,619	GR	1,125	18	10	30
Yates Petroleum Corporation, One Tree Unit #2	YPCOTU2	3000562276	468582	3619170	1,529	KB	928	18	16	29
TEXACO Inc., Federal (USA) "G" #1	TEXIFG1	3003520004	394443	3619379	1,540	GR	1,396	18	8	33
Marathon Oil Co., Mesa Verde Ranch #1	MOCMVR1	3003520022	455326	3618246	1,554	? (BH)	1,557	18	14	35
Yates Petroleum Corp., Buckhorn AYU State Com #1	YPCBAYU	3000560541	506142	3613140	1,529	? (BH)	1,407	19	20	18
Texas Oil & Gas Corp., Federal "A" #1	TO&GFA1	3000510431	506950	3613041	1,648	KB	1,643	19	20	17
Yates Petroleum Corporation (aka Phoenix Resources Co.), Bullis "AVW" State Com (aka Ranch Road) #1	YPCBAVW	3000560557	507355	3612640	1,824	GR	1,203	19	20	20
Sun Oil Co., Pinon Unit #2	SOCPIU2	3000500007	478157	3612259	1,767	DF	563	19	17	20
Sun Oil Co., Pinon Unit #1	SOCPIU1	3000500006	476922	3611828	1,574	DF	1,802	19	17	19
U.V. Industries, Inc., Long Canyon Unit #1	UVILCU1	3000560411	502547	3610225	1,330	KB	2,137	19	19	26
Gulf Oil Corp., Federal Munson #1	GOCFMU1	3000510075	489407	3609839	1,538	DF	1,677	19	18	28
Plymouth Oil Co., Evans (aka Federal D) #1	PLOCEV1	3003500003	404731	3604561	1,649	DF	1,481	20	9	15

Table 3.1 continued.

Well Name, Lease	Well ID	API Number	Easting	Northing	Well Elevation (m)	Reference Level (Source)	Well Depth (m)	Township (S)	Range (E)	Section
Texas Oil & Gas Corp., Federal "B" #1	TO&GFB1	NA	510832	3603835	1,511	?	3,003	20	20	15
Atlantic Refining Co., State "AV" #1	ARCSAV1	3003510001	461443	3603143	1,440	? (BH)	2,852	20	15	16
Zapata Petroleum Corp., Federal 14 #1	ZPCF141	3003500006	454127	3603086	1,373	DF	2,892	20	14	14
Sun Oil Company, T.J. Pearson #1	SOCTJP1	3003500005	416750	3598464	1,619	?	1,125	20	10	35
Terra Resources, Inc., Burro Canyon Unit #1-Y	TRBCU1Y	3003520017	511686	3596471	1,529	? (BH)	928	21	20	2
Stanolind Oil & Gas, Thorn Unit #1	SO&GTU1	3003500007	453419	3593869	1,540	Topo	1,396	21	14	15
Standard of Texas, Scarp Unit #1	SOTSCU1	3003500009	487438	3593394	1,554	DF	1,557	21	18	18
Lefors Petroleum Co., Federal #1	LEPCFE1	3003500008	471863	3592611	1,529	KB	1,407	21	16	22
Yates Petroleum Corporation, Brainerd "IO" Federal #1	YPCBIOF	3001522149	523000	3587630	1,648	KB	1,643	22	21	1
Tri-Service Drilling Co., Little Dog Federal #1	TSDLDF1	3003520008	496060	3586992	1,824	GR	1,203	22	19	6
Otero Oil Co., McGregor #1	OTOCMC1	3003500010	412151	3586894	1,767	?	563	22	10	5
Brainerd Corp. (aka Continental Oil Co.), Federal "A" (aka East Texas Hill Unit) #1	BRCFEA1	3001500005	523406	3586429	1,574	DF	1,802	22	21	1
Continental Oil Co., H.W. Bass #1	COCHWB1	3001500004	516898	3586367	1,330	?	2,137	22	21	5
Marathon Oil Company, Box Canyon Unit #1	MOCBCU1	3001510012	522193	3586059	1,538	DF	1,677	22	21	12
Pitts Energy Co., Federal "9" #1	PIECF91	3001527563	518567	3585218	1,649	KB	1,481	22	21	9

Table 3.1 continued.

Well Name, Lease	Well ID	API Number	Easting	Northing	Well Elevation (m)	Reference Level (Source)	Well Depth (m)	Township (S)	Range (E)	Section
Sinclair Oil & Gas Company, Federal Eddy 193 #1	SO&GFE1	3001500001	518145	3580901	1,511	DF	3,003	22	21	28
E.P. Campbell, Hurley #1	EPCAHU1	3003500012	447355	3580223	1,440	DF	2,852	22	14	30
Tom L. Ingram, State "E" #1	TLISTE1	3001520003	523070	3579540	1,373	GR	2,892	22	21	36
Fred Turner, Jr., Everett #1	FTUEVE1	NA	443146	3579159	1,619	? (BH)	1,125	22	13	34
E.P. Campbell, Liberman State #1	EPCALI1	3003500014	457361	3576570	1,529	DF	928	23	15	7
W.R. Weaver, Thompson #1	WRWETH1	3003500017	499785	3575900	1,540	DF	1,396	23	19	9
E.P. Campbell, Lois Spanel #1	EPCALS1	3003500015	467947	3575324	1,554	DF (Est.)	1,557	23	16	7
Presco, Inc., Indian Creek Federal #1	PRIICF1	3003520030	511700	3573937	1,529	GR	1,407	23	20	14
E.P. Campbell, McMillan Federal #1	EPCAMF1	3003500018	500598	3573842	1,648	DF	1,643	23	19	15
Humble Oil & Refining Co., Huapache Oil Unit #2	HO&RHO2	3001500013	530547	3572779	1,824	DF	1,203	23	22	23
Coral Oil & Gas Co., Warren #1	CO&GCW1	3003500016	487264	3571960	1,767	Topo	563	23	18	19
Inexco Oil Company, Sitting Bull Unit #1	IOCSBU1	3001520752	527152	3568073	1,574	GR	1,802	24	22	4
Coral Oil & Gas Company, Ann Spanel #1	CO&GAS1	3003500021	451716	3566857	1,330	DF	2,137	24	14	9
Atlantic Refining Co., Huapache Unit #9	ARCHUU9	3001500016	527053	3566737	1,538	DF	1,677	24	22	9
Skelly Oil Co., Las Cruces "D" #1	SOCLCD1	3001500003	522240	3565867	1,649	DF	1,481	24	21	12
Union Oil Co., Federal White #1	UNOCFW1	3001500019	525449	3565154	1,545	DF	1,617	24	22	17

Table 3.1 continued.

Well Name, Lease	Well ID	API Number	Easting	Northing	Well Elevation (m)	Reference Level (Source)	Well Depth (m)	Township (S)	Range (E)	Section
Humble Oil & Refining Co., Huapache Unit #5	HO&RHU5	3001500018	531153	3564735	1,511	DF	3,003	24	22	14
Threshold Development Co., Chiricahua R 21 Federal #1	TDCR21F	3003520034	489264	3563381	1,440	GR	2,852	24	18	21
Fred Turner, Jr. (aka Pasotero Pet. Corp.), Evans #1	FTUJEV1	3003500020	433355	3563003	1,373	? (BH)	2,892	24	12	22
E.P. Campbell (aka John J. Eisner), Federal #1	EPCAFE1	3003500019	432641	3562887	1,619	DF	1,125	24	12	21
Flynn, Welch, Yates, Donahue #1	FWYDON1	NA	460768	3561350	1,529	? (Dunn)	928	24	15	28
Franklin, Aston & Fair, Inc., Turkey Draw Unit #1	FA&FTD1	3001521378	524583	3560015	1,540	GR	1,396	24	22	31
Union Oil Co., McMillan #1	UNOCMC1	3003500028	440825	3557266	1,554	Topo	1,557	25	13	9
Union Oil Co., Verse 7 Federal #1	UOCV7F1	3001520591	524435	3556316	1,529	GR	1,407	25	22	7
W.W. West, West Dog Canyon Unit #1	WWWWDC1	3003520007	505979	3555044	1,648	GR	1,643	25	20	18
Transocean Oil, G.J. Ablah #1	TROGJA1	3003520018	442810	3554817	1,824	GR	1,203	25	13	15
R.H. Ernest, Located Land Co. #1	RHELLC1	3003500023	382791	3553354	1,767	USGS	563	25	7	20
Threshold Development Co., Mescalero 28 Federal #1	TDM28F1	3003520033	489514	3552255	1,574	GR	1,802	25	18	28
Beard Oil Company, Ridge USA #1	BOCRUS1	3001522547	524447	3551405	1,330	GR	2,137	25	22	30
Pennzoil Co., Southland "28" State #1	PCS28S1	3003520019	479573	3551070	1,538	GR	1,677	25	17	28
Fred Turner, Jr., State #1	FTUJST1	3003500027	475070	3550274	1,649	DF	1,481	25	16	36

Table 3.1 continued.

Well Name, Lease	Well ID	API Number	Easting	Northing	Well Elevation (m)	Reference Level (Source)	Well Depth (m)	Township (S)	Range (E)	Section
E.J. Dunigan, Alpha Federal #1	EJDALF1	3003520002	496594	3549815	1,511	KB	3,003	25	19	31
GDP 61-6	GDP61-6	NA	390213	3549130	1,440	WH	2,852	26	8	6
GDP 45-5	GDP45-5	NA	391837	3549102	1,373	WH	2,892	26	8	5
GDP 46-6	GDP46-6	NA	390223	3549119	1,619	WH	1,125	26	8	6
Hunt Oil Co., McMillan-Turner #1	HUOCMT1	3003500029	469015	3547882	1,529	? (Dunn)	928	26	16	5
Harvey E. Yates Co., Bennett Ranch Unit #1	HEYBRU1	3003520027	435547	3545814	1,540	GR	1,396	26	12	14
Seaboard Oil Co., Trigg-Federal #1	SEOCTF1	3003500032	418801	3545797	1,554	DF	1,557	26	11	18
GDP 51-8	GDP51-8	NA	393417	3545870	1,529	WH	1,407	26	8	16
E.P. Campbell, Spiegel-Federal #1	EPCSPF1	3003510002	511803	3544568	1,648	Topo	1,643	26	20	14
Sinclair Oil & Gas Co., Guadalupe Ridge Unit #1	SO&GGR1	3001520176	519670	3543204	1,824	GR	1,203	26	21	22
Harvey E. Yates Co., Bennett Ranch Unit 25 #1	HEYBR25	3003520031	437133	3542284	1,767	?	563	26	12	25

Table 3.1 continued:

API Number Key: NA = Not applicable.

Reference Level (Source) Key: GR = Ground surface, KB = Kelley bushing, TH = Tubing head, DF = Derrick floor, WH = Well head, ? = unknown if elevation is from GR, KB, TH, DF, or WH, DEM = from USGS NED, Topo = GR from topo. map, BH = from Broadhead (2007), Est. = Estimated, Dunn = from Dunn NMGS (1954), USGS = from USGS.

Well Name, Lease	Well ID	API Number	Easting	Northing	Well Elevation (m)	Reference Level (Source)	Well Depth (m)	Section	Block	Survey
Hunt Petroleum Corp., C.L. Ranch "5" #1	HPCCL51	4222930011	496478	3539912	1,110	? (K&H)	1,678	5	67	T-1, T&P
TEXACO, Inc., State of Texas "FO" "3" #1	TSTFO31	4222930005	421857	3539803	1,580	?	2,647	3	A	UL
Chesapeake Operating, Inc., DF Ranch State 63-12 #1	CODFRS1	4210932302	543327	3538510	1,211	GR	2,780	12	63	T-1, T&P
Magnolia Petr. Co., U-Tex Lease #39881 #1	MPCUTL1	4222900015	443219	3536988	1,533	DF	1,652	19	C	UL
EOG Resources, Inc., Rector Canyon 24 State #1	EOGRC24	4210932250	544329	3534119	1,200	GR	3,024	24	63	T-1, T&P
Pan American Petroleum Corporation, List Anderson #1	PAPCLA1	NA	491521	3533849	1,108	? (V&K)	2,021	23	68	T-1, T&P
Bonanza Co., Pierson	BONCOPI	NA	531346	3532226	1,346	? (V&K)	2,142	26	64	T-1, T&P
Pure Oil Co., Hunter #1	PUOCHU1	NA	509809	3531380	1,625	? (K&H)	2,027	34	66	T-1, T&P
Hunt Oil Co., Dyer #1	HUOCDY1	4222930007	485477	3530917	1,119	? (K&H)	898	31	68	T-1, T&P
Hueco Basin, University #1	HUBAUN1	NA	421896	3530405	1,558	DEM	765	39	A	UL
Trail Mountain, Inc., University Big Iron "C45" #1	TMUBIC1	4222900029	440743	3529232	1,516	GR	965	45	C	UL
Hunt Petroleum Corp., C.L. Ranch #1	HPCCLR1	4222930010	496475	3528252	1,105	? (K&H)	1,595	44	67	T-1, T&P
TEXACO Inc., Culberson "L" Fee #1	TEXCLF1	NA	519234	3527336	1,564	? (K&H)	2,652	45	65	T-1, T&P
Tenneco Oil Co., TXL Fee #1	TOTXLF1	4210931401	563041	3526975	1,086	KB	4,095	1	61	T-2, T&P
Pan American Petroleum Corporation, Ed Hammock #1	PAPCEH1	NA	499124	3526693	1,110	GR	2,152	4	67	T-2, T&P
Trail Mountain, Inc., University Sizzler D5 #1	TMUSD51	4222930227	437784	3526650	1,437	GR	1,774	5	D	UL
TXL Corp., Culberson "C" Fee #1	TXLCCF1	NA	523721	3526221	1,515	? (V&K)	2,362	1	65	T-2, T&P

Table 3.2: Texas oil-and-gas exploratory wells used in this study. Key at bottom of table.

Well Name, Lease	Well ID	API Number	Easting	Northing	Well Elevation (m)	Reference Level (Source)	Well Depth (m)	Section	Block	Survey
General Crude Oil Company, Merrill and Voyles et al. #1	GCOCMV1	NA	477481	3524877	1,580	DF	2,647	8	69	T-2, T&P
Magnolia Petro., No. A-1 Homer, Cowden	MPNA1HC	NA	544286	3524346	1,211	? (V&K)	2,780	12	63	T-2, T&P
EOG Resources, Inc., Kenney 16 State #1H	EOGKS1H	4210932270	527946	3523355	1,533	GR	1,652	16	64	T-2, T&P
EOG Resources, Inc., Kenney 16 State #2	EOGKES2	4210932269	528404	3522559	1,200	GR	3,024	16	64	T-2, T&P
California Standard of Texas, Theisen #1	CASATT1	NA	426103	3521248	1,108	?	2,021	19	E	UL
D & J Equip Co., J.C. Hunter, Jr. #2	DJJCHJ2	NA	512403	3519886	1,346	? (V&K)	2,142	2	120	PSL
Trail Mountain, Inc., University Felina "D27" #1	TMUFD27	4222930006	439917	3518350	1,625	GR	2,027	27	D	UL
Border Exploration Co., Hammack et al. CT-1	BECHCT1	4222930196	505172	3518026	1,119	? (K&H)	898	20	120	PSL
TXL Oil Corp., Culberson B-T Fee #1	TXLCBT1	NA	550456	3517797	1,558	? (V&K)	765	33	62	T-2, T&P
A.R. Jones Co., E.C. Mowry #1	ARJECM1	NA	474192	3516927	1,516	DF	965	36	70	T-2, T&P
Tipperary Corp., ST-1 Billye Sparks	TCST1BS	4222930195	474281	3516816	1,105	GR	1,595	36	70	T-2, T&P
J.L. Cowley, E.C. Mowry #1	JLCECM1	NA	473079	3515907	1,564	?	2,652	37	70	T-2, T&P
Border Exploration Co., J.J. McAdoo 7 #1	BECJJM1	4222930200	505794	3514682	1,086	? (K&H)	4,095	7	119	PSL
T.E. Robertson Co., Inc., Mowry et al. #2	TERCMO2	NA	471217	3514010	1,110	DF	2,152	47	70	T-2, T&P
The Superior Oil Company, Covington State #1	TSOCCS1	4210931405	565213	3512927	1,437	GR	1,774	1	115	PSL
Chesapeake Operating, Inc., Dela Minerals "3" State #701	COIDM3S	4210932268	566918	3512065	1,515	GR	2,362	7	114	PSL
Trail Mountain, Inc., University Devil Woman L5 #1	TMUDWL5	4222930253	477595	3510876	1,181	GR	1,461	5	L	UL

Table 3.2 continued.

274

Well Name, Lease	Well ID	API Number	Easting	Northing	Well Elevation (m)	Reference Level (Source)	Well Depth (m)	Section	Block	Survey
Samson Lone Star, L.L.C., University Lands 46-14 #2	SALSUL2	4210932278	551660	3509591	1,110	KB	1,678	14	46	UL
Humble Oil & Ref. Co., M.C. Sibley #1	HORMCS1	NA	533795	3508569	1,580	? (V&K)	2,647	24	68	PSL
N. Amer. Royalties, Inc., Potter #1	NARIPO1	NA	511738	3508091	1,211	? (V&K)	2,780	31	119	PSL
Chesapeake Operating, Inc., University Lands 4627 #1	COUL462	4210932287	550571	3507028	1,533	GR	1,652	27	46	UL
J.M. Huber Corp., Tom Potter #1	JMHCTP1	NA	514111	3505748	1,200	? (V&K)	3,024	2	118	PSL
EnCana Oil & Gas (USA) Inc., Sibley Ranch 47 State "25" #1	EOGSR47	4210932251	544180	3505778	1,108	KB	2,021	25	47	PSL
Anderson & Prichard, Bordens #1	A&PBOR1	NA	521137	3505265	1,346	? (V&K)	2,142	34	69	PSL
Trail Mountain, Inc., University Ooby Dooby L35 #1	TMUODL1	4222930261	482251	3502319	1,625	KB	2,027	35	L	UL
Petro-Hunt, L.L.C., Melissa Taylor State 27 #1-H	PHMTS27	4210932255	563684	3501318	1,119	GR	898	27	109	PSL
Faith Minerals, Inc., Wesley West #1	FMINWW1	4222930012	503401	3499500	1,558	GR	765	36	118	PSL
American Quasar Pet. Co., V.C. Rounsaville #1	AQPVCR1	NA	563477	3498883	1,516	? (V&K)	965	13	108	PSL
Hassle Hunt Trust, Univ. "M-49" #1	HHUM491	NA	450328	3497929	1,105	DF	1,595	9	M	UL
EOG Resources, Inc., Wild Horse Draw 7 #1	EOGWHD7	4210932256	536584	3497771	1,564	GR	2,652	7	106	PSL
Pan American Pet. Corp., Phillip F. Hass #1	PAPPFH1	NA	422942	3494846	1,086	DF	4,095	14	13	PSL
Chesapeake Operating, Inc., Melissa Taylor State 105-3	COMT105	4210932297	541293	3493028	1,110	GR	2,152	3	105	PSL
Transocean Oil, Inc., 36-1 MSA Trustee, Inc.	TO36MSA	4222930192	424652	3490962	1,437	KB	1,774	36	13	PSL
El Paso Co., No. 1 Montgomery	EPCN1MO	NA	546957	3484390	1,515	? (V&K)	2,362	17	100	PSL

Table 3.2 continued.

Well Name, Lease	Well ID	API Number	Easting	Northing	Well Elevation (m)	Reference Level (Source)	Well Depth (m)	Section	Block	Survey
Gulf Oil Corp., M.A. Grisham #1	GOCMAG1	NA	535928	3484129	1,110	? (V&K)	1,678	18	99	PSL
Hassle Hunt Trust, Mosely #1	HAHUTM1	NA	449636	3483385	1,580	GR	2,647	27	24	PSL
Lockhart, Roseborough & Benton, Gardner & Mosely #1 or Western States Oil, Gardner & Moseley #1	LR&BGM1 or WSOG&M1	NA	442367	3480668	1,211	DF	2,780	12	18	PSL
Chesapeake Operating, Inc., State Street State #701	COSS701	4210932271	546492	3478738	1,533	GR	1,652	7	97	PSL
Sinclair, Looney	SINCLOO	NA	551319	3475371	1,200	? (V&K)	3,024	22	97	PSL
Gulf Oil Corp., J. Burner-State "B" #1	GOCJBS1	NA	441556	3472050	1,108	DF	2,021	14	19	PSL
Lockhart Bros., Gardner & Mosely (Formerly Public School) #1	LOBG&M1	NA	446485	3468512	1,346	?	2,142	5	21	PSL
Stanolind Oil & Gas Co. American Land, No. 1 Roseborough	SOGAL1R	NA	444464	3467169	1,625	? (V&K)	2,027	7	21	PSL
J.P. Hurndall & R.A. Gray, J.S. Pierce #1	H&GJSP1	NA	479266	3465692	1,119	DEM	898	8	46	PSL
Fred A. Davis West and Armour, Davis #1	FADWAD1	NA	528309	3464645	1,558	? (V&K)	765	5	86	PSL

Table 3.2 continued:

API Number Key: NA = Not applicable.

Reference Level (Source) Key: GR = Ground surface, KB = Kelley bushing, DF = Derrick floor, ? = unknown if elevation is from GR, KB, or DF, DEM = from USGS NED, K&H = from King and Harder (1985), V&K = from Veldhuis and Keller (1980).

Well ID	Distance Along Cross Section (m)	Well Elevation (m)	Well Depth (m)
SPCCLU1	0	2,859	1,433
YPCDCF1	27,841	1,946	2,569
YPCOTU1	32,348	1,876	1,992
YPCOTU2	36,933	2,010	908
SOCPIU2	48,742	1,925	506
LEPCFE1	71,399	1,642	686
CO&GCW1	97,263	1,186	717
TDCR21F	106,121	1,133	1,834
EJDALF1	121,541	1,159	1,523
HPCCL51	131,444	1,110	1,678
HPCCLR1	143,104	1,105	1,595

Table 3.21: Subsurface oil-and-gas exploratory wells along cross-section A - A'.

Well ID	Distance Along Cross Section (m)	Well Elevation (m)	Well Depth (m)
SPCCLU1	0	2,859	1,433
MOCMVR1	35,636	2,143	2,137
ARCSAV1	51,931	1,921	1,227
EPCALS1	81,521	1,408	817
PCS28S1	108,977	1,206	905
HPCCL51	129,671	1,110	1,678

Table 3.22: Subsurface oil-and-gas exploratory wells along cross-section B - B'.

Well ID	Distance Along Cross Section (m)	Well Elevation (m)	Well Depth (m)
PLOCEV1	0	1,233	2,312
SOCTJP1	13,477	1,344	1,362
ZPCF141	51,139	2,109	1,537
ARCSAV1	58,455	1,921	1,227
LEPCFE1	73,270	1,642	686
SOTSCU1	88,865	1,628	812
TSDLDF1	99,604	1,940	1,259
TRBCU1Y	117,881	1,572	1,704
TO&GFB1	125,294	1,463	2,480

Table 3.23: Subsurface oil-and-gas exploratory wells along cross-section C - C'.

Well ID	Distance Along Cross Section (m)	Well Elevation (m)	Well Depth (m)
OTOCMC1	0	1,295	527
FTUEVE1	31,946	1,476	1,202
EPCAHU1	36,287	1,404	742
EPCALI1	46,939	1,326	823
EPCALS1	57,597	1,408	817
CO&GCW1	77,205	1,186	717
EPCAMF1	90,671	1,319	972
PRIICF1	101,774	1,767	1,454
SO&GFE1	111,262	1,582	1,524
BRCFEA1	118,893	1,397	3,230

Table 3.24: Subsurface oil-and-gas exploratory wells along cross-section D - D'.

Well ID	Distance Along Cross Section (m)	Well Elevation (m)	Well Depth (m)
GDP 45-5	0	1,255	1,207
SEOCTF1	27,166	1,618	1,707
HEYBRU1	43,911	1,554	2,156
TROGJA1	55,479	1,509	1,617
HUOCMT1	83,689	1,269	663
FTUJST1	90,199	1,317	1,583
PCS28S1	94,772	1,206	905
TDM28F1	104,784	1,219	1,409
EJDALF1	112,272	1,159	1,523
WWWWDC1	123,016	1,771	1,390
UNOCFW1	144,954	1,740	2,053
HO&RHO2	154,127	1,358	3,835

Table 3.25: Subsurface oil-and-gas exploratory wells along cross-section E - E'.

Groundwater Well ID	Source	Distance Along Cross Section (m)	^{14}C Activity from Exponential Trend [A] (pmC)	$[HCO_3^-]$ from Linear Trend (mmoles/L)	$[Mg^{2+}]$ from Linear Trend (mmoles/L)	^{14}C Activity Calculated Using Dedolomitization Model $[A_0]$ (pmC)	^{14}C Age (yr)
SM-0085	SMHS	537	84.4	6.4	0.3	NA	
SM-0044	SMHS	20,294	64.1	6.0	0.8	82.3	2,067
Doll Day	A&S	56,137	39.0	5.1	1.7	70.6	4,916
Uña	A&S	66,705	33.6	4.8	2.0	69.9	6,049
Runyan	A&S	71,399	31.5	4.7	2.1	69.8	6,572
Cauhape	A&S	77,842	28.8	4.6	2.3	69.5	7,280
Harvey Lewis Well	A&S	97,882	21.8	4.1	2.8	65.4	9,077
Evrage House	A&S	118,245	16.4	3.6	3.3	59.9	10,694

Table 3.29: Continuous parameters used in stoichiometric dedolomitization model, and resultant ^{14}C activities and groundwater ages.

Source Key: SMHS = New Mexico Bureau of Geology & Mineral Resources' Sacramento Mountains Hydrogeology Study, A&S = This study.

Geologic Unit	Sample Depth (m)	n (%)	k (mD)	K (m/day)
Yeso	405	1.7	NA	NA
Yeso	430	18.3	NA	NA
Yeso	456	0	0.01	7.E-06
Yeso	470	12	NA	NA
Yeso	482	5.1	0.01	7.E-06
Yeso	488	9.9	0	0
Yeso	519	9.5	0.15	1.1E-04
Yeso	546	8.8	0.43	3.2E-04
Yeso	564	0	0	0
Yeso	581	0	0.01	7.E-06
Yeso	588	0.2	NA	NA
Abo	596	0	0	0
Abo	629	NA	1.75	1.30E-03
Abo	639	0.1	NA	NA
Abo	641	0	0	0
Abo	648	0.1	0.01	7.E-06
El Paso/Ellenburger	691	No visible porosity.	NA	NA
El Paso/Ellenburger	693	Minor porosity.	NA	NA
El Paso/Ellenburger	710	0.3	0.000342	2.54E-07
Bliss	823	2.5	NA	NA
Precambrian	833	0	0	0
Precambrian	841	0	0	0
Precambrian	849	0	0	0
Precambrian	858	0	0	0

Table 3.30: Wellsite core analysis porosity [n] and permeability [k], and calculated
hydraulic conductivity [K] data from the Yates Petroleum Corporation, One Tree Unit #2
(YPCOTU2) well along cross-section A - A'.

Cross Section Interval	K with n = 6.95% (m/day)	K with n = 0.1% (m/day)	K with n = 18.3% (m/day)
SM-0085 to SM-0044	6.38E-02	9.18E-04	1.68E-01
SM-0044 to Doll Day	1.51E-01	2.18E-03	3.98E-01
Doll Day to Uña	3.38E-01	4.86E-03	8.90E-01
Uña to Runyan	4.78E-02	6.88E-04	1.26E-01
Runyan to Cauhape	1.66E-01	2.39E-03	4.37E-01
Cauhape to Harvey Lewis Well	4.46E+00	6.42E-02	1.17E+01
Harvey Lewis Well to Evrage House	1.44E+00	2.08E-02	3.80E+00

Table 3.31: Range of hydraulic conductivity [K] values calculated from stoichiometric dedolomitization model groundwater ages along cross-section A - A'.

Cross Section Interval	Average Saturated Aquifer Thickness Over Each Interval (m)	T with n = 6.95% (m²/day)	T with n = 0.1% (m²/day)	T with n = 18.3% (m²/day)
SM-0085 to SM-0044	763	4.87E+01	7.00E-01	1.28E+02
SM-0044 to Doll Day	564	8.53E+01	1.23E+00	2.25E+02
Doll Day to Uña	142	4.78E+01	6.88E-01	1.26E+02
Uña to Runyan	152	7.26E+00	1.04E-01	1.91E+01
Runyan to Cauhape	160	2.66E+01	3.82E-01	6.99E+01
Cauhape to Harvey Lewis Well	438	1.95E+03	2.81E+01	5.14E+03
Harvey Lewis Well to Evrage House	840	1.21E+03	1.74E+01	3.19E+03

Table 3.32: Range of transmissivity [T] values calculated from stoichiometric dedolomitization model groundwater ages along cross-section A - A'.

Groundwater Well ID/ State Well Number	Maximum Groundwater Level Change 2003 (m)	Minimum Groundwater Level Change 2003 (m)	Maximum Groundwater Level Change 2004 (m)	Average Amplitude of Water Level Fluctuation 2003 $[s_0]$ for 4807516 and $[s_T]$ for H&C 1, 2, and 3 (m)	S/T (day/m^2)
4807516	5.43E-01	-7.78E+00	-1.80E-01	3.98E+00	NA
H&C 1	9.34E-02	-3.33E+00	-4.72E-01	1.57E+00	4.52E-06
H&C 2	4.08E-01	-1.14E+00	-2.28E-01	6.16E-01	1.26E-06
H&C 3	2.56E-01	-5.03E-01	7.58E-02	3.35E-01	1.40E-06
H&C 4	NA	NA	1.03E-02	NA	NA

Table 3.33: Maximum and minimum groundwater level change, average amplitude of water level fluctuation, and S/T values for 2003.

Groundwater Well ID/ State Well Number	Maximum Groundwater Level Change 2004 (m)	Minimum Groundwater Level Change 2004 (m)	Maximum Groundwater Level Change 2005 (m)	Average Amplitude of Water Level Fluctuation 2004 $[s_0]$ for 4807516 and $[s_T]$ for H&C 1, 2, 3, and 4 (m)	S/T (day/m^2)
4807516	-1.80E-01	-5.87E+00	5.73E-01	3.03E+00	NA
H&C 1	-4.72E-01	-2.98E+00	-7.36E-02	1.35E+00	3.88E-06
H&C 2	-2.28E-01	-1.42E+00	-4.99E-01	5.30E-01	1.14E-06
H&C 3	7.58E-02	-5.62E-01	1.70E-01	3.42E-01	1.15E-06
H&C 4	1.03E-02	-3.71E-02	6.18E-02	3.66E-02	3.63E-06

Table 3.34: Maximum and minimum groundwater level change, average amplitude of water level fluctuation, and S/T values for 2004.

Groundwater Well ID/ State Well Number	Maximum Groundwater Level Change 2005 (m)	Minimum Groundwater Level Change 2005 (m)	Maximum Groundwater Level Change 2006 (m)	Average Amplitude of Water Level Fluctuation 2005 [s_0] for 4807516 and [s_T] for H&C 1, 2, 3, and 4 (m)	S/T (day/m^2)
4807516	5.73E-01	-6.46E+00	-6.10E-03	3.37E+00	NA
H&C 1	-7.36E-02	-3.12E+00	-5.07E-01	1.42E+00	4.18E-06
H&C 2	-4.99E-01	-1.99E+00	-1.19E+00	5.73E-01	1.17E-06
H&C 3	1.70E-01	-6.40E-01	-8.10E-02	3.42E-01	1.24E-06
H&C 4	6.18E-02	-2.90E-02	1.80E-02	3.45E-02	3.87E-06

Table 3.35: Maximum and minimum groundwater level change, average amplitude of water level fluctuation, and S/T values for 2005.

Groundwater Well ID/ State Well Number	Distance from Dell City (m)	s_T/s_0 2003	S/T 2003 (day/m^2)	s_T/s_0 2004	S/T 2004 (day/m^2)	s_T/s_0 2005	S/T 2005 (day/m^2)
4807516	NA	NA	NA	NA	NA	NA	NA
H&C 1	8,224	3.95E-01	NA	4.45E-01	NA	4.20E-01	NA
H&C 2	24,591	1.55E-01	NA	1.75E-01	NA	1.70E-01	NA
H&C 3	28,920	8.40E-02	NA	1.13E-01	NA	1.01E-01	NA
H&C 4	47,476	NA	NA	1.20E-02	NA	1.02E-02	NA
			5.68E-07		1.00E-06		1.07E-06

Table 3.36: Values of s_T/s_0 for each year, and values of S/T calculated from exponential trends of s_T/s_0 versus distance for each year.

Groundwater Well ID	Distance from H&C 1 (m)	Average Annual Phase Lag between H&C 1 and Indicated Well [t_L] 2003 (days)	S/T 2003 (day/m^2)	Average Annual Phase Lag between H&C 1 and Indicated Well [t_L] 2004 (days)	S/T 2004 (day/m^2)	Average Annual Phase Lag between H&C 1 and Indicated Well [t_L] 2005 (days)	S/T 2005 (day/m^2)
H&C 2	16,367	8	NA	19	NA	21	NA
H&C 3	20,696	17	NA	32	NA	34	NA
H&C 4	39,252	NA	NA	81	NA	104	NA
			1.30E-07		2.52E-07		4.65E-07

Table 3.37: Average annual phase lag [t_L] between each well pair for each year, and values of S/T calculated from linear trends of t_L versus distance for each year.

Year	S/T from the Attenuation of the Amplitude of the Periodic Water Level Fluctuations (day/m^2)	Median T from ^{14}C Groundwater Ages Along Cross Section A to A' (m^2/day)	S Using Median T	Minimum T from ^{14}C Groundwater Ages Along Cross Section A to A' (m^2/day)	S Using Minimum T	Maximum T from ^{14}C Groundwater Ages Along Cross Section A to A' (m^2/day)	S Using Maximum T
2003	5.68E-07	4.78E+01	2.72E-05	1.04E-01	5.93E-08	5.14E+03	2.92E-03
2004	1.00E-06	4.78E+01	4.79E-05	1.04E-01	1.05E-07	5.14E+03	5.15E-03
2005	1.07E-06	4.78E+01	5.10E-05	1.04E-01	1.11E-07	5.14E+03	5.48E-03

Table 3.38: Values of S calculated using S/T values estimated from the attenuation of the amplitude of the periodic water level fluctuations.

Year	S/T from the Phase Lag of the Periodic Water Level Fluctuations (day/m^2)	Median T from ^{14}C Groundwater Ages Along Cross Section A to A' (m^2/day)	S Using Median T	Minimum T from ^{14}C Groundwater Ages Along Cross Section A to A' (m^2/day)	S Using Minimum T	Maximum T from ^{14}C Groundwater Ages Along Cross Section A to A' (m^2/day)	S Using Maximum T
2003	1.30E-07	4.78E+01	6.23E-06	1.04E-01	1.36E-08	5.14E+03	6.69E-04
2004	2.52E-07	4.78E+01	1.21E-05	1.04E-01	2.64E-08	5.14E+03	1.30E-03
2005	4.65E-07	4.78E+01	2.22E-05	1.04E-01	4.85E-08	5.14E+03	2.39E-03

Table 3.39: Values of S calculated using S/T values estimated from the phase lag of the periodic water level fluctuations.

Minimum S	Maximum S	Average S	Aquifer	Source
		8.5E-04	Yeso Fm. (unfractured siltstone and gypsum)	Wasiolek (1991)
1.0E-05	1.0E-03	NA	Confined	Schwartz and Zhang (2003)
3.5E-04	2.E-03	NA	Madison aquifer system	Greene (1993)
1.E-05	1.E-04	NA	Confined portion of Edwards-Trinity aquifer system	Ryder (1996)

Table 3.40: Range of S values reported in the scientific literature for confined and/or predominantly carbonate aquifers.

CHAPTER 4: 3-D FINITE DIFFERENCE GROUNDWATER FLOW MODEL

In order to test the conceptual model of groundwater flow presented in the preceding chapter and better constrain the permeability distribution of the aquifer system, a 3-D finite difference groundwater flow model of the northern Salt Basin watershed was developed with MODFLOW-2000, the U.S. Geological Survey's modular groundwater flow model (Harbaugh et al., 2000). MODFLOW-2000 solves the 3-D groundwater flow equation for a porous medium:

$$\frac{\partial}{\partial x}\left(K_{xx}\frac{\partial h}{\partial x}\right)+\frac{\partial}{\partial y}\left(K_{yy}\frac{\partial h}{\partial y}\right)+\frac{\partial}{\partial z}\left(K_{zz}\frac{\partial h}{\partial z}\right)+W=S_{s}\frac{\partial h}{\partial t}, \quad [11]$$

where

K_{xx}, K_{yy}, and K_{zz} = Hydraulic conductivity along the x, y, and z coordinate axes, respectively, which are assumed to be parallel to the major axes of hydraulic conductivity (L/t),

h = Potentiometric head (L),

W = Volumetric flux per unit volume representing sources and/or sinks of water (t^{-1}),

S_S = Specific storage of the porous material (L^{-1}), and

t = time (t),

using the finite difference method (McDonald and Harbaugh, 1988). When combined

286

with boundary and initial conditions, [11] describes transient 3-D groundwater flow in a heterogeneous and anisotropic medium (Harbaugh et al., 2000).

4.1: Model Development

Groundwater Modeling System (GMS) provides a graphical pre- and post-processor for MODFLOW-2000. As discussed in Chapter 3.2.c, GMS version 6.5 was used to construct a 3-D hydrogeologic framework model of the Salt Basin. The 3-D hydrogeologic framework solid model was used to aid in the development of a 3-D finite difference groundwater flow model of the Salt Basin. However, for simplicity, and to minimize model run times, only 6 hydrogeologic groupings from the framework solid model were incorporated into the groundwater flow model, including, from oldest to youngest, the Precambrian, the Paleozoic (the Cambrian through the Pennsylvanian), the Permian (Lower Abo/Pow Wow Conglomerate through Artesia Group), the Cretaceous, Cenozoic intrusions, and Cenozoic alluvium. Similar to the 17 hydrogeologic groupings used for the 3-D hydrogeologic framework model, the 6 hydrogeologic groupings used in the groundwater flow model were chosen such that hydrogeologic units with similar lithologies and facies, and thus probably similar hydraulic properties, were combined.

Also, for simplicity, and to minimize model run times, a cell size of 1,000 by 1,000 meters (3,280 by 3,280 feet) was used for the 3-D MODFLOW grid, in contrast to 500 by 500 meters (1,640 by 1,640 feet) cell size used for the 3-D hydrogeologic framework model. In order to facilitate the assignment of hydrogeologic units to the 3-D MODFLOW grid, a simplified 3-D hydrogeologic framework solid model was created. The simplified 3-D framework solid model consisted of the 6 hydrogeologic units listed above, and a cell size of 1,000 by 1,000 meters (3,280 by 3,280 feet). Using the same

method as described in Chapter 3.2.c, a GMS grid was assigned 6 layers to represent the 6 hydrogeologic units, and the elevation values from the 6 ArcGIS raster surfaces were used to define the elevation values of the 6 layers in the GMS grid.

However, unlike the 500 by 500 meters (1,640 by 1,640 feet) solid model, described in Chapter 3, the cell size of the simplified solid model did not match the cell size of the ArcGIS raster surfaces representing the elevation of the top of the hydrogeologic units. As a result, the elevation values from the ArcGIS raster surfaces could not be directly used to define the elevation of the 6 layers in the GMS grid. Instead, the elevation values from the ArcGIS raster surfaces were interpolated to the GMS grid layers using a natural neighbor interpolation scheme to create the simplified 3-D framework solid model.

The active portion of the 3-D MODFLOW grid consisted of 6 layers, 146 rows, 130 columns, and 72,366 cells. The top of the MODFLOW grid was set at the top of the simplified 3-D hydrogeologic framework solid model (i.e. the land surface elevation). Layer 1 was given a variable thickness, as discussed in more detail below, while layers 2 through 6 were assigned a constant thickness of 50, 250, 500, 1,000, and 1,500 meters (160, 820, 1,600, 3,300, and 4,900 feet), respectively. As a result, the MODFLOW grid layers crosscut the hydrogeologic units within the 3-D framework solid model. The simplified 3-D framework solid model was used to assign a hydrogeologic unit to each cell within the MODFLOW model domain. The hydrogeologic unit assigned to each cell in the MODFLOW grid was chosen as the hydrogeologic unit from the simplified 3-D framework solid model occupying the majority of each MODFLOW cell.

In addition to the 6 hydrogeologic units from the 3-D framework solid model, several other units were incorporated into the MODFLOW grid. The Cenozoic intrusive mass postulated by Nutt et al. (1997) to exist beneath the Cornudas Mountains was included in the groundwater flow model from layer 3 to the top of the Precambrian. The lateral extent of this mass within the groundwater flow model domain corresponds to the residual gravity low, as defined by the 0 mGal contour, presented in Nutt et al. (1997). The intrusive mass was grouped with the Cenozoic intrusions hydrogeologic unit. In an attempt to model the confined to semi-confined Cretaceous aquifer overlying the regional Permian aquifer in the southwestern portion of the Diablo Plateau, a low permeability confining unit was inserted in layer 2 beneath the Cretaceous hydrogeologic unit in layer 1. As a result, the MODFLOW grid consists of 7 hydrogeologic units.

The base of layer 1 was originally defined as 100 meters (330 feet) below the groundwater surface depicted in Figure 3.42. However, initial model runs reveled that numerous cells in layer 1 would become dry. Original versions of MODFLOW allowed variable-head model cells to become desaturated, in which case they were converted to no-flow cells, but did not allow them to become resaturated and converted back to variable-head cells (McDonald et al., 1998). Variable-head cells can incorrectly become dry during the iterative solution process (McDonald et al., 1998). MODFLOW-2000 includes an option to allow dry cells to be converted to variable-head cells (termed "wetting") based on the head in variable-head cells immediately below and/or horizontally adjacent to the dry cells, but enabling this feature can lead to instability in the convergence of the iterative solution process (McDonald et al., 1998).

As mentioned in the preceding paragraph, during initial model runs numerous cells in layer 1would become dry during the solution process. The wetting capability was enabled in subsequent model runs to allow variable-head cells that may have been incorrectly converted to no-flow cells to become re-wetted. However, enabling the wetting capability produced instability in the iterative solution process, and convergence could not be achieved. Therefore, in order to ensure that variable-head cells would not incorrectly become dry during the solution process the thickness of layer 1 was increased so that the heads in layer 1 would not fall below the bottom of layer 1 during the solution process. As a result, the wetting capability wasn't needed, and the stability of the solution was re-established. The base of layer 1 was re-defined as 100 meters (330 feet) below a subdued version of the groundwater surface depicted in Figure 3.42, in which the subdued groundwater surface was up to 685 meters (2,250 feet) lower than the groundwater surface in Figure 3.42. The re-defined thickness of layer 1 ranged from 100 to 1,470 meters (330 to 4,820 feet).

Figure 4.1 presents the locations and an oblique view of the 5 cross-sections, as discussed in Chapter 3.3, within the 3-D hydrogeologic framework solid model, and the 3-D groundwater flow model. Figures 4.2 through 4.6 compare side views of the 5 cross-sections through the 3-D hydrogeologic framework solid model, and the 3-D groundwater flow model. Figure 4.7 presents the locations and an oblique view of the 5 cross-sections within the simplified 3-D hydrogeologic framework solid model, and the 3-D groundwater flow model. Figures 4.8 through 4.12 compare side views of the 5 cross-sections through the simplified 3-D hydrogeologic framework solid model, and the 3-D groundwater flow model to illustrate how hydrogeologic units from the simplified solid

model were assigned to cells within the 6 layer groundwater flow model. Figures 4.13 through 4.18 show the distribution of the 6 hydrogeologic units from the simplified 3-D hydrogeologic framework solid model, and the low permeability Cretaceous confining unit, within layers 1 through 6 of the groundwater flow model grid. Faults are represented within the 3-D groundwater flow model solely through juxtaposition of the hydrogeologic units, as defined by the simplified 3-D framework solid model.

Model length is in meters, and time is in days. The Layer-Property Flow (LPF) Package was used as the internal flow package. The LPF Package assumes that a node is located at the center of each model cell (Harbaugh et al., 2000). Layer 1 was defined as convertible, in which case cell thickness depends on the computed hydraulic head in the cell. If the head is above the elevation of the top of the cell, the cell thickness is calculated as the elevation of the top of the cell minus the elevation of the bottom of the cell (Harbaugh et al., 2000). If the head is below the top of the cell, the cell thickness is calculated as the head minus the elevation of the bottom of the cell (Harbaugh et al., 2000). Layers 2 through 6 were set as confined, in which case cell thickness is calculated as the elevation of the top of the cell minus the elevation of the bottom of the cell (Harbaugh et al., 2000).

MODFLOW-2000 includes several solver packages, each of which can be used to solve the set of simultaneous finite difference equations for head at each cell by iteration. Initial model runs were attempted with the strongly implicit procedure (SIP) and preconditioned Conjugate Gradient (PCG) solvers, but convergence could not be achieved with either of these two solvers. The slice successive overrelaxtion (SOR) solver proved to be the most stable and capable of converging. The SOR technique

divides the finite difference grid into vertical "slices," and groups the node equations from each slice into discrete sets (McDonald and Harbaugh, 1988). During every iteration, these sets of equations are processed in turn, resulting in a new set of estimated head values for each slice (McDonald and Harbaugh, 1988). The head change criterion for convergence was set at 0.001 meters (0.003 feet).

4.1.a: Boundary and Initial Conditions

The domain of the 3-D solid and groundwater flow models was defined using the groundwater surface shown in Figure 3.42. The boundary was drawn to correspond to the groundwater divides as indicated by the groundwater surface, except in the southeastern portion of the domain where the boundary corresponds to the groundwater divide associated with the Bitterwell Break. Also, the northwestern portion of the domain encompasses a part of the Peñasco Basin, as suggested by the groundwater surface. As a result, the entire domain of the groundwater flow model is surrounded by a no-flow boundary. (Figure 4.19) As mentioned above, the active portion of the groundwater flow model grid consists of 6 layers, 146 rows, 130 columns, and 72,366 cells, each with a plan view area of 1.0 km^2 (0.39 mi^2). (Figure 4.19) The groundwater surface depicted in Figure 3.42 was used as the starting head for all 6 layers.

-Recharge Distributions

The Recharge (RCH) Package was used to apply areal recharge to layer 1 of the groundwater flow model domain. Two different recharge distributions were investigated for this modeling exercise: a water-balance based and an elevation-dependent distribution. Each recharge distribution was hand-calibrated to steady-state groundwater elevations in 378 wells throughout the model domain by varying the horizontal hydraulic

conductivity of the hydrogeologic units. More detail on the calibration process is provided in Chapter 4.2.a. The appropriateness of the two recharge distributions was tested by comparing radiocarbon groundwater ages from wells within the Salt Basin, as presented in Sigstedt (2010), to MODPATH particle-tracking ages calculated from the hand-calibrated MODFLOW solutions for each recharge distribution. The MODPARTH particle-tracking setup is discussed in more detail in Chapter 4.2.b, and the results are presented in Chapter 4.3.b.

-Water-balance Based Recharge Distribution

For the water-balance based recharge distribution, recharge was applied to the sub-basins delineated by JSAI (2010). (Figure 4.19) The recharge rates applied to the sub-basins were derived from visual inspection of the figures depicting the net infiltration simulated by the water-balance recharge modeling conducted by DBS&A (2010a). (Figures 4.20 through 4.25, and Table 4.1) The sub-basins delineated by JSAI (2010) were placed over the top of the DBS&A (2010a) net infiltration figures, and a recharge rate was selected for each sub-basin based on the average net infiltration simulated over the entire area of each sub-basin. DBS&A (2010a) simulated net infiltration for minimum, average, and maximum water years. Thus, three different recharge scenarios were examined for the water-balance based recharge distribution, incorporating the recharge rates and areal distribution of recharge derived from the DBS&A (2010a) simulated net infiltration for the minimum, average, and maximum water years. (Figures 4.20 through 4.25, and Table 4.1)

As discussed in Chapter 3.1, DBS&A (2010a) conceptualized the recharge mechanisms in the Salt Basin to include: mountain block recharge, mountain front

recharge, local recharge, and diffuse recharge. DBS&A (2010a) only estimated recharge within the Salt Basin watershed boundary. However, the groundwater flow model domain was defined using the groundwater surface, and thus does not correspond exactly to the watershed boundary. For those regions of the model domain not incorporated in the DBS&A (2010a) study, the distribution and amount of recharge was estimated to be similar to the neighboring regions included in the DBS&A (2010a) study. For the portion of the Peñasco Basin included in the model domain, recharge was assumed to be equal to the subsurface flux through the eastern portion of the Salt Basin calculated by Sigstedt (2010) using apparent groundwater ages estimated from the ^{14}C data. Sigstedt (2010) calculated a minimum, average, and maximum subsurface flux, and these values were incorporated into the three recharge scenarios.

The recharge rates and areal recharge applied to the sub-basins for the minimum, average, and maximum recharge scenarios of the water-balance based recharge distribution are summarized in Table 4.1. Total recharge to the groundwater flow model domain using the water-balance based recharge distribution ranged from 160,000 m^3/day (49,000 acre-feet/year) for the minimum recharge scenario to 350,000 m^3/day (110,000 acre-feet/year) for the maximum recharge scenario, with the average recharge scenario producing 270,000 m^3/day (81,000 acre-feet/year). These values for total recharge to the Salt Basin are on the upper end of the range of values reported in previous studies, as discussed in Chapter 3.1. Figures 4.20, 4.21, and 4.22 show the distribution of recharge rates for the minimum, average, and maximum recharge scenarios. Figures 4.23, 4.24, and 4.25 present the distribution of areal recharge for the minimum, average, and maximum recharge scenarios. The sub-basins contributing the most to total recharge

included those sub-basins encompassing the Sacramento and Guadalupe Mountains, and the region to the southwest and northeast of the Otero Break.

One of the shortcomings of the water-balance based recharge distribution is that it appears to overestimate recharge in the lower elevation regions of the Salt Basin. In the DBS&A (2010a) study most recharge to the groundwater system is concentrated along sinkholes to the southwest of the Otero Break and on the Chert Plateau and Otero Hills to the northeast of the Otero Break, while the high mountain region of the Sacramento Mountains contributes almost no recharge. Several sources of hydrogeologic evidence suggest that regions to the southwest and northeast of the Otero Break receive much less recharge than the Sacramento Mountains. Depth to the regional groundwater surface in the region around the Otero Break ranges from 76 meters (250 feet) to greater than 300 meters (1,000 feet), while in the Sacramento Mountains depths are generally less than 76 meters (250 feet). (Figure 3.43) Tritium levels in wells to the northeast of the Otero Break are low, ranging from 0.24 to 1.6 Tritium Units (TU), while tritium levels in wells and springs within the Sacramento Mountains generally range from 2.97 to 10.4 TU, indicating groundwater is typically less than 50 years old (Newton et al., 2009; Sigstedt, 2010). Also, radiocarbon groundwater ages in wells to the northeast of the Otero Break are greater than 1,000 years old, with some ages near or greater than 10,000 years old (Sigstedt, 2010).

-Elevation-dependent Recharge Distribution

For the elevation-dependent recharge distribution, recharge was applied to the high mountain regions of the Sacramento and Guadalupe Mountains, as well as the regions around the Cornudas Mountains and the southwest portion of the Diablo Plateau

where the depth-to-groundwater map [Figure 3.43] indicates areas of shallower groundwater. Again, three different recharge scenarios, minimum, average, and maximum, were examined for the elevation-dependent recharge distribution. The recharge rates applied to the Sacramento and Guadalupe Mountains regions of the groundwater flow model domain were derived using data presented in Newton et al. (2011).

Based on water level, geochemistry, and stable isotope data, Newton et al. (2011) determined that the main recharge source areas for the High Mountain, Pecos Slope, and Salt Basin aquifer systems are located in the high mountain areas of the Sacramento Mountains above a surface elevation of approximately 2,500 meters (8,200 feet). Using the chloride mass balance method, Newton et al. (2011) estimated the relative recharge rate within this area to range from 4 to 44%, with a mean value of 22%, of average annual precipitation. (Table 4.2) The recharge factors presented in Newton et al. (2011) were multiplied by the average annual precipitation, obtained from PRISM [Figure 1.11], to calculate the minimum, average, and maximum recharge rates that were applied to the Sacramento and Guadalupe Mountains regions of the groundwater flow model domain above a surface elevation of 2,500 meters (8,200 feet).

On the Otero Mesa/Diablo Plateau recharge rates were based on soil chloride profile data from the Diablo Plateau collected by Kreitler et al. (1987), as cited in Mayer (1995). Kreitler et al. (1987) concluded that on the Diablo Plateau the main recharge mechanism is through fractures in creek beds and closed depressions during occasional flash floods (Mayer, 1995). On the basis of soil chloride profiles, Kreitler et al. (1987) calculated recharge for creek beds and depressions to range from 0.028 to 0.457 cm/year

(0.011 to 0.180 inches/year), and for areas outside creek beds to range from 0.005 to 0.020 cm/year (0.002 to 0.0079 inches/year) (Mayer, 1995). (Table 4.3) The minimum and maximum of each range were used for the minimum and maximum recharge scenarios, respectively, while the midpoint of each range was used for the average recharge scenario. As mentioned above, these recharge rates were applied to the region of shallow groundwater around the Cornudas Mountains and on the southwest portion of the Diablo Plateau. On the basis of digitized topography and stream courses, and assuming a stream-bed width of 10 meters (33 feet), Mayer (1995) calculated creek beds and depressions to occupy only 3% of the total area of the Otero Mesa/Diablo Plateau. Thus, the creek bed and depression recharge rate was applied to only 3% of the area of the Cornudas Mountains and Diablo Plateau recharge zones within the groundwater flow model domain.

The recharge rates and areal recharge applied to the Sacramento and Guadalupe Mountains, and Cornudas Mountains and Diablo Plateau recharge zones for the minimum, average, and maximum recharge scenarios of the elevation-dependent recharge distribution are summarized in Tables 4.4 and 4.5, respectively. Total recharge to the groundwater flow model domain using the elevation-dependent recharge distribution ranged from 9,100 m^3/day (2,700 acre-feet/year) for the minimum recharge scenario to 99,000 m^3/day (29,000 acre-feet/year) for the maximum recharge scenario, with the average recharge scenario producing 50,000 m^3/day (15,000 acre-feet/year). Figures 4.26, 4.27, and 4.28 show the distribution of recharge rates for the minimum, average, and maximum recharge scenarios. Figures 4.29, 4.30, and 4.31 present the

distribution of areal recharge for the minimum, average, and maximum recharge scenarios.

Recharge to the Sacramento Mountains recharge zone ranged from 7,400 m^3/day (2,200 acre-feet/year) for the minimum recharge scenario to 81,000 m^3/day (24,000 acre-feet/year) for the maximum recharge scenario, with the average recharge scenario resulting in 41,000 m^3/day (12,000 acre-feet/year). These values for the Sacramento Mountains recharge zone compare favorably to the subsurface flux from the Sacramento Mountains through the eastern portion of the Salt Basin, calculated by Sigstedt (2010) using radiocarbon groundwater ages. Sigstedt (2010) estimated the subsurface flux to range from 20,000 m^3/day (6,000 acre-feet/year) to 37,000 m^3/day (11,000 acre-feet/year). Recharge to the Guadalupe Mountains recharge zone ranged from 1,600 m^3/day (470 acre-feet/year) for the minimum recharge scenario to 17,000 m^3/day (5,100 acre-feet/year) for the maximum recharge scenario, with the average recharge scenario resulting in 8,600 m^3/day (2,600 acre-feet/year). These values for the Guadalupe Mountains recharge zone seem reasonable compared to the recharge values for the Sacramento Mountains recharge zone.

Abundant hydrogeologic evidence exists to indicate that the Guadalupe Mountains receive much less recharge than the Sacramento Mountains. The northern portion of the Guadalupe Mountains (i.e. the portion that extends in a general northwest direction from Guadalupe Ridge along the Algerita and Buckhorn Escarpments), and the Brokeoff Mountains and Dog Canyon areas contain no springs or perennial streams (Hayes, 1964). In contrast, the Sacramento Mountains contain numerous springs, and several perennial streams, including the upper portions of the Sacramento River, and the

Rio Peñasco (Newton et al., 2009). In addition, depth to the regional groundwater surface is generally greater than 230 meters (750 feet) in the Guadalupe Mountains, while in the Sacramento Mountains depths are generally less than 76 meters (250 feet). (Figure 3.43) Tritium levels in wells near the base of the Guadalupe and Brokeoff Mountains are low (< 1 TU), while tritium levels in wells and springs within the Sacramento Mountains generally range from 2.97 to 10.4 TU, indicating groundwater is typically less than 50 years old (Newton et al., 2009; Sigstedt, 2010). Also, radiocarbon groundwater ages calculated by Sigstedt (2010) for wells near the base of the Guadalupe and Brokeoff Mountains are greater than 10,000 years old. All of this evidence suggests the Guadalupe and Brokeoff Mountains do not contribute significant recharge to the Salt Basin groundwater system.

Recharge to the Cornudas Mountains and Diablo Plateau recharge zones ranged from 140 m^3/day (41 acre-feet/year) for the minimum recharge scenario to 1,000 m^3/day (300 acre-feet/year) for the maximum recharge scenario, with the average recharge scenario resulting in 580 m^3/day (170 acre-feet/year). Hydrogeologic evidence suggests that these relatively low recharge values are reasonable. Sigstedt (2010) produced groundwater chemistry contours of magnesium and sulfate concentration for the Salt Basin in New Mexico and Texas. Although radiocarbon groundwater ages were not obtained from the Otero Mesa/Diablo Plateau region, the groundwater chemistry contours, along with correlations between increasing radiocarbon groundwater age and increasing magnesium and sulfate concentrations on the eastern side of the basin, have implications for relative fluxes on the western side of the basin (Sigstedt, 2010). In addition, radiocarbon groundwater ages from two wells just to the east of the Cornudas

Mountains are older than any of the wells on the eastern side of the basin, and are located within a region of high magnesium and sulfate concentrations (Sigstedt, 2010). All of this evidence indicates that recharge and the groundwater flux from the Otero Mesa/Diablo Plateau region is relatively low.

-Discharge

Discharge from the Salt Flats region was modeled using the Well (WEL) Package. The region of discharge from the playa was assumed to correspond to the area of depth-to-water less than 15 meters (50 feet) from Figure 3.43. (Figure 4.19) Pumping wells discharging at the same flow rate were placed in each layer 1 cell within this region, resulting in a total of 1,118 wells. For the steady-state groundwater flow model it was assumed that recharge equals discharge, and all groundwater discharges at the Salt Flats playa.

4.1.b: Model-assigned Hydraulic Properties

The hydraulic properties (horizontal hydraulic conductivity and vertical anisotropy) assigned to each cell within the model domain were controlled by the hydrogeologic unit of each cell [Figures 4.13 through 4.18], as well the location of each cell within the structural zones delineated in Figure 3.1. The LPF Package allows vertical hydraulic conductivity to be entered either as actual hydraulic conductivity values, or as anisotropy factors defined as horizontal hydraulic conductivity divided by vertical hydraulic conductivity. In general, cells within the structural zones corresponding to the "graben" southwest of the Otero Break, the Cornucopia Draw and Piñon Creek drainages, the Dell Valley region, and the Salt Basin graben were assigned higher horizontal hydraulic conductivities and lower vertical anisotropies than surrounding cells

due to the greater density of faulting and fracturing within these blocks, as discussed in Chapter 2.

The hydraulic property data presented in Chapter 3.6 and Tables A-3.27 and A-3.28, and displayed graphically in Figures 3.57 and 3.58, along with the permeability distribution from previous groundwater flow modeling efforts, as discussed in Chapter 3.1, were used to guide the initial values and distribution of horizontal hydraulic conductivity assigned to each hydrogeologic unit. The bulk of the published hydraulic property data presented in Chapter 3 were transmissivity values estimated from specific capacity or aquifer tests performed on wells completed in a particular aquifer or hydrogeologic facies. In order to calculate hydraulic conductivity from this data, the transmissivity values were divided by the saturated aquifer thickness, which was assumed to be equal to the length of the screened and/or open interval for each well. The use of the screened/open interval, along with the fact that most wells are open to the most productive intervals in a heterogeneous aquifer may bias the hydraulic conductivity estimates towards larger values. Thus, the range of hydraulic conductivity values calculated from published transmissivity values were used to constrain the maximum value of horizontal hydraulic conductivity assigned to each hydrogeologic unit.

The majority of the transmissivity data were obtained from wells for which screened and open intervals were commonly available in the TWDB's database. If a well contained multiple screened and/or open intervals, the bottom of the deepest screened or open interval was used as the bottom of the screened/open interval and the top of the shallowest screened or open interval was used as the top of the screened/open interval. For wells in which screened or open intervals were not available (i.e. wells located in

New Mexico, as well as some wells in Texas), the aquifer thickness was assumed to be equal to the length from the mean water level to the bottom of the well. In situations were no water levels were available, or well depth was not given, the aquifer thickness was assumed to be 30 meters (98 feet), which approximately corresponds to the minimum length of screened interval for all wells with screen data. Assuming the minimum screen length maximizes the estimate of hydraulic conductivity, but none of the hydraulic conductivity values estimated in this way produced the maximum estimate of hydraulic conductivity for a particular aquifer or hydrogeologic facies. The hydraulic conductivity values estimated from the transmissivity data are presented in Table A-4.6 and Figure 4.32.

Cenozoic alluvium in layers 1 through 3 was assigned an initial horizontal hydraulic conductivity of 1 meters/day (3 feet/day). The Cretaceous in layer 1 was given an initial horizontal hydraulic conductivity of 0.01 meters/day (0.03 feet/day). The Permian in layers 1 through 5 within the structural zones associated with a high density of faulting and fracturing was assigned an initial horizontal hydraulic conductivity ranging from 1 to 10 meters/day (3 to 30 feet/day), while the surrounding Permian units were assigned an initial horizontal hydraulic conductivity ranging from 0.01 to 0.1 meters/day (0.03 to 0.3 feet/day). The Permian within the higher permeability structural zones was given a vertical anisotropy of 10, while the other units described above were given a vertical anisotropy of 100.

The low permeability confining unit inserted in layer 2 beneath the Cretaceous was assigned an initial horizontal hydraulic conductivity of 0.000001 meters/day (0.000003 feet/day), and a vertical anisotropy of 1,000. The Paleozoic (Cambrian through

Pennsylvanian) in layers 2 through 6 was assigned an initial horizontal hydraulic conductivity of 0.001 meters/day (0.003 feet/day). The Precambrian in layers 1 through 6 was assigned an initial horizontal hydraulic conductivity of 0.001 meters/day (0.003 feet/day). The Cenozoic intrusions in layers 1 through 5, including the Cenozoic mass in layers 3 through 5, were given an initial horizontal hydraulic conductivity of 0.0001 meters/day (0.0003 feet/day). The Paleozoic, Precambrian, and Cenozoic intrusions were assigned a vertical anisotropy of 1,000.

4.2: Model Calibration and MODPATH Particle-tracking Setup

4.2.a: Model Calibration

A subset of the groundwater wells used to contour the groundwater surface displayed in Figure 3.42 (i.e. those wells within the groundwater flow model domain) were used as calibration targets. (Figure 4.33) Both recharge distribution models were calibrated to steady-state conditions. Model calibration involved manually varying only the horizontal hydraulic conductivity of each hydrogeologic unit to attempt to minimize the sum of the squares of the residuals for all groundwater well calibration points. The range of hydraulic conductivity values presented in Figures 3.57 and 4.32, and Tables A-3.27 and A-4.6 were used to constrain the minimum and maximum horizontal hydraulic conductivity of each unit during model calibration.

Model calibration was achieved by manually increasing or decreasing the horizontal hydraulic conductivity of each hydrogeologic unit from the initial value assigned to each unit [Tables 4.7 and 4.8], through the range of possible conductivity values for each unit [Figures 3.57 and 4.32, and Tables A-3.27 and A-4.6], until the sum of the squares of the residuals for all calibration points was minimized or stable. If the

sum of the squares of the residuals became stable (i.e. unchanging) during calibration, and remained stable through the range of possible conductivity values, the horizontal hydraulic conductivity value associated with the initial stabilization of the sum of the squares of the residuals was assigned to the unit being calibrated. If increasing and decreasing the horizontal hydraulic conductivity value of a unit through the range of possible conductivity values didn't result in a reduction of the sum of the squares of the residuals, the initial horizontal hydraulic conductivity value [Tables 4.7 and 4.8] was restored to that unit. Another constraint maintained throughout the calibration process was the horizontal hydraulic conductivity assigned to a hydrogeologic unit in the average recharge scenario model must be greater than or equal to the conductivity assigned to the same unit in the minimum recharge scenario model, and less than or equal to the conductivity assigned to the same unit in the maximum recharge scenario model.

In general, calibration proceeded from the youngest to the oldest hydrogeologic unit: Cenozoic alluvium, the Cretaceous, the low permeability Cretaceous confining, the Permian, the Paleozoic (the Cambrian through the Pennsylvanian), and the Precambrian. The one exception was Cenozoic intrusions, which were calibrated after the Precambrian. For Cenozoic alluvium, the Cretaceous, the low permeability Cretaceous confining, and the Permian hydrogeologic units, the horizontal hydraulic conductivity was varied in increments of a quarter of an order-of-magnitude (e.g. 1 to 2.5, or 0.1 to 0.075). For the Paleozoic hydrogeologic unit, the horizontal hydraulic conductivity was varied in increments of a half of an order-of-magnitude (e.g. 1 to 5, or 0.1 to 0.05). For Cenozoic intrusions and the Precambrian hydrogeologic units, the horizontal hydraulic conductivity was varied in increments of an order-of-magnitude (e.g. 1 to 10, or 0.1 to 0.01).

The residual for a calibration, also referred to as an observation, point was defined as the hydraulic head computed by the groundwater flow model minus the observed head. If multiple water levels measurements were available for a groundwater well, the observed head was set as the mean groundwater elevation, relative to mean sea level. However, numerous wells, especially those located in the New Mexico portion of the model domain, had only one water level measurement available. Refer to Chapter 3.3 for more information on the groundwater wells used in this study.

GMS 6.5 can determine the location of an observation point within the 3-D MODFLOW grid in several ways: 1) the user defines an elevation for the point and this elevation is compared to the layer elevations to determine which layer the point is in, 2) the user automatically assigns the point to a layer, or 3) the user defines a top and bottom elevation representing the screened interval of the well and this interval is compared to the layer elevations to determine which layer or layers the point is in. The third method listed was used for this modeling exercise. The criteria used to define the length of the screened interval assigned to each well was the same as that described above in Chapter 4.1.b. The groundwater wells used as calibration targets within the groundwater flow model are displayed in Figure 4.33. Table A-4.9 lists the groundwater wells used as calibration targets, including the row and column location of each well within the model domain, the model layer or layers intersected by the screened interval of each well, the top and bottom elevation of the screened interval, and the observed groundwater elevation.

Model calibration was first performed for the minimum recharge scenario of both the water-balance based recharge distribution and the elevation-dependent recharge

distribution. The quality of the calibration was assessed through several statistics, including the sum of the residuals, the sum of the absolute values of the residuals, the sum of the squares of the residuals, and the root-mean-square (RMS) error, as well as visual inspection of a plot of the observed versus computed heads. In addition to the sum of the residuals, the sum of the absolute values of the residuals, the sum of the squares of the residuals, and the RMS error, calculated calibration statistics included the mean of the residuals, the mean of the absolute values of the residuals, the standard deviation of the residuals, the standard deviation of the residuals divided by the range of observed hydraulic head, and the mean of the residuals divided by the range of observed hydraulic head.

4.2.b: MODPATH Particle-tracking Setup

After an adequate calibration to the groundwater level observation points had been achieved for all recharge scenarios of both recharge distributions, MODPATH was used to simulate groundwater residence times. As mentioned in Chapter 4.1.a, the purpose of the MODPATH particle-tracking exercise was to test the appropriateness of the two recharge distributions. This was accomplished by comparing radiocarbon groundwater ages from wells within the Salt Basin, as presented in Sigstedt (2010), to MODPATH particle-tracking ages calculated from the hand-calibrated MODFLOW solutions for each recharge distribution. Chapter 4.3.b summarizes the results of the MODPATH particle-tracking exercise.

MODPATH is a post-processing program designed to use output from steady-state or transient MODFLOW simulations to compute 3-D flow paths and travel times for imaginary "particles" of water moving through the simulated groundwater system

(Pollock, 1994). MODPATH calculates the average linear groundwater velocity vector field within each cell based on the intercell flow rates calculated by MODFLOW, and uses this field to compute particle path lines (Pollock, 1994). Thus, MODPATH only simulates advective transport, and the groundwater ages calculated using this method are advective ages.

In order to calculate the average linear groundwater velocity within each cell, MODPATH requires porosity values to be assigned to each hydrogeologic unit. Sigstedt (2010) referenced porosity and depth relationships for a major west Texas oil field from Galloway (1983). The data presented in Galloway (1983) included a plot of depth versus average porosity for the Permian San Andres and Abo Formations, the Siluro-Devonian, and the Ordovician. The porosity data in Galloway (1983) and the wellsite core analysis porosity data from the Yates Petroleum Corporation, One Tree Unit #2 well [Table 3.30] were used to assign a minimum, average, and maximum porosity value to each MODFLOW hydrogeologic unit. The minimum, average, and maximum porosity values were used to compute particle flow paths and travel times for the minimum, average, and maximum recharge scenario models of both recharge distributions. Table 4.10 lists the minimum, average, and maximum porosity values used for each hydrogeologic unit.

MODPATH can perform either forward or reverse particle tracking. Reverse particle tracking was used for this modeling exercise, and involved generating particles in the MODFLOW grid cells corresponding to the location of 13 of the 15 wells for which radiocarbon groundwater ages were calculated by Sigstedt (2010) [Figure 4.34] and tracking them backward to their origins. Particle origins refers to their position within the MODFLOW grid when they reached the simulated groundwater surface (i.e. recharged

the groundwater system). Two of the radiocarbon groundwater age wells from Sigstedt (2010), Hunt C13 and Hunt House, were not included because they are very close to, and have similar groundwater ages to the included Hunt 8 well, and they are located in grid cells which already contain pumping wells used to simulate discharge from the groundwater system at the Salt Flats.

The total depths of 12 of the 13 radiocarbon groundwater age wells do not exceed the bottom of layer 1 in the MODFLOW grid, and thus particles were generated in layer 1 for these wells. The total depth of Butterfield Well extends into layer 2 of the MODFLOW grid, and thus particles were generated in layer 2 for this well. Table 4.11 lists the groundwater age wells used, including the NMOSE POD Number (if available), the UTM coordinates using the NAD 83 coordinate system, the row and column location within the MODFLOW domain, the layer location within the MODFLOW domain, the ground surface elevation in meters derived from the 1-arc second NED discussed above in Chapter 3.2.a, the total well depth in meters, and the elevation of the total well depth in meters. Figure 4.34 displays the location of the groundwater age wells within the MODFLOW model domain.

MODPATH can generate particles at a MODFLOW grid cell in several ways: 1) on the computed groundwater surface within the cell, 2) in the interior of the cell, or 3) on the cell faces. The vertical position of particles generated in the interior of the cell is set at the midpoint between the computed groundwater surface within the cell and the bottom of the cell. The computed groundwater surface within each cell varied between the different recharge scenarios of both recharge distributions, and therefore the vertical

position of particles generated using methods 1) and 2) also varied between the different models.

Using 1), 2), or 3), particles could be generated on the computed groundwater surface within each cell, at the midpoint between the computed groundwater surface and the bottom of each cell, or on the bottom cell face, respectively. In general, particles were generated in two of these three positions within the MODFLOW cells in order to bound the vertical position of the elevation, relative to mean sea level, of the total depth of the radiocarbon groundwater age wells. However, if the elevation of the total depth of a groundwater age well was higher than the computed groundwater surface within the MODFLOW cell, only particles generated on the groundwater surface were deemed to represent the pathlines of groundwater sampled at the well. If the elevation of the total depth of a groundwater age well was located between the computed groundwater surface and the midpoint, or the midpoint and the bottom cell face, the particles generated at the corresponding two vertical positions which bound the elevation of the total depth of the well were chosen to represent the potential pathlines and residence times of groundwater sampled at the well. Tables 4.12 and 4.13 list the elevation of the total depth of each groundwater age well as well as the elevations of the three vertical positions within each cell for the calibrated minimum, average, and maximum recharge scenario models of the water-balance based and elevation-dependent recharge distributions, respectively. Tables 4.12 and 4.13 also designate which vertical positions were chosen to represent the potential pathlines and residence times of groundwater sampled at each well.

A maximum of 100 particles could be generated in the interior of the cell. As a result, 100 particles were generated at each selected vertical position within the cells

corresponding to the location of the radiocarbon groundwater age wells. The mean, median, and standard deviation of the particle travel times (i.e. ages) were calculated for each selected vertical position within the cells. The median of the particle travel times for each selected vertical position within the cells were used for graphical comparison to the radiocarbon groundwater ages presented in Sigstedt (2010).

4.3: Model Results

4.3.a: MODFLOW

The mass balances for the calibrated minimum, average, and maximum recharge scenario models of the water-balance based and elevation-dependent recharge distributions are presented in Tables A-4.14 and A-4.15, respectively. Figures 4.35 through 4.37, and Figures 4.38 through 4.40 compare model computed heads in layer 1 for the calibrated recharge scenario models of the water-balance based and elevation-dependent recharge distributions, respectively, to the groundwater surface depicted in Figure 3.42. In general, model computed heads for both recharge distributions represent the overall configuration of the groundwater surface displayed in Figure 3.42, and the model computed heads for both recharge distributions are similar.

Plots of model computed head versus observed head at all calibration points for the minimum, average, and maximum recharge scenario models of the water-balance based and elevation-dependent recharge distributions are presented in Figures 4.41 through 4.43, and Figures 4.44 through 4.46, respectively. Figures 4.47 through 4.49, and Figures 4.50 through 4.52 plot residual head versus observed head at all calibration points for the minimum, average, and maximum recharge scenario models of the water-balance based and elevation-dependent recharge distributions, respectively. Visual inspection of

Figures 4.41 through 4.52 reveal that model computed heads for both recharge distributions provide a reasonably close match to observed heads throughout the range of observed heads. Residual hydraulic head statistics for the calibrated recharge scenario models of the water-balance based and elevation-dependent recharge distributions are presented in Tables 4.16 and 4.17, respectively. Figures 4.53 and 4.54, and Figures 4.55 and 4.56 graphically compare the sum of the residuals, the sum of the absolute values of the residuals, and the sum of the squares of the residuals between the calibrated minimum, average, and maximum recharge scenario models of the water-balance based and elevation-dependent recharge distributions, respectively.

Tables 4.7 and 4.8 summarize the initial horizontal hydraulic conductivity values assigned to each hydrogeologic unit, as discussed in Chapter 4.1.b, and the final horizontal hydraulic conductivity values for the calibrated minimum, average, and maximum recharge scenario models of the water-balance based and elevation-dependent recharge distributions, respectively. Tables 4.7 and 4.8 also summarize the vertical anisotropy factors applied to each hydrogeologic unit. As mentioned in Chapter 4.2.a, the vertical anisotropy factors were not varied during model calibration.

Figure 4.57 and Figures A-4.58 through A-4.62, Figure 4.63 and Figures A-4.64 through A-4.68, and Figure 4.69 and Figures A-4.70 through A-4.74 display the range of horizontal hydraulic conductivities within layers 1 through 6 for the calibrated minimum, average, and maximum recharge scenario models, respectively, of the water-balance based recharge distribution. Figure 4.75 and Figures A-4.76 through A-4.80, Figure 4.81 and Figures A-4.82 through A-4.86, and Figure 4.87 and Figures A-4.88 through A-4.92 present the same range of horizontal hydraulic conductivities for the calibrated elevation-

dependent recharge distribution models. Figures 4.93 through 4.95, and Figures 4.96 through 4.98 plot the range of horizontal hydraulic conductivities assigned to each hydrogeologic unit for the calibrated minimum, average, and maximum recharge scenario models of the water-balance based and elevation-dependent recharge distributions, respectively. These plots can be compared to the range of hydraulic conductivity values from previous studies, as presented in Figure 3.57.

Horizontal hydraulic conductivities from the calibrated minimum, average, and maximum recharge scenario models were used to derive the distribution of aquifer transmissivity within Cenozoic alluvium and the Permian hydrogeologic units. Under the assumption that groundwater flow is parallel to unit layering, the transmissivity of an aquifer containing layers with different hydraulic conductivities is equal to the sum of the transmissivities of each unit (Oosterbaan and Nijland, 1994). The transmissivity of Cenozoic alluvium and the Permian hydrogeologic units was calculated by multiplying the saturated thickness of each cell occupied by either Cenozoic alluvium or the Permian unit by the hydraulic conductivity assigned to that cell. The transmissivities calculated for a particular row and column location within the model domain were then summed over the range of layers occupied by either Cenozoic alluvium or the Permian hydrogeologic units to arrive at the aquifer transmissivity for that row and column location.

Figures 4.99, 4.100, and 4.101 show the distribution of aquifer transmissivity for the calibrated minimum, average, and maximum recharge scenario models, respectively, of the water-balance based recharge distribution. The distribution of aquifer transmissivity for the calibrated elevation-dependent recharge distribution models are displayed in Figures 4.102, 4.103, and 4.104. Figures 4.105 and 4.106 plot the range of

transmissivities derived from the calibrated minimum, average, and maximum recharge scenario models of the water-balance based and elevation-dependent recharge distributions, respectively. These plots can be compared to the range of transmissivity values from previous studies, as presented in Figure 3.58. The range of transmissivities derived from the two recharge distributions are very similar to previous estimates, including the transmissivity values calculated using the ^{14}C groundwater ages along cross-section A to A', as discussed in Chapter 3.6.b. The range of transmissivities derived from the water-balance based and elevation-dependent recharge distributions are further summarized in Tables 4.18 and 4.19, respectively.

As indicated by the distribution of horizontal hydraulic conductivity and transmissivity within the groundwater flow model domain, the highest permeability zones correspond to regions of extensive faulting and fracturing. These heavily faulted regions include the Otero Break, the Salt Basin graben, and the subsurface Pedernal uplift. In contrast, the Otero Mesa and Diablo Plateau regions, which have experienced relatively little faulting and fracturing, correspond to the lowest permeability zones.

4.3.b: MODPATH

Tables 4.20 through 4.22, and Tables 4.23 through 4.25 list the median MODPATH particle ages derived from the three calibrated recharge scenario models of the water-balance based and elevation-dependent recharge distributions, respectively, using the minimum, average, and maximum porosity values presented in Table 4.10. Tables 4.20 through 4.25 also present the radiocarbon groundwater ages calculated by Sigstedt (2010) using inverse geochemical modeling in NETPATH. Figures 4.107 through 4.109, and Figures 4.110 through 4.112 plot the NETPATH ages versus the

median MODPATH particle ages derived from the three calibrated recharge scenario models of the water-balance based and elevation-dependent recharge distributions, respectively, using minimum, average, and maximum porosities. Figures 4.113 through 4.115, and Figures 4.116 through 4.118 display the pathlines and origins of all particles derived from the three calibrated recharge scenario models of the water-balance based and elevation-dependent recharge distributions, respectively, using average porosity values.

The standard deviation of the MODPATH particle ages derived from the three calibrated recharge scenario models of the water-balance based and elevation-dependent recharge distributions using minimum, average, and maximum porosity values are presented in Tables A-4.26 through A-4.28, and Tables A-4.29 through A-4.31, respectively. Tables A-4.32 through A-4.34, and Tables A-4.35 through A-4.37 list the residual ages (i.e. the MODPATH ages minus the NETPATH ages) for the three calibrated recharge scenario models of the water-balance based and elevation-dependent recharge distributions, respectively, using minimum, average, and maximum porosity values. Tables 4.38 and 4.39 present residual age statistics (i.e. the sum of the residuals, the sum of the absolute values of the residuals, the sum of the squares of the residuals, and the root-mean-square [RMS] error) for the three calibrated recharge scenario models of the water-balance based and elevation-dependent recharge distributions, respectively, using minimum, average, and maximum porosity values. These residual age statistics for the water-balance based and elevation-dependent recharge distributions are displayed graphically in Figures 4.119 through 4.121, and Figures 4.122 through 4.124, respectively.

As can be seen in Figures 4.107 through 4.109, and Figure 4.119 (sum of residuals), the ages derived from MODPATH using the MODFLOW solution for the three calibrated recharge scenario models of the water-balance based recharge distribution are generally younger than the NETPATH ages presented in Sigstedt (2010). In contrast, Figures 4.110 through 4.112, and Figure 4.122 (sum of residuals) show that the MODPATH ages derived from the three calibrated recharge scenario models of the elevation-dependent recharge distribution are generally older than the NETPATH ages presented in Sigstedt (2010). Upon initial inspection of the residual age statistics [Tables 4.38 and 4.39], MODPATH particle ages derived from the water-balance based recharge distribution models appear to more closely match the radiocarbon groundwater ages calculated by Sigstedt (2010). However, MODPATH particle ages derived from the elevation-dependent recharge distribution models at the Evrage House and Collins wells are generally over one order of magnitude larger than the particle ages at the other wells, ranging from 390,000 to 4,600,000 years. (Figures 4.110 through 4.112, and Tables 4.23 through 4.25) If the MODPATH particle ages from the Evrage House and Collins wells are treated as outliers, the residual age statistics indicate that MODPATH particle ages derived from the average recharge scenario/minimum porosity model and the maximum recharge scenario/minimum and average porosity models of the elevation-dependent recharge distribution produce a better match to the radiocarbon groundwater ages, as compared to the water-balance based recharge distribution. (Tables 4.38 and 4.39)

4.4: Model Discussion

Both the water-balance based and elevation-dependent recharge distribution models produced a reasonably good match to observed groundwater levels and regional

groundwater flow. However, MODPATH particle ages derived from the average recharge scenario/minimum porosity model and the maximum recharge scenario/minimum and average porosity models of the elevation-dependent recharge distribution resulted in a statistically better match to radiocarbon groundwater ages calculated by Sigstedt (2010), as compared to the water-balance based recharge distribution. In general, MODPATH particle ages derived from the water-balance based recharge distribution models ranged from one to three orders of magnitude younger than the radiocarbon groundwater ages.

The MODFLOW solutions for the two recharge distributions tested in this thesis illustrate the non-uniqueness of the solutions. An adequate match to observed groundwater levels was achieved by either increasing hydraulic conductivity and recharge, as seen in the water-balance based recharge distribution, or decreasing hydraulic conductivity and recharge, as seen in the elevation-dependent recharge distribution. This issue of non-uniqueness is similar to the one discussed by Mayer (1995) concerning his modeling exercise. In addition, the MODPATH particle-tracking ages depend upon the distribution of hydrogeologic units within the groundwater flow model, as defined by the 3-D hydrogeologic framework model, as well as the hydraulic conductivity and recharge values assigned to the model. Thus, it is not possible to definitively say that the statistically better match between MODPATH particle ages derived from the elevation-dependent recharge distribution and the radiocarbon groundwater ages is the result of either the recharge distribution, or the distribution of hydrogeologic units. However, abundant hydrogeologic evidence, and the statistically better agreement between MODPATH and radiocarbon ages suggest that the elevation-dependent recharge distribution is a better representation of recharge in the Salt Basin.

FIGURES – CHAPTER 4
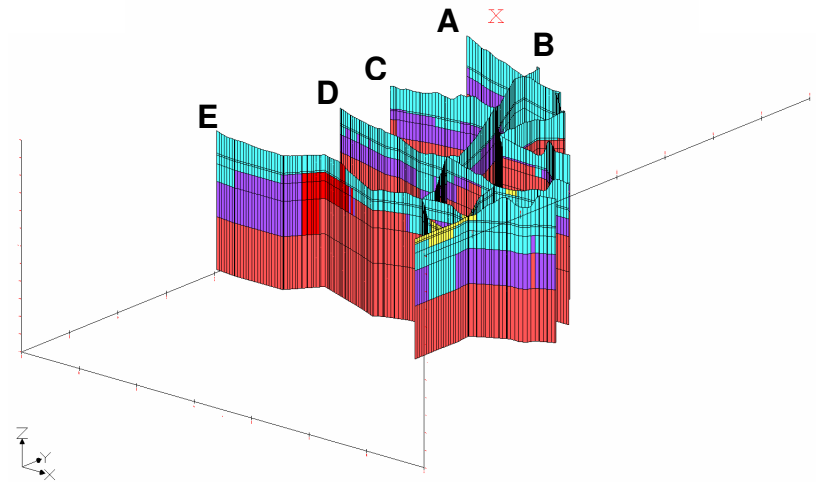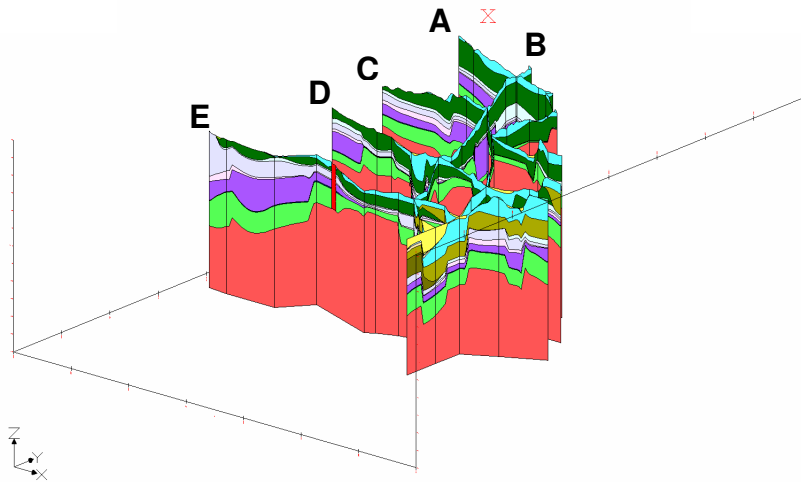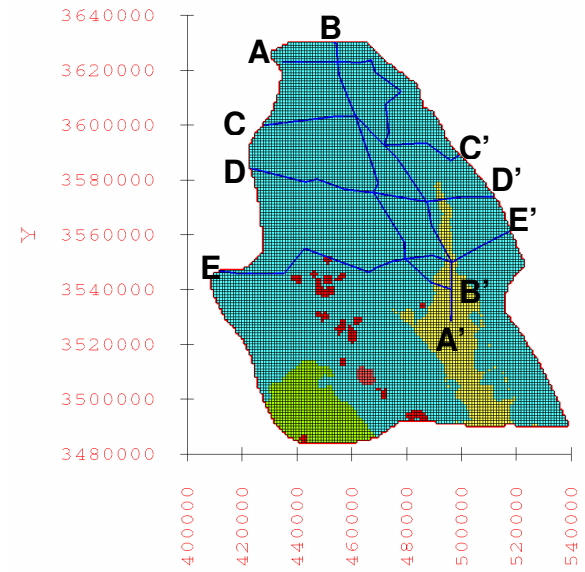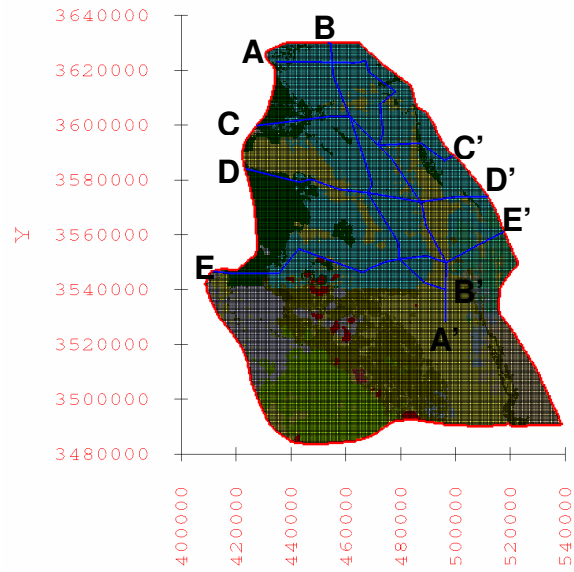
Figure 4.1: Locations and an oblique view of the five cross-sections within the solid model on left and groundwater flow model on right.
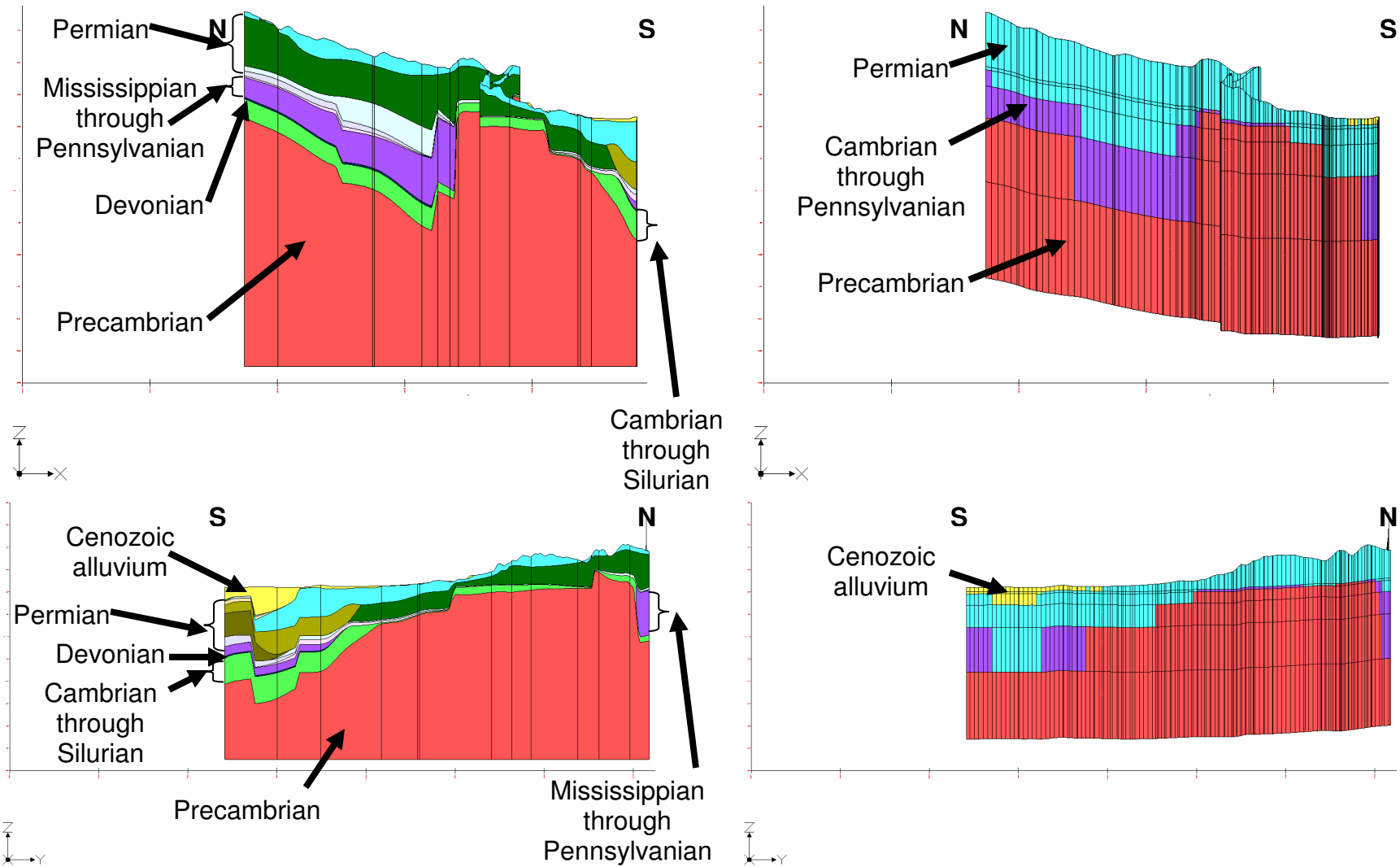
Figure 4.2: Side views along cross-section A - A' of the solid model on left and groundwater flow model on right. Vertical exaggeration 10×.
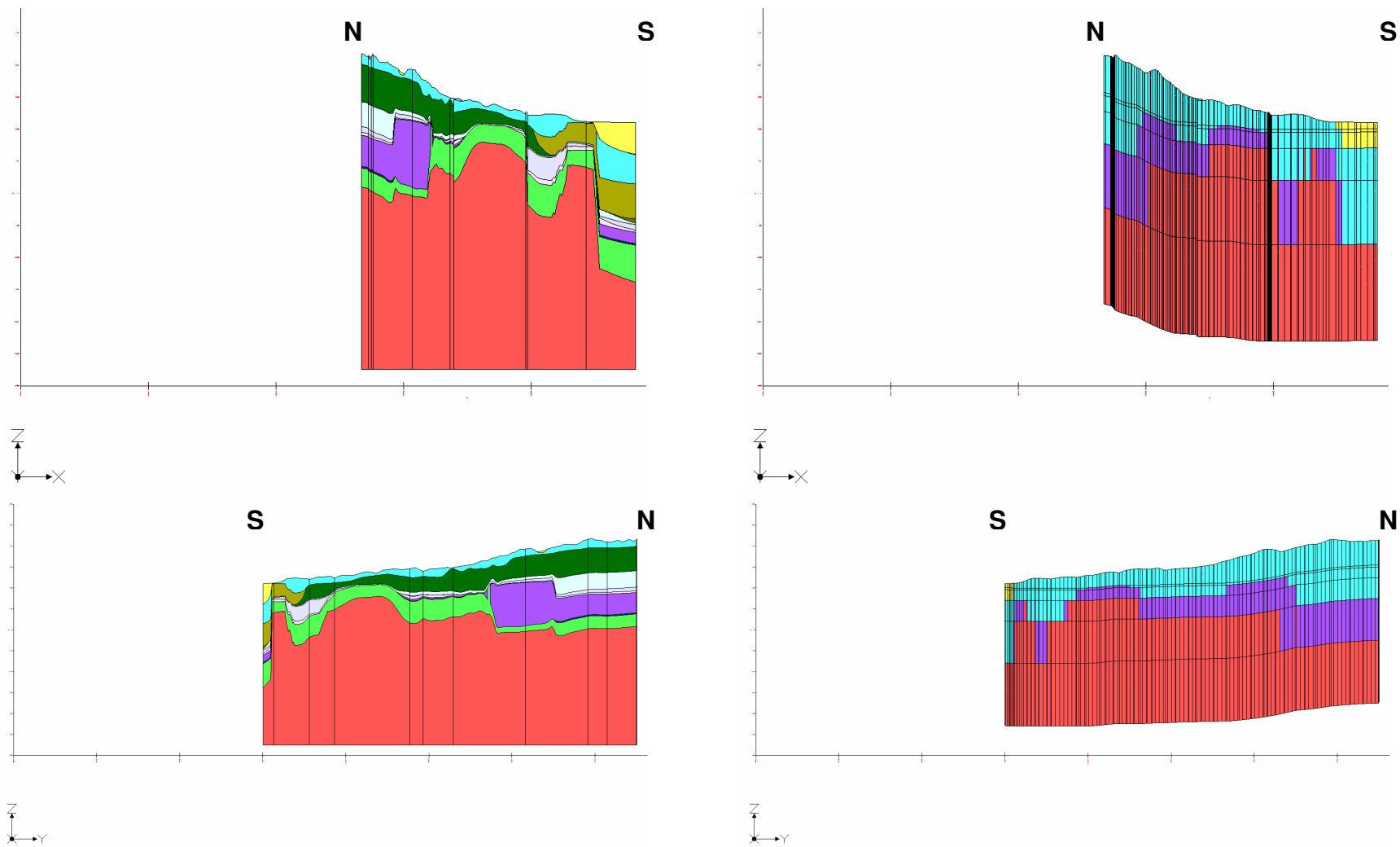
Figure 4.3: Side views along cross-section B - B' of the solid model on left and groundwater flow model on right. Vertical exaggeration 10×.
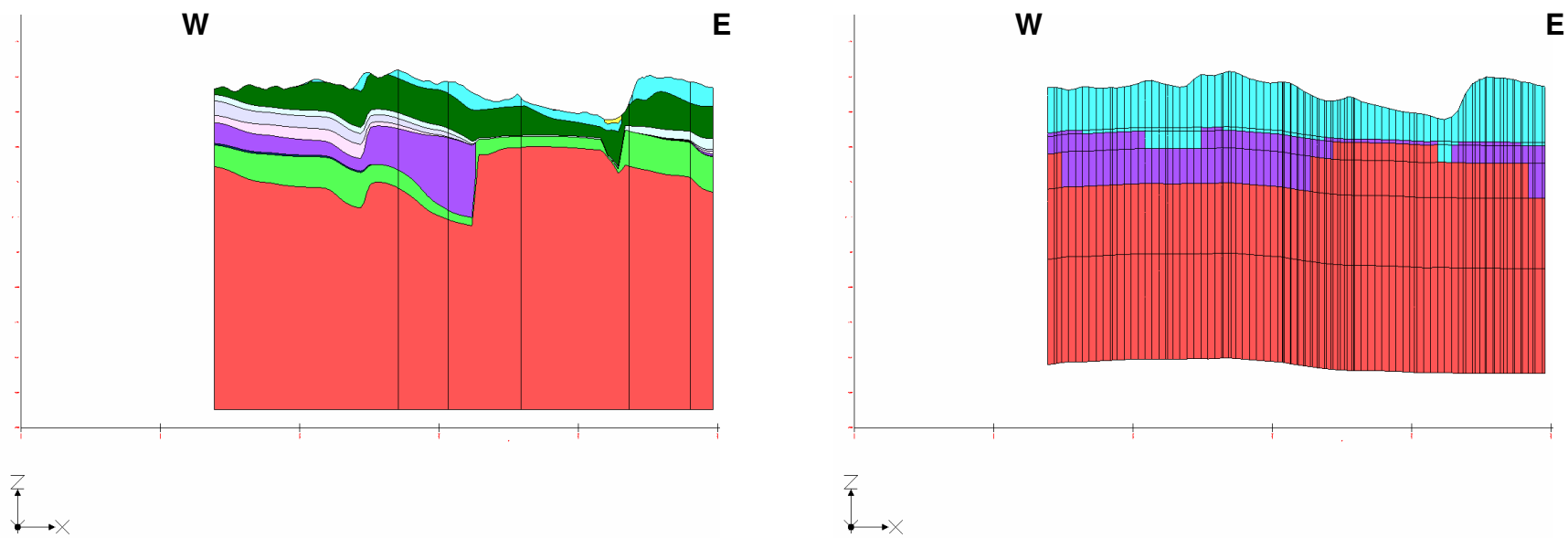
Figure 4.4: Side view along cross-section C - C' of the solid model on left and groundwater flow model on right. Vertical exaggeration 10×.

321
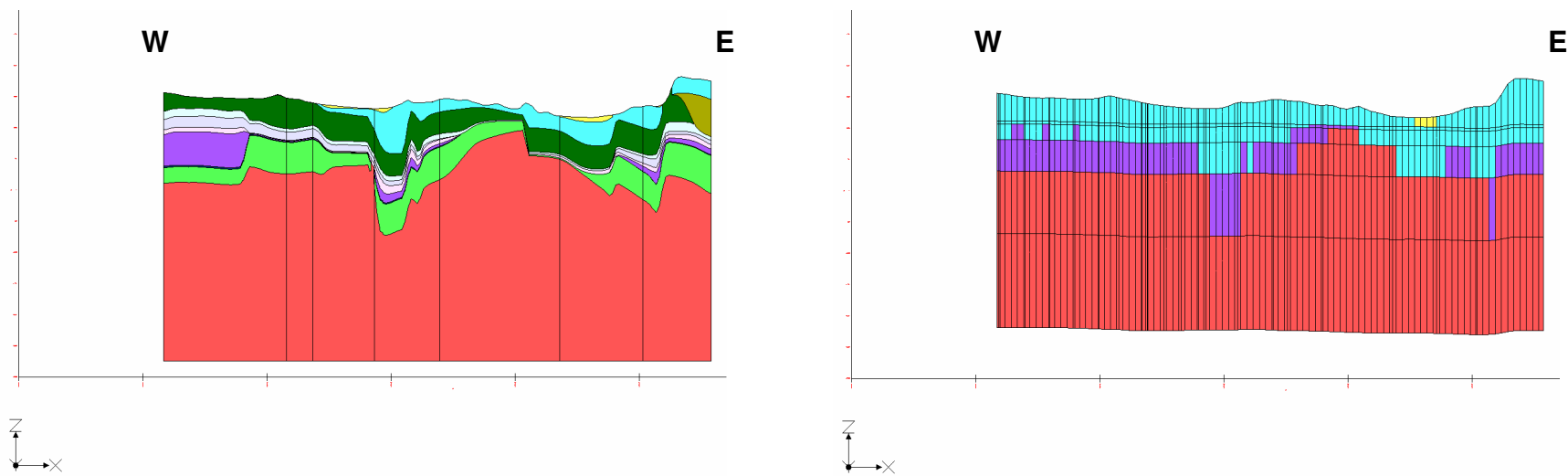
Figure 4.5: Side view along cross-section D - D' of the solid model on left and groundwater flow model on right. Vertical exaggeration 10×.
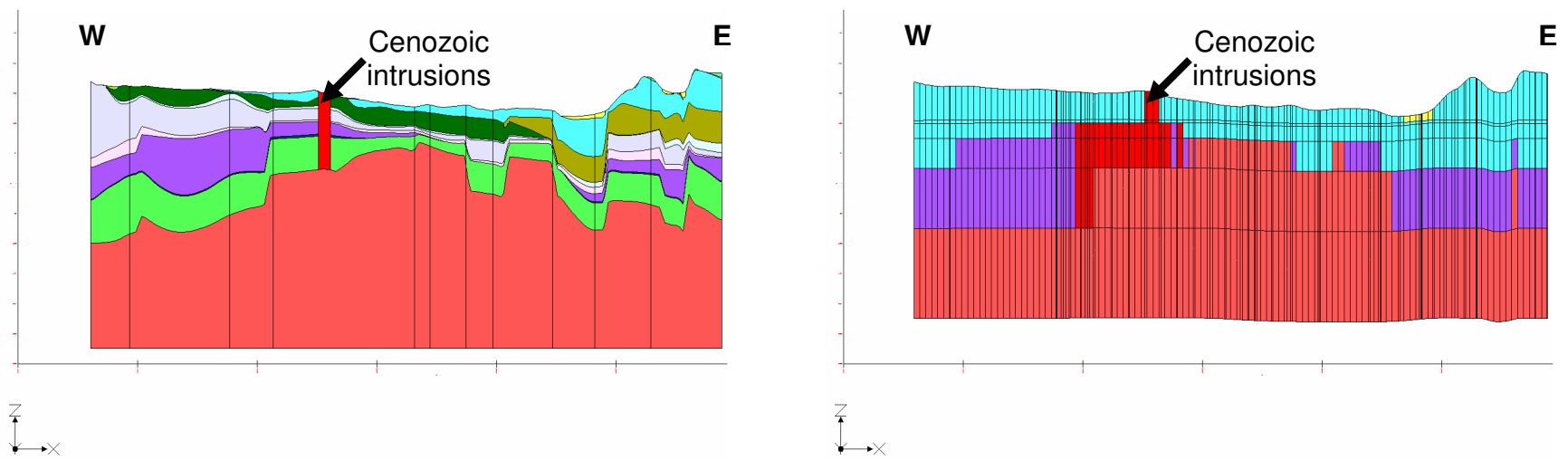
Figure 4.6: Side view along cross-section E - E' of the solid model on left and groundwater flow model on right. Vertical exaggeration 10×.
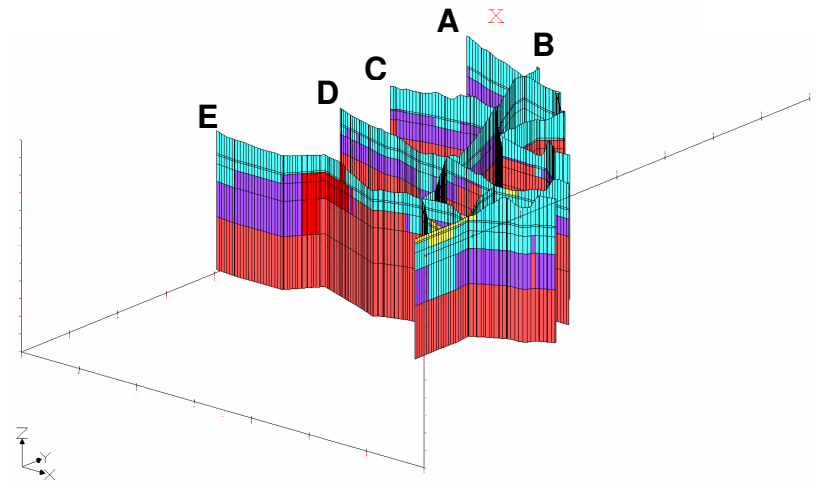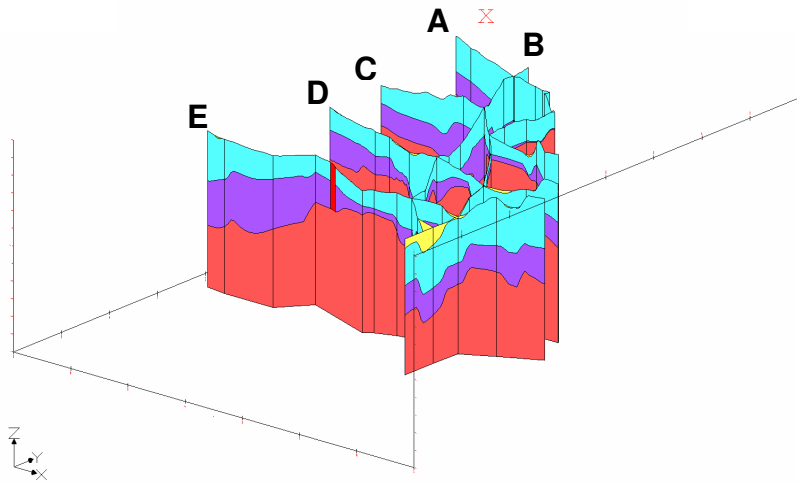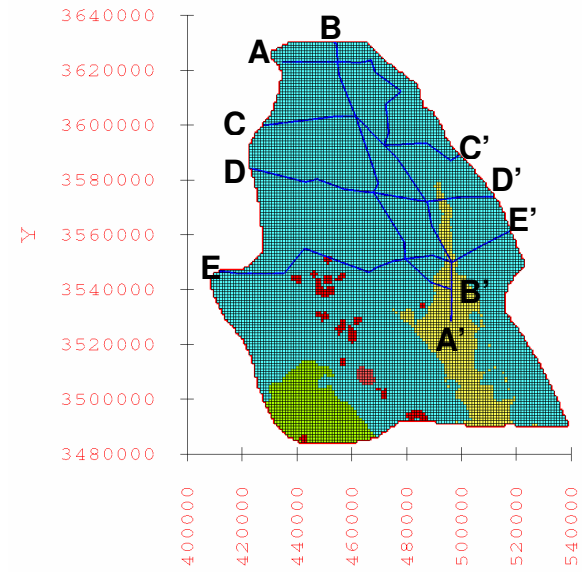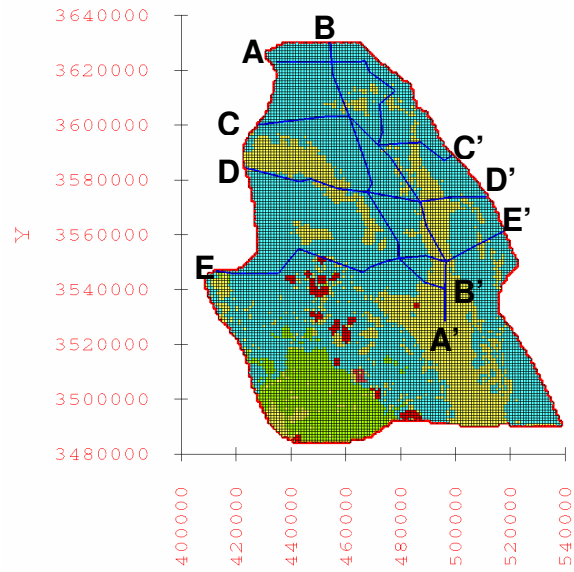
Figure 4.7 Locations and an oblique view of the five cross-sections within the simplified solid model on left and groundwater flow model on right.
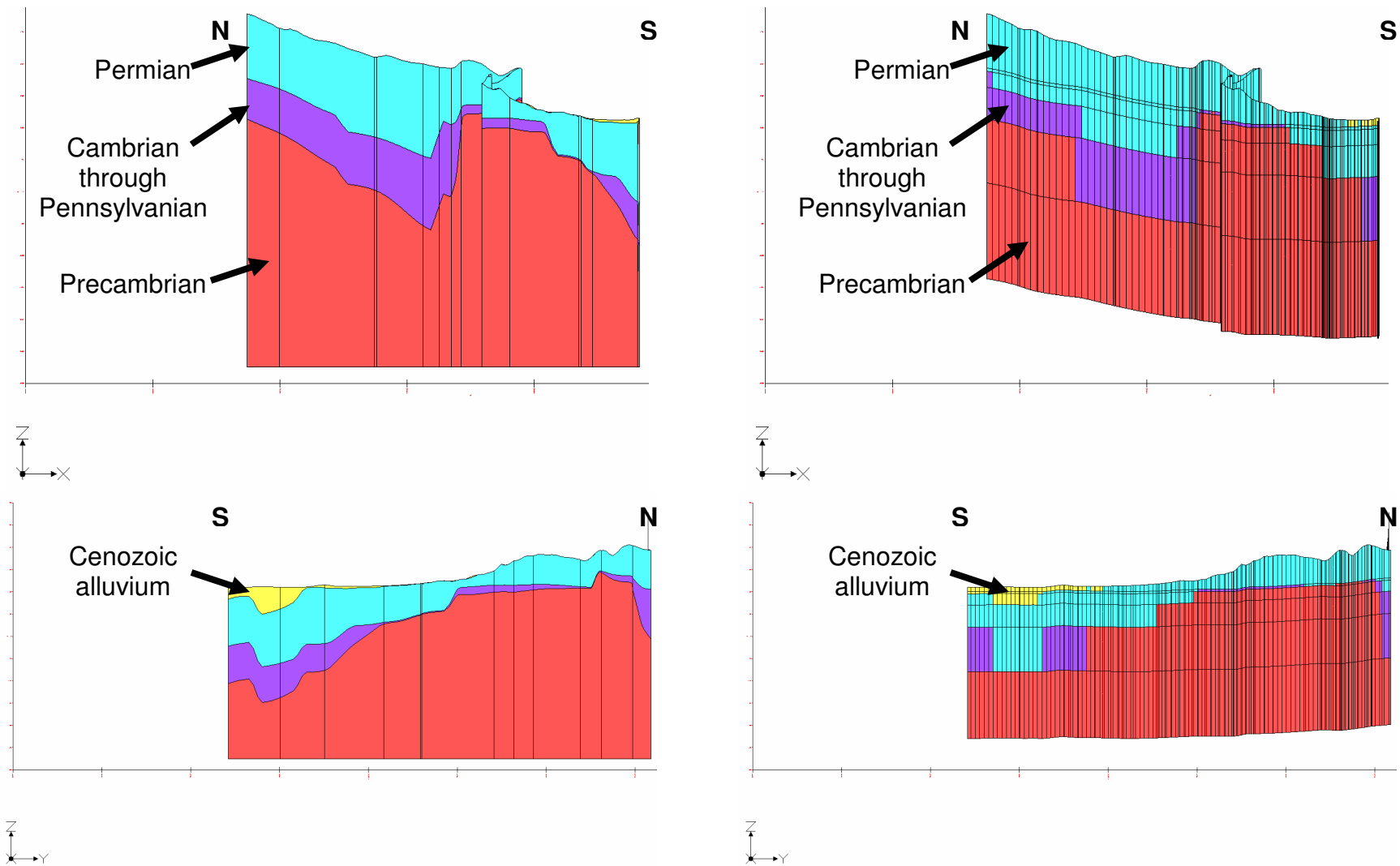
Figure 4.8: Side views along cross-section A - A' of the simplified solid model on left and groundwater flow model on right. Vertical exaggeration 10×.
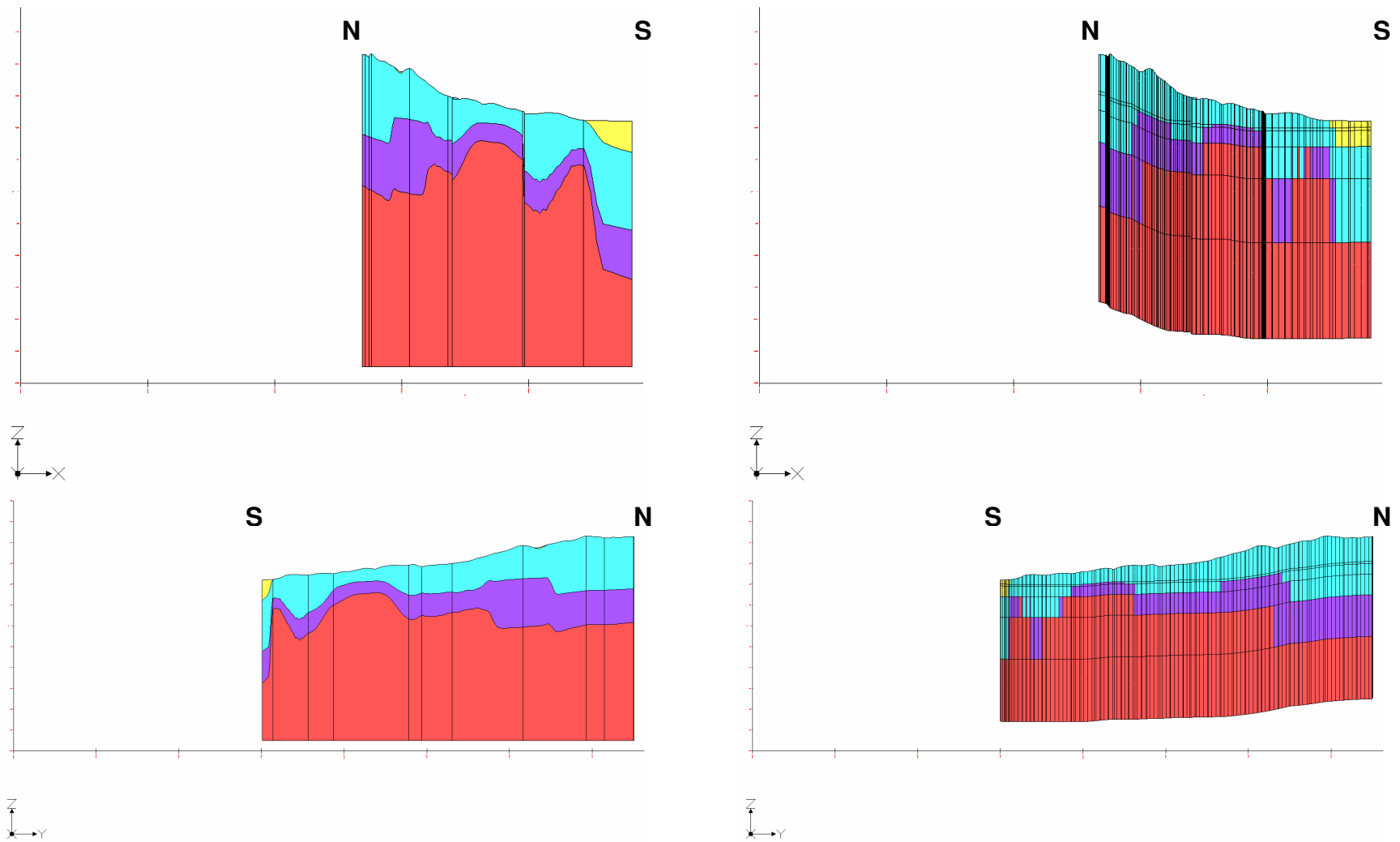
Figure 4.9: Side views along cross-section B - B' of the simplified solid model on left and groundwater flow model on right. Vertical exaggeration 10×.
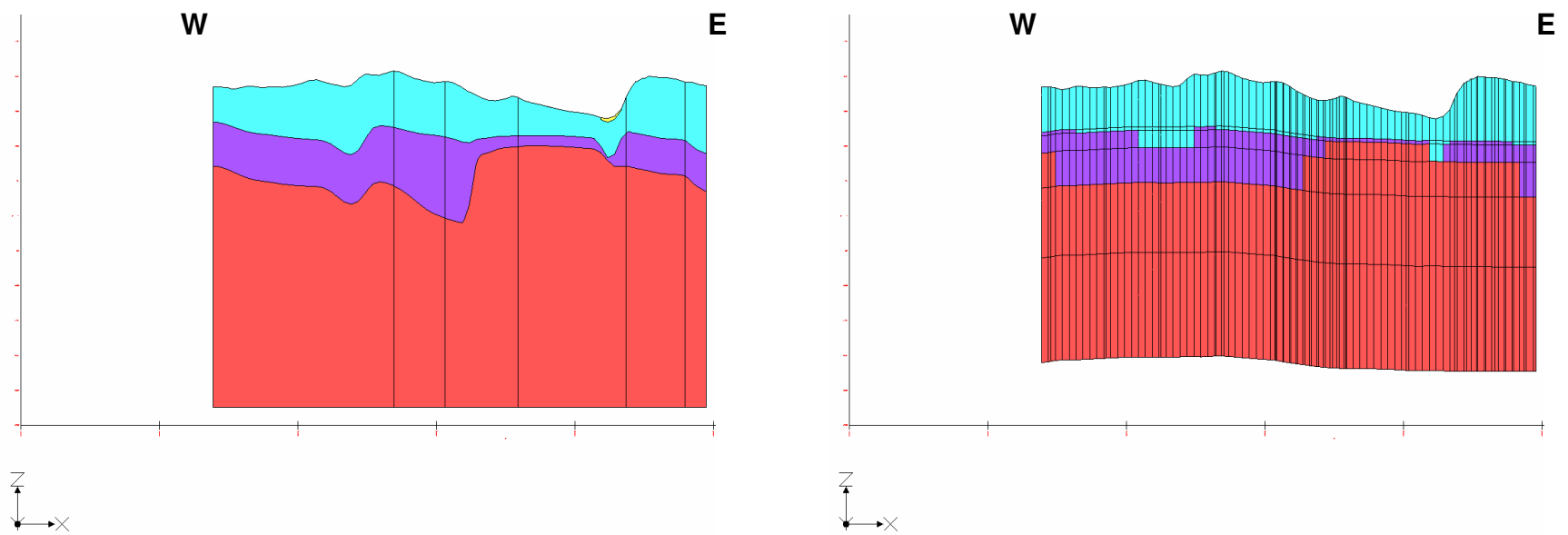
Figure 4.10: Side view along cross-section C - C' of the simplified solid model on left and groundwater flow model on right. Vertical exaggeration 10×.
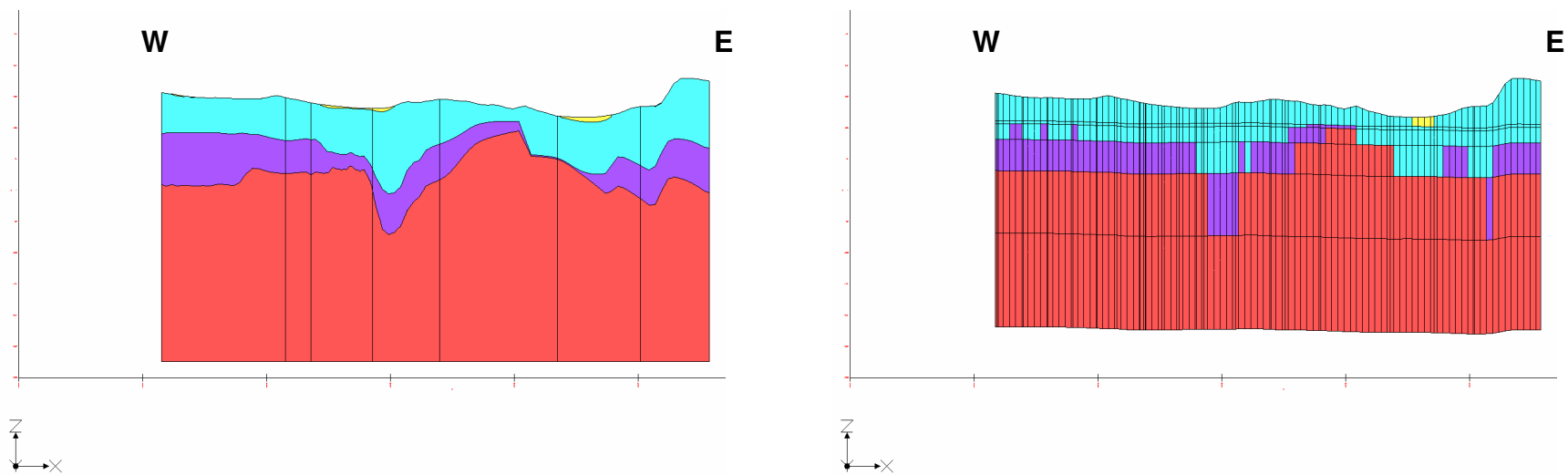
Figure 4.11: Side view along cross-section D - D' of the simplified solid model on left and groundwater flow model on right. Vertical exaggeration 10×.
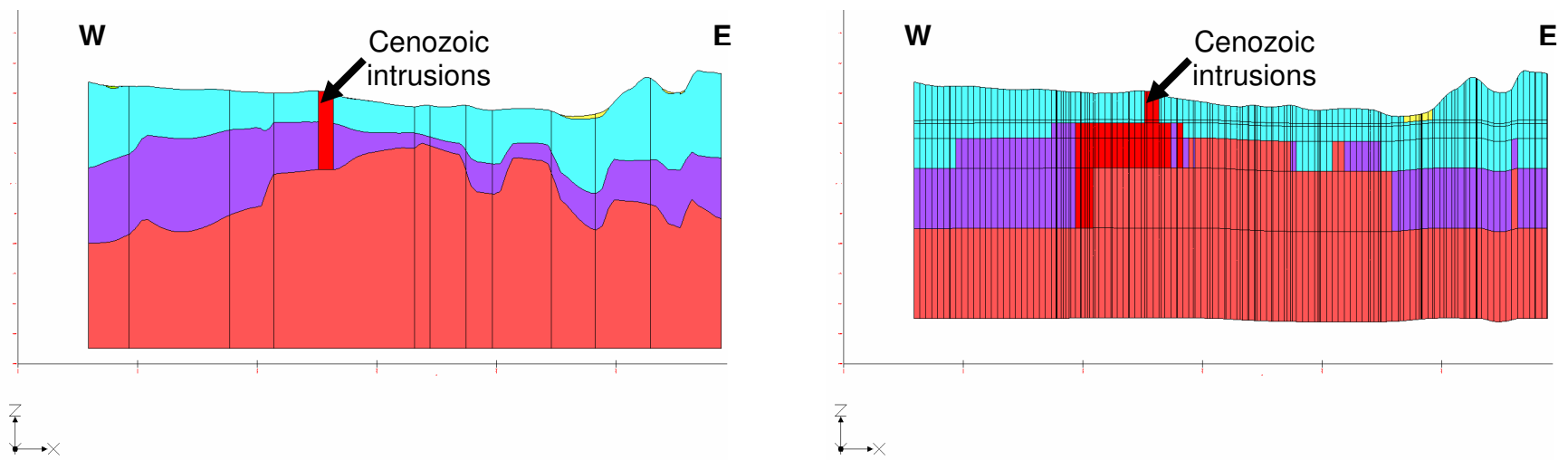
Figure 4.12: Side view along cross-section E - E' of the simplified solid model on left and groundwater flow model on right. Vertical exaggeration 10×.
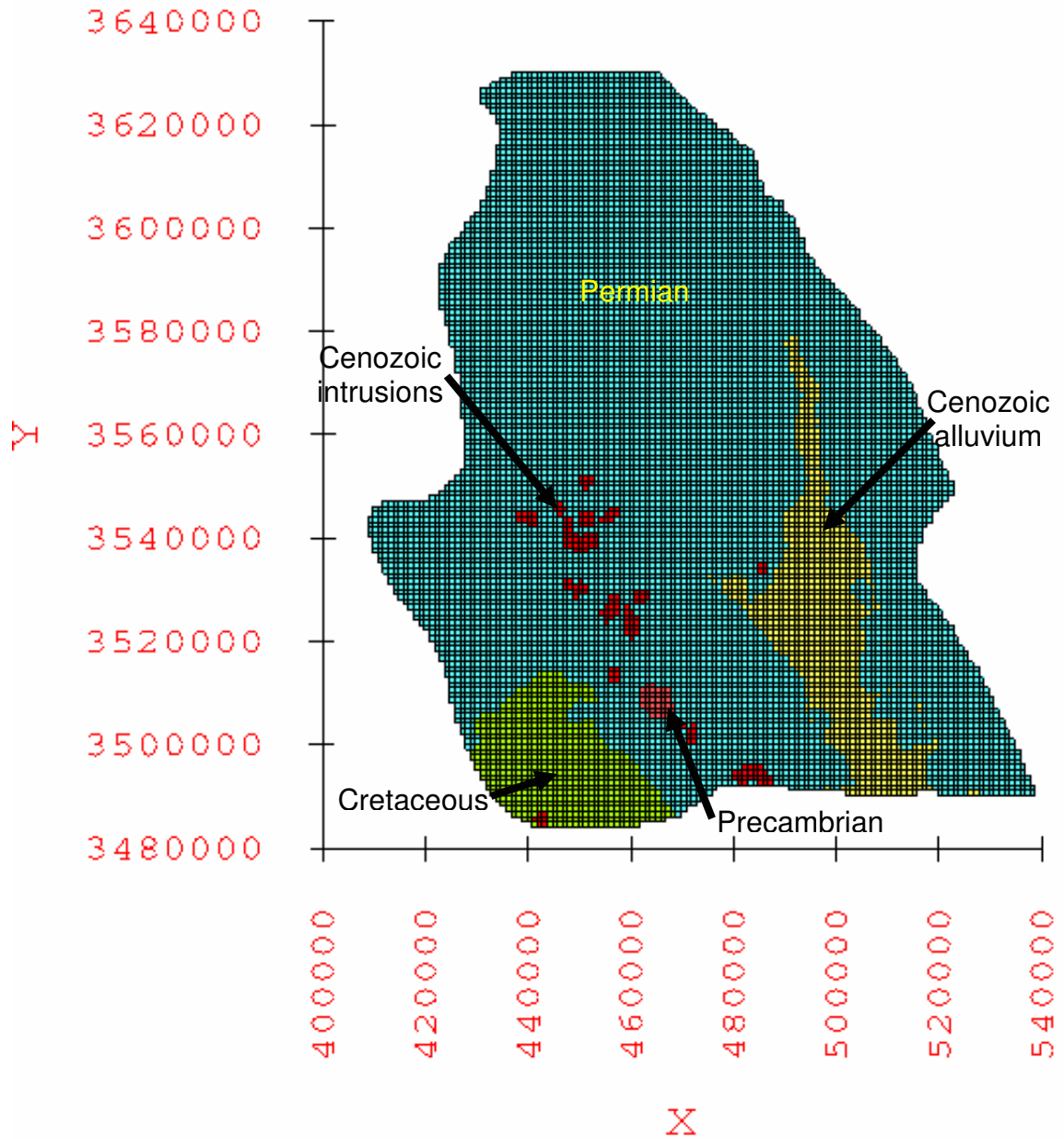
Figure 4.13: Distribution of hydrogeologic units within layer 1 of the groundwater flow model grid.
Axes scale is in UTM NAD83 Zone 13 North coordinates.
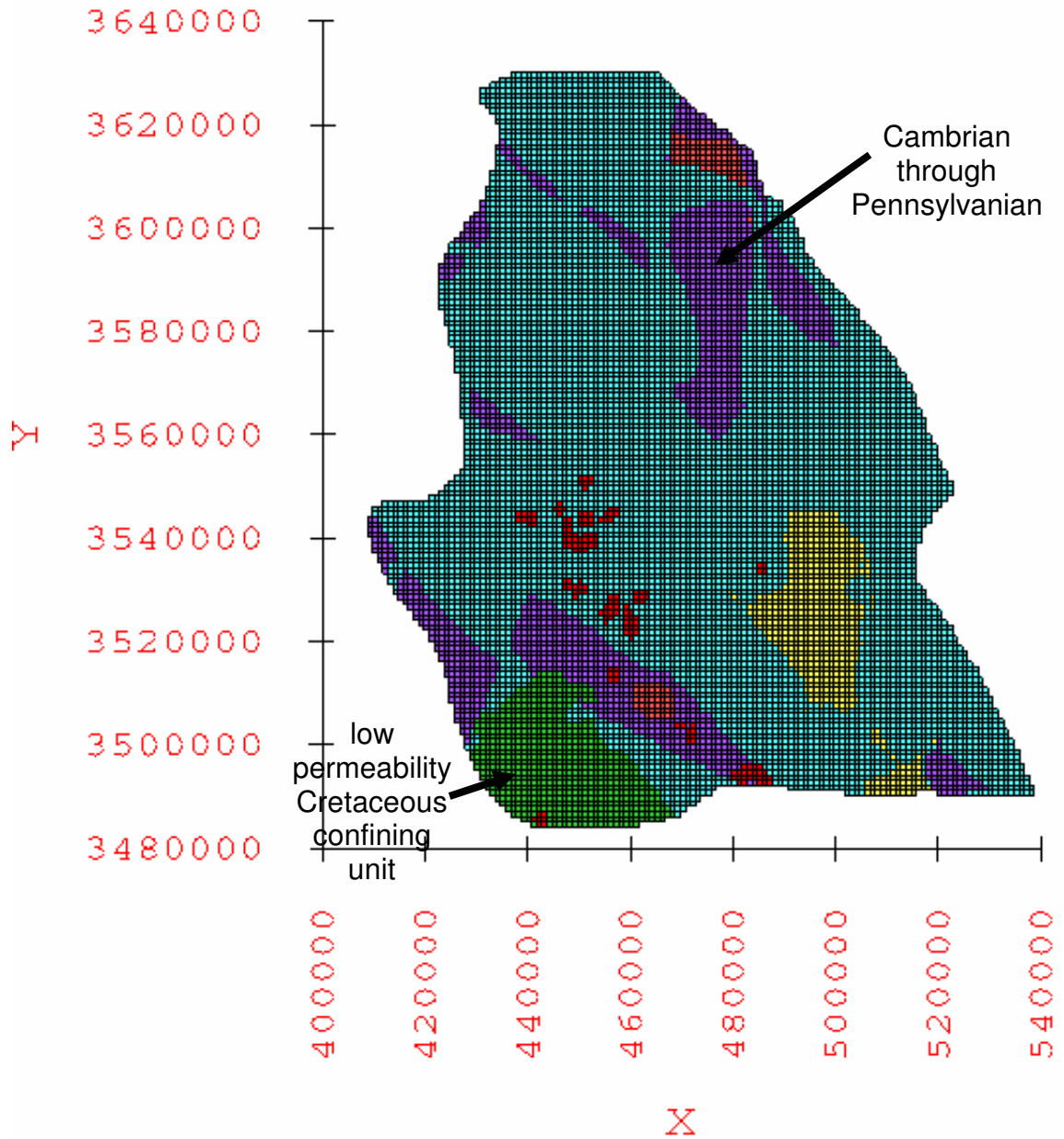
Figure 4.14: Distribution of hydrogeologic units within layer 2 of the groundwater flow model grid.
Axes scale is in UTM NAD83 Zone 13 North coordinates.
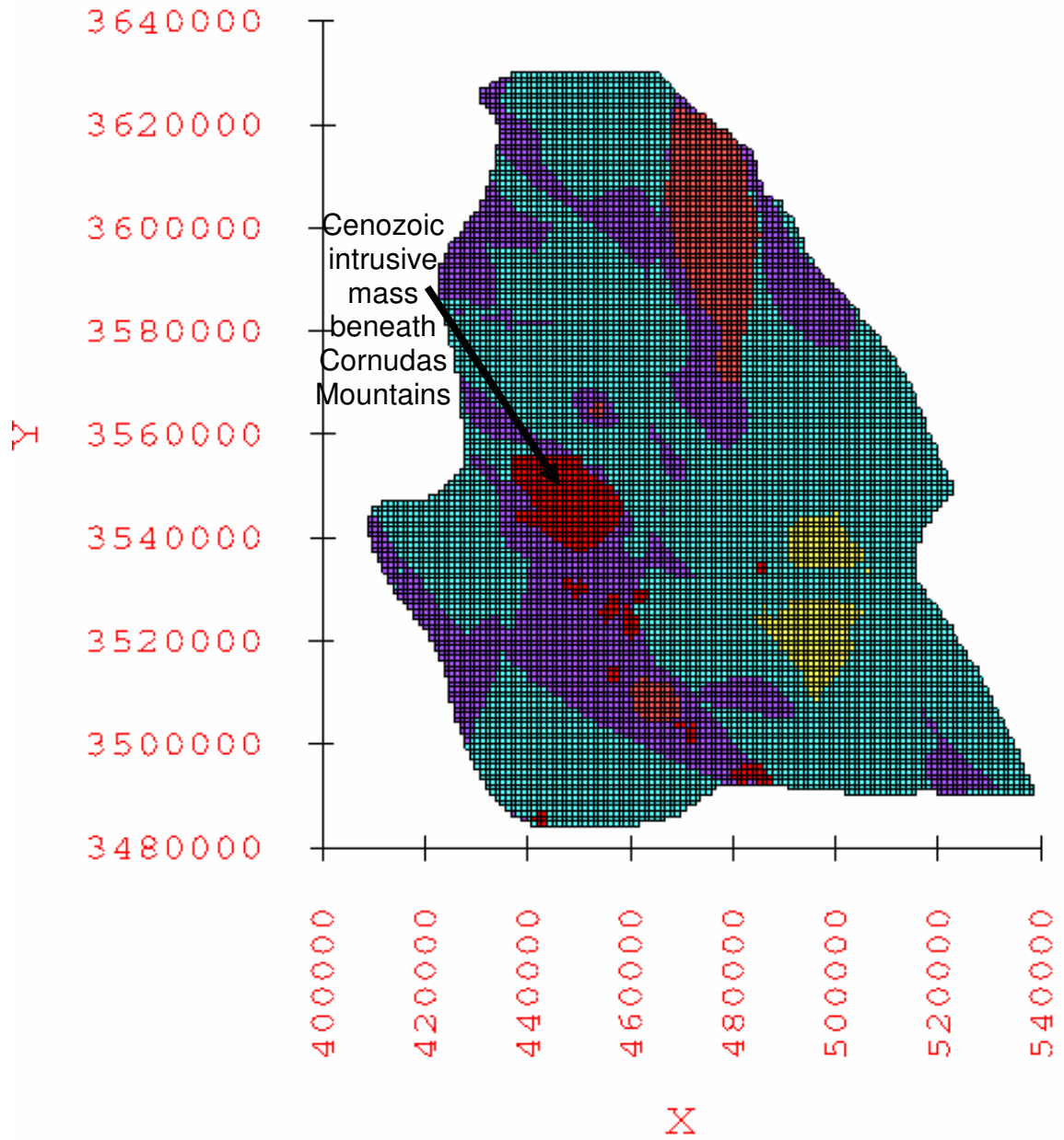
Figure 4.15: Distribution of hydrogeologic units within layer 3 of the groundwater flow model grid.
Axes scale is in UTM NAD83 Zone 13 North coordinates.
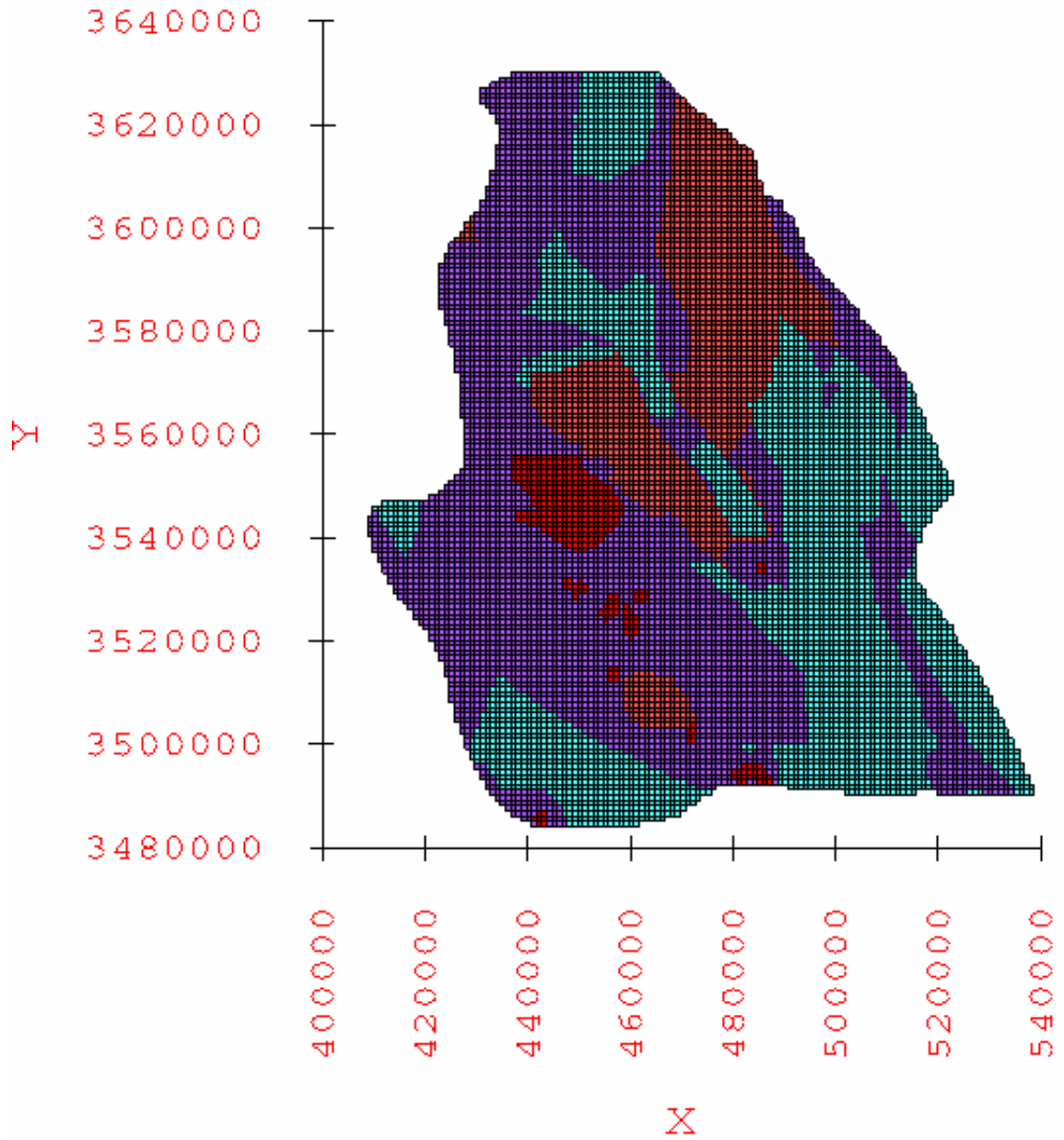
Figure 4.16: Distribution of hydrogeologic units within layer 4 of the groundwater flow
model grid.
Axes scale is in UTM NAD83 Zone 13 North coordinates.
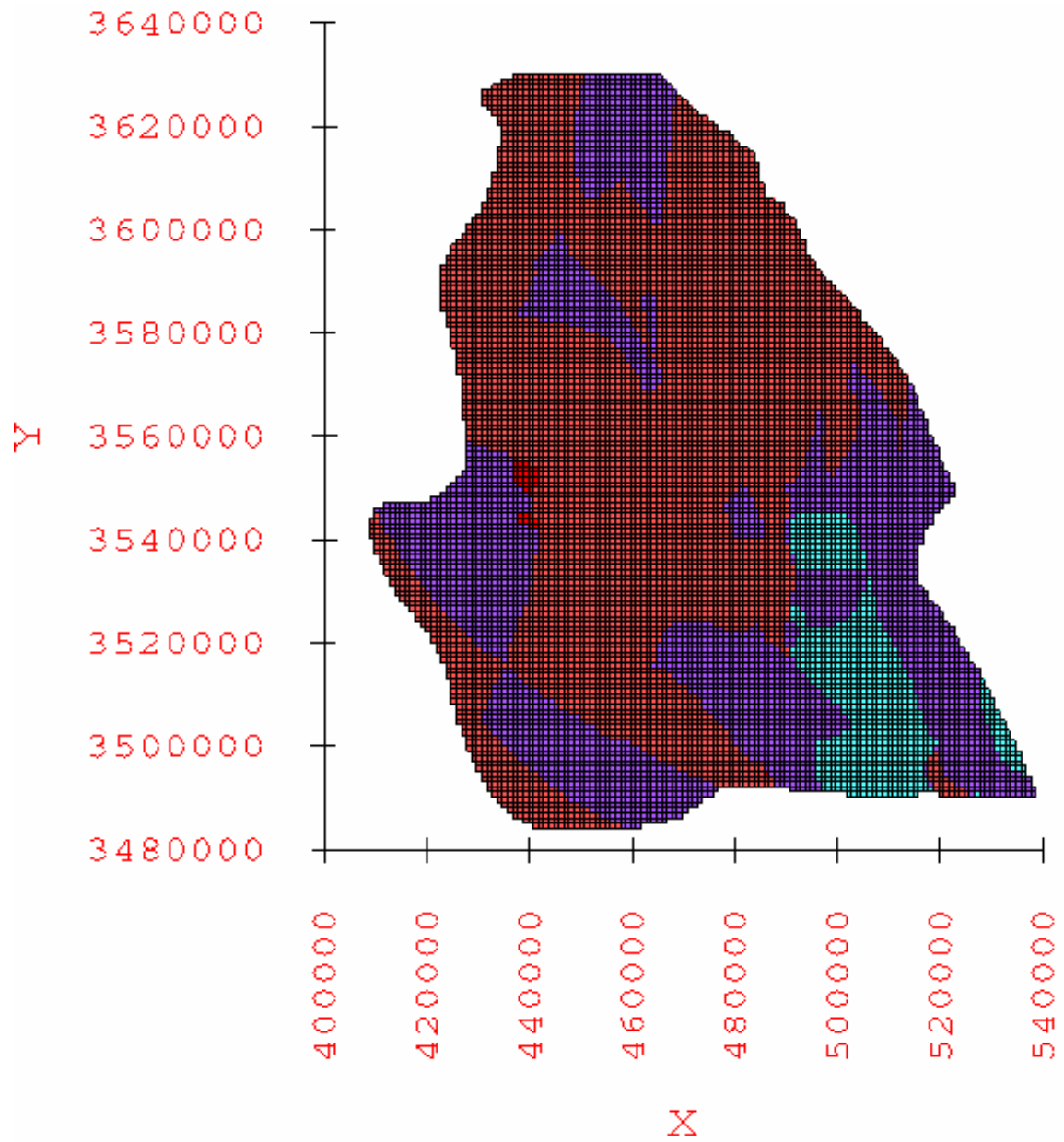
Figure 4.17: Distribution of hydrogeologic units within layer 5 of the groundwater flow model grid.
Axes scale is in UTM NAD83 Zone 13 North coordinates.
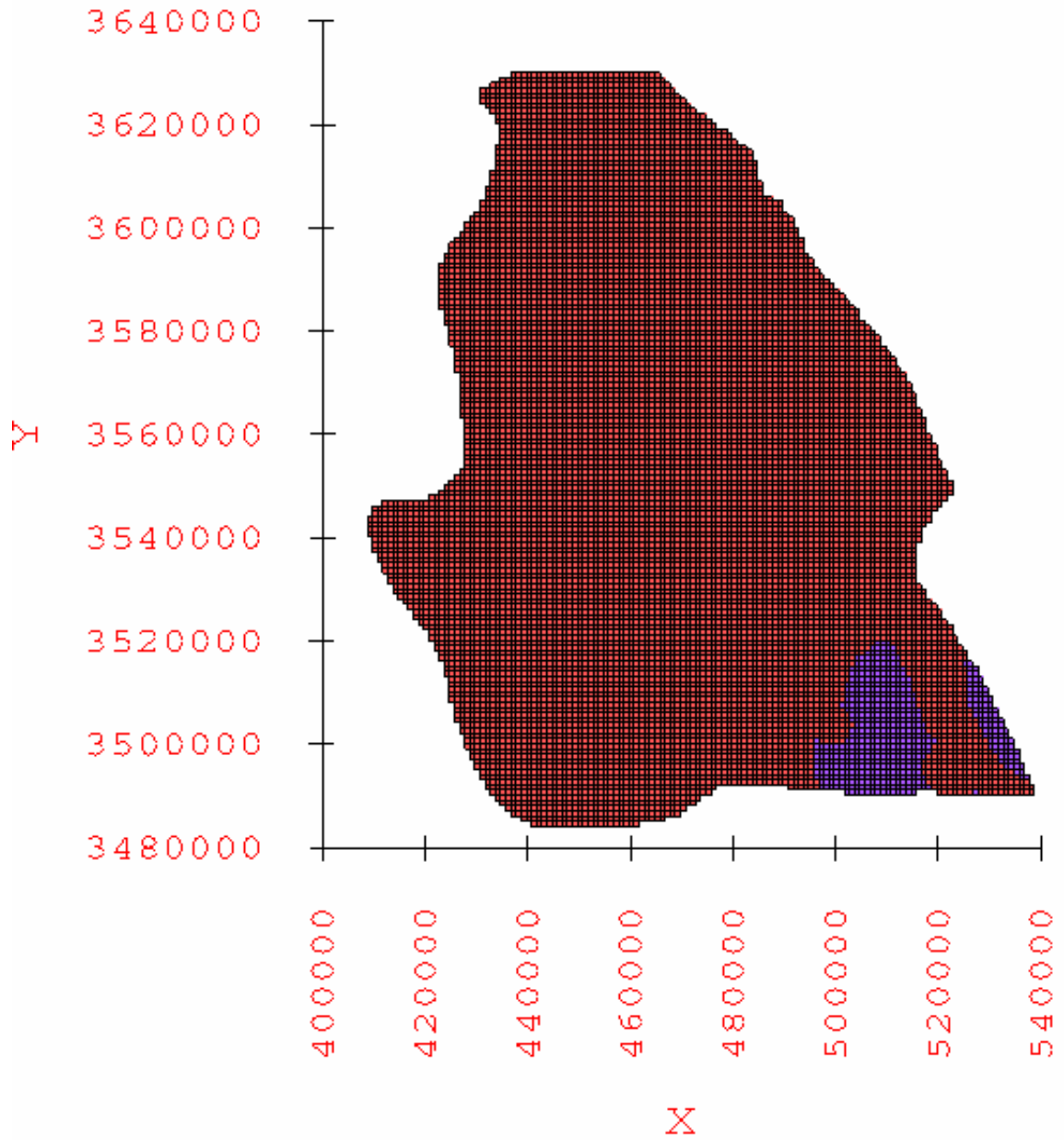
Figure 4.18: Distribution of hydrogeologic units within layer 6 of the groundwater flow model grid.
Axes scale is in UTM NAD83 Zone 13 North coordinates.
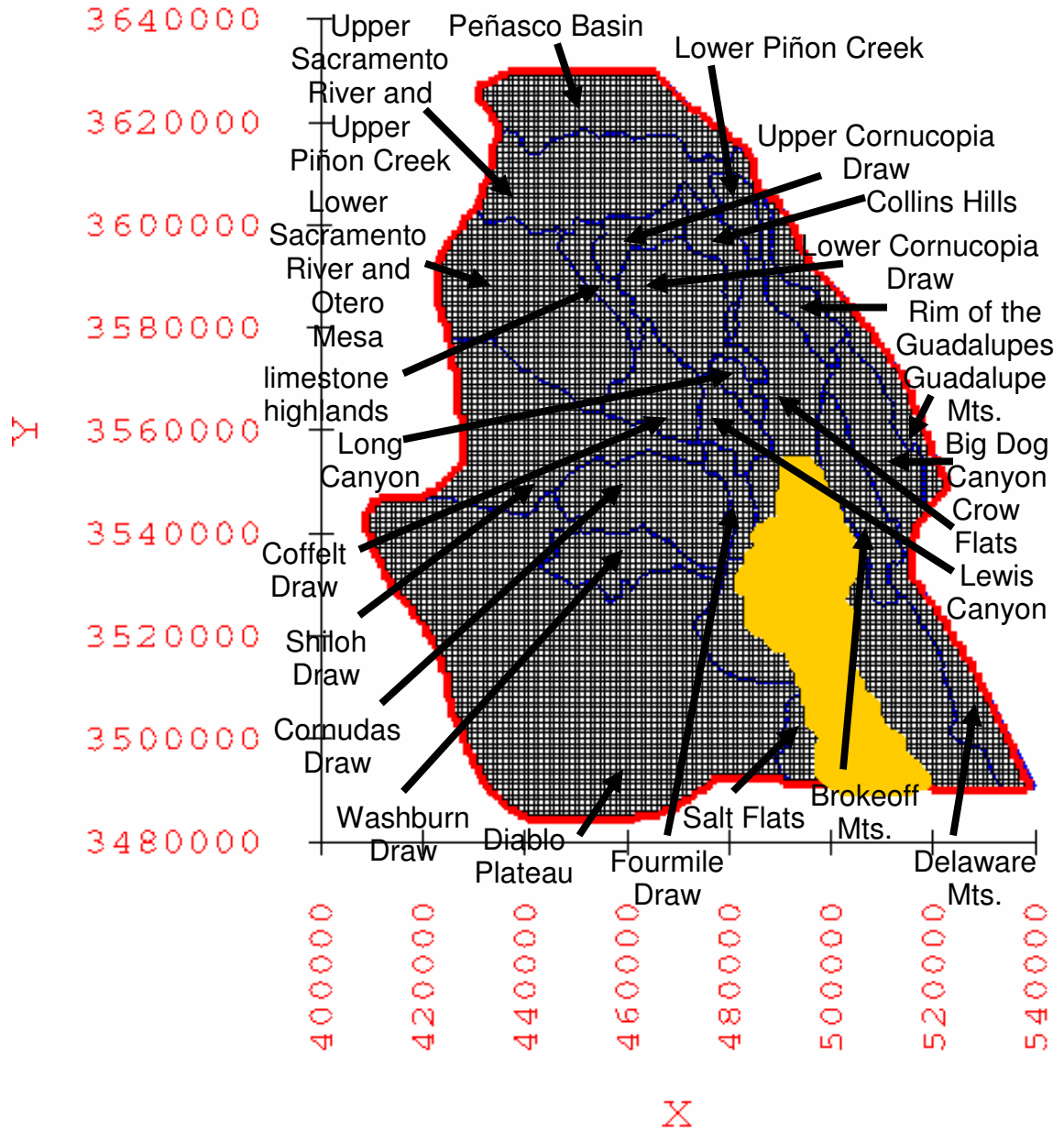
Figure 4.19: Groundwater flow model domain, plan view of model grid, recharge zones derived from sub-basins delineated by JSAI (2010), and discharge zone at Salt Flats playa.

Axes scale is in UTM NAD83 Zone 13 North coordinates. Red line along perimeter of model domain designates no-flow boundary. Areas enclosed by blue lines indicate recharge zones. Grid cells highlighted with yellow specify discharge zone.
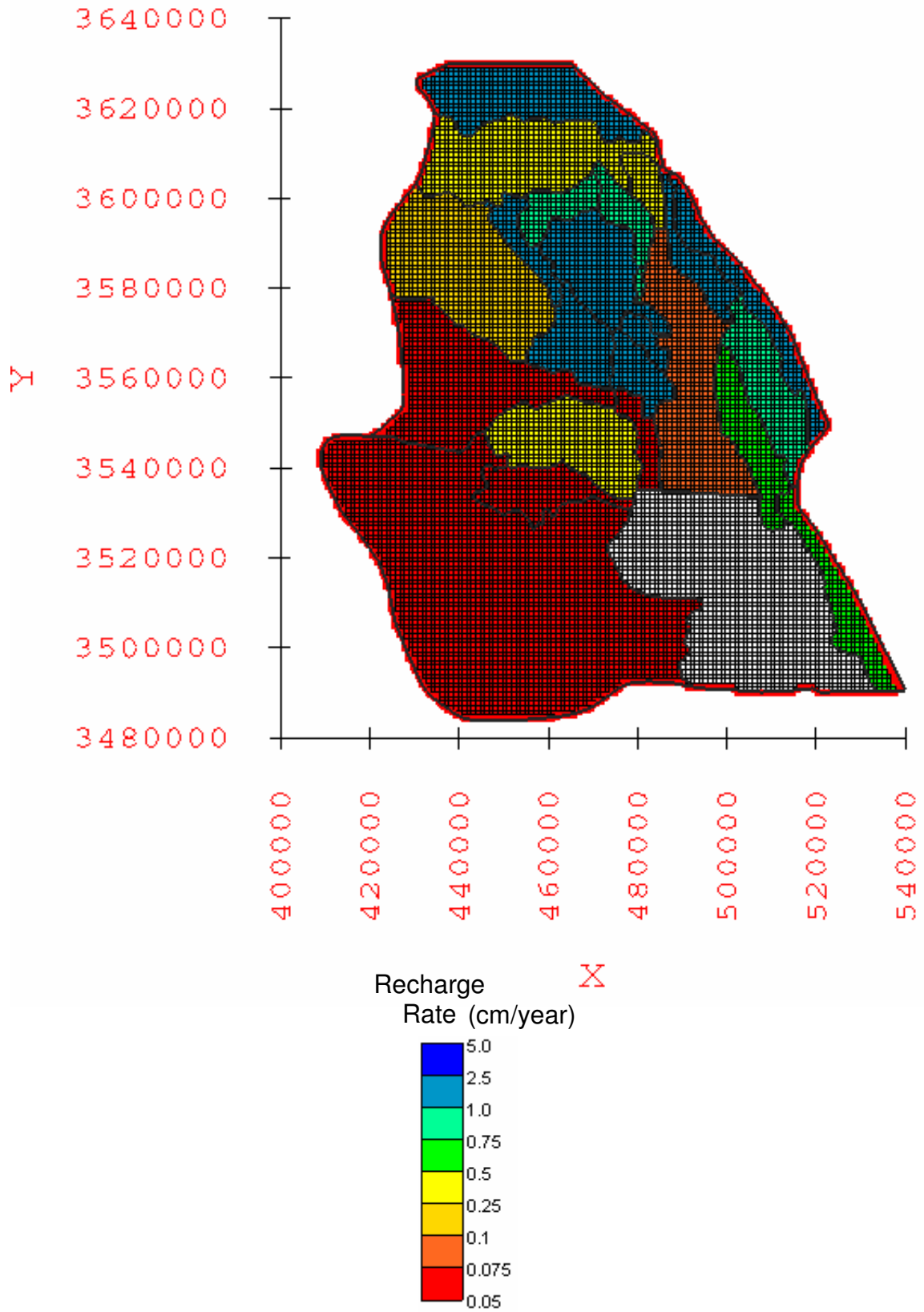
Figure 4.20: Water-balance based minimum recharge rates applied to the sub-basins within the groundwater flow model domain.
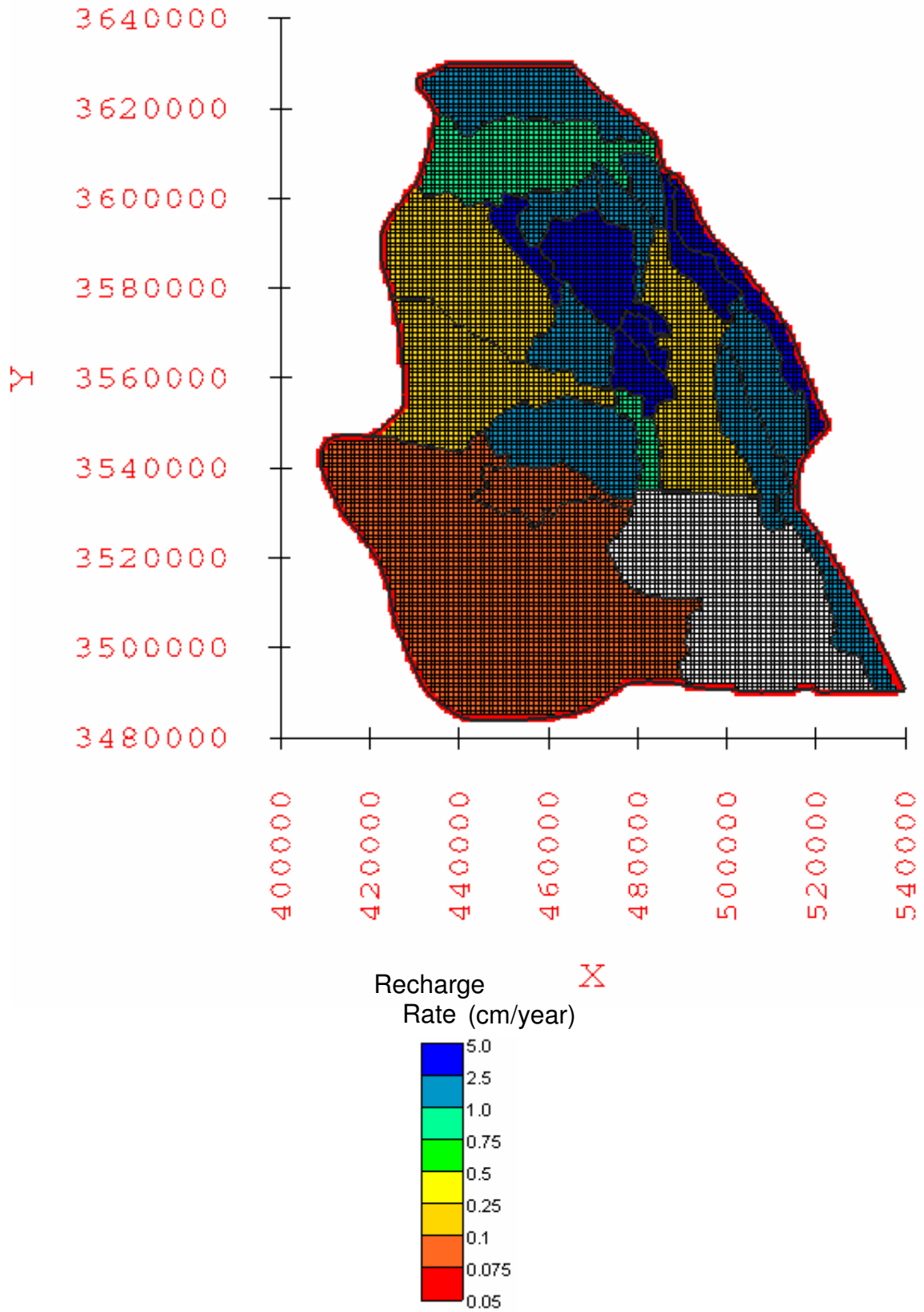
Figure 4.21: Water-balance based average recharge rates applied to the sub-basins within the groundwater flow model domain.
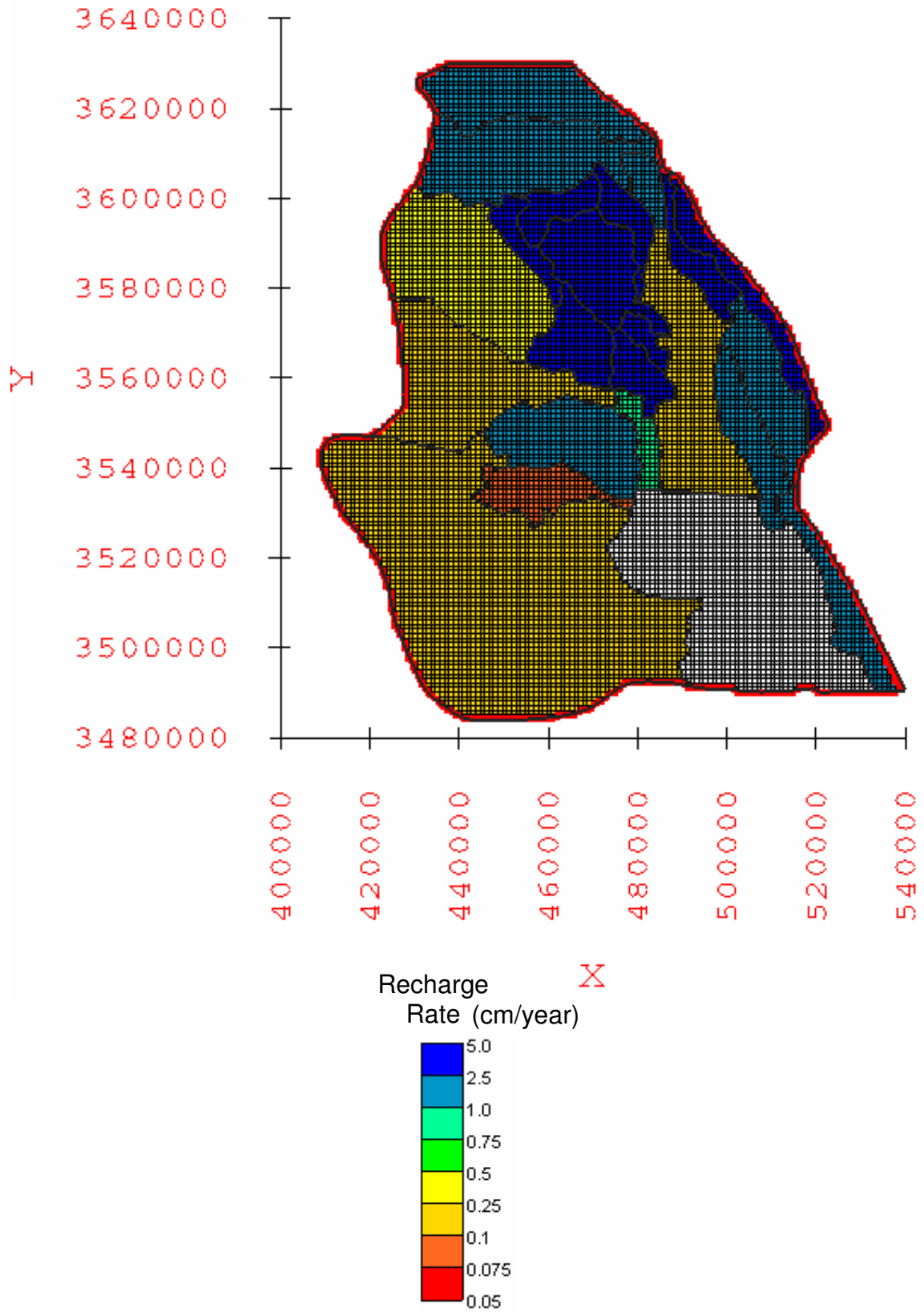
Figure 4.22: Water-balance based maximum recharge rates applied to the sub-basins within the groundwater flow model domain.
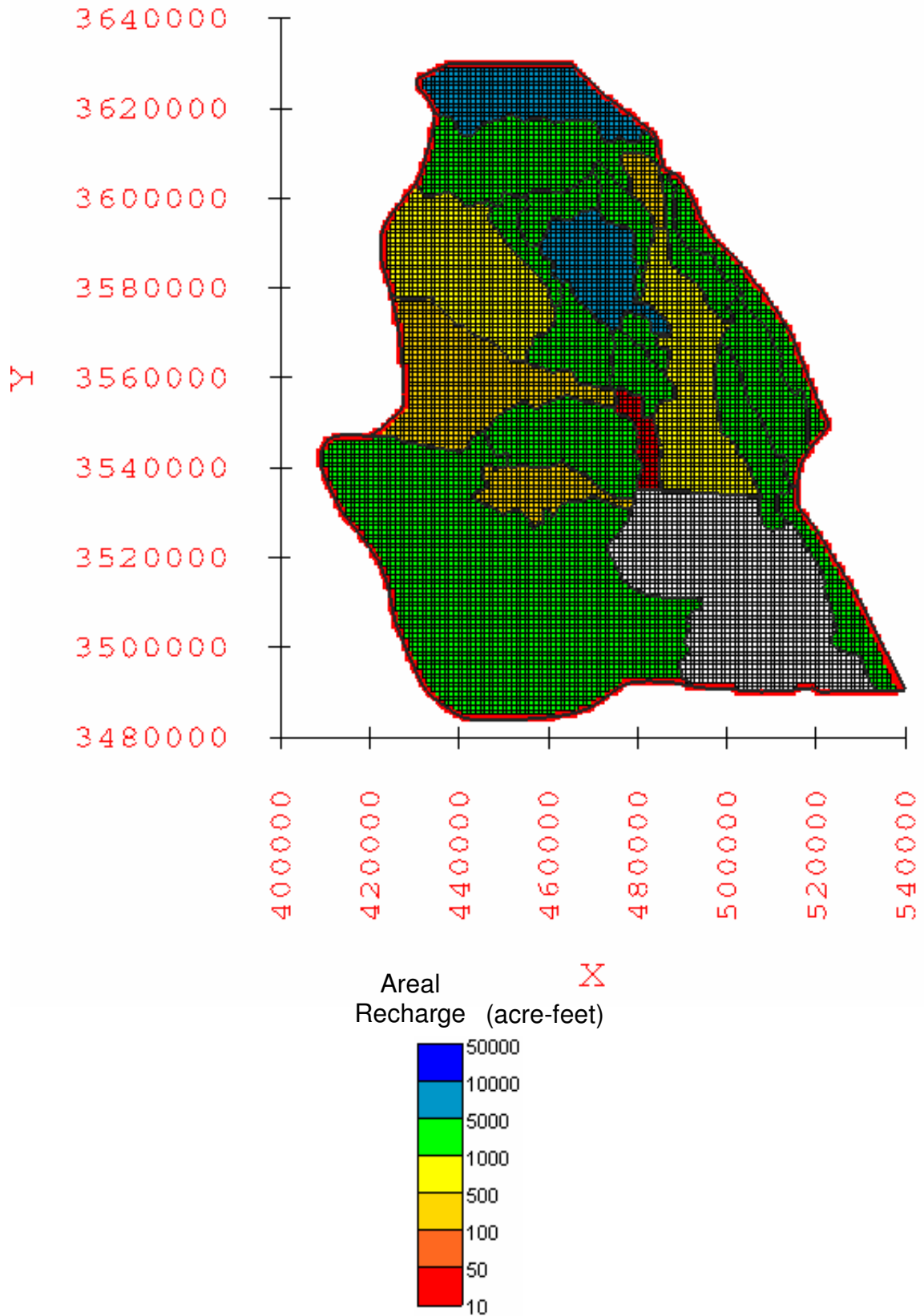
Figure 4.23: Water-balance based minimum areal recharge applied to the sub-basins within the groundwater flow model domain.
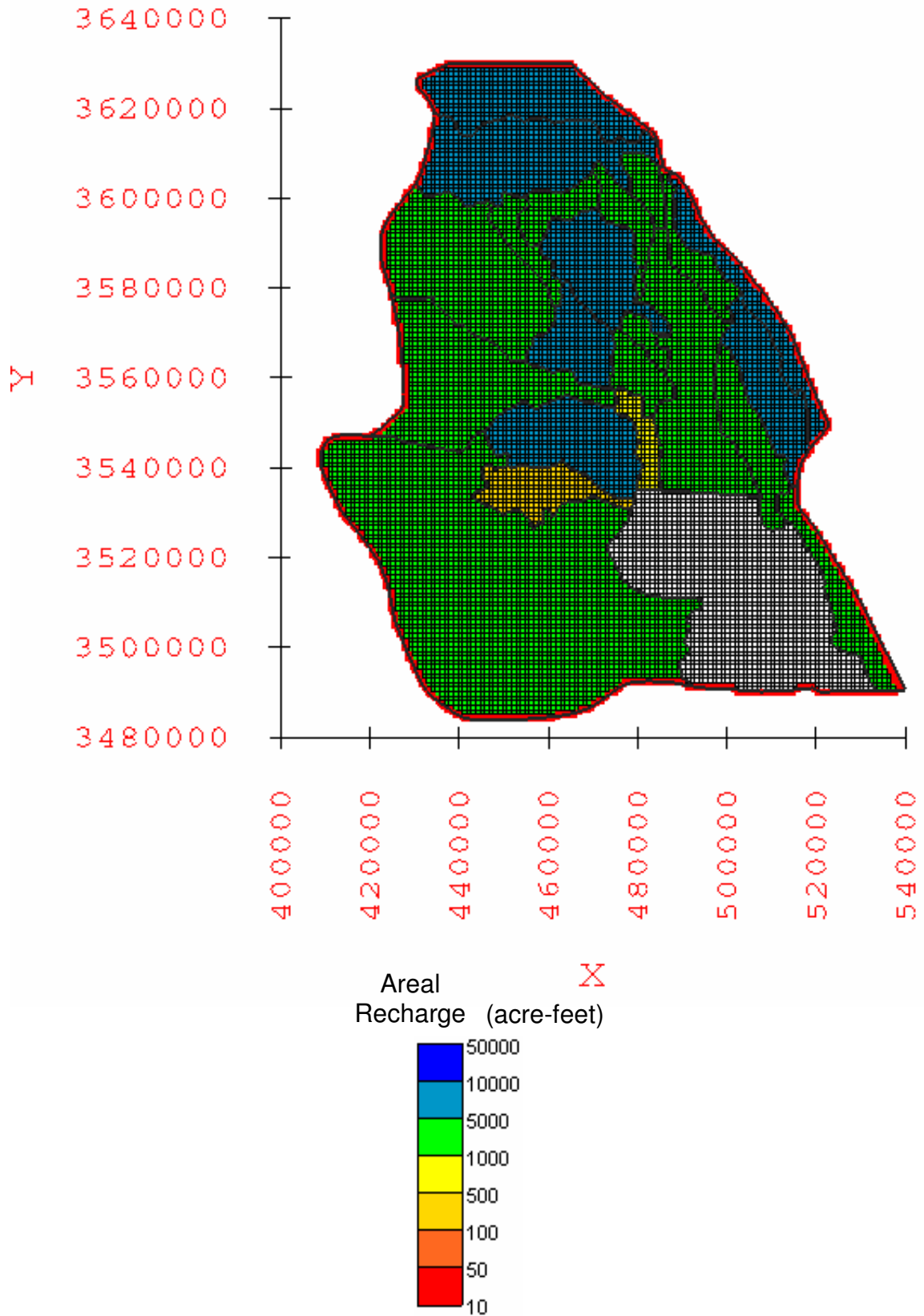
Figure 4.24: Water-balance based average areal recharge applied to the sub-basins within the groundwater flow model domain.
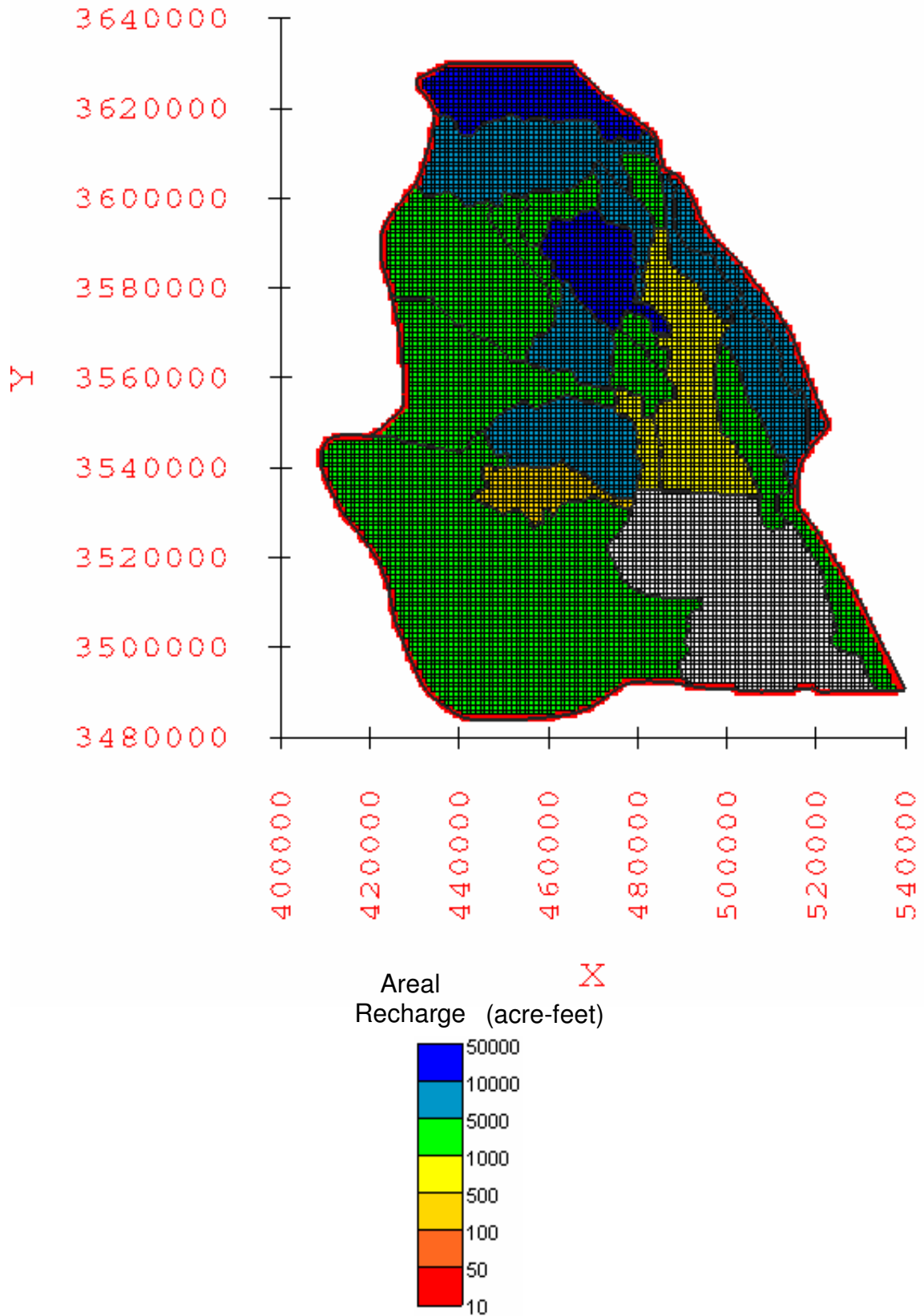
Figure 4.25: Water-balance based maximum areal recharge applied to the sub-basins within the groundwater flow model domain.
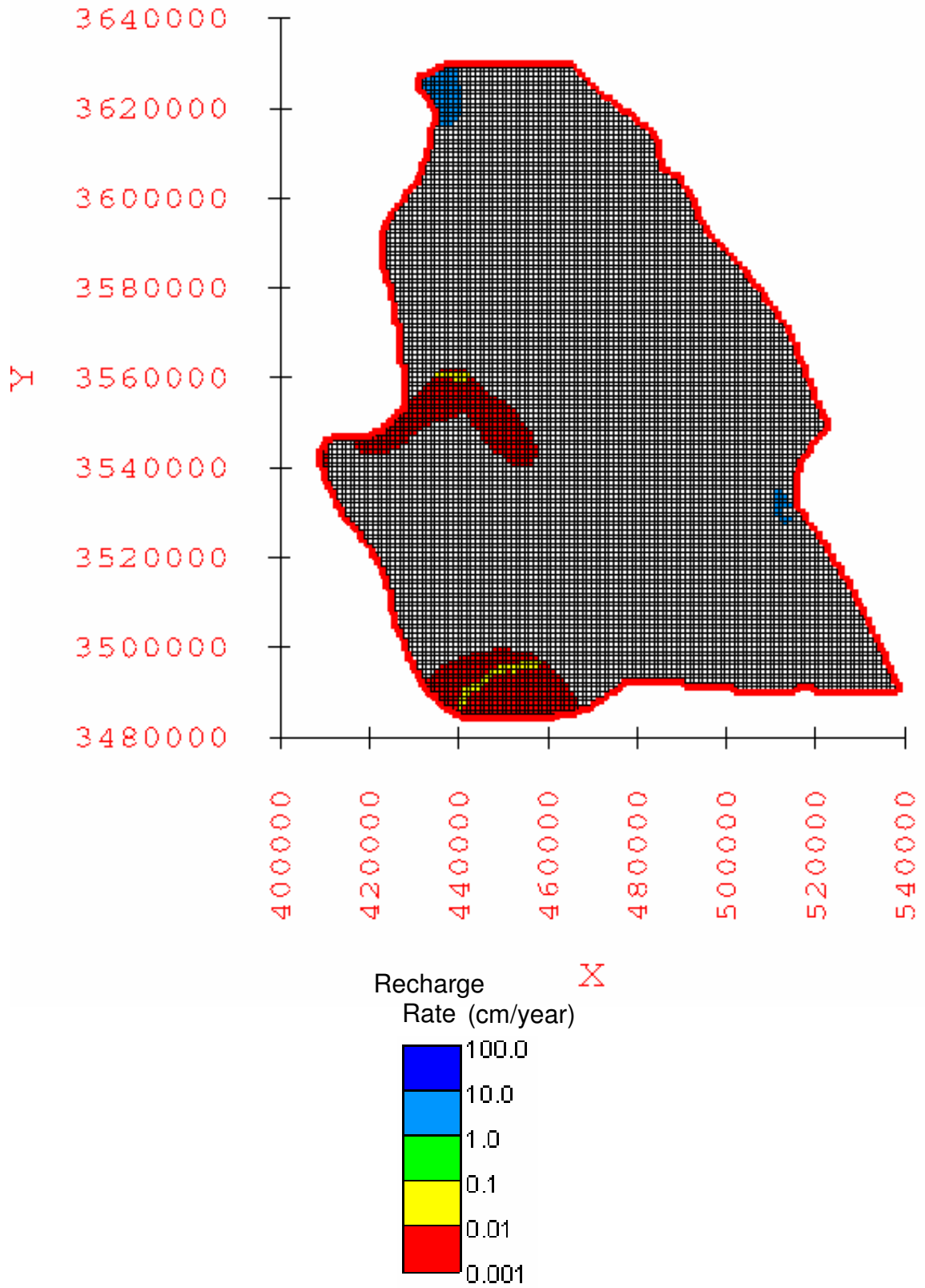
Figure 4.26: Elevation-dependent minimum recharge rates applied to the recharge zones within the groundwater flow model domain.
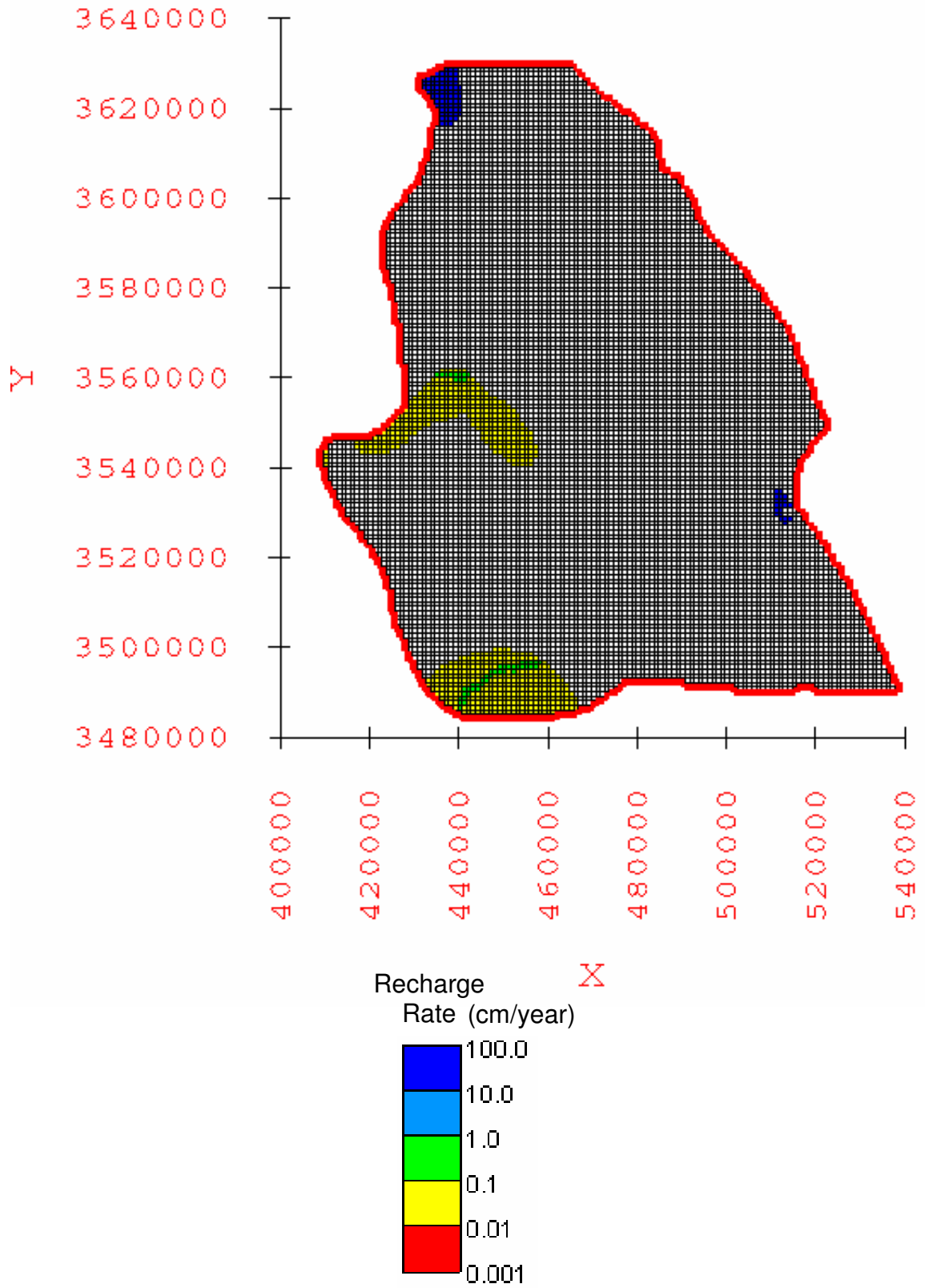
Figure 4.27: Elevation-dependent average recharge rates applied to the recharge zones within the groundwater flow model domain.
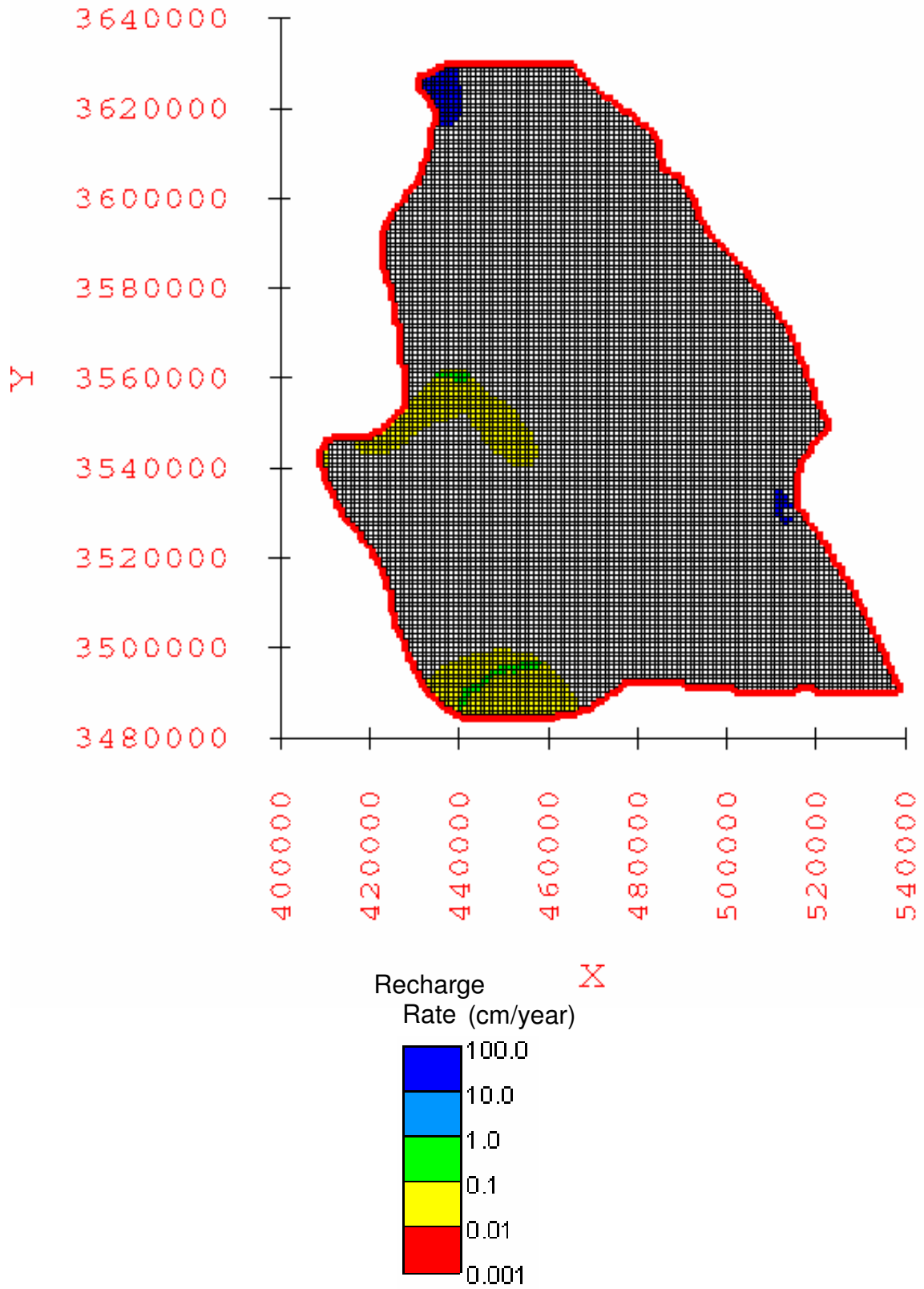
Figure 4.28: Elevation-dependent maximum recharge rates applied to the recharge zones within the groundwater flow model domain.
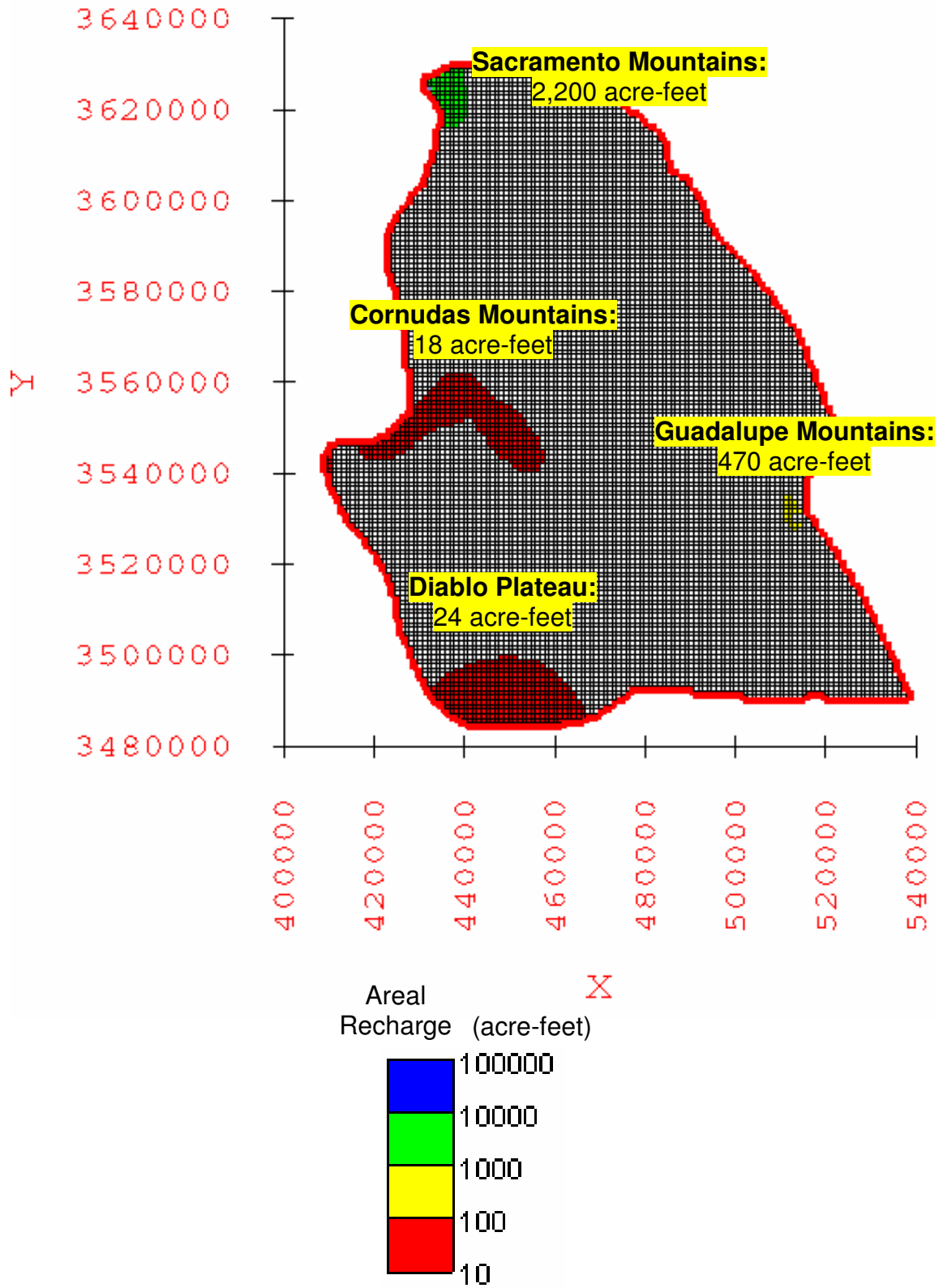
Figure 4.29: Elevation-dependent minimum areal recharge applied to the recharge zones within the groundwater flow model domain.
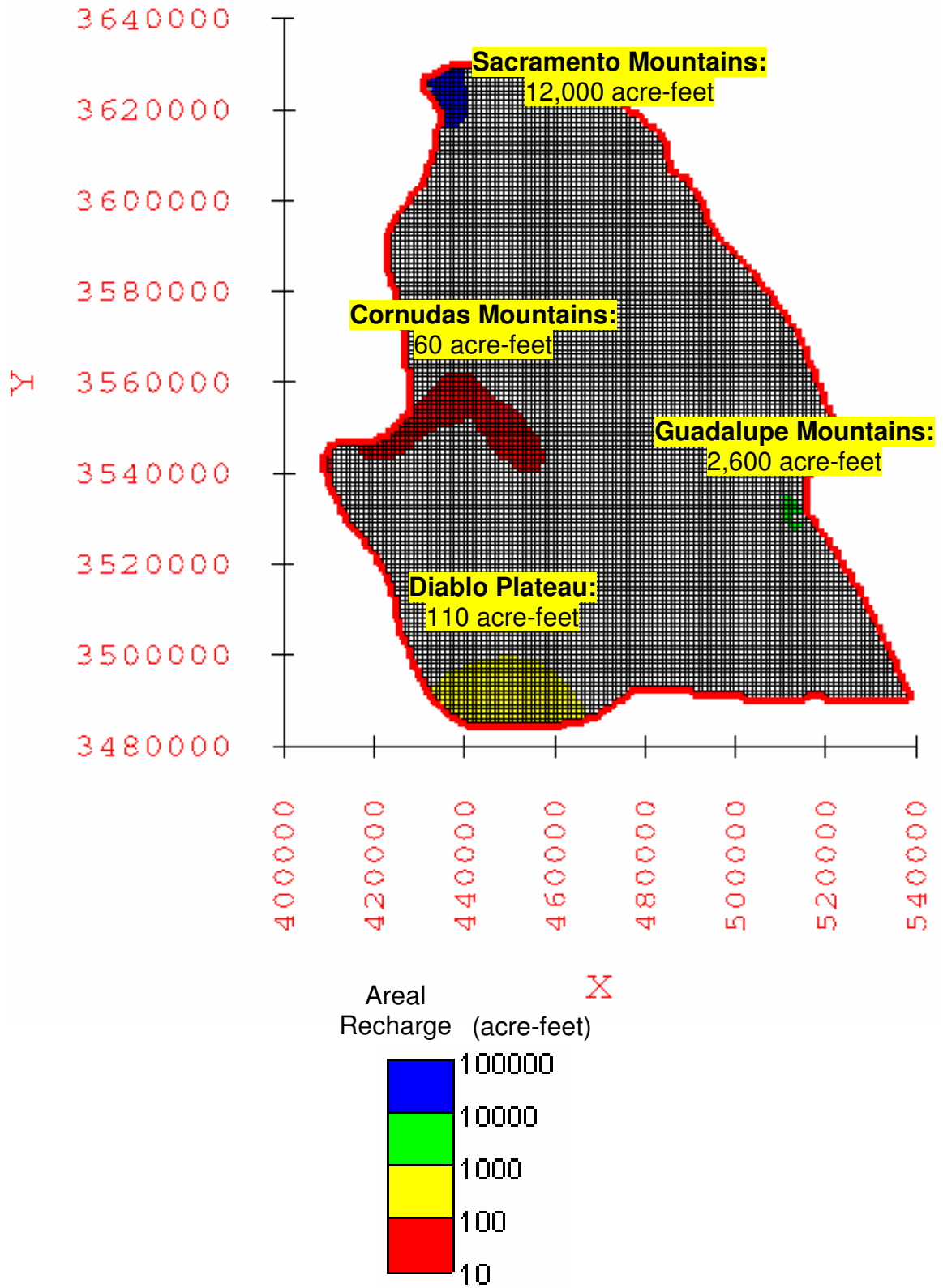
Figure 4.30: Elevation-dependent average areal recharge applied to the recharge zones within the groundwater flow model domain.
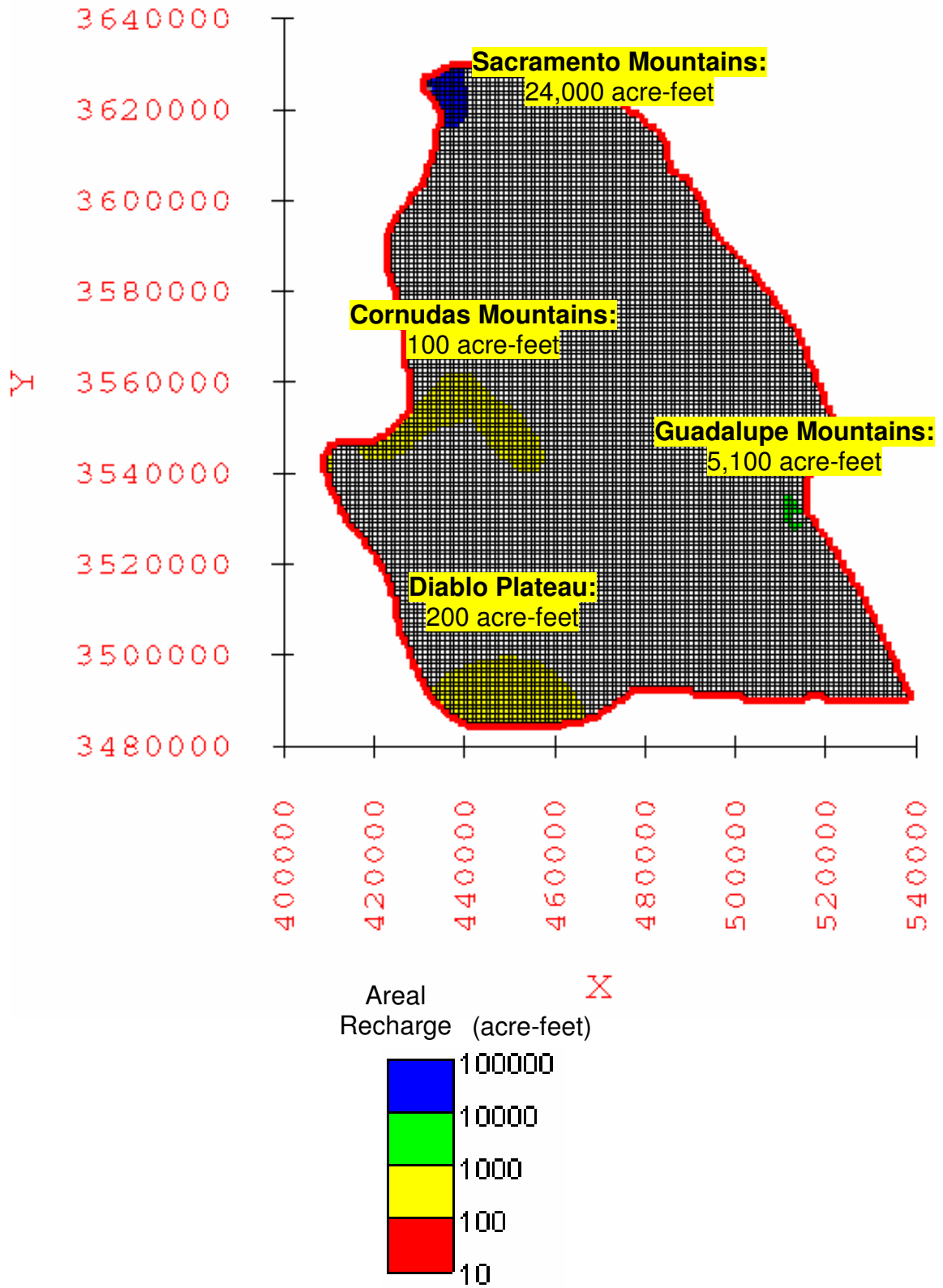
Figure 4.31: Elevation-dependent maximum areal recharge applied to the recharge zones within the groundwater flow model domain.
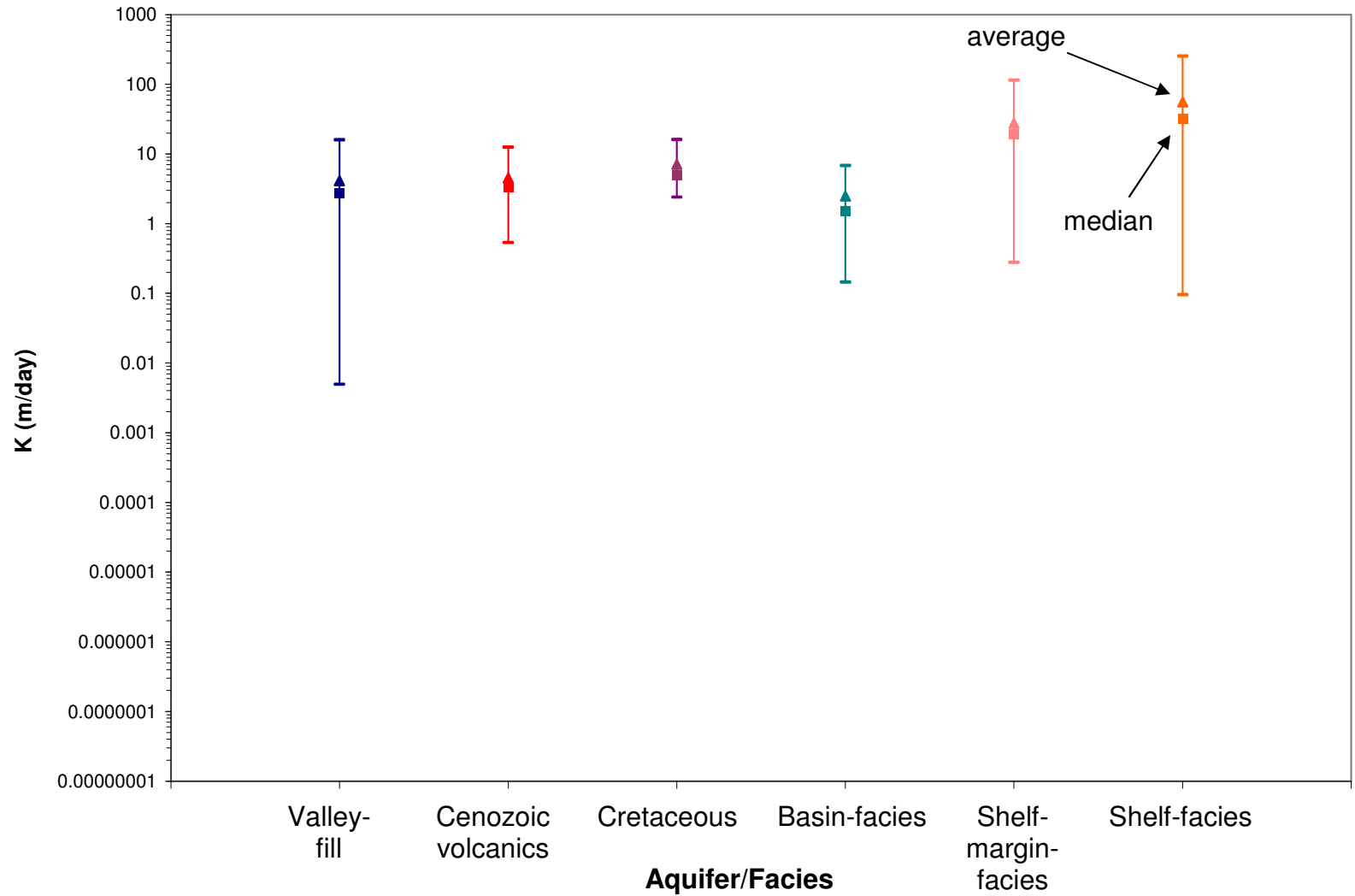
Figure 4.32: Range of hydraulic conductivity [K] values calculated from transmissivity [T].
Vertical axis is logarithmic scale. Squares indicate median values, and triangles indicate average values.
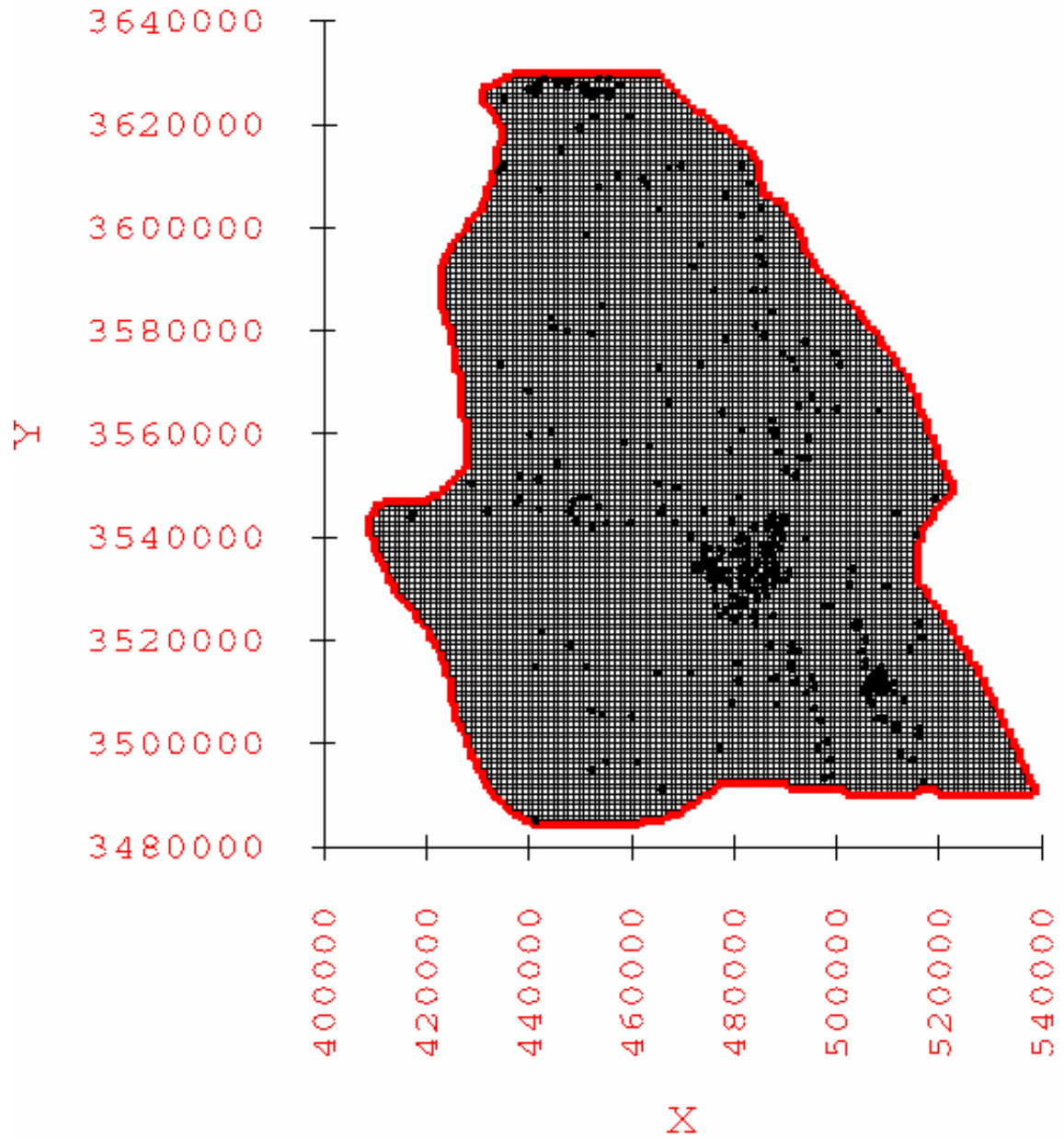
Figure 4.33: Calibration targets within the groundwater flow model domain. Axes scale is in UTM NAD83 Zone 13 North coordinates.
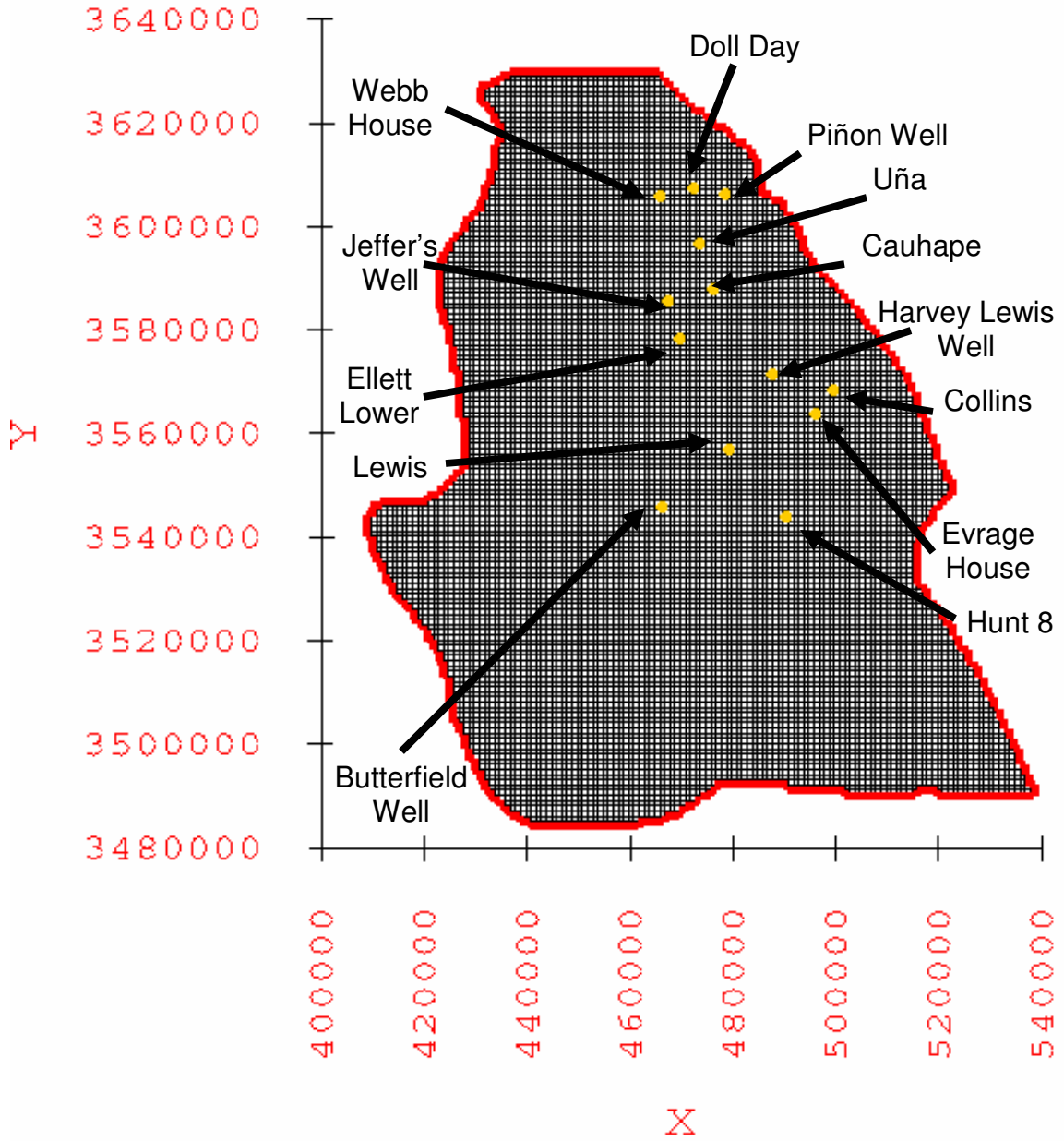
Figure 4.34: Location of the groundwater age wells within the MODFLOW model domain.
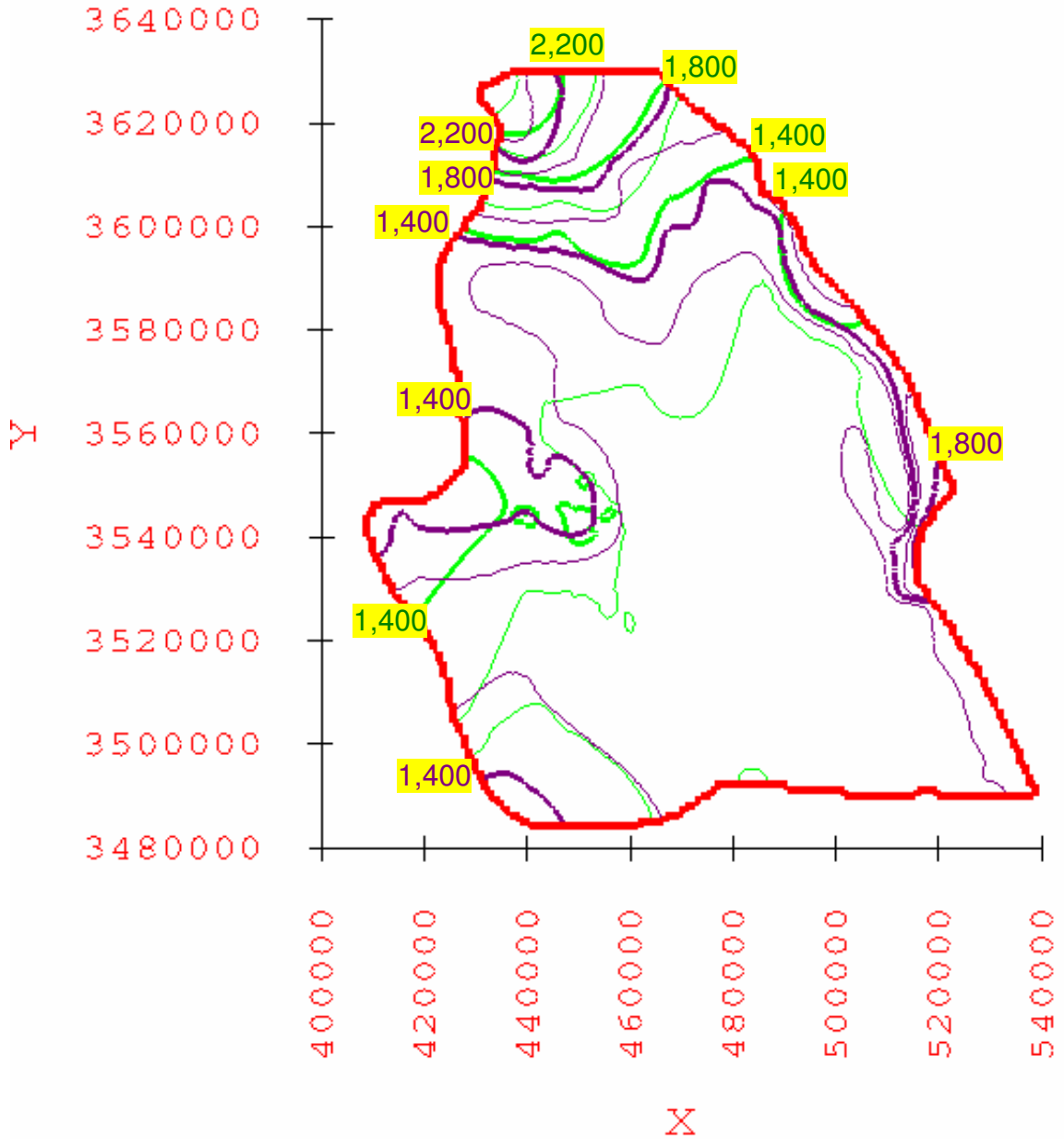
Figure 4.35: Comparison of the computed hydraulic head in layer 1 for the calibrated water-balance based minimum recharge scenario model and the observed groundwater surface.

Green lines are the model computed head contours. Purple dashed lines are the observed groundwater surface contours. Contour elevations are in meters above mean sea level. Contour interval is 200 meters.
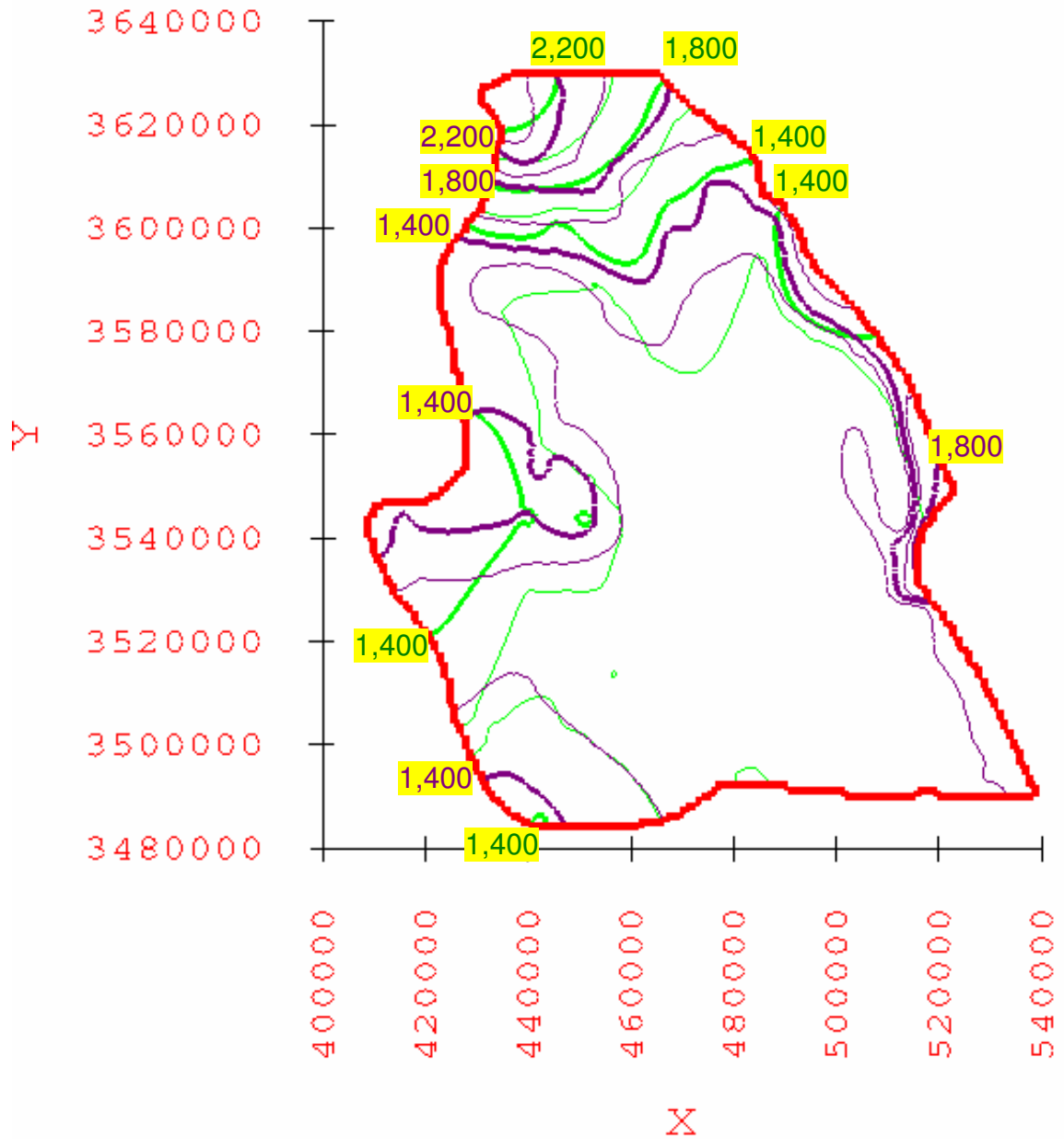
Figure 4.36: Comparison of the computed hydraulic head in layer 1 for the calibrated
water-balance based average recharge scenario model and the observed groundwater
surface.
Green lines are the model computed head contours. Purple dashed lines are the observed
groundwater surface contours. Contour elevations are in meters above mean sea level.
Contour interval is 200 meters.
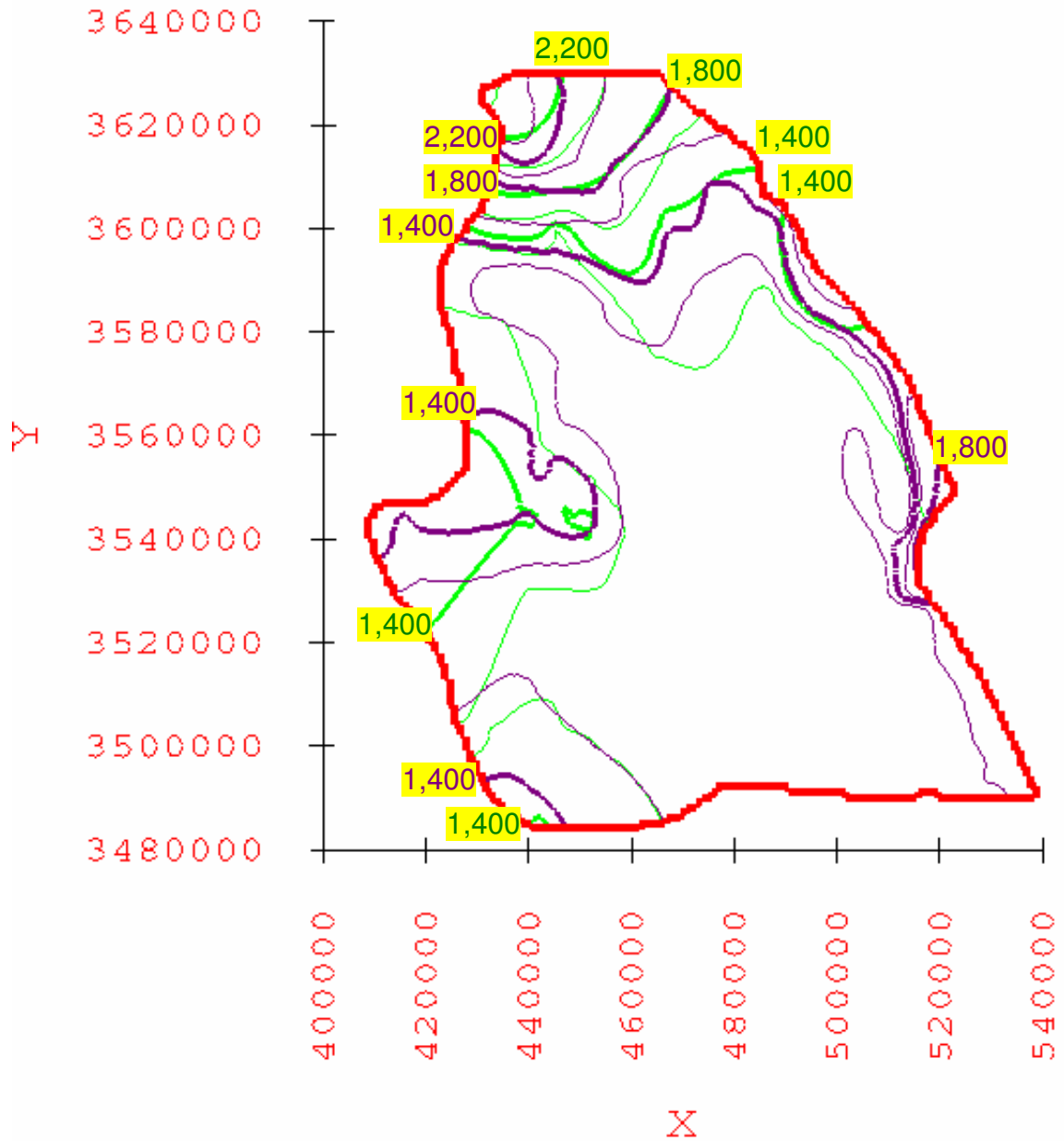
Figure 4.37: Comparison of the computed hydraulic head in layer 1 for the calibrated water-balance based maximum recharge scenario model and the observed groundwater surface.

Green lines are the model computed head contours. Purple dashed lines are the observed groundwater surface contours. Contour elevations are in meters above mean sea level. Contour interval is 200 meters.
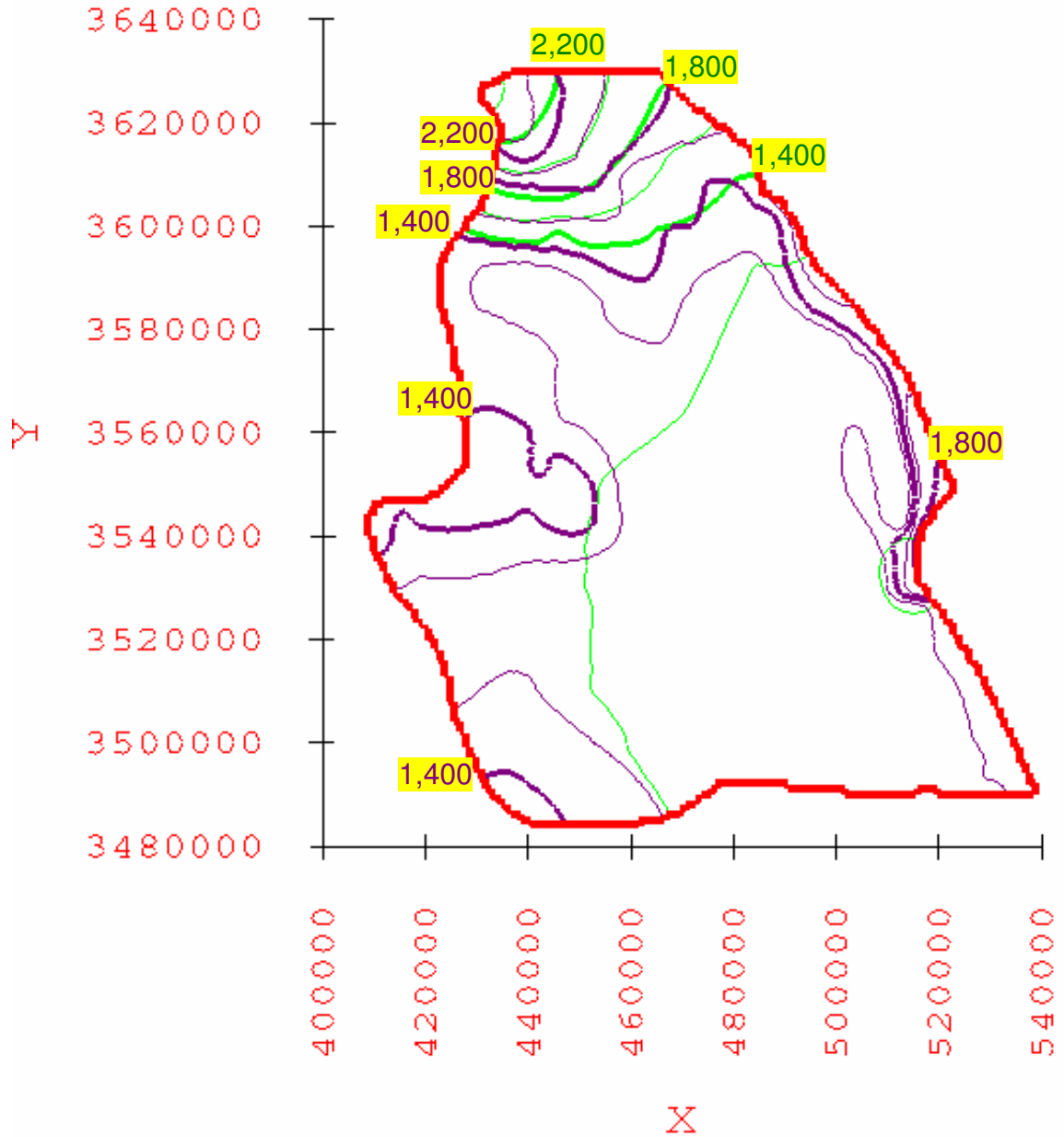
Figure 4.38: Comparison of the computed hydraulic head in layer 1 for the calibrated elevation-dependent minimum recharge scenario model and the observed groundwater surface.

Green lines are the model computed head contours. Purple dashed lines are the observed groundwater surface contours. Contour elevations are in meters above mean sea level. Contour interval is 200 meters.
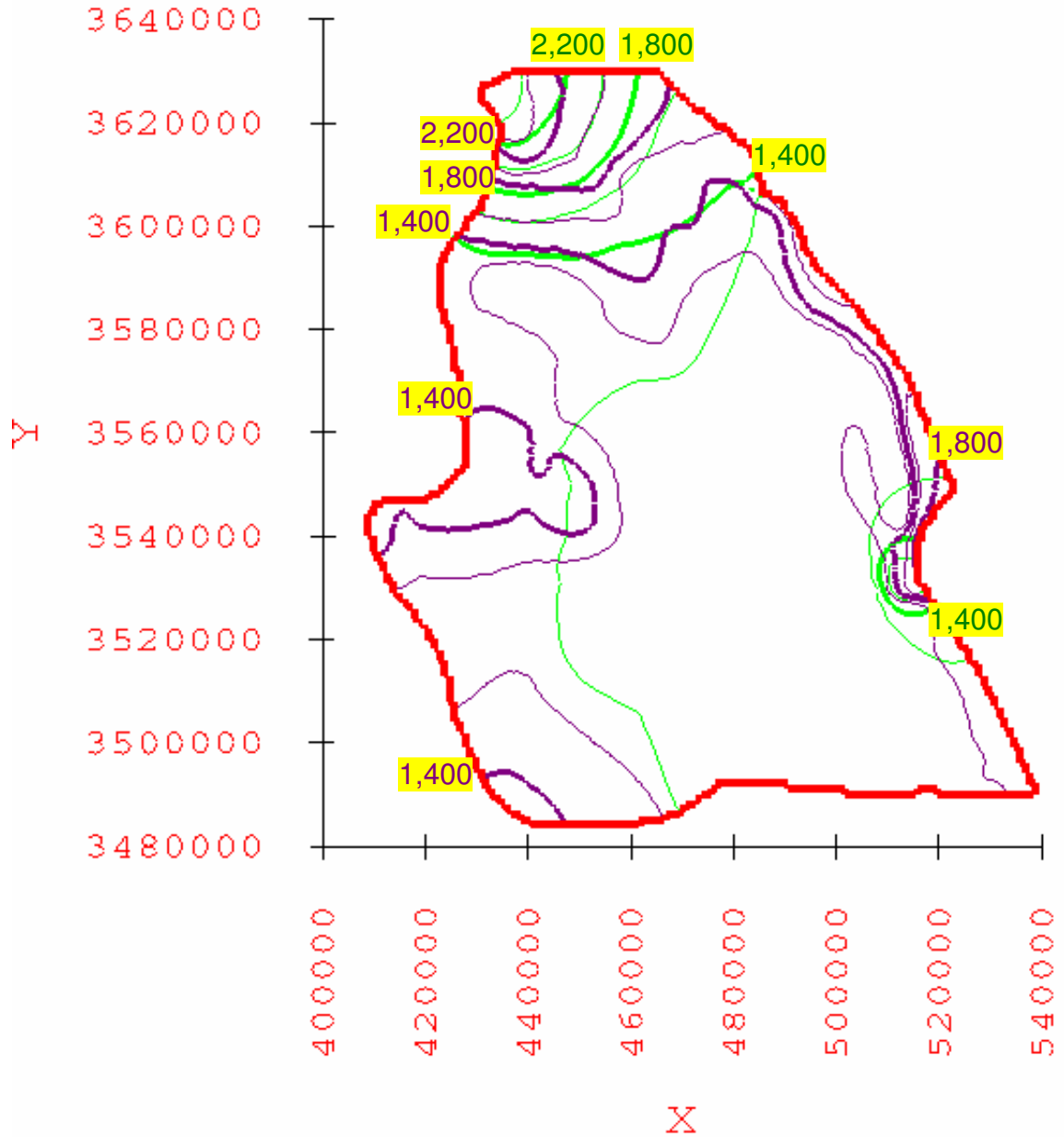
Figure 4.39: Comparison of the computed hydraulic head in layer 1 for the calibrated elevation-dependent average recharge scenario model and the observed groundwater surface.

Green lines are the model computed head contours. Purple dashed lines are the observed groundwater surface contours. Contour elevations are in meters above mean sea level. Contour interval is 200 meters.
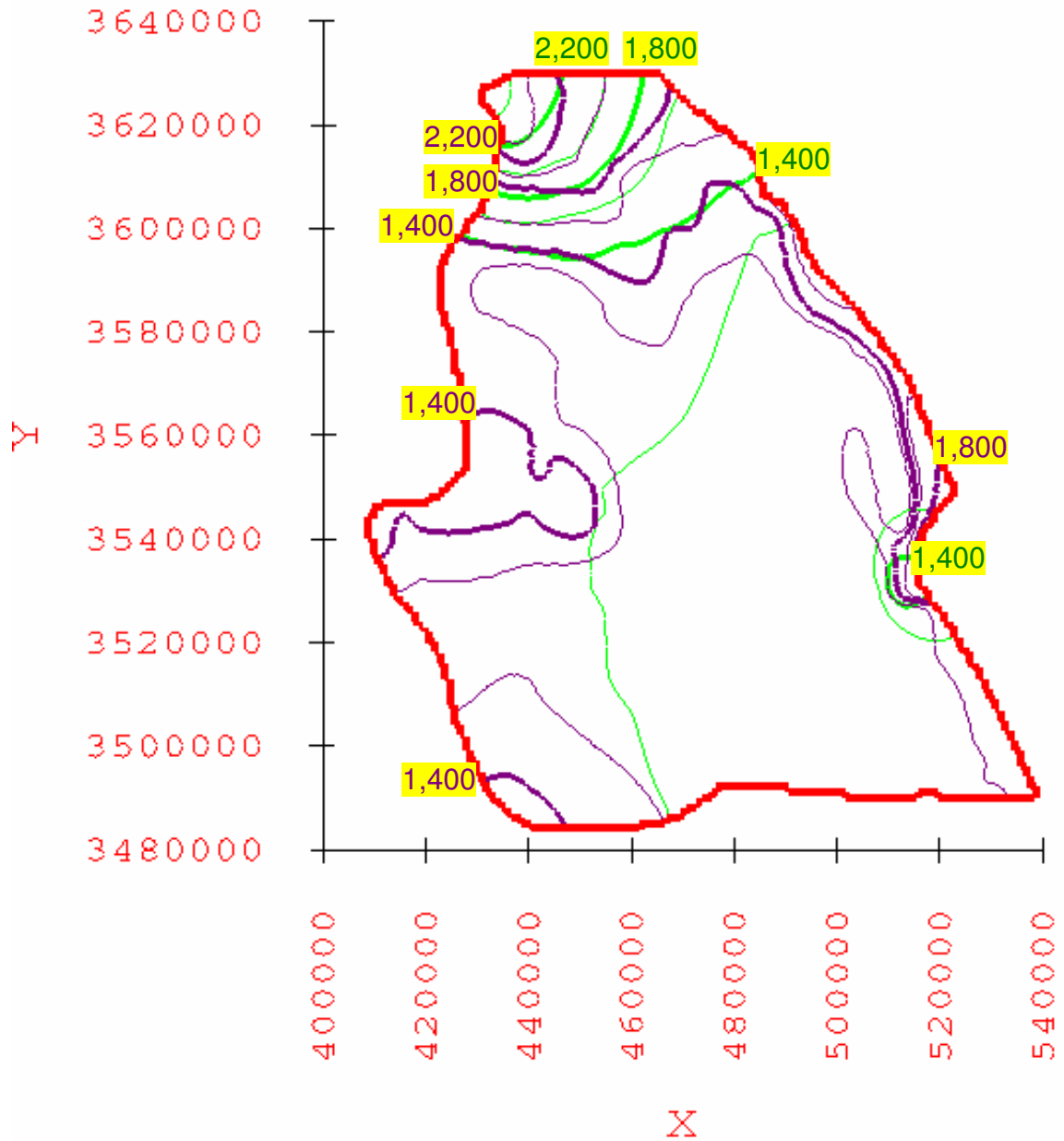
Figure 4.40: Comparison of the computed hydraulic head in layer 1 for the calibrated elevation-dependent maximum recharge scenario model and the observed groundwater surface.

Green lines are the model computed head contours. Purple dashed lines are the observed groundwater surface contours. Contour elevations are in meters above mean sea level. Contour interval is 200 meters.
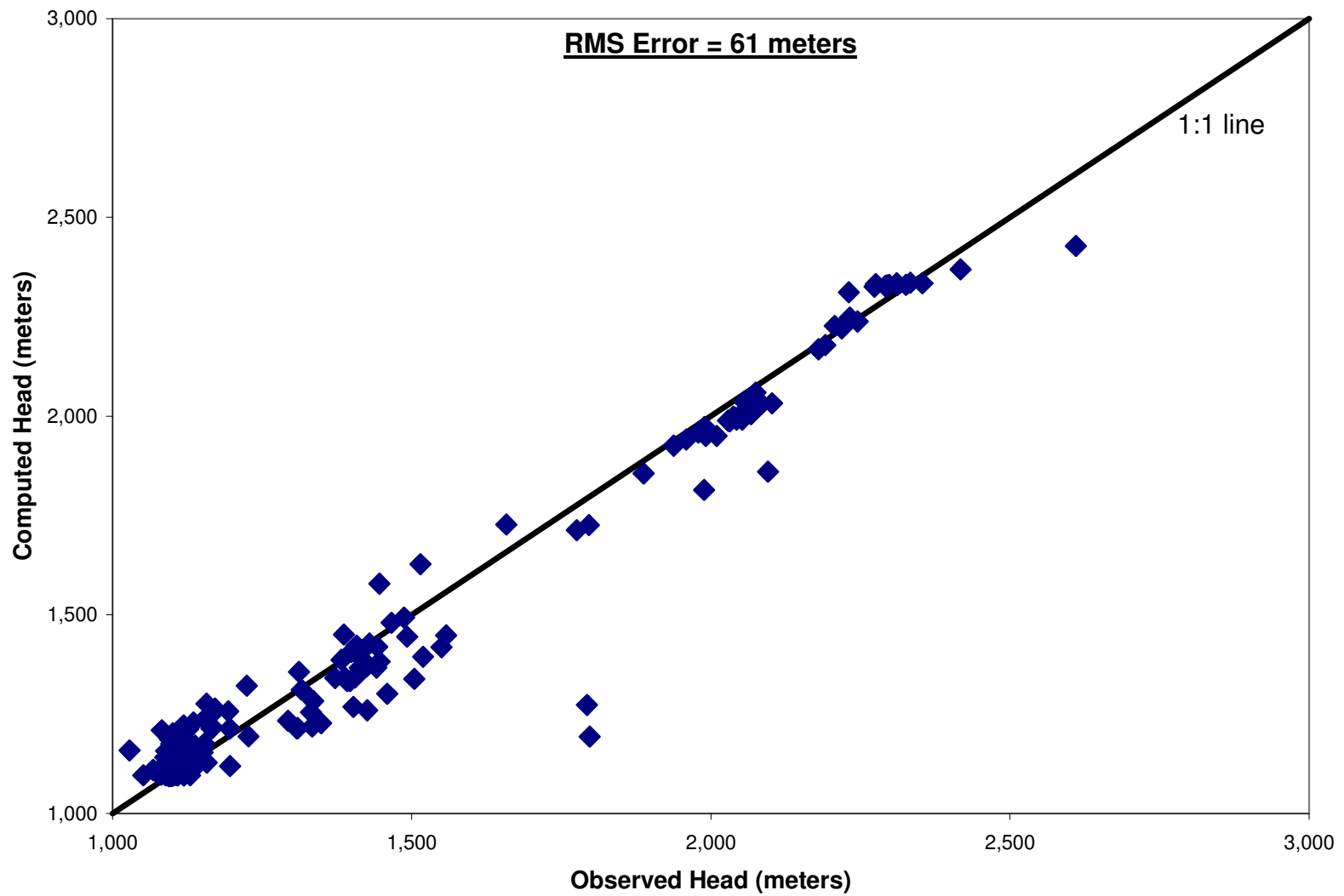
Figure 4.41: Computed versus observed hydraulic head for the calibrated water-balance based minimum recharge scenario model.
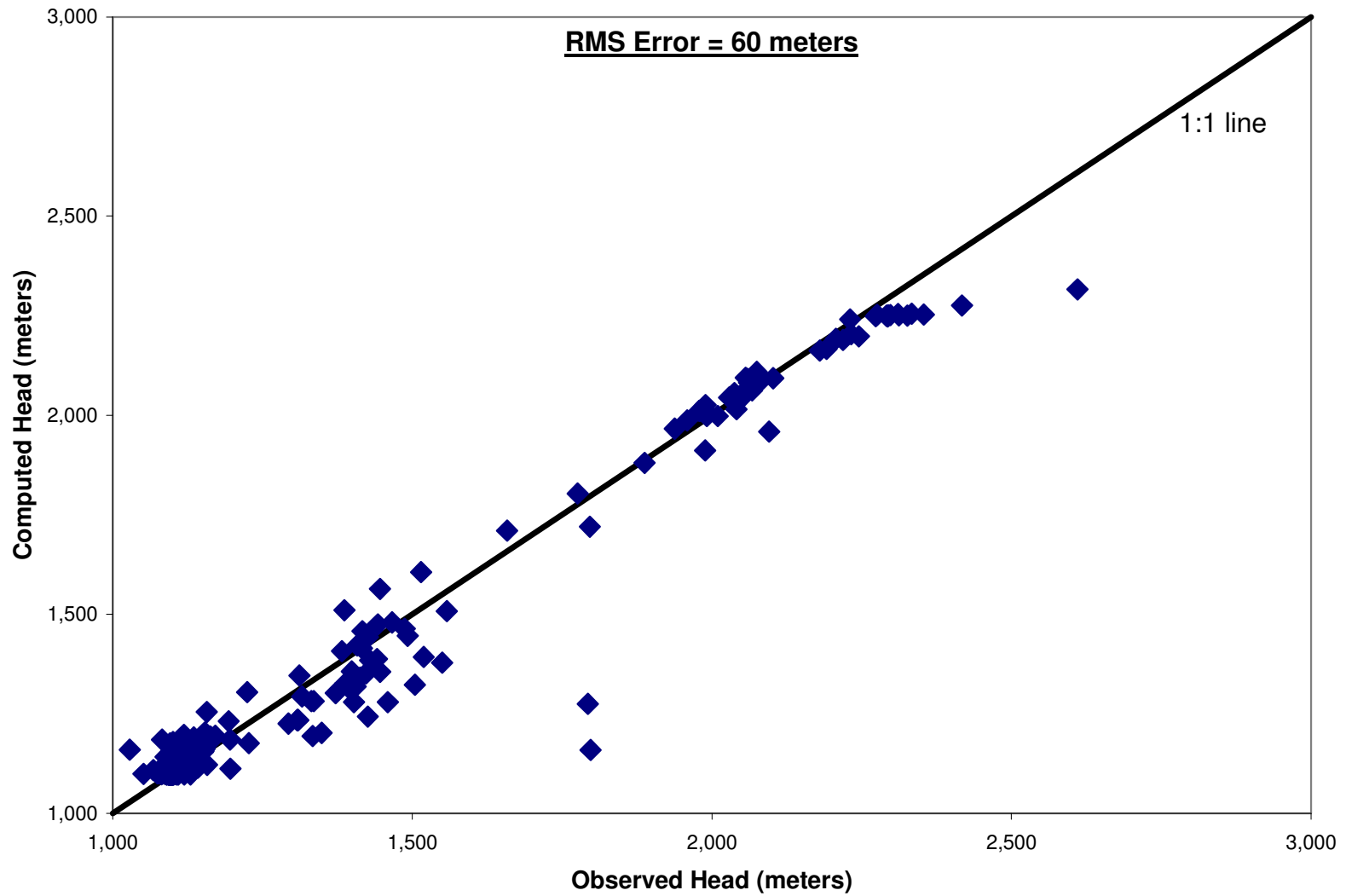
Figure 4.42: Computed versus observed hydraulic head for the calibrated water-balance based average recharge scenario model.
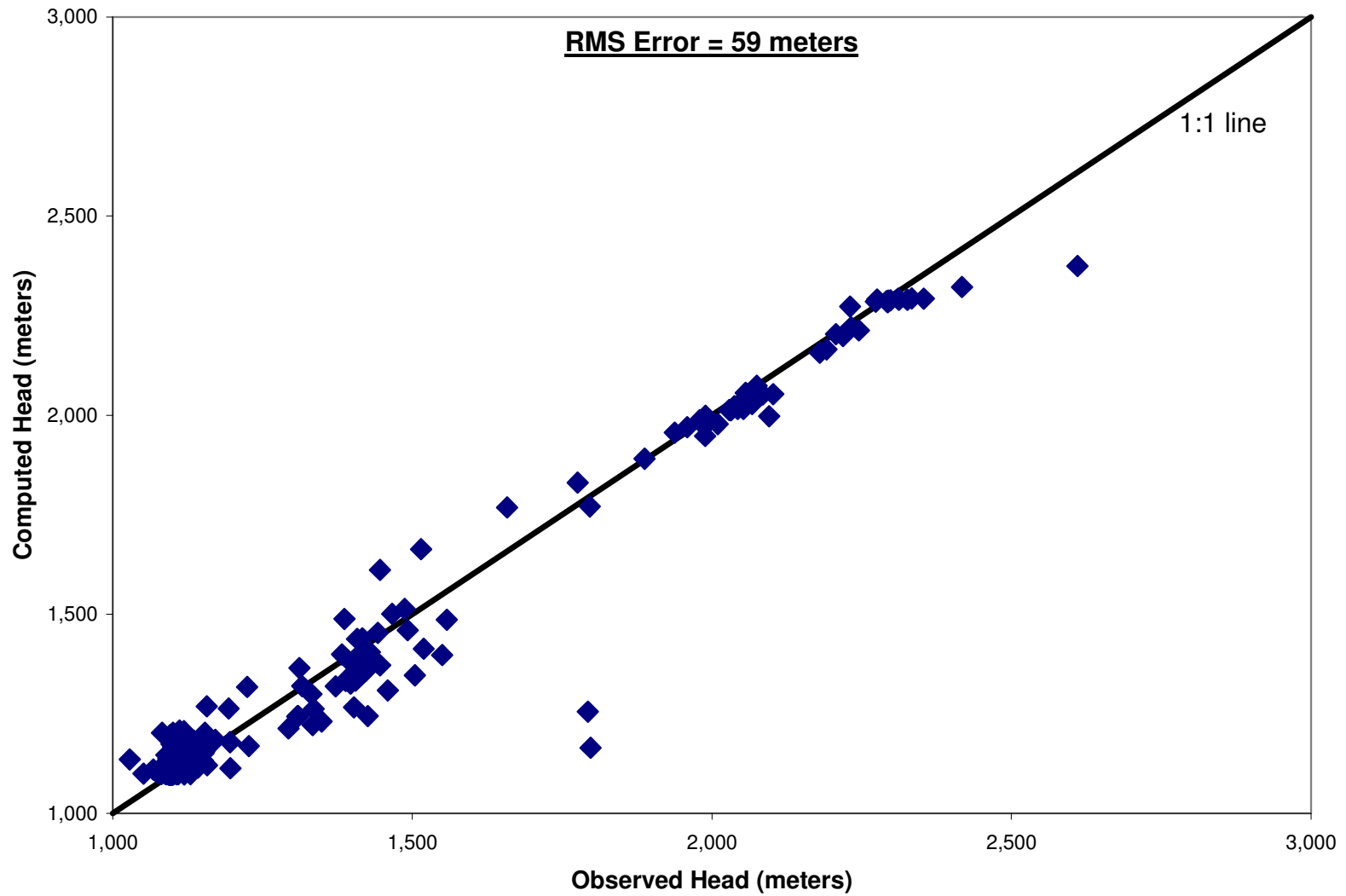
Figure 4.43: Computed versus observed hydraulic head for the calibrated water-balance based maximum recharge scenario model.
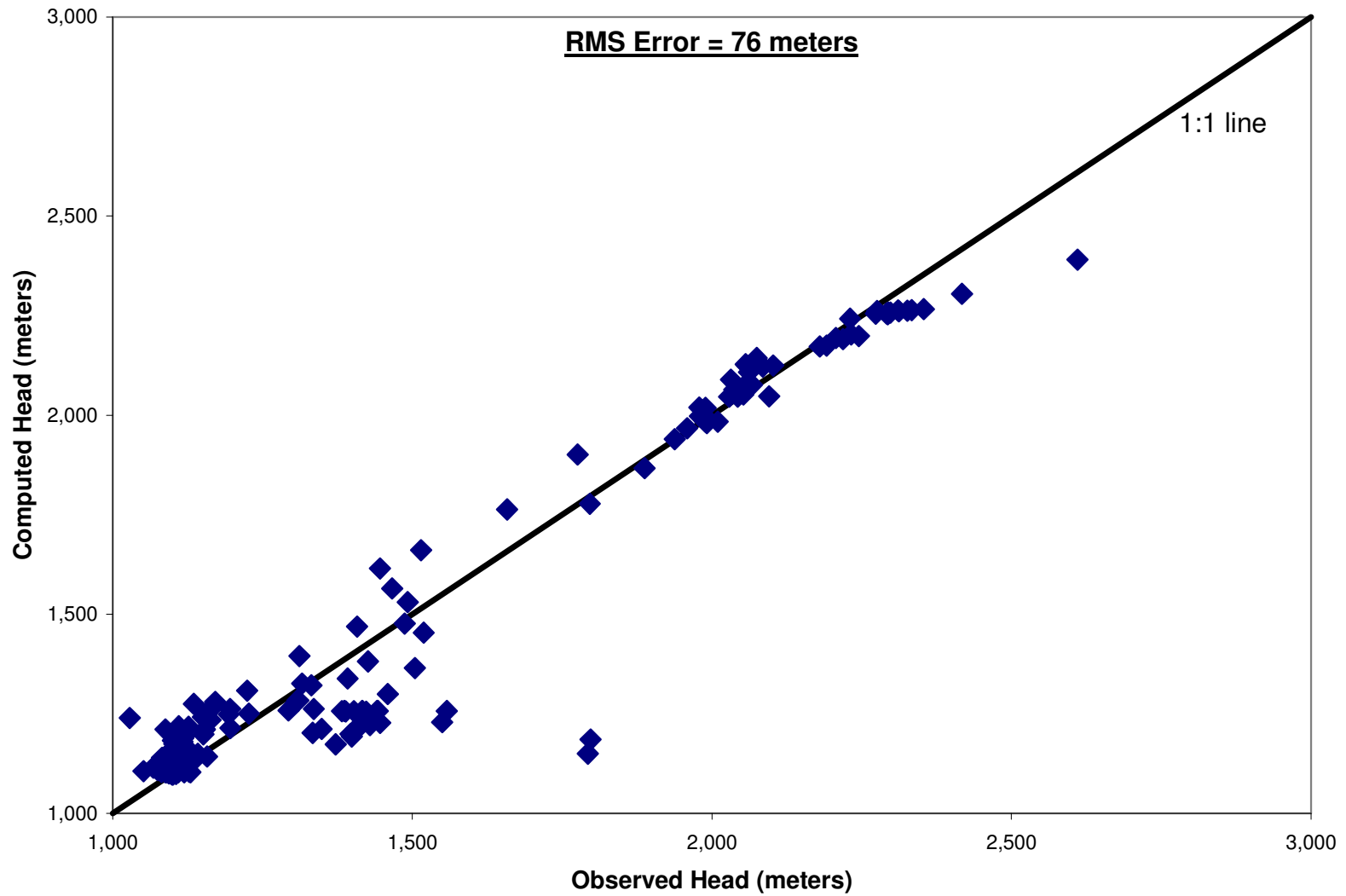
Figure 4.44: Computed versus observed hydraulic head for the calibrated elevation-dependent minimum recharge scenario model.
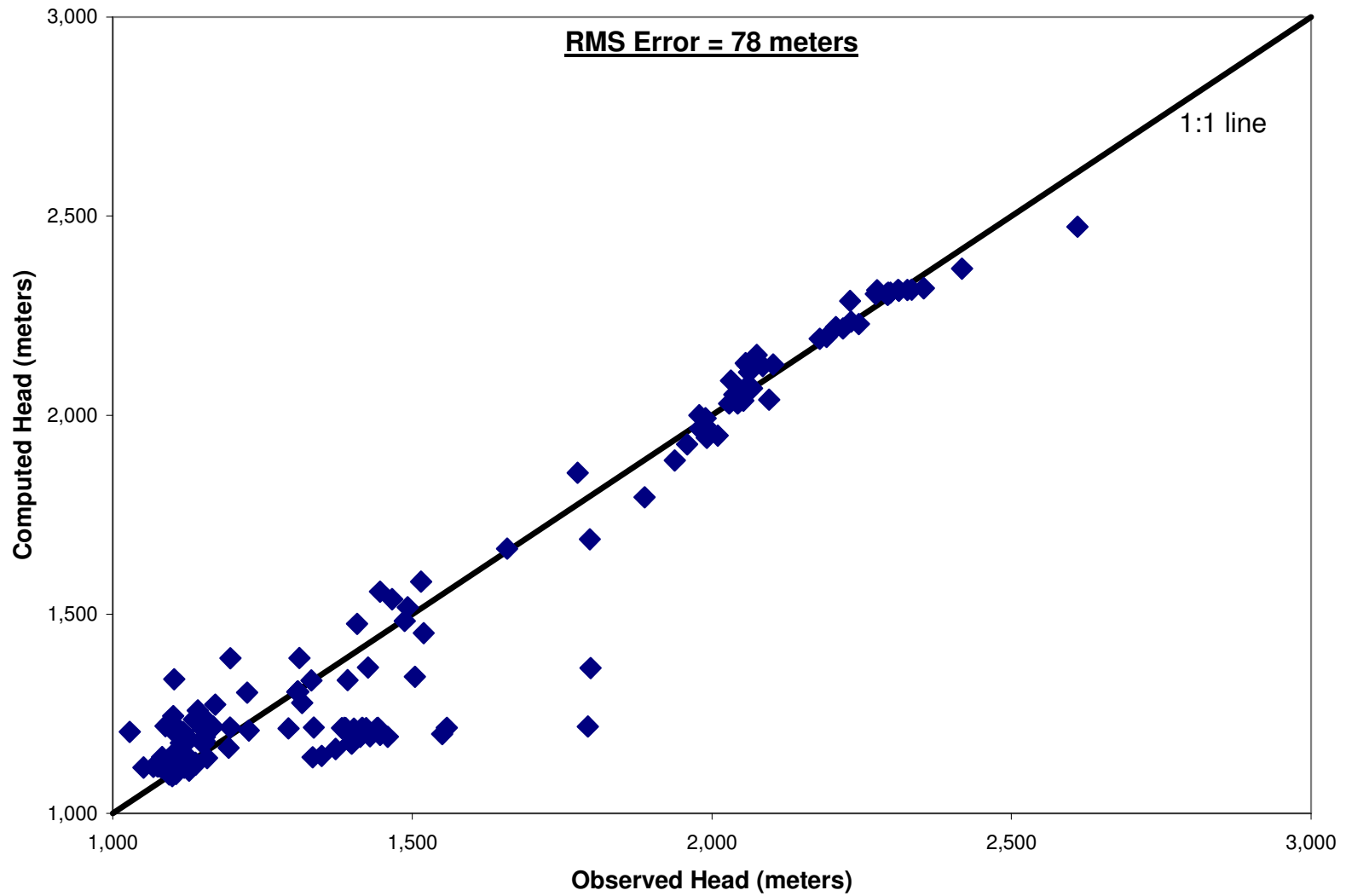
Figure 4.45: Computed versus observed hydraulic head for the calibrated elevation-dependent average recharge scenario model.
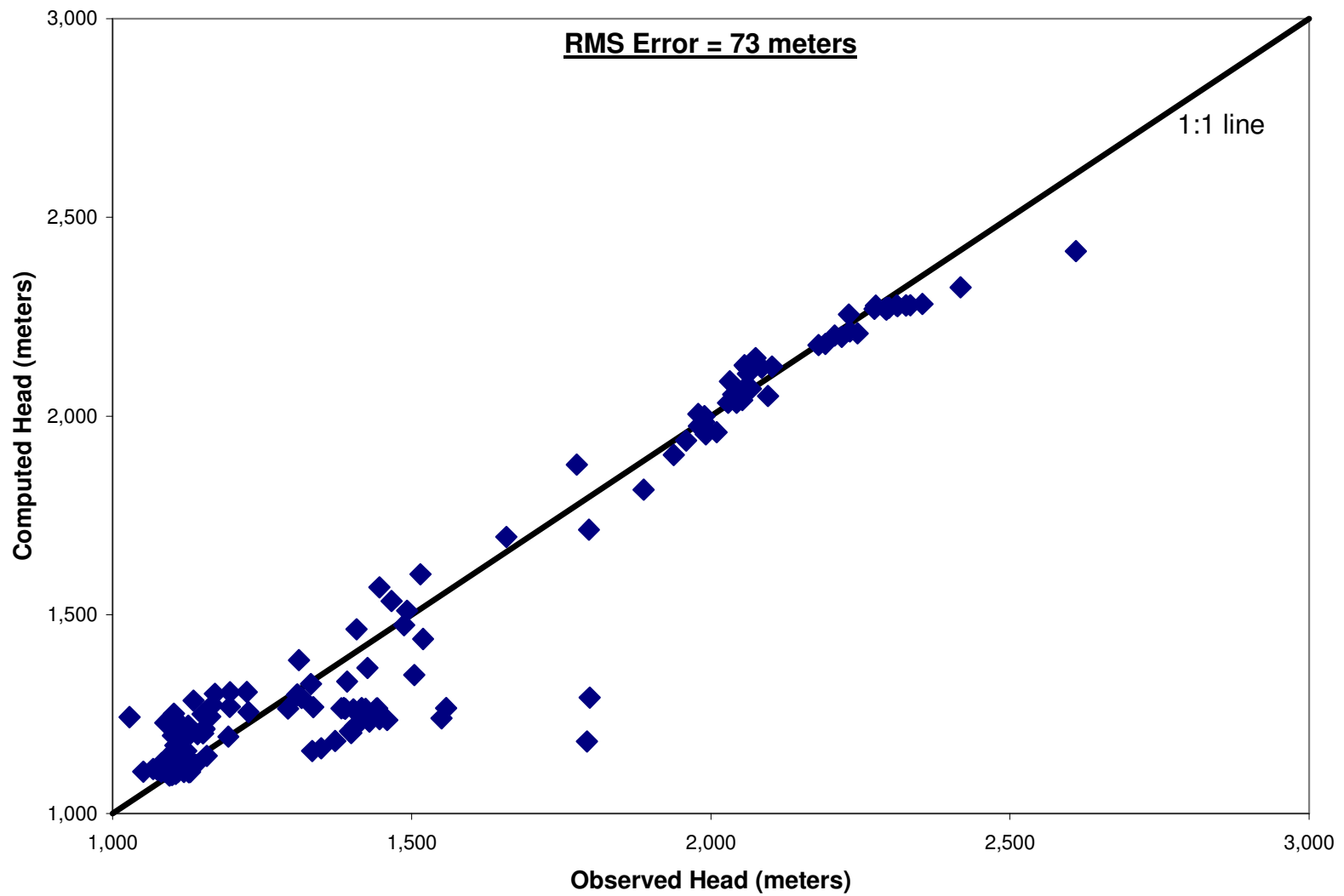
Figure 4.46: Computed versus observed hydraulic head for the calibrated elevation-dependent maximum recharge scenario model.
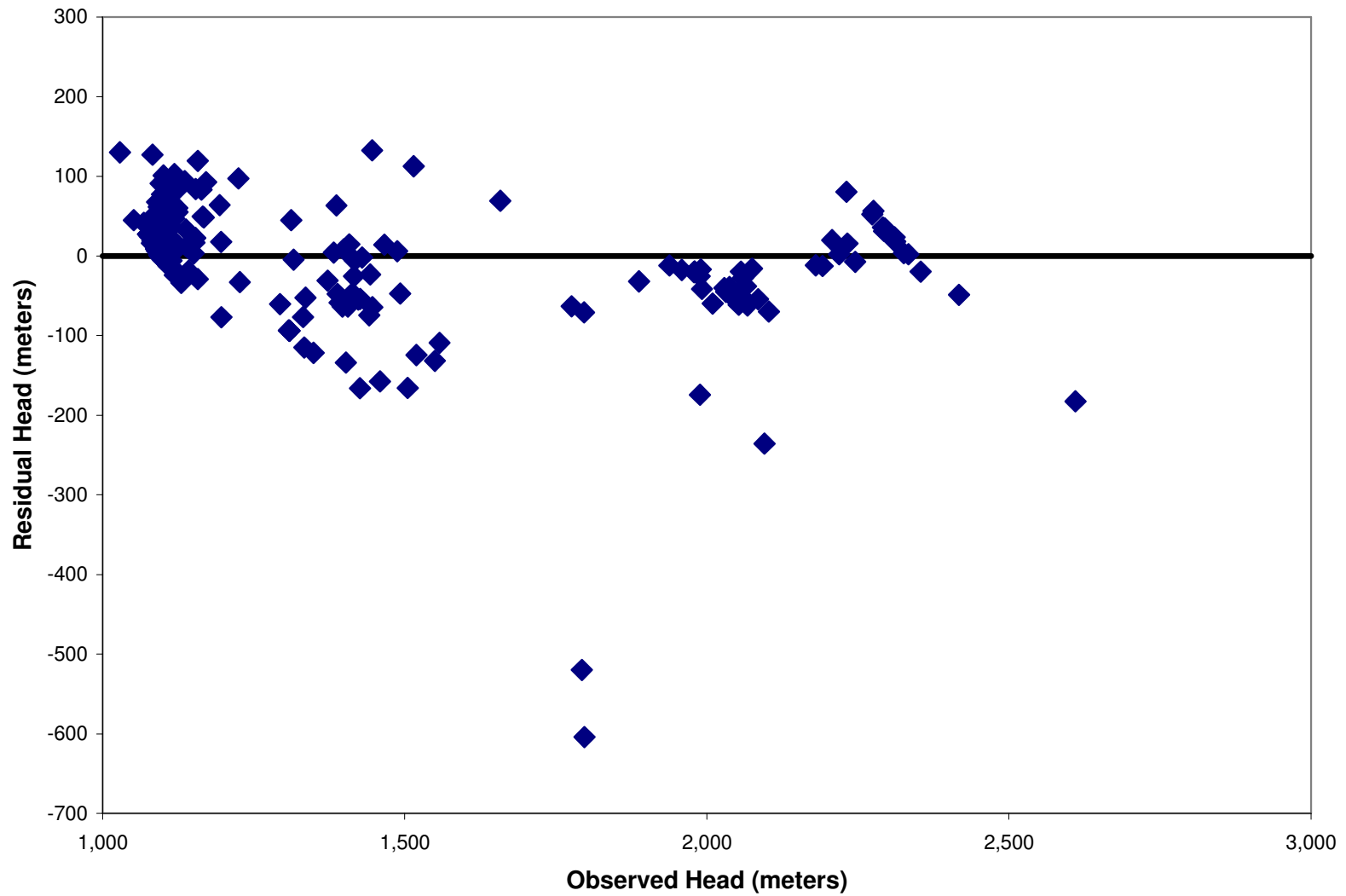
Figure 4.47: Residual versus observed hydraulic head for the calibrated water-balance based minimum recharge scenario model.
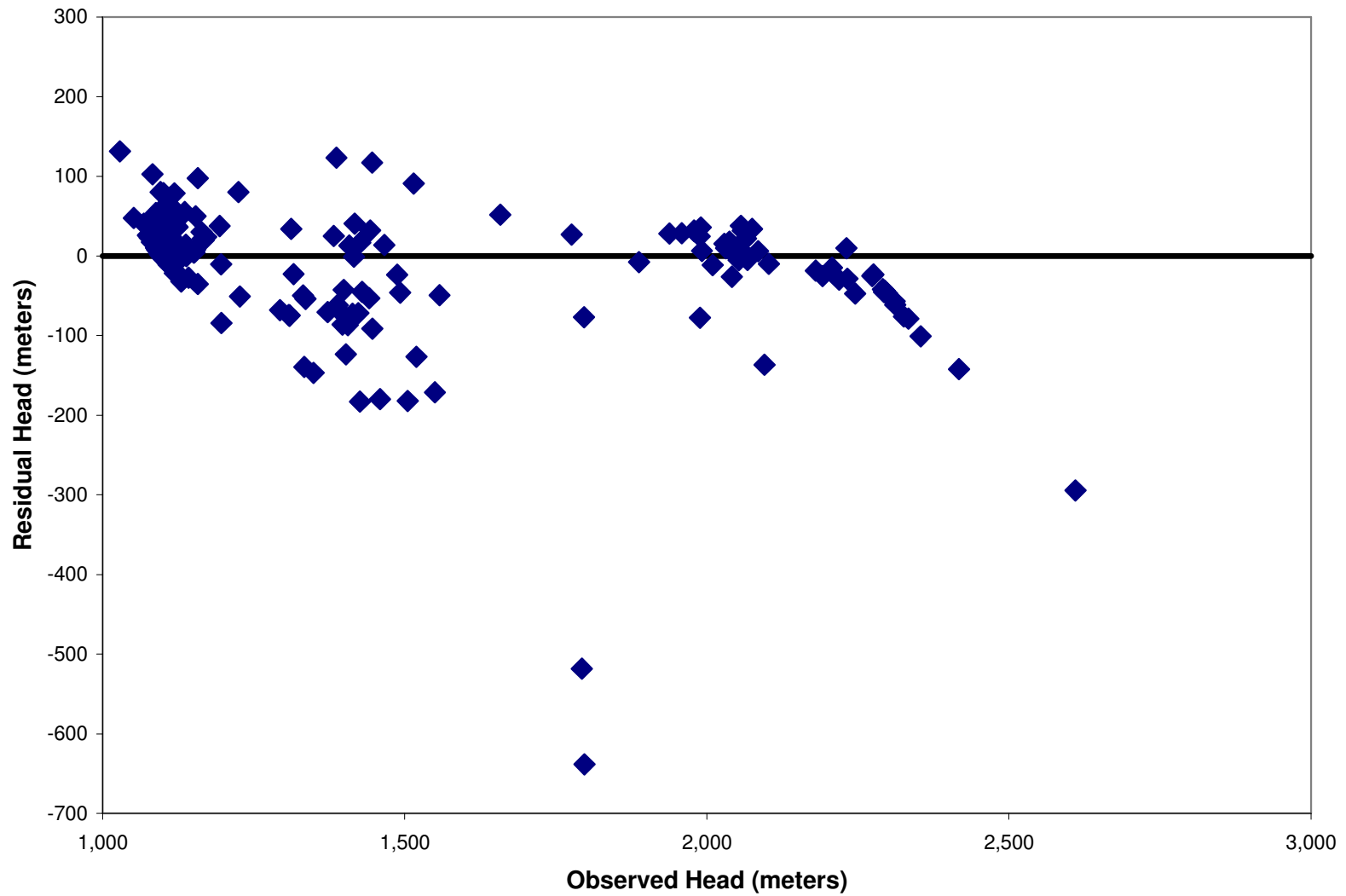
Figure 4.48: Residual versus observed hydraulic head for the calibrated water-balance based average recharge scenario model.
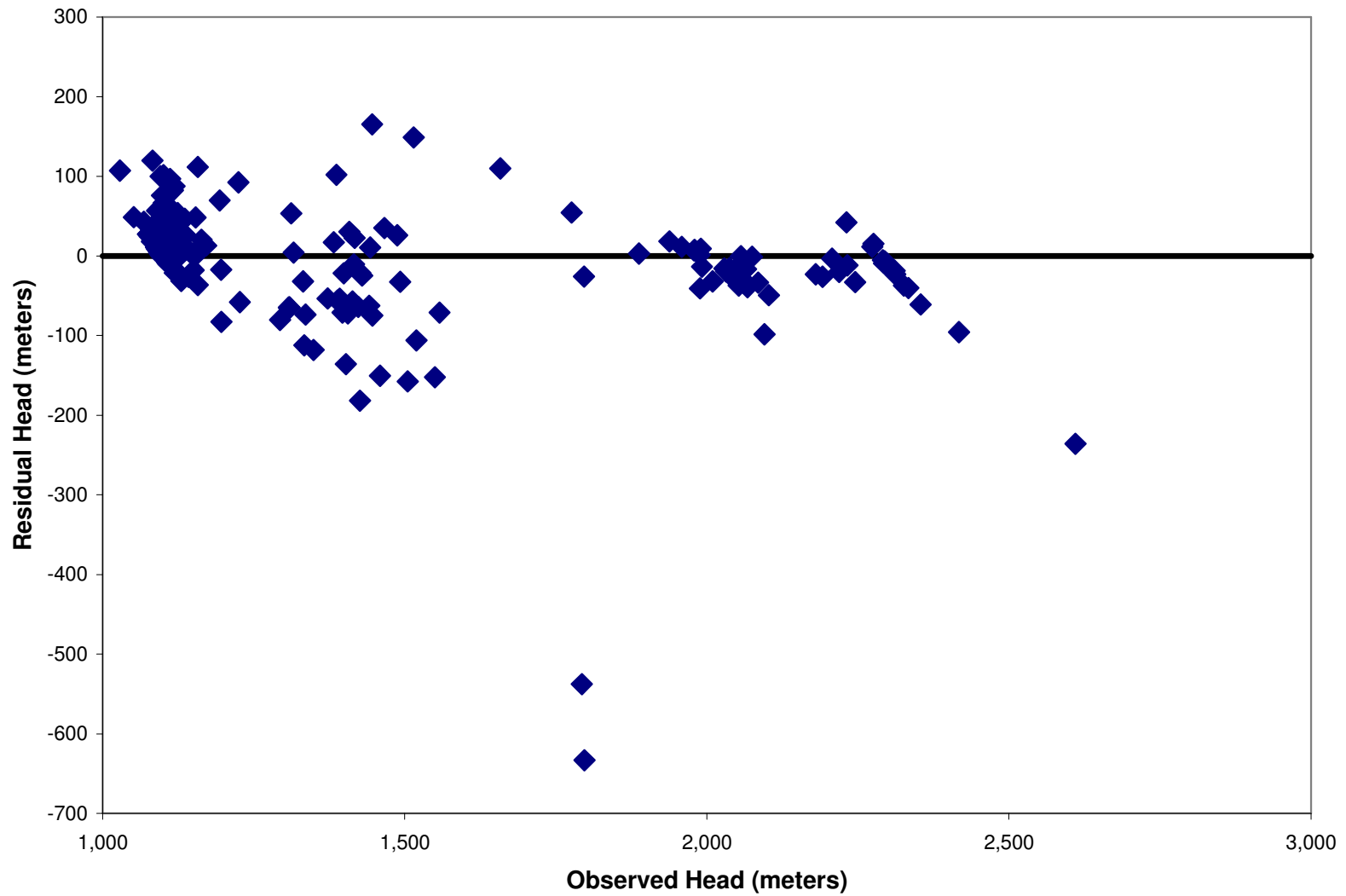
Figure 4.49: Residual versus observed hydraulic head for the calibrated water-balance based maximum recharge scenario model.
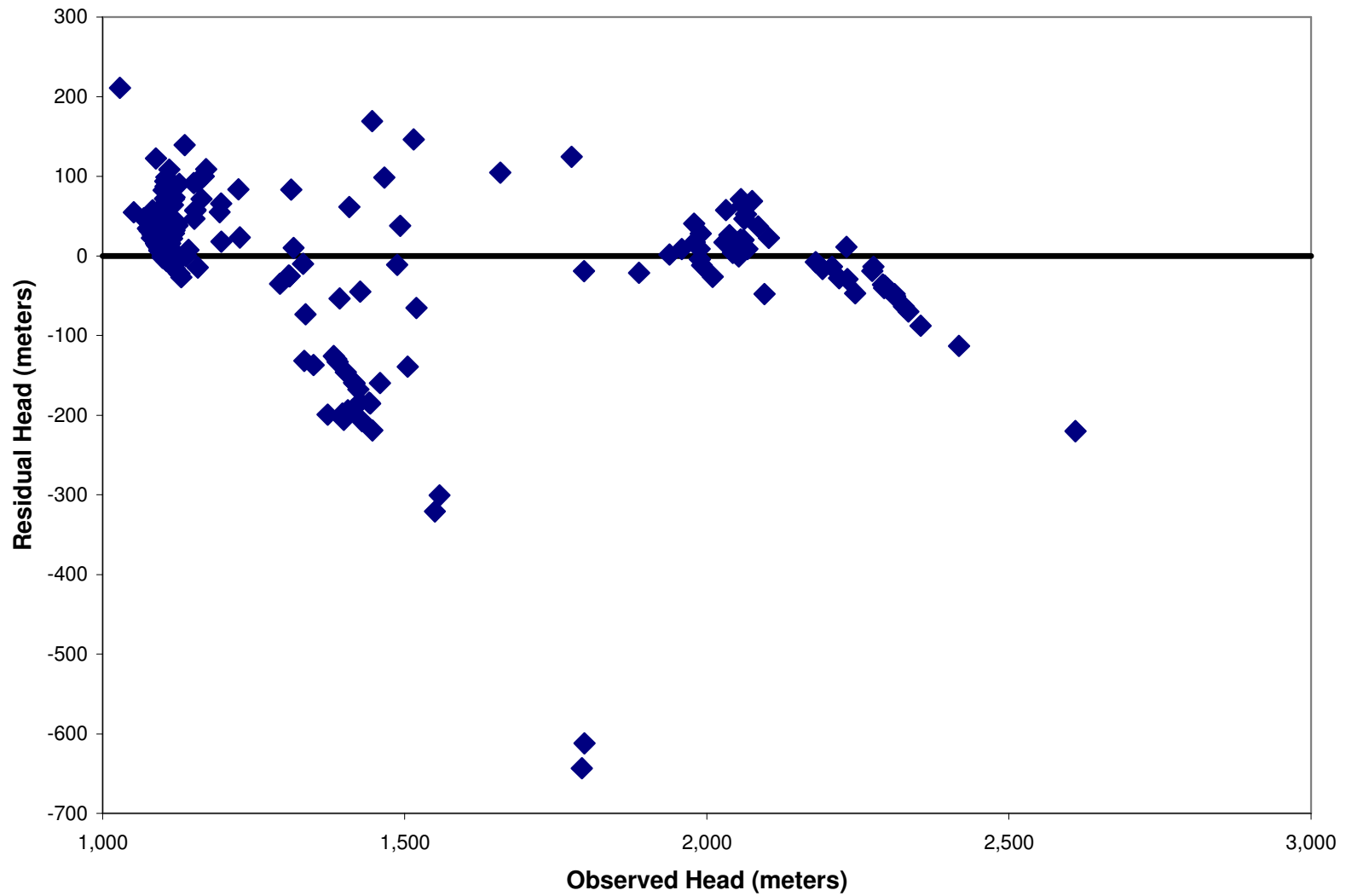
Figure 4.50: Residual versus observed hydraulic head for the calibrated elevation-dependent minimum recharge scenario model.
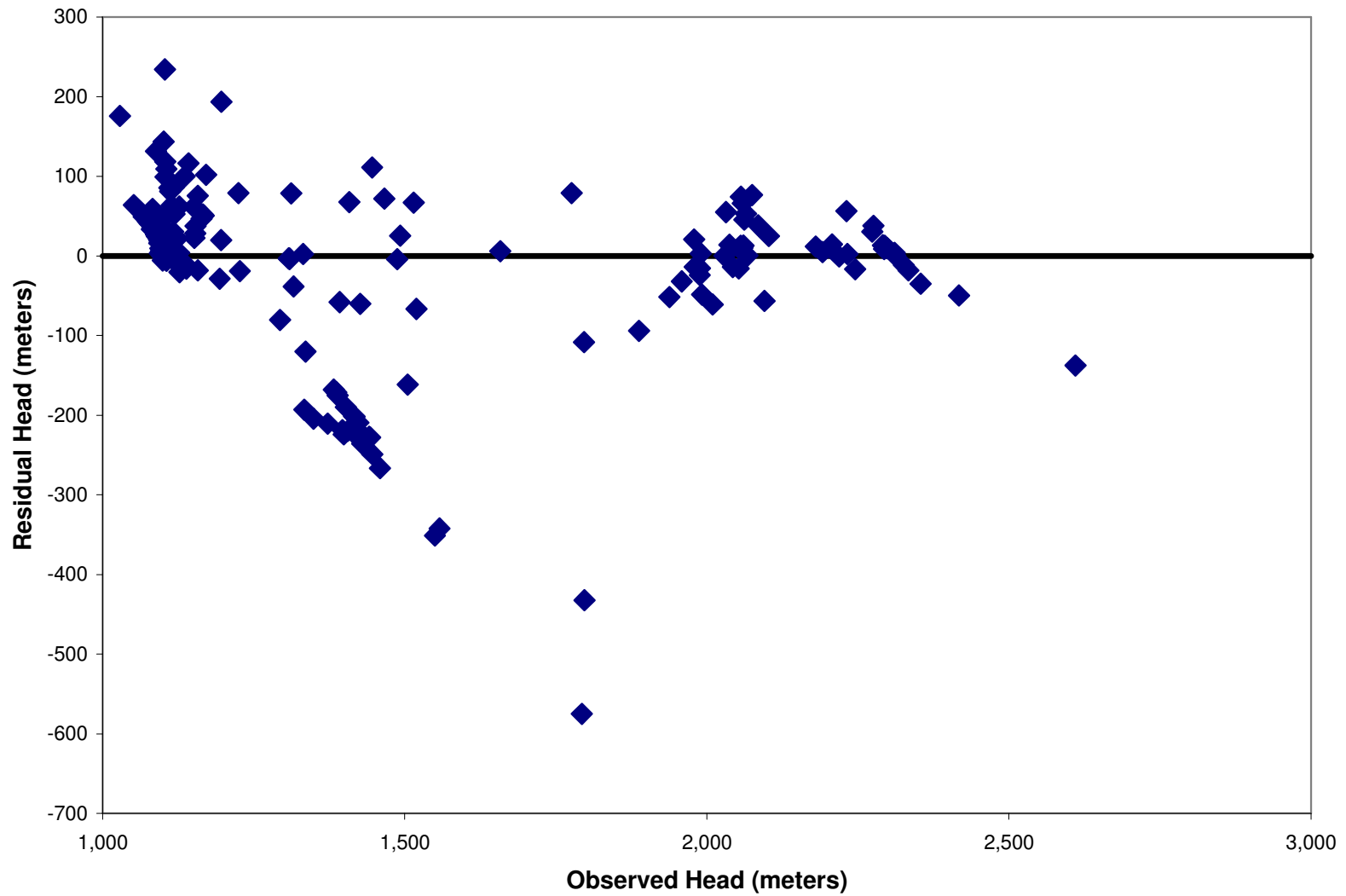
Figure 4.51: Residual versus observed hydraulic head for the calibrated elevation-dependent average recharge scenario model.
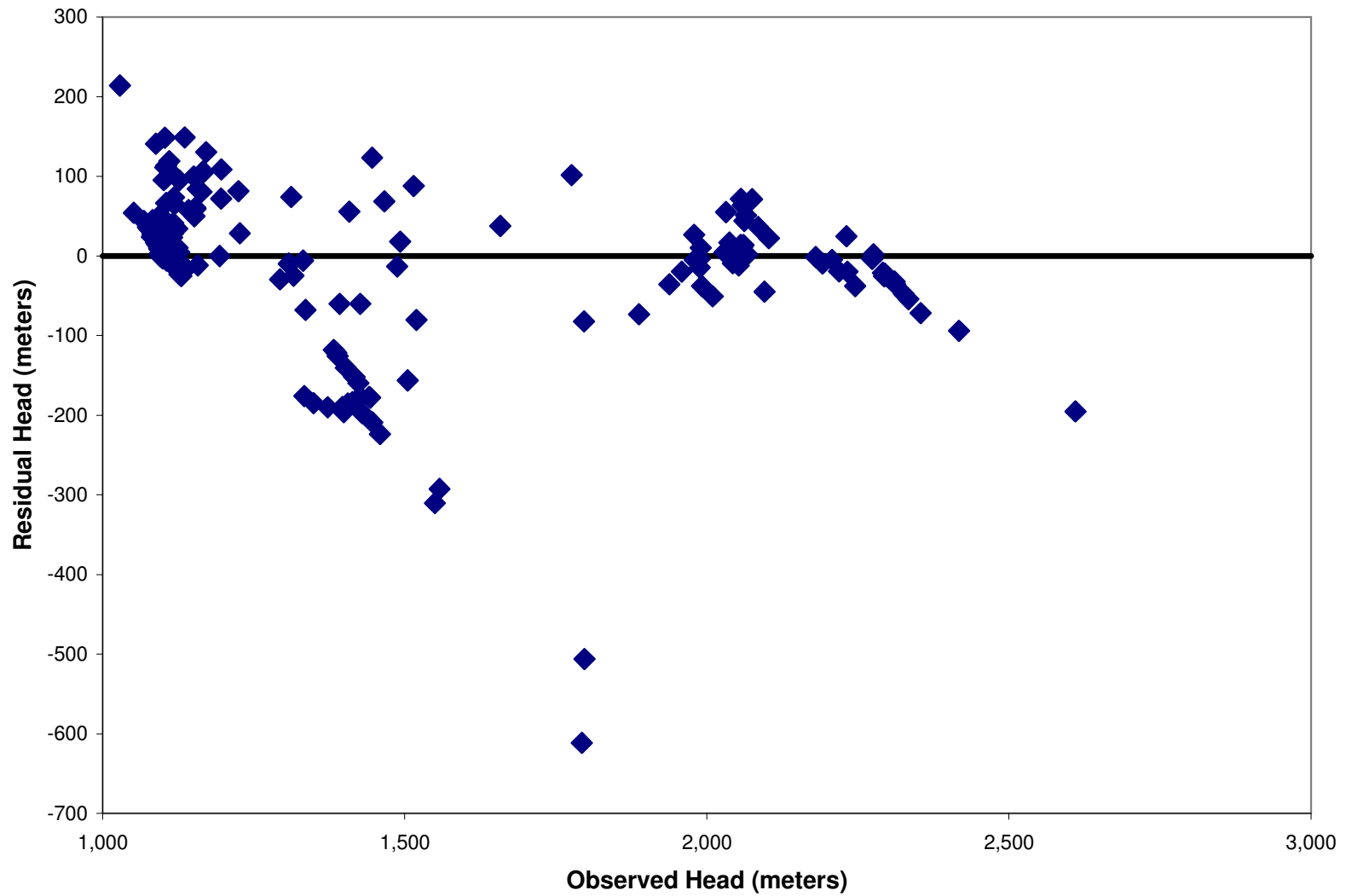
Figure 4.52: Residual versus observed hydraulic head for the calibrated elevation-dependent maximum recharge scenario model.
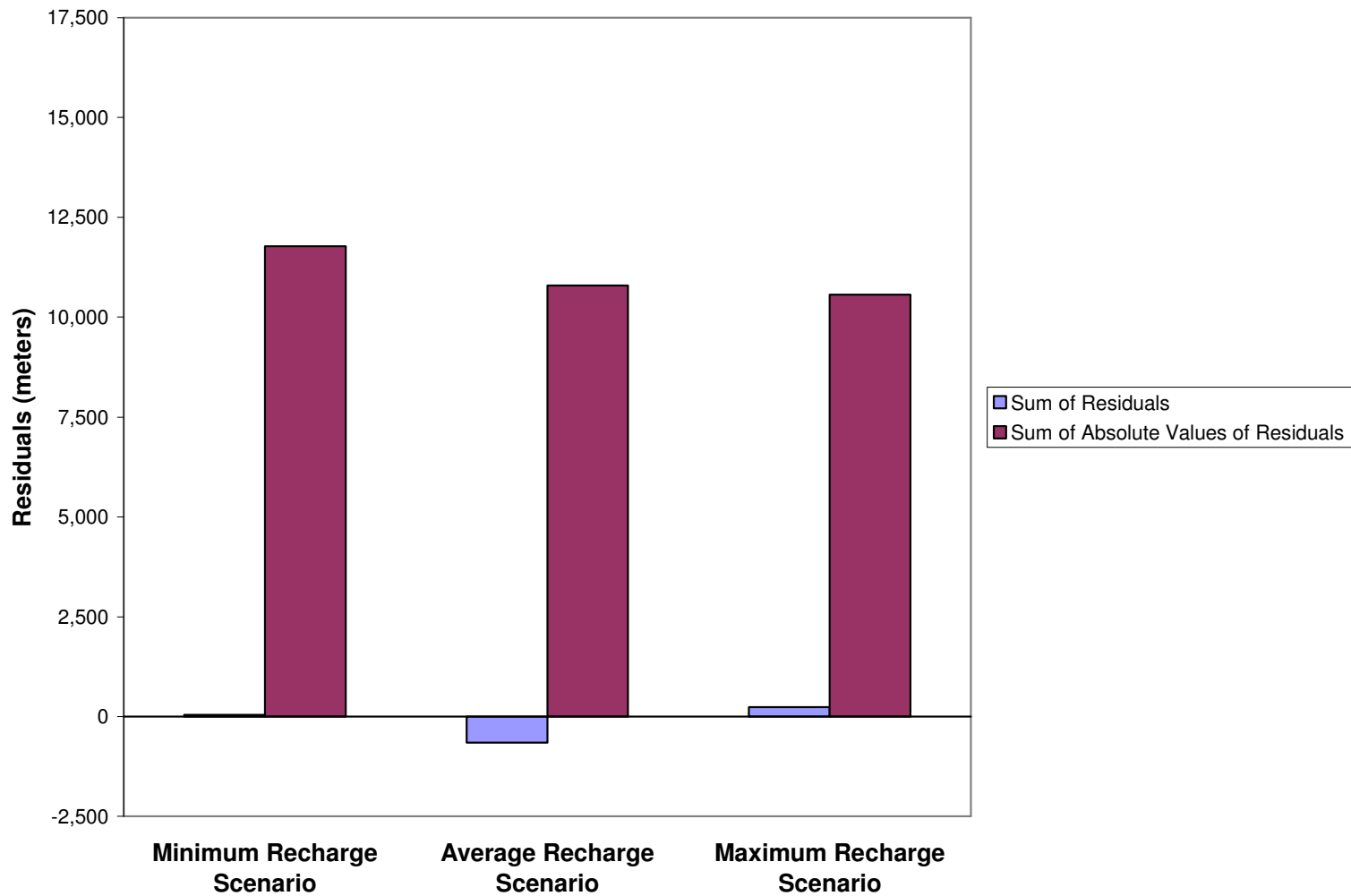
Figure 4.53: Sum of the residuals and sum of the absolute values of the residuals between observed and computed hydraulic heads for the calibrated water-balance based minimum, average, and maximum recharge scenario models.
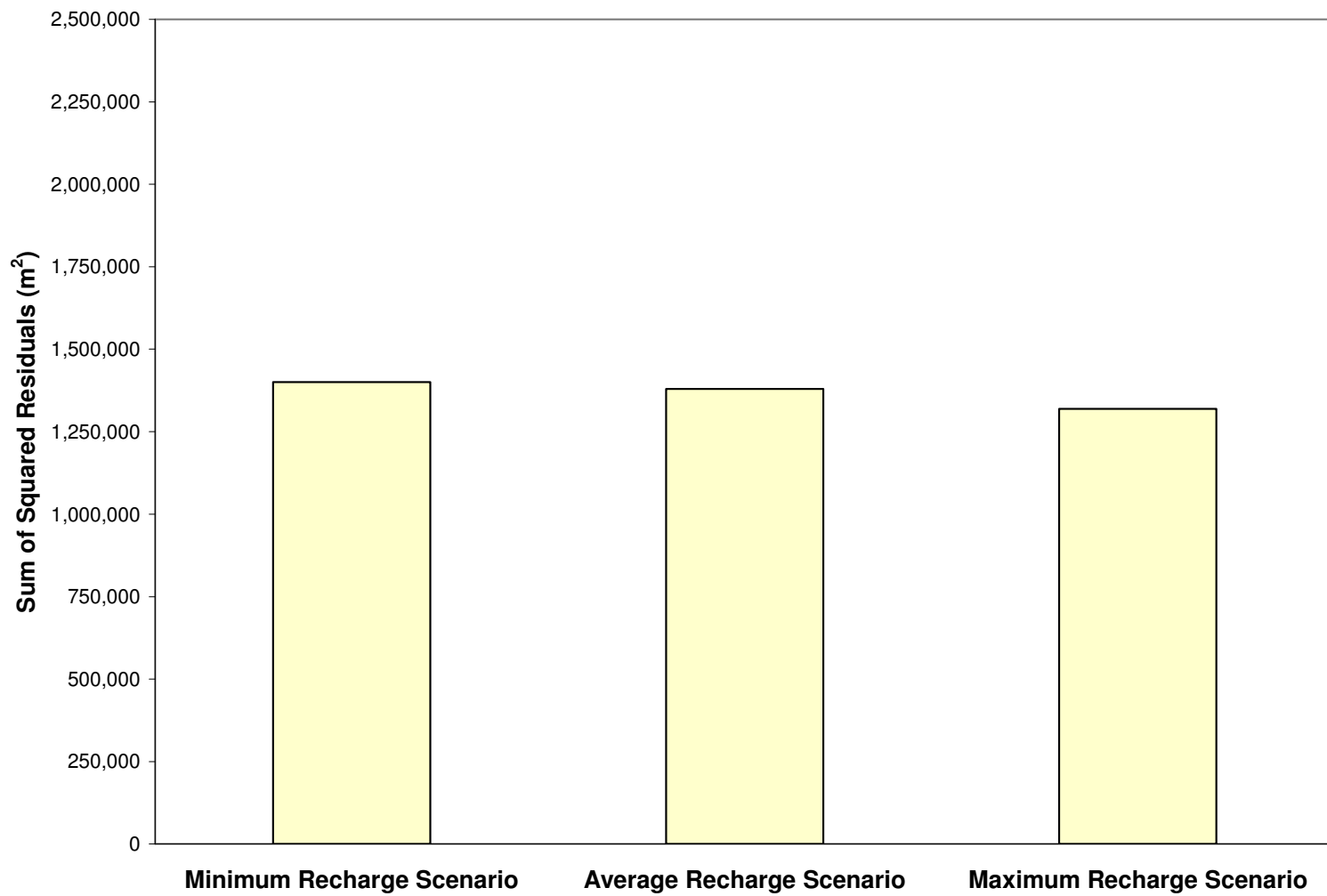
Figure 4.54: Sum of the squares of the residuals between observed and computed hydraulic heads for the calibrated water-balance based minimum, average, and maximum recharge scenario models.
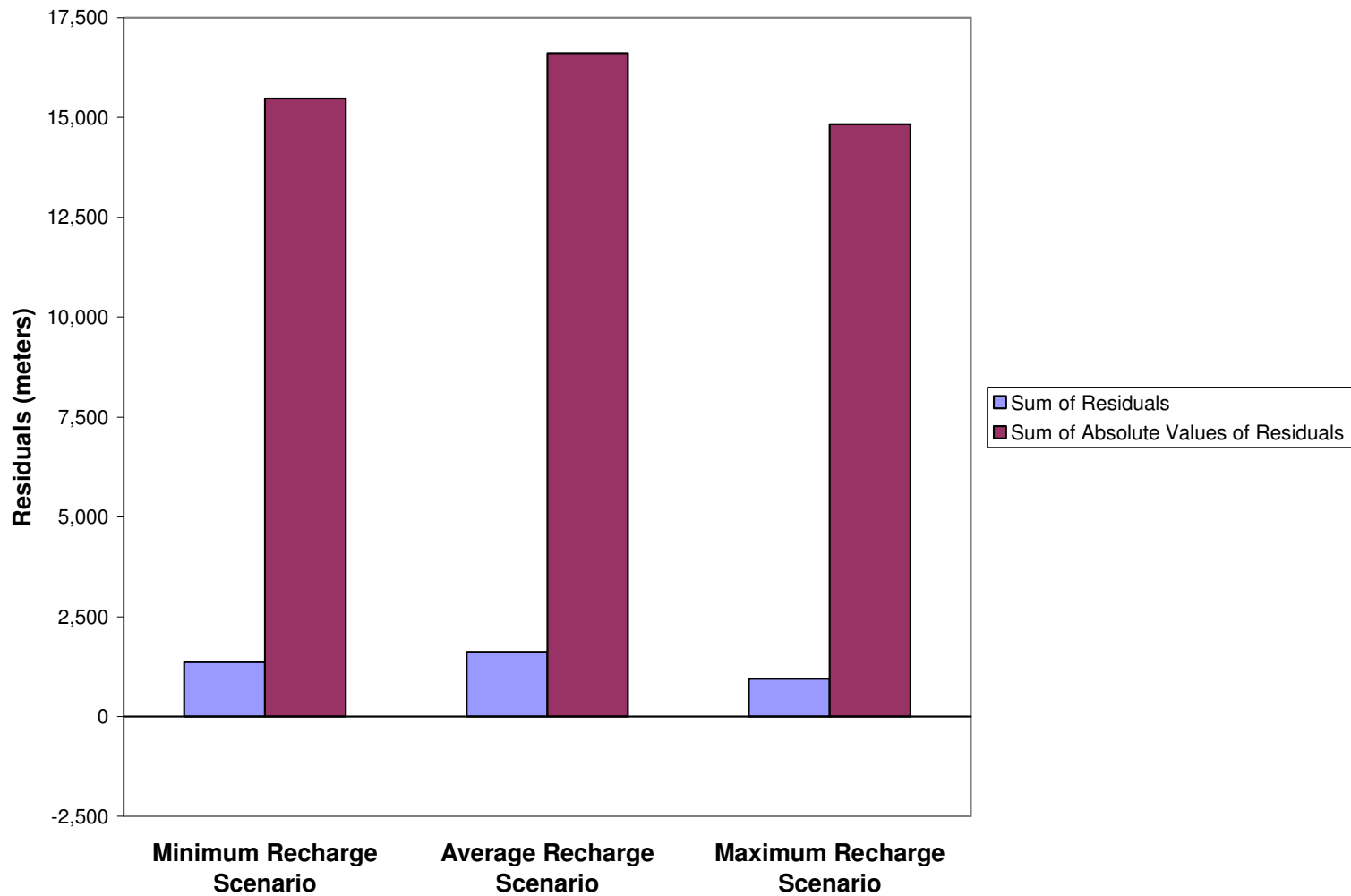
Figure 4.55: Sum of the residuals and sum of the absolute values of the residuals between observed and computed hydraulic heads for the calibrated elevation-dependent minimum, average, and maximum recharge scenario models.
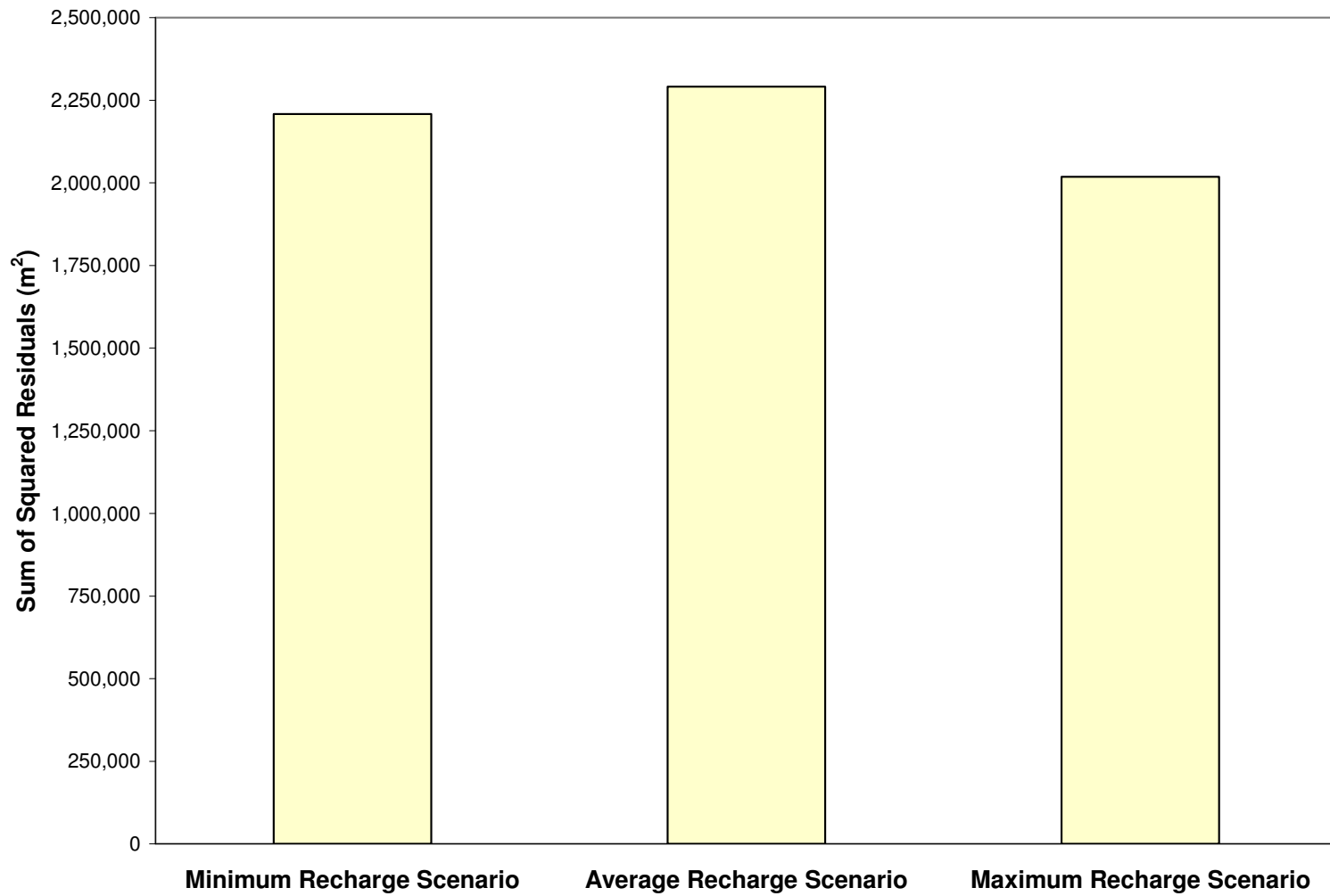
Figure 4.56: Sum of the squares of the residuals between observed and computed hydraulic heads for the calibrated elevation-dependent minimum, average, and maximum recharge scenarios models.
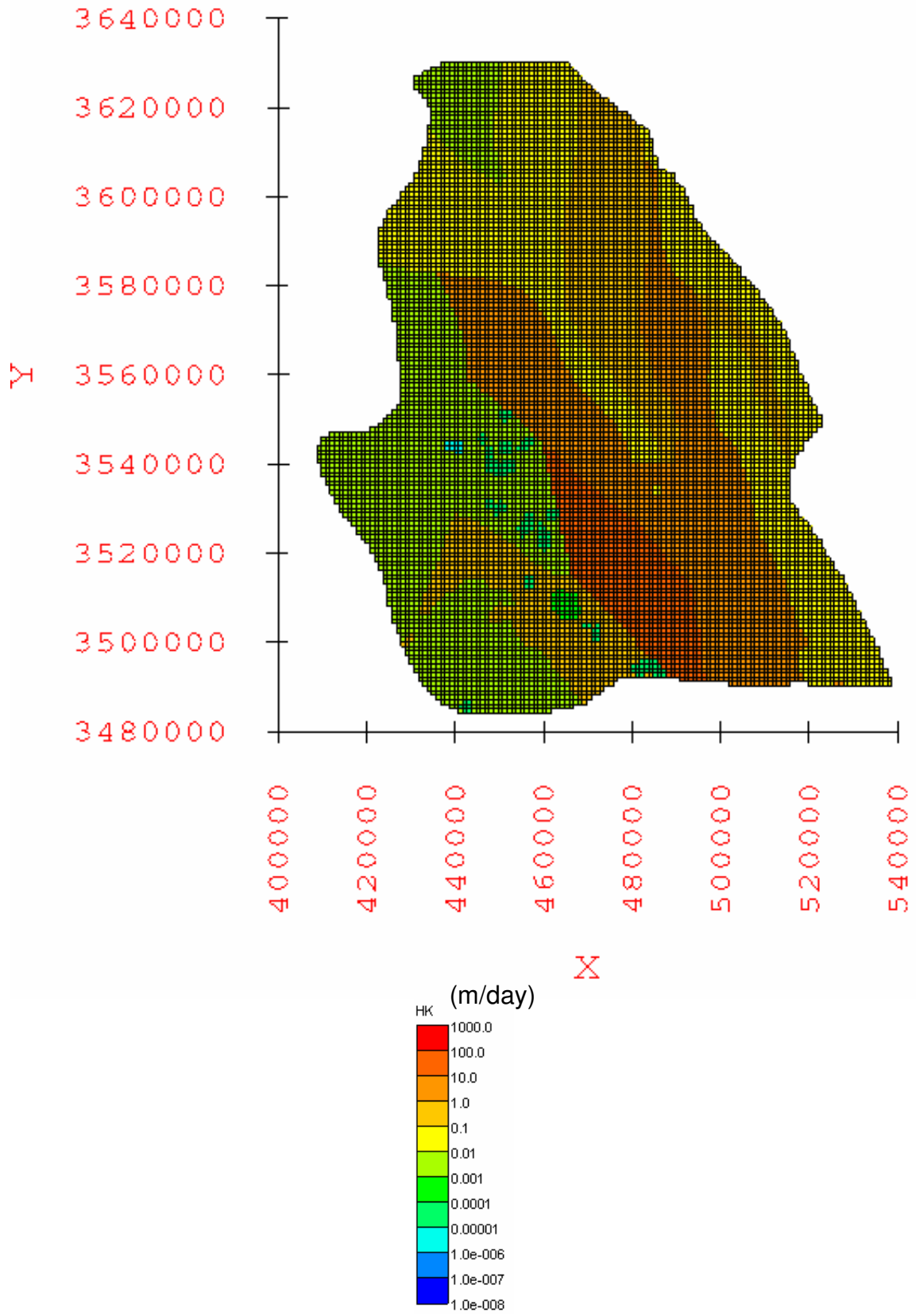
Figure 4.57: Horizontal hydraulic conductivity [HK] distribution in layer 1 for the calibrated water-balance based minimum recharge scenario groundwater flow model.
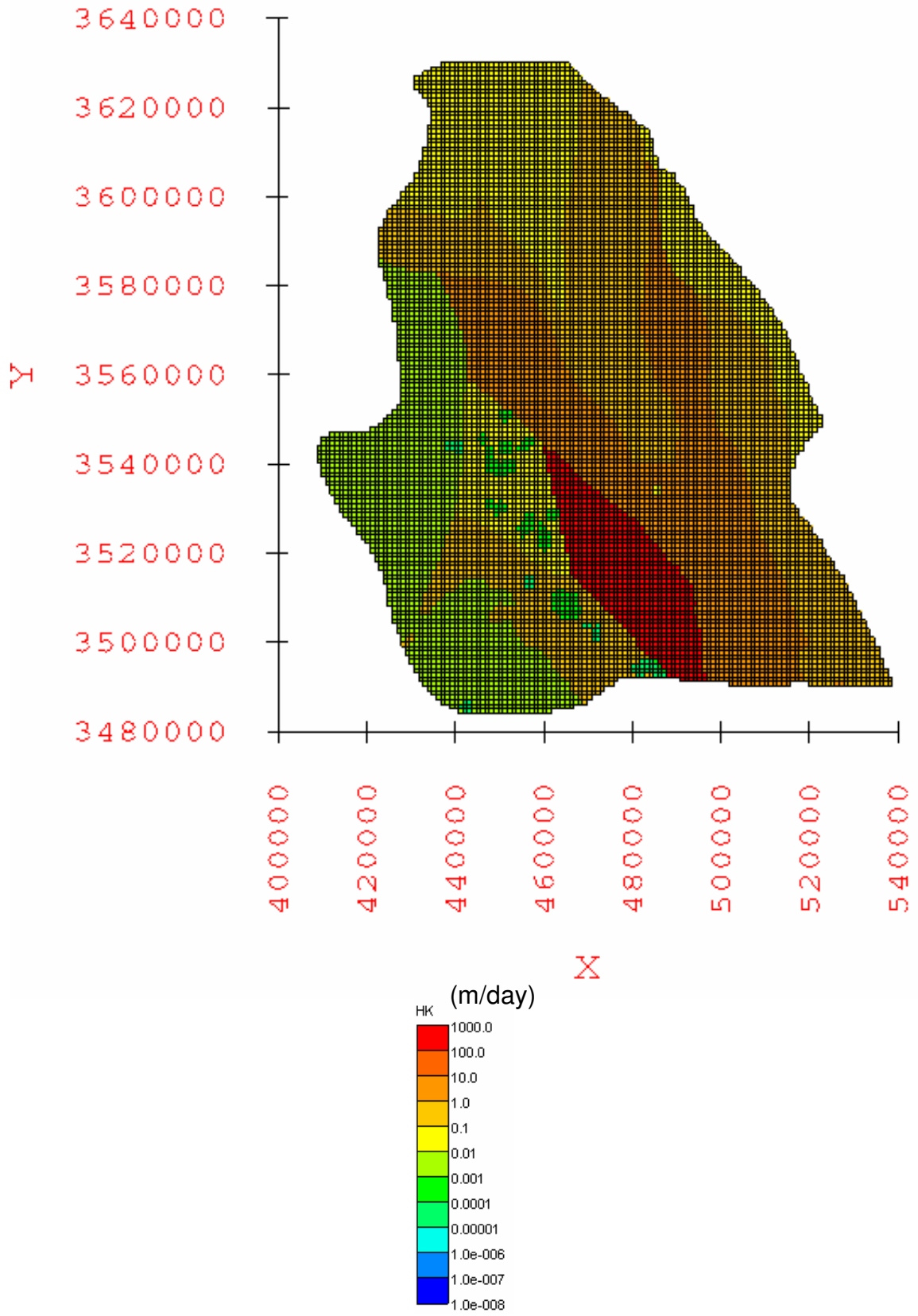
Figure 4.63: Horizontal hydraulic conductivity [HK] distribution in layer 1 for the calibrated water-balance based average recharge scenario groundwater flow model.

375
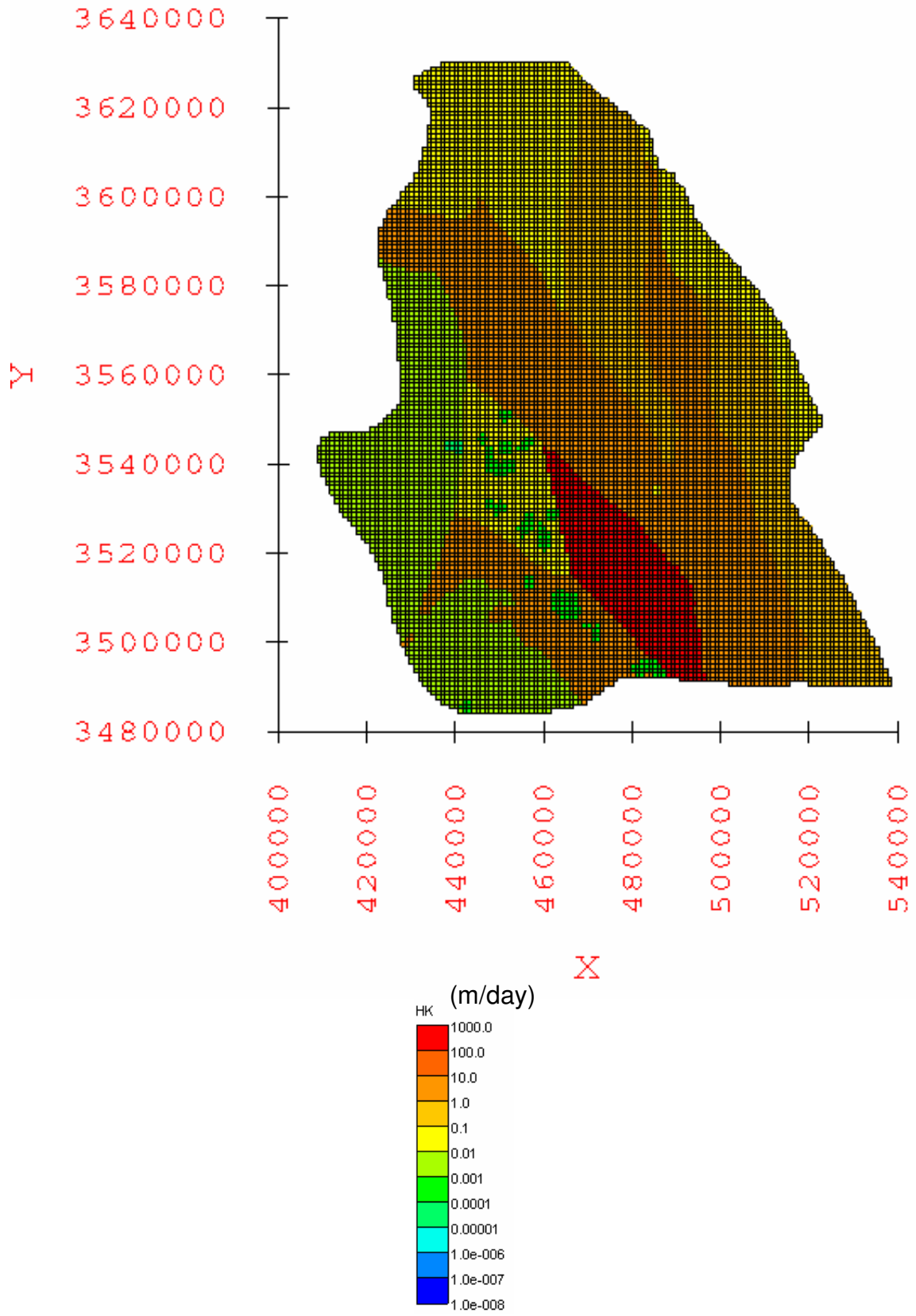
Figure 4.69: Horizontal hydraulic conductivity [HK] distribution in layer 1 for the calibrated water-balance based maximum recharge scenario groundwater flow model.
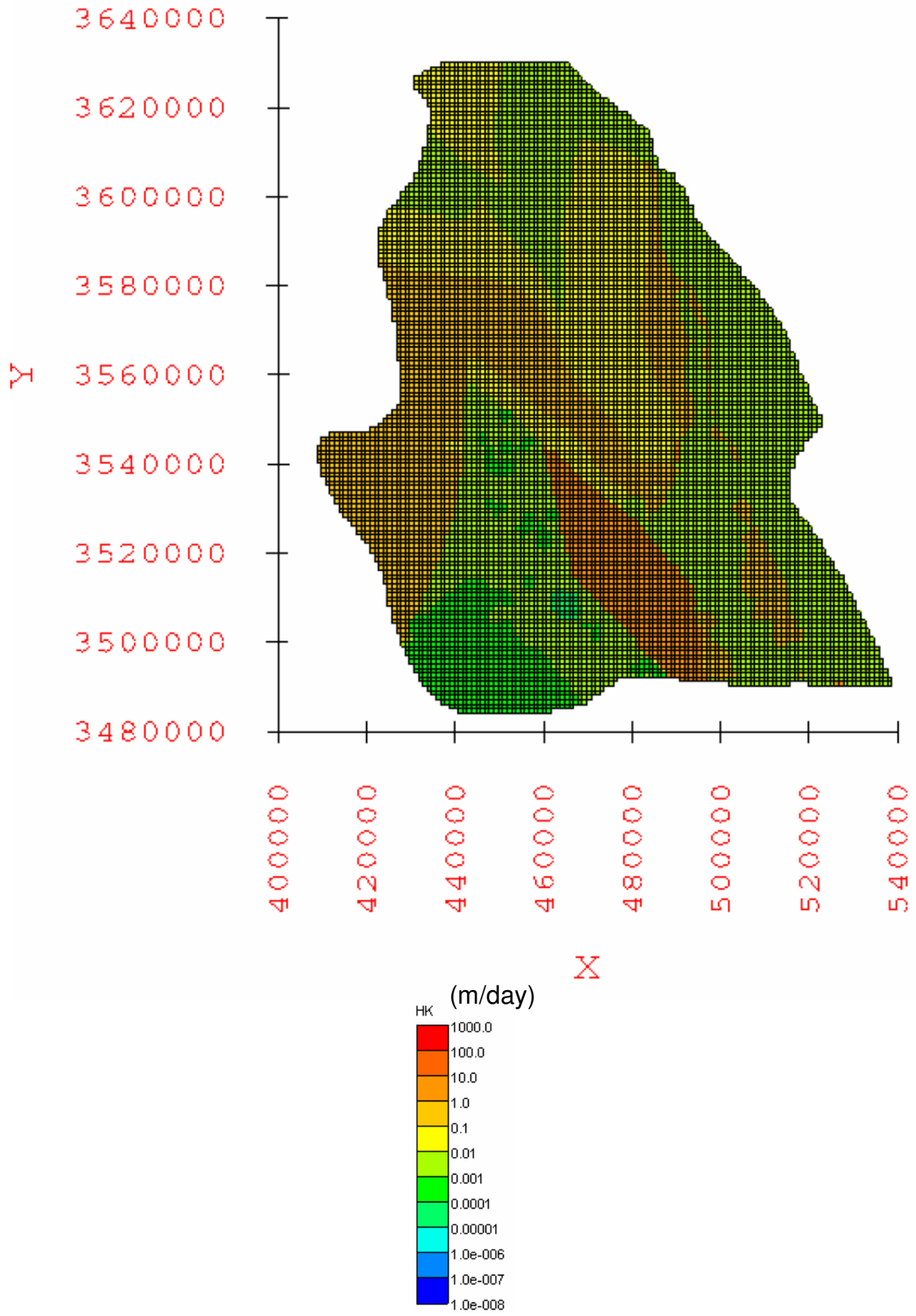
Figure 4.75: Horizontal hydraulic conductivity [HK] distribution in layer 1 for the calibrated elevation-dependent minimum recharge scenario groundwater flow model.
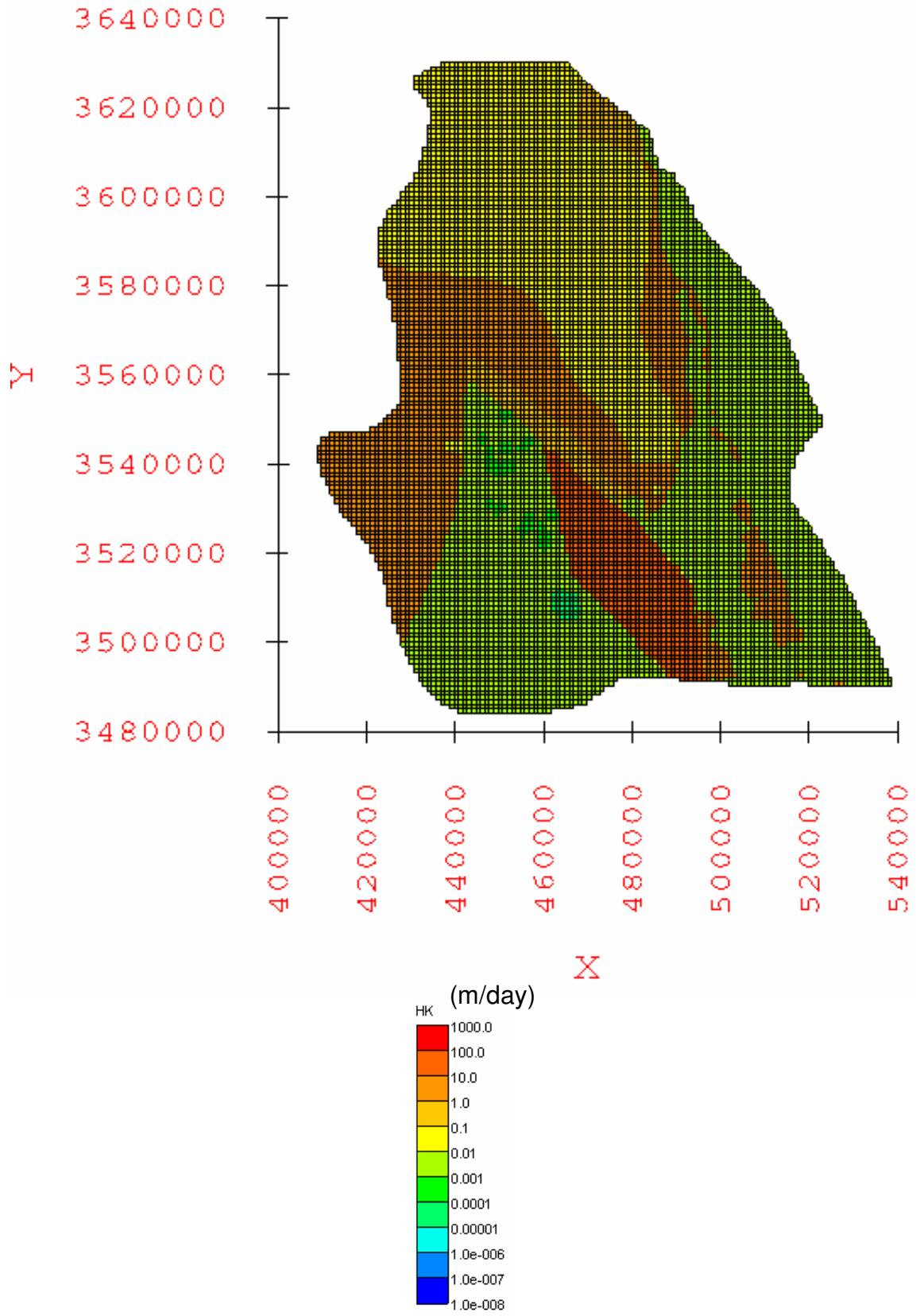
Figure 4.81: Horizontal hydraulic conductivity [HK] distribution in layer 1 for the calibrated elevation-dependent average recharge scenario groundwater flow model.
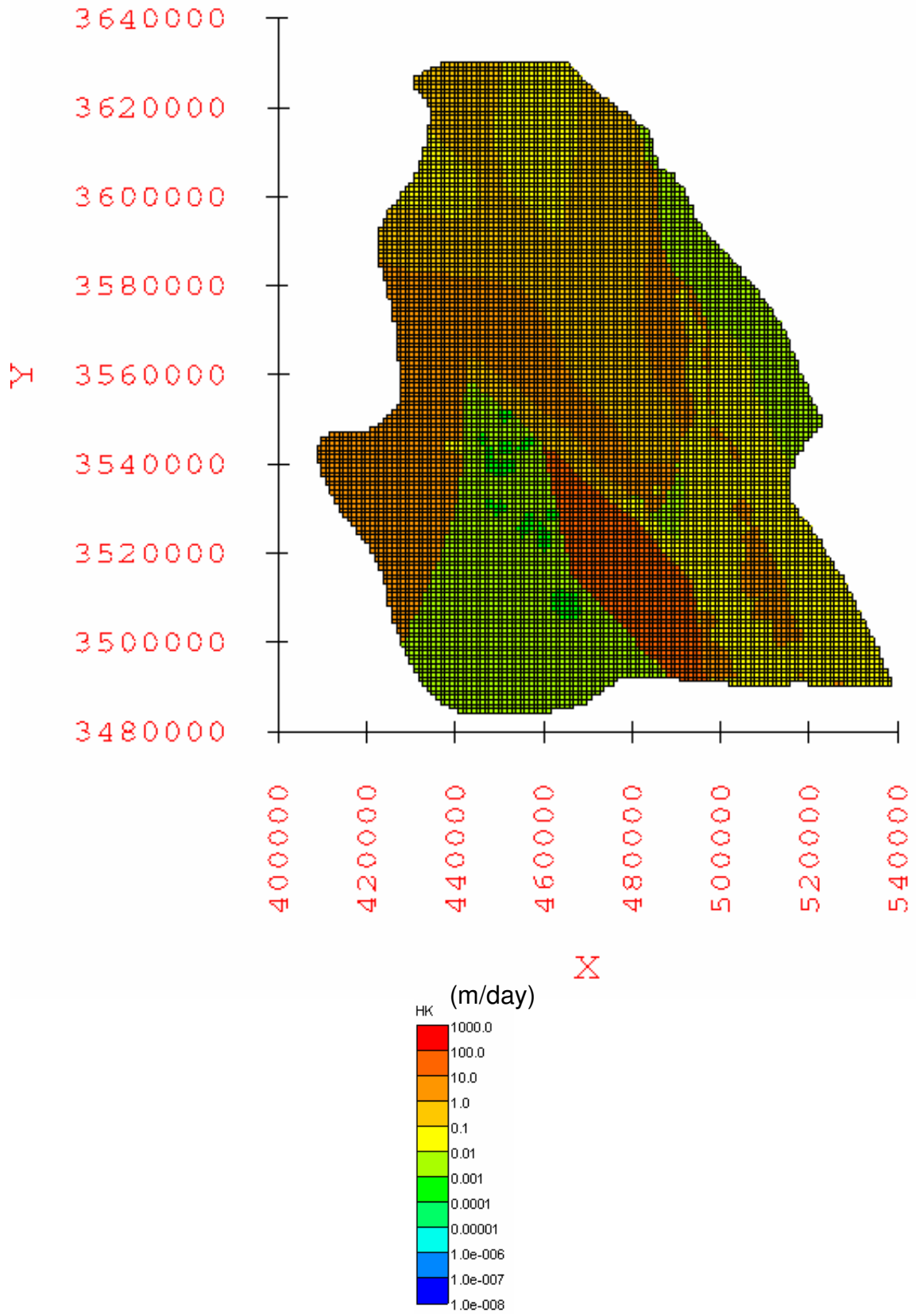
Figure 4.87: Horizontal hydraulic conductivity [HK] distribution in layer 1 for the calibrated elevation-dependent maximum recharge scenario groundwater flow model.
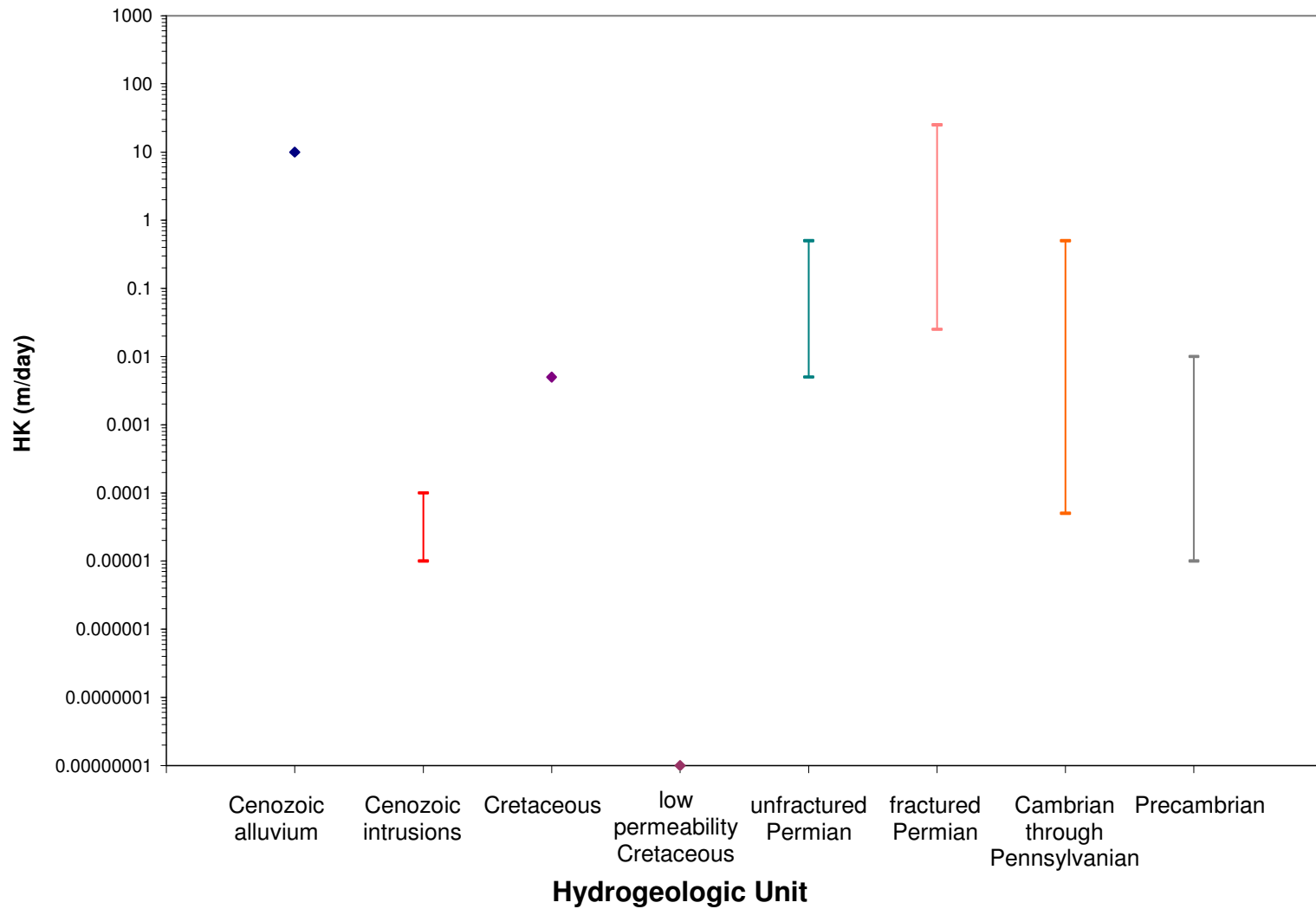
Figure 4.93: Range of horizontal hydraulic conductivity [HK] values for the calibrated water-balance based minimum recharge scenario model.
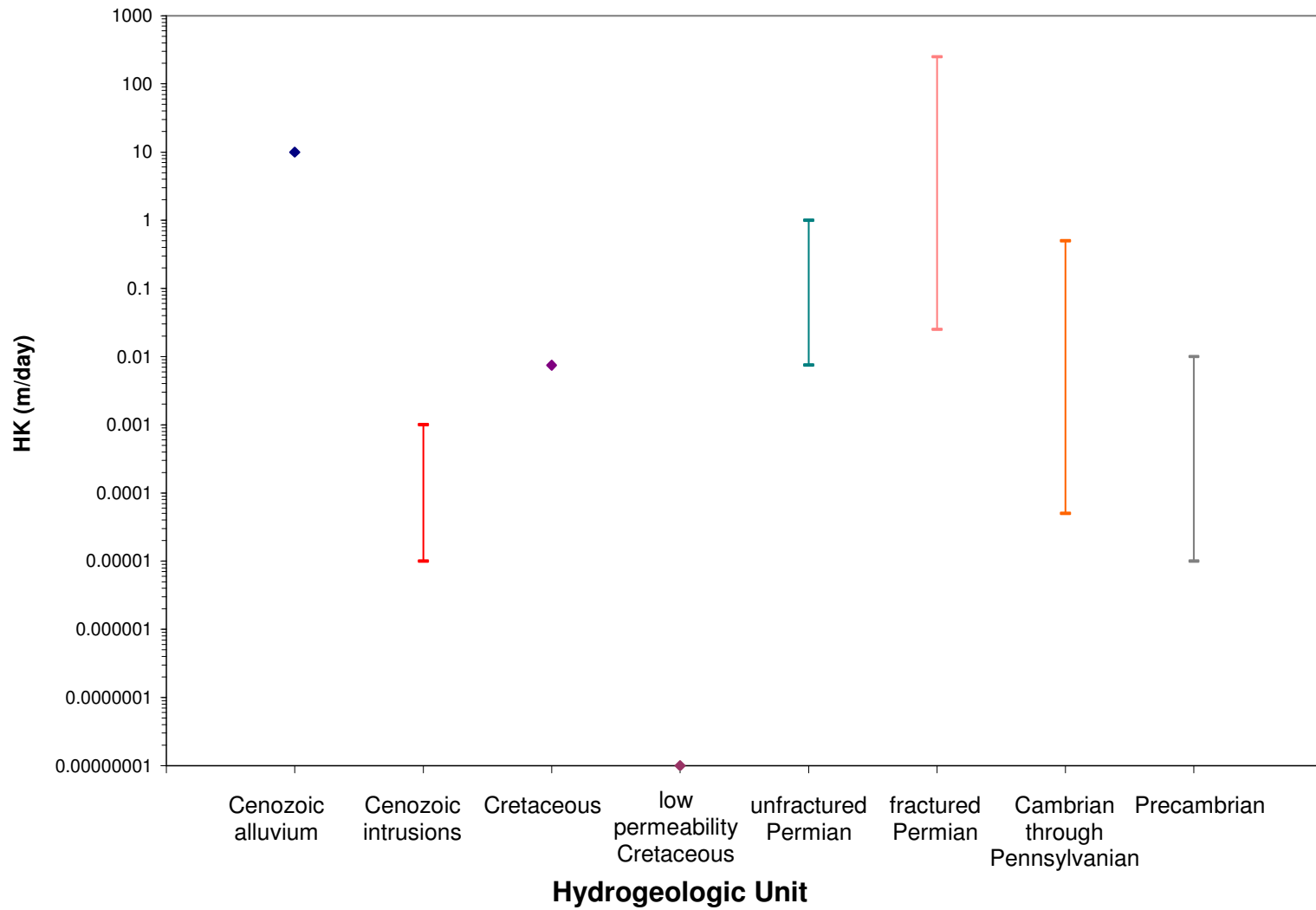
Figure 4.94: Range of horizontal hydraulic conductivity [HK] values for the calibrated water-balance based average recharge scenario model.
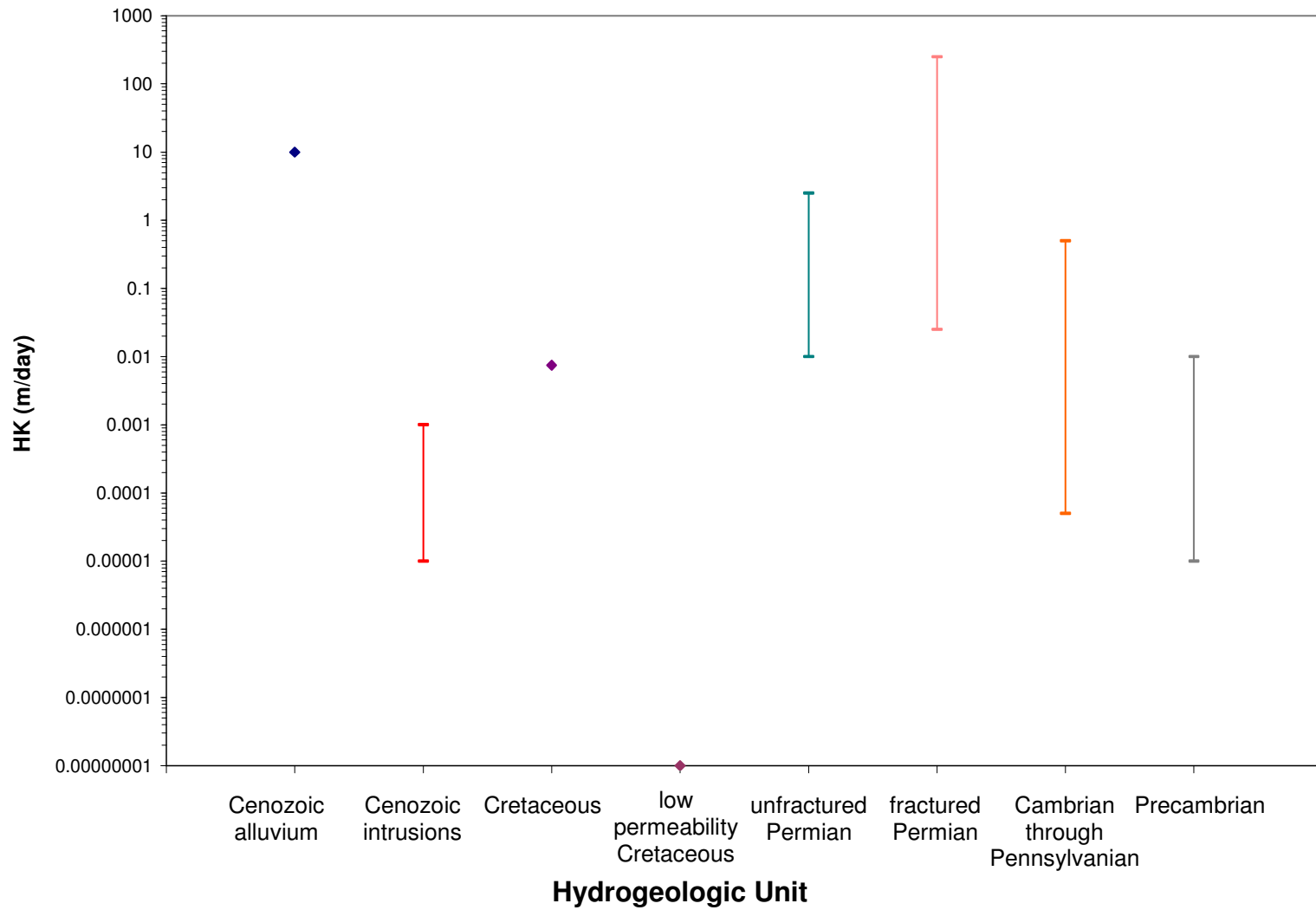
Figure 4.95: Range of horizontal hydraulic conductivity [HK] values for the calibrated water-balance based maximum recharge scenario model.
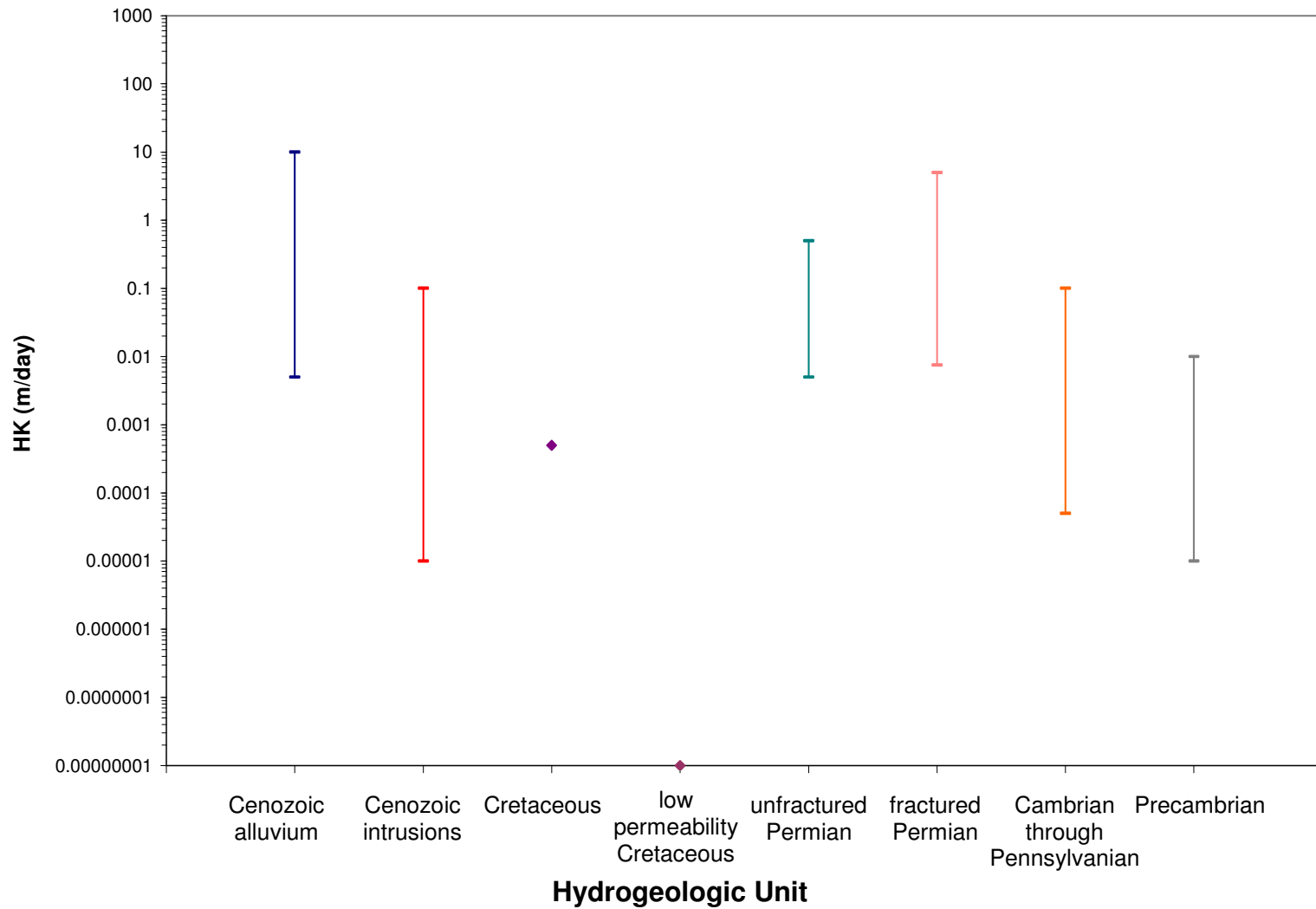
Figure 4.96: Range of horizontal hydraulic conductivity [HK] values for the calibrated elevation-dependent minimum recharge scenario model.
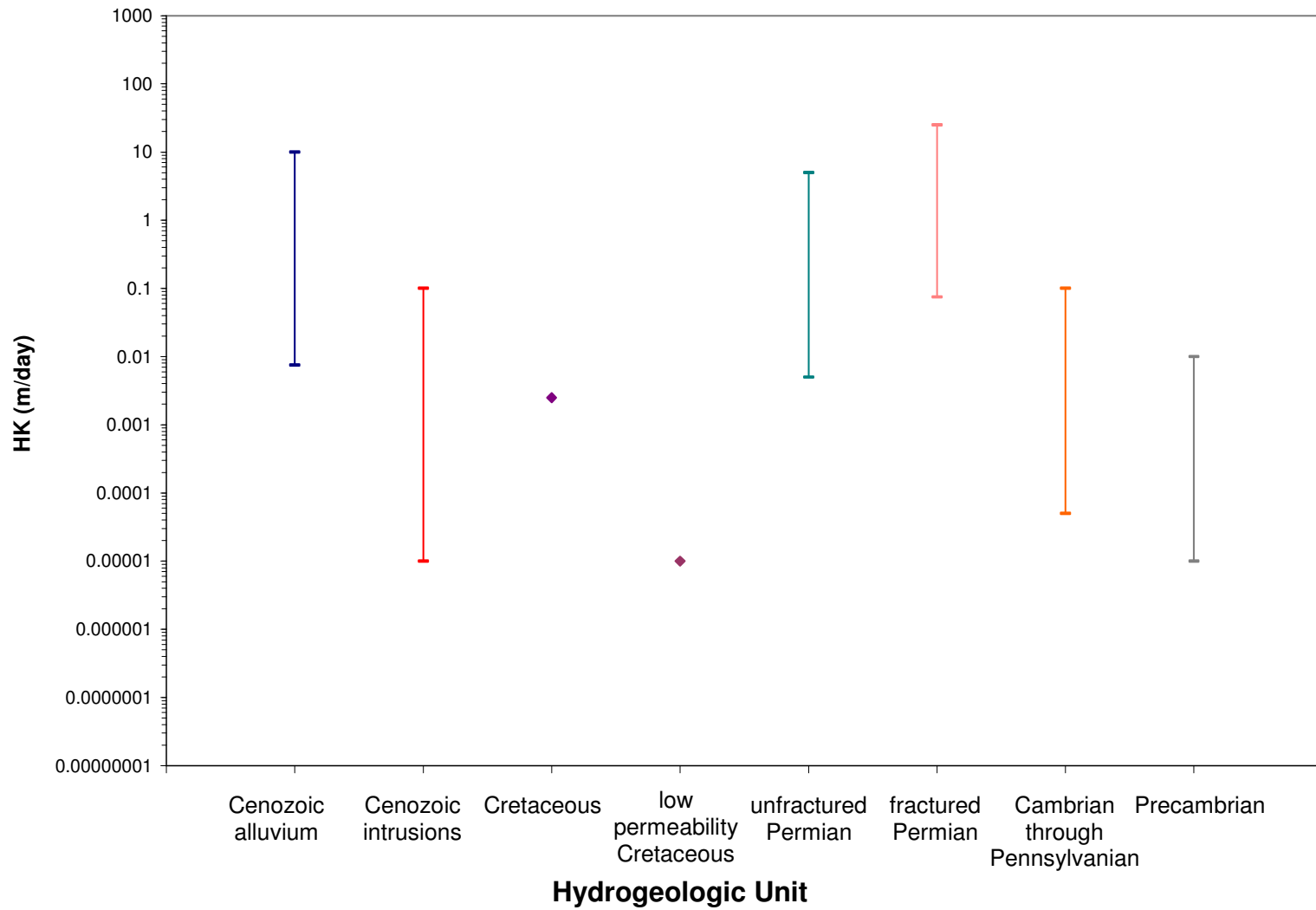
Figure 4.97: Range of horizontal hydraulic conductivity [HK] values for the calibrated elevation-dependent average recharge scenario model.
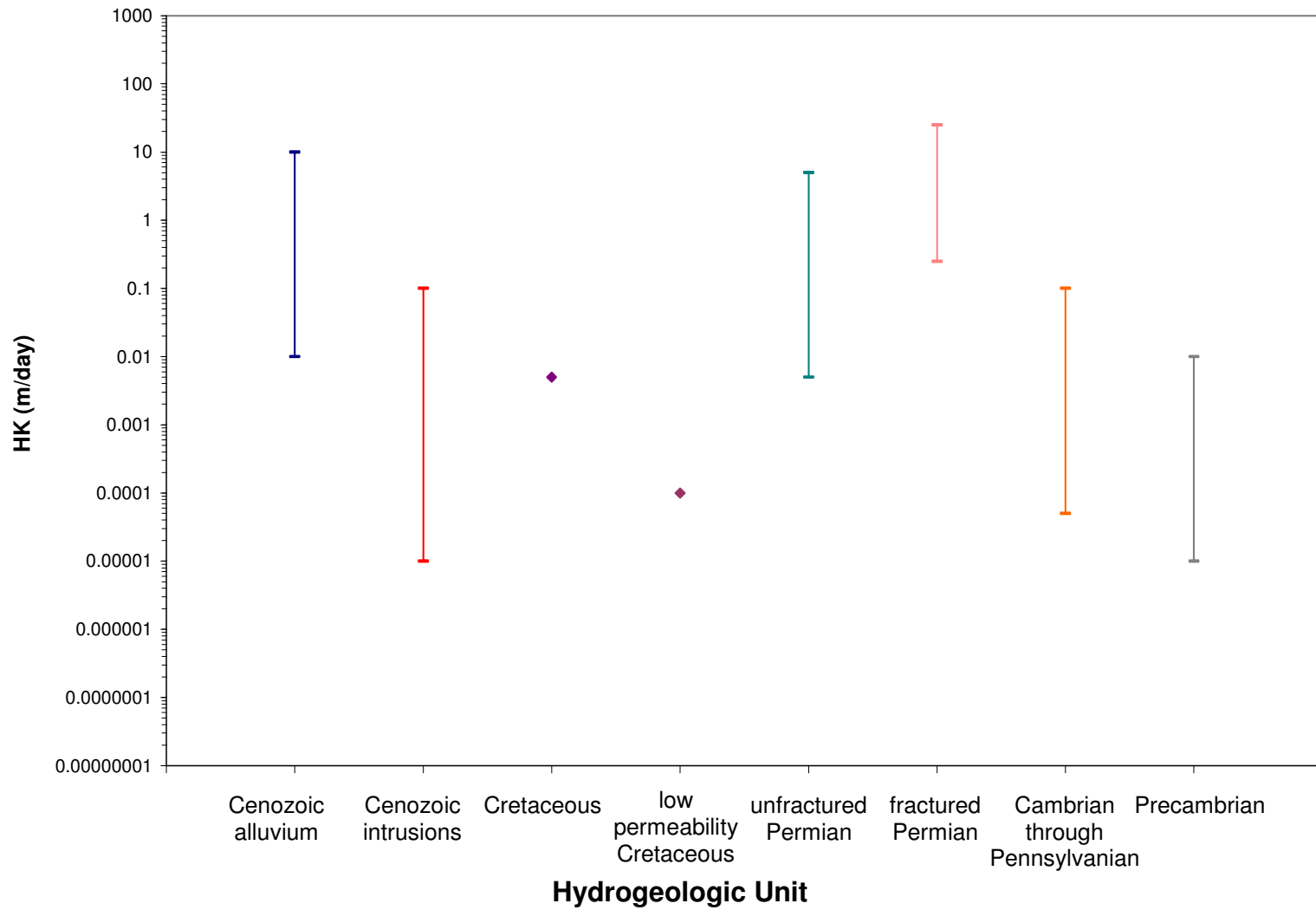
Figure 4.98: Range of horizontal hydraulic conductivity [HK] values for the calibrated elevation-dependent maximum recharge scenario model.
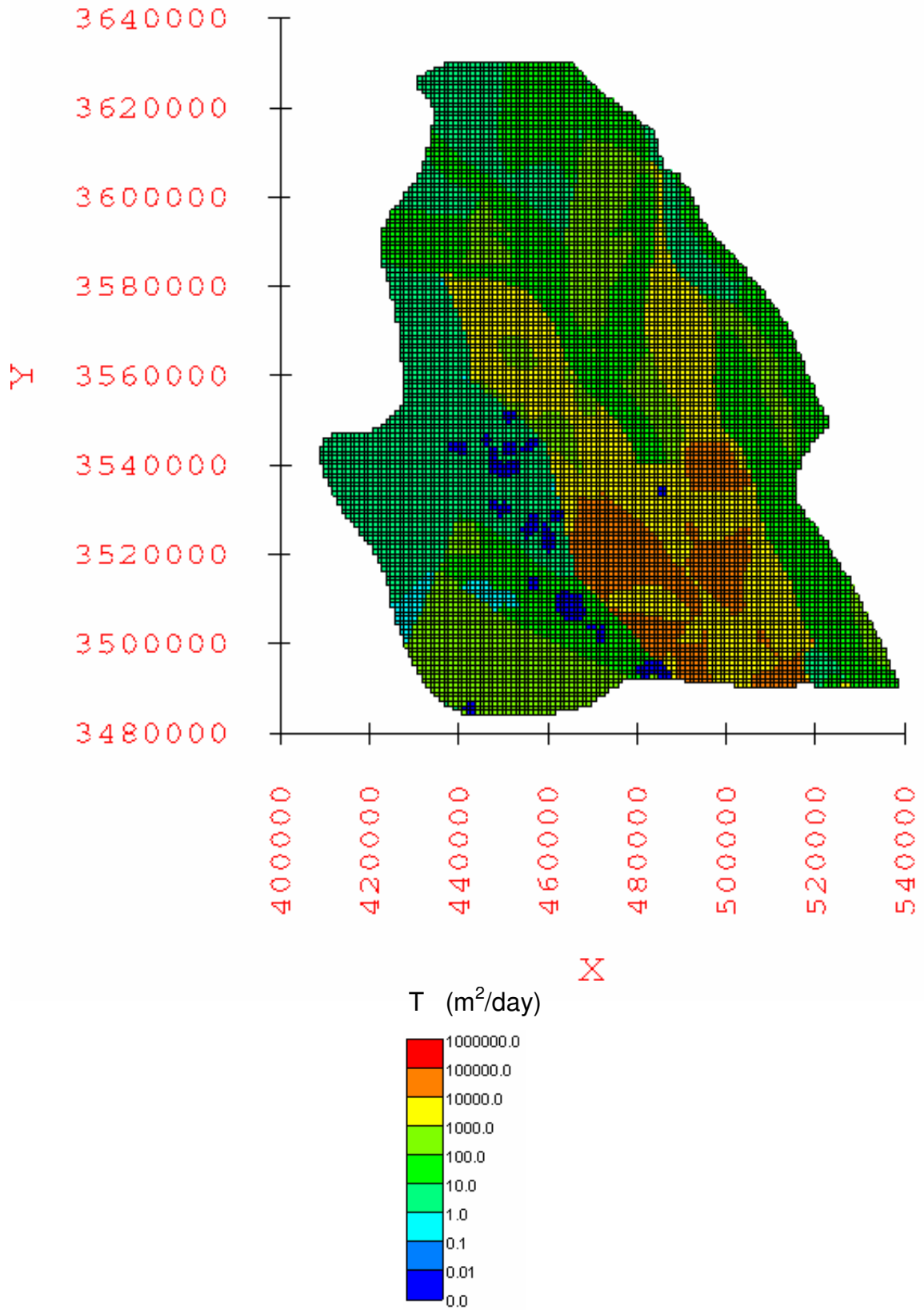
Figure 4.99: Distribution of aquifer transmissivity [T] for the calibrated water-balance based minimum recharge scenario groundwater flow model.
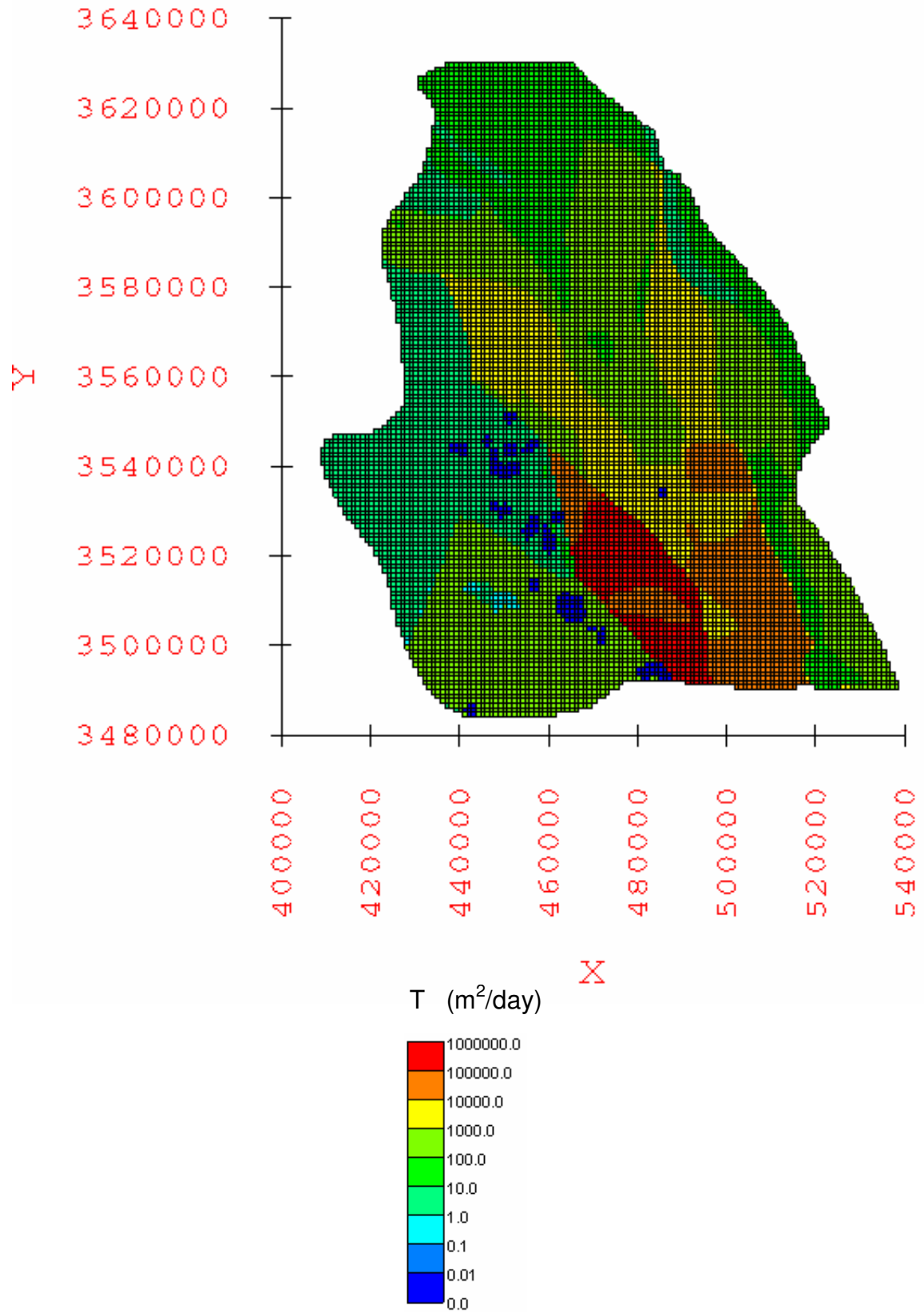
Figure 4.100: Distribution of aquifer transmissivity [T] for the calibrated water-balance based average recharge scenario groundwater flow model.
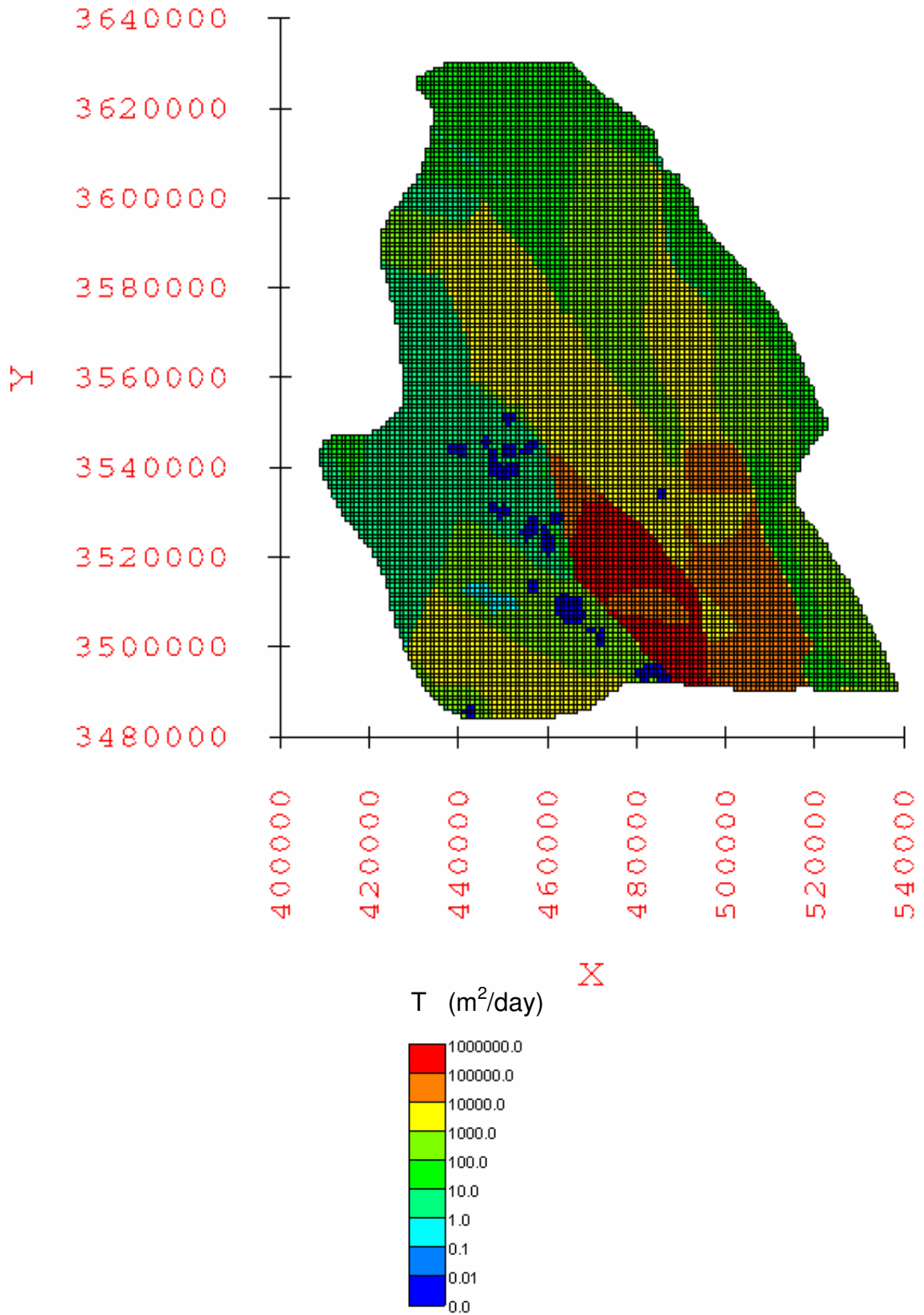
Figure 4.101: Distribution of aquifer transmissivity [T] for the calibrated water-balance based maximum recharge scenario groundwater flow model.
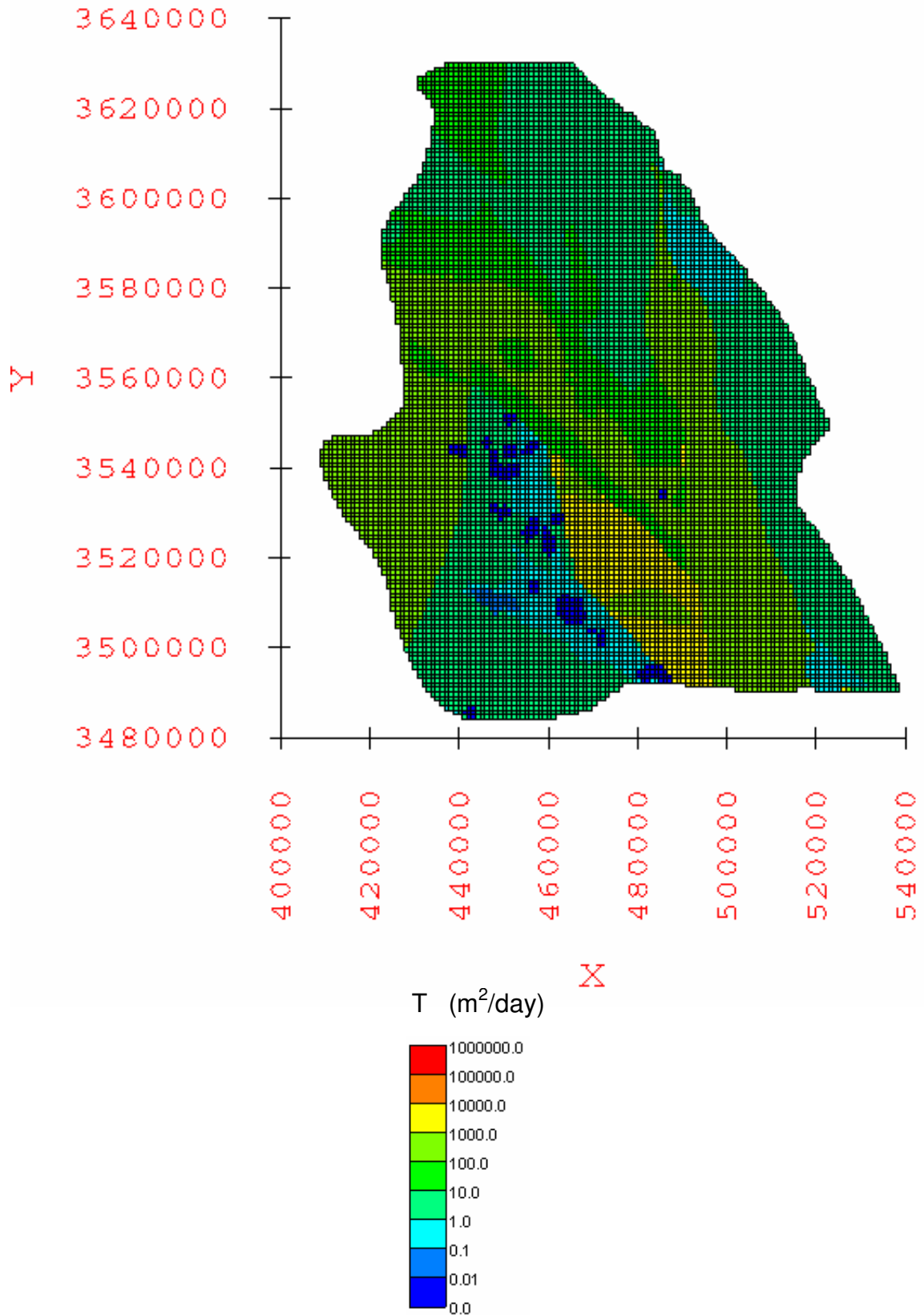
Figure 4.102: Distribution of aquifer transmissivity [T] for the calibrated elevation-dependent minimum recharge scenario groundwater flow model.
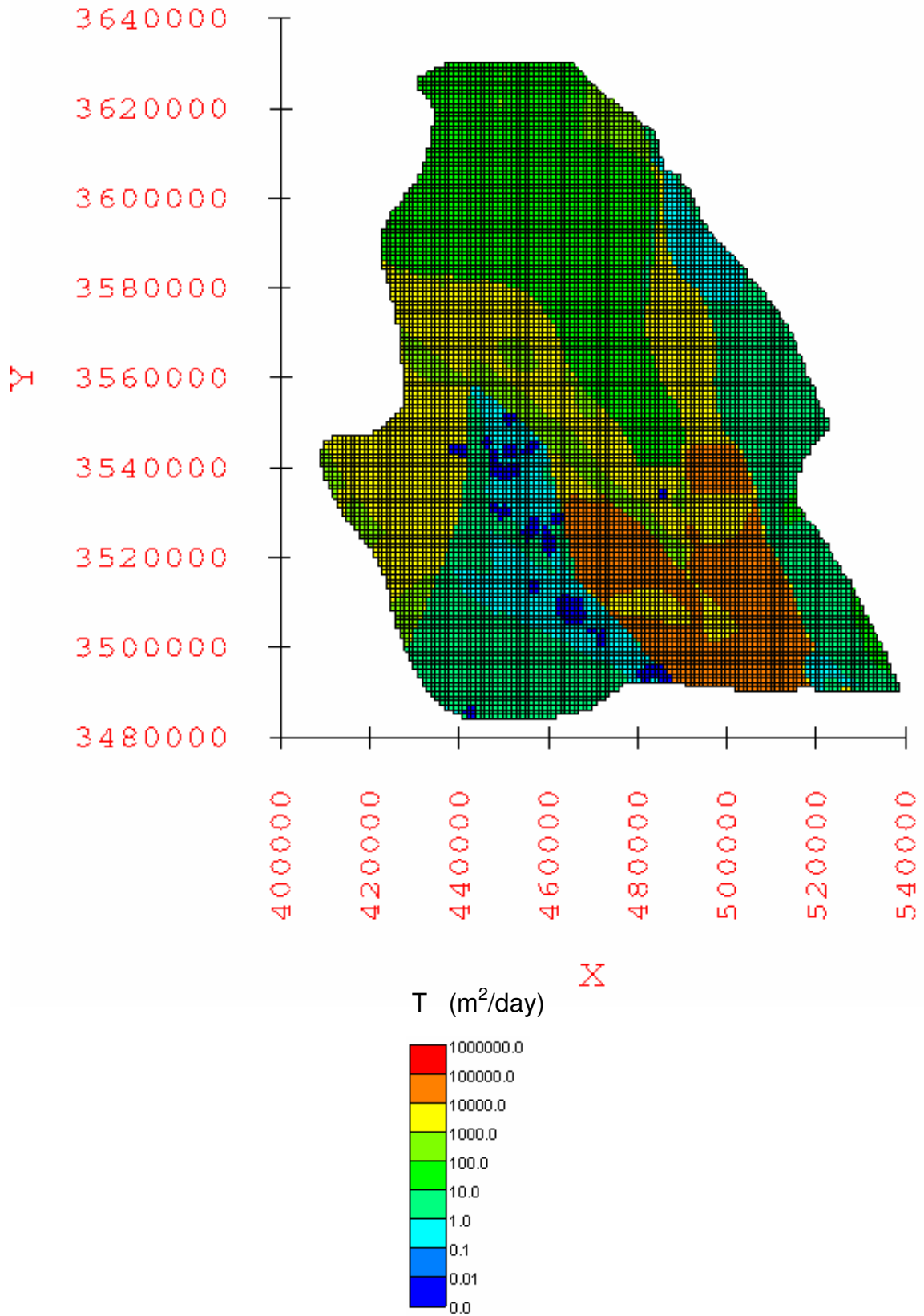
Figure 4.103: Distribution of aquifer transmissivity [T] for the calibrated elevation-
dependent average recharge scenario groundwater flow model.
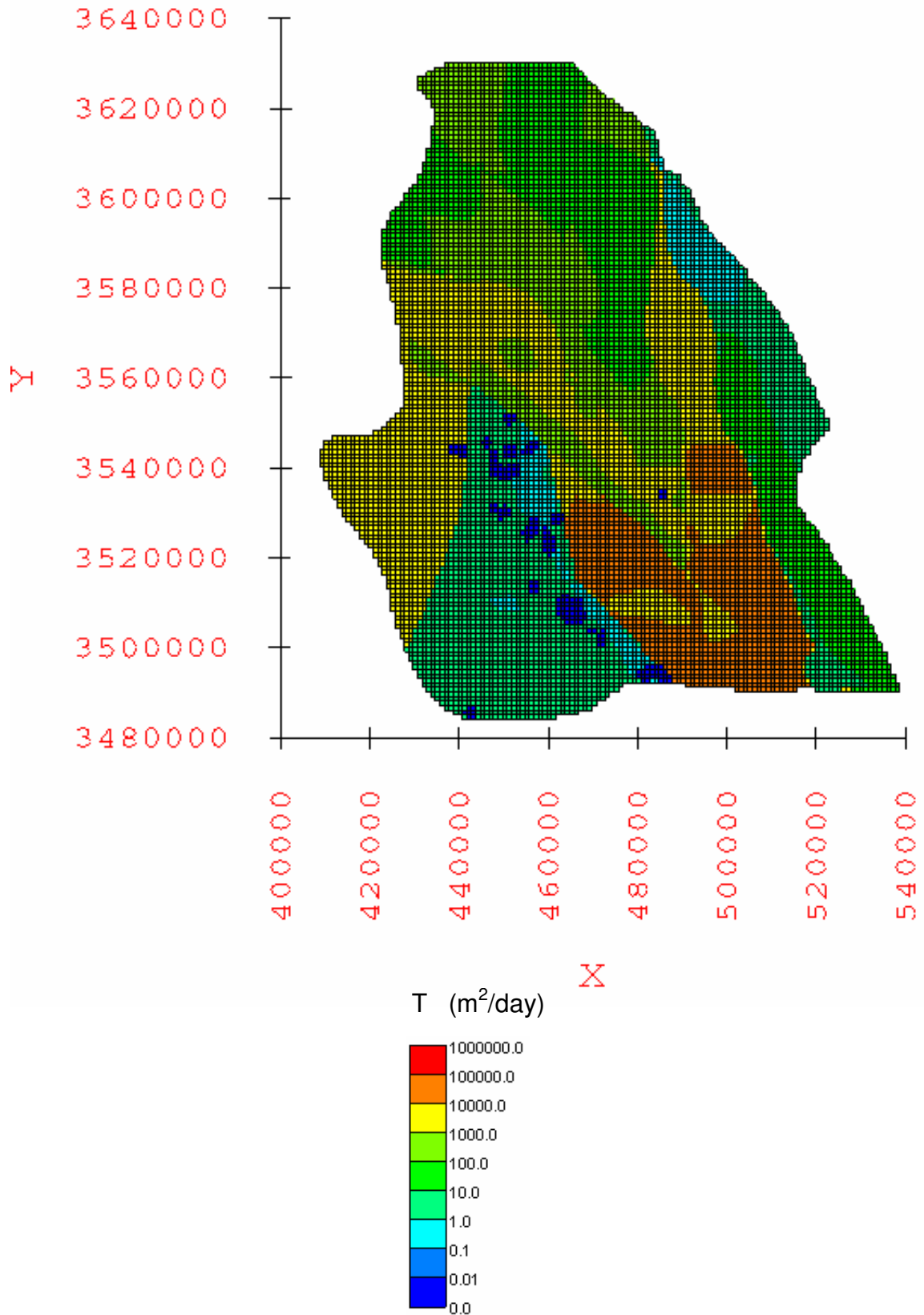
Figure 4.104: Distribution of aquifer transmissivity [T] for the calibrated elevation-dependent maximum recharge scenario groundwater flow model.
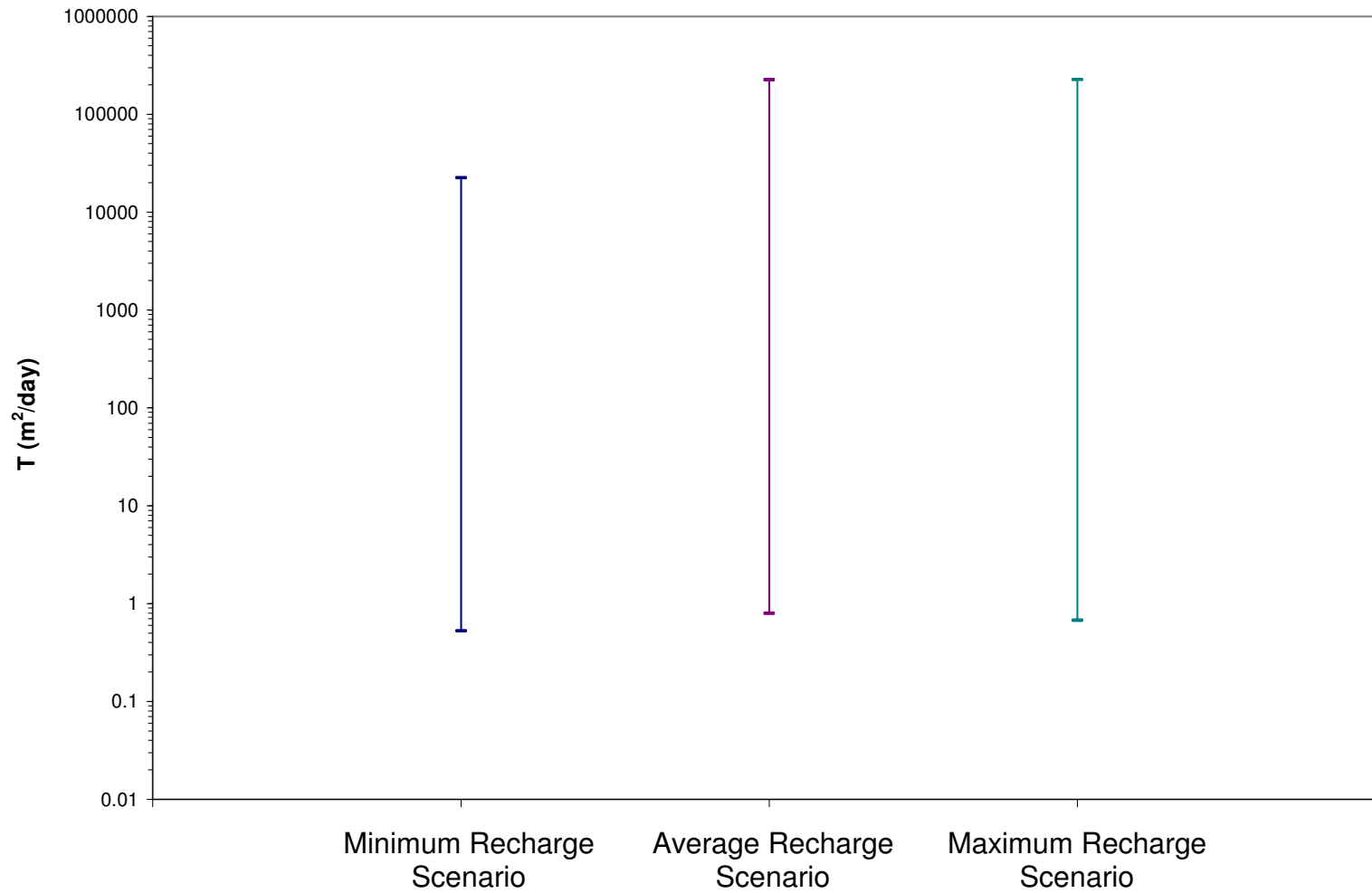
Figure 4.105: Range of transmissivities [T] derived from the calibrated water-balance based minimum, average, and maximum recharge scenario models.
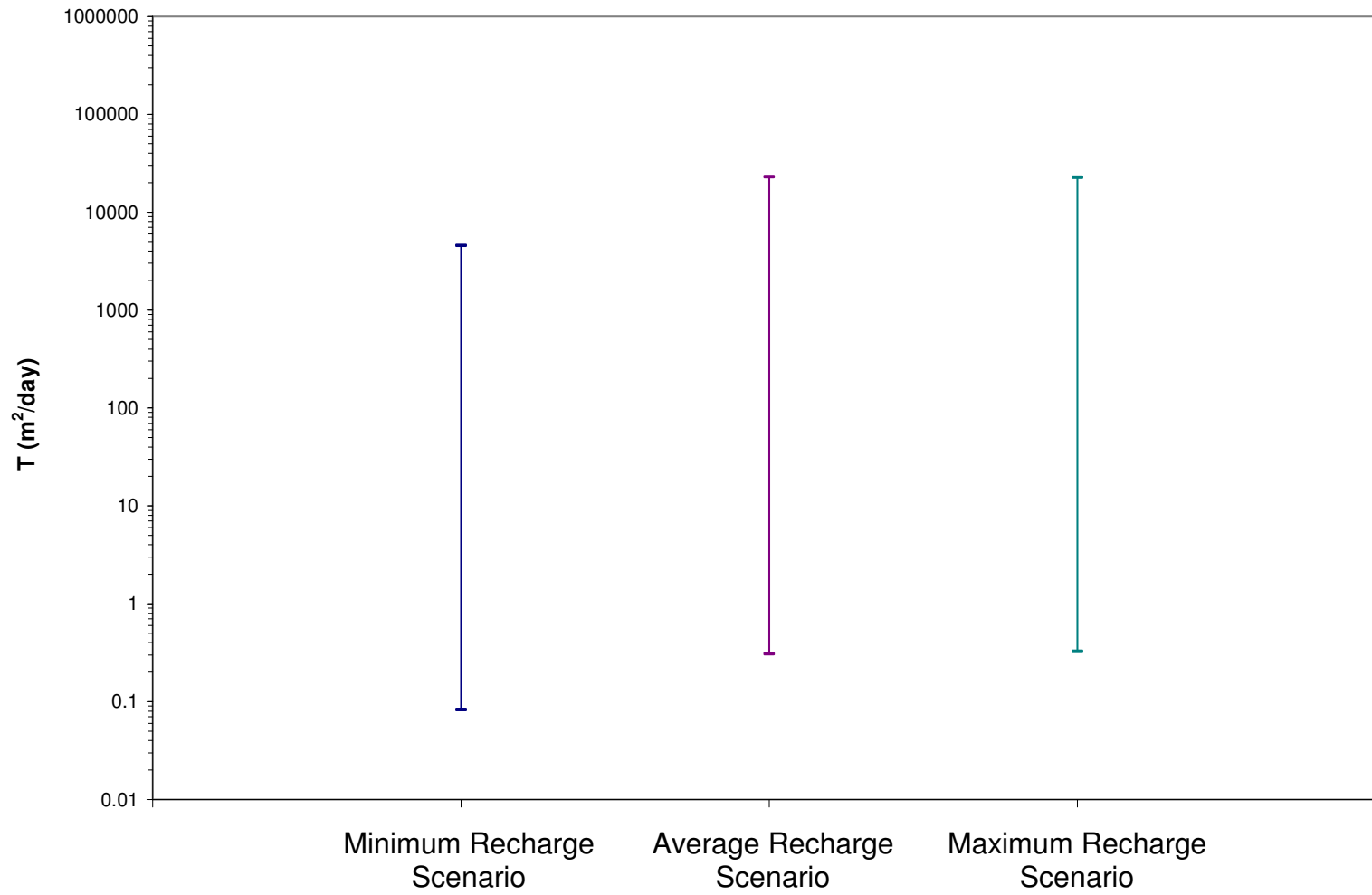
Figure 4.106: Range of transmissivities [T] derived from the calibrated elevation-dependent minimum, average, and maximum recharge scenario models.
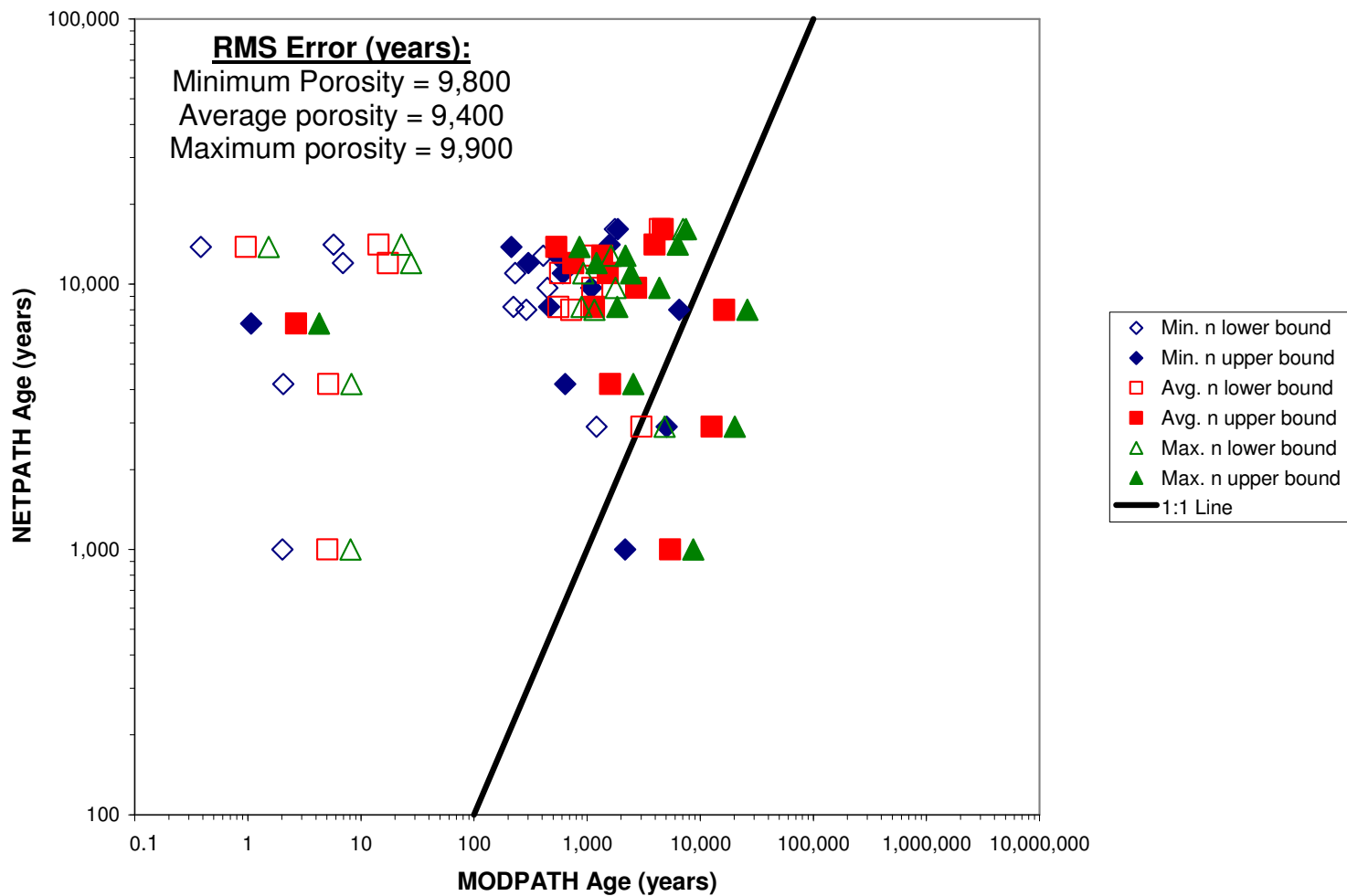
Figure 4.107: NETPATH versus MODPATH ages for the calibrated water-balance based minimum recharge scenario model using minimum, average, and maximum porosities.
Vertical and horizontal axes are logarithmic scale.
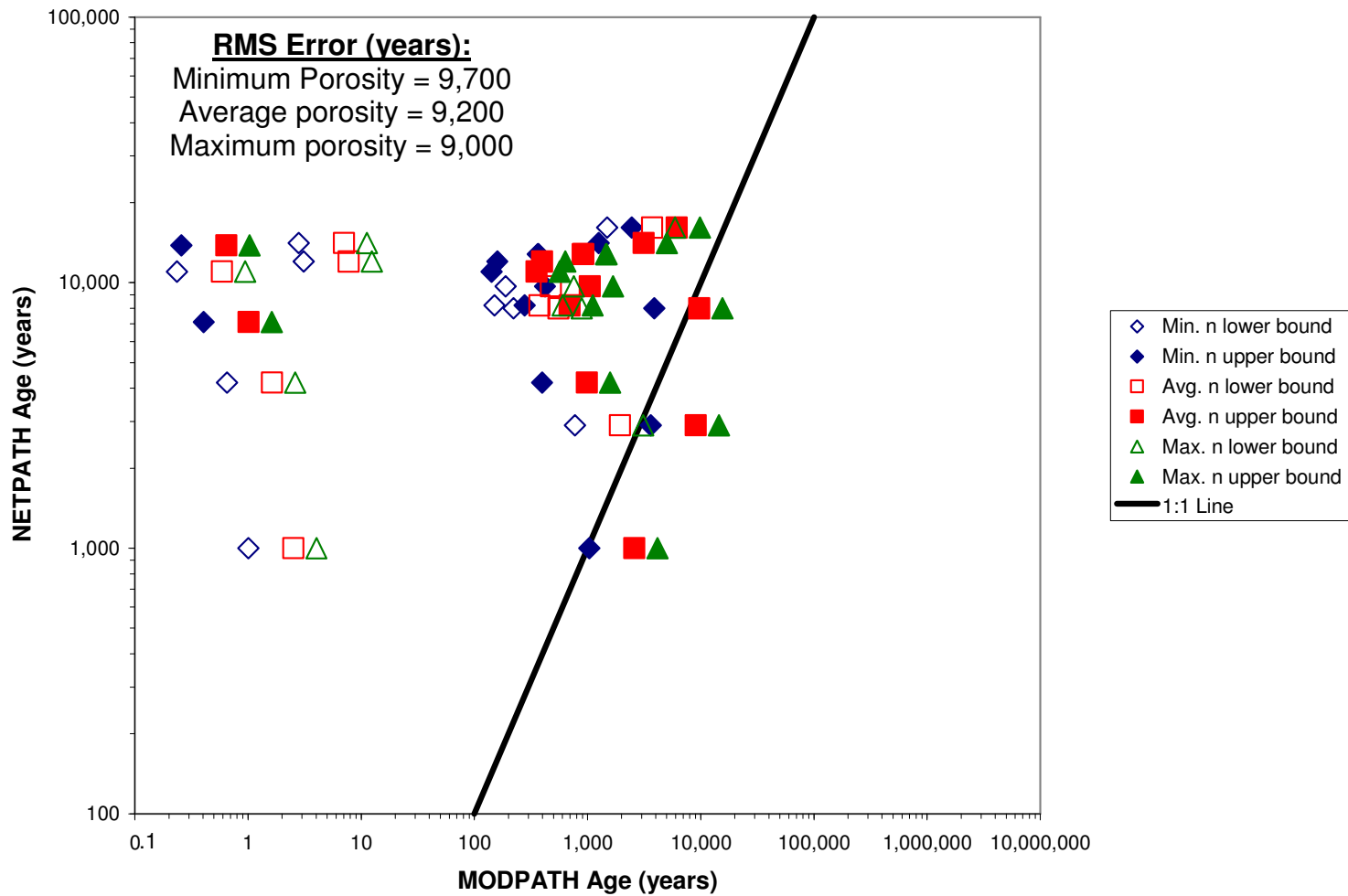
Figure 4.108: NETPATH versus MODPATH ages for the calibrated water-balance based average recharge scenario model using minimum, average, and maximum porosities.

Vertical and horizontal axes are logarithmic scale.
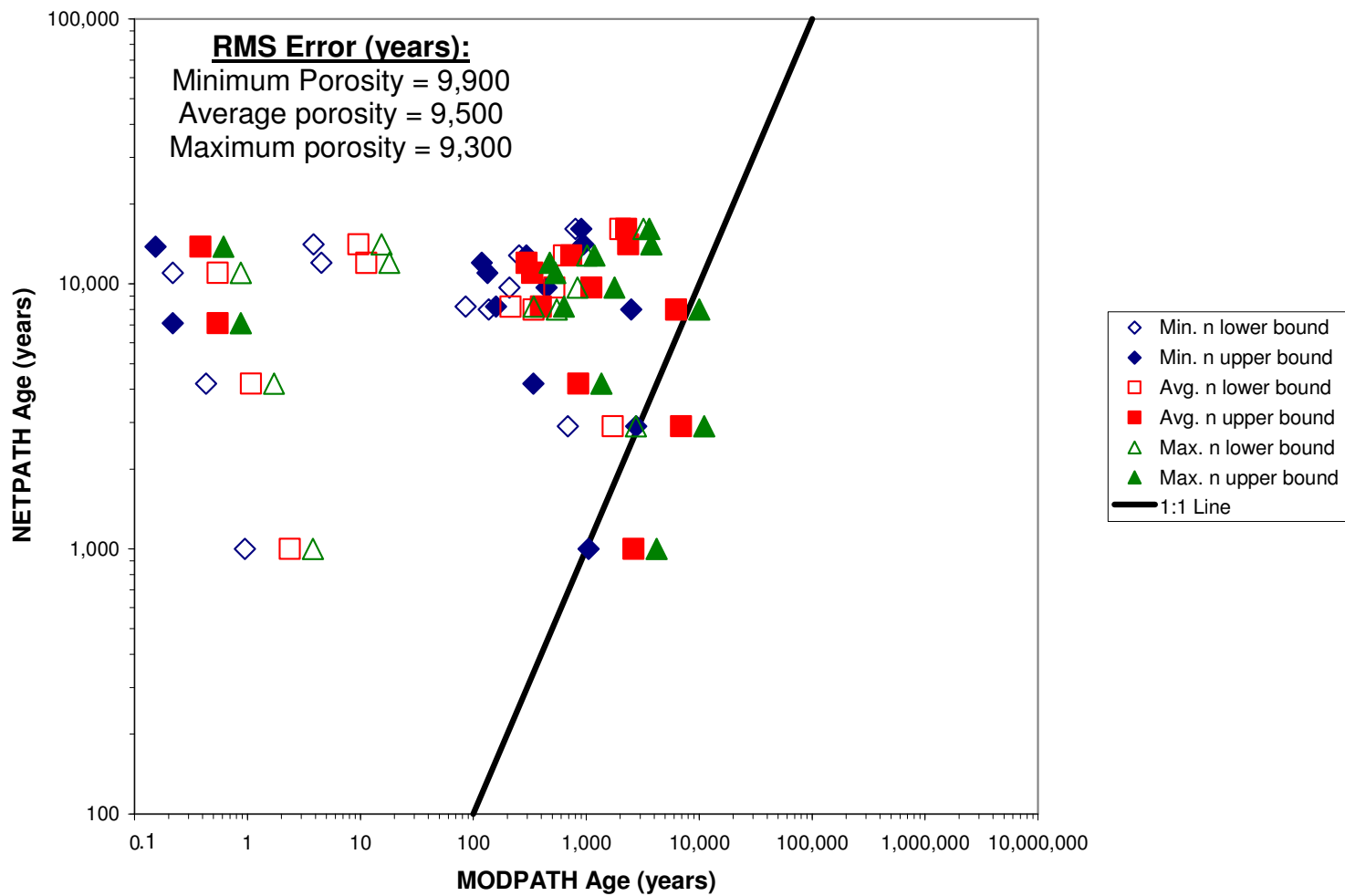
Figure 4.109: NETPATH versus MODPATH ages for the calibrated water-balance based maximum recharge scenario model using minimum, average, and maximum porosities.
Vertical and horizontal axes are logarithmic scale.
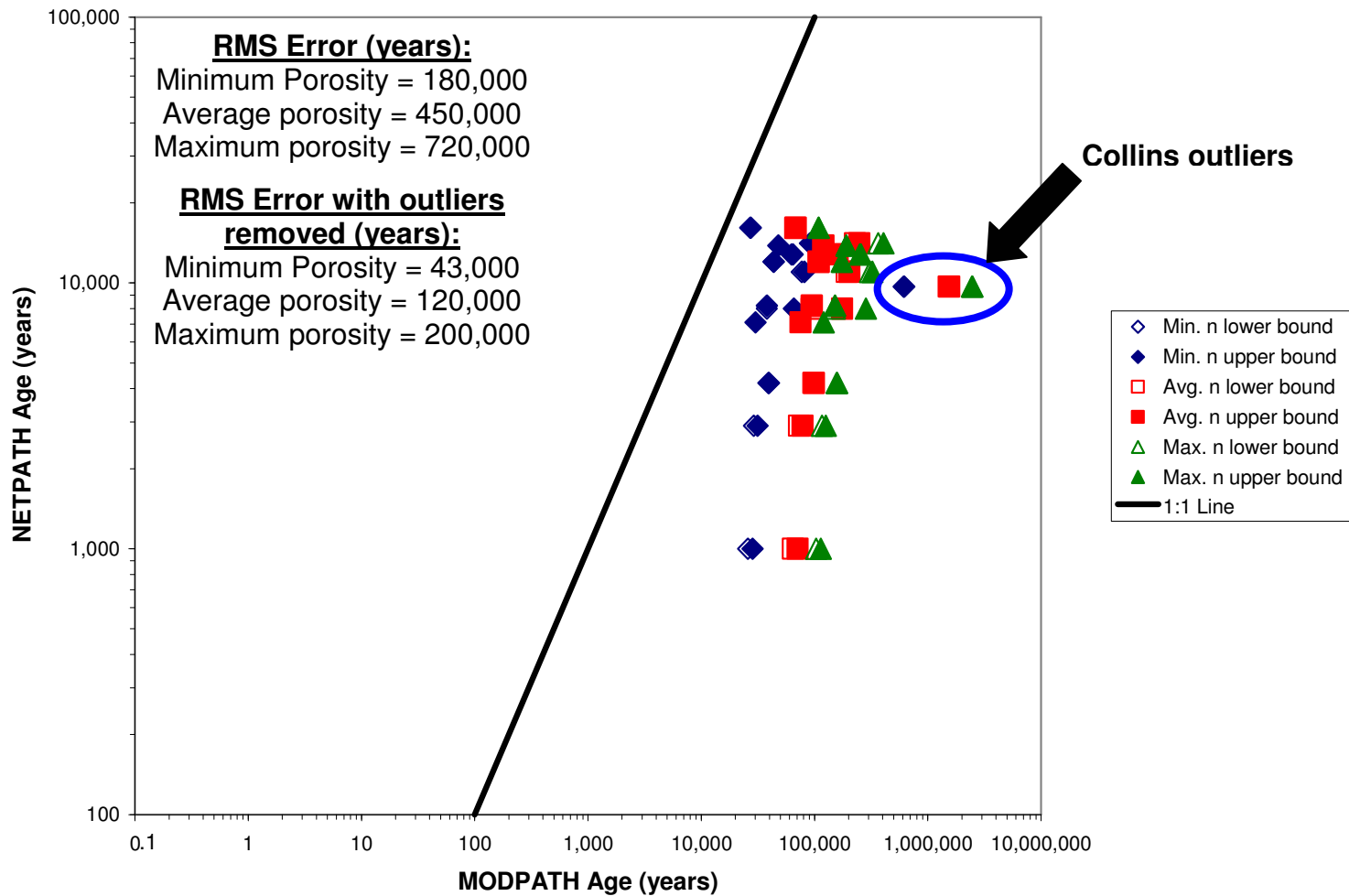
Figure 4.110: NETPATH versus MODPATH ages for the calibrated elevation-dependent minimum recharge scenario model using minimum, average, and maximum porosities.
Vertical and horizontal axes are logarithmic scale.
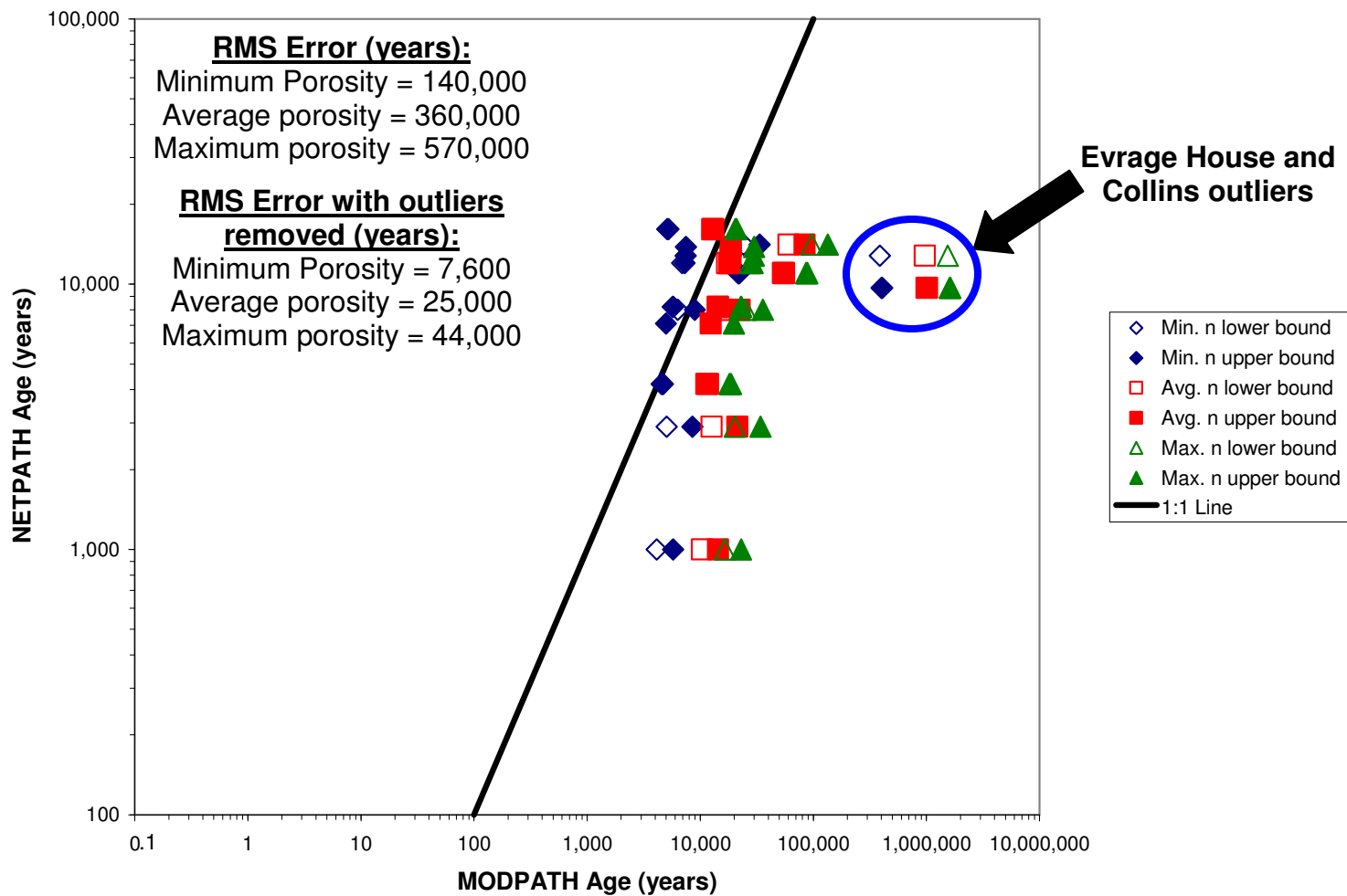
Figure 4.111: NETPATH versus MODPATH ages for the calibrated elevation-dependent average recharge scenario model using minimum, average, and maximum porosities.
Vertical and horizontal axes are logarithmic scale.
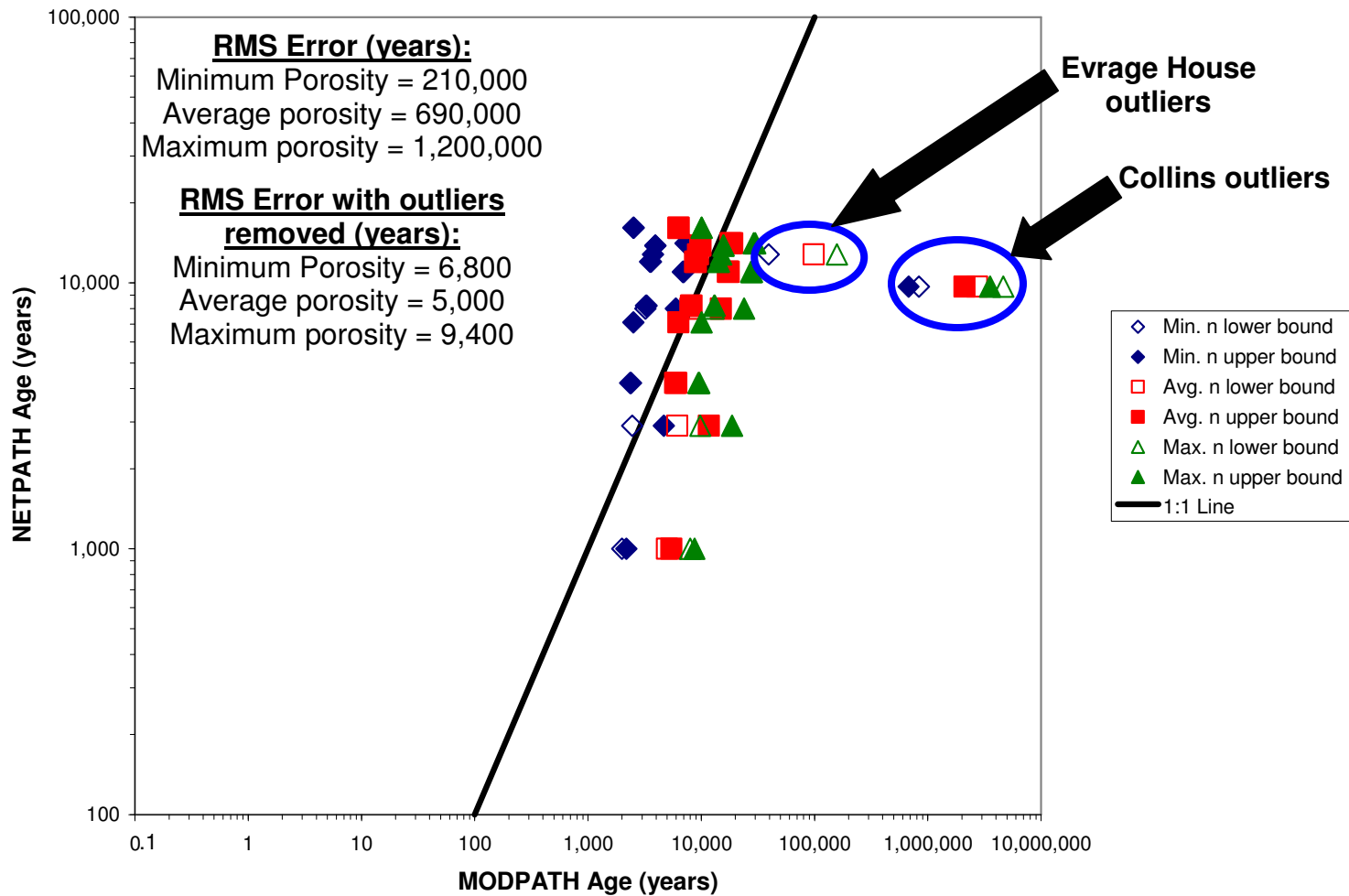
Figure 4.112: NETPATH versus MODPATH ages for the calibrated elevation-dependent maximum recharge scenario model using minimum, average, and maximum porosities.
Vertical and horizontal axes are logarithmic scale.
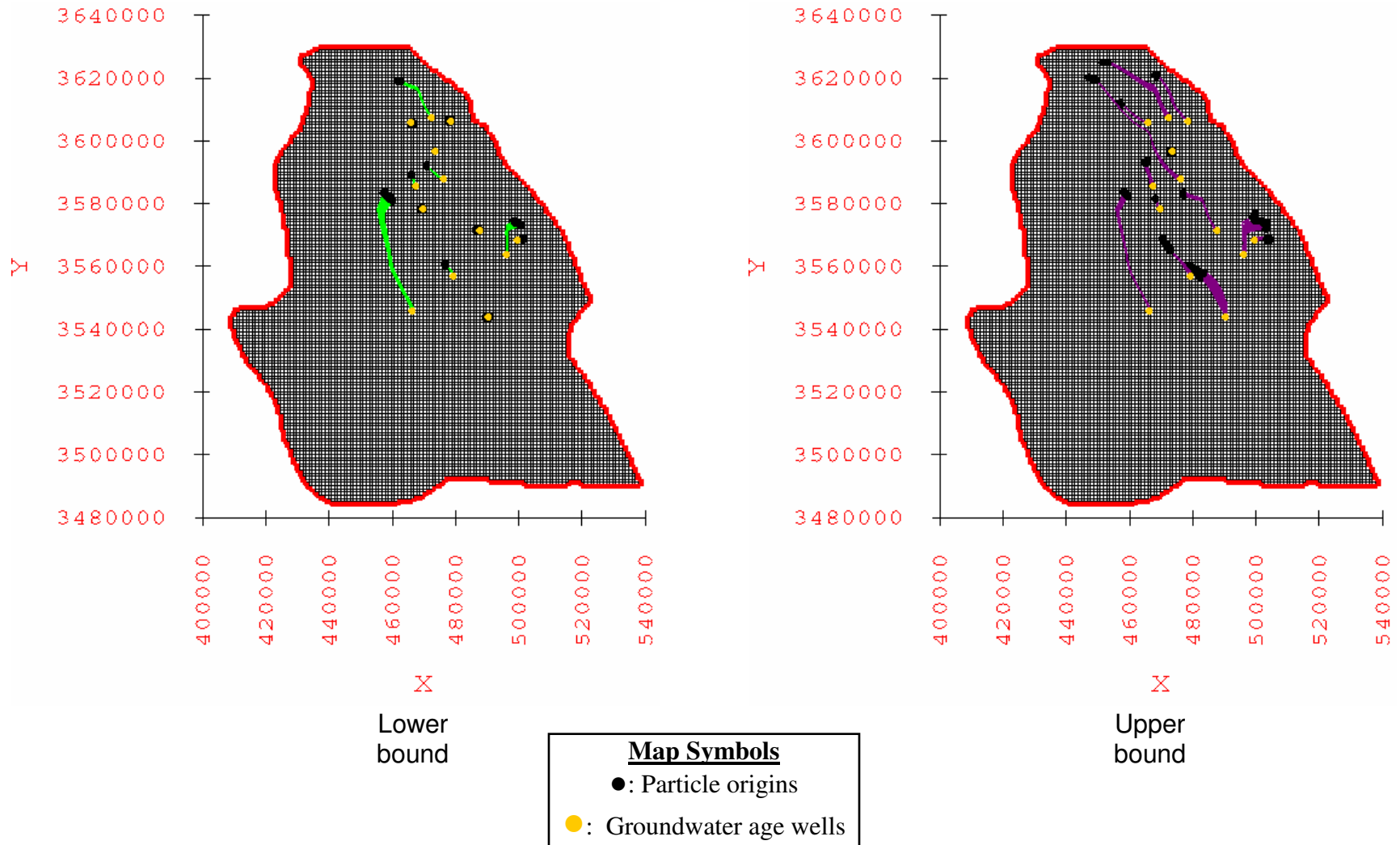
Figure 4.113: MODPATH pathlines and origins of particles for the water-balance based minimum recharge scenario using average porosity values.
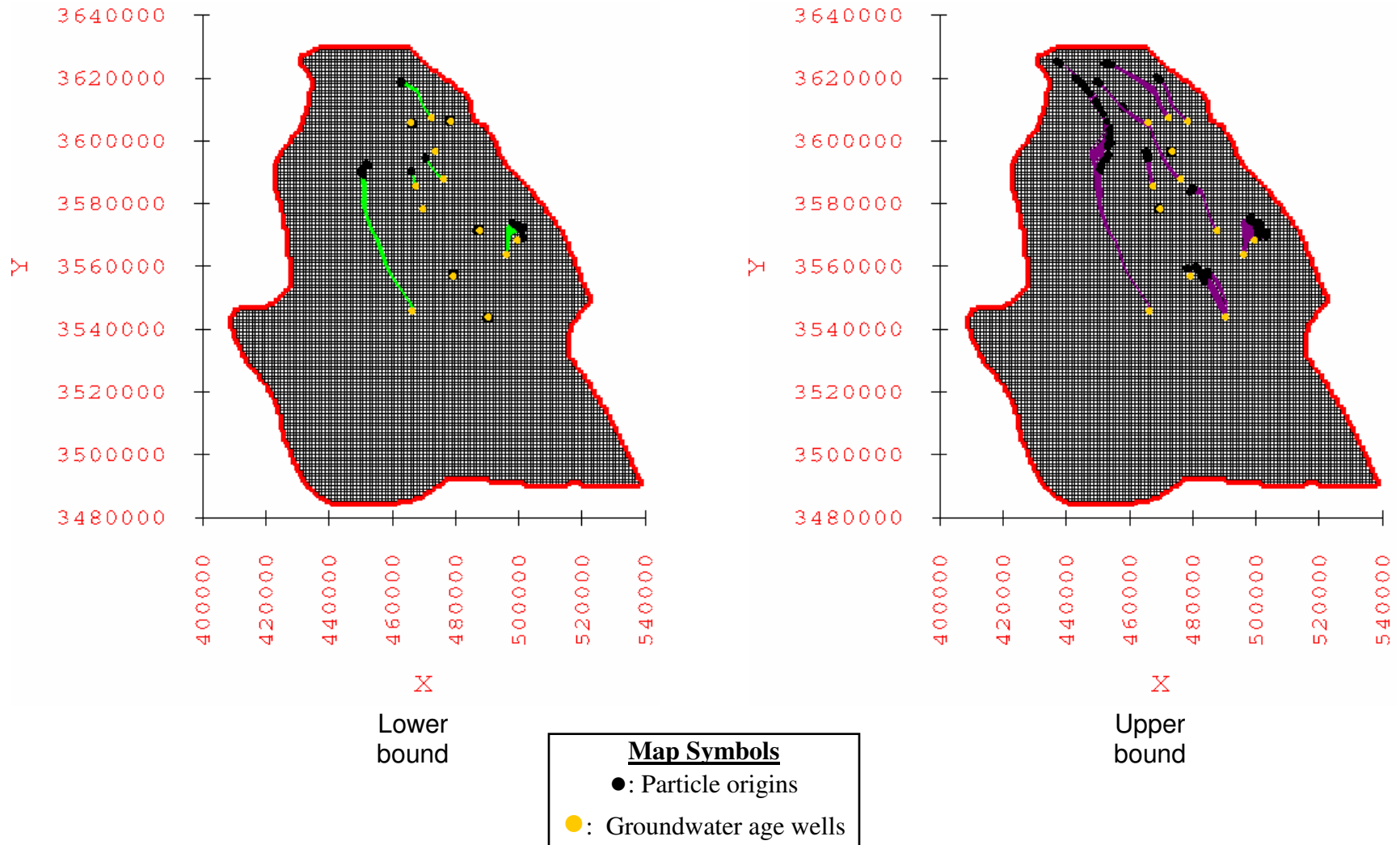
Figure 4.114: MODPATH pathlines and origins of particles for the water-balance based average recharge scenario using average porosity values.
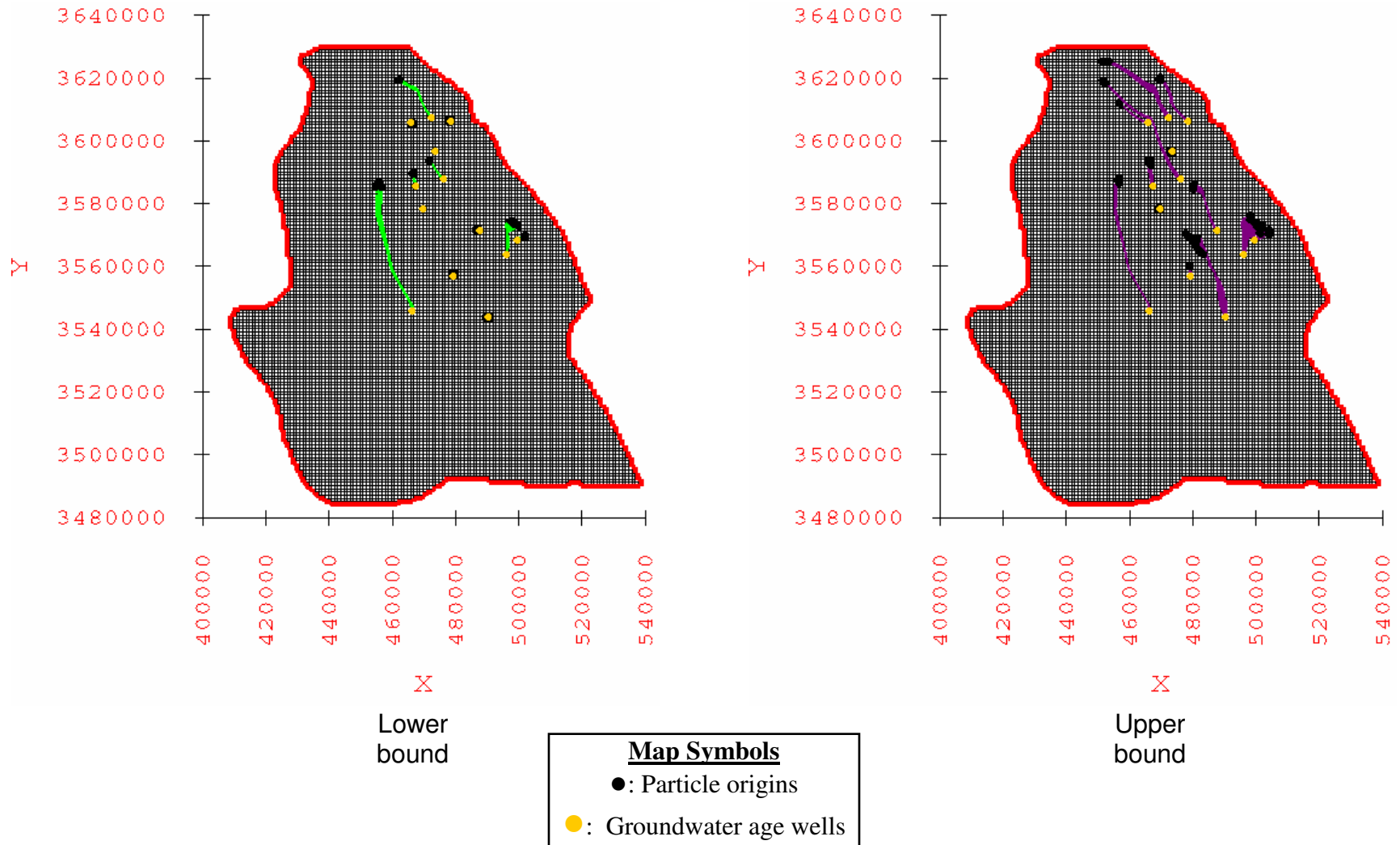
Figure 4.115: MODPATH pathlines and origins of particles for the water-balance based maximum recharge scenario using average porosity values.
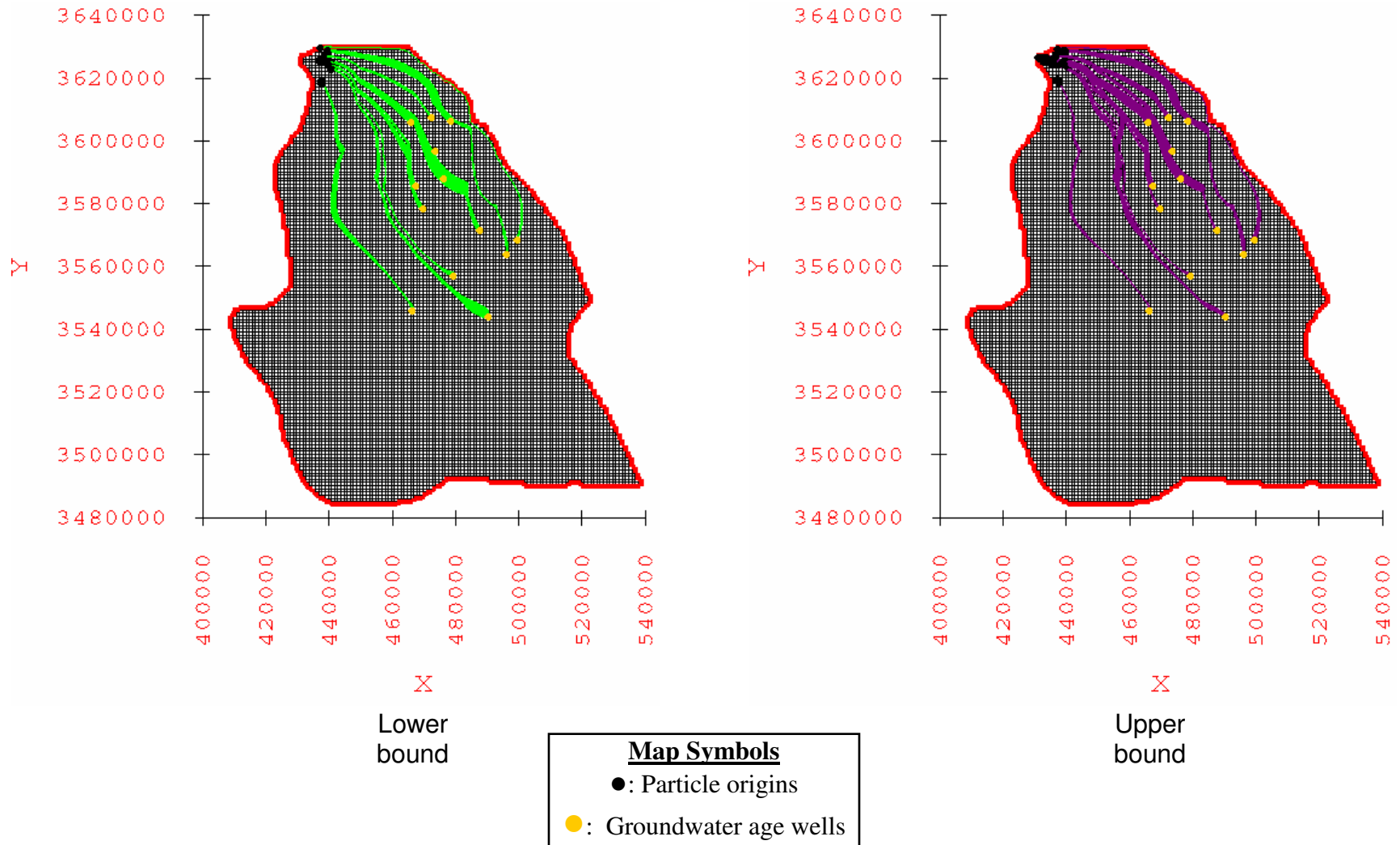
Figure 4.116: MODPATH pathlines and origins of particles for the elevation-dependent minimum recharge scenario using average porosity values.
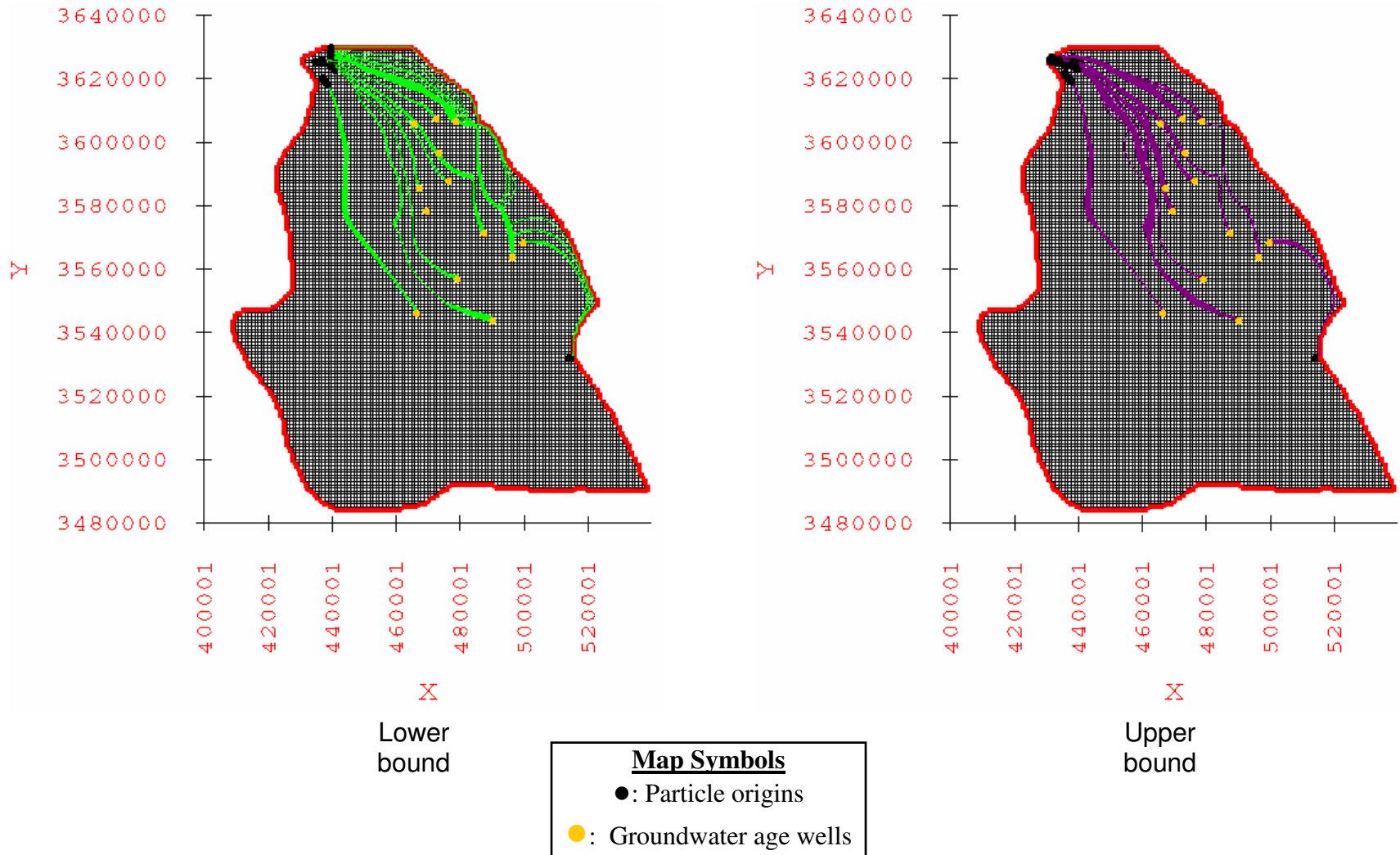
Figure 4.117: MODPATH pathlines and origins of particles for the elevation-dependent average recharge scenario using average porosity values.
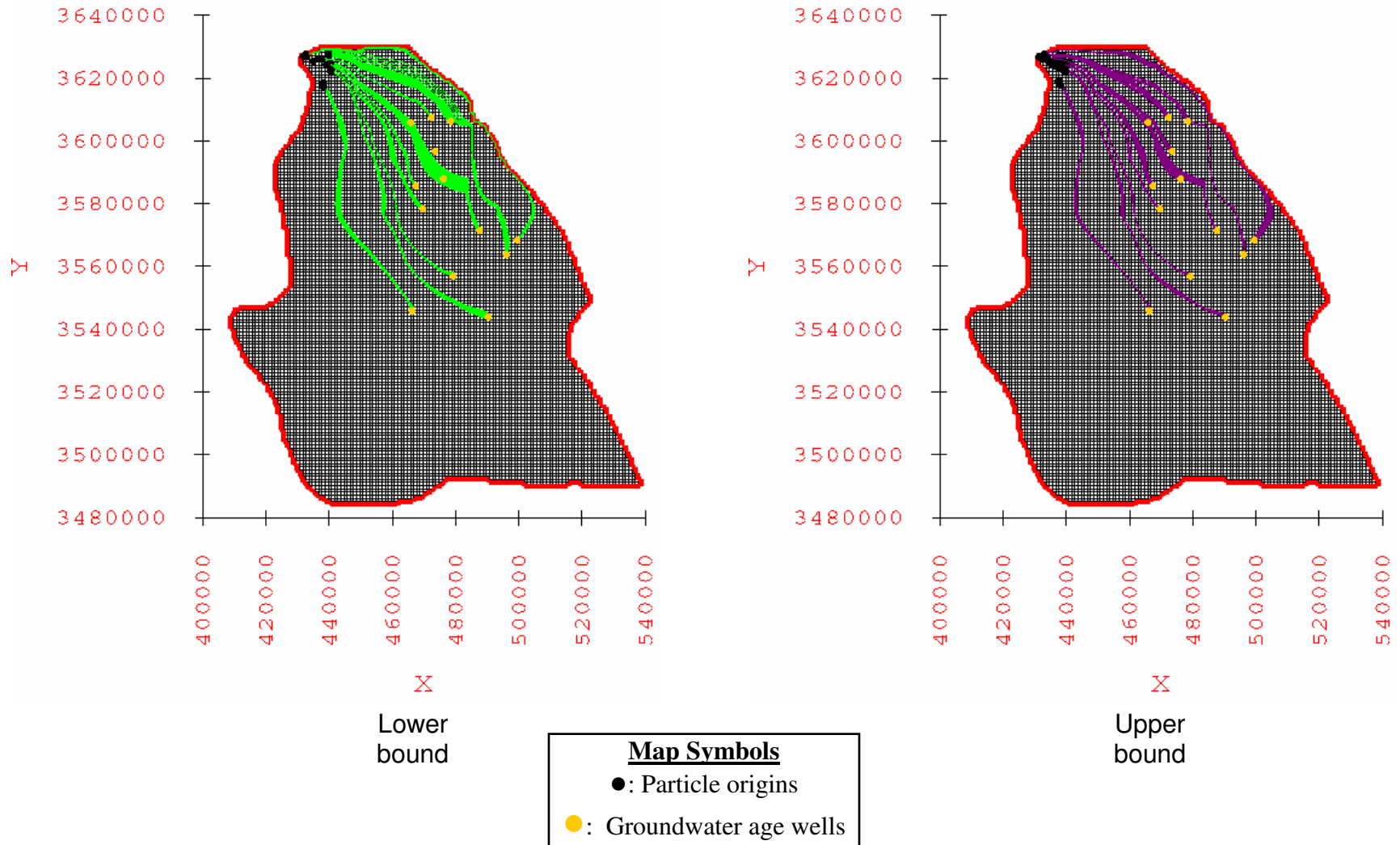
Figure 4.118: MODPATH pathlines and origins of particles for the elevation-dependent maximum recharge scenario using average porosity values.
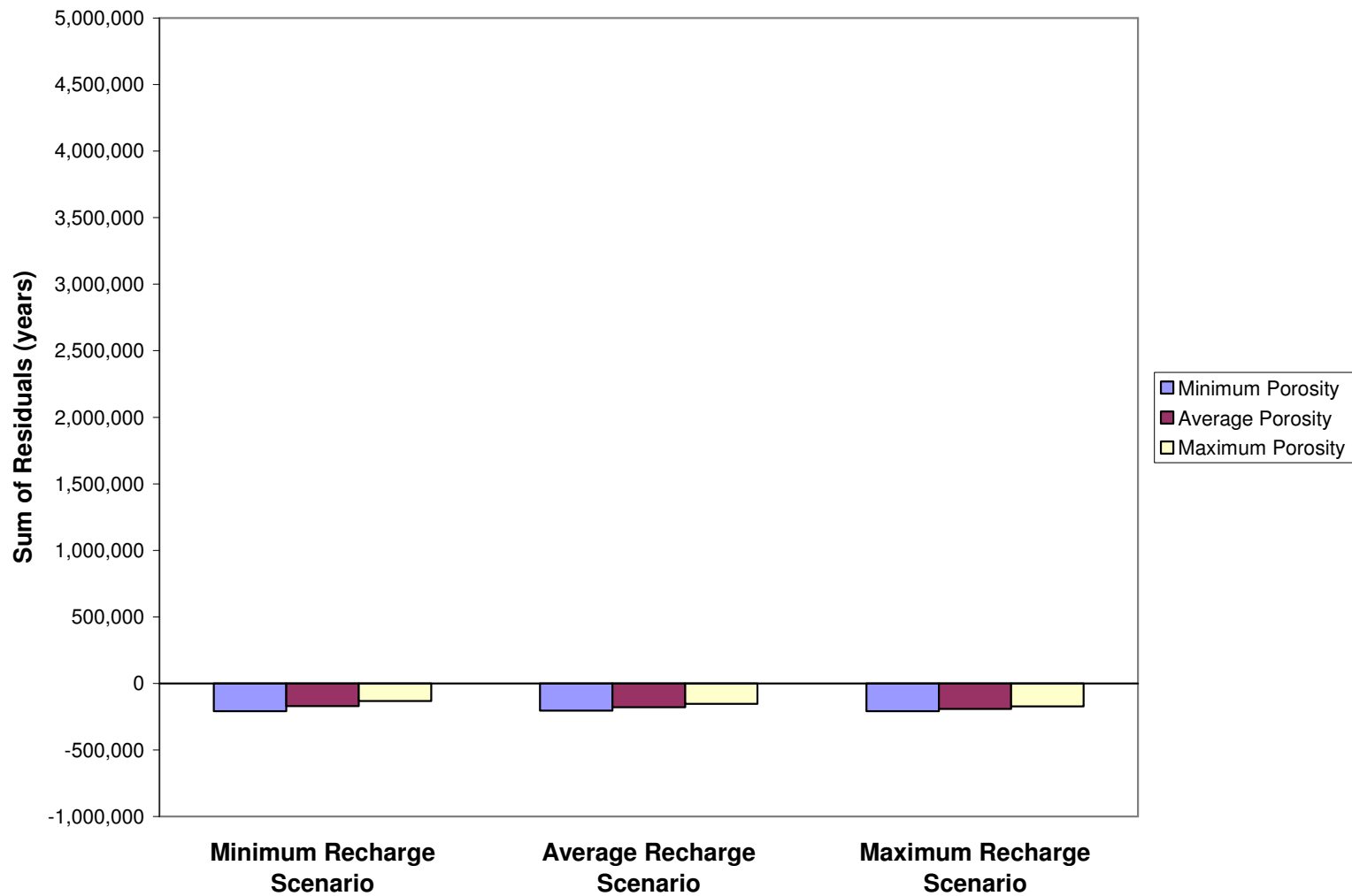
Figure 4.119: Sum of the residuals between MODPATH and NETPATH ages for the water-balance based minimum, average, and maximum recharge scenarios using minimum, average, and maximum porosities.
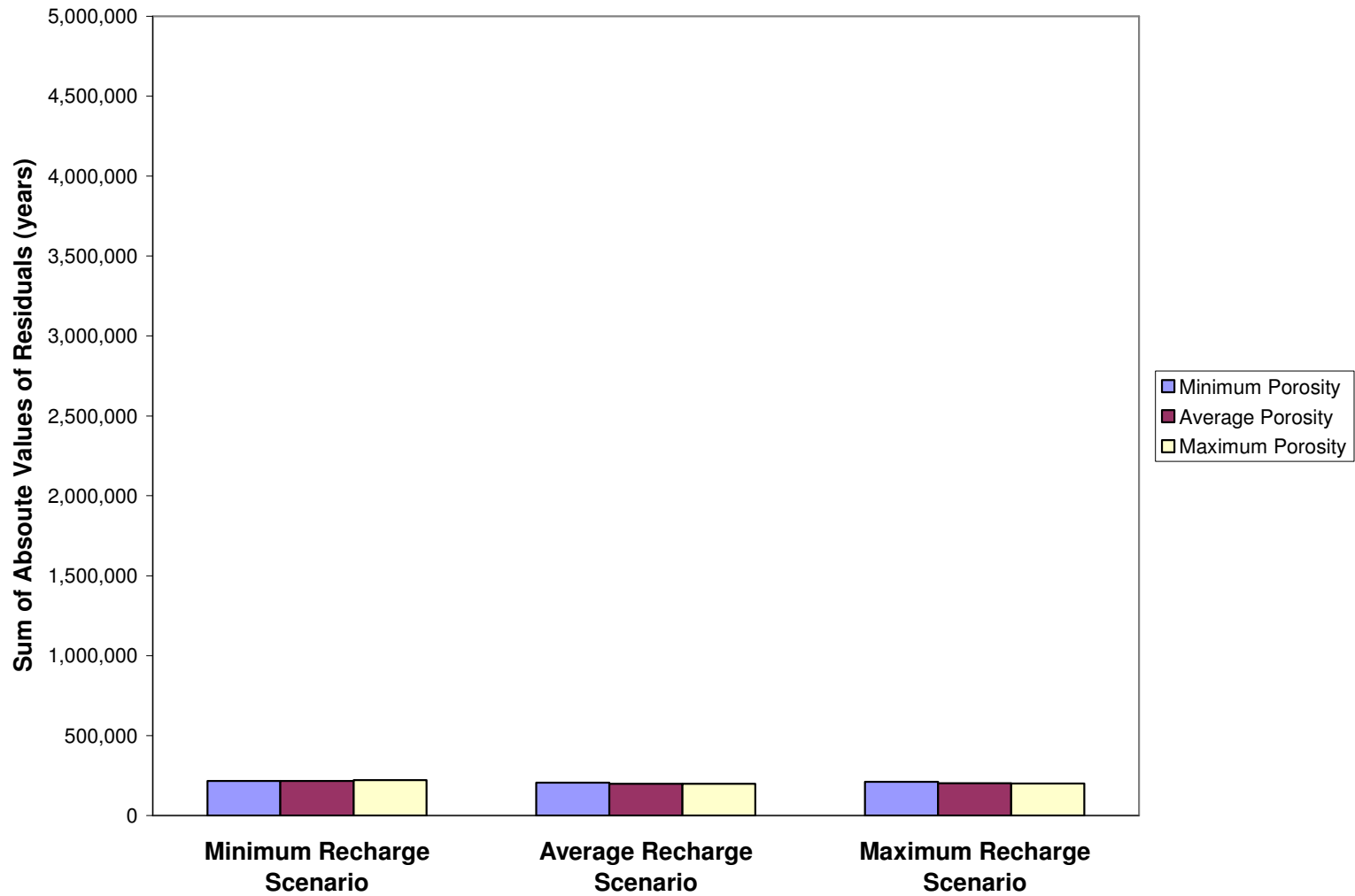
Figure 4.120: Sum of the absolute values of the residuals between MODPATH and NETPATH ages for the water-balance based minimum, average, and maximum recharge scenarios using minimum, average, and maximum porosities.
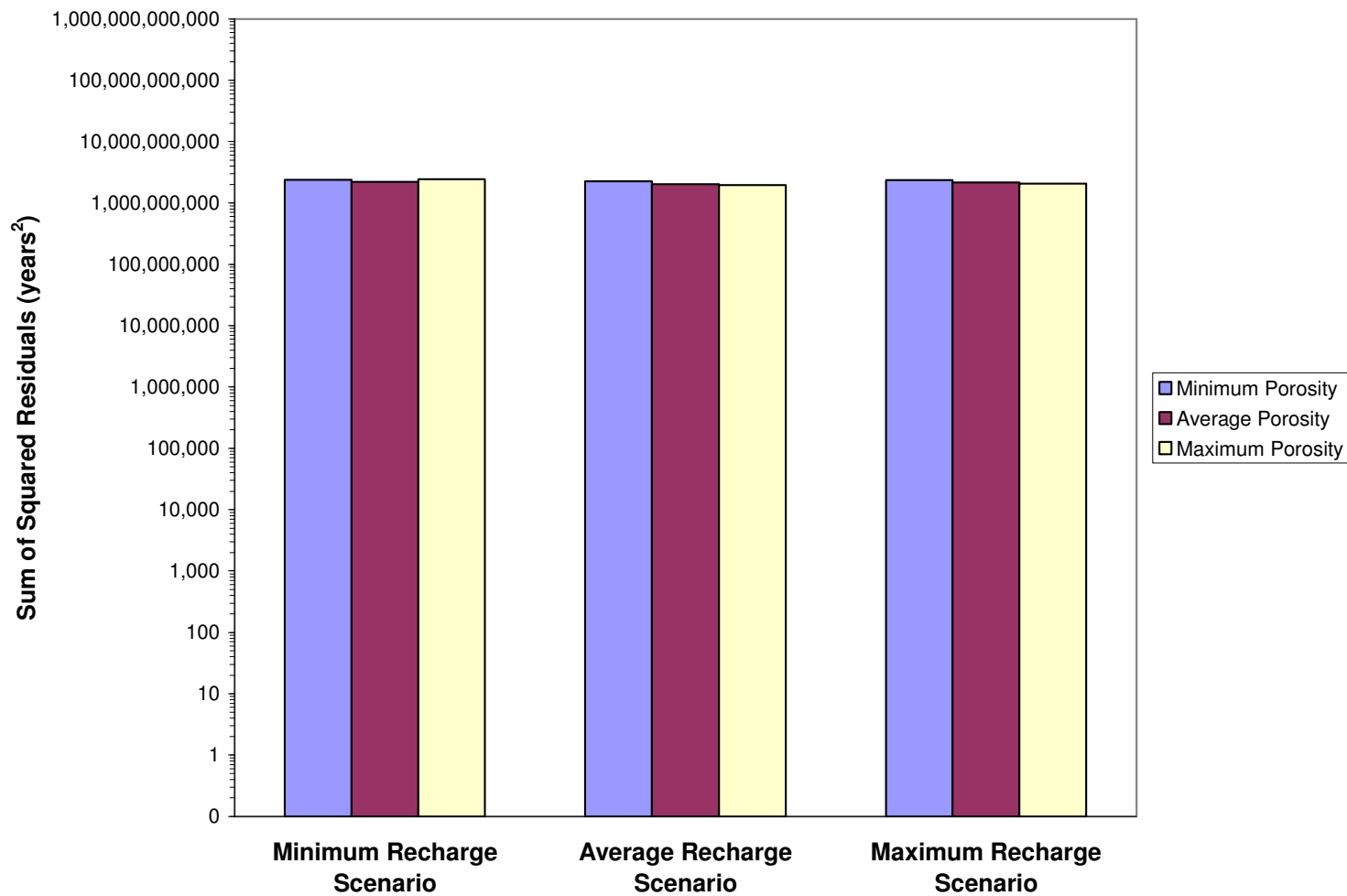
Figure 4.121: Sum of the squares of the residuals between MODPATH and NETPATH ages for the water-balance based minimum, average, and maximum recharge scenarios using minimum, average, and maximum porosities. Vertical axis is logarithmic scale.
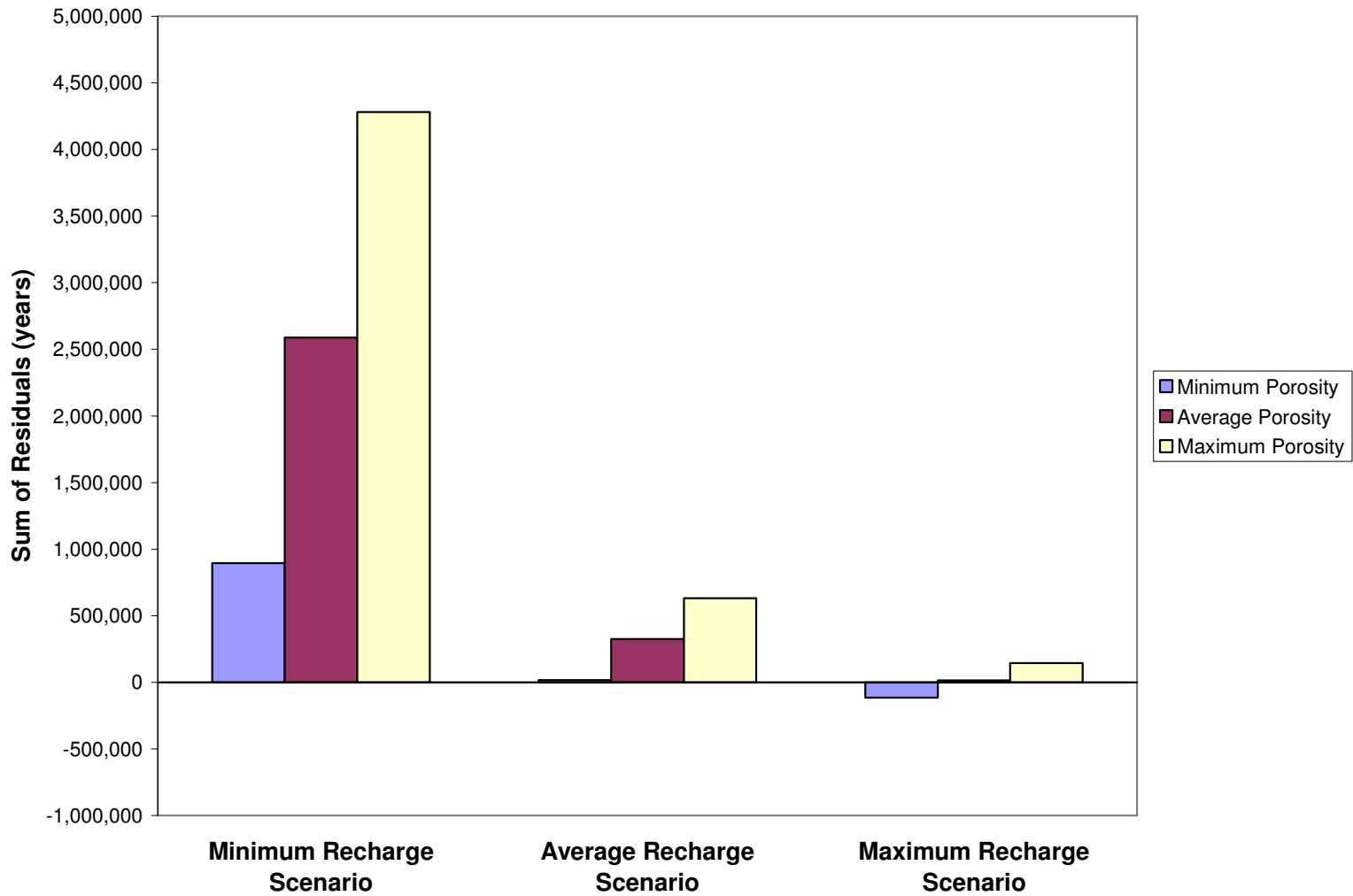
Figure 4.122: Sum of the residuals between MODPATH and NETPATH ages for the elevation-dependent minimum, average, and maximum recharge scenarios using minimum, average, and maximum porosities.
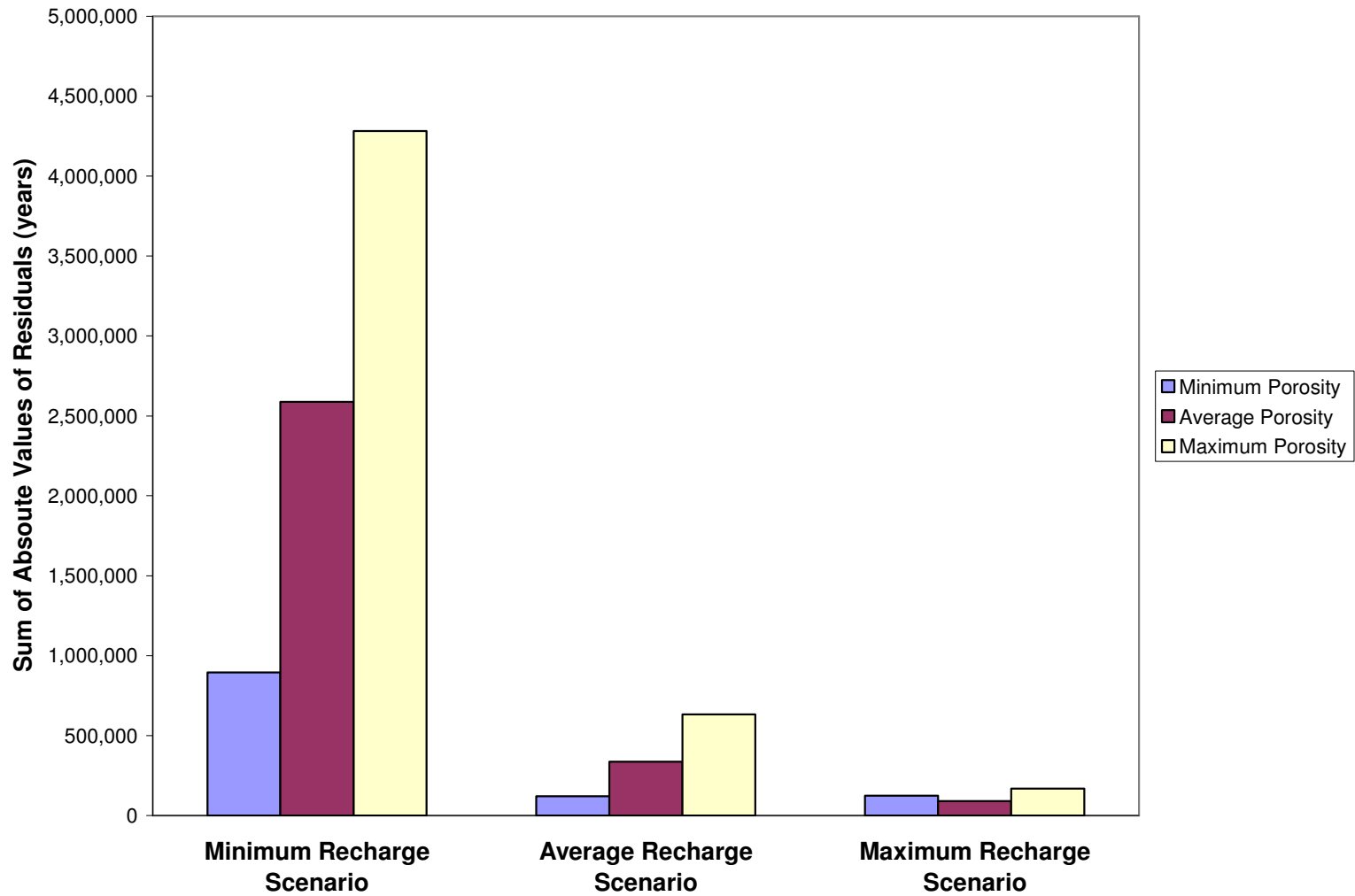
Figure 4.123: Sum of the absolute values of the residuals between MODPATH and NETPATH ages for the elevation-dependent minimum, average, and maximum recharge scenarios using minimum, average, and maximum porosities.
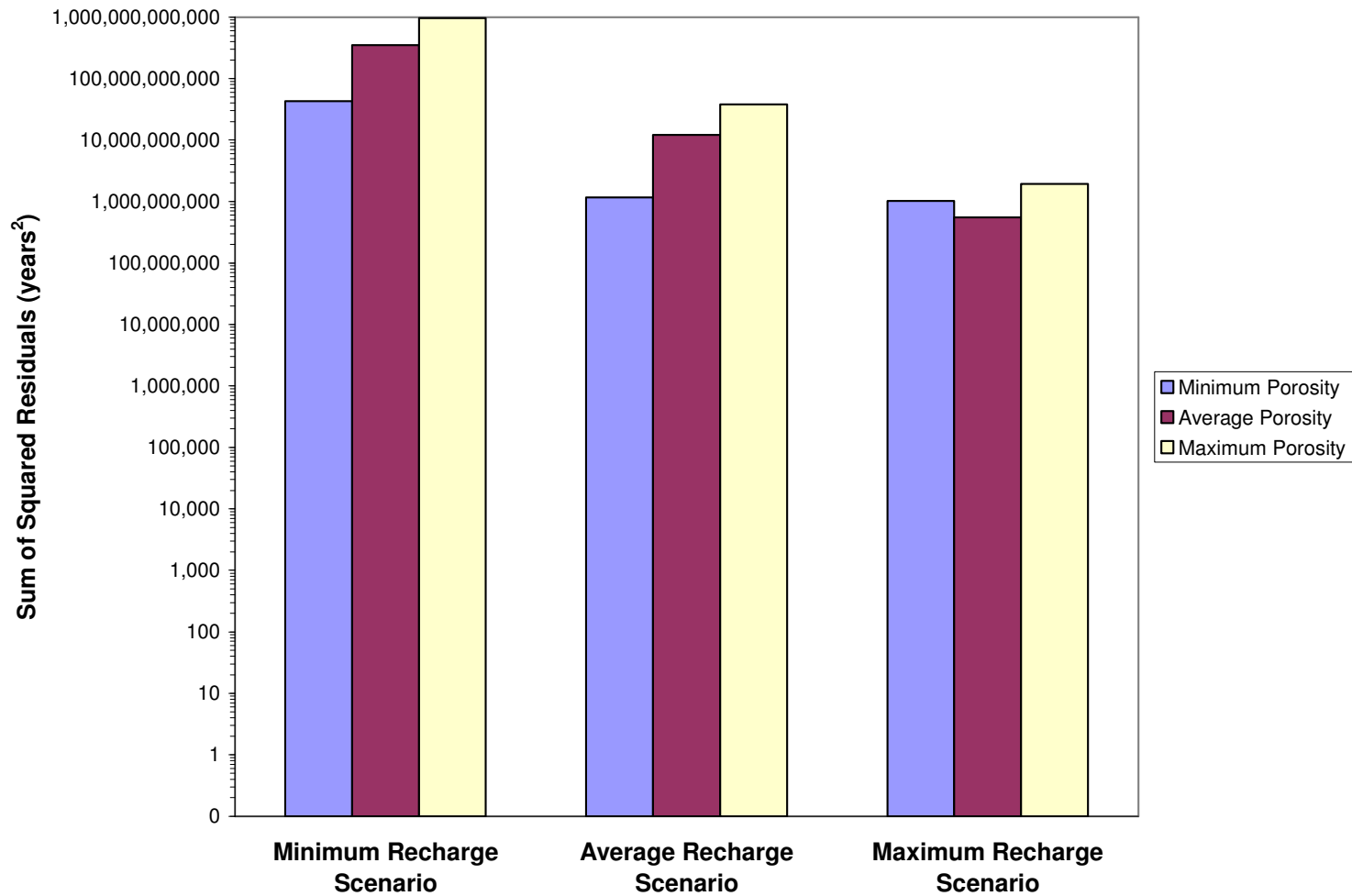
Figure 4.124: Sum of the squares of the residuals between MODPATH and NETPATH ages for the elevation-dependent minimum, average, and maximum recharge scenarios using minimum, average, and maximum porosities. Vertical axis is logarithmic scale.

TABLES – CHAPTER 4

Salt Basin Sub-basins Delineated by JSAI (2010)	Minimum Recharge Rate (cm/year)	Average Recharge Rate (cm/year)	Maximum Recharge Rate (cm/year)	Minimum Recharge (m³/day)	Average Recharge (m³/day)	Maximum Recharge (m³/day)	Minimum Recharge (acre-feet/year)	Average Recharge (acre-feet/year)	Maximum Recharge (acre-feet/year)
Peñasco Basin	1.3	1.9	2.4	19,842	28,523	37,204	5,875	8,446	11,016
Upper Sacramento River and Upper Piñon Creek	0.5	1.0	1.2	9,637	19,275	22,166	2,854	5,707	6,564
Lower Piñon Creek	0.5	1.5	2.5	1,342	4,025	6,708	397	1,192	1,986
Collins Hills	1.0	2.5	5.0	3,970	9,925	19,850	1,176	2,939	5,878
Rim of the Guadalupes	2.0	2.8	4.0	8,542	11,746	17,085	2,529	3,478	5,059
Guadalupe Mountains	2.0	2.8	4.0	16,482	22,663	32,964	4,880	6,711	9,761
Upper Cornucopia Draw	1.0	2.5	3.5	3,888	9,720	13,607	1,151	2,878	4,029
limestone highlands	2.5	3.0	5.0	8,282	9,939	16,564	2,452	2,943	4,905
Lower Sacramento River and Otero Mesa	0.1	0.3	0.3	2,988	5,976	6,573	885	1,769	1,946
Lower Cornucopia Draw	2.5	3.0	5.0	28,064	33,676	56,127	8,310	9,972	16,620
Crow Flats	0.1	0.2	0.2	2,015	4,030	3,023	597	1,193	895
Shiloh Draw	0.1	0.2	0.2	1,655	4,413	4,965	490	1,307	1,470
Coffelt Draw	2.0	2.5	2.8	13,909	17,386	19,124	4,118	5,148	5,663
Big Dog Canyon	1.0	2.0	2.0	9,254	18,508	18,508	2,740	5,480	5,480
Long Canyon	2.0	3.0	3.3	3,559	5,339	5,784	1,054	1,581	1,713
Lewis Canyon	2.0	3.0	3.3	8,268	12,403	13,436	2,448	3,673	3,979
Brokeoff Mountains	0.8	1.5	1.5	5,709	11,417	11,417	1,690	3,381	3,381
Fourmile Draw	0.1	1.0	1.0	145	2,902	2,902	43	859	859
Cornudas Draw	0.5	1.5	1.8	6,817	20,452	23,861	2,019	6,056	7,065
Washburn Draw	0.1	0.1	0.1	348	695	695	103	206	206
Diablo Plateau	0.1	0.1	0.1	4,325	8,649	10,811	1,281	2,561	3,201
Delaware Mountains	0.8	1.5	1.5	5,647	11,294	11,294	1,672	3,344	3,344
Salt Flats	0.0	0.0	0.0	0	0	0	0	0	0
Sum all sub-basins				**164,688**	**272,956**	**354,670**	**48,765**	**80,824**	**105,020**

Table 4.1: Water-balance based minimum, average, and maximum recharge rates and areal recharge applied to the Salt Basin sub-basins within the 3-D MODFLOW groundwater flow model domain.

413

Minimum Sacramento Mountains Recharge Factor (%)	Average Sacramento Mountains Recharge Factor (%)	Maximum Sacramento Mountains Recharge Factor (%)
4	22	44

Table 4.2: Sacramento Mountains recharge factors from Newton et al. (2011).

Location	Minimum Recharge Rate (cm/year)	Average Recharge Rate (cm/year)	Maximum Recharge Rate (cm/year)
Creek beds and depressions	0.028	0.242	0.457
Outside creek beds	0.005	0.0125	0.020

Table 4.3: Kreitler et al. (1987) recharge rates for Diablo Plateau from Mayer (1995).

Range of Average Annual Precipitation in Figure 1.11 Polygons (cm/year)	Median Average Annual Precipitation in Figure 1.11 Polygons (cm/year)	Minimum Recharge Factor (%)	Average Recharge Factor (%)	Maximum Recharge Factor (%)	Minimum Recharge Rate (cm/year)	Average Recharge Rate (cm/year)	Maximum Recharge Rate (cm/year)	Minimum Recharge (m³/day)	Average Recharge (m³/day)	Maximum Recharge (m³/day)	Minimum Recharge (acre-feet/year)	Average Recharge (acre-feet/year)	Maximum Recharge (acre-feet/year)
61 to 66	64	4	22	44	2.5	14.0	27.9						
66 to 71	69	4	22	44	2.7	15.1	30.2						
71 to 76	74	4	22	44	2.9	16.2	32.4						
76 to 81	79	4	22	44	3.1	17.3	34.6						
Sum Sacramento Mountains recharge zone								7,366	40,513	81,026	2,181	11,996	23,992
61 to 66	64	4	22	44	2.5	14.0	27.9						
66 to 71	69	4	22	44	2.7	15.1	30.2						
71 to 76	74	4	22	44	2.9	16.2	32.4						
Sum Guadalupe Mountains recharge zone								1,572	8,644	17,288	465	2,560	5,119

Table 4.4: Elevation-dependent minimum, average, and maximum recharge rates and areal recharge applied to the recharge zones within the 3-D MODFLOW groundwater flow model domain in the Sacramento and Guadalupe Mountains.

Location	Minimum Recharge Rate (cm/year)	Average Recharge Rate (cm/year)	Maximum Recharge Rate (cm/year)	Minimum Recharge (m³/day)	Average Recharge (m³/day)	Maximum Recharge (m³/day)	Minimum Recharge (acre-feet/year)	Average Recharge (acre-feet/year)	Maximum Recharge (acre-feet/year)
Creek beds and depressions	0.028	0.242	0.457						
Outside creek beds	0.005	0.0125	0.020						
Sum Cornudas Mountains recharge zone				60	202	344	18	60	102
Creek beds and depressions	0.028	0.242	0.457						
Outside creek beds	0.005	0.0125	0.020						
Sum Diablo Plateau recharge zone				80	380	679	24	112	201

Table 4.5: Elevation-dependent minimum, average, and maximum recharge rates and areal recharge applied to the recharge zones within the 3-D MODFLOW groundwater flow model domain in around the Cornudas Mountains and on the Diablo Plateau.

Hydrogeologic Unit	Model Layers	Initial Horizontal K (m/day)	Vertical Anisotropy	Calibrated Water-balance Based Minimum Recharge Scenario Horizontal K (m/day)	Calibrated Water-balance Based Average Recharge Scenario Horizontal K (m/day)	Calibrated Water-balance Based Maximum Recharge Scenario Horizontal K (m/day)
Cenozoic alluvium	1, 2, and 3	1	100	10	10	10
Cenozoic intrusions	1, 2, 3, 4, and 5	0.0001	1,000	0.00001 to 0.0001	0.00001 to 0.001	0.00001 to 0.001
Cretaceous	1	0.01	100	0.005	0.0075	0.0075
Low permeability confining unit beneath Cretaceous	2	0.000001	1,000	0.00000001	0.00000001	0.00000001
Unfractured Permian	1, 2, 3, 4, and 5	0.01 to 0.1	100	0.005 to 0.5	0.0075 to 1	0.01 to 2.5
Fractured Permian	1, 2, 3, 4, and 5	1 to 10	10	0.025 to 25	0.025 to 250	0.025 to 250
Paleozoic (Cambrian through Pennslyvanian)	2, 3, 4, 5, and 6	0.001	1,000	0.00005 to 0.5	0.00005 to 0.5	0.00005 to 0.5
Precambrian	1, 2, 3, 4, 5, and 6	0.001	1,000	0.00001 to 0.01	0.00001 to 0.01	0.00001 to 0.01

Table 4.7: Initial horizontal hydraulic conductivity [K], vertical anisotropy, and final horizontal K assigned to each hydrogeologic unit for the calibrated water-balance based minimum, average, and maximum recharge scenario models.

Hydrogeologic Unit	Model Layers	Initial Horizontal K (m/day)	Vertical Anisotropy	Calibrated Elevation-dependent Minimum Recharge Scenario Horizontal K (m/day)	Calibrated Elevation-dependent Average Recharge Scenario Horizontal K (m/day)	Calibrated Elevation-dependent Maximum Recharge Scenario Horizontal K (m/day)
Cenozoic alluvium	1, 2, and 3	1	100	0.005 to 10	0.0075 to 10	0.01 to 10
Cenozoic intrusions	1, 2, 3, 4, and 5	0.0001	1,000	0.00001 to 0.1	0.00001 to 0.1	0.00001 to 0.1
Cretaceous	1	0.01	100	0.0005	0.0025	0.005
Low permeability confining unit beneath Cretaceous	2	0.000001	1,000	0.00000001	0.00001	0.0001
Unfractured Permian	1, 2, 3, 4, and 5	0.01 to 0.1	100	0.005 to 0.5	0.005 to 5	0.005 to 5
Fractured Permian	1, 2, 3, 4, and 5	1 to 10	10	0.0075 to 5	0.075 to 25	0.25 to 25
Paleozoic (Cambrian through Pennslyvanian)	2, 3, 4, 5, and 6	0.001	1,000	0.00005 to 0.1	0.00005 to 0.1	0.00005 to 0.1
Precambrian	1, 2, 3, 4, 5, and 6	0.001	1,000	0.00001 to 0.01	0.00001 to 0.01	0.00001 to 0.01

Table 4.8: Initial horizontal hydraulic conductivity [K], vertical anisotropy, and final horizontal K assigned to each hydrogeologic unit for the calibrated elevation-dependent minimum, average, and maximum recharge scenario models.

Hydrogeologic Unit	Minimum Porosity (%)	Averge Porosity (%)	Maximum Porosity (%)
Cenozoic alluvium	5	12.5	20
Cenozoic intrusions	0.1	0.5	1
Cretaceous	5	12.5	20
Low permeability confining unit beneath Cretaceous	5	12.5	20
Unfractured Permian	5	12.5	20
Fractured Permian	5	12.5	20
Paleozoic (Cambrian through Pennslyvanian)	1	5.5	10
Precambrian	0.1	0.5	1

Table 4.10: Minimum, average, and maximum porosity values used for MODPATH solution.

Groundwater Age Well ID	POD Number	Easting	Northing	Model Row	Model Column	Model Layer	Ground Surface Elevation (m)	Well Depth (m)	Elevation of Well Depth (m)	Note
Doll Day	ST 00241 POD1	472590	3607544	79	44	1	1,718	475	1,243	Well depth from well owner
Piñon Well	ST 00003	478550	3606619	73	45	1	1,623	335	1,287	Well depth from NMOSE
Webb House	NA	465825	3606007	85	46	1	1,815	457	1,358	Well depth unkown; estimated
Uña	ST 00018	473476	3596830	78	55	1	1,743	390	1,353	Well depth from NMOSE
Cauhape	ST 00019	476365	3588074	75	64	1	1,447	315	1,131	Well depth from NMOSE
Jeffer's Well	NA	467327	3585742	84	66	1	1,481	305	1,177	Well depth from well owner
Ellett Lower	NA	469670	3578554	82	73	1	1,397	160	1,237	Well depth from well owner
Harvey Lewis Well	ST 00014	487565	3571656	64	80	1	1,181	91	1,090	Well depth from NMOSE
Collins	NA	499579	3568454	52	83	1	1,238	183	1,055	Well depth from well owner
Evrage House	ST 00050	496187	3563804	55	88	1	1,147	61	1,086	Well depth from NMOSE
Lewis	ST 00163	479239	3557196	72	94	1	1,230	154	1,076	Well depth from NMOSE
Butterfield Well	ST 00044	466258	3546182	85	105	2	1,268	244	1,024	Well depth from NMOSE
Hunt 8	ST 00057	490345	3544103	61	108	1	1,114	48	1,066	Well depth from NMOSE

Table 4.11: Groundwater age wells incorporated into MODPATH particle tracking exercise.

POD Number Key: NA = Not applicable.

Groundwater Age Well ID	Elevation of Well Depth (m)	Water-balance Based Minimum Recharge Scenario			Water-balance Based Average Recharge Scenario			Water-balance Based Maximum Recharge Scenario		
		Elevation of Computed Groundwater Surface (m)	Elevation of Midpoint (m)	Elevation of Bottom of Cell (m)	Elevation of Computed Groundwater Surface (m)	Elevation of Midpoint (m)	Elevation of Bottom of Cell (m)	Elevation of Computed Groundwater Surface (m)	Elevation of Midpoint (m)	Elevation of Bottom of Cell (m)
Doll Day	1,243	1,401	1,297	1,192	1,398	1,295	1,192	1,412	1,302	1,192
Pinon Well	1,287	1,359	1,256	1,154	1,349	1,251	1,154	1,368	1,261	1,154
Webb House	1,358	1,429	1,328	1,227	1,428	1,328	1,227	1,445	1,336	1,227
Una	1,353	1,334	1,227	1,120	1,323	1,222	1,120	1,338	1,229	1,120
Cauhape	1,131	1,276	1,167	1,058	1,254	1,156	1,058	1,267	1,163	1,058
Jeffer's Well	1,177	1,301	1,201	1,101	1,272	1,186	1,101	1,276	1,189	1,101
Ellett Lower	1,237	1,269	1,173	1,077	1,231	1,154	1,077	1,230	1,154	1,077
Harvey Lewis Well	1,090	1,157	1,087	1,018	1,143	1,080	1,018	1,154	1,086	1,018
Collins	1,055	1,169	1,093	1,018	1,152	1,085	1,018	1,164	1,091	1,018
Evrage House	1,086	1,146	1,093	1,040	1,135	1,088	1,040	1,144	1,092	1,040
Lewis	1,076	1,155	1,076	997	1,139	1,068	997	1,139	1,068	997
Butterfield Well	1,024	1,031	1,006	981	1,031	1,006	981	1,031	1,006	981
Hunt 8	1,066	1,110	1,054	997	1,109	1,053	997	1,111	1,054	997

Table 4.12: Elevations at which MODPATH particles were generated for the calibrated water-balance based minimum, average, and maximum recharge scenario models.

Orange highlighted rectangles indicate the vertical position of generated MODPATH particles chosen to represent the potential pathlines and residence times of groundwater sampled at each well.

Groundwater Age Well ID	Elevation of Well Depth (m)	Elevation-dependent Minimum Recharge Scenario			Elevation-dependent Average Recharge Scenario			Elevation-dependent Maximum Recharge Scenario		
		Elevation of Computed Groundwater Surface (m)	Elevation of Midpoint (m)	Elevation of Bottom of Cell (m)	Elevation of Computed Groundwater Surface (m)	Elevation of Midpoint (m)	Elevation of Bottom of Cell (m)	Elevation of Computed Groundwater Surface (m)	Elevation of Midpoint (m)	Elevation of Bottom of Cell (m)
Doll Day	1,243	1,462	1,327	1,192	1,464	1,328	1,192	1,454	1,323	1,192
Pinon Well	1,287	1,399	1,276	1,154	1,396	1,275	1,154	1,390	1,272	1,154
Webb House	1,358	1,491	1,359	1,227	1,495	1,361	1,227	1,483	1,355	1,227
Una	1,353	1,338	1,229	1,120	1,334	1,227	1,120	1,332	1,226	1,120
Cauhape	1,131	1,248	1,153	1,058	1,231	1,145	1,058	1,240	1,149	1,058
Jeffer's Well	1,177	1,274	1,188	1,101	1,267	1,184	1,101	1,284	1,193	1,101
Ellett Lower	1,237	1,243	1,160	1,077	1,226	1,152	1,077	1,251	1,164	1,077
Harvey Lewis Well	1,090	1,143	1,081	1,018	1,123	1,071	1,018	1,125	1,071	1,018
Collins	1,055	1,140	1,079	1,018	1,125	1,072	1,018	1,123	1,071	1,018
Evrage House	1,086	1,136	1,088	1,040	1,122	1,081	1,040	1,121	1,081	1,040
Lewis	1,076	1,149	1,073	997	1,135	1,066	997	1,142	1,070	997
Butterfield Well	1,024	1,031	1,006	981	1,031	1,006	981	1,031	1,006	981
Hunt 8	1,066	1,113	1,055	997	1,114	1,056	997	1,110	1,054	997

Table 4.13: Elevations at which MODPATH particles were generated for the calibrated elevation-dependent minimum, average, and maximum recharge scenario models.

Orange highlighted rectangles indicate the vertical position of generated MODPATH particles chosen to represent the potential pathlines and residence times of groundwater sampled at each well.

Water-balance Based Minimum Recharge Scenario	
Sum Residuals (m)	44
Sum Absolute Residuals (m)	11,780
Sum Squared Residuals (m^2)	1,400,350
RMS Error (m)	61
Residual Mean (m)	0.1
Absolute Residual Mean (m)	16
Residual Standard Deviation (m)	61
Minimum Observed Hydraulic Head (m)	1,029
Maximum Observed Hydraulic Head (m)	2,610
Residual Standard Deviation/Range	0.039
Residual Mean/Range	0.00007
Water-balance Based Average Recharge Scenario	
Sum Residuals (m)	-649
Sum Absolute Residuals (m)	10,793
Sum Squared Residuals (m^2)	1,379,233
RMS Error (m)	60
Residual Mean (m)	-2
Absolute Residual Mean (m)	13
Residual Standard Deviation (m)	60
Minimum Observed Hydraulic Head (m)	1,029
Maximum Observed Hydraulic Head (m)	2,610
Residual Standard Deviation/Range	0.038
Residual Mean/Range	-0.001
Water-balance Based Maximum Recharge Scenario	
Sum Residuals (m)	236
Sum Absolute Residuals (m)	10,568
Sum Squared Residuals (m^2)	1,318,998
RMS Error (m)	59
Residual Mean (m)	0.6
Absolute Residual Mean (m)	14
Residual Standard Deviation (m)	59
Minimum Observed Hydraulic Head (m)	1,029
Maximum Observed Hydraulic Head (m)	2,610
Residual Standard Deviation/Range	0.037
Residual Mean/Range	0.0004

Table 4.16: Residual hydraulic head statistics for the calibrated water-balance based minimum, average, and maximum recharge scenario models.

Elevation-dependent Minimum Recharge Scenario	
Sum Residuals (m)	1,364
Sum Absolute Residuals (m)	15,478
Sum Squared Residuals (m^2)	2,208,280
RMS Error (m)	76
Residual Mean (m)	4
Absolute Residual Mean (m)	22
Residual Standard Deviation (m)	76
Minimum Observed Hydraulic Head (m)	1,029
Maximum Observed Hydraulic Head (m)	2,610
Residual Standard Deviation/Range	0.048
Residual Mean/Range	0.002

Elevation-dependent Average Recharge Scenario	
Sum Residuals (m)	1,621
Sum Absolute Residuals (m)	16,612
Sum Squared Residuals (m^2)	2,291,432
RMS Error (m)	78
Residual Mean (m)	4
Absolute Residual Mean (m)	24
Residual Standard Deviation (m)	78
Minimum Observed Hydraulic Head (m)	1,029
Maximum Observed Hydraulic Head (m)	2,610
Residual Standard Deviation/Range	0.049
Residual Mean/Range	0.003

Elevation-dependent Maximum Recharge Scenario	
Sum Residuals (m)	951
Sum Absolute Residuals (m)	14,836
Sum Squared Residuals (m^2)	2,018,583
RMS Error (m)	73
Residual Mean (m)	3
Absolute Residual Mean (m)	21
Residual Standard Deviation (m)	73
Minimum Observed Hydraulic Head (m)	1,029
Maximum Observed Hydraulic Head (m)	2,610
Residual Standard Deviation/Range	0.046
Residual Mean/Range	0.002

Table 4.17: Residual hydraulic head statistics for the calibrated elevation-dependent minimum, average, and maximum recharge scenario models.

Recharge Scenario	Minimum T (m^2/day)	Maximum T (m^2/day)
Water-balance Based Minimum	0.53	23,000
Water-balance Based Average	0.80	230,000
Water-balance Based Maximum	0.68	230,000

Table 4.18: Range of transmissivity [T] values derived from the calibrated water-balance based minimum, average, and maximum recharge scenario models.

Recharge Scenario	Minimum T (m^2/day)	Maximum T (m^2/day)
Elevation-dependent Minimum	0.083	4,500
Elevation-dependent Average	0.31	23,000
Elevation-dependent Maximum	0.33	23,000

Table 4.19: Range of transmissivity [T] values derived from the calibrated elevation-dependent minimum, average, and maximum recharge scenario models.

Water-balance Based Minimum Recharge Scenario									
		Minimum Porosity			Average Porosity			Maximum Porosity		
Groundwater Age Well ID	NETPATH Age (years)	MODPATH Age on Computed Groundwater Surface (years)	MODPATH Age on Midpoint (years)	MODPATH Age on Bottom of Cell (years)	MODPATH Age on Computed Groundwater Surface (years)	MODPATH Age on Midpoint (years)	MODPATH Age on Bottom of Cell (years)	MODPATH Age on Computed Groundwater Surface (years)	MODPATH Age on Midpoint (years)	MODPATH Age on Bottom of Cell (years)
Doll Day	2,900	NA	1,211	5,051	NA	3,027	12,627	NA	4,844	20,203
Pinon Well	4,200	2	639	NA	5	1,599	NA	8	2,558	NA
Webb House	1,000	2	2,163	NA	5	5,409	NA	8	8,654	NA
Una	7,100	1	NA	NA	3	NA	NA	4	NA	NA
Cauhape	8,000	NA	290	6,541	NA	726	16,351	NA	1,161	26,162
Jeffer's Well	8,200	NA	223	462	NA	558	1,155	NA	893	1,848
Ellett Lower	13,800	0	214	NA	1	535	NA	2	856	NA
Harvey Lewis Well	12,000	7	301	NA	17	753	NA	28	1,204	NA
Collins	9,700	NA	447	1,087	NA	1,116	2,719	NA	1,786	4,350
Evrage House	12,800	NA	409	543	NA	1,023	1,358	NA	1,636	2,174
Lewis	11,000	NA	231	609	NA	577	1,523	NA	924	2,437
Butterfield Well	16,100	1,758	1,870	NA	4,396	4,675	NA	7,033	7,480	NA
Hunt 8	14,100	6	1,585	NA	14	3,961	NA	23	6,338	NA

Table 4.20: NETPATH ages from Sigstedt (2010) and MODPATH ages from the calibrated water-balance based minimum recharge scenario MODFLOW solution using minimum, average, and maximum porosities.

Orange highlighted rectangles indicate the MODPATH ages chosen to bound the residence time of groundwater sampled at each well.

		Water-balance Based Average Recharge Scenario								
		Minimum Porosity			Average Porosity			Maximum Porosity		
Groundwater Age Well ID	NETPATH Age (years)	MODPATH Age on Computed Groundwater Surface (years)	MODPATH Age on Midpoint (years)	MODPATH Age on Bottom of Cell (years)	MODPATH Age on Computed Groundwater Surface (years)	MODPATH Age on Midpoint (years)	MODPATH Age on Bottom of Cell (years)	MODPATH Age on Computed Groundwater Surface (years)	MODPATH Age on Midpoint (years)	MODPATH Age on Bottom of Cell (years)
Doll Day	2,900	NA	772	3,631	NA	1,930	9,078	NA	3,087	14,525
Pinon Well	4,200	1	395	NA	2	989	NA	3	1,582	NA
Webb House	1,000	1	1,035	NA	3	2,588	NA	4	4,141	NA
Una	7,100	0	NA	NA	1	NA	NA	2	NA	NA
Cauhape	8,000	NA	222	3,886	NA	554	9,716	NA	886	15,546
Jeffer's Well	8,200	NA	151	277	NA	377	692	NA	603	1,108
Ellett Lower	13,800	0	NA	NA	1	NA	NA	1	NA	NA
Harvey Lewis Well	12,000	3	159	NA	8	397	NA	12	636	NA
Collins	9,700	NA	189	421	NA	472	1,052	NA	756	1,683
Evrage House	12,800	NA	365	368	NA	912	919	NA	1,459	1,471
Lewis	11,000	0	142	NA	1	356	NA	1	569	NA
Butterfield Well	16,100	1,483	2,462	NA	3,706	6,157	NA	5,930	9,850	NA
Hunt 8	14,100	3	1,254	NA	7	3,136	NA	11	5,017	NA

Table 4.21: NETPATH ages from Sigstedt (2010) and MODPATH ages from the calibrated water-balance based average recharge scenario MODFLOW solution using minimum, average, and maximum porosities.

Orange highlighted rectangles indicate the MODPATH ages chosen to bound the residence time of groundwater sampled at each well.

| Water-balance Based Maximum Recharge Scenario | | | | | | | | | |
| Groundwater Age Well ID | NETPATH Age (years) | Minimum Porosity | | | Average Porosity | | | Maximum Porosity | | |
		MODPATH Age on Computed Groundwater Surface (years)	MODPATH Age on Midpoint (years)	MODPATH Age on Bottom of Cell (years)	MODPATH Age on Computed Groundwater Surface (years)	MODPATH Age on Midpoint (years)	MODPATH Age on Bottom of Cell (years)	MODPATH Age on Computed Groundwater Surface (years)	MODPATH Age on Midpoint (years)	MODPATH Age on Bottom of Cell (years)
Doll Day	2,900	NA	686	2,776	NA	1,715	6,939	NA	2,744	11,103
Pinon Well	4,200	0	339	NA	1	848	NA	2	1,357	NA
Webb House	1,000	1	1,053	NA	2	2,633	NA	4	4,212	NA
Una	7,100	0	NA	NA	1	NA	NA	1	NA	NA
Cauhape	8,000	NA	137	2,499	NA	342	6,248	NA	547	9,997
Jeffer's Well	8,200	NA	85	159	NA	213	397	NA	341	634
Ellett Lower	13,800	0	NA	NA	0	NA	NA	1	NA	NA
Harvey Lewis Well	12,000	5	119	NA	11	297	NA	18	476	NA
Collins	9,700	NA	210	445	NA	524	1,112	NA	838	1,779
Evrage House	12,800	NA	254	296	NA	635	739	NA	1,016	1,182
Lewis	11,000	0	134	NA	1	334	NA	1	534	NA
Butterfield Well	16,100	801	906	NA	2,002	2,265	NA	3,203	3,624	NA
Hunt 8	14,100	4	943	NA	10	2,359	NA	15	3,774	NA

Table 4.22: NETPATH ages from Sigstedt (2010) and MODPATH ages from the calibrated water-balance based maximum recharge scenario MODFLOW solution using minimum, average, and maximum porosities.

Orange highlighted rectangles indicate the MODPATH ages chosen to bound the residence time of groundwater sampled at each well.

Groundwater Age Well ID	NETPATH Age (years)	Elevation-dependent Minimum Recharge Scenario								
		Minimum Porosity			Average Porosity			Maximum Porosity		
		MODPATH Age on Computed Groundwater Surface (years)	MODPATH Age on Midpoint (years)	MODPATH Age on Bottom of Cell (years)	MODPATH Age on Computed Groundwater Surface (years)	MODPATH Age on Midpoint (years)	MODPATH Age on Bottom of Cell (years)	MODPATH Age on Computed Groundwater Surface (years)	MODPATH Age on Midpoint (years)	MODPATH Age on Bottom of Cell (years)
Doll Day	2,900	NA	29,209	31,326	NA	73,024	78,315	NA	116,838	125,304
Pinon Well	4,200	39,254	39,614	NA	98,136	99,034	NA	157,017	158,455	NA
Webb House	1,000	NA	25,841	28,442	NA	64,603	71,104	NA	103,365	113,767
Una	7,100	30,123	NA	NA	75,308	NA	NA	120,492	NA	NA
Cauhape	8,000	NA	37,965	65,573	NA	94,912	174,911	NA	151,860	284,339
Jeffer's Well	8,200	NA	37,819	38,024	NA	94,548	95,061	NA	151,277	152,097
Ellett Lower	13,800	47,809	47,940	NA	119,524	119,850	NA	191,238	191,761	NA
Harvey Lewis Well	12,000	43,494	43,553	NA	108,736	108,882	NA	173,978	174,210	NA
Collins	9,700	NA	619,774	611,088	NA	1,552,414	1,530,378	NA	2,485,056	2,450,553
Evrage House	12,800	NA	64,322	62,917	NA	160,806	157,294	NA	257,290	251,670
Lewis	11,000	77,238	81,206	NA	193,095	203,015	NA	308,953	324,823	NA
Butterfield Well	16,100	27,025	27,276	NA	67,562	68,191	NA	108,100	109,106	NA
Hunt 8	14,100	91,061	92,916	NA	227,653	248,452	NA	364,245	406,894	NA

Table 4.23: NETPATH ages from Sigstedt (2010) and MODPATH ages from the calibrated elevation-dependent minimum recharge scenario MODFLOW solution using minimum, average, and maximum porosities.

Orange highlighted rectangles indicate the MODPATH ages chosen to bound the residence time of groundwater sampled at each well.

Elevation-dependent Average Recharge Scenario									
		Minimum Porosity			Average Porosity			Maximum Porosity		
Groundwater Age Well ID	NETPATH Age (years)	MODPATH Age on Computed Groundwater Surface (years)	MODPATH Age on Midpoint (years)	MODPATH Age on Bottom of Cell (years)	MODPATH Age on Computed Groundwater Surface (years)	MODPATH Age on Midpoint (years)	MODPATH Age on Bottom of Cell (years)	MODPATH Age on Computed Groundwater Surface (years)	MODPATH Age on Midpoint (years)	MODPATH Age on Bottom of Cell (years)
Doll Day	2,900	NA	5,057	8,541	NA	12,642	21,352	NA	20,227	34,163
Pinon Well	4,200	4,558	4,688	NA	11,396	11,721	NA	18,233	18,753	NA
Webb House	1,000	NA	4,131	5,751	NA	10,328	14,376	NA	16,525	23,002
Una	7,100	4,973	NA	NA	12,434	NA	NA	19,894	NA	NA
Cauhape	8,000	NA	6,352	8,984	NA	15,880	22,459	NA	25,408	35,935
Jeffer's Well	8,200	NA	5,721	5,776	NA	14,303	14,439	NA	22,885	23,103
Ellett Lower	13,800	7,474	NA	NA	18,685	NA	NA	29,896	NA	NA
Harvey Lewis Well	12,000	6,924	7,281	NA	17,311	18,203	NA	27,697	29,125	NA
Collins	9,700	NA	401,260	406,635	NA	1,003,149	1,016,589	NA	1,605,040	1,626,542
Evrage House	12,800	387,340	7,445	NA	968,351	18,612	NA	1,549,362	29,780	NA
Lewis	11,000	21,646	22,039	NA	54,115	55,098	NA	86,585	88,157	NA
Butterfield Well	16,100	5,094	5,217	NA	12,736	13,043	NA	20,377	20,869	NA
Hunt 8	14,100	24,184	33,523	NA	60,459	83,808	NA	96,734	134,093	NA

Table 4.24: NETPATH ages from Sigstedt (2010) and MODPATH ages from the calibrated elevation-dependent average recharge scenario MODFLOW solution using minimum, average, and maximum porosities.

Orange highlighted rectangles indicate the MODPATH ages chosen to bound the residence time of groundwater sampled at each well.

Groundwater Age Well ID	NETPATH Age (years)	Minimum Porosity			Average Porosity			Maximum Porosity		
		MODPATH Age on Computed Groundwater Surface (years)	MODPATH Age on Midpoint (years)	MODPATH Age on Bottom of Cell (years)	MODPATH Age on Computed Groundwater Surface (years)	MODPATH Age on Midpoint (years)	MODPATH Age on Bottom of Cell (years)	MODPATH Age on Computed Groundwater Surface (years)	MODPATH Age on Midpoint (years)	MODPATH Age on Bottom of Cell (years)
Doll Day	2,900	NA	2,446	4,669	NA	6,116	11,672	NA	9,785	18,675
Pinon Well	4,200	2,353	2,408	NA	5,882	6,020	NA	9,411	9,632	NA
Webb House	1,000	2,001	2,174	NA	5,002	5,435	NA	8,004	8,696	NA
Una	7,100	2,515	NA	NA	6,287	NA	NA	10,060	NA	NA
Cauhape	8,000	NA	3,216	5,989	NA	8,039	14,971	NA	12,863	23,954
Jeffer's Well	8,200	NA	3,256	3,279	NA	8,140	8,197	NA	13,024	13,115
Ellett Lower	13,800	3,929	3,948	NA	9,824	9,871	NA	15,718	15,794	NA
Harvey Lewis Well	12,000	3,540	3,580	NA	8,851	8,950	NA	14,161	14,321	NA
Collins	9,700	NA	836,078	676,253	NA	2,734,009	2,107,019	NA	4,638,479	3,543,782
Evrage House	12,800	39,353	3,748	NA	98,381	9,370	NA	157,410	14,992	NA
Lewis	11,000	6,904	7,009	NA	17,259	17,522	NA	27,615	28,035	NA
Butterfield Well	16,100	2,512	2,520	NA	6,279	6,301	NA	10,046	10,081	NA
Hunt 8	14,100	7,254	7,517	NA	18,136	18,792	NA	29,017	30,067	NA

Table 4.25: NETPATH ages from Sigstedt (2010) and MODPATH ages from the calibrated elevation-dependent maximum recharge scenario MODFLOW solution using minimum, average, and maximum porosities.

Orange highlighted rectangles indicate the MODPATH ages chosen to bound the residence time of groundwater sampled at each well.

Water-balance Based Minimum Recharge Scenario			
Statistic	Minimum Porosity	Average Porosity	Maximum Porosity
Sum Residuals (years)	-209,047	-170,567	-132,087
Sum Absolute Residuals (years)	215,675	215,796	222,213
Sum Squared Residuals (years^2)	2,382,279,439	2,216,152,581	2,440,163,800
RMS Error (years)	9,762	9,415	9,880

Water-balance Based Average Recharge Scenario			
Statistic	Minimum Porosity	Average Porosity	Maximum Porosity
Sum Residuals (years)	-203,679	-177,848	-152,017
Sum Absolute Residuals (years)	205,212	196,812	197,014
Sum Squared Residuals (years^2)	2,256,174,267	2,013,764,816	1,954,184,998
RMS Error (years)	9,696	9,160	9,024

Water-balance Based Maximum Recharge Scenario			
Statistic	Minimum Porosity	Average Porosity	Maximum Porosity
Sum Residuals (years)	-209,049	-191,273	-173,496
Sum Absolute Residuals (years)	209,155	202,616	200,321
Sum Squared Residuals (years^2)	2,352,235,737	2,170,874,905	2,072,649,619
RMS Error (years)	9,900	9,511	9,293

Table 4.38: Residual age statistics for the calibrated water-balance based minimum, average, and maximum recharge scenario MODFLOW solutions using minimum, average, and maximum porosities.

Elevation-dependent Minimum Recharge Scenario			
Statistic	Minimum Porosity	Average Porosity	Maximum Porosity
Sum Residuals (years)	894,651	2,586,717	4,281,779
Sum Absolute Residuals (years)	894,651	2,586,717	4,281,779
Sum Squared Residuals (years^2)	43,034,332,815	352,316,919,807	963,202,659,626
RMS Error (years)	176,283	449,210	722,450
RMS Error with outliers removed (years)	43,256	123,766	204,642

Elevation-dependent Average Recharge Scenario			
Statistic	Minimum Porosity	Average Porosity	Maximum Porosity
Sum Residuals (years)	16,661	324,702	632,743
Sum Absolute Residuals (years)	120,743	337,545	632,743
Sum Squared Residuals (years^2)	1,159,868,251	12,142,411,637	38,117,422,665
RMS Error (years)	140,235	356,675	573,260
RMS Error with outliers removed (years)	7,615	24,640	43,656

Elevation-dependent Maximum Recharge Scenario			
Statistic	Minimum Porosity	Average Porosity	Maximum Porosity
Sum Residuals (years)	-115,734	14,416	144,565
Sum Absolute Residuals (years)	123,621	90,478	168,711
Sum Squared Residuals (years^2)	1,019,805,143	553,112,221	1,934,670,863
RMS Error (years)	212,501	687,851	1,165,130
RMS Error with outliers removed (years)	6,808	5,014	9,378

Table 4.39: Residual age statistics for the calibrated elevation-dependent minimum, average, and maximum recharge scenario MODFLOW solutions using minimum, average, and maximum porosities.

CONCLUSION

The Salt Basin region experienced a long and complex geologic history. Four main episodes of deformation from the Pennsylvanian to the Cenozoic affected the depositional environments and resulting facies distributions of the rocks within the basin. The collision of the southern margin of North America with South America-Africa during the Pennsylvanian-to-Early Permian Ouachita-Marathon orogeny resulted in the differential uplift and subsidence of the Pedernal landmass, and Diablo and Central Basin Platforms, and the Orogrande, Delaware, and Midland Basins, respectively (Dickerson, 1989). Mid-to-Late Permian structural features outlined the margins of the subsiding Delaware Basin (Black, 1973; Dickerson, 1989; King, 1948). East-west oriented compression during the Late Cretaceous Laramide orogeny produced northwest trending thrust faults and northwest to westerly trending folds in the Otero Mesa region (Black, 1973; Broadhead, 2002). Finally, Cenozoic Basin-and-Range extension overprinted all these former structures with the formation of horst and graben structures bounded by high-angle normal faults (Goetz, 1977).

The primary aquifer is found in Permian rocks that were deposited on a shallow marine shelf adjacent to the Delaware Basin to the southeast. The permeability of these rocks is highly dependent upon fracture density. Groundwater flow is concentrated in fractures and solution channels formed in limestones and dolomites within these rocks. The majority of the faulting and fracturing within these rocks is the result of deformation

associated with the Late Cretaceous Laramide orogeny and Cenozoic Basin-and-Range extension. Interbedded, less permeable lithologies act as barriers to groundwater movement, causing groundwater to flow at different stratigraphic levels within the same unit.

The primary aquifer units are the San Andres and Yeso Formations, which transition to the Victorio Peak and Bone Spring Limestones/Formations toward the southeast. These units are hydraulically connected to each other, and to the Cenozoic valley-fill deposits within the Salt Basin graben. Perched aquifers occur in localized Cretaceous deposits above the regional Permian aquifer, and also in alluvial deposits associated with ephemeral drainages. Previous studies, as well as the 3-D groundwater flow modeling presented in this thesis, indicate that a zone of high permeability associated with the heavily faulted and fractured Otero Break extends from the southern Sacramento Mountains southeastward towards Dell City, Texas and the Salt Basin graben. High permeabilities in the Permian and valley-fill aquifers extending northward from, and surrounding, the Dell City region are also suggested by the 3-D groundwater flow modeling results.

The range of transmissivity values calculated using ^{14}C groundwater ages and 3-D groundwater flow modeling vary up to more than six orders of magnitude. Transmissivity values estimated using ^{14}C groundwater ages along cross-section A to A' to the northeast of the Otero Break ranged from 0.10 to 5,100 m^2/day (1.1 to 55,000 ft^2/day). Using a more reasonable range of formation-scale porosities, the transmissivity values along cross-section A to A' ranged from 8.4 to 4,200 m^2/day (90 to 45,000 ft^2/day). Transmissivity values derived from the 3-D groundwater flow modeling ranged from

0.083 to 230,000 m^2/day (0.89 to 2,500,000 ft^2/day), with the highest transmissivity zones concentrated around the densely faulted and fractured regions of the Otero Break, the Salt Basin graben, and the subsurface Pedernal uplift. These transmissivities compare favorably to the range of published transmissivity values derived from aquifer tests or specific capacity data for groundwater wells completed in shelf-facies rocks within the Salt Basin region.

Analysis of the northward propagation of the periodic rise and fall in groundwater levels associated with seasonal groundwater withdrawals for irrigation near Dell City, Texas indicates that the Salt Basin aquifer system is confined, and the fracture systems which act as conduits for groundwater flow are highly connected. The seasonal fluctuation in groundwater levels was recorded in four wells, the farthest being 47.48 km (29.50 miles) away from Dell City. The values of storage coefficient estimated using the attenuation of the amplitude of the periodic water level fluctuations and the phase lag in the arrival time of the periodic water level fluctuations vary over a large range of up to five orders of magnitude due to the fact that the range of transmissivity values obtained from the ^{14}C groundwater ages along cross-section A to A' were used to calculate them.

Storage coefficient values calculated using the attenuation of the amplitude of the periodic water level fluctuations ranged from 0.000000059 to 0.0055, with a median of 0.000048 and an average of 0.0015. Using the range of transmissivity values calculated from more reasonable formation-scale porosities, the storage coefficient values obtained using the attenuation of the amplitude ranged from 0.0000047 to 0.0045. Storage coefficient values calculated using the phase lag in the arrival time of the periodic water level fluctuations ranged from 0.000000014 to 0.0024, with a median of 0.000012 and an

average of 0.00049. Using the range of transmissivity values calculated from more reasonable formation-scale porosities, the storage coefficient values obtained using the phase lag ranged from 0.0000011 to 0.0020. These values encompass the range of storage coefficient values reported in the scientific literature for confined, predominantly carbonate aquifers in the Western United States.

Two recharge distributions (water-balance based and elevation-dependent) were tested using MODFLOW-2000 in an attempt to match observed groundwater levels from wells throughout the Salt Basin, and radiocarbon groundwater ages from wells predominantly in the eastern half of the New Mexico portion of the Salt Basin. For the water-balance based recharge distribution, recharge was applied to the sub-basins delineated by JSAI (2010). The recharge rates applied to the sub-basins were derived from visual inspection of the figures depicting the net infiltration simulated by the water-balance recharge modeling conducted by DBS&A (2010a). For the elevation-dependent recharge distribution, recharge was applied to the high mountain regions of the Sacramento and Guadalupe Mountains above a surface elevation of 2,500 meters (8,200 feet), as well as the regions around the Cornudas Mountains and the southwest portion of the Diablo Plateau where depth-to-groundwater is shallow. Both recharge distribution models were calibrated to steady-state groundwater levels in 378 wells by varying the distribution of horizontal hydraulic conductivity within the groundwater flow model domain.

Total recharge to the groundwater flow model domain using the water-balance based recharge distribution ranged from 160,000 m^3/day (49,000 acre-feet/year) for the minimum recharge scenario to 350,000 m^3/day (110,000 acre-feet/year) for the maximum

436

recharge scenario, with the average recharge scenario producing 270,000 m^3/day (81,000 acre-feet/year). These values for total recharge to the Salt Basin are on the upper end of the range of values reported in previous studies. One of the shortcomings of the water-balance based recharge distribution is that most recharge to the groundwater system is concentrated along sinkholes to the southwest of the Otero Break and on the Chert Plateau and Otero Hills to the northeast of the Otero Break, while the high mountain region of the Sacramento Mountains contributes almost no recharge, despite abundant hydrogeologic evidence to the contrary.

Total recharge to the groundwater flow model domain using the elevation-dependent recharge distribution ranged from 9,100 m^3/day (2,700 acre-feet/year) for the minimum recharge scenario to 99,000 m^3/day (29,000 acre-feet/year) for the maximum recharge scenario, with the average recharge scenario producing 50,000 m^3/day (15,000 acre-feet/year). Recharge to the Sacramento Mountains recharge zone ranged from 7,400 m^3/day (2,200 acre-feet/year) for the minimum recharge scenario to 81,000 m^3/day (24,000 acre-feet/year) for the maximum recharge scenario, with the average recharge scenario resulting in 41,000 m^3/day (12,000 acre-feet/year). These values for the Sacramento Mountains recharge zone compare favorably to the subsurface flux from the Sacramento Mountains through the eastern portion of the Salt Basin, calculated by Sigstedt (2010) using radiocarbon groundwater ages. Sigstedt (2010) estimated the subsurface flux to range from 20,000 m^3/day (6,000 acre-feet/year) to 37,000 m^3/day (11,000 acre-feet/year).

Recharge to the Guadalupe Mountains recharge zone ranged from 1,600 m^3/day (470 acre-feet/year) for the minimum recharge scenario to 17,000 m^3/day (5,100 acre-

feet/year) for the maximum recharge scenario, with the average recharge scenario resulting in 8,600 m^3/day (2,600 acre-feet/year). These values for the Guadalupe Mountains recharge zone seem reasonable, based on abundant hydrogeologic evidence that indicates the Guadalupe Mountains receive much less recharge than the Sacramento Mountains. Recharge to the Cornudas Mountains and Diablo Plateau recharge zones ranged from 140 m^3/day (41 acre-feet/year) for the minimum recharge scenario to 1,000 m^3/day (300 acre-feet/year) for the maximum recharge scenario, with the average recharge scenario resulting in 580 m^3/day (170 acre-feet/year). Again, hydrogeologic evidence suggests that these relatively low recharge values are reasonable.

Both the calibrated water-balance based and elevation-dependent recharge distribution models produced a reasonably good match to observed groundwater levels and regional groundwater flow. However, MODPATH particle ages derived from the average recharge scenario/minimum porosity model and the maximum recharge scenario/minimum and average porosity models of the elevation-dependent recharge distribution resulted in a statistically better match to radiocarbon groundwater ages calculated by Sigstedt (2010), as compared to the water-balance based recharge distribution. In general, MODPATH particle ages derived from the water-balance based recharge distribution models ranged from one to three orders of magnitude younger than the radiocarbon groundwater ages.

The groundwater flow modeling discussed in this thesis suffers from several issues of non-uniqueness. As illustrated by the MODFLOW solutions for the two recharge distributions, an adequate match to observed groundwater levels was achieved by either increasing hydraulic conductivity and recharge (water-balance based recharge

distribution), or decreasing hydraulic conductivity and recharge (elevation-dependent recharge distribution). This issue of non-uniqueness is similar to the one discussed by Mayer (1995) concerning his modeling exercise. In addition, the MODPATH particle-tracking ages depend upon the distribution of hydrogeologic units within the groundwater flow model, as defined by the 3-D hydrogeologic framework model, as well as the hydraulic conductivity and recharge values assigned to the model. Thus, it is not possible to definitively say that the statistically better match between MODPATH particle ages derived from the elevation-dependent recharge distribution and the radiocarbon groundwater ages is the result of either the recharge distribution, or the distribution of hydrogeologic units. However, the abundant hydrogeologic evidence discussed in this thesis, along with the statistically better agreement between MODPATH particle ages derived from the elevation-dependent recharge distribution and radiocarbon groundwater ages suggest that the elevation-dependent recharge distribution is a better representation of recharge to the Salt Basin aquifer, as compared to the water-balance based recharge distribution.

REFERENCES

Adams, J. E. (1965). Stratigraphic-Tectonic Development of Delaware Basin. *American Association of Petroleum Geologists Bulletin, 49*(11), 2140-2148.

Adams, D. C., Ouimette, M. A., and Moreno, F. (1993). Middle-Late Proterozoic Extension in the Carlsbad Region of Southeastern New Mexico and West Texas. *New Mexico Geological Society Guidebook, 44*th *Field Conference, Carlsbad Region,* 137-144.

Angle, E. S. (2001). Hydrogeology of the Salt Basin. In Mace, R. E., Mullican, W. F. III, and Angle, E. S. (Eds.), *Aquifers of West Texas: Texas Water Development Board Report, 356*, 232-247.

Ashworth, J. B. (1995). Ground-Water Resources of the Bone Spring - Victorio Peak Aquifer in the Dell Valley Area, Texas. *Texas Water Development Board Report, 344*, 42 p.

Ashworth, J. B. (2001). Bone Spring-Victorio Peak Aquifer of the Dell Valley Region of Texas. In Mace, R. E., Mullican, W. F. III, and Angle, E. S. (Eds.), *Aquifers of West Texas: Texas Water Development Board Report, 356*, 135-152.

Bachman, G. O., and Haves, P. T. (1958). Stratigraphy of Upper Pennsylvanian and Lower Permian Rocks in the Sand Canyon Area, Otero County, New Mexico. *Bulletin of the Geological Society of America, 69*, 689-700.

Back, W., Hanshaw, B. B., Plummer, L. N., Rahn, P. H., Rightmire, C. T., and Rubin, M. (1983). Process and Rate of Dedolomitization: Mass Transfer and ^{14}C Dating in a Regional Carbonate Aquifer. *Bulletin of the Geological Society of America, 94*, 1415-1429.

Barker, D. S., Long, L. E., Hoops, G. K., and Hodges, F. N. (1977). Petrology and Rb-Sr Isotope Geochemistry of Intrusions in the Diablo Plateau, Northern Trans-Pecos Magmatic Province, Texas and New Mexico. *Geological Society of America Bulletin, 88*(10), 1437-1446.

Betancourt, J. L., Rylander, K. A., Peñalba, C., and McVickar, J. L. (2001). Late Quaternary Vegetation History of Rough Canyon, South-Central New Mexico, USA. *Palaeogeography, Palaeoclimatology, Palaeoecology, 165*(1), 71-95.

Bjorklund, L. J. (1957). Reconnaissance of Ground-Water Conditions in the Crow Flats Area, Otero County, New Mexico. *State of New Mexico State Engineer Office Technical Report, 8*, 26 p.

Black, B. A. (1973). Geology of the Northern and Eastern Parts of the Otero Platform, Otero and Chaves Counties, New Mexico. *Dissertation*, 170 p.

Black, B. A. (1975) Geology and Oil and Gas Potential of the Northeast Otero Platform Area, New Mexico. *New Mexico Geological Society Guidebook, 26th Field Conference, Las Cruces Country,* 323-333.

Black, B. A. (1976). Tectonics of the Northern and Eastern Parts of the Otero Platform, Otero and Chaves Counties, New Mexico. In Woodward, L. A. and Northrop, S. A. (Eds.), *Tectonics and Mineral Resources in Southwestern North America: New Mexico Geological Society Special Publication, 61*, 39-45.

Blakey, R. (2009a). [JPEG images and text modified from a poster session presented to

    the Annual Meeting of the Geological Society of America, Salt Lake City, Oct.

    2005]. *Paleogeography and Tectonic Evolution of Late Paleozoic Sedimentary*

    Basins, Southwestern North America. Retrieved from

    http://jan.ucc.nau.edu/~rcb7/garm.html.

Blakey, R. (2009b). [JPEG images that track the ancient landscapes of North America].

    Paleogeography and Geologic Evolution of North America. Retrieved from

    http://jan.ucc.nau.edu/~rcb7/nam.html.

Boyd, D. W. (1958). Permian Sedimentary Facies, Central Guadalupe Mountains, New

    Mexico. New Mexico Institute of Mining & Technology State Bureau of Mines

    and Mineral Resources Bulletin, 49, 100 p.

Boyd, F. M. (1982). Hydrogeology of the Northern Salt Basin of West Texas and New

    Mexico. *Thesis*, 135 p.

Boyd, F. M. and Kreitler, C. W. (1986a). Hydrogeology of a Gypsum Playa, Northern

    Salt Basin, Texas. *Bureau of Economic Geology Report of Investigations, 158*, 37

    p.

Boyd, F. M. and Kreitler, C. W. (1986b). Hydrogeology of a Gypsum Playa, Northern

    Salt Basin, Texas. *El Paso Geological Society Guidebook, 18*, 170-183.

Broadhead, R. F. (2002). Petroleum Geology of the McGregor Range, Otero County,

    New Mexico. *New Mexico Geological Society Guidebook, 53rd Field Conference,*

    Geology of White Sands, 331-338.

Broadhead, R. F. (2007). Personal Communication.

Brown, L. D., Reilinger, R. E., and Hagstrum, J. R. (1978). Contemporary Uplift of the Diablo Plateau, West Texas, From Leveling Measurements. *Journal of Geophysical Research, 83*(811), 5465-5471.

Cather, S. M. and Harrison, R. W. (2002). Lower Paleozoic Isopach Maps of Southern New Mexico and Their Implications for Laramide and Ancestral Rocky Mountain Tectonism. *New Mexico Geological Society Guidebook, 53rd Field Conference, Geology of White Sands,* 85-101.

Chace, D. A. and Roberts, R. M. (2004). South-Central Salt Basin Groundwater Characterization. *El Paso Geological Society Field Guide Book for the Otero Mesa Area, New Mexico*, 47-61.

Chapman, J. (1984). Hydrogeochemistry of the Unsaturated Zone of a Salt Flat in Hudspeth County, Texas. *Thesis*, 132 p.

Chowdhury, A. H., Ridgeway, C., and Mace, R. E.. (2004). Origin of the Waters in the San Solomon Spring System, Trans-Pecos Texas. In Mace, R. E., Angle, E. S., and Mullican, W. F. III (Eds.), *Aquifers of the Edwards Plateau: Texas Water Development Board Report, 360*, 315-344.

Collins, E. W. and Raney, J. A. (1991). Tertiary and Quaternary Structure and Paleotectonics of the Hueco Basin, Trans-Pecos Texas and Chihuahua, Mexico. *Bureau of Economic Geology: Geological Circular, 91-2*, 44 p.

Collins, E. W. and Raney, J. A. (1997). Quaternary Faults Within Intermontane Basins of Northwest Trans-Pecos Texas and Chihuahua, Mexico. *Bureau of Economic Geology: Report of Investigations, 245*, 59 p.

Daly, C., Neilson, R. P., and Phillips, D. L. (1994). A Statistical-Topographic Model for Mapping Climatological Precipitation over Mountainous Terrain. *Journal of Applied Meteorology, 33*(2), 140-158.

Daniel B. Stephens & Associates, Inc. (2010a). Recharge Modeling Study, Salt Basin of Southeastern New Mexico. *Daniel B. Stephens & Associates, Inc. Draft Report, Prepared for New Mexico Interstate Stream Commission*, 34 p.

Daniel B. Stephens & Associates, Inc. (2010b). Salt Basin Historical Playa Evaporation Study. *Daniel B. Stephens & Associates, Inc. Draft Report, Prepared for New Mexico Interstate Stream Commission*, 28 p.

Denison, R. E. and Hetherington, E. A., Jr. (1969). Basement Rocks in Far West Texas and South-central New Mexico. In Kottlowski, F. E. and LeMone, D. V. (Eds.), *Border Stratigraphy Symposium: New Mexico Bureau of Mines and Mineral Resources Circular*, 104, 1-16.

Denison, R. E., Lidiak, E. G., Bickford, M. E., and Kisvarsanyi, E. B. (1984). Geology and Geochronology of Precambrian Rocks in the Central Interior Region of the United States. *U.S. Geological Survey Professional Paper 1241-C*, 25 p.

Dickerson, P. W. (1989). Evolution of the Delaware Basin. In Muehlberger, R. W. and Dickerson, P. W. (Eds.), *Structure and Stratigraphy of Trans-Pecos Texas; American Geophysical Union, 28th International Geological Congress Field Trip Guidebook*, T137, 113-124.

Dickerson, P. W. and Muehlberger, W. R. (1994). Basins in the Big Bend Segment of the Rio Grande Rift, Trans Pecos, Texas. In Keller, G. R., and Cather, S. M. (Eds.),

Basins of the Rio Grande Rift-Structure, Stratigraphy, and Tectonic Setting: Geological Society of America Special Paper, 291, 283-297.

Fenneman, N. M. and Johnson, D. W. (1946). Physical Divisions of the United States. *U.S. Geological Survey Special Map*.

Ferris, J. G. (1963). Cyclic Water-Level Fluctuations as a Basis for Determining Aquifer Transmissibility. In Bentall, R. (Compiler), *Methods of Determining Permeability, Transmissibility and Drawdown: U. S. Geological Survey Water-Supply Paper 1536-I*, 305-318.

Finch, S. T., Jr. (2010). Personal Communication.

Finger, J. T. and Jacobson, R. D. (1997). Fort Bliss Exploratory Slimholes: Drilling and Testing. *Sandia National Laboratories Report, SAND97-3075*, 17 p.

Foster, R. W. (1978). Oil and Gas Evaluation of White Sands Missile Range and Fort Bliss Military Reservation, South-central New Mexico. *New Mexico Bureau of Mines and Mineral Resources Open file report, 92*, 60 p.

Gates, J. S., White, D. E., Stanley, W. D., and Ackermann, H. D. (1980). Availability of Fresh and Slightly Saline Ground-Water in the Basins of Westernmost Texas. *Texas Department of Water Resources Report, 256*, 108 p.

George, P., Mace, R. E., and Mullican, W. F. (2005). The Hydrogeology of Hudspeth County, Texas. *Texas Water Development Board Report, 364*, 95 p.

Goetz, L. K. (1977). Quaternary Faulting in the Salt Basin Graben, West Texas. *Thesis*, 136 p.

Goetz, L. K. (1980). Quaternary Faulting in Salt Basin Graben, West Texas. *New Mexico Geological Society Guidebook, 31st Field Conference, Trans-Pecos Region,* 83-92.

Goetz, L. K. (1985). Salt Basin Graben: A Basin and Range Right-lateral Transtensional Fault Zone, Some Speculations. In Dickerson, P. W. and Muehlberger, R. W. (Eds.), *Structure and Tectonics of Trans-Pecos Texas: West Texas Geological Society Publication, 85-81*, 165-168.

Greene, E. A. (1993). Hydraulic Properties of the Madison Aquifer System in the Western Rapid City Area, South Dakota. *U. S. Geological Survey Water-Resources Investigations Report, 93-4008*, 56 p.

Haenggi, W. T. (2002). Tectonic History of the Chihuahua Trough, Mexico and Adjacent USA, Part II: Mesozoic and Cenozoic. *Boletín de la Sociedad Geológica Mexicana, 55*(1), 38-94.

Harbaugh, A. W., Banta, E. R., Hill, M. C., and McDonald, M. G. (2000). MODFLOW-2000, The U.S. Geological Survey Modular Ground-Water Model – User Guide to Modularization Concepts and the Ground-Water Flow Process. *U. S. Geological Survey Open-File Report, 00-92*, 121 p.

Hawley, J. W. (1993). Geomorphic Setting and Late Quaternary History of Pluvial-Lake Basins in the Southern New Mexico Region. *New Mexico Bureau of Mines and Mineral Resources Open-File Report, 391*, 28 p.

Hayes, P. T. (1964). Geology of the Guadalupe Mountains, New Mexico. *U.S. Geological Survey Professional Paper, 446*, 68 p.

Hiss, W. L. (1980). Movement of Groundwater in Permian Guadalupian Aquifer Systems, Southeastern New Mexico and Western Texas. *New Mexico Geological Society Guidebook, 31ˢᵗ Field Conference, Trans-Pecos Region,* 85-90.

Hsieh, P. A. and Freckleton, J. R. (1993). Documentation of a Computer Program to Simulate Horizontal-Flow Barriers Using the U.S. Geological Survey's Modular Three-Dimensional Finite-Difference Ground-Water Flow Model. *U. S. Geological Survey Open-File Report, 92-477*, 32 p.

Huff, G. F. and Chace, D. A. (2006). Knowledge and Understanding of the Hydrogeology of the Salt Basin in South-central New Mexico and Future Study Needs. *U.S. Geological Survey Open-File Report, 2006-1358*, 17 p.

Hussain, M., Rohr, D. M., and Warren, J. K. (1988). Depositional Environments and Facies in a Quaternary Continental Sabkha, West Texas. In Reid, S. T., Bass, R. O., and Welch, P. (Eds.), *Guadalupe Mountains Revisited, Texas and New Mexico: West Texas Geological Society Publication, 88-84*, 177-185.

Hutchison, W. R. (2006). Groundwater Management in El Paso, Texas. *Dissertation*, 329 p.

Hutchison, W. R. (2008). Preliminary Groundwater Flow Model, Dell City Area, Hudspeth and Culberson Counties, Texas. *El Paso Water Utilities Hydrogeology Report, 08-01*, 435 p.

John Shomaker & Associates, Inc. (2002). Hydrogeologic Framework of the Salt Basin and Development of Three-Dimensional Ground-Water Flow Model. *John Shomaker & Associates, Inc. Final Report, Prepared for New Mexico Interstate Stream Commission*, 28 p.

John Shomaker & Associates, Inc. (2010). Revised Hydrogeologic Framework and

    Updated Groundwater-Flow Model of the Salt Basin, New Mexico. *John*

    Shomaker & Associates, Inc. Draft Report, Prepared for New Mexico Interstate

    Stream Commission, 68 p.

Kalin, R. M. (2000). Radiocarbon Dating of Groundwater Systems. In Cook, P.G. and

    Herczeg, A.L. (Eds.), *Environmental Tracers in Subsurface Hydrology* (111-144).

    Netherlands: Springer.

Keller, G. R. and Cather, S. M. (1994). Introduction. In Keller, G. R. and Cather, S. M.

    (Eds.), *Basins of the Rio Grande Rift-Structure, Stratigraphy, and Tectonic*

    Setting: Geological Society of America Special Paper, 291, 1-3.

Keller, G. R., Veldhuis, J. H., and Powers, D. W. (1983). An Analysis of Gravity and

    Magnetic Anomalies in the Diablo Plateau Area. In Meader-Roberts, S. J. (Ed.),

    Geology of the Sierra Diablo and Southern Hueco Mountains West Texas:

    Permian Basin Section Society of Economic Paleontologists and Mineralogists

    Field Conference Guidebook, 83-22, 152-165.

Kelley, V. C. (1971). Geology of the Pecos Country, Southeastern New Mexico. *New*

    Mexico Bureau of Mines & Mineral Resources Memoir, 24, 75 p.

King, P. B. (1942). Permian of West Texas and southeastern New Mexico. *American*

    Association of Petroleum Geologists Bulletin, 26(4), 535-763.

King, P. B. (1948). Geology of the Southern Guadalupe Mountains, Texas. *U.S.*

    Geological Survey Professional Paper, 215, 183 p.

King, P. B. (1965). Geology of the Sierra Diablo Region Texas. *U.S. Geological Survey*

    Professional Paper, 480, 185 p.

King, P. B. (1983). Leonard and Wolfcamp Series of Sierra Diablo, Texas. In Meader-Roberts, S. J. (Ed.), *Geology of the Sierra Diablo and Southern Hueco Mountains West Texas: Permian Basin Section Society of Economic Paleontologists and Mineralogists Field Conference Guidebook, 83-22*, 80-96.

King, P. B., King, R. E., and Knight, J. B. (1945). Geology of the Hueco Mountains, El Paso and Hudspeth Counties, Texas. *U.S. Geological Survey Oil and Gas Inv. Prelim. Map, 36*, 2 sheets.

King, W. E. and Harder, V. M. (1985). Oil and Gas Potential of the Tularosa Basin-Otero Platform-Salt Basin Graben Area, New Mexico and Texas. *New Mexico Bureau of Mines and Mineral Resources Circular, 198*, 36 p.

Kluth, C. F. and Coney, P. J. (1981). Plate Tectonics of the Ancestral Rocky Mountains. *Geology*, (9), 10-15.

Kottlowski, F. E. (1963). Paleozoic and Mesozoic Strata of Southwestern and South-Central New Mexico. *New Mexico Institute of Mining & Technology State Bureau of Mines and Mineral Resources Bulletin, 79*, 100 p.

Kottlowski, F. E. (1969). Summary of Late Paleozoic in El Paso Border Region. In Kottlowski, F. E. and LeMone, D. V. (Eds.), *Border Stratigraphy Symposium; State Bureau of Mines and Mineral Resources, New Mexico Institute of Mining and Technology Circular, 104*, 38-51.

Kreitler, C. W., Mullican, W. F., and Nativ, R. (1990). Hydrogeology of the Diablo Plateau, Trans-Pecos Texas. In Kreitler, C. W. and Sharp, J. M., Jr. (Eds.), *Hydrology of Trans-Pecos Texas: Texas Bureau of Economic Geology Guidebook, 25*, 49-58.

Kreitler, C. W., Raney, J. A., Nativ, R., Collins, E. W., Mullican, W. F., III, Gustavson, T. C., and Henry, C. D. (1987). *Siting a Low-level Radioactive Waste Disposal Facility in Texas: Geological and Hydrological Investigations of State of Texas and the University of Texas Lands: Austin, Texas Bureau of Economic Geology, University of Texas, Report to the Texas Low-level Radioactive Waste Disposal Authority, 4*, 330 p.

LeMone, D. V. (1969). Cambrian-Ordovician in El Paso Border Region. In Kottlowski, F. E. and LeMone, D. V. (Eds.), *Border Stratigraphy Symposium; State Bureau of Mines and Mineral Resources, New Mexico Institute of Mining and Technology Circular, 104*, 17-25.

Mace, R. E. (2001). Estimating Transmissivity Using Specific-Capacity Data. *Bureau of Economic Geology Geological Circular, 01-2*, 44 p.

Machette, M. N., Personius, S. F., Kelson, K. I., Haller, K. M., and Dart, R. L. (1998). Map and Data for Quaternary Faults and Folds in New Mexico. *U.S. Geological Survey Open-File Report, 98-521*, 443 p.

Masson, P. H. (1956). Age of Igneous Rocks at Pump Station Hills, Hudspeth County, Texas. *Bulletin of the American Association of Petroleum Geologists, 40*(3), 501-518.

Maxey, G. B. and Eakin, T. E. (1949). Ground Water in White River Valley, White Pine, Nye, and Lincoln Counties, Nevada. *State of Nevada Office of the State Engineer Water Resources Bulletin, 8*, 59 p.

Mayer, J. R. (1995). The Role of Fractures in Regional Groundwater Flow: Field Evidence and Model Results from the Basin and Range of Texas and New Mexico. *Thesis*, 218 p.

Mayer, J. R. and Sharp, J. M., Jr. (1995). The Role of Fractures in Regional Groundwater Flow. In Rossmanith, H. (Ed.), *Mechanics of Jointed and Faulted Rock*, 375-380.

Mayer, J. R. and Sharp, J. M., Jr. (1998). Fracture Control of Regional Ground-Water Flow in a Carbonate Aquifer in a Semi-Arid Region. *GSA Bulletin, 110*(2), 269–283.

McAnulty, N. (1976). Resurgent Cauldrons and Associated Mineralization, Trans-Pecos Texas. *Tectonics and Mineral Resources in Southwestern North America: New Mexico Geological Society Special Publication, 61*, 180-186.

McDonald, M. G. and Harbaugh, A. W. (1988). A Modular Three-Dimensional Finite-Difference Ground-Water Flow Model. *Techniques of Water-Resources Investigations of the U. S. Geological Survey, Book 6, Chapter A1*, 586 p.

McDonald, M. G., Harbaugh, A. W., Orr, B. R., and Ackerman, D. J. (1998). A Method of Converting No-Flow Cells to Variable-Head Cells for the U.S. Geological Survey Modular Finite-Difference Ground-Water Flow Model. *U. S. Geological Survey Open-File Report, 91-536*, 56 p.

McGlasson, E. H. (1969). Siluro-Devonian of West Texas and Southeastern New Mexico. In Kottlowski, F. E. and LeMone, D. V. (Eds.), *Border Stratigraphy Symposium; State Bureau of Mines and Mineral Resources, New Mexico Institute of Mining and Technology Circular, 104*, 26-37.

McKnight, C. L. (1986). Descriptive Geomorphology of the Guadalupe Mountains, South-Central New Mexico and West Texas. *Baylor Geological Studies Bulletin, 43*, 40 p.

McLemore, V. T. and Guilinger, J. R. (1993). Geology and Mineral Resources of the Cornudas Mountains, Otero County, New Mexico and Hudspeth County, Texas. *New Mexico Geological Society Guidebook, 44th Field Conference, Carlsbad Region,* 145-153.

Menking, K. M., Anderson, R. Y., Shafike, N. G., Syed, K. H., and Allen, B. D. (2004). Wetter or Colder During the Last Glacial Maximum? Revisiting the Pluvial Lake Question in Southwestern North America. *Quaternary Research, 62*(3), 280-288.

Meyer, R. F. (1968). Geology of Pennsylvanian and Wolfcampian Rocks in Southeastern New Mexico. *Dissertation,* 186 p.

Miller, W. R. (1997). Environmental Geochemistry and Processes Controlling Water Chemistry, Cornudas Mountains, New Mexico. *U.S. Geological Survey Open-File Report, 97-158*, 27 p.

Morse, J. T. (2010). The Hydrogeology of the Sacramento Mountains Using Environmental Tracers. *Thesis,* 120 p.

Muehlberger, W. R. (1980). Texas Lineament Revisited. *New Mexico Geological Society Guidebook, 31st Field Conference, Trans-Pecos Region,* 113-121.

Muehlberger, W. R., Belcher, R. C., and Goetz, L. K. (1978). Quaternary Faulting in Trans-Pecos Texas. *Geology, 6*, 337-340.

Mullican, W. F. III and Mace, R. E. (2001). The Diablo Plateau Aquifer. *Aquifers of West Texas: Texas Water Development Board Report, 356*, 248-258.

Newell, N. D., Rigby, J. K., Fischer, A. G., Whiteman, A. J., Hickox, J. E., and Bradley, J. S. (1972). The Permian Reef Complex of the Guadalupe Mountains Region, Texas and New Mexico A Study in Paleoecology. *Hafner Publishing Company, Inc., New York*, 236 p.

Newton, B. T., Timmons, S. S., Rawling, G., Land, L., Kludt, T., and Timmons, J. M. (2011). Sacramento Mountains Hydrogeology Study, *New Mexico Bureau of Geology and Mineral Resources Open File Report, 538*.

Newton, B. T., Timmons, S. S., Rawling, G., Partey, F., Kludt, T., Land, L., Timmons, J. M., and Walsh, P. (2009). Sacramento Mountains Hydrogeology Study, *New Mexico Bureau of Mines and Mineral Resources: Aquifer Mapping Program Open File Report, 518*, 63 p.

Nielson, P. D. and Sharp, J. M., Jr. (1985). Tectonic Controls on the Hydrogeology of the Salt Basin, Trans-Pecos Texas. *Structure and Tectonics of Trans-Pecos Texas: West Texas Geological Society Publication, 85-81*, 231-234.

Nutt, C. J., O'Neill, J. M., Kleinkopf, M. D., Klein, D. P., Miller, W. R., Rodriquez, B. D., and McLemore, V. T. (1997). Geology and Mineral Resources of the Cornudas Mountains, New Mexico. *U.S. Geological Survey Open-File Report, 97-282*, 46 p.

Nutt, C. J. and O'Neill, J. M. (1998). Geologic Framework of Tertiary Intrusions of the Cornudas Mountains, Southern New Mexico. In Mack, G. H., Austin, G. S., and Barker, J. M. (Eds.), *New Mexico Geological Society Guidebook, 49th Field Conference, Las Cruces Country II*, 129-134.

O'Neill, J. M. and Nutt, C. J. (1998). Geologic Map of the Cornudas Mountains, New Mexico. *U.S. Geological Survey, Geologic Investigations Map GI, 2631*, scale 1:24,000.

Oosterbaan, R. J. and Nijland, H. J. (1994). Chapter 12: Determining the Saturated Hydraulic Conductivity. In Ritzema, H. P. (Ed.), *Drainage Principles and Applications, International Institute for Land Reclamation and Improvement (ILRI) Publication 16,* 38 p.

Peckham, R. C. (1963). Summary of the Ground-water Aquifers in the Rio Grande Basin. *Texas Water Commission Circular, 63-05*, 18 p.

Pollock, D. W. (1994). User's Guide for MODPATH/MODPATH-PLOT, Version 3: A Particle Tracking Post-Processing Package for MODFLOW, the U.S. Geological Survey Finite-Difference Ground-Water Flow Model. *U. S. Geological Survey Open-File Report, 94-464*, 249 p.

Pray, L. C. (1961). Geology of the Sacramento Mountains Escarpment, Otero County, New Mexico. *New Mexico Institute of Mining & Technology State Bureau of Mines and Mineral Resources Bulletin, 35*, 144 p.

Ross, C. A. and Ross, J. R. P. (1985). Paleozoic Tectonics and Sedimentation in West Texas, Southern New Mexico, and Southern Arizona. In Dickerson, P. W. and Muehlberger, W. R. (Eds.), *Structure and Tectonics of Trans-Pecos Texas: West Texas Geological Society Field Conference, West Texas Geological Society Publication 85-81,* 221-230.

Ryder, P. D. (1996). Ground Water Atlas of the United States: Oklahoma, Texas. *U.S. Geological Survey, Hydrologic Investigations Atlas 730-E*. http://pubs.usgs.gov/ha/ha730/ch_e/index.html.

Scalapino, R. A. (1950). Development of Groundwater for Irrigation in the Dell City Area, Hudspeth County, Texas. *Texas Board of Water Engineers Bulletin, 5004*, 38 p.

Schruben, P. G., Arndt, R. E., and Bawiec, W. J. (1994). Geology of the Conterminous United States at 1:2,500,000 Scale – A Digital Representation of the 1974 P. B. King and H. M. Beikman Map. *U.S. Geological Survey Digital Data Series 11, Release 2*. http://tin.er.usgs.gov/geology/us/.

Schwartz, F. W. and Zhang, H. (2003). *Fundamentals of Groundwater*. New York, NY: John Wiley & Sons, Inc.

Seager, W. R., Hawley, J. W., Kottlowski, F. E., and Kelley, S. A. (1987). Geology of East Half of Las Cruces and Northeast El Paso 1º x 2º Sheets, New Mexico. *New Mexico Bureau of Mines & Mineral Resources Geologic Map, 57*.

Sharp, J. M., Jr. (1989). Regional Ground-Water Systems in Northern Trans-Pecos Texas. In Dickerson, P. W., and Muehlberger, W. R. (Eds.), *Structure and Stratigraphy of Trans-Pecos Texas: American Geophysical Union Field Trip Guidebook*, T317, 123-130.

Sharp, J. M., Jr. (2001). Regional Groundwater Flow Systems in Trans-Pecos Texas. In Mace, R. E., Mullican, W. F. III, and Angle, E. S. (Eds.), *Aquifers of West Texas: Texas Water Development Board Report, 356*, 41-75.

Sharp, J. M., Jr., Mayer, J. R., and McCutcheon, E. (1993). Hydrogeologic Trends in the Dell City Area, Hudspeth County, Texas. *New Mexico Geological Society Guidebook, 44th Field Conference, Carlsbad Region,* 327-330.

Shepard, T. M. and Walper, J. L. (1982). Tectonic Evolution of Trans-Pecos, Texas. In Meader-Roberts, S. J. (Ed.), *Geology of the Sierra Diablo and Southern Hueco Mountains West Texas: Permian Basin Section Society of Economic Paleontologists and Mineralogists Field Conference Guidebook, 83-22*, 131-140.

Sigstedt, S. C. (2010). Environmental Tracers in Groundwater of the Salt Basin, New Mexico, and Implications for Water Resources. *Thesis,* 190 p.

South Central Mountain RC&D Council, Inc. (2002). Tularosa Basin and Salt Basin Regional Water Plan 2000-2040 Executive Summary. 33 p.

Spirakis, C. S., O'Neill, J. M., and Kleinkopf, M. D. (1997). Geology and Mineral Resources of Salt Flats and Surrounding Area, Cienega School 7.5' Quadrangle, New Mexico and Texas. *U.S. Geological Survey Open-File Report, 97-281*, 25 p.

Standen, A., Finch, S., Williams, R., and Lee-Brand, B. (2009). Capitan Reef Complex Structure and Stratigraphy. *Texas Water Development Board, Contract Number 0804830794*, 53 p.

Stoeser, D. B., Green, G. N., Morath, L. C., Heran, W. D., Wilson, A. B., Moore, D. W., and Van Gosen, B. S. (2007). Preliminary Integrated Geologic Map Databases for the United States: Central States: Montana, Wyoming, Colorado, New Mexico, North Dakota, South Dakota, Nebraska, Kansas, Oklahoma, Texas, Iowa, Missouri, Arkansas, and Louisiana. *U.S. Geological Survey Open-File Report, 2005-1351, Version 1.2*. http://pubs.usgs.gov/of/2005/1351/.

Uliana, M. M. (2000). Delineation of Regional Groundwater Flow Paths and their Relation to Structural Features in the Salt and Toyah Basins, Trans-Pecos Texas. *Dissertation*, 215 p.

Uliana, M. M. (2001). The Geology and Hydrogeology of the Capitan Aquifer: A Brief Overview. In Mace, R. E., Mullican, W. F. III, and Angle, E. S. (Eds.), *Aquifers of West Texas: Texas Water Development Board Report, 356*, 153-166.

Uliana, M. M. and Sharp, J. M., Jr. (2001). Tracing Regional Flow Paths to Major Springs in Trans-Pecos Texas Using Geochemical Data and Geochemical Models. *Chemical Geology, 179*, 53-72.

Uliana, M. M., Banner, J. L., and Sharp, J. M., Jr. (2007). Regional Groundwater Flow Paths in Trans-Pecos, Texas Inferred From Oxygen, Hydrogen, and Strontium Isotopes. *Journal of Hydrology, 334*, 334-346.

Veldhuis, J. H. and Keller, G. R. (1980). An Integrated Geologic and Geophysical Study of the Salt Basin Graben, West Texas. *New Mexico Geological Society Guidebook, 31st Field Conference, Trans-Pecos Region,* 141-150.

Vogel, J. C. (1970). Carbon-14 Dating of Groundwater. In International Atomic Energy Agency (Ed.), *Isotope Hydrology 1970,* 225-239.

Wasiolek, M. (1991). The Hydrogeology of the Permian Yeso Formation Within the Upper Rio Hondo Basin and the Eastern Mescalero Apache Indian Reservation, Lincoln and Otero Counties, New Mexico. *New Mexico Geological Society Guidebook, 42nd Field Conference, Sierra Blanca, Sacramento, Capitan Ranges,* 343-351.

White, D. E., et al. (1980). Ground-Water Data for the Salt Basin, Eagle Flat, Red Light

     Draw, Green River Valley and Presidio Bolson in Westernmost Texas. *Texas*

     Department of Water Resources Report, 259, 97 p.

Wilkins, D. E. and Currey, D. R. (1997). Timing and Extent of Late Quaternary

     Paleolakes in the Trans-Pecos Closed Basin, West Texas and South-Central New

     Mexico. *Quaternary Research, 47*(3), 306-315.

Wilkins, D. E. and Currey, D. R. (1999). Radiocarbon Chronology and d[13]C Analysis of

     Mid- to Late-Holocene Aeolian Environments, Guadalupe Mountains National

     Park, Texas, USA. *The Holocene, 9*(3), 363-371.

APPENDIX

FIGURES – CHAPTER 1
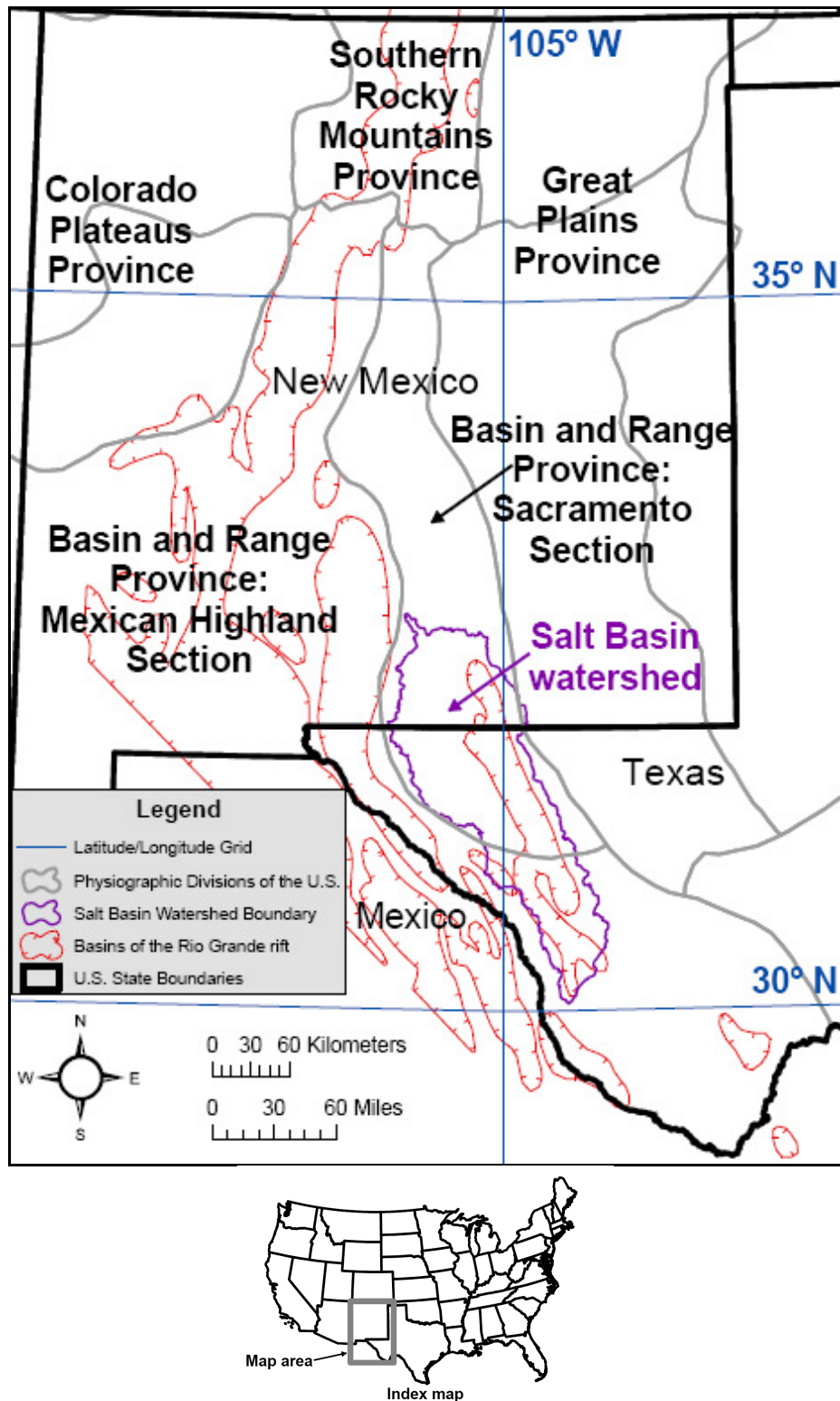
Figure A-1.1: Location of Salt Basin watershed with respect to physiographic divisions of the U.S., from Fenneman and Johnson (1946), and basins of the Rio Grande rift, from Keller and Cather (1994).

Salt Basin watershed boundary taken from U.S. Department of Agriculture (USDA). U.S. state boundaries taken from the National Atlas.
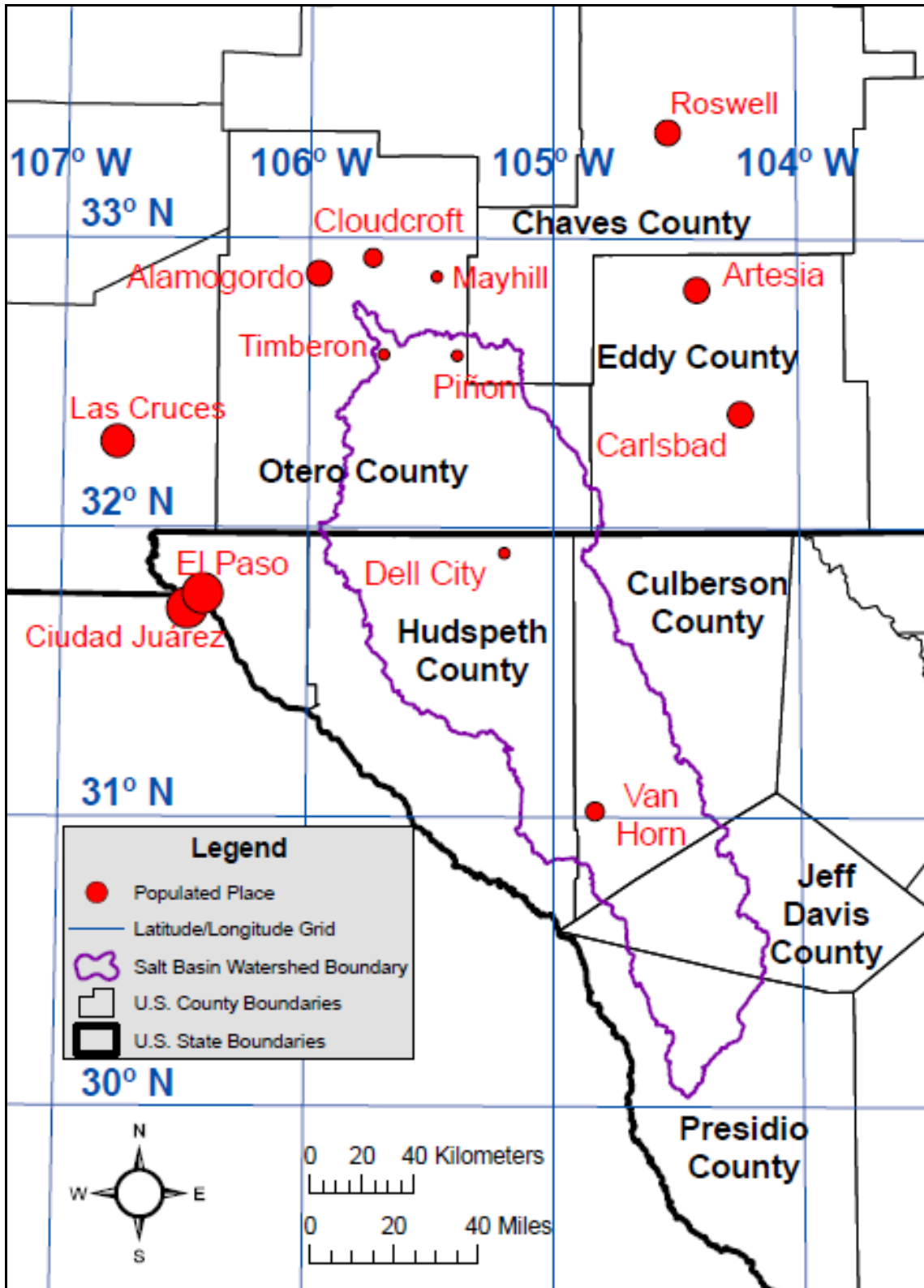
Figure A-1.2: Location map of Salt Basin watershed with respect to populated places and U.S. counties of New Mexico and Texas.
Location of populated places, and U.S. county boundaries taken from the National Atlas.
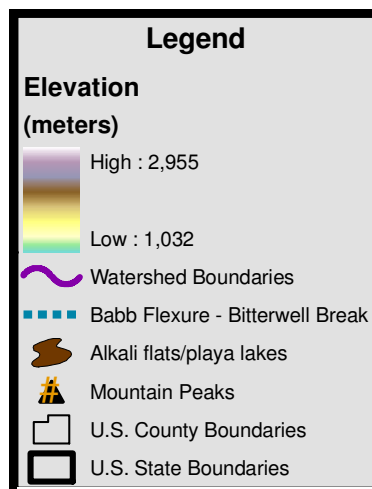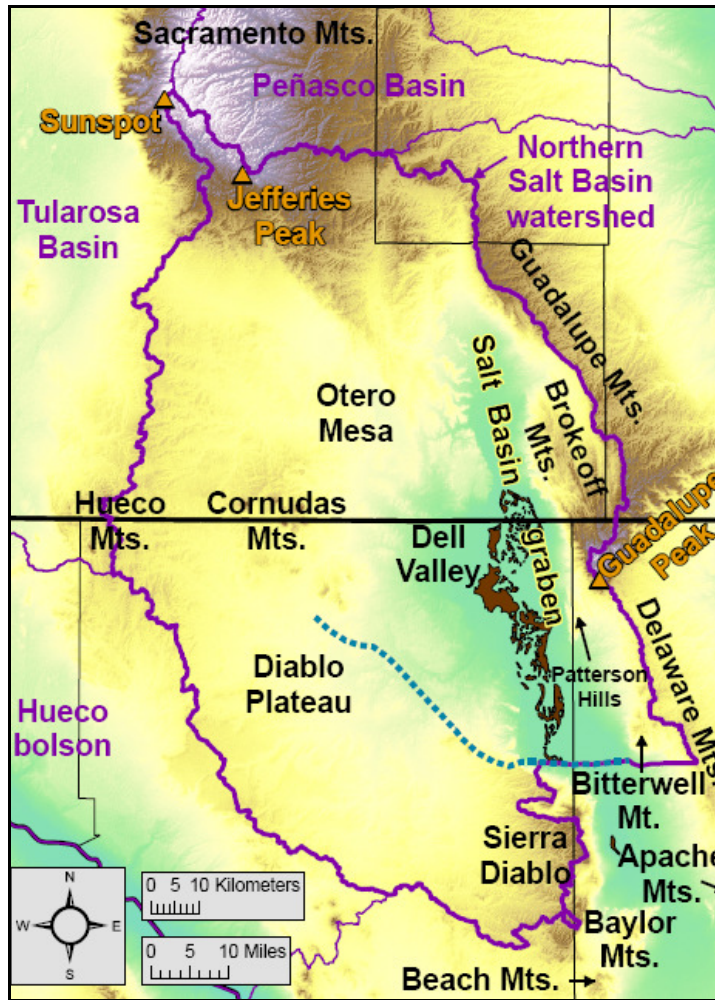
Figure A-1.3: Location map of northern Salt Basin watershed, after Hutchison (2006). Elevation taken from the National Elevation Dataset (NED) 1-arc second DEM. Watershed boundaries taken from USDA. Location of Babb Flexure - Bitterwell Break taken from Goetz (1985). Location of alkali flats/playa lakes taken from National Hydrography Dataset (NHD) for New Mexico, and from Stoeser et al. (2005) for Texas.
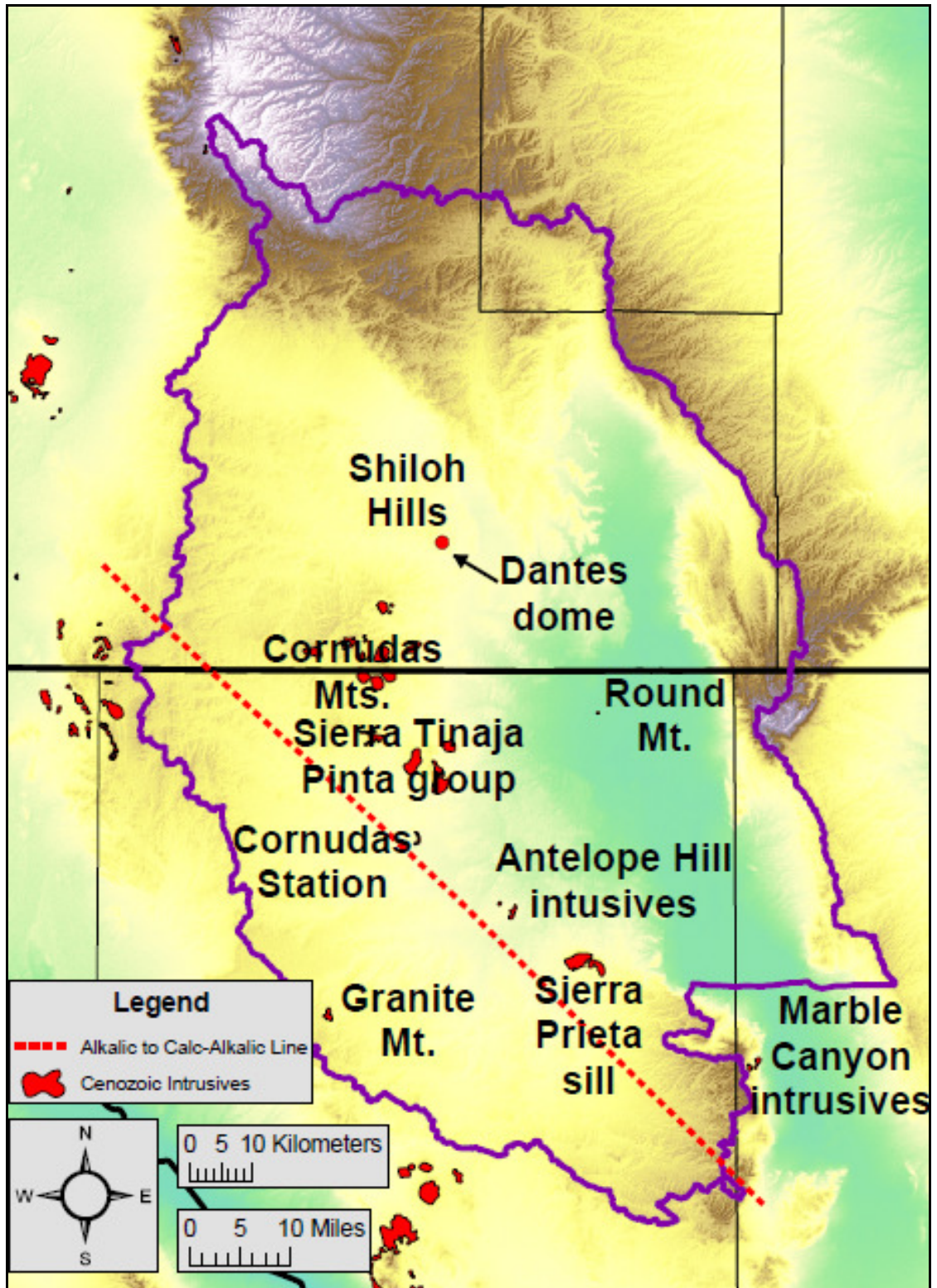
Figure A-1.4: Cenozoic intrusions in the Salt Basin region.
Location of Cenozoic intrusives taken from Stoeser et al. (2005). Alkalic to Calc-Alkalic Line separates calc-alkalic magmatism to the west from alkalic magmatism to the east, from McLemore and Guilinger (1993).
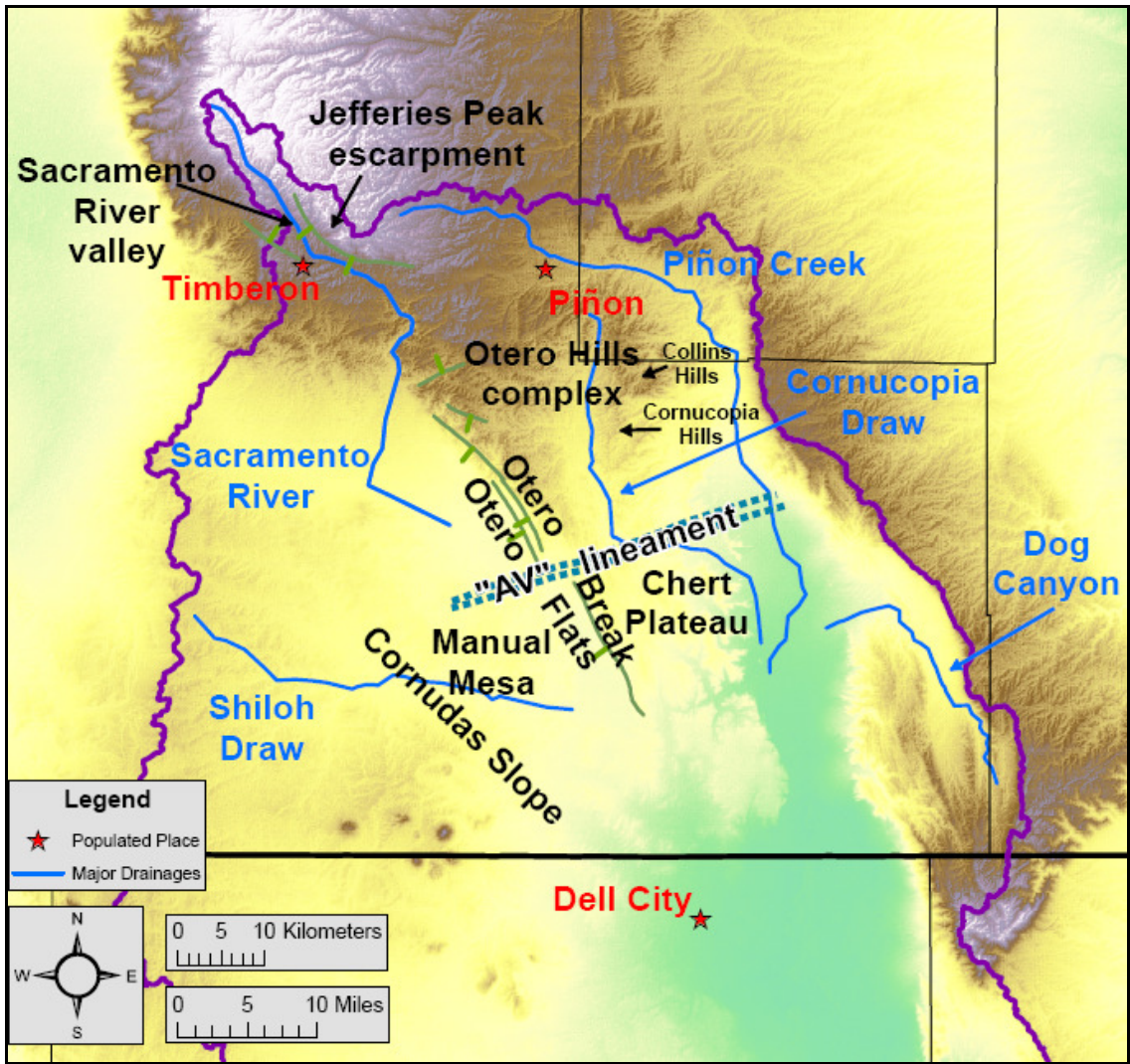
Figure A-1.5: Physiographic features of the north and northeast portions of Otero Mesa, from Black (1973).

Bar on downthrown side of normal or high angle faults. Location of major drainages taken from the National Atlas.
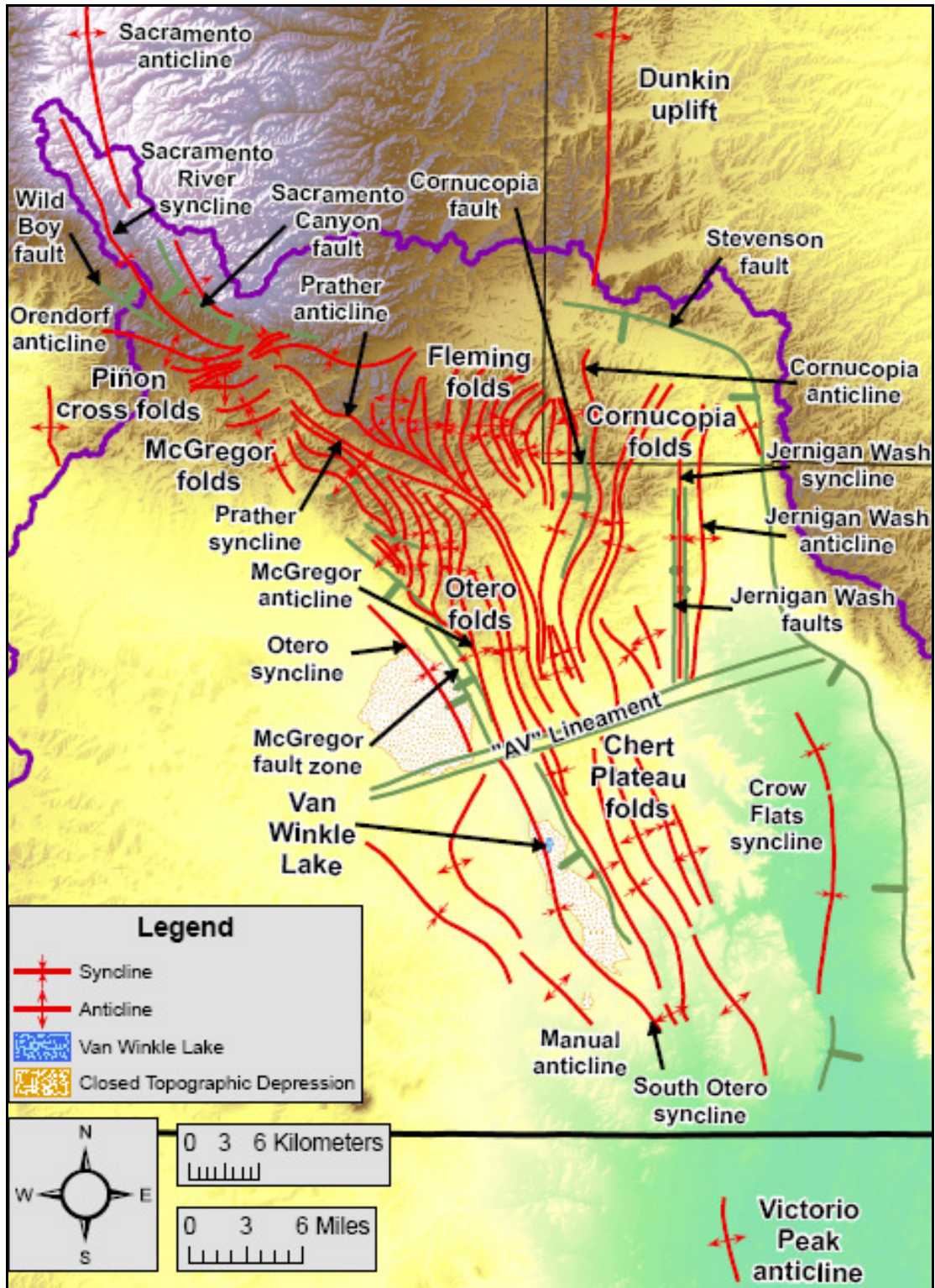
Figure A-1.6: Structural features of the north and northeast portions of Otero Mesa, from Black (1973), Broadhead (2002), Goetz (1985), and Kelley (1971). Bar on downthrown side of normal or high angle faults. Location of Van Winkle Lake and closed topographic depressions taken from the U. S. Geological Survey's 1:100,000-scale metric topographic map of Crow Flats, NM-TX.

Legend

Average Annual Temperature (1971-2000)

Median value for each area in ºC (ºF)

	17 (63)
	16 (61)
	15 (59)
	14 (57)
	13 (55)
	12 (53)
	11 (51)
	9.4 (49)
	8.3 (47)
	7.2 (45)
	6.1 (43)
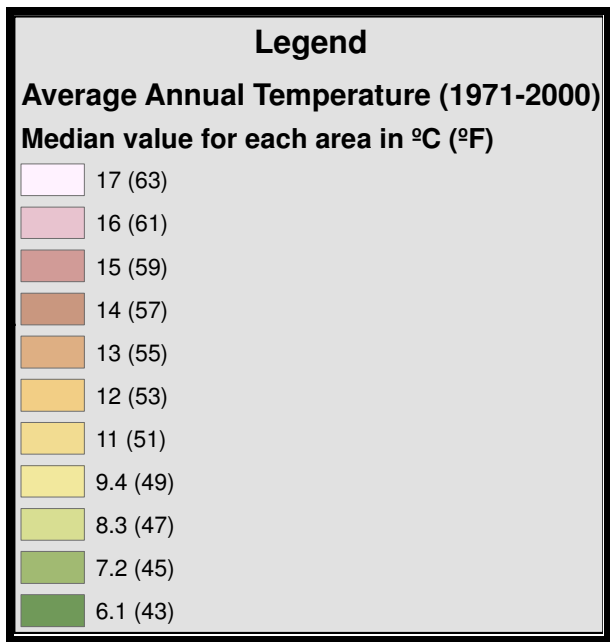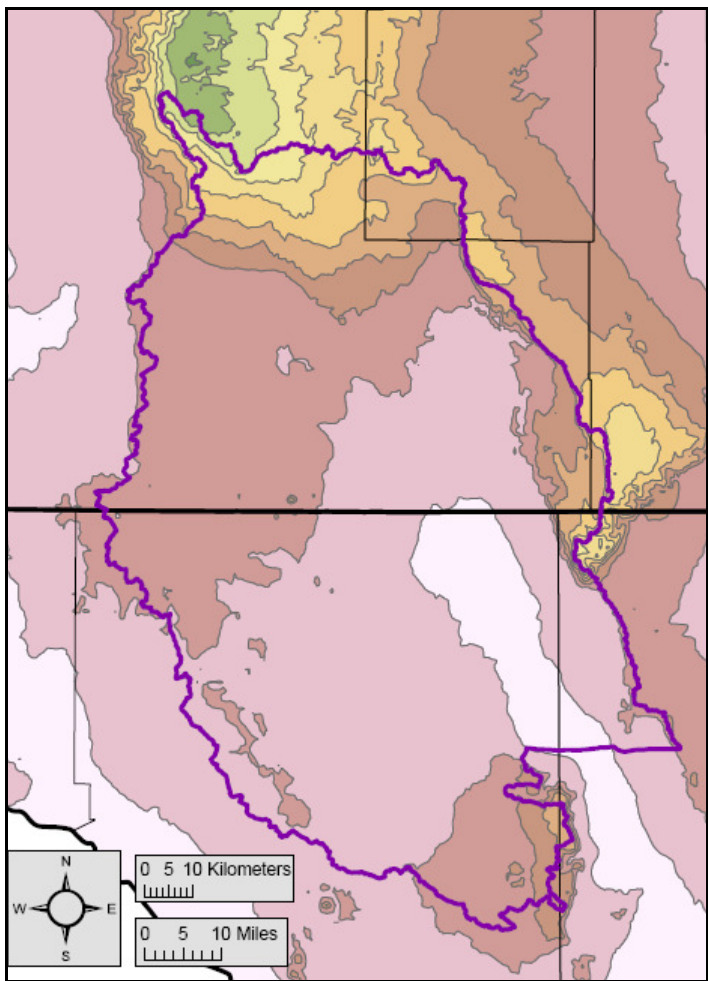
Figure A-1.7: Average annual temperature (1971-2000), from USDA.
Source scale: 1:250,000. Horizontal resolution: ~800 meters.
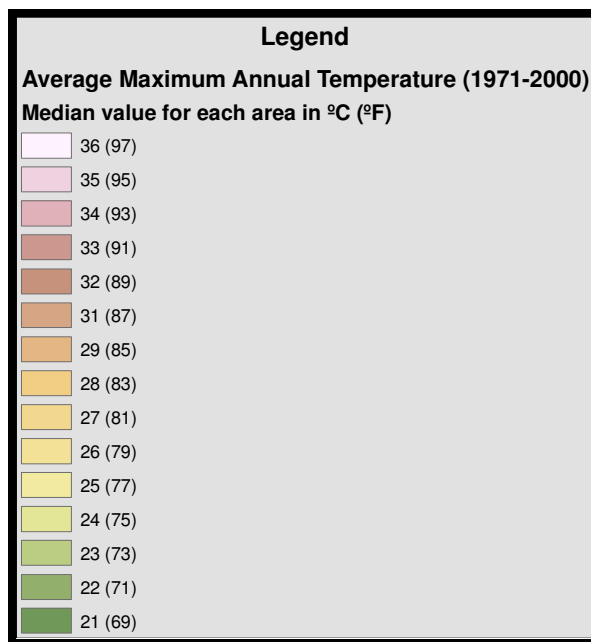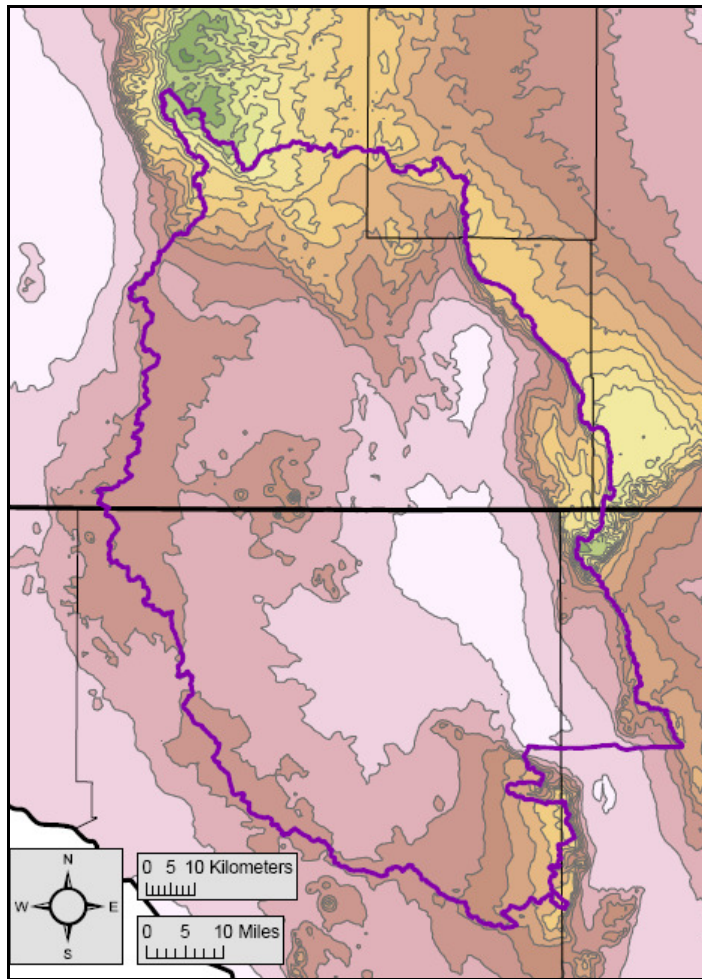
Figure A-1.8: Average maximum annual temperature (1971-2000), from USDA.
Source scale: 1:250,000. Horizontal resolution: ~800 meters.

Legend

Average Minimum Annual Temperature (1971-2000)

Median value for each area in ºC (ºF)

	1 (33)
	-1 (31)
	-2 (29)
	-3 (27)
	-4 (25)
	-5 (23)
	-6 (21)
	-7 (19)
	-8 (17)
	-9 (15)
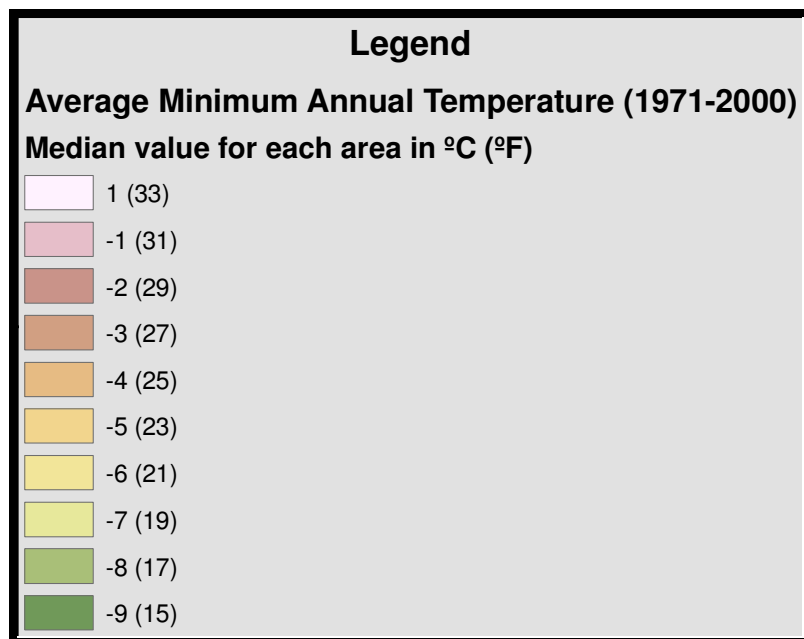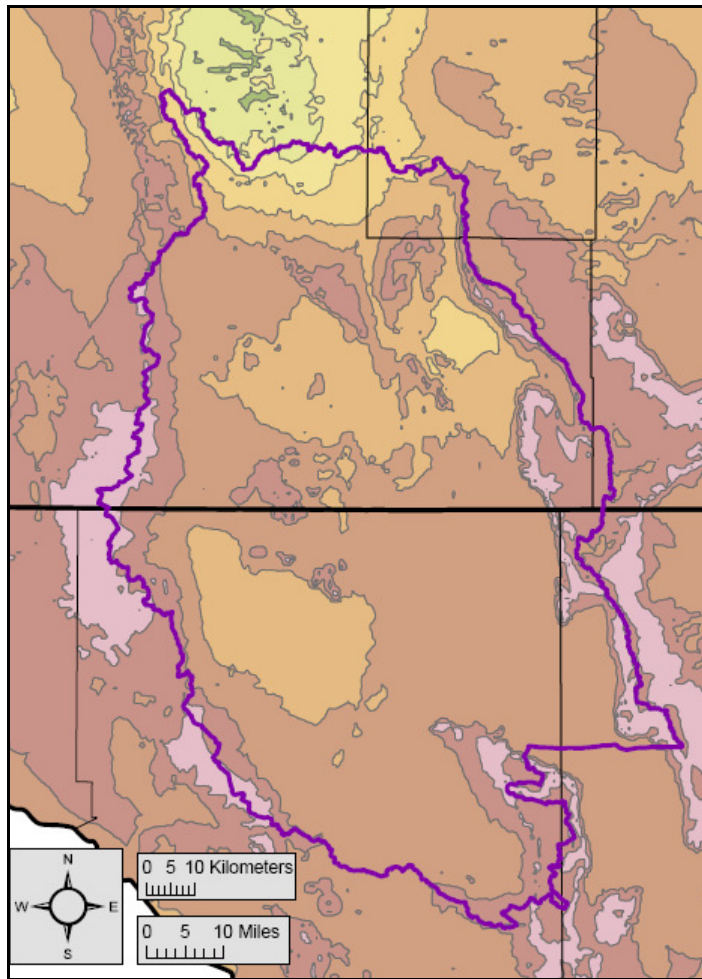
Figure A-1.9: Average minimum annual temperature (1971-2000), from USDA.
Source scale: 1:250,000. Horizontal resolution: ~800 meters.
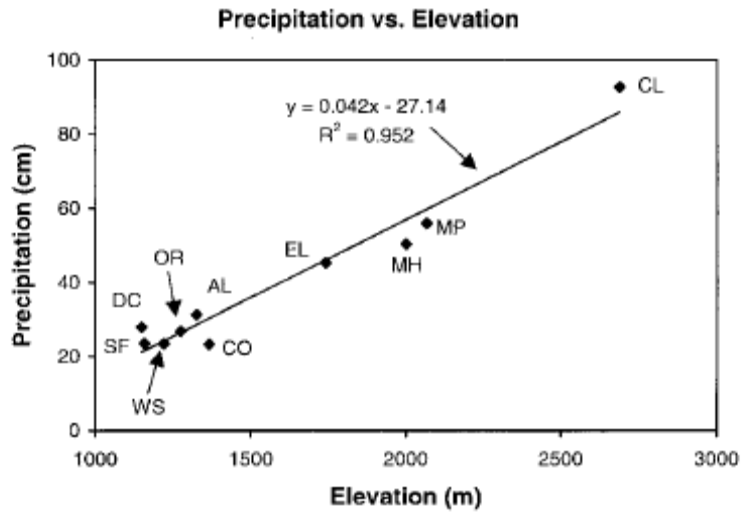
Figure A-1.10: Precipitation (cm) as a function of elevation (m) for recording stations in and near the northern Salt Basin watershed, from Mayer and Sharp (1998). Recording stations are: AL – Alamogordo; CL – Cloudcroft; CO – Cornudas; DC – Dell City; EL – Elk; MH – Mayhill; MP – Mountain Park; OR – Orogrande; SF – Salt Flat; WS – White Sands.

Legend

Average Annual Precipitation (1971-2000)

Median value for each area in cm (in)

- 84 (33)
- 79 (31)
- 74 (29)
- 69 (27)
- 64 (25)
- 58 (23)
- 53 (21)
- 48 (19)
- 43 (17)
- 38 (15)
- 33 (13)
- 28 (11)
- 23 (9)
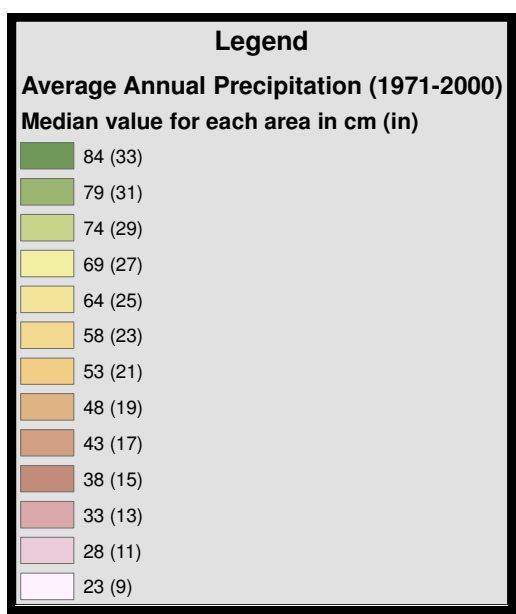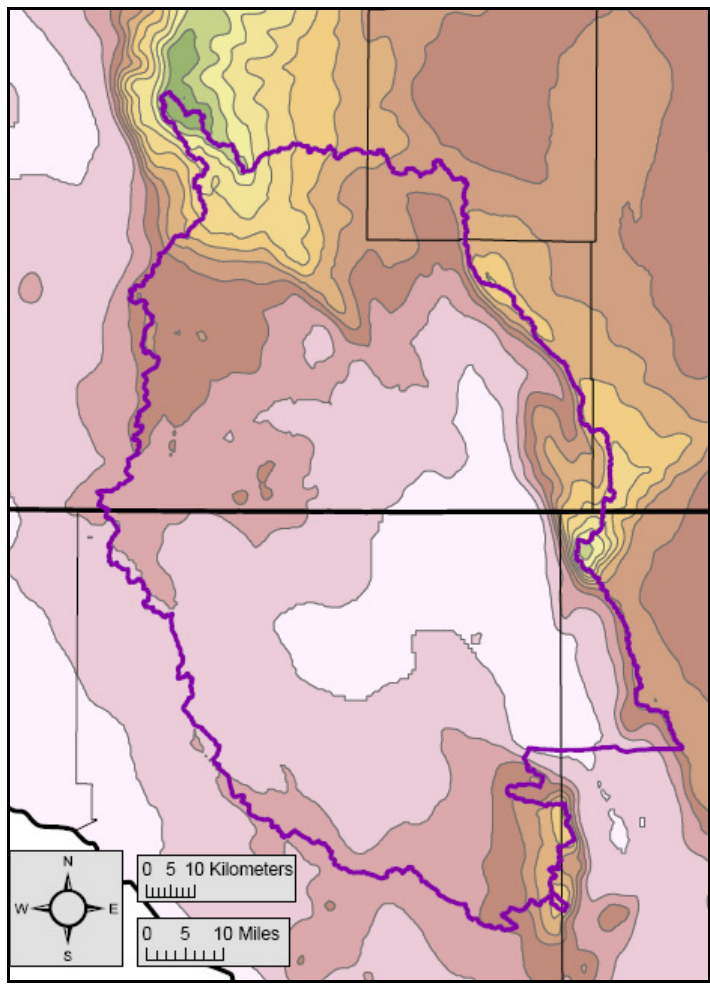
Figure A-1.11: Average annual precipitation (1971-2000), from USDA.
Mean monthly precipitation was calculated using PRISM, and then summed to produce
the above map. Source scale: 1:250,000. Horizontal resolution: ~800 meters.
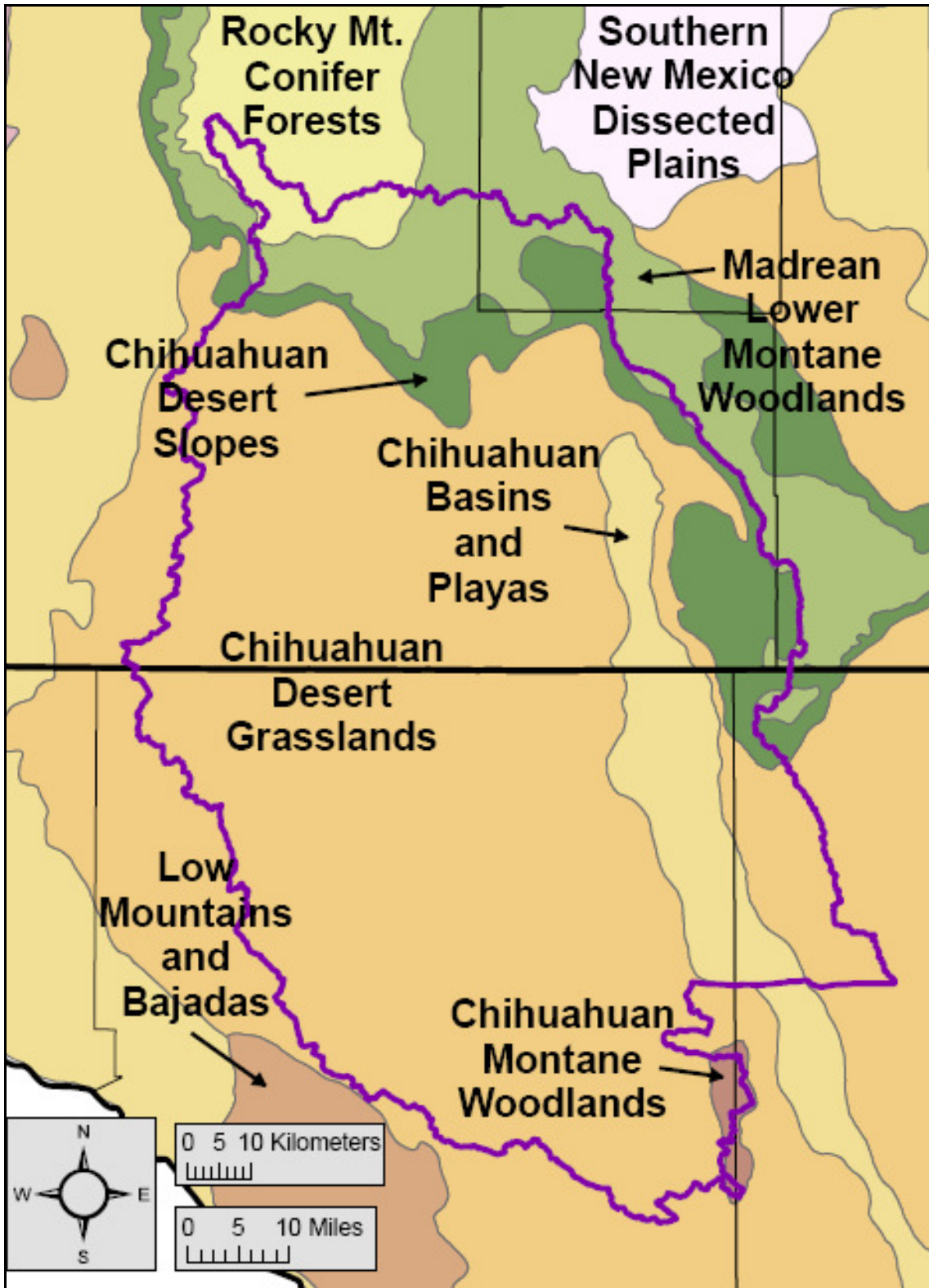
Figure A-1.12: Level IV ecoregions within the northern Salt Basin watershed. Ecoregions from the U.S. Environmental Protection Agency (EPA).
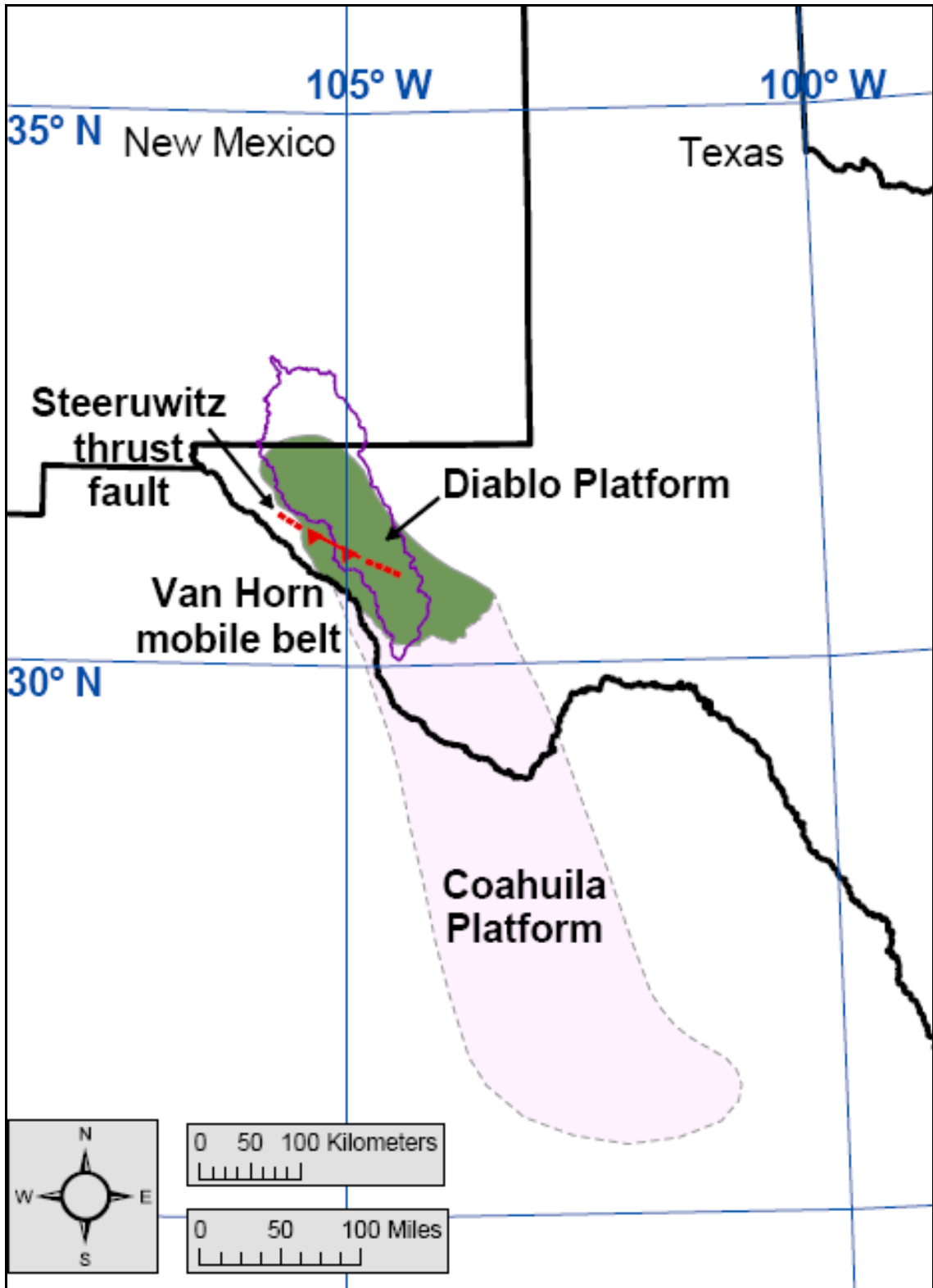
Figure A-1.13: Location of the Diablo and Coahuila Platforms, from Shepard and Walper (1982).
Location of Steeruwitz thrust fault taken from Goetz (1977). Features formed about 1.25 Ga.
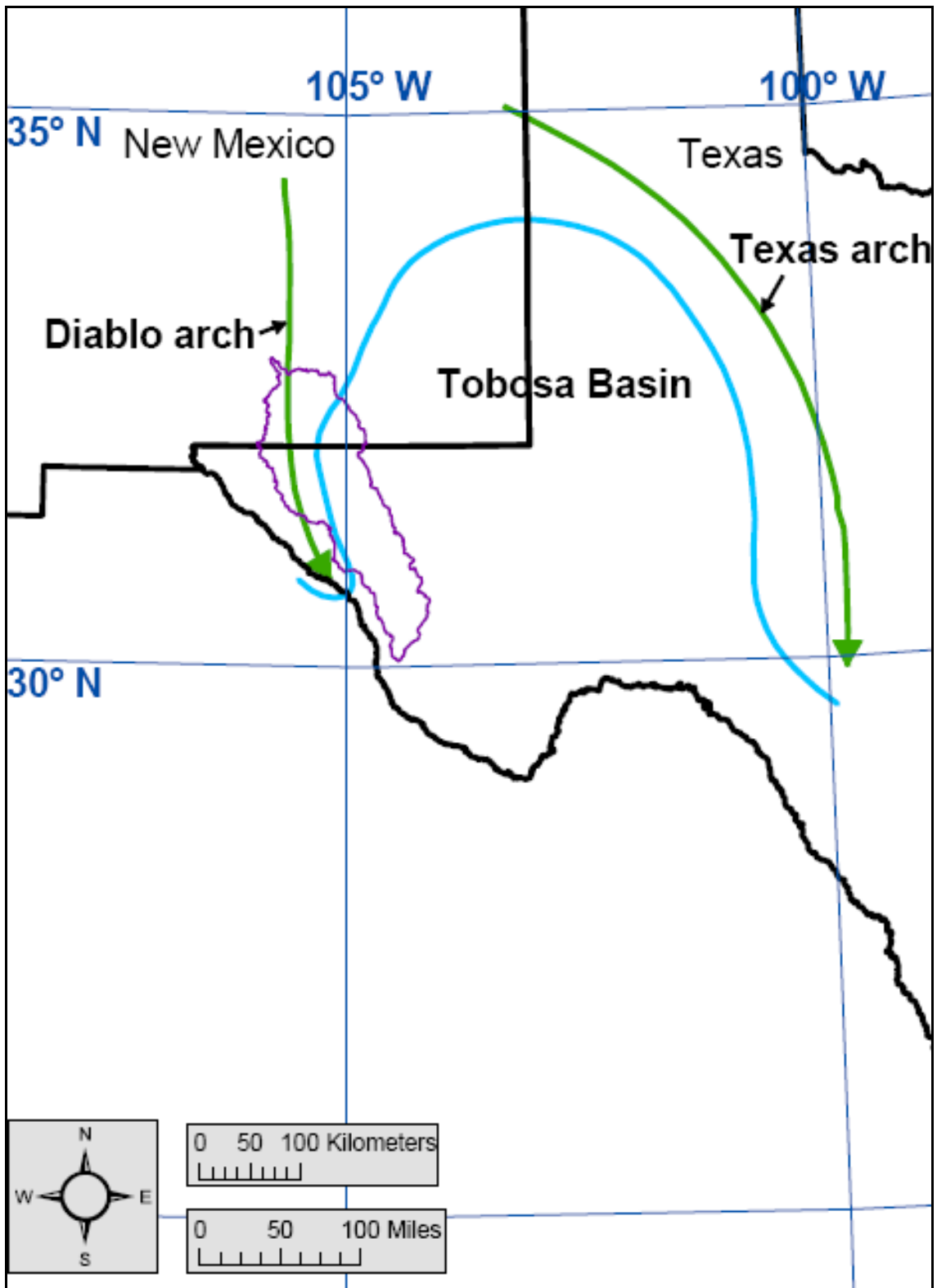
Figure A-1.14: Location of the Diablo and Texas Arches, and the Tobosa Basin, from Adams (1965).
Features formed during the Late Precambrian to Early Cambrian (550 to 510 Ma).
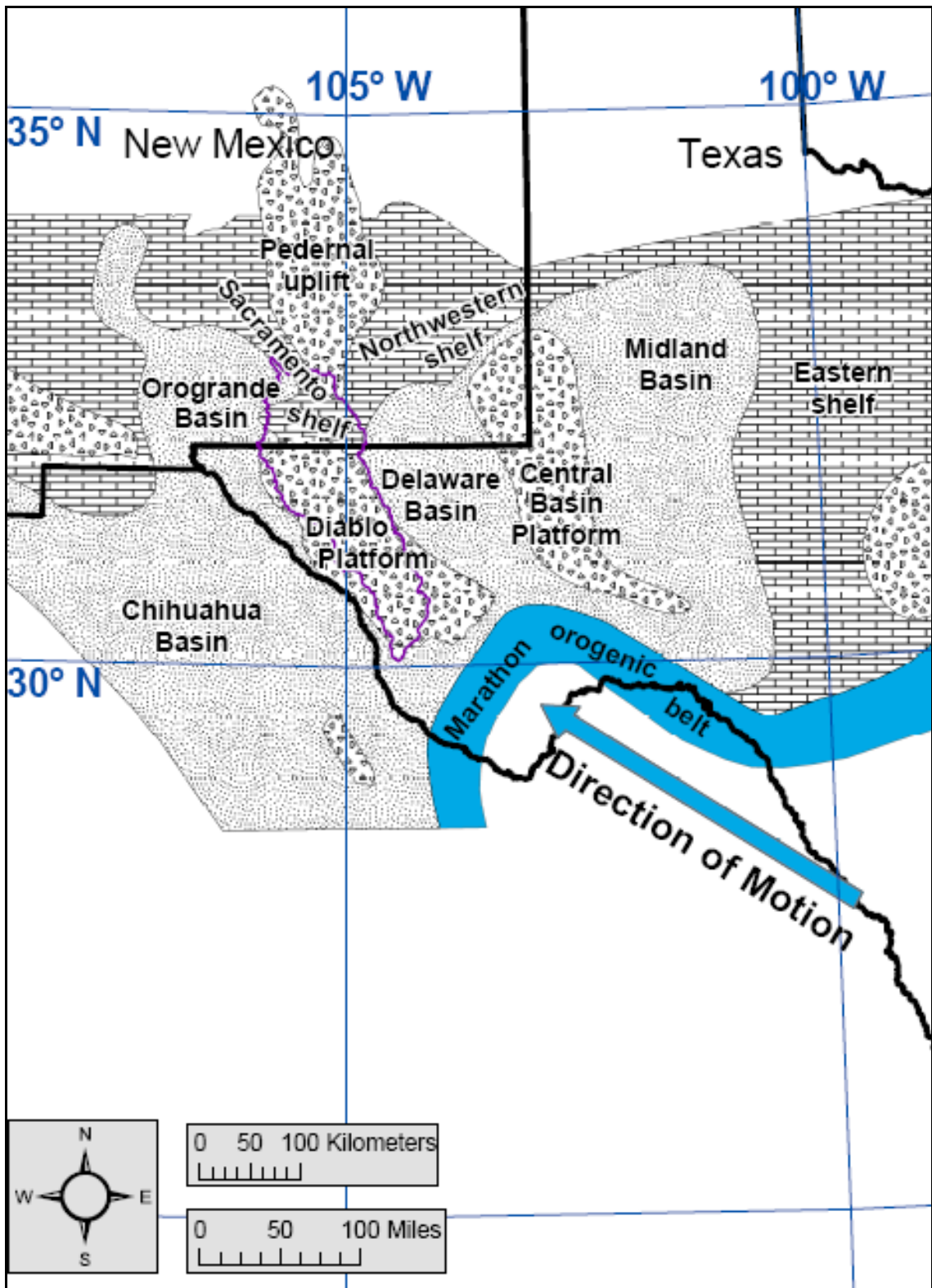
Figure A-1.15: Late-Pennsylvanian-to-Early-Permian tectonic features of the Salt Basin region, from Ross and Ross (1985).
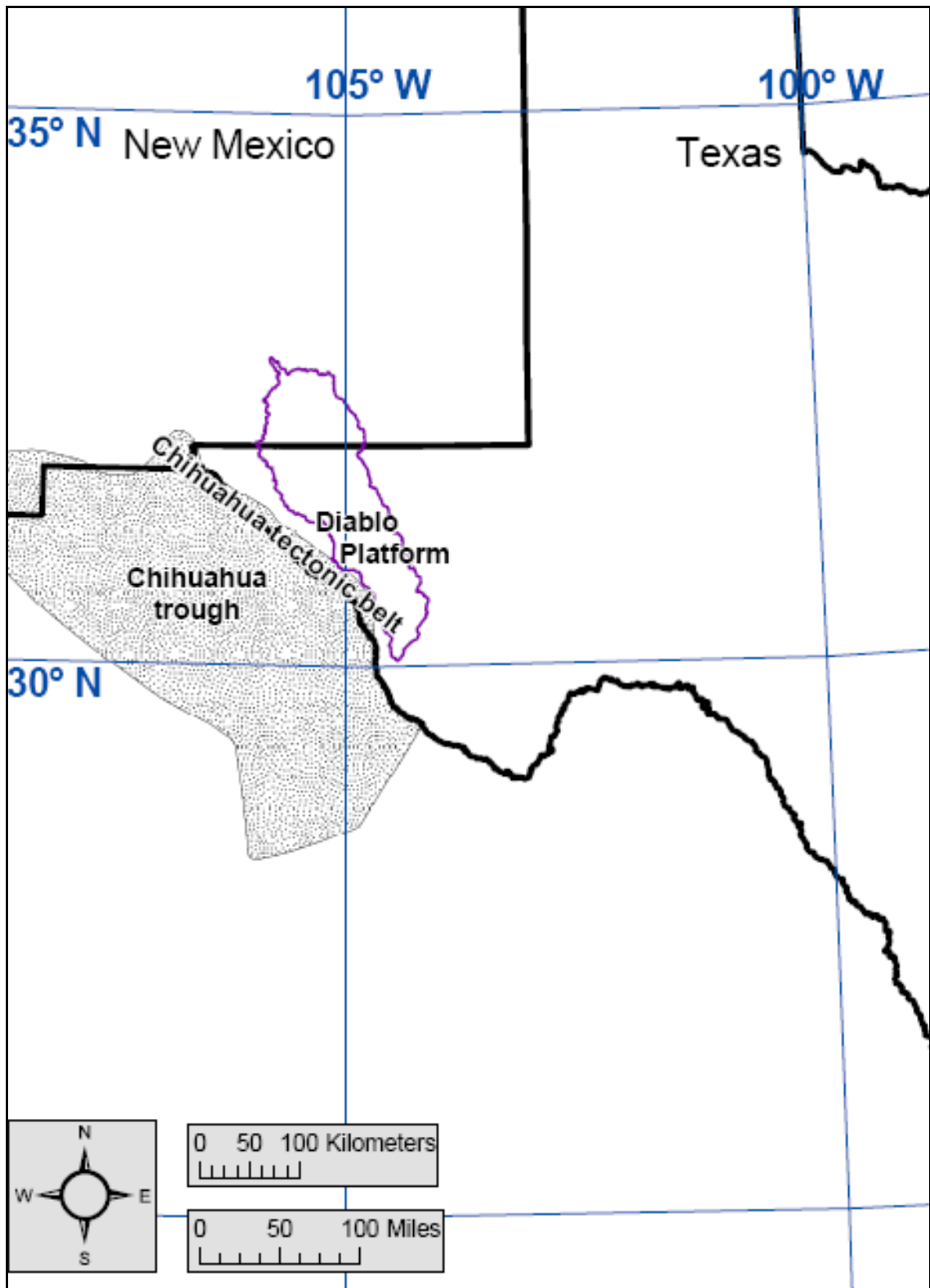
Figure A-1.16: Location of the Mesozoic Chihuahua trough and Chihuahua tectonic belt, from Haenggi (2002).

FIGURES – CHAPTER 2
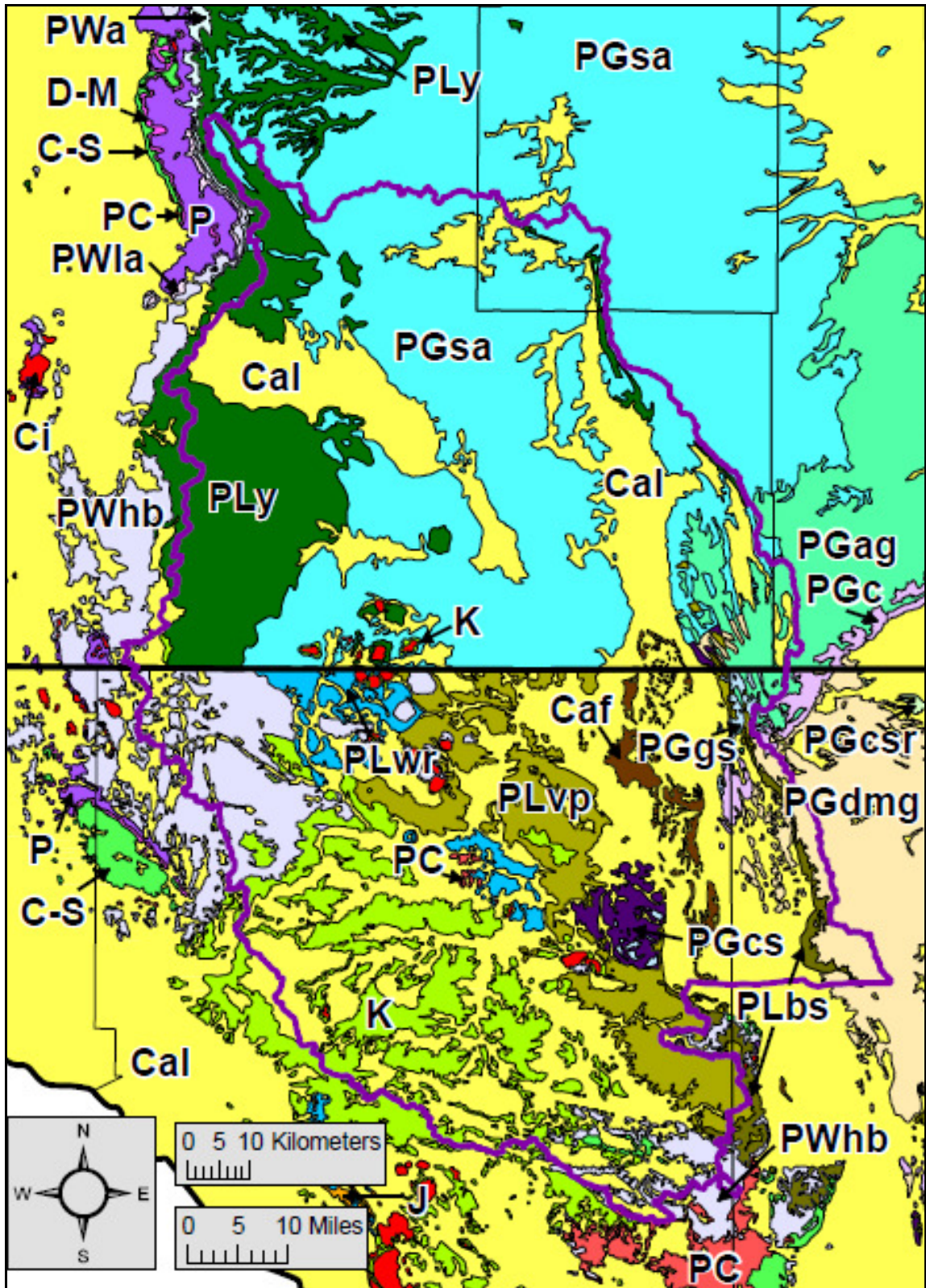
Figure A-2.1: Surface geology of the northern Salt Basin watershed.
Geology from Stoeser et al. (2005), with location of alkali flats/playa lakes for New
Mexico taken from NHD.

Figure A-2.1: Legend

Eon	Era	Period	Legend

Cenozoic

Mesozoic

Phanerozoic

Paleozoic

Permian

Proterozoic

Legend

- Alkali Flats/Playa Lakes (Caf)
- Cenozoic Alluvial Deposits (Cal)
- Cenozoic Intrusives (Ci)
- Cretaceous (K)
- Jurassic (J)
- Castile, Salado, and Rustler Formations (POcsr)
- Artesia Group (PGag)
- Capitan Limestone/Formation (PGc)
- Goat Seep Dolomite/Limestone/Formation (PGgs)
- Delaware Mountain Group (PGdmg)
- San Andres Formation (PGsa)
- Cutoff Shale (PLcs)
- Victorio Peak Limestone/Formation (PLvp)
- Wilke Ranch Formation [Leonardian] (PLwr)
- Yeso Formation (PLy)
- Bone Spring Limestone/Formation (PLbs)
- Abo Formation (PWa)
- Hueco Limestone/Formation / Bursum Formation (PWhb)
- Lower Abo / Pow Wow Conglomerate (PWla)
- Pennsylvanian (P)
- Devonian - Mississippian (D-M)
- Cambrian - Silurian (C-S)
- Precambrian (PC)

Ma	System	Series	Stage	Northwestern and Sacramento Shelves (Sacramento Mountains, Otero Mesa/Diablo Plateau, Hueco Mountains)		Shelf Margin (Guadalupe Mountains, Sierra Diablo)	Delaware Basin
2.588 – Present	Quaternary			In mountains and mesas, alluvium, colluvium, terrace gravels, and spring deposits; in grabens, bolson deposits, lacustrine deposits, fanglomerate, and drifted sand.			
65.5 – 2.588	Neogene Paleogene			Intrusive igneous rocks		//////	//////
99.6 – 65.5	Cretaceous		Gulfian	Mesaverde Fm.		//////	//////
				Mancos Fm.			
				Dakota Fm.			
127 – 99.6	Cretaceous		Comanchean	Washita Group		Also present in the Sierra Diablo	//////
				Fredericksburg Group	Finlay Limestone		
				Trinity Group	Cox Sandstone		
					Campagrande Cong.		
199.6 – 145.5	Jurassic			//////		//////	//////
251 – 199.6	Triassic			//////		//////	//////

Age (Ma)	Period	Series						
260.4 – 251	Permian	Ochoan	//////// (hatched)					Rustler Fm.
								Salado Fm.
								Castile Fm.
270.6 – 260.4		Guadalupian	Artesia Group	Tansill Fm.	Carlsbad Group	Capitan Lm./Fm.	Bell Canyon Fm.	Delaware Mountain Group
				Yates Fm.				
				Seven Rivers Fm.				
				Queen Fm.		Goat Seep Do./Lm./Fm.	Cherry Canyon Fm.	
				Grayburg Fm.				
			San Andres Fm.	Fourmile Draw		Cherry Canyon		
				Bonney Canyon		//////// (hatched)	Brushy Canyon Fm.	
				Rio Bonito				
				Glorieta		Cutoff Shale		
280 – 270.6		Leonardian		Yeso Fm.		Victorio Peak Lm./Fm.		Bone Spring Lm./Fm.
						Bone Spring		

Age (Ma)	Period	Subperiod	Stage	Magdalena Fm./Group		Wolfcamp Series (Hueco Lm./Fm. and Pow Wow Cong.)	
299 – 280	Permian		Wolfcampian	Abo Fm. — Lee Ranch tongue / Pendejo tongue / Danley Ranch tongue	Hueco Lm./Fm / Pow Wow Cong.	Wolfcamp Series (Hueco Lm./Fm. and Pow Wow Cong.)	Wolfcamp Fm.
					Bursum / Laborcita Fm.		
305 – 299	Carboniferous	Pennsylvanian	Virgilian	Magdalena Fm./Group	Holder Fm.	Unnamed	Cisco
306.5 – 305			Missourian		Beeman Fm.	Unnamed	Canyon
308 – 306.5			Desmoinesian		Gobbler Fm.	Unnamed	Strawn
311.7 – 308			Atokan/Derryan			Unnamed	Bend
318.1 – 311.7			Morrowan			Unnamed?	

Age	Period	Series	Stage	Formation	
333 – 318.1	Carboniferous	Mississippian	Chesterian	Helms Fm.	Barnett Shale
340 – 333			Meramecian	Rancheria Fm.	"Mississippian Limestone"
348 – 340			Osagean	Lake Valley Fm.	
359.2 – 348			Kinderhookian	Caballero Fm.	
385.3 – 359.2	Devonian	Upper		Sly Gap Fm.	Percha / Woodford Shale
				Oñate Fm. / Percha Shale	
				Canutillo Fm.	
397.5 – 385.3		Middle		//////	"Devonian"
416 – 397.5		Lower		//////	
438 – 421.3	Silurian		Niagaran	Fusselman Fm.	

				Valmont Dolomite	Montoya Group
451 – 443.7	Ordovician		Cincinnatian	Montoya Group	
488.3 – 471.8			Canadian	El Paso / Ellenburger Group	
501 – 488.3	Cambrian		Croixian	Bliss Sandstone	
	Precambrian				

Figure A-2.2: Generalized stratigraphic chart of the Salt Basin region.

Adapted from numerous sources, including Black (1973), Boyd (1958), Foster (1978), Hayes (1964), Kelley (1971), Kottlowski (1963), LeMone (1969), McGlasson (1969), Newell et al. (1972), and Pray (1961).
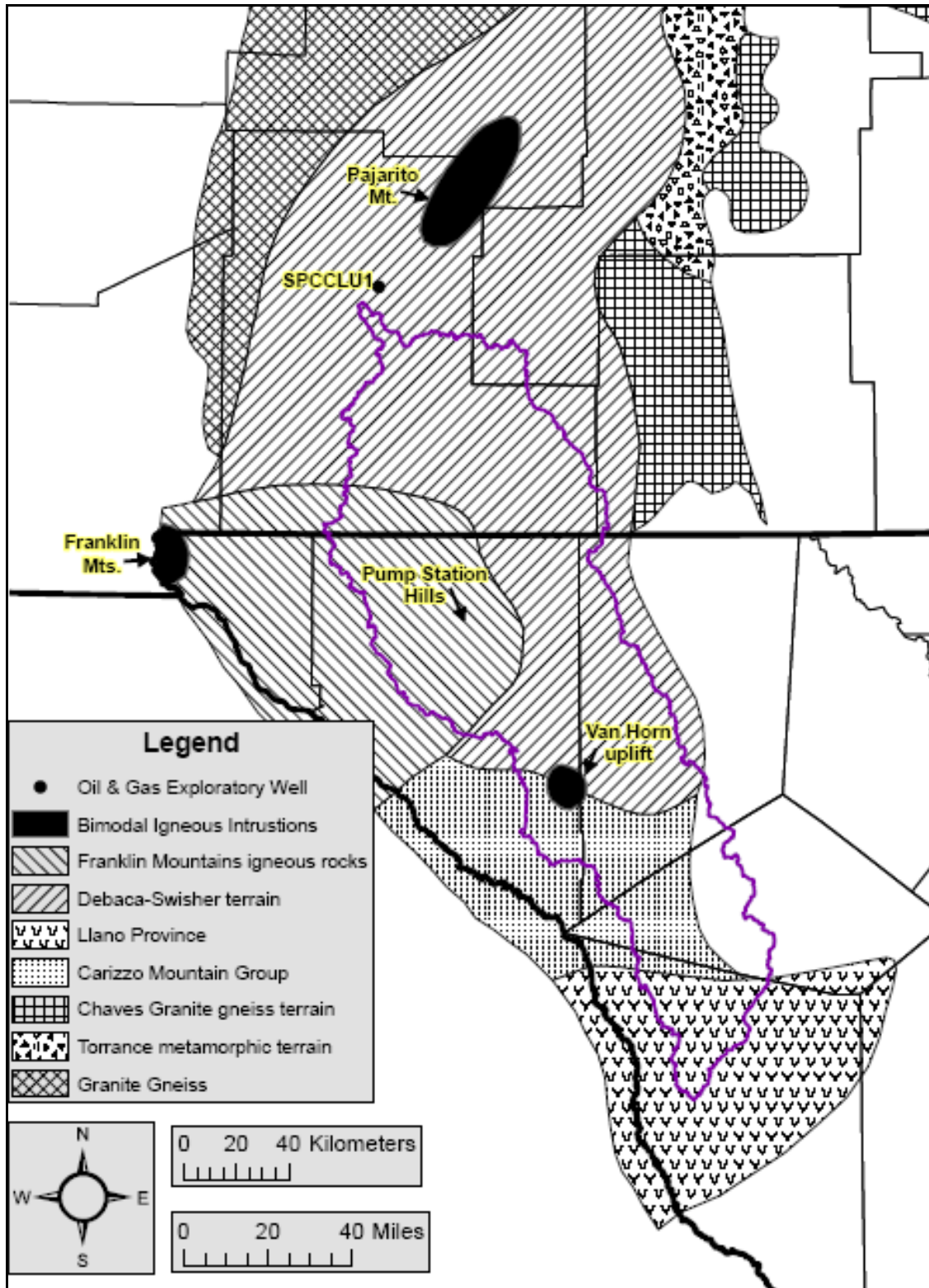
Figure A-2.3: Precambrian basement rocks of the Salt Basin region, from Adams et al. (1993) and Denison et al. (1984).
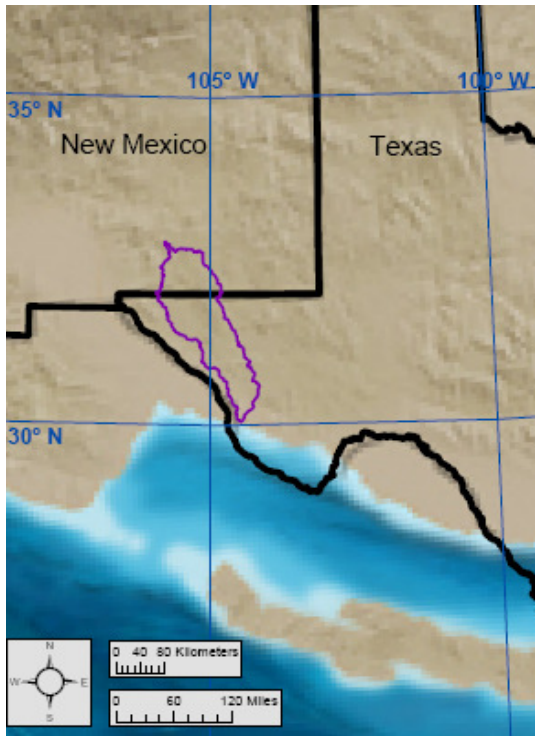
a: Late Precambrian (550 Ma)
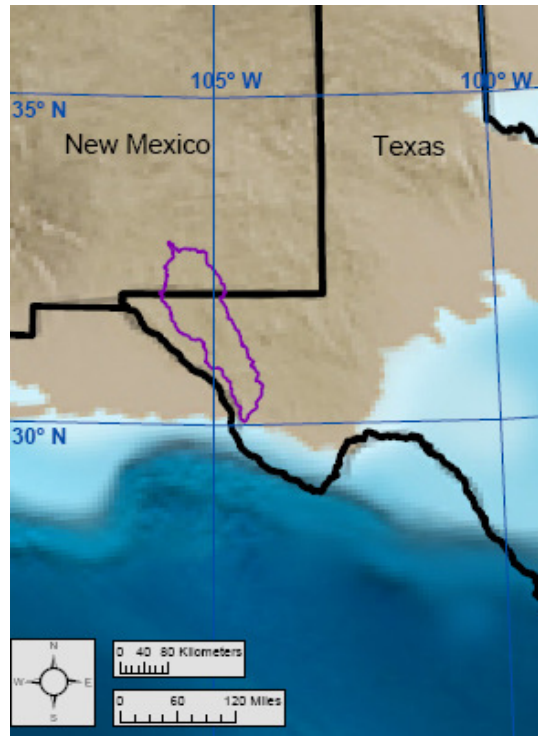
b: Middle Cambrian (510 Ma)
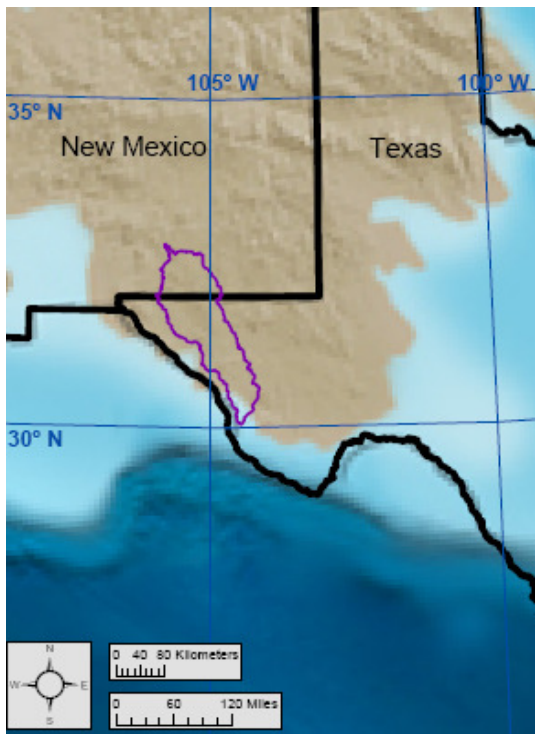
c: Late Cambrian (500 Ma)
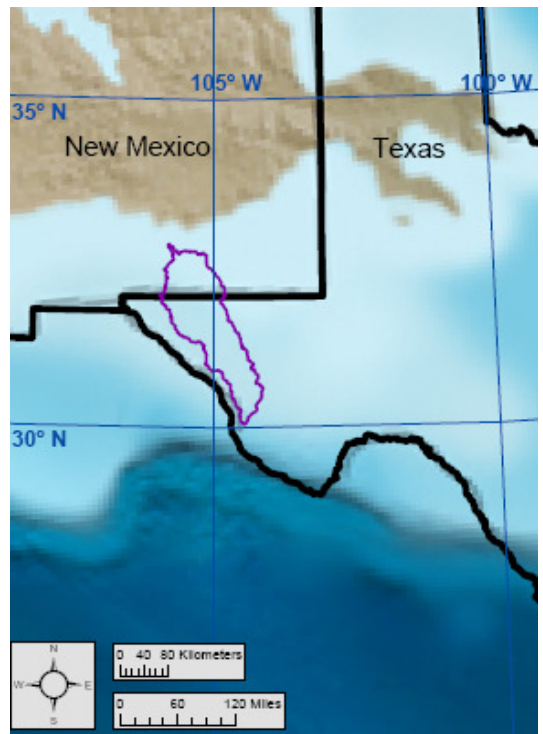
d: Early Ordovician (485 Ma)

Figure A-2.4: Late-Precambrian-to-Early-Ordovician paleogeography of the Salt Basin region, from Blakey (2009b).
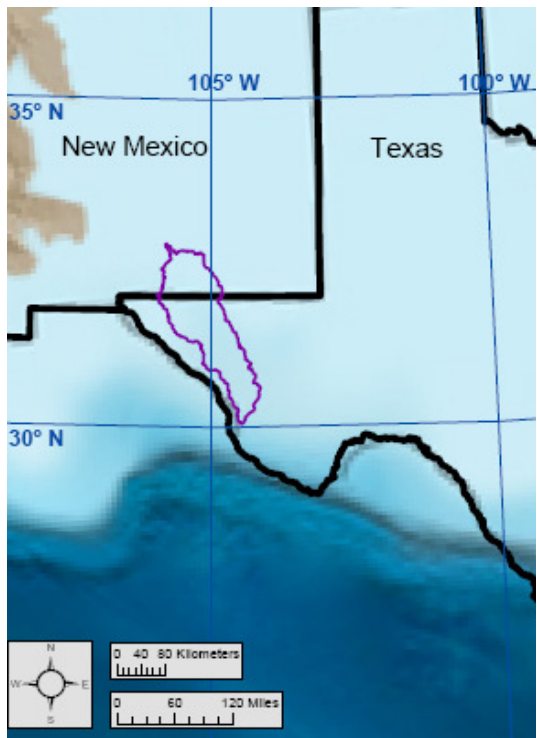
a: Middle Ordovician (470 Ma)
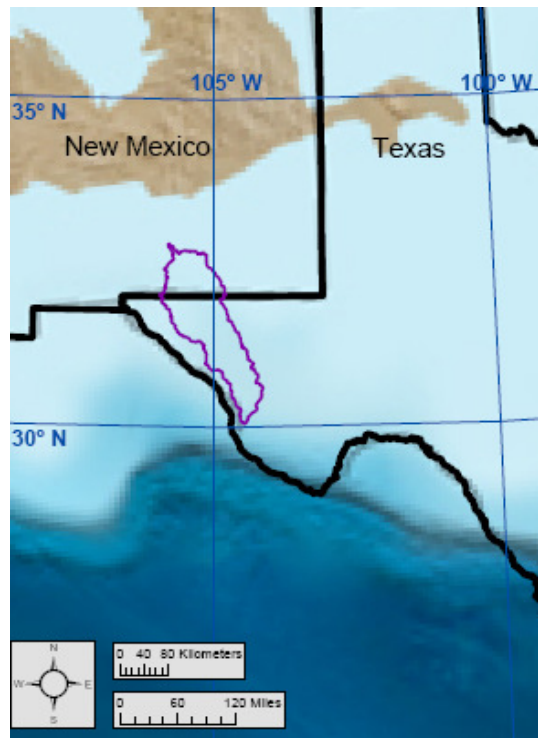
b: Late Ordovician (450 Ma)
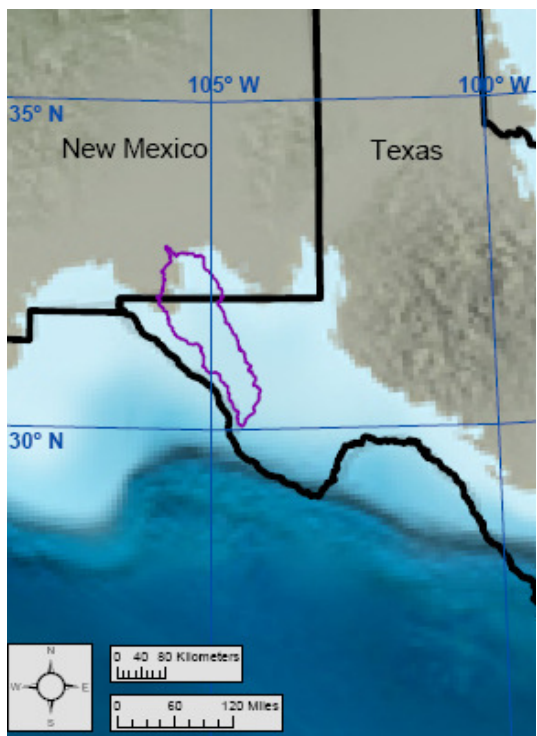
c: Early Silurian (430 Ma)
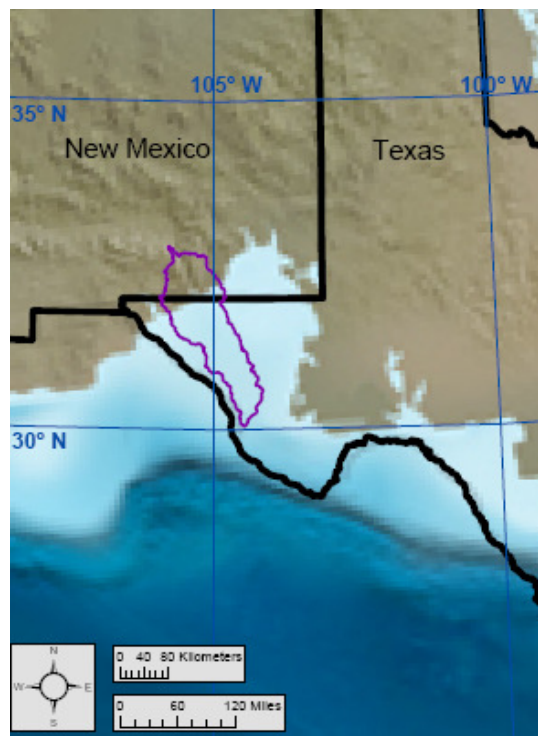
d: Late Silurian (420 Ma)

Figure A-2.5: Middle-Ordovician-to-Late-Silurian paleogeography of the Salt Basin region, from Blakey (2009b).

a: Early Devonian (400 Ma)
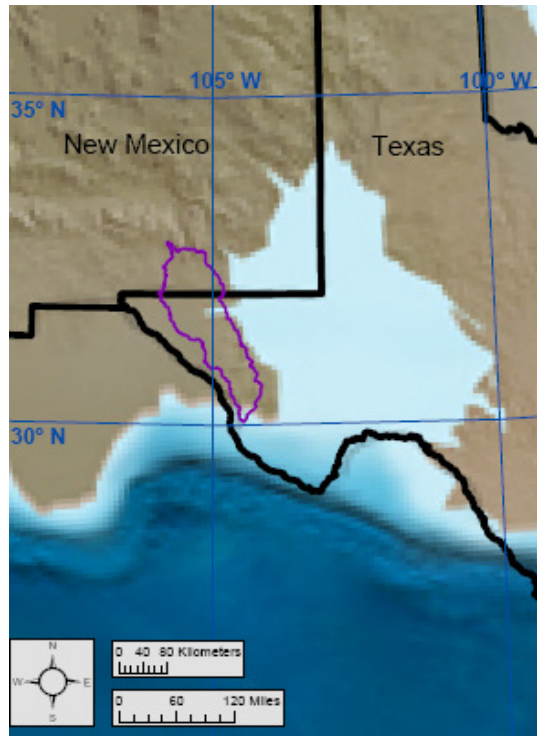
b: Middle Devonian (385 Ma)
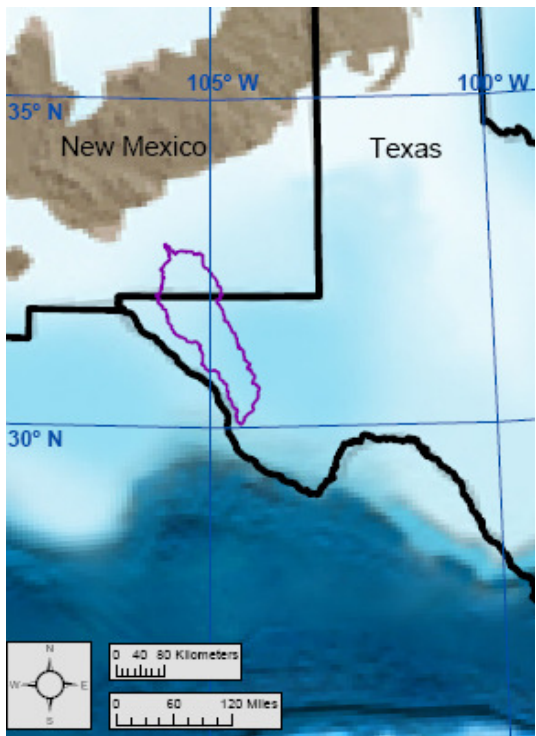
c: Late Devonian (360 Ma)
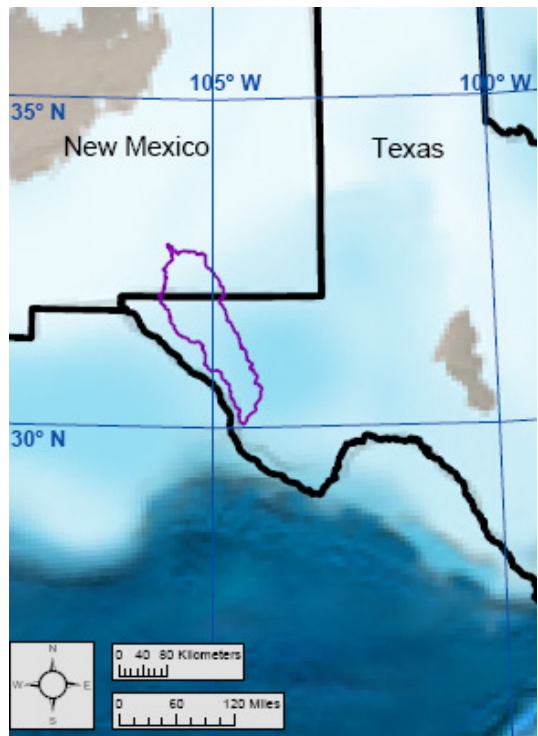
d: Early Mississippian (345 Ma)

Figure A-2.6: Early-Devonian-to-Early-Mississippian paleogeography of the Salt Basin region, from Blakey (2009b).
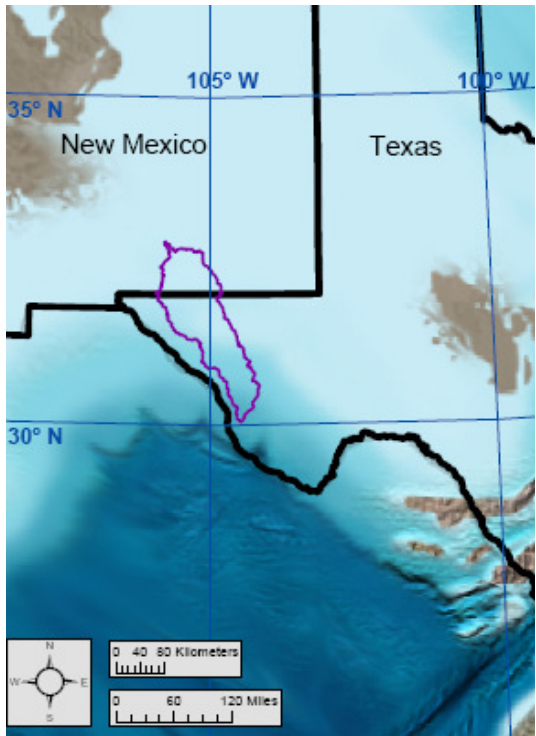
a: Early Mississippian (340 Ma)
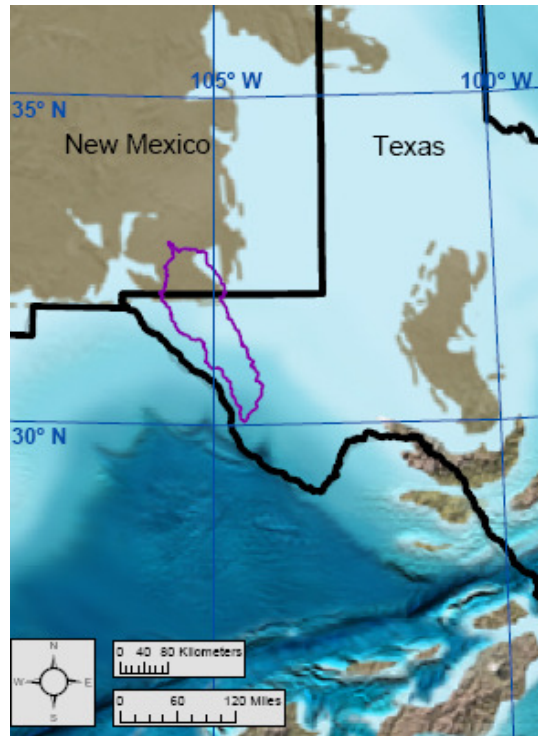
b: Late Mississippian (325 Ma)
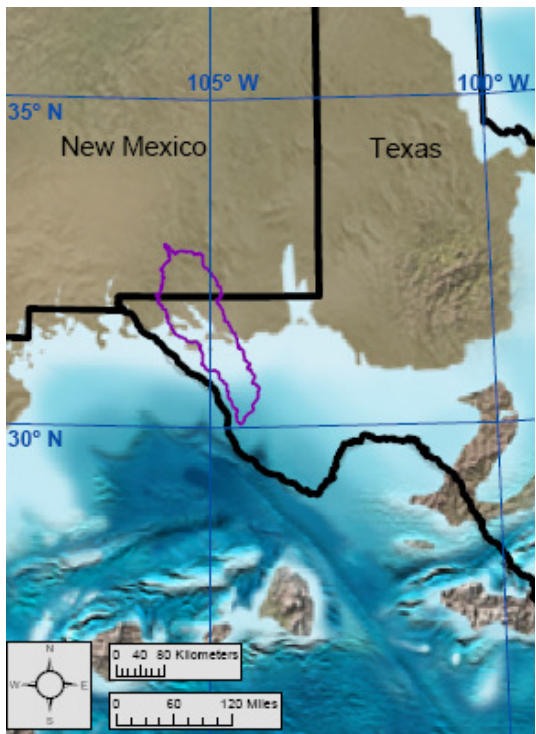
c: Miss.-Penn. lowstand (320 Ma)
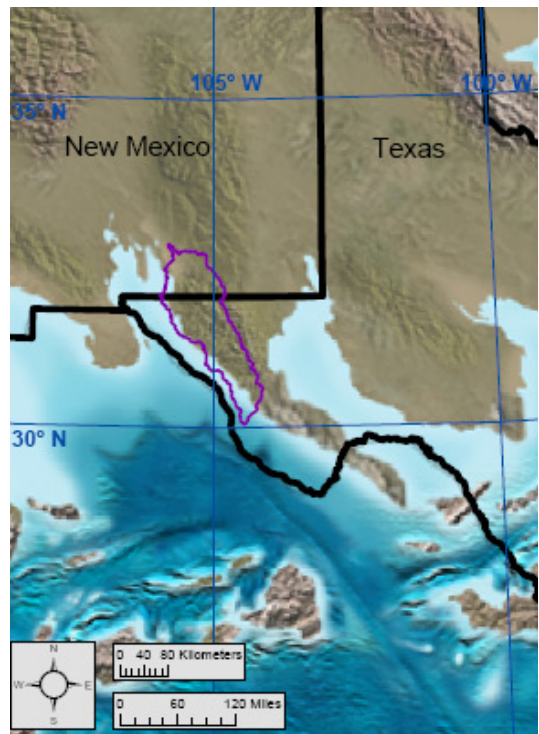
d: Pennsylvanian Morrowan (318 Ma)

Figure A-2.7: Early-Mississippian-to-Pennsylvanian-Morrowan paleogeography of the Salt Basin region, from Blakey (2009a).
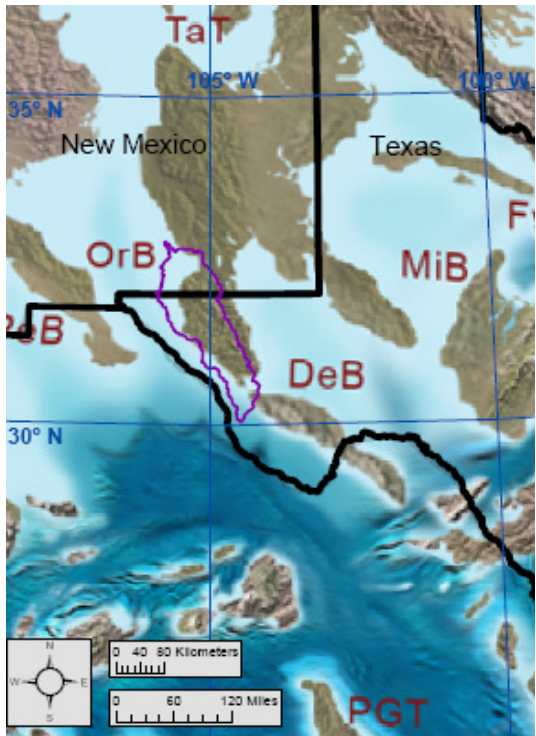
a: Pennsylvanian Atokan (315 Ma)

b: Pennsylvanian Desmoinian (310 Ma)

c: Pennsylvanian Missourian (300 Ma)

d: Pennsylvanian Virgilian (295 Ma)

Figure A-2.8: Pennsylvanian-Atokan-to-Pennsylvanian-Virgilian paleogeography of the Salt Basin region, from Blakey (2009a).
OrB = Orogrande Basin, DeB = Delaware Basin, MiB = Midland Basin.

a: Early Permian (290 Ma)

b: Early Permian (287 Ma)

c: Early Permian (285 Ma)

d: Early Permian (280 Ma)

Figure A-2.9: Early-Permian paleogeography of the Salt Basin region, from Blakey (2009a).
OrB = Orogrande Basin, DeB = Delaware Basin, MiB = Midland Basin.
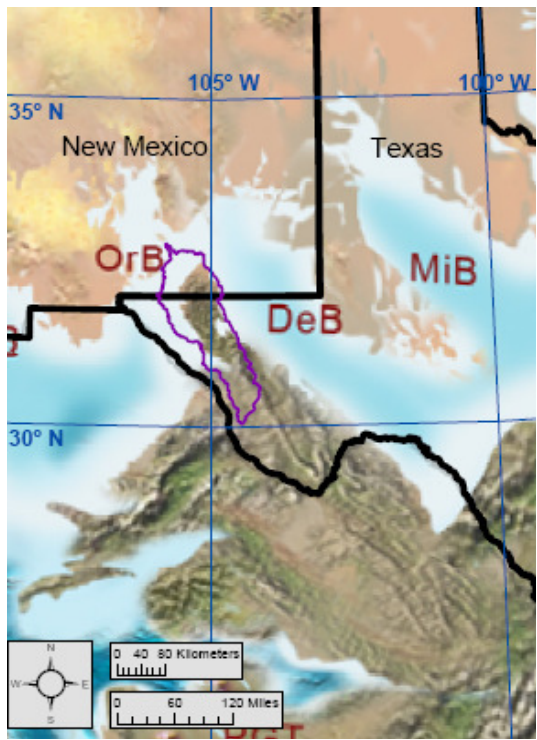
a: Early Permian (278 Ma)
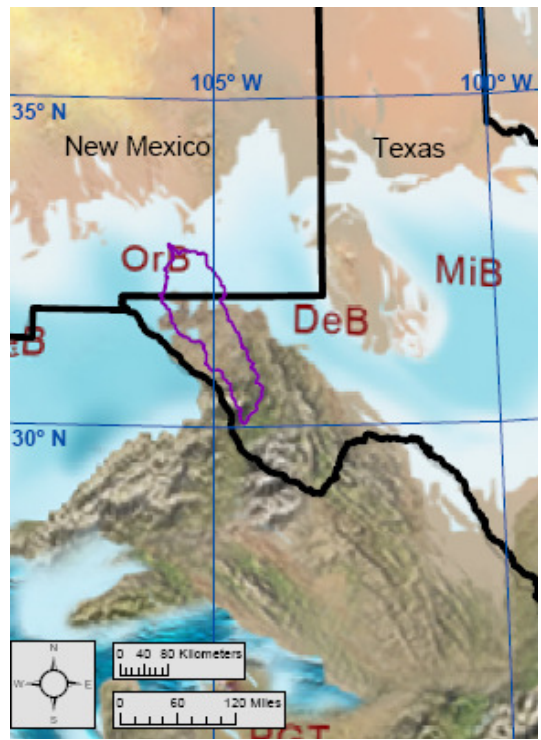
b: Early Permian (275 Ma)
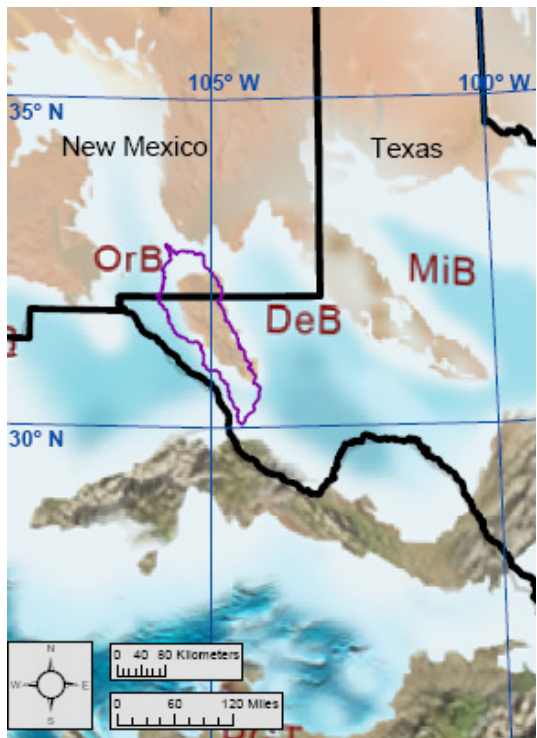
c: Middle Permian (270 Ma)

d: Late Permian (260 Ma)

Figure A-2.10: Early-Permian-to-Late-Permian paleogeography of the Salt Basin region, from Blakey (2009a).

OrB = Orogrande Basin, DeB = Delaware Basin, MiB = Midland Basin.
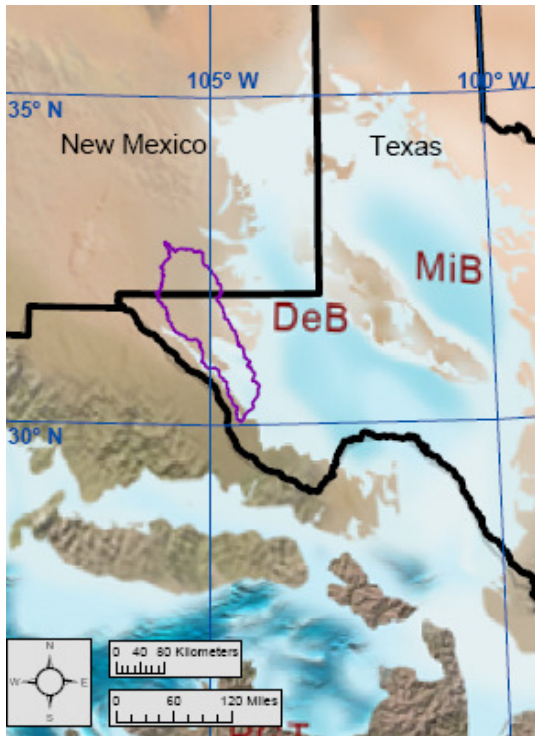
a: Late Permian (255 Ma)

b: Early Triassic (240 Ma)
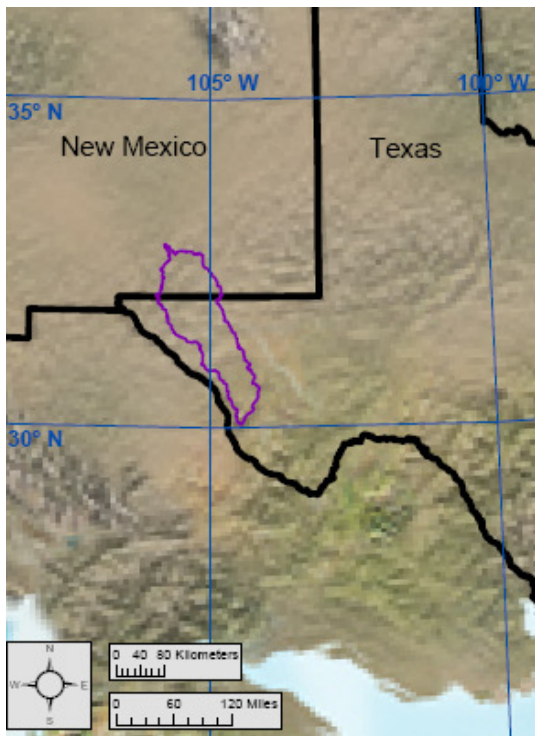
c: Middle Triassic (230 Ma)

d: Late Triassic (210 Ma)

Figure A-2.11: Late-Permian-to-Late-Triassic paleogeography of the Salt Basin region, from Blakey (2009a) and Blakey (2009b).
DeB = Delaware Basin, MiB = Midland Basin.

493

a: Early Jurassic (195 Ma)
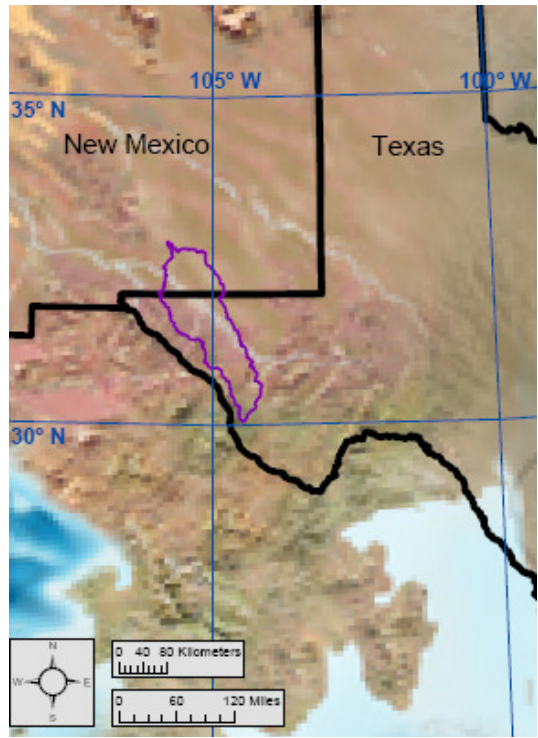
b: Early Jurassic (180 Ma)
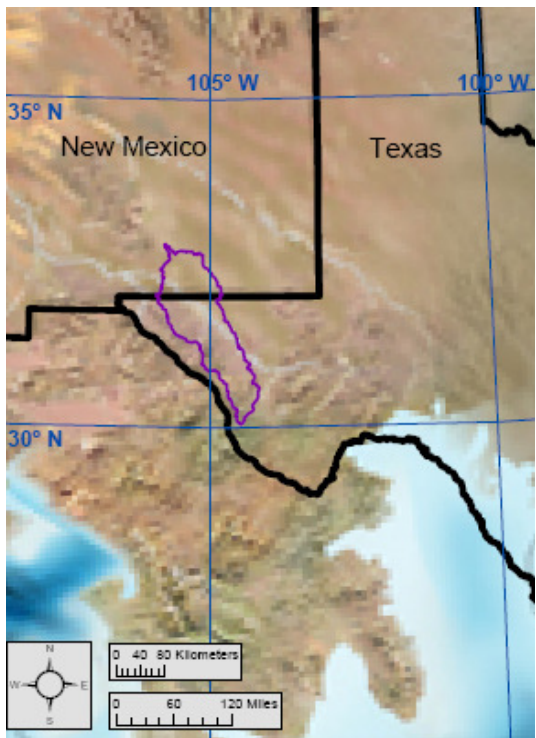
c: Middle Jurassic (170 Ma)

d: Late Jurassic (150 Ma)

Figure A-2.12: Early-Jurassic-to-Late-Jurassic paleogeography of the Salt Basin region, from Blakey (2009b).

a: Early Cretaceous (140 Ma)
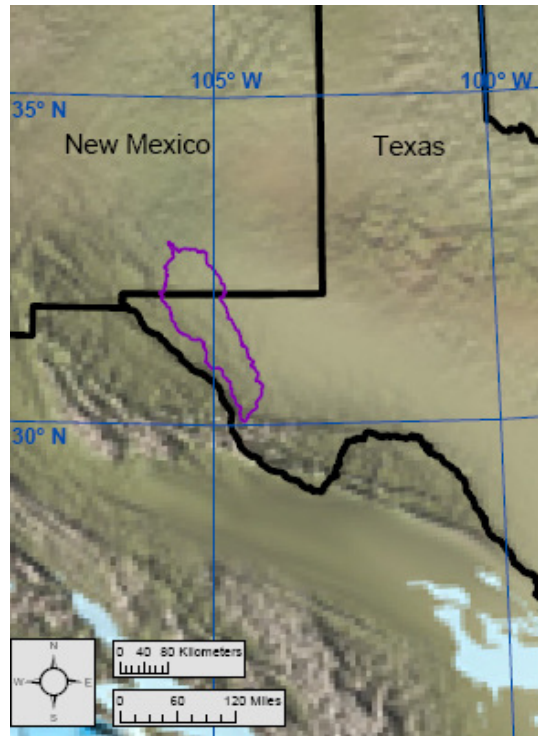
b: Early Cretaceous (130 Ma)

c: Early Cretaceous (115 Ma)

d: Late Cretaceous (100 Ma)

Figure A-2.13: Early-Cretaceous-to-Late-Cretaceous paleogeography of the Salt Basin region, from Blakey (2009b).

a: Late Cretaceous (85 Ma)

b: Late Cretaceous (75 Ma)

c: Cretaceous-Paleogene (65 Ma)
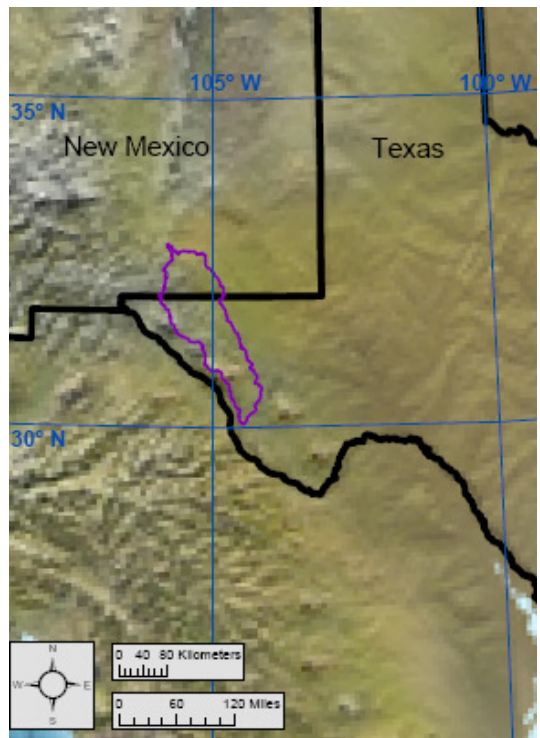
d: Paleogene Paleocene (60 Ma)

Figure A-2.14: Late-Cretaceous-to-Paleogene-Paleocene paleogeography of the Salt Basin region, from Blakey (2009b).

a: Paleogene Eocene (50 Ma) b: Paleogene Eocene (40 Ma)
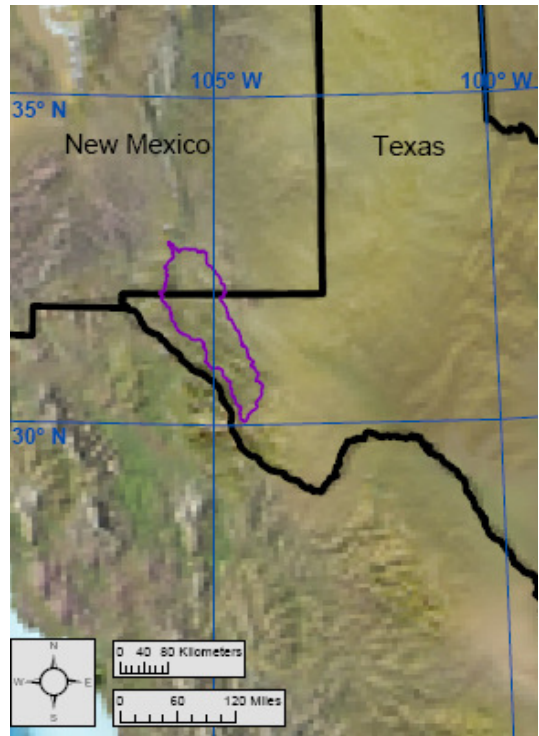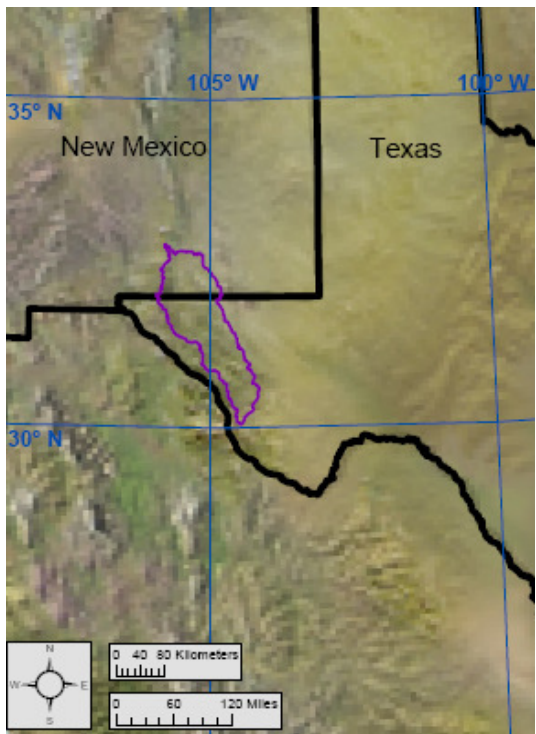
c: Paleogene Oligocene (25 Ma) d: Neogene Miocene (15 Ma)

Figure A-2.15: Paleogene-Eocene-to-Neogene-Miocene paleogeography of the Salt Basin region, from Blakey (2009b).

a: Neogene Miocene (8 Ma)   b: Neogene Pliocene (3 Ma)

c: Quaternary Glacial (0.126 Ma)   d: Present

Figure A-2.16: Neogene-Miocene-to-Present paleogeography of the Salt Basin region, from Blakey (2009b).

a: Wolfcampian facies

b: Early Leonardian facies

Legend

Sandstone, fine- to coarse-grained, including some conglomerate	Limestone, thick- to thin-bedded, calcitic or dolomitic
Anhydrite, generally interbedded with dominant facies	Shale, dark gray to black, and thin-bedded black limestone
Red beds, in part shaly, in part sandy	
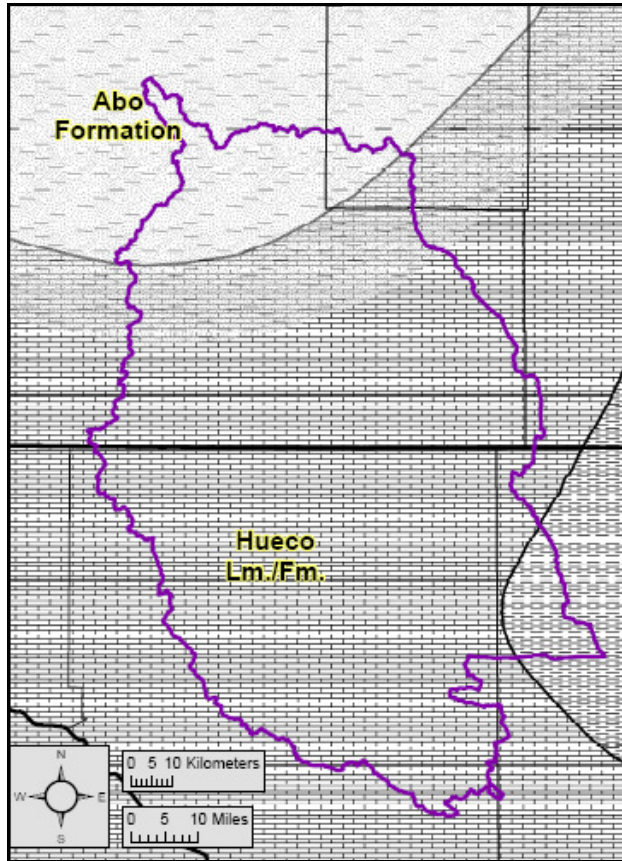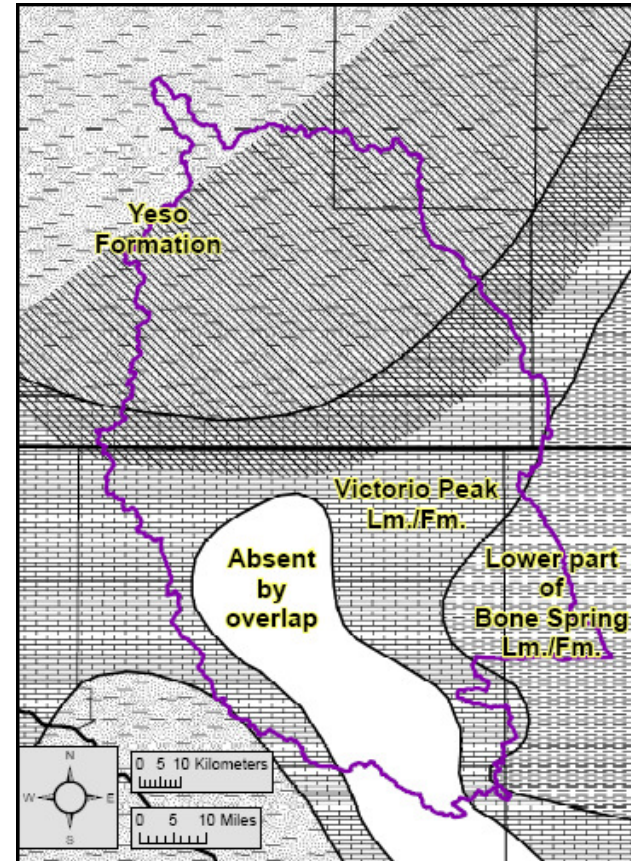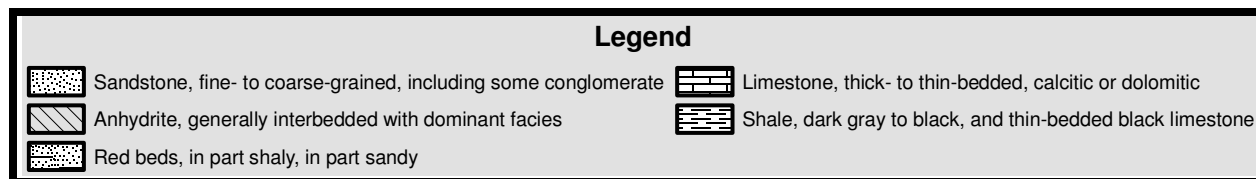
Figure A-2.17: Wolfcampian-to-Early-Leonardian facies, from King (1942) and King (1948).

a: Late Leonardian facies   b: Early Guadalupian facies

Legend

Sandstone, fine- to coarse-grained, including some conglomerate	Limestone, thick- to thin-bedded, calcitic or dolomitic
Anhydrite, generally interbedded with dominant facies	Shale, dark gray to black, and thin-bedded black limestone
Red beds, in part shaly, in part sandy	
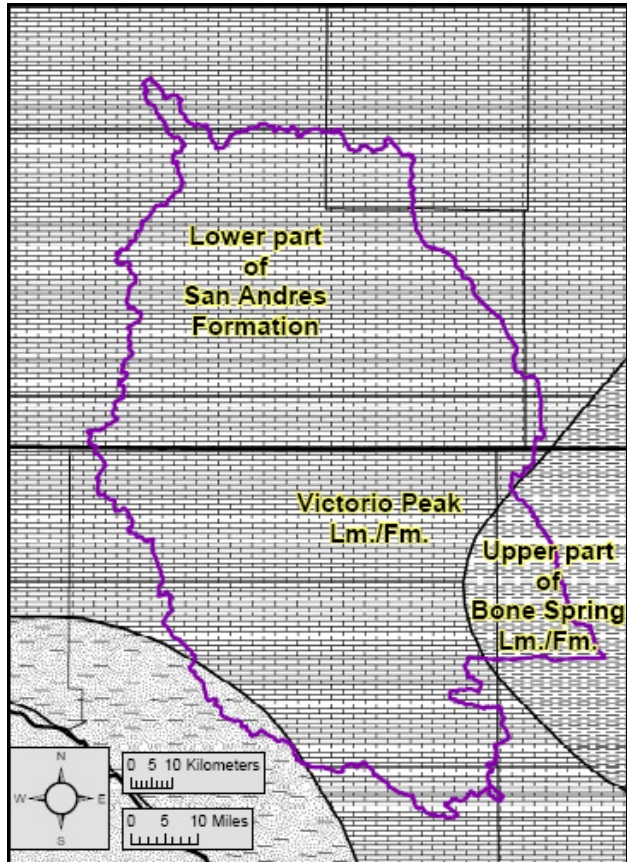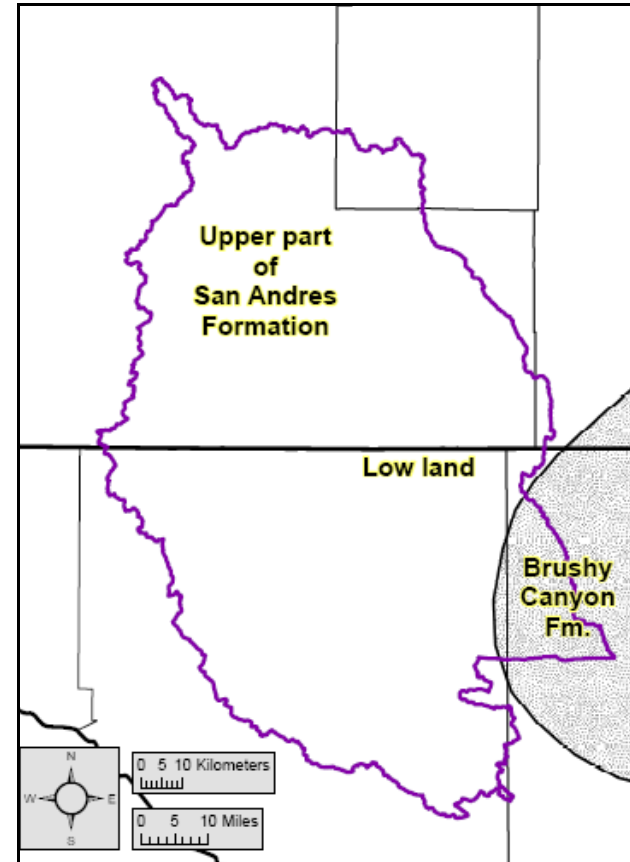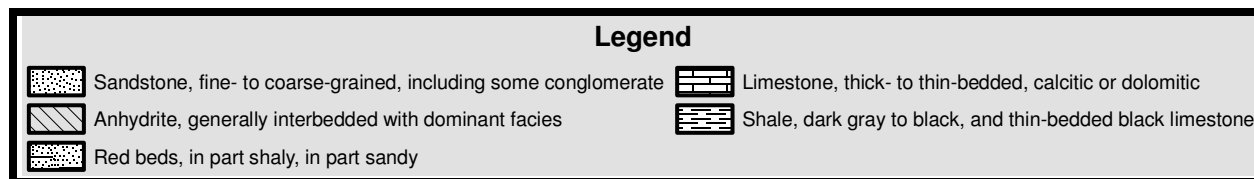
Figure A-2.18: Late-Leonardian-to-Early-Guadalupian facies, from King (1942) and King (1948).

a: Middle Guadalupian facies

b: Late Guadalupian facies

Legend

Sandstone, fine- to coarse-grained, including some conglomerate	Limestone, thick- to thin-bedded, calcitic or dolomitic
Anhydrite, generally interbedded with dominant facies	Shale, dark gray to black, and thin-bedded black limestone
Red beds, in part shaly, in part sandy	
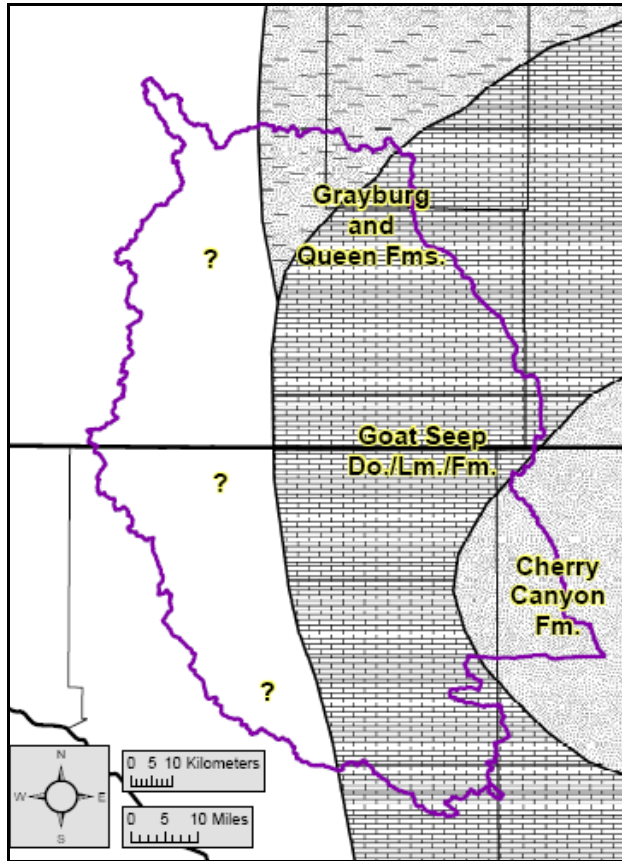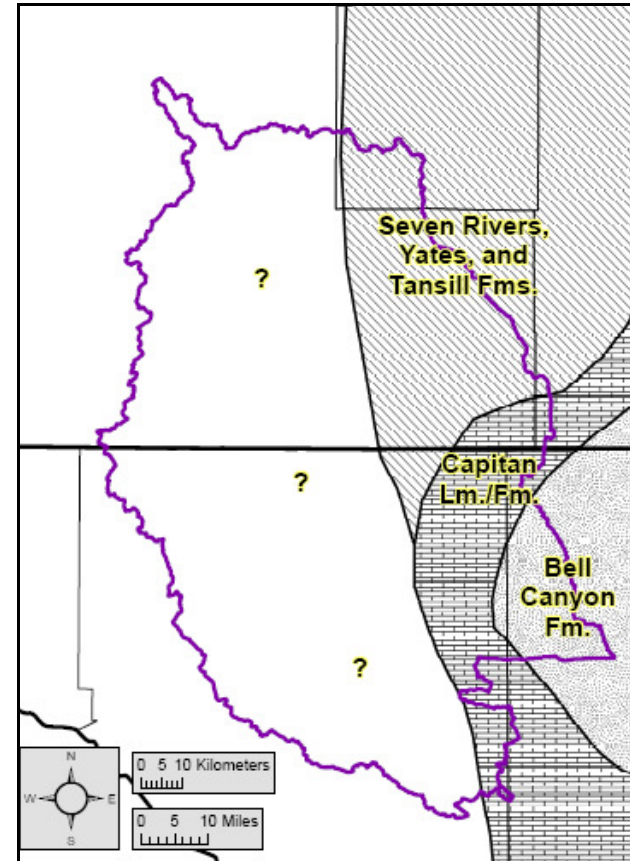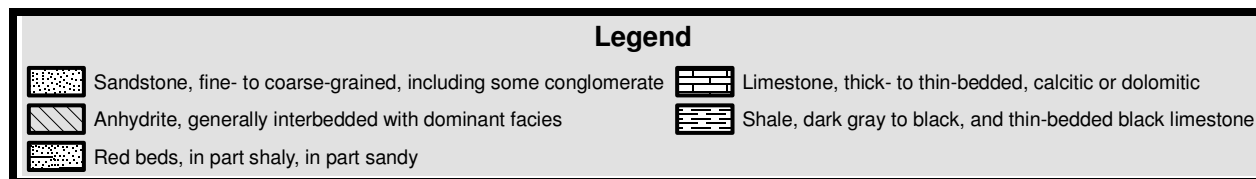
Figure A-2.19: Middle-Guadalupian-to-Late-Guadalupian facies, from King (1942) and King (1948).
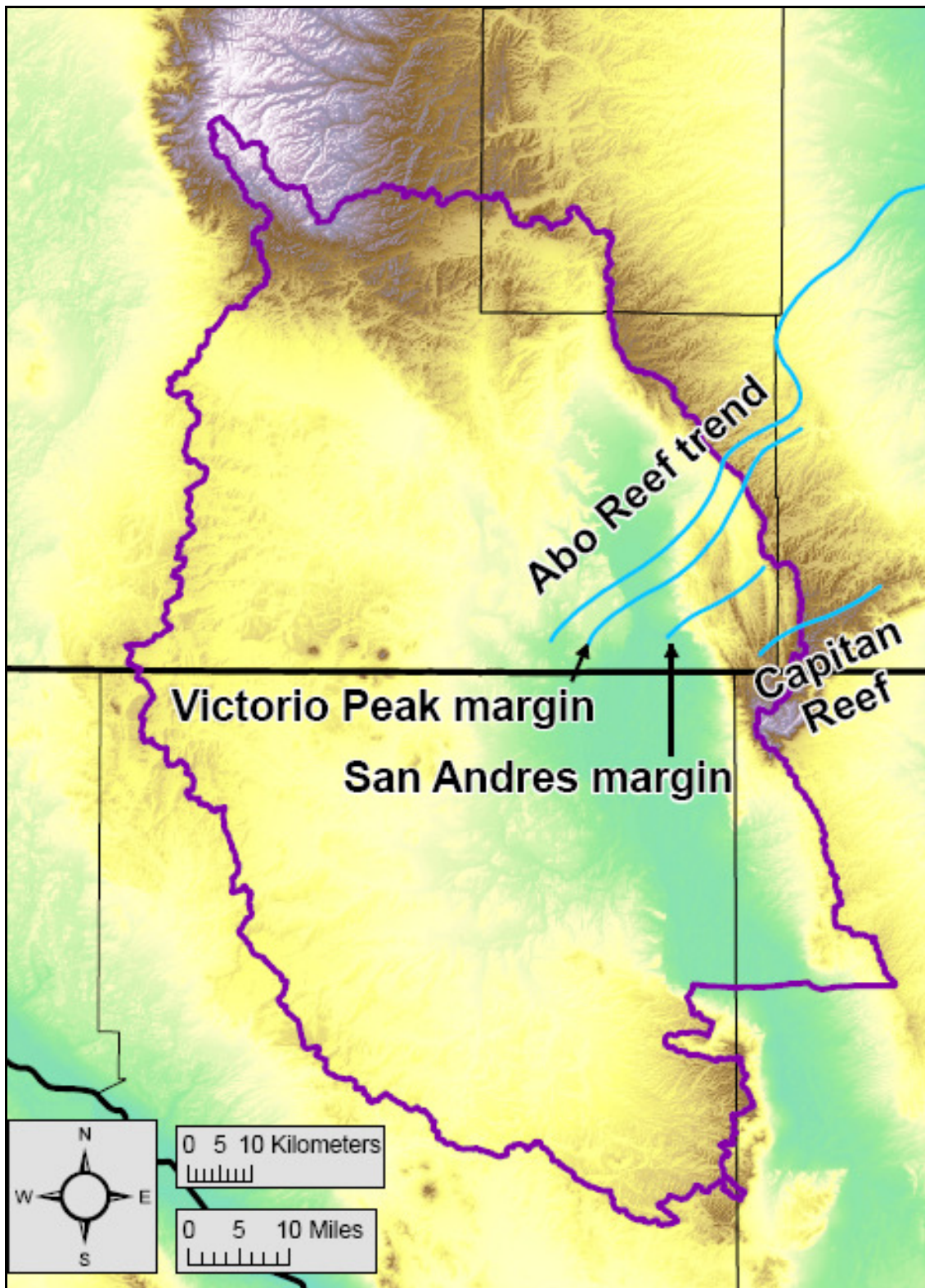
Figure A-2.20: Permian shelf-margin trends, from Black (1975).
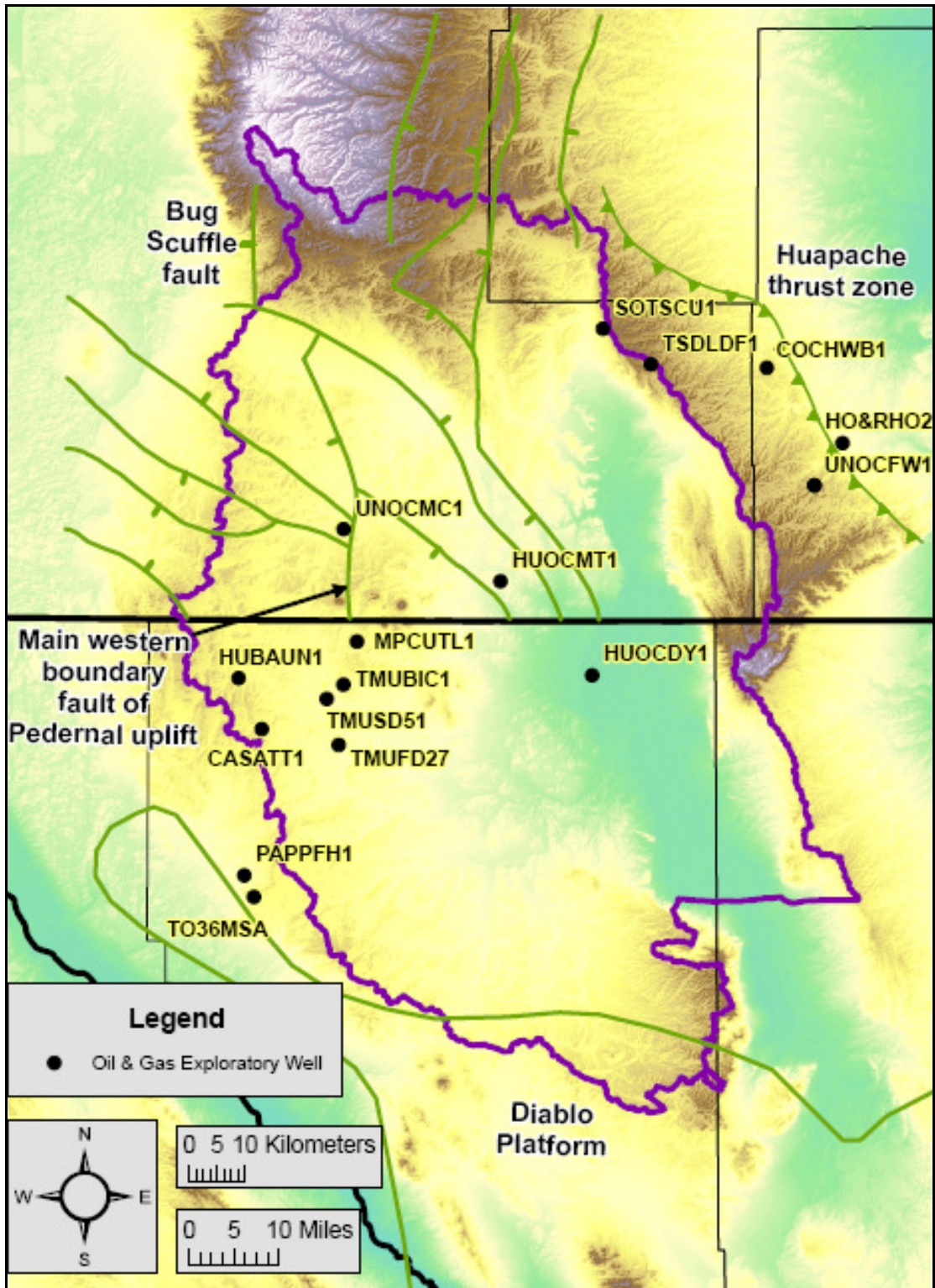
Figure A-2.21: Pennsylvanian-to-Early-Permian structural features of the northern Salt Basin watershed.

Bar on downthrown side of normal or high angle faults, triangles on upthrown side of thrust zone. Location of structures in New Mexico taken from Broadhead (2002). Location of Diablo Platform taken from Kottlowski (1969).
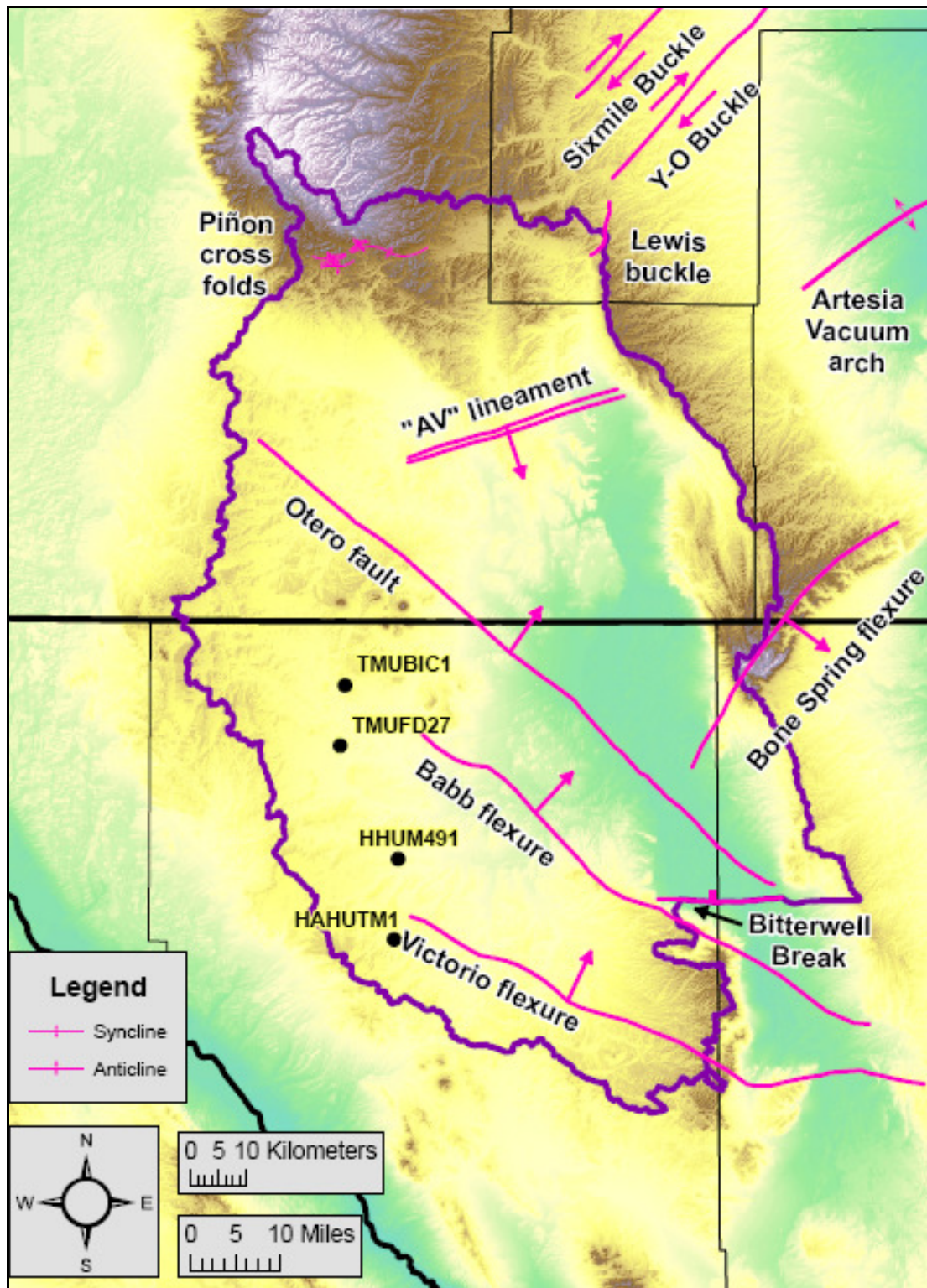
Figure A-2.22: Mid-to-Late-Permian structural features of the northern Salt Basin watershed.
Arrows indicate sense of displacement. Bar on downthrown side of Bitterwell Break.
Location of structures taken from Black (1976), Goetz (1985), and Kelley (1971).
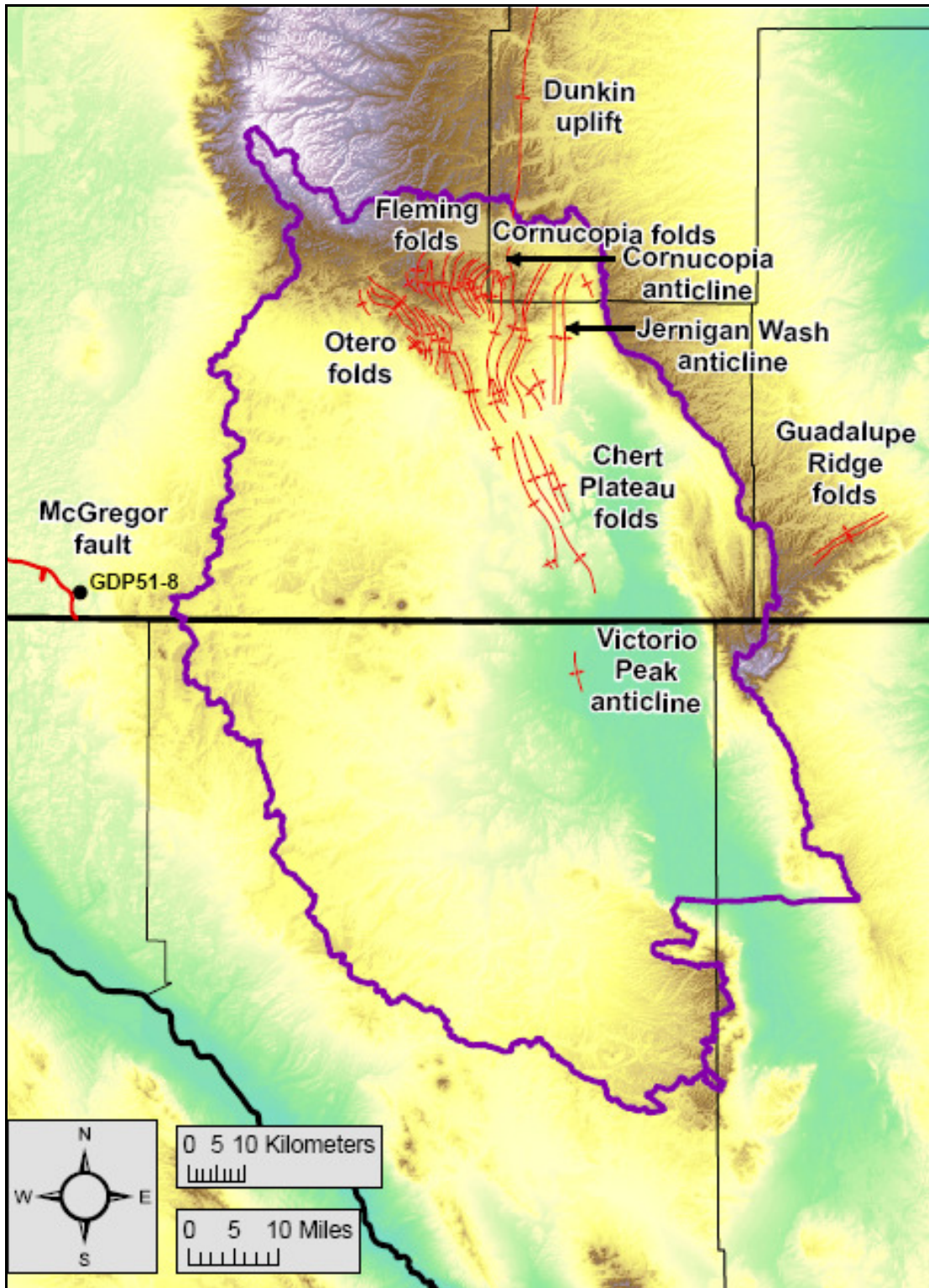
Figure A-2.23: Late-Cretaceous (Laramide) structural features of the northern Salt Basin watershed.
Syncline and anticline symbols are the same as those used on Figure A-2.22. Bar on downthrown side of McGregor fault. Location of structures taken from Black (1976), Goetz (1985), Kelley (1971), and Seager et al. (1987).
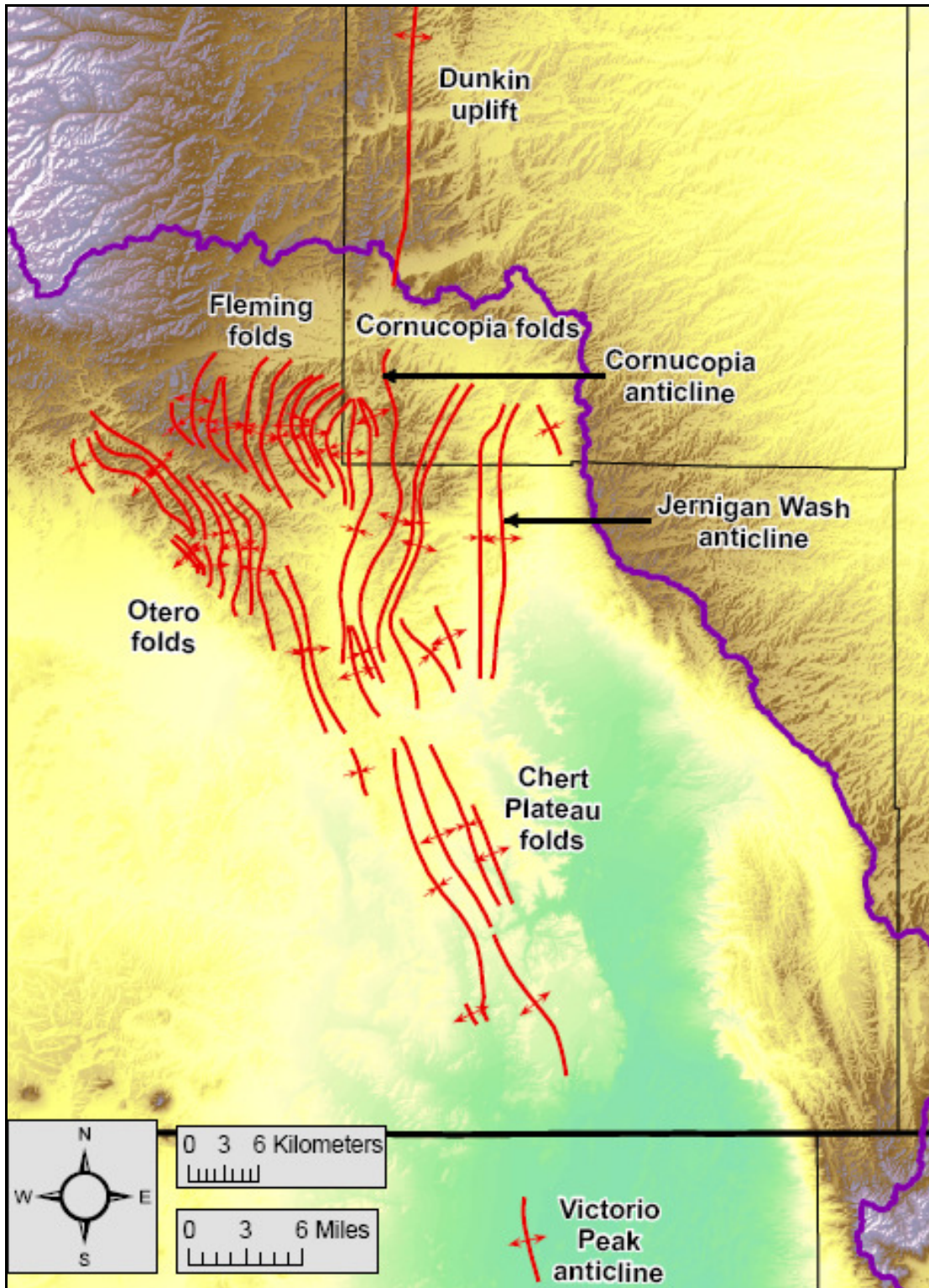
Figure A-2.24: Late-Cretaceous (Laramide) structural features of the north and northeast portions of Otero Mesa.
Syncline and anticline symbols are the same as those used on Figure A-2.22. Location of structures taken from Black (1976), Goetz (1985), and Kelley (1971).
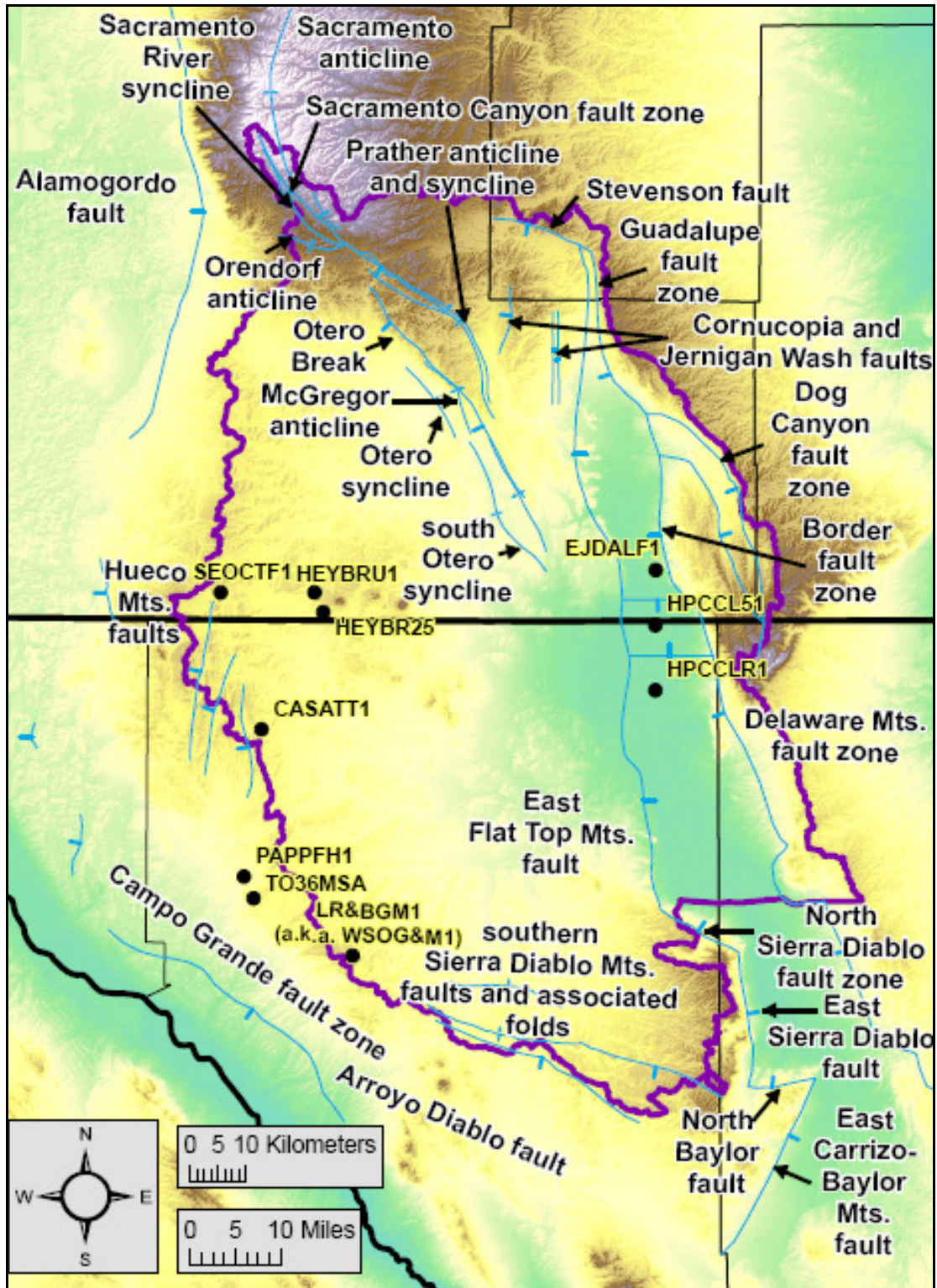
Figure A-2.25: Cenozoic structural features of the northern Salt Basin watershed. Syncline and anticline symbols are the same as those used on Figure A-2.22. Bar on downthrown side of normal or high angle faults. Location of structures taken from Black (1976), Broadhead (2002), Cather and Harrison (2002), Collins and Raney (1991), Goetz (1985), Pray (1961), Schruben et al. (1994), and Seager et al. (1987).

FIGURES – CHAPTER 3
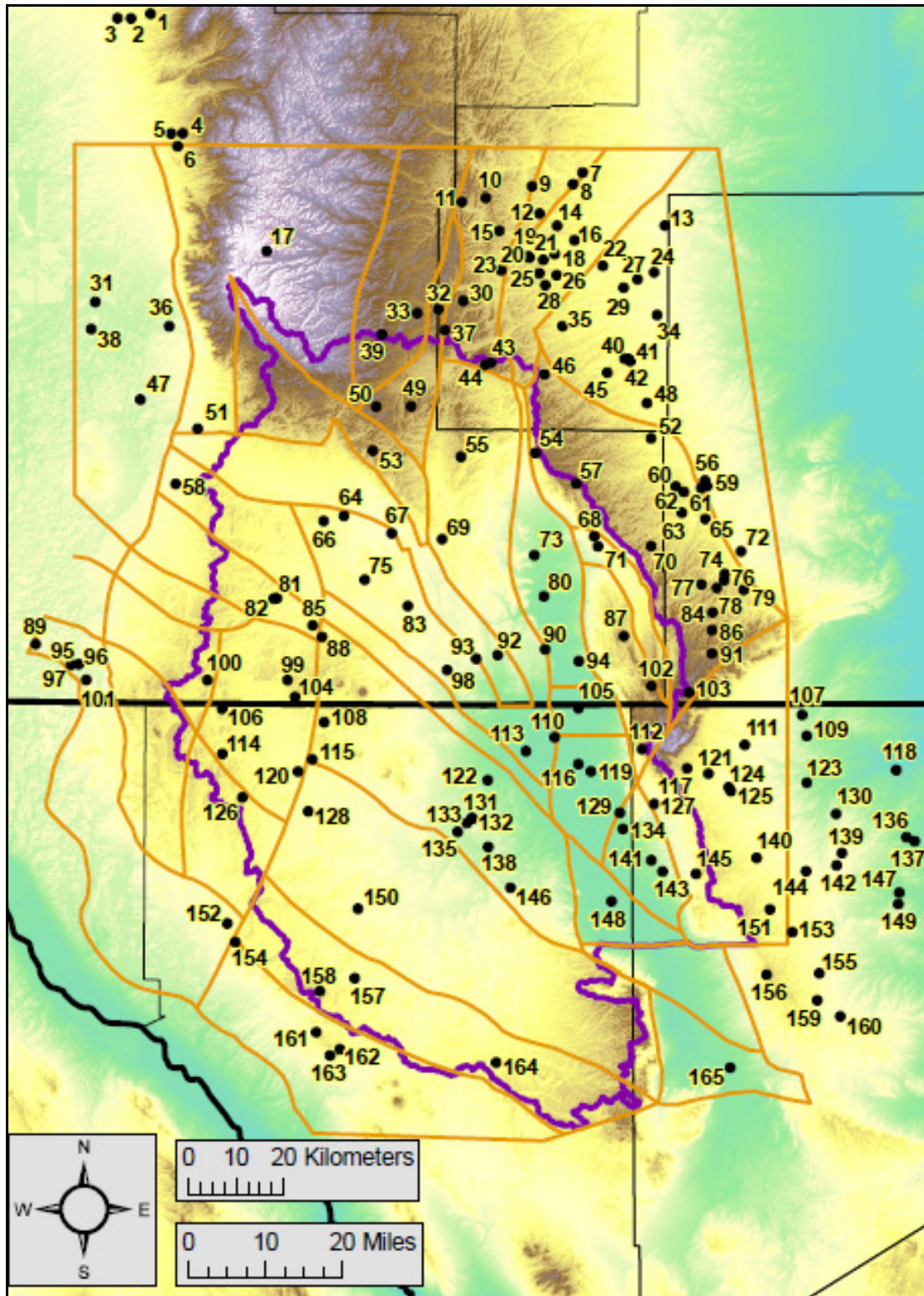
Figure A-3.1: Structural zones/blocks used in 3-D hydrogeologic framework model. Black circles indicate the location of all oil-and-gas exploratory wells used in this study as control on the subsurface geology. Oil-and-gas exploratory well key on next page.

Figure A-3.1: Key

#	Well ID
1	HO&MSL1
2	HO&MJL1
3	HO&MCL2
4	HO&MFA1
5	LAHTHO1
6	HO&MS31
7	MCOCFH1
8	MCOCGB1
9	HO&RYF1
10	JCTSA61
11	LM&SAR1
12	HO&RHY1
13	WHBDCS1
14	COCSNN1
15	JCTFA28
16	C&KSLS1
17	SPCCLU1
18	YPCDNU1
19	YPCDDU2
20	YPCDDU1
21	SE&PJT1
22	C&KLCS1
23	LO&GTLW
24	MAGHEF2
25	YPCLCU1
26	SOCSAV1
27	WHIBHU1
28	YPCLCU2
29	MAGBLHI
30	GOCCSU1
31	TEXIFE1
32	YPCOTU1
33	YPCDCF1
34	TO&GFC1
35	KOCFMU1
36	TEXIFF1
37	YPCOTU2
38	TEXIFG1
39	MOCMVR1
40	YPCBAYU
41	TO&GFA1
42	YPCBAVW
43	SOCPIU2
44	SOCPIU1
45	UVILCU1
46	GOCFMU1
47	PLOCEV1

#	Well ID
48	TO&GFB1
49	ARCSAV1
50	ZPCF141
51	SOCTJP1
52	TRBCU1Y
53	SO&GTU1
54	SOTSCU1
55	LEPCFE1
56	YPCBIOF
57	TSDLDF1
58	OTOCMC1
59	BRCFEA1
60	COCHWB1
61	MOCBCU1
62	PIECF91
63	SO&GFE1
64	EPCAHU1
65	TLISTE1
66	FTUEVE1
67	EPCALI1
68	WRWETH1
69	EPCALS1
70	PRIICF1
71	EPCAMF1
72	HO&RHO2
73	CO&GCW1
74	IOCSBU1
75	CO&GAS1
76	ARCHUU9
77	SOCLCD1
78	UNOCFW1
79	HO&RHU5
80	TDCR21F
81	FTUJEV1
82	EPCAFE1
83	FWYDON1
84	FA&FTD1
85	UNOCMC1
86	UOCV7F1
87	WWWWDC1
88	TROGJA1
89	RHELLC1
90	TDM28F1
91	BOCRUS1
92	PCS28S1
93	FTUJST1
94	EJDALF1

#	Well ID
95	GDP61-6
96	GDP45-5
97	GDP46-6
98	HUOCMT1
99	HEYBRU1
100	SEOCTF1
101	GDP51-8
102	EPCSPF1
103	SO&GGR1
104	HEYBR25
105	HPCCL51
106	TSTFO31
107	CODFRS1
108	MPCUTL1
109	EOGRC24
110	PAPCLA1
111	BONCOPI
112	PUOCHU1
113	HUOCDY1
114	HUBAUN1
115	TMUBIC1
116	HPCCLR1
117	TEXCLF1
118	TOTXLF1
119	PAPCEH1
120	TMUSD51
121	TXLCCF1
122	GCOCMV1
123	MPNA1HC
124	EOGKS1H
125	EOGKES2
126	CASATT1
127	DJJCHJ2
128	TMUFD27
129	BECHCT1
130	TXLCBT1
131	ARJECM1
132	TCST1BS
133	JLCECM1
134	BECJJM1
135	TERCMO2
136	TSOCCS1
137	COIDM3S
138	TMUDWL5
139	SALSUL2
140	HORMCS1
141	NARIPO1

#	Well ID
142	COUL462
143	JMHCTP1
144	EOGSR47
145	A&PBOR1
146	TMUODL1
147	PHMTS27
148	FMINWW1
149	AQPVCR1
150	HHUM491
151	EOGWHD7
152	PAPPFH1
153	COMT105
154	TO36MSA
155	EPCN1MO
156	GOCMAG1
157	HAHUTM1
158	LR&BGM1/ WSOG&M1
159	COSS701
160	SINCLOO
161	GOCJBS1
162	LOBG&M1
163	SOGAL1R
164	H&GJSP1
165	FADWAD1
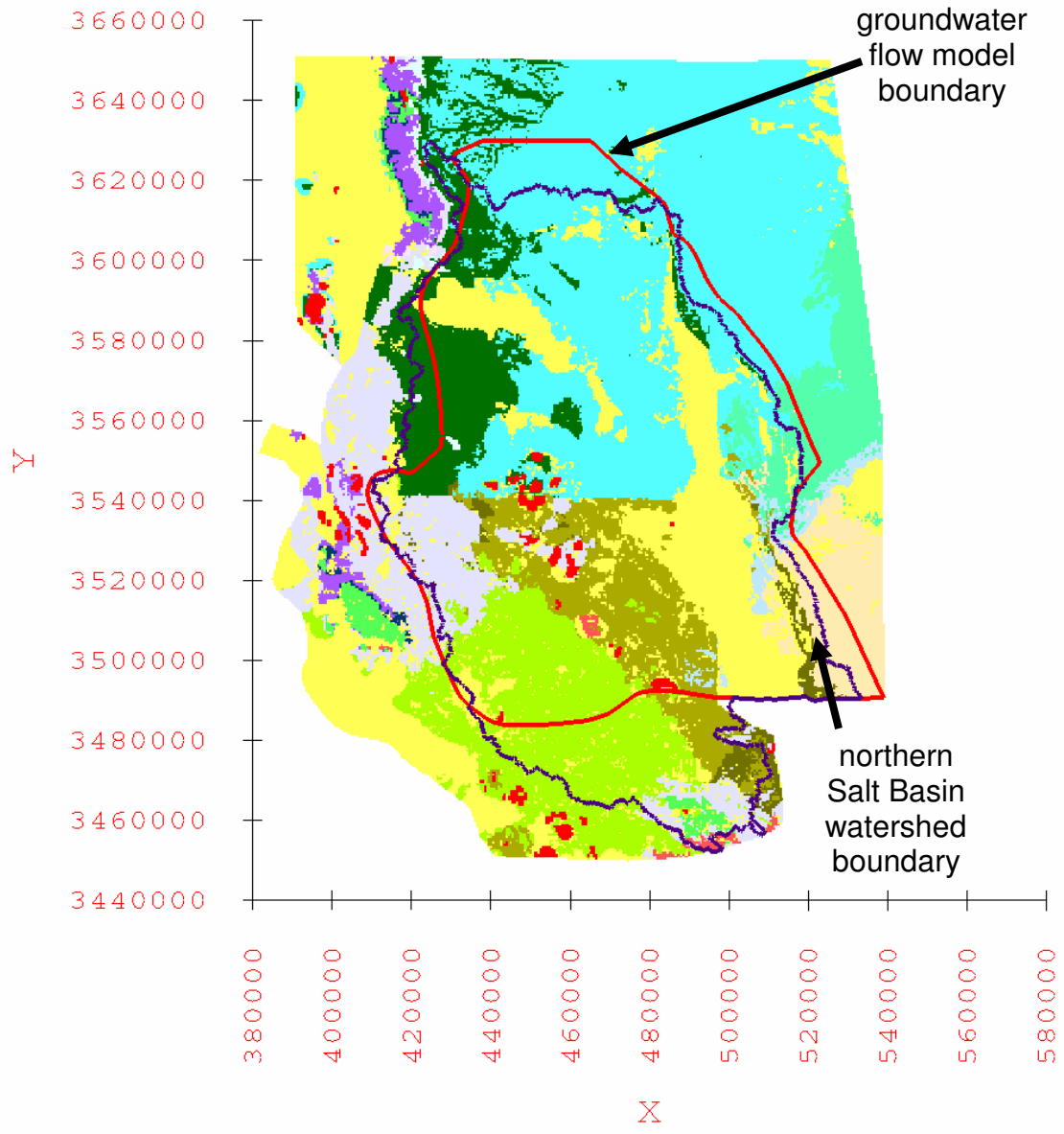
Figure A-3.2: Land surface expression of the 3-D hydrogeologic framework solid model. Color-coding of hydrogeologic units corresponds to that used in Figure A-2.1. Purple line indicates northern Salt Basin watershed boundary. Red line designates groundwater flow model boundary.
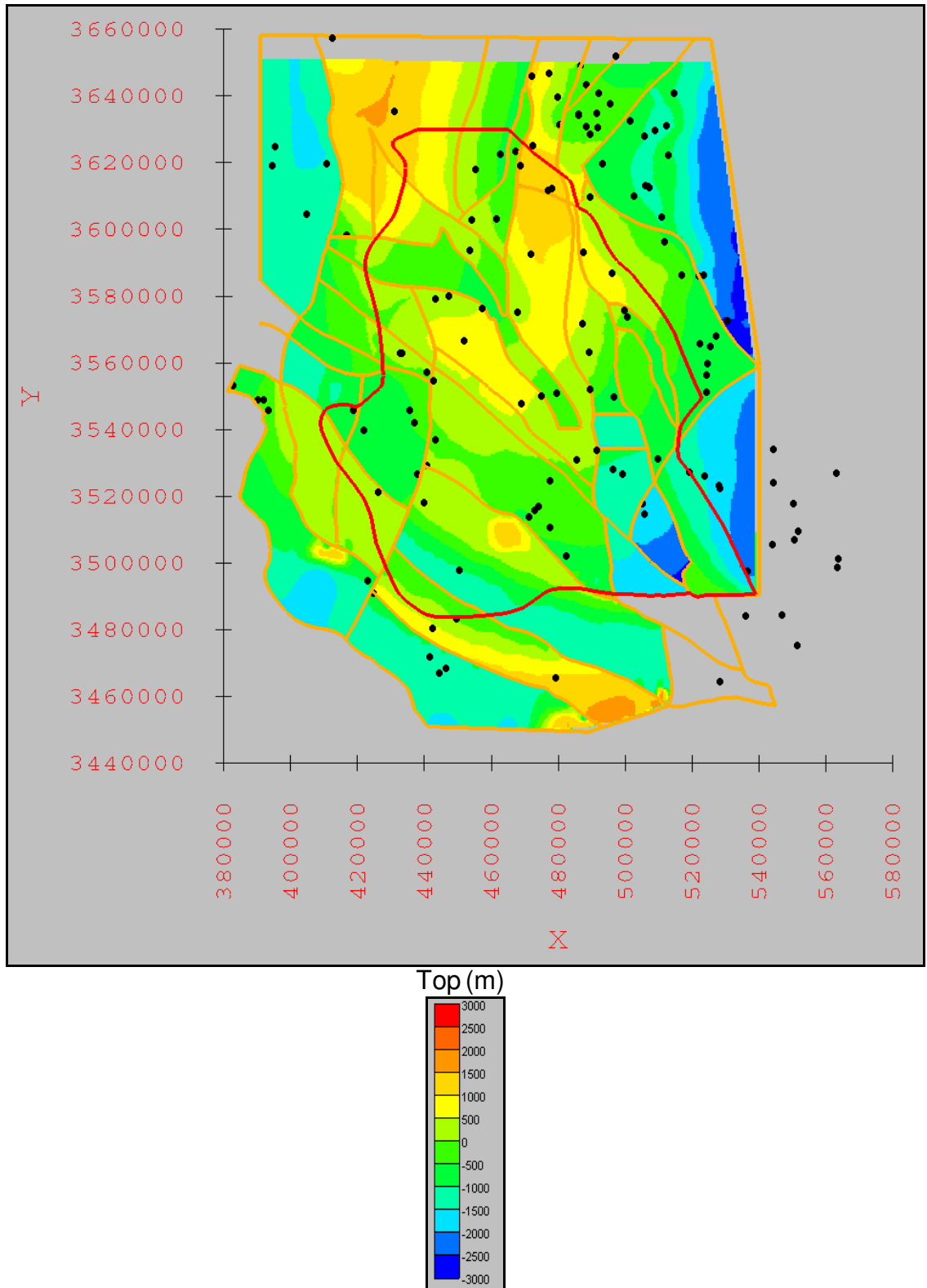
Figure A-3.3: Elevation of the top of the Precambrian.
Elevations are in meters relative to mean sea level. Contour interval is 500 meters (1,640 feet). Black circles indicate the oil-and-gas exploratory wells used as control for the unit.
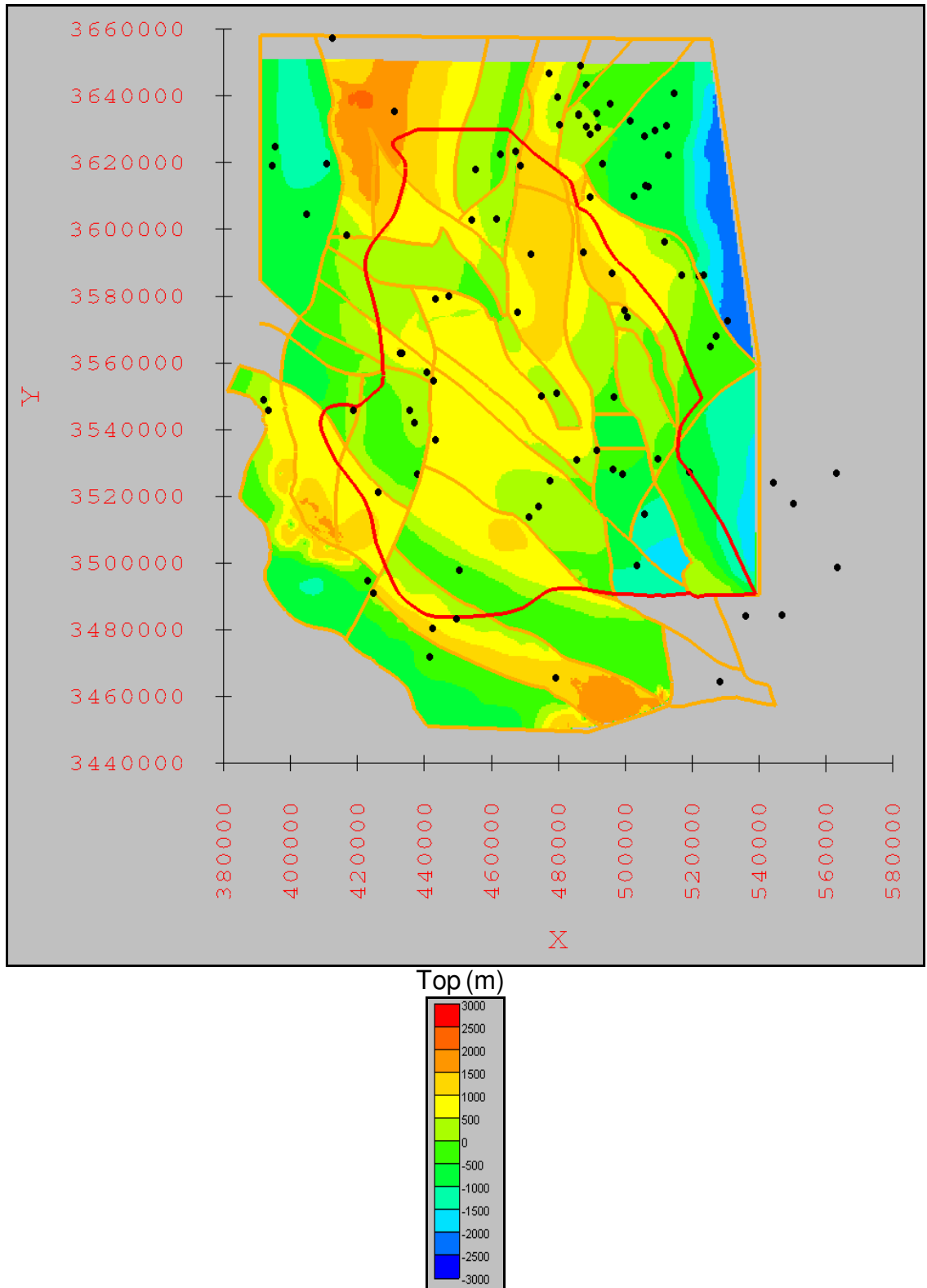
Figure A-3.4: Elevation of the top of the Cambrian through the Silurian. Elevations are in meters relative to mean sea level. Contour interval is 500 meters (1,640 feet). Black circles indicate the oil-and-gas exploratory wells used as control for the unit.

513

Figure A-3.5: Elevation of the top of the Devonian.
Elevations are in meters relative to mean sea level. Contour interval is 500 meters (1,640 feet). Black circles indicate the oil-and-gas exploratory wells used as control for the unit.

Figure A-3.6: Elevation of the top of the Mississippian through the Pennsylvanian. Elevations are in meters relative to mean sea level. Contour interval is 500 meters (1,640 feet). Black circles indicate the oil-and-gas exploratory wells used as control for the unit.
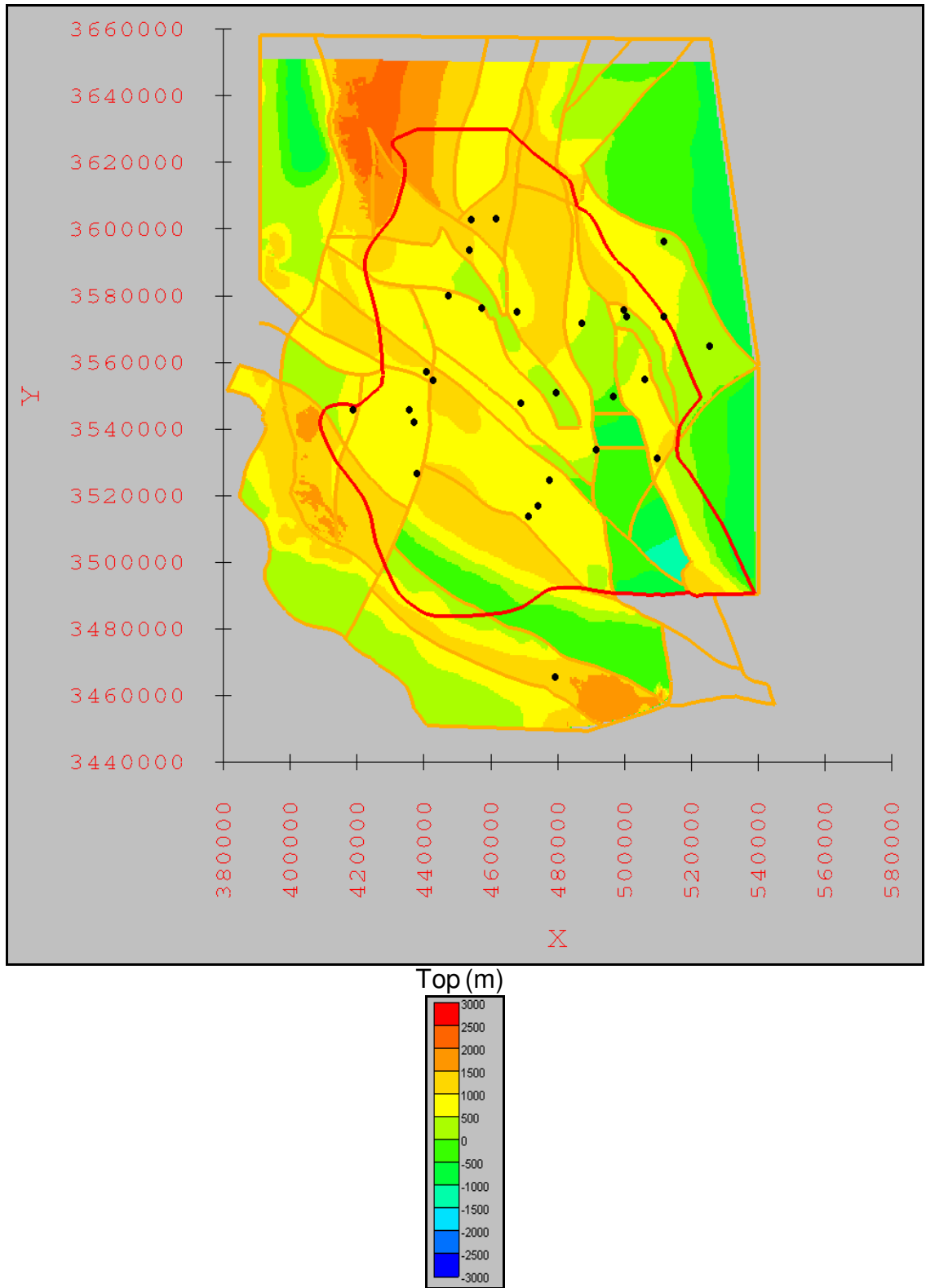
Figure A-3.7: Elevation of the top of Lower Abo/Pow Wow Conglomerate. Elevations are in meters relative to mean sea level. Contour interval is 500 meters (1,640 feet). Black circles indicate the oil-and-gas exploratory wells used as control for the unit.
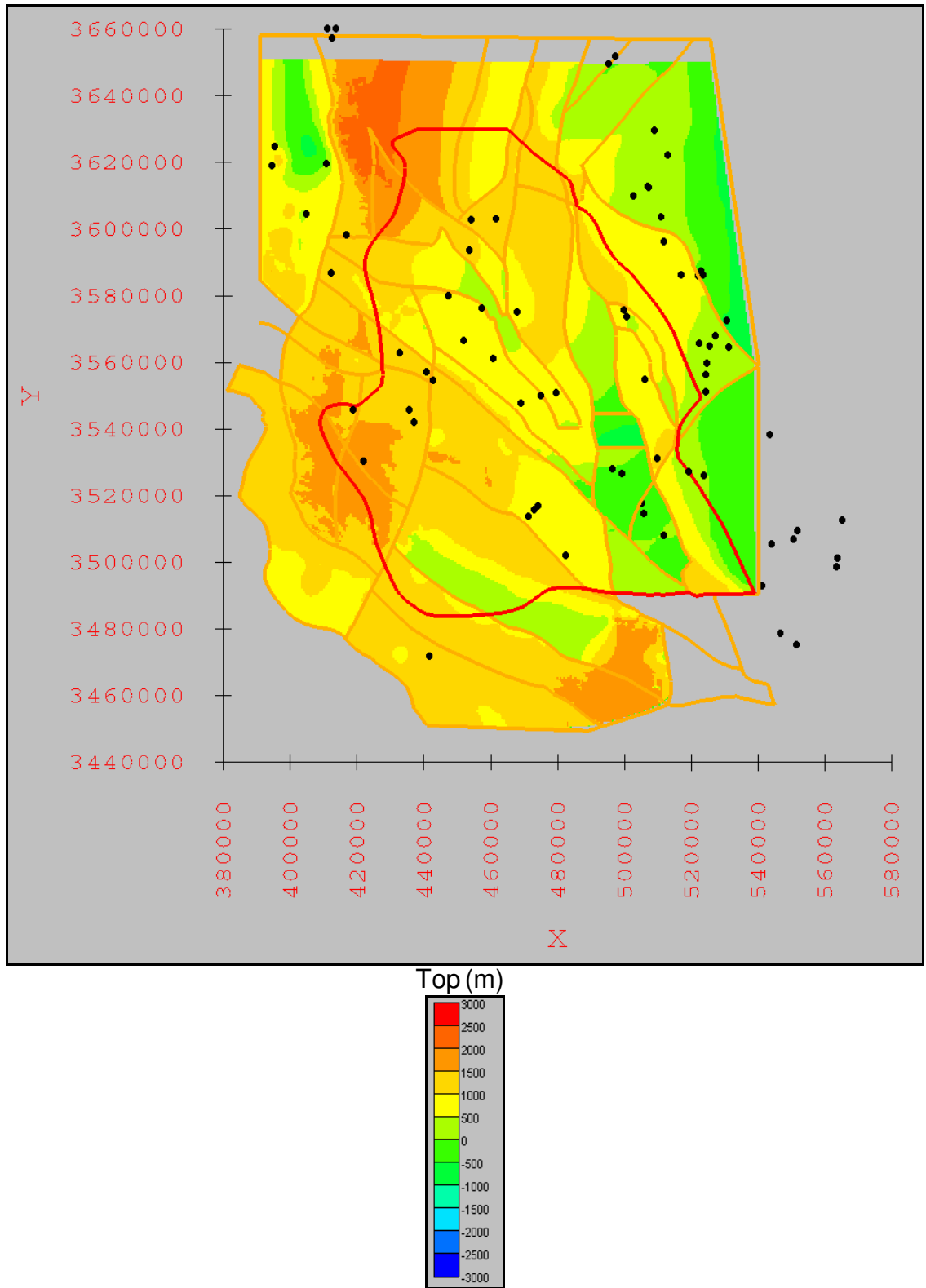
Figure A-3.8: Elevation of the top of Hueco Limestone/Formation (or Bursum Formation) and Wolfcamp Formation.

Elevations are in meters relative to mean sea level. Contour interval is 500 meters (1,640 feet). Black circles indicate the oil-and-gas exploratory wells used as control for the unit.
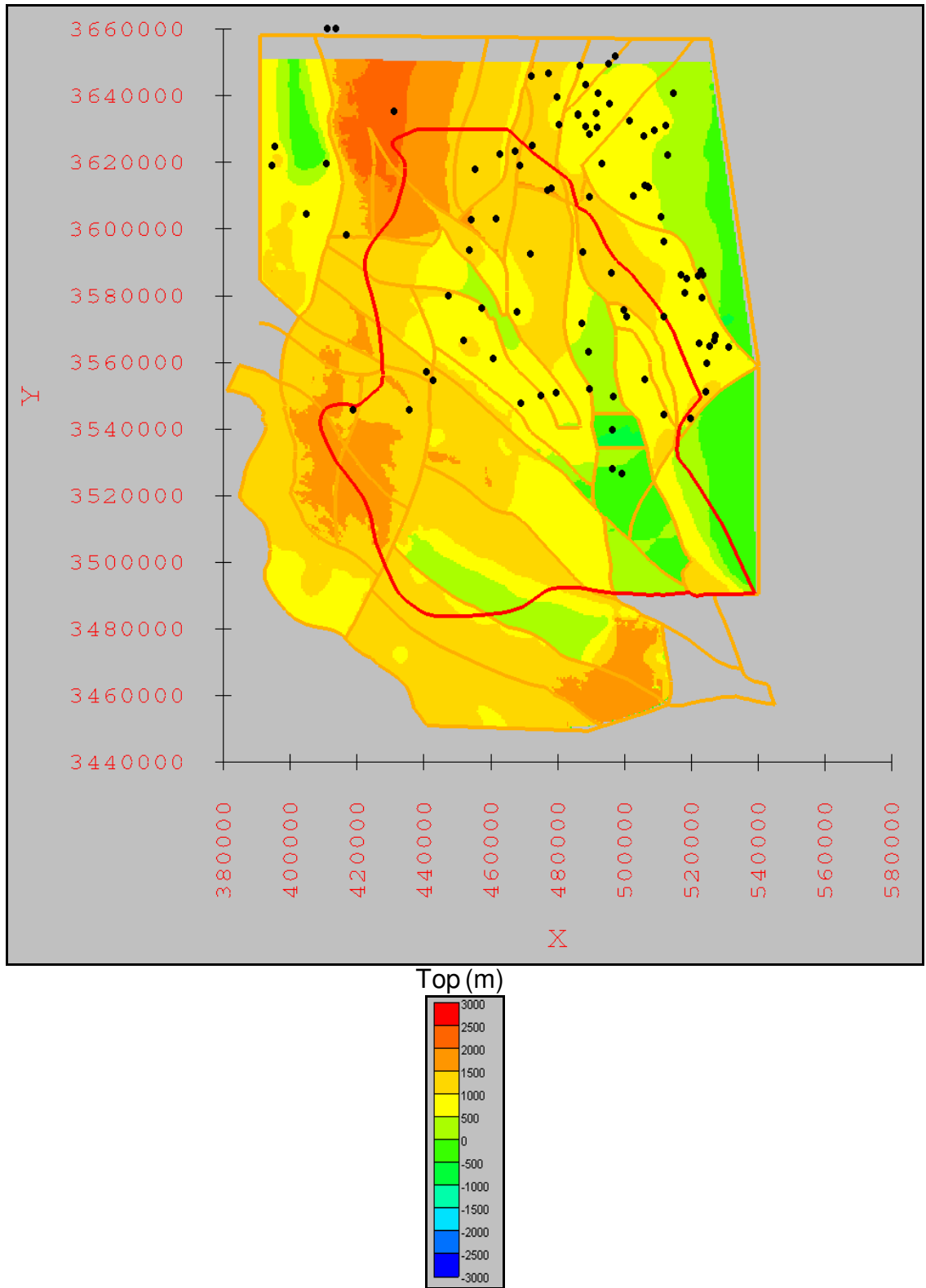
Figure A-3.9: Elevation of the top of Abo Formation.
Elevations are in meters relative to mean sea level. Contour interval is 500 meters (1,640 feet). Black circles indicate the oil-and-gas exploratory wells used as control for the unit.
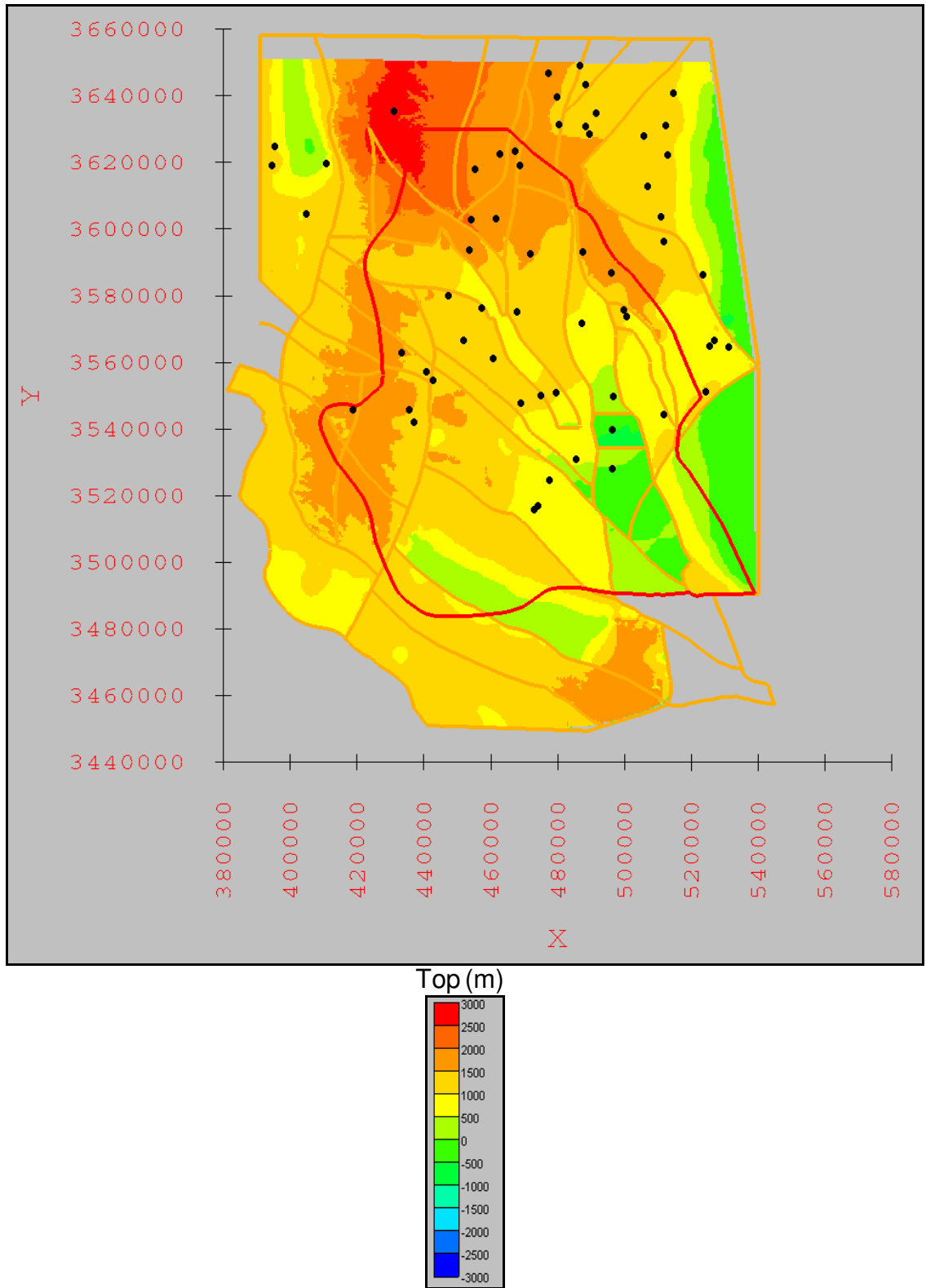
Figure A-3.10: Elevation of the top of Yeso Formation.
Elevations are in meters relative to mean sea level. Contour interval is 500 meters (1,640 feet). Black circles indicate the oil-and-gas exploratory wells used as control for the unit.
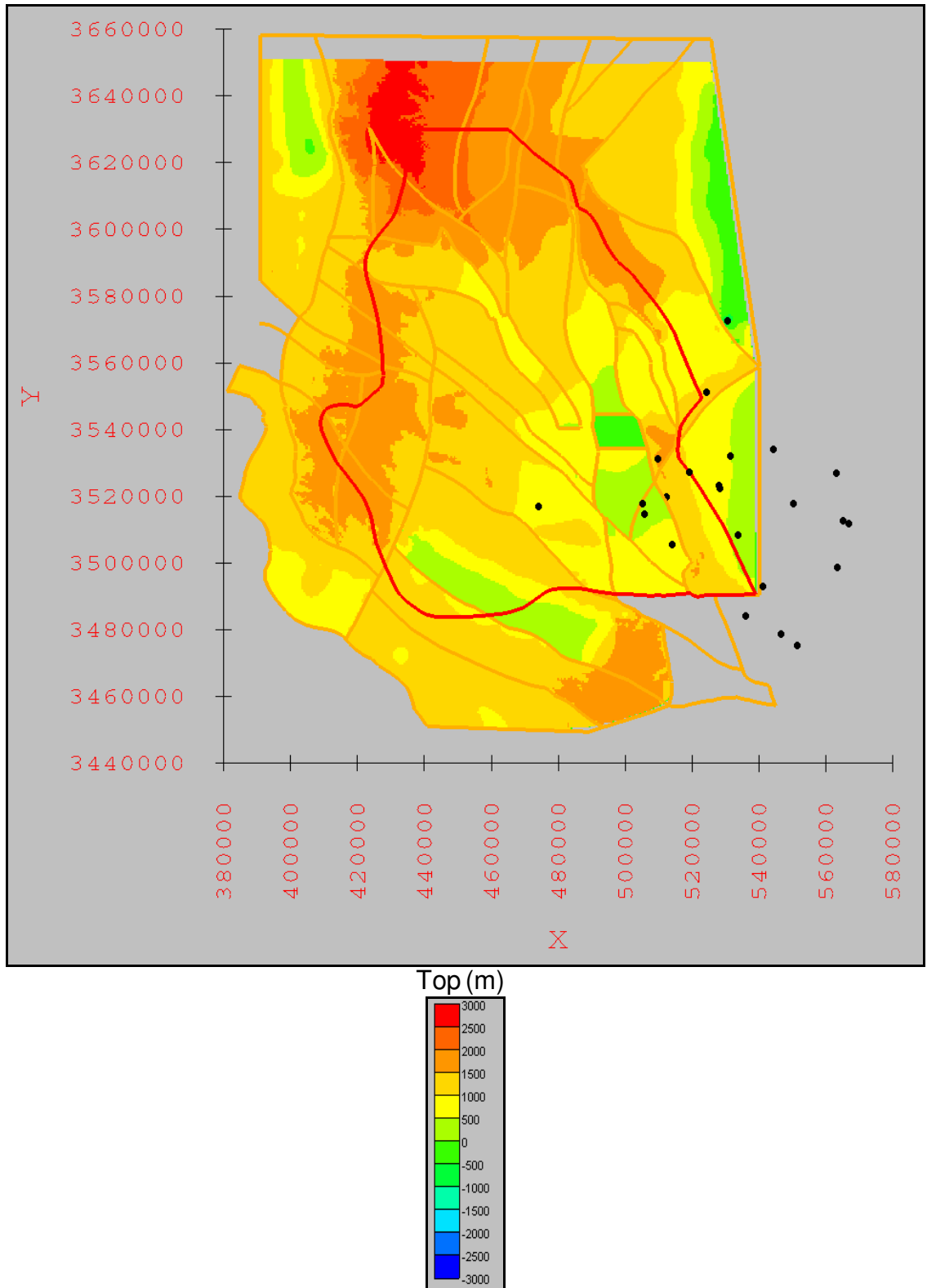
Figure A-3.11: Elevation of the top of Bone Spring Limestone/Formation. Elevations are in meters relative to mean sea level. Contour interval is 500 meters (1,640 feet). Black circles indicate the oil-and-gas exploratory wells used as control for the unit.
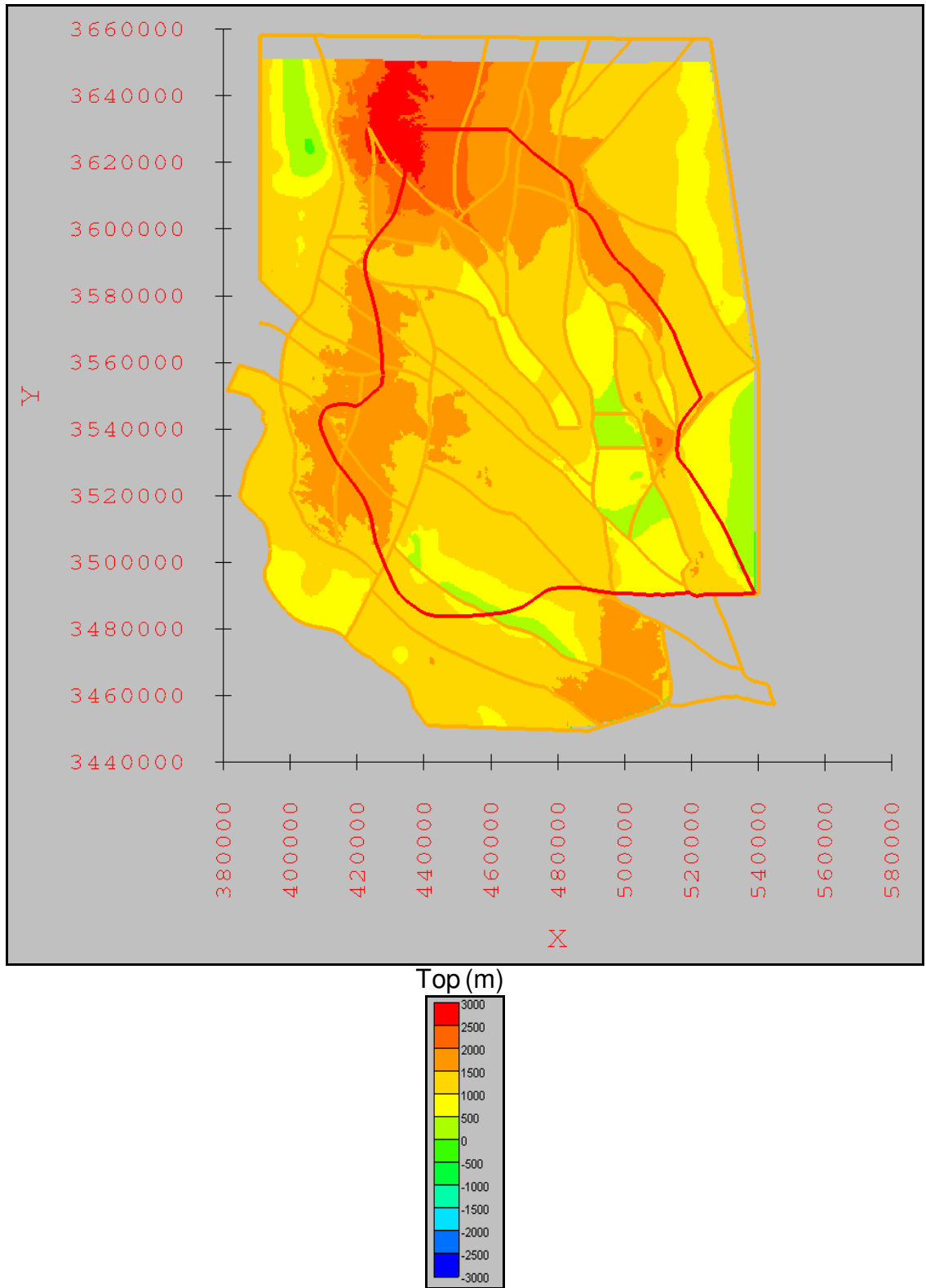
Figure A-3.12: Elevation of the top of Victorio Peak Limestone/Formation and Cutoff Shale and Wilke Ranch Formation.

Elevations are in meters relative to mean sea level. Contour interval is 500 meters (1,640 feet). Black circles indicate the oil-and-gas exploratory wells used as control for the unit.
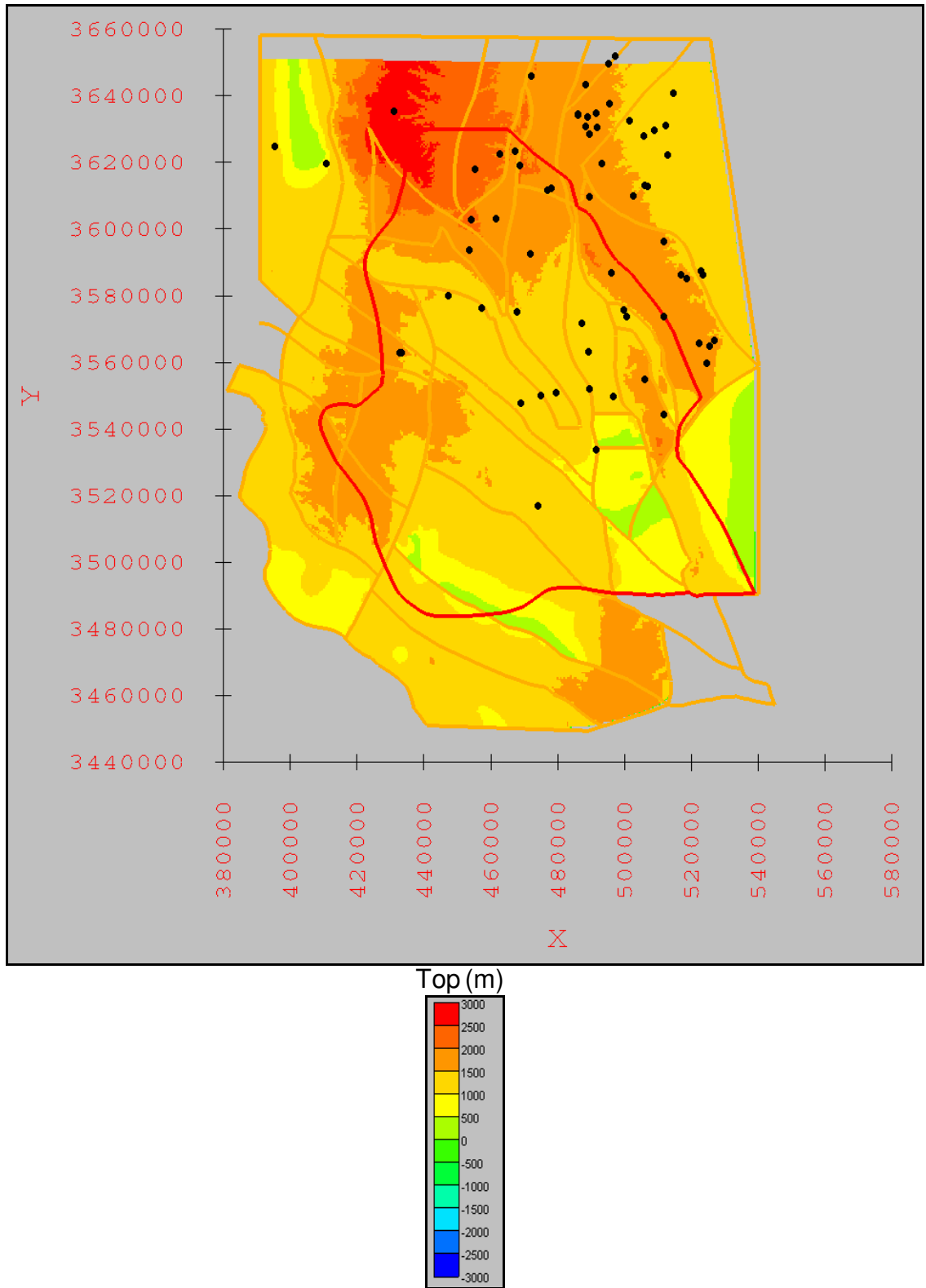
Figure A-3.13: Elevation of the top of San Andres Formation.
Elevations are in meters relative to mean sea level. Contour interval is 500 meters (1,640 feet). Black circles indicate the oil-and-gas exploratory wells used as control for the unit.

Figure A-3.14: Elevation of the top of Delaware Mountain Group.
Elevations are in meters relative to mean sea level. Contour interval is 500 meters (1,640 feet). Black circles indicate the oil-and-gas exploratory wells used as control for the unit.
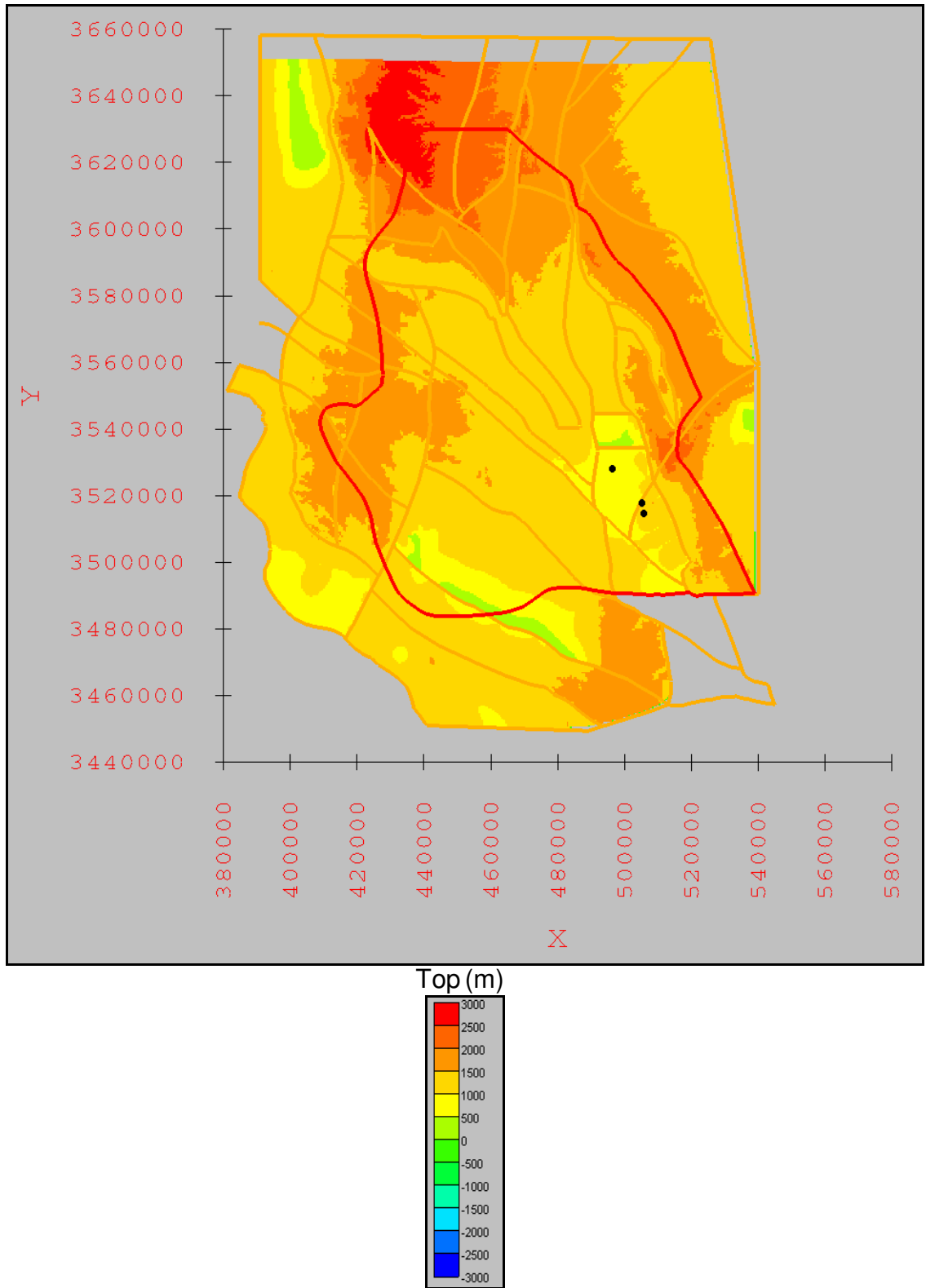
Figure A-3.15: Elevation of the top of Goat Seep Dolomite/Limestone/Formation and Capitan Limestone/Formation.
Elevations are in meters relative to mean sea level. Contour interval is 500 meters (1,640 feet). Black circles indicate the oil-and-gas exploratory wells used as control for the unit.
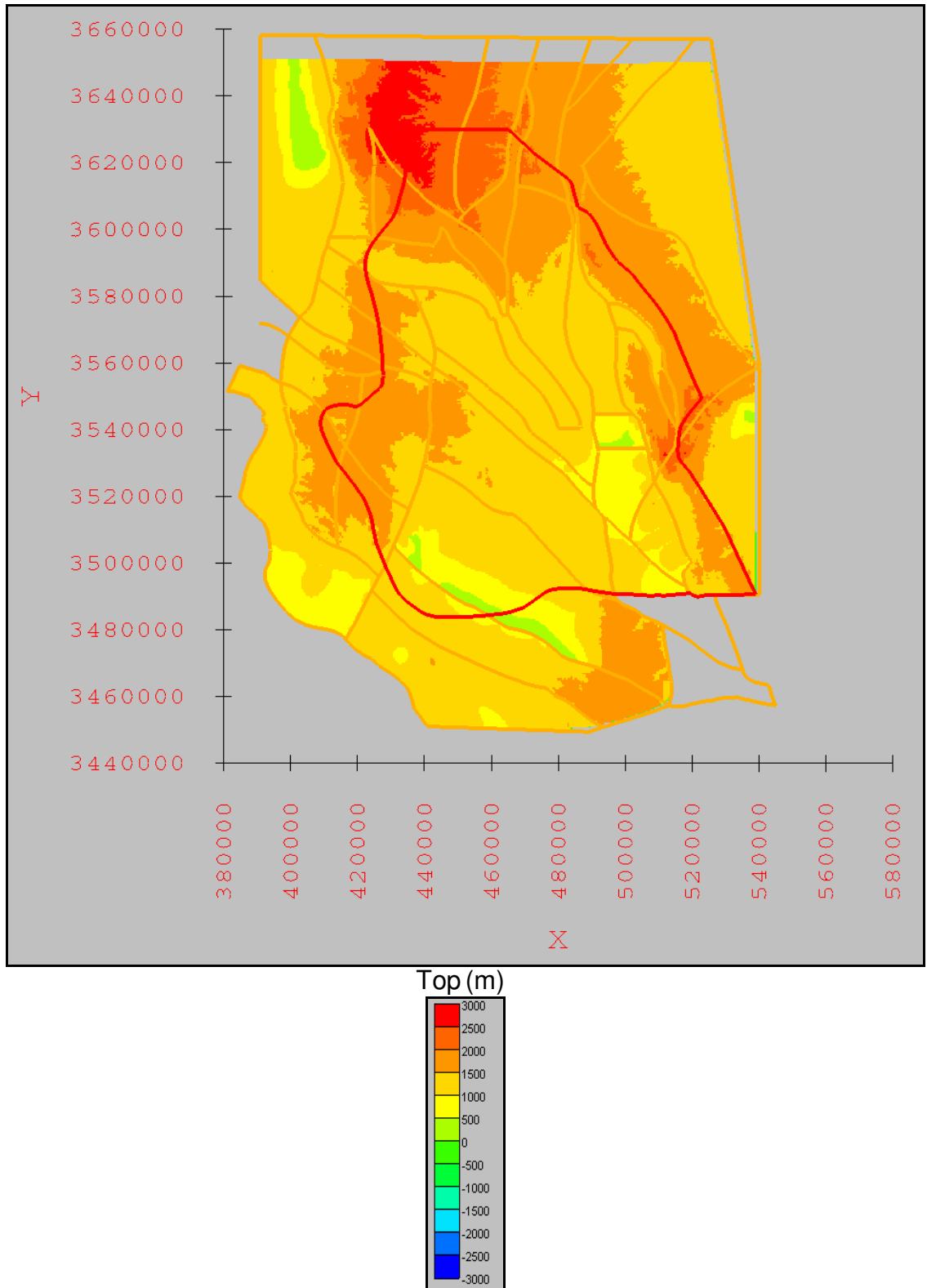
Figure A-3.16: Elevation of the top of Artesia Group.
Elevations are in meters relative to mean sea level. Contour interval is 500 meters (1,640 feet). Black circles indicate the oil-and-gas exploratory wells used as control for the unit.
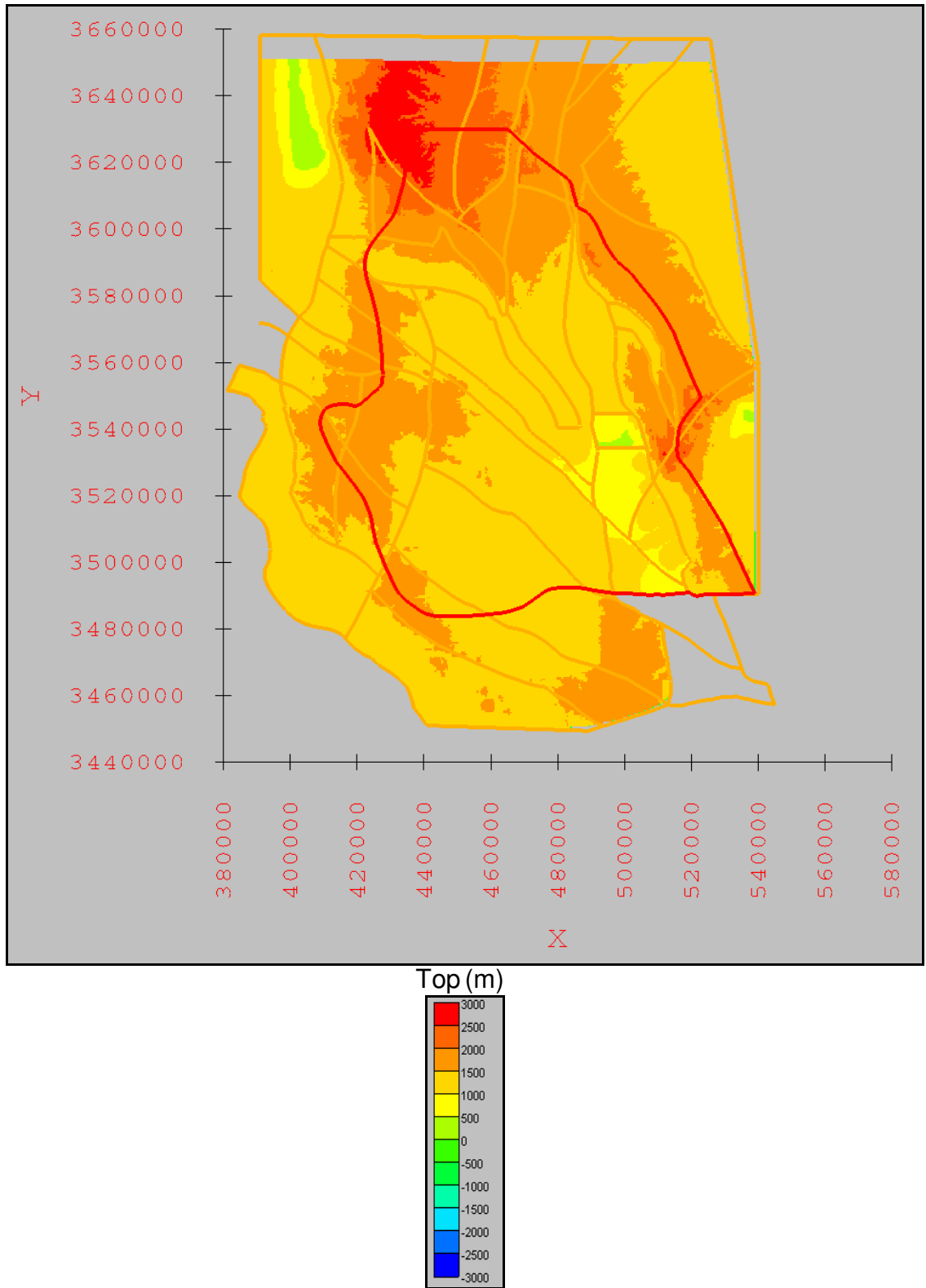
Figure A-3.17: Elevation of the top of the Cretaceous.
Elevations are in meters relative to mean sea level. Contour interval is 500 meters (1,640 feet). Black circles indicate the oil-and-gas exploratory wells used as control for the unit.

Figure A-3.18: Elevation of the top of Cenozoic alluvium.
Elevations are in meters relative to mean sea level. Contour interval is 500 meters (1,640 feet). Black circles indicate the oil-and-gas exploratory wells used as control for the unit.
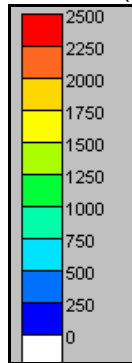
Figure A-3.19: Thickness of the Cambrian through the Silurian.
Contour interval is 250 meters (820 feet). White color indicates unit is not present. Black circles indicate the oil-and-gas exploratory wells used as control for the unit.
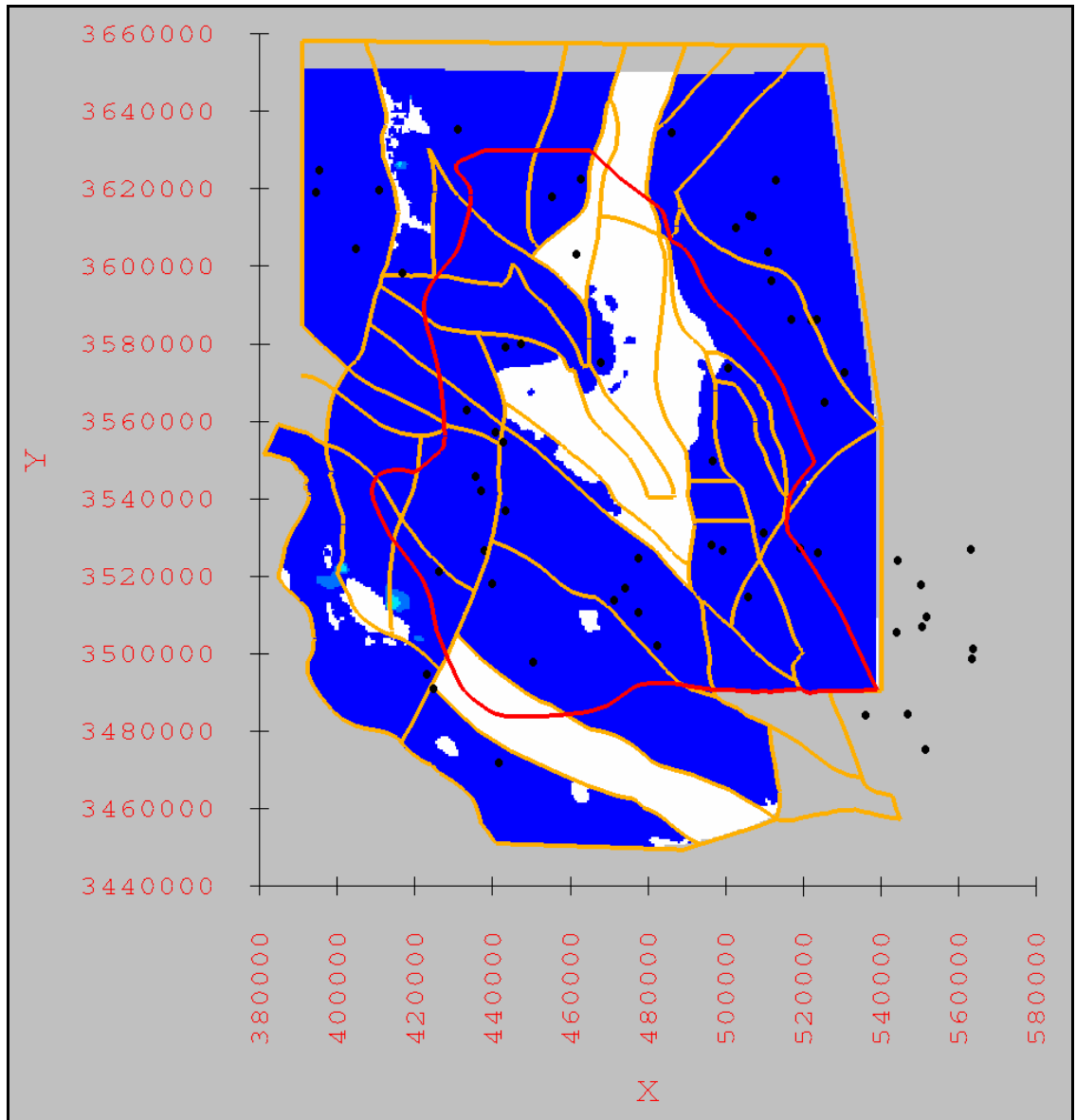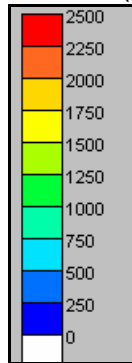
Figure A-3.20: Thickness of the Devonian.
Contour interval is 250 meters (820 feet). White color indicates unit is not present. Black circles indicate the oil-and-gas exploratory wells used as control for the unit.

Figure A-3.21: Thickness of the Mississippian through the Pennsylvanian.
Contour interval is 250 meters (820 feet). White color indicates unit is not present. Black circles indicate the oil-and-gas exploratory wells used as control for the unit.

Figure A-3.22: Thickness of Lower Abo/Pow Wow Conglomerate.
Contour interval is 250 meters (820 feet). White color indicates unit is not present. Black circles indicate the oil-and-gas exploratory wells used as control for the unit.

Figure A-3.23: Thickness of Hueco Limestone/Formation (or Bursum Formation) and Wolfcamp Formation.
Contour interval is 250 meters (820 feet). White color indicates unit is not present. Black circles indicate the oil-and-gas exploratory wells used as control for the unit.

Figure A-3.24: Thickness of Abo Formation.
Contour interval is 250 meters (820 feet). White color indicates unit is not present. Black circles indicate the oil-and-gas exploratory wells used as control for the unit.
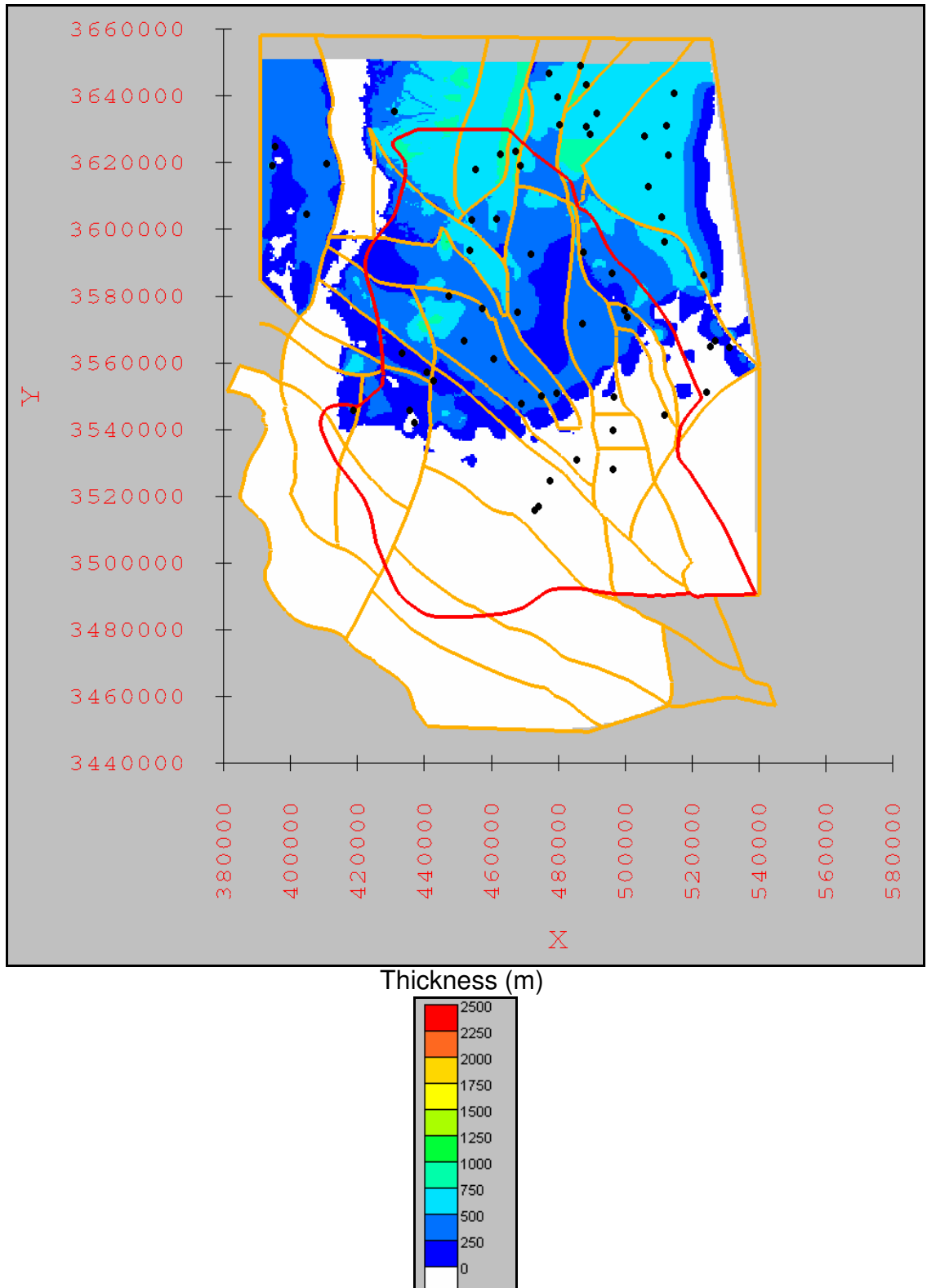
Figure A-3.25: Thickness of Yeso Formation.
Contour interval is 250 meters (820 feet). White color indicates unit is not present. Black circles indicate the oil-and-gas exploratory wells used as control for the unit.
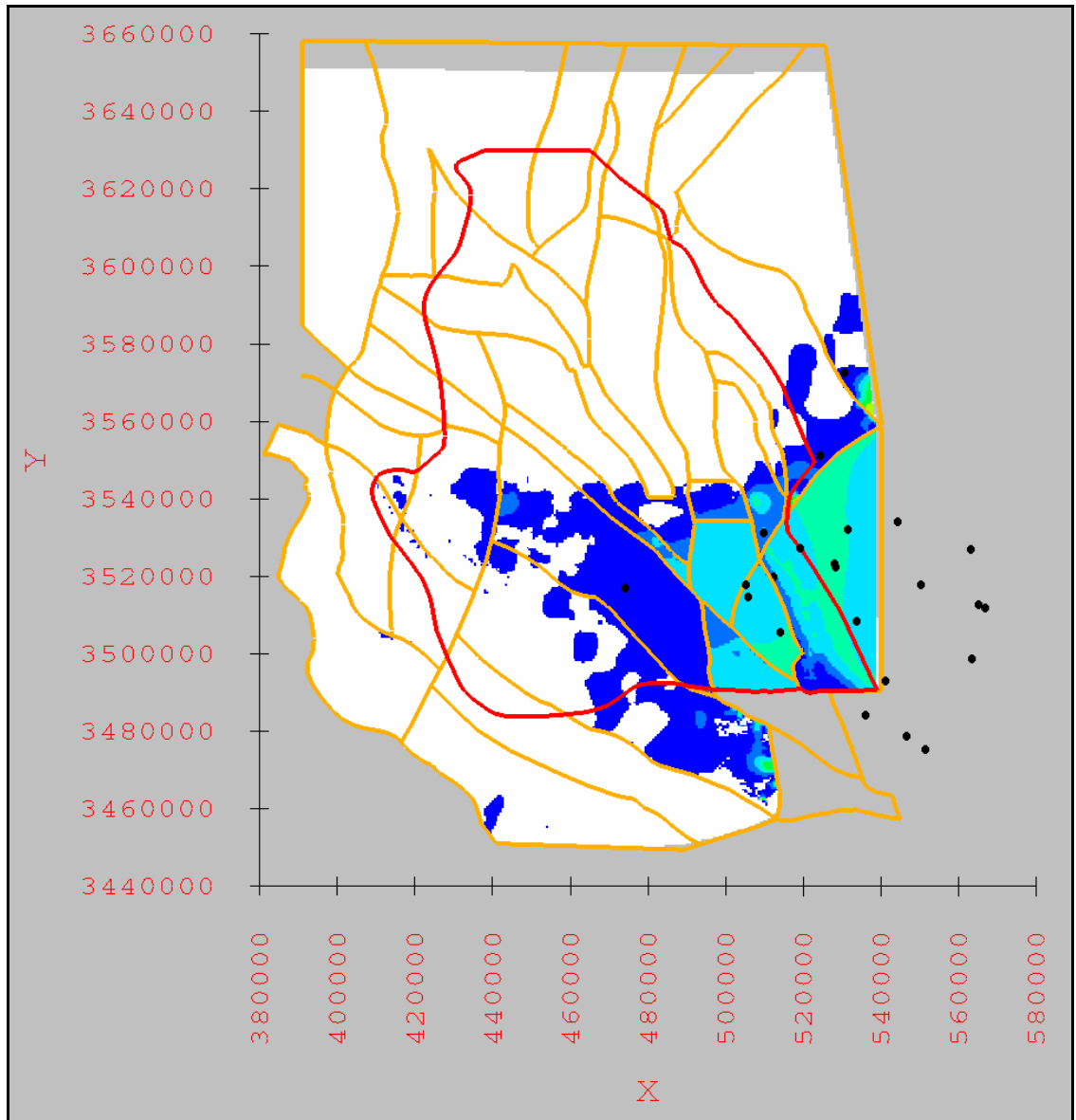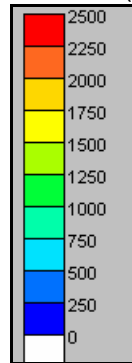
Figure A-3.26: Thickness of Bone Spring Limestone/Formation.
Contour interval is 250 meters (820 feet). White color indicates unit is not present. Black
circles indicate the oil-and-gas exploratory wells used as control for the unit.

Figure A-3.27: Thickness of Victorio Peak Limestone/Formation and Cutoff Shale and Wilke Ranch Formation.
Contour interval is 250 meters (820 feet). White color indicates unit is not present. Black circles indicate the oil-and-gas exploratory wells used as control for the unit.

536
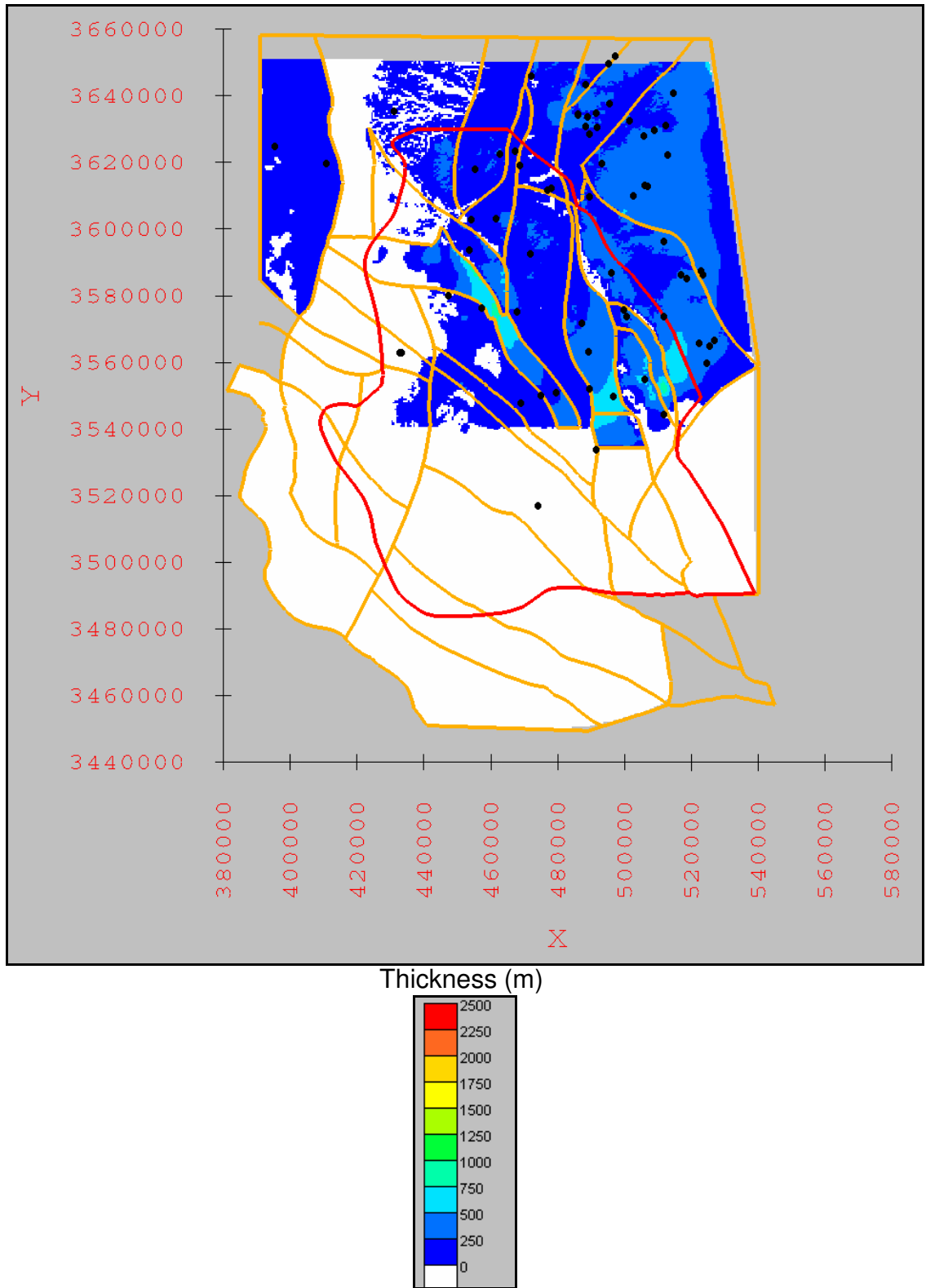
Figure A-3.28: Thickness of San Andres Formation.
Contour interval is 250 meters (820 feet). White color indicates unit is not present. Black
circles indicate the oil-and-gas exploratory wells used as control for the unit.

Figure A-3.29: Thickness of Delaware Mountain Group.
Contour interval is 250 meters (820 feet). White color indicates unit is not present. Black circles indicate the oil-and-gas exploratory wells used as control for the unit.
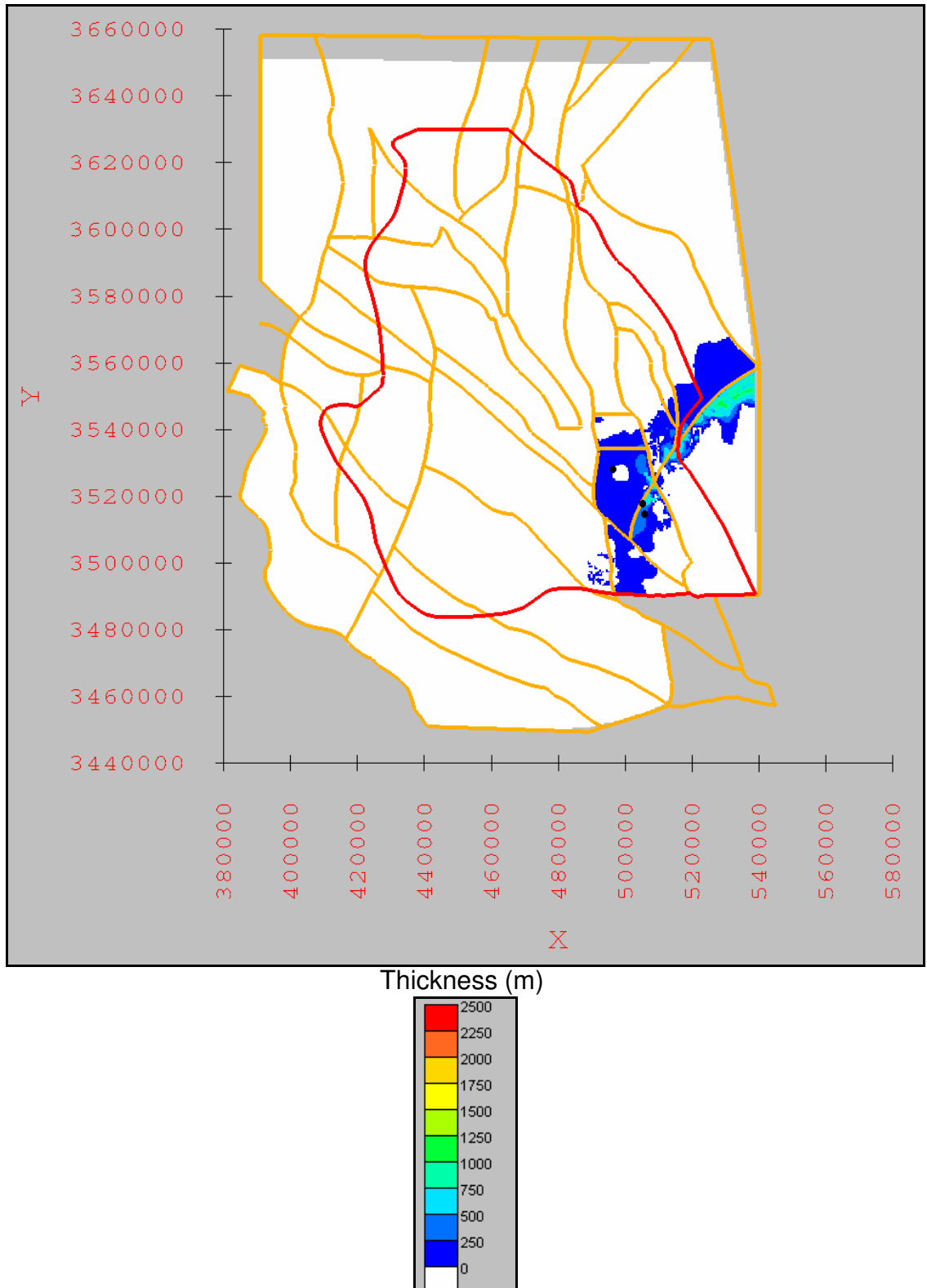
Figure A-3.30: Thickness of Goat Seep Dolomite/Limestone/Formation and Capitan Limestone/Formation.

Contour interval is 250 meters (820 feet). White color indicates unit is not present. Black circles indicate the oil-and-gas exploratory wells used as control for the unit.
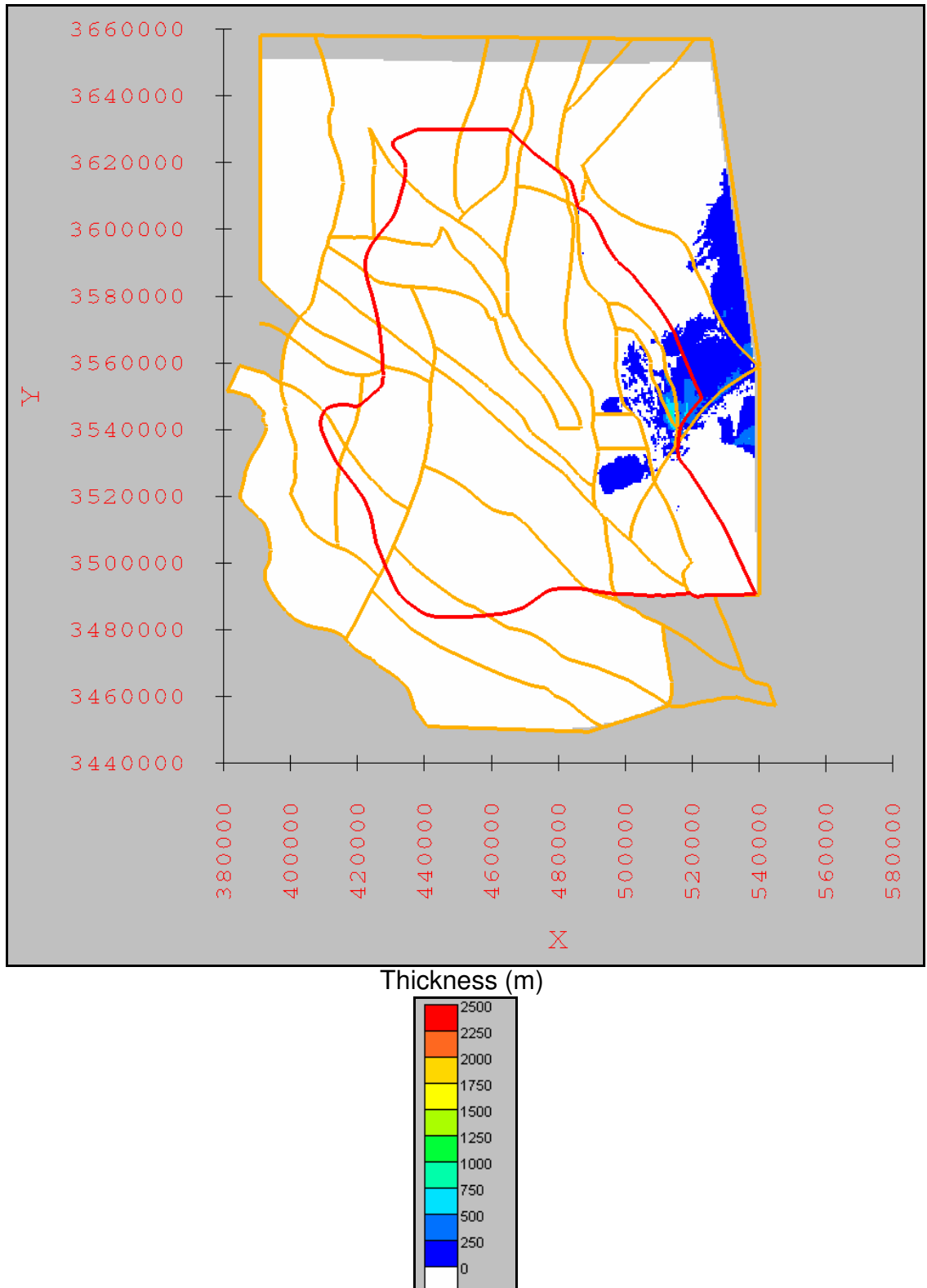
Figure A-3.31: Thickness of Artesia Group.
Contour interval is 250 meters (820 feet). White color indicates unit is not present. Black circles indicate the oil-and-gas exploratory wells used as control for the unit.
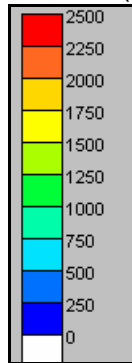
Figure A-3.32: Thickness of the Cretaceous.
Contour interval is 250 meters (820 feet). White color indicates unit is not present. Black circles indicate the oil-and-gas exploratory wells used as control for the unit.

Figure A-3.33: Thickness of Cenozoic alluvium.
Contour interval is 250 meters (820 feet). White color indicates unit is not present. Black circles indicate the oil-and-gas exploratory wells used as control for the unit.
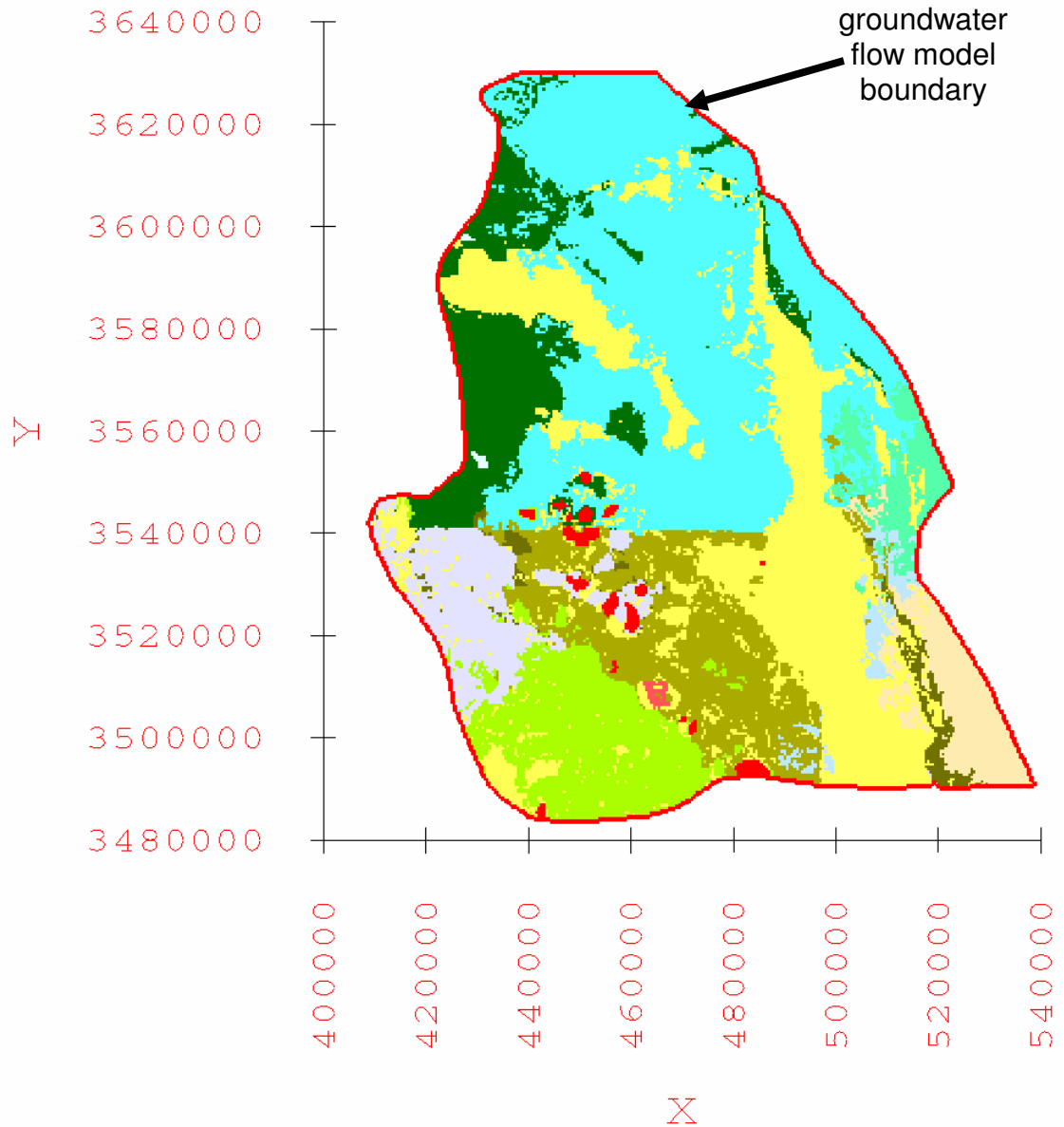
Figure A-3.34: Land surface expression of the 3-D hydrogeologic framework solid model clipped to the groundwater flow model boundary.
Color-coding of hydrogeologic units corresponds to that used in Figure A-2.1. Red line designates groundwater flow model boundary.

Figure A-3.35: Oblique views of the 3-D hydrogeologic framework solid model clipped to the groundwater flow model boundary.
Color-coding of hydrogeologic units corresponds to that used in Figure A-2.1. Vertical exaggeration 10×.

Figure A-3.36: Location of the five hydrogeologic cross-sections.
Also includes the location of the groundwater wells sampled during this study along each cross-section, the subsurface geologic control points along each cross-section, and the groundwater surface contours produced for this study.
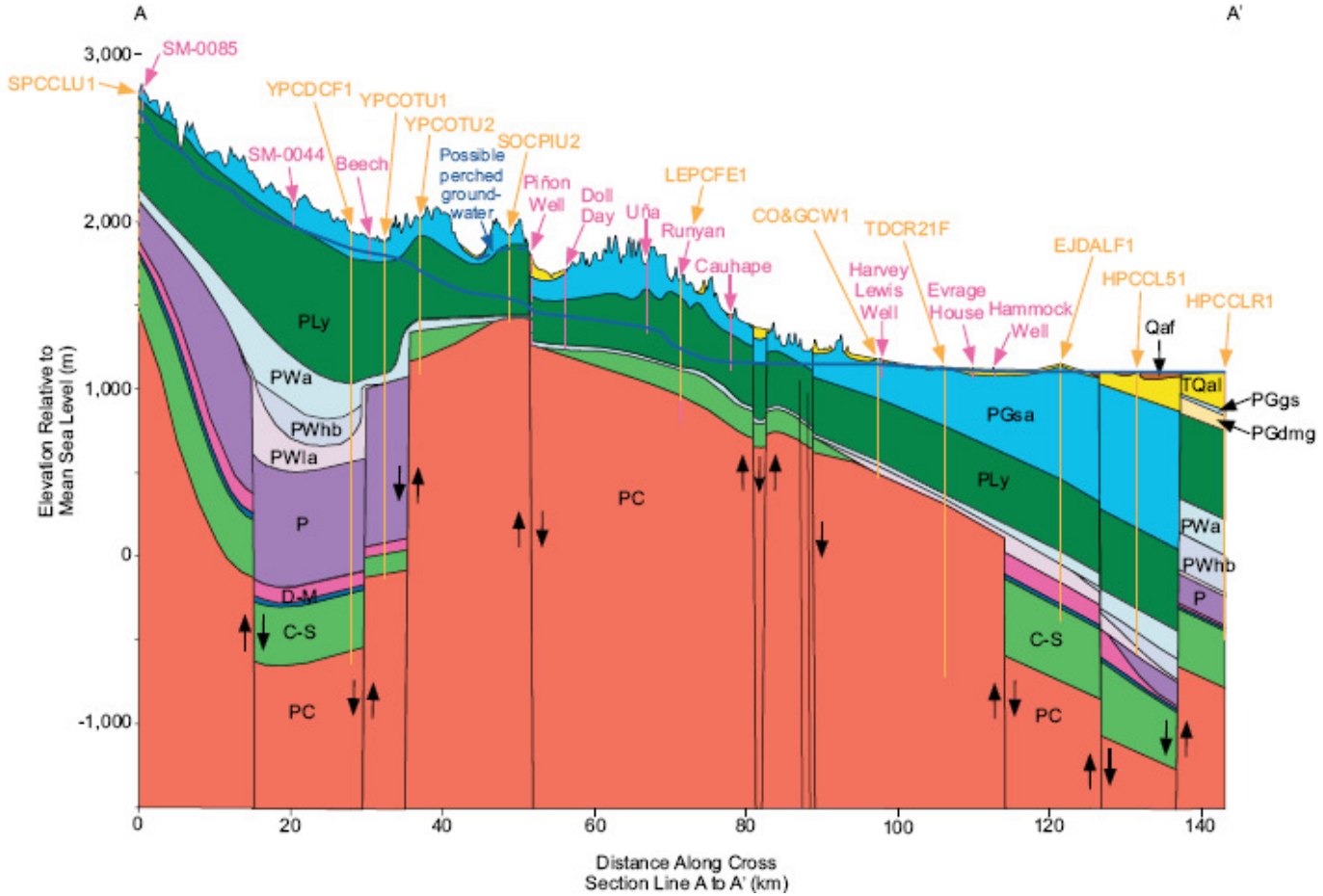
Figure A-3.37: North-South cross-section A - A'.

Vertical exaggeration 23×.

On all cross-sections, the light brown vertical lines are oil-and-gas exploratory well subsurface control points, the pink vertical lines are groundwater wells sampled during this study and by the SMHS, and the arrows indicate the sense of displacement on faults. Dashed lines for wells indicate that the well was projected to the line of cross-section. The groundwater surface is represented by the dark blue line. Color-coding of hydrogeologic units and unit labels corresponds to that used in Figure A-2.1.

Figure A-3.38: North-South cross-section B - B'.

Vertical exaggeration 18×.

547
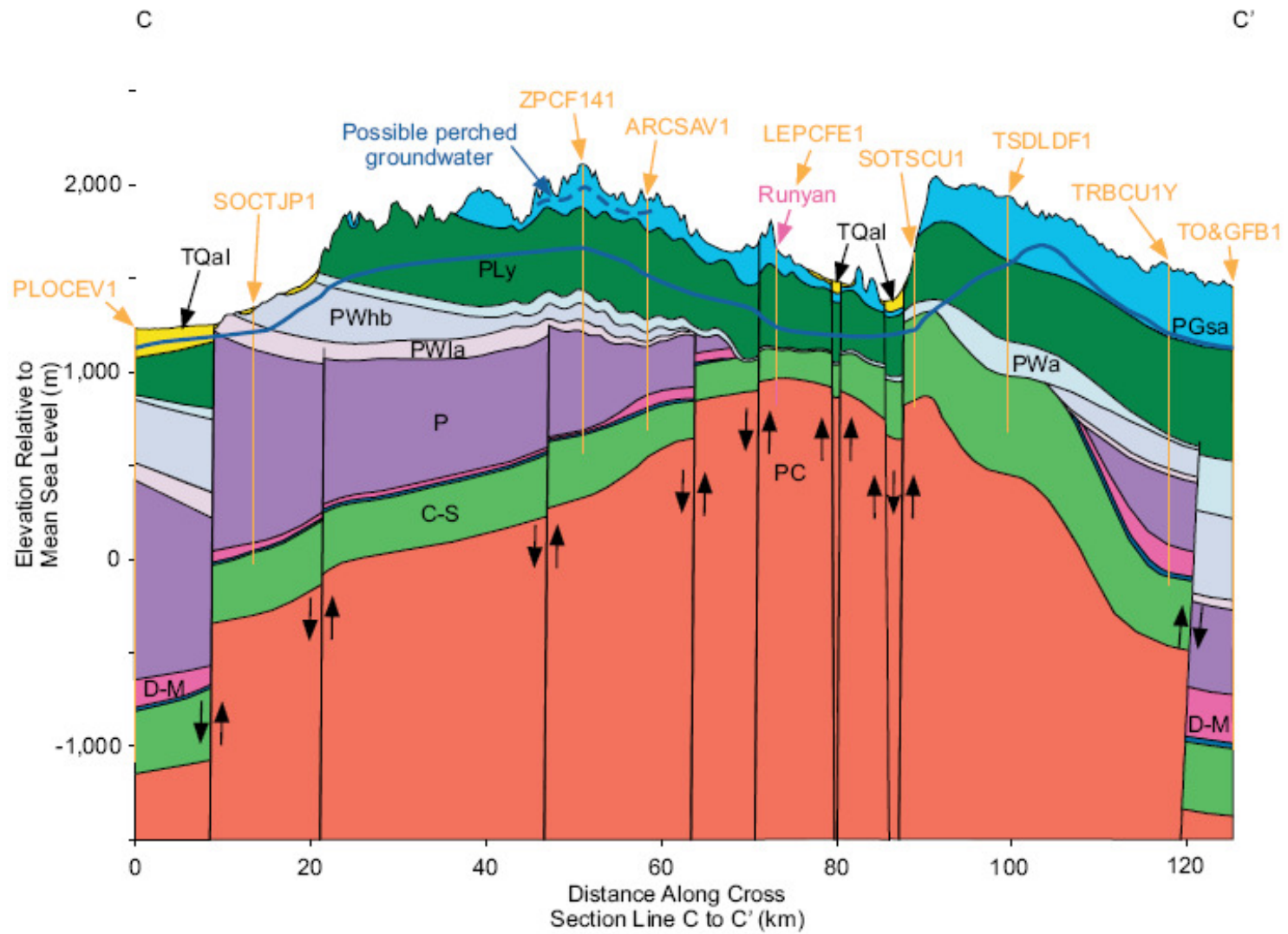
Figure A-3.39: West-East cross-section C - C'.

Vertical exaggeration 22×.

548
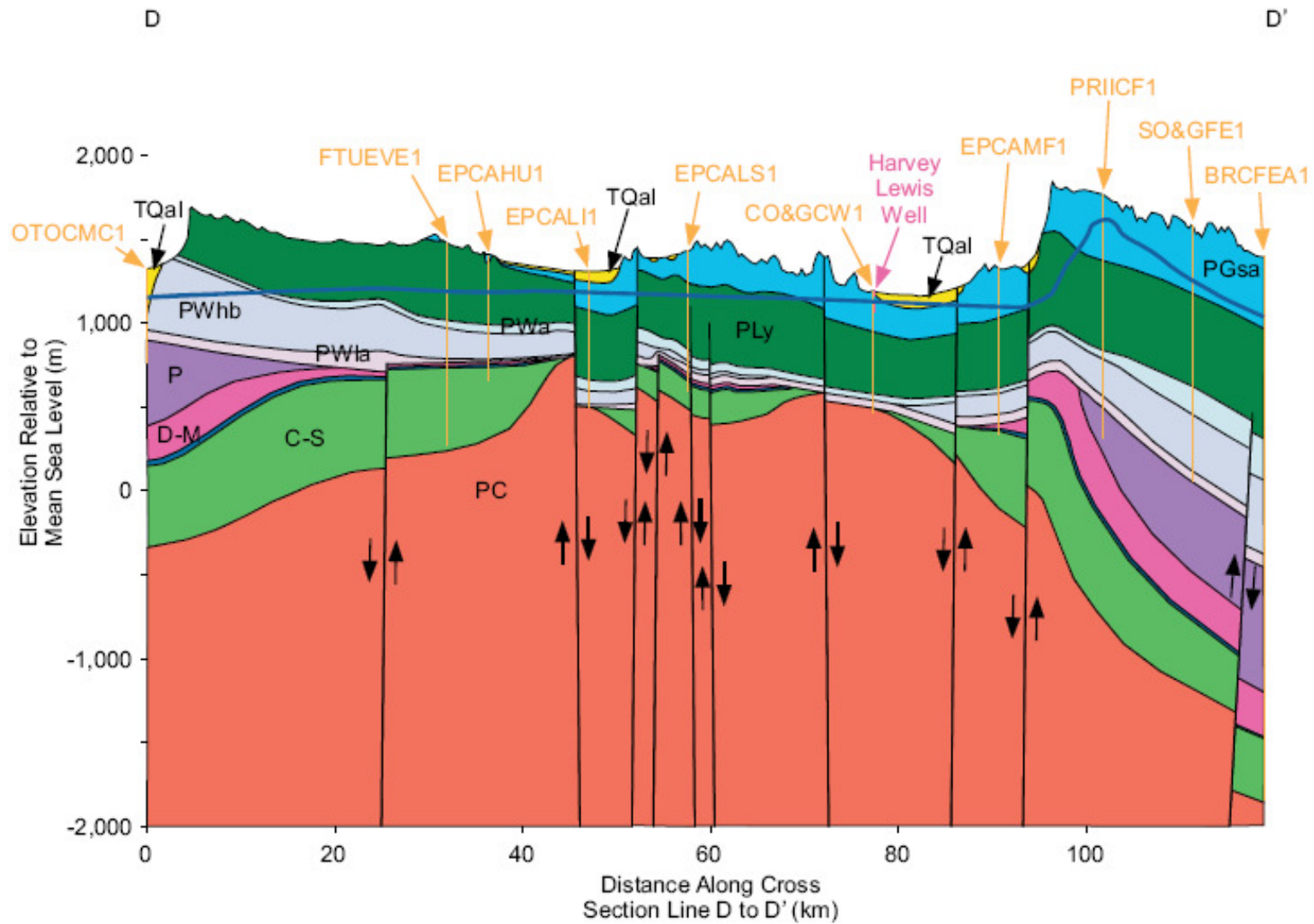
Figure A-3.40: West-East cross-section D - D'.

Vertical exaggeration 18×.

549

Figure A-3.41: West-East cross-section E - E'.

Vertical exaggeration 15×.
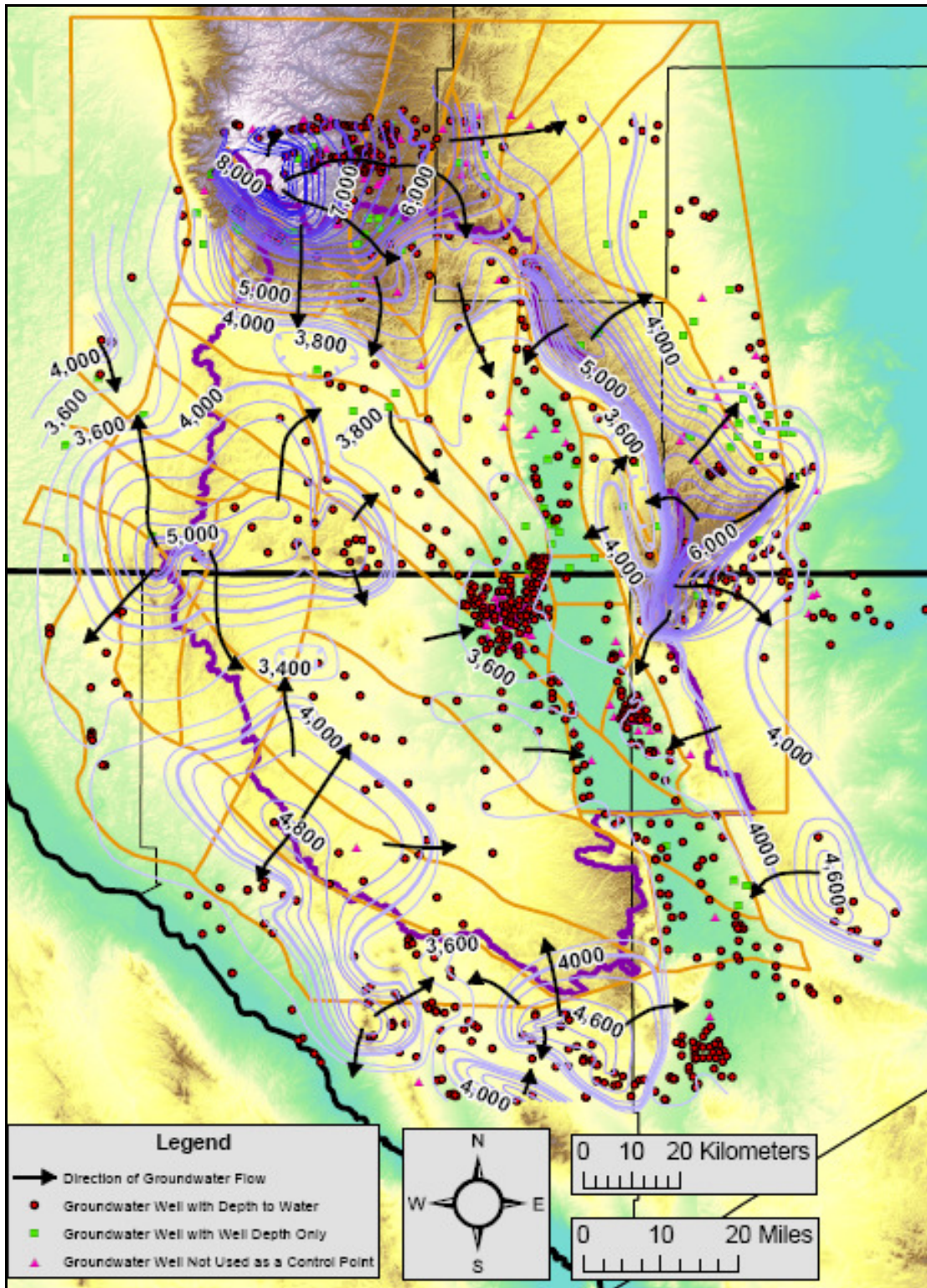
Figure A-3.42: Groundwater elevation contours for the Salt Basin region. Elevations are in feet above mean sea level. Contour interval is 200 feet. Hachured contours indicate groundwater depressions. The red circle and green square symbols indicate groundwater wells used as control for the contours, while the pink triangle symbols indicate groundwater wells not used as control points.
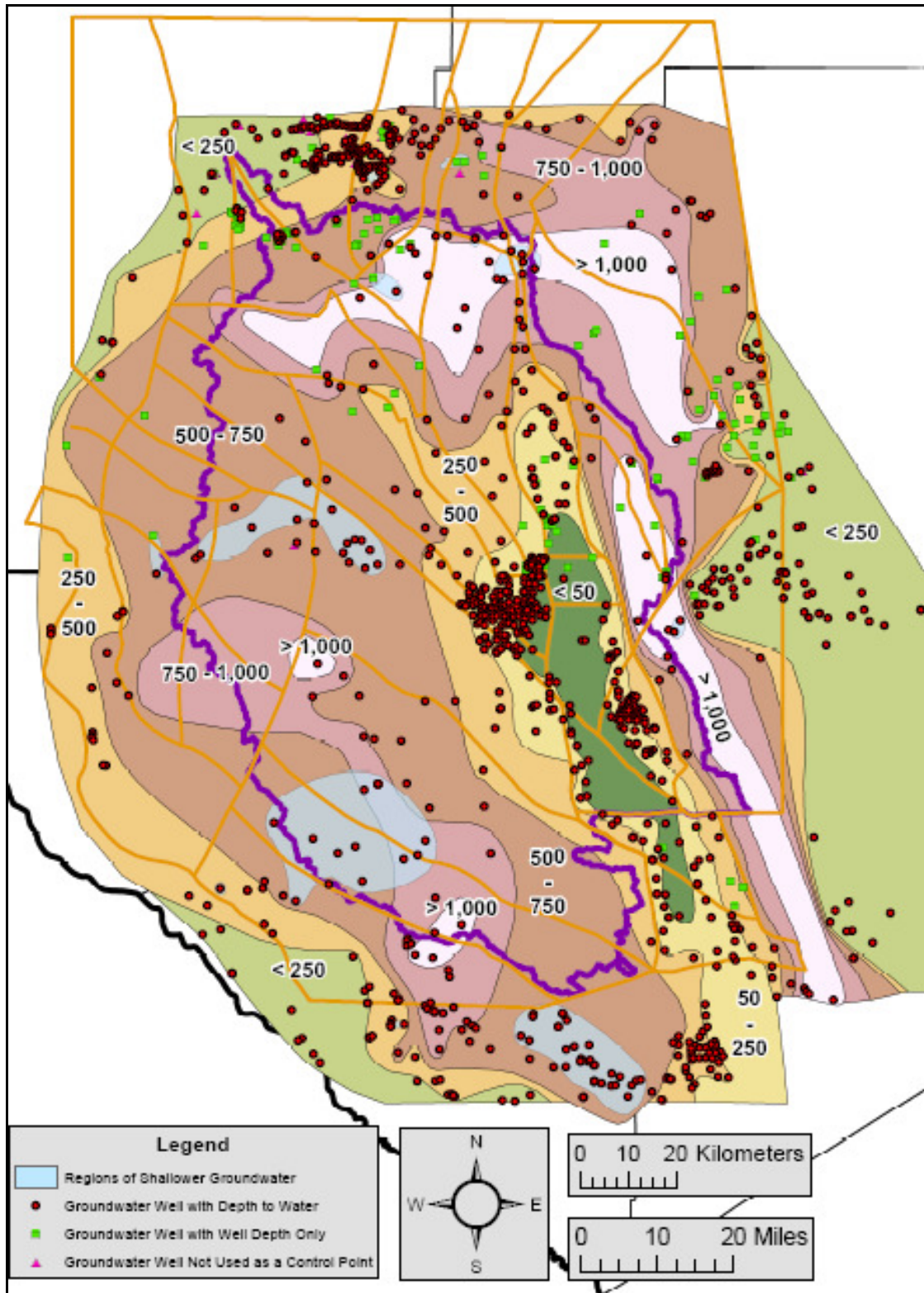
Figure A-3.43: Depth-to-groundwater for the Salt Basin region.
Depths are in feet. Groundwater well symbology is the same as Figure A-3.42. Light blue regions delineate zones of shallower groundwater than is indicated by the surrounding depth-to-groundwater polygons.
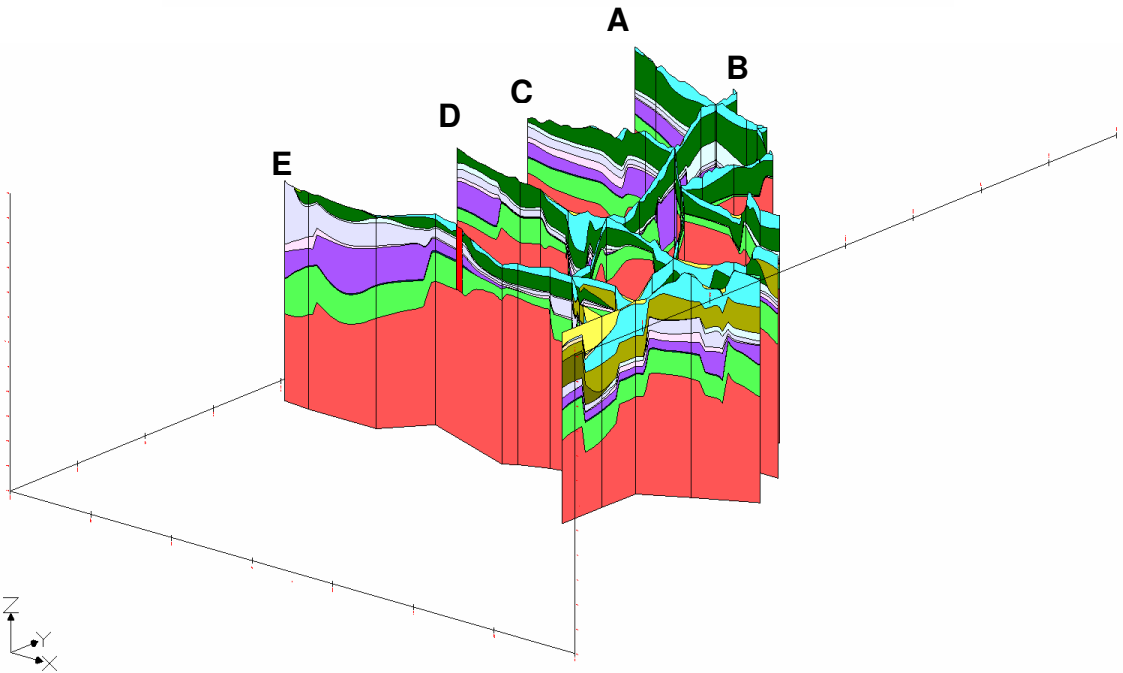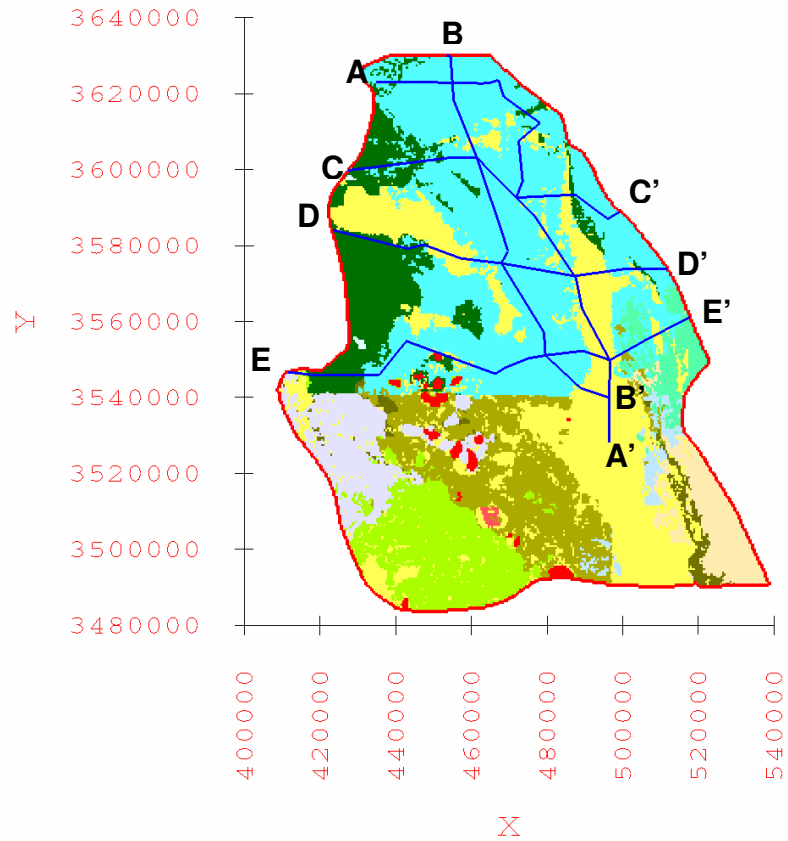
Figure A-3.44: Locations and an oblique view of the five cross-sections within the 3-D hydrogeologic framework solid model.
Color-coding of hydrogeologic units corresponds to that used in Figure A-2.1, and Figures A-3.37 through A-3.41. Red line designates groundwater flow model boundary. Blue lines indicate cross-sections. Vertical exaggeration 10×.

Figure A-3.45: Side views along cross-section A - A' of the 3-D framework solid model on left and hand-drawn cross-section on right. Vertical exaggeration 10× on 3-D framework solid model cross-sections. Vertical exaggeration 23× on hand-drawn cross-section.

554
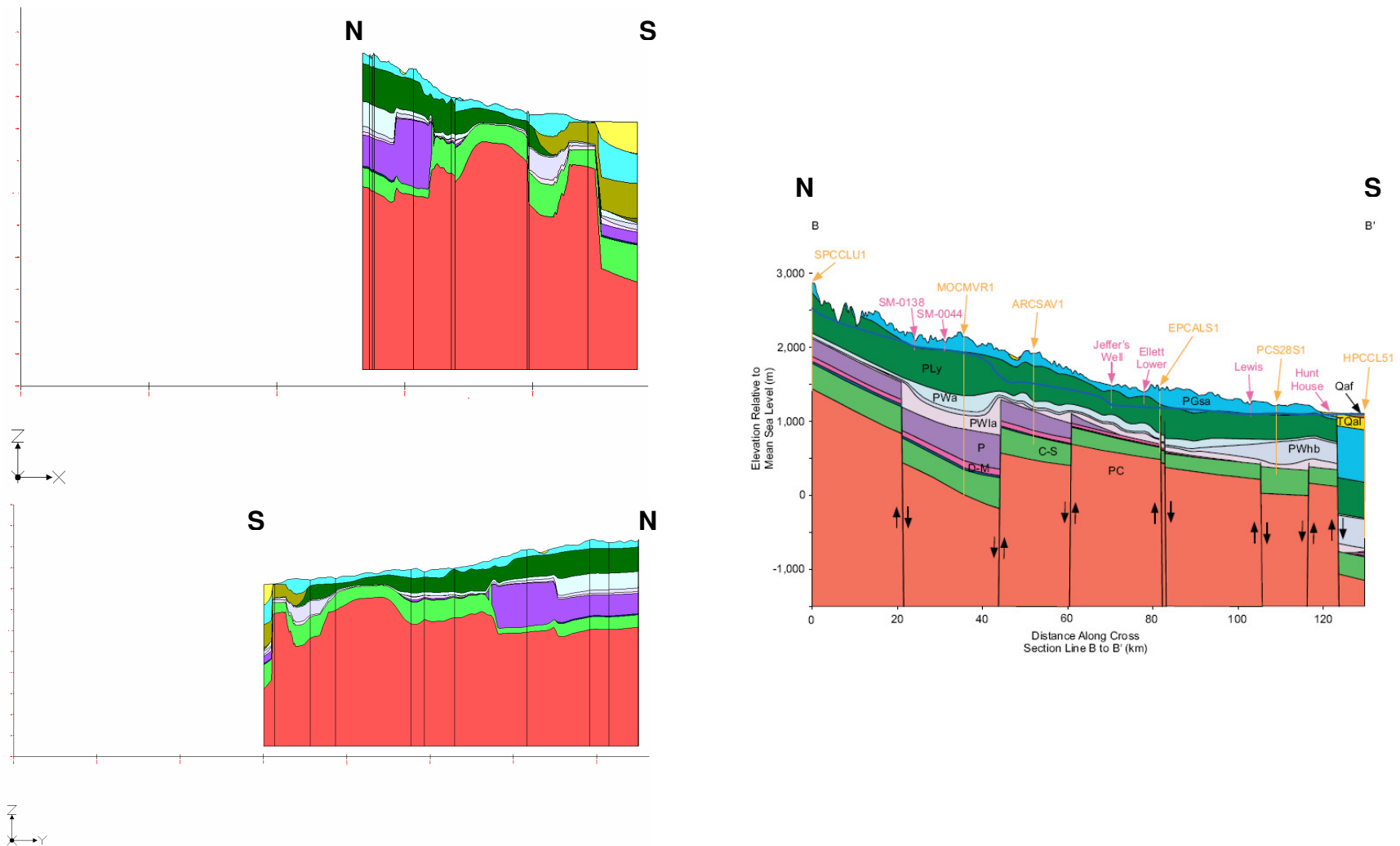
Figure A-3.46: Side views along cross-section B - B' of the 3-D framework solid model on left and hand-drawn cross-section on right. Vertical exaggeration 10× on 3-D framework solid model cross-sections. Vertical exaggeration 18× on hand-drawn cross-section.
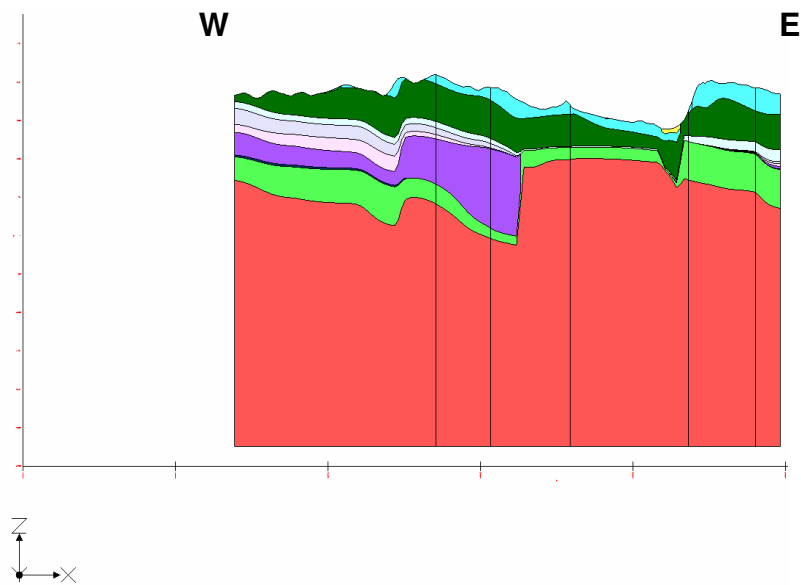
Figure A-3.47: Side views along cross-section C - C' of the 3-D framework solid model on left and hand-drawn cross-section on right. Vertical exaggeration 10× on 3-D framework solid model cross-section. Vertical exaggeration 22× on hand-drawn cross-section.
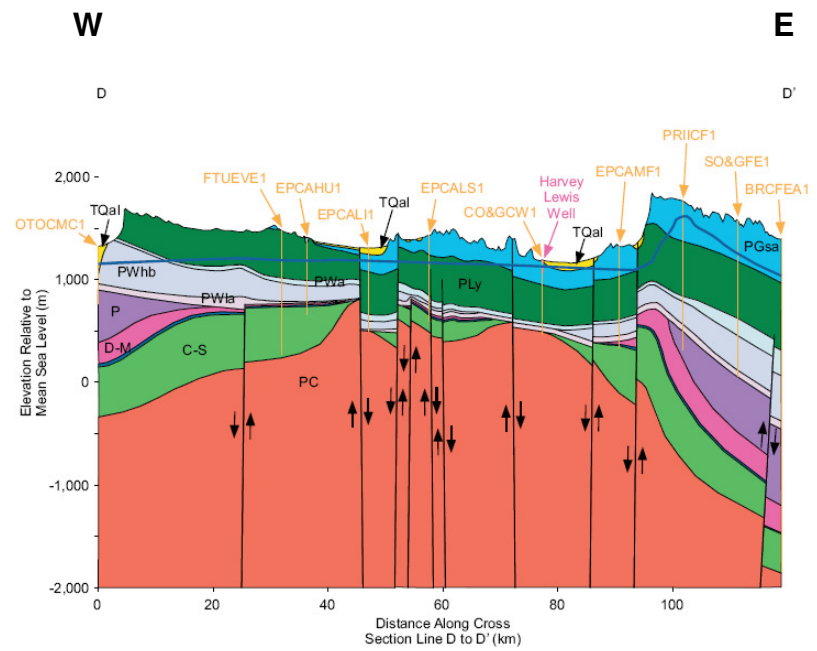
Figure A-3.48: Side views along cross-section D - D' of the 3-D framework solid model on left and hand-drawn cross-section on right. Vertical exaggeration 10× on 3-D framework solid model cross-section. Vertical exaggeration 18× on hand-drawn cross-section.

557
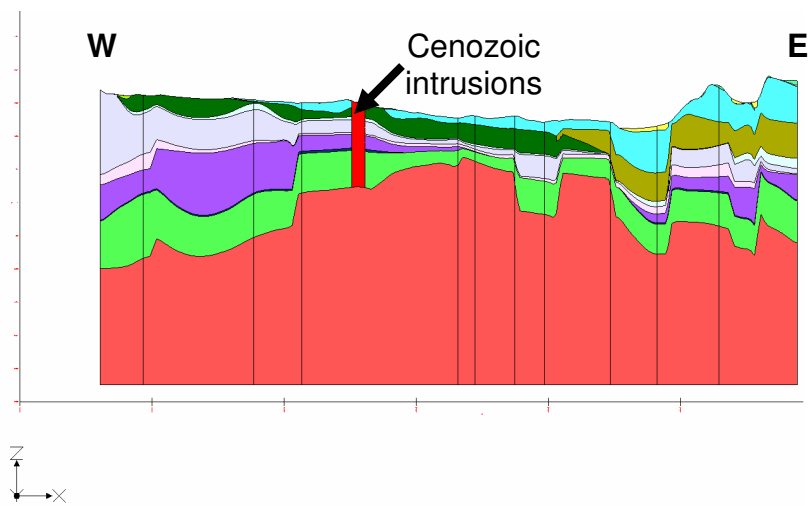
Figure A-3.49: Side views along cross-section E - E' of the 3-D framework solid model on left and hand-drawn cross-section on right. Vertical exaggeration 10× on 3-D framework solid model cross-section. Vertical exaggeration 15× on hand-drawn cross-section.

Figure A-3.50: Aquifers in the Salt Basin region.
Location of high mountain and Pecos slope aquifers from SMHS. Location of Bone Spring-Victorio Peak and Hueco bolson aquifers from TWDB. Location of Capitan Reef Complex aquifer from Uliana (2001). Location of Cretaceous aquifer from Sharp (1989).

Figure A-3.51: Predevelopment groundwater elevation contours, from JSAI (2002). Elevations are in feet above mean sea level. Contour interval is 200 feet.

560

Figure A-3.52: Predevelopment groundwater elevation contours for the valley-fill aquifer within the Salt Basin graben, from Sharp (1989).
Elevations are in feet above mean sea level. Contour interval is 10 feet. Also illustrates the structural features associated with groundwater divides in the valley-fill aquifer.
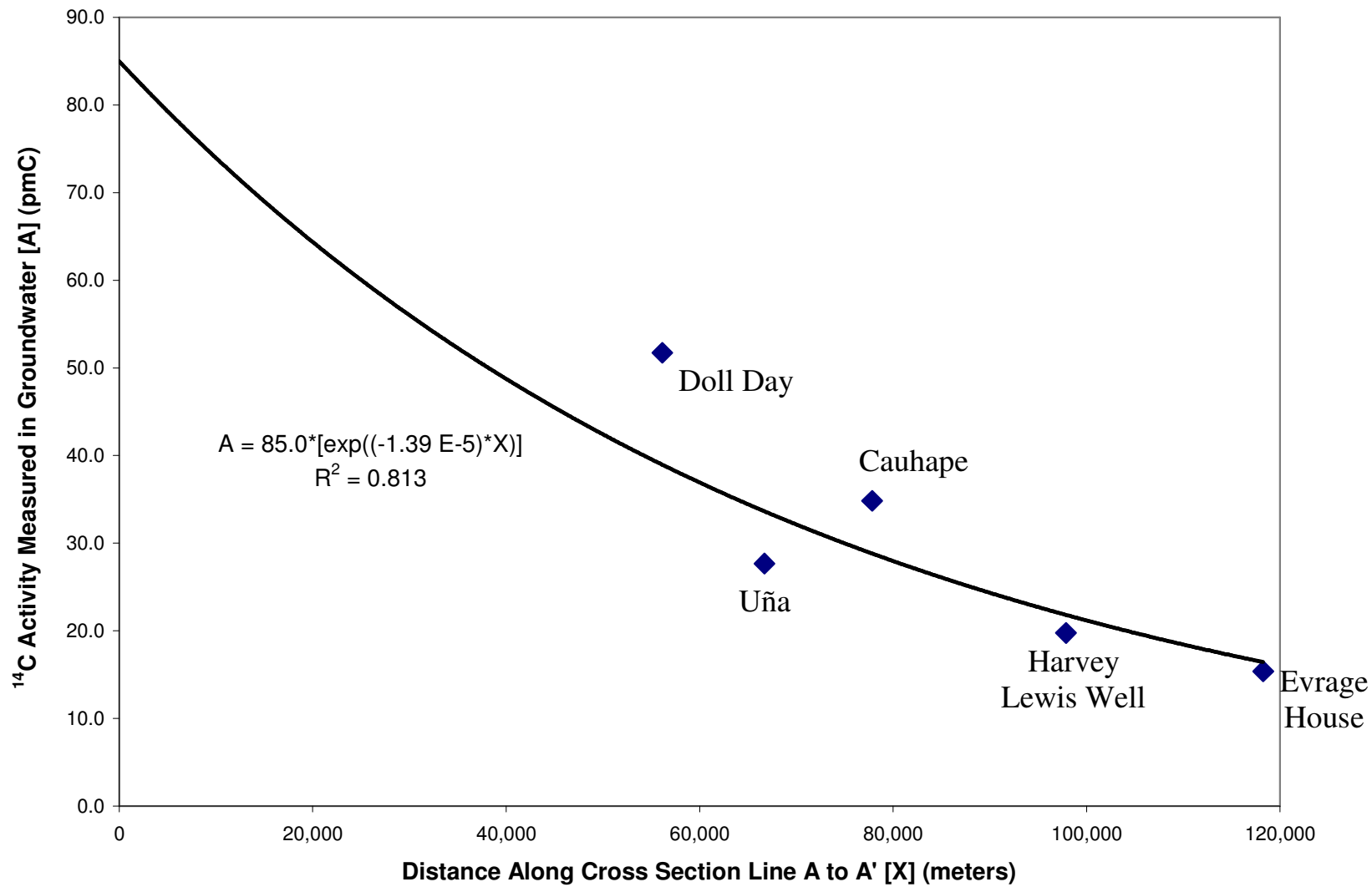
Figure A-3.53: ^{14}C activity measured in groundwater versus distance along cross-section line A - A'.
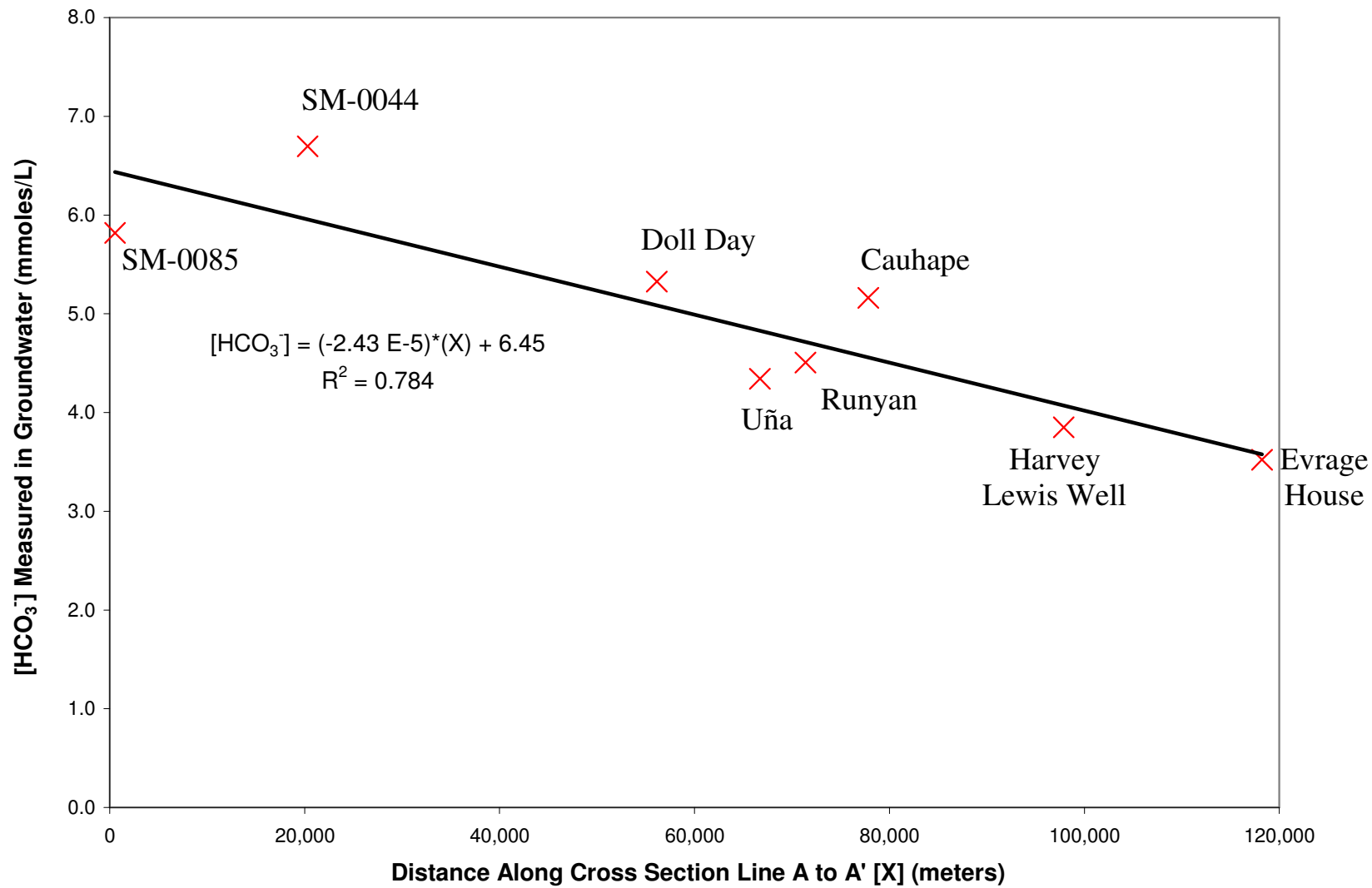
Figure A-3.54: [HCO$_3^-$] measured in groundwater versus distance along cross-section line A - A'.
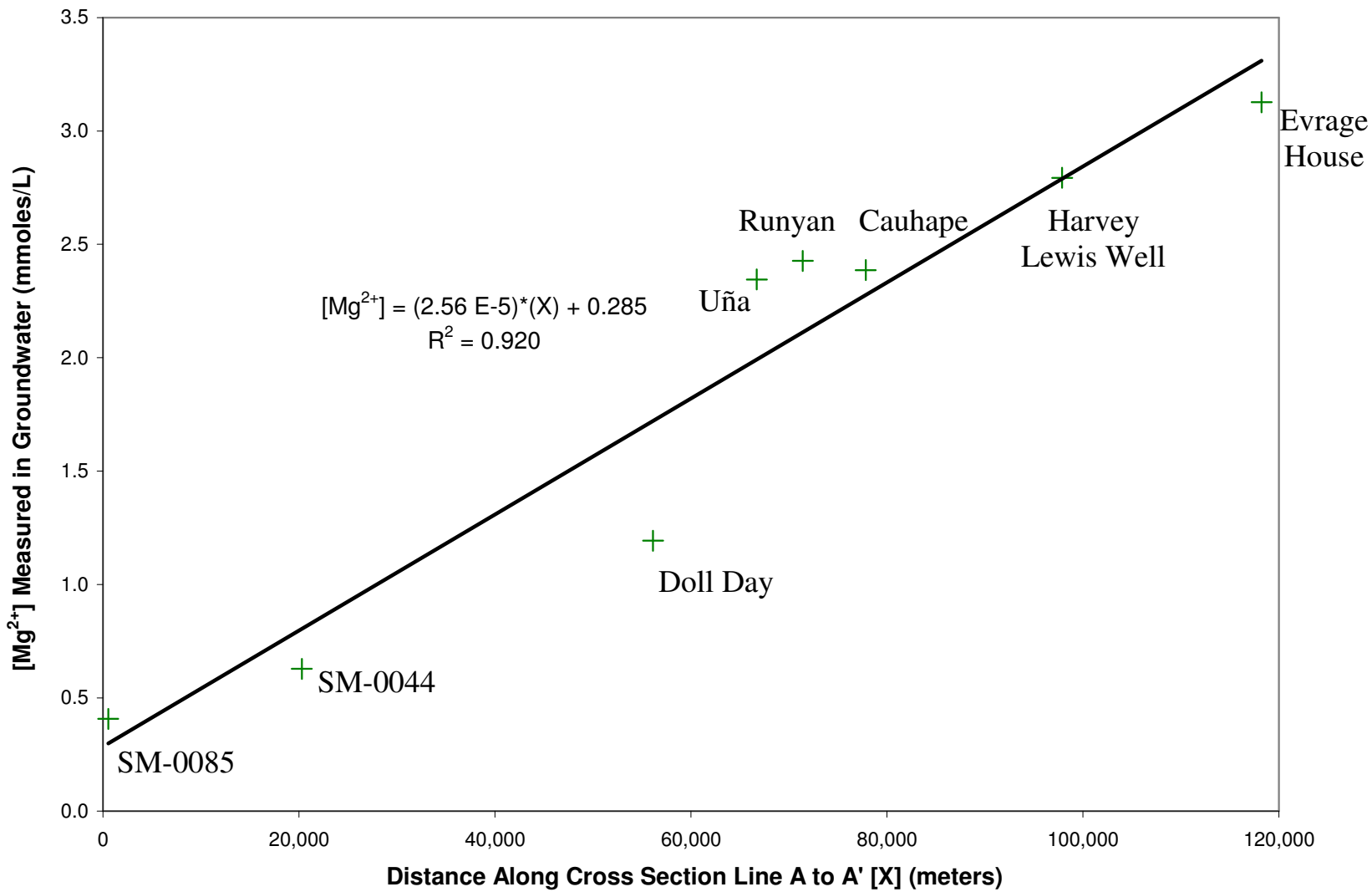
Figure A-3.55: [Mg^{2+}] measured in groundwater versus distance along cross-section line A - A'.
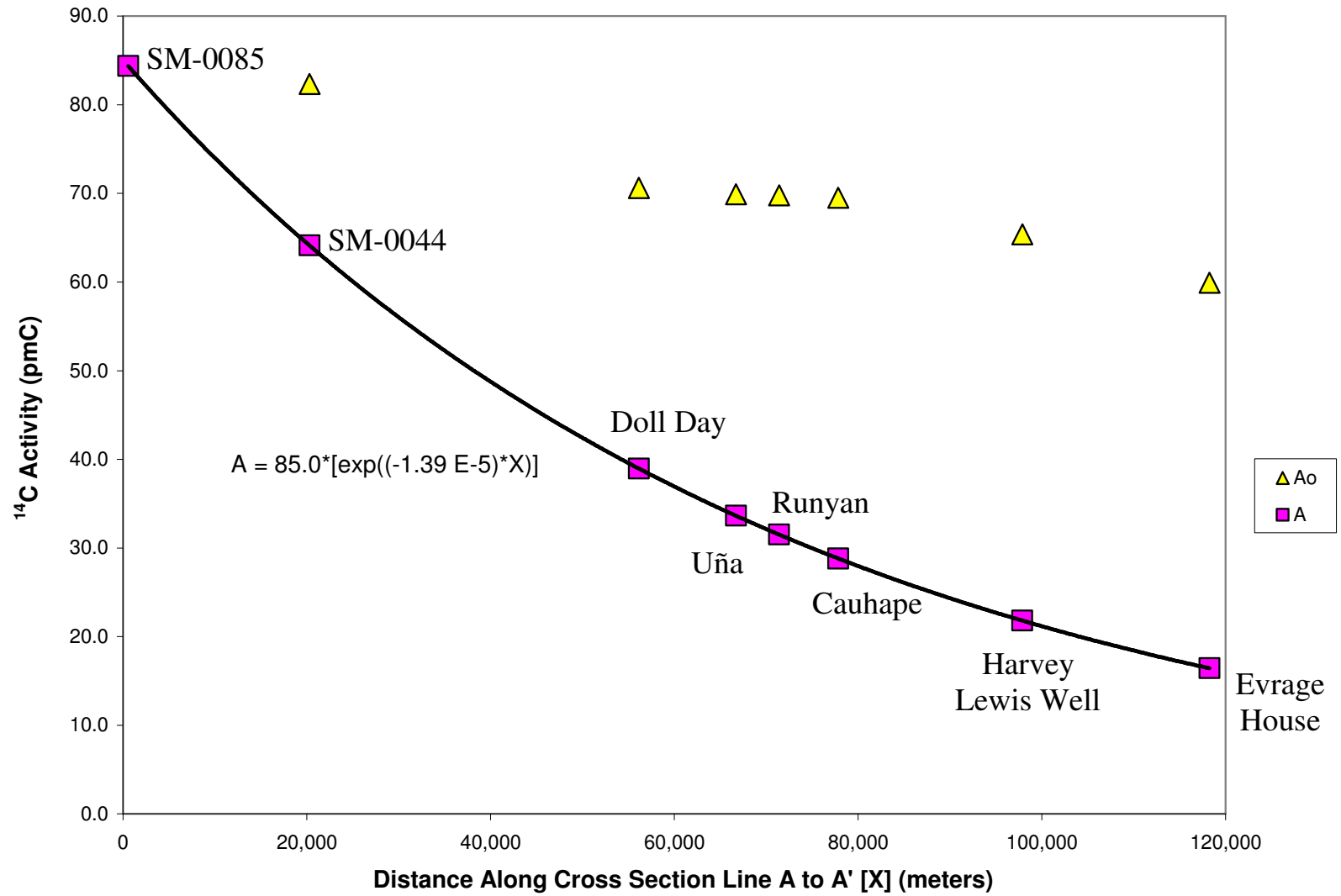
Figure A-3.56: ^{14}C activity [A] and [A_0] versus distance along cross-section line A - A'.
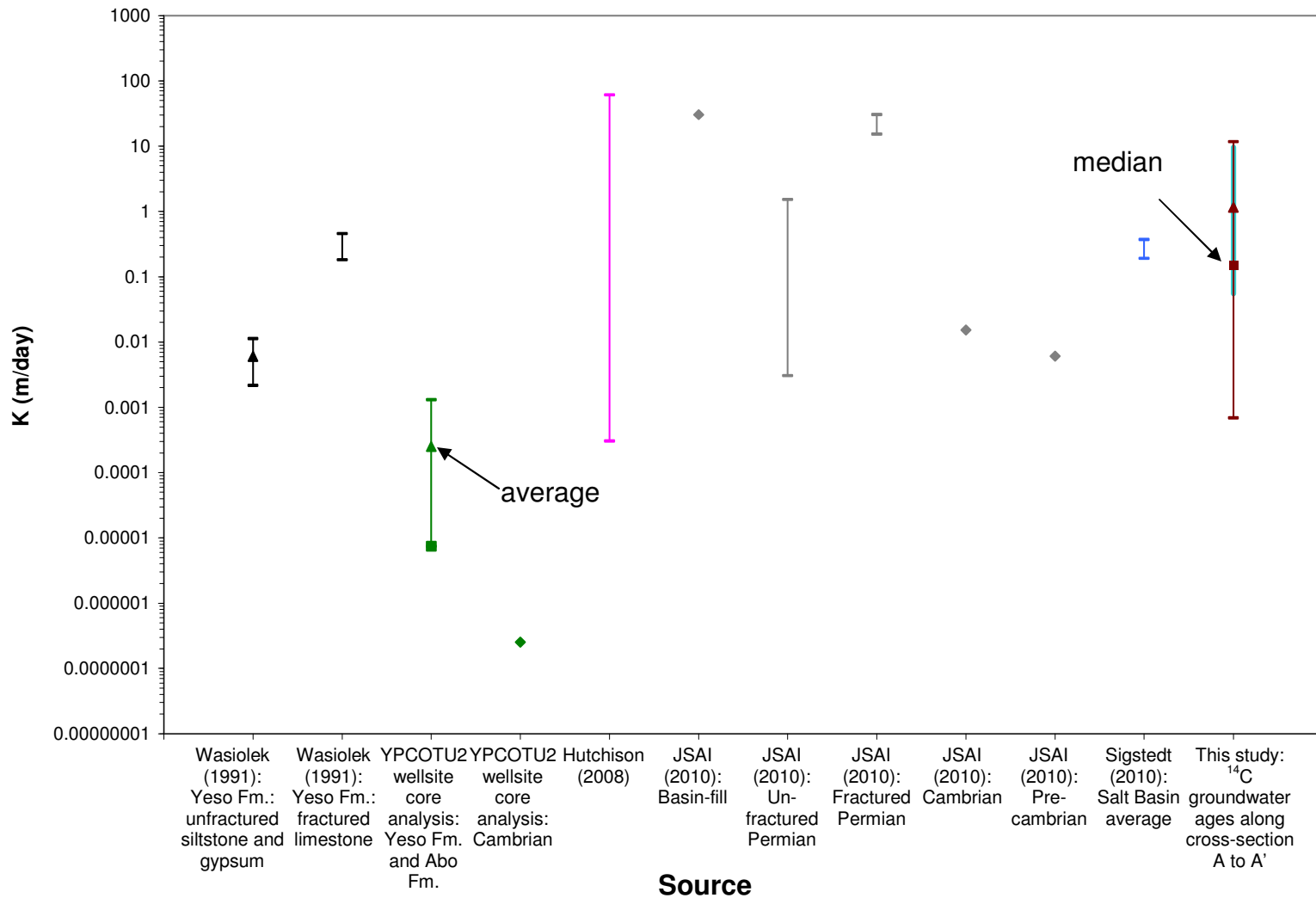
Figure A-3.57: Range of hydraulic conductivity [K] values from previous studies and this study. Vertical axis is logarithmic scale. Squares indicate median values, and triangles indicate average values.
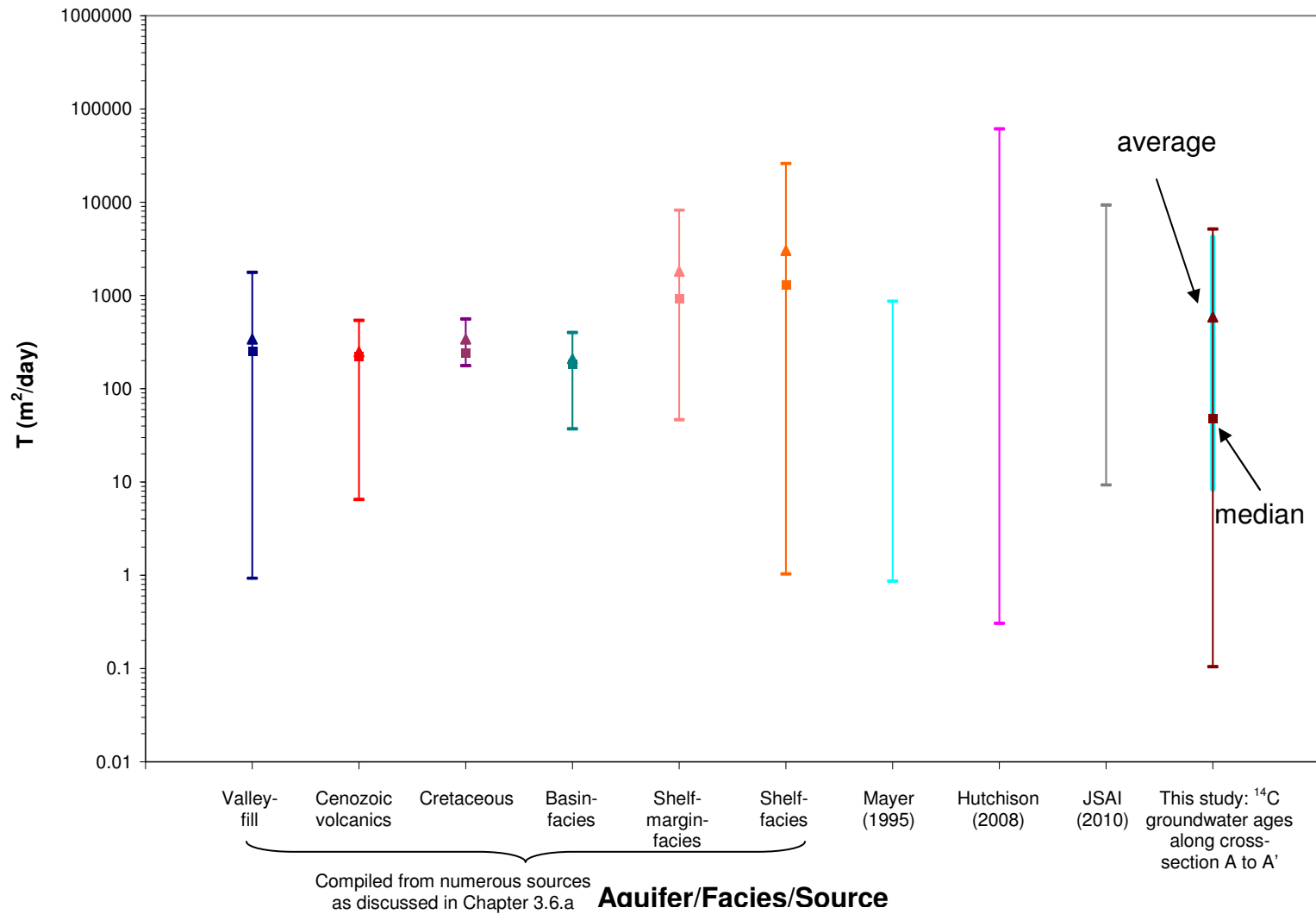
Figure A-3.58: Range of transmissivity [T] values from previous studies and this study.
Vertical axis is logarithmic scale. Squares indicate median values, and triangles indicate average values.

Figure A-3.59: Location of the four groundwater wells in the New Mexico portion of the Salt Basin watershed with continuous water level measurements from 2003 to the middle of 2006, as presented in Huff and Chace (2006), and the TWDB's State Well Number 4807516.

Figure A-3.60: Change in groundwater levels versus time for wells H&C 1, H&C 2, H&C 3, and H&C 4.

Figure A-3.61: Change in groundwater levels versus time for wells H&C 1, H&C 2, H&C 3, H&C 4, and 4807516.

Figure A-3.62: Location of maximum and minimum change in groundwater levels used to calculate the average annual amplitude of water level fluctuations in wells H&C 1, 2, 3, and 4, and 4807516.
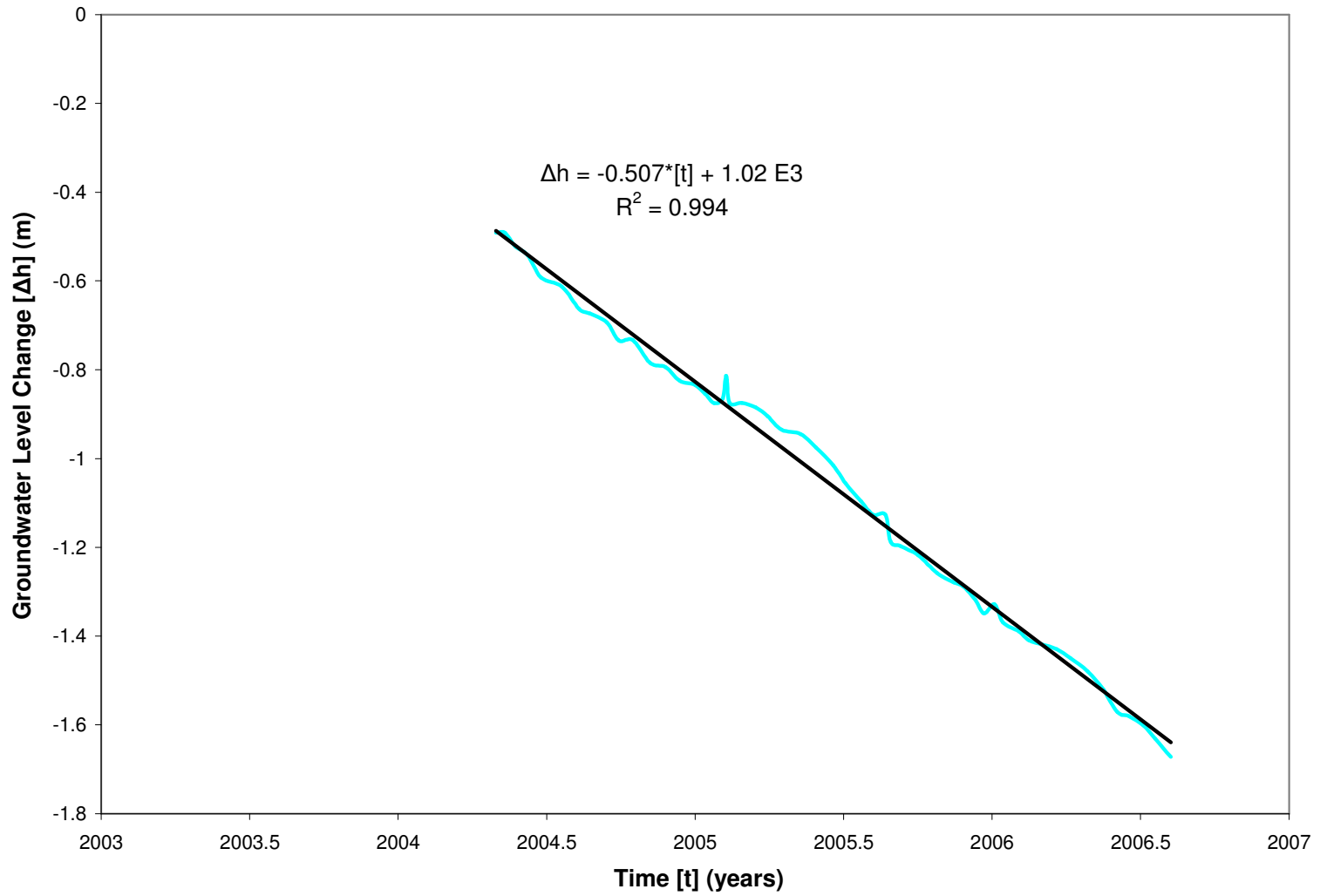
Figure A-3.63: Change in groundwater level versus time for well H&C 4.
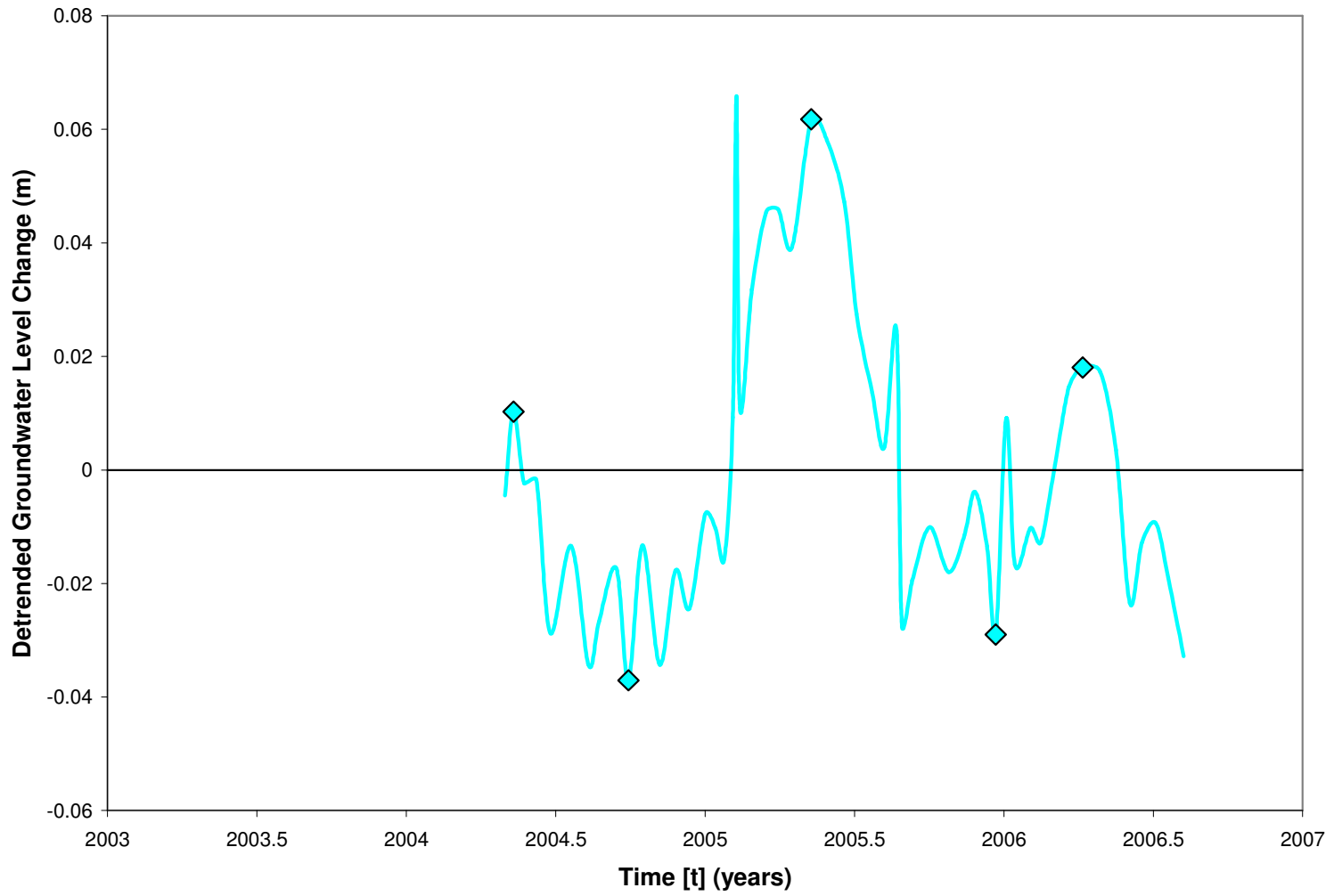
Figure A-3.64: Detrended change in groundwater level versus time for well H&C 4.
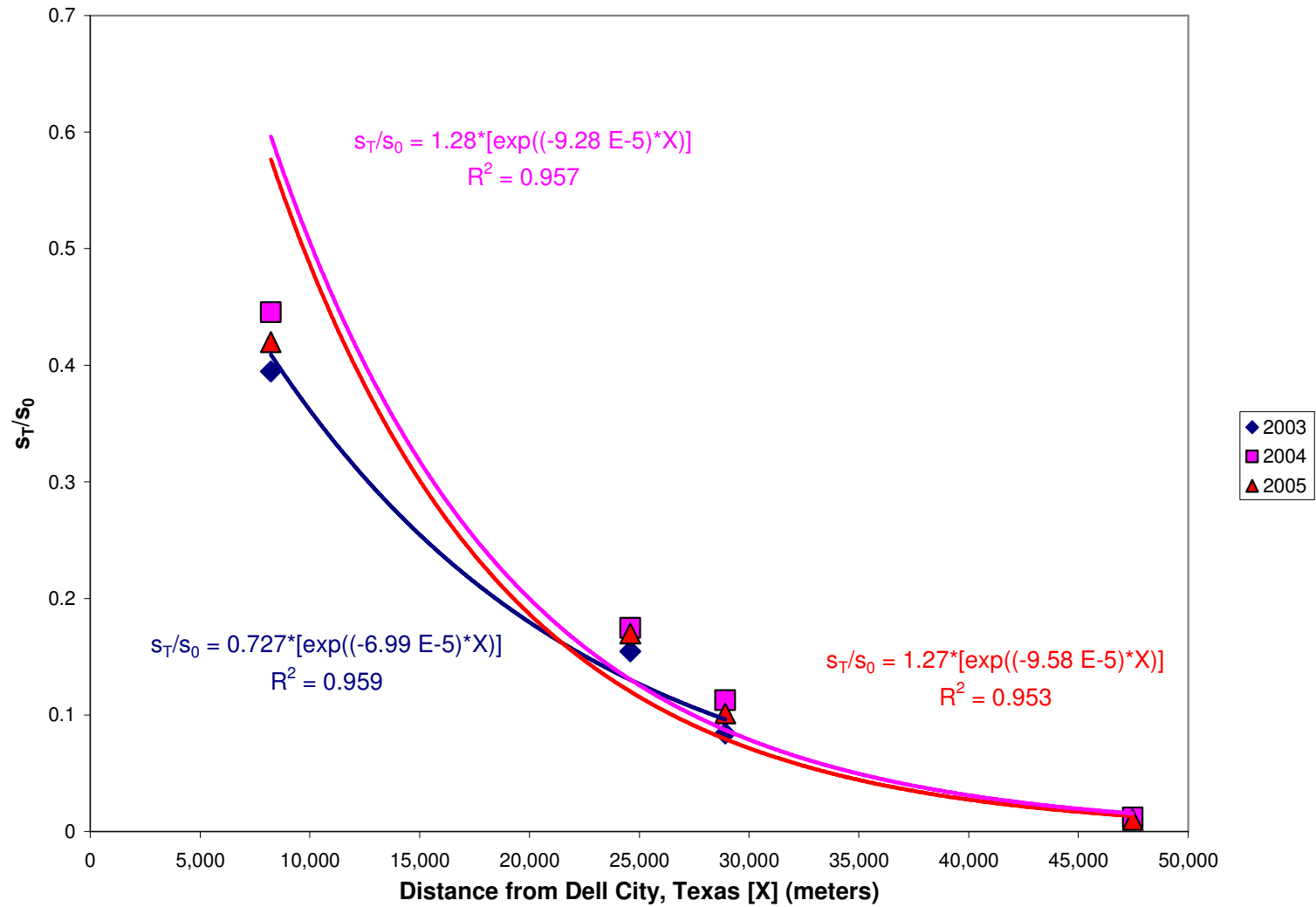
Figure A-3.65: s_T/s_0 calculated from water level fluctuations in 2003 at wells H&C 1, 2, and 3, and 4807516, and in 2004 and 2005 at wells H&C 1, 2, 3, and 4, and 4807516 versus distance from Dell City, Texas.
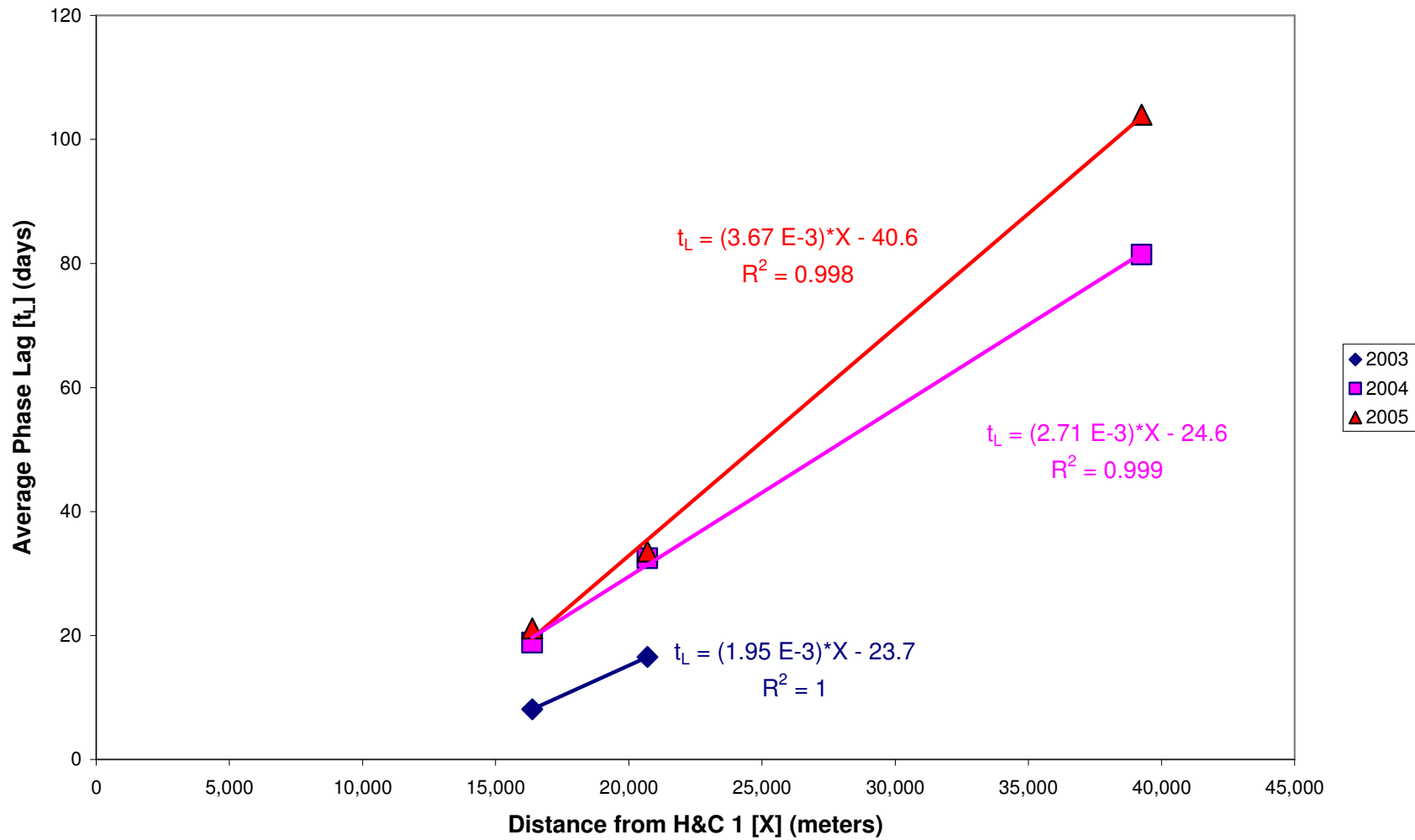
Figure A-3.66: Average phase lag between well H&C 1 and wells H&C 2 and 3 in 2003, and well H&C 1 and wells H&C 2, 3, and 4 in 2004 and 2005 versus distance from well H&C 1.

575
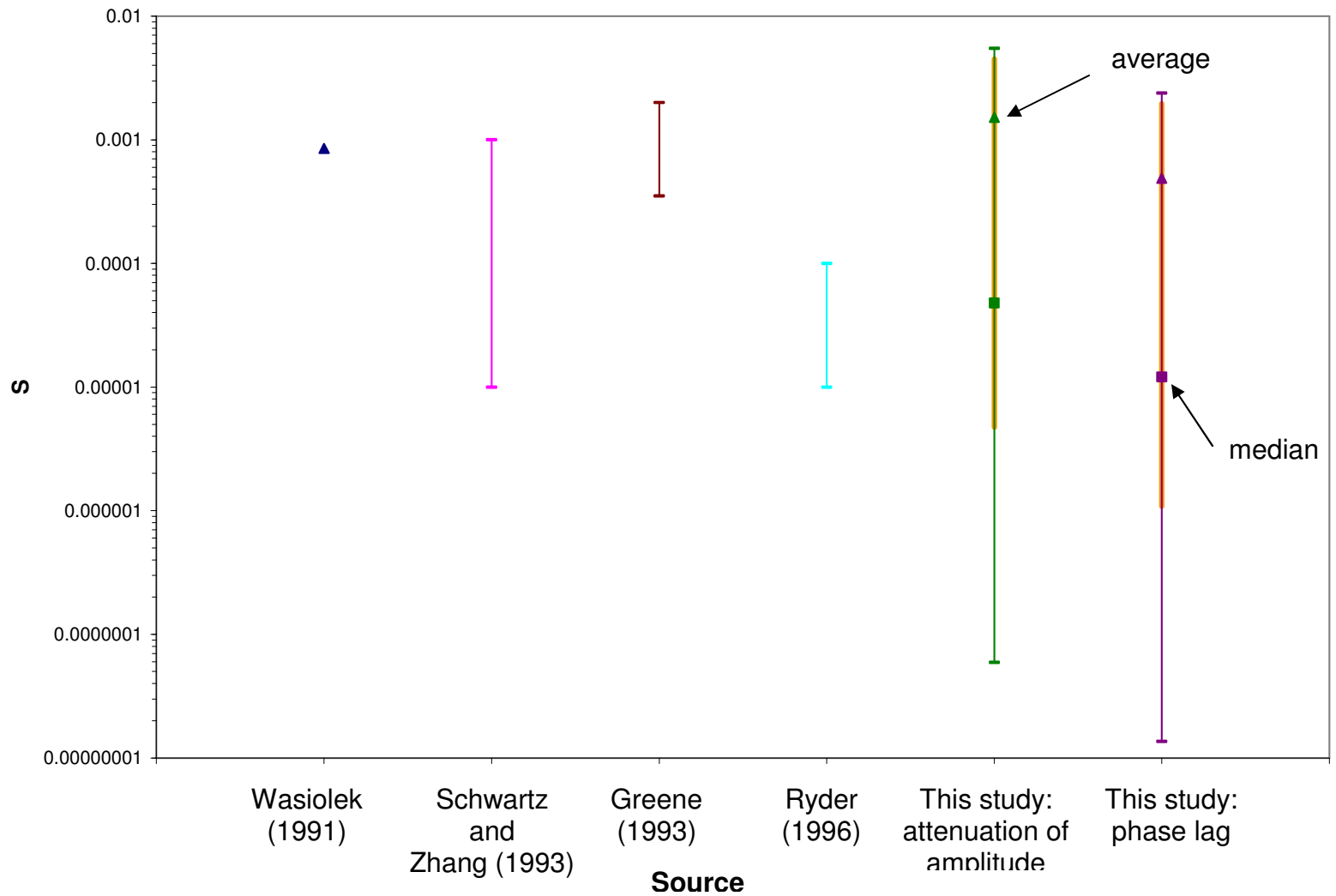
Figure A-3.67: Range of storage coefficient [S] values from previous studies and this study.
Vertical axis is logarithmic scale. Squares indicate median values, and triangles indicate average values.

FIGURES – CHAPTER 4
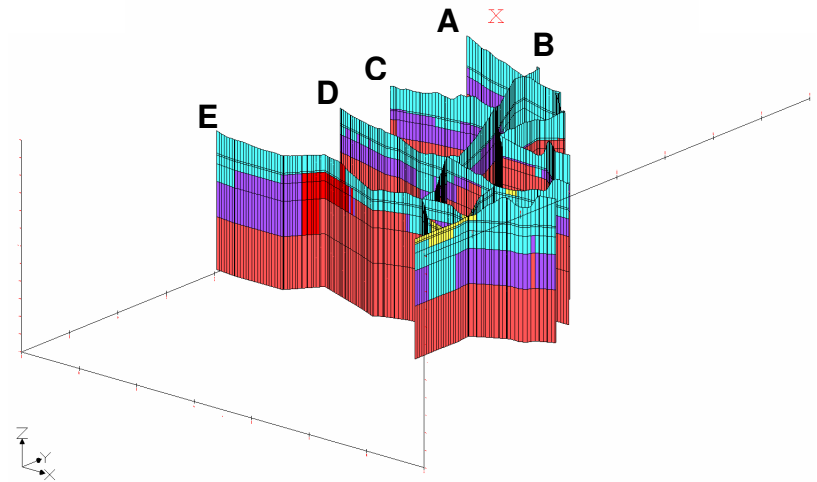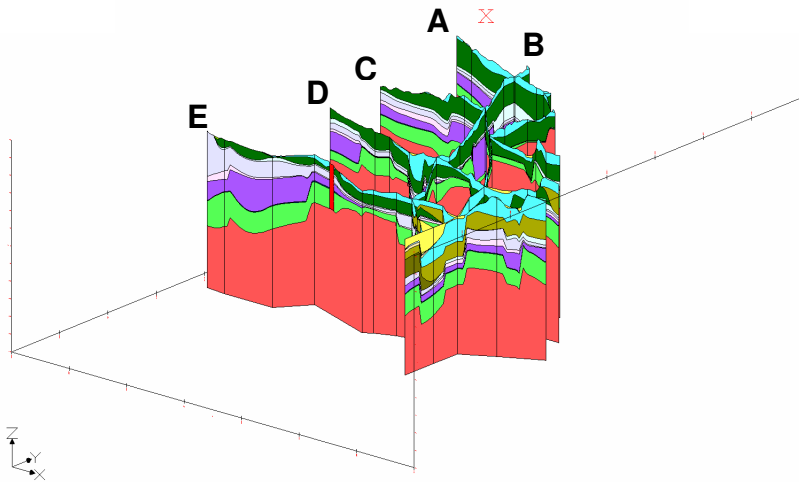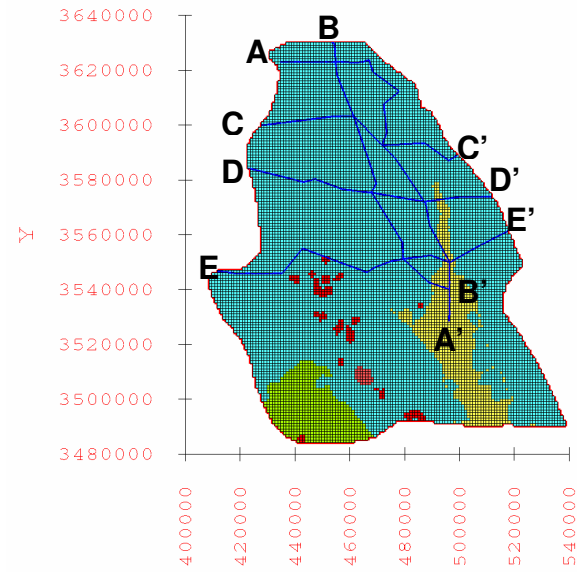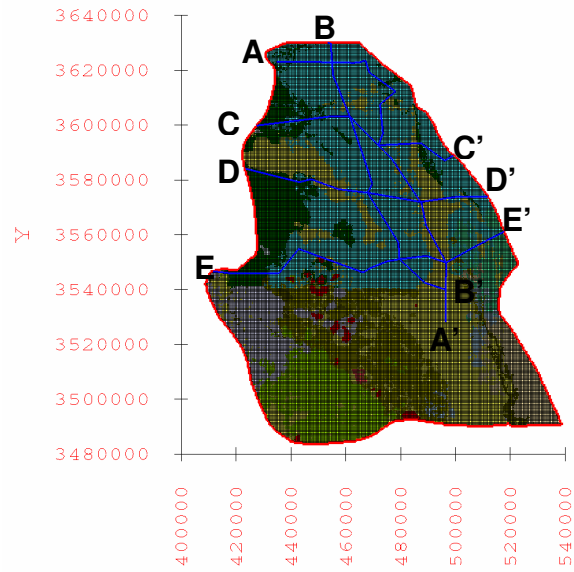
Figure A-4.1: Locations and an oblique view of the five cross-sections within the solid model on left and groundwater flow model on right.

578
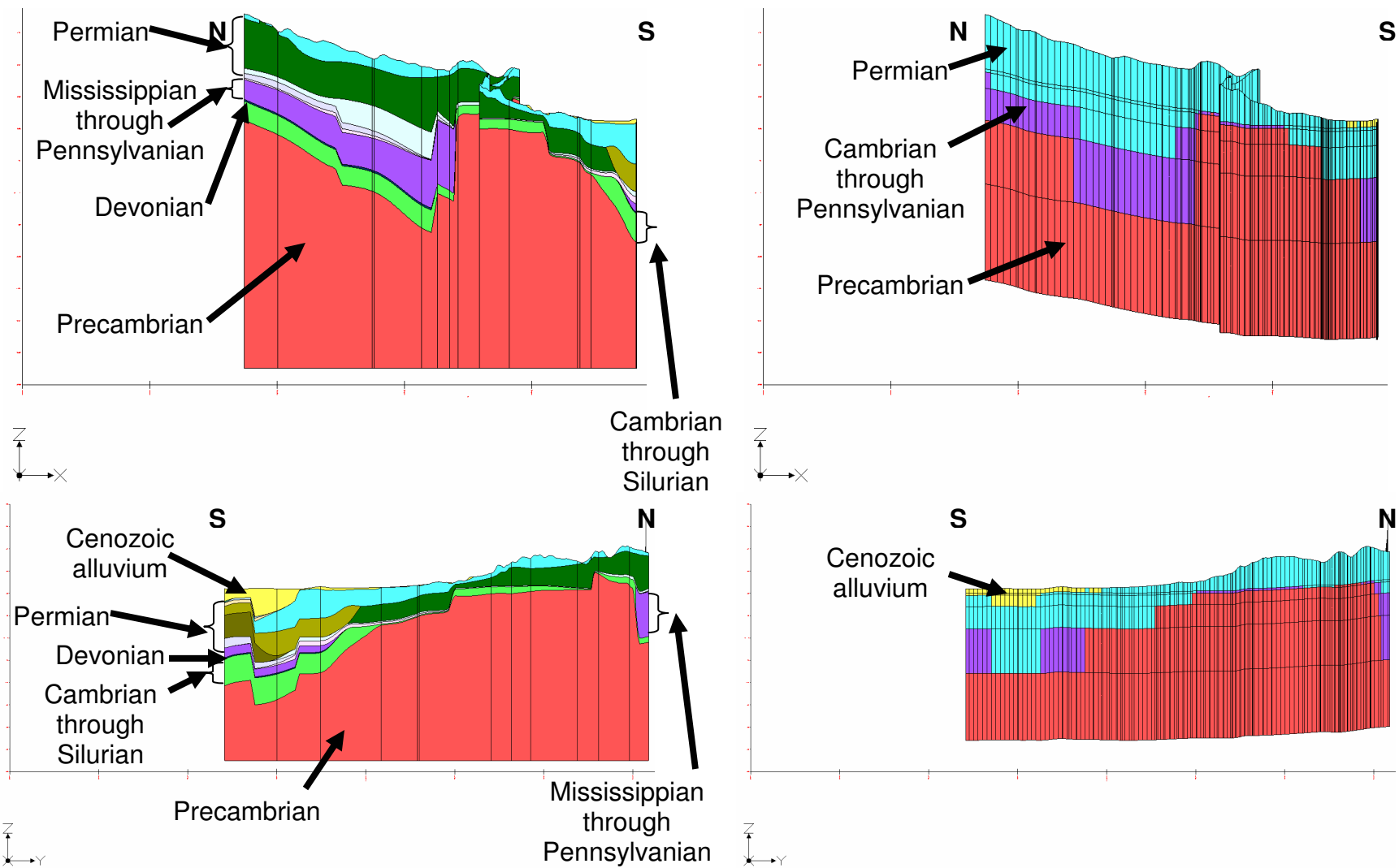
Figure A-4.2: Side views along cross-section A - A' of the solid model on left and groundwater flow model on right. Vertical exaggeration 10×.
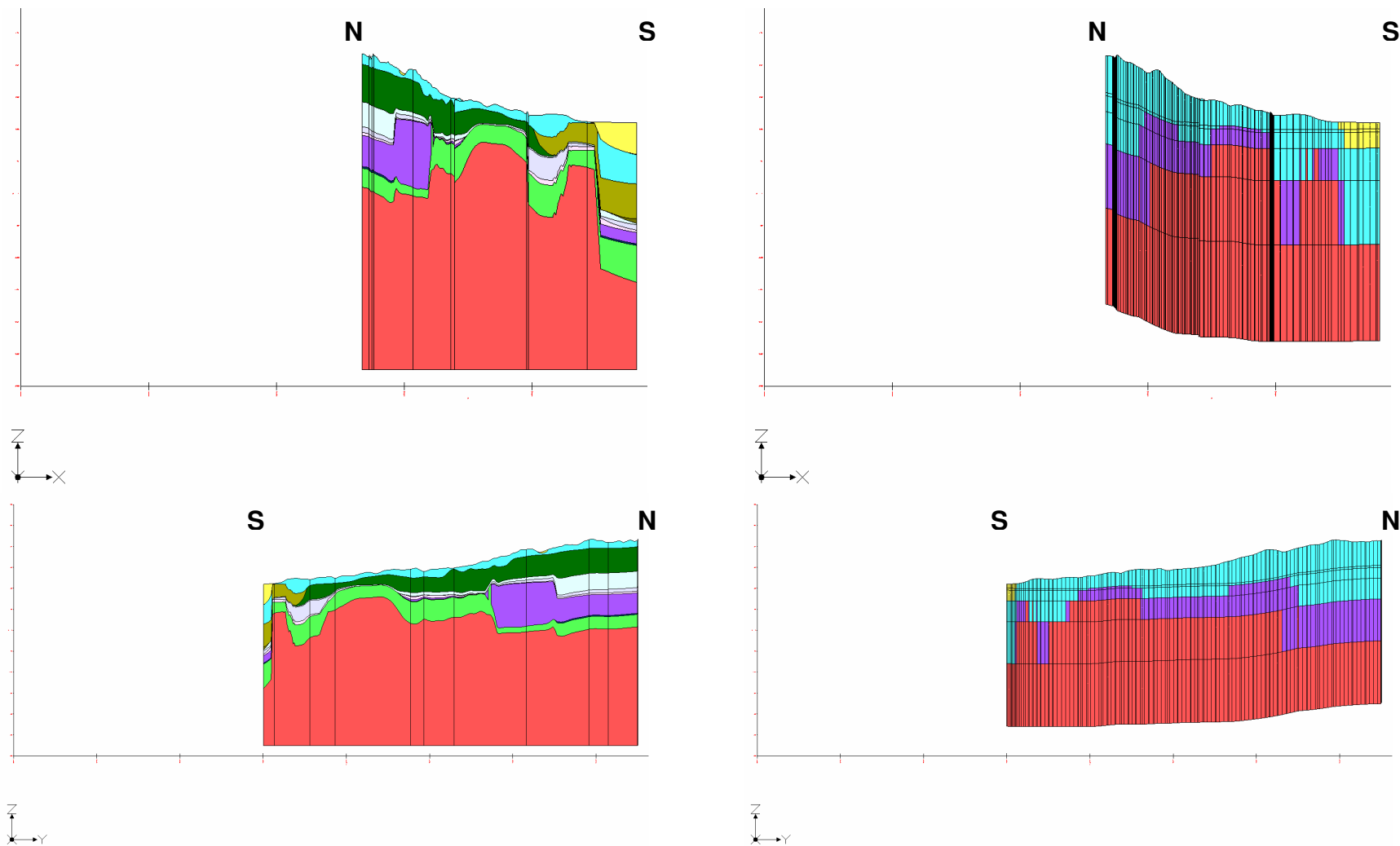
Figure A-4.3: Side views along cross-section B - B' of the solid model on left and groundwater flow model on right. Vertical exaggeration 10×.
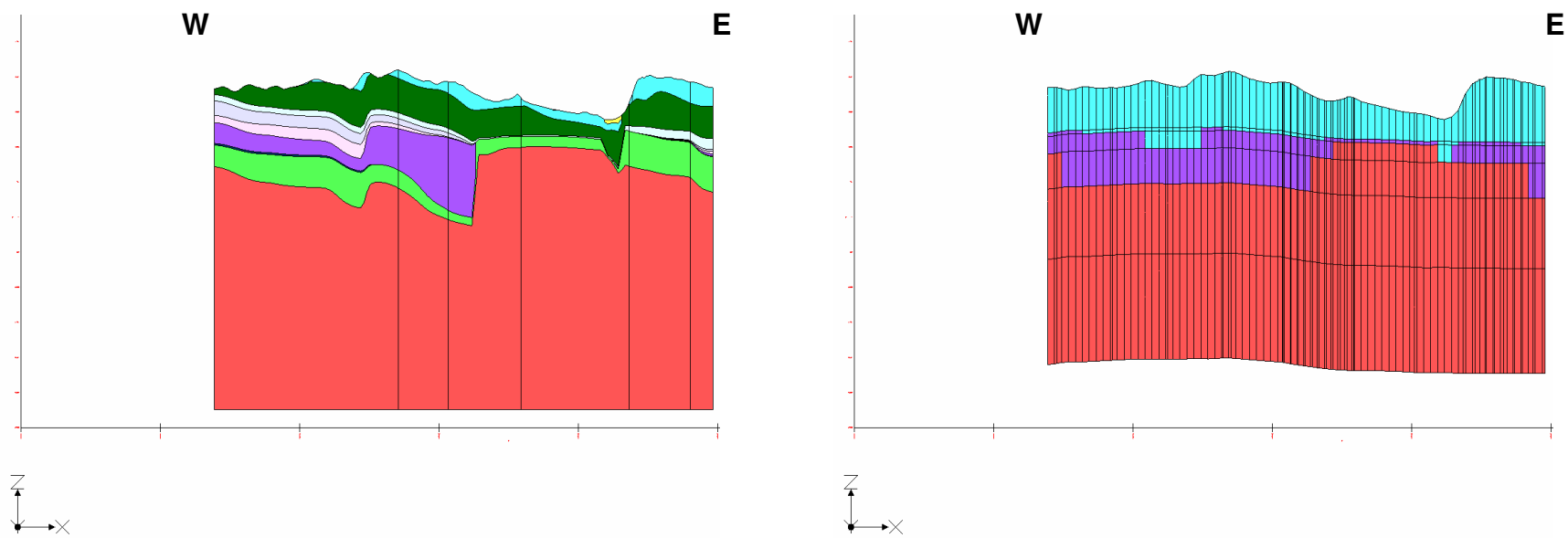
Figure A-4.4: Side view along cross-section C - C' of the solid model on left and groundwater flow model on right. Vertical exaggeration 10×.

581
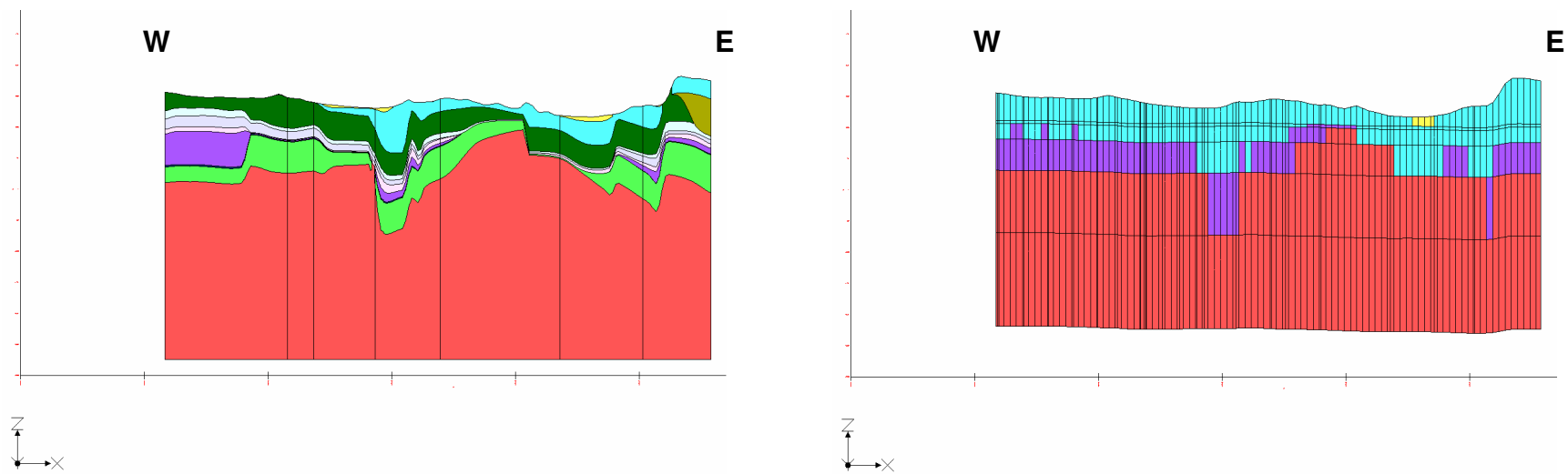
Figure A-4.5: Side view along cross-section D - D' of the solid model on left and groundwater flow model on right. Vertical exaggeration 10×.
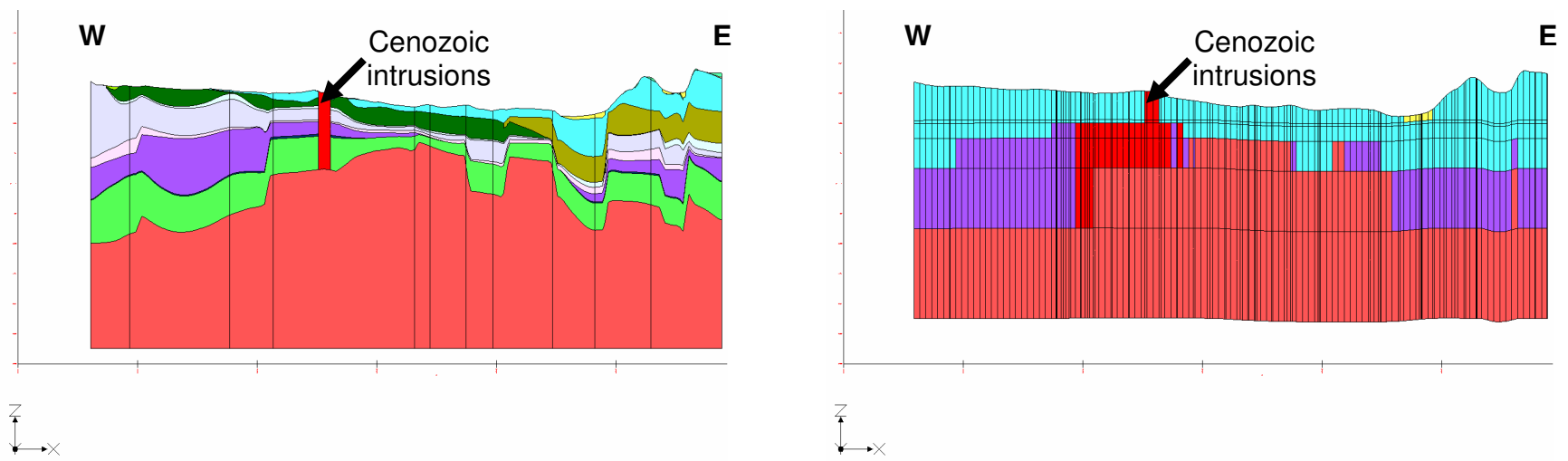
Figure A-4.6: Side view along cross-section E - E' of the solid model on left and groundwater flow model on right. Vertical exaggeration 10×.
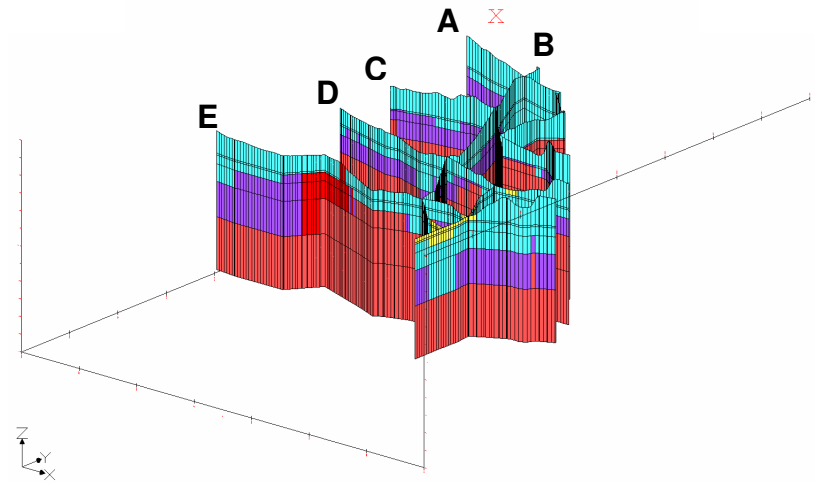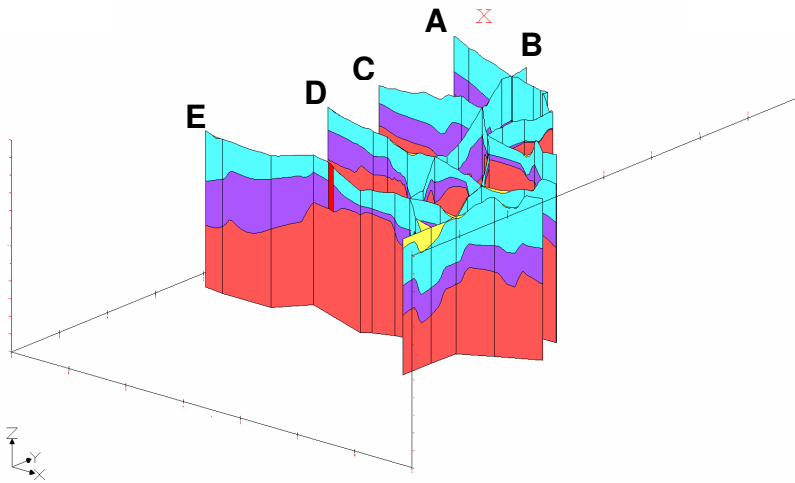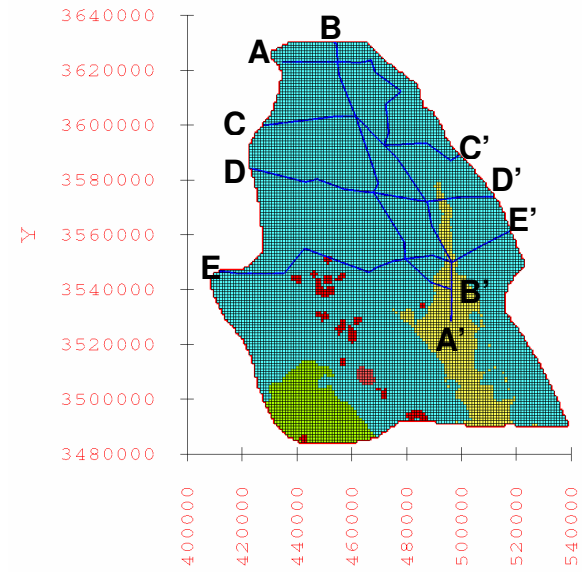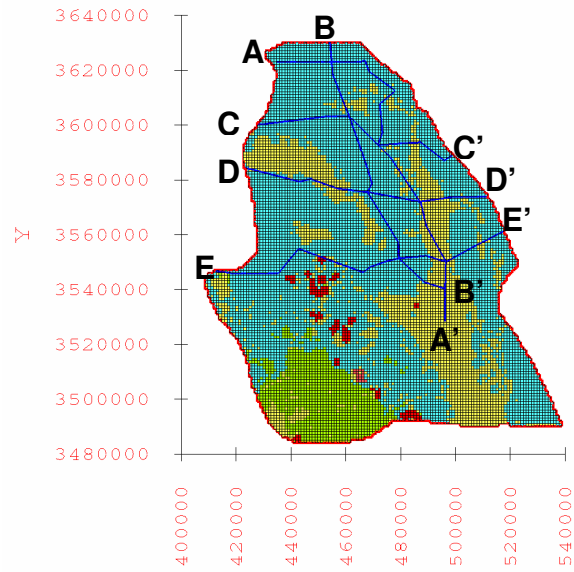
Figure A-4.7 Locations and an oblique view of the five cross-sections within the simplified solid model on left and groundwater flow model on right.

584
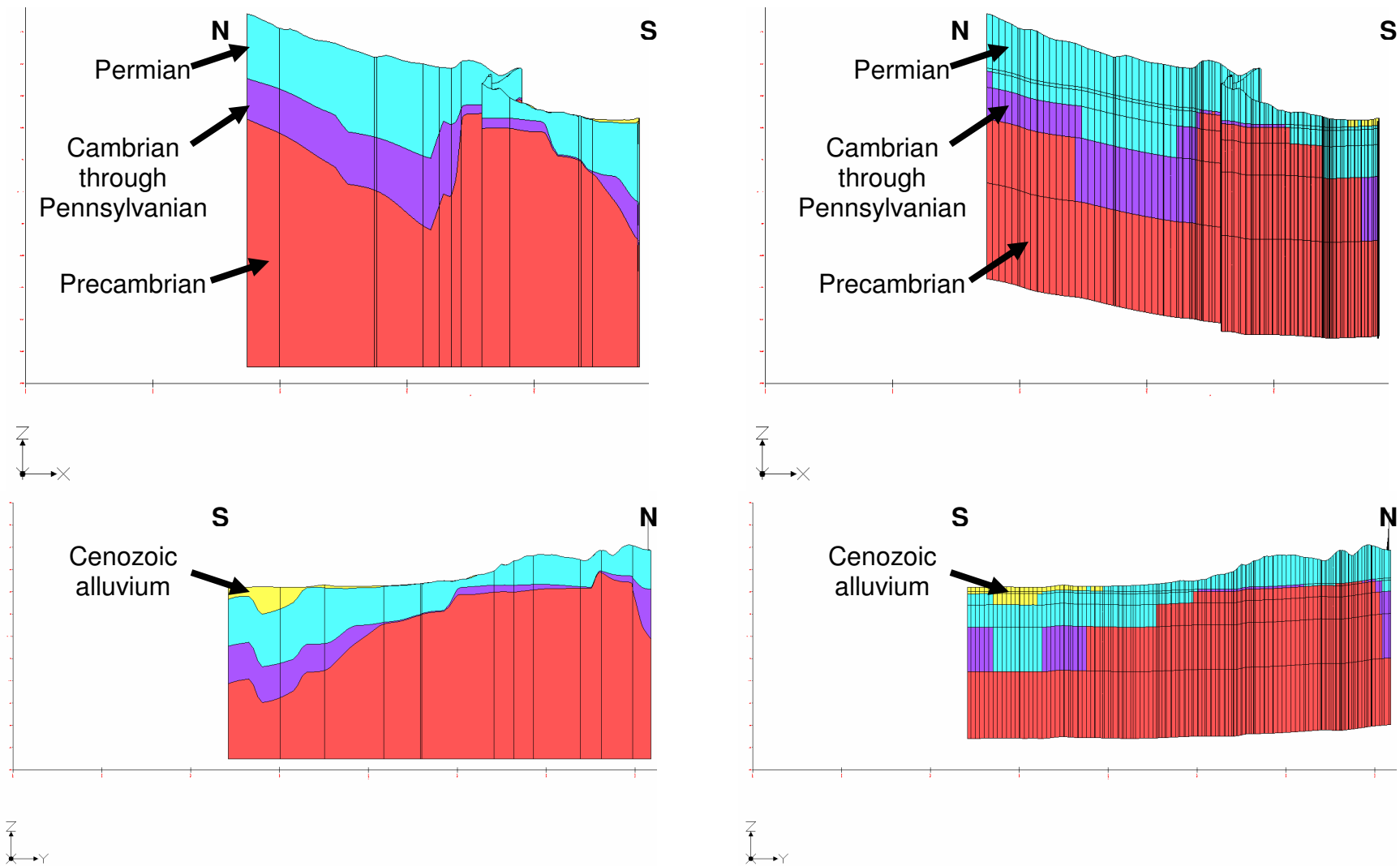
Figure A-4.8: Side views along cross-section A - A' of the simplified solid model on left and groundwater flow model on right. Vertical exaggeration 10×.
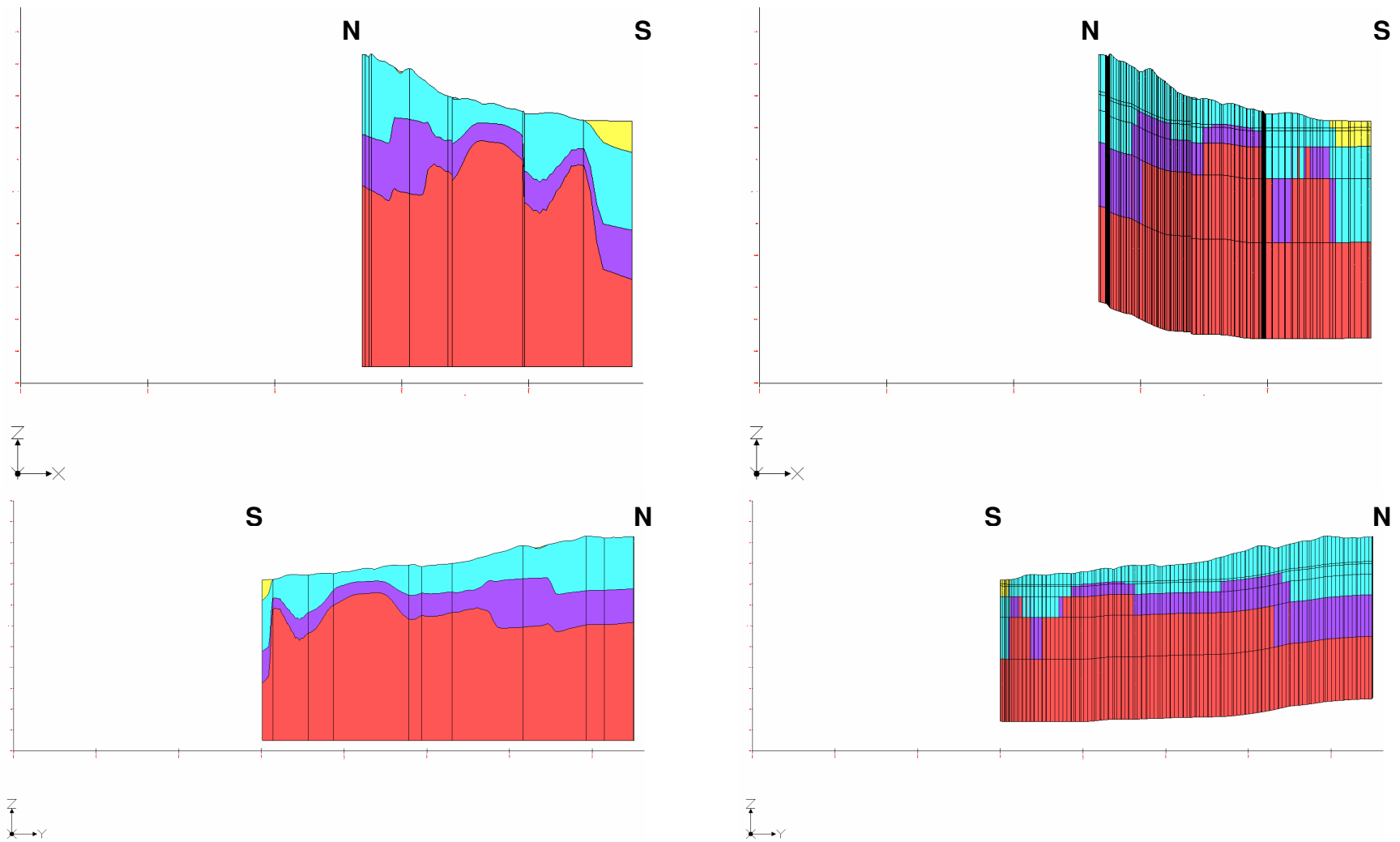
Figure A-4.9: Side views along cross-section B - B' of the simplified solid model on left and groundwater flow model on right. Vertical exaggeration 10×.
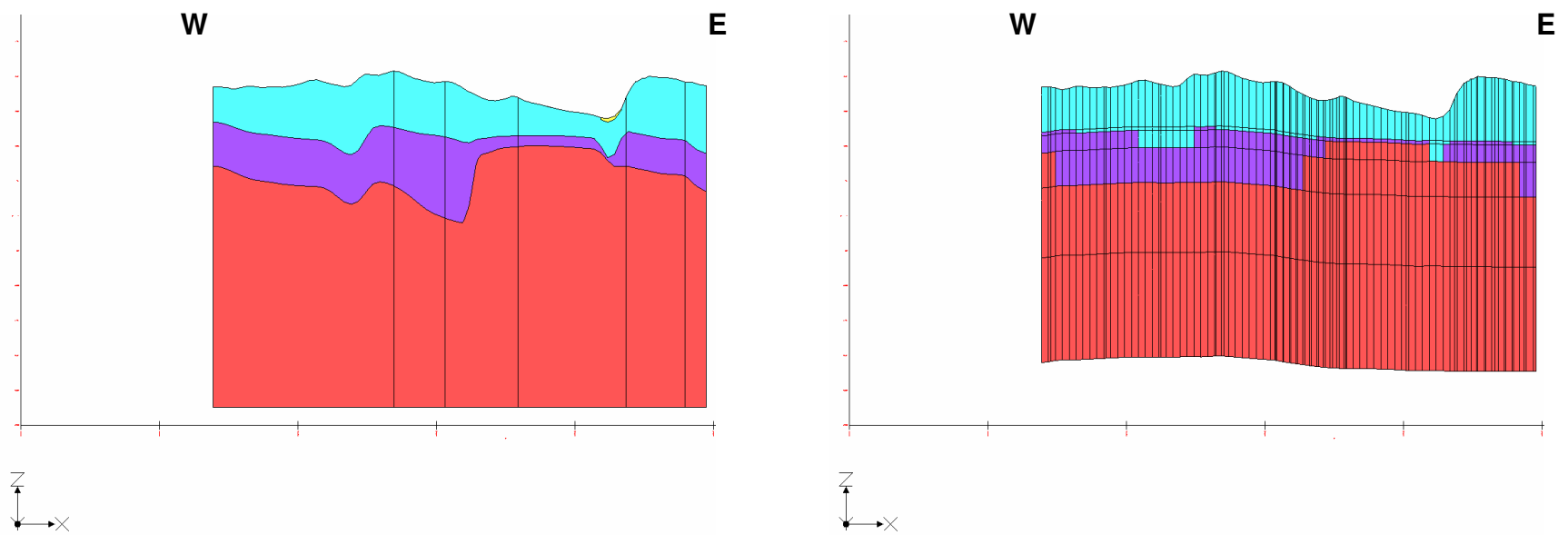
Figure A-4.10: Side view along cross-section C - C' of the simplified solid model on left and groundwater flow model on right. Vertical exaggeration 10×.
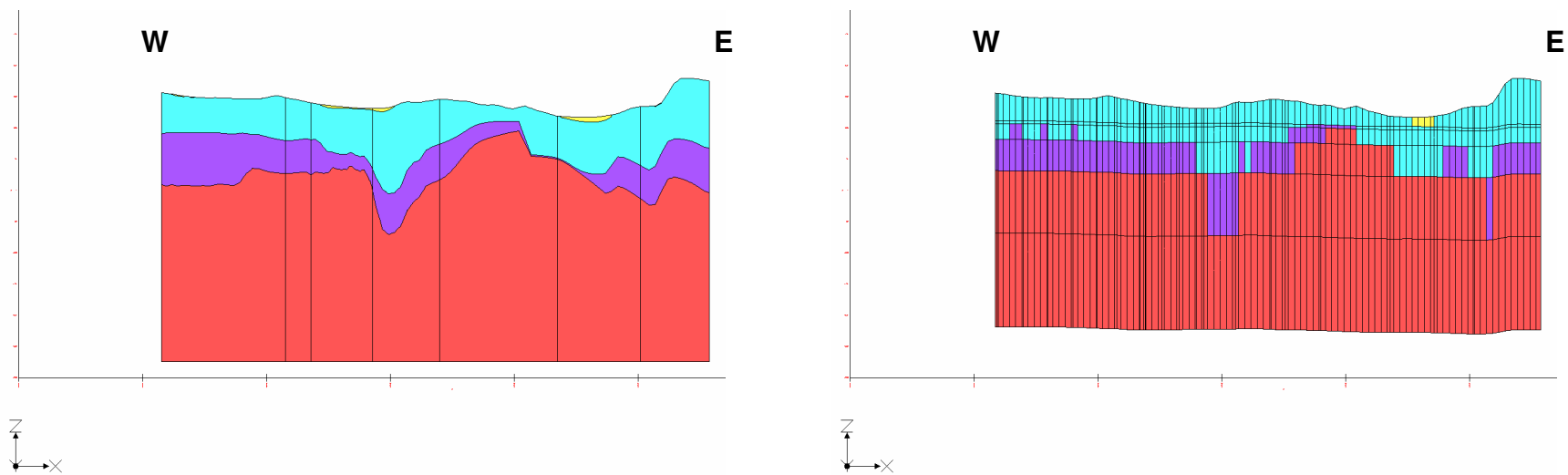
Figure A-4.11: Side view along cross-section D - D' of the simplified solid model on left and groundwater flow model on right. Vertical exaggeration 10×.
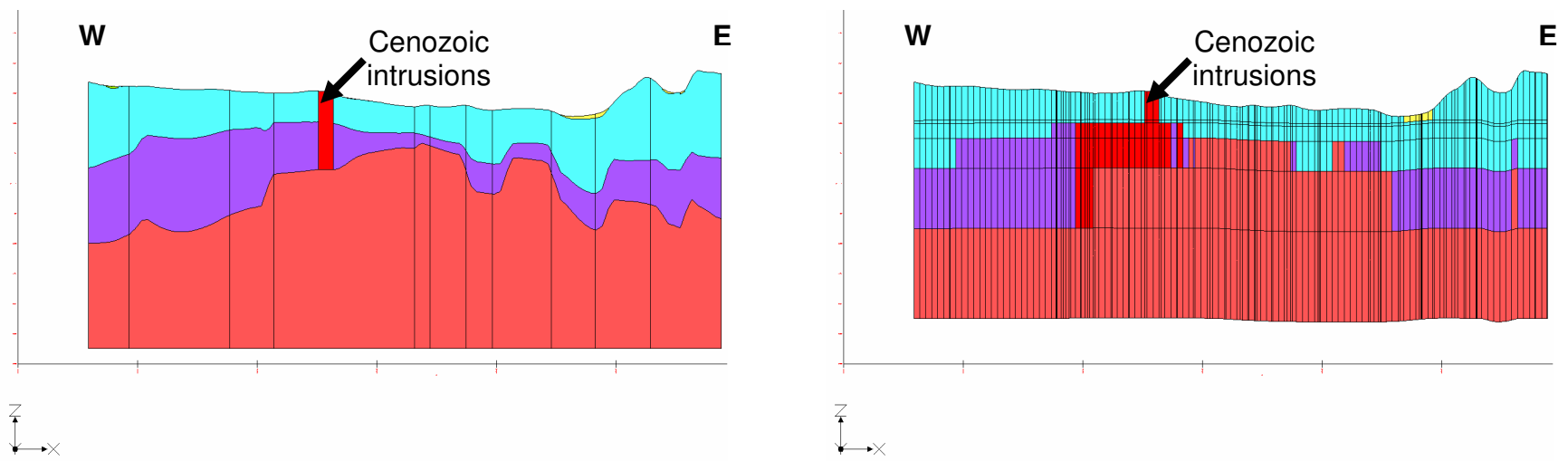
Figure A-4.12: Side view along cross-section E - E' of the simplified solid model on left and groundwater flow model on right. Vertical exaggeration 10×.
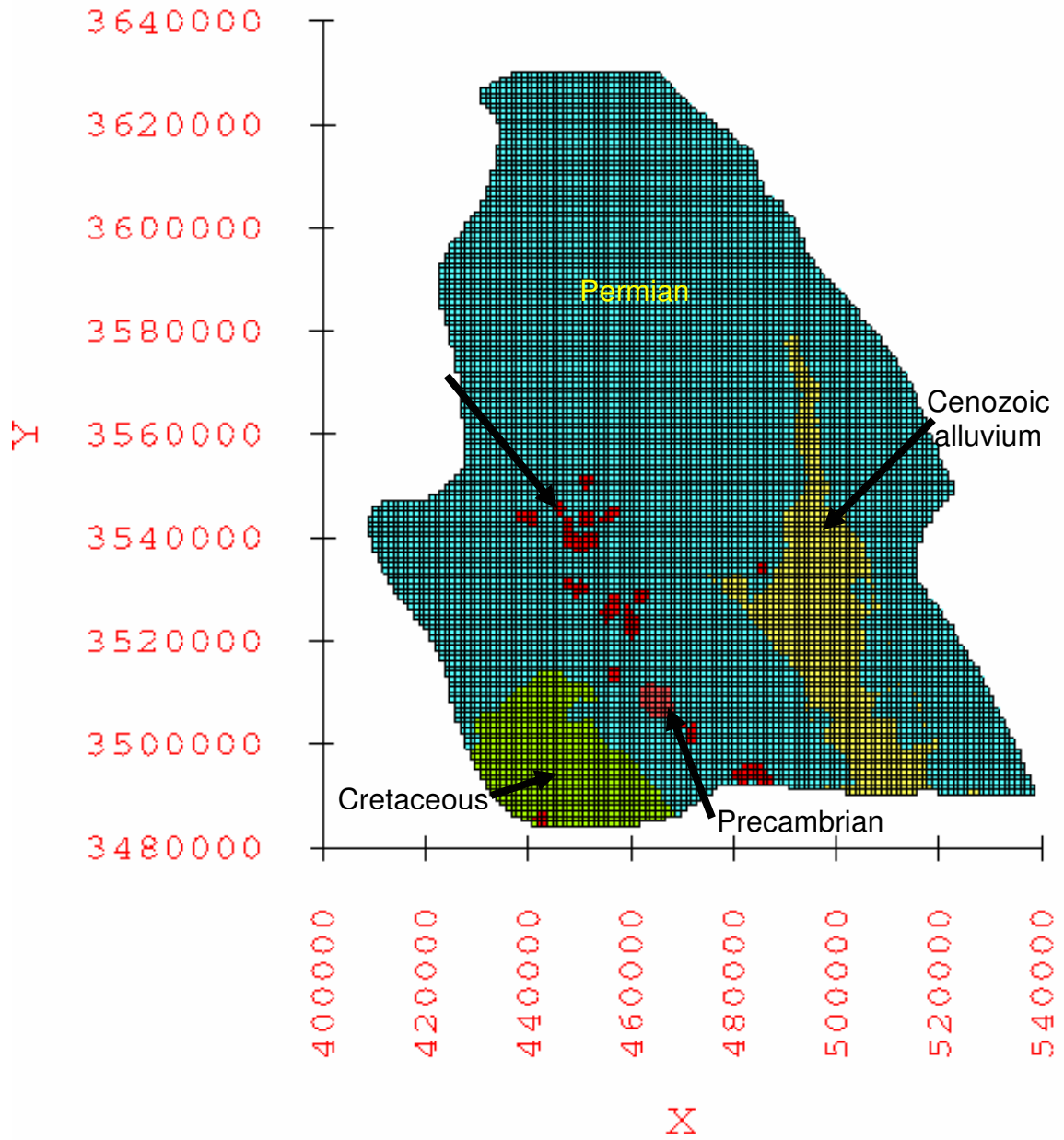
Figure A-4.13: Distribution of hydrogeologic units within layer 1 of the groundwater flow model grid.
Axes scale is in UTM NAD83 Zone 13 North coordinates.
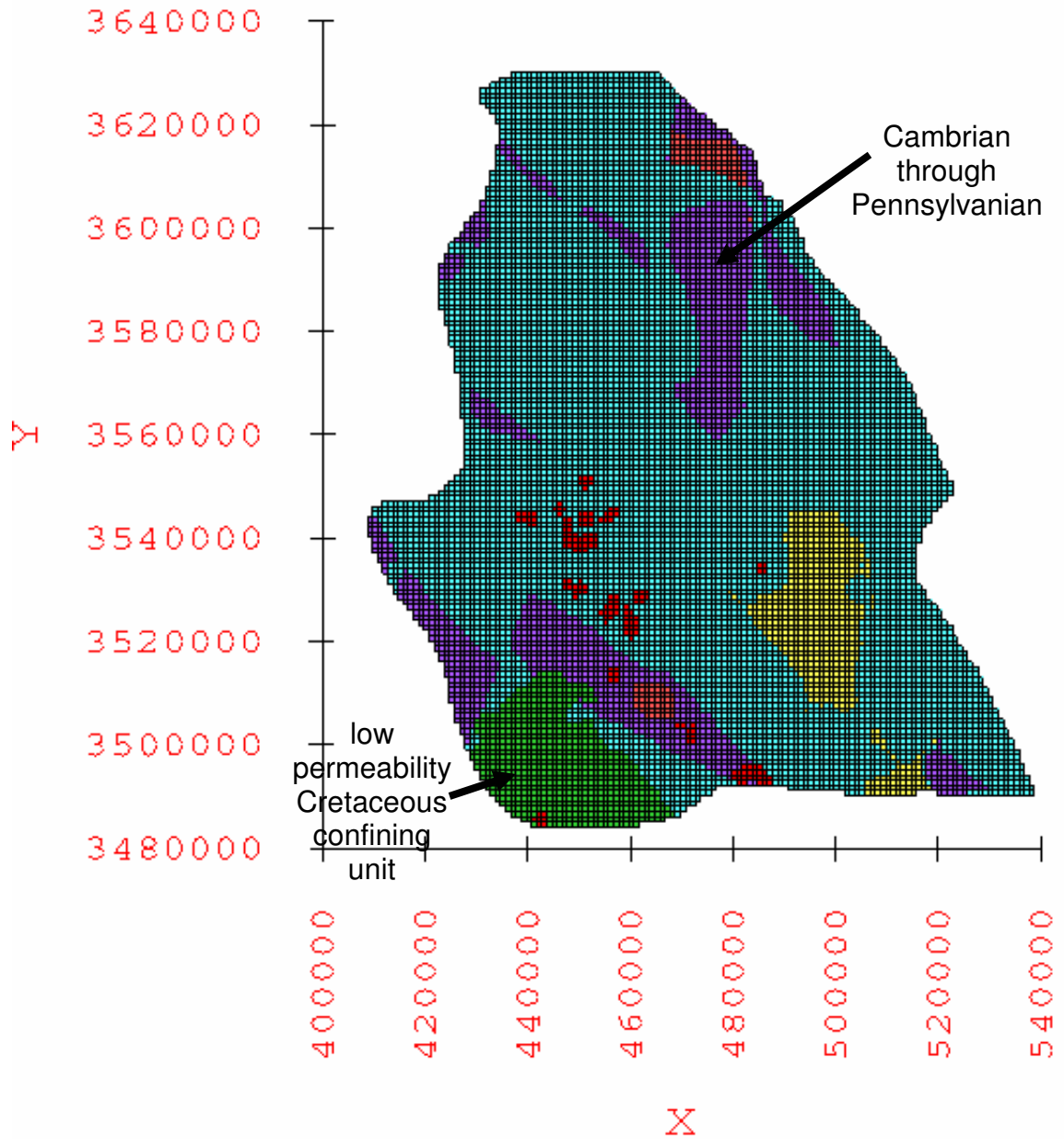
Figure A-4.14: Distribution of hydrogeologic units within layer 2 of the groundwater flow model grid.
Axes scale is in UTM NAD83 Zone 13 North coordinates.

591
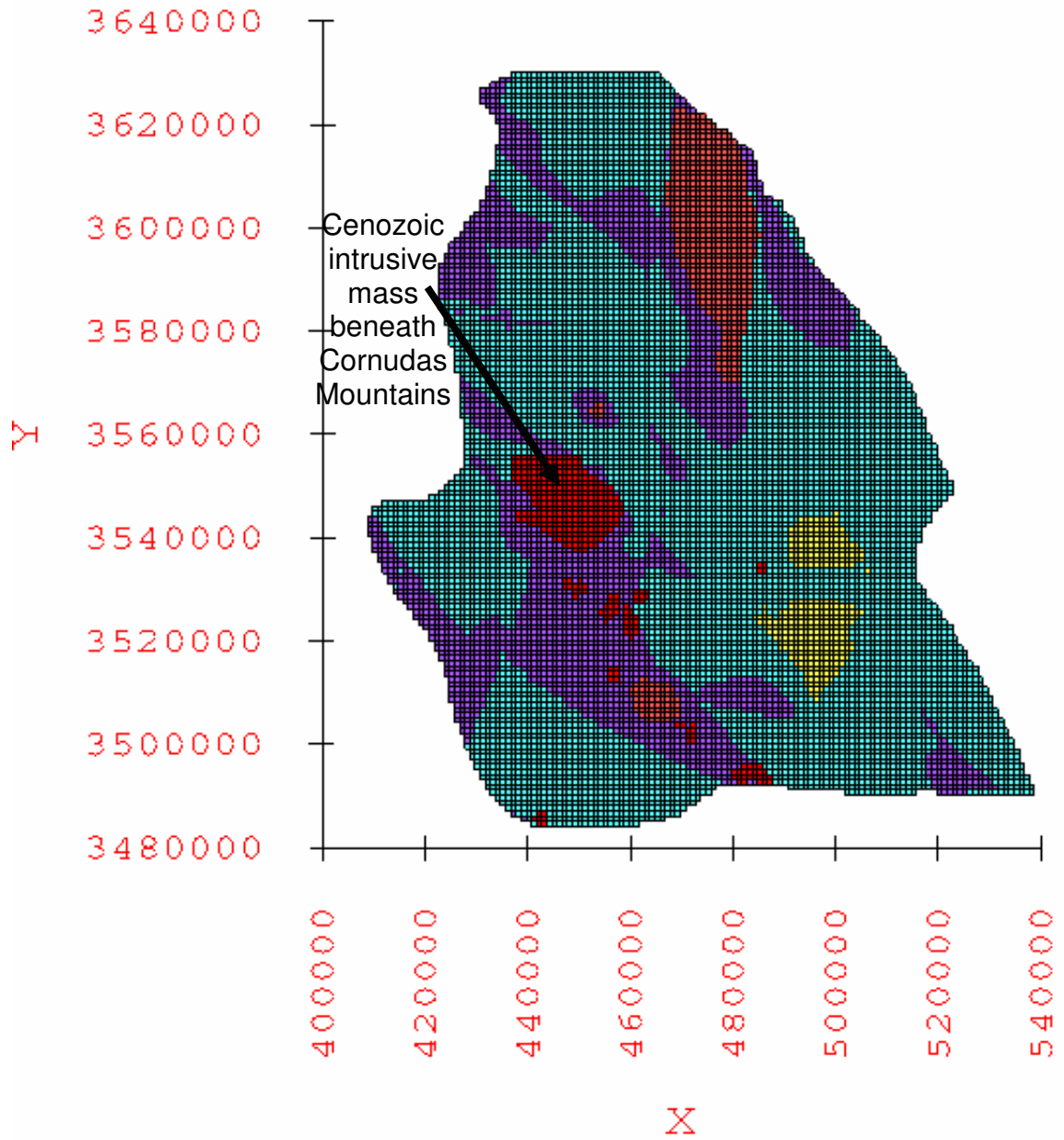
Figure A-4.15: Distribution of hydrogeologic units within layer 3 of the groundwater flow model grid.
Axes scale is in UTM NAD83 Zone 13 North coordinates.

592
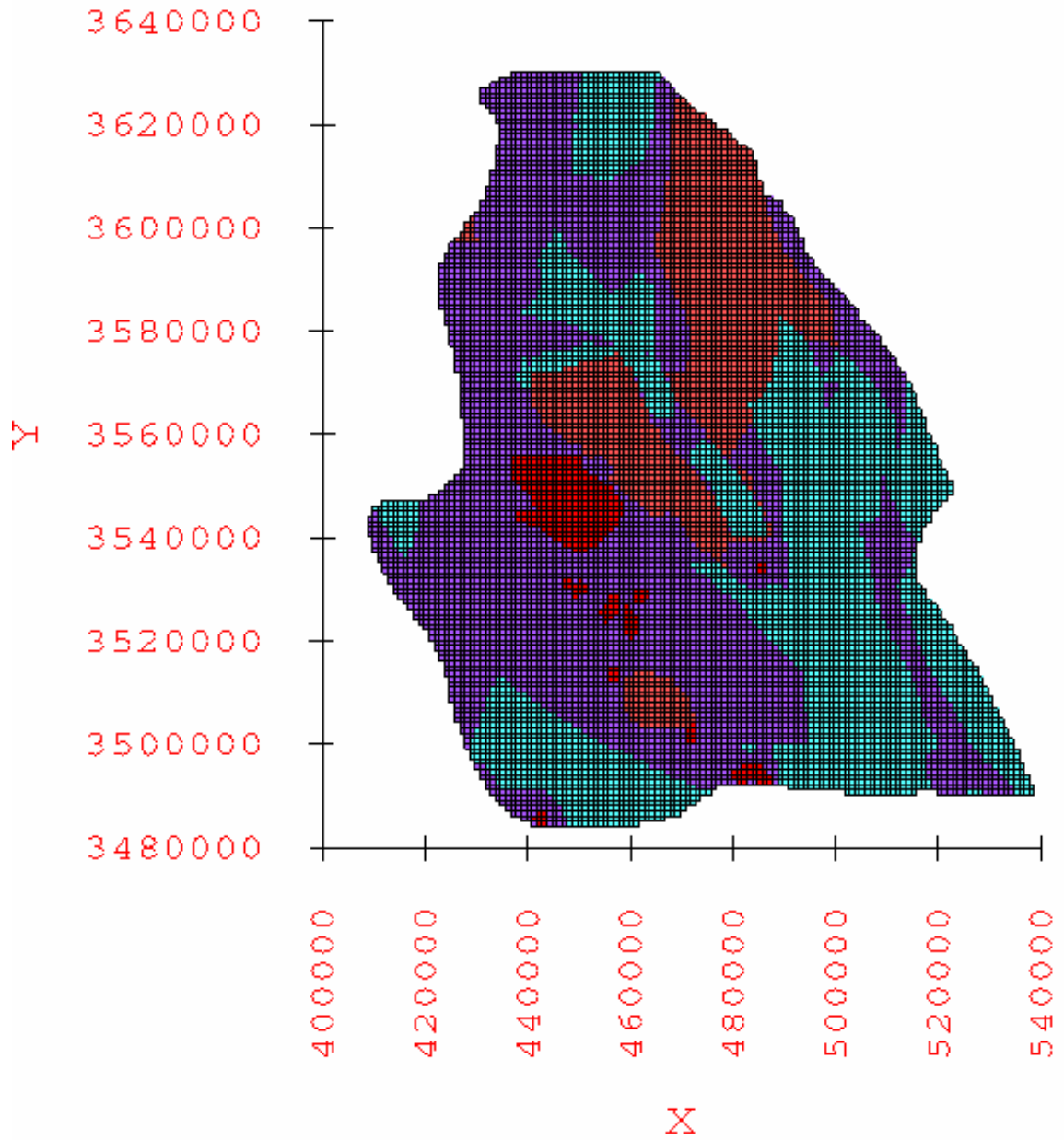
Figure A-4.16: Distribution of hydrogeologic units within layer 4 of the groundwater flow model grid.
Axes scale is in UTM NAD83 Zone 13 North coordinates.
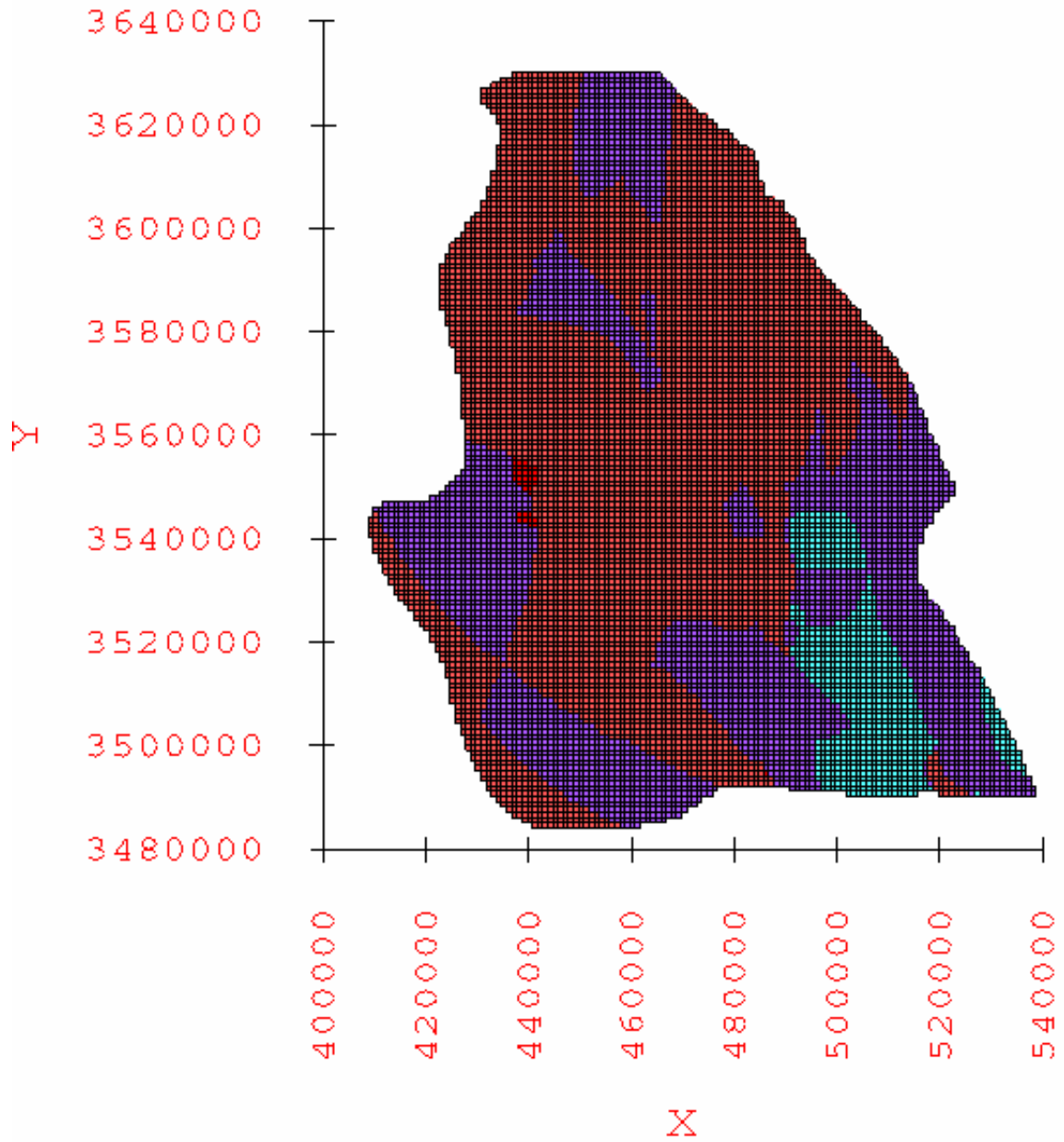
Figure A-4.17: Distribution of hydrogeologic units within layer 5 of the groundwater flow model grid.
Axes scale is in UTM NAD83 Zone 13 North coordinates.
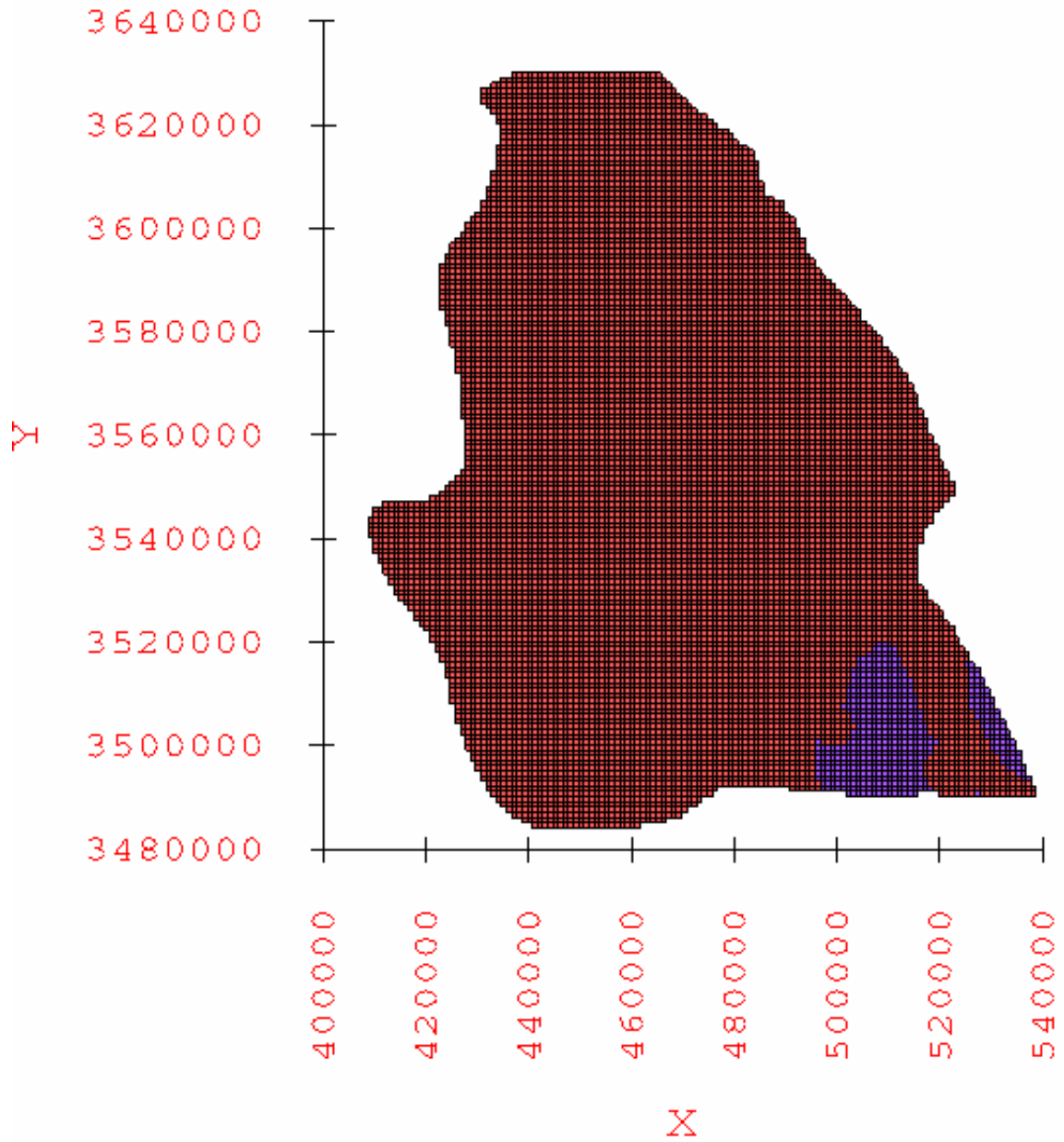
Figure A-4.18: Distribution of hydrogeologic units within layer 6 of the groundwater flow model grid.

Axes scale is in UTM NAD83 Zone 13 North coordinates.
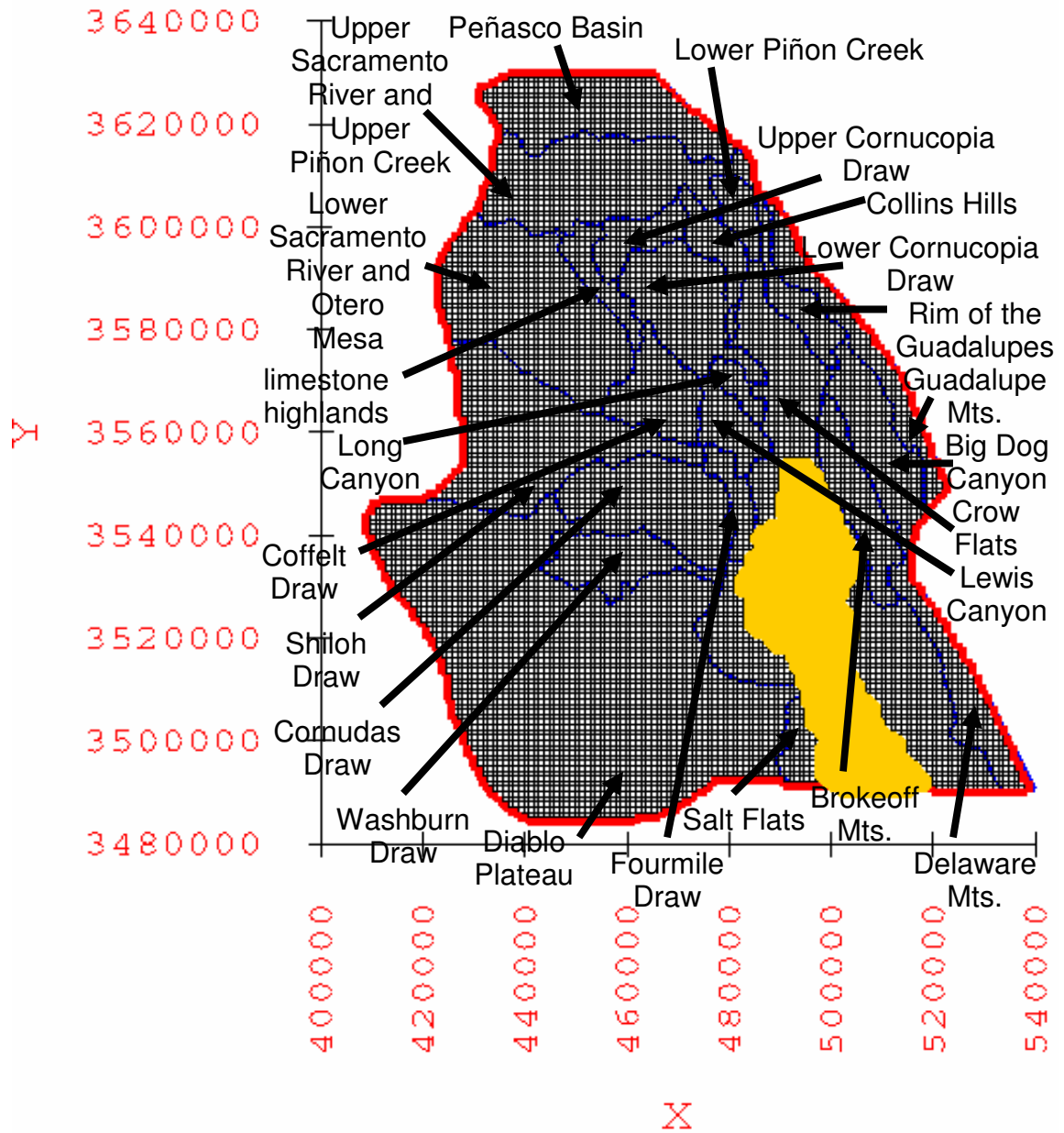
Figure A-4.19: Groundwater flow model domain, plan view of model grid, recharge zones derived from sub-basins delineated by JSAI (2010), and discharge zone at Salt Flats playa.

Axes scale is in UTM NAD83 Zone 13 North coordinates. Red line along perimeter of model domain designates no-flow boundary. Areas enclosed by blue lines indicate recharge zones. Grid cells highlighted with yellow specify discharge zone.
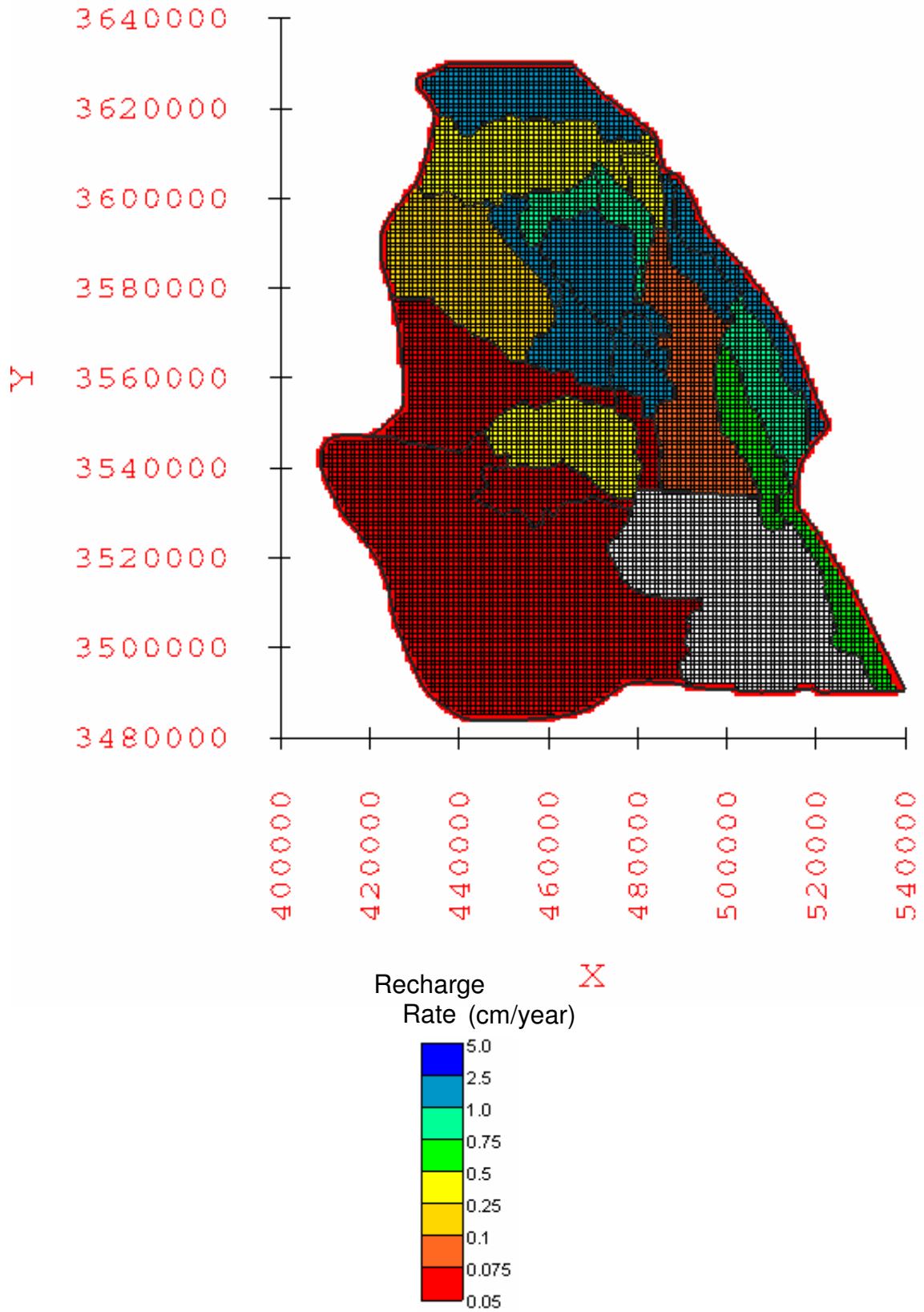
Figure A-4.20: Water-balance based minimum recharge rates applied to the sub-basins within the groundwater flow model domain.
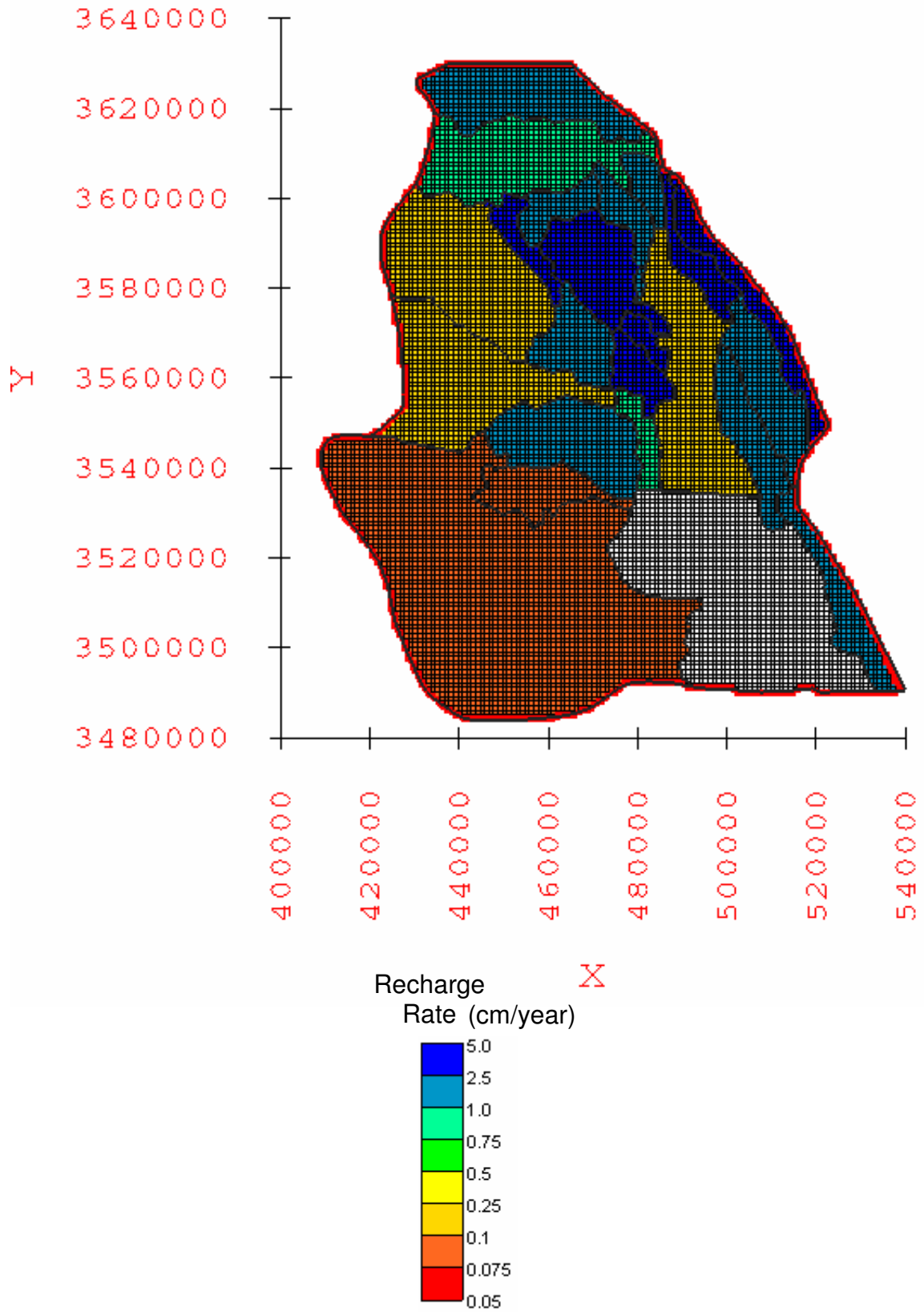
Figure A-4.21: Water-balance based average recharge rates applied to the sub-basins within the groundwater flow model domain.
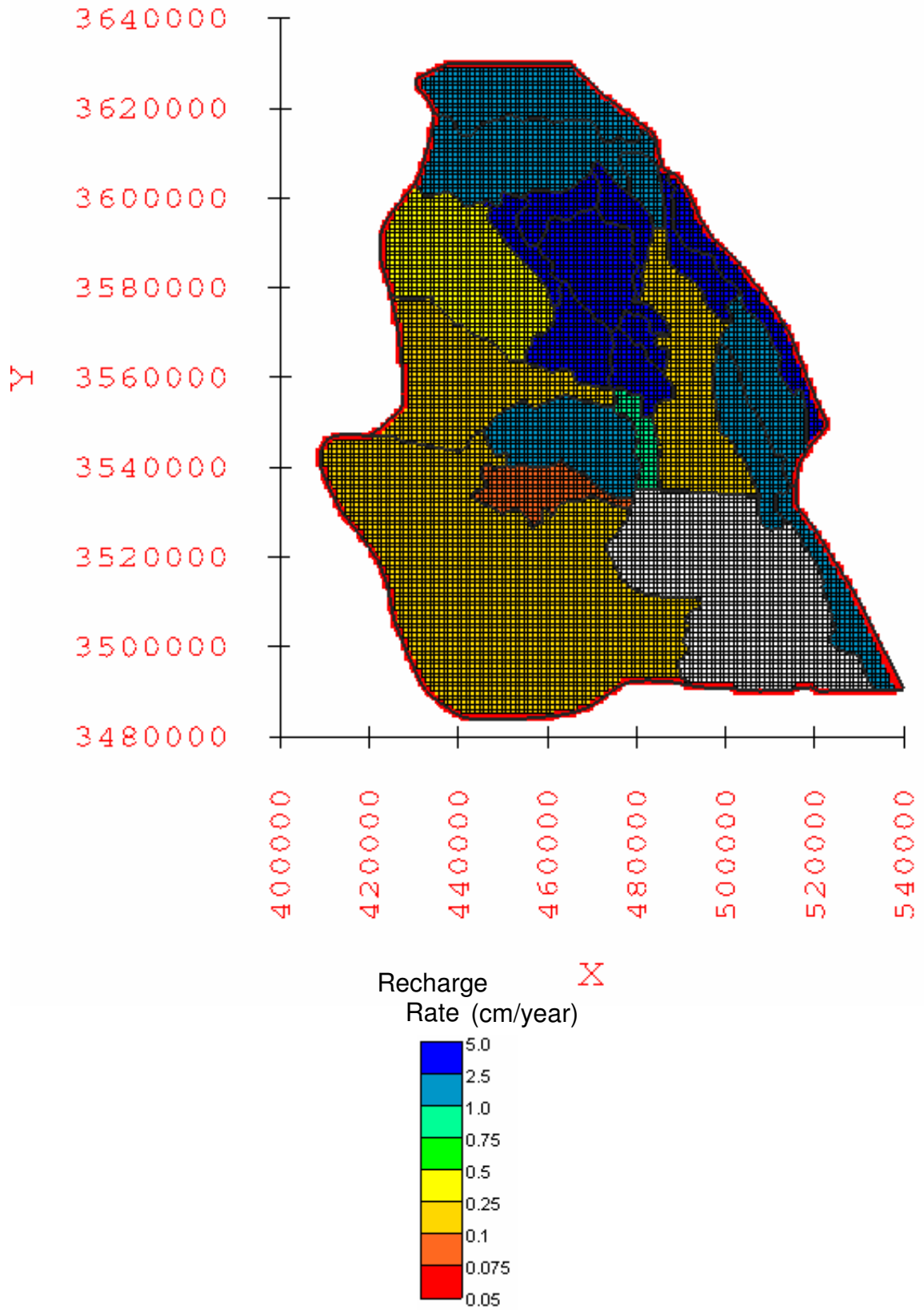
Figure A-4.22: Water-balance based maximum recharge rates applied to the sub-basins within the groundwater flow model domain.
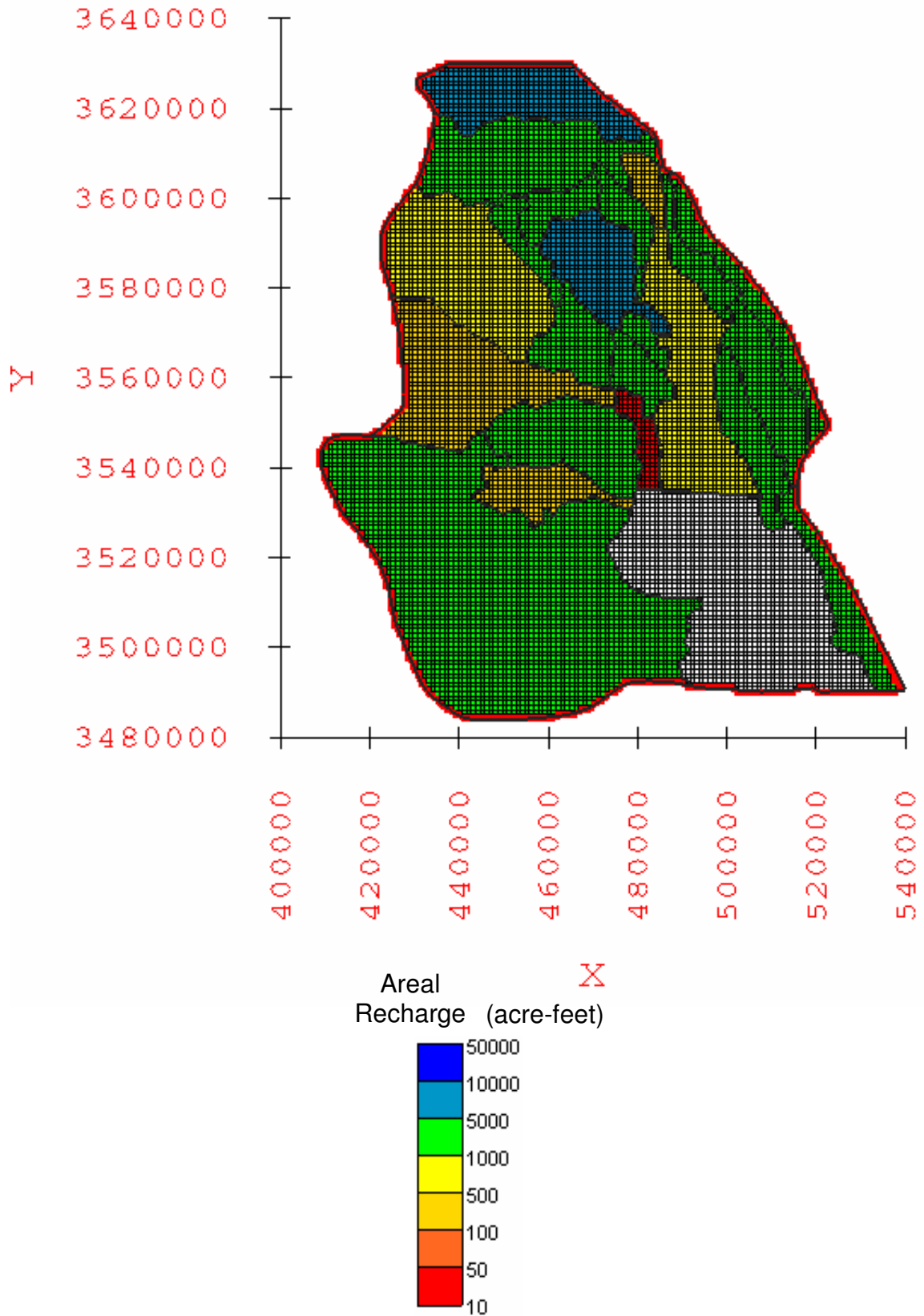
Figure A-4.23: Water-balance based minimum areal recharge applied to the sub-basins within the groundwater flow model domain.
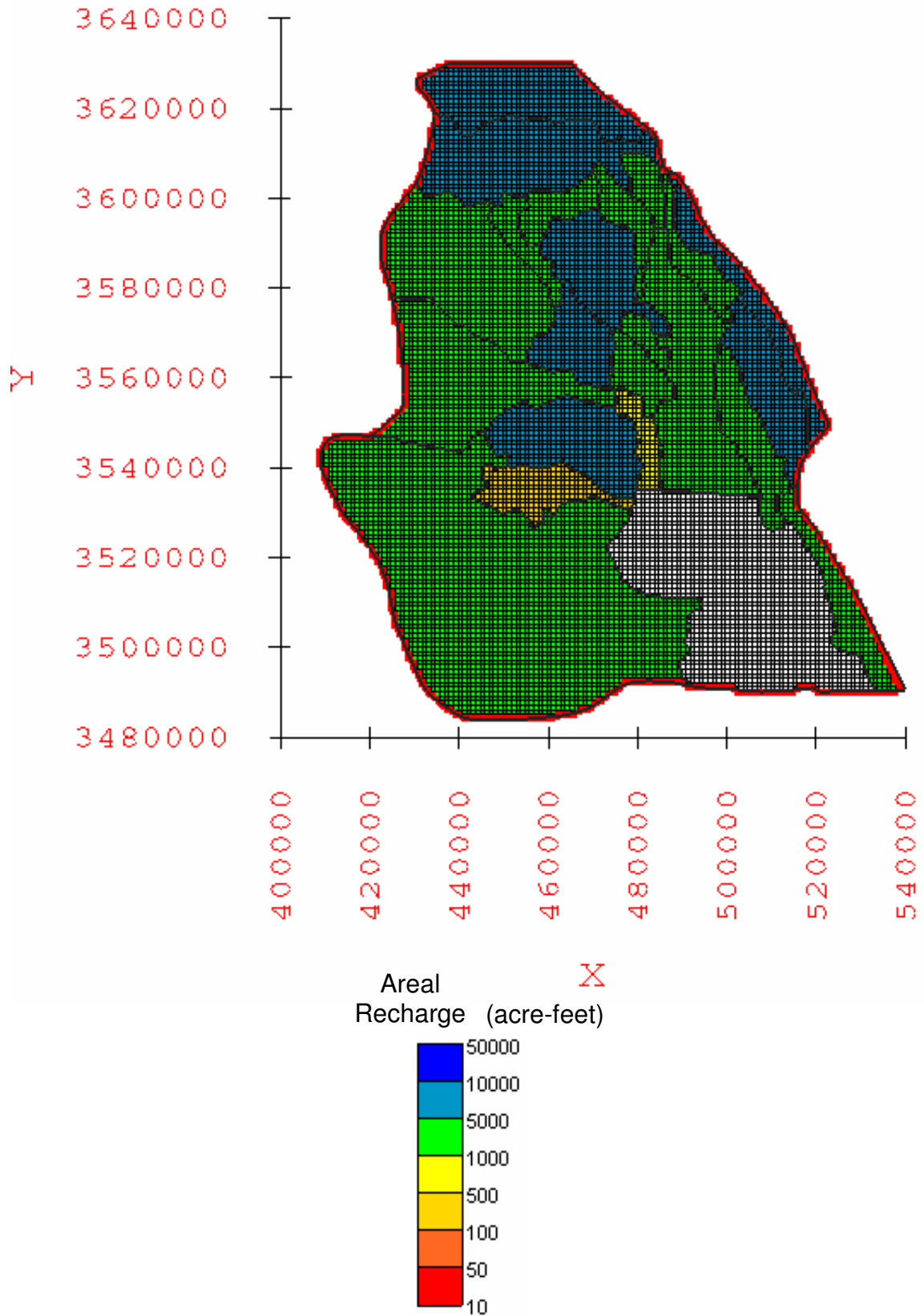
Figure A-4.24: Water-balance based average areal recharge applied to the sub-basins within the groundwater flow model domain.
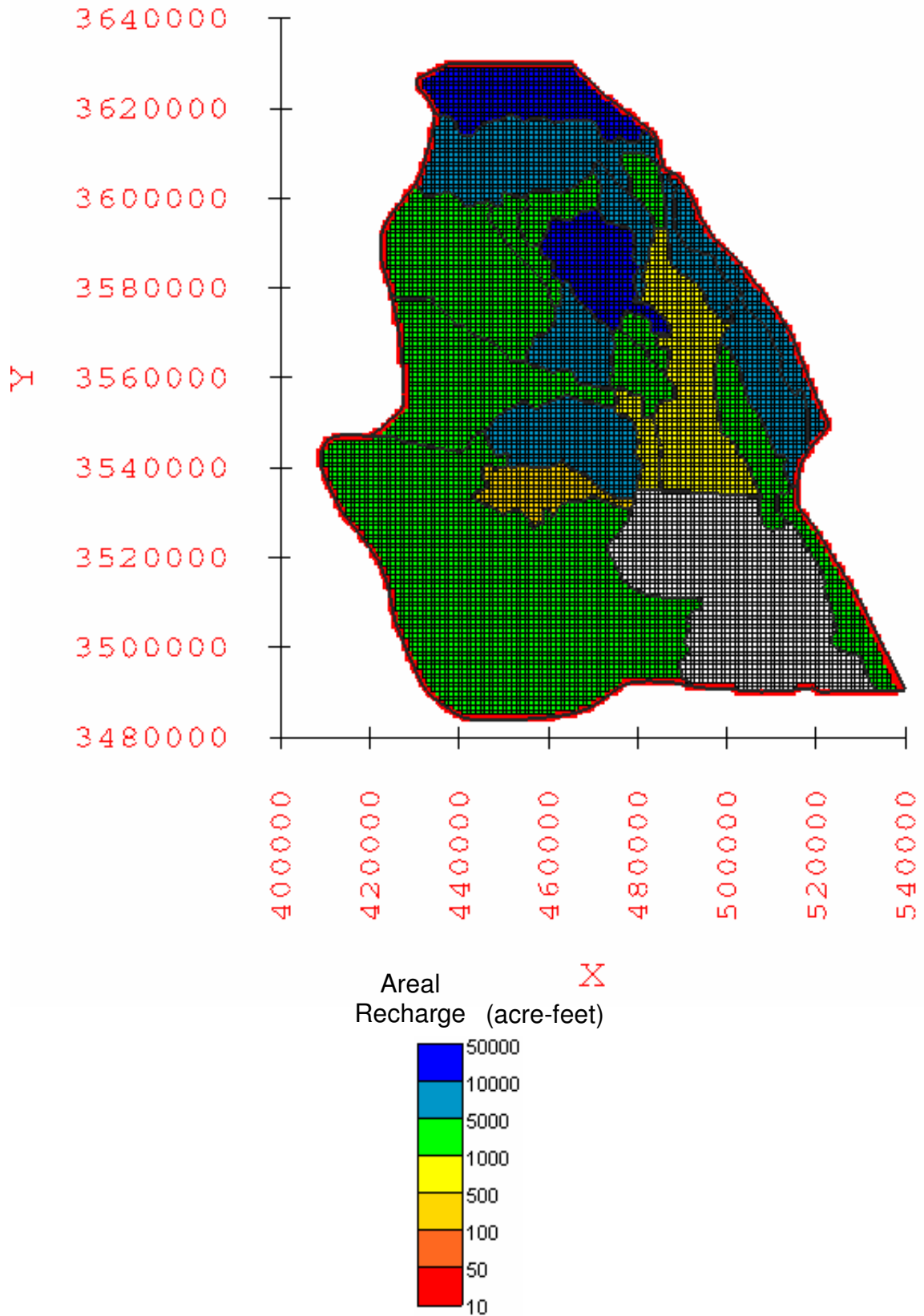
Figure A-4.25: Water-balance based maximum areal recharge applied to the sub-basins within the groundwater flow model domain.
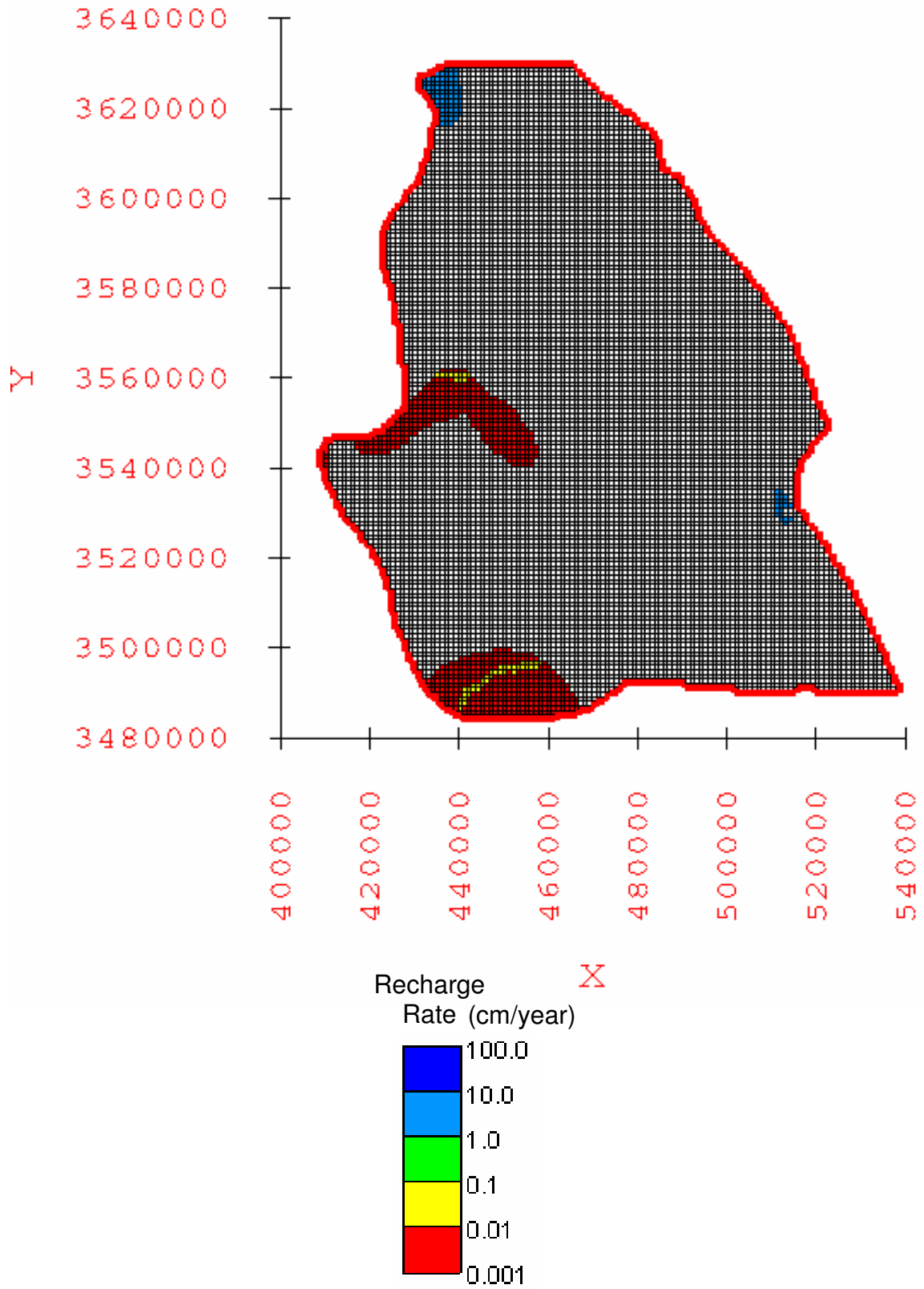
Figure A-4.26: Elevation-dependent minimum recharge rates applied to the recharge zones within the groundwater flow model domain.
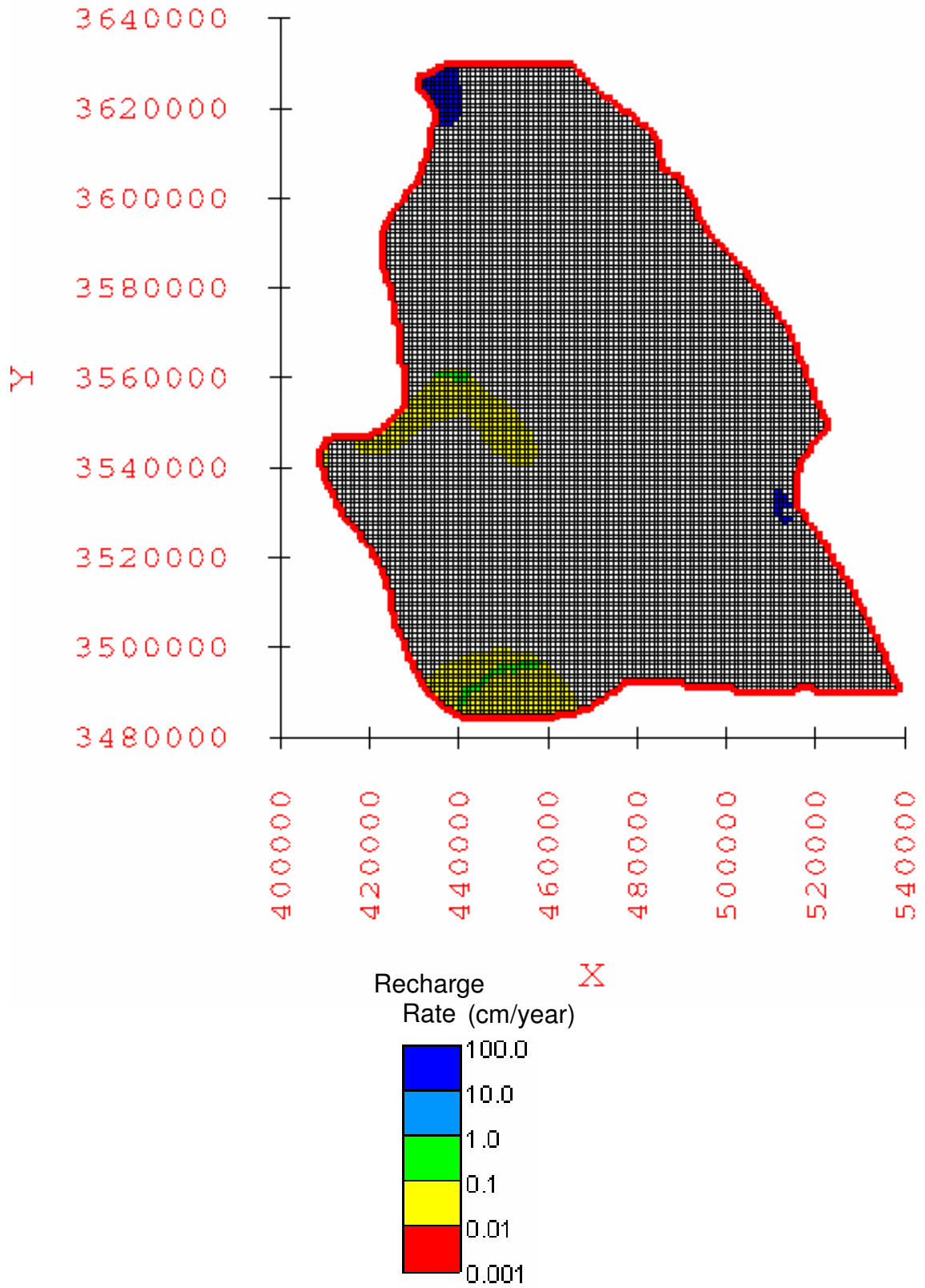
Figure A-4.27: Elevation-dependent average recharge rates applied to the recharge zones within the groundwater flow model domain.
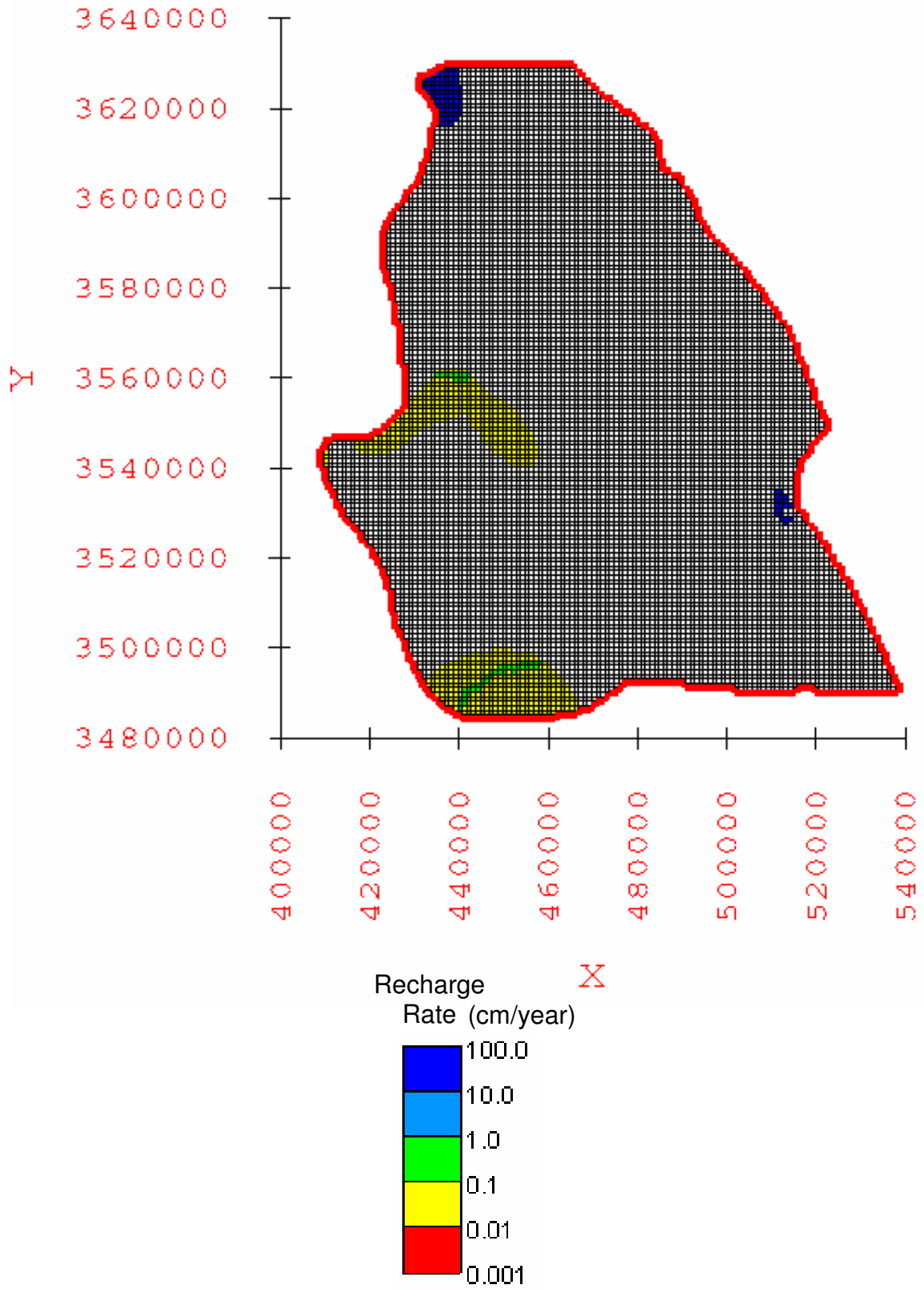
Figure A-4.28: Elevation-dependent maximum recharge rates applied to the recharge zones within the groundwater flow model domain.
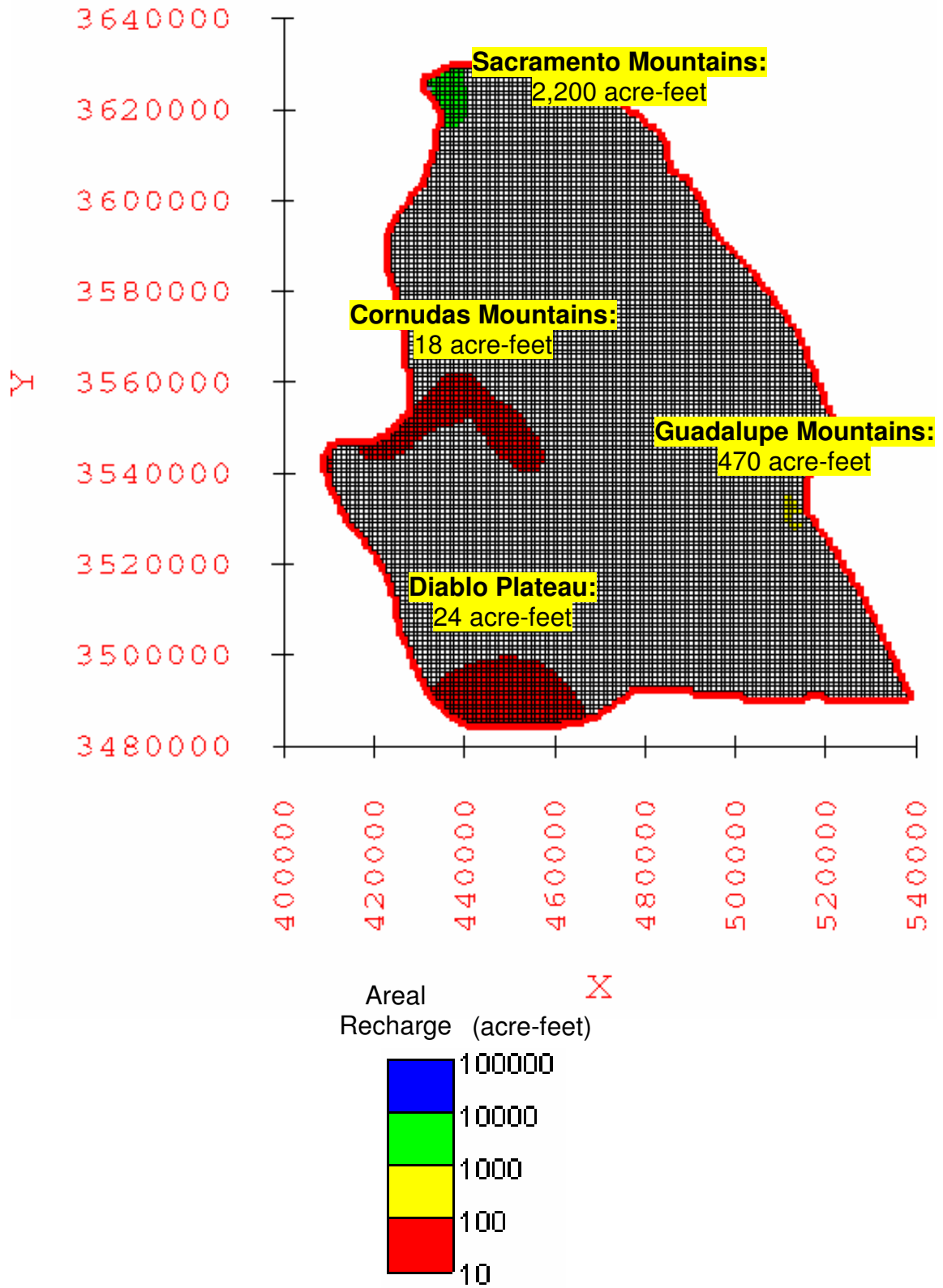
Figure A-4.29: Elevation-dependent minimum areal recharge applied to the recharge zones within the groundwater flow model domain.
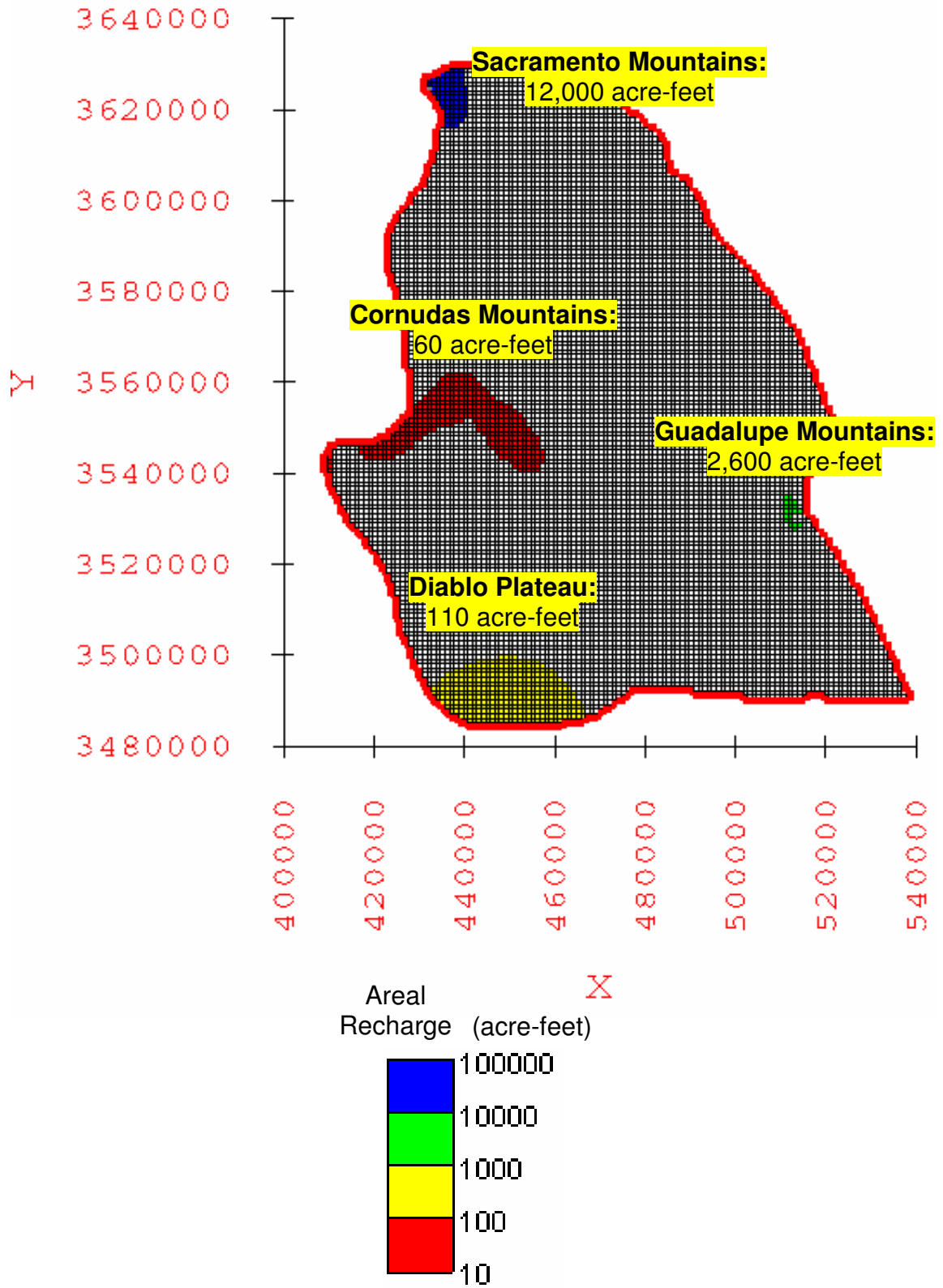
Figure A-4.30: Elevation-dependent average areal recharge applied to the recharge zones within the groundwater flow model domain.
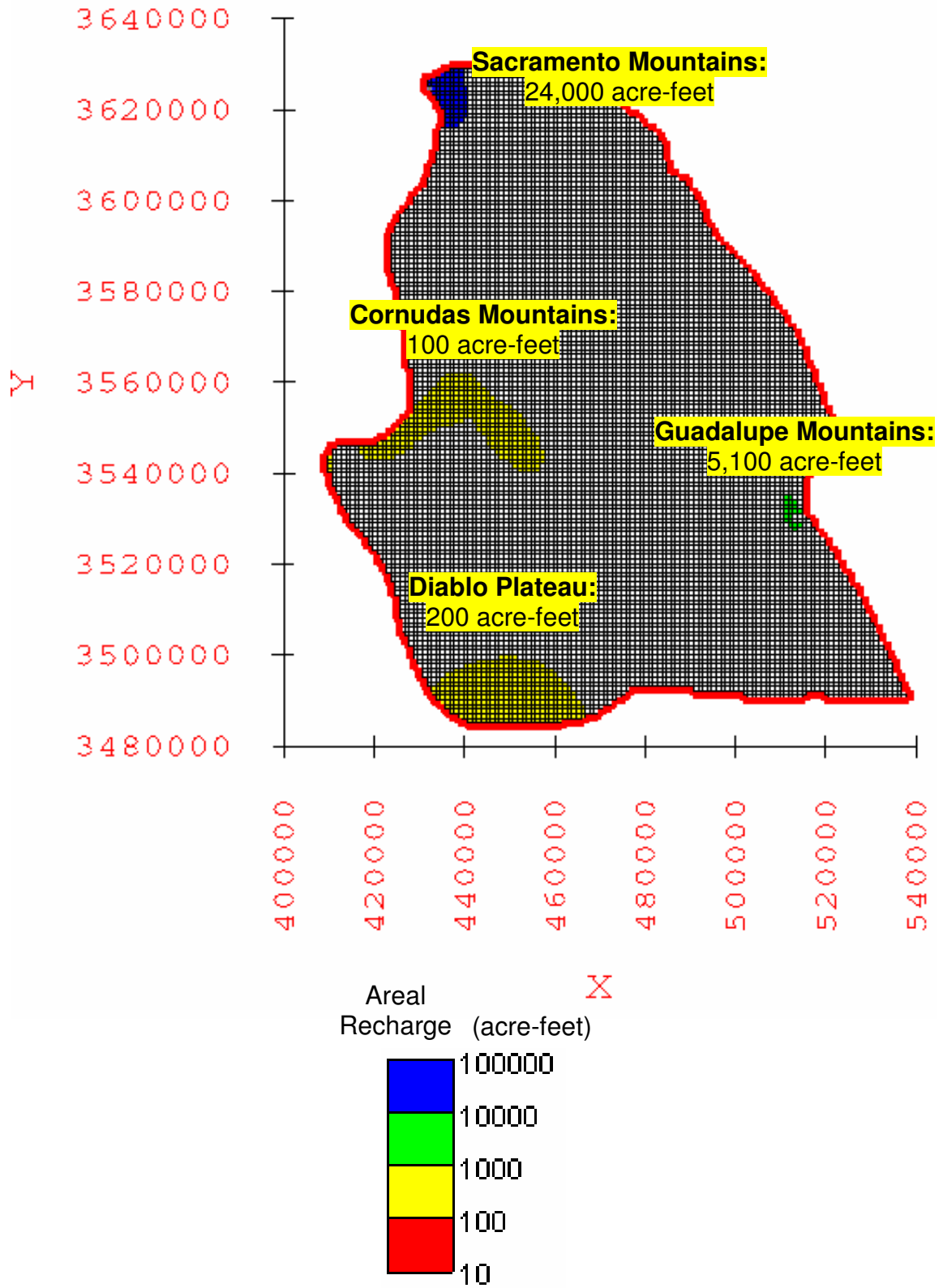
Figure A-4.31: Elevation-dependent maximum areal recharge applied to the recharge zones within the groundwater flow model domain.
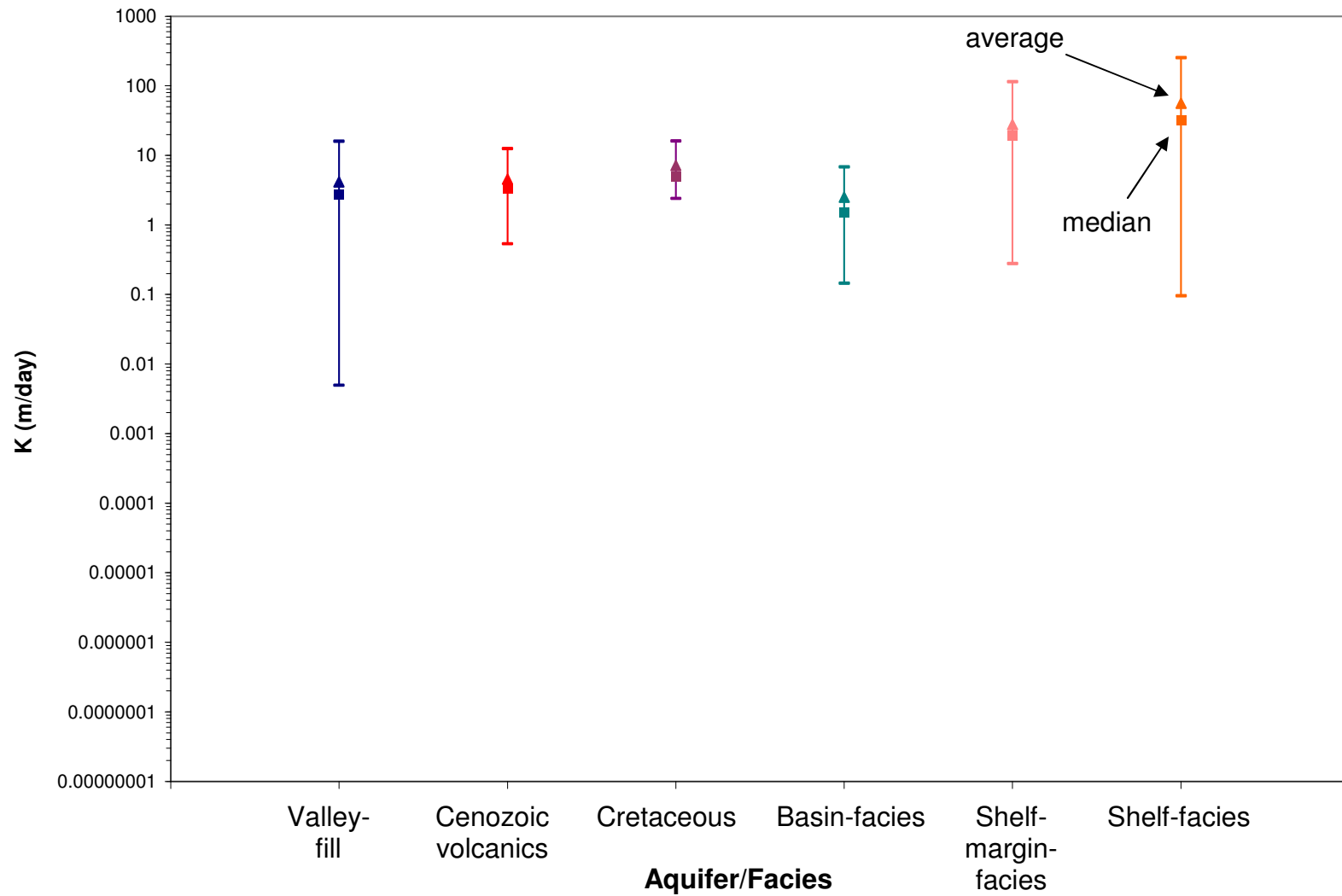
Figure A-4.32: Range of hydraulic conductivity [K] values calculated from transmissivity [T].
Vertical axis is logarithmic scale. Squares indicate median values, and triangles indicate average values.

609
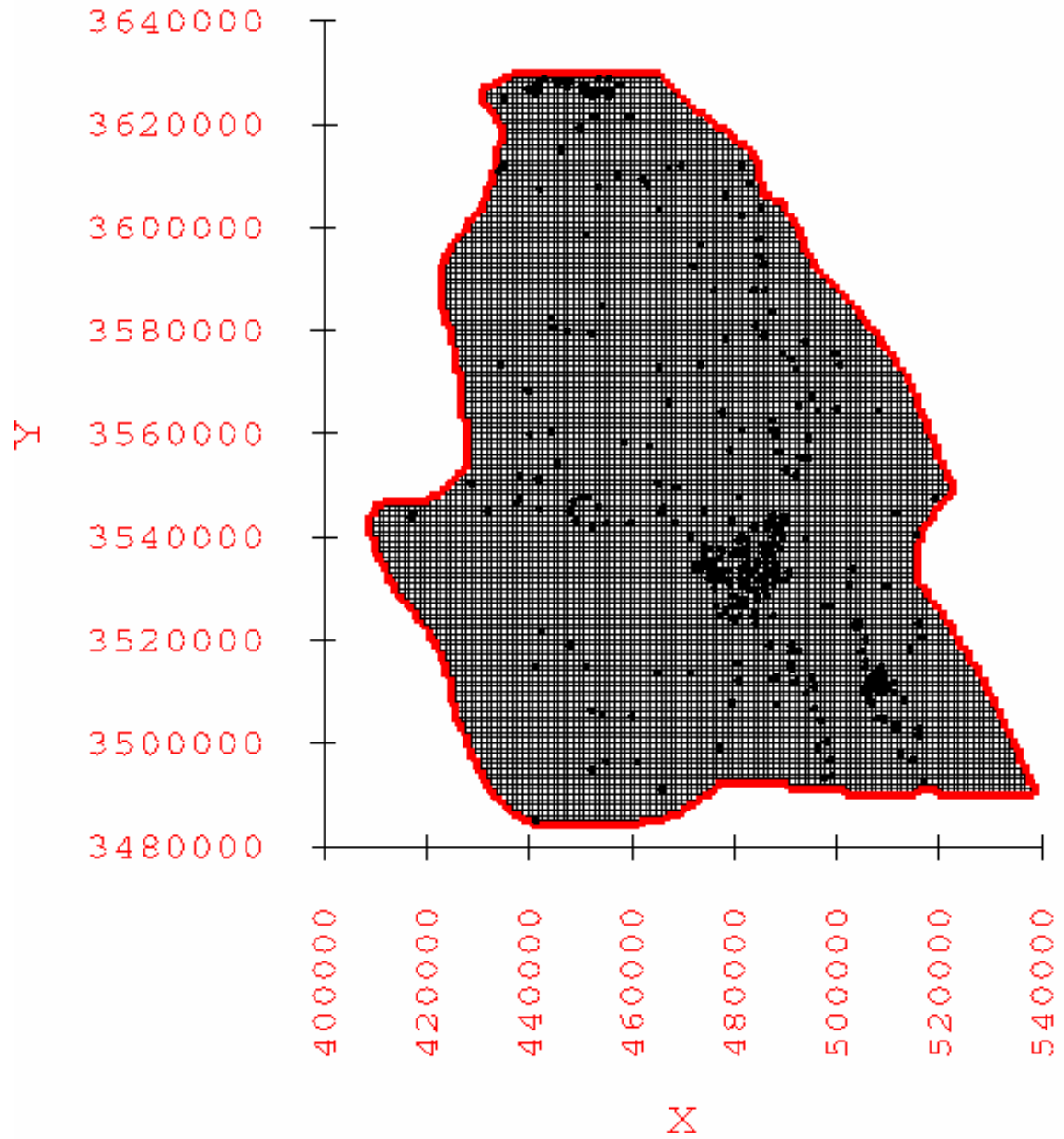
Figure A-4.33: Calibration targets within the groundwater flow model domain.
Axes scale is in UTM NAD83 Zone 13 North coordinates.
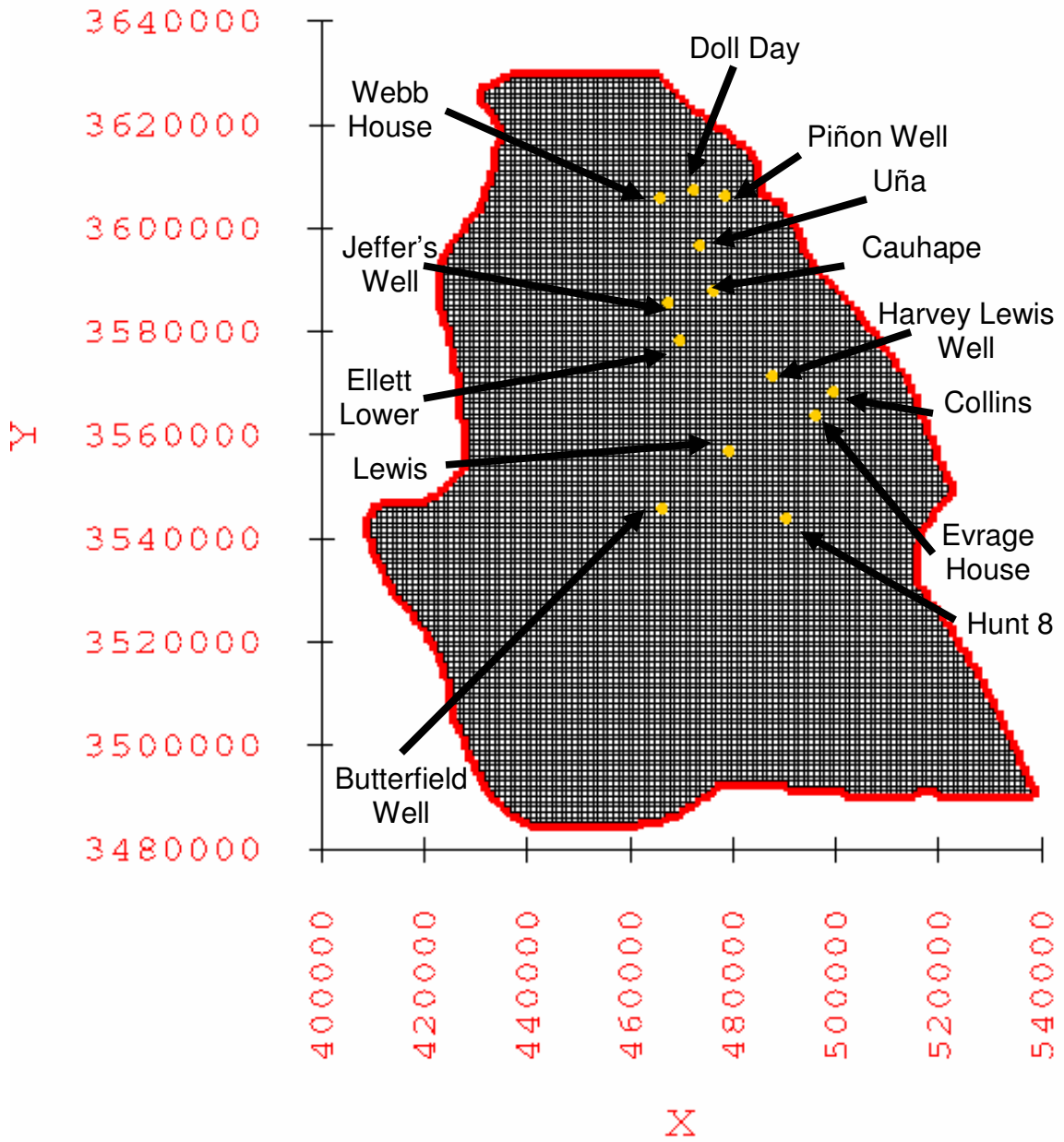
Figure A-4.34: Location of the groundwater age wells within the MODFLOW model domain.
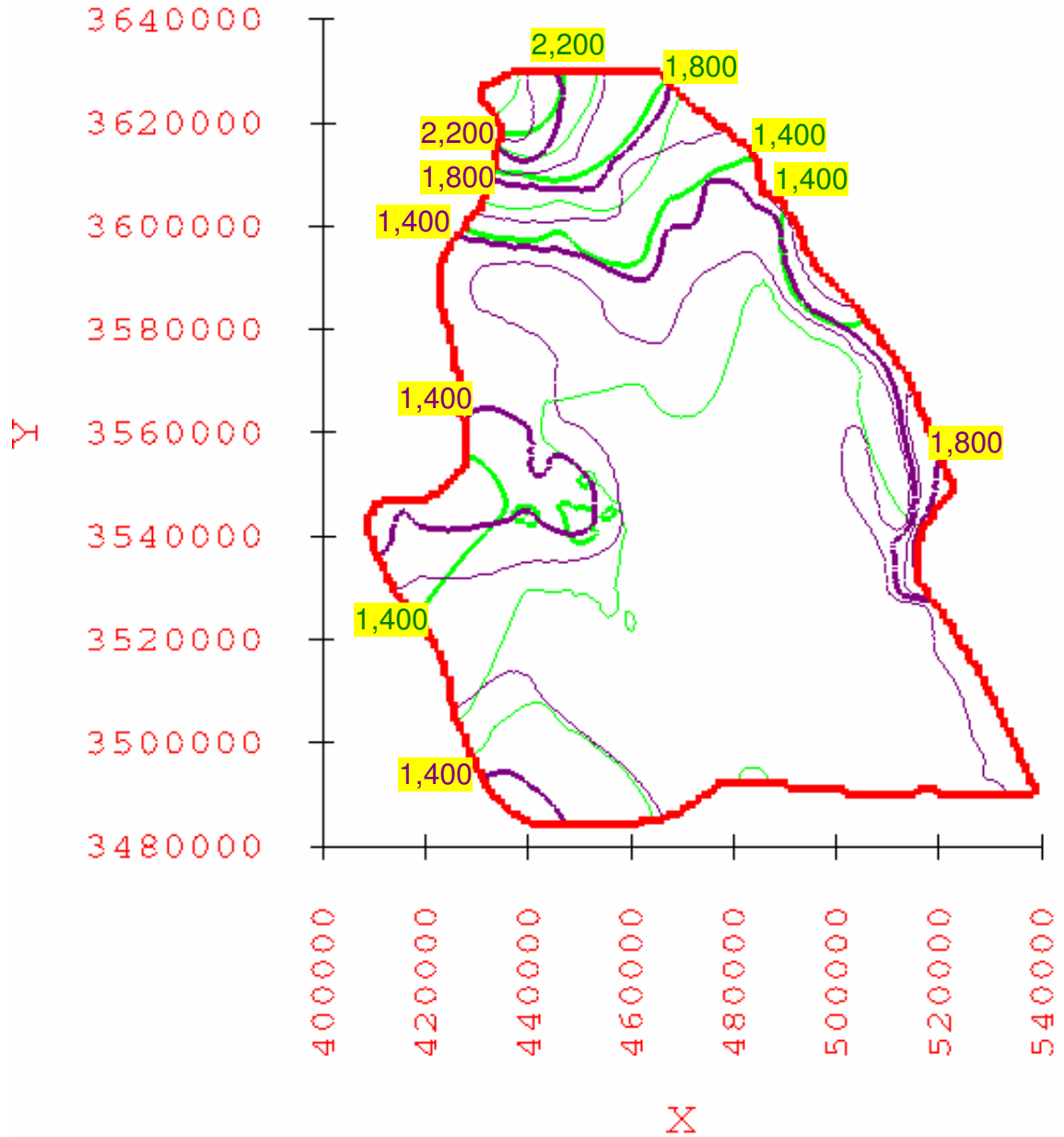
Figure A-4.35: Comparison of the computed hydraulic head in layer 1 for the calibrated water-balance based minimum recharge scenario model and the observed groundwater surface.

Green lines are the model computed head contours. Purple dashed lines are the observed groundwater surface contours. Contour elevations are in meters above mean sea level. Contour interval is 200 meters.
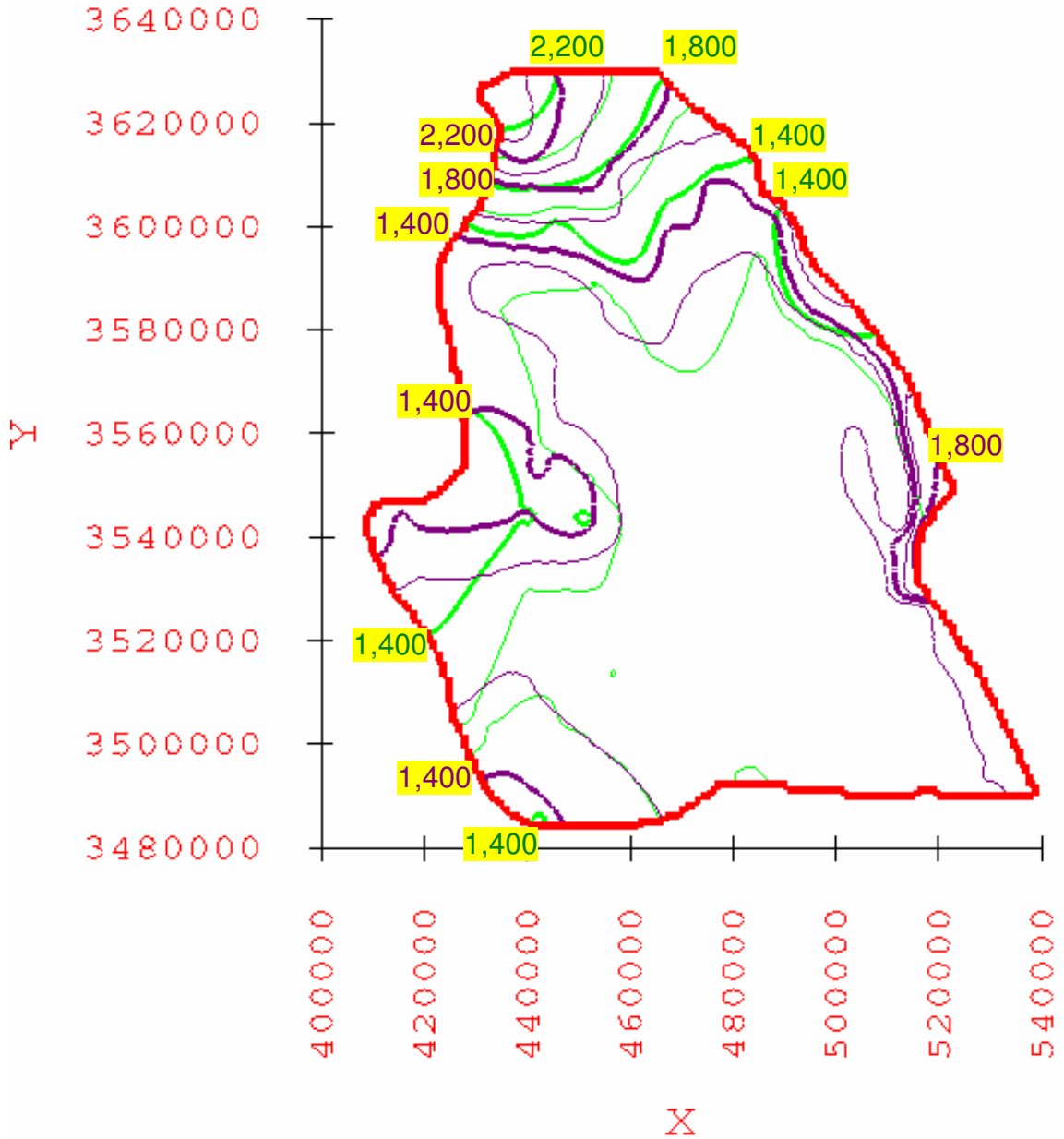
Figure A-4.36: Comparison of the computed hydraulic head in layer 1 for the calibrated water-balance based average recharge scenario model and the observed groundwater surface.

Green lines are the model computed head contours. Purple dashed lines are the observed groundwater surface contours. Contour elevations are in meters above mean sea level. Contour interval is 200 meters.
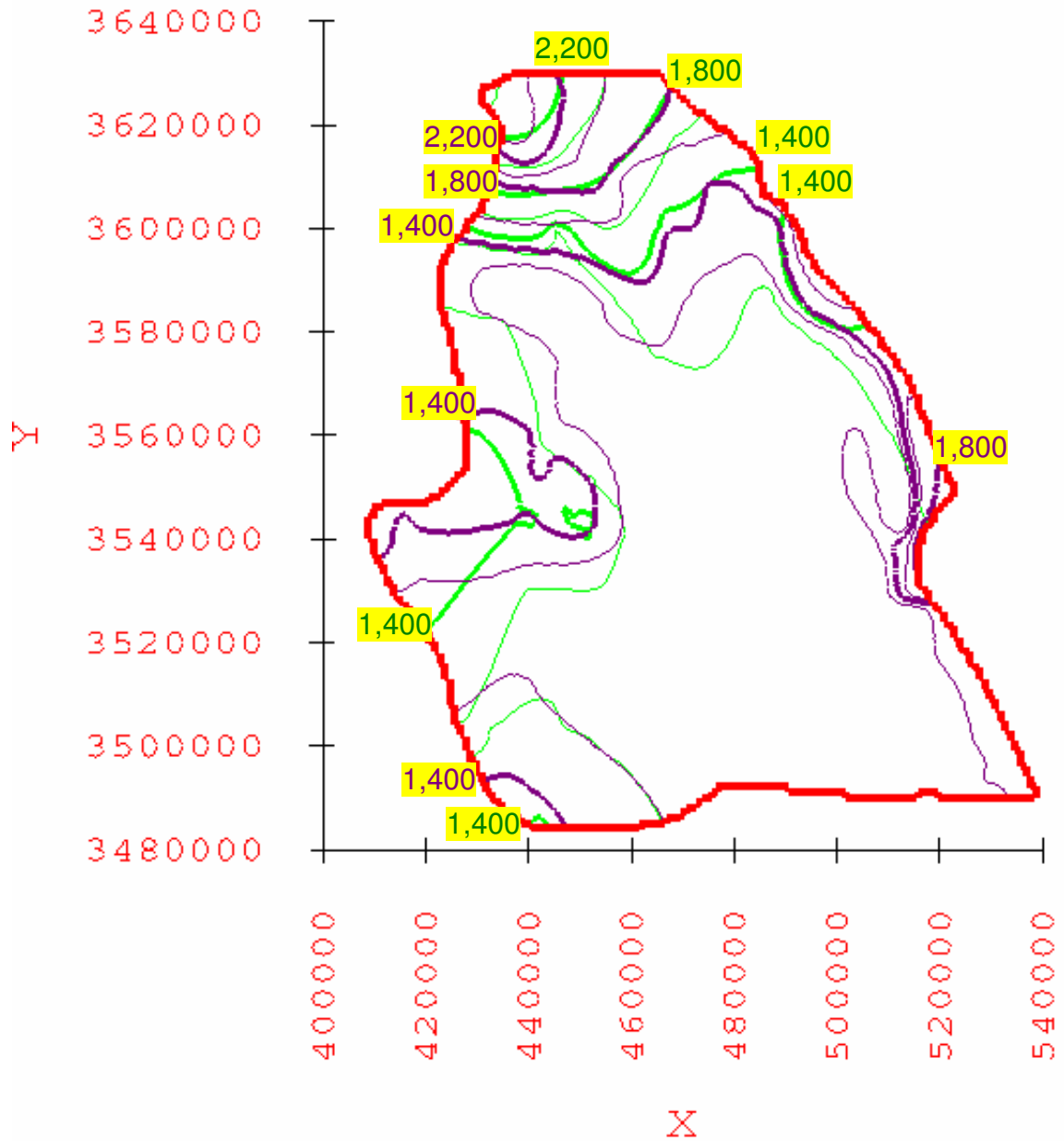
Figure A-4.37: Comparison of the computed hydraulic head in layer 1 for the calibrated water-balance based maximum recharge scenario model and the observed groundwater surface.

Green lines are the model computed head contours. Purple dashed lines are the observed groundwater surface contours. Contour elevations are in meters above mean sea level. Contour interval is 200 meters.
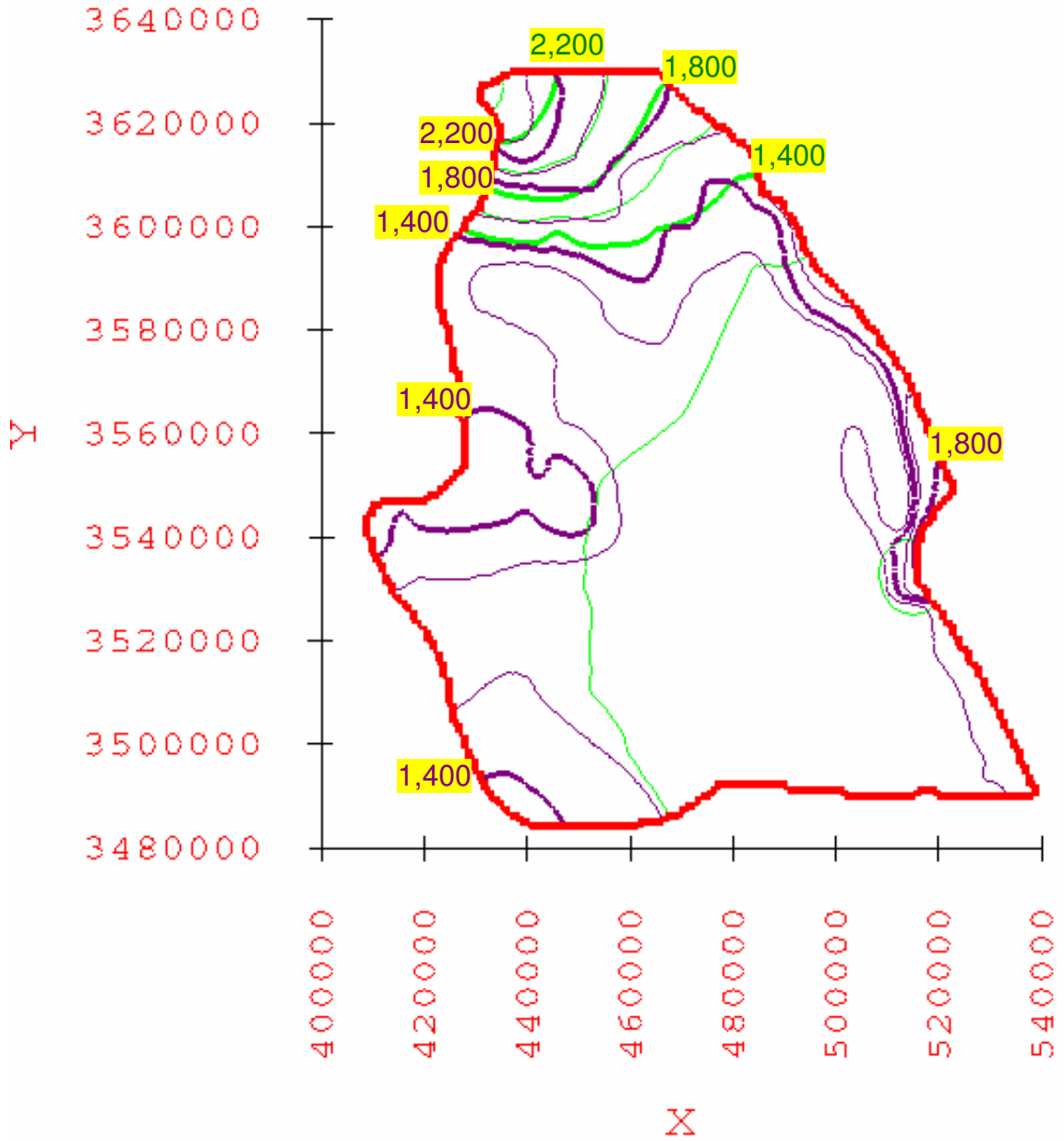
Figure A-4.38: Comparison of the computed hydraulic head in layer 1 for the calibrated elevation-dependent minimum recharge scenario model and the observed groundwater surface.

Green lines are the model computed head contours. Purple dashed lines are the observed groundwater surface contours. Contour elevations are in meters above mean sea level. Contour interval is 200 meters.
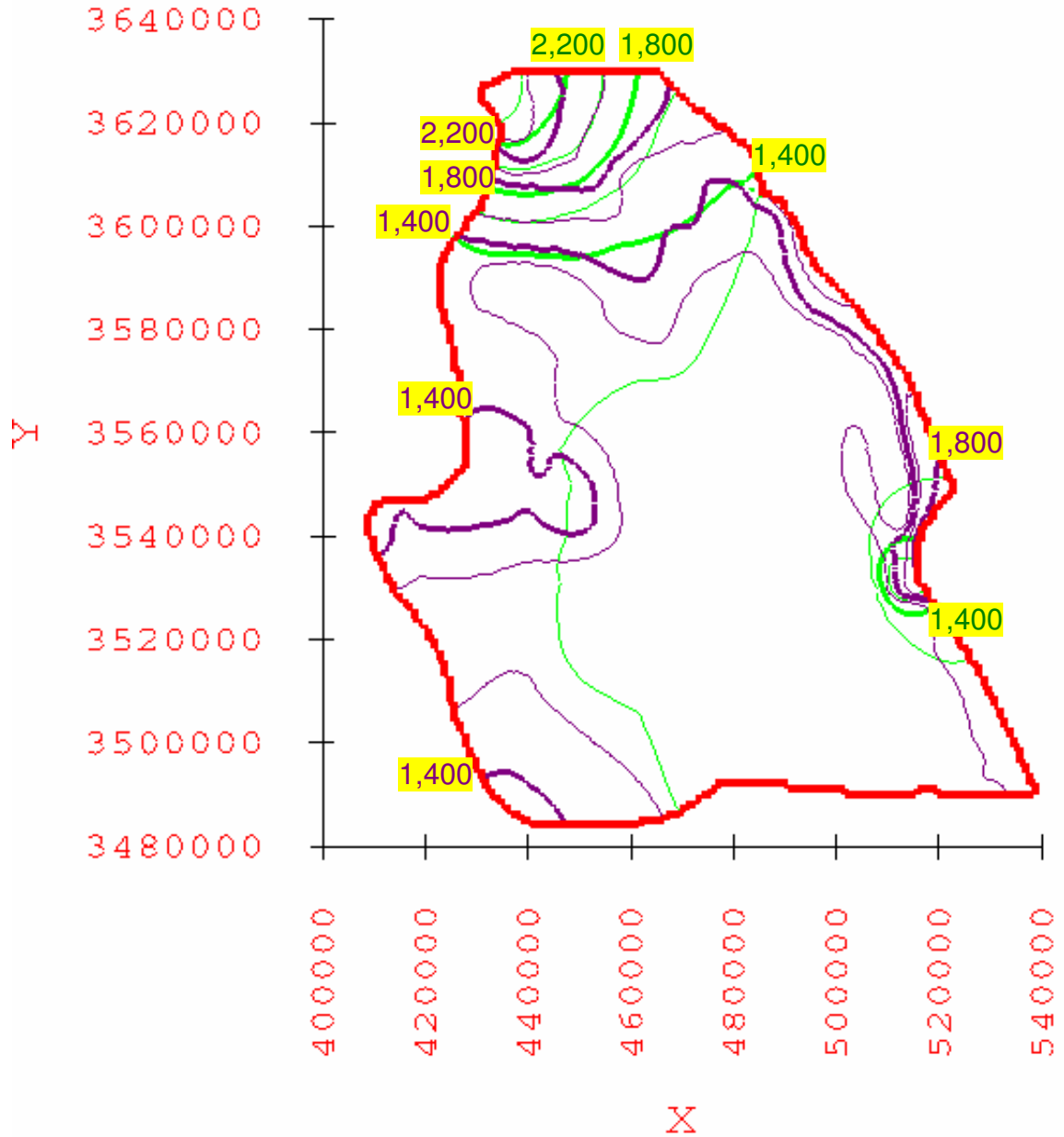
Figure A-4.39: Comparison of the computed hydraulic head in layer 1 for the calibrated elevation-dependent average recharge scenario model and the observed groundwater surface.

Green lines are the model computed head contours. Purple dashed lines are the observed groundwater surface contours. Contour elevations are in meters above mean sea level. Contour interval is 200 meters.
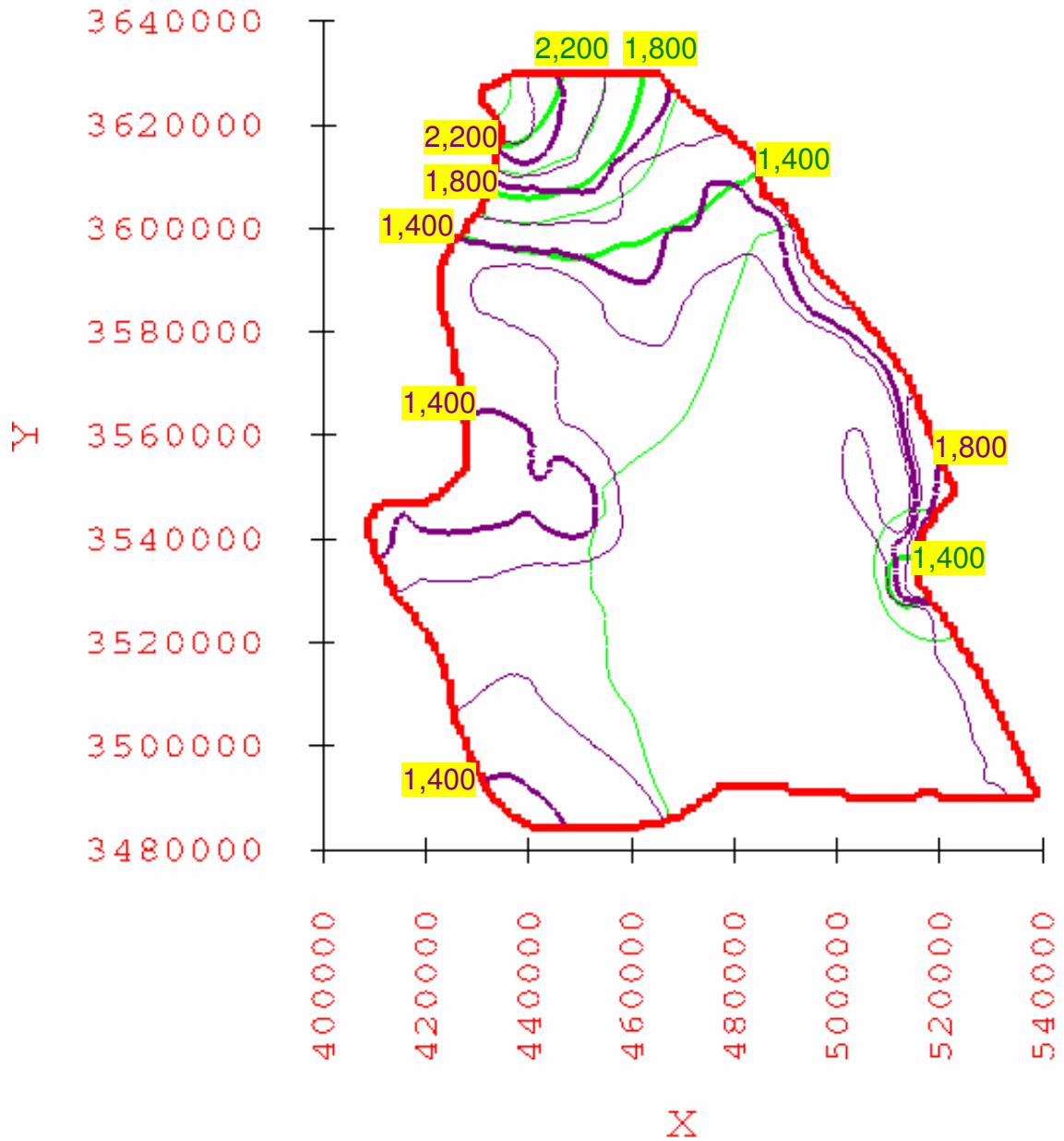
Figure A-4.40: Comparison of the computed hydraulic head in layer 1 for the calibrated elevation-dependent maximum recharge scenario model and the observed groundwater surface.

Green lines are the model computed head contours. Purple dashed lines are the observed groundwater surface contours. Contour elevations are in meters above mean sea level. Contour interval is 200 meters.
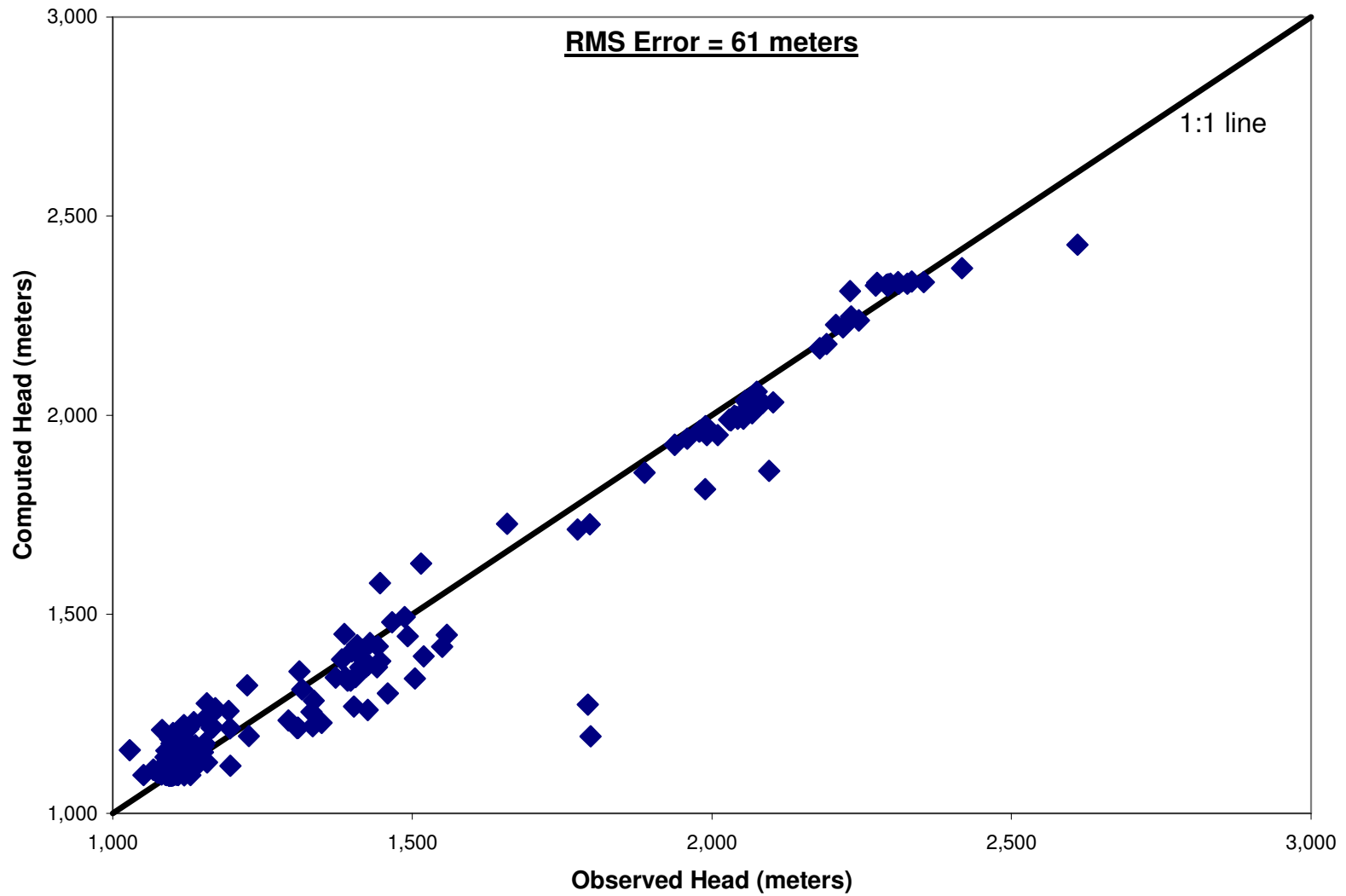
Figure A-4.41: Computed versus observed hydraulic head for the calibrated water-balance based minimum recharge scenario model.
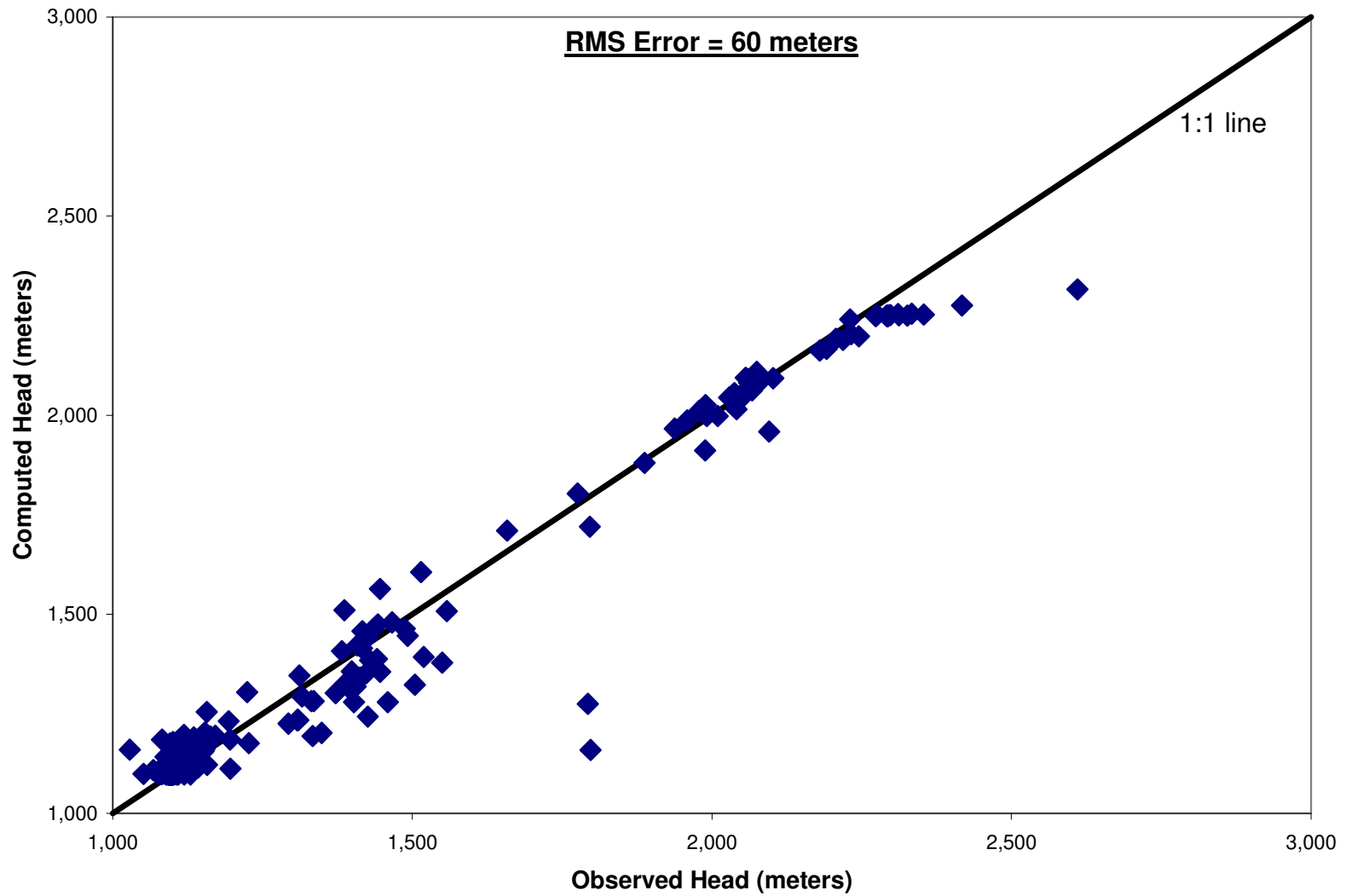
Figure A-4.42: Computed versus observed hydraulic head for the calibrated water-balance based average recharge scenario model.
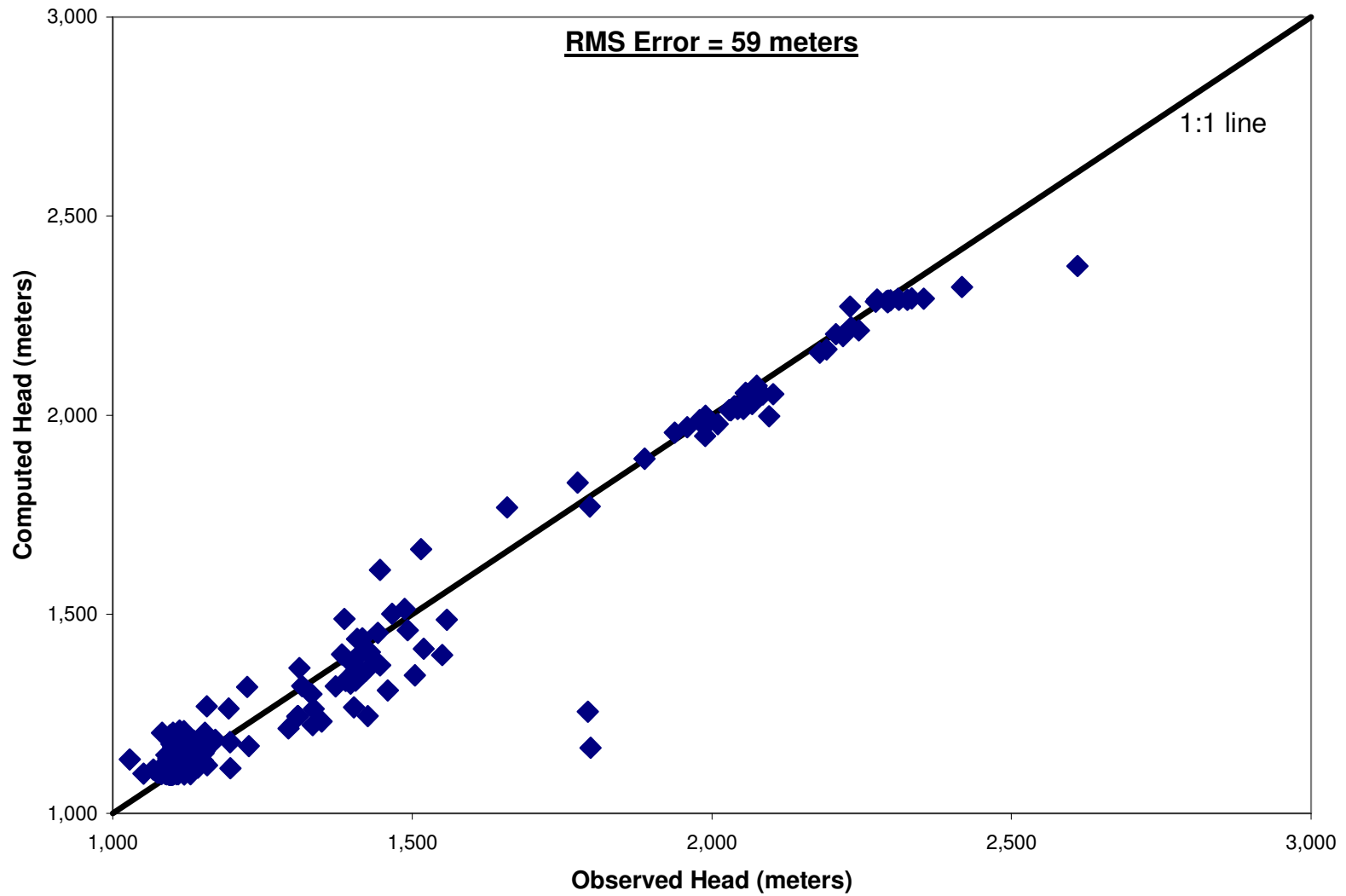
Figure A-4.43: Computed versus observed hydraulic head for the calibrated water-balance based maximum recharge scenario model.
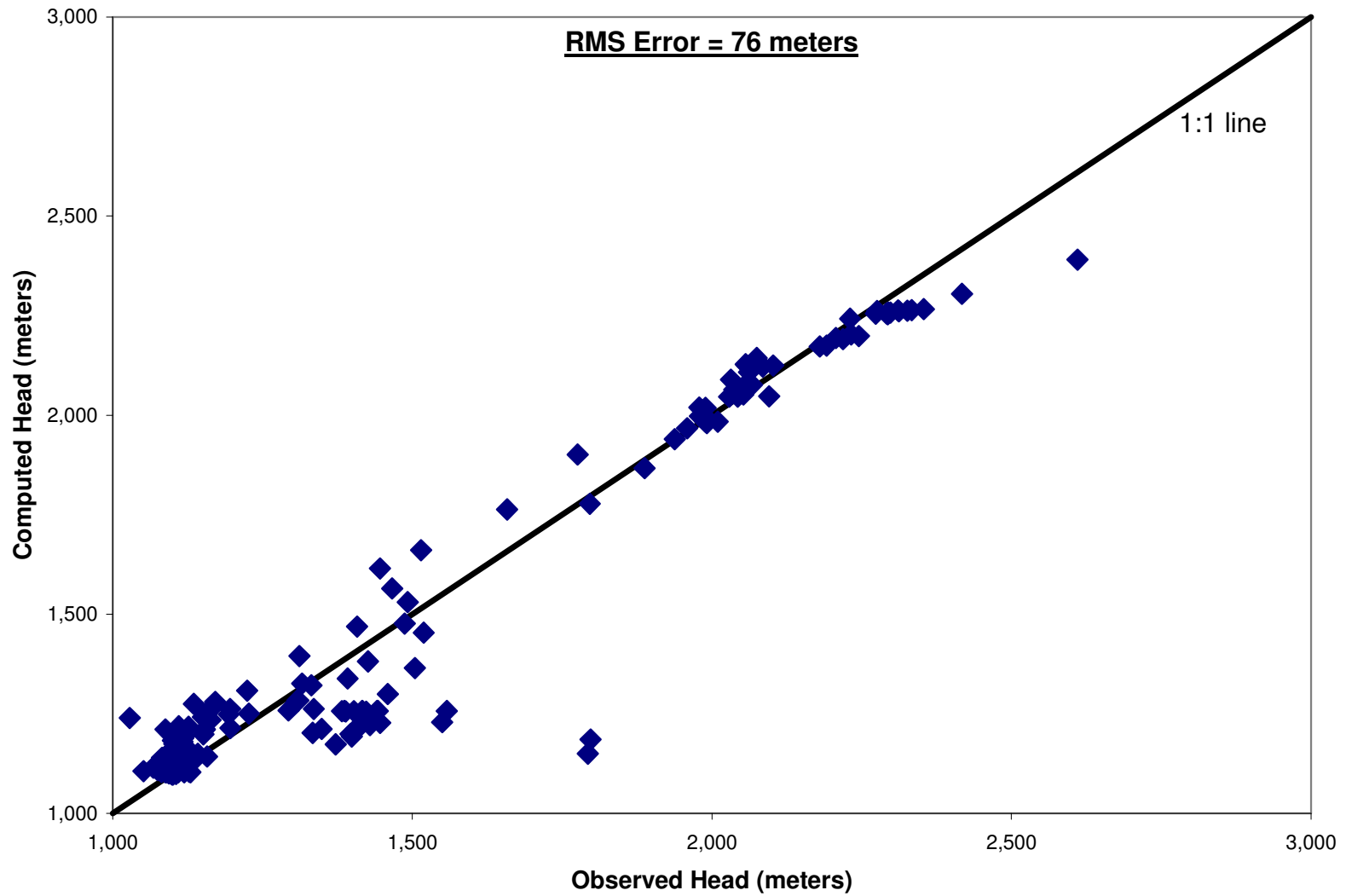
Figure A-4.44: Computed versus observed hydraulic head for the calibrated elevation-dependent minimum recharge scenario model.
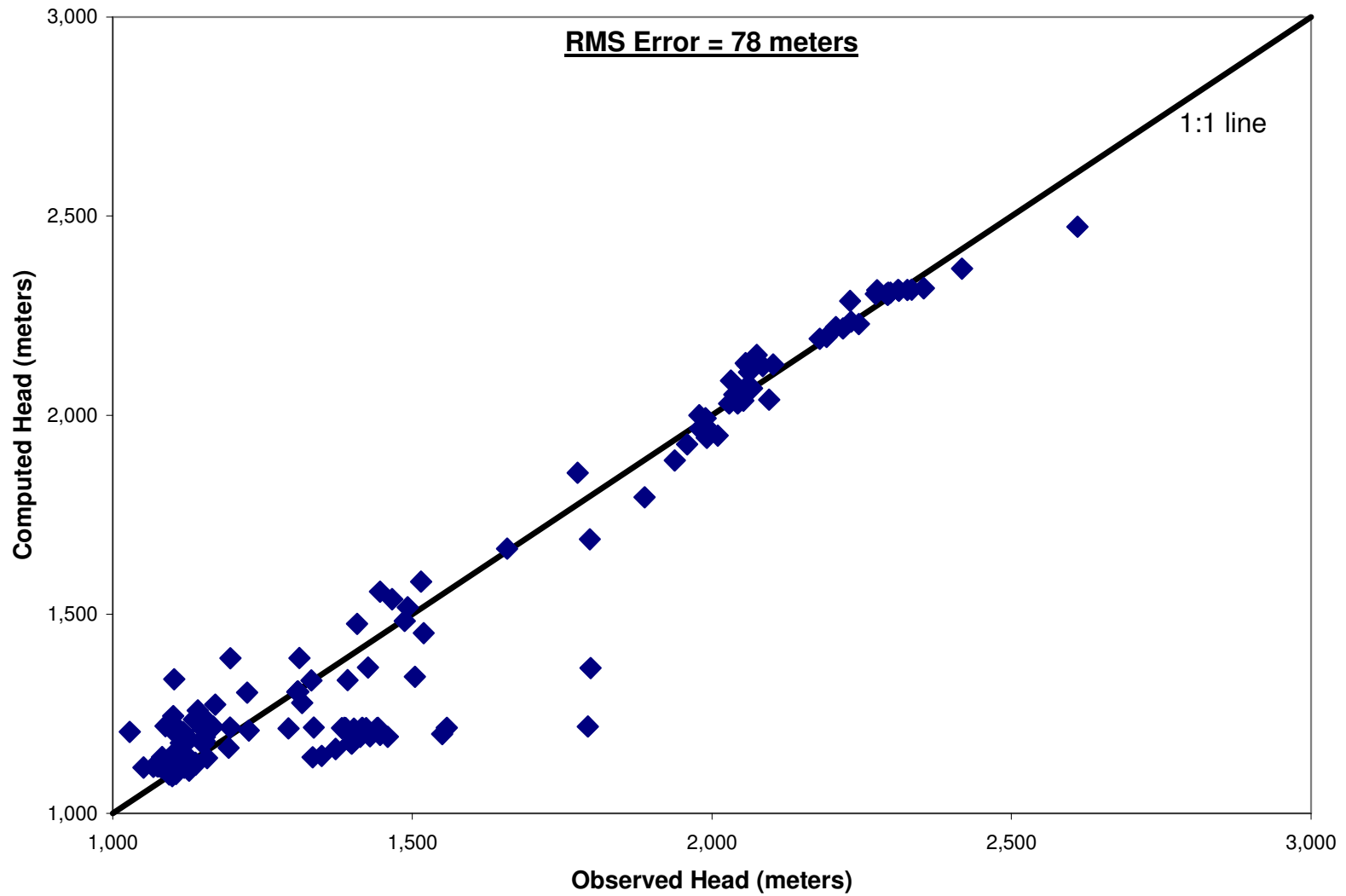
Figure A-4.45: Computed versus observed hydraulic head for the calibrated elevation-dependent average recharge scenario model.
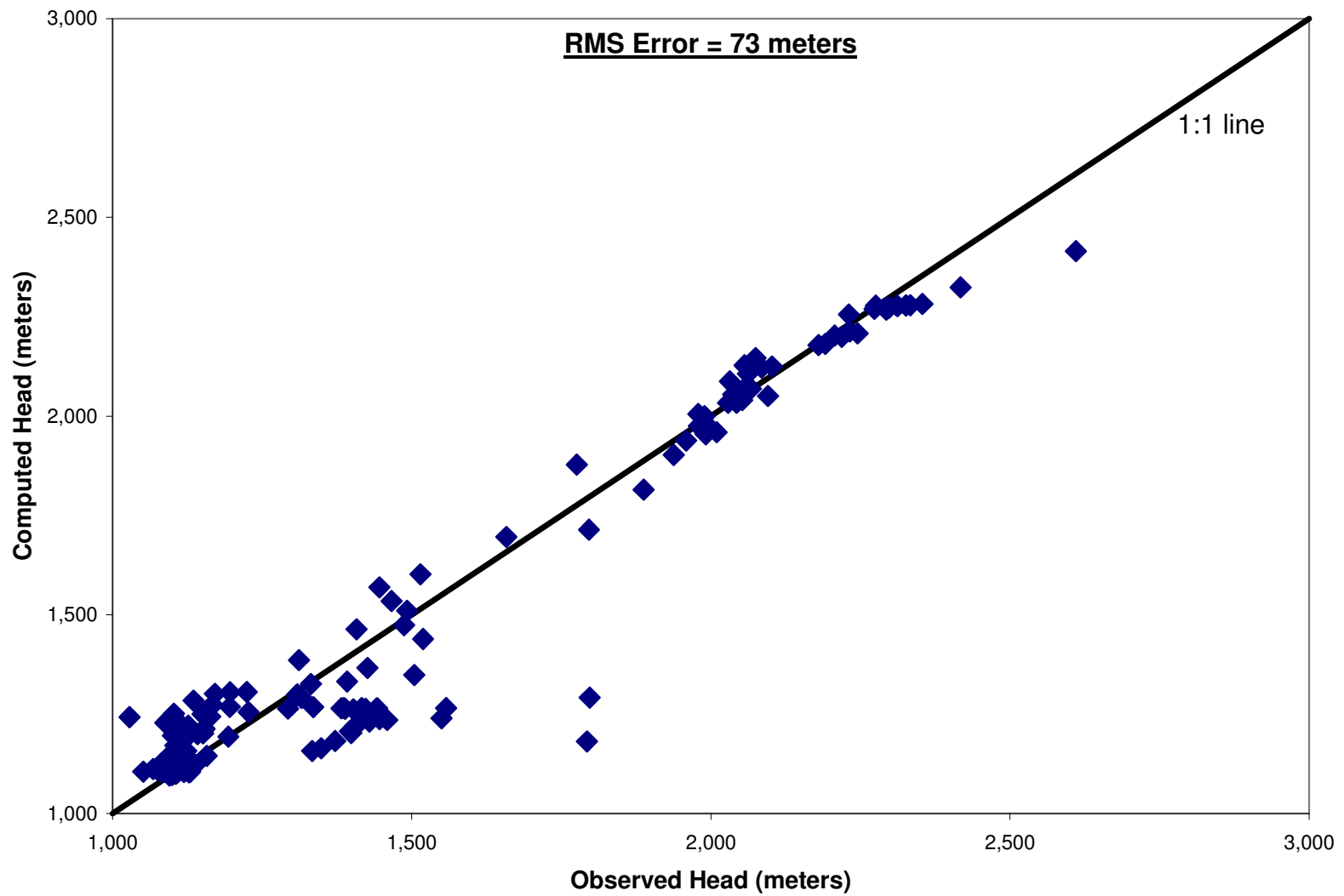
Figure A-4.46: Computed versus observed hydraulic head for the calibrated elevation-dependent maximum recharge scenario model.
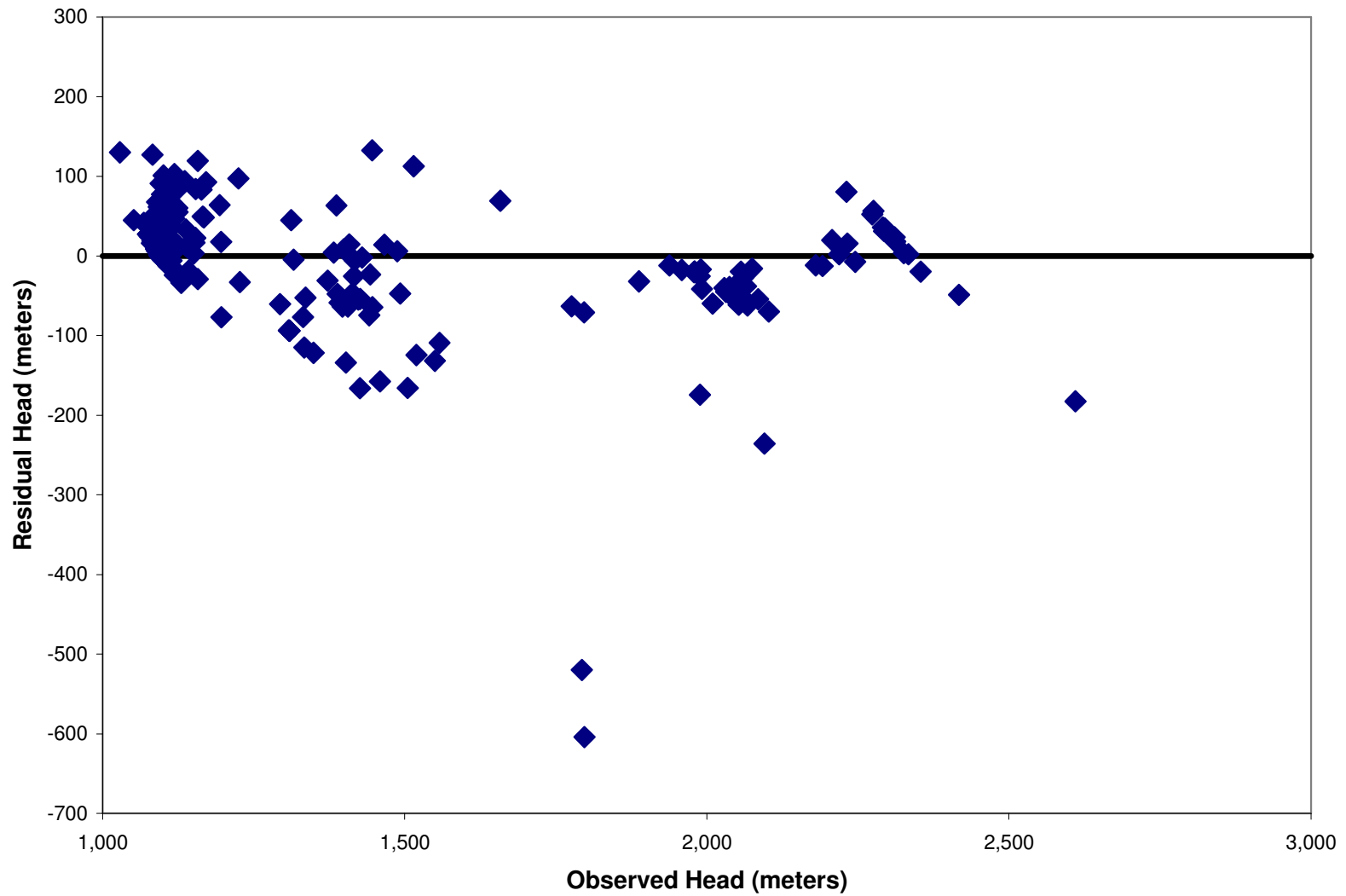
Figure A-4.47: Residual versus observed hydraulic head for the calibrated water-balance based minimum recharge scenario model.
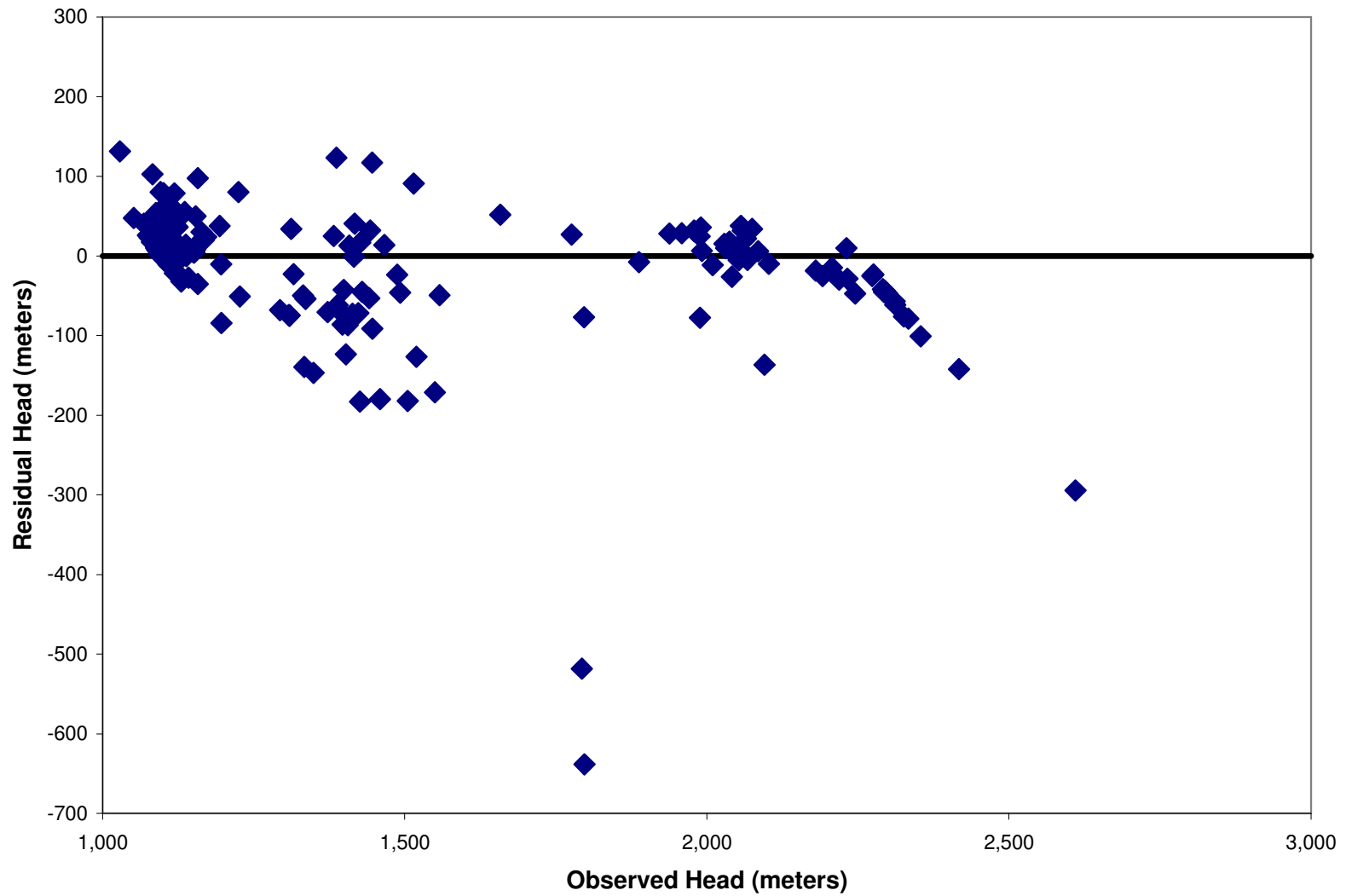
Figure A-4.48: Residual versus observed hydraulic head for the calibrated water-balance based average recharge scenario model.
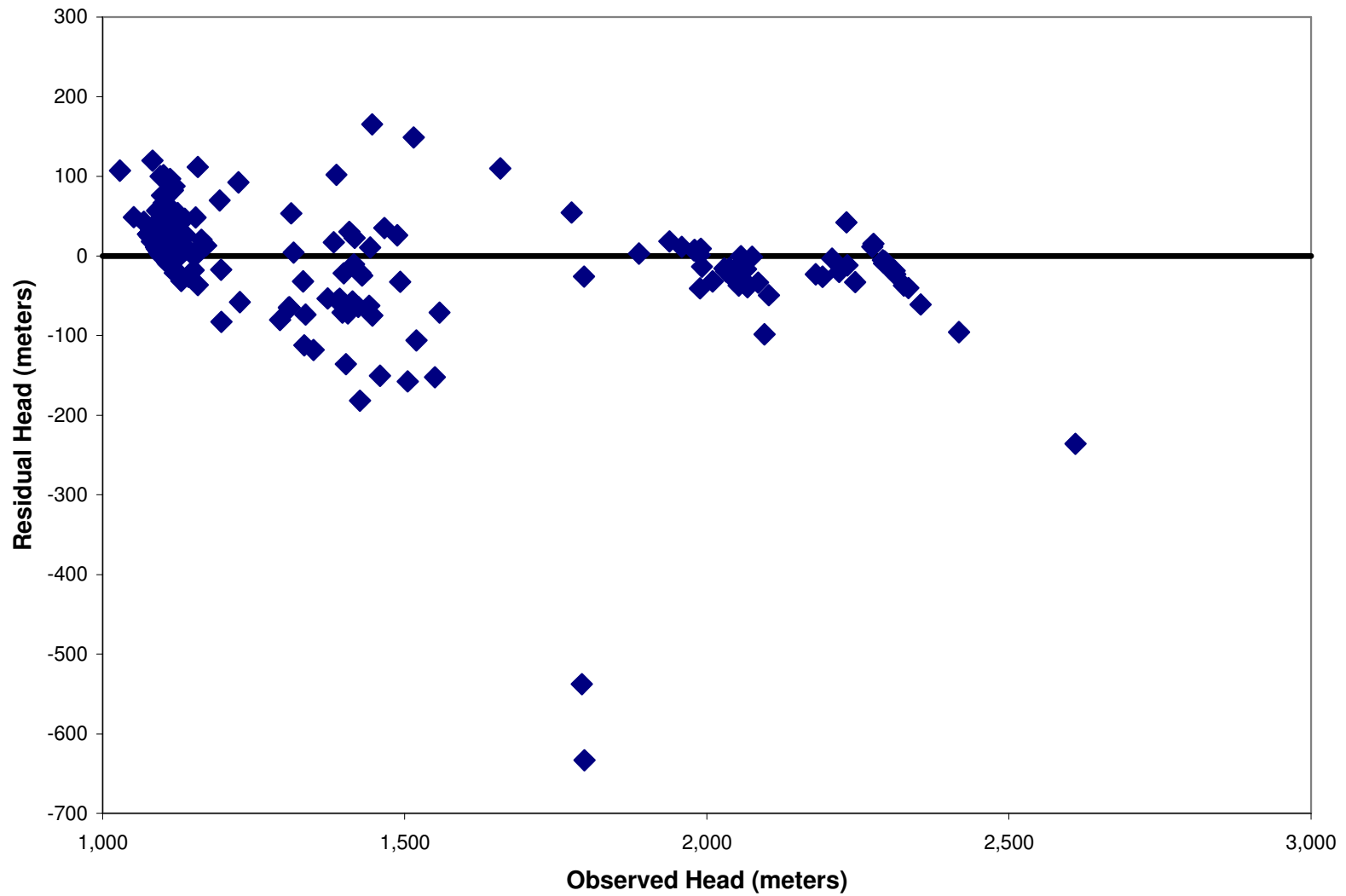
Figure A-4.49: Residual versus observed hydraulic head for the calibrated water-balance based maximum recharge scenario model.
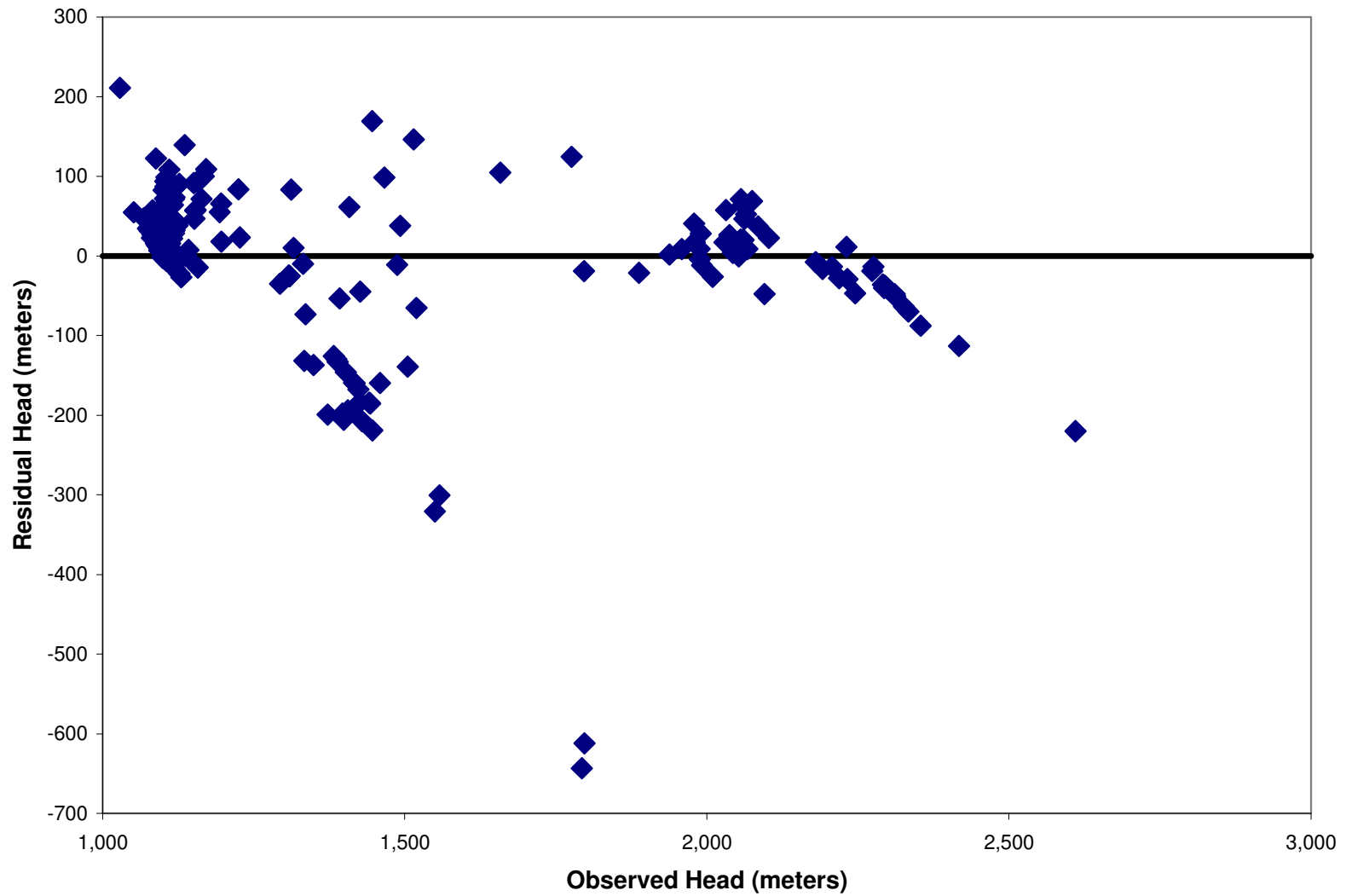
Figure A-4.50: Residual versus observed hydraulic head for the calibrated elevation-dependent minimum recharge scenario model.
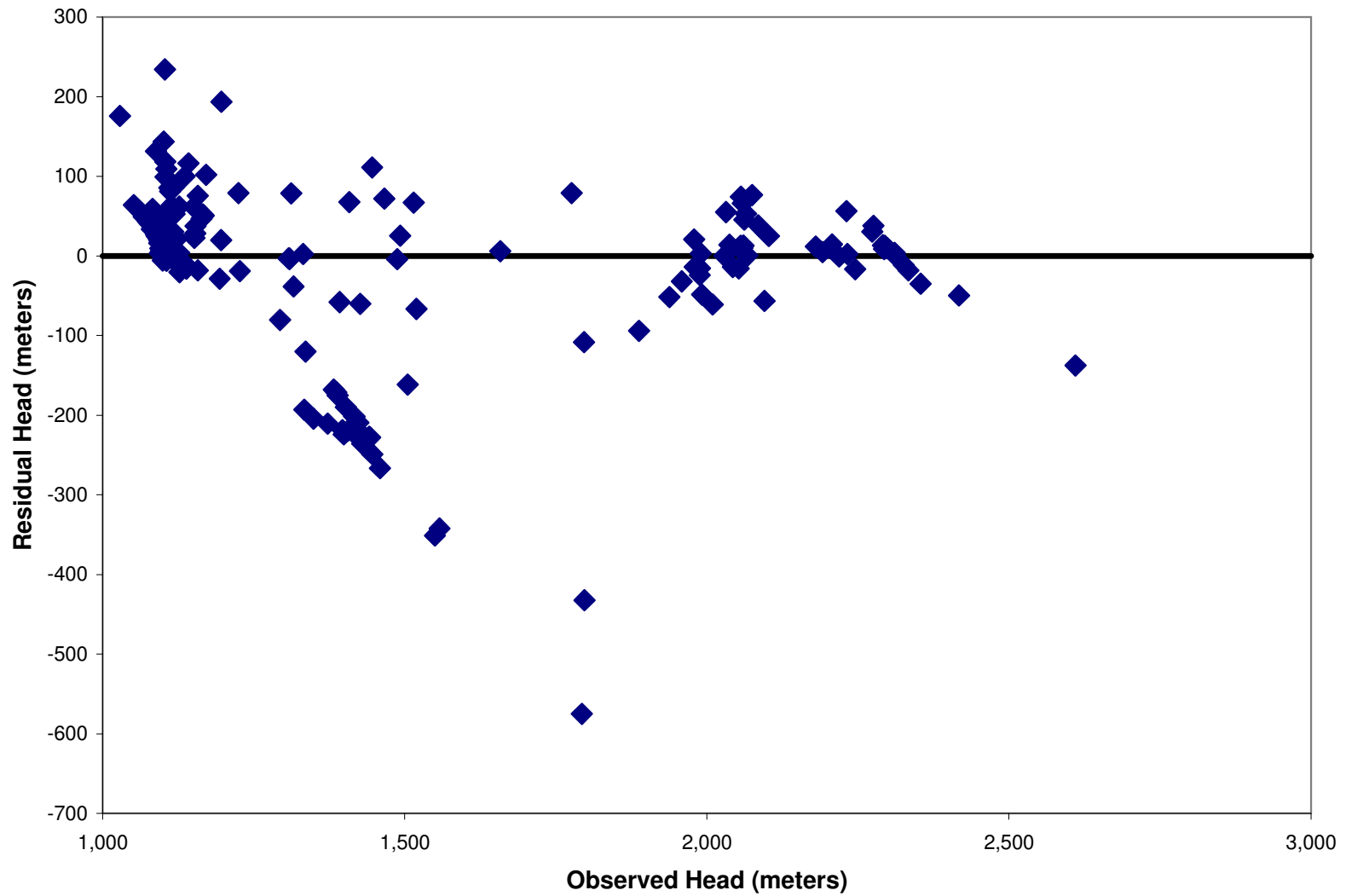
Figure A-4.51: Residual versus observed hydraulic head for the calibrated elevation-dependent average recharge scenario model.
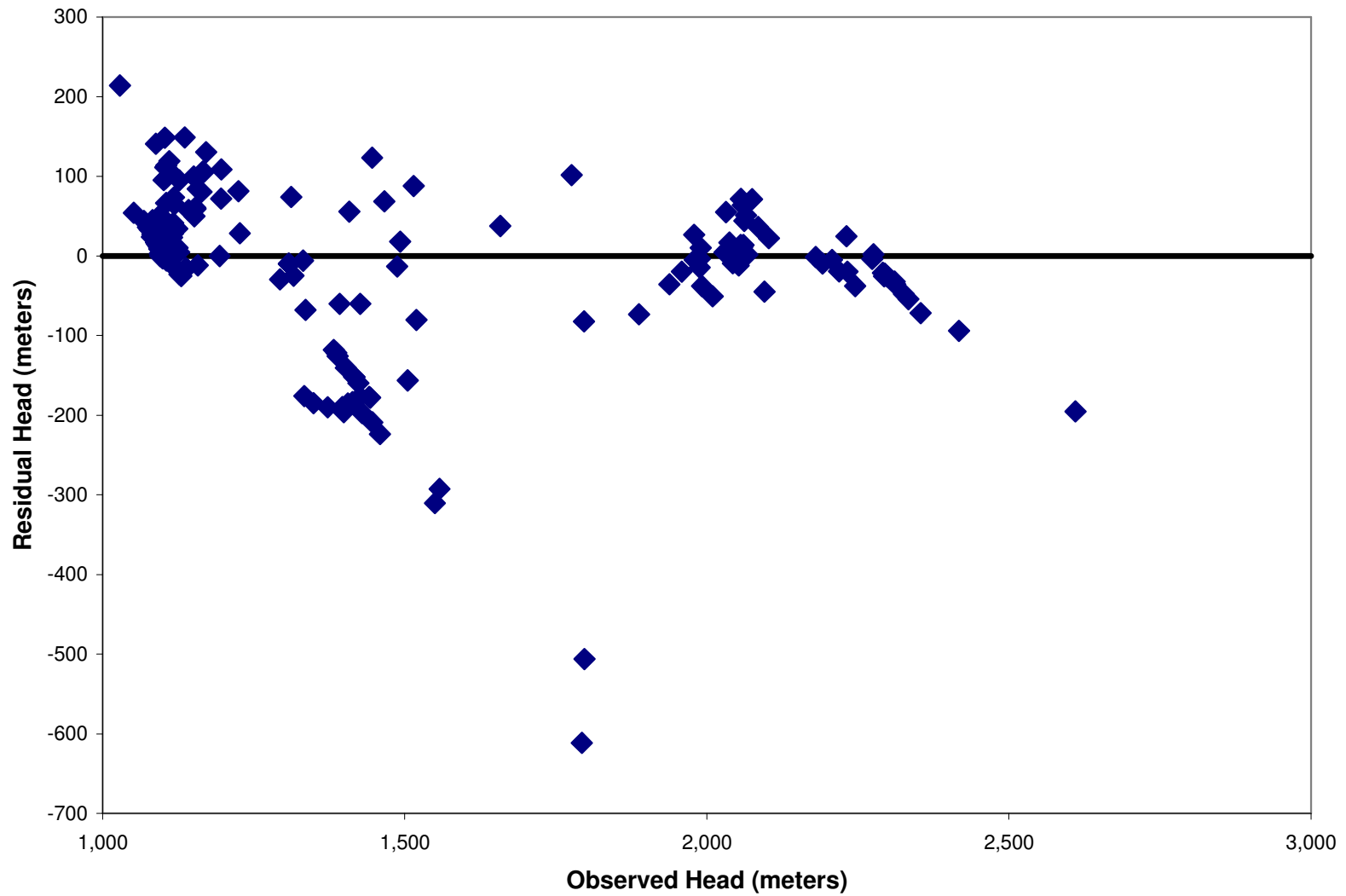
Figure A-4.52: Residual versus observed hydraulic head for the calibrated elevation-dependent maximum recharge scenario model.
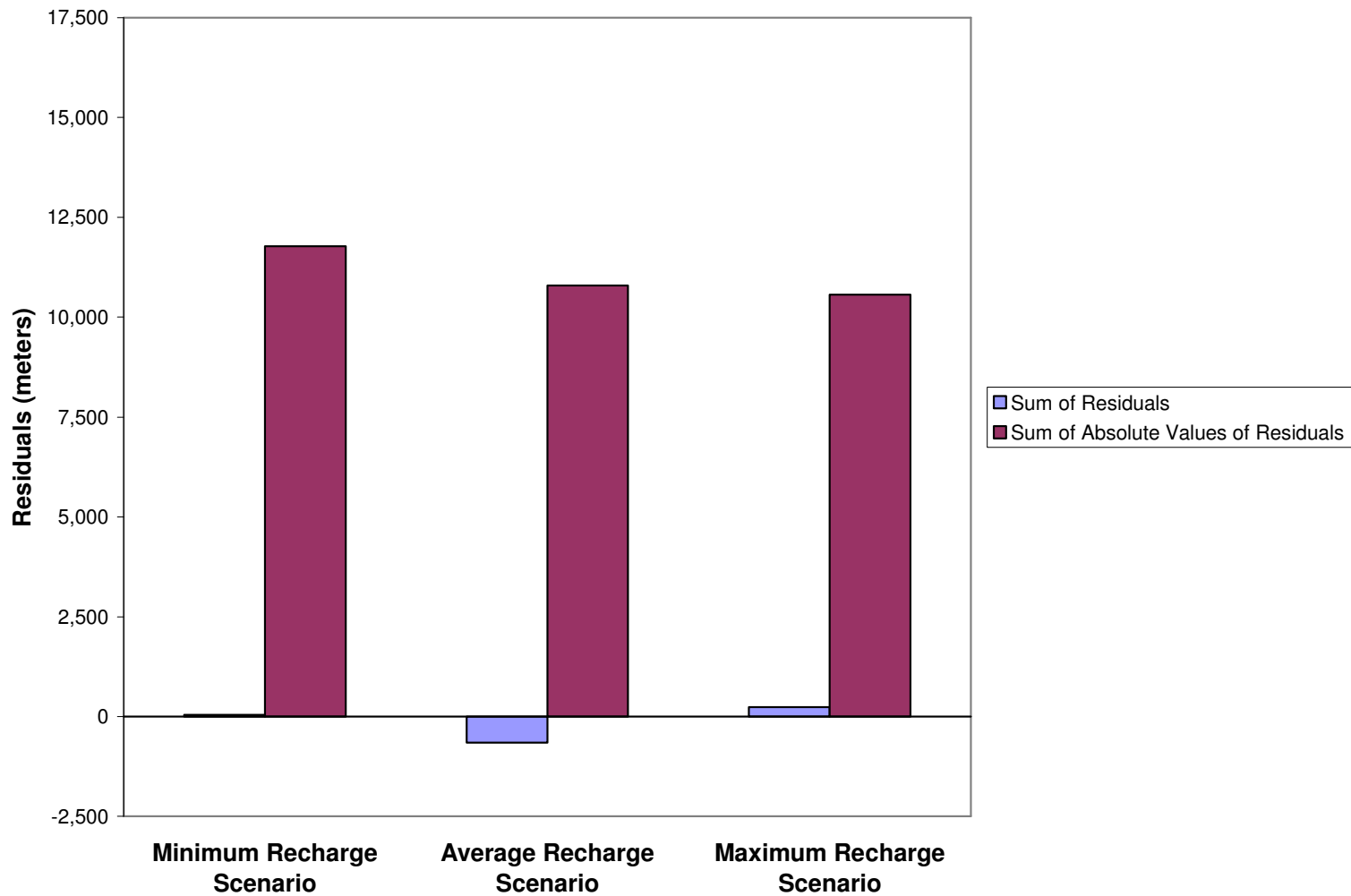
Figure A-4.53: Sum of the residuals and sum of the absolute values of the residuals between observed and computed hydraulic heads for the calibrated water-balance based minimum, average, and maximum recharge scenario models.
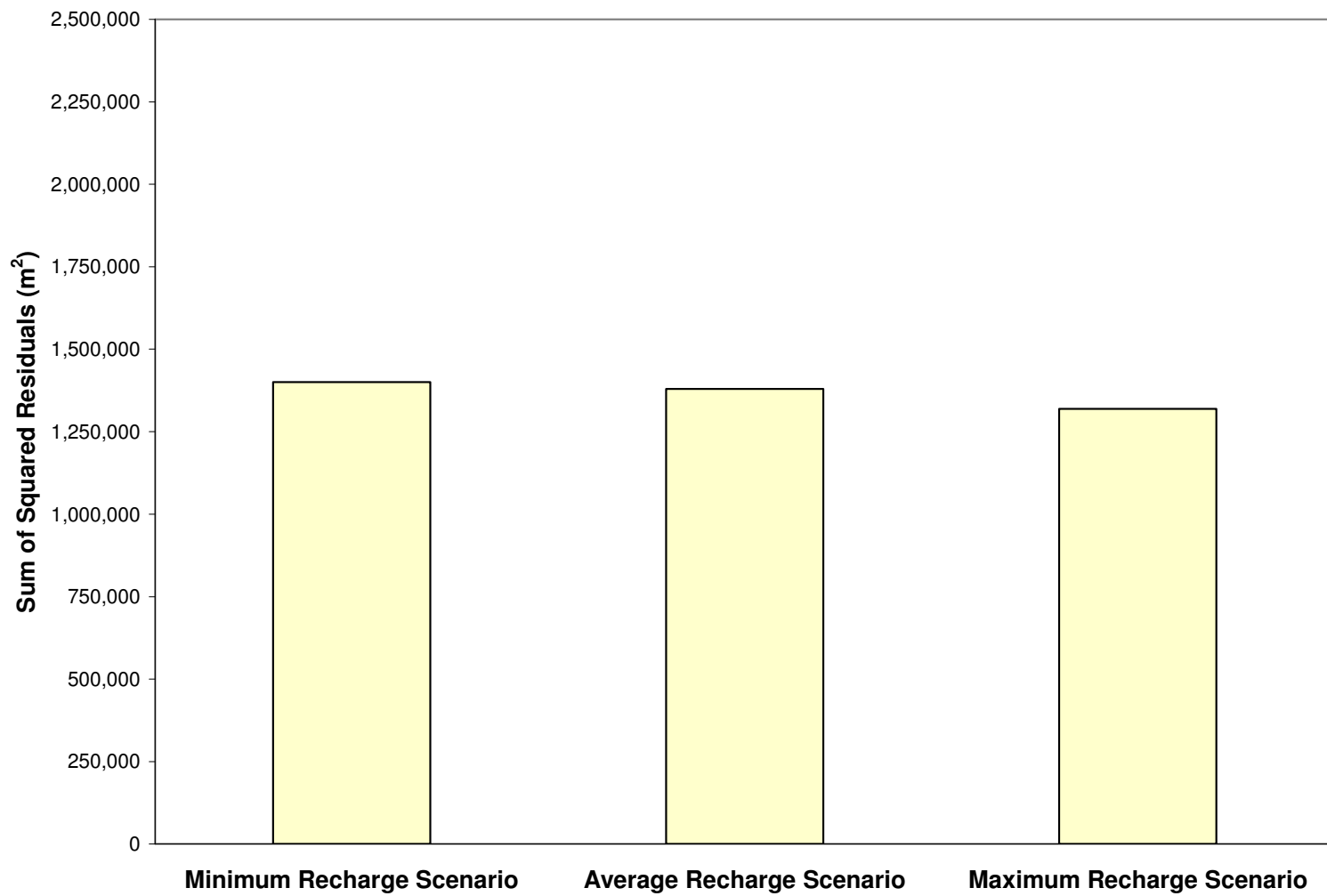
Figure A-4.54: Sum of the squares of the residuals between observed and computed hydraulic heads for the calibrated water-balance based minimum, average, and maximum recharge scenario models.
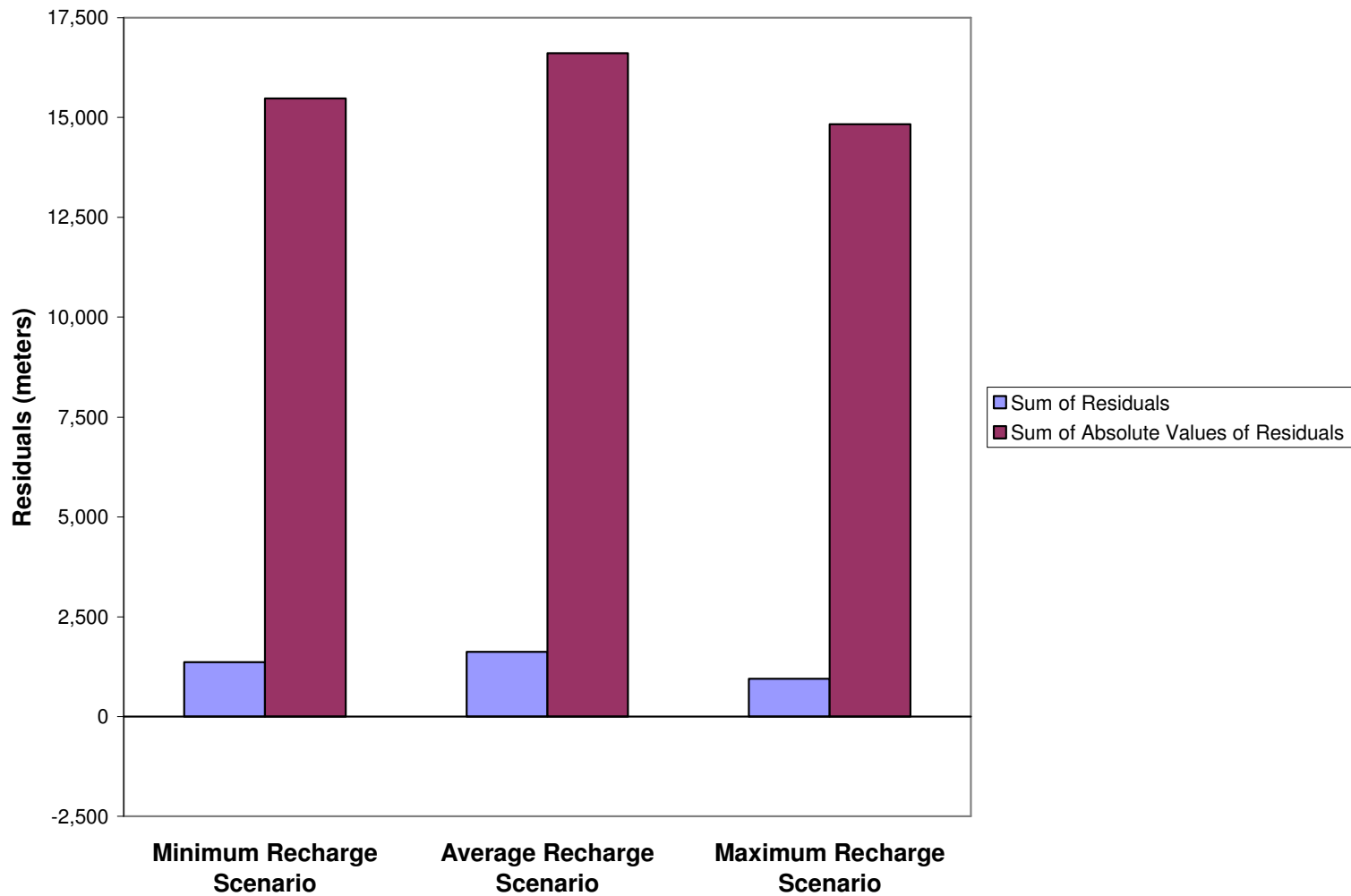
Figure A-4.55: Sum of the residuals and sum of the absolute values of the residuals between observed and computed hydraulic heads for the calibrated elevation-dependent minimum, average, and maximum recharge scenario models.
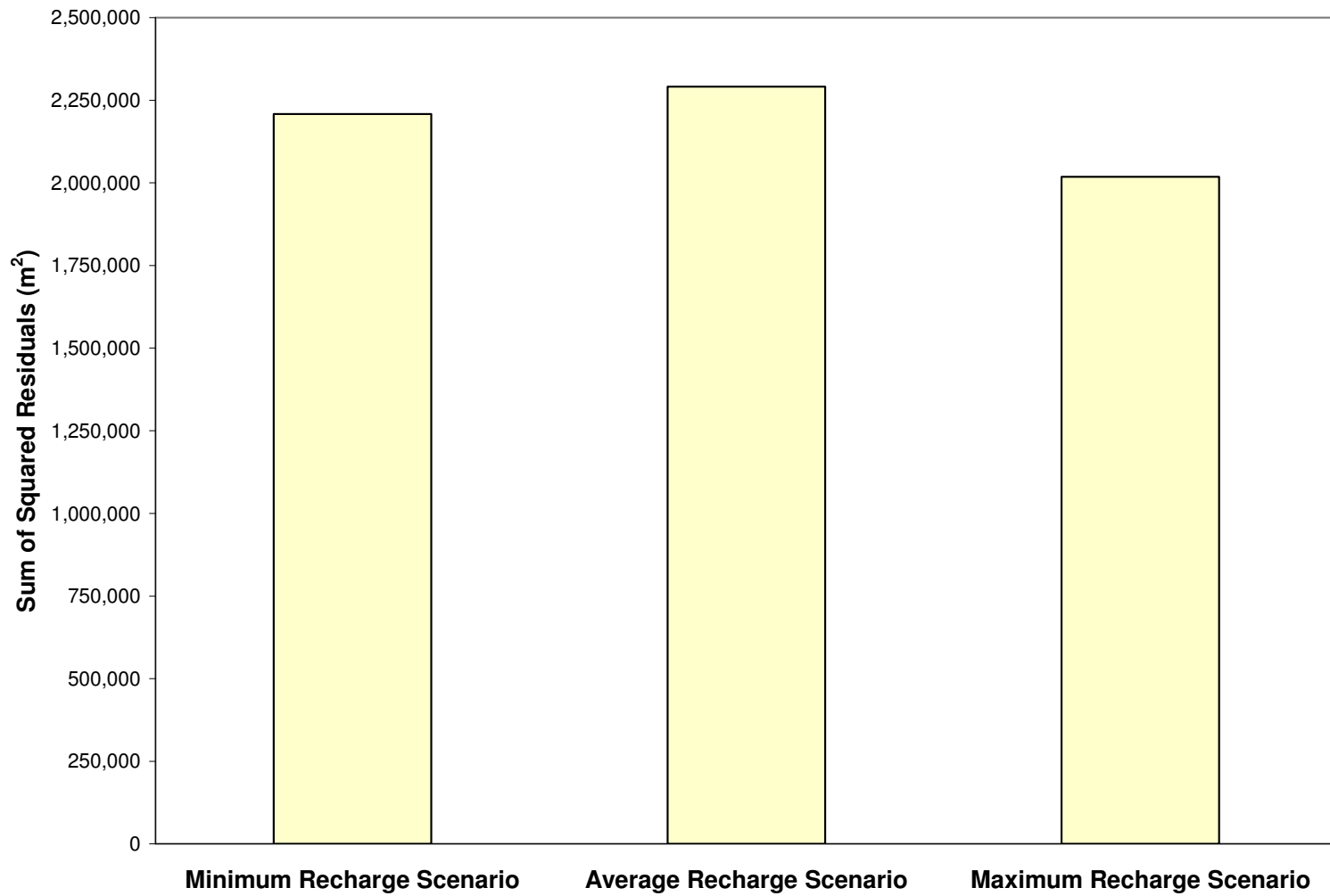
Figure A-4.56: Sum of the squares of the residuals between observed and computed hydraulic heads for the calibrated elevation-dependent minimum, average, and maximum recharge scenarios models.
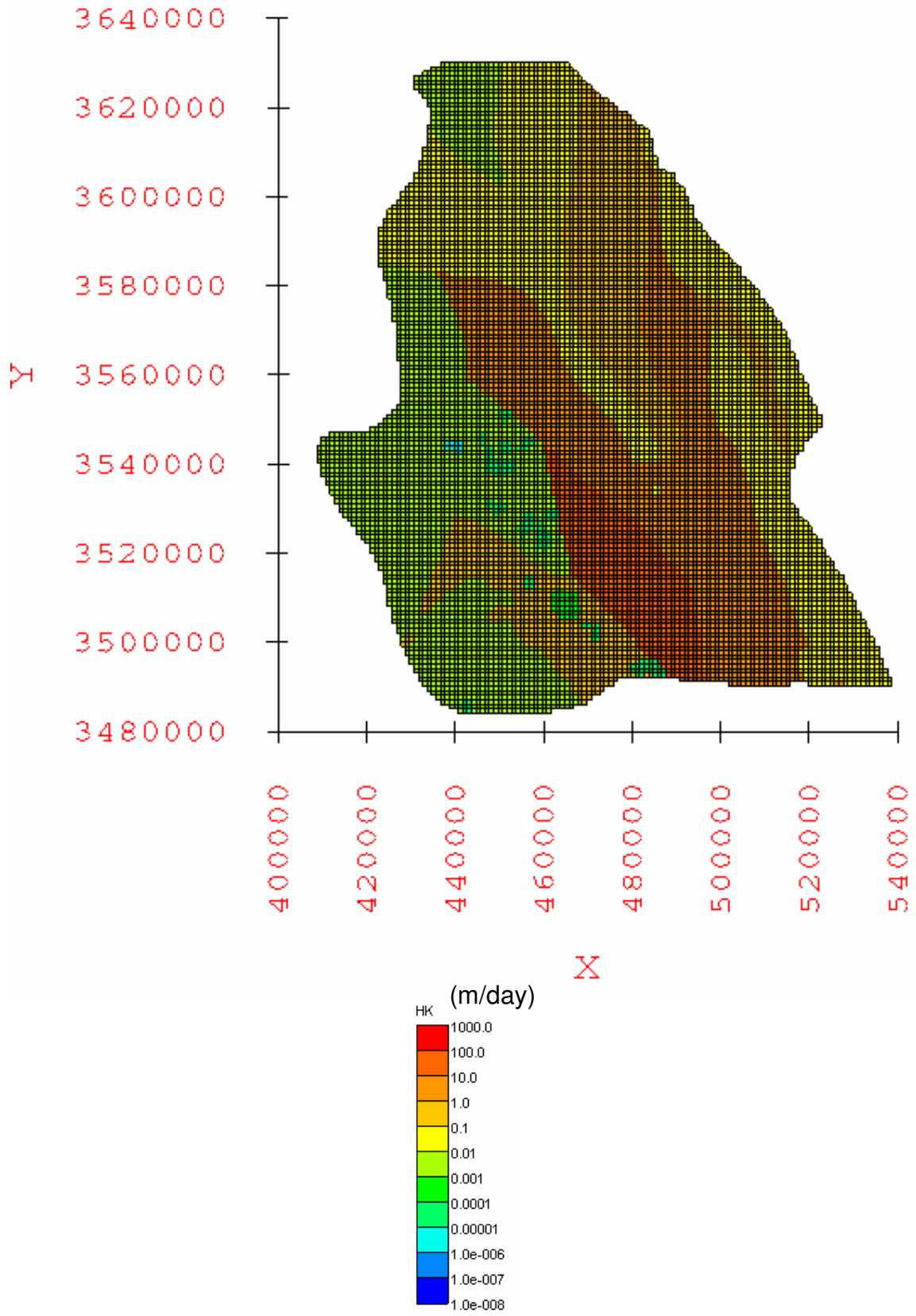
Figure A-4.57: Horizontal hydraulic conductivity [HK] distribution in layer 1 for the calibrated water-balance based minimum recharge scenario groundwater flow model.
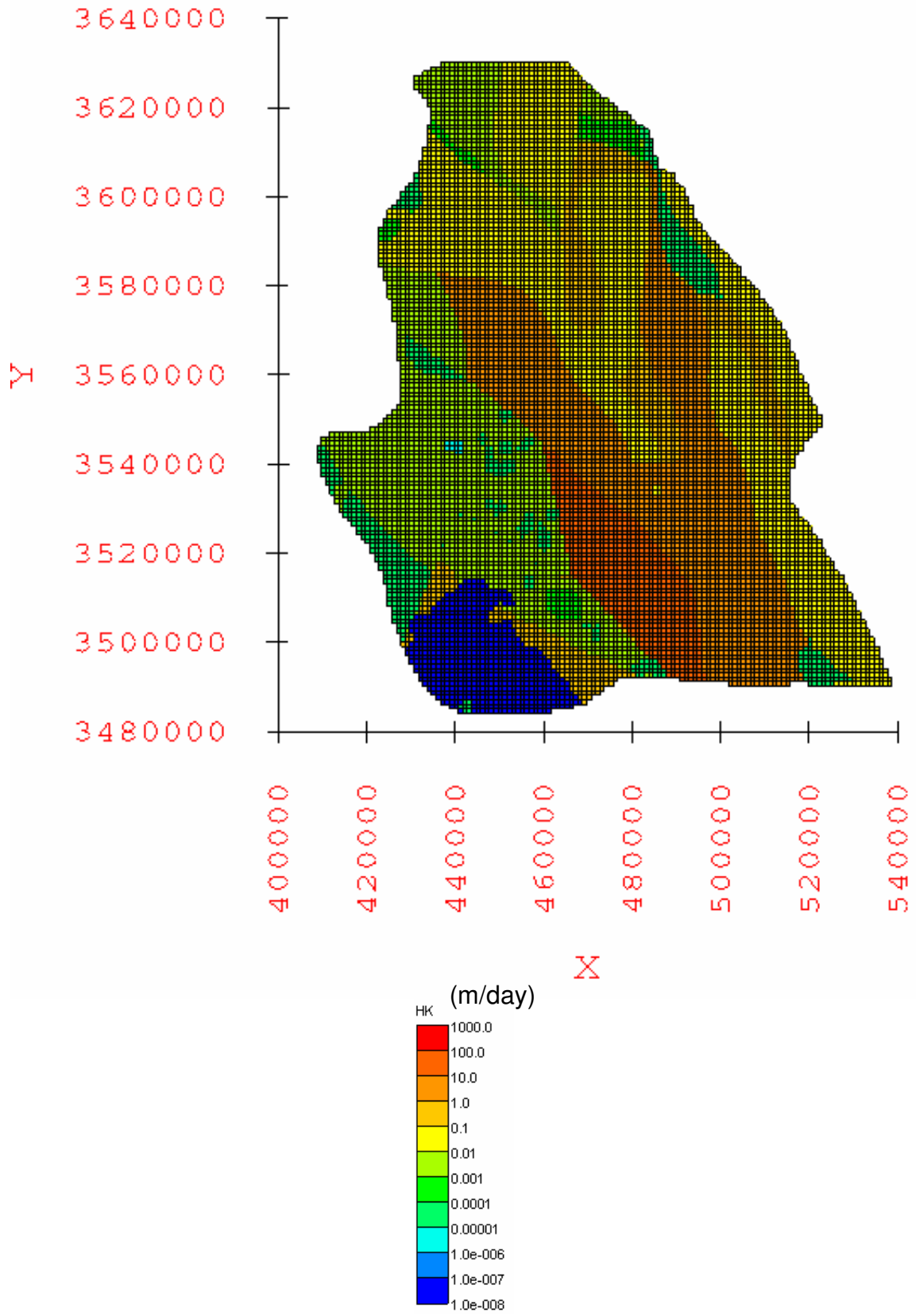
Figure A-4.58: Horizontal hydraulic conductivity [HK] distribution in layer 2 for the calibrated water-balance based minimum recharge scenario groundwater flow model.
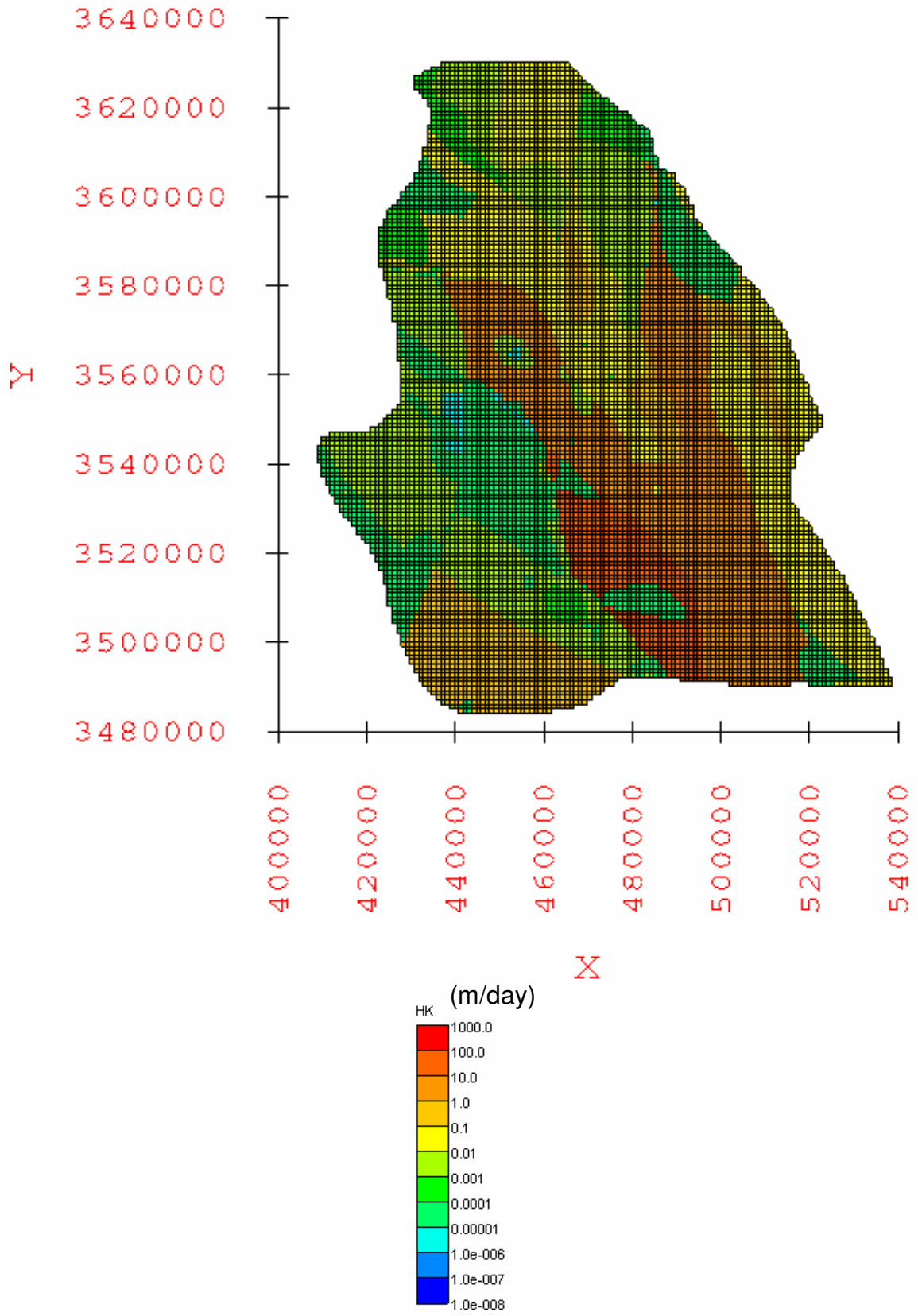
Figure A-4.59: Horizontal hydraulic conductivity [HK] distribution in layer 3 for the calibrated water-balance based minimum recharge scenario groundwater flow model.
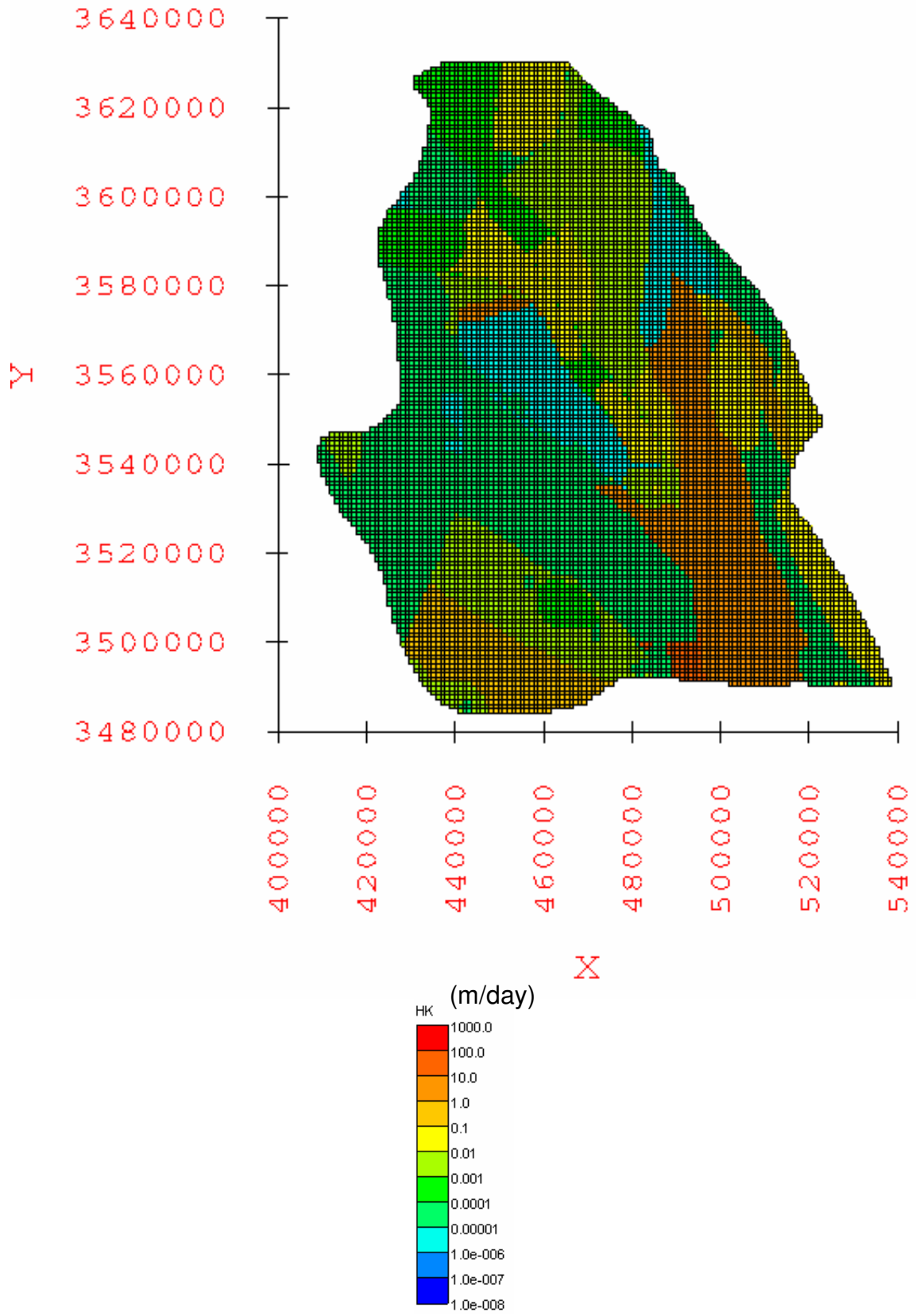
Figure A-4.60: Horizontal hydraulic conductivity [HK] distribution in layer 4 for the calibrated water-balance based minimum recharge scenario groundwater flow model.
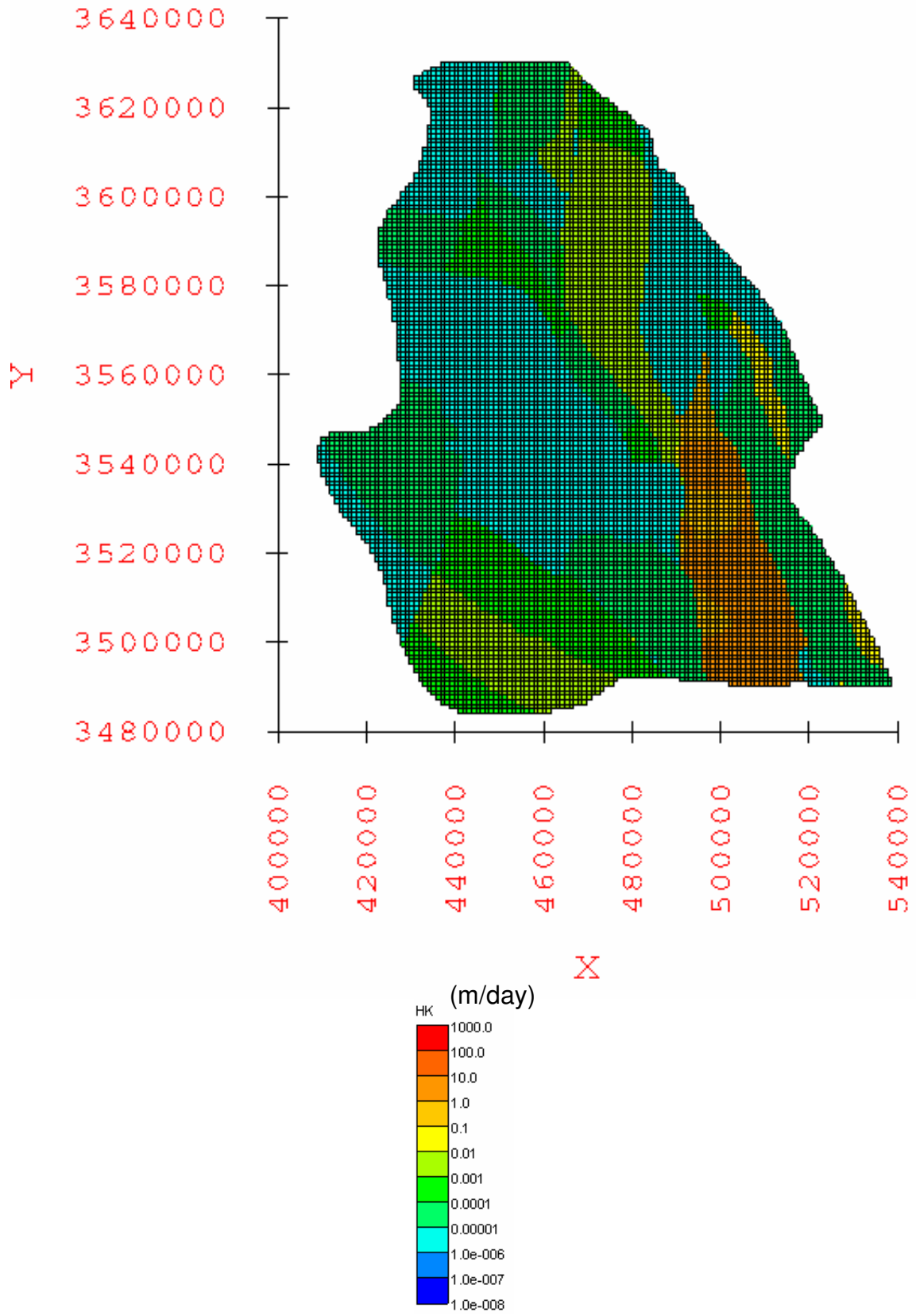
Figure A-4.61: Horizontal hydraulic conductivity [HK] distribution in layer 5 for the calibrated water-balance based minimum recharge scenario groundwater flow model.
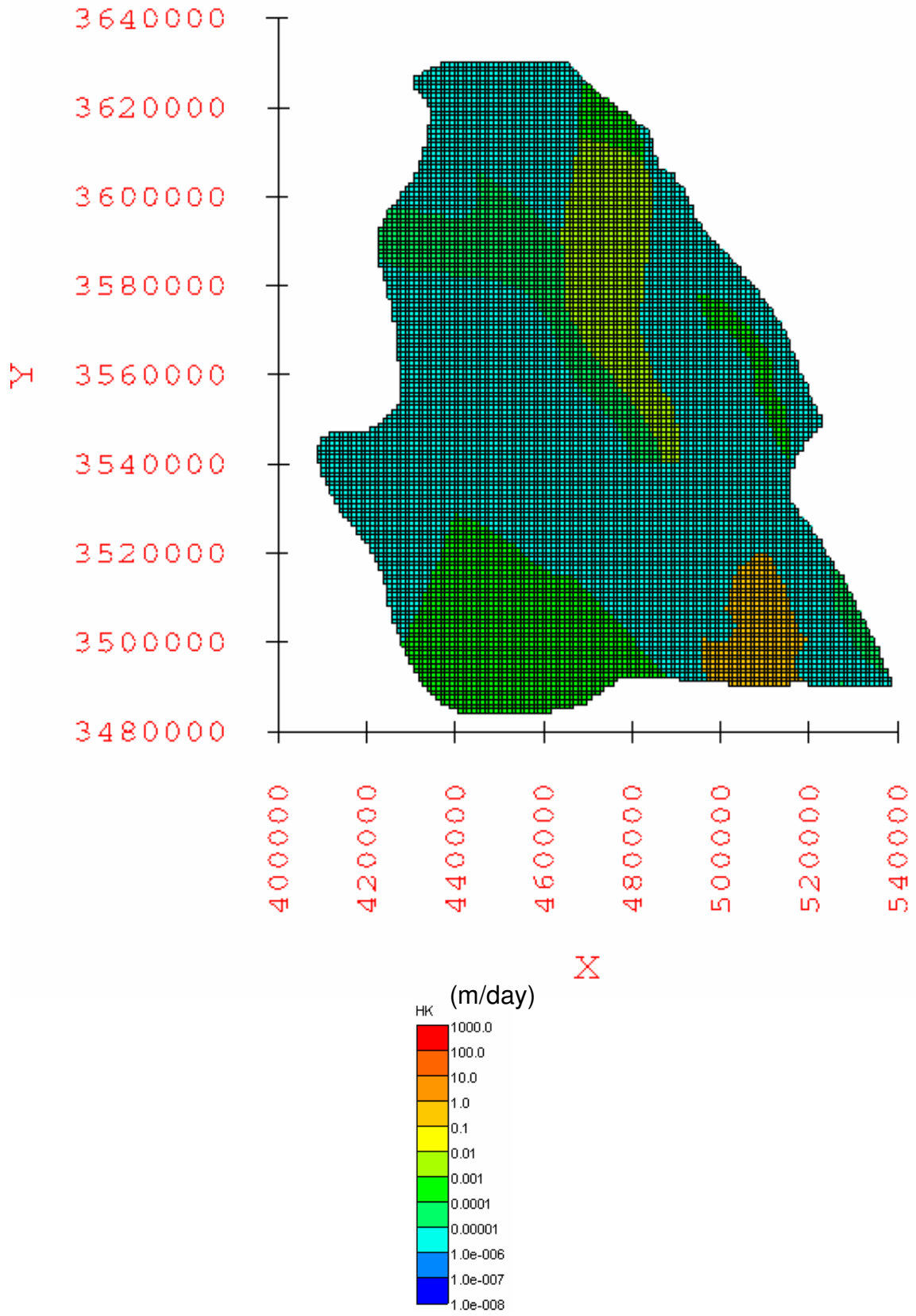
Figure A-4.62: Horizontal hydraulic conductivity [HK] distribution in layer 6 for the calibrated water-balance based minimum recharge scenario groundwater flow model.
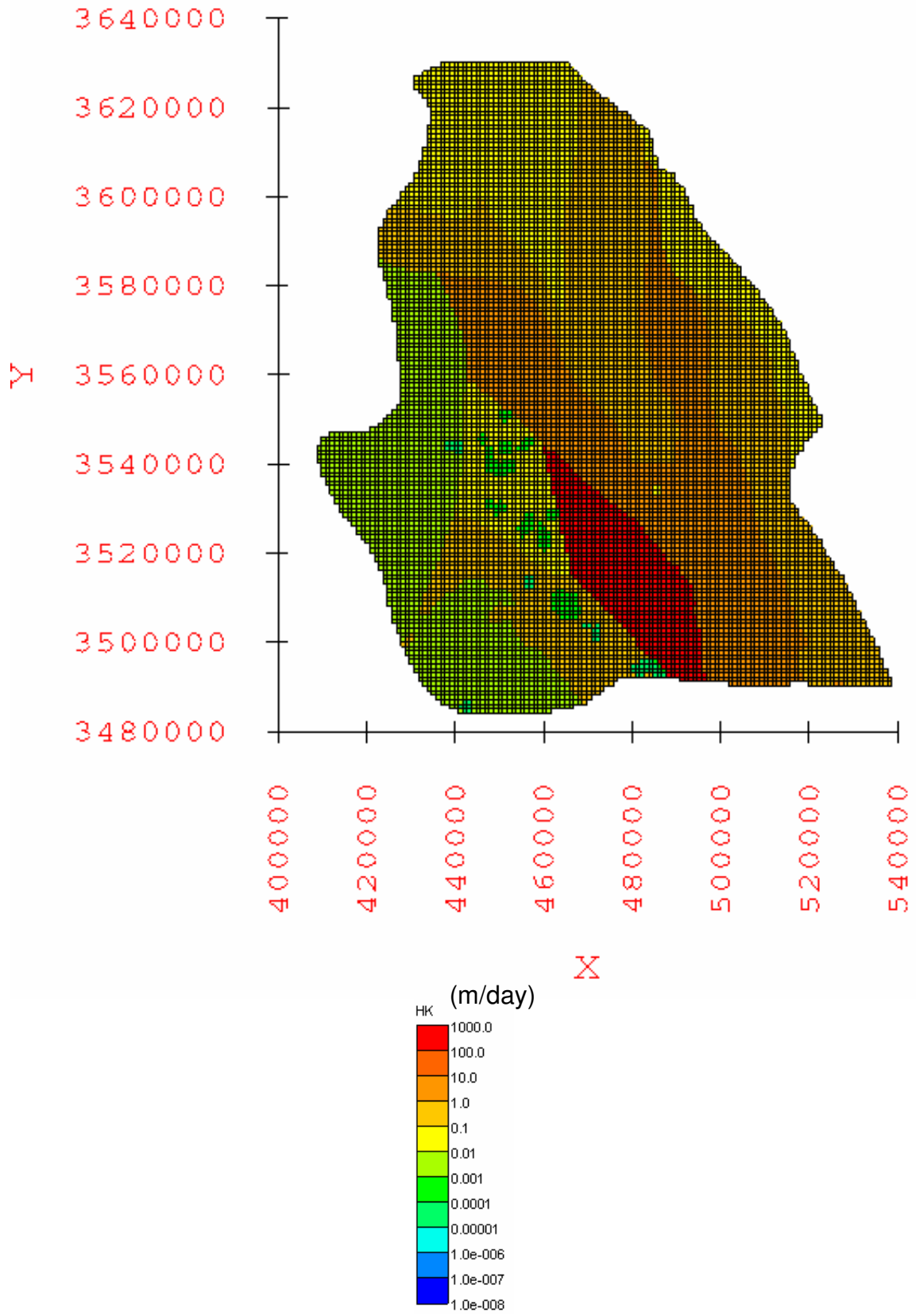
Figure A-4.63: Horizontal hydraulic conductivity [HK] distribution in layer 1 for the calibrated water-balance based average recharge scenario groundwater flow model.
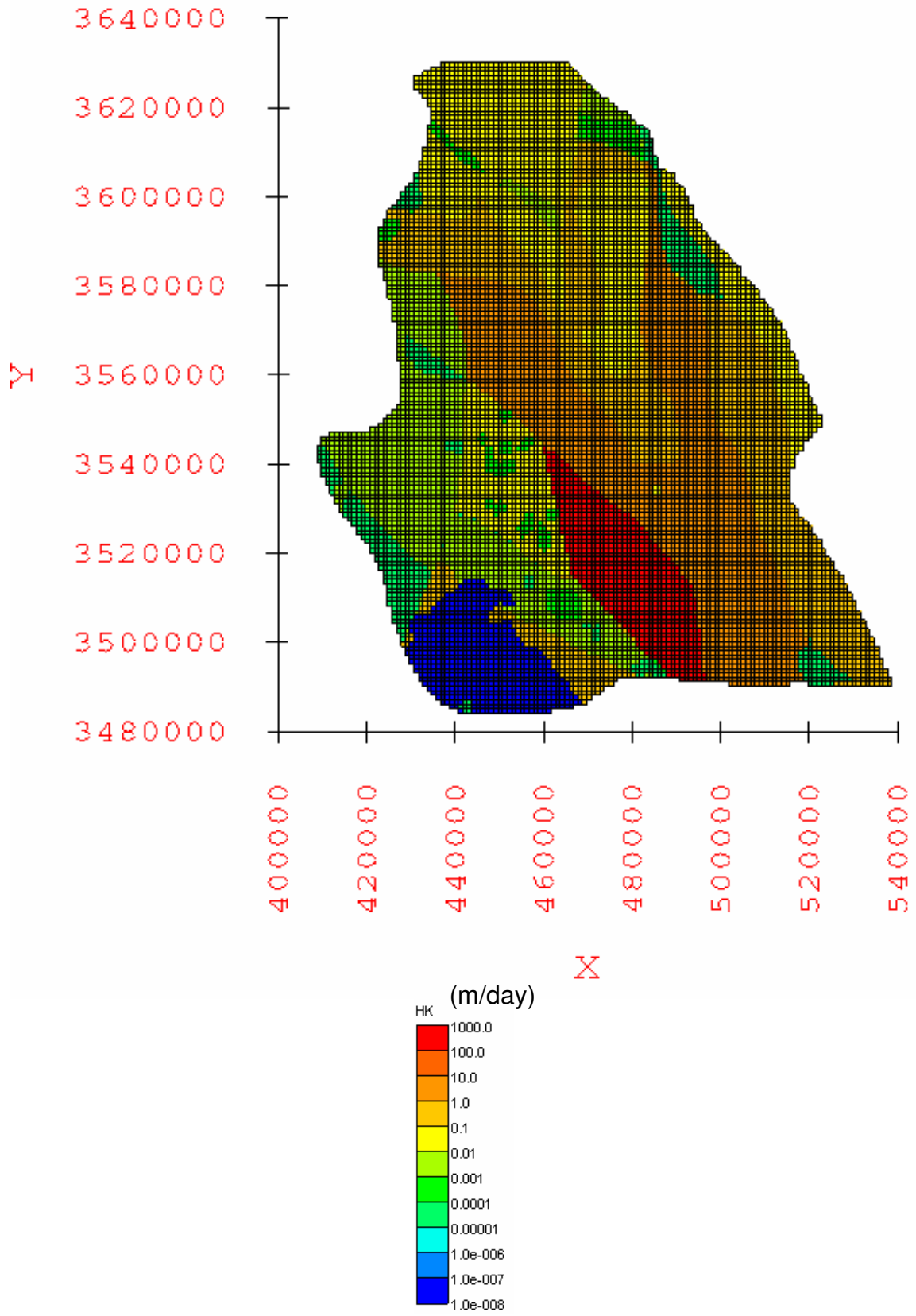
Figure A-4.64: Horizontal hydraulic conductivity [HK] distribution in layer 2 for the calibrated water-balance based average recharge scenario groundwater flow model.
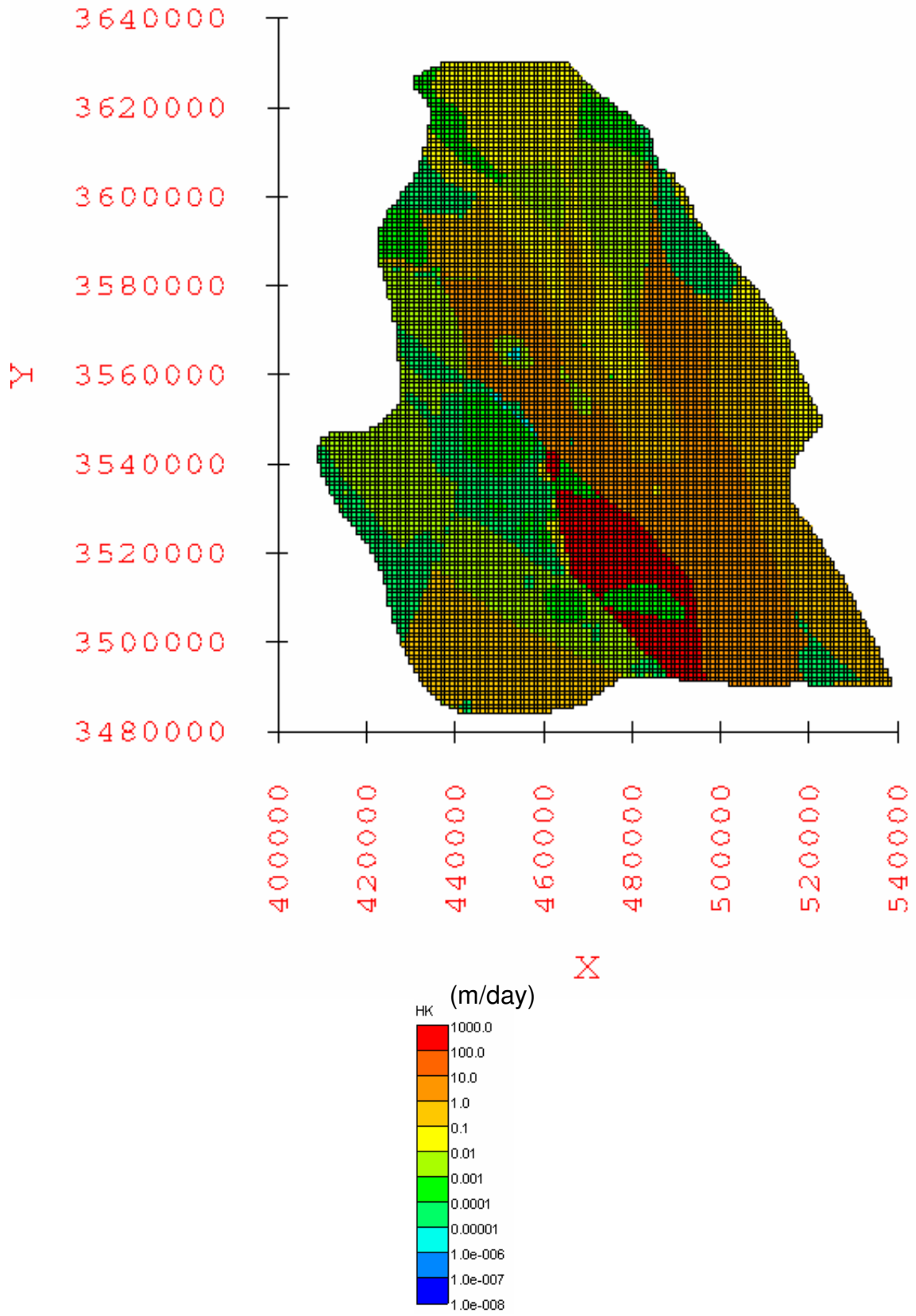
Figure A-4.65: Horizontal hydraulic conductivity [HK] distribution in layer 3 for the calibrated water-balance based average recharge scenario groundwater flow model.
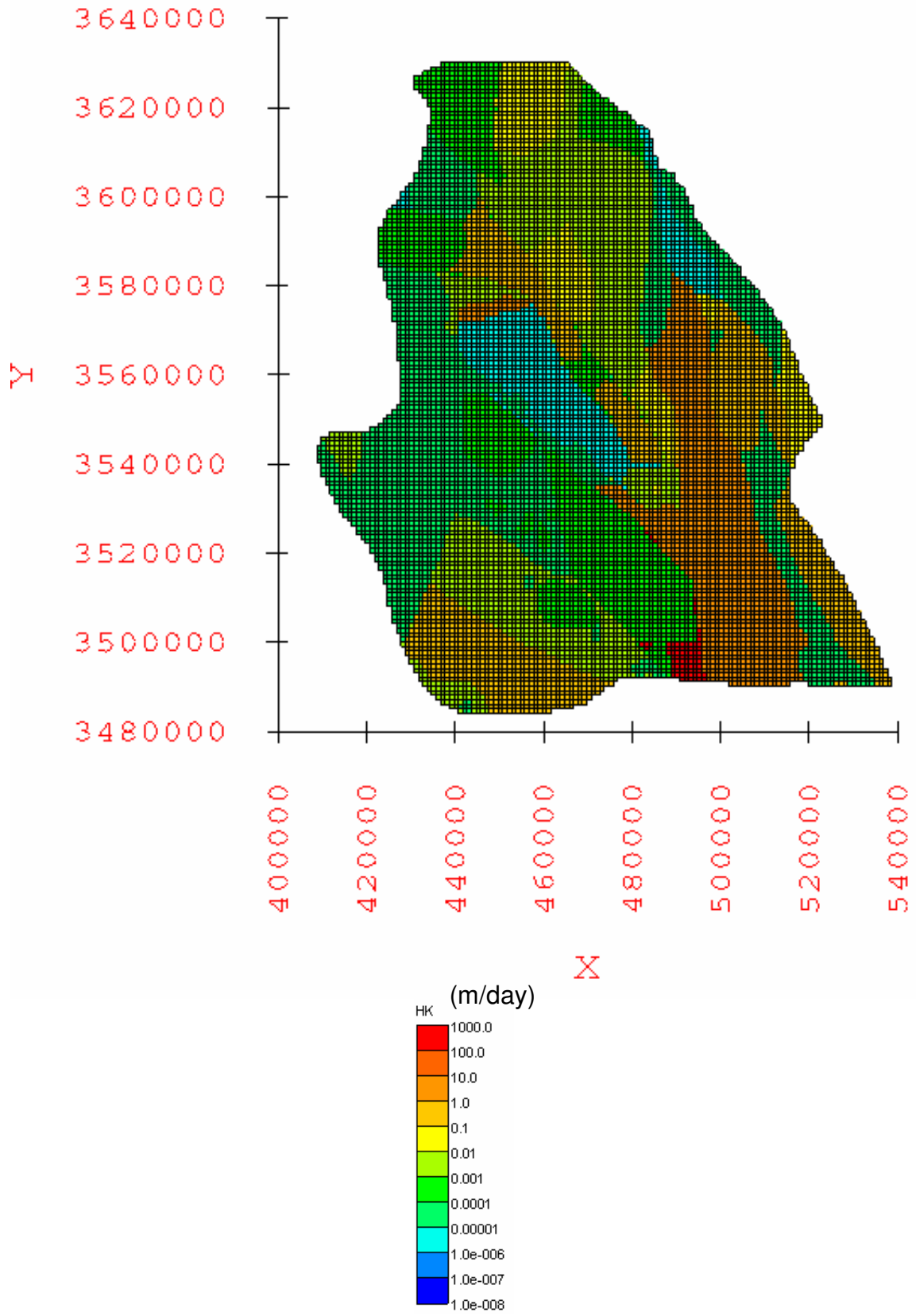
Figure A-4.66: Horizontal hydraulic conductivity [HK] distribution in layer 4 for the calibrated water-balance based average recharge scenario groundwater flow model.
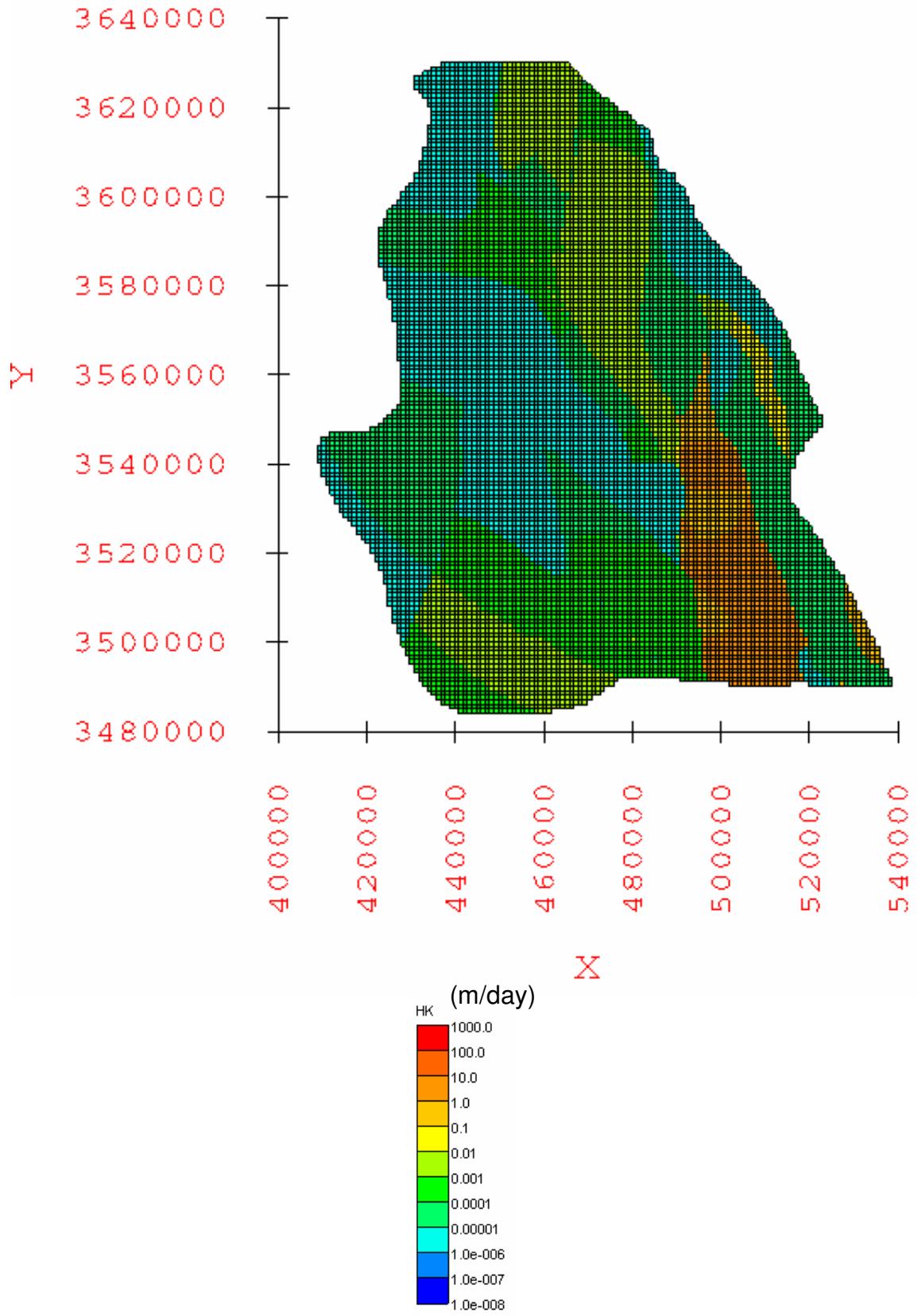
Figure A-4.67: Horizontal hydraulic conductivity [HK] distribution in layer 5 for the calibrated water-balance based average recharge scenario groundwater flow model.
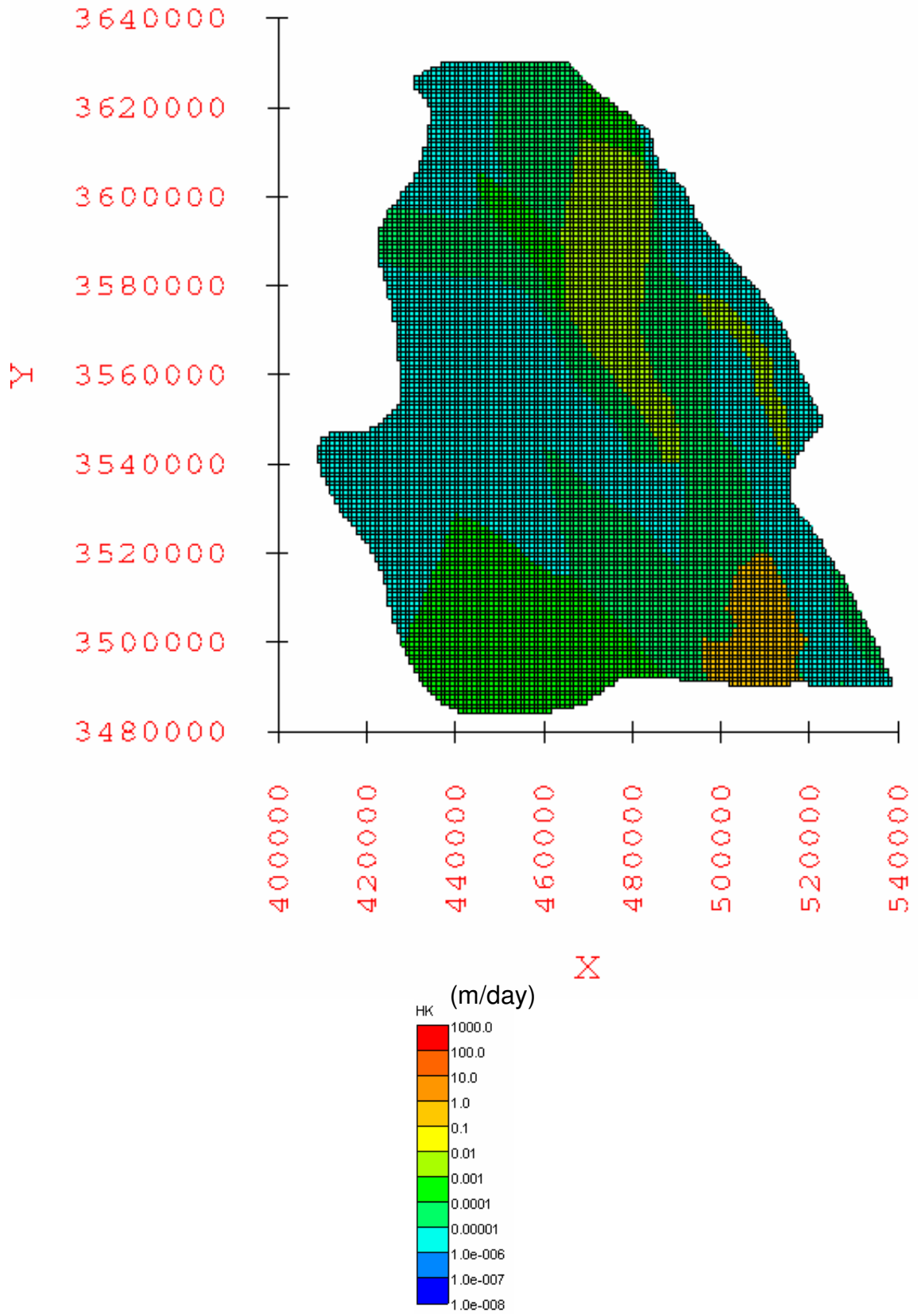
Figure A-4.68: Horizontal hydraulic conductivity [HK] distribution in layer 6 for the calibrated water-balance based average recharge scenario groundwater flow model.
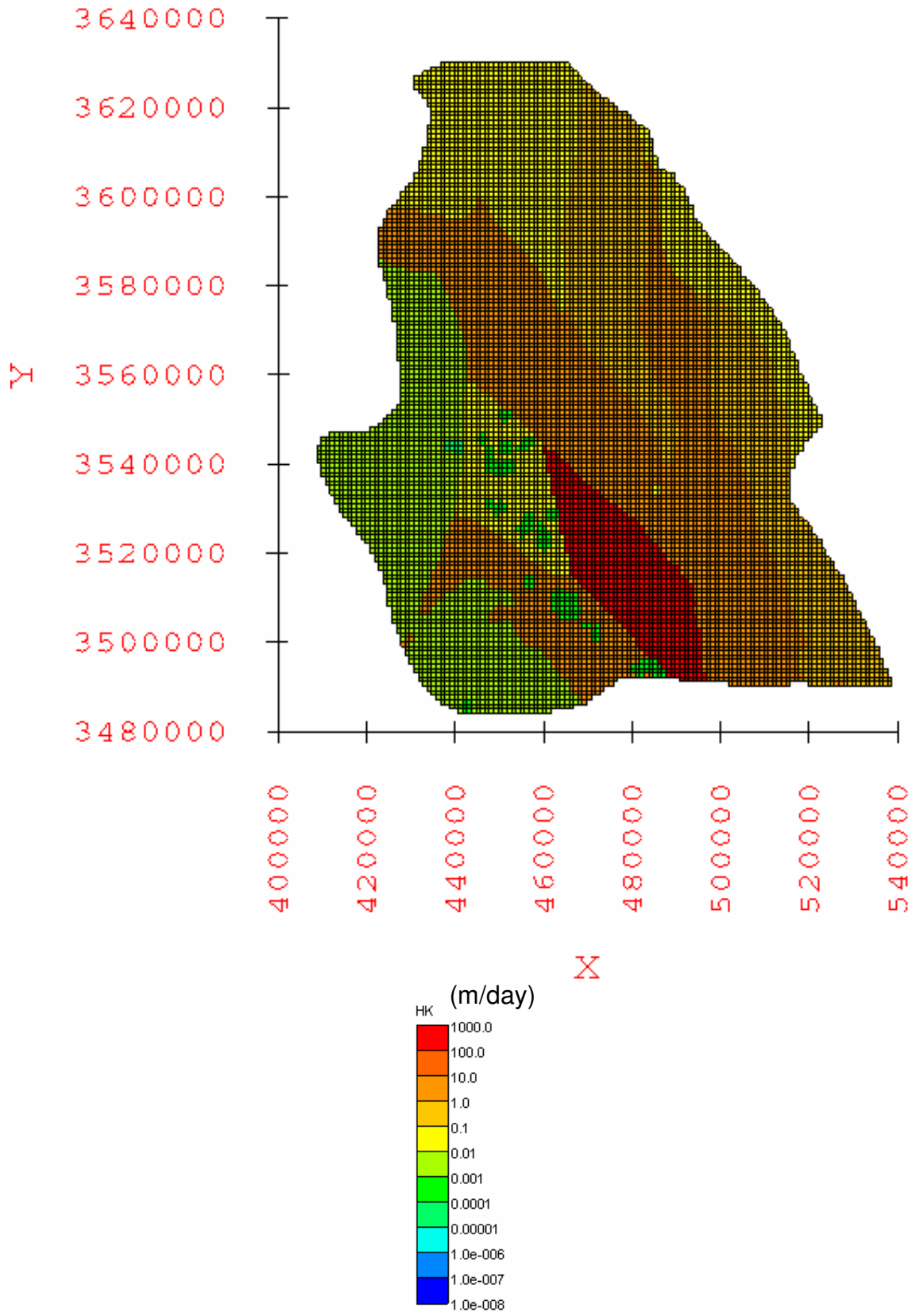
Figure A-4.69: Horizontal hydraulic conductivity [HK] distribution in layer 1 for the calibrated water-balance based maximum recharge scenario groundwater flow model.
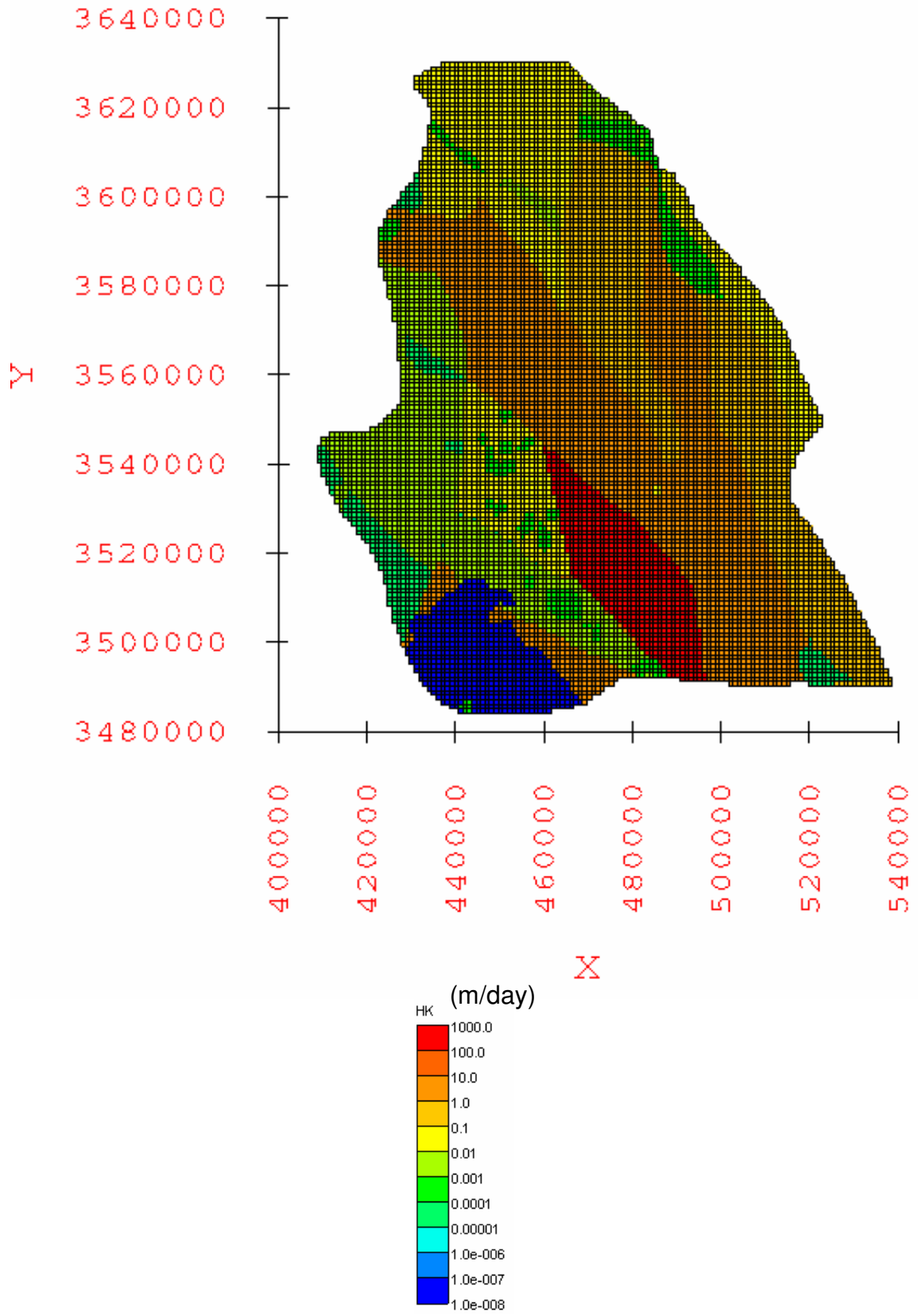
Figure A-4.70: Horizontal hydraulic conductivity [HK] distribution in layer 2 for the calibrated water-balance based maximum recharge scenario groundwater flow model.
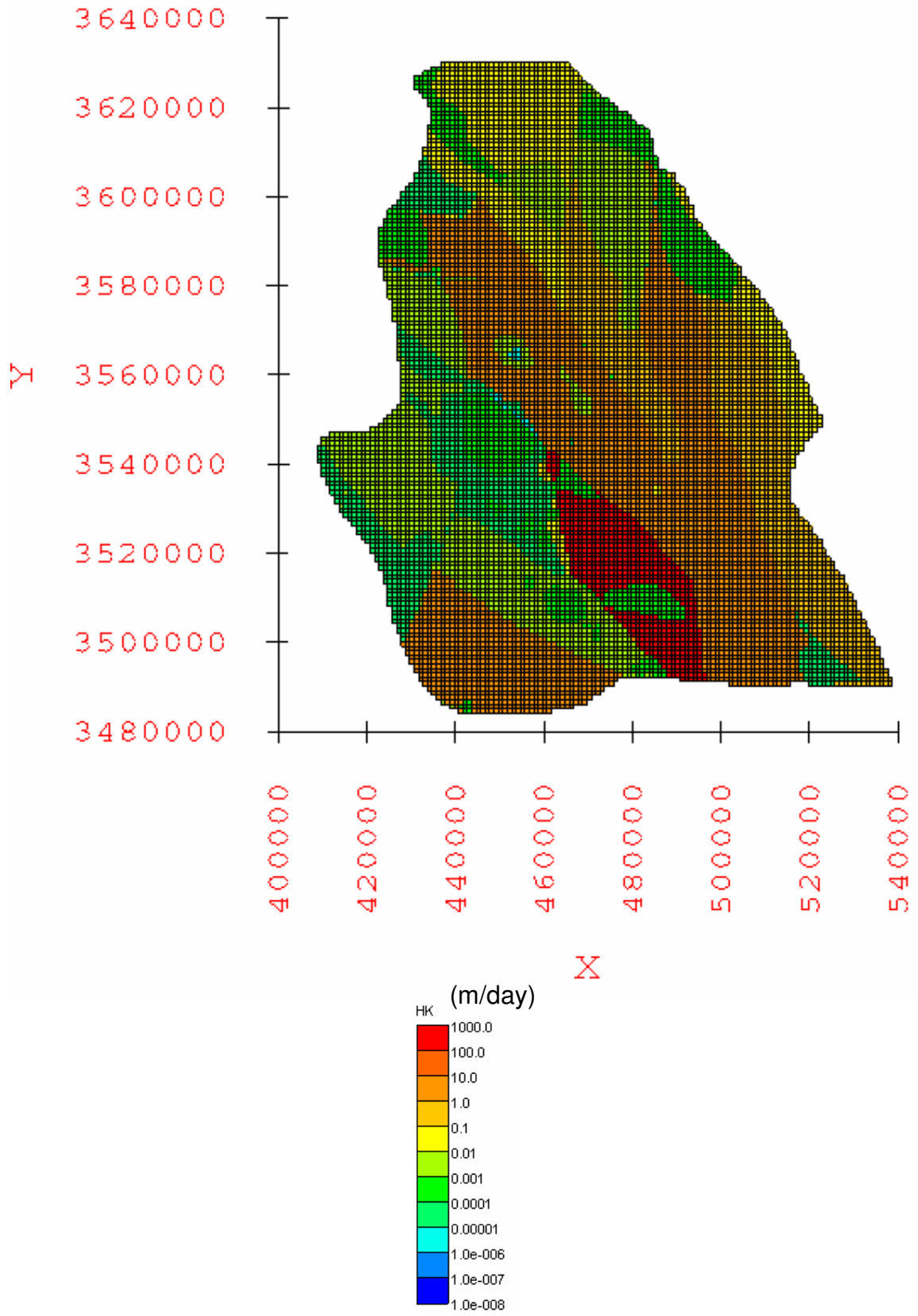
Figure A-4.71: Horizontal hydraulic conductivity [HK] distribution in layer 3 for the calibrated water-balance based maximum recharge scenario groundwater flow model.
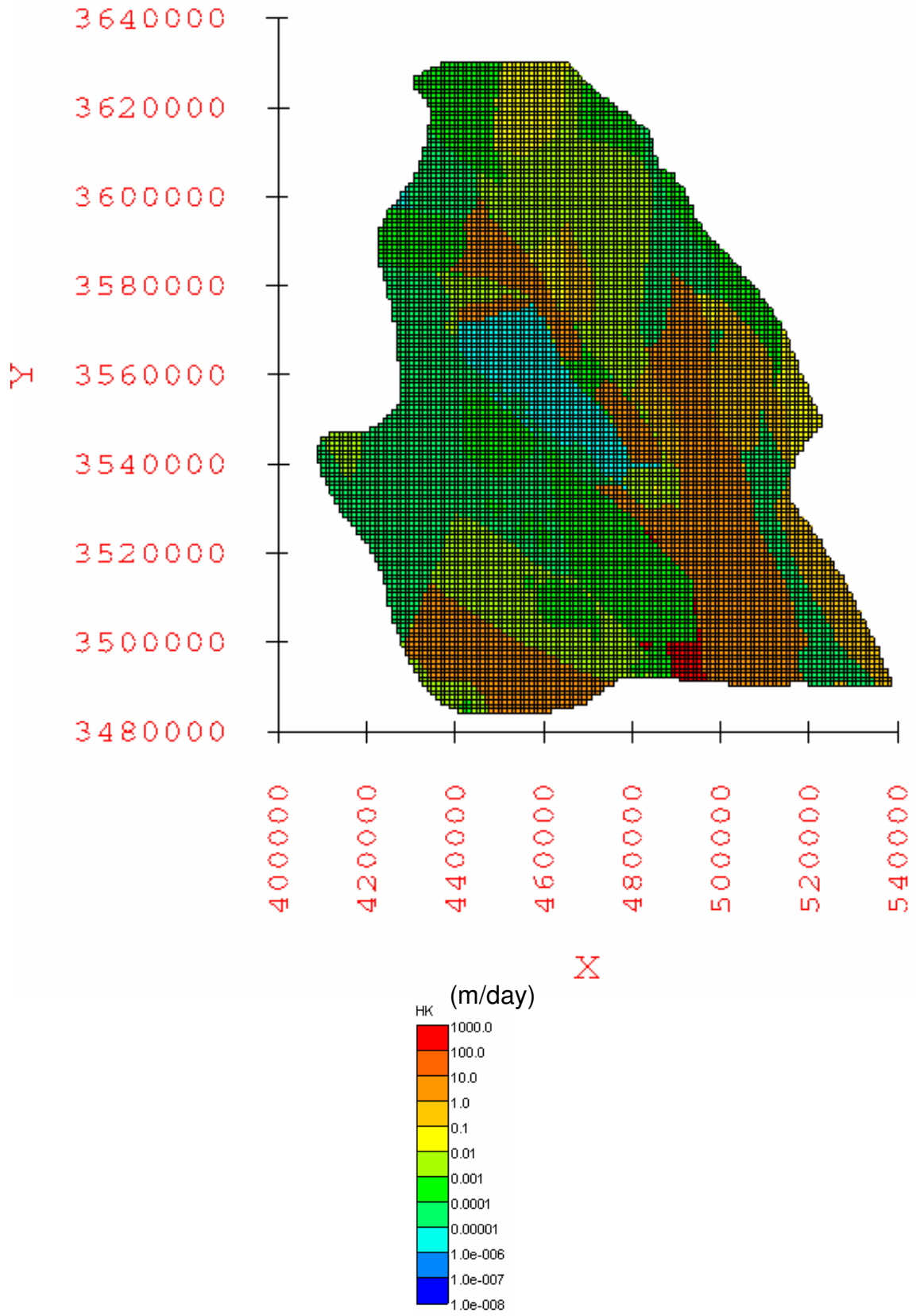
Figure A-4.72: Horizontal hydraulic conductivity [HK] distribution in layer 4 for the calibrated water-balance based maximum recharge scenario groundwater flow model.
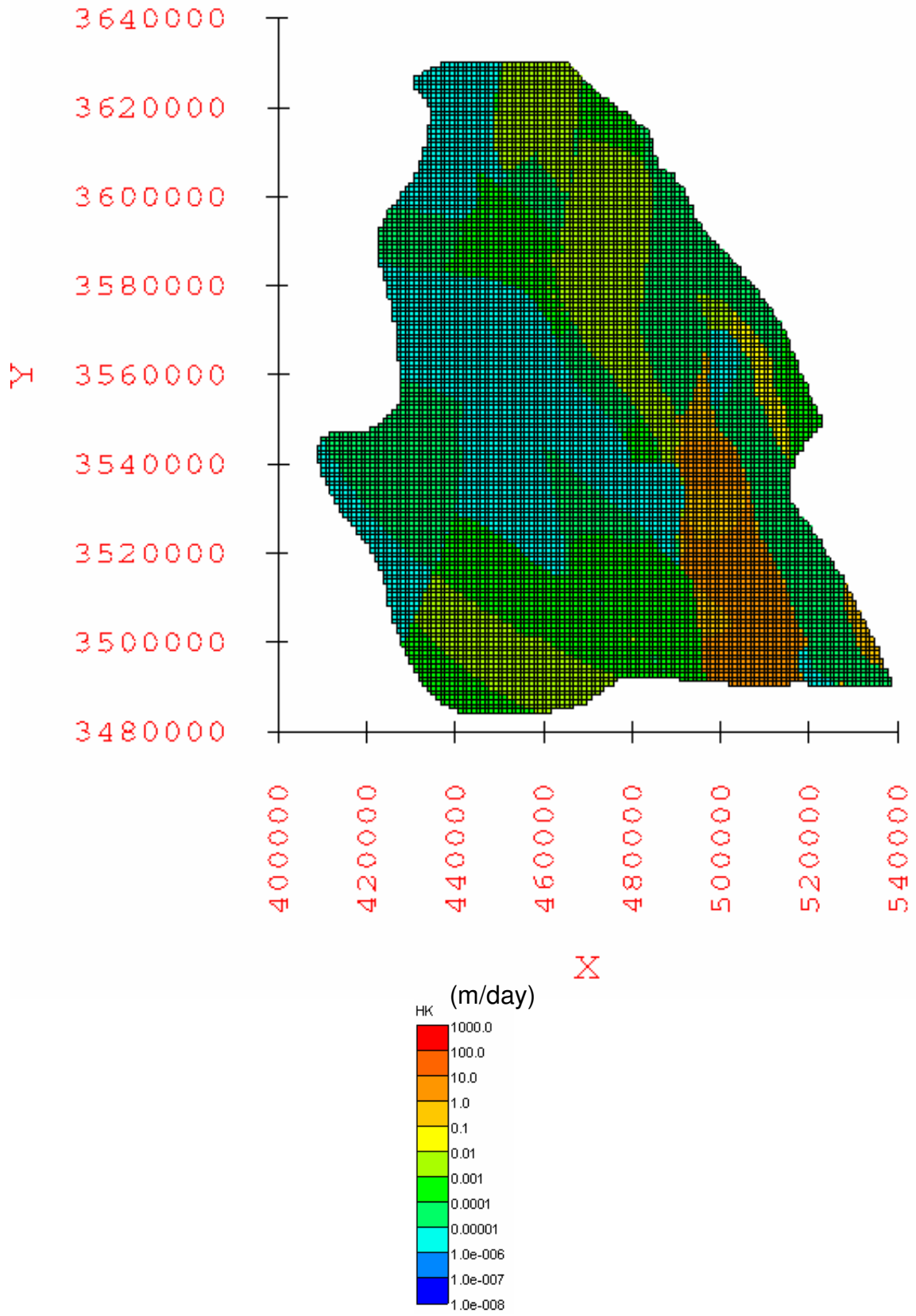
Figure A-4.73: Horizontal hydraulic conductivity [HK] distribution in layer 5 for the calibrated water-balance based maximum recharge scenario groundwater flow model.
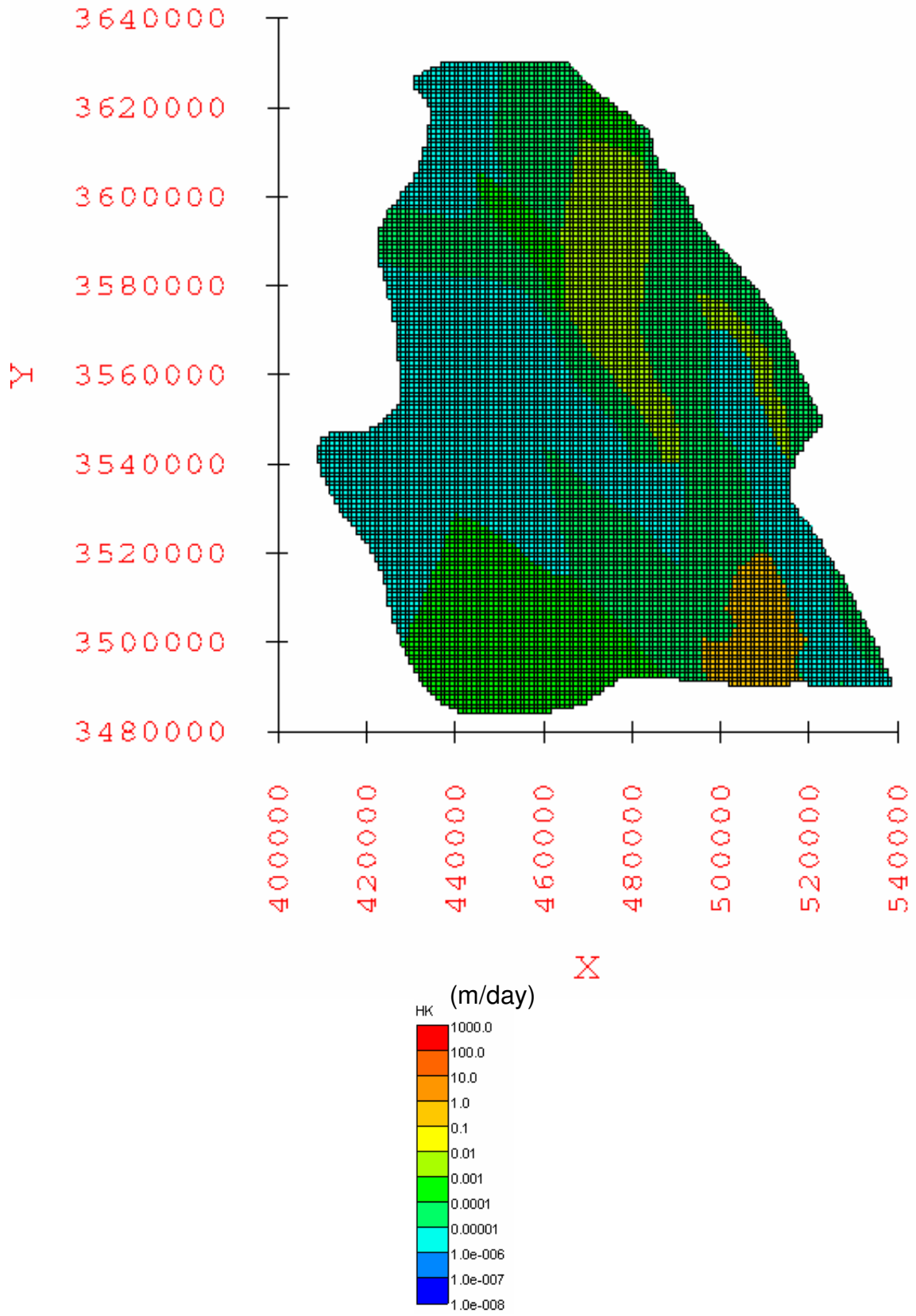
Figure A-4.74: Horizontal hydraulic conductivity [HK] distribution in layer 6 for the calibrated water-balance based maximum recharge scenario groundwater flow model.
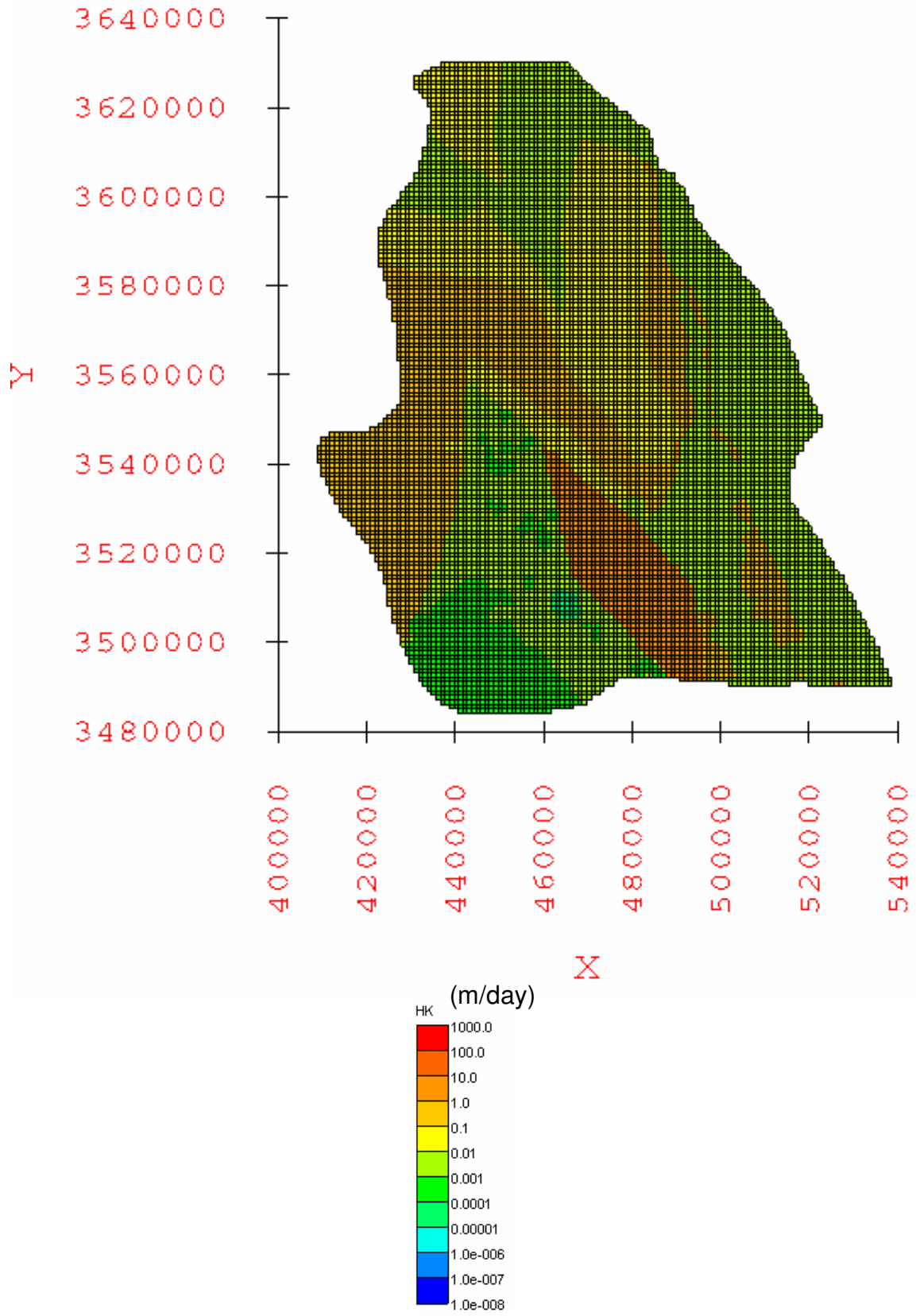
Figure A-4.75: Horizontal hydraulic conductivity [HK] distribution in layer 1 for the calibrated elevation-dependent minimum recharge scenario groundwater flow model.
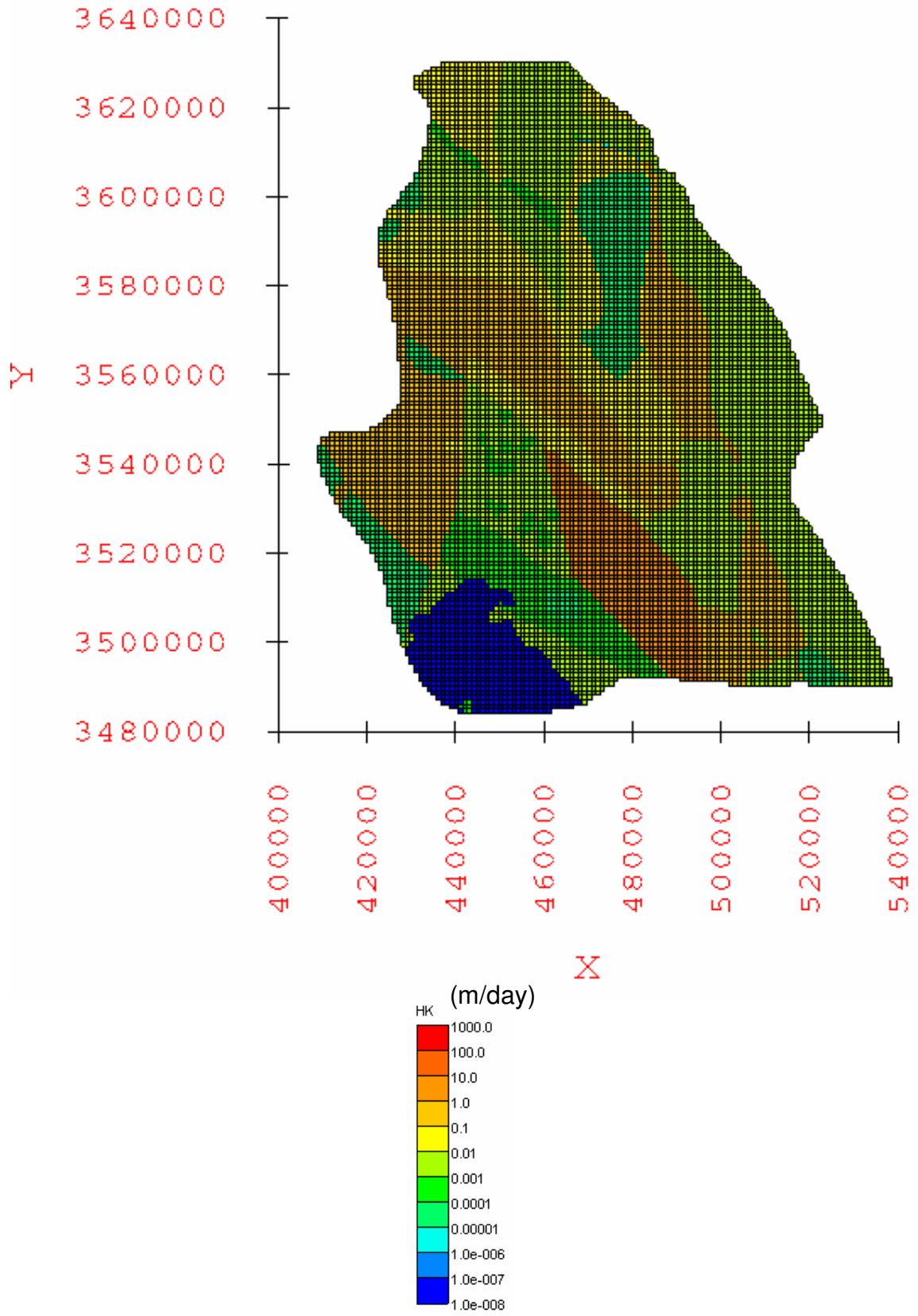
Figure A-4.76: Horizontal hydraulic conductivity [HK] distribution in layer 2 for the calibrated elevation-dependent minimum recharge scenario groundwater flow model.
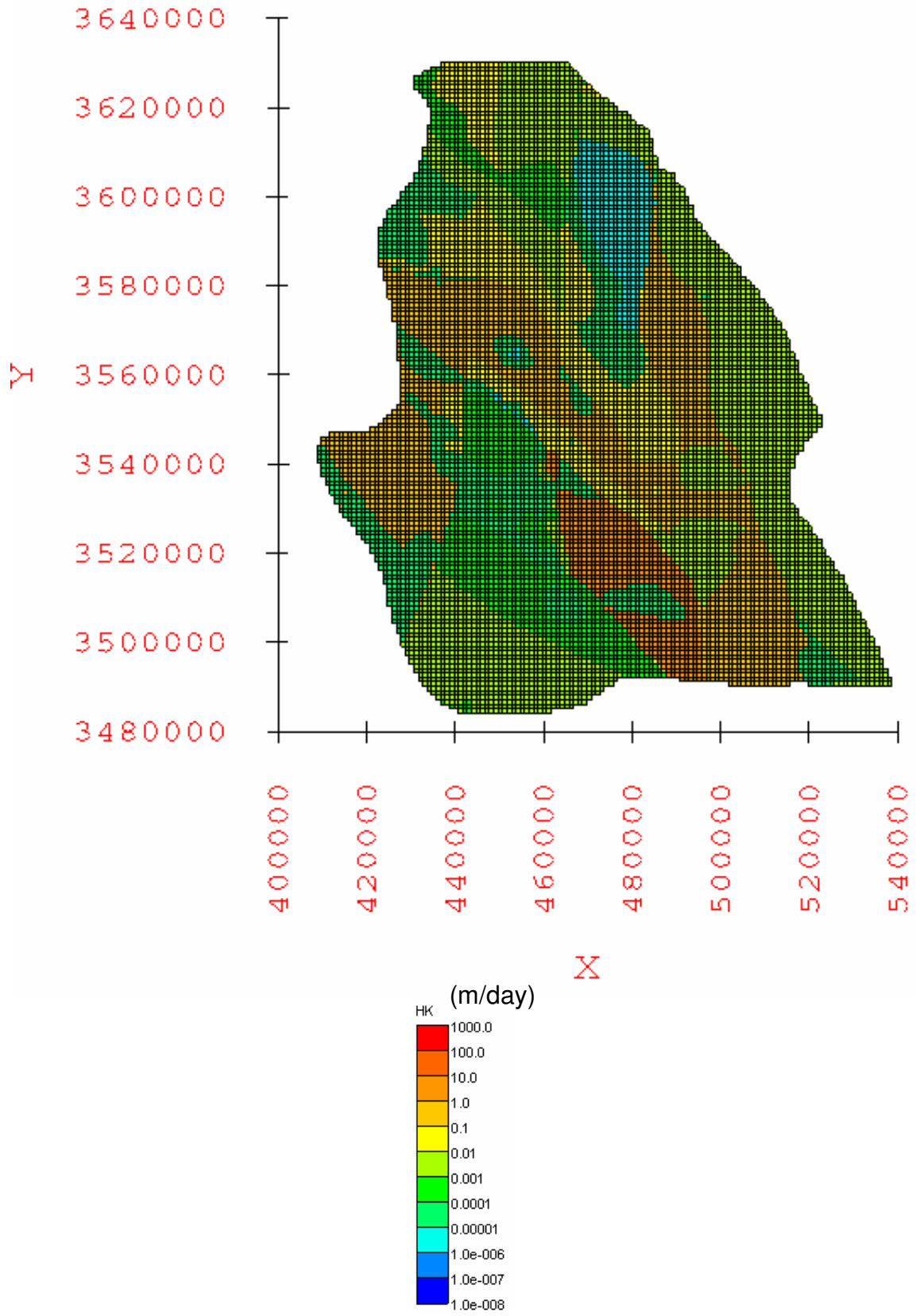
Figure A-4.77: Horizontal hydraulic conductivity [HK] distribution in layer 3 for the calibrated elevation-dependent minimum recharge scenario groundwater flow model.

654
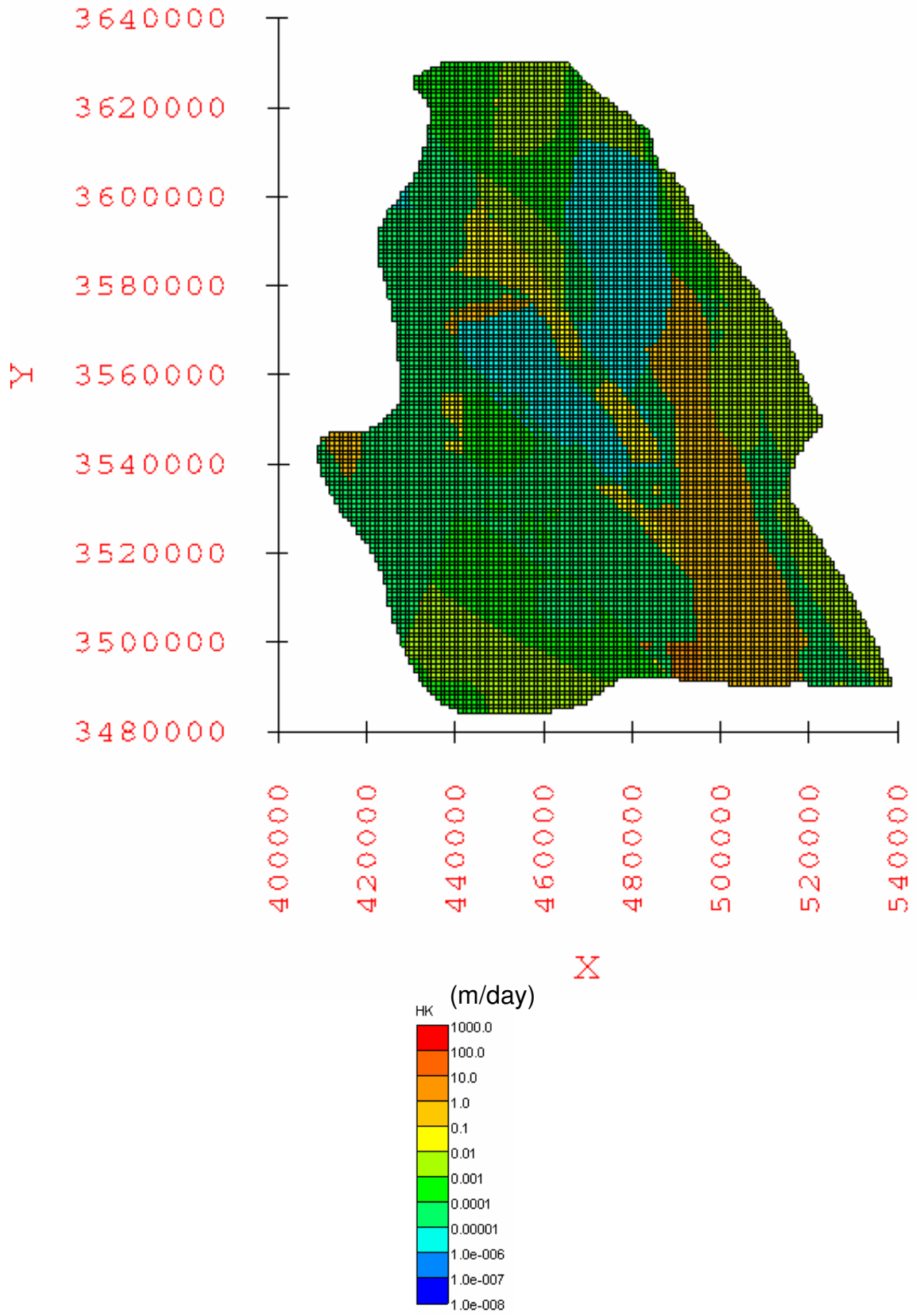
Figure A-4.78: Horizontal hydraulic conductivity [HK] distribution in layer 4 for the calibrated elevation-dependent minimum recharge scenario groundwater flow model.
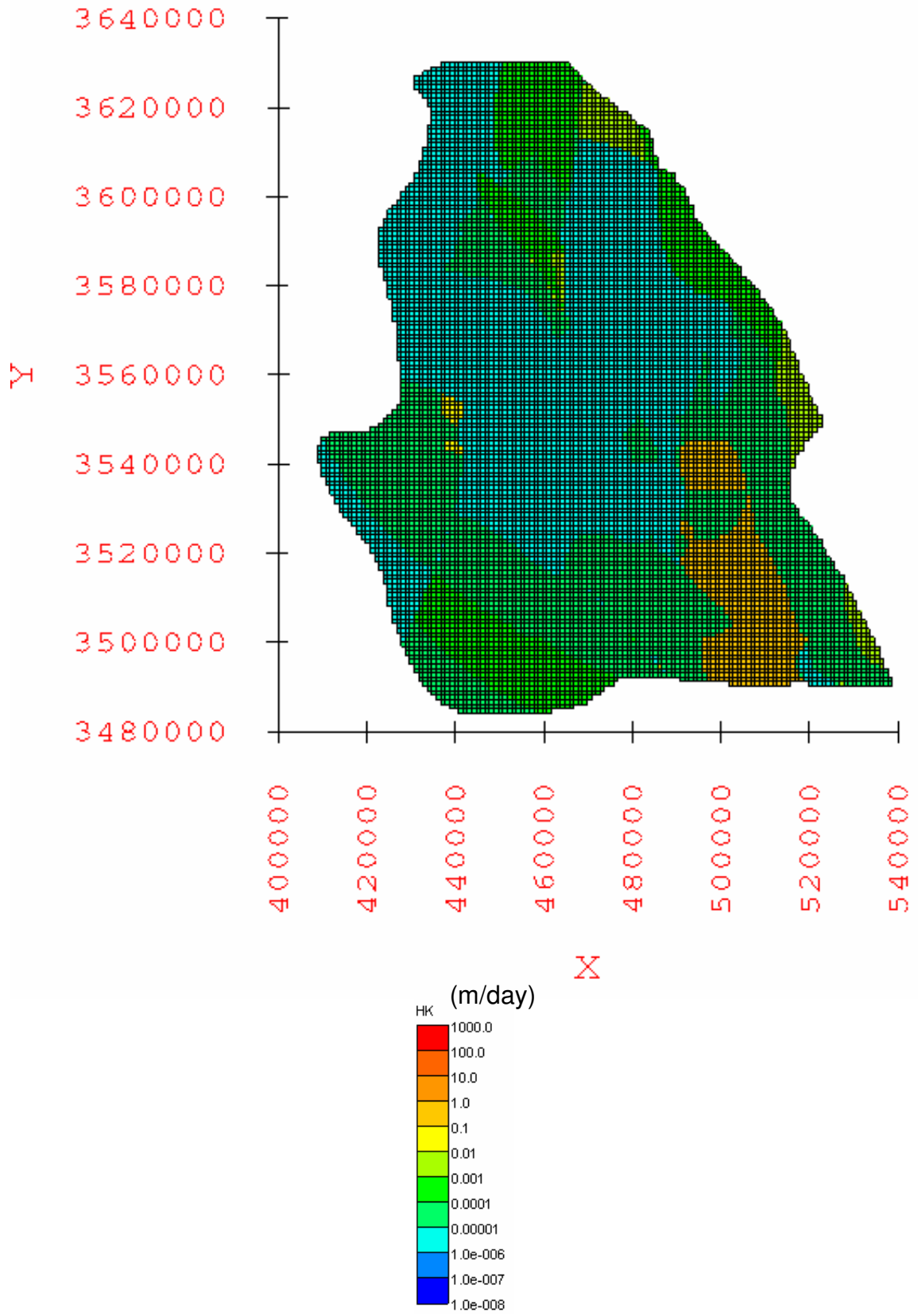
Figure A-4.79: Horizontal hydraulic conductivity [HK] distribution in layer 5 for the calibrated elevation-dependent minimum recharge scenario groundwater flow model.
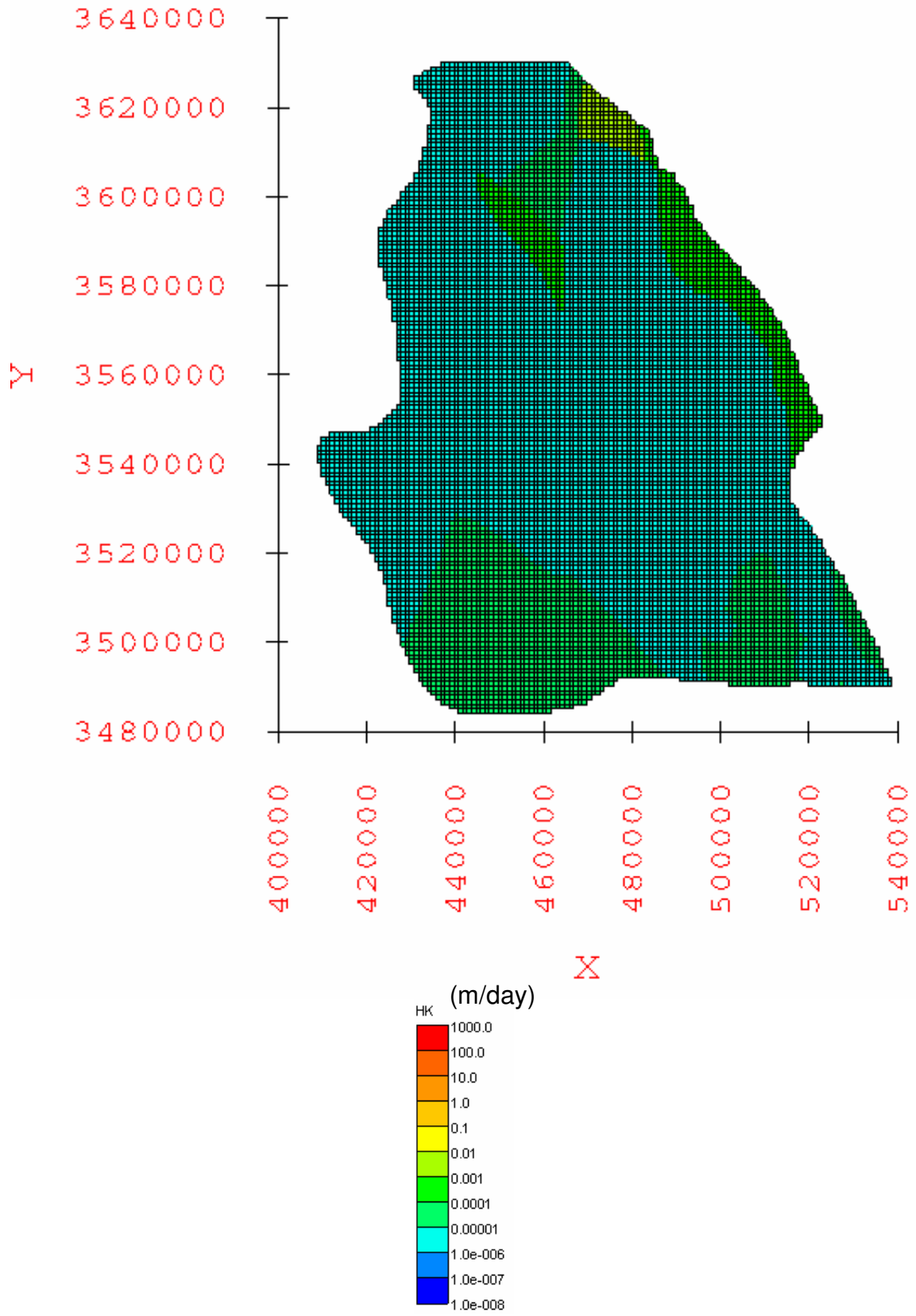
Figure A-4.80: Horizontal hydraulic conductivity [HK] distribution in layer 6 for the calibrated elevation-dependent minimum recharge scenario groundwater flow model.

Figure A-4.81: Horizontal hydraulic conductivity [HK] distribution in layer 1 for the calibrated elevation-dependent average recharge scenario groundwater flow model.

658
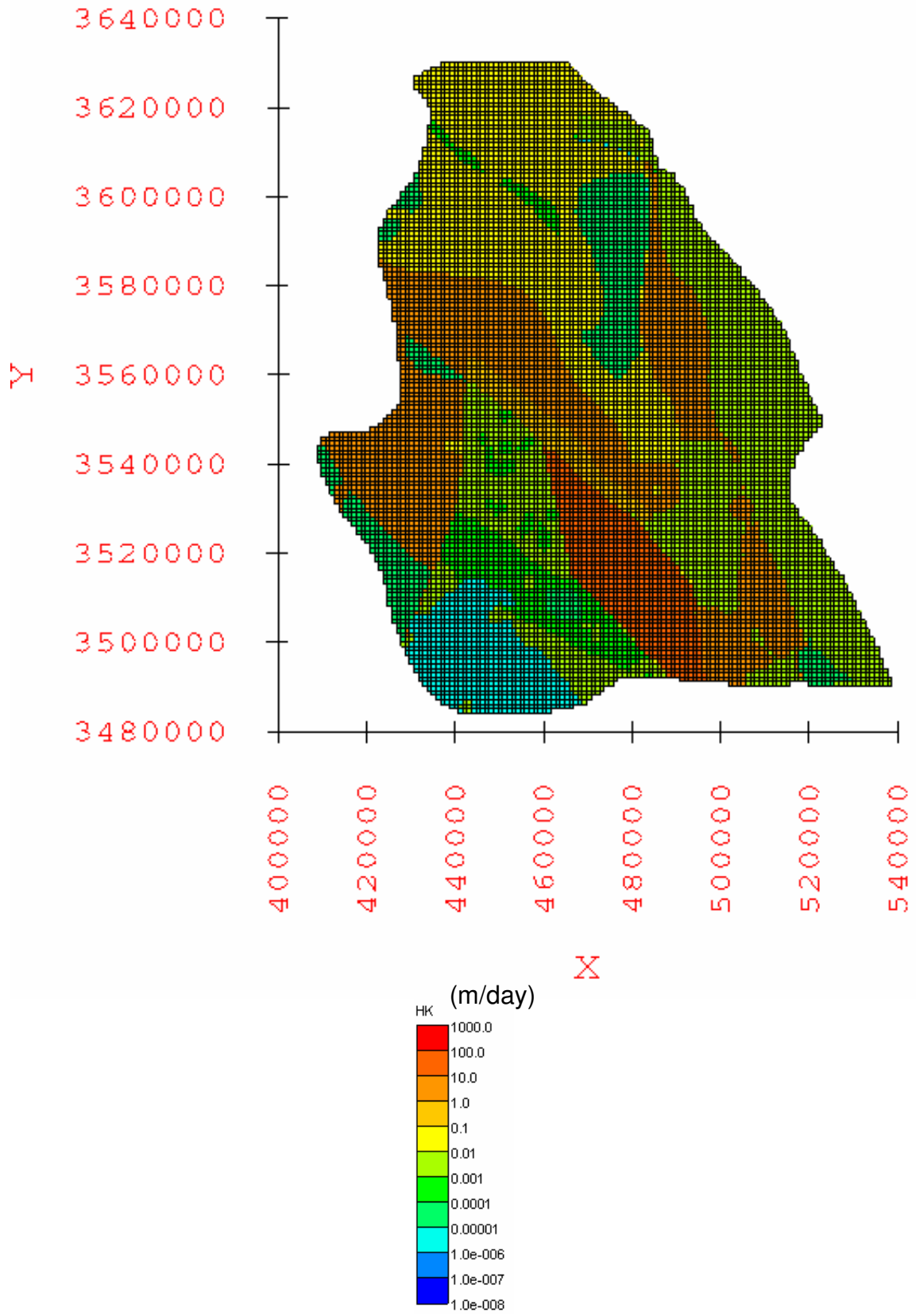
Figure A-4.82: Horizontal hydraulic conductivity [HK] distribution in layer 2 for the calibrated elevation-dependent average recharge scenario groundwater flow model.
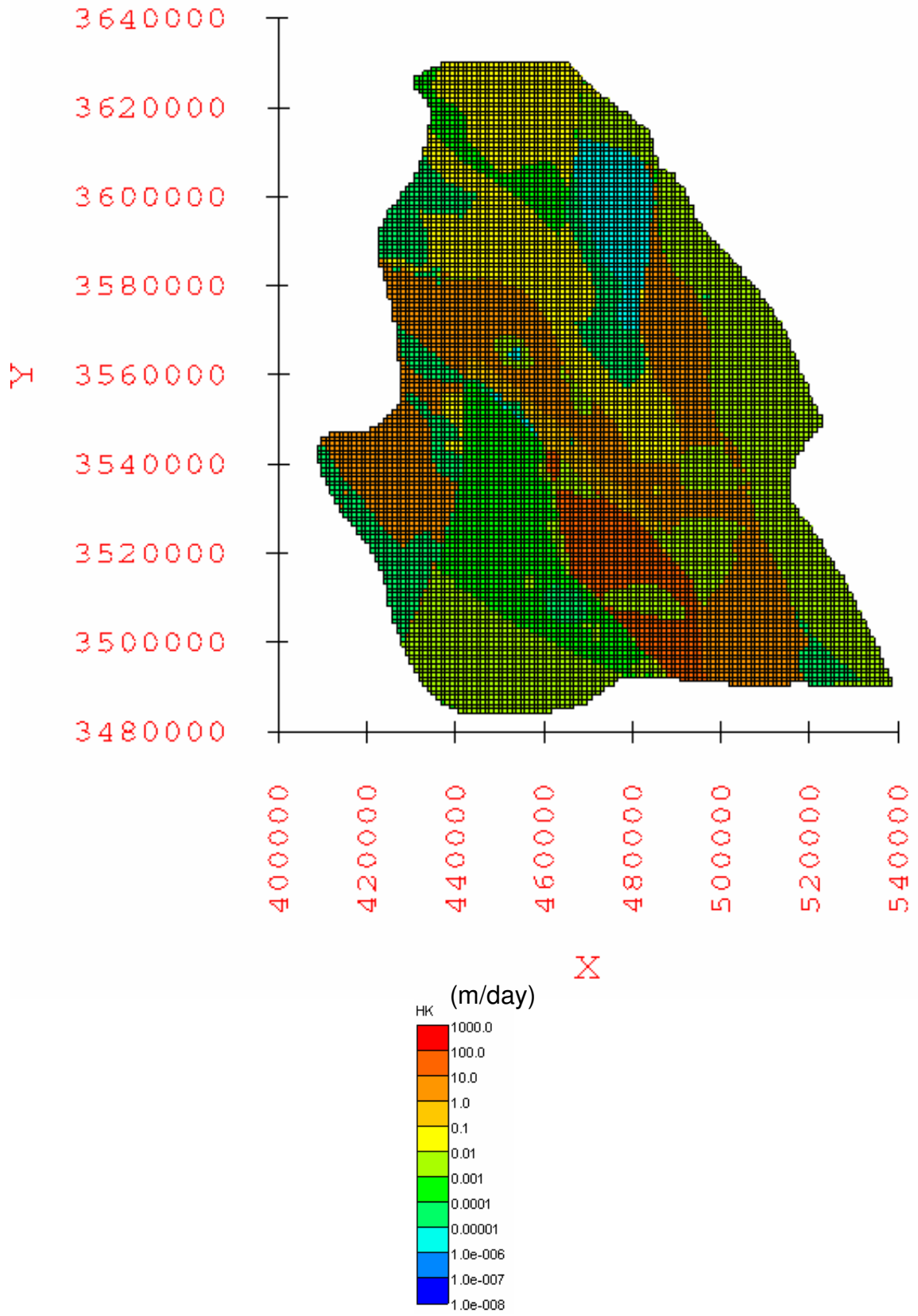
Figure A-4.83: Horizontal hydraulic conductivity [HK] distribution in layer 3 for the calibrated elevation-dependent average recharge scenario groundwater flow model.
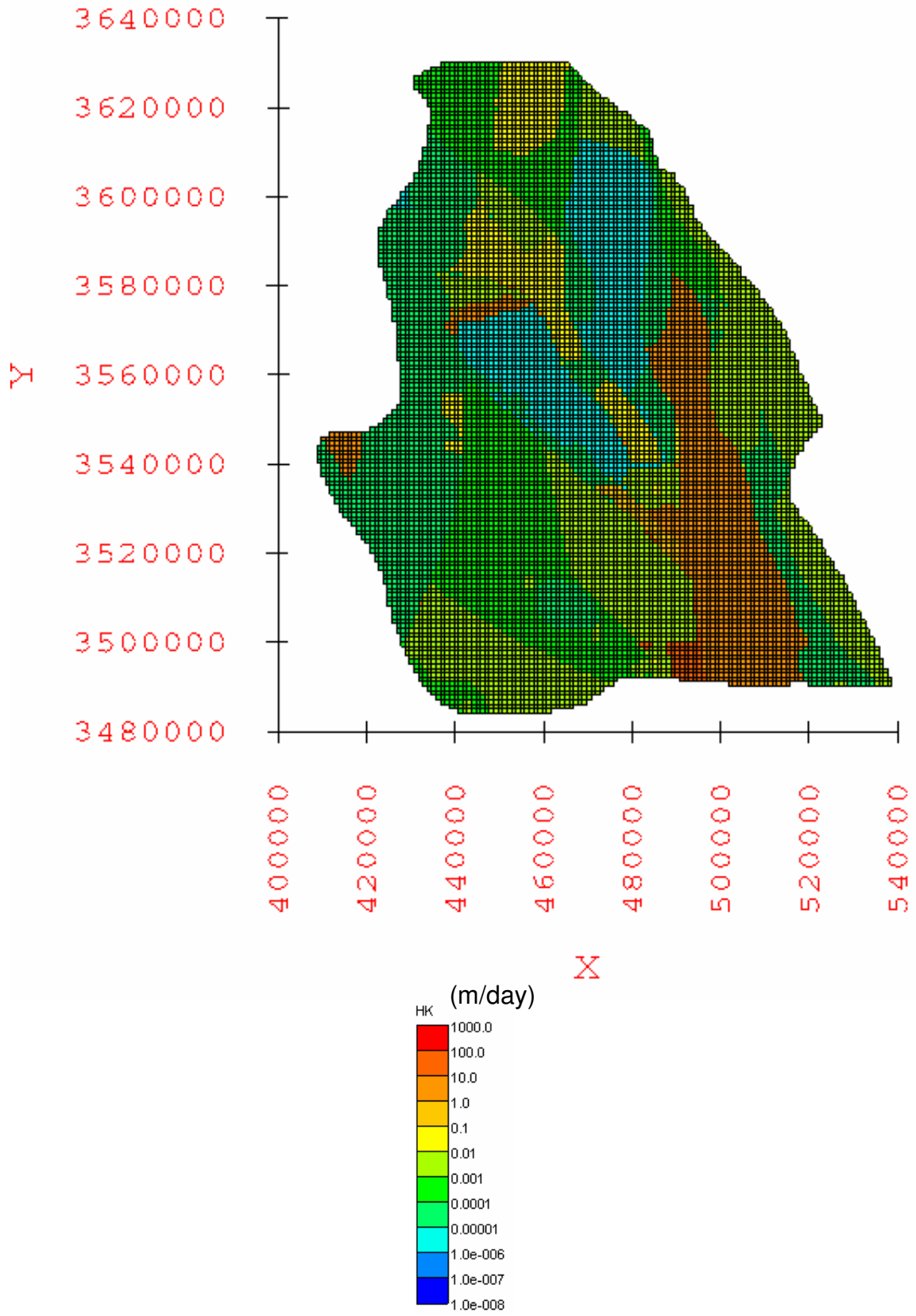
Figure A-4.84: Horizontal hydraulic conductivity [HK] distribution in layer 4 for the calibrated elevation-dependent average recharge scenario groundwater flow model.
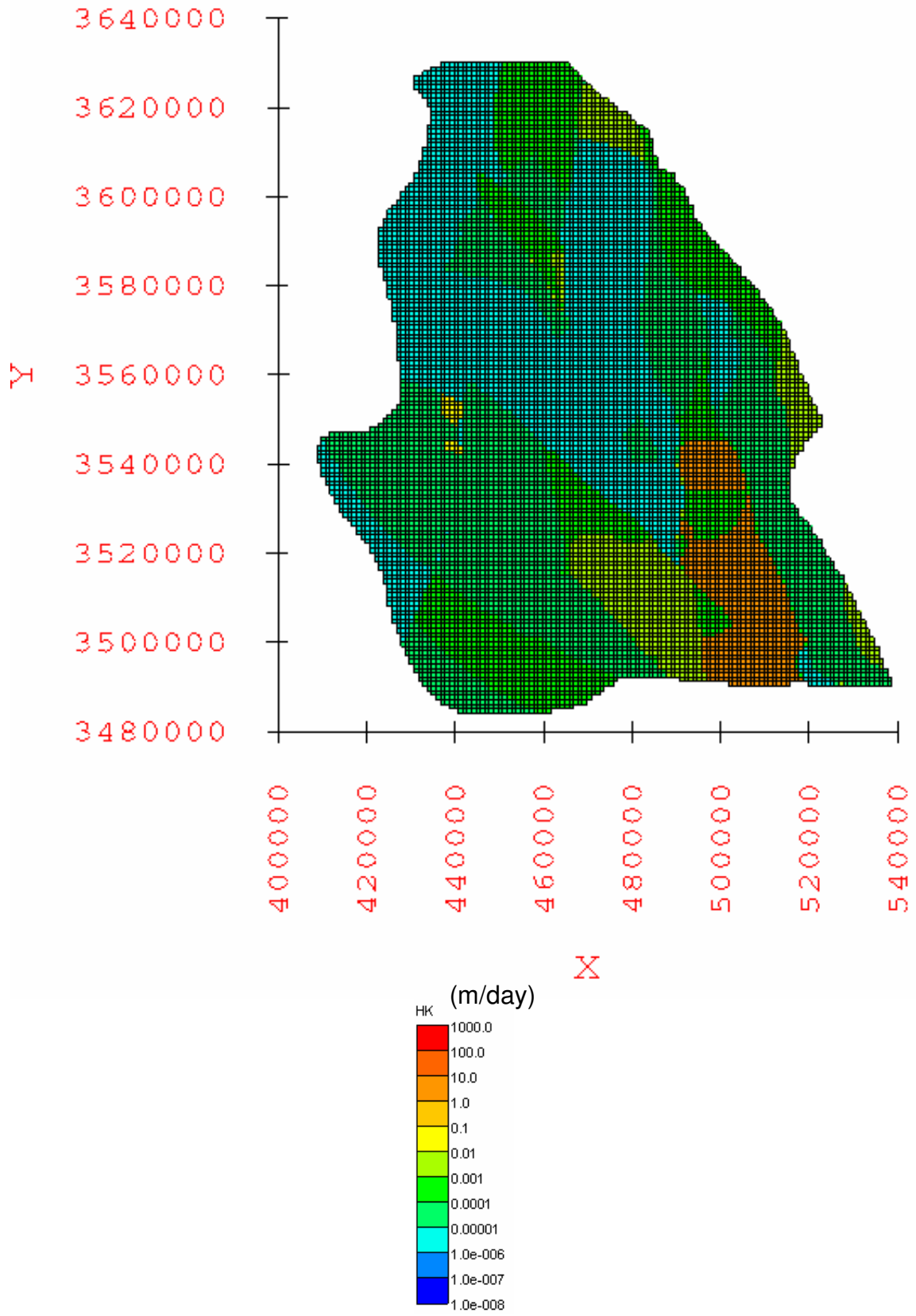
Figure A-4.85: Horizontal hydraulic conductivity [HK] distribution in layer 5 for the calibrated elevation-dependent average recharge scenario groundwater flow model.
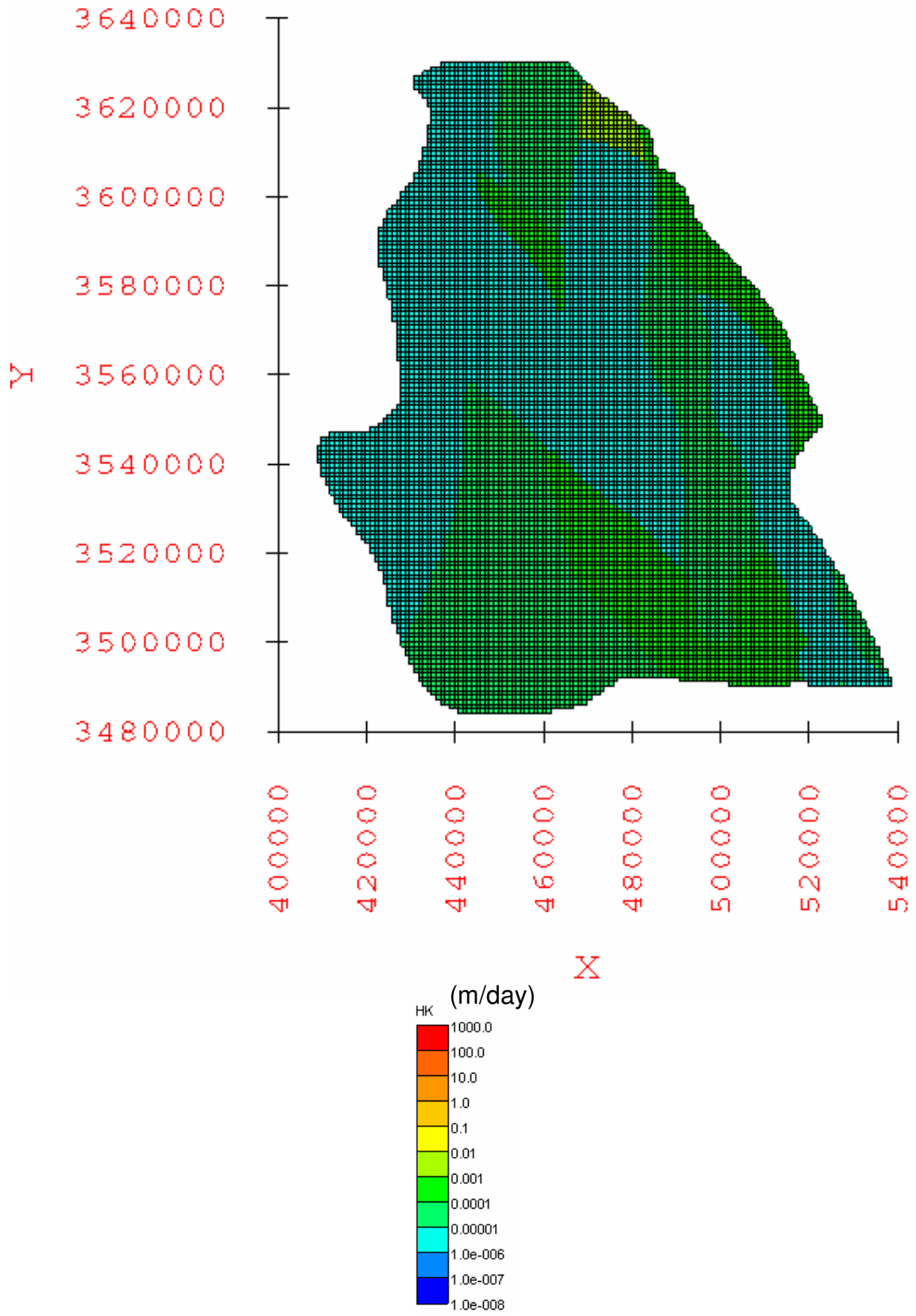
Figure A-4.86: Horizontal hydraulic conductivity [HK] distribution in layer 6 for the calibrated elevation-dependent average recharge scenario groundwater flow model.
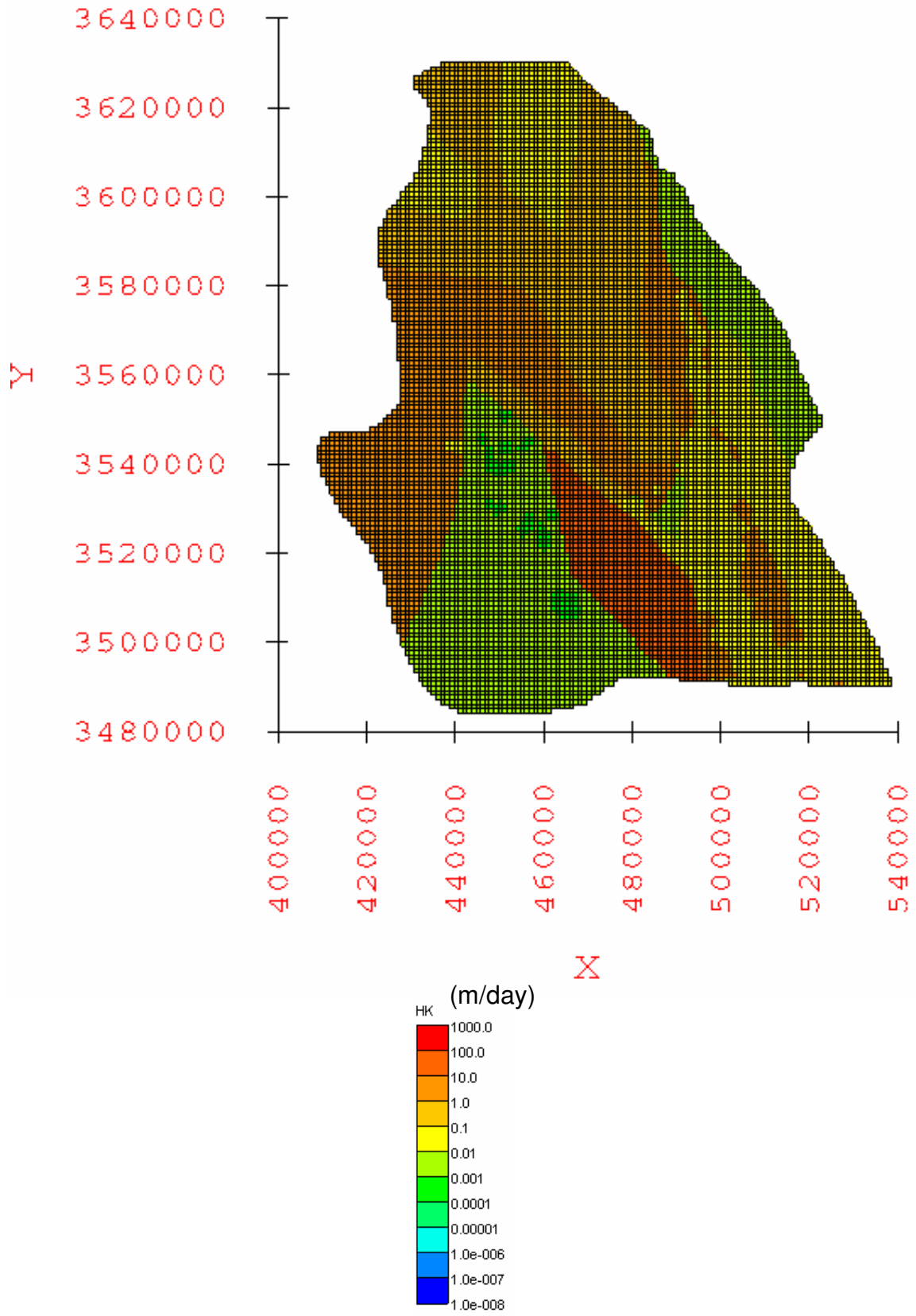
Figure A-4.87: Horizontal hydraulic conductivity [HK] distribution in layer 1 for the calibrated elevation-dependent maximum recharge scenario groundwater flow model.
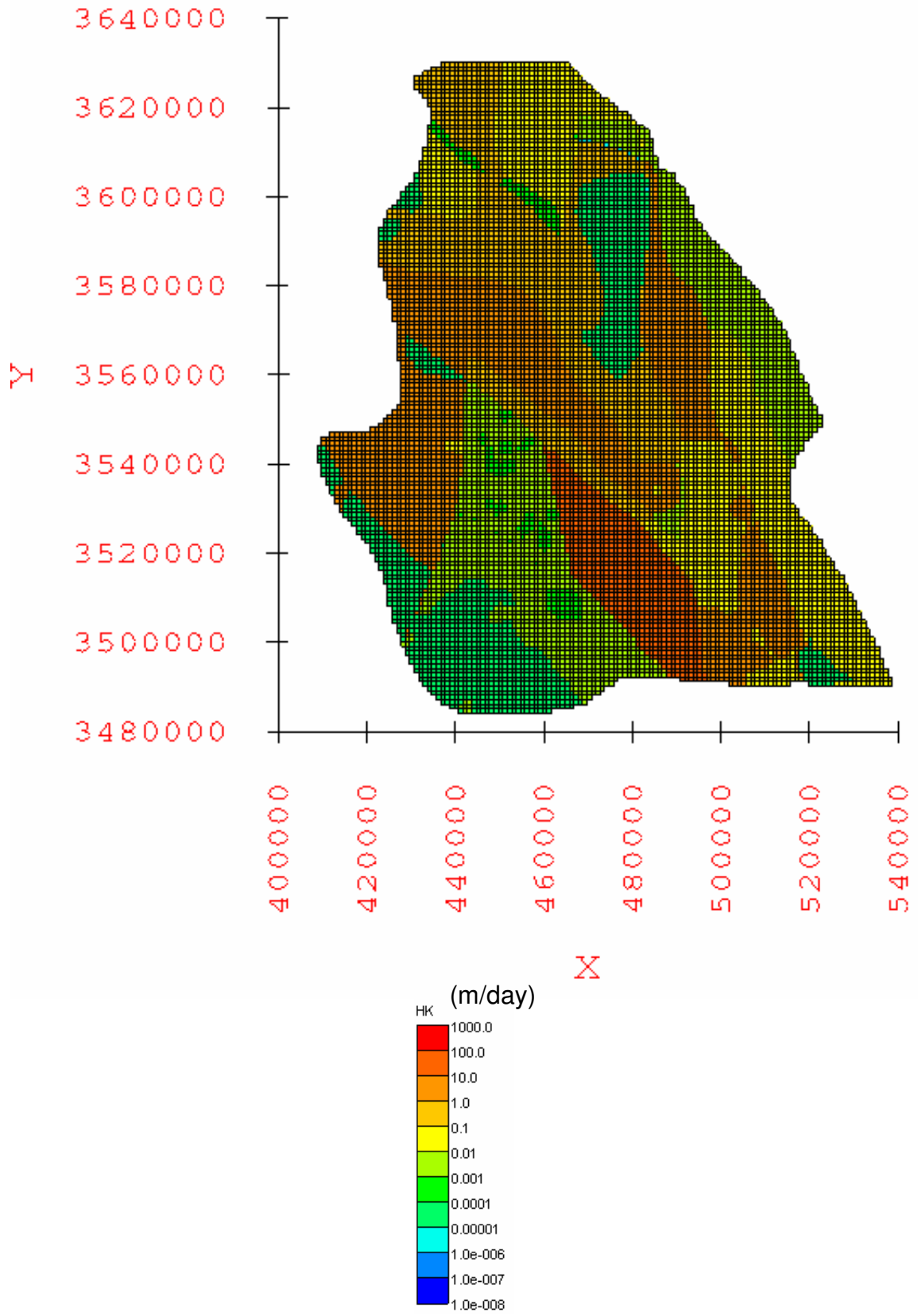
Figure A-4.88: Horizontal hydraulic conductivity [HK] distribution in layer 2 for the calibrated elevation-dependent maximum recharge scenario groundwater flow model.
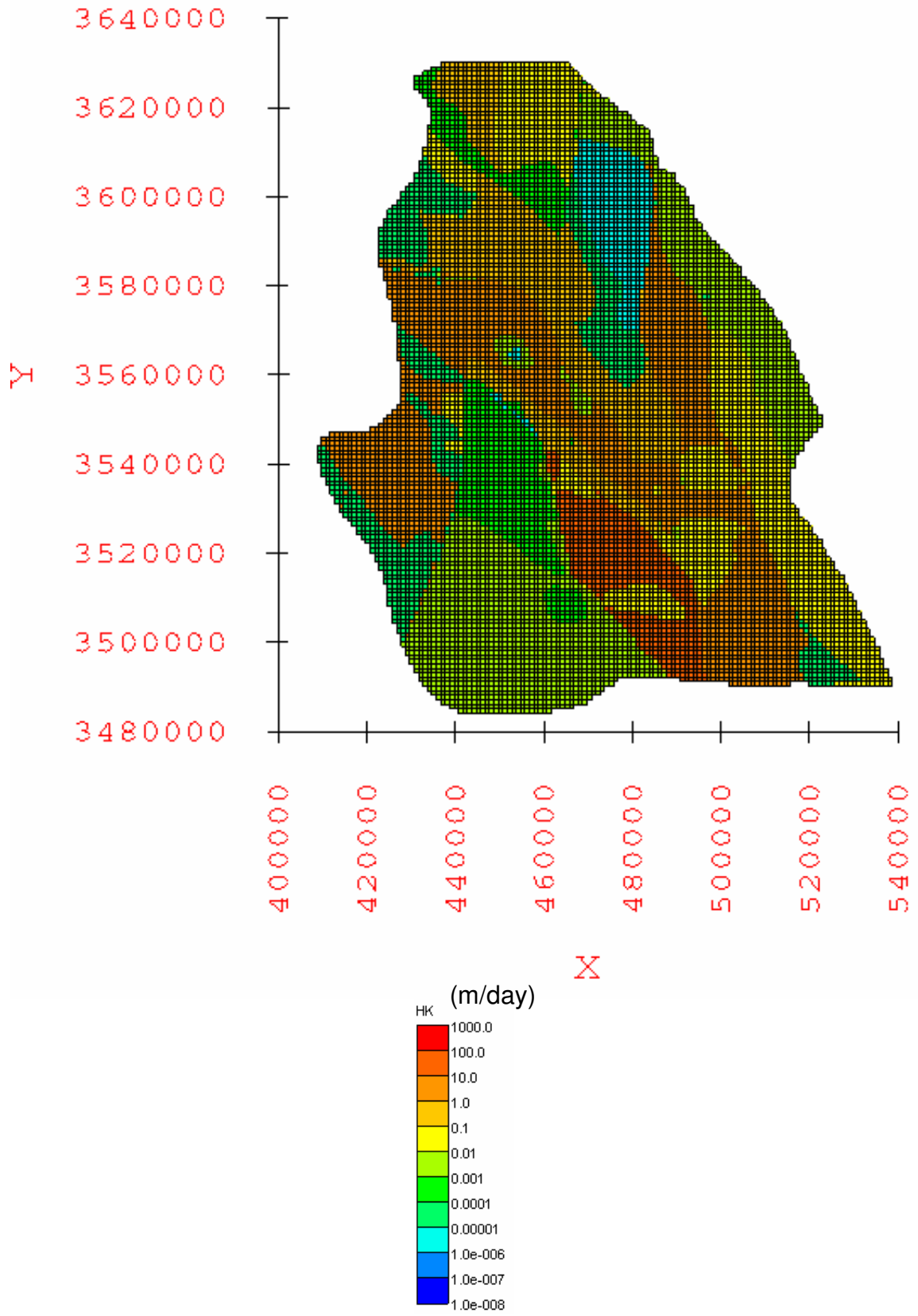
Figure A-4.89: Horizontal hydraulic conductivity [HK] distribution in layer 3 for the calibrated elevation-dependent maximum recharge scenario groundwater flow model.
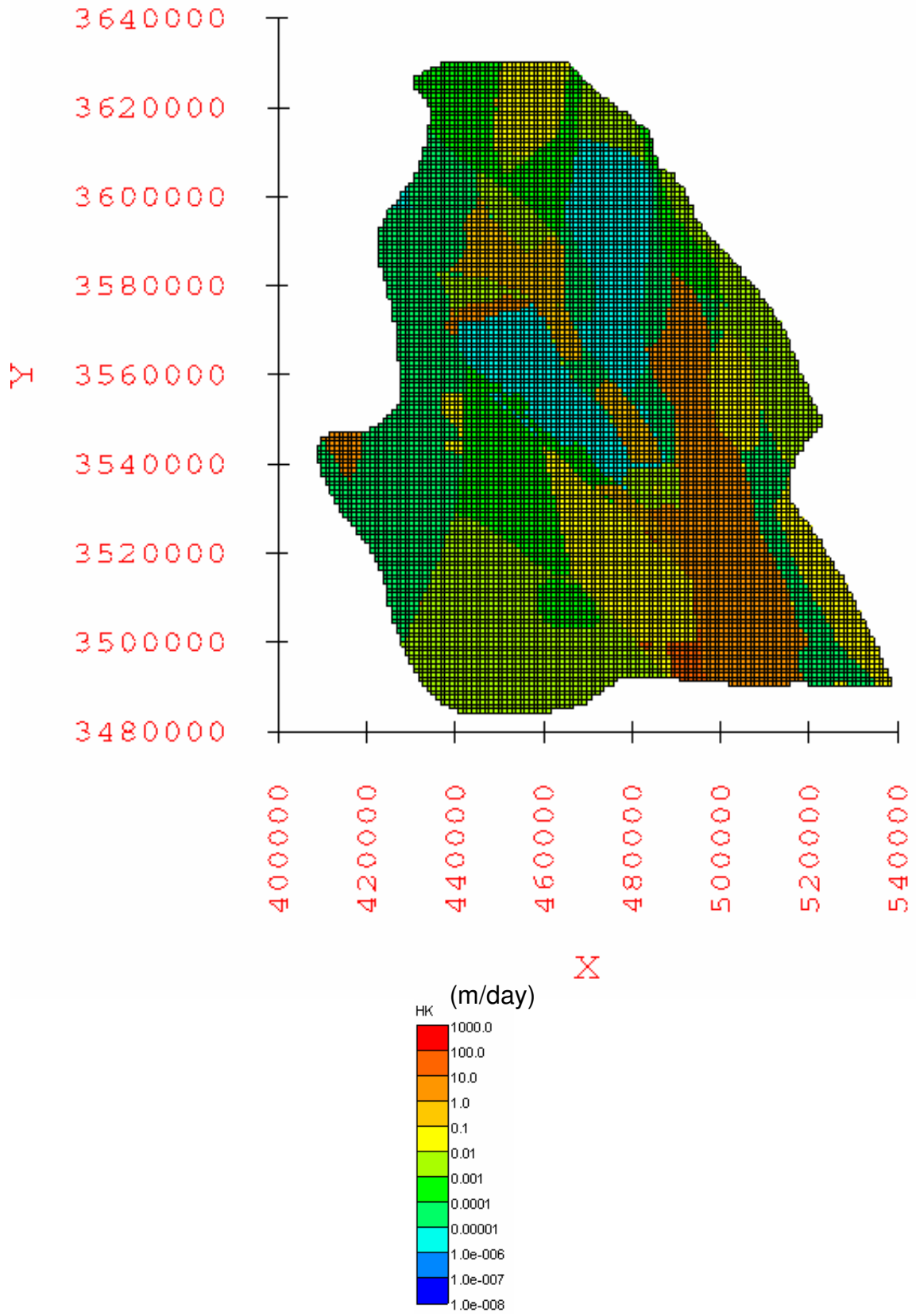
Figure A-4.90: Horizontal hydraulic conductivity [HK] distribution in layer 4 for the calibrated elevation-dependent maximum recharge scenario groundwater flow model.
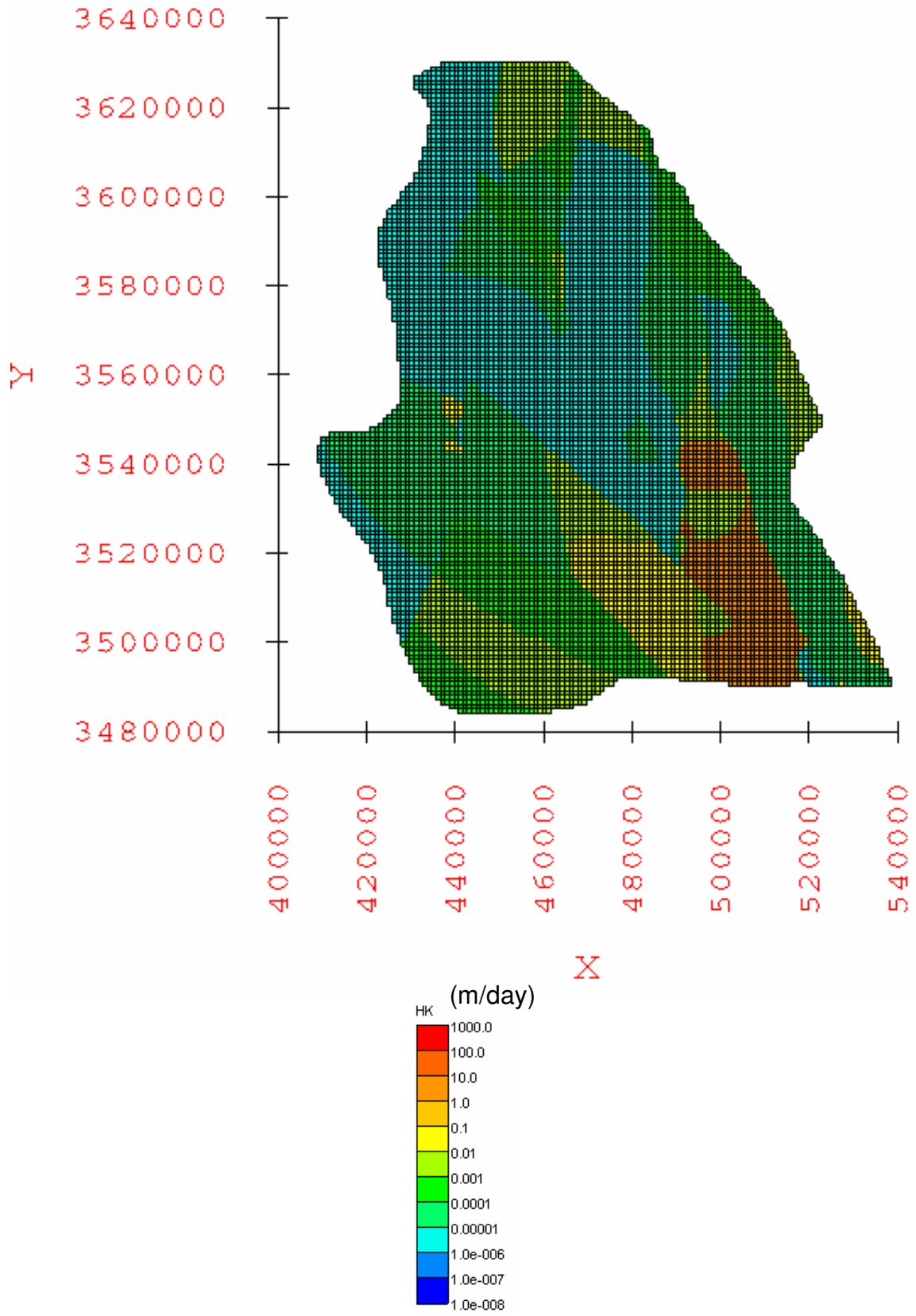
Figure A-4.91: Horizontal hydraulic conductivity [HK] distribution in layer 5 for the calibrated elevation-dependent maximum recharge scenario groundwater flow model.
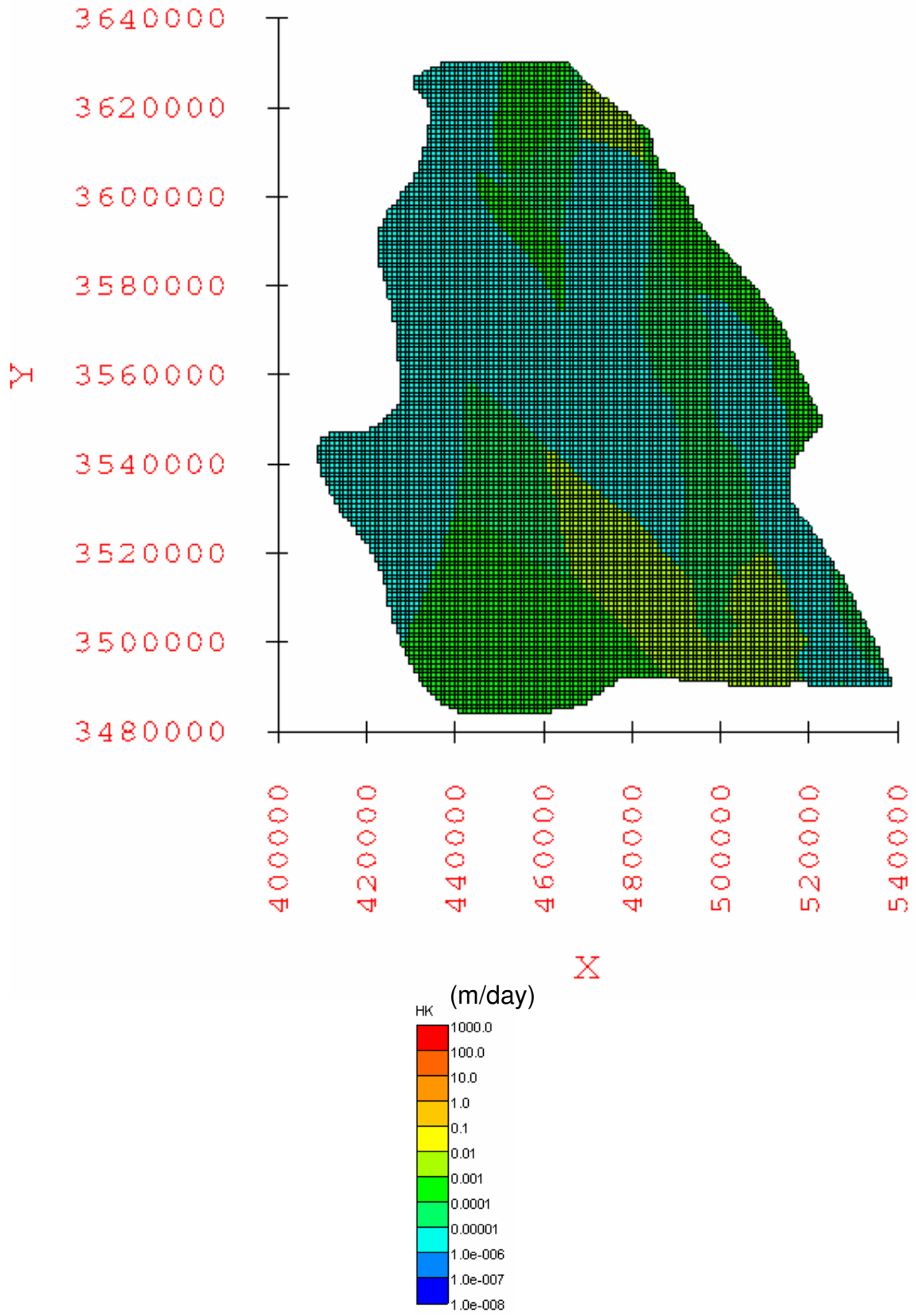
Figure A-4.92: Horizontal hydraulic conductivity [HK] distribution in layer 6 for the calibrated elevation-dependent maximum recharge scenario groundwater flow model.
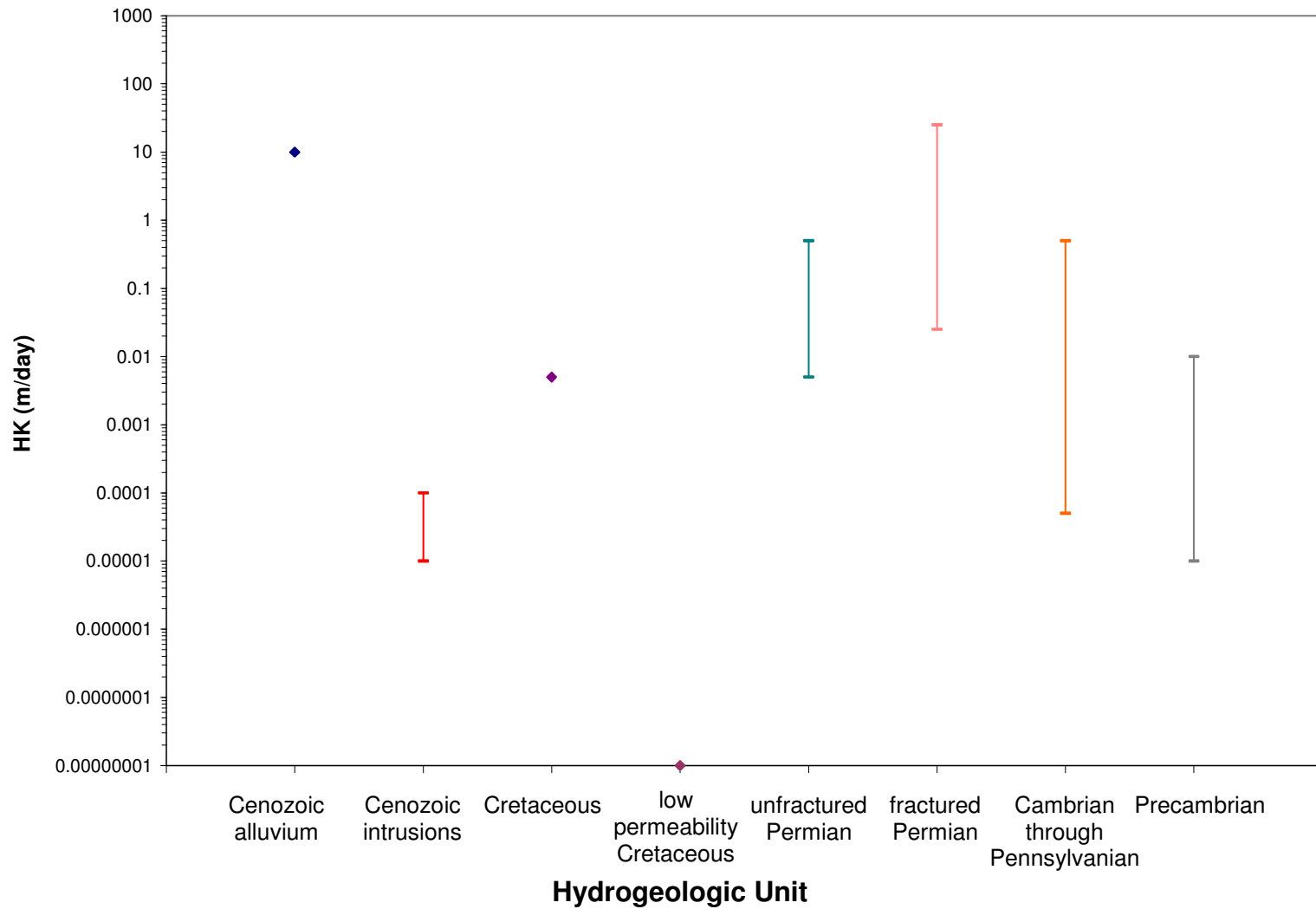
Figure A-4.93: Range of horizontal hydraulic conductivity [HK] values for the calibrated water-balance based minimum recharge scenario model.
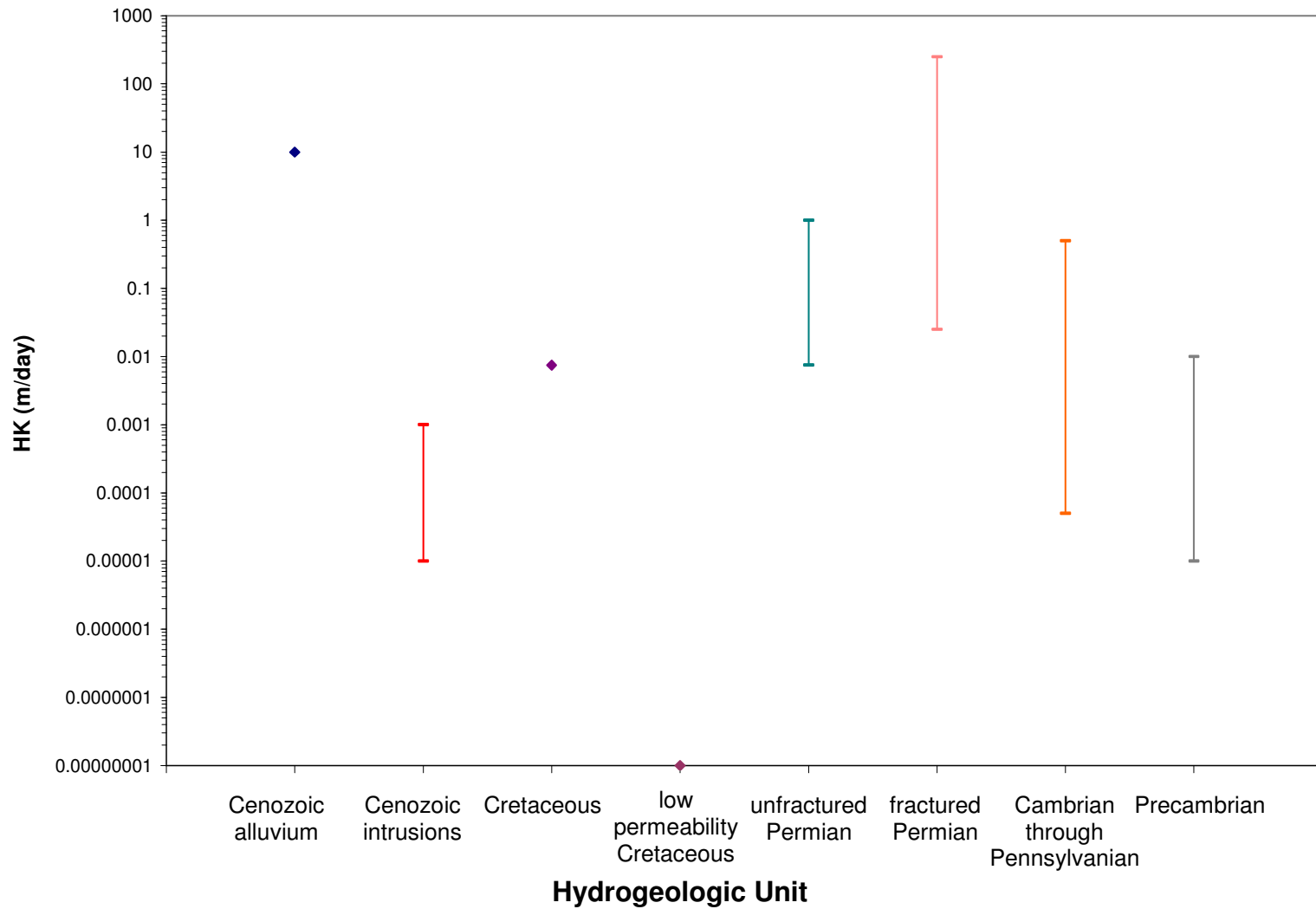
Figure A-4.94: Range of horizontal hydraulic conductivity [HK] values for the calibrated water-balance based average recharge scenario model.
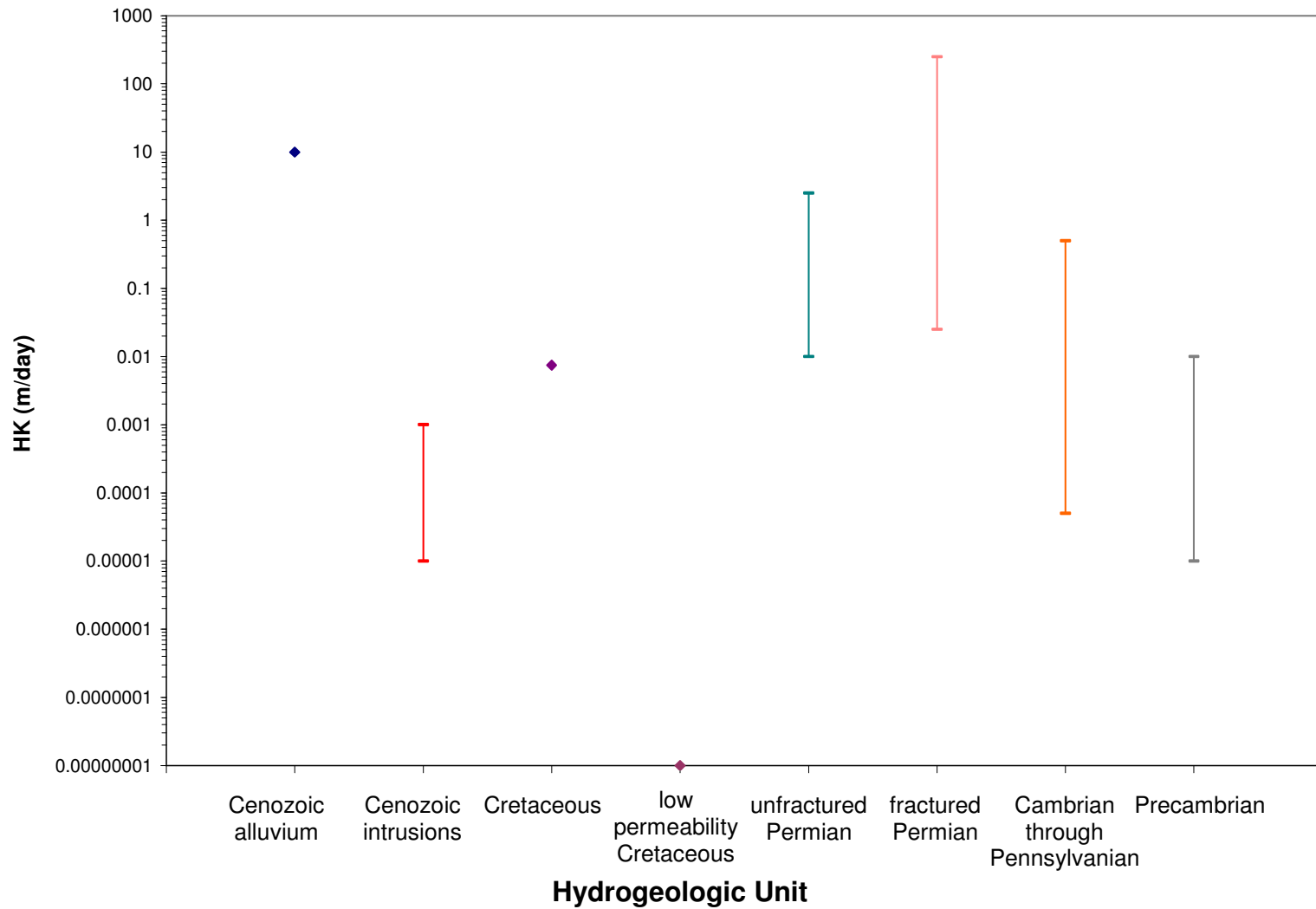
Figure A-4.95: Range of horizontal hydraulic conductivity [HK] values for the calibrated water-balance based maximum recharge scenario model.
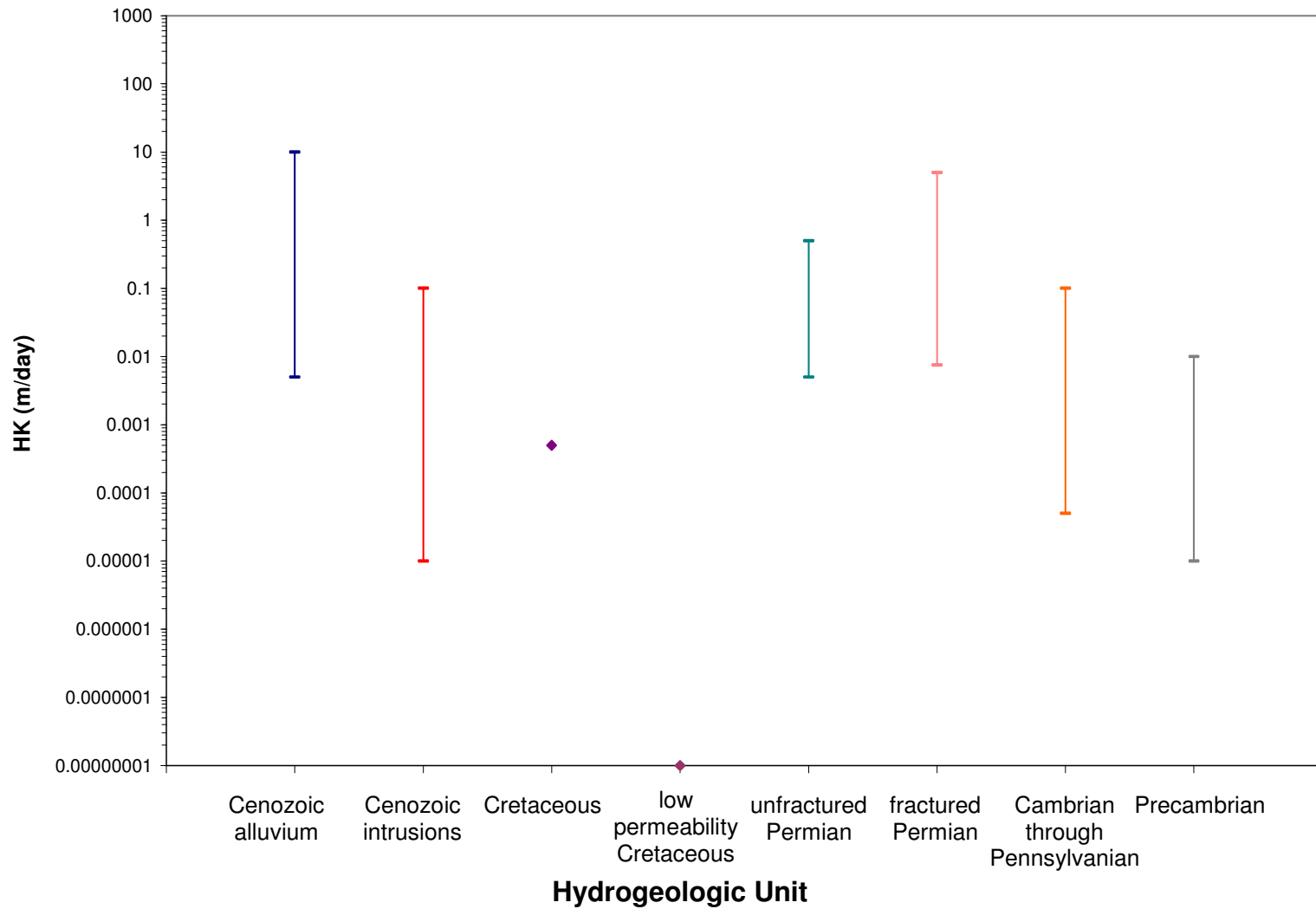
Figure A-4.96: Range of horizontal hydraulic conductivity [HK] values for the calibrated elevation-dependent minimum recharge scenario model.
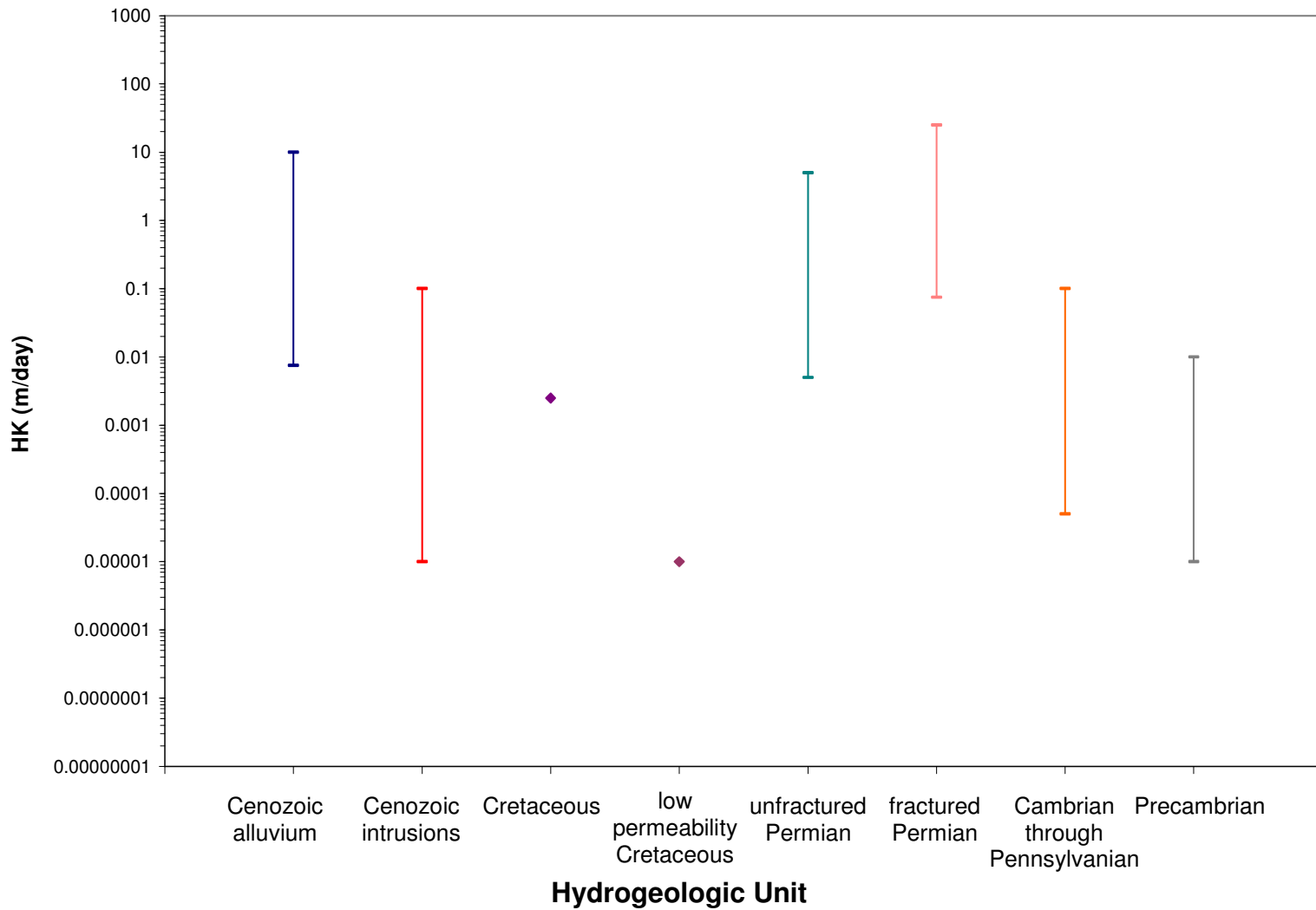
Figure A-4.97: Range of horizontal hydraulic conductivity [HK] values for the calibrated elevation-dependent average recharge scenario model.
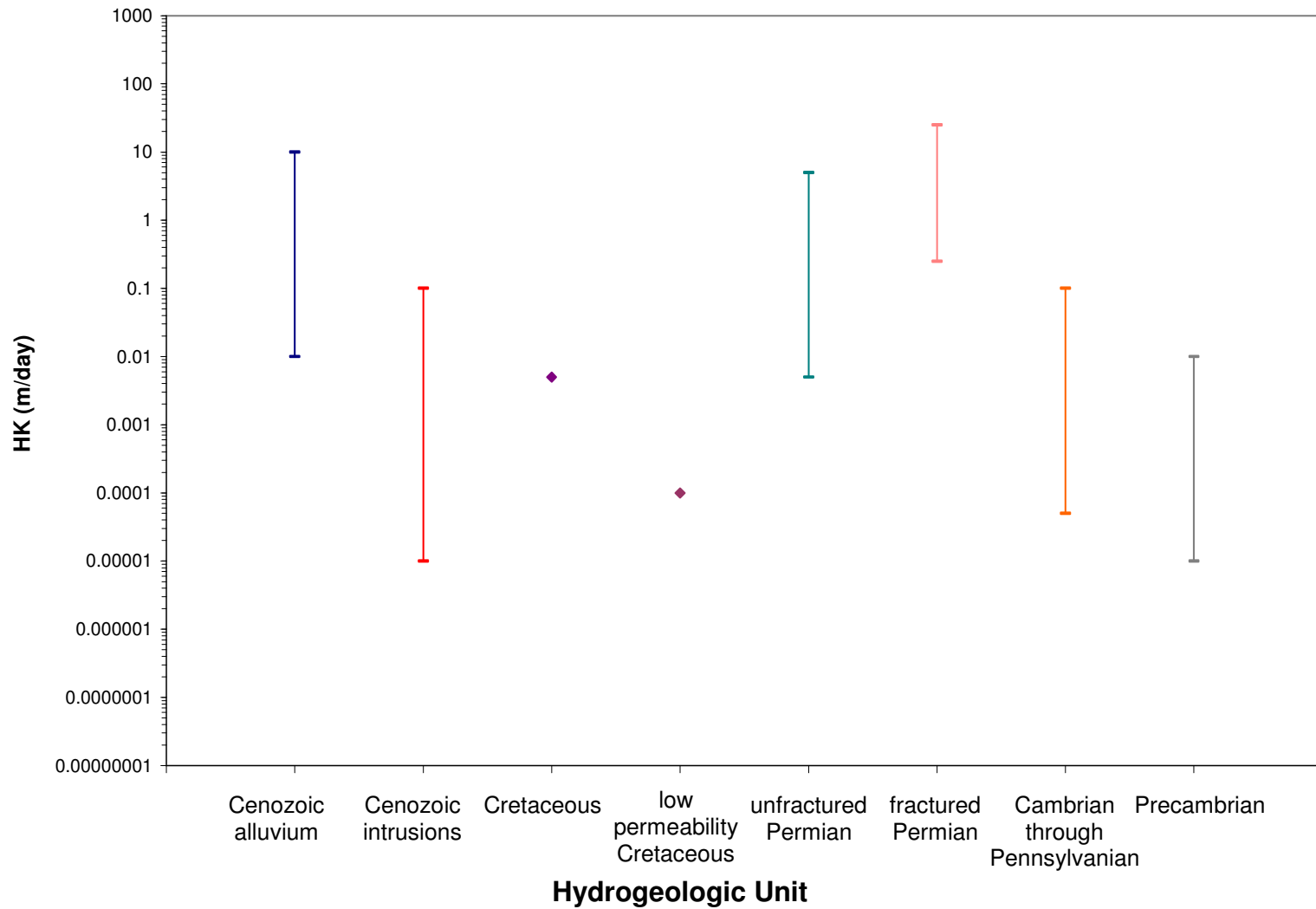
Figure A-4.98: Range of horizontal hydraulic conductivity [HK] values for the calibrated elevation-dependent maximum recharge scenario model.
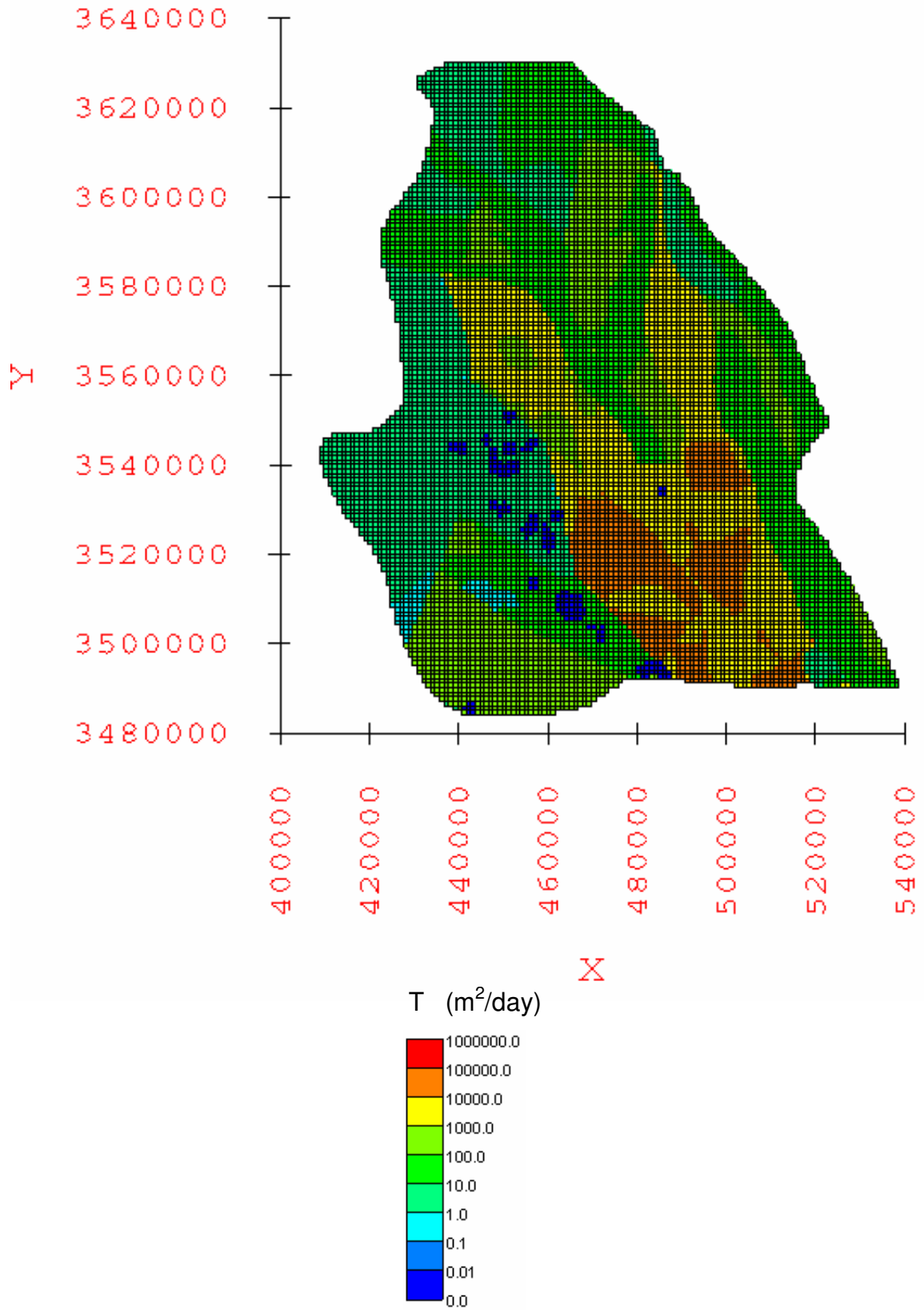
Figure A-4.99: Distribution of aquifer transmissivity [T] for the calibrated water-balance based minimum recharge scenario groundwater flow model.
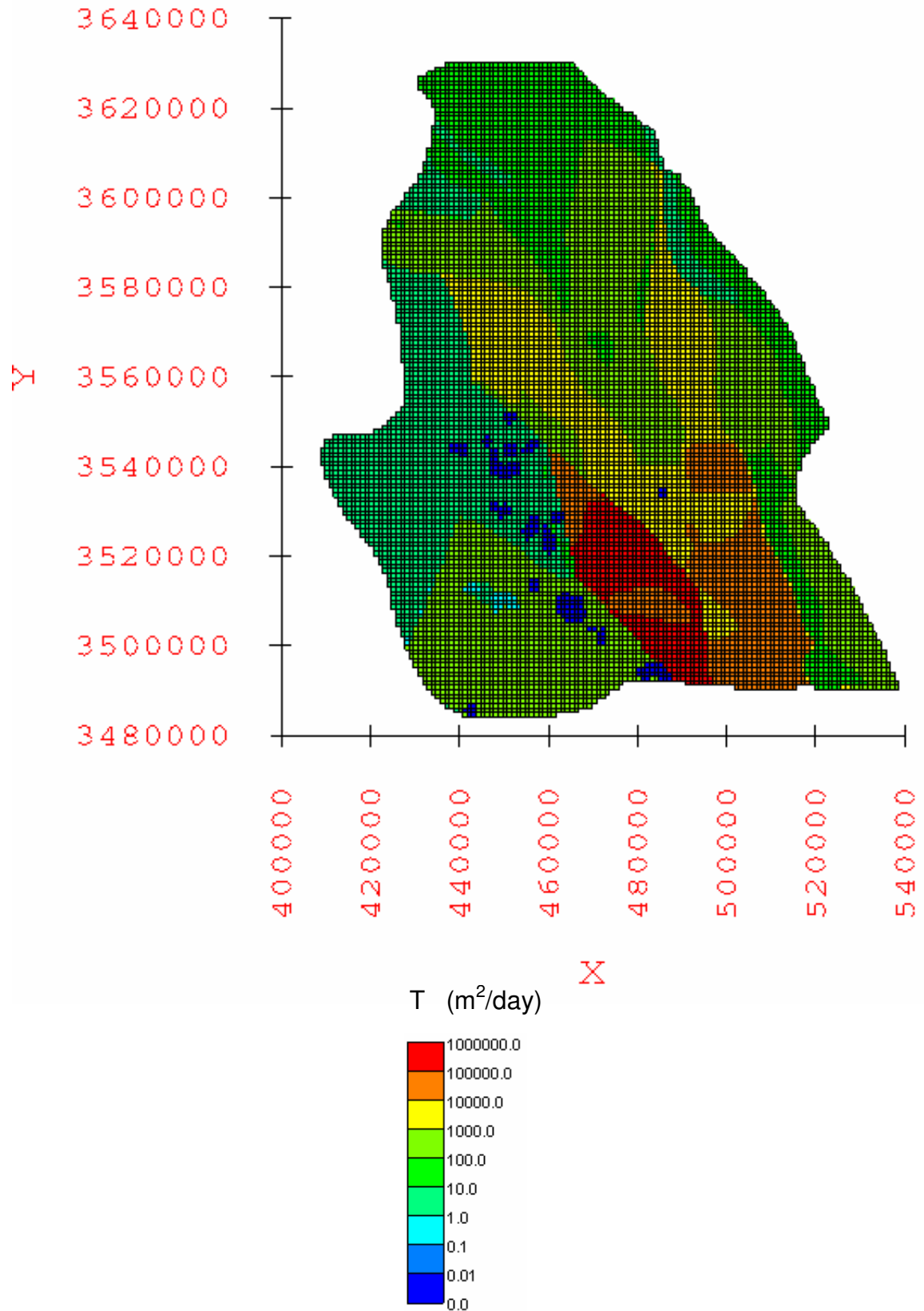
Figure A-4.100: Distribution of aquifer transmissivity [T] for the calibrated water-balance based average recharge scenario groundwater flow model.
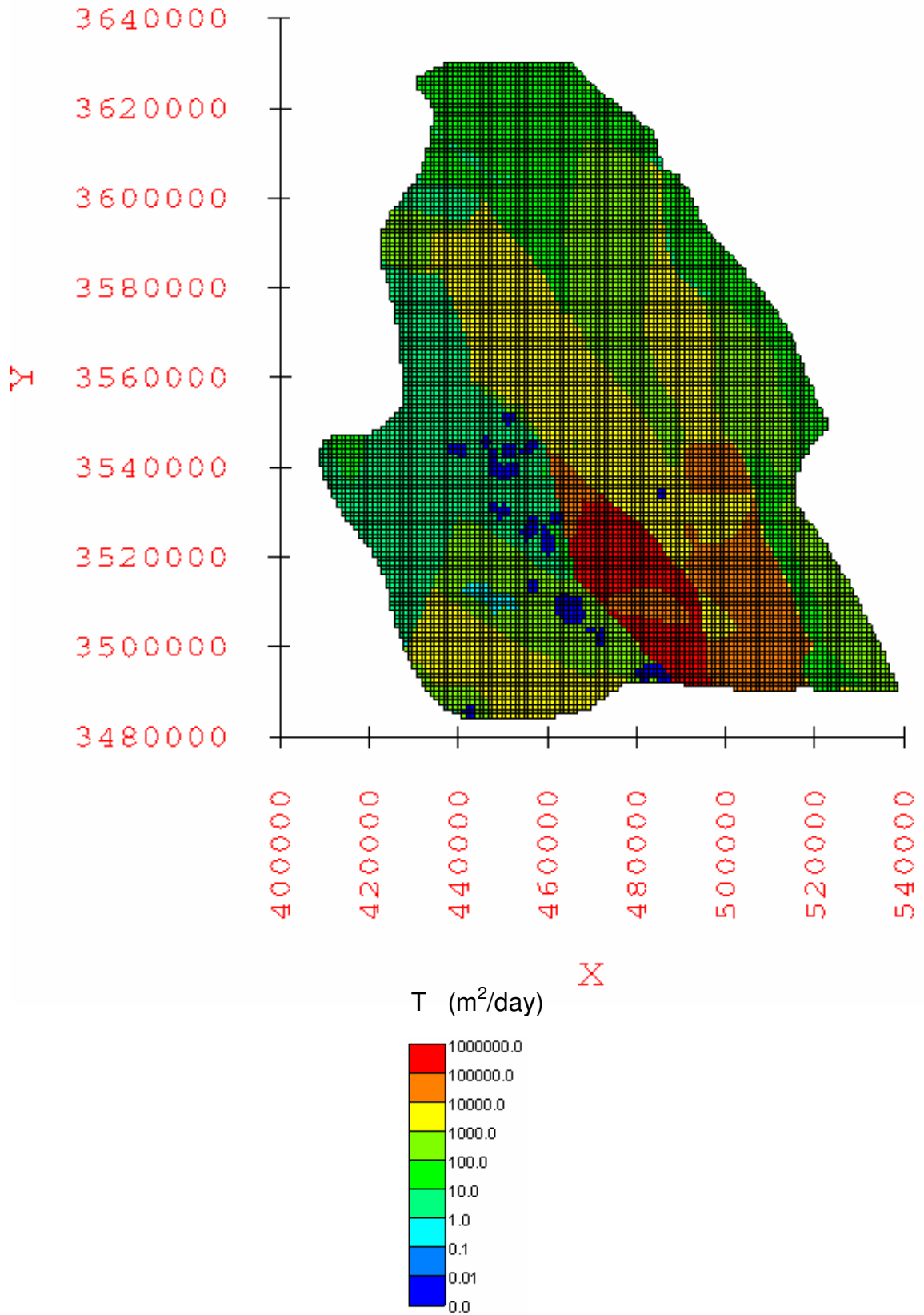
Figure A-4.101: Distribution of aquifer transmissivity [T] for the calibrated water-balance based maximum recharge scenario groundwater flow model.
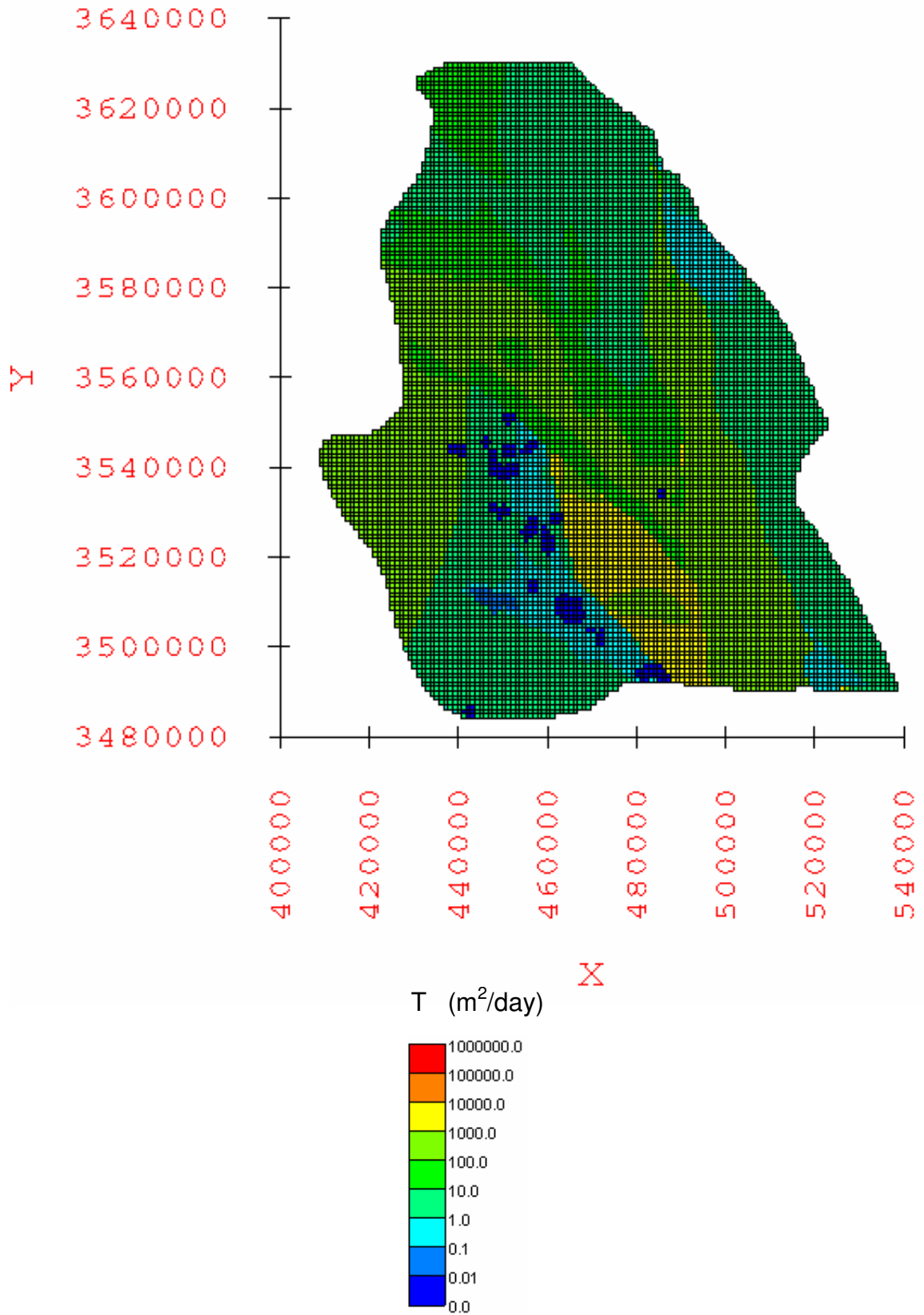
Figure A-4.102: Distribution of aquifer transmissivity [T] for the calibrated elevation-dependent minimum recharge scenario groundwater flow model.
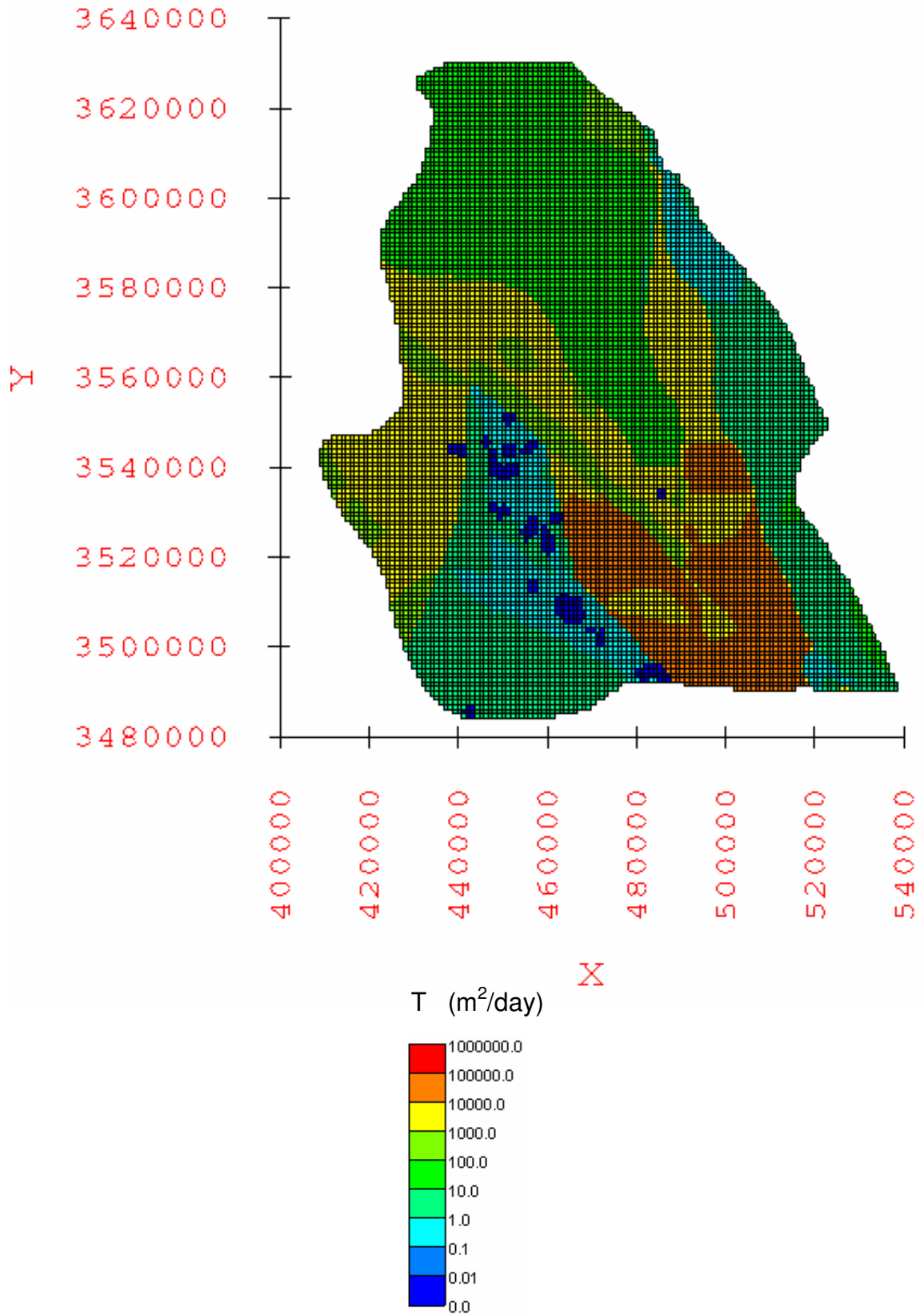
Figure A-4.103: Distribution of aquifer transmissivity [T] for the calibrated elevation-dependent average recharge scenario groundwater flow model.
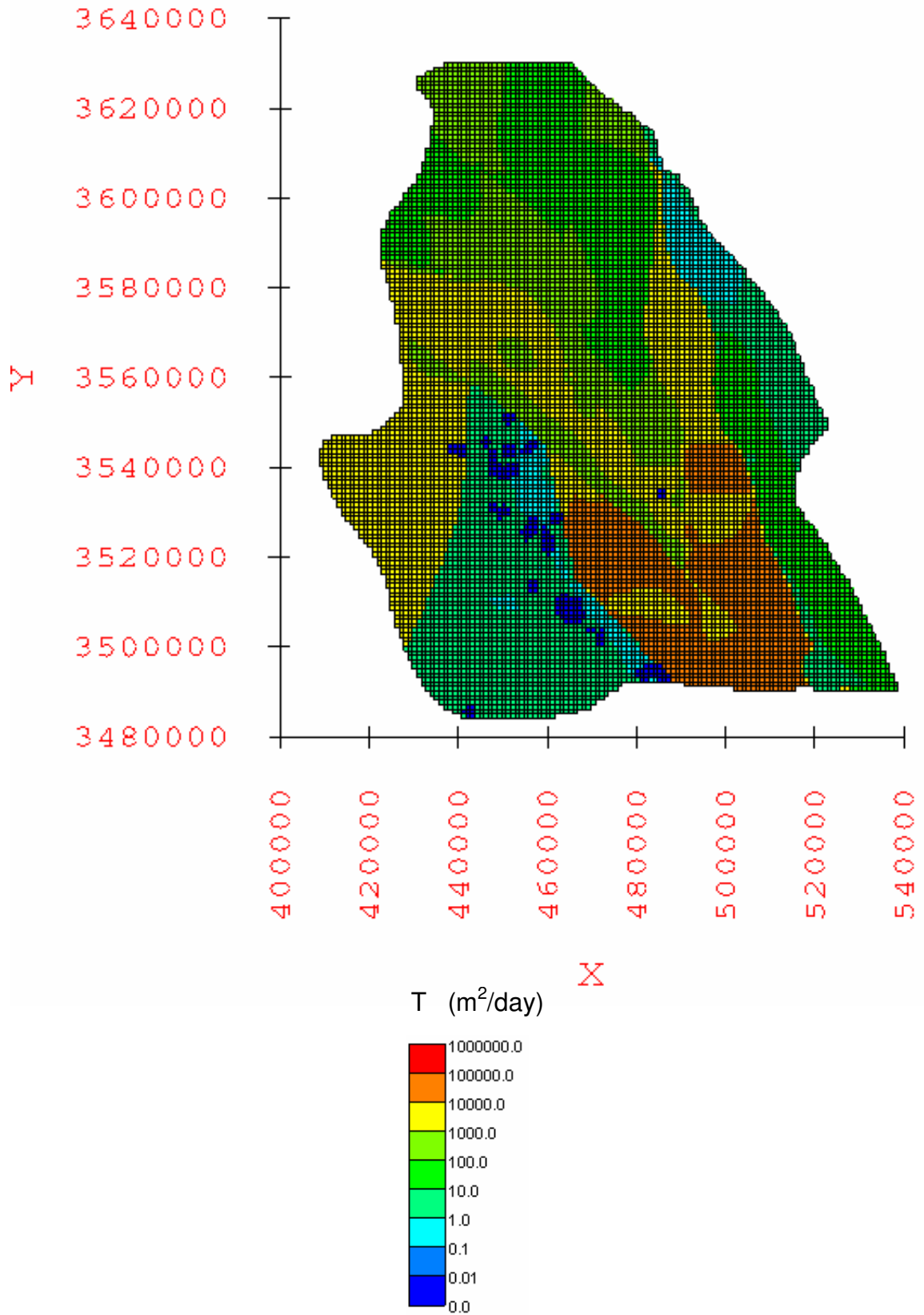
Figure A-4.104: Distribution of aquifer transmissivity [T] for the calibrated elevation-dependent maximum recharge scenario groundwater flow model.
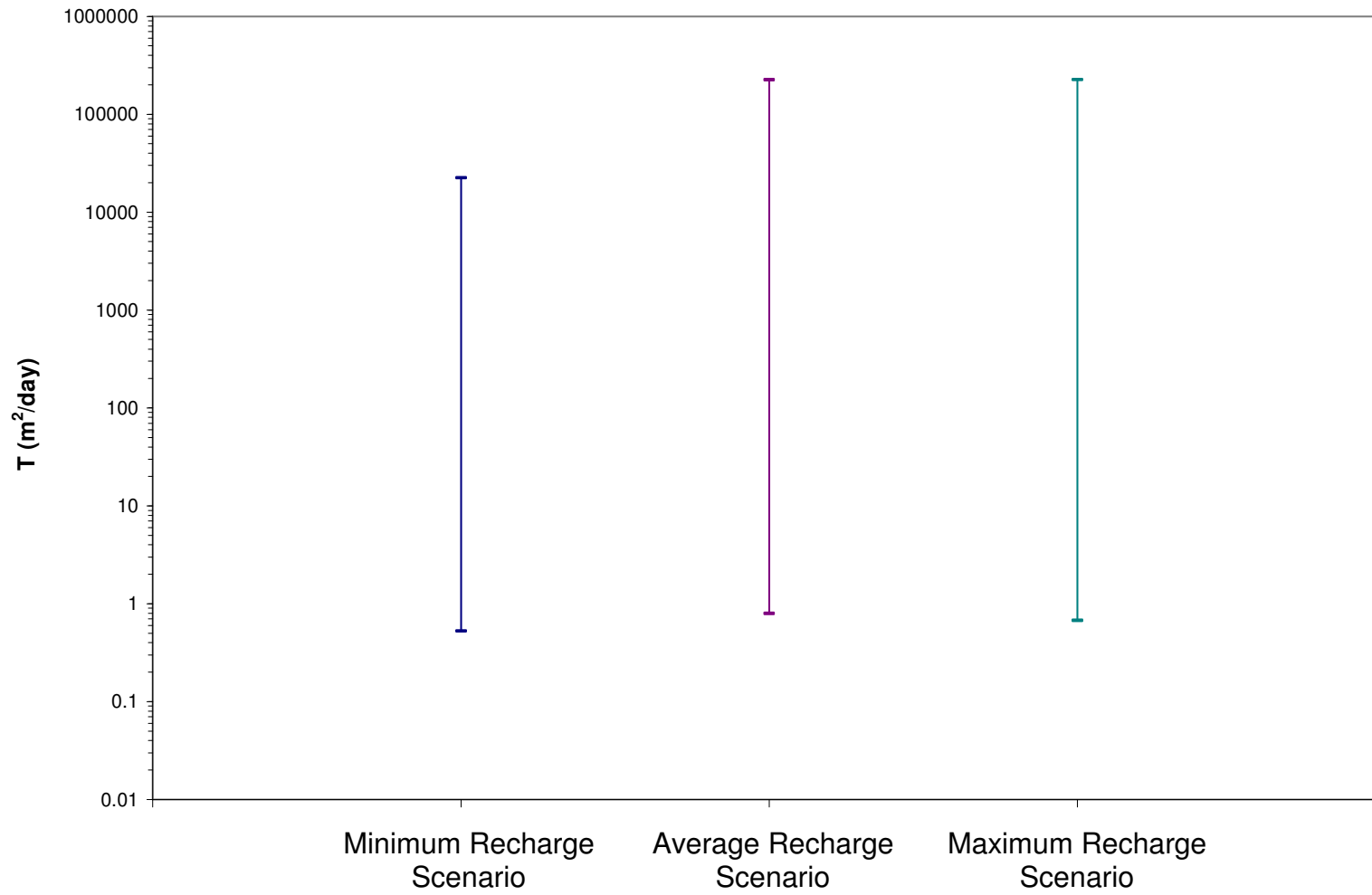
Figure A-4.105: Range of transmissivities [T] derived from the calibrated water-balance based minimum, average, and maximum recharge scenario models.
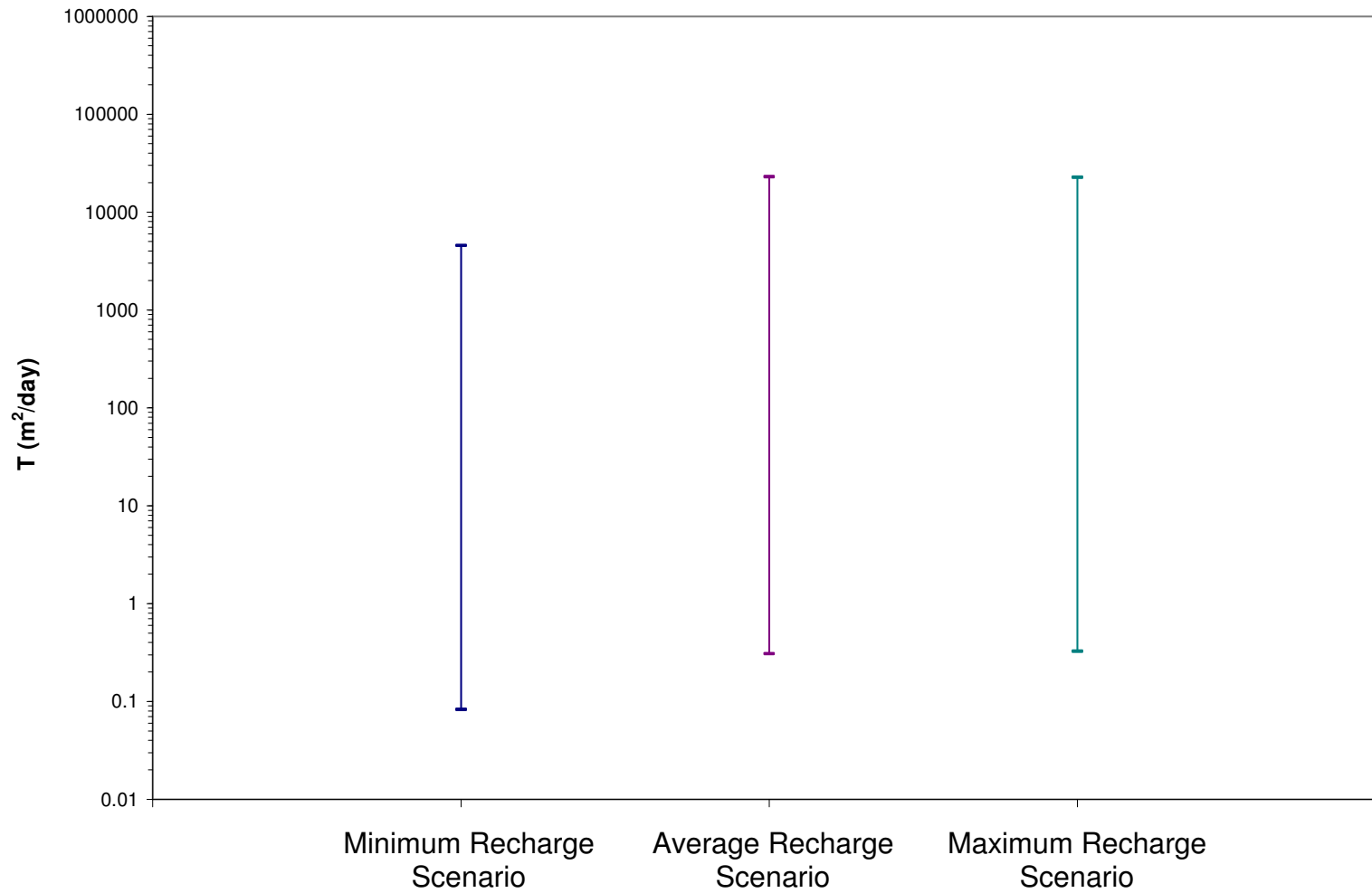
Figure A-4.106: Range of transmissivities [T] derived from the calibrated elevation-dependent minimum, average, and maximum recharge scenario models.
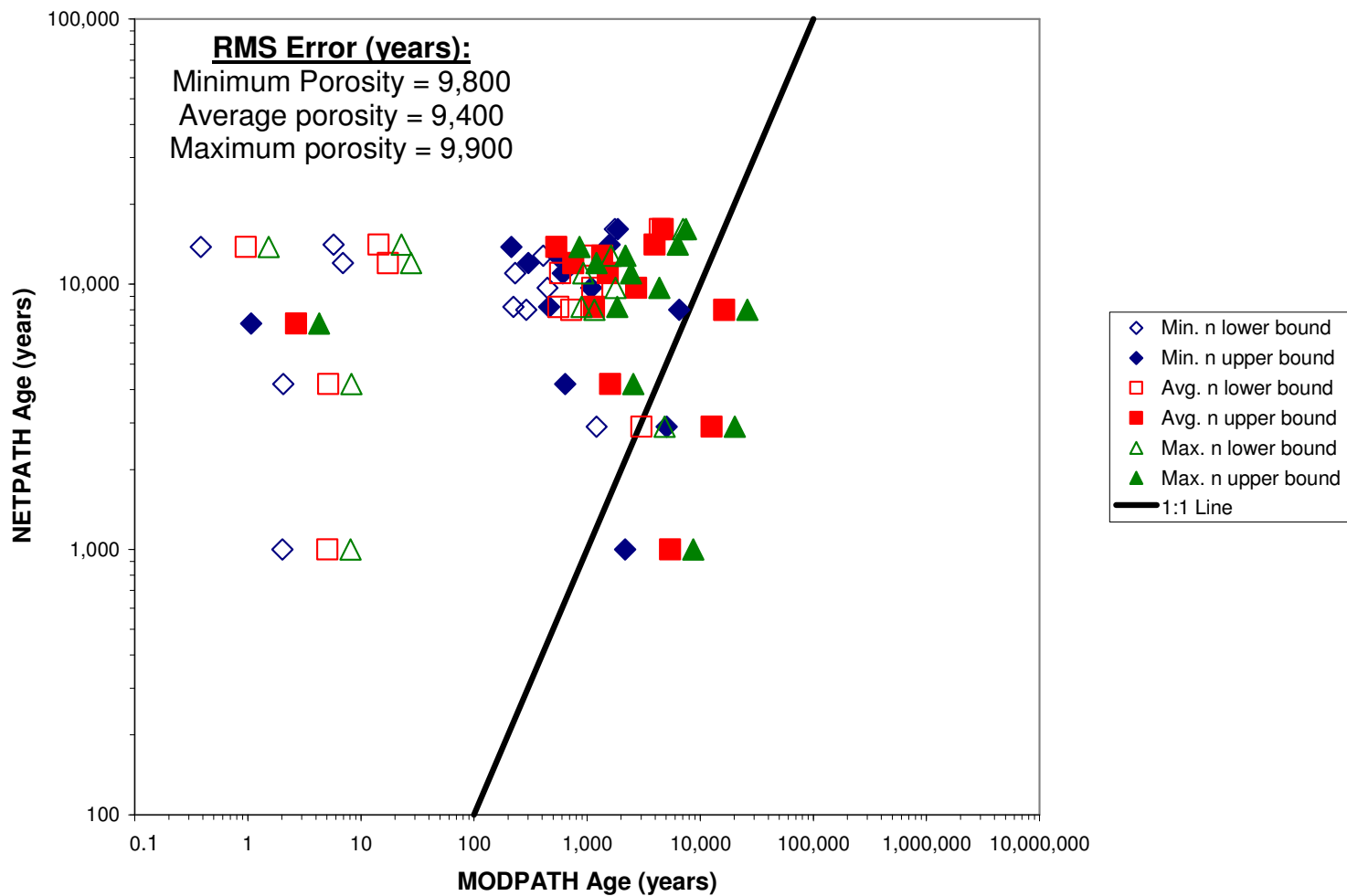
Figure A-4.107: NETPATH versus MODPATH ages for the calibrated water-balance based minimum recharge scenario model using minimum, average, and maximum porosities.
Vertical and horizontal axes are logarithmic scale.
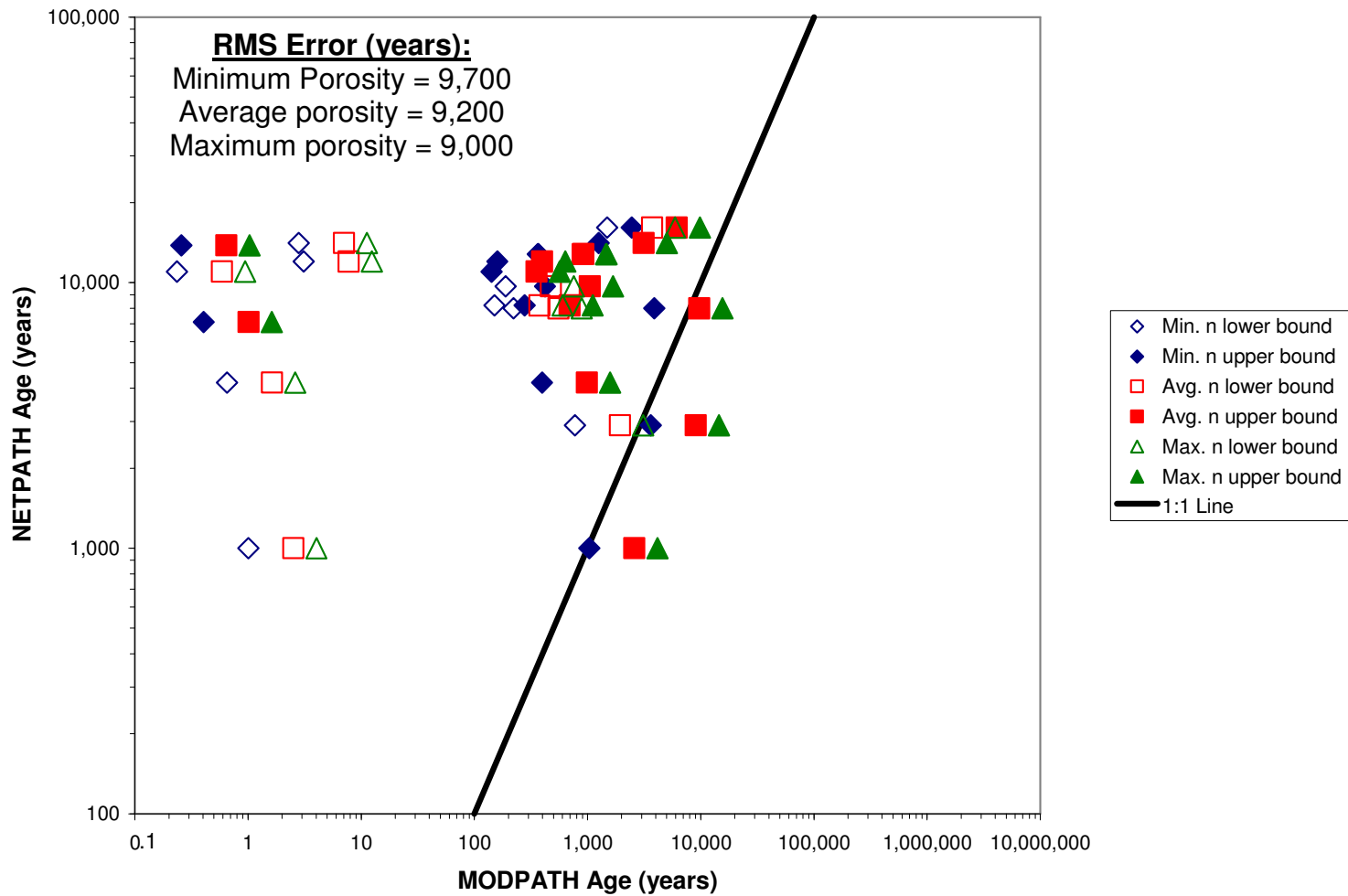
Figure A-4.108: NETPATH versus MODPATH ages for the calibrated water-balance based average recharge scenario model using minimum, average, and maximum porosities.
Vertical and horizontal axes are logarithmic scale.
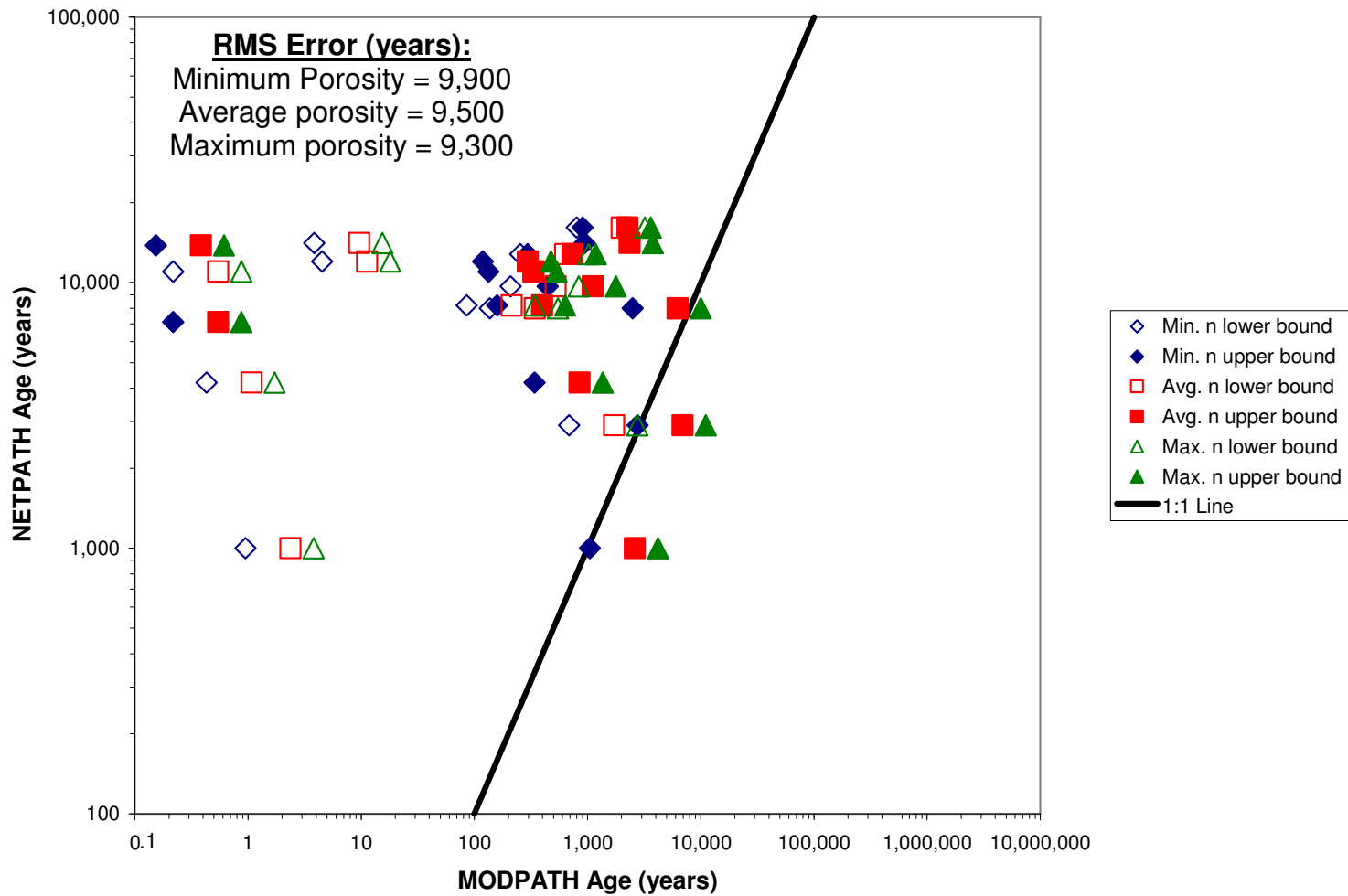
Figure A-4.109: NETPATH versus MODPATH ages for the calibrated water-balance based maximum recharge scenario model using minimum, average, and maximum porosities.
Vertical and horizontal axes are logarithmic scale.
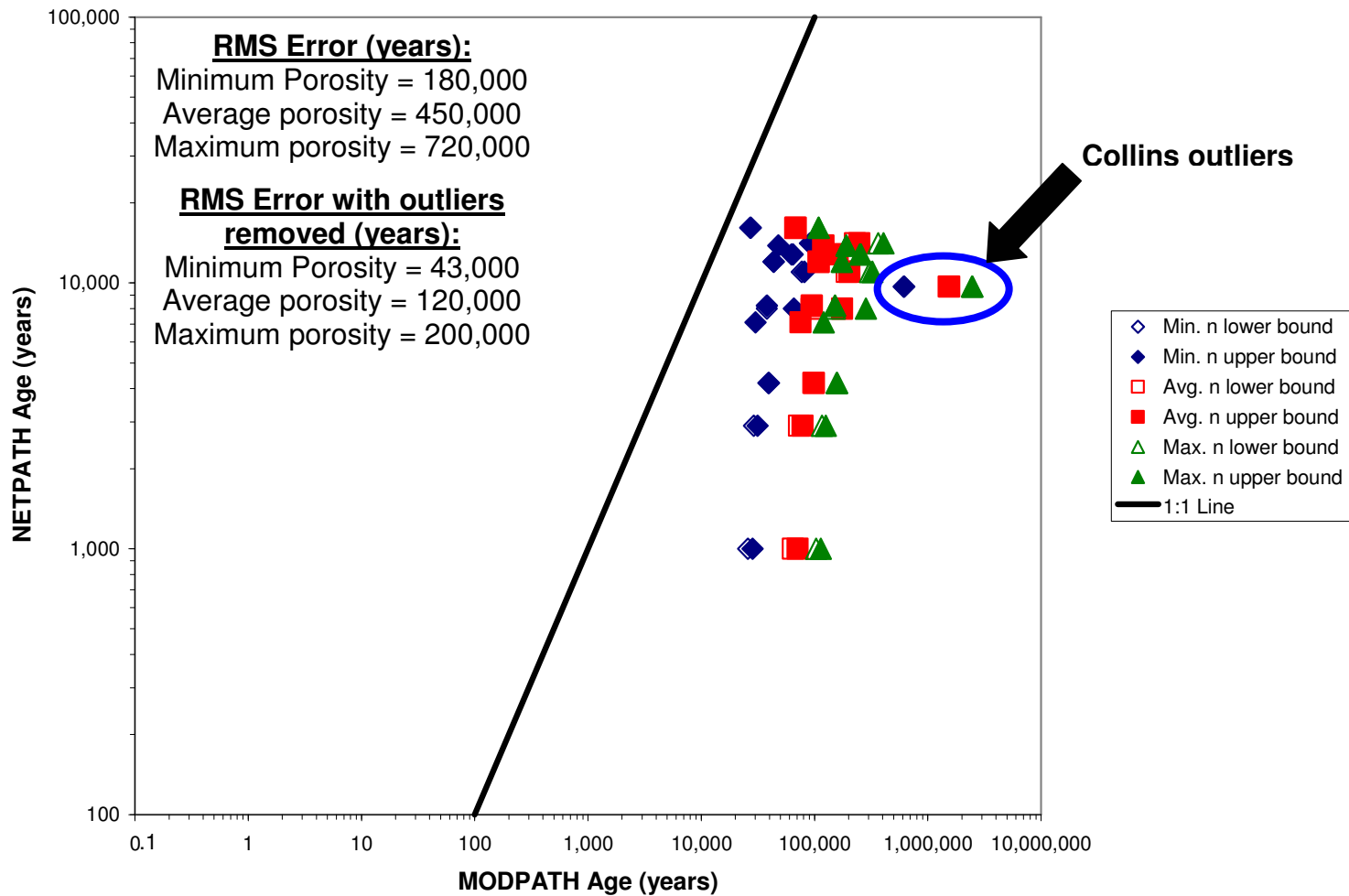
Figure A-4.110: NETPATH versus MODPATH ages for the calibrated elevation-dependent minimum recharge scenario model using minimum, average, and maximum porosities.
Vertical and horizontal axes are logarithmic scale.
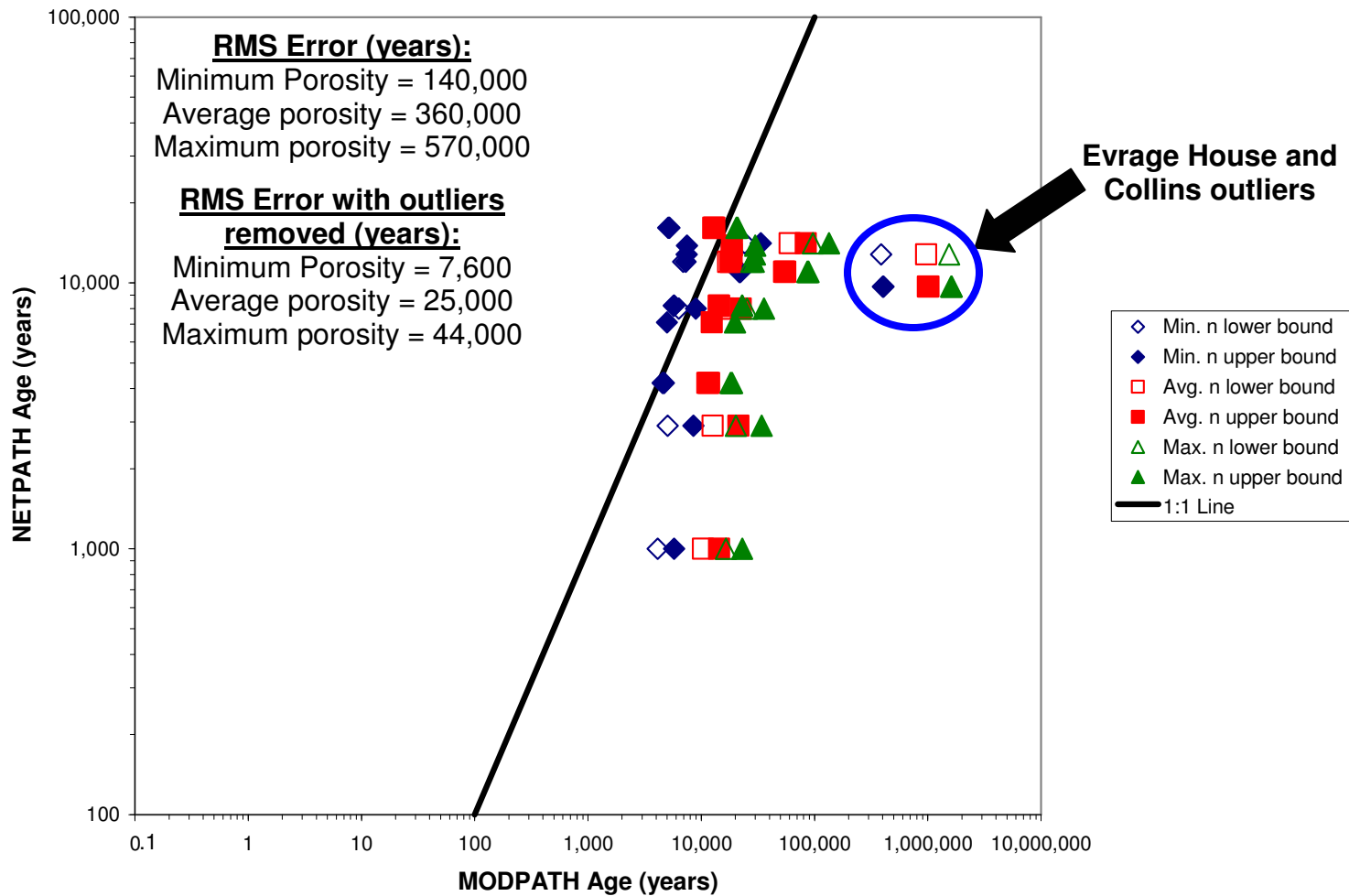
Figure A-4.111: NETPATH versus MODPATH ages for the calibrated elevation-dependent average recharge scenario model using minimum, average, and maximum porosities.
Vertical and horizontal axes are logarithmic scale.
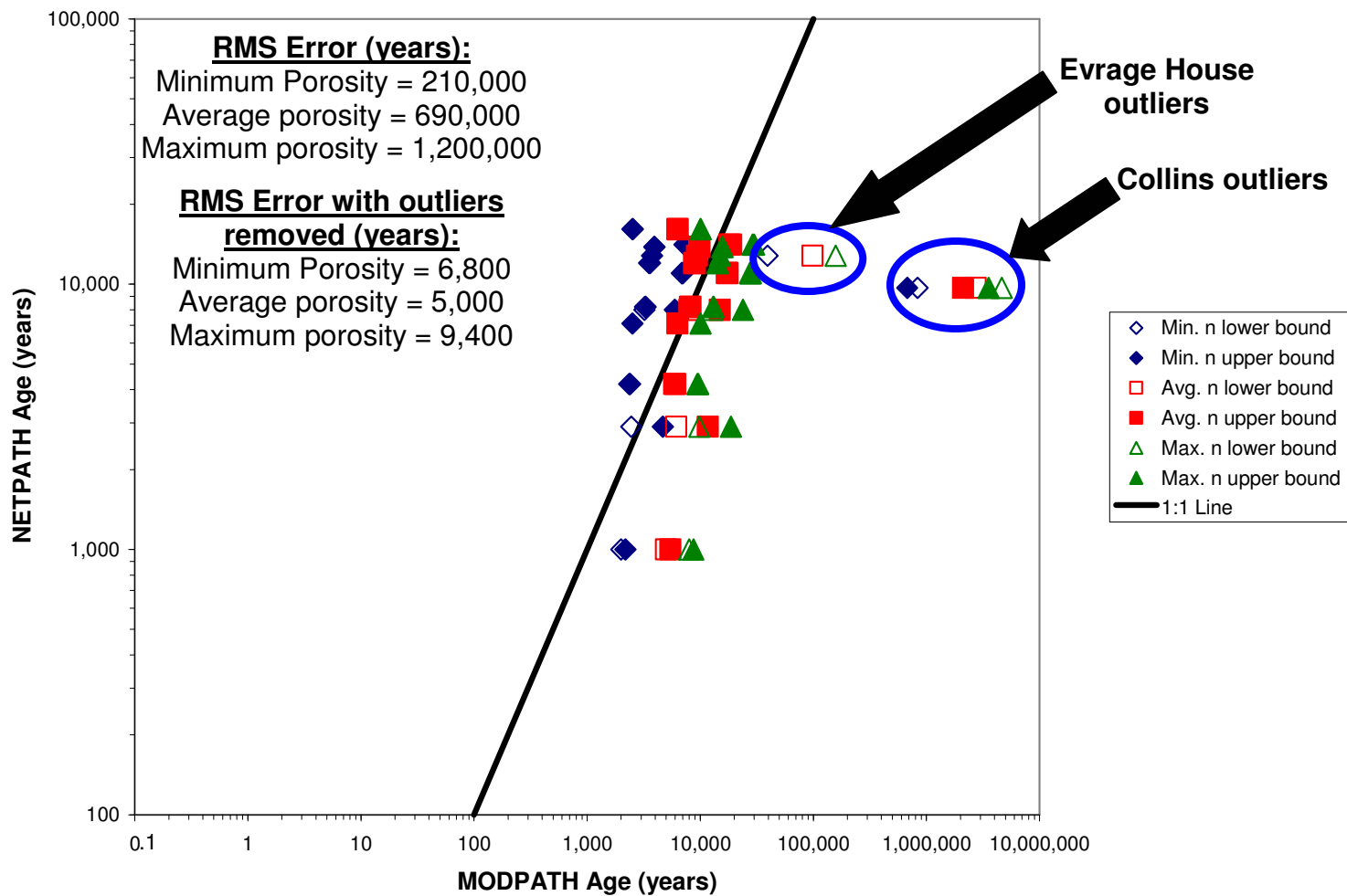
Figure A-4.112: NETPATH versus MODPATH ages for the calibrated elevation-dependent maximum recharge scenario model using minimum, average, and maximum porosities.

Vertical and horizontal axes are logarithmic scale.
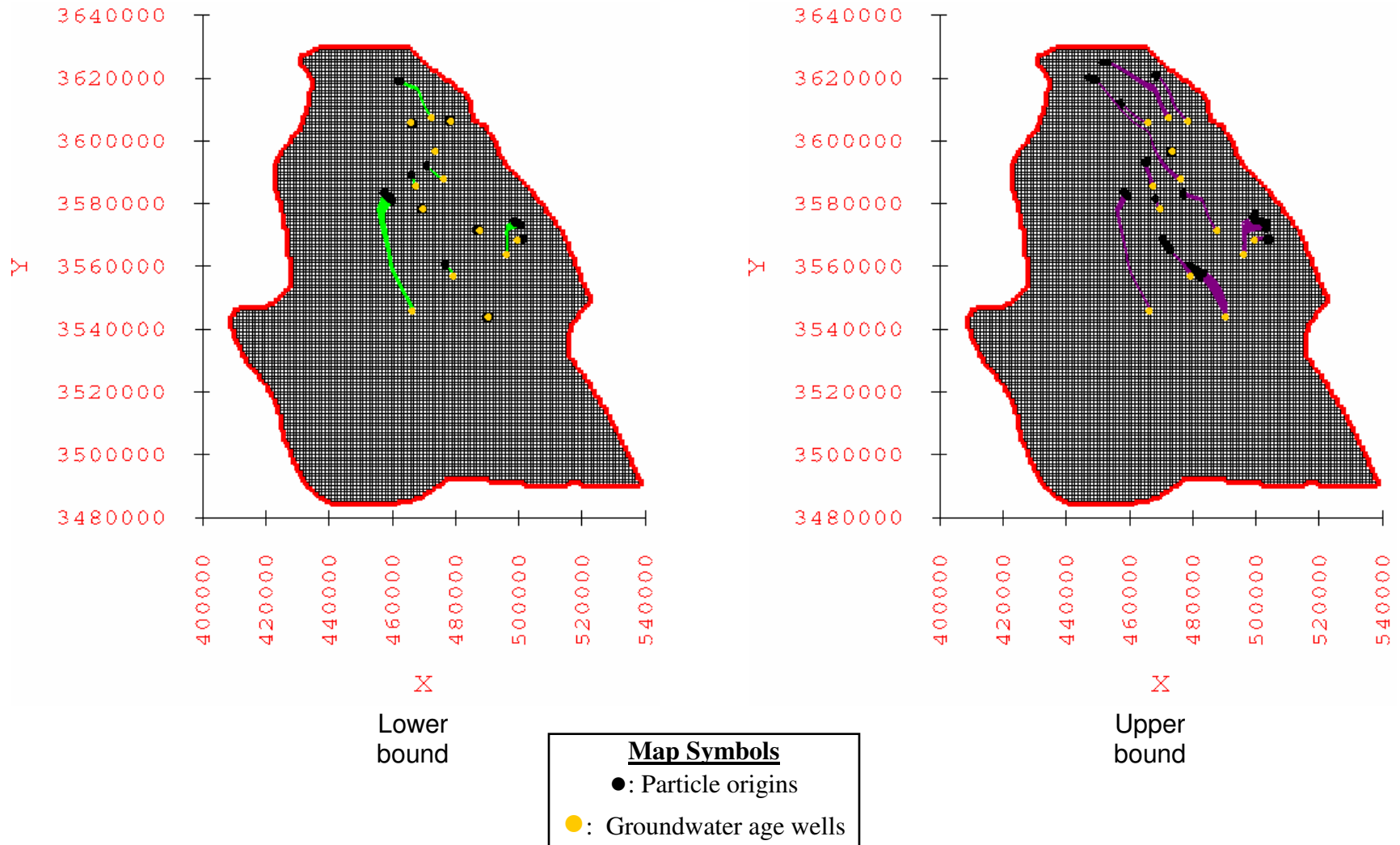
Figure A-4.113: MODPATH pathlines and origins of particles for the water-balance based minimum recharge scenario using average porosity values.

690
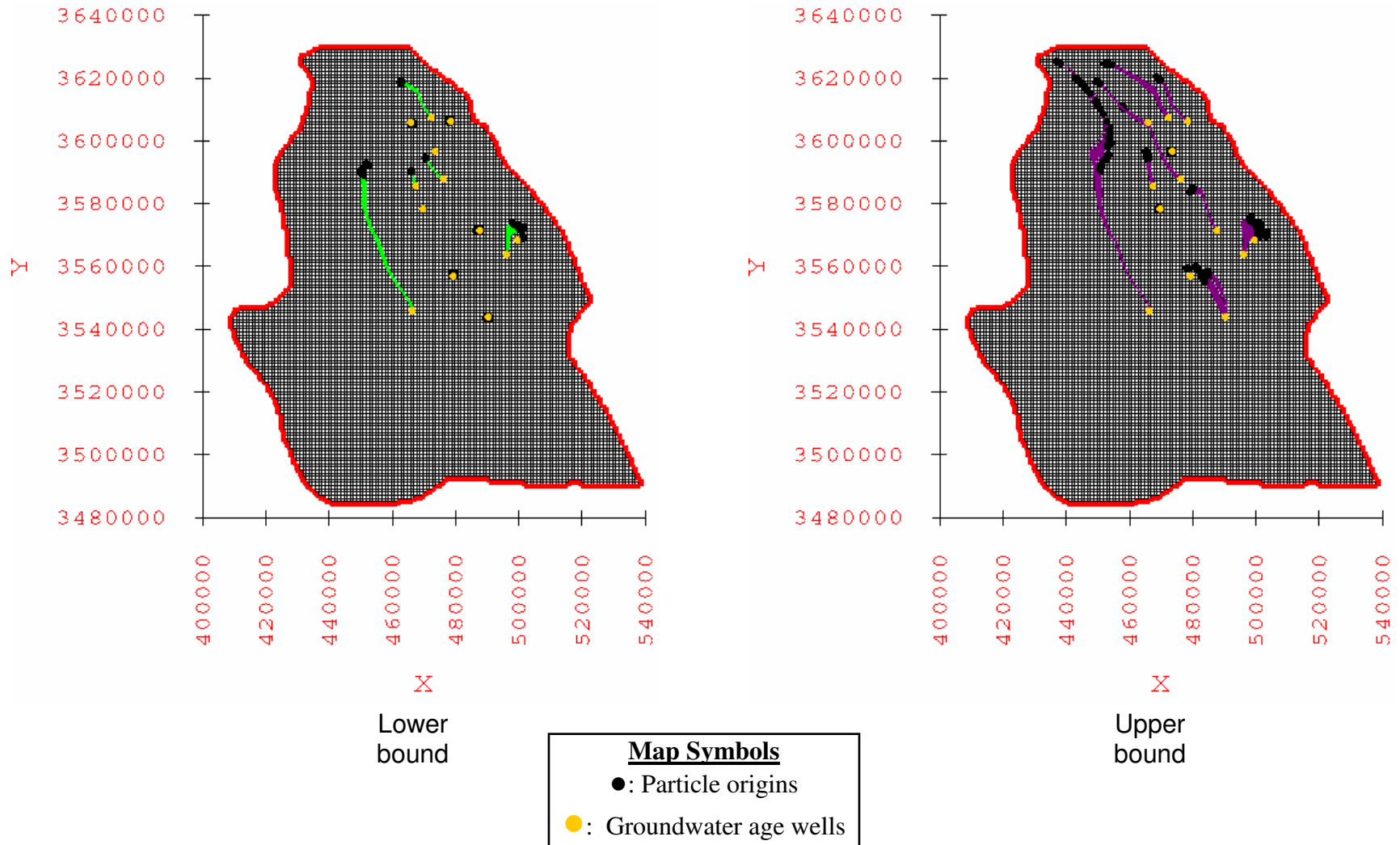
Figure A-4.114: MODPATH pathlines and origins of particles for the water-balance based average recharge scenario using average porosity values.
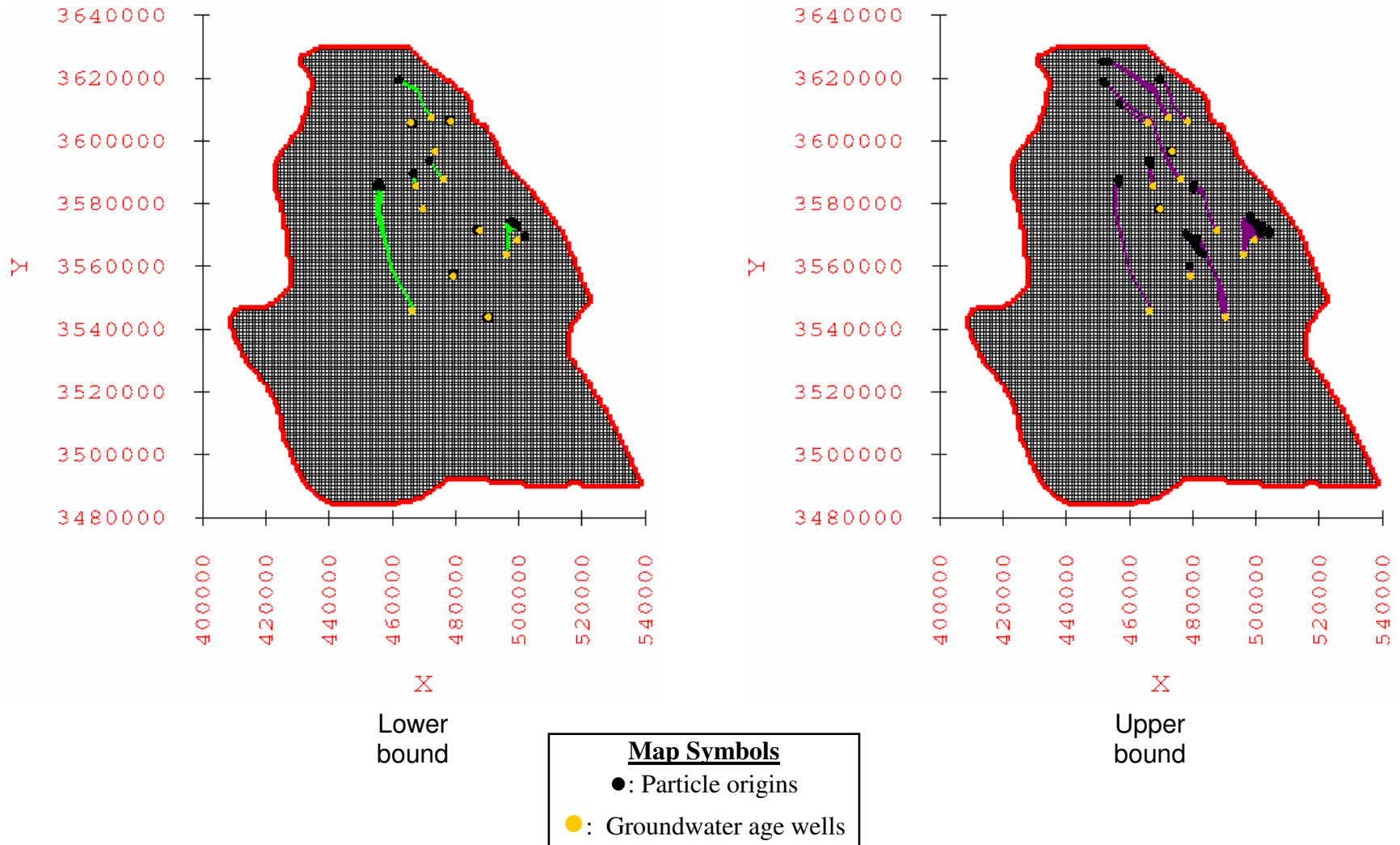
Figure A-4.115: MODPATH pathlines and origins of particles for the water-balance based maximum recharge scenario using average porosity values.

Map Symbols

●: Particle origins

🟠: Groundwater age wells
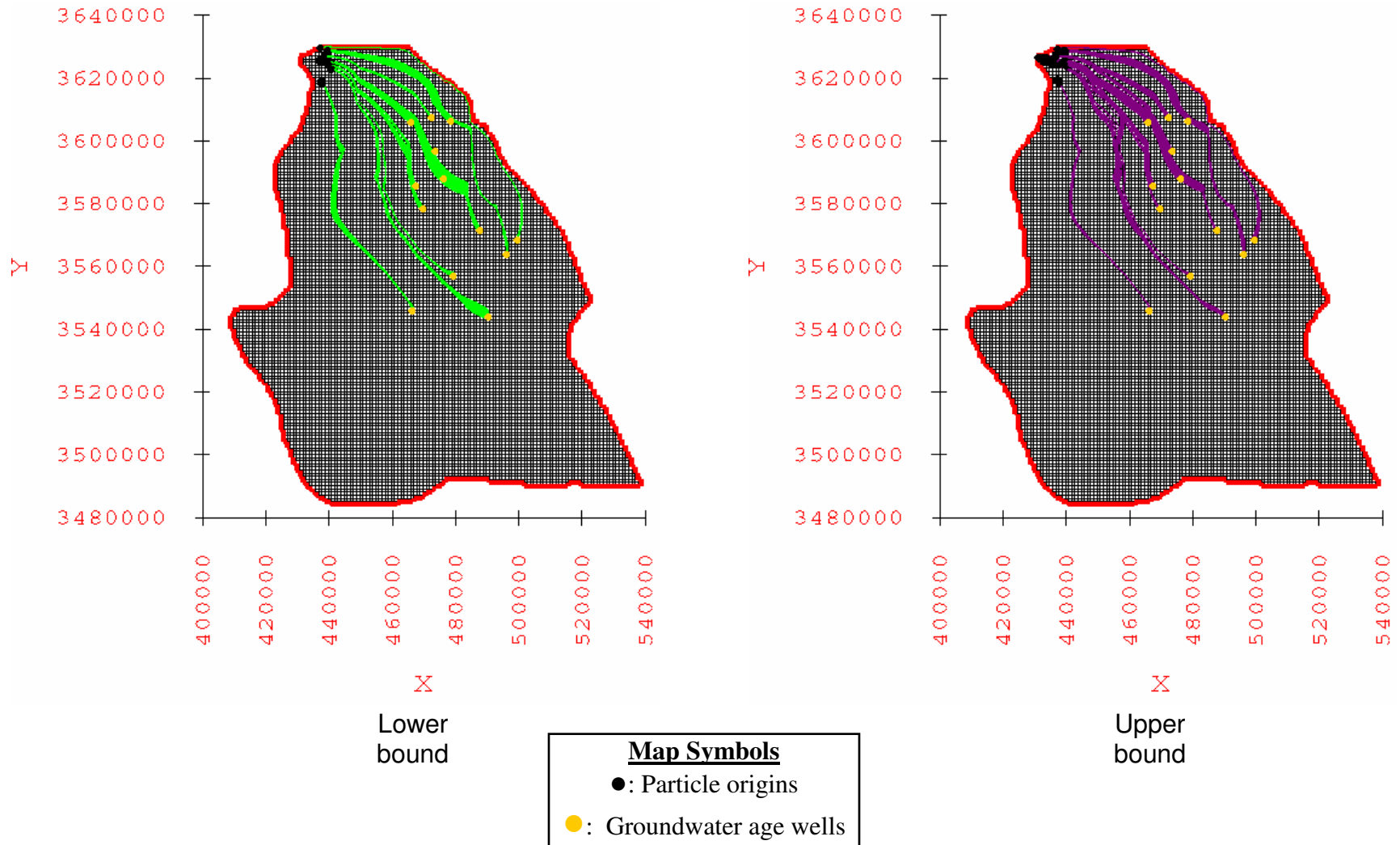
Figure A-4.116: MODPATH pathlines and origins of particles for the elevation-dependent minimum recharge scenario using average porosity values.
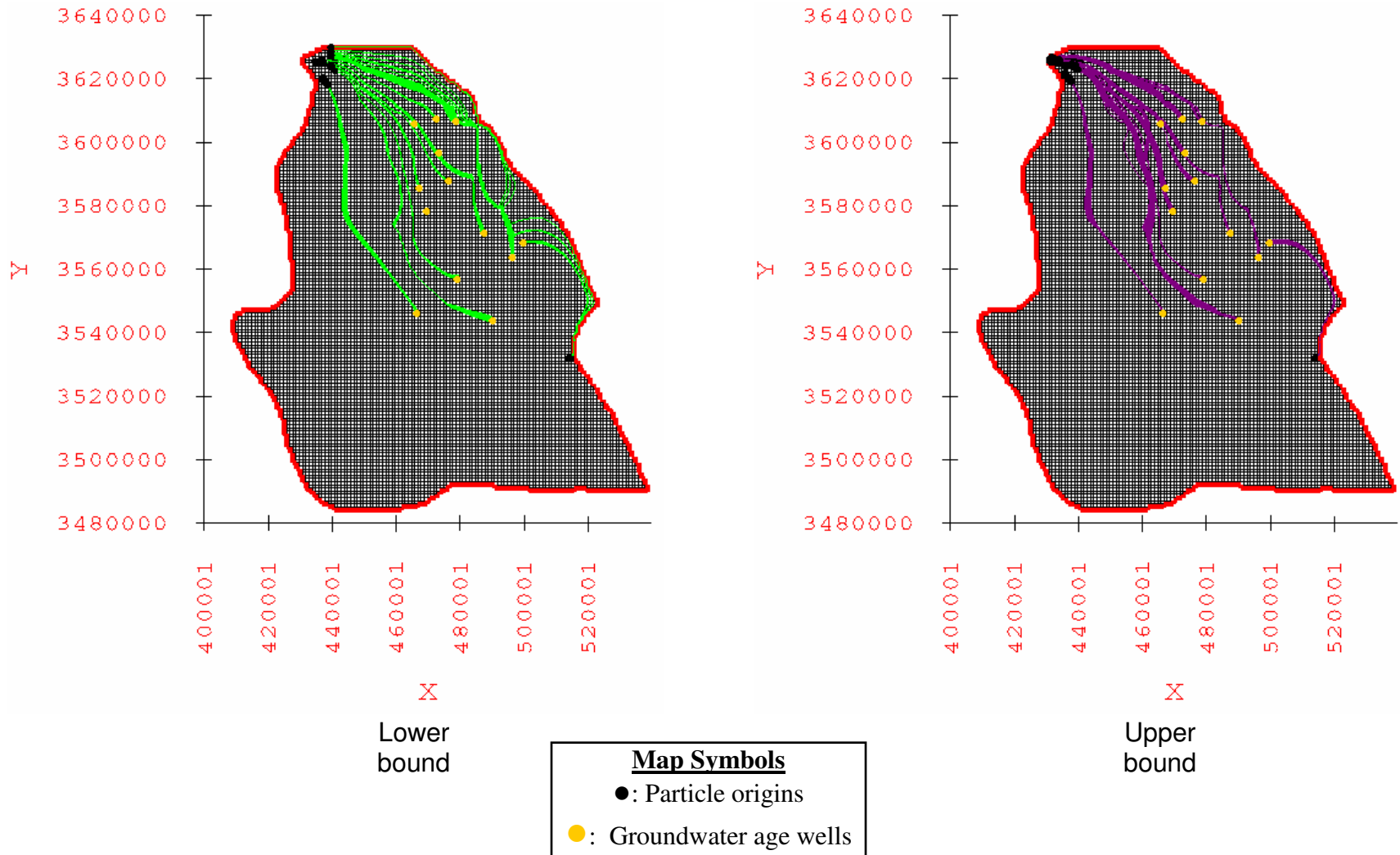
Figure A-4.117: MODPATH pathlines and origins of particles for the elevation-dependent average recharge scenario using average porosity values.

694
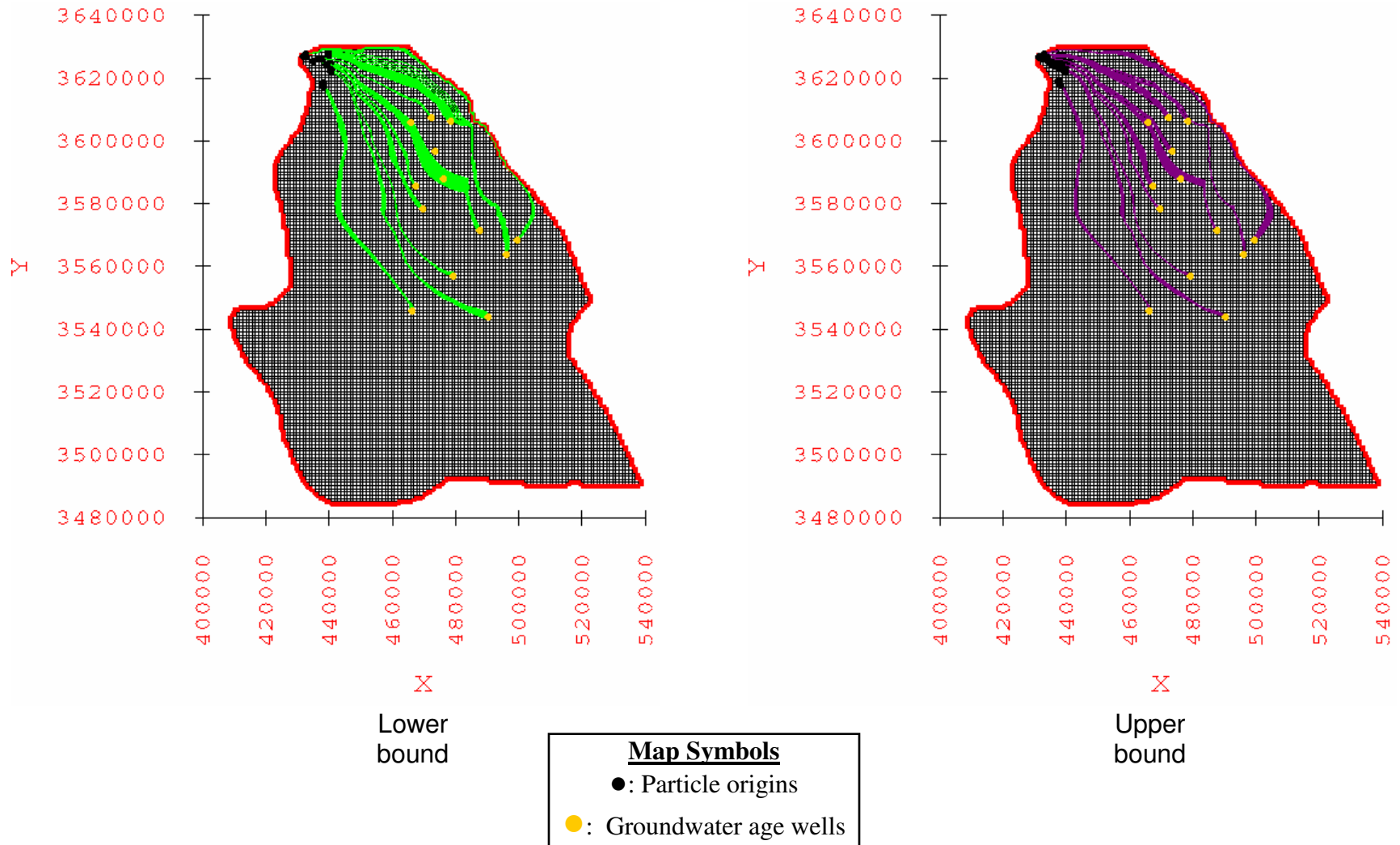
Figure A-4.118: MODPATH pathlines and origins of particles for the elevation-dependent maximum recharge scenario using average porosity values.
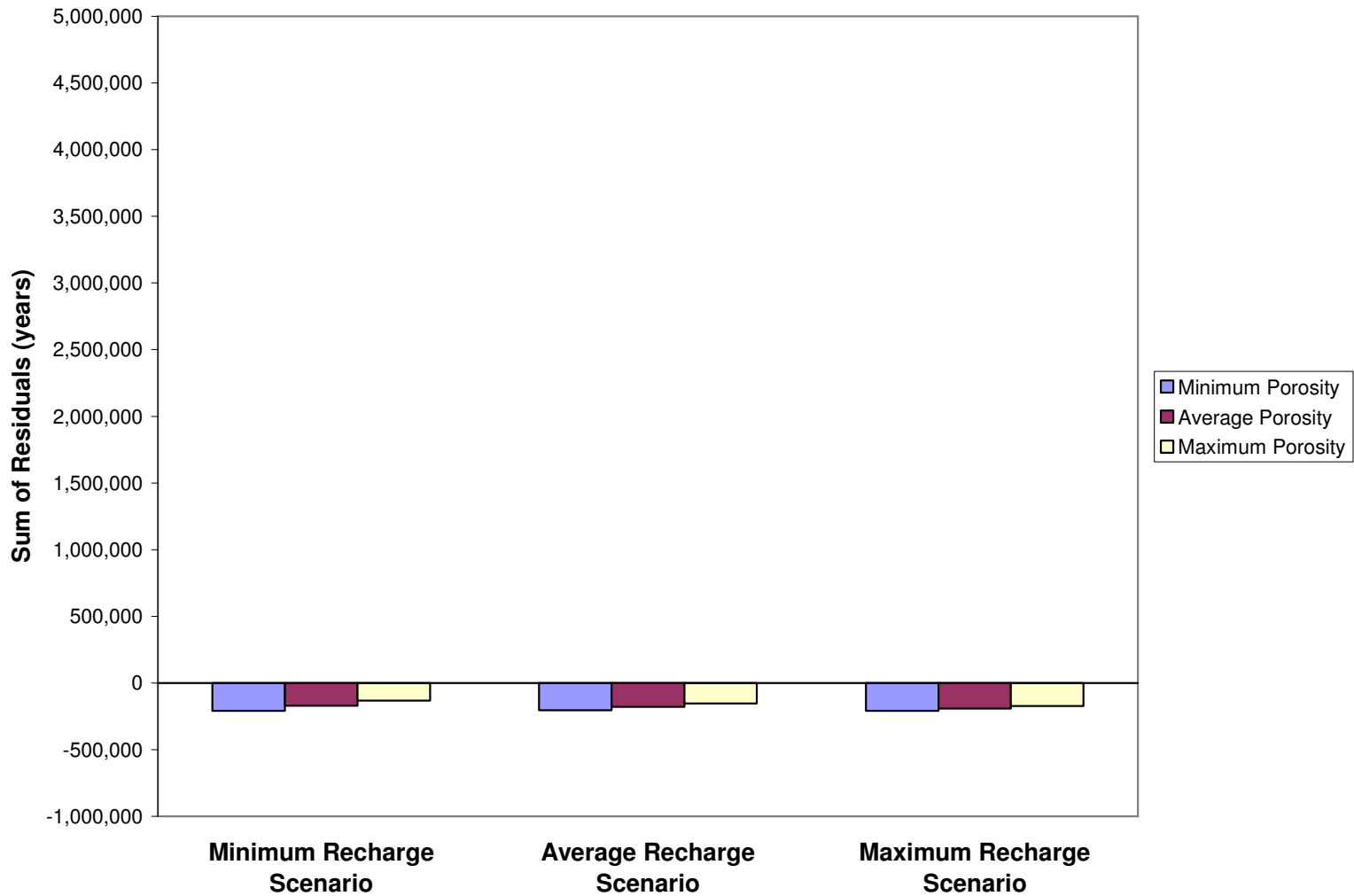
Figure A-4.119: Sum of the residuals between MODPATH and NETPATH ages for the water-balance based minimum, average, and maximum recharge scenarios using minimum, average, and maximum porosities.
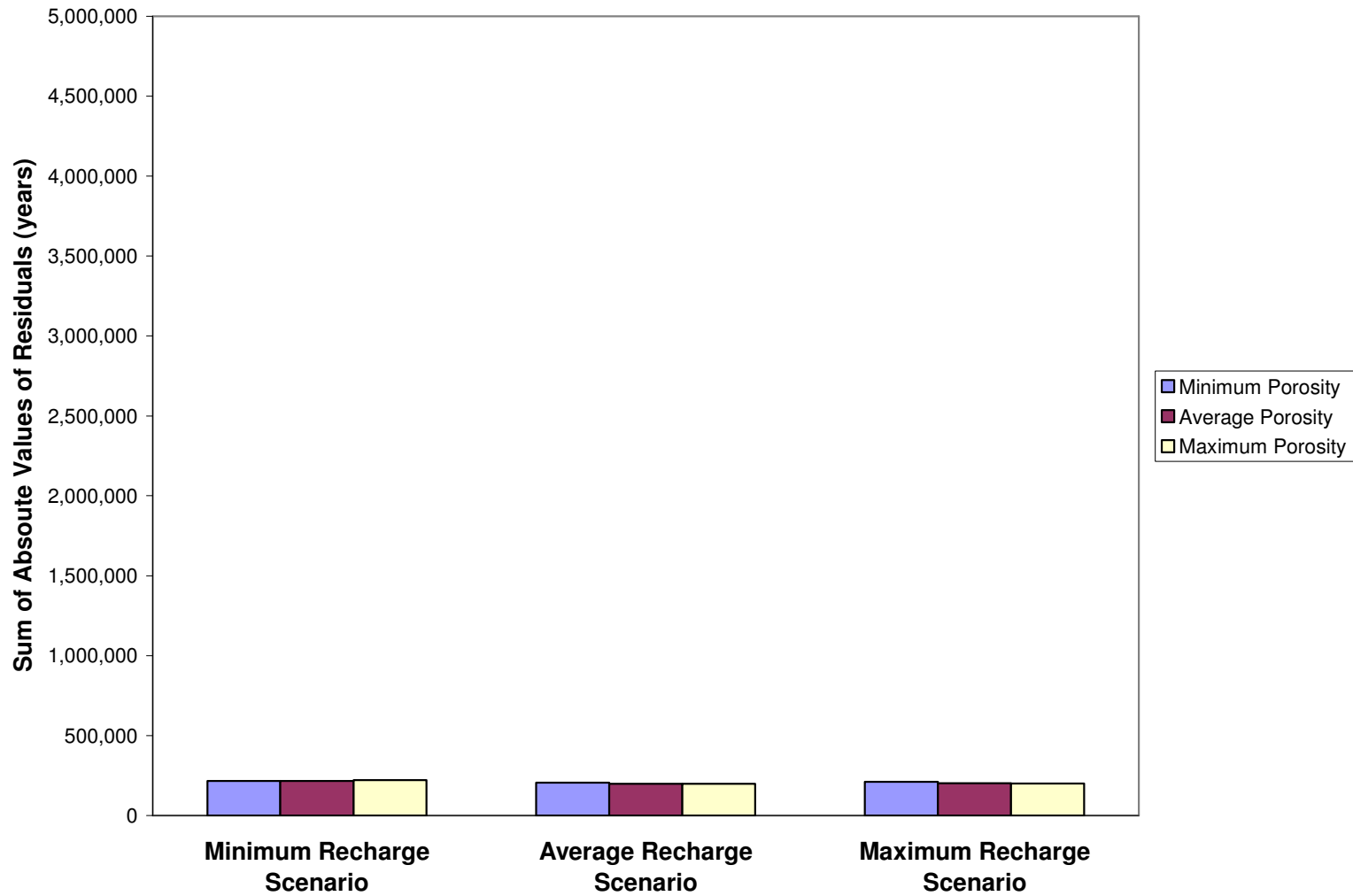
Figure A-4.120: Sum of the absolute values of the residuals between MODPATH and NETPATH ages for the water-balance based minimum, average, and maximum recharge scenarios using minimum, average, and maximum porosities.
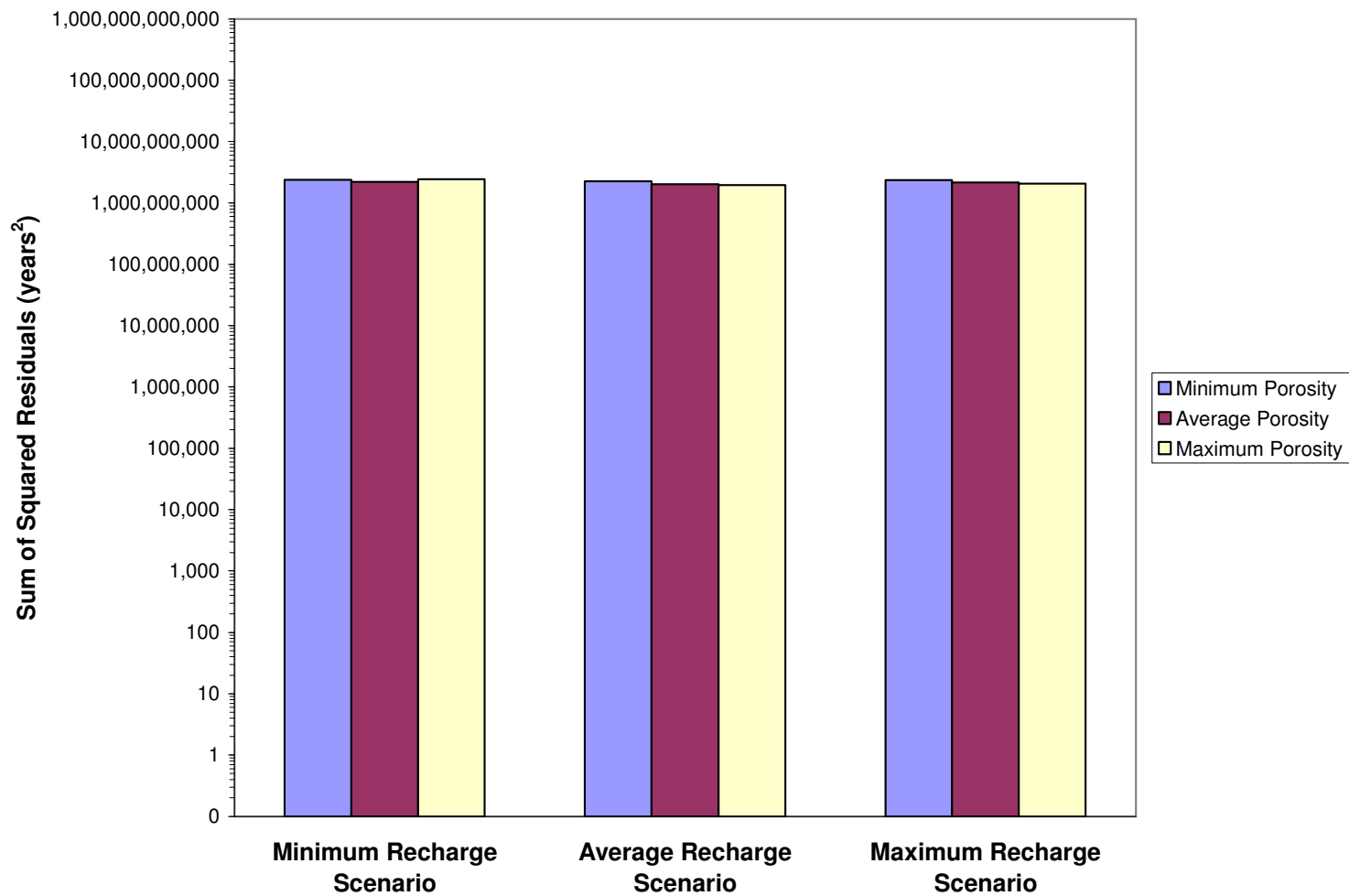
Figure A-4.121: Sum of the squares of the residuals between MODPATH and NETPATH ages for the water-balance based minimum, average, and maximum recharge scenarios using minimum, average, and maximum porosities. Vertical axis is logarithmic scale.
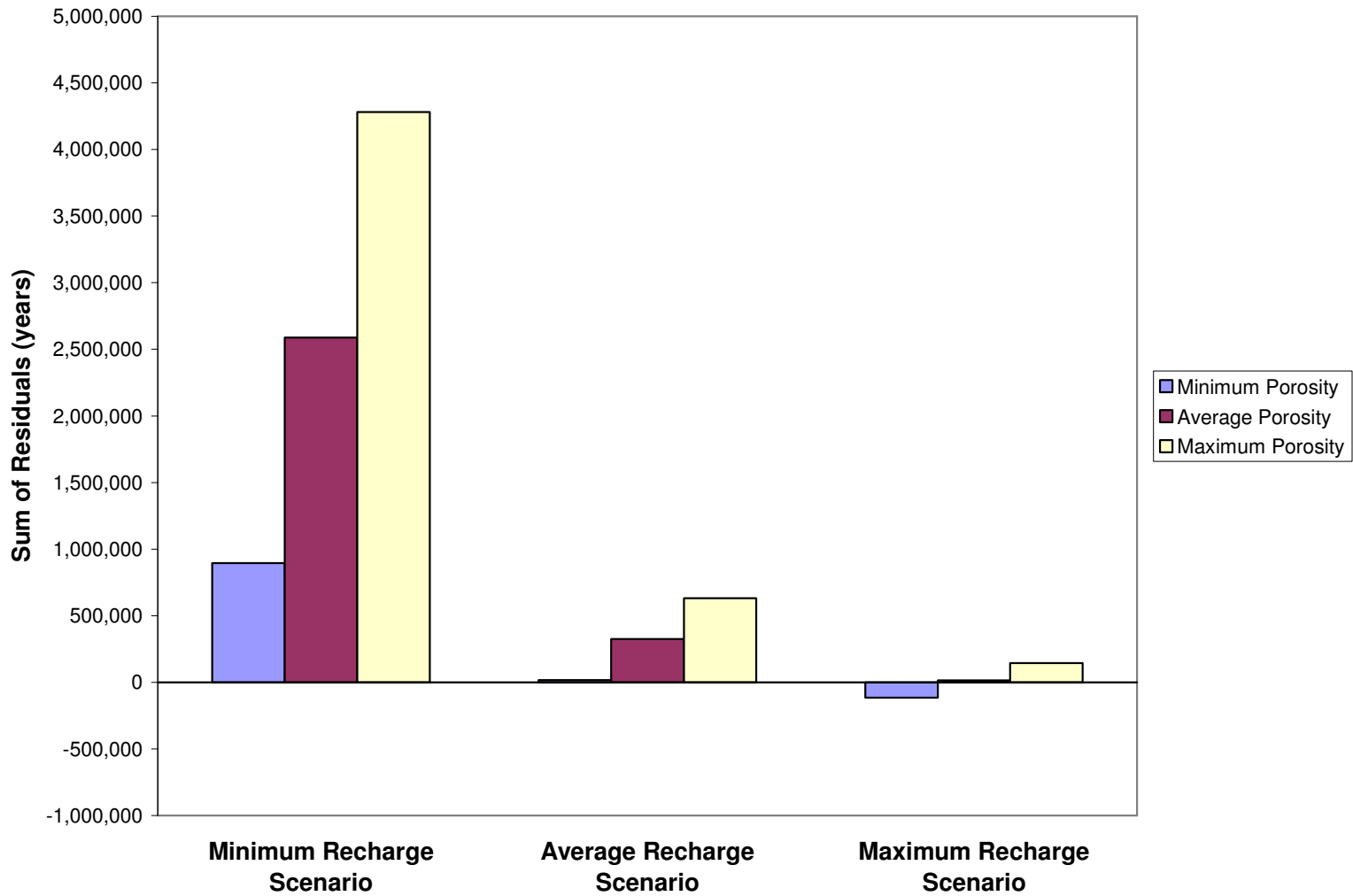
Figure A-4.122: Sum of the residuals between MODPATH and NETPATH ages for the elevation-dependent minimum, average, and maximum recharge scenarios using minimum, average, and maximum porosities.
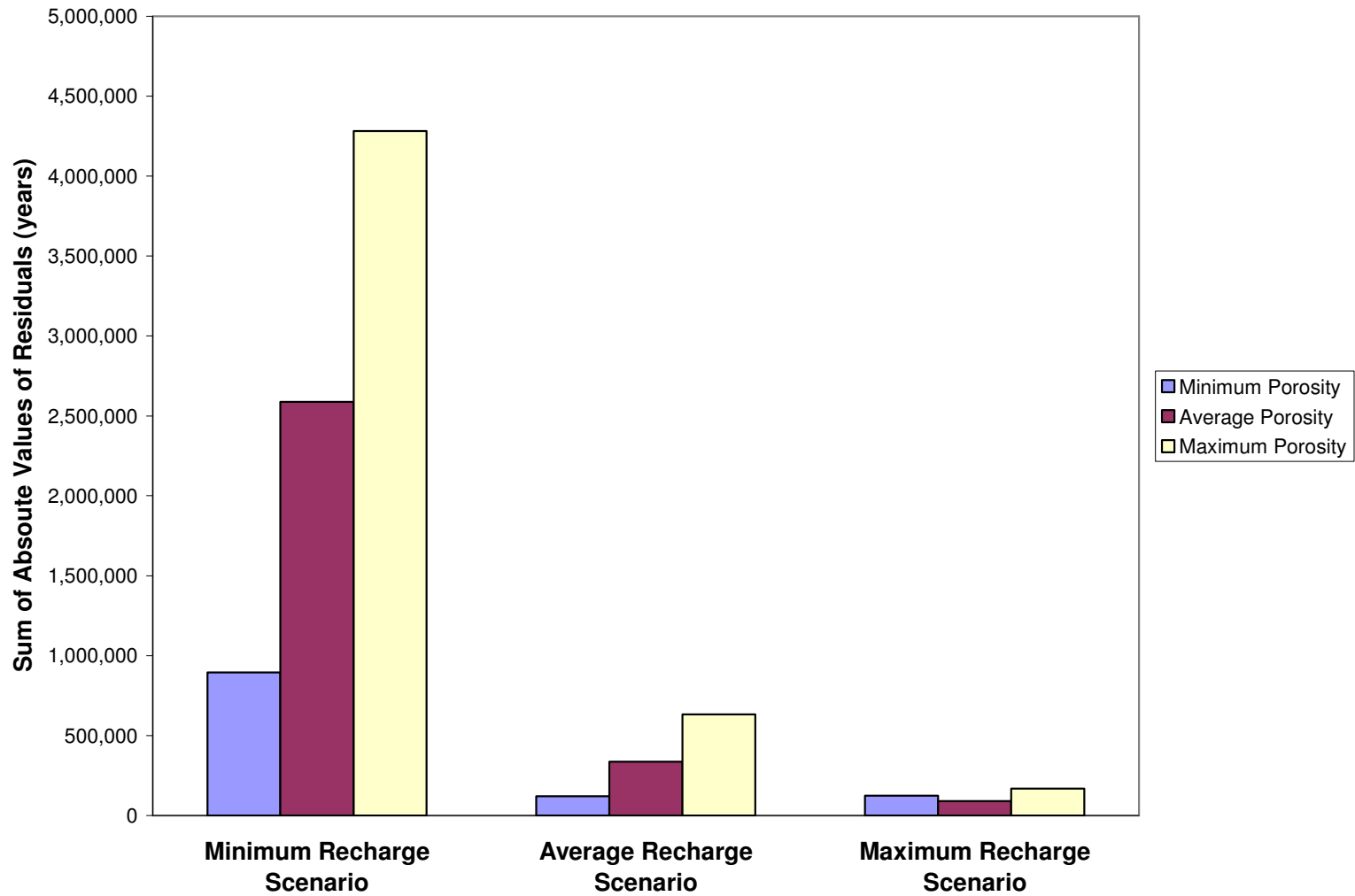
Figure A-4.123: Sum of the absolute values of the residuals between MODPATH and NETPATH ages for the elevation-dependent minimum, average, and maximum recharge scenarios using minimum, average, and maximum porosities.
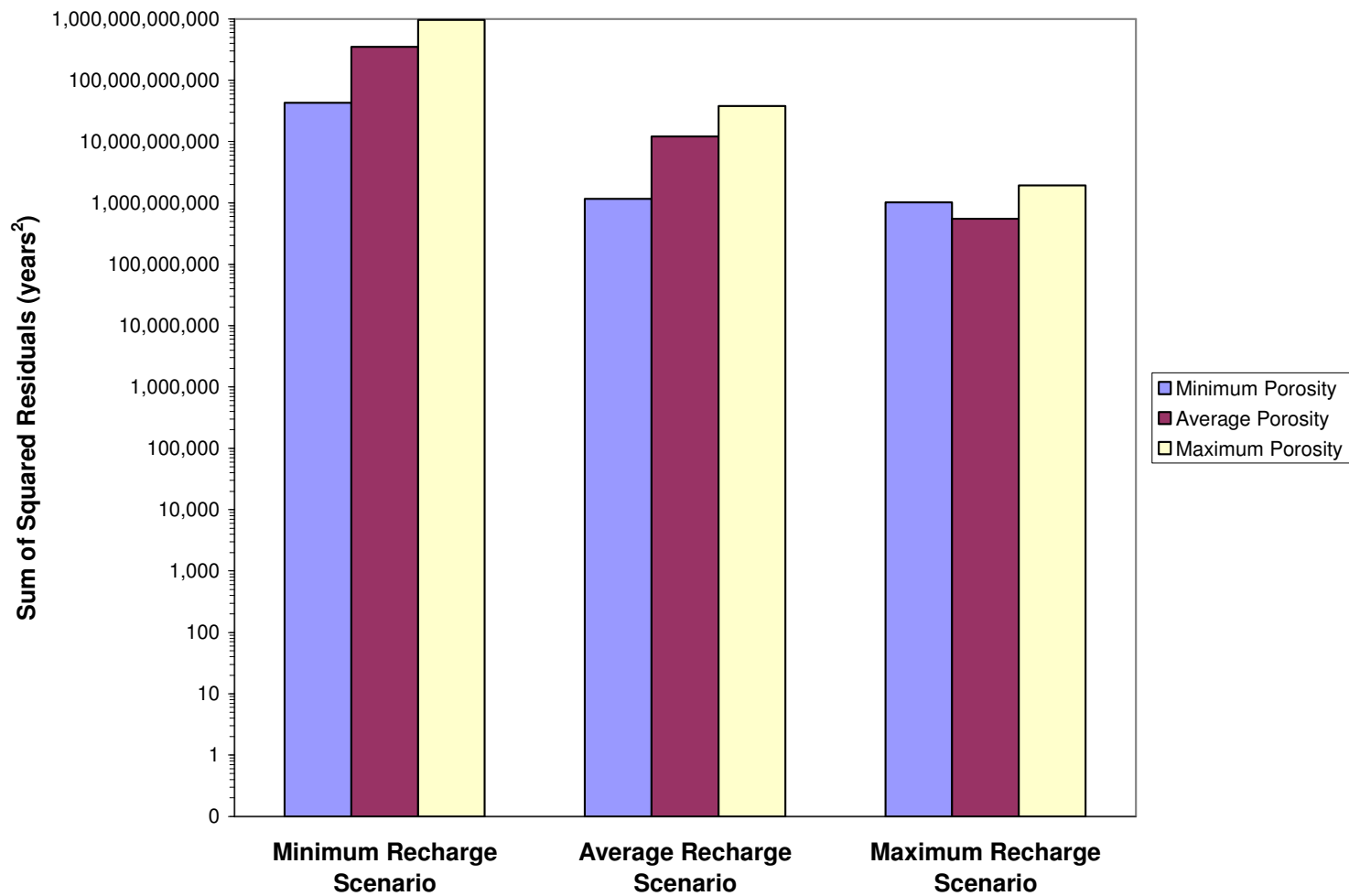
Figure A-4.124: Sum of the squares of the residuals between MODPATH and NETPATH ages for the elevation-dependent minimum, average, and maximum recharge scenarios using minimum, average, and maximum porosities. Vertical axis is logarithmic scale.

TABLES – CHAPTER 3

Well Name, Lease	Well ID	API Number	Easting	Northing	Well Elevation (m)	Reference Level (Source)	Well Depth (m)	Township (S)	Range (E)	Section
Houston Oil & Minerals Corp., State L.G. "1453" #1	HO&MSL1	3003520013	406876	3685414	1,511	GR	3,003	12	10	5
Houston Oil & Minerals Corp., J.M. Lewelling #1	HO&MJL1	3003520010	402778	3684425	1,440	KB	2,852	12	9	12
Houston Oil & Minerals Corp., Lewelling #2	HO&MCL2	3003520015	399960	3684444	1,373	GR	2,892	12	9	10
Houston Oil & Minerals Corp., Federal "A" #1	HO&MFA1	3003520009	413617	3660369	1,619	GR	1,125	14	10	24
Leland A. Hodges, Trustee, Houston #1	LAHTHO1	3003520005	411157	3660302	1,529	GR	928	14	10	23
Houston Oil & Minerals Corp., State 3724 #1	HO&MS31	3003520011	412512	3657622	1,540	GR	1,396	14	10	36
McClellan Oil Corp., Flying "H" Ranch Unit Tract 3 #1	MCOCFH1	3000562244	497349	3652108	1,554	GR	1,557	15	19	14
McClellan Oil Corp., Gragg B #1	MCOCGB1	3000561993	495371	3649683	1,529	GR	1,407	15	19	27
Humble Oil & Refining Co., Yates Federal #1	HO&RYF1	3000560015	486777	3649300	1,648	GR	1,643	15	18	26
J. Cleo Thompson, State A-6 #1	JCTSA61	3000562988	477111	3646836	1,824	GR	1,203	16	17	6
Lubbook Machine & Supply Co., Inc., Anderson-Randell #1	LM&SAR1	3000500003	472069	3645946	1,767	TH	563	16	16	3
Humble Oil & Refining Co., Humble-Yates N.M. State #1	HO&RHY1	3000510521	488336	3643533	1,574	DF	1,802	16	18	8
W.H. Black Drilling Co., Shildneck #1	WHBDCS1	3000500012	514561	3641046	1,330	?	2,137	16	20	24
Continental Oil Company, State NN #1	COCSNN1	3000560185	492051	3640997	1,538	DF	1,677	16	18	22
J. Cleo Thompson, Federal A-28 #1	JCTFA28	3000562915	479948	3639939	1,649	GR	1,481	16	17	28
C & K Petroleum, Inc., Singer Lake State #1	C&KSLS1	3000560320	495659	3637945	1,545	KB	1,617	16	19	31

Table A-3.1: New Mexico oil-and-gas exploratory wells used in this study. Key at bottom of table.

Well Name, Lease	Well ID	API Number	Easting	Northing	Well Elevation (m)	Reference Level (Source)	Well Depth (m)	Township (S)	Range (E)	Section
Southern Production Co., Cloudcroft Unit #1	SPCCLU1	3003500002	431152	3635650	1,511	? (BH)	3,003	17	12	5
Yates Petroleum Corporation, Dunken Nose Unit #1	YPCDNU1	3000560383	491492	3635055	1,440	GR	2,852	17	18	10
Yates Petroleum Corporation, Dunken Dome Unit #2	YPCDDU2	3000560397	485994	3634588	1,373	GR	2,892	17	18	7
Yates Petroleum Corporation, Dunken Dome Unit #1	YPCDDU1	3000560374	486211	3634277	1,619	GR	1,125	17	18	7
Sun Exploration & Production Co., J.T. Jennings #1	SE&PJT1	3000561103	489093	3633855	1,529	GR	928	17	18	9
C & K Petroleum, Inc., Little Cuevo State #1	C&KLCS1	3000560324	501605	3632606	1,540	GR	1,396	17	19	15
Liberty Oil & Gas Corp., T.L. Watts #1	LO&GTLW	3000560766	480341	3631643	1,554	? (BH)	1,557	17	17	21
Magnolia, Headley Federal #2	MAGHEF2	NA	512347	3631229	1,529	?	1,407	17	20	23
Yates Petroleum Corporation, Little Cuevo Unit #1	YPCLCU1	3000561785	488273	3631027	1,648	GR	1,643	17	18	20
Sunray DX Oil Company, N.M. State "AV" #1	SOCSAV1	3000510144	491916	3630614	1,824	GR	1,203	17	18	22
Westcoast Hydrocarbons, Inc., Black Hills Unit #1	WHIBHU1	3000500013	508897	3629768	1,767	?	563	17	20	28
Yates Petroleum Corporation, Little Cuevo Unit #2	YPCLCU2	3000562268	489571	3628557	1,574	GR	1,802	17	18	33
Magnolia, Black Hills	MAGBLHI	NA	505927	3627975	1,330	?	2,137	17	20	31
Gulf Oil Corporation, Chaves State "U" #1	GOCCSU1	3000500002	472386	3625264	1,538	DF	1,677	18	16	10
TEXACO Inc., Federal (USA) "E" #1	TEXIFE1	3003520001	395308	3624999	1,649	GR	1,481	18	8	10
Yates Petroleum Corporation, One Tree Unit #1	YPCOTU1	3000562259	467160	3623529	1,545	KB	1,617	18	16	18

Table A-3.1 continued.

Well Name, Lease	Well ID	API Number	Easting	Northing	Well Elevation (m)	Reference Level (Source)	Well Depth (m)	Township (S)	Range (E)	Section
Yates Petroleum Corporation, Dog Canyon "YF" Federal #1	YPCDCF1	3003520024	462754	3622676	1,511	KB	3,003	18	15	15
Texas Oil & Gas Corp., Federal "C" #1	TO&GFC1	3000560017	512954	3622309	1,440	GR	2,852	18	20	23
Kewanee Oil Co., F-M Unit #1	KOCFMU1	3000500009	493140	3619927	1,373	?	2,892	18	18	26
TEXACO Inc., Federal (USA) "F" #1	TEXIFF1	3003520006	410790	3619951	1,619	GR	1,125	18	10	30
Yates Petroleum Corporation, One Tree Unit #2	YPCOTU2	3000562276	468582	3619170	1,529	KB	928	18	16	29
TEXACO Inc., Federal (USA) "G" #1	TEXIFG1	3003520004	394443	3619379	1,540	GR	1,396	18	8	33
Marathon Oil Co., Mesa Verde Ranch #1	MOCMVR1	3003520022	455326	3618246	1,554	? (BH)	1,557	18	14	35
Yates Petroleum Corp., Buckhorn AYU State Com #1	YPCBAYU	3000560541	506142	3613140	1,529	? (BH)	1,407	19	20	18
Texas Oil & Gas Corp., Federal "A" #1	TO&GFA1	3000510431	506950	3613041	1,648	KB	1,643	19	20	17
Yates Petroleum Corporation (aka Phoenix Resources Co.), Bullis "AVW" State Com (aka Ranch Road) #1	YPCBAVW	3000560557	507355	3612640	1,824	GR	1,203	19	20	20
Sun Oil Co., Pinon Unit #2	SOCPIU2	3000500007	478157	3612259	1,767	DF	563	19	17	20
Sun Oil Co., Pinon Unit #1	SOCPIU1	3000500006	476922	3611828	1,574	DF	1,802	19	17	19
U.V. Industries, Inc., Long Canyon Unit #1	UVILCU1	3000560411	502547	3610225	1,330	KB	2,137	19	19	26
Gulf Oil Corp., Federal Munson #1	GOCFMU1	3000510075	489407	3609839	1,538	DF	1,677	19	18	28
Plymouth Oil Co., Evans (aka Federal D) #1	PLOCEV1	3003500003	404731	3604561	1,649	DF	1,481	20	9	15

Table A-3.1 continued.

705

Well Name, Lease	Well ID	API Number	Easting	Northing	Well Elevation (m)	Reference Level (Source)	Well Depth (m)	Township (S)	Range (E)	Section
Texas Oil & Gas Corp., Federal "B" #1	TO&GFB1	NA	510832	3603835	1,511	?	3,003	20	20	15
Atlantic Refining Co., State "AV" #1	ARCSAV1	3003510001	461443	3603143	1,440	? (BH)	2,852	20	15	16
Zapata Petroleum Corp., Federal 14 #1	ZPCF141	3003500006	454127	3603086	1,373	DF	2,892	20	14	14
Sun Oil Company, T.J. Pearson #1	SOCTJP1	3003500005	416750	3598464	1,619	?	1,125	20	10	35
Terra Resources, Inc., Burro Canyon Unit #1-Y	TRBCU1Y	3003520017	511686	3596471	1,529	? (BH)	928	21	20	2
Stanolind Oil & Gas, Thorn Unit #1	SO&GTU1	3003500007	453419	3593869	1,540	Topo	1,396	21	14	15
Standard of Texas, Scarp Unit #1	SOTSCU1	3003500009	487438	3593394	1,554	DF	1,557	21	18	18
Lefors Petroleum Co., Federal #1	LEPCFE1	3003500008	471863	3592611	1,529	KB	1,407	21	16	22
Yates Petroleum Corporation, Brainerd "IO" Federal #1	YPCBIOF	3001522149	523000	3587630	1,648	KB	1,643	22	21	1
Tri-Service Drilling Co., Little Dog Federal #1	TSDLDF1	3003520008	496060	3586992	1,824	GR	1,203	22	19	6
Otero Oil Co., McGregor #1	OTOCMC1	3003500010	412151	3586894	1,767	?	563	22	10	5
Brainerd Corp. (aka Continental Oil Co.), Federal "A" (aka East Texas Hill Unit) #1	BRCFEA1	3001500005	523406	3586429	1,574	DF	1,802	22	21	1
Continental Oil Co., H.W. Bass #1	COCHWB1	3001500004	516898	3586367	1,330	?	2,137	22	21	5
Marathon Oil Company, Box Canyon Unit #1	MOCBCU1	3001510012	522193	3586059	1,538	DF	1,677	22	21	12
Pitts Energy Co., Federal "9" #1	PIECF91	3001527563	518567	3585218	1,649	KB	1,481	22	21	9

Table A-3.1 continued.

706

Well Name, Lease	Well ID	API Number	Easting	Northing	Well Elevation (m)	Reference Level (Source)	Well Depth (m)	Township (S)	Range (E)	Section
Sinclair Oil & Gas Company, Federal Eddy 193 #1	SO&GFE1	3001500001	518145	3580901	1,511	DF	3,003	22	21	28
E.P. Campbell, Hurley #1	EPCAHU1	3003500012	447355	3580223	1,440	DF	2,852	22	14	30
Tom L. Ingram, State "E" #1	TLISTE1	3001520003	523070	3579540	1,373	GR	2,892	22	21	36
Fred Turner, Jr., Everett #1	FTUEVE1	NA	443146	3579159	1,619	? (BH)	1,125	22	13	34
E.P. Campbell, Liberman State #1	EPCALI1	3003500014	457361	3576570	1,529	DF	928	23	15	7
W.R. Weaver, Thompson #1	WRWETH1	3003500017	499785	3575900	1,540	DF	1,396	23	19	9
E.P. Campbell, Lois Spanel #1	EPCALS1	3003500015	467947	3575324	1,554	DF (Est.)	1,557	23	16	7
Presco, Inc., Indian Creek Federal #1	PRIICF1	3003520030	511700	3573937	1,529	GR	1,407	23	20	14
E.P. Campbell, McMillan Federal #1	EPCAMF1	3003500018	500598	3573842	1,648	DF	1,643	23	19	15
Humble Oil & Refining Co., Huapache Oil Unit #2	HO&RHO2	3001500013	530547	3572779	1,824	DF	1,203	23	22	23
Coral Oil & Gas Co., Warren #1	CO&GCW1	3003500016	487264	3571960	1,767	Topo	563	23	18	19
Inexco Oil Company, Sitting Bull Unit #1	IOCSBU1	3001520752	527152	3568073	1,574	GR	1,802	24	22	4
Coral Oil & Gas Company, Ann Spanel #1	CO&GAS1	3003500021	451716	3566857	1,330	DF	2,137	24	14	9
Atlantic Refining Co., Huapache Unit #9	ARCHUU9	3001500016	527053	3566737	1,538	DF	1,677	24	22	9
Skelly Oil Co., Las Cruces "D" #1	SOCLCD1	3001500003	522240	3565867	1,649	DF	1,481	24	21	12
Union Oil Co., Federal White #1	UNOCFW1	3001500019	525449	3565154	1,545	DF	1,617	24	22	17

Table A-3.1 continued.

707

Well Name, Lease	Well ID	API Number	Easting	Northing	Well Elevation (m)	Reference Level (Source)	Well Depth (m)	Township (S)	Range (E)	Section
Humble Oil & Refining Co., Huapache Unit #5	HO&RHU5	3001500018	531153	3564735	1,511	DF	3,003	24	22	14
Threshold Development Co., Chiricahua R 21 Federal #1	TDCR21F	3003520034	489264	3563381	1,440	GR	2,852	24	18	21
Fred Turner, Jr. (aka Pasotero Pet. Corp.), Evans #1	FTUJEV1	3003500020	433355	3563003	1,373	? (BH)	2,892	24	12	22
E.P. Campbell (aka John J. Eisner), Federal #1	EPCAFE1	3003500019	432641	3562887	1,619	DF	1,125	24	12	21
Flynn, Welch, Yates, Donahue #1	FWYDON1	NA	460768	3561350	1,529	? (Dunn)	928	24	15	28
Franklin, Aston & Fair, Inc., Turkey Draw Unit #1	FA&FTD1	3001521378	524583	3560015	1,540	GR	1,396	24	22	31
Union Oil Co., McMillan #1	UNOCMC1	3003500028	440825	3557266	1,554	Topo	1,557	25	13	9
Union Oil Co., Verse 7 Federal #1	UOCV7F1	3001520591	524435	3556316	1,529	GR	1,407	25	22	7
W.W. West, West Dog Canyon Unit #1	WWWWDC1	3003520007	505979	3555044	1,648	GR	1,643	25	20	18
Transocean Oil, G.J. Ablah #1	TROGJA1	3003520018	442810	3554817	1,824	GR	1,203	25	13	15
R.H. Ernest, Located Land Co. #1	RHELLC1	3003500023	382791	3553354	1,767	USGS	563	25	7	20
Threshold Development Co., Mescalero 28 Federal #1	TDM28F1	3003520033	489514	3552255	1,574	GR	1,802	25	18	28
Beard Oil Company, Ridge USA #1	BOCRUS1	3001522547	524447	3551405	1,330	GR	2,137	25	22	30
Pennzoil Co., Southland "28" State #1	PCS28S1	3003520019	479573	3551070	1,538	GR	1,677	25	17	28
Fred Turner, Jr., State #1	FTUJST1	3003500027	475070	3550274	1,649	DF	1,481	25	16	36

Table A-3.1 continued.

Well Name, Lease	Well ID	API Number	Easting	Northing	Well Elevation (m)	Reference Level (Source)	Well Depth (m)	Township (S)	Range (E)	Section
E.J. Dunigan, Alpha Federal #1	EJDALF1	3003520002	496594	3549815	1,511	KB	3,003	25	19	31
GDP 61-6	GDP61-6	NA	390213	3549130	1,440	WH	2,852	26	8	6
GDP 45-5	GDP45-5	NA	391837	3549102	1,373	WH	2,892	26	8	5
GDP 46-6	GDP46-6	NA	390223	3549119	1,619	WH	1,125	26	8	6
Hunt Oil Co., McMillan-Turner #1	HUOCMT1	3003500029	469015	3547882	1,529	? (Dunn)	928	26	16	5
Harvey E. Yates Co., Bennett Ranch Unit #1	HEYBRU1	3003520027	435547	3545814	1,540	GR	1,396	26	12	14
Seaboard Oil Co., Trigg-Federal #1	SEOCTF1	3003500032	418801	3545797	1,554	DF	1,557	26	11	18
GDP 51-8	GDP51-8	NA	393417	3545870	1,529	WH	1,407	26	8	16
E.P. Campbell, Spiegel-Federal #1	EPCSPF1	3003510002	511803	3544568	1,648	Topo	1,643	26	20	14
Sinclair Oil & Gas Co., Guadalupe Ridge Unit #1	SO&GGR1	3001520176	519670	3543204	1,824	GR	1,203	26	21	22
Harvey E. Yates Co., Bennett Ranch Unit 25 #1	HEYBR25	3003520031	437133	3542284	1,767	?	563	26	12	25

Table A-3.1 continued:

API Number Key: NA = Not applicable.

Reference Level (Source) Key: GR = Ground surface, KB = Kelley bushing, TH = Tubing head, DF = Derrick floor, WH = Well head, ? = unknown if elevation is from GR, KB, TH, DF, or WH, DEM = from USGS NED, Topo = GR from topo. map, BH = from Broadhead (2007), Est. = Estimated, Dunn = from Dunn NMGS (1954), USGS = from USGS.

Well Name, Lease	Well ID	API Number	Easting	Northing	Well Elevation (m)	Reference Level (Source)	Well Depth (m)	Section	Block	Survey
Hunt Petroleum Corp., C.L. Ranch "5" #1	HPCCL51	4222930011	496478	3539912	1,110	? (K&H)	1,678	5	67	T-1, T&P
TEXACO, Inc., State of Texas "FO" "3" #1	TSTFO31	4222930005	421857	3539803	1,580	?	2,647	3	A	UL
Chesapeake Operating, Inc., DF Ranch State 63-12 #1	CODFRS1	4210932302	543327	3538510	1,211	GR	2,780	12	63	T-1, T&P
Magnolia Petr. Co., U-Tex Lease #39881 #1	MPCUTL1	4222900015	443219	3536988	1,533	DF	1,652	19	C	UL
EOG Resources, Inc., Rector Canyon 24 State #1	EOGRC24	4210932250	544329	3534119	1,200	GR	3,024	24	63	T-1, T&P
Pan American Petroleum Corporation, List Anderson #1	PAPCLA1	NA	491521	3533849	1,108	? (V&K)	2,021	23	68	T-1, T&P
Bonanza Co., Pierson	BONCOPI	NA	531346	3532226	1,346	? (V&K)	2,142	26	64	T-1, T&P
Pure Oil Co., Hunter #1	PUOCHU1	NA	509809	3531380	1,625	? (K&H)	2,027	34	66	T-1, T&P
Hunt Oil Co., Dyer #1	HUOCDY1	4222930007	485477	3530917	1,119	? (K&H)	898	31	68	T-1, T&P
Hueco Basin, University #1	HUBAUN1	NA	421896	3530405	1,558	DEM	765	39	A	UL
Trail Mountain, Inc., University Big Iron "C45" #1	TMUBIC1	4222900029	440743	3529232	1,516	GR	965	45	C	UL
Hunt Petroleum Corp., C.L. Ranch #1	HPCCLR1	4222930010	496475	3528252	1,105	? (K&H)	1,595	44	67	T-1, T&P
TEXACO Inc., Culberson "L" Fee #1	TEXCLF1	NA	519234	3527336	1,564	? (K&H)	2,652	45	65	T-1, T&P
Tenneco Oil Co., TXL Fee #1	TOTXLF1	4210931401	563041	3526975	1,086	KB	4,095	1	61	T-2, T&P
Pan American Petroleum Corporation, Ed Hammock #1	PAPCEH1	NA	499124	3526693	1,110	GR	2,152	4	67	T-2, T&P
Trail Mountain, Inc., University Sizzler D5 #1	TMUSD51	4222930227	437784	3526650	1,437	GR	1,774	5	D	UL
TXL Corp., Culberson "C" Fee #1	TXLCCF1	NA	523721	3526221	1,515	? (V&K)	2,362	1	65	T-2, T&P

Table A-3.2: Texas oil-and-gas exploratory wells used in this study. Key at bottom of table.

Well Name, Lease	Well ID	API Number	Easting	Northing	Well Elevation (m)	Reference Level (Source)	Well Depth (m)	Section	Block	Survey
General Crude Oil Company, Merrill and Voyles et al. #1	GCOCMV1	NA	477481	3524877	1,580	DF	2,647	8	69	T-2, T&P
Magnolia Petro., No. A-1 Homer, Cowden	MPNA1HC	NA	544286	3524346	1,211	? (V&K)	2,780	12	63	T-2, T&P
EOG Resources, Inc., Kenney 16 State #1H	EOGKS1H	4210932270	527946	3523355	1,533	GR	1,652	16	64	T-2, T&P
EOG Resources, Inc., Kenney 16 State #2	EOGKES2	4210932269	528404	3522559	1,200	GR	3,024	16	64	T-2, T&P
California Standard of Texas, Theisen #1	CASATT1	NA	426103	3521248	1,108	?	2,021	19	E	UL
D & J Equip Co., J.C. Hunter, Jr. #2	DJJCHJ2	NA	512403	3519886	1,346	? (V&K)	2,142	2	120	PSL
Trail Mountain, Inc., University Felina "D27" #1	TMUFD27	4222930006	439917	3518350	1,625	GR	2,027	27	D	UL
Border Exploration Co., Hammack et al. CT-1	BECHCT1	4222930196	505172	3518026	1,119	? (K&H)	898	20	120	PSL
TXL Oil Corp., Culberson B-T Fee #1	TXLCBT1	NA	550456	3517797	1,558	? (V&K)	765	33	62	T-2, T&P
A.R. Jones Co., E.C. Mowry #1	ARJECM1	NA	474192	3516927	1,516	DF	965	36	70	T-2, T&P
Tipperary Corp., ST-1 Billye Sparks	TCST1BS	4222930195	474281	3516816	1,105	GR	1,595	36	70	T-2, T&P
J.L. Cowley, E.C. Mowry #1	JLCECM1	NA	473079	3515907	1,564	?	2,652	37	70	T-2, T&P
Border Exploration Co., J.J. McAdoo 7 #1	BECJJM1	4222930200	505794	3514682	1,086	? (K&H)	4,095	7	119	PSL
T.E. Robertson Co., Inc., Mowry et al. #2	TERCMO2	NA	471217	3514010	1,110	DF	2,152	47	70	T-2, T&P
The Superior Oil Company, Covington State #1	TSOCCS1	4210931405	565213	3512927	1,437	GR	1,774	1	115	PSL
Chesapeake Operating, Inc., Dela Minerals "3" State #701	COIDM3S	4210932268	566918	3512065	1,515	GR	2,362	7	114	PSL
Trail Mountain, Inc., University Devil Woman L5 #1	TMUDWL5	4222930253	477595	3510876	1,181	GR	1,461	5	L	UL

Table A-3.2 continued.

711

Well Name, Lease	Well ID	API Number	Easting	Northing	Well Elevation (m)	Reference Level (Source)	Well Depth (m)	Section	Block	Survey
Samson Lone Star, L.L.C., University Lands 46-14 #2	SALSUL2	4210932278	551660	3509591	1,110	KB	1,678	14	46	UL
Humble Oil & Ref. Co., M.C. Sibley #1	HORMCS1	NA	533795	3508569	1,580	? (V&K)	2,647	24	68	PSL
N. Amer. Royalties, Inc., Potter #1	NARIPO1	NA	511738	3508091	1,211	? (V&K)	2,780	31	119	PSL
Chesapeake Operating, Inc., University Lands 4627 #1	COUL462	4210932287	550571	3507028	1,533	GR	1,652	27	46	UL
J.M. Huber Corp., Tom Potter #1	JMHCTP1	NA	514111	3505748	1,200	? (V&K)	3,024	2	118	PSL
EnCana Oil & Gas (USA) Inc., Sibley Ranch 47 State "25" #1	EOGSR47	4210932251	544180	3505778	1,108	KB	2,021	25	47	PSL
Anderson & Prichard, Bordens #1	A&PBOR1	NA	521137	3505265	1,346	? (V&K)	2,142	34	69	PSL
Trail Mountain, Inc., University Ooby Dooby L35 #1	TMUODL1	4222930261	482251	3502319	1,625	KB	2,027	35	L	UL
Petro-Hunt, L.L.C., Melissa Taylor State 27 #1-H	PHMTS27	4210932255	563684	3501318	1,119	GR	898	27	109	PSL
Faith Minerals, Inc., Wesley West #1	FMINWW1	4222930012	503401	3499500	1,558	GR	765	36	118	PSL
American Quasar Pet. Co., V.C. Rounsaville #1	AQPVCR1	NA	563477	3498883	1,516	? (V&K)	965	13	108	PSL
Hassle Hunt Trust, Univ. "M-49" #1	HHUM491	NA	450328	3497929	1,105	DF	1,595	9	M	UL
EOG Resources, Inc., Wild Horse Draw 7 #1	EOGWHD7	4210932256	536584	3497771	1,564	GR	2,652	7	106	PSL
Pan American Pet. Corp., Phillip F. Hass #1	PAPPFH1	NA	422942	3494846	1,086	DF	4,095	14	13	PSL
Chesapeake Operating, Inc., Melissa Taylor State 105-3	COMT105	4210932297	541293	3493028	1,110	GR	2,152	3	105	PSL
Transocean Oil, Inc., 36-1 MSA Trustee, Inc.	TO36MSA	4222930192	424652	3490962	1,437	KB	1,774	36	13	PSL
El Paso Co., No. 1 Montgomery	EPCN1MO	NA	546957	3484390	1,515	? (V&K)	2,362	17	100	PSL

Table A-3.2 continued.

Well Name, Lease	Well ID	API Number	Easting	Northing	Well Elevation (m)	Reference Level (Source)	Well Depth (m)	Section	Block	Survey
Gulf Oil Corp., M.A. Grisham #1	GOCMAG1	NA	535928	3484129	1,110	? (V&K)	1,678	18	99	PSL
Hassle Hunt Trust, Mosely #1	HAHUTM1	NA	449636	3483385	1,580	GR	2,647	27	24	PSL
Lockhart, Roseborough & Benton, Gardner & Mosely #1 or Western States Oil, Gardner & Moseley #1	LR&BGM1 or WSOG&M1	NA	442367	3480668	1,211	DF	2,780	12	18	PSL
Chesapeake Operating, Inc., State Street State #701	COSS701	4210932271	546492	3478738	1,533	GR	1,652	7	97	PSL
Sinclair, Looney	SINCLOO	NA	551319	3475371	1,200	? (V&K)	3,024	22	97	PSL
Gulf Oil Corp., J. Burner-State "B" #1	GOCJBS1	NA	441556	3472050	1,108	DF	2,021	14	19	PSL
Lockhart Bros., Gardner & Mosely (Formerly Public School) #1	LOBG&M1	NA	446485	3468512	1,346	?	2,142	5	21	PSL
Stanolind Oil & Gas Co. American Land, No. 1 Roseborough	SOGAL1R	NA	444464	3467169	1,625	? (V&K)	2,027	7	21	PSL
J.P. Hurndall & R.A. Gray, J.S. Pierce #1	H&GJSP1	NA	479266	3465692	1,119	DEM	898	8	46	PSL
Fred A. Davis West and Armour, Davis #1	FADWAD1	NA	528309	3464645	1,558	? (V&K)	765	5	86	PSL

Table A-3.2 continued:

API Number Key: NA = Not applicable.

Reference Level (Source) Key: GR = Ground surface, KB = Kelley bushing, DF = Derrick floor, ? = unknown if elevation is from GR, KB, or DF, DEM = from USGS NED, K&H = from King and Harder (1985), V&K = from Veldhuis and Keller (1980).

Well Name, Lease	Well ID	API Number	Easting	Northing	Well Elevation (m)	Depth to Top of Precambrian (m)	Elevation of Top of Precambrian (m)	Source	Note
Houston Oil & Minerals Corp., State L.G. "1453" #1	HO&MSL1	3003520013	406876	3685414	1,511	2,999	-1,489	NMBG DL	
Houston Oil & Minerals Corp., Lewelling #2	HO&MCL2	3003520015	399960	3684444	1,373	2,713	-1,339	OCD	
Houston Oil & Minerals Corp., J.M. Lewelling #1	HO&MJL1	3003520010	402778	3684425	1,434	Est.	-1,425	F	Estimate from Foster (1978)
Houston Oil & Minerals Corp., State 3724 #1	HO&MS31	3003520011	412512	3657622	1,540	1,372	169	OCD	
McClellan Oil Corp., Flying "H" Ranch Unit Tract 3 #1	MCOCFH1	3000562244	497349	3652108	1,554	1,432	122	OCD	
Humble Oil & Refining Co., Yates Federal #1	HO&RYF1	3000560015	486777	3649300	1,648	Est.	-30	BH	Estimate from Broadhead (2007)
J. Cleo Thompson, State A-6 #1	JCTSA61	3000562988	477111	3646836	1,824	1,180	644	OCD	
Lubbook Machine & Supply Co., Inc., Anderson-Randell #1	LM&SAR1	3000500003	472069	3645946	1,767	539	1,228	OCD	
Humble Oil & Refining Co., Humble-Yates N.M. State #1	HO&RHY1	3000510521	488336	3643533	1,574	1,798	-225	OCD	
W.H. Black Drilling Co., Shildneck #1	WHBDCS1	3000500012	514561	3641046	1,330	2,131	-801	NMBG SC	
Continental Oil Company, State NN #1	COCSNN1	3000560185	492051	3640997	1,538	1,822	-284	OCD	Estimate based on nearby wells
J. Cleo Thompson, Federal A-28 #1	JCTFA28	3000562915	479948	3639939	1,649	1,461	188	OCD	
C & K Petroleum, Inc., Singer Lake State #1	C&KSLS1	3000560320	495659	3637945	1,545	1,830	-285	OCD	Estimate based on nearby wells
Southern Production Co., Cloudcroft Unit #1	SPCCLU1	3003500002	431152	3635650	2,859	1,402	1,457	BH	
Yates Petroleum Corporation, Dunken Nose Unit #1	YPCDNU1	3000560383	491492	3635055	1,602	1,860	-258	OCD	Estimate based on nearby wells
Yates Petroleum Corporation, Dunken Dome Unit #2	YPCDDU2	3000560397	485994	3634588	1,631	1,726	-95	OCD	Estimate based on nearby wells
Yates Petroleum Corporation, Dunken Dome Unit #1	YPCDDU1	3000560374	486211	3634277	1,643	1,763	-119	OCD	
C & K Petroleum, Inc., Little Cuevo State #1	C&KLCS1	3000560324	501605	3632606	1,464	2,152	-689	OCD	Estimate based on nearby wells
Liberty Oil & Gas Corp., T.L. Watts #1	LO&GTLW	3000560766	480341	3631643	1,633	1,751	-118	BH	
Magnolia, Headley Federal #2	MAGHEF2	NA	512347	3631229	1,510	1,749	-239	BH	Estimate based on nearby wells
Yates Petroleum Corporation, Little Cuevo Unit #1	YPCLCU1	3000561785	488273	3631027	1,633	1,751	-118	NMBG SC	

Table A-3.3: Oil-and-gas exploratory wells used as control for the top of the Precambrian. Key at bottom of table.

Well Name, Lease	Well ID	API Number	Easting	Northing	Well Elevation (m)	Depth to Top of Precambrian (m)	Elevation of Top of Precambrian (m)	Source	Note
Sunray DX Oil Company, N.M. State "AV" #1	SOCSAV1	3000510144	491916	3630614	1,582	1,795	-213	OCD	
Westcoast Hydrocarbons, Inc., Black Hills Unit #1	WHIBHU1	3000500013	508897	3629768	1,453	1,748	-295	NMBG SC	Estimate based on nearby wells
Yates Petroleum Corporation, Little Cuevo Unit #2	YPCLCU2	3000562268	489571	3628557	1,618	1,666	-48	OCD	Estimate based on nearby wells
Magnolia, Black Hills	MAGBLHI	NA	505927	3627975	1,494	Est.	-229	BH	Estimate from Broadhead (2007)
Gulf Oil Corporation, Chaves State "U" #1	GOCCSU1	3000500002	472386	3625264	1,907	905	1,002	OCD	
TEXACO Inc., Federal (USA) "E" #1	TEXIFE1	3003520001	395308	3624999	1,219	Est.	-1,285	F	
Yates Petroleum Corporation, One Tree Unit #1	YPCOTU1	3000562259	467160	3623529	1,876	1,976	-100	NMBG SC	
Yates Petroleum Corporation, Dog Canyon "YF" Federal #1	YPCDCF1	3003520024	462754	3622676	1,946	2,512	-566	NMBG SC	
Texas Oil & Gas Corp., Federal "C" #1	TO&GFC1	3000560017	512954	3622309	1,359	Est.	-1,054	BH	Estimate from Broadhead (2007)
TEXACO Inc., Federal (USA) "F" #1	TEXIFF1	3003520006	410790	3619951	1,232	Est.	-1,481	F	Estimate from Foster (1978)
Kewanee Oil Co., F-M Unit #1	KOCFMU1	3000500009	493140	3619927	1,579	2,307	-728	NMBG SC	Estimate based on nearby wells
TEXACO Inc., Federal (USA) "G" #1	TEXIFG1	3003520004	394443	3619379	1,276	Est.	-1,242	F	Estimate from Foster (1978)
Yates Petroleum Corporation, One Tree Unit #2	YPCOTU2	3000562276	468582	3619170	2,010	824	1,185	NMBG SC	
Marathon Oil Co., Mesa Verde Ranch #1	MOCMVR1	3003520022	455326	3618246	2,143	2,123	20	NMBG SC	
Yates Petroleum Corp., Buckhorn AYU State Com #1	YPCBAYU	3000560541	506142	3613140	1,440	Est.	-962	BH	Estimate from Broadhead (2007)
Texas Oil & Gas Corp., Federal "A" #1	TO&GFA1	3000510431	506950	3613041	1,442	2,496	-1,054	BH	Estimate based on nearby wells
Yates Petroleum Corporation (aka Phoenix Resources Co.), Bullis "AVW" State Com (aka Ranch Road) #1	YPCBAVW	3000560557	507355	3612640	1,478	2,553	-1,075	NMBG SC	Estimate based on nearby wells
Sun Oil Co., Pinon Unit #2	SOCPIU2	3000500007	478157	3612259	1,925	501	1,424	NMBG SC	
Sun Oil Co., Pinon Unit #1	SOCPIU1	3000500006	476922	3611828	1,995	526	1,469	NMBG SC	
U.V. Industries, Inc., Long Canyon Unit #1	UVILCU1	3000560411	502547	3610225	1,536	Est.	-1,072	BH	Estimate from Broadhead (2007)

Table A-3.3 continued.

715

Well Name, Lease	Well ID	API Number	Easting	Northing	Well Elevation (m)	Depth to Top of Precambrian (m)	Elevation of Top of Precambrian (m)	Source	Note
Gulf Oil Corp., Federal Munson #1	GOCFMU1	3000510075	489407	3609839	1,723	1,402	321	NMBG SC	
Plymouth Oil Co., Evans (aka Federal D) #1	PLOCEV1	3003500003	404731	3604561	1,233	Est.	-1,141	F	Estimate from Foster (1978)
Texas Oil & Gas Corp., Federal "B" #1	TO&GFB1	NA	510832	3603835	1,463	2,837	-1,374	NMBG SC	Estimate based on nearby wells
Atlantic Refining Co., State "AV" #1	ARCSAV1	3003510001	461443	3603143	1,921	Est.	-100	BH	Estimate from Broadhead (2007)
Zapata Petroleum Corp., Federal 14 #1	ZPCF141	3003500006	454127	3603086	2,109	Est.	326	F	Estimate from Foster (1978)
Sun Oil Company, T.J. Pearson #1	SOCTJP1	3003500005	416750	3598464	1,344	Est.	-302	F	Estimate from Foster (1978)
Terra Resources, Inc., Burro Canyon Unit #1-Y	TRBCU1Y	3003520017	511686	3596471	1,572	Est.	-466	BH	Estimate from Broadhead (2007)
Stanolind Oil & Gas, Thorn Unit #1	SO&GTU1	3003500007	453419	3593869	1,914	Est.	72	F	Estimate from Foster (1978)
Standard of Texas, Scarp Unit #1	SOTSCU1	3003500009	487438	3593394	1,628	786	842	NMBG SC	
Lefors Petroleum Co., Federal #1	LEPCFE1	3003500008	471863	3592611	1,642	677	964	NMBG SC	
Tri-Service Drilling Co., Little Dog Federal #1	TSDLDF1	3003520008	496060	3586992	1,940	Est.	451	BH	Estimate from Broadhead (2007)
Brainerd Corp. (aka Continental Oil Co.), Federal "A" (aka East Texas Hill Unit) #1	BRCFEA1	3001500005	523406	3586429	1,397	3,248	-1,851	NMBG SC	Estimate based on nearby wells
Continental Oil Co., H.W. Bass #1	COCHWB1	3001500004	516898	3586367	1,680	1,636	43	NMBG SC	Estimate based on nearby wells
Marathon Oil Company, Box Canyon Unit #1	MOCBCU1	3001510012	522193	3586059	1,426	3,206	-1,780	OCD	Estimate based on nearby wells
E.P. Campbell, Hurley #1	EPCAHU1	3003500012	447355	3580223	1,404	Est.	198	F	Estimate from Foster (1978)
Fred Turner, Jr., Everett #1	FTUEVE1	NA	443146	3579159	1,476	Est.	248	F	Estimate from Foster (1978)
E.P. Campbell, Liberman State #1	EPCALI1	3003500014	457361	3576570	1,326	819	507	K&H	
W.R. Weaver, Thompson #1	WRWETH1	3003500017	499785	3575900	1,386	Est.	14	BH	Estimate from Broadhead (2007)
E.P. Campbell, Lois Spanel #1	EPCALS1	3003500015	467947	3575324	1,408	908	500	K&H	Estimate based on nearby wells
E.P. Campbell, McMillan Federal #1	EPCAMF1	3003500018	500598	3573842	1,319	Est.	-98	BH	Estimate from Broadhead (2007)
Humble Oil & Refining Co., Huapache Oil Unit #2	HO&RHO2	3001500013	530547	3572779	1,358	3,823	-2,465	OCD	

Table A-3.3 continued.

716

Well Name, Lease	Well ID	API Number	Easting	Northing	Well Elevation (m)	Depth to Top of Precambrian (m)	Elevation of Top of Precambrian (m)	Source	Note
Coral Oil & Gas Co., Warren #1	CO&GCW1	3003500016	487264	3571960	1,186	687	499	K&H	
Inexco Oil Company, Sitting Bull Unit #1	IOCSBU1	3001520752	527152	3568073	1,650	2,329	-679	OCD	Estimate based on nearby wells
Coral Oil & Gas Company, Ann Spanel #1	CO&GAS1	3003500021	451716	3566857	1,391	556	835	OCD	
Skelly Oil Co., Las Cruces "D" #1	SOCLCD1	3001500003	522240	3565867	1,749	2,411	-663	NMBG SC	Estimate based on nearby wells
Union Oil Co., Federal White #1	UNOCFW1	3001500019	525449	3565154	1,740	Est.	-714	BH	Estimate from Broadhead (2007)
Threshold Development Co., Chiricahua R 21 Federal #1	TDCR21F	3003520034	489264	3563381	1,133	816	317	OCD	
Fred Turner, Jr. (aka Pasotero Pet. Corp.), Evans #1	FTUJEV1	3003500020	433355	3563003	1,545	Est.	370	F	Estimate from Foster (1978)
E.P. Campbell (aka John J. Eisner), Federal #1	EPCAFE1	3003500019	432641	3562887	1,497	1,138	358	NMBG SC	Estimate based on nearby wells
Franklin, Aston & Fair, Inc., Turkey Draw Unit #1	FA&FTD1	3001521378	524583	3560015	1,776	2,786	-1,010	OCD	Estimate based on nearby wells
Union Oil Co., McMillan #1	UNOCMC1	3003500028	440825	3557266	1,522	Est.	-27	F	Estimate from Foster (1978)
Union Oil Co., Verse 7 Federal #1	UOCV7F1	3001520591	524435	3556316	1,801	2,842	-1,041	OCD	Estimate based on nearby wells
Transocean Oil, G.J. Ablah #1	TROGJA1	3003520018	442810	3554817	1,509	1,376	133	K&H	
R.H. Ernest, Located Land Co. #1	RHELLC1	3003500023	382791	3553354	1,249	Est.	-987	F	Estimate from Foster (1978)
Threshold Development Co., Mescalero 28 Federal #1	TDM28F1	3003520033	489514	3552255	1,219	831	387	OCD	
Beard Oil Company, Ridge USA #1	BOCRUS1	3001522547	524447	3551405	1,896	3,164	-1,267	OCD	Estimate based on nearby wells
Pennzoil Co., Southland "28" State #1	PCS28S1	3003520019	479573	3551070	1,206	1,181	25	K&H	Estimate based on nearby wells
Fred Turner, Jr., State #1	FTUJST1	3003500027	475070	3550274	1,317	939	379	K&H	
E.J. Dunigan, Alpha Federal #1	EJDALF1	3003520002	496594	3549815	1,159	Est.	-755	BH	Estimate from Broadhead (2007)
GDP 61-6	GDP61-6	NA	390213	3549130	1,254	1,859	-605	F&J	Estimate based on nearby wells
GDP 46-6	GDP46-6	NA	390223	3549119	1,252	1,853	-601	F&J	Estimate based on nearby wells
GDP 45-5	GDP45-5	NA	391837	3549102	1,255	Est.	-432	BH	Estimate from Broadhead (2007)
Hunt Oil Co., McMillan-Turner #1	HUOCMT1	3003500029	469015	3547882	1,269	573	696	BH	
GDP 51-8	GDP51-8	NA	393417	3545870	1,253	Est.	223	BH	Estimate from Broadhead (2007)

Table A-3.3 continued.

Well Name, Lease	Well ID	API Number	Easting	Northing	Well Elevation (m)	Depth to Top of Precambrian (m)	Elevation of Top of Precambrian (m)	Source	Note
Harvey E. Yates Co., Bennett Ranch Unit #1	HEYBRU1	3003520027	435547	3545814	1,554	2,154	-599	OCD	
Seaboard Oil Co., Trigg-Federal #1	SEOCTF1	3003500032	418801	3545797	1,618	Est.	-894	F	Estimate from Foster (1978)
Harvey E. Yates Co., Bennett Ranch Unit 25 #1	HEYBR25	3003520031	437133	3542284	1,533	1,962	-429	OCD	Estimate based on nearby wells
TEXACO, Inc., State of Texas "FO" "3" #1	TSTFO31	4222930005	421857	3539803	1,580	2,647	-1,066	BEG SC	In Precambrian at total well depth
Magnolia Petr. Co., U-Tex Lease #39881 #1	MPCUTL1	4222900015	443219	3536988	1,533	1,654	-121	BEG SC	Estimate based on nearby wells
EOG Resources, Inc., Rector Canyon 24 State #1	EOGRC24	4210932250	544329	3534119	1,200	3,630	-2,430	RRC	Estimate based on nearby wells
Pan American Petroleum Corporation, List Anderson #1	PAPCLA1	NA	491521	3533849	1,108	905	203	V&K	
Pure Oil Co., Hunter #1	PUOCHU1	NA	509809	3531380	1,625	2,149	-524	K&H	Estimate based on nearby wells
Hunt Oil Co., Dyer #1	HUOCDY1	4222930007	485477	3530917	1,119	1,212	-93	K&H	Estimate based on nearby wells
Trail Mountain, Inc., University Big Iron "C45" #1	TMUBIC1	4222900029	440743	3529232	1,516	1,667	-151	RRC	Estimate based on nearby wells
Hunt Petroleum Corp., C.L. Ranch #1	HPCCLR1	4222930010	496475	3528252	1,105	2,206	-1,101	K&H	Estimate based on nearby wells
TEXACO Inc., Culberson "L" Fee #1	TEXCLF1	NA	519234	3527336	1,564	2,850	-1,286	K&H	Estimate based on nearby wells
Tenneco Oil Co., TXL Fee #1	TOTXLF1	4210931401	563041	3526975	1,086	4,291	-3,205	RRC	Estimate based on nearby wells
Pan American Petroleum Corporation, Ed Hammock #1	PAPCEH1	NA	499124	3526693	1,110	2,245	-1,135	V&K	Estimate based on nearby wells
Trail Mountain, Inc., University Sizzler D5 #1	TMUSD51	4222930227	437784	3526650	1,437	2,468	-1,031	RRC	Estimate based on nearby wells
TXL Corp., Culberson "C" Fee #1	TXLCCF1	NA	523721	3526221	1,515	2,943	-1,429	V&K	Estimate based on nearby wells
General Crude Oil Company, Merrill and Voyles et al. #1	GCOCMV1	NA	477481	3524877	1,181	1,443	-262	BEG WR	
Magnolia Petro., No. A-1 Homer, Cowden	MPNA1HC	NA	544286	3524346	1,194	3,722	-2,528	V&K	Estimate based on nearby wells
EOG Resources, Inc., Kenney 16 State #1H	EOGKS1H	4210932270	527946	3523355	1,372	2,999	-1,628	RRC	Estimate based on nearby wells
EOG Resources, Inc., Kenney 16 State #2	EOGKES2	4210932269	528404	3522559	1,365	3,076	-1,711	RRC	Estimate based on nearby wells
California Standard of Texas, Theisen #1	CASATT1	NA	426103	3521248	1,557	1,439	119	BEG WR	

Table A-3.3 continued.

Well Name, Lease	Well ID	API Number	Easting	Northing	Well Elevation (m)	Depth to Top of Precambrian (m)	Elevation of Top of Precambrian (m)	Source	Note
Trail Mountain, Inc., University Felina "D27" #1	TMUFD27	4222930006	439917	3518350	1,427	1,292	134	RRC	Estimate based on nearby wells
Border Exploration Co., Hammack et al. CT-1	BECHCT1	4222930196	505172	3518026	1,107	2,987	-1,880	K&H	Estimate based on nearby wells
TXL Oil Corp., Culberson B-T Fee #1	TXLCBT1	NA	550456	3517797	1,236	4,072	-2,836	V&K	Estimate based on nearby wells
A.R. Jones Co., E.C. Mowry #1	ARJECM1	NA	474192	3516927	1,230	1,577	-347	BEG SC	Estimate based on nearby wells
J.L. Cowley, E.C. Mowry #1	JLCECM1	NA	473079	3515907	1,234	1,432	-198	BEG SC	Estimate based on nearby wells
Border Exploration Co., J.J. McAdoo 7 #1	BECJJM1	4222930200	505794	3514682	1,143	2,811	-1,668	K&H	Estimate based on nearby wells
T.E. Robertson Co., Inc., Mowry et al. #2	TERCMO2	NA	471217	3514010	1,222	1,512	-290	BEG SC	Estimate based on nearby wells
Trail Mountain, Inc., University Devil Woman L5 #1	TMUDWL5	4222930253	477595	3510876	1,221	1,745	-524	RRC	Estimate based on nearby wells
Samson Lone Star, L.L.C., University Lands 46-14 #2	SALSUL2	4210932278	551660	3509591	1,310	4,317	-3,007	RRC	Estimate based on nearby wells
Chesapeake Operating, Inc., University Lands 4627 #1	COUL462	4210932287	550571	3507028	1,300	4,295	-2,996	RRC	Estimate based on nearby wells
EnCana Oil & Gas (USA) Inc., Sibley Ranch 47 State "25" #1	EOGSR47	4210932251	544180	3505778	1,332	3,965	-2,633	RRC	Estimate based on nearby wells
Trail Mountain, Inc., University Ooby Dooby L35 #1	TMUODL1	4222930261	482251	3502319	1,230	2,050	-820	RRC	Estimate based on nearby wells
Petro-Hunt, L.L.C., Melissa Taylor State 27 #1-H	PHMTS27	4210932255	563684	3501318	1,150	4,779	-3,629	RRC	Estimate based on nearby wells
American Quasar Pet. Co., V.C. Rounsaville #1	AQPVCR1	NA	563477	3498883	1,178	4,833	-3,655	V&K	Estimate based on nearby wells
Hassle Hunt Trust, Univ. "M-49" #1	HHUM491	NA	450328	3497929	1,497	2,505	-1,009	V&K	
EOG Resources, Inc., Wild Horse Draw 7 #1	EOGWHD7	4210932256	536584	3497771	1,510	3,464	-1,954	RRC	Estimate based on nearby wells
Pan American Pet. Corp., Phillip F. Hass #1	PAPPFH1	NA	422942	3494846	1,373	2,282	-910	BEG SC	
Transocean Oil, Inc., 36-1 MSA Trustee, Inc.	TO36MSA	4222930192	424652	3490962	1,551	2,290	-739	BEG SC	Estimate based on nearby wells
El Paso Co., No. 1 Montgomery	EPCN1MO	NA	546957	3484390	1,370	2,265	-895	V&K	Estimate based on nearby wells
Gulf Oil Corp., M.A. Grisham #1	GOCMAG1	NA	535928	3484129	1,729	2,060	-331	V&K	Estimate based on nearby wells
Hassle Hunt Trust, Mosely #1	HAHUTM1	NA	449636	3483385	1,447	1,706	-259	V&K	Estimate based on nearby wells

Table A-3.3 continued.

719

Well Name, Lease	Well ID	API Number	Easting	Northing	Well Elevation (m)	Depth to Top of Precambrian (m)	Elevation of Top of Precambrian (m)	Source	Note
Lockhart, Roseborough & Benton, Gardner & Mosely #1 or Western States Oil, Gardner & Moseley #1	LR&BGM1 or WSOG&M1	NA	442367	3480668	1,531	1,023	508	BEG SC	Estimate based on nearby wells
Sinclair, Looney	SINCLOO	NA	551319	3475371	1,310	3,220	-1,910	V&K	Estimate based on nearby wells
Gulf Oil Corp., J. Burner-State "B" #1	GOCJBS1	NA	441556	3472050	1,418	2,786	-1,369	BEG SC	
Lockhart Bros., Gardner & Mosely (Formerly Public School) #1	LOBG&M1	NA	446485	3468512	1,481	543	938	BEG SC	
Stanolind Oil & Gas Co. American Land, No. 1 Roseborough	SOGAL1R	NA	444464	3467169	1,463	488	975	V&K	
J.P. Hurndall & R.A. Gray, J.S. Pierce #1	H&GJSP1	NA	479266	3465692	1,488	456	1,032	BEG SC	Estimate based on nearby wells
Fred A. Davis West and Armour, Davis #1	FADWAD1	NA	528309	3464645	1,146	1,417	-271	V&K	Estimate based on nearby wells

Table A-3.3 continued.

API Number Key: NA = Not applicable.

Depth to Top of … Key: Est. = Estimate.

Source Key: BEG SC = Scout cards from the Bureau of Economic Geology's Austin Core Research Center, BEG WR = Well records from the Bureau of Economic Geology's Austin Core Research Center, BH = Broadhead (2007), F = Foster (1978), F&J = Finger and Jacobson (1997), K&H = King and Harder (1985), NMBG DL = Driller's logs from the New Mexico Subsurface Data Library at the New Mexico Bureau of Geology and Mineral Resources, NMBG SC = Scout cards from the New Mexico Subsurface Data Library at the New Mexico Bureau of Geology and Mineral Resources, OCD = Oil Conservation Division online well files, RRC = Railroad Commission of Texas, V&K = Veldhuis and Keller (1980).

Well Name, Lease	Well ID	API Number	Easting	Northing	Well Elevation (m)	Depth to Top of Bliss Sandstone (m)	Elevation of Top of Bliss Sandstone (m)	Source	Note
Houston Oil & Minerals Corp., J.M. Lewelling #1	HO&MJL1	3003520010	402778	3684425	1,440	2,841	-1,401	NMBG SC	
Houston Oil & Minerals Corp., State 3724 #1	HO&MS31	3003520011	412512	3657622	1,540	1,344	196	OCD	
Humble Oil & Refining Co., Yates Federal #1	HO&RYF1	3000560015	486777	3649300	1,648	1,631	17	OCD	
J. Cleo Thompson, State A-6 #1	JCTSA61	3000562988	477111	3646836	1,824	1,140	684	OCD	
Humble Oil & Refining Co., Humble-Yates N.M. State #1	HO&RHY1	3000510521	488336	3643533	1,574	1,766	-193	OCD	
W.H. Black Drilling Co., Shildneck #1	WHBDCS1	3000500012	514561	3641046	1,330	2,027	-696	NMBG SC	
J. Cleo Thompson, Federal A-28 #1	JCTFA28	3000562915	479948	3639939	1,649	1,420	229	OCD	
Southern Production Co., Cloudcroft Unit #1	SPCCLU1	3003500002	431152	3635650	2,859	1,373	1,486	BH	
Yates Petroleum Corporation, Dog Canyon "YF" Federal #1	YPCDCF1	3003520024	462754	3622676	1,946	2,492	-545	NMBG SC	
Yates Petroleum Corporation, One Tree Unit #2	YPCOTU2	3000562276	468582	3619170	2,010	800	1,210	NMBG SC	
Marathon Oil Co., Mesa Verde Ranch #1	MOCMVR1	3003520022	455326	3618246	2,143	2,070	73	BH	
Standard of Texas, Scarp Unit #1	SOTSCU1	3003500009	487438	3593394	1,628	721	906	BH	
Lefors Petroleum Co., Federal #1	LEPCFE1	3003500008	471863	3592611	1,642	606	1,036	NMBG SC	
Fred Turner, Jr., Everett #1	FTUEVE1	NA	443146	3579159	1,476	Est.	336	K&H	Estimated from K&H (1985)
Transocean Oil, G.J. Ablah #1	TROGJA1	3003520018	442810	3554817	1,509	1,334	176	K&H	
Fred Turner, Jr., State #1	FTUJST1	3003500027	475070	3550274	1,317	905	412	K&H	
Harvey E. Yates Co., Bennett Ranch Unit #1	HEYBRU1	3003520027	435547	3545814	1,554	2,108	-553	OCD	
Magnolia Petr. Co., U-Tex Lease #39881 #1	MPCUTL1	4222900015	443219	3536988	1,533	1,633	-99	BEG SC	
General Crude Oil Company, Merrill and Voyles et al. #1	GCOCMV1	NA	477481	3524877	1,181	1,425	-244	BEG WR	
California Standard of Texas, Theisen #1	CASATT1	NA	426103	3521248	1,557	1,333	224	BEG WR	
Hassle Hunt Trust, Univ. "M-49" #1	HHUM491	NA	450328	3497929	1,497	2,401	-905	BEG SC	

Table A-3.4: Oil-and-gas exploratory wells used as control for the top of the Bliss Sandstone. See key at bottom of Table A-3.3.

Well Name, Lease	Well ID	API Number	Easting	Northing	Well Elevation (m)	Depth to Top of Bliss Sandstone (m)	Elevation of Top of Bliss Sandstone (m)	Source	Note
Pan American Pet. Corp., Phillip F. Hass #1	PAPPFH1	NA	422942	3494846	1,373	2,198	-826	BEG SC	
Lockhart, Roseborough & Benton, Gardner & Mosely #1 or Western States Oil, Gardner & Moseley #1	LR&BGM1 or WSOG&M1	NA	442367	3480668	1,531	914	617	BEG SC	
Gulf Oil Corp., J. Burner-State "B" #1	GOCJBS1	NA	441556	3472050	1,418	2,611	-1,193	BEG SC	
J.P. Hurndall & R.A. Gray, J.S. Pierce #1	H&GJSP1	NA	479266	3465692	1,488	316	1,172	BEG SC	

Table A-3.4 continued.

Well Name, Lease	Well ID	API Number	Easting	Northing	Well Elevation (m)	Depth to Top of El Paso/ Ellenburger Group (m)	Elevation of Top of El Paso/ Ellenburger Group (m)	Source	Note
Houston Oil & Minerals Corp., State L.G. "1453" #1	HO&MSL1	3003520013	406876	3685414	1,511	2,979	-1,469	NMBG DL	
Houston Oil & Minerals Corp., J.M. Lewelling #1	HO&MJL1	3003520010	402778	3684425	1,440	2,804	-1,365	OCD	
Houston Oil & Minerals Corp., State 3724 #1	HO&MS31	3003520011	412512	3657622	1,540	1,301	239	OCD	
Humble Oil & Refining Co., Yates Federal #1	HO&RYF1	3000560015	486777	3649300	1,648	1,581	67	OCD	
J. Cleo Thompson, State A-6 #1	JCTSA61	3000562988	477111	3646836	1,824	1,074	750	OCD	
W.H. Black Drilling Co., Shildneck #1	WHBDCS1	3000500012	514561	3641046	1,330	1,935	-605	NMBG SC	
J. Cleo Thompson, Federal A-28 #1	JCTFA28	3000562915	479948	3639939	1,649	1,351	297	OCD	
Southern Production Co., Cloudcroft Unit #1	SPCCLU1	3003500002	431152	3635650	2,859	1,148	1,711	BH	
Yates Petroleum Corporation, Dunken Dome Unit #1	YPCDDU1	3000560374	486211	3634277	1,643	1,644	0	OCD	
Liberty Oil & Gas Corp., T.L. Watts #1	LO&GTLW	3000560766	480341	3631643	1,633	1,590	44	BH	
Yates Petroleum Corporation, Little Cuevo Unit #1	YPCLCU1	3000561785	488273	3631027	1,633	1,590	44	NMBG SC	
Sunray DX Oil Company, N.M. State "AV" #1	SOCSAV1	3000510144	491916	3630614	1,582	1,639	-57	OCD	
Westcoast Hydrocarbons, Inc., Black Hills Unit #1	WHIBHU1	3000500013	508897	3629768	1,453	1,619	-166	NMBG SC	
Magnolia, Black Hills	MAGBLHI	NA	505927	3627975	1,494	1,661	-167	NMBG SC	
TEXACO Inc., Federal (USA) "E" #1	TEXIFE1	3003520001	395308	3624999	1,219	2,300	-1,082	K&H	
Yates Petroleum Corporation, Dog Canyon "YF" Federal #1	YPCDCF1	3003520024	462754	3622676	1,946	2,363	-417	NMBG SC	
TEXACO Inc., Federal (USA) "F" #1	TEXIFF1	3003520006	410790	3619951	1,232	2,508	-1,276	K&H	
Yates Petroleum Corporation, One Tree Unit #2	YPCOTU2	3000562276	468582	3619170	2,010	655	1,354	NMBG SC	
Marathon Oil Co., Mesa Verde Ranch #1	MOCMVR1	3003520022	455326	3618246	2,143	1,885	258	BH	
Plymouth Oil Co., Evans (aka Federal D) #1	PLOCEV1	3003500003	404731	3604561	1,233	2,214	-982	BH	
Standard of Texas, Scarp Unit #1	SOTSCU1	3003500009	487438	3593394	1,628	582	1,045	BH	

Table A-3.5: Oil-and-gas exploratory wells used as control for the top of the El Paso/Ellenburger Group. See key at bottom of Table A-3.3.

Well Name, Lease	Well ID	API Number	Easting	Northing	Well Elevation (m)	Depth to Top of El Paso/ Ellenburger Group (m)	Elevation of Top of El Paso/ Ellenburger Group (m)	Source	Note
Lefors Petroleum Co., Federal #1	LEPCFE1	3003500008	471863	3592611	1,642	527	1,115	NMBG SC	
Tri-Service Drilling Co., Little Dog Federal #1	TSDLDF1	3003520008	496060	3586992	1,940	1,205	735	NMBG SC	
Brainerd Corp. (aka Continental Oil Co.), Federal "A" (aka East Texas Hill Unit) #1	BRCFEA1	3001500005	523406	3586429	1,397	3,190	-1,793	NMBG SC	
Continental Oil Co., H.W. Bass #1	COCHWB1	3001500004	516898	3586367	1,680	1,551	129	NMBG SC	
Fred Turner, Jr., Everett #1	FTUEVE1	NA	443146	3579159	1,476	Est.	515	K&H	Estimated from K&H (1985)
W.R. Weaver, Thompson #1	WRWETH1	3003500017	499785	3575900	1,386	1,122	264	NMBG SC	
Humble Oil & Refining Co., Huapache Oil Unit #2	HO&RHO2	3001500013	530547	3572779	1,358	3,628	-2,270	OCD	
Fred Turner, Jr. (aka Pasotero Pet. Corp.), Evans #1	FTUJEV1	3003500020	433355	3563003	1,545	841	704	BH	
Fred Turner, Jr., State #1	FTUJST1	3003500027	475070	3550274	1,317	647	671	K&H	
Harvey E. Yates Co., Bennett Ranch Unit #1	HEYBRU1	3003520027	435547	3545814	1,554	1,774	-219	OCD	
Harvey E. Yates Co., Bennett Ranch Unit 25 #1	HEYBR25	3003520031	437133	3542284	1,533	1,582	-49	OCD	
Magnolia Petr. Co., U-Tex Lease #39881 #1	MPCUTL1	4222900015	443219	3536988	1,533	1,274	259	BEG SC	
Pan American Petroleum Corporation, List Anderson #1	PAPCLA1	NA	491521	3533849	1,108	774	334	V&K	
Pure Oil Co., Hunter #1	PUOCHU1	NA	509809	3531380	1,625	2,018	-393	K&H	
TEXACO Inc., Culberson "L" Fee #1	TEXCLF1	NA	519234	3527336	1,564	2,560	-997	K&H	
Tenneco Oil Co., TXL Fee #1	TOTXLF1	4210931401	563041	3526975	1,086	4,001	-2,916	RRC	
Pan American Petroleum Corporation, Ed Hammock #1	PAPCEH1	NA	499124	3526693	1,110	2,114	-1,004	V&K	
General Crude Oil Company, Merrill and Voyles et al. #1	GCOCMV1	NA	477481	3524877	1,181	1,125	56	BEG WR	
Magnolia Petro., No. A-1 Homer, Cowden	MPNA1HC	NA	544286	3524346	1,194	3,432	-2,238	V&K	
California Standard of Texas, Theisen #1	CASATT1	NA	426103	3521248	1,557	936	621	BEG WR	
TXL Oil Corp., Culberson B-T Fee #1	TXLCBT1	NA	550456	3517797	1,236	3,783	-2,546	V&K	

Table A-3.5 continued.

724

Well Name, Lease	Well ID	API Number	Easting	Northing	Well Elevation (m)	Depth to Top of El Paso/ Ellenburger Group (m)	Elevation of Top of El Paso/ Ellenburger Group (m)	Source	Note
A.R. Jones Co., E.C. Mowry #1	ARJECM1	NA	474192	3516927	1,230	1,259	-30	BEG SC	
T.E. Robertson Co., Inc., Mowry et al. #2	TERCMO2	NA	471217	3514010	1,222	1,194	28	BEG SC	
Faith Minerals, Inc., Wesley West #1	FMINWW1	4222930012	503401	3499500	1,104	3,274	-2,170	BEG SC	In Ellenburger at total well depth
Hassle Hunt Trust, Univ. "M-49" #1	HHUM491	NA	450328	3497929	1,497	2,094	-597	BEG SC	
Pan American Pet. Corp., Phillip F. Hass #1	PAPPFH1	NA	422942	3494846	1,373	1,875	-503	BEG SC	
El Paso Co., No. 1 Montgomery	EPCN1MO	NA	546957	3484390	1,370	1,975	-605	V&K	
Gulf Oil Corp., M.A. Grisham #1	GOCMAG1	NA	535928	3484129	1,729	1,771	-41	V&K	
Hassle Hunt Trust, Mosely #1	HAHUTM1	NA	449636	3483385	1,447	1,228	219	V&K	
Lockhart, Roseborough & Benton, Gardner & Mosely #1 or Western States Oil, Gardner & Moseley #1	LR&BGM1 or WSOG&M1	NA	442367	3480668	1,531	479	1,053	BEG SC	
Gulf Oil Corp., J. Burner-State "B" #1	GOCJBS1	NA	441556	3472050	1,418	2,242	-824	BEG SC	
J.P. Hurndall & R.A. Gray, J.S. Pierce #1	H&GJSP1	NA	479266	3465692	1,488	117	1,371	BEG SC	
Fred A. Davis West and Armour, Davis #1	FADWAD1	NA	528309	3464645	1,146	1,128	18	V&K	Approximate

Table A-3.5 continued.

Well Name, Lease	Well ID	API Number	Easting	Northing	Well Elevation (m)	Depth to Top of Montoya Group (m)	Elevation of Top of Montoya Group (m)	Source	Note
Houston Oil & Minerals Corp., State L.G. "1453" #1	HO&MSL1	3003520013	406876	3685414	1,511	2,880	-1,370	NMBG DL	
Houston Oil & Minerals Corp., J.M. Lewelling #1	HO&MJL1	3003520010	402778	3684425	1,440	2,731	-1,291	OCD	
Houston Oil & Minerals Corp., State 3724 #1	HO&MS31	3003520011	412512	3657622	1,540	1,198	342	OCD	
Humble Oil & Refining Co., Yates Federal #1	HO&RYF1	3000560015	486777	3649300	1,648	1,539	109	OCD	
J. Cleo Thompson, State A-6 #1	JCTSA61	3000562988	477111	3646836	1,824	992	832	OCD	
W.H. Black Drilling Co., Shildneck #1	WHBDCS1	3000500012	514561	3641046	1,330	1,835	-504	NMBG SC	
J. Cleo Thompson, Federal A-28 #1	JCTFA28	3000562915	479948	3639939	1,649	1,263	386	OCD	
Southern Production Co., Cloudcroft Unit #1	SPCCLU1	3003500002	431152	3635650	2,859	1,114	1,745	BH	
Liberty Oil & Gas Corp., T.L. Watts #1	LO&GTLW	3000560766	480341	3631643	1,633	1,508	125	BH	
Yates Petroleum Corporation, Little Cuevo Unit #1	YPCLCU1	3000561785	488273	3631027	1,633	1,508	125	NMBG SC	
Sunray DX Oil Company, N.M. State "AV" #1	SOCSAV1	3000510144	491916	3630614	1,582	1,569	13	OCD	
Westcoast Hydrocarbons, Inc., Black Hills Unit #1	WHIBHU1	3000500013	508897	3629768	1,453	1,573	-119	NMBG SC	
Magnolia, Black Hills	MAGBLHI	NA	505927	3627975	1,494	1,559	-65	NMBG SC	
TEXACO Inc., Federal (USA) "E" #1	TEXIFE1	3003520001	395308	3624999	1,219	2,216	-997	K&H	
Yates Petroleum Corporation, Dog Canyon "YF" Federal #1	YPCDCF1	3003520024	462754	3622676	1,946	2,215	-268	NMBG SC	
TEXACO Inc., Federal (USA) "F" #1	TEXIFF1	3003520006	410790	3619951	1,232	2,407	-1,175	K&H	
TEXACO Inc., Federal (USA) "G" #1	TEXIFG1	3003520004	394443	3619379	1,276	Est.	-1,124	F	Estimated from Foster (1978)
Plymouth Oil Co., Evans (aka Federal D) #1	PLOCEV1	3003500003	404731	3604561	1,233	2,124	-892	BH	
Zapata Petroleum Corp., Federal 14 #1	ZPCF141	3003500006	454127	3603086	2,109	1,512	597	OCD	
Standard of Texas, Scarp Unit #1	SOTSCU1	3003500009	487438	3593394	1,628	509	1,119	BH	
Tri-Service Drilling Co., Little Dog Federal #1	TSDLDF1	3003520008	496060	3586992	1,940	1,108	832	OCD	

Table A-3.6: Oil-and-gas exploratory wells used as control for the top of the Montoya Group. See key at bottom of Table A-3.3.

Well Name, Lease	Well ID	API Number	Easting	Northing	Well Elevation (m)	Depth to Top of Montoya Group (m)	Elevation of Top of Montoya Group (m)	Source	Note
Brainerd Corp. (aka Continental Oil Co.), Federal "A" (aka East Texas Hill Unit) #1	BRCFEA1	3001500005	523406	3586429	1,397	3,053	-1,656	NMBG SC	
Continental Oil Co., H.W. Bass #1	COCHWB1	3001500004	516898	3586367	1,680	1,433	247	NMBG SC	
Fred Turner, Jr., Everett #1	FTUEVE1	NA	443146	3579159	1,476	Est.	619	K&H	Estimated from K&H (1985)
W.R. Weaver, Thompson #1	WRWETH1	3003500017	499785	3575900	1,386	1,033	353	NMBG SC	
Humble Oil & Refining Co., Huapache Oil Unit #2	HO&RHO2	3001500013	530547	3572779	1,358	3,486	-2,128	OCD	
Fred Turner, Jr. (aka Pasotero Pet. Corp.), Evans #1	FTUJEV1	3003500020	433355	3563003	1,545	664	881	BH	
Fred Turner, Jr., State #1	FTUJST1	3003500027	475070	3550274	1,317	597	720	K&H	
GDP 45-5	GDP45-5	NA	391837	3549102	1,255	1,109	146	F&J	
Harvey E. Yates Co., Bennett Ranch Unit #1	HEYBRU1	3003520027	435547	3545814	1,554	1,669	-114	OCD	
Harvey E. Yates Co., Bennett Ranch Unit 25 #1	HEYBR25	3003520031	437133	3542284	1,533	1,451	82	OCD	
Magnolia Petr. Co., U-Tex Lease #39881 #1	MPCUTL1	4222900015	443219	3536988	1,533	1,174	360	BEG SC	
Pure Oil Co., Hunter #1	PUOCHU1	NA	509809	3531380	1,625	1,912	-287	K&H	
TEXACO Inc., Culberson "L" Fee #1	TEXCLF1	NA	519234	3527336	1,564	2,424	-860	K&H	
General Crude Oil Company, Merrill and Voyles et al. #1	GCOCMV1	NA	477481	3524877	1,181	1,053	128	BEG WR	
Magnolia Petro., No. A-1 Homer, Cowden	MPNA1HC	NA	544286	3524346	1,194	3,289	-2,095	V&K	
California Standard of Texas, Theisen #1	CASATT1	NA	426103	3521248	1,557	859	699	BEG WR	
A.R. Jones Co., E.C. Mowry #1	ARJECM1	NA	474192	3516927	1,230	1,197	33	BEG SC	
T.E. Robertson Co., Inc., Mowry et al. #2	TERCMO2	NA	471217	3514010	1,222	1,152	70	BEG SC	
Hassle Hunt Trust, Univ. "M-49" #1	HHUM491	NA	450328	3497929	1,497	1,881	-384	BEG SC	
El Paso Co., No. 1 Montgomery	EPCN1MO	NA	546957	3484390	1,370	1,774	-404	V&K	
Gulf Oil Corp., M.A. Grisham #1	GOCMAG1	NA	535928	3484129	1,729	1,620	109	V&K	

Table A-3.6 continued.

Well Name, Lease	Well ID	API Number	Easting	Northing	Well Elevation (m)	Depth to Top of Montoya Group (m)	Elevation of Top of Montoya Group (m)	Source	Note
Lockhart, Roseborough & Benton, Gardner & Mosely #1 or Western States Oil, Gardner & Moseley #1	LR&BGM1 or WSOG&M1	NA	442367	3480668	1,531	399	1,132	BEG SC	
Gulf Oil Corp., J. Burner-State "B" #1	GOCJBS1	NA	441556	3472050	1,418	2,164	-746	BEG SC	
Fred A. Davis West and Armour, Davis #1	FADWAD1	NA	528309	3464645	1,146	488	658	V&K	Approximate

Table A-3.6 continued.

Well Name, Lease	Well ID	API Number	Easting	Northing	Well Elevation (m)	Depth to Top of Fusselman Formation (m)	Elevation of Top of Fusselman Formation (m)	Source	Note
Houston Oil & Minerals Corp., State L.G. "1453" #1	HO&MSL1	3003520013	406876	3685414	1,511	2,848	-1,338	NMBG DL	
Houston Oil & Minerals Corp., J.M. Lewelling #1	HO&MJL1	3003520010	402778	3684425	1,440	2,701	-1,261	OCD	
Houston Oil & Minerals Corp., State 3724 #1	HO&MS31	3003520011	412512	3657622	1,540	1,161	379	OCD	
J. Cleo Thompson, State A-6 #1	JCTSA61	3000562988	477111	3646836	1,824	969	855	OCD	
Humble Oil & Refining Co., Humble-Yates N.M. State #1	HO&RHY1	3000510521	488336	3643533	1,574	1,591	-17	OCD	
W.H. Black Drilling Co., Shildneck #1	WHBDCS1	3000500012	514561	3641046	1,330	1,801	-471	NMBG SC	
J. Cleo Thompson, Federal A-28 #1	JCTFA28	3000562915	479948	3639939	1,649	1,216	433	OCD	
C & K Petroleum, Inc., Singer Lake State #1	C&KSLS1	3000560320	495659	3637945	1,545	1,571	-26	OCD	
Southern Production Co., Cloudcroft Unit #1	SPCCLU1	3003500002	431152	3635650	2,859	1,072	1,787	BH	
Yates Petroleum Corporation, Dunken Nose Unit #1	YPCDNU1	3000560383	491492	3635055	1,602	1,601	1	OCD	
Yates Petroleum Corporation, Dunken Dome Unit #2	YPCDDU2	3000560397	485994	3634588	1,631	1,457	174	OCD	
Yates Petroleum Corporation, Dunken Dome Unit #1	YPCDDU1	3000560374	486211	3634277	1,643	1,494	150	OCD	
C & K Petroleum, Inc., Little Cuevo State #1	C&KLCS1	3000560324	501605	3632606	1,464	1,923	-459	OCD	
Liberty Oil & Gas Corp., T.L. Watts #1	LO&GTLW	3000560766	480341	3631643	1,633	1,472	162	BH	
Magnolia, Headley Federal #2	MAGHEF2	NA	512347	3631229	1,510	1,460	50	BH	
Yates Petroleum Corporation, Little Cuevo Unit #1	YPCLCU1	3000561785	488273	3631027	1,633	1,472	162	NMBG SC	
Sunray DX Oil Company, N.M. State "AV" #1	SOCSAV1	3000510144	491916	3630614	1,582	1,536	46	OCD	
Westcoast Hydrocarbons, Inc., Black Hills Unit #1	WHIBHU1	3000500013	508897	3629768	1,453	1,453	0	BH	
Yates Petroleum Corporation, Little Cuevo Unit #2	YPCLCU2	3000562268	489571	3628557	1,618	1,397	220	OCD	
Magnolia, Black Hills	MAGBLHI	NA	505927	3627975	1,494	1,494	1	NMBG SC	
TEXACO Inc., Federal (USA) "E" #1	TEXIFE1	3003520001	395308	3624999	1,219	2,154	-935	K&H	

Table A-3.7: Oil-and-gas exploratory wells used as control for the top of the Fusselman Formation. See key at bottom of Table A-3.3.

Well Name, Lease	Well ID	API Number	Easting	Northing	Well Elevation (m)	Depth to Top of Fusselman Formation (m)	Elevation of Top of Fusselman Formation (m)	Source	Note
Yates Petroleum Corporation, One Tree Unit #1	YPCOTU1	3000562259	467160	3623529	1,876	1,856	20	BH	
Yates Petroleum Corporation, Dog Canyon "YF" Federal #1	YPCDCF1	3003520024	462754	3622676	1,946	2,165	-219	NMBG SC	
Texas Oil & Gas Corp., Federal "C" #1	TO&GFC1	3000560017	512954	3622309	1,359	2,063	-704	BH	
Kewanee Oil Co., F-M Unit #1	KOCFMU1	3000500009	493140	3619927	1,579	1,993	-414	NMBG SC	
TEXACO Inc., Federal (USA) "F" #1	TEXIFF1	3003520006	410790	3619951	1,232	2,353	-1,120	K&H	
TEXACO Inc., Federal (USA) "G" #1	TEXIFG1	3003520004	394443	3619379	1,276	Est.	-1,091	F	Estimated from Foster (1978)
Marathon Oil Co., Mesa Verde Ranch #1	MOCMVR1	3003520022	455326	3618246	2,143	1,797	346	NMBG SC	
Yates Petroleum Corp., Buckhorn AYU State Com #1	YPCBAYU	3000560541	506142	3613140	1,440	2,033	-593	NMBG SC	
Texas Oil & Gas Corp., Federal "A" #1	TO&GFA1	3000510431	506950	3613041	1,442	2,128	-685	BH	
U.V. Industries, Inc., Long Canyon Unit #1	UVILCU1	3000560411	502547	3610225	1,536	2,240	-703	BH	
Gulf Oil Corp., Federal Munson #1	GOCFMU1	3000510075	489407	3609839	1,723	1,033	690	BH	
Plymouth Oil Co., Evans (aka Federal D) #1	PLOCEV1	3003500003	404731	3604561	1,233	2,043	-811	BH	
Atlantic Refining Co., State "AV" #1	ARCSAV1	3003510001	461443	3603143	1,921	1,128	793	OCD	
Zapata Petroleum Corp., Federal 14 #1	ZPCF141	3003500006	454127	3603086	2,109	1,445	664	NMBG SC	
Sun Oil Company, T.J. Pearson #1	SOCTJP1	3003500005	416750	3598464	1,344	1,308	36	BH	
Terra Resources, Inc., Burro Canyon Unit #1-Y	TRBCU1Y	3003520017	511686	3596471	1,572	1,665	-93	BH	
Standard of Texas, Scarp Unit #1	SOTSCU1	3003500009	487438	3593394	1,628	337	1,291	BH	
Tri-Service Drilling Co., Little Dog Federal #1	TSDLDF1	3003520008	496060	3586992	1,940	962	978	NMBG SC	
Brainerd Corp. (aka Continental Oil Co.), Federal "A" (aka East Texas Hill Unit) #1	BRCFEA1	3001500005	523406	3586429	1,397	2,875	-1,478	NMBG SC	
Continental Oil Co., H.W. Bass #1	COCHWB1	3001500004	516898	3586367	1,680	1,263	416	NMBG SC	
Marathon Oil Company, Box Canyon Unit #1	MOCBCU1	3001510012	522193	3586059	1,426	2,833	-1,407	OCD	

Table A-3.7 continued.

Well Name, Lease	Well ID	API Number	Easting	Northing	Well Elevation (m)	Depth to Top of Fusselman Formation (m)	Elevation of Top of Fusselman Formation (m)	Source	Note
E.P. Campbell, Hurley #1	EPCAHU1	3003500012	447355	3580223	1,404	666	737	K&H	
Fred Turner, Jr., Everett #1	FTUEVE1	NA	443146	3579159	1,476	Est.	735	K&H	Estimated from K&H (1985)
W.R. Weaver, Thompson #1	WRWETH1	3003500017	499785	3575900	1,386	924	462	NMBG SC	
E.P. Campbell, Lois Spanel #1	EPCALS1	3003500015	467947	3575324	1,408	758	650	K&H	
E.P. Campbell, McMillan Federal #1	EPCAMF1	3003500018	500598	3573842	1,319	961	358	K&H	
Inexco Oil Company, Sitting Bull Unit #1	IOCSBU1	3001520752	527152	3568073	1,650	1,820	-170	OCD	
Union Oil Co., Federal White #1	UNOCFW1	3001500019	525449	3565154	1,740	2,006	-265	BH	
Fred Turner, Jr. (aka Pasotero Pet. Corp.), Evans #1	FTUJEV1	3003500020	433355	3563003	1,545	600	945	BH	
E.P. Campbell (aka John J. Eisner), Federal #1	EPCAFE1	3003500019	432641	3562887	1,497	564	933	NMBG SC	
Union Oil Co., McMillan #1	UNOCMC1	3003500028	440825	3557266	1,522	1,079	443	BH	
Transocean Oil, G.J. Ablah #1	TROGJA1	3003520018	442810	3554817	1,509	787	722	K&H	
Pennzoil Co., Southland "28" State #1	PCS28S1	3003520019	479573	3551070	1,206	839	367	K&H	
E.J. Dunigan, Alpha Federal #1	EJDALF1	3003520002	496594	3549815	1,159	1,464	-304	K&H	
GDP 45-5	GDP45-5	NA	391837	3549102	1,255	950	305	F&J	
Harvey E. Yates Co., Bennett Ranch Unit #1	HEYBRU1	3003520027	435547	3545814	1,554	1,516	38	OCD	
Seaboard Oil Co., Trigg-Federal #1	SEOCTF1	3003500032	418801	3545797	1,618	1,502	116	K&H	
GDP 51-8	GDP51-8	NA	393417	3545870	1,253	455	798	F&J	
Harvey E. Yates Co., Bennett Ranch Unit 25 #1	HEYBR25	3003520031	437133	3542284	1,533	1,298	234	OCD	
Magnolia Petr. Co., U-Tex Lease #39881 #1	MPCUTL1	4222900015	443219	3536988	1,533	973	561	BEG SC	
Pure Oil Co., Hunter #1	PUOCHU1	NA	509809	3531380	1,625	1,630	-5	K&H	
Hunt Oil Co., Dyer #1	HUOCDY1	4222930007	485477	3530917	1,119	552	567	K&H	
Hunt Petroleum Corp., C.L. Ranch #1	HPCCLR1	4222930010	496475	3528252	1,105	1,546	-441	K&H	

Table A-3.7 continued.

Well Name, Lease	Well ID	API Number	Easting	Northing	Well Elevation (m)	Depth to Top of Fusselman Formation (m)	Elevation of Top of Fusselman Formation (m)	Source	Note
TEXACO Inc., Culberson "L" Fee #1	TEXCLF1	NA	519234	3527336	1,564	2,154	-590	K&H	
Tenneco Oil Co., TXL Fee #1	TOTXLF1	4210931401	563041	3526975	1,086	3,512	-2,427	RRC	
Trail Mountain, Inc., University Sizzler D5 #1	TMUSD51	4222930227	437784	3526650	1,437	1,768	-331	RRC	
General Crude Oil Company, Merrill and Voyles et al. #1	GCOCMV1	NA	477481	3524877	1,181	783	398	BEG WR	
California Standard of Texas, Theisen #1	CASATT1	NA	426103	3521248	1,557	677	881	BEG WR	
A.R. Jones Co., E.C. Mowry #1	ARJECM1	NA	474192	3516927	1,230	935	295	BEG SC	
Border Exploration Co., J.J. McAdoo 7 #1	BECJJM1	4222930200	505794	3514682	1,143	2,151	-1,008	K&H	
T.E. Robertson Co., Inc., Mowry et al. #2	TERCMO2	NA	471217	3514010	1,222	882	340	BEG SC	
American Quasar Pet. Co., V.C. Rounsaville #1	AQPVCR1	NA	563477	3498883	1,178	4,239	-3,061	V&K	
Hassle Hunt Trust, Univ. "M-49" #1	HHUM491	NA	450328	3497929	1,497	1,647	-151	BEG SC	
Pan American Pet. Corp., Phillip F. Hass #1	PAPPFH1	NA	422942	3494846	1,373	1,524	-151	BEG SC	
Transocean Oil, Inc., 36-1 MSA Trustee, Inc.	TO36MSA	4222930192	424652	3490962	1,551	1,532	20	BEG SC	
Hassle Hunt Trust, Mosely #1	HAHUTM1	NA	449636	3483385	1,447	954	493	V&K	
Lockhart, Roseborough & Benton, Gardner & Mosely #1 or Western States Oil, Gardner & Moseley #1	LR&BGM1 or WSOG&M1	NA	442367	3480668	1,531	317	1,214	BEG SC	
Gulf Oil Corp., J. Burner-State "B" #1	GOCJBS1	NA	441556	3472050	1,418	1,842	-424	BEG SC	

Table A-3.7 continued.

Well Name, Lease	Well ID	API Number	Easting	Northing	Well Elevation (m)	Depth to Top of Devonian (m)	Elevation of Top of Devonian (m)	Source	Note
Southern Production Co., Cloudcroft Unit #1	SPCCLU1	3003500002	431152	3635650	2,859	1,047	1,812	BH	
Yates Petroleum Corporation, Dunken Dome Unit #2	YPCDDU2	3000560397	485994	3634588	1,631	1,455	176	OCD	
TEXACO Inc., Federal (USA) "E" #1	TEXIFE1	3003520001	395308	3624999	1,219	2,138	-919	K&H	
Yates Petroleum Corporation, Dog Canyon "YF" Federal #1	YPCDCF1	3003520024	462754	3622676	1,946	2,137	-191	NMBG SC	
Texas Oil & Gas Corp., Federal "C" #1	TO&GFC1	3000560017	512954	3622309	1,359	2,048	-689	NMBG SC	
TEXACO Inc., Federal (USA) "F" #1	TEXIFF1	3003520006	410790	3619951	1,232	2,322	-1,089	K&H	
TEXACO Inc., Federal (USA) "G" #1	TEXIFG1	3003520004	394443	3619379	1,276	Est.	-1,070	F	Estimated from Foster (1978)
Marathon Oil Co., Mesa Verde Ranch #1	MOCMVR1	3003520022	455326	3618246	2,143	1,769	374	BH	
Yates Petroleum Corp., Buckhorn AYU State Com #1	YPCBAYU	3000560541	506142	3613140	1,440	2,019	-579	NMBG SC	
Texas Oil & Gas Corp., Federal "A" #1	TO&GFA1	3000510431	506950	3613041	1,442	2,114	-671	NMBG SC	
U.V. Industries, Inc., Long Canyon Unit #1	UVILCU1	3000560411	502547	3610225	1,536	2,226	-689	NMBG SC	
Plymouth Oil Co., Evans (aka Federal D) #1	PLOCEV1	3003500003	404731	3604561	1,233	2,028	-796	BH	
Texas Oil & Gas Corp., Federal "B" #1	TO&GFB1	NA	510832	3603835	1,463	2,451	-988	NMBG SC	
Atlantic Refining Co., State "AV" #1	ARCSAV1	3003510001	461443	3603143	1,921	1,109	811	NMBG SC	
Sun Oil Company, T.J. Pearson #1	SOCTJP1	3003500005	416750	3598464	1,344	1,305	39	BH	
Terra Resources, Inc., Burro Canyon Unit #1-Y	TRBCU1Y	3003520017	511686	3596471	1,572	1,647	-76	BH	
Brainerd Corp. (aka Continental Oil Co.), Federal "A" (aka East Texas Hill Unit) #1	BRCFEA1	3001500005	523406	3586429	1,397	2,867	-1,470	NMBG SC	
Continental Oil Co., H.W. Bass #1	COCHWB1	3001500004	516898	3586367	1,680	1,251	429	NMBG SC	
Marathon Oil Company, Box Canyon Unit #1	MOCBCU1	3001510012	522193	3586059	1,426	2,827	-1,401	OCD	
E.P. Campbell, Hurley #1	EPCAHU1	3003500012	447355	3580223	1,404	653	750	K&H	
Fred Turner, Jr., Everett #1	FTUEVE1	NA	443146	3579159	1,476	Est.	741	K&H	Estimated from K&H (1985)

Table A-3.8: Oil-and-gas exploratory wells used as control for the top of the Devonian. See key at bottom of Table A-3.3.

Well Name, Lease	Well ID	API Number	Easting	Northing	Well Elevation (m)	Depth to Top of Devonian (m)	Elevation of Top of Devonian (m)	Source	Note
E.P. Campbell, Lois Spanel #1	EPCALS1	3003500015	467947	3575324	1,408	745	663	K&H	
E.P. Campbell, McMillan Federal #1	EPCAMF1	3003500018	500598	3573842	1,319	956	363	K&H	
Humble Oil & Refining Co., Huapache Oil Unit #2	HO&RHO2	3001500013	530547	3572779	1,358	3,292	-1,934	OCD	
Union Oil Co., Federal White #1	UNOCFW1	3001500019	525449	3565154	1,740	1,985	-245	BH	
Fred Turner, Jr. (aka Pasotero Pet. Corp.), Evans #1	FTUJEV1	3003500020	433355	3563003	1,545	576	969	BH	
Union Oil Co., McMillan #1	UNOCMC1	3003500028	440825	3557266	1,522	1,062	460	BH	
Transocean Oil, G.J. Ablah #1	TROGJA1	3003520018	442810	3554817	1,509	754	756	K&H	
E.J. Dunigan, Alpha Federal #1	EJDALF1	3003520002	496594	3549815	1,159	1,440	-281	K&H	
Harvey E. Yates Co., Bennett Ranch Unit #1	HEYBRU1	3003520027	435547	3545814	1,554	1,495	59	OCD	
Harvey E. Yates Co., Bennett Ranch Unit 25 #1	HEYBR25	3003520031	437133	3542284	1,533	1,250	283	OCD	
Magnolia Petr. Co., U-Tex Lease #39881 #1	MPCUTL1	4222900015	443219	3536988	1,533	933	600	BEG SC	
Pure Oil Co., Hunter #1	PUOCHU1	NA	509809	3531380	1,625	1,587	39	K&H	
Hunt Petroleum Corp., C.L. Ranch #1	HPCCLR1	4222930010	496475	3528252	1,105	1,529	-424	K&H	
TEXACO Inc., Culberson "L" Fee #1	TEXCLF1	NA	519234	3527336	1,564	2,115	-551	K&H	
Tenneco Oil Co., TXL Fee #1	TOTXLF1	4210931401	563041	3526975	1,086	3,477	-2,391	RRC	
Pan American Petroleum Corporation, Ed Hammock #1	PAPCEH1	NA	499124	3526693	1,110	1,691	-581	V&K	
Trail Mountain, Inc., University Sizzler D5 #1	TMUSD51	4222930227	437784	3526650	1,437	1,747	-309	RRC	
TXL Corp., Culberson "C" Fee #1	TXLCCF1	NA	523721	3526221	1,515	2,319	-804	V&K	
General Crude Oil Company, Merrill and Voyles et al. #1	GCOCMV1	NA	477481	3524877	1,181	720	461	BEG WR	
Magnolia Petro., No. A-1 Homer, Cowden	MPNA1HC	NA	544286	3524346	1,194	2,935	-1,741	V&K	
California Standard of Texas, Theisen #1	CASATT1	NA	426103	3521248	1,557	642	916	BEG WR	

Table A-3.8 continued.

Well Name, Lease	Well ID	API Number	Easting	Northing	Well Elevation (m)	Depth to Top of Devonian (m)	Elevation of Top of Devonian (m)	Source	Note
Trail Mountain, Inc., University Felina "D27" #1	TMUFD27	4222930006	439917	3518350	1,427	495	931	RRC	
TXL Oil Corp., Culberson B-T Fee #1	TXLCBT1	NA	550456	3517797	1,236	3,256	-2,020	V&K	
A.R. Jones Co., E.C. Mowry #1	ARJECM1	NA	474192	3516927	1,230	886	344	BEG SC	
Border Exploration Co., J.J. McAdoo 7 #1	BECJJM1	4222930200	505794	3514682	1,143	2,093	-950	K&H	
T.E. Robertson Co., Inc., Mowry et al. #2	TERCMO2	NA	471217	3514010	1,222	829	393	BEG SC	
Trail Mountain, Inc., University Devil Woman L5 #1	TMUDWL5	4222930253	477595	3510876	1,221	1,022	199	RRC	
Samson Lone Star, L.L.C., University Lands 46-14 #2	SALSUL2	4210932278	551660	3509591	1,310	3,692	-2,382	RRC	
Chesapeake Operating, Inc., University Lands 4627 #1	COUL462	4210932287	550571	3507028	1,300	3,670	-2,371	RRC	
EnCana Oil & Gas (USA) Inc., Sibley Ranch 47 State "25" #1	EOGSR47	4210932251	544180	3505778	1,332	3,341	-2,008	RRC	
Trail Mountain, Inc., University Ooby Dooby L35 #1	TMUODL1	4222930261	482251	3502319	1,230	1,327	-97	RRC	
Petro-Hunt, L.L.C., Melissa Taylor State 27 #1-H	PHMTS27	4210932255	563684	3501318	1,150	4,154	-3,004	RRC	
American Quasar Pet. Co., V.C. Rounsaville #1	AQPVCR1	NA	563477	3498883	1,178	4,184	-3,006	V&K	
Hassle Hunt Trust, Univ. "M-49" #1	HHUM491	NA	450328	3497929	1,497	1,592	-96	BEG SC	
Pan American Pet. Corp., Phillip F. Hass #1	PAPPFH1	NA	422942	3494846	1,373	1,433	-61	BEG SC	
Transocean Oil, Inc., 36-1 MSA Trustee, Inc.	TO36MSA	4222930192	424652	3490962	1,551	1,455	96	BEG SC	
El Paso Co., No. 1 Montgomery	EPCN1MO	NA	546957	3484390	1,370	1,428	-58	V&K	
Gulf Oil Corp., M.A. Grisham #1	GOCMAG1	NA	535928	3484129	1,729	1,210	519	V&K	
Sinclair, Looney	SINCLOO	NA	551319	3475371	1,310	2,595	-1,285	V&K	
Gulf Oil Corp., J. Burner-State "B" #1	GOCJBS1	NA	441556	3472050	1,418	1,835	-417	BEG SC	

Table A-3.8 continued.

Well Name, Lease	Well ID	API Number	Easting	Northing	Well Elevation (m)	Depth to Top of Mississippian (m)	Elevation of Top of Mississippian (m)	Source	Note
Houston Oil & Minerals Corp., State L.G. "1453" #1	HO&MSL1	3003520013	406876	3685414	1,511	2,781	-1,271	NMBG DL	
Houston Oil & Minerals Corp., J.M. Lewelling #1	HO&MJL1	3003520010	402778	3684425	1,440	2,643	-1,203	OCD	
Houston Oil & Minerals Corp., State 3724 #1	HO&MS31	3003520011	412512	3657622	1,540	1,015	525	OCD	
J. Cleo Thompson, State A-6 #1	JCTSA61	3000562988	477111	3646836	1,824	944	880	OCD	
W.H. Black Drilling Co., Shildneck #1	WHBDCS1	3000500012	514561	3641046	1,330	1,747	-416	NMBG SC	
Continental Oil Company, State NN #1	COCSNN1	3000560185	492051	3640997	1,538	1,478	60	OCD	
J. Cleo Thompson, Federal A-28 #1	JCTFA28	3000562915	479948	3639939	1,649	1,186	463	OCD	
C & K Petroleum, Inc., Singer Lake State #1	C&KSLS1	3000560320	495659	3637945	1,545	1,539	6	OCD	
Southern Production Co., Cloudcroft Unit #1	SPCCLU1	3003500002	431152	3635650	2,859	979	1,880	BH	
Yates Petroleum Corporation, Dunken Nose Unit #1	YPCDNU1	3000560383	491492	3635055	1,602	1,540	62	OCD	
Yates Petroleum Corporation, Dunken Dome Unit #2	YPCDDU2	3000560397	485994	3634588	1,631	1,420	211	OCD	
Yates Petroleum Corporation, Dunken Dome Unit #1	YPCDDU1	3000560374	486211	3634277	1,643	1,447	197	OCD	
C & K Petroleum, Inc., Little Cuevo State #1	C&KLCS1	3000560324	501605	3632606	1,464	1,811	-348	OCD	
Liberty Oil & Gas Corp., T.L. Watts #1	LO&GTLW	3000560766	480341	3631643	1,633	1,433	200	BH	
Magnolia, Headley Federal #2	MAGHEF2	NA	512347	3631229	1,510	1,390	119	NMBG SC	
Yates Petroleum Corporation, Little Cuevo Unit #1	YPCLCU1	3000561785	488273	3631027	1,633	1,433	200	NMBG SC	
Sunray DX Oil Company, N.M. State "AV" #1	SOCSAV1	3000510144	491916	3630614	1,582	1,451	131	OCD	
Yates Petroleum Corporation, Little Cuevo Unit #2	YPCLCU2	3000562268	489571	3628557	1,618	1,329	288	OCD	
Magnolia, Black Hills	MAGBLHI	NA	505927	3627975	1,494	1,422	72	NMBG SC	
TEXACO Inc., Federal (USA) "E" #1	TEXIFE1	3003520001	395308	3624999	1,219	2,016	-797	K&H	
Yates Petroleum Corporation, One Tree Unit #1	YPCOTU1	3000562259	467160	3623529	1,876	1,786	90	NMBG SC	

Table A-3.9: Oil-and-gas exploratory wells used as control for the top of the Mississippian. See key at bottom of Table A-3.3.

Well Name, Lease	Well ID	API Number	Easting	Northing	Well Elevation (m)	Depth to Top of Mississippian (m)	Elevation of Top of Mississippian (m)	Source	Note
Yates Petroleum Corporation, Dog Canyon "YF" Federal #1	YPCDCF1	3003520024	462754	3622676	1,946	2,051	-105	NMBG SC	
Texas Oil & Gas Corp., Federal "C" #1	TO&GFC1	3000560017	512954	3622309	1,359	1,934	-575	NMBG SC	
Kewanee Oil Co., F-M Unit #1	KOCFMU1	3000500009	493140	3619927	1,579	1,862	-283	NMBG SC	
TEXACO Inc., Federal (USA) "F" #1	TEXIFF1	3003520006	410790	3619951	1,232	2,225	-993	K&H	
TEXACO Inc., Federal (USA) "G" #1	TEXIFG1	3003520004	394443	3619379	1,276	Est.	-978	F	Estimated from Foster (1978)
Marathon Oil Co., Mesa Verde Ranch #1	MOCMVR1	3003520022	455326	3618246	2,143	1,675	468	NMBG SC	
Yates Petroleum Corp., Buckhorn AYU State Com #1	YPCBAYU	3000560541	506142	3613140	1,440	1,881	-441	NMBG SC	
Texas Oil & Gas Corp., Federal "A" #1	TO&GFA1	3000510431	506950	3613041	1,442	1,973	-530	NMBG SC	
Yates Petroleum Corporation (aka Phoenix Resources Co.), Bullis "AVW" State Com (aka Ranch Road) #1	YPCBAVW	3000560557	507355	3612640	1,478	2,033	-555	NMBG SC	
U.V. Industries, Inc., Long Canyon Unit #1	UVILCU1	3000560411	502547	3610225	1,536	2,083	-546	NMBG SC	
Gulf Oil Corp., Federal Munson #1	GOCFMU1	3000510075	489407	3609839	1,723	908	815	NMBG SC	
Plymouth Oil Co., Evans (aka Federal D) #1	PLOCEV1	3003500003	404731	3604561	1,233	1,878	-646	BH	
Texas Oil & Gas Corp., Federal "B" #1	TO&GFB1	NA	510832	3603835	1,463	2,192	-728	NMBG SC	
Atlantic Refining Co., State "AV" #1	ARCSAV1	3003510001	461443	3603143	1,921	1,044	877	NMBG SC	
Zapata Petroleum Corp., Federal 14 #1	ZPCF141	3003500006	454127	3603086	2,109	1,430	679	NMBG SC	
Sun Oil Company, T.J. Pearson #1	SOCTJP1	3003500005	416750	3598464	1,344	1,259	85	BH	
Terra Resources, Inc., Burro Canyon Unit #1-Y	TRBCU1Y	3003520017	511686	3596471	1,572	1,493	79	OCD	
Yates Petroleum Corporation, Brainerd "IO" Federal #1	YPCBIOF	3001522149	523000	3587630	1,406	2,753	-1,347	OCD	
Brainerd Corp. (aka Continental Oil Co.), Federal "A" (aka East Texas Hill Unit) #1	BRCFEA1	3001500005	523406	3586429	1,397	2,798	-1,401	NMBG SC	
Continental Oil Co., H.W. Bass #1	COCHWB1	3001500004	516898	3586367	1,680	1,163	517	NMBG SC	
Marathon Oil Company, Box Canyon Unit #1	MOCBCU1	3001510012	522193	3586059	1,426	2,710	-1,284	OCD	

Table A-3.9 continued.

Well Name, Lease	Well ID	API Number	Easting	Northing	Well Elevation (m)	Depth to Top of Mississippian (m)	Elevation of Top of Mississippian (m)	Source	Note
E.P. Campbell, Hurley #1	EPCAHU1	3003500012	447355	3580223	1,404	638	766	K&H	
E.P. Campbell, Lois Spanel #1	EPCALS1	3003500015	467947	3575324	1,408	708	700	K&H	
E.P. Campbell, McMillan Federal #1	EPCAMF1	3003500018	500598	3573842	1,319	925	394	K&H	
Humble Oil & Refining Co., Huapache Oil Unit #2	HO&RHO2	3001500013	530547	3572779	1,358	3,199	-1,841	OCD	
Inexco Oil Company, Sitting Bull Unit #1	IOCSBU1	3001520752	527152	3568073	1,650	1,716	-66	OCD	
Skelly Oil Co., Las Cruces "D" #1	SOCLCD1	3001500003	522240	3565867	1,749	1,798	-50	NMBG SC	
Union Oil Co., Federal White #1	UNOCFW1	3001500019	525449	3565154	1,740	1,841	-101	BH	
Flynn, Welch, Yates, Donahue #1	FWYDON1	NA	460768	3561350	1,303	439	864	BH	
Franklin, Aston & Fair, Inc., Turkey Draw Unit #1	FA&FTD1	3001521378	524583	3560015	1,776	2,173	-397	OCD	
Union Oil Co., McMillan #1	UNOCMC1	3003500028	440825	3557266	1,522	975	547	BH	
Union Oil Co., Verse 7 Federal #1	UOCV7F1	3001520591	524435	3556316	1,801	2,229	-428	OCD	
Transocean Oil, G.J. Ablah #1	TROGJA1	3003520018	442810	3554817	1,509	686	823	K&H	
Beard Oil Company, Ridge USA #1	BOCRUS1	3001522547	524447	3551405	1,896	2,551	-654	OCD	
E.J. Dunigan, Alpha Federal #1	EJDALF1	3003520002	496594	3549815	1,159	1,317	-157	K&H	
GDP 61-6	GDP61-6	NA	390213	3549130	1,254	533	721	F&J	
GDP 45-5	GDP45-5	NA	391837	3549102	1,255	361	894	F&J	
GDP 46-6	GDP46-6	NA	390223	3549119	1,252	527	725	F&J	
Harvey E. Yates Co., Bennett Ranch Unit #1	HEYBRU1	3003520027	435547	3545814	1,554	1,350	204	OCD	
Seaboard Oil Co., Trigg-Federal #1	SEOCTF1	3003500032	418801	3545797	1,618	1,431	187	K&H	
GDP 51-8	GDP51-8	NA	393417	3545870	1,253	231	1,021	F&J	
Harvey E. Yates Co., Bennett Ranch Unit 25 #1	HEYBR25	3003520031	437133	3542284	1,533	1,138	394	OCD	
Magnolia Petr. Co., U-Tex Lease #39881 #1	MPCUTL1	4222900015	443219	3536988	1,533	639	895	BEG SC	
EOG Resources, Inc., Rector Canyon 24 State #1	EOGRC24	4210932250	544329	3534119	1,200	2,853	-1,653	RRC	Estimate

Table A-3.9 continued.

738

Well Name, Lease	Well ID	API Number	Easting	Northing	Well Elevation (m)	Depth to Top of Mississippian (m)	Elevation of Top of Mississippian (m)	Source	Note
Pure Oil Co., Hunter #1	PUOCHU1	NA	509809	3531380	1,625	1,485	140	K&H	
Trail Mountain, Inc., University Big Iron "C45" #1	TMUBIC1	4222900029	440743	3529232	1,516	864	652	RRC	
Hunt Petroleum Corp., C.L. Ranch #1	HPCCLR1	4222930010	496475	3528252	1,105	1,515	-410	K&H	
TEXACO Inc., Culberson "L" Fee #1	TEXCLF1	NA	519234	3527336	1,564	2,020	-456	K&H	
Trail Mountain, Inc., University Sizzler D5 #1	TMUSD51	4222930227	437784	3526650	1,437	1,574	-137	RRC	
TXL Corp., Culberson "C" Fee #1	TXLCCF1	NA	523721	3526221	1,515	2,244	-729	V&K	
General Crude Oil Company, Merrill and Voyles et al. #1	GCOCMV1	NA	477481	3524877	1,181	683	498	BEG WR	
EOG Resources, Inc., Kenney 16 State #1H	EOGKS1H	4210932270	527946	3523355	1,372	2,222	-850	RRC	
EOG Resources, Inc., Kenney 16 State #2	EOGKES2	4210932269	528404	3522559	1,365	2,298	-934	RRC	
California Standard of Texas, Theisen #1	CASATT1	NA	426103	3521248	1,557	507	1,050	BEG WR	
Trail Mountain, Inc., University Felina "D27" #1	TMUFD27	4222930006	439917	3518350	1,427	360	1,066	RRC	
Border Exploration Co., Hammack et al. CT-1	BECHCT1	4222930196	505172	3518026	1,107	2,227	-1,120	K&H	
A.R. Jones Co., E.C. Mowry #1	ARJECM1	NA	474192	3516927	1,230	689	541	BEG SC	
J.L. Cowley, E.C. Mowry #1	JLCECM1	NA	473079	3515907	1,234	672	561	BEG SC	
Border Exploration Co., J.J. McAdoo 7 #1	BECJJM1	4222930200	505794	3514682	1,143	1,983	-840	K&H	
T.E. Robertson Co., Inc., Mowry et al. #2	TERCMO2	NA	471217	3514010	1,222	694	528	BEG SC	
Trail Mountain, Inc., University Devil Woman L5 #1	TMUDWL5	4222930253	477595	3510876	1,221	696	525	RRC	
Samson Lone Star, L.L.C., University Lands 46-14 #2	SALSUL2	4210932278	551660	3509591	1,310	3,419	-2,110	RRC	
Trail Mountain, Inc., University Ooby Dooby L35 #1	TMUODL1	4222930261	482251	3502319	1,230	1,192	38	RRC	
Petro-Hunt, L.L.C., Melissa Taylor State 27 #1-H	PHMTS27	4210932255	563684	3501318	1,150	3,874	-2,724	RRC	
Hassle Hunt Trust, Univ. "M-49" #1	HHUM491	NA	450328	3497929	1,497	1,561	-64	BEG SC	

Table A-3.9 continued.

739

Well Name, Lease	Well ID	API Number	Easting	Northing	Well Elevation (m)	Depth to Top of Mississippian (m)	Elevation of Top of Mississippian (m)	Source	Note
EOG Resources, Inc., Wild Horse Draw 7 #1	EOGWHD7	4210932256	536584	3497771	1,510	2,687	-1,177	RRC	Estimate
Pan American Pet. Corp., Phillip F. Hass #1	PAPPFH1	NA	422942	3494846	1,373	1,345	28	BEG SC	
Transocean Oil, Inc., 36-1 MSA Trustee, Inc.	TO36MSA	4222930192	424652	3490962	1,551	1,411	140	BEG SC	
Gulf Oil Corp., J. Burner-State "B" #1	GOCJBS1	NA	441556	3472050	1,418	1,718	-301	BEG SC	

Table A-3.9 continued.

Well Name, Lease	Well ID	API Number	Easting	Northing	Well Elevation (m)	Depth to Top of Pennsylvanian (m)	Elevation of Top of Pennsylvanian (m)	Source	Note
Houston Oil & Minerals Corp., State L.G. "1453" #1	HO&MSL1	3003520013	406876	3685414	1,511	2,201	-690	NMBG DL	
Houston Oil & Minerals Corp., J.M. Lewelling #1	HO&MJL1	3003520010	402778	3684425	1,440	2,094	-654	OCD	
Houston Oil & Minerals Corp., Federal "A" #1	HO&MFA1	3003520009	413617	3660369	1,619	553	1,066	K&H	
Leland A. Hodges, Trustee, Houston #1	LAHTHO1	3003520005	411157	3660302	1,529	416	1,113	K&H	
Houston Oil & Minerals Corp., State 3724 #1	HO&MS31	3003520011	412512	3657622	1,540	515	1,025	OCD	
McClellan Oil Corp., Flying "H" Ranch Unit Tract 3 #1	MCOCFH1	3000562244	497349	3652108	1,554	1,301	253	OCD	
J. Cleo Thompson, State A-6 #1	JCTSA61	3000562988	477111	3646836	1,824	796	1,029	OCD	
W.H. Black Drilling Co., Shildneck #1	WHBDCS1	3000500012	514561	3641046	1,330	1,548	-218	NMBG SC	
Southern Production Co., Cloudcroft Unit #1	SPCCLU1	3003500002	431152	3635650	2,859	735	2,124	NMBG SC	
Yates Petroleum Corporation, Dunken Nose Unit #1	YPCDNU1	3000560383	491492	3635055	1,602	1,355	247	OCD	
Yates Petroleum Corporation, Dunken Dome Unit #2	YPCDDU2	3000560397	485994	3634588	1,631	1,227	403	OCD	
Yates Petroleum Corporation, Dunken Dome Unit #1	YPCDDU1	3000560374	486211	3634277	1,643	1,247	397	OCD	
Liberty Oil & Gas Corp., T.L. Watts #1	LO&GTLW	3000560766	480341	3631643	1,633	1,265	368	BH	
Magnolia, Headley Federal #2	MAGHEF2	NA	512347	3631229	1,510	1,298	211	NMBG SC	
Yates Petroleum Corporation, Little Cuevo Unit #1	YPCLCU1	3000561785	488273	3631027	1,633	1,265	368	NMBG SC	
Sunray DX Oil Company, N.M. State "AV" #1	SOCSAV1	3000510144	491916	3630614	1,582	1,291	291	OCD	
Yates Petroleum Corporation, Little Cuevo Unit #2	YPCLCU2	3000562268	489571	3628557	1,618	1,215	403	OCD	
Magnolia, Black Hills	MAGBLHI	NA	505927	3627975	1,494	1,335	159	NMBG SC	
TEXACO Inc., Federal (USA) "E" #1	TEXIFE1	3003520001	395308	3624999	1,219	1,010	209	K&H	
Yates Petroleum Corporation, One Tree Unit #1	YPCOTU1	3000562259	467160	3623529	1,876	835	1,041	NMBG SC	
Yates Petroleum Corporation, Dog Canyon "YF" Federal #1	YPCDCF1	3003520024	462754	3622676	1,946	1,381	566	BH	

Table A-3.10: Oil-and-gas exploratory wells used as control for the top of the Pennsylvanian. See key at bottom of Table A-3.3.

Well Name, Lease	Well ID	API Number	Easting	Northing	Well Elevation (m)	Depth to Top of Pennsylvanian (m)	Elevation of Top of Pennsylvanian (m)	Source	Note
Texas Oil & Gas Corp., Federal "C" #1	TO&GFC1	3000560017	512954	3622309	1,359	1,570	-211	NMBG SC	
Kewanee Oil Co., F-M Unit #1	KOCFMU1	3000500009	493140	3619927	1,579	1,506	73	NMBG SC	
TEXACO Inc., Federal (USA) "F" #1	TEXIFF1	3003520006	410790	3619951	1,232	1,817	-584	KH	
TEXACO Inc., Federal (USA) "G" #1	TEXIFG1	3003520004	394443	3619379	1,276	Est.	19	F	Estimated from Foster (1978)
Marathon Oil Co., Mesa Verde Ranch #1	MOCMVR1	3003520022	455326	3618246	2,143	1,243	900	BH	
Yates Petroleum Corp., Buckhorn AYU State Com #1	YPCBAYU	3000560541	506142	3613140	1,440	1,503	-63	NMBG SC	
Texas Oil & Gas Corp., Federal "A" #1	TO&GFA1	3000510431	506950	3613041	1,442	1,587	-144	OCD	
Yates Petroleum Corporation (aka Phoenix Resources Co.), Bullis "AVW" State Com (aka Ranch Road) #1	YPCBAVW	3000560557	507355	3612640	1,478	1,602	-124	NMBG SC	
U.V. Industries, Inc., Long Canyon Unit #1	UVILCU1	3000560411	502547	3610225	1,536	1,798	-262	OCD	
Plymouth Oil Co., Evans (aka Federal D) #1	PLOCEV1	3003500003	404731	3604561	1,233	796	436	BH	
Texas Oil & Gas Corp., Federal "B" #1	TO&GFB1	NA	510832	3603835	1,463	1,728	-265	NMBG SC	
Atlantic Refining Co., State "AV" #1	ARCSAV1	3003510001	461443	3603143	1,921	777	1,144	NMBG SC	
Zapata Petroleum Corp., Federal 14 #1	ZPCF141	3003500006	454127	3603086	2,109	886	1,223	NMBG SC	
Sun Oil Company, T.J. Pearson #1	SOCTJP1	3003500005	416750	3598464	1,344	591	752	BH	
Terra Resources, Inc., Burro Canyon Unit #1-Y	TRBCU1Y	3003520017	511686	3596471	1,572	1,110	461	OCD	
Stanolind Oil & Gas, Thorn Unit #1	SO&GTU1	3003500007	453419	3593869	1,914	1,186	728	BH	
Yates Petroleum Corporation, Brainerd "IO" Federal #1	YPCBIOF	3001522149	523000	3587630	1,406	1,844	-438	OCD	
Otero Oil Co., McGregor #1	OTOCMC1	3003500010	412151	3586894	1,295	396	899	BH	
Marathon Oil Company, Box Canyon Unit #1	MOCBCU1	3001510012	522193	3586059	1,426	2,308	-882	OCD	
Presco, Inc., Indian Creek Federal #1	PRIICF1	3003520030	511700	3573937	1,767	1,277	490	OCD	
Humble Oil & Refining Co., Huapache Oil Unit #2	HO&RHO2	3001500013	530547	3572779	1,358	2,090	-732	OCD	

Table A-3.10 continued.

Well Name, Lease	Well ID	API Number	Easting	Northing	Well Elevation (m)	Depth to Top of Pennsylvanian (m)	Elevation of Top of Pennsylvanian (m)	Source	Note
Inexco Oil Company, Sitting Bull Unit #1	IOCSBU1	3001520752	527152	3568073	1,650	1,385	264	OCD	
Skelly Oil Co., Las Cruces "D" #1	SOCLCD1	3001500003	522240	3565867	1,749	1,393	356	NMBG SC	
Union Oil Co., Federal White #1	UNOCFW1	3001500019	525449	3565154	1,740	1,420	320	BH	
Humble Oil & Refining Co., Huapache Unit #5	HO&RHU5	3001500018	531153	3564735	1,631	1,429	202	OCD	
Franklin, Aston & Fair, Inc., Turkey Draw Unit #1	FA&FTD1	3001521378	524583	3560015	1,776	1,561	216	OCD	
Union Oil Co., McMillan #1	UNOCMC1	3003500028	440825	3557266	1,522	683	840	BH	
Union Oil Co., Verse 7 Federal #1	UOCV7F1	3001520591	524435	3556316	1,801	1,592	210	OCD	
Transocean Oil, G.J. Ablah #1	TROGJA1	3003520018	442810	3554817	1,509	529	980	K&H	
Beard Oil Company, Ridge USA #1	BOCRUS1	3001522547	524447	3551405	1,896	1,856	40	NMBG SC	
GDP 61-6	GDP61-6	NA	390213	3549130	1,254	433	822	F&J	
GDP 45-5	GDP45-5	NA	391837	3549102	1,255	6	1,249	F&J	
GDP 46-6	GDP46-6	NA	390223	3549119	1,252	205	1,047	F&J	
Harvey E. Yates Co., Bennett Ranch Unit #1	HEYBRU1	3003520027	435547	3545814	1,554	744	811	OCD	
Seaboard Oil Co., Trigg-Federal #1	SEOCTF1	3003500032	418801	3545797	1,618	1,156	462	K&H	
GDP 51-8	GDP51-8	NA	393417	3545870	1,253	196	1,056	F&J	
E.P. Campbell, Spiegel-Federal #1	EPCSPF1	3003510002	511803	3544568	1,868	1,369	499	K&H	
Sinclair Oil & Gas Co., Guadalupe Ridge Unit #1	SO&GGR1	3001520176	519670	3543204	2,215	2,222	-7	OCD	
Harvey E. Yates Co., Bennett Ranch Unit 25 #1	HEYBR25	3003520031	437133	3542284	1,533	529	1,004	OCD	
Chesapeake Operating, Inc., DF Ranch State 63-12 #1	CODFRS1	4210932302	543327	3538510	1,211	2,286	-1,075	RRC	
EOG Resources, Inc., Rector Canyon 24 State #1	EOGRC24	4210932250	544329	3534119	1,200	2,334	-1,134	RRC	Estimate
Bonanza Co., Pierson	BONCOPI	NA	531346	3532226	1,346	1,943	-597	V&K	
Pure Oil Co., Hunter #1	PUOCHU1	NA	509809	3531380	1,625	1,011	614	K&H	
Hueco Basin, University #1	HUBAUN1	NA	421896	3530405	1,558	754	805	BEG WR	

Table A-3.10 continued.

Well Name, Lease	Well ID	API Number	Easting	Northing	Well Elevation (m)	Depth to Top of Pennsylvanian (m)	Elevation of Top of Pennsylvanian (m)	Source	Note
Trail Mountain, Inc., University Big Iron "C45" #1	TMUBIC1	4222900029	440743	3529232	1,516	520	996	RRC	
Hunt Petroleum Corp., C.L. Ranch #1	HPCCLR1	4222930010	496475	3528252	1,105	1,339	-235	K&H	
TEXACO Inc., Culberson "L" Fee #1	TEXCLF1	NA	519234	3527336	1,564	1,346	217	K&H	
Tenneco Oil Co., TXL Fee #1	TOTXLF1	4210931401	563041	3526975	1,086	2,846	-1,760	RRC	
Trail Mountain, Inc., University Sizzler D5 #1	TMUSD51	4222930227	437784	3526650	1,437	725	712	RRC	
EOG Resources, Inc., Kenney 16 State #1H	EOGKS1H	4210932270	527946	3523355	1,372	1,662	-290	RRC	
EOG Resources, Inc., Kenney 16 State #2	EOGKES2	4210932269	528404	3522559	1,365	1,662	-297	RRC	
California Standard of Texas, Theisen #1	CASATT1	NA	426103	3521248	1,557	158	1,399	BEG WR	
Trail Mountain, Inc., University Felina "D27" #1	TMUFD27	4222930006	439917	3518350	1,427	273	1,153	RRC	
Border Exploration Co., Hammack et al. CT-1	BECHCT1	4222930196	505172	3518026	1,107	1,573	-466	K&H	
A.R. Jones Co., E.C. Mowry #1	ARJECM1	NA	474192	3516927	1,230	647	583	BEG SC	
Tipperary Corp., ST-1 Billye Sparks	TCST1BS	4222930195	474281	3516816	1,230	930	300	BEG SC	In Penn. at total well depth
J.L. Cowley, E.C. Mowry #1	JLCECM1	NA	473079	3515907	1,234	604	630	BEG SC	
Border Exploration Co., J.J. McAdoo 7 #1	BECJJM1	4222930200	505794	3514682	1,143	1,646	-503	K&H	
T.E. Robertson Co., Inc., Mowry et al. #2	TERCMO2	NA	471217	3514010	1,222	529	693	BEG SC	
The Superior Oil Company, Covington State #1	TSOCCS1	4210931405	565213	3512927	1,140	3,314	-2,174	RRC	
Trail Mountain, Inc., University Devil Woman L5 #1	TMUDWL5	4222930253	477595	3510876	1,221	457	764	RRC	
Samson Lone Star, L.L.C., University Lands 46-14 #2	SALSUL2	4210932278	551660	3509591	1,310	3,214	-1,904	RRC	
Humble Oil & Ref. Co., M.C. Sibley #1	HORMCS1	NA	533795	3508569	1,458	2,301	-844	V&K	
Chesapeake Operating, Inc., University Lands 4627 #1	COUL462	4210932287	550571	3507028	1,300	3,167	-1,868	RRC	
EnCana Oil & Gas (USA) Inc., Sibley Ranch 47 State "25" #1	EOGSR47	4210932251	544180	3505778	1,332	2,804	-1,472	RRC	

Table A-3.10 continued.

Well Name, Lease	Well ID	API Number	Easting	Northing	Well Elevation (m)	Depth to Top of Pennsylvanian (m)	Elevation of Top of Pennsylvanian (m)	Source	Note
Anderson & Prichard, Bordens #1	A&PBOR1	NA	521137	3505265	1,391	1,524	-133	V&K	In Penn. at total well depth
Trail Mountain, Inc., University Ooby Dooby L35 #1	TMUODL1	4222930261	482251	3502319	1,230	775	455	RRC	
Petro-Hunt, L.L.C., Melissa Taylor State 27 #1-H	PHMTS27	4210932255	563684	3501318	1,150	3,841	-2,691	RRC	
EOG Resources, Inc., Wild Horse Draw 7 #1	EOGWHD7	4210932256	536584	3497771	1,510	2,298	-788	RRC	Estimate
Pan American Pet. Corp., Phillip F. Hass #1	PAPPFH1	NA	422942	3494846	1,373	701	671	BEG SC	
Transocean Oil, Inc., 36-1 MSA Trustee, Inc.	TO36MSA	4222930192	424652	3490962	1,551	878	673	BEG SC	
Chesapeake Operating, Inc., State Street State #701	COSS701	4210932271	546492	3478738	1,422	1,520	-98	RRC	
Gulf Oil Corp., J. Burner-State "B" #1	GOCJBS1	NA	441556	3472050	1,418	799	619	BEG SC	

Table A-3.10 continued.

Well Name, Lease	Well ID	API Number	Easting	Northing	Well Elevation (m)	Depth to Top of Pow Wow Conglomerate (m)	Elevation of Top of Pow Wow Conglomerate (m)	Source	Note
Atlantic Refining Co., State "AV" #1	ARCSAV1	3003510001	461443	3603143	1,921	766	1,155	NMBG SC	
Zapata Petroleum Corp., Federal 14 #1	ZPCF141	3003500006	454127	3603086	2,109	835	1,273	BH	
Terra Resources, Inc., Burro Canyon Unit #1-Y	TRBCU1Y	3003520017	511686	3596471	1,572	1,089	483	BH	
Stanolind Oil & Gas, Thorn Unit #1	SO&GTU1	3003500007	453419	3593869	1,914	986	928	BH	
E.P. Campbell, Hurley #1	EPCAHU1	3003500012	447355	3580223	1,404	633	771	K&H	
E.P. Campbell, Liberman State #1	EPCALI1	3003500014	457361	3576570	1,326	807	518	K&H	
W.R. Weaver, Thompson #1	WRWETH1	3003500017	499785	3575900	1,386	861	525	NMBG SC	
E.P. Campbell, Lois Spanel #1	EPCALS1	3003500015	467947	3575324	1,408	649	759	K&H	
Presco, Inc., Indian Creek Federal #1	PRIICF1	3003520030	511700	3573937	1,767	1,194	573	OCD	
E.P. Campbell, McMillan Federal #1	EPCAMF1	3003500018	500598	3573842	1,319	855	464	K&H	
Coral Oil & Gas Co., Warren #1	CO&GCW1	3003500016	487264	3571960	1,186	641	544	K&H	
Union Oil Co., Federal White #1	UNOCFW1	3001500019	525449	3565154	1,740	1,380	361	BH	
Union Oil Co., McMillan #1	UNOCMC1	3003500028	440825	3557266	1,522	584	938	BH	
W.W. West, West Dog Canyon Unit #1	WWWWDC1	3003520007	505979	3555044	1,771	1,167	603	OCD	
Transocean Oil, G.J. Ablah #1	TROGJA1	3003520018	442810	3554817	1,509	503	1,006	K&H	
Pennzoil Co., Southland "28" State #1	PCS28S1	3003520019	479573	3551070	1,206	787	419	K&H	
E.J. Dunigan, Alpha Federal #1	EJDALF1	3003520002	496594	3549815	1,159	1,208	-49	K&H	
Hunt Oil Co., McMillan-Turner #1	HUOCMT1	3003500029	469015	3547882	1,269	533	736	BH	
Harvey E. Yates Co., Bennett Ranch Unit #1	HEYBRU1	3003520027	435547	3545814	1,554	668	887	OCD	
Seaboard Oil Co., Trigg-Federal #1	SEOCTF1	3003500032	418801	3545797	1,618	936	683	K&H	
Harvey E. Yates Co., Bennett Ranch Unit 25 #1	HEYBR25	3003520031	437133	3542284	1,533	524	1,008	OCD	

Table A-3.11: Oil-and-gas exploratory wells used as control for the top of the Pow Wow Conglomerate. See key at bottom of Table A-3.3.

Well Name, Lease	Well ID	API Number	Easting	Northing	Well Elevation (m)	Depth to Top of Pow Wow Conglomerate (m)	Elevation of Top of Pow Wow Conglomerate (m)	Source	Note
Pan American Petroleum Corporation, List Anderson #1	PAPCLA1	NA	491521	3533849	1,108	753	355	V&K	
Pure Oil Co., Hunter #1	PUOCHU1	NA	509809	3531380	1,625	499	1,126	K&H	
Trail Mountain, Inc., University Sizzler D5 #1	TMUSD51	4222930227	437784	3526650	1,437	668	770	RRC	
General Crude Oil Company, Merrill and Voyles et al. #1	GCOCMV1	NA	477481	3524877	1,181	632	548	BEG WR	
A.R. Jones Co., E.C. Mowry #1	ARJECM1	NA	474192	3516927	1,230	596	634	BEG SC	
T.E. Robertson Co., Inc., Mowry et al. #2	TERCMO2	NA	471217	3514010	1,222	445	777	BEG SC	
J.P. Hurndall & R.A. Gray, J.S. Pierce #1	H&GJSP1	NA	479266	3465692	1,488	112	1,376	BEG SC	

Table A-3.11 continued.

Well Name, Lease	Well ID	API Number	Easting	Northing	Well Elevation (m)	Depth to Top of Hueco Lm./Fm. and Wolfcamp (m)	Elevation of Top of Hueco Lm./Fm. and Wolfcamp (m)	Source	Note
Houston Oil & Minerals Corp., State L.G. "1453" #1	HO&MSL1	3003520013	406876	3685414	1,511	1,945	-434	NMBG DL	
Houston Oil & Minerals Corp., J.M. Lewelling #1	HO&MJL1	3003520010	402778	3684425	1,440	1,317	123	OCD	
Houston Oil & Minerals Corp., Federal "A" #1	HO&MFA1	3003520009	413617	3660369	1,619	273	1,346	K&H	
Leland A. Hodges, Trustee, Houston #1	LAHTHO1	3003520005	411157	3660302	1,529	131	1,399	K&H	
Houston Oil & Minerals Corp., State 3724 #1	HO&MS31	3003520011	412512	3657622	1,540	148	1,392	OCD	
McClellan Oil Corp., Flying "H" Ranch Unit Tract 3 #1	MCOCFH1	3000562244	497349	3652108	1,554	991	563	OCD	
McClellan Oil Corp., Gragg B #1	MCOCGB1	3000561993	495371	3649683	1,529	1,022	508	OCD	
Westcoast Hydrocarbons, Inc., Black Hills Unit #1	WHIBHU1	3000500013	508897	3629768	1,453	1,308	146	NMBG SC	
TEXACO Inc., Federal (USA) "E" #1	TEXIFE1	3003520001	395308	3624999	1,219	618	600	K&H	
Texas Oil & Gas Corp., Federal "C" #1	TO&GFC1	3000560017	512954	3622309	1,359	1,195	164	NMBG SC	
TEXACO Inc., Federal (USA) "F" #1	TEXIFF1	3003520006	410790	3619951	1,232	1,423	-190	K&H	
TEXACO Inc., Federal (USA) "G" #1	TEXIFG1	3003520004	394443	3619379	1,276	Est.	436	F	Estimated from Foster (1978)
Texas Oil & Gas Corp., Federal "A" #1	TO&GFA1	3000510431	506950	3613041	1,442	1,122	321	NMBG SC	
Yates Petroleum Corporation (aka Phoenix Resources Co.), Bullis "AVW" State Com (aka Ranch Road) #1	YPCBAVW	3000560557	507355	3612640	1,478	1,187	291	NMBG SC	
U.V. Industries, Inc., Long Canyon Unit #1	UVILCU1	3000560411	502547	3610225	1,536	1,140	397	NMBG SC	
Plymouth Oil Co., Evans (aka Federal D) #1	PLOCEV1	3003500003	404731	3604561	1,233	576	657	BH	
Texas Oil & Gas Corp., Federal "B" #1	TO&GFB1	NA	510832	3603835	1,463	1,247	216	NMBG SC	
Atlantic Refining Co., State "AV" #1	ARCSAV1	3003510001	461443	3603143	1,921	711	1,210	NMBG SC	
Zapata Petroleum Corp., Federal 14 #1	ZPCF141	3003500006	454127	3603086	2,109	747	1,362	NMBG SC	
Sun Oil Company, T.J. Pearson #1	SOCTJP1	3003500005	416750	3598464	1,344	390	953	BH	

Table A-3.12: Oil-and-gas exploratory wells used as control for the top of the Hueco Limestone/Formation and Wolfcamp Formation. See key at bottom of Table A-3.3.

Well Name, Lease	Well ID	API Number	Easting	Northing	Well Elevation (m)	Depth to Top of Hueco Lm./Fm. and Wolfcamp (m)	Elevation of Top of Hueco Lm./Fm. and Wolfcamp (m)	Source	Note
Terra Resources, Inc., Burro Canyon Unit #1-Y	TRBCU1Y	3003520017	511686	3596471	1,572	932	639	BH	
Stanolind Oil & Gas, Thorn Unit #1	SO&GTU1	3003500007	453419	3593869	1,914	838	1,076	BH	
Yates Petroleum Corporation, Brainerd "IO" Federal #1	YPCBIOF	3001522149	523000	3587630	1,406	1,423	-18	OCD	
Otero Oil Co., McGregor #1	OTOCMC1	3003500010	412151	3586894	1,295	250	1,045	BH	
Brainerd Corp. (aka Continental Oil Co.), Federal "A" (aka East Texas Hill Unit) #1	BRCFEA1	3001500005	523406	3586429	1,397	1,421	-24	NMBG SC	
Continental Oil Co., H.W. Bass #1	COCHWB1	3001500004	516898	3586367	1,680	1,140	540	NMBG SC	
Marathon Oil Company, Box Canyon Unit #1	MOCBCU1	3001510012	522193	3586059	1,426	1,439	-13	OCD	
E.P. Campbell, Hurley #1	EPCAHU1	3003500012	447355	3580223	1,404	468	936	K&H	
E.P. Campbell, Liberman State #1	EPCALI1	3003500014	457361	3576570	1,326	728	598	K&H	
W.R. Weaver, Thompson #1	WRWETH1	3003500017	499785	3575900	1,386	771	615	BH	
E.P. Campbell, Lois Spanel #1	EPCALS1	3003500015	467947	3575324	1,408	639	770	K&H	
E.P. Campbell, McMillan Federal #1	EPCAMF1	3003500018	500598	3573842	1,319	747	572	BH	
Humble Oil & Refining Co., Huapache Oil Unit #2	HO&RHO2	3001500013	530547	3572779	1,358	1,826	-468	OCD	
Inexco Oil Company, Sitting Bull Unit #1	IOCSBU1	3001520752	527152	3568073	1,650	1,342	307	OCD	
Coral Oil & Gas Company, Ann Spanel #1	CO&GAS1	3003500021	451716	3566857	1,391	425	966	OCD	
Skelly Oil Co., Las Cruces "D" #1	SOCLCD1	3001500003	522240	3565867	1,749	1,337	412	NMBG SC	
Union Oil Co., Federal White #1	UNOCFW1	3001500019	525449	3565154	1,740	1,144	596	BH	
Humble Oil & Refining Co., Huapache Unit #5	HO&RHU5	3001500018	531153	3564735	1,631	1,382	250	NMBG SC	
E.P. Campbell (aka John J. Eisner), Federal #1	EPCAFE1	3003500019	432641	3562887	1,497	170	1,327	NMBG SC	
Flynn, Welch, Yates, Donahue #1	FWYDON1	NA	460768	3561350	1,303	415	888	BH	
Franklin, Aston & Fair, Inc., Turkey Draw Unit #1	FA&FTD1	3001521378	524583	3560015	1,776	1,405	371	OCD	

Table A-3.12 continued.

Well Name, Lease	Well ID	API Number	Easting	Northing	Well Elevation (m)	Depth to Top of Hueco Lm./Fm. and Wolfcamp (m)	Elevation of Top of Hueco Lm./Fm. and Wolfcamp (m)	Source	Note
Union Oil Co., McMillan #1	UNOCMC1	3003500028	440825	3557266	1,522	259	1,263	BH	
Union Oil Co., Verse 7 Federal #1	UOCV7F1	3001520591	524435	3556316	1,801	1,418	383	OCD	
W.W. West, West Dog Canyon Unit #1	WWWWDC1	3003520007	505979	3555044	1,771	869	902	OCD	
Transocean Oil, G.J. Ablah #1	TROGJA1	3003520018	442810	3554817	1,509	315	1,194	K&H	
Beard Oil Company, Ridge USA #1	BOCRUS1	3001522547	524447	3551405	1,896	1,743	153	NMBG SC	
Pennzoil Co., Southland "28" State #1	PCS28S1	3003520019	479573	3551070	1,206	473	733	K&H	
Fred Turner, Jr., State #1	FTUJST1	3003500027	475070	3550274	1,317	561	756	K&H	
Hunt Oil Co., McMillan-Turner #1	HUOCMT1	3003500029	469015	3547882	1,269	393	876	BH	
Harvey E. Yates Co., Bennett Ranch Unit #1	HEYBRU1	3003520027	435547	3545814	1,554	201	1,353	OCD	
Seaboard Oil Co., Trigg-Federal #1	SEOCTF1	3003500032	418801	3545797	1,618	223	1,395	K&H	
Harvey E. Yates Co., Bennett Ranch Unit 25 #1	HEYBR25	3003520031	437133	3542284	1,533	64	1,469	OCD	
Chesapeake Operating, Inc., DF Ranch State 63-12 #1	CODFRS1	4210932302	543327	3538510	1,211	1,943	-732	RRC	
Pure Oil Co., Hunter #1	PUOCHU1	NA	509809	3531380	1,625	421	1,204	K&H	
Hueco Basin, University #1	HUBAUN1	NA	421896	3530405	1,558	137	1,421	BEG WR	
Hunt Petroleum Corp., C.L. Ranch #1	HPCCLR1	4222930010	496475	3528252	1,105	1,093	12	K&H	
TEXACO Inc., Culberson "L" Fee #1	TEXCLF1	NA	519234	3527336	1,564	1,198	365	K&H	
Pan American Petroleum Corporation, Ed Hammock #1	PAPCEH1	NA	499124	3526693	1,110	1,169	-59	V&K	
TXL Corp., Culberson "C" Fee #1	TXLCCF1	NA	523721	3526221	1,515	1,466	49	V&K	
Border Exploration Co., Hammack et al. CT-1	BECHCT1	4222930196	505172	3518026	1,107	1,395	-288	K&H	
A.R. Jones Co., E.C. Mowry #1	ARJECM1	NA	474192	3516927	1,230	501	728	BEG SC	
J.L. Cowley, E.C. Mowry #1	JLCECM1	NA	473079	3515907	1,234	454	779	BEG SC	

Table A-3.12 continued.

750

Well Name, Lease	Well ID	API Number	Easting	Northing	Well Elevation (m)	Depth to Top of Hueco Lm./Fm. and Wolfcamp (m)	Elevation of Top of Hueco Lm./Fm. and Wolfcamp (m)	Source	Note
Border Exploration Co., J.J. McAdoo 7 #1	BECJJM1	4222930200	505794	3514682	1,143	1,396	-253	K&H	
T.E. Robertson Co., Inc., Mowry et al. #2	TERCMO2	NA	471217	3514010	1,222	384	839	BEG SC	
The Superior Oil Company, Covington State #1	TSOCCS1	4210931405	565213	3512927	1,140	2,295	-1,155	RRC	
Samson Lone Star, L.L.C., University Lands 46-14 #2	SALSUL2	4210932278	551660	3509591	1,310	1,990	-680	RRC	
N. Amer. Royalties, Inc., Potter #1	NARIPO1	NA	511738	3508091	1,186	1,115	71	V&K	
Chesapeake Operating, Inc., University Lands 4627 #1	COUL462	4210932287	550571	3507028	1,300	1,952	-652	RRC	
EnCana Oil & Gas (USA) Inc., Sibley Ranch 47 State "25" #1	EOGSR47	4210932251	544180	3505778	1,332	1,670	-338	RRC	
Trail Mountain, Inc., University Ooby Dooby L35 #1	TMUODL1	4222930261	482251	3502319	1,230	427	803	RRC	
Petro-Hunt, L.L.C., Melissa Taylor State 27 #1-H	PHMTS27	4210932255	563684	3501318	1,150	2,234	-1,084	RRC	
American Quasar Pet. Co., V.C. Rounsaville #1	AQPVCR1	NA	563477	3498883	1,178	2,718	-1,540	V&K	
Chesapeake Operating, Inc., Melissa Taylor State 105-3	COMT105	4210932297	541293	3493028	1,437	1,513	-76	RRC	
Chesapeake Operating, Inc., State Street State #701	COSS701	4210932271	546492	3478738	1,422	1,216	206	RRC	
Sinclair, Looney	SINCLOO	NA	551319	3475371	1,310	1,539	-229	V&K	
Gulf Oil Corp., J. Burner-State "B" #1	GOCJBS1	NA	441556	3472050	1,418	79	1,339	BEG SC	

Table A-3.12 continued.

751

Well Name, Lease	Well ID	API Number	Easting	Northing	Well Elevation (m)	Depth to Top of Abo Formation (m)	Elevation of Top of Abo Formation (m)	Source	Note
Houston Oil & Minerals Corp., State L.G. "1453" #1	HO&MSL1	3003520013	406876	3685414	1,511	1,280	230	NMBG DL	
Houston Oil & Minerals Corp., J.M. Lewelling #1	HO&MJL1	3003520010	402778	3684425	1,440	991	449	OCD	
Houston Oil & Minerals Corp., Federal "A" #1	HO&MFA1	3003520009	413617	3660369	1,619	0	1,619	K&H	
Leland A. Hodges, Trustee, Houston #1	LAHTHO1	3003520005	411157	3660302	1,529	0	1,529	K&H	
McClellan Oil Corp., Flying "H" Ranch Unit Tract 3 #1	MCOCFH1	3000562244	497349	3652108	1,554	834	721	OCD	
McClellan Oil Corp., Gragg B #1	MCOCGB1	3000561993	495371	3649683	1,529	788	741	OCD	
Humble Oil & Refining Co., Yates Federal #1	HO&RYF1	3000560015	486777	3649300	1,648	856	792	OCD	
J. Cleo Thompson, State A-6 #1	JCTSA61	3000562988	477111	3646836	1,824	685	1,139	OCD	
Lubbook Machine & Supply Co., Inc., Anderson-Randell #1	LM&SAR1	3000500003	472069	3645946	1,767	503	1,264	OCD	
Humble Oil & Refining Co., Humble-Yates N.M. State #1	HO&RHY1	3000510521	488336	3643533	1,574	826	748	OCD	
W.H. Black Drilling Co., Shildneck #1	WHBDCS1	3000500012	514561	3641046	1,330	954	376	NMBG SC	
Continental Oil Company, State NN #1	COCSNN1	3000560185	492051	3640997	1,538	823	715	OCD	
J. Cleo Thompson, Federal A-28 #1	JCTFA28	3000562915	479948	3639939	1,649	604	1,045	OCD	
C & K Petroleum, Inc., Singer Lake State #1	C&KSLS1	3000560320	495659	3637945	1,545	870	675	OCD	
Southern Production Co., Cloudcroft Unit #1	SPCCLU1	3003500002	431152	3635650	2,859	658	2,201	BH	
Yates Petroleum Corporation, Dunken Nose Unit #1	YPCDNU1	3000560383	491492	3635055	1,602	884	718	OCD	
Yates Petroleum Corporation, Dunken Dome Unit #2	YPCDDU2	3000560397	485994	3634588	1,631	832	799	OCD	
Yates Petroleum Corporation, Dunken Dome Unit #1	YPCDDU1	3000560374	486211	3634277	1,643	850	794	OCD	
C & K Petroleum, Inc., Little Cuevo State #1	C&KLCS1	3000560324	501605	3632606	1,464	942	522	OCD	
Liberty Oil & Gas Corp., T.L. Watts #1	LO&GTLW	3000560766	480341	3631643	1,633	933	700	BH	
Magnolia, Headley Federal #2	MAGHEF2	NA	512347	3631229	1,510	891	619	NMBG SC	

Table A-3.13: Oil-and-gas exploratory wells used as control for the top of the Abo Formation. See key at bottom of Table A-3.3.

Well Name, Lease	Well ID	API Number	Easting	Northing	Well Elevation (m)	Depth to Top of Abo Formation (m)	Elevation of Top of Abo Formation (m)	Source	Note
Yates Petroleum Corporation, Little Cuevo Unit #1	YPCLCU1	3000561785	488273	3631027	1,633	933	700	NMBG SC	
Sunray DX Oil Company, N.M. State "AV" #1	SOCSAV1	3000510144	491916	3630614	1,582	847	735	OCD	
Westcoast Hydrocarbons, Inc., Black Hills Unit #1	WHIBHU1	3000500013	508897	3629768	1,453	900	553	NMBG SC	
Yates Petroleum Corporation, Little Cuevo Unit #2	YPCLCU2	3000562268	489571	3628557	1,618	910	707	OCD	
Magnolia, Black Hills	MAGBLHI	NA	505927	3627975	1,494	905	589	NMBG SC	
Gulf Oil Corporation, Chaves State "U" #1	GOCCSU1	3000500002	472386	3625264	1,907	544	1,363	OCD	
TEXACO Inc., Federal (USA) "E" #1	TEXIFE1	3003520001	395308	3624999	1,219	467	752	K&H	
Yates Petroleum Corporation, One Tree Unit #1	YPCOTU1	3000562259	467160	3623529	1,876	789	1,087	NMBG SC	
Yates Petroleum Corporation, Dog Canyon "YF" Federal #1	YPCDCF1	3003520024	462754	3622676	1,946	921	1,025	NMBG SC	
Texas Oil & Gas Corp., Federal "C" #1	TO&GFC1	3000560017	512954	3622309	1,359	954	405	NMBG SC	
Kewanee Oil Co., F-M Unit #1	KOCFMU1	3000500009	493140	3619927	1,579	911	668	NMBG SC	
TEXACO Inc., Federal (USA) "F" #1	TEXIFF1	3003520006	410790	3619951	1,232	1,238	-6	K&H	
Yates Petroleum Corporation, One Tree Unit #2	YPCOTU2	3000562276	468582	3619170	2,010	594	1,415	NMBG SC	
TEXACO Inc., Federal (USA) "G" #1	TEXIFG1	3003520004	394443	3619379	1,276	Est.	714	F	Estimated from Foster (1978)
Marathon Oil Co., Mesa Verde Ranch #1	MOCMVR1	3003520022	455326	3618246	2,143	794	1,349	NMBG SC	
Yates Petroleum Corp., Buckhorn AYU State Com #1	YPCBAYU	3000560541	506142	3613140	1,440	895	545	NMBG SC	
Texas Oil & Gas Corp., Federal "A" #1	TO&GFA1	3000510431	506950	3613041	1,442	908	534	NMBG SC	
Yates Petroleum Corporation (aka Phoenix Resources Co.), Bullis "AVW" State Com (aka Ranch Road) #1	YPCBAVW	3000560557	507355	3612640	1,478	957	521	NMBG SC	
Sun Oil Co., Pinon Unit #2	SOCPIU2	3000500007	478157	3612259	1,925	492	1,433	NMBG SC	
Sun Oil Co., Pinon Unit #1	SOCPIU1	3000500006	476922	3611828	1,995	508	1,487	NMBG SC	
U.V. Industries, Inc., Long Canyon Unit #1	UVILCU1	3000560411	502547	3610225	1,536	933	603	NMBG SC	

Table A-3.13 continued.

Well Name, Lease	Well ID	API Number	Easting	Northing	Well Elevation (m)	Depth to Top of Abo Formation (m)	Elevation of Top of Abo Formation (m)	Source	Note
Gulf Oil Corp., Federal Munson #1	GOCFMU1	3000510075	489407	3609839	1,723	707	1,016	NMBG SC	
Plymouth Oil Co., Evans (aka Federal D) #1	PLOCEV1	3003500003	404731	3604561	1,233	355	878	BH	
Texas Oil & Gas Corp., Federal "B" #1	TO&GFB1	NA	510832	3603835	1,463	942	521	NMBG SC	
Atlantic Refining Co., State "AV" #1	ARCSAV1	3003510001	461443	3603143	1,921	641	1,279	NMBG SC	
Zapata Petroleum Corp., Federal 14 #1	ZPCF141	3003500006	454127	3603086	2,109	671	1,438	NMBG SC	
Sun Oil Company, T.J. Pearson #1	SOCTJP1	3003500005	416750	3598464	1,344	250	1,094	BH	
Terra Resources, Inc., Burro Canyon Unit #1-Y	TRBCU1Y	3003520017	511686	3596471	1,572	902	669	BH	
Stanolind Oil & Gas, Thorn Unit #1	SO&GTU1	3003500007	453419	3593869	1,914	746	1,169	BH	
Standard of Texas, Scarp Unit #1	SOTSCU1	3003500009	487438	3593394	1,628	259	1,369	BH	
Lefors Petroleum Co., Federal #1	LEPCFE1	3003500008	471863	3592611	1,642	509	1,133	NMBG SC	
Yates Petroleum Corporation, Brainerd "IO" Federal #1	YPCBIOF	3001522149	523000	3587630	1,406	1,067	338	OCD	
Tri-Service Drilling Co., Little Dog Federal #1	TSDLDF1	3003520008	496060	3586992	1,940	777	1,163	NMBG SC	
Brainerd Corp. (aka Continental Oil Co.), Federal "A" (aka East Texas Hill Unit) #1	BRCFEA1	3001500005	523406	3586429	1,397	1,081	316	NMBG SC	
Continental Oil Co., H.W. Bass #1	COCHWB1	3001500004	516898	3586367	1,680	870	810	NMBG SC	
Marathon Oil Company, Box Canyon Unit #1	MOCBCU1	3001510012	522193	3586059	1,426	1,077	349	OCD	
Pitts Energy Co., Federal "9" #1	PIECF91	3001527563	518567	3585218	1,619	943	675	OCD	
Sinclair Oil & Gas Company, Federal Eddy 193 #1	SO&GFE1	3001500001	518145	3580901	1,582	958	624	OCD	
E.P. Campbell, Hurley #1	EPCAHU1	3003500012	447355	3580223	1,404	419	985	K&H	
Tom L. Ingram, State "E" #1	TLISTE1	3001520003	523070	3579540	1,390	725	664	OCD	
E.P. Campbell, Liberman State #1	EPCALI1	3003500014	457361	3576570	1,326	662	663	K&H	
W.R. Weaver, Thompson #1	WRWETH1	3003500017	499785	3575900	1,386	736	650	NMBG SC	

Table A-3.13 continued.

Well Name, Lease	Well ID	API Number	Easting	Northing	Well Elevation (m)	Depth to Top of Abo Formation (m)	Elevation of Top of Abo Formation (m)	Source	Note
E.P. Campbell, Lois Spanel #1	EPCALS1	3003500015	467947	3575324	1,408	562	847	K&H	
Presco, Inc., Indian Creek Federal #1	PRIICF1	3003520030	511700	3573937	1,767	931	836	OCD	
E.P. Campbell, McMillan Federal #1	EPCAMF1	3003500018	500598	3573842	1,319	712	607	K&H	
Coral Oil & Gas Co., Warren #1	CO&GCW1	3003500016	487264	3571960	1,186	609	577	K&H	
Inexco Oil Company, Sitting Bull Unit #1	IOCSBU1	3001520752	527152	3568073	1,650	1,062	588	OCD	
Coral Oil & Gas Company, Ann Spanel #1	CO&GAS1	3003500021	451716	3566857	1,391	376	1,014	OCD	
Atlantic Refining Co., Huapache Unit #9	ARCHUU9	3001500016	527053	3566737	1,686	978	708	NMBG SC	
Skelly Oil Co., Las Cruces "D" #1	SOCLCD1	3001500003	522240	3565867	1,749	1,050	699	NMBG SC	
Union Oil Co., Federal White #1	UNOCFW1	3001500019	525449	3565154	1,740	1,077	663	BH	
Humble Oil & Refining Co., Huapache Unit #5	HO&RHU5	3001500018	531153	3564735	1,631	1,064	568	OCD	
Threshold Development Co., Chiricahua R 21 Federal #1	TDCR21F	3003520034	489264	3563381	1,133	758	374	NMBG SC	
Flynn, Welch, Yates, Donahue #1	FWYDON1	NA	460768	3561350	1,303	355	948	BH	
Franklin, Aston & Fair, Inc., Turkey Draw Unit #1	FA&FTD1	3001521378	524583	3560015	1,776	1,087	690	OCD	
Union Oil Co., McMillan #1	UNOCMC1	3003500028	440825	3557266	1,522	212	1,311	BH	
W.W. West, West Dog Canyon Unit #1	WWWWDC1	3003520007	505979	3555044	1,771	863	908	OCD	
Transocean Oil, G.J. Ablah #1	TROGJA1	3003520018	442810	3554817	1,509	278	1,231	K&H	
Threshold Development Co., Mescalero 28 Federal #1	TDM28F1	3003520033	489514	3552255	1,219	469	749	OCD	
Beard Oil Company, Ridge USA #1	BOCRUS1	3001522547	524447	3551405	1,896	1,184	712	OCD	
Pennzoil Co., Southland "28" State #1	PCS28S1	3003520019	479573	3551070	1,206	454	753	K&H	
Fred Turner, Jr., State #1	FTUJST1	3003500027	475070	3550274	1,317	493	824	K&H	
E.J. Dunigan, Alpha Federal #1	EJDALF1	3003520002	496594	3549815	1,159	1,129	31	K&H	

Table A-3.13 continued.

Well Name, Lease	Well ID	API Number	Easting	Northing	Well Elevation (m)	Depth to Top of Abo Formation (m)	Elevation of Top of Abo Formation (m)	Source	Note
Hunt Oil Co., McMillan-Turner #1	HUOCMT1	3003500029	469015	3547882	1,269	375	895	BH	
Harvey E. Yates Co., Bennett Ranch Unit #1	HEYBRU1	3003520027	435547	3545814	1,554	104	1,451	OCD	
Seaboard Oil Co., Trigg-Federal #1	SEOCTF1	3003500032	418801	3545797	1,618	168	1,450	K&H	
E.P. Campbell, Spiegel-Federal #1	EPCSPF1	3003510002	511803	3544568	1,868	1,033	835	K&H	
Sinclair Oil & Gas Co., Guadalupe Ridge Unit #1	SO&GGR1	3001520176	519670	3543204	2,215	1,009	1,206	OCD	
Hunt Petroleum Corp., C.L. Ranch "5" #1	HPCCL51	4222930011	496478	3539912	1,110	1,418	-308	K&H	
Hunt Petroleum Corp., C.L. Ranch #1	HPCCLR1	4222930010	496475	3528252	1,105	881	223	K&H	
Pan American Petroleum Corporation, Ed Hammock #1	PAPCEH1	NA	499124	3526693	1,110	977	133	V&K	

Table A-3.13 continued.

756

Well Name, Lease	Well ID	API Number	Easting	Northing	Well Elevation (m)	Depth to Top of Yeso Formation (m)	Elevation of Top of Yeso Formation (m)	Source	Note
Houston Oil & Minerals Corp., Lewelling #2	HO&MCL2	3003520015	399960	3684444	1,373	2,252	-879	OCD	
Humble Oil & Refining Co., Yates Federal #1	HO&RYF1	3000560015	486777	3649300	1,648	253	1,395	OCD	
J. Cleo Thompson, State A-6 #1	JCTSA61	3000562988	477111	3646836	1,824	146	1,679	OCD	
Humble Oil & Refining Co., Humble-Yates N.M. State #1	HO&RHY1	3000510521	488336	3643533	1,574	224	1,350	OCD	
W.H. Black Drilling Co., Shildneck #1	WHBDCS1	3000500012	514561	3641046	1,330	313	1,018	NMBG SC	
J. Cleo Thompson, Federal A-28 #1	JCTFA28	3000562915	479948	3639939	1,649	50	1,599	OCD	
Southern Production Co., Cloudcroft Unit #1	SPCCLU1	3003500002	431152	3635650	2,859	116	2,743	BH	
Yates Petroleum Corporation, Dunken Nose Unit #1	YPCDNU1	3000560383	491492	3635055	1,602	274	1,327	OCD	
Liberty Oil & Gas Corp., T.L. Watts #1	LO&GTLW	3000560766	480341	3631643	1,633	255	1,378	BH	
Magnolia, Headley Federal #2	MAGHEF2	NA	512347	3631229	1,510	282	1,228	NMBG SC	
Yates Petroleum Corporation, Little Cuevo Unit #1	YPCLCU1	3000561785	488273	3631027	1,633	255	1,378	NMBG SC	
Yates Petroleum Corporation, Little Cuevo Unit #2	YPCLCU2	3000562268	489571	3628557	1,618	230	1,387	OCD	
Magnolia, Black Hills	MAGBLHI	NA	505927	3627975	1,494	262	1,232	NMBG SC	
TEXACO Inc., Federal (USA) "E" #1	TEXIFE1	3003520001	395308	3624999	1,219	214	1,005	KH	
Yates Petroleum Corporation, One Tree Unit #1	YPCOTU1	3000562259	467160	3623529	1,876	109	1,767	NMBG SC	
Yates Petroleum Corporation, Dog Canyon "YF" Federal #1	YPCDCF1	3003520024	462754	3622676	1,946	163	1,783	NMBG SC	
Texas Oil & Gas Corp., Federal "C" #1	TO&GFC1	3000560017	512954	3622309	1,359	334	1,025	OCD	
TEXACO Inc., Federal (USA) "F" #1	TEXIFF1	3003520006	410790	3619951	1,232	931	301	K&H	
Yates Petroleum Corporation, One Tree Unit #2	YPCOTU2	3000562276	468582	3619170	2,010	91	1,918	NMBG SC	
TEXACO Inc., Federal (USA) "G" #1	TEXIFG1	3003520004	394443	3619379	1,276	Est.	1,067	F	Estimated from Foster (1978)
Marathon Oil Co., Mesa Verde Ranch #1	MOCMVR1	3003520022	455326	3618246	2,143	199	1,944	BH	

Table A-3.14: Oil-and-gas exploratory wells used as control for the top of the Yeso Formation. See key at bottom of Table A-3.3.

Well Name, Lease	Well ID	API Number	Easting	Northing	Well Elevation (m)	Depth to Top of Yeso Formation (m)	Elevation of Top of Yeso Formation (m)	Source	Note
Texas Oil & Gas Corp., Federal "A" #1	TO&GFA1	3000510431	506950	3613041	1,442	337	1,106	NMBG SC	
Plymouth Oil Co., Evans (aka Federal D) #1	PLOCEV1	3003500003	404731	3604561	1,233	158	1,074	BH	
Texas Oil & Gas Corp., Federal "B" #1	TO&GFB1	NA	510832	3603835	1,463	344	1,119	NMBG SC	
Atlantic Refining Co., State "AV" #1	ARCSAV1	3003510001	461443	3603143	1,921	172	1,749	BH	
Zapata Petroleum Corp., Federal 14 #1	ZPCF141	3003500006	454127	3603086	2,109	233	1,876	BH	
Terra Resources, Inc., Burro Canyon Unit #1-Y	TRBCU1Y	3003520017	511686	3596471	1,572	381	1,191	BH	
Stanolind Oil & Gas, Thorn Unit #1	SO&GTU1	3003500007	453419	3593869	1,914	223	1,692	BH	
Standard of Texas, Scarp Unit #1	SOTSCU1	3003500009	487438	3593394	1,628	0	1,628	BH	
Lefors Petroleum Co., Federal #1	LEPCFE1	3003500008	471863	3592611	1,642	91	1,551	NMBG SC	
Tri-Service Drilling Co., Little Dog Federal #1	TSDLDF1	3003520008	496060	3586992	1,940	344	1,596	OCD	
Brainerd Corp. (aka Continental Oil Co.), Federal "A" (aka East Texas Hill Unit) #1	BRCFEA1	3001500005	523406	3586429	1,397	433	964	NMBG SC	
E.P. Campbell, Hurley #1	EPCAHU1	3003500012	447355	3580223	1,404	51	1,352	K&H	
E.P. Campbell, Liberman State #1	EPCALI1	3003500014	457361	3576570	1,326	245	1,081	K&H	
W.R. Weaver, Thompson #1	WRWETH1	3003500017	499785	3575900	1,386	290	1,096	NMBG SC	
E.P. Campbell, Lois Spanel #1	EPCALS1	3003500015	467947	3575324	1,408	172	1,236	K&H	
E.P. Campbell, McMillan Federal #1	EPCAMF1	3003500018	500598	3573842	1,319	288	1,031	K&H	
Coral Oil & Gas Co., Warren #1	CO&GCW1	3003500016	487264	3571960	1,186	235	950	K&H	
Coral Oil & Gas Company, Ann Spanel #1	CO&GAS1	3003500021	451716	3566857	1,390	0	1,390	OCD	
Atlantic Refining Co., Huapache Unit #9	ARCHUU9	3001500016	527053	3566737	1,686	501	1,185	OCD	
Union Oil Co., Federal White #1	UNOCFW1	3001500019	525449	3565154	1,740	533	1,207	BH	
Humble Oil & Refining Co., Huapache Unit #5	HO&RHU5	3001500018	531153	3564735	1,631	495	1,136	OCD	

Table A-3.14 continued.

758

Well Name, Lease	Well ID	API Number	Easting	Northing	Well Elevation (m)	Depth to Top of Yeso Formation (m)	Elevation of Top of Yeso Formation (m)	Source	Note
Fred Turner, Jr. (aka Pasotero Pet. Corp.), Evans #1	FTUJEV1	3003500020	433355	3563003	1,545	85	1,460	BH	
Flynn, Welch, Yates, Donahue #1	FWYDON1	NA	460768	3561350	1,303	0	1,303	BH	
Union Oil Co., McMillan #1	UNOCMC1	3003500028	440825	3557266	1,522	0	1,522	BH	
Transocean Oil, G.J. Ablah #1	TROGJA1	3003520018	442810	3554817	1,509	0	1,509	K&H	
Beard Oil Company, Ridge USA #1	BOCRUS1	3001522547	524447	3551405	1,896	647	1,249	OCD	
Pennzoil Co., Southland "28" State #1	PCS28S1	3003520019	479573	3551070	1,206	117	1,089	K&H	
Fred Turner, Jr., State #1	FTUJST1	3003500027	475070	3550274	1,317	195	1,123	K&H	
E.J. Dunigan, Alpha Federal #1	EJDALF1	3003520002	496594	3549815	1,159	694	465	K&H	
Hunt Oil Co., McMillan-Turner #1	HUOCMT1	3003500029	469015	3547882	1,269	81	1,189	BH	
Harvey E. Yates Co., Bennett Ranch Unit #1	HEYBRU1	3003520027	435547	3545814	1,554	0	1,554	OCD	
Seaboard Oil Co., Trigg-Federal #1	SEOCTF1	3003500032	418801	3545797	1,616	0	1,616	K&H	
E.P. Campbell, Spiegel-Federal #1	EPCSPF1	3003510002	511803	3544568	1,868	650	1,219	K&H	
Harvey E. Yates Co., Bennett Ranch Unit 25 #1	HEYBR25	3003520031	437133	3542284	1,533	0	1,533	OCD	
Hunt Petroleum Corp., C.L. Ranch "5" #1	HPCCL51	4222930011	496478	3539912	1,110	936	174	K&H	
Hunt Oil Co., Dyer #1	HUOCDY1	4222930007	485477	3530917	1,119	27	1,092	K&H	
Hunt Petroleum Corp., C.L. Ranch #1	HPCCLR1	4222930010	496475	3528252	1,105	347	758	K&H	
General Crude Oil Company, Merrill and Voyles et al. #1	GCOCMV1	NA	477481	3524877	1,181	353	828	BEG WR	
A.R. Jones Co., E.C. Mowry #1	ARJECM1	NA	474192	3516927	1,230	333	897	BEG SC	
J.L. Cowley, E.C. Mowry #1	JLCECM1	NA	473079	3515907	1,234	338	895	BEG SC	

Table A-3.14 continued.

Well Name, Lease	Well ID	API Number	Easting	Northing	Well Elevation (m)	Depth to Top of Bone Spring Lm./Fm. (m)	Elevation of Top of Bone Spring Lm./Fm. (m)	Source	Note
Humble Oil & Refining Co., Huapache Oil Unit #2	HO&RHO2	3001500013	530547	3572779	1,358	341	1,017	OCD	
Beard Oil Company, Ridge USA #1	BOCRUS1	3001522547	524447	3551405	1,896	434	1,463	OCD	
EOG Resources, Inc., Rector Canyon 24 State #1	EOGRC24	4210932250	544329	3534119	1,200	1,267	-67	RRC	Estimate
Bonanza Co., Pierson	BONCOPI	NA	531346	3532226	1,346	905	441	V&K	
Pure Oil Co., Hunter #1	PUOCHU1	NA	509809	3531380	1,625	0	1,625	K&H	
TEXACO Inc., Culberson "L" Fee #1	TEXCLF1	NA	519234	3527336	1,564	477	1,087	K&H	
Tenneco Oil Co., TXL Fee #1	TOTXLF1	4210931401	563041	3526975	1,086	1,417	-332	RRC	
EOG Resources, Inc., Kenney 16 State #1H	EOGKS1H	4210932270	527946	3523355	1,372	1,349	23	RRC	
EOG Resources, Inc., Kenney 16 State #2	EOGKES2	4210932269	528404	3522559	1,365	1,349	16	RRC	
D & J Equip Co., J.C. Hunter, Jr. #2	DJJCHJ2	NA	512403	3519886	1,234	1,551	-317	V&K	Approximate
Border Exploration Co., Hammack et al. CT-1	BECHCT1	4222930196	505172	3518026	1,107	846	261	K&H	
TXL Oil Corp., Culberson B-T Fee #1	TXLCBT1	NA	550456	3517797	1,236	1,120	116	V&K	
A.R. Jones Co., E.C. Mowry #1	ARJECM1	NA	474192	3516927	1,230	378	852	BEG SC	
Border Exploration Co., J.J. McAdoo 7 #1	BECJJM1	4222930200	505794	3514682	1,143	860	283	K&H	
The Superior Oil Company, Covington State #1	TSOCCS1	4210931405	565213	3512927	1,140	1,436	-296	RRC	
Chesapeake Operating, Inc., Dela Minerals "3" State #701	COIDM3S	4210932268	566918	3512065	1,142	1,490	-348	RRC	
Humble Oil & Ref. Co., M.C. Sibley #1	HORMCS1	NA	533795	3508569	1,458	559	898	V&K	
J.M. Huber Corp., Tom Potter #1	JMHCTP1	NA	514111	3505748	1,202	566	636	V&K	
American Quasar Pet. Co., V.C. Rounsaville #1	AQPVCR1	NA	563477	3498883	1,178	1,380	-202	V&K	
Chesapeake Operating, Inc., Melissa Taylor State 105-3	COMT105	4210932297	541293	3493028	1,437	697	740	RRC	
Gulf Oil Corp., M.A. Grisham #1	GOCMAG1	NA	535928	3484129	1,729	341	1,388	V&K	

Table A-3.15: Oil-and-gas exploratory wells used as control for the top of the Bone Spring Limestone/Formation. See key at bottom of Table A-3.3.

Well Name, Lease	Well ID	API Number	Easting	Northing	Well Elevation (m)	Depth to Top of Bone Spring Lm./Fm. (m)	Elevation of Top of Bone Spring Lm./Fm. (m)	Source	Note
Chesapeake Operating, Inc., State Street State #701	COSS701	4210932271	546492	3478738	1,422	649	773	RRC	
Sinclair, Looney	SINCLOO	NA	551319	3475371	1,310	905	405	V&K	

Table A-3.15 continued.

Well Name, Lease	Well ID	API Number	Easting	Northing	Well Elevation (m)	Depth to Top of San Andres Formation (m)	Elevation of Top of San Andres Formation (m)	Source	Note
Houston Oil & Minerals Corp., State L.G. "1453" #1	HO&MSL1	3003520013	406876	3685414	1,511	402	1,108	NMBG DL	
Houston Oil & Minerals Corp., J.M. Lewelling #1	HO&MJL1	3003520010	402778	3684425	1,440	250	1,190	OCD	
Houston Oil & Minerals Corp., Lewelling #2	HO&MCL2	3003520015	399960	3684444	1,373	2,042	-669	OCD	
McClellan Oil Corp., Flying "H" Ranch Unit Tract 3 #1	MCOCFH1	3000562244	497349	3652108	1,554	0	1,554	OCD	
McClellan Oil Corp., Gragg B #1	MCOCGB1	3000561993	495371	3649683	1,529	0	1,529	OCD	
Lubbook Machine & Supply Co., Inc., Anderson-Randell #1	LM&SAR1	3000500003	472069	3645946	1,767	0	1,767	OCD	
Humble Oil & Refining Co., Humble-Yates N.M. State #1	HO&RHY1	3000510521	488336	3643533	1,571	0	1,571	OCD	
W.H. Black Drilling Co., Shildneck #1	WHBDCS1	3000500012	514561	3641046	1,330	0	1,330	NMBG SC	
C & K Petroleum, Inc., Singer Lake State #1	C&KSLS1	3000560320	495659	3637945	1,541	0	1,541	OCD	
Southern Production Co., Cloudcroft Unit #1	SPCCLU1	3003500002	431152	3635650	2,859	0	2,859	NMBG SC	
Yates Petroleum Corporation, Dunken Nose Unit #1	YPCDNU1	3000560383	491492	3635055	1,602	0	1,602	OCD	
Yates Petroleum Corporation, Dunken Dome Unit #2	YPCDDU2	3000560397	485994	3634588	1,631	0	1,631	OCD	
Yates Petroleum Corporation, Dunken Dome Unit #1	YPCDDU1	3000560374	486211	3634277	1,643	0	1,643	OCD	
Sun Exploration & Production Co., J.T. Jennings #1	SE&PJT1	3000561103	489093	3633855	1,579	0	1,579	OCD	
C & K Petroleum, Inc., Little Cuevo State #1	C&KLCS1	3000560324	501605	3632606	1,464	0	1,464	OCD	
Magnolia, Headley Federal #2	MAGHEF2	NA	512347	3631229	1,510	0	1,510	NMBG SC	
Yates Petroleum Corporation, Little Cuevo Unit #1	YPCLCU1	3000561785	488273	3631027	1,633	0	1,633	NMBG SC	
Sunray DX Oil Company, N.M. State "AV" #1	SOCSAV1	3000510144	491916	3630614	1,582	0	1,582	OCD	
Westcoast Hydrocarbons, Inc., Black Hills Unit #1	WHIBHU1	3000500013	508897	3629768	1,453	0	1,453	NMBG SC	
Yates Petroleum Corporation, Little Cuevo Unit #2	YPCLCU2	3000562268	489571	3628557	1,618	0	1,618	OCD	
Magnolia, Black Hills	MAGBLHI	NA	505927	3627975	1,494	0	1,494	NMBG SC	

Table A-3.16: Oil-and-gas exploratory wells used as control for the top of the San Andres Formation. See key at bottom of Table A-3.3.

Well Name, Lease	Well ID	API Number	Easting	Northing	Well Elevation (m)	Depth to Top of San Andres Formation (m)	Elevation of Top of San Andres Formation (m)	Source	Note
TEXACO Inc., Federal (USA) "E" #1	TEXIFE1	3003520001	395308	3624999	1,219	58	1,161	K&H	
Yates Petroleum Corporation, One Tree Unit #1	YPCOTU1	3000562259	467160	3623529	1,872	0	1,872	NMBG SC	
Yates Petroleum Corporation, Dog Canyon "YF" Federal #1	YPCDCF1	3003520024	462754	3622676	1,942	0	1,942	NMBG SC	
Texas Oil & Gas Corp., Federal "C" #1	TO&GFC1	3000560017	512954	3622309	1,359	0	1,359	NMBG SC	
Kewanee Oil Co., F-M Unit #1	KOCFMU1	3000500009	493140	3619927	1,579	0	1,579	NMBG SC	
TEXACO Inc., Federal (USA) "F" #1	TEXIFF1	3003520006	410790	3619951	1,232	744	488	K&H	
Yates Petroleum Corporation, One Tree Unit #2	YPCOTU2	3000562276	468582	3619170	2,007	0	2,007	NMBG SC	
Marathon Oil Co., Mesa Verde Ranch #1	MOCMVR1	3003520022	455326	3618246	2,134	0	2,134	NMBG SC	
Yates Petroleum Corp., Buckhorn AYU State Com #1	YPCBAYU	3000560541	506142	3613140	1,440	0	1,440	NMBG SC	
Texas Oil & Gas Corp., Federal "A" #1	TO&GFA1	3000510431	506950	3613041	1,439	0	1,439	NMBG SC	
Sun Oil Co., Pinon Unit #2	SOCPIU2	3000500007	478157	3612259	1,925	0	1,925	NMBG SC	
Sun Oil Co., Pinon Unit #1	SOCPIU1	3000500006	476922	3611828	1,994	0	1,994	NMBG SC	
U.V. Industries, Inc., Long Canyon Unit #1	UVILCU1	3000560411	502547	3610225	1,533	0	1,533	NMBG SC	
Gulf Oil Corp., Federal Munson #1	GOCFMU1	3000510075	489407	3609839	1,723	0	1,723	NMBG SC	
Atlantic Refining Co., State "AV" #1	ARCSAV1	3003510001	461443	3603143	1,917	0	1,917	NMBG SC	
Zapata Petroleum Corp., Federal 14 #1	ZPCF141	3003500006	454127	3603086	2,105	0	2,105	NMBG SC	
Terra Resources, Inc., Burro Canyon Unit #1-Y	TRBCU1Y	3003520017	511686	3596471	1,568	0	1,568	OCD	
Stanolind Oil & Gas, Thorn Unit #1	SO&GTU1	3003500007	453419	3593869	1,914	0	1,914	NMBG SC	
Lefors Petroleum Co., Federal #1	LEPCFE1	3003500008	471863	3592611	1,639	0	1,639	OCD	
Yates Petroleum Corporation, Brainerd "IO" Federal #1	YPCBIOF	3001522149	523000	3587630	1,402	0	1,402	OCD	
Tri-Service Drilling Co., Little Dog Federal #1	TSDLDF1	3003520008	496060	3586992	1,940	0	1,940	NMBG SC	

Table A-3.16 continued.

763

Well Name, Lease	Well ID	API Number	Easting	Northing	Well Elevation (m)	Depth to Top of San Andres Formation (m)	Elevation of Top of San Andres Formation (m)	Source	Note
Brainerd Corp. (aka Continental Oil Co.), Federal "A" (aka East Texas Hill Unit) #1	BRCFEA1	3001500005	523406	3586429	1,390	0	1,390	NMBG SC	
Continental Oil Co., H.W. Bass #1	COCHWB1	3001500004	516898	3586367	1,680	0	1,680	NMBG SC	
Pitts Energy Co., Federal "9" #1	PIECF91	3001527563	518567	3585218	1,615	0	1,615	OCD	
E.P. Campbell, Hurley #1	EPCAHU1	3003500012	447355	3580223	1,404	0	1,404	K&H	
E.P. Campbell, Liberman State #1	EPCALI1	3003500014	457361	3576570	1,326	0	1,326	K&H	
W.R. Weaver, Thompson #1	WRWETH1	3003500017	499785	3575900	1,386	0	1,386	NMBG SC	
E.P. Campbell, Lois Spanel #1	EPCALS1	3003500015	467947	3575324	1,408	0	1,408	K&H	
Presco, Inc., Indian Creek Federal #1	PRIICF1	3003520030	511700	3573937	1,767	0	1,767	OCD	
E.P. Campbell, McMillan Federal #1	EPCAMF1	3003500018	500598	3573842	1,319	0	1,319	K&H	
Coral Oil & Gas Co., Warren #1	CO&GCW1	3003500016	487264	3571960	1,186	0	1,186	K&H	
Atlantic Refining Co., Huapache Unit #9	ARCHUU9	3001500016	527053	3566737	1,686	158	1,528	OCD	
Skelly Oil Co., Las Cruces "D" #1	SOCLCD1	3001500003	522240	3565867	1,749	111	1,637	NMBG SC	
Union Oil Co., Federal White #1	UNOCFW1	3001500019	525449	3565154	1,740	0	1,740	BH	
Threshold Development Co., Chiricahua R 21 Federal #1	TDCR21F	3003520034	489264	3563381	1,133	0	1,133	OCD	
Fred Turner, Jr. (aka Pasotero Pet. Corp.), Evans #1	FTUJEV1	3003500020	433355	3563003	1,545	0	1,545	BH	
E.P. Campbell (aka John J. Eisner), Federal #1	EPCAFE1	3003500019	432641	3562887	1,496	0	1,496	NMBG SC	
Franklin, Aston & Fair, Inc., Turkey Draw Unit #1	FA&FTD1	3001521378	524583	3560015	1,776	640	1,136	OCD	
W.W. West, West Dog Canyon Unit #1	WWWWDC1	3003520007	505979	3555044	1,771	44	1,726	OCD	
Threshold Development Co., Mescalero 28 Federal #1	TDM28F1	3003520033	489514	3552255	1,219	0	1,219	OCD	
Pennzoil Co., Southland "28" State #1	PCS28S1	3003520019	479573	3551070	1,206	0	1,206	K&H	
Fred Turner, Jr., State #1	FTUJST1	3003500027	475070	3550274	1,315	0	1,315	K&H	

Table A-3.16 continued.

764

Well Name, Lease	Well ID	API Number	Easting	Northing	Well Elevation (m)	Depth to Top of San Andres Formation (m)	Elevation of Top of San Andres Formation (m)	Source	Note
E.J. Dunigan, Alpha Federal #1	EJDALF1	3003520002	496594	3549815	1,159	18	1,141	K&H	
Hunt Oil Co., McMillan-Turner #1	HUOCMT1	3003500029	469015	3547882	1,269	0	1,269	BH	
E.P. Campbell, Spiegel-Federal #1	EPCSPF1	3003510002	511803	3544568	1,868	40	1,828	K&H	
Pan American Petroleum Corporation, List Anderson #1	PAPCLA1	NA	491521	3533849	1,108	176	931	V&K	
A.R. Jones Co., E.C. Mowry #1	ARJECM1	NA	474192	3516927	1,230	0	1,230	BEG SC	

Table A-3.16 continued.

Well Name, Lease	Well ID	API Number	Easting	Northing	Well Elevation (m)	Depth to Top of Delaware Mountain Group (m)	Elevation of Top of Delaware Mountain Group (m)	Source	Note
Hunt Petroleum Corp., C.L. Ranch #1	HPCCLR1	4222930010	496475	3528252	1,105	269	836	K&H	
TEXACO Inc., Culberson "L" Fee #1	TEXCLF1	NA	519234	3527336	1,564	0	1,564	K&H	
Tenneco Oil Co., TXL Fee #1	TOTXLF1	4210931401	563041	3526975	1,086	353	733	RRC	
Border Exploration Co., Hammack et al. CT-1	BECHCT1	4222930196	505172	3518026	1,107	587	521	K&H	
Border Exploration Co., J.J. McAdoo 7 #1	BECJJM1	4222930200	505794	3514682	1,143	407	736	K&H	
The Superior Oil Company, Covington State #1	TSOCCS1	4210931405	565213	3512927	1,140	644	496	RRC	
Chesapeake Operating, Inc., Dela Minerals "3" State #701	COIDM3S	4210932268	566918	3512065	1,142	700	442	RRC	
EnCana Oil & Gas (USA) Inc., Sibley Ranch 47 State "25" #1	EOGSR47	4210932251	544180	3505778	1,332	202	1,131	RRC	

Table A-3.17: Oil-and-gas exploratory wells used as control for the top of the Delaware Mountain Group. See key at bottom of Table A-3.3.

Well Name, Lease	Well ID	API Number	Easting	Northing	Well Elevation (m)	Depth to Top of Goat Seep Dolomite/Lm./Fm. (m)	Elevation of Top of Goat Seep Dolomite/Lm./Fm. (m)	Source	Note
Hunt Petroleum Corp., C.L. Ranch #1	HPCCLR1	4222930010	496475	3528252	1,105	230	875	K&H	
Border Exploration Co., Hammack et al. CT-1	BECHCT1	4222930196	505172	3518026	1,107	571	536	K&H	

Table A-3.18: Oil-and-gas exploratory wells used as control for the top of the Goat Seep Dolomite/Limestone/Formation. See key at bottom of Table A-3.3.

Well Name, Lease	Well ID	API Number	Easting	Northing	Well Elevation (m)	Depth to Top of Capitan Lm./Fm. (m)	Elevation of Top of Capitan Lm./Fm. (m)	Source	Note
Border Exploration Co., Hammack et al. CT-1	BECHCT1	4222930196	505172	3518026	1,107	0	1,107	K&H	
Border Exploration Co., J.J. McAdoo 7 #1	BECJJM1	4222930200	505794	3514682	1,143	0	1,143	K&H	

Table A-3.19: Oil-and-gas exploratory wells used as control for the top of the Capitan Limestone/Formation. See key at bottom of Table A-3.3.

Well Name, Lease	Well ID	API Number	Easting	Northing	Well Elevation (m)	Depth to Top of Cenozoic Alluvium (m)	Elevation of Top of Cenozoic Alluvium (m)	Source	Note
Houston Oil & Minerals Corp., Lewelling #2	HO&MCL2	3003520015	399960	3684444	1,373	0	1,373	OCD	
TEXACO Inc., Federal (USA) "E" #1	TEXIFE1	3003520001	395308	3624999	1,219	0	1,219	K&H	
TEXACO Inc., Federal (USA) "F" #1	TEXIFF1	3003520006	410790	3619951	1,232	0	1,232	K&H	
Plymouth Oil Co., Evans (aka Federal D) #1	PLOCEV1	3003500003	404731	3604561	1,233	0	1,233	BH	
Otero Oil Co., McGregor #1	OTOCMC1	3003500010	412151	3586894	1,289	0	1,289	BH	
W.W. West, West Dog Canyon Unit #1	WWWWDC1	3003520007	505979	3555044	1,771	0	1,771	OCD	
E.J. Dunigan, Alpha Federal #1	EJDALF1	3003520002	496594	3549815	1,156	0	1,156	K&H	
GDP 61-6	GDP61-6	NA	390213	3549130	1,254	0	1,254	F&J	
GDP 45-5	GDP45-5	NA	391837	3549102	1,255	0	1,255	F&J	
GDP 46-6	GDP46-6	NA	390223	3549119	1,252	0	1,252	F&J	
GDP 51-8	GDP51-8	NA	393417	3545870	1,253	0	1,253	F&J	
E.P. Campbell, Spiegel-Federal #1	EPCSPF1	3003510002	511803	3544568	1,868	0	1,868	K&H	
Hunt Petroleum Corp., C.L. Ranch "5" #1	HPCCL51	4222930011	496478	3539912	1,110	0	1,110	K&H	
Hunt Oil Co., Dyer #1	HUOCDY1	4222930007	485477	3530917	1,119	0	1,119	K&H	
Hunt Petroleum Corp., C.L. Ranch #1	HPCCLR1	4222930010	496475	3528252	1,105	0	1,105	K&H	

Table A-3.20: Oil-and-gas exploratory wells used as control for the top of the Cenozoic alluvium. See key at bottom of Table A-3.3.

Well ID	Distance Along Cross Section (m)	Well Elevation (m)	Well Depth (m)
SPCCLU1	0	2,859	1,433
YPCDCF1	27,841	1,946	2,569
YPCOTU1	32,348	1,876	1,992
YPCOTU2	36,933	2,010	908
SOCPIU2	48,742	1,925	506
LEPCFE1	71,399	1,642	686
CO&GCW1	97,263	1,186	717
TDCR21F	106,121	1,133	1,834
EJDALF1	121,541	1,159	1,523
HPCCL51	131,444	1,110	1,678
HPCCLR1	143,104	1,105	1,595

Table A-3.21: Subsurface oil-and-gas exploratory wells along cross-section A - A'.

Well ID	Distance Along Cross Section (m)	Well Elevation (m)	Well Depth (m)
SPCCLU1	0	2,859	1,433
MOCMVR1	35,636	2,143	2,137
ARCSAV1	51,931	1,921	1,227
EPCALS1	81,521	1,408	817
PCS28S1	108,977	1,206	905
HPCCL51	129,671	1,110	1,678

Table A-3.22: Subsurface oil-and-gas exploratory wells along cross-section B - B'.

Well ID	Distance Along Cross Section (m)	Well Elevation (m)	Well Depth (m)
PLOCEV1	0	1,233	2,312
SOCTJP1	13,477	1,344	1,362
ZPCF141	51,139	2,109	1,537
ARCSAV1	58,455	1,921	1,227
LEPCFE1	73,270	1,642	686
SOTSCU1	88,865	1,628	812
TSDLDF1	99,604	1,940	1,259
TRBCU1Y	117,881	1,572	1,704
TO&GFB1	125,294	1,463	2,480

Table A-3.23: Subsurface oil-and-gas exploratory wells along cross-section C - C'.

Well ID	Distance Along Cross Section (m)	Well Elevation (m)	Well Depth (m)
OTOCMC1	0	1,295	527
FTUEVE1	31,946	1,476	1,202
EPCAHU1	36,287	1,404	742
EPCALI1	46,939	1,326	823
EPCALS1	57,597	1,408	817
CO&GCW1	77,205	1,186	717
EPCAMF1	90,671	1,319	972
PRIICF1	101,774	1,767	1,454
SO&GFE1	111,262	1,582	1,524
BRCFEA1	118,893	1,397	3,230

Table A-3.24: Subsurface oil-and-gas exploratory wells along cross-section D - D'.

Well ID	Distance Along Cross Section (m)	Well Elevation (m)	Well Depth (m)
GDP 45-5	0	1,255	1,207
SEOCTF1	27,166	1,618	1,707
HEYBRU1	43,911	1,554	2,156
TROGJA1	55,479	1,509	1,617
HUOCMT1	83,689	1,269	663
FTUJST1	90,199	1,317	1,583
PCS28S1	94,772	1,206	905
TDM28F1	104,784	1,219	1,409
EJDALF1	112,272	1,159	1,523
WWWWDC1	123,016	1,771	1,390
UNOCFW1	144,954	1,740	2,053
HO&RHO2	154,127	1,358	3,835

Table A-3.25: Subsurface oil-and-gas exploratory wells along cross-section E - E'.

POD Number/ Well ID/ State Well Number	Easting	Northing	Ground Surface Elevation (m)	Elevation of Well Depth (m)	Groundwater Elevation (m)	Aquifer	County	Depth-to-Groundwater Control Point	Groundwater Surface Control Point	Source	Note
PN 00007	460240	3638479	2,000	1,787	1,791	NA	Otero	Y	Y	NMOSE	*
SM-0098	476159	3637546	1,719	1,613	1,628	NA	Chaves	Y	N	SMHS	*
PN 00058	482719	3637520	1,645	1,534	1,543	NA	Eddy	Y	N	NMOSE	*
PN 01036 POD1	442482	3636947	2,291	2,154	2,200	NA	Otero	Y	Y	NMOSE	*
PN 00737	445116	3636923	2,346	2,316	NA	NA	Otero	Y	N	NMOSE	*
PN 00049	453268	3636885	2,036	2,001	2,008	NA	Otero	Y	Y	NMOSE	*
PN 00842	439450	3636685	2,501	2,410	NA	NA	Otero	N	N	NMOSE	*
RA 03777	497585	3636663	1,536	1,297	1,310	NA	Chaves	Y	Y	NMOSE	*
PN 00079	462708	3636475	1,923	1,783	1,808	NA	Otero	Y	Y	NMOSE	*
PN 00822	439437	3636284	2,371	2,187	2,206	NA	Otero	N	N	NMOSE	*
SM-0144	470081	3636255	2,042	1,740	1,788	NA	Chaves	Y	Y	SMHS	*
PN 00630	452766	3636193	2,058	2,053	2,053	NA	Otero	Y	N	NMOSE	*
PN 00044	452865	3636092	2,056	2,006	2,019	NA	Otero	Y	Y	NMOSE	*
SM-0135	472964	3636058	1,839	1,625	1,656	NA	Chaves	Y	Y	SMHS	*
PN 01003	443816	3636026	2,249	2,172	2,197	NA	Otero	Y	Y	NMOSE	*
PN 01090 POD1	452699	3636003	2,074	2,019	2,039	NA	Otero	Y	Y	NMOSE	*
RA 11168 POD1	508183	3635914	1,432	1,173	1,237	NA	Chaves	Y	Y	NMOSE	*
PN 00667 POD2	452861	3635895	2,056	2,020	2,041	NA	Otero	Y	N	NMOSE	*
PN 00602	446786	3635832	2,218	2,197	2,203	NA	Otero	Y	N	NMOSE	*
PN 00635	452762	3635796	2,058	2,040	2,052	NA	Otero	Y	N	NMOSE	*
PN 00722	446292	3635739	2,145	2,111	2,127	NA	Otero	Y	Y	NMOSE	*
PN 00865	446092	3635739	2,169	2,079	2,139	NA	Otero	Y	Y	NMOSE	*
PN 00670	452661	3635695	2,061	1,963	2,018	NA	Otero	Y	Y	NMOSE	*
PN 00667	452958	3635600	2,098	2,082	2,090	NA	Otero	Y	N	NMOSE	*
PN 00217	425332	3635555	2,793	2,688	2,717	NA	Otero	Y	Y	NMOSE	*
PN 00661	456937	3635554	2,071	1,888	1,934	NA	Otero	Y	Y	NMOSE	*
PN 00031 A	445304	3635500	2,180	2,113	2,125	NA	Otero	Y	N	NMOSE	*
PN 00219 POD2	425635	3635450	2,774	2,655	2,688	NA	Otero	N	Y	NMOSE	*

Table A-3.26: Groundwater surface and depth-to-groundwater control wells. Key at bottom of table.

POD Number/ Well ID/ State Well Number	Easting	Northing	Ground Surface Elevation (m)	Elevation of Well Depth (m)	Groundwater Elevation (m)	Aquifer	County	Depth-to-Groundwater Control Point	Groundwater Surface Control Point	Source	Note
PN 00080	486788	3635392	1,561	1,449	1,468	NA	Chaves	Y	N	NMOSE	*
RA 03836	513345	3635360	1,364	1,083	1,102	NA	Chaves	Y	Y	NMOSE	*
PN 00201	446482	3635350	2,153	2,120	2,129	NA	Otero	Y	Y	NMOSE	*
PN 00077	447796	3635323	2,108	2,073	2,103	NA	Otero	Y	Y	NMOSE	*
PN 00039	448555	3635276	2,103	2,071	2,097	NA	Otero	Y	Y	NMOSE	*
SM-0133	475444	3635270	1,785	1,480	1,511	NA	Chaves	Y	Y	SMHS	*
PN 00217 POD2	426036	3635242	2,761	2,627	2,674	NA	Otero	N	Y	NMOSE	*
PN 00806	457244	3635239	2,038	1,858	1,917	NA	Otero	Y	Y	NMOSE	*
PN 00031	444293	3635234	2,227	2,150	2,208	NA	Otero	Y	N	NMOSE	*
PN 00754	457654	3635225	2,032	1,849	NA	NA	Otero	Y	Y	NMOSE	*
PN 00585	443691	3635217	2,192	2,182	2,188	NA	Otero	Y	Y	NMOSE	*
PN 00124 POD2	450135	3635156	2,079	2,049	2,077	NA	Otero	Y	Y	NMOSE	*
PN 00956	451657	3635122	2,202	2,117	2,166	NA	Otero	Y	N	NMOSE	*
PN 00089	450641	3635119	2,106	2,068	2,104	NA	Otero	Y	N	NMOSE	*
PN 00307	440858	3635117	2,270	2,215	2,255	NA	Otero	Y	Y	NMOSE	*
PN 00983	450221	3635109	2,076	2,040	2,064	NA	Otero	Y	Y	NMOSE	*
PN 00124	450012	3635101	2,078	2,059	2,074	NA	Otero	Y	Y	NMOSE	*
PN 00019	449812	3635101	2,082	2,050	2,072	NA	Otero	Y	N	NMOSE	*
PN 00175	449604	3635092	2,086	2,058	2,080	NA	Otero	Y	Y	NMOSE	*
PN 00860	448972	3635070	2,123	2,075	2,090	NA	Otero	Y	Y	NMOSE	*
PN 00912	441365	3635033	2,278	2,231	2,248	NA	Otero	Y	Y	NMOSE	*
PN 00050	451558	3635023	2,144	2,082	2,093	NA	Otero	Y	N	NMOSE	*
PN 00781	440959	3635018	2,239	2,162	2,192	NA	Otero	Y	N	NMOSE	*
PN 00043	452751	3634995	2,079	2,039	2,047	NA	Otero	Y	Y	NMOSE	*
PN 00266	439730	3634978	2,305	2,258	2,272	NA	Otero	Y	Y	NMOSE	*
PN 00756	451262	3634929	2,087	2,062	2,076	NA	Otero	Y	N	NMOSE	*
PN 00778	441058	3634917	2,241	2,160	2,194	NA	Otero	Y	N	NMOSE	*
PN 00413	439421	3634864	2,282	2,224	2,270	NA	Otero	Y	Y	NMOSE	*

Table A-3.26 continued.

POD Number/ Well ID/ State Well Number	Easting	Northing	Ground Surface Elevation (m)	Elevation of Well Depth (m)	Groundwater Elevation (m)	Aquifer	County	Depth-to-Groundwater Control Point	Groundwater Surface Control Point	Source	Note
PN 00639 POD2	439221	3634864	2,324	2,236	2,266	NA	Otero	Y	Y	NMOSE	*
PN 00639	439013	3634851	2,340	2,282	2,309	NA	Otero	Y	Y	NMOSE	*
SM-0134	473847	3634846	1,842	1,705	1,723	NA	Chaves	Y	N	SMHS	*
PN 00703	451363	3634832	2,061	1,981	2,033	NA	Otero	Y	Y	NMOSE	*
SM-0151	465000	3634677	2,026	1,808	1,815	NA	Otero	Y	Y	SMHS	*
PN 00256	442578	3634664	2,205	2,095	2,114	NA	Otero	Y	N	NMOSE	*
PN 00412	468408	3634588	1,945	1,805	1,823	NA	Otero	Y	N	NMOSE	*
RA 05467	490603	3634559	1,538	1,363	1,363	NA	Chaves	Y	Y	NMOSE	*
PN 00796	438911	3634546	2,355	2,240	2,276	NA	Otero	N	Y	NMOSE	*
PN 00360	438508	3634534	2,300	2,178	NA	NA	Otero	N	N	NMOSE	*
PN 00675 POD2	438028	3634534	2,356	2,247	2,300	NA	Otero	Y	Y	NMOSE	*
PN 00675	428756	3634521	2,857	2,791	2,808	NA	Otero	Y	N	NMOSE	*
PN 00510	455964	3634444	2,077	1,880	1,921	NA	Otero	N	Y	NMOSE	*
PN 00352	437133	3634435	2,442	2,330	2,369	NA	Otero	Y	Y	NMOSE	*
PN 00407	438425	3634427	2,320	2,202	2,231	NA	Otero	N	N	NMOSE	*
PN 00695	442225	3634406	2,302	2,223	2,238	NA	Otero	Y	Y	NMOSE	*
PN 00198	442161	3634253	2,308	2,177	NA	NA	Otero	Y	Y	NMOSE	*
PN 01073 POD1	458646	3634238	2,028	1,852	1,892	NA	Otero	Y	N	NMOSE	*
PN 00795	456185	3634233	2,090	1,907	NA	NA	Otero	Y	Y	NMOSE	*
PN 00895	458651	3634205	2,025	1,857	1,882	NA	Otero	Y	Y	NMOSE	*
RA 03407	510105	3634187	1,402	1,147	1,161	NA	Eddy	Y	Y	NMOSE	*
PN 00510 POD2	441013	3634150	2,395	2,193	2,242	NA	Otero	N	Y	NMOSE	*
T 01737	422914	3633828	2,304	2,230	2,265	NA	Otero	Y	Y	NMOSE	*
PN 00392	434027	3633750	2,426	2,382	2,410	NA	Otero	Y	Y	NMOSE	*
PN 00381	433827	3633750	2,400	2,354	2,391	NA	Otero	Y	Y	NMOSE	*
PN 00881	462920	3633625	2,039	1,807	1,828	NA	Otero	Y	Y	NMOSE	*
PN 00631	457024	3633611	2,067	1,864	1,899	NA	Otero	N	Y	NMOSE	*
PN 01037 POD1	458019	3633590	2,029	1,846	1,889	NA	Otero	Y	Y	NMOSE	*

Table A-3.26 continued.

POD Number/ Well ID/ State Well Number	Easting	Northing	Ground Surface Elevation (m)	Elevation of Well Depth (m)	Groundwater Elevation (m)	Aquifer	County	Depth-to-Groundwater Control Point	Groundwater Surface Control Point	Source	Note
PN 00265	457552	3633285	2,037	1,853	1,885	NA	Otero	Y	N	NMOSE	*
PN 01066 POD1	457632	3633191	2,043	1,860	1,902	NA	Otero	Y	Y	NMOSE	*
PN 00844	457451	3633184	2,056	1,843	1,912	NA	Otero	Y	Y	NMOSE	*
PN 00220 POD2	455975	3633018	2,124	1,936	1,962	NA	Otero	N	Y	NMOSE	*
PN 00343 POD2	457020	3632990	2,061	1,854	1,878	NA	Otero	N	N	NMOSE	*
PN 00343	456694	3632900	2,078	1,891	1,904	NA	Otero	N	Y	NMOSE	*
PN 00245	457121	3632891	2,077	1,874	1,908	NA	Otero	N	Y	NMOSE	*
PN 00345	456384	3632808	2,105	2,075	NA	NA	Otero	Y	N	NMOSE	*
PN 00882	458234	3632785	2,006	1,829	1,884	NA	Otero	Y	Y	NMOSE	*
PN 00126	448392	3632652	2,356	2,092	2,113	NA	Otero	N	Y	NMOSE	*
PN 00282	430011	3632612	2,497	2,445	2,476	NA	Otero	Y	Y	NMOSE	*
PN 00499	449708	3632571	2,242	2,106	2,127	NA	Otero	Y	Y	NMOSE	*
PN 00009	450106	3632566	2,285	2,155	2,163	NA	Otero	Y	N	NMOSE	*
SM-0150	467259	3632518	1,977	1,785	1,807	NA	Chaves	Y	Y	SMHS	*
PN 01032 POD1	459566	3632490	2,038	1,777	1,911	NA	Otero	Y	N	NMOSE	*
RA 06874 POD2	512800	3632324	1,329	1,098	1,143	NA	Chaves	Y	Y	NMOSE	*
PN 00666	458018	3632173	2,017	1,829	1,901	NA	Otero	Y	Y	NMOSE	*
PN 00546	457650	3632172	2,029	1,864	1,878	NA	Otero	Y	N	NMOSE	*
PN 00768	449107	3632170	2,252	2,069	2,206	NA	Otero	Y	N	NMOSE	*
RA 03675	506224	3632085	1,369	1,125	1,227	NA	Chaves	Y	Y	NMOSE	*
PN 00489	462307	3631988	2,013	1,774	1,800	NA	Otero	Y	Y	NMOSE	*
PN 00123	448907	3631970	2,266	2,220	NA	NA	Otero	Y	N	NMOSE	*
PN 01006 POD1	448290	3631954	2,280	2,140	2,173	NA	Otero	Y	Y	NMOSE	*
PN 00036	476427	3631844	1,740	1,494	1,512	NA	Chaves	Y	Y	NMOSE	*
PN 00676 POD2	448622	3631773	2,276	2,017	NA	NA	Otero	Y	Y	NMOSE	*
PN 01041 POD1	448528	3631684	2,287	2,086	2,125	NA	Otero	N	Y	NMOSE	*
PN 00676	448602	3631656	2,270	1,995	2,053	NA	Otero	N	N	NMOSE	*
PN 00261	448186	3631243	2,304	2,199	2,211	NA	Otero	Y	N	NMOSE	*

Table A-3.26 continued.

773

POD Number/ Well ID/ State Well Number	Easting	Northing	Ground Surface Elevation (m)	Elevation of Well Depth (m)	Groundwater Elevation (m)	Aquifer	County	Depth-to-Groundwater Control Point	Groundwater Surface Control Point	Source	Note
PN 01025 POD1	457816	3631165	2,025	1,879	1,927	NA	Otero	Y	Y	NMOSE	*
PN 00310	464326	3631160	1,995	1,752	1,858	NA	Otero	Y	Y	NMOSE	*
PN 00609	450011	3631044	2,241	2,160	2,168	NA	Otero	Y	N	NMOSE	*
PN 00311	466125	3630937	1,991	1,703	1,808	NA	Otero	Y	Y	NMOSE	*
PN 01031 POD1	453015	3630869	2,145	2,030	2,054	NA	Otero	Y	Y	NMOSE	*
PN 00032 POD1	481051	3630828	1,668	1,394	NA	NA	Chaves	Y	Y	NMOSE	*
PN 00032	481152	3630729	1,662	1,388	1,403	NA	Chaves	Y	Y	NMOSE	*
PN 00112	441444	3630676	2,377	2,286	NA	NA	Otero	Y	Y	NMOSE	*
PN 00608	444188	3630649	2,422	2,248	2,312	NA	Otero	Y	N	NMOSE	*
PN 00829	449712	3630539	2,231	2,174	2,207	NA	Otero	Y	N	NMOSE	*
PN 00047	452294	3630371	2,165	2,040	2,074	NA	Otero	Y	Y	NMOSE	*
PN 00879	449507	3630340	2,213	2,200	2,209	NA	Otero	Y	N	NMOSE	*
PN 00730	449307	3630340	2,216	2,179	2,188	NA	Otero	Y	N	NMOSE	*
PN 00122	450316	3630337	2,183	2,106	NA	NA	Otero	Y	Y	NMOSE	*
PN 00216	450721	3630335	2,204	2,154	2,174	NA	Otero	Y	N	NMOSE	*
PN 00127	451698	3630149	2,173	2,089	2,122	NA	Otero	Y	Y	NMOSE	*
PN 00804	450722	3630119	2,156	2,102	2,120	NA	Otero	Y	Y	NMOSE	*
PN 00361	450926	3630115	2,158	2,091	2,108	NA	Otero	Y	Y	NMOSE	*
PN 00200	452202	3630056	2,144	2,042	2,063	NA	Otero	Y	Y	NMOSE	*
PN 00329	449410	3630031	2,182	2,044	2,057	NA	Otero	Y	N	NMOSE	*
PN 00297	452924	3629955	2,163	2,041	2,056	NA	Otero	Y	Y	NMOSE	*
PN 00298	451898	3629949	2,143	2,036	2,067	NA	Otero	Y	Y	NMOSE	*
PN 00171	451512	3629932	2,179	2,121	2,139	NA	Otero	Y	N	NMOSE	*
PN 00507	450423	3629810	2,183	2,077	2,169	NA	Otero	Y	N	NMOSE	*
PN 00763	442570	3629791	2,356	2,235	2,311	NA	Otero	Y	Y	NMOSE	*
PN 00817	437004	3629732	2,638	2,620	2,631	NA	Otero	Y	N	NMOSE	*
PN 00443	451319	3629711	2,144	2,018	2,109	NA	Otero	Y	Y	NMOSE	*
PN 00989	454590	3629707	2,095	1,962	1,983	NA	Otero	Y	Y	NMOSE	*

Table A-3.26 continued.

POD Number/ Well ID/ State Well Number	Easting	Northing	Ground Surface Elevation (m)	Elevation of Well Depth (m)	Groundwater Elevation (m)	Aquifer	County	Depth-to-Groundwater Control Point	Groundwater Surface Control Point	Source	Note
PN 00203	437505	3629632	2,536	2,493	2,501	NA	Otero	Y	Y	NMOSE	*
PN 00783	437404	3629531	2,539	2,484	2,510	NA	Otero	Y	Y	NMOSE	*
PN 00061	451711	3629525	2,148	2,071	2,087	NA	Otero	Y	Y	NMOSE	*
PN 00176	451319	3629511	2,171	2,044	2,110	NA	Otero	Y	Y	NMOSE	*
PN 01001	449106	3629511	2,179	2,141	2,158	NA	Otero	Y	Y	NMOSE	*
PN 00223	451632	3629411	2,155	2,036	2,046	NA	Otero	Y	N	NMOSE	*
PN 00731	450016	3629402	2,300	2,226	2,272	NA	Otero	Y	N	NMOSE	*
PN 00834	451923	3629312	2,208	2,132	NA	NA	Otero	Y	N	NMOSE	*
PN 00299	451325	3629307	2,177	2,085	NA	NA	Otero	Y	Y	NMOSE	*
PN 01019 POD1	449107	3629302	2,207	2,146	2,168	NA	Otero	Y	Y	NMOSE	*
PN 01002	448704	3629296	2,192	2,134	2,173	NA	Otero	Y	Y	NMOSE	*
PN 00911	455633	3629273	2,083	1,870	1,916	NA	Otero	N	N	NMOSE	*
PN 00682	477102	3629119	1,721	1,446	NA	NA	Chaves	Y	Y	NMOSE	*
PN 00005	447085	3629047	2,374	2,343	2,356	NA	Otero	Y	N	NMOSE	*
PN 00239	435673	3629038	2,632	2,615	2,621	NA	Otero	Y	Y	NMOSE	*
PN 00209	464199	3629035	2,020	1,775	1,829	NA	Otero	Y	Y	NMOSE	*
PN 00308	442967	3628994	2,302	2,213	2,231	NA	Otero	Y	Y	NMOSE	*
PN 00237	435787	3628929	2,618	2,603	2,613	NA	Otero	Y	Y	NMOSE	*
PN 00119	453798	3628887	2,122	1,919	2,043	NA	Otero	Y	Y	NMOSE	*
PN 00966	455641	3628866	2,078	1,932	1,988	NA	Otero	Y	Y	NMOSE	*
PN 00071	451029	3628808	2,207	2,133	2,141	NA	Otero	Y	N	NMOSE	*
PN 00962	445691	3628786	2,247	2,155	2,193	NA	Otero	Y	N	NMOSE	*
PN 00087	447801	3628775	2,207	2,181	2,205	NA	Otero	Y	N	NMOSE	*
PN 00225	447398	3628755	2,234	2,218	2,233	NA	Otero	Y	N	NMOSE	*
PN 00856	435787	3628729	2,689	2,627	2,652	NA	Otero	Y	N	NMOSE	*
PN 00046	449109	3628694	2,316	2,262	2,289	NA	Otero	Y	N	NMOSE	*
PN 00561	445394	3628678	2,238	2,207	2,233	NA	Otero	Y	Y	NMOSE	*
PN 00417	446288	3628596	2,225	2,199	2,219	NA	Otero	Y	Y	NMOSE	*

Table A-3.26 continued.

POD Number/ Well ID/ State Well Number	Easting	Northing	Ground Surface Elevation (m)	Elevation of Well Depth (m)	Groundwater Elevation (m)	Aquifer	County	Depth-to-Groundwater Control Point	Groundwater Surface Control Point	Source	Note
PN 00949	446088	3628596	2,232	2,189	2,207	NA	Otero	Y	Y	NMOSE	*
SM-0075	447829	3628594	2,207	2,153	2,180	NA	Otero	Y	Y	SMHS	*
PN 00872	445891	3628586	2,228	2,107	NA	NA	Otero	Y	Y	NMOSE	*
PN 00018	447500	3628450	2,219	2,182	NA	NA	Otero	Y	Y	NMOSE	*
PN 00857	447300	3628450	2,235	2,191	2,217	NA	Otero	Y	N	NMOSE	*
PN 00750	445692	3628385	2,271	2,240	2,245	NA	Otero	Y	Y	NMOSE	*
PN 00014	446998	3628333	2,243	2,193	2,229	NA	Otero	Y	N	NMOSE	*
PN 00835	438193	3628324	2,567	2,421	NA	NA	Otero	Y	Y	NMOSE	*
PN 00196 POD2	442050	3628215	2,374	2,237	2,298	NA	Otero	Y	Y	NMOSE	*
PN 00196	442155	3628153	2,361	2,286	2,292	NA	Otero	Y	Y	NMOSE	*
PN 00708	441748	3628136	2,368	2,321	2,334	NA	Otero	Y	Y	NMOSE	*
PN 00526	442254	3628052	2,324	2,263	2,294	NA	Otero	Y	Y	NMOSE	*
PN 00594	442054	3628052	2,362	2,288	2,295	NA	Otero	Y	Y	NMOSE	*
PN 00357	458020	3627889	2,109	1,915	1,938	NA	Otero	Y	Y	NMOSE	*
PN 00681	473462	3627768	1,762	1,738	NA	NA	Chaves	Y	N	NMOSE	*
PN 00129	456540	3627762	2,119	2,072	2,087	NA	Otero	Y	N	NMOSE	*
PN 00202	442148	3627748	2,309	2,270	2,274	NA	Otero	Y	Y	NMOSE	*
PN 00174	441744	3627731	2,326	2,294	2,311	NA	Otero	Y	Y	NMOSE	*
PN 00073	451331	3627670	2,164	2,062	2,085	NA	Otero	Y	Y	NMOSE	*
PN 00679	471776	3627604	1,790	1,699	NA	NA	Chaves	Y	Y	NMOSE	*
PN 00004	447404	3627541	2,313	2,183	2,191	NA	Otero	Y	Y	NMOSE	*
PN 00786	443258	3627488	2,380	2,360	2,371	NA	Otero	Y	N	NMOSE	*
PN 00775	444171	3627420	2,356	2,311	2,347	NA	Otero	Y	N	NMOSE	*
PN 00552	450369	3627370	2,240	2,054	2,075	NA	Otero	N	Y	NMOSE	*
PN 00016	451191	3627359	2,179	2,077	2,102	NA	Otero	Y	Y	NMOSE	*
PN 00587	441735	3627325	2,321	2,224	2,276	NA	Otero	Y	Y	NMOSE	*
PN 00296	450990	3627158	2,244	2,141	2,145	NA	Otero	Y	N	NMOSE	*
PN 00799	439811	3627141	2,432	2,396	2,418	NA	Otero	Y	Y	NMOSE	*

Table A-3.26 continued.

POD Number/ Well ID/ State Well Number	Easting	Northing	Ground Surface Elevation (m)	Elevation of Well Depth (m)	Groundwater Elevation (m)	Aquifer	County	Depth-to-Groundwater Control Point	Groundwater Surface Control Point	Source	Note
PN 00929	441727	3626918	2,330	2,282	2,312	NA	Otero	Y	Y	NMOSE	*
PN 00383	454601	3626841	2,075	1,984	1,990	NA	Otero	Y	Y	NMOSE	*
PN 00500	455220	3626840	2,066	1,988	2,063	NA	Otero	Y	N	NMOSE	*
PN 00715	451553	3626829	2,186	2,095	2,114	NA	Otero	Y	N	NMOSE	*
PN 00700	451138	3626824	2,189	2,022	2,060	NA	Otero	Y	Y	NMOSE	*
PN 00659	451039	3626725	2,173	2,082	2,108	NA	Otero	Y	N	NMOSE	*
PN 00253	454601	3626641	2,071	1,992	2,016	NA	Otero	Y	N	NMOSE	*
PN 00810	453553	3626641	2,092	2,011	2,029	NA	Otero	Y	Y	NMOSE	*
PN 00677	452954	3626641	2,100	2,012	2,038	NA	Otero	Y	Y	NMOSE	*
PN 00616	456041	3626639	2,044	1,971	1,992	NA	Otero	Y	Y	NMOSE	*
PN 00595	451351	3626632	2,152	2,081	2,097	NA	Otero	Y	N	NMOSE	*
PN 01016 POD1	451138	3626624	2,154	1,971	NA	NA	Otero	Y	Y	NMOSE	*
PN 01027 POD1	450938	3626624	2,163	1,995	2,056	NA	Otero	Y	Y	NMOSE	*
PN 00152	441442	3626588	2,378	2,348	2,354	NA	Otero	Y	Y	NMOSE	*
PN 00717	441242	3626588	2,404	2,313	NA	NA	Otero	Y	Y	NMOSE	*
PN 00808	441637	3626578	2,340	2,321	NA	NA	Otero	Y	Y	NMOSE	*
PN 00166	455330	3626534	2,059	1,962	1,980	NA	Otero	Y	Y	NMOSE	*
PN 00236	451289	3626498	2,156	1,961	2,065	NA	Otero	Y	Y	NMOSE	*
PN 00183	456045	3626424	2,062	1,894	2,034	NA	Otero	Y	N	NMOSE	*
PN 00182	441562	3626354	2,348	2,313	2,326	NA	Otero	Y	Y	NMOSE	*
PN 00847	453052	3626336	2,093	1,989	NA	NA	Otero	Y	Y	NMOSE	*
PN 00669	451477	3626306	2,173	1,998	2,062	NA	Otero	Y	Y	NMOSE	*
PN 00424	456551	3626125	2,034	1,912	2,009	NA	Otero	Y	N	NMOSE	*
PN 00426	453238	3626121	2,098	1,992	2,053	NA	Otero	Y	Y	NMOSE	*
PN 00338 POD2	452541	3626026	2,105	1,965	2,012	NA	Otero	Y	N	NMOSE	*
PN 00211	456449	3626025	2,039	1,942	1,959	NA	Otero	Y	Y	NMOSE	*
PN 00704	452352	3626017	2,111	1,958	2,059	NA	Otero	Y	Y	NMOSE	*
PN 00719	451963	3626009	2,122	2,070	2,085	NA	Otero	Y	N	NMOSE	*

Table A-3.26 continued.

POD Number/ Well ID/ State Well Number	Easting	Northing	Ground Surface Elevation (m)	Elevation of Well Depth (m)	Groundwater Elevation (m)	Aquifer	County	Depth-to-Groundwater Control Point	Groundwater Surface Control Point	Source	Note
PN 00702	451763	3626009	2,128	2,037	NA	NA	Otero	Y	Y	NMOSE	*
PN 00195	441972	3625956	2,504	2,469	2,483	NA	Otero	Y	N	NMOSE	*
PN 00660	452253	3625918	2,139	2,085	2,098	NA	Otero	Y	N	NMOSE	*
PN 00184	456653	3625828	2,037	1,903	NA	NA	Otero	Y	Y	NMOSE	*
PN 00841	452352	3625817	2,118	2,048	2,067	NA	Otero	Y	Y	NMOSE	*
PN 01015 POD1	452152	3625817	2,160	1,944	1,976	NA	Otero	N	N	NMOSE	*
PN 00393	451288	3625692	2,148	2,071	2,099	NA	Otero	Y	N	NMOSE	*
PN 00871	452147	3625610	2,148	2,017	2,061	NA	Otero	Y	Y	NMOSE	*
PN 00738	452248	3625511	2,119	2,030	2,056	NA	Otero	Y	Y	NMOSE	*
PN 00729	455646	3625420	2,107	1,964	2,010	NA	Otero	Y	Y	NMOSE	*
PN 00758	452347	3625410	2,110	1,999	2,057	NA	Otero	Y	Y	NMOSE	*
PN 00780	452147	3625410	2,133	2,050	2,079	NA	Otero	Y	N	NMOSE	*
PN 00720	451373	3625397	2,236	2,114	2,151	NA	Otero	Y	N	NMOSE	*
T 04695	421163	3625340	2,219	2,119	2,128	NA	Otero	N	Y	NMOSE	*
T 04207	420963	3625340	2,203	2,050	NA	NA	Otero	N	Y	NMOSE	*
T 04186	420671	3625247	2,199	2,107	NA	NA	Otero	Y	Y	NMOSE	*
T 04443	420276	3625246	2,234	2,173	2,214	NA	Otero	Y	N	NMOSE	*
PN 00683	472375	3625165	1,948	988	NA	NA	Chaves	N	N	NMOSE	*
PN 00382	435462	3625068	2,634	2,587	2,610	NA	Otero	Y	Y	NMOSE	*
T 04187	420369	3624953	2,153	1,924	NA	NA	Otero	N	Y	NMOSE	*
T 03353	420169	3624953	2,155	2,094	NA	NA	Otero	Y	Y	NMOSE	*
T 04424	420270	3624854	2,147	2,088	2,127	NA	Otero	Y	N	NMOSE	*
PN 00684	477394	3624730	1,751	1,553	NA	NA	Chaves	Y	Y	NMOSE	*
PN 00747	456761	3624707	2,024	1,982	NA	NA	Otero	Y	N	NMOSE	*
PN 00753	456660	3624606	2,035	1,989	2,006	NA	Otero	Y	N	NMOSE	*
PN 00557	452126	3624101	2,181	2,062	2,102	NA	Otero	Y	N	NMOSE	*
PN 00831	456030	3623803	2,053	1,977	2,004	NA	Otero	Y	N	NMOSE	*
PN 00755	455225	3622995	2,074	1,976	2,016	NA	Otero	Y	N	NMOSE	*

Table A-3.26 continued.

POD Number/ Well ID/ State Well Number	Easting	Northing	Ground Surface Elevation (m)	Elevation of Well Depth (m)	Groundwater Elevation (m)	Aquifer	County	Depth-to-Groundwater Control Point	Groundwater Surface Control Point	Source	Note
PN 00761	454834	3622797	2,091	1,999	2,045	NA	Otero	Y	N	NMOSE	*
ST 00062	432133	3621977	2,714	2,625	2,645	NA	Otero	Y	Y	NMOSE	*
PN 00942	459827	3621825	2,023	1,846	1,888	NA	Otero	Y	Y	NMOSE	*
T 01386	413314	3621642	1,251	1,179	1,179	NA	Otero	Y	Y	NMOSE	*
T 01925	418686	3621600	2,178	2,138	2,160	NA	Otero	Y	N	NMOSE	*
PN 00511	453047	3621586	2,142	1,959	1,979	NA	Otero	Y	Y	NMOSE	*
PN 00224	477378	3620705	1,823	1,604	1,671	NA	Chaves	Y	Y	NMOSE	*
RA 09265	484620	3620287	1,653	1,409	1,507	NA	Chaves	Y	Y	NMOSE	*
PN 00787	449823	3619557	2,218	1,936	2,032	NA	Otero	Y	Y	NMOSE	*
RA 04570	520714	3619405	1,287	1,073	1,089	NA	Eddy	Y	Y	NMOSE	*
RA 05465	521117	3619405	1,282	1,046	1,072	NA	Eddy	Y	Y	NMOSE	*
T 05008 POD1	425564	3617902	2,107	2,040	2,061	NA	Otero	Y	Y	NMOSE	*
T 05126 POD1	425166	3617518	2,123	2,102	NA	NA	Otero	N	N	NMOSE	*
RA 05487	517807	3617479	1,325	1,046	1,085	NA	Eddy	Y	Y	NMOSE	*
T 04531	424589	3617331	2,064	1,942	NA	NA	Otero	Y	Y	NMOSE	*
T 04385	425370	3617301	2,091	1,908	1,973	NA	Otero	Y	Y	NMOSE	*
T 04137	425561	3617286	2,063	1,941	NA	NA	Otero	Y	Y	NMOSE	*
T 04530	424198	3617146	2,047	1,926	NA	NA	Otero	Y	N	NMOSE	*
T 04389	426542	3617057	2,112	2,021	2,032	NA	Otero	Y	Y	NMOSE	*
T 04781	424592	3616921	2,058	1,869	NA	NA	Otero	Y	Y	NMOSE	*
T 03800	417107	3616826	1,281	976	NA	NA	Otero	N	Y	NMOSE	*
RA 07804	525020	3616698	1,246	1,035	1,090	NA	Eddy	Y	Y	NMOSE	*
RA 06189	510157	3616661	1,407	1,355	NA	NA	Chaves	Y	Y	NMOSE	*
T 04329	425770	3616471	2,013	1,830	NA	NA	Otero	Y	Y	NMOSE	*
T 03040	414185	3616346	1,252	1,206	1,222	NA	Otero	Y	Y	NMOSE	*
RA 10997 POD1	523043	3616281	1,270	986	1,111	NA	Eddy	Y	Y	NMOSE	*
RA 05236	524162	3615894	1,247	827	1,083	NA	Eddy	Y	Y	NMOSE	*
ST 00115 S-6	455056	3615809	2,048	1,834	NA	NA	Otero	Y	Y	NMOSE	*

Table A-3.26 continued.

POD Number/ Well ID/ State Well Number	Easting	Northing	Ground Surface Elevation (m)	Elevation of Well Depth (m)	Groundwater Elevation (m)	Aquifer	County	Depth-to-Groundwater Control Point	Groundwater Surface Control Point	Source	Note
T 04783	425578	3615659	1,947	1,825	NA	NA	Otero	Y	Y	NMOSE	*
T 04150	426363	3615631	1,989	1,873	1,903	NA	Otero	Y	Y	NMOSE	*
ST 00115 S-4	452993	3615570	2,100	1,886	NA	NA	Otero	Y	Y	NMOSE	*
ST 00115 S-7	458842	3615492	1,976	1,763	NA	NA	Otero	Y	Y	NMOSE	*
ST 00115 S-10	446461	3615401	2,267	1,961	2,041	NA	Otero	Y	Y	NMOSE	*
ST 00231	458447	3615297	2,004	1,821	NA	NA	Otero	Y	Y	NMOSE	*
ST 00115 S	446659	3614999	2,293	2,080	NA	NA	Otero	Y	N	NMOSE	*
T 04532	426179	3614833	1,931	1,742	NA	NA	Otero	Y	Y	NMOSE	*
T 04468	426373	3614819	1,952	1,831	NA	NA	Otero	Y	Y	NMOSE	*
ST 00115 S-2	446459	3614799	2,308	2,094	NA	NA	Otero	Y	N	NMOSE	*
T 04538	425790	3614441	1,932	1,810	NA	NA	Otero	Y	Y	NMOSE	*
T 04533	425984	3614427	1,887	1,765	NA	NA	Otero	Y	Y	NMOSE	*
RA 03458	508453	3614347	1,415	1,073	1,112	NA	Chaves	Y	Y	NMOSE	*
T 04782	425196	3614255	1,940	1,623	NA	NA	Otero	Y	Y	NMOSE	*
T 04534	426188	3614022	1,922	1,800	NA	NA	Otero	Y	Y	NMOSE	*
T 04535	426192	3613617	1,884	1,793	NA	NA	Otero	Y	Y	NMOSE	*
ST 00115 S-8	455267	3613559	2,067	1,853	NA	NA	Otero	Y	Y	NMOSE	*
T 04537	425798	3613431	1,892	1,770	NA	NA	Otero	Y	Y	NMOSE	*
ST 00246	435898	3612934	2,232	2,110	NA	NA	Otero	Y	Y	NMOSE	*
ST 00112	437925	3612859	2,236	2,205	2,228	NA	Otero	Y	N	NMOSE	*
ST 00130	437721	3612712	2,230	2,211	2,222	NA	Otero	Y	N	NMOSE	*
ST 00225	437319	3612712	2,212	2,166	NA	NA	Otero	Y	Y	NMOSE	*
ST 00115 S-5	452208	3612559	2,124	1,911	NA	NA	Otero	Y	Y	NMOSE	*
RA 11072 POD1	515918	3612553	1,346	910	1,091	NA	Eddy	Y	Y	NMOSE	*
ST 00230	436113	3612527	2,221	2,038	NA	NA	Otero	Y	N	NMOSE	*
ST 00226	437519	3612512	2,230	2,184	NA	NA	Otero	Y	Y	NMOSE	*
ST 00111 S-3	434091	3612380	2,181	1,815	2,016	NA	Otero	Y	N	NMOSE	*
ST 00168	434497	3612371	2,151	1,968	2,037	NA	Otero	Y	N	NMOSE	*

Table A-3.26 continued.

POD Number/ Well ID/ State Well Number	Easting	Northing	Ground Surface Elevation (m)	Elevation of Well Depth (m)	Groundwater Elevation (m)	Aquifer	County	Depth- to- Groundwater Control Point	Groundwater Surface Control Point	Source	Note
ST 00190	434497	3612171	2,159	2,109	2,141	NA	Otero	Y	N	NMOSE	*
ST 00111	434903	3612163	2,129	1,980	2,096	NA	Otero	Y	Y	NMOSE	*
ST 00005	481574	3612051	1,824	1,474	1,519	NA	Chaves	Y	Y	NMOSE	*
ST 00008	469786	3612015	1,777	1,480	1,492	NA	Chaves	Y	Y	NMOSE	*
ST 00009	467376	3611968	1,817	1,448	1,466	NA	Chaves	Y	Y	NMOSE	*
ST 00205	434185	3611875	2,172	2,080	NA	NA	Otero	Y	N	NMOSE	*
ST 00142	434084	3611774	2,171	2,049	2,118	NA	Otero	Y	N	NMOSE	*
ST 00111 S	435098	3611759	2,123	2,001	2,108	NA	Otero	Y	N	NMOSE	*
ST 00185	431660	3611748	2,200	2,017	NA	NA	Otero	Y	N	NMOSE	*
ST 00010	475764	3611561	1,837	1,800	1,819	NA	Chaves	Y	N	NMOSE	*
ST 00013	475555	3611403	1,885	1,874	1,876	NA	Chaves	Y	N	NMOSE	*
ST 00111 S-4	434269	3610961	2,159	1,946	1,989	NA	Otero	Y	Y	NMOSE	*
ST 00144	434069	3610961	2,160	2,023	NA	NA	Otero	Y	N	NMOSE	*
ST 00172	434679	3610957	2,162	2,028	2,114	NA	Otero	Y	N	NMOSE	*
ST 00143	434871	3610745	2,147	1,965	NA	NA	Otero	Y	Y	NMOSE	*
T 01400	415047	3610599	1,295	1,099	1,225	NA	Otero	Y	Y	NMOSE	*
ST 00119	461982	3610457	1,873	1,416	NA	NA	Otero	Y	Y	NMOSE	*
RA 07122	502745	3610425	1,519	970	NA	NA	Chaves	Y	Y	NMOSE	*
ST 00115	450857	3610382	2,152	1,939	NA	NA	Otero	Y	Y	NMOSE	*
ST 00165	457467	3610375	1,987	1,553	1,658	NA	Otero	Y	Y	NMOSE	*
ST 00115 S-3	450788	3610184	2,135	1,922	NA	NA	Otero	Y	Y	NMOSE	*
ST 00115 S-9	450405	3610184	2,160	1,946	NA	NA	Otero	Y	Y	NMOSE	*
T 01412	418461	3610174	1,372	1,245	NA	NA	Otero	Y	Y	NMOSE	*
ST 00145	434214	3609956	2,118	1,981	NA	NA	Otero	Y	N	NMOSE	*
ST 00166	461985	3609637	1,865	1,448	1,515	NA	Otero	Y	Y	NMOSE	*
ST 00113	437897	3609513	2,071	1,888	NA	NA	Otero	Y	Y	NMOSE	*
ST 00220	459873	3609158	1,932	1,413	NA	NA	Otero	Y	Y	NMOSE	*
ST 00006	483181	3608828	1,688	1,425	1,505	NA	Chaves	Y	Y	NMOSE	*

Table A-3.26 continued.

POD Number/ Well ID/ State Well Number	Easting	Northing	Ground Surface Elevation (m)	Elevation of Well Depth (m)	Groundwater Elevation (m)	Aquifer	County	Depth-to-Groundwater Control Point	Groundwater Surface Control Point	Source	Note
ST 00221	463074	3608381	1,831	1,332	1,446	NA	Otero	Y	Y	NMOSE	*
ST 00001	485497	3608120	1,667	1,662	1,666	NA	Chaves	Y	N	NMOSE	*
ST 00020	453685	3607880	1,995	1,666	1,797	NA	Otero	Y	Y	NMOSE	*
SM-0046	442173	3607555	1,959	1,715	1,776	NA	Otero	Y	Y	SMHS	*
ST 00003	478550	3606619	1,623	1,287	1,312	NA	Chaves	Y	Y	NMOSE	*
ST 00002	485697	3606511	1,642	1,505	1,551	NA	Chaves	Y	Y	NMOSE	*
RA 11056	488112	3605092	1,850	1,669	1,674	NA	Chaves	Y	Y	NMOSE	*
RA 11074 POD1	516938	3604883	1,393	966	1,076	NA	Eddy	Y	Y	NMOSE	*
ST 00007	485591	3603997	1,599	1,421	1,459	NA	Chaves	Y	Y	NMOSE	*
ST 00021	465694	3603733	1,835	1,399	1,408	NA	Otero	Y	Y	NMOSE	*
T 02408	403609	3603266	1,229	926	1,133	NA	Otero	Y	Y	NMOSE	*
ST 00208	454125	3603086	2,091	1,848	NA	NA	Otero	Y	N	NMOSE	*
ST 00004	480157	3602997	1,560	1,362	1,392	NA	Chaves	Y	N	NMOSE	*
ST 00236 POD1	481499	3602715	1,629	1,244	1,316	NA	Chaves	Y	Y	NMOSE	*
ST 00098	450214	3601975	1,889	1,605	NA	NA	Otero	Y	Y	NMOSE	*
RA 10444	530277	3600916	1,299	970	1,093	NA	Eddy	Y	Y	NMOSE	*
RA 06432	528356	3600600	1,289	695	NA	NA	Chaves	Y	Y	NMOSE	*
ST 00011	459040	3600344	1,899	1,582	1,853	NA	Otero	Y	N	NMOSE	*
RA 06725	522565	3599257	1,353	1,201	NA	NA	Eddy	Y	N	NMOSE	*
ST 00080	451407	3598958	1,832	1,481	1,487	NA	Otero	Y	Y	NMOSE	*
ST 00194 S	484877	3598063	1,453	1,178	1,194	NA	Chaves	Y	Y	NMOSE	*
ST 00018	473476	3596830	1,743	1,353	1,392	NA	Otero	Y	Y	NMOSE	*
RA 11300 POD1	533742	3595158	1,213	1,045	1,094	NA	Eddy	Y	Y	NMOSE	*
ST 00194	484918	3594393	1,395	NA	1,349	NA	Otero	Y	Y	NMOSE	*
RA 09633	520766	3593858	1,408	1,149	NA	NA	Eddy	Y	Y	NMOSE	*
ST 00068	485622	3592884	1,400	1,326	1,334	NA	Otero	Y	Y	NMOSE	*
ST 00022	471858	3592609	1,648	825	1,225	NA	Otero	Y	Y	NMOSE	*
RA 09961	500975	3592119	1,841	1,536	NA	NA	Otero	Y	Y	NMOSE	*

Table A-3.26 continued.

782

POD Number/ Well ID/ State Well Number	Easting	Northing	Ground Surface Elevation (m)	Elevation of Well Depth (m)	Groundwater Elevation (m)	Aquifer	County	Depth-to-Groundwater Control Point	Groundwater Surface Control Point	Source	Note
RA 09631	500474	3591418	1,858	1,599	NA	NA	Otero	Y	Y	NMOSE	*
RA 08610	518659	3591136	1,440	1,078	NA	NA	Eddy	Y	Y	NMOSE	*
T 02263	397286	3590033	1,335	1,159	1,313	NA	Otero	Y	Y	NMOSE	*
T 03849	399296	3589611	1,294	1,196	1,273	NA	Otero	Y	Y	NMOSE	*
T 03846	399499	3589607	1,292	975	1,170	NA	Otero	Y	Y	NMOSE	*
RA 09741	534813	3589438	1,217	1,156	1,162	NA	Eddy	Y	Y	NMOSE	*
RA 09632	497261	3589022	1,919	1,660	NA	NA	Otero	Y	Y	NMOSE	*
RA 10046	532553	3588361	1,240	1,165	1,175	NA	Eddy	Y	Y	NMOSE	*
ST 00200	483909	3588157	1,314	1,094	1,101	NA	Otero	Y	Y	NMOSE	*
ST 00196	486119	3588154	1,342	1,108	1,116	NA	Otero	Y	Y	NMOSE	*
ST 00019	476365	3588074	1,447	1,131	1,157	NA	Otero	Y	Y	NMOSE	*
RA 05566	533690	3586838	1,264	1,193	1,221	NA	Chaves	Y	N	NMOSE	*
RA 05242	535603	3586131	1,274	1,077	1,083	NA	Eddy	Y	Y	NMOSE	*
ST 00081	454291	3584921	1,365	1,167	1,171	NA	Otero	Y	Y	NMOSE	*
ST 00134	463908	3584910	1,642	1,449	NA	NA	Otero	Y	N	NMOSE	*
ST 00131	442247	3583759	1,435	1,106	NA	NA	Otero	Y	Y	NMOSE	*
ST 00075	487572	3583723	1,246	1,093	1,124	NA	Otero	Y	Y	NMOSE	*
RA 09271	529149	3583521	1,310	1,054	1,103	NA	Eddy	Y	Y	NMOSE	*
T 01680	397033	3582862	1,287	1,056	1,129	NA	Otero	Y	Y	NMOSE	*
RA 05256	535796	3582806	1,267	1,102	1,106	NA	Eddy	Y	Y	NMOSE	*
ST 00055	444554	3582645	1,416	1,106	1,136	NA	Otero	Y	Y	NMOSE	*
T 05626 POD1	396643	3582089	1,277	1,094	NA	NA	Otero	Y	Y	NMOSE	*
RA 10184	526538	3581912	1,336	1,295	NA	NA	Eddy	Y	N	NMOSE	*
ST 00195	484099	3581318	1,232	1,095	1,098	NA	Otero	Y	Y	NMOSE	*
ST 00132	444847	3580934	1,435	1,153	1,168	NA	Otero	Y	Y	NMOSE	*
RA 10185	530765	3580706	1,332	1,095	NA	NA	Eddy	Y	Y	NMOSE	*
RA 06763	533616	3580505	1,288	1,255	1,261	NA	Eddy	Y	N	NMOSE	*
ST 00056	447353	3580223	1,401	1,127	1,165	NA	Otero	Y	Y	NMOSE	*

Table A-3.26 continued.

783

POD Number/ Well ID/ State Well Number	Easting	Northing	Ground Surface Elevation (m)	Elevation of Well Depth (m)	Groundwater Elevation (m)	Aquifer	County	Depth-to-Groundwater Control Point	Groundwater Surface Control Point	Source	Note
ST 00133	452054	3579701	1,341	1,158	1,196	NA	Otero	Y	Y	NMOSE	*
ST 00198	485704	3579307	1,209	1,096	1,102	NA	Otero	Y	Y	NMOSE	*
RA 10183	520481	3579285	1,430	1,244	NA	NA	Eddy	Y	Y	NMOSE	*
RA 06149	520279	3579284	1,439	1,249	1,263	NA	Chaves	Y	Y	NMOSE	*
ST 00135	458662	3578880	1,311	1,165	NA	NA	Otero	Y	Y	NMOSE	*
ST 00254 POD1	478461	3578608	1,297	1,053	1,119	NA	Otero	Y	Y	NMOSE	*
RA 10186	525743	3578291	1,387	1,109	NA	NA	Eddy	Y	N	NMOSE	*
ST 00052	494206	3578272	1,226	1,089	1,104	NA	Otero	Y	Y	NMOSE	*
RA 05937	534375	3578180	1,303	1,202	1,213	NA	Chaves	Y	Y	NMOSE	*
ST 00072	493805	3578067	1,210	1,057	1,118	NA	Otero	Y	Y	NMOSE	*
RA 10188	531179	3577689	1,323	1,228	NA	NA	Eddy	Y	Y	NMOSE	*
RA 05904	534942	3576386	1,281	1,191	1,202	NA	Eddy	Y	Y	NMOSE	*
ST 00137	457256	3576067	1,307	1,171	NA	NA	Otero	Y	Y	NMOSE	*
ST 00078	489782	3575872	1,175	1,084	1,106	NA	Otero	Y	Y	NMOSE	*
ST 00069	499785	3575849	1,386	1,099	1,112	NA	Otero	Y	Y	NMOSE	*
RA 10187	522705	3575479	1,558	1,357	NA	NA	Eddy	Y	Y	NMOSE	*
ST 00197	482280	3575089	1,243	1,075	1,083	NA	Otero	Y	N	NMOSE	*
ST 00136	449823	3575088	1,361	1,138	NA	NA	Otero	Y	Y	NMOSE	*
ST 00071	490990	3574863	1,169	986	1,100	NA	Otero	Y	Y	NMOSE	*
C 01485	540578	3574395	1,236	1,202	1,215	NA	Eddy	Y	Y	NMOSE	*
T 01015	406098	3574332	1,304	1,060	NA	NA	Otero	Y	Y	NMOSE	*
RA 10193	536455	3574279	1,265	1,208	NA	NA	Eddy	Y	Y	NMOSE	*
RA 10189	527569	3574079	1,426	1,083	NA	NA	Eddy	Y	N	NMOSE	*
ST 00102	434576	3573550	1,485	1,317	1,336	NA	Otero	Y	Y	NMOSE	*
ST 00199	473613	3573502	1,390	1,146	1,154	NA	Otero	Y	Y	NMOSE	*
ST 00070	500796	3573438	1,317	1,088	1,096	NA	Otero	Y	Y	NMOSE	*
RA 10191	533007	3573334	1,309	1,225	NA	NA	Eddy	Y	Y	NMOSE	*
ST 00035	465493	3573243	1,346	1,148	1,163	NA	Otero	Y	Y	NMOSE	*

Table A-3.26 continued.

POD Number/ Well ID/ State Well Number	Easting	Northing	Ground Surface Elevation (m)	Elevation of Well Depth (m)	Groundwater Elevation (m)	Aquifer	County	Depth-to-Groundwater Control Point	Groundwater Surface Control Point	Source	Note
ST 00053	492193	3572648	1,159	1,058	1,103	NA	Otero	Y	Y	NMOSE	*
RA 10190	530196	3572471	1,369	1,170	NA	NA	Eddy	Y	Y	NMOSE	*
RA 10391	527178	3572272	1,535	394	1,145	NA	Eddy	Y	N	NMOSE	*
RA 06403	535860	3572265	1,293	1,154	1,206	NA	Eddy	Y	Y	NMOSE	*
RA 10194	539885	3572082	1,245	1,197	NA	NA	Eddy	Y	Y	NMOSE	*
ST 00017	481172	3571976	1,315	1,113	1,177	NA	Otero	Y	N	NMOSE	*
ST 00014	487565	3571656	1,181	1,090	1,148	NA	Otero	Y	N	NMOSE	*
ST 00076	491992	3571643	1,160	977	1,008	NA	Otero	Y	N	NMOSE	*
RA 10197	534862	3570855	1,292	1,273	NA	NA	Eddy	Y	Y	NMOSE	*
RA 10195	541298	3570677	1,303	1,200	NA	NA	Eddy	Y	Y	NMOSE	*
RA 10196	539489	3570472	1,306	1,237	NA	NA	Eddy	Y	Y	NMOSE	*
ST 00016	486459	3570354	1,198	1,107	1,156	NA	Otero	Y	N	NMOSE	*
RA 06204	518897	3570045	1,757	1,345	NA	NA	Chaves	Y	N	NMOSE	*
RA 10192	530018	3569865	1,433	1,334	NA	NA	Eddy	Y	Y	NMOSE	*
RA 09962	520110	3569851	1,743	1,439	NA	NA	Eddy	Y	Y	NMOSE	*
RA 09634	520011	3569749	1,743	1,484	NA	NA	Eddy	Y	Y	NMOSE	*
RA 11307 POD 1	517952	3569172	1,721	1,340	1,368	NA	Eddy	Y	N	NMOSE	*
ST 00103	439978	3568708	1,443	1,272	1,294	NA	Otero	Y	Y	NMOSE	*
ST 00073	494200	3568627	1,160	1,008	1,023	NA	Otero	Y	N	NMOSE	*
C 02887	534069	3567939	1,340	1,295	NA	NA	Eddy	Y	Y	NMOSE	*
T 03875	389700	3567825	1,249	1,065	NA	NA	Otero	Y	Y	NMOSE	*
RA 05498	528556	3567464	1,461	1,407	NA	NA	Eddy	Y	Y	NMOSE	*
ST 00048	495206	3567420	1,167	1,133	1,138	NA	Otero	Y	Y	NMOSE	*
ST 00036	467360	3566280	1,273	1,105	1,127	NA	Otero	Y	Y	NMOSE	*
C 02247	537627	3565738	1,405	1,314	1,370	NA	Eddy	Y	Y	NMOSE	*
ST 00086	492587	3565618	1,144	1,089	1,110	NA	Otero	Y	Y	NMOSE	*
ST 00015	492488	3565519	1,143	1,089	1,113	NA	Otero	Y	Y	NMOSE	*
C 02888	534480	3565392	1,418	1,319	NA	NA	Eddy	Y	Y	NMOSE	*

Table A-3.26 continued.

785

POD Number/ Well ID/ State Well Number	Easting	Northing	Ground Surface Elevation (m)	Elevation of Well Depth (m)	Groundwater Elevation (m)	Aquifer	County	Depth-to-Groundwater Control Point	Groundwater Surface Control Point	Source	Note
ST 00037	500007	3565208	1,353	1,079	1,138	NA	Otero	Y	Y	NMOSE	*
ST 00148	490272	3564919	1,138	955	NA	NA	Otero	Y	Y	NMOSE	*
RA 09964	521338	3564671	1,697	1,392	NA	NA	Eddy	Y	N	NMOSE	*
ST 00074	496386	3564607	1,154	1,016	1,108	NA	Otero	Y	Y	NMOSE	*
ST 00077	508213	3564589	1,418	1,037	1,082	NA	Otero	Y	Y	NMOSE	*
ST 00161	477637	3564446	1,276	1,029	1,124	NA	Otero	Y	Y	NMOSE	*
ST 00095	508515	3564286	1,414	1,094	NA	NA	Otero	Y	Y	NMOSE	*
ST 00050	496187	3563804	1,147	1,086	NA	NA	Otero	Y	Y	NMOSE	*
RA 10121	526156	3563653	1,744	1,523	1,576	NA	Eddy	Y	Y	NMOSE	*
C 02129	545792	3563338	1,268	1,218	1,241	NA	Chaves	Y	Y	NMOSE	*
ST 00088	487550	3563011	1,132	1,025	1,098	NA	Otero	Y	Y	NMOSE	*
RA 09620	526061	3562945	1,752	1,508	1,543	NA	Eddy	Y	Y	NMOSE	*
RA 08041	526761	3562645	1,745	1,522	1,566	NA	Eddy	Y	Y	NMOSE	*
RA 09403	525659	3562543	1,762	1,564	1,587	NA	Eddy	Y	N	NMOSE	*
C 02496	544400	3562541	1,307	940	968	NA	Chaves	N	N	NMOSE	*
RA 06737	533128	3562459	1,639	1,411	1,431	NA	Eddy	Y	Y	NMOSE	*
RA 10056	526563	3562444	1,745	1,515	1,570	NA	Eddy	Y	Y	NMOSE	*
RA 09089	525759	3562442	1,759	1,522	1,573	NA	Eddy	Y	Y	NMOSE	*
RA 09932	525557	3562441	1,765	1,497	1,574	NA	Eddy	Y	Y	NMOSE	*
RA 09628	525860	3562343	1,756	1,603	NA	NA	Eddy	Y	N	NMOSE	*
C 01394	543997	3562337	1,340	1,181	1,284	NA	Chaves	Y	Y	NMOSE	*
RA 10198	524554	3562251	1,772	1,577	NA	NA	Eddy	Y	Y	NMOSE	*
RA 09920	526563	3562244	1,740	1,541	NA	NA	Eddy	Y	Y	NMOSE	*
RA 10126	526763	3562244	1,731	1,509	1,568	NA	Eddy	Y	Y	NMOSE	*
RA 09040	526161	3562243	1,743	1,506	1,564	NA	Eddy	Y	Y	NMOSE	*
RA 09993	525759	3562242	1,760	1,530	1,595	NA	Eddy	Y	N	NMOSE	*
RA 09161	525959	3562242	1,754	1,524	1,577	NA	Eddy	Y	Y	NMOSE	*
RA 10017	525357	3562241	1,769	1,524	1,578	NA	Eddy	Y	Y	NMOSE	*

Table A-3.26 continued.

POD Number/ Well ID/ State Well Number	Easting	Northing	Ground Surface Elevation (m)	Elevation of Well Depth (m)	Groundwater Elevation (m)	Aquifer	County	Depth-to-Groundwater Control Point	Groundwater Surface Control Point	Source	Note
RA 08043	525557	3562241	1,769	1,546	NA	NA	Eddy	Y	Y	NMOSE	*
RA 10008	524154	3562053	1,770	1,525	1,587	NA	Eddy	Y	Y	NMOSE	*
RA 09401	524354	3562053	1,772	1,536	1,574	NA	Eddy	Y	N	NMOSE	*
RA 09027	524556	3562050	1,774	1,522	1,592	NA	Eddy	Y	Y	NMOSE	*
RA 10462	524756	3562050	1,773	1,530	1,563	NA	Eddy	Y	N	NMOSE	*
RA 10704 POD1	524154	3561853	1,778	1,534	NA	NA	Eddy	Y	Y	NMOSE	*
RA 10517	524556	3561850	1,771	1,521	1,587	NA	Eddy	Y	Y	NMOSE	*
RA 09055	524357	3561451	1,772	1,527	1,594	NA	Eddy	Y	Y	NMOSE	*
RA 09963	513828	3561357	1,840	1,535	NA	NA	Eddy	Y	Y	NMOSE	*
C 01489	541999	3561329	1,369	1,292	NA	NA	Eddy	Y	Y	NMOSE	*
C 01519	541495	3561223	1,381	1,343	1,350	NA	Eddy	Y	Y	NMOSE	*
RA 09830	523867	3561153	1,777	1,548	NA	NA	Eddy	Y	Y	NMOSE	*
ST 00162	481454	3561014	1,212	1,075	1,090	NA	Otero	Y	Y	NMOSE	*
ST 00084	487747	3561001	1,136	1,064	1,102	NA	Otero	Y	Y	NMOSE	*
ST 00087	487547	3561001	1,137	1,076	1,103	NA	Otero	Y	Y	NMOSE	*
ST 00089	487950	3561000	1,134	1,004	1,100	NA	Otero	Y	Y	NMOSE	*
RA 09635	513931	3560856	1,853	1,594	NA	NA	Eddy	Y	Y	NMOSE	*
ST 00092	444365	3560630	1,410	1,166	1,227	NA	Otero	Y	Y	NMOSE	*
ST 00097	440344	3560061	1,430	1,278	1,403	NA	Otero	Y	Y	NMOSE	*
ST 00141 S	488452	3559894	1,129	1,022	NA	NA	Otero	Y	Y	NMOSE	*
ST 00141	488248	3559694	1,129	855	NA	NA	Otero	Y	Y	NMOSE	*
ST 00180 S	488148	3559592	1,130	947	1,109	NA	Otero	Y	Y	NMOSE	*
ST 00049	494596	3559387	1,131	1,104	1,106	NA	Otero	Y	Y	NMOSE	*
C 01327	546421	3558638	1,412	1,384	1,387	NA	Chaves	Y	N	NMOSE	*
ST 00038	458735	3558565	1,336	1,032	1,154	NA	Otero	Y	Y	NMOSE	*
ST 00042	463561	3557747	1,304	1,121	1,152	NA	Otero	Y	Y	NMOSE	*
ST 00163	479239	3557196	1,230	1,076	1,093	NA	Otero	Y	Y	NMOSE	*
ST 00164	488754	3556577	1,126	1,088	1,106	NA	Otero	Y	Y	NMOSE	*

Table A-3.26 continued.

787

POD Number/ Well ID/ State Well Number	Easting	Northing	Ground Surface Elevation (m)	Elevation of Well Depth (m)	Groundwater Elevation (m)	Aquifer	County	Depth-to-Groundwater Control Point	Groundwater Surface Control Point	Source	Note
ST 00192	493185	3555562	1,121	1,030	1,102	NA	Otero	Y	Y	NMOSE	*
ST 00191	494594	3555559	1,130	1,039	1,112	NA	Otero	Y	Y	NMOSE	*
ST 00138	506116	3555044	1,754	901	NA	NA	Otero	Y	Y	NMOSE	*
RA 05286 REPAR	535065	3554824	1,792	1,706	1,733	NA	Eddy	Y	Y	NMOSE	*
ST 00025	425104	3554803	1,584	1,419	1,431	NA	Otero	Y	Y	NMOSE	*
ST 00147	489461	3554468	1,127	983	NA	NA	Otero	Y	Y	NMOSE	*
ST 00028	445541	3554322	1,482	1,421	1,426	NA	Otero	Y	Y	NMOSE	*
ST 00054	489965	3553359	1,128	1,037	1,106	NA	Otero	Y	Y	NMOSE	*
ST 00152	490568	3552754	1,120	1,044	NA	NA	Otero	Y	Y	NMOSE	*
ST 00033	492178	3552346	1,116	1,025	1,104	NA	Otero	Y	Y	NMOSE	*
ST 00182	492380	3552344	1,116	1,070	1,101	NA	Otero	Y	Y	NMOSE	*
ST 00026	438231	3552247	1,487	1,426	1,441	NA	Otero	Y	Y	NMOSE	*
ST 00093	491775	3552147	1,116	1,076	NA	NA	Otero	Y	Y	NMOSE	*
ST 00110	491775	3551945	1,117	965	1,103	NA	Otero	Y	Y	NMOSE	*
ST 00151	490771	3551748	1,122	970	NA	NA	Otero	Y	Y	NMOSE	*
ST 00027	441810	3551427	1,538	1,371	1,389	NA	Otero	Y	Y	NMOSE	*
ST 00155	491877	3551242	1,117	1,099	NA	NA	Otero	Y	Y	NMOSE	*
ST 00212	490771	3551143	1,139	987	NA	NA	Otero	Y	Y	NMOSE	*
ST 00096	513359	3550998	1,657	1,123	NA	NA	Otero	Y	Y	NMOSE	*
ST 00153	485681	3550966	1,243	1,090	NA	NA	Otero	Y	Y	NMOSE	*
C 03116	544325	3550819	1,200	1,118	1,131	NA	Chaves	Y	Y	NMOSE	*
C 02816	543319	3550626	1,212	1,132	1,154	NA	Chaves	Y	Y	NMOSE	*
ST 00107	428705	3550603	1,528	1,412	1,443	NA	Otero	Y	Y	NMOSE	*
ST 00043	465163	3550511	1,288	1,044	1,105	NA	Otero	Y	Y	NMOSE	*
ST 00040	469119	3549792	1,269	1,086	1,117	NA	Otero	Y	Y	NMOSE	*
ST 00158	492678	3549631	1,113	1,095	NA	NA	Otero	Y	Y	NMOSE	*
C 01392	538058	3549100	1,313	1,252	1,259	NA	Eddy	Y	Y	NMOSE	*
T 03499	407862	3548799	1,549	1,465	NA	NA	Otero	Y	Y	NMOSE	*

Table A-3.26 continued.

POD Number/ Well ID/ State Well Number	Easting	Northing	Ground Surface Elevation (m)	Elevation of Well Depth (m)	Groundwater Elevation (m)	Aquifer	County	Depth-to-Groundwater Control Point	Groundwater Surface Control Point	Source	Note
ST 00041	450338	3548063	1,490	1,398	1,413	NA	Otero	Y	Y	NMOSE	*
C 00910	534470	3548020	1,403	1,345	NA	NA	Eddy	Y	Y	NMOSE	*
ST 00051	451746	3547855	1,468	1,389	1,406	NA	Otero	Y	Y	NMOSE	*
ST 00187 S	481046	3547755	1,188	1,084	1,105	NA	Otero	Y	Y	NMOSE	*
C 01025	533621	3547538	1,420	1,343	1,413	NA	Eddy	Y	N	NMOSE	*
C 02318	519164	3547455	2,046	1,776	1,793	NA	Eddy	Y	Y	NMOSE	*
ST 00024	438171	3547423	1,546	1,375	1,383	NA	Otero	Y	Y	NMOSE	*
ST 00039	448727	3547265	1,532	1,425	1,447	NA	Otero	Y	Y	NMOSE	*
ST 00154	491062	3547222	1,118	1,097	NA	NA	Otero	Y	Y	NMOSE	*
C 02267	533207	3547130	1,418	1,360	1,368	NA	Eddy	Y	Y	NMOSE	*
ST 00106	437663	3546802	1,544	1,370	1,416	NA	Otero	N	Y	NMOSE	*
ST 00044	466258	3546182	1,268	1,024	1,119	NA	Otero	Y	Y	NMOSE	*
C 02411	536795	3545970	1,327	1,269	1,278	NA	Eddy	Y	Y	NMOSE	*
ST 00032	453546	3545833	1,454	1,359	1,397	NA	Otero	Y	Y	NMOSE	*
ST 00101	442084	3545493	1,609	1,365	1,423	NA	Otero	Y	Y	NMOSE	*
ST 00046	474148	3545352	1,207	1,077	1,100	NA	Otero	Y	Y	NMOSE	*
ST 00099	447914	3545254	1,596	1,535	1,550	NA	Otero	Y	Y	NMOSE	*
ST 00108	432019	3545238	1,582	1,396	1,417	NA	Otero	Y	Y	NMOSE	*
C 01285	535549	3544971	1,341	1,260	1,309	NA	Eddy	Y	Y	NMOSE	*
ST 00090	417884	3544898	1,606	1,545	1,558	NA	Otero	Y	Y	NMOSE	*
C 02252	533078	3544781	1,384	1,380	1,382	NA	Eddy	Y	N	NMOSE	*
ST 00045	465851	3544774	1,264	1,002	1,157	NA	Otero	Y	Y	NMOSE	*
ST 00160	511665	3544666	1,866	988	1,101	NA	Otero	Y	Y	NMOSE	*
C 01008	539332	3544643	1,263	1,202	1,221	NA	Eddy	Y	Y	NMOSE	*
ST 00186 S	487526	3544312	1,138	1,055	1,080	NA	Otero	Y	Y	NMOSE	*
ST 00066	500206	3544281	1,118	1,096	NA	NA	Otero	Y	Y	NMOSE	*
T 05304 POD1	390017	3544257	1,246	1,124	NA	NA	Otero	Y	Y	NMOSE	*
C 02255	533069	3544175	1,374	1,317	1,336	NA	Eddy	Y	Y	NMOSE	*

Table A-3.26 continued.

POD Number/ Well ID/ State Well Number	Easting	Northing	Ground Surface Elevation (m)	Elevation of Well Depth (m)	Groundwater Elevation (m)	Aquifer	County	Depth-to-Groundwater Control Point	Groundwater Surface Control Point	Source	Note
ST 00253 POD1	489252	3544154	1,121	1,060	1,091	NA	Otero	Y	Y	NMOSE	*
ST 00186	487526	3544112	1,130	1,053	1,096	NA	Otero	Y	Y	NMOSE	*
ST 00123	489740	3544106	1,116	1,045	1,095	NA	Otero	Y	Y	NMOSE	*
ST 00057	490345	3544103	1,114	1,066	1,090	NA	Otero	Y	Y	NMOSE	*
ST 00091	416873	3544102	1,603	1,329	1,387	NA	Otero	Y	Y	NMOSE	*
ST 00059	489135	3543905	1,117	986	1,092	NA	Otero	Y	Y	NMOSE	*
ST 00116 B	487724	3543709	1,126	1,048	1,091	NA	Otero	Y	Y	NMOSE	*
ST 00058	489939	3543499	1,114	983	1,092	NA	Otero	Y	Y	NMOSE	*
ST 00187	479815	3543323	1,153	1,077	1,100	NA	Otero	Y	Y	NMOSE	*
ST 00116	487320	3543307	1,124	1,069	1,090	NA	Otero	Y	Y	NMOSE	*
ST 00034	449111	3543234	1,597	1,414	1,429	NA	Otero	Y	Y	NMOSE	*
C 02185	543727	3542935	1,186	1,140	1,168	NA	Chaves	Y	Y	NMOSE	*
ST 00116 S	486716	3542904	1,125	1,088	1,091	NA	Otero	Y	Y	NMOSE	*
ST 00059 S-3	489332	3542899	1,113	806	1,092	NA	Otero	Y	Y	NMOSE	*
ST 00031	455145	3542811	1,408	1,362	1,372	NA	Otero	Y	Y	NMOSE	*
ST 00029	459818	3542789	1,331	1,117	1,127	NA	Otero	Y	Y	NMOSE	*
ST 00047	468499	3542756	1,234	1,106	1,115	NA	Otero	Y	Y	NMOSE	*
ST 00150	486311	3542703	1,129	1,015	NA	NA	Otero	Y	Y	NMOSE	*
ST 00060 S-2	487519	3542699	1,118	950	1,092	NA	Otero	Y	Y	NMOSE	*
ST 00125	488927	3542696	1,120	NA	1,068	NA	Otero	Y	Y	NMOSE	*
ST 00058 S-2	490136	3542693	1,112	1,072	NA	NA	Otero	Y	Y	NMOSE	*
ST 00060	487519	3542499	1,116	958	1,091	NA	Otero	Y	Y	NMOSE	*
ST 00187 S-2	483837	3542303	1,169	1,049	1,095	NA	Otero	Y	Y	NMOSE	*
ST 00120	486712	3542298	1,119	1,043	1,092	NA	Otero	Y	Y	NMOSE	*
ST 00059 S	489128	3542292	1,113	982	1,088	NA	Otero	Y	Y	NMOSE	*
ST 00159	494968	3542280	1,106	954	NA	NA	Otero	Y	Y	NMOSE	*
ST 00030	452522	3542012	1,490	1,394	1,399	NA	Otero	Y	Y	NMOSE	*
C 02254	531230	3541986	1,408	1,353	1,362	NA	Eddy	Y	Y	NMOSE	*

Table A-3.26 continued.

POD Number/ Well ID/ State Well Number	Easting	Northing	Ground Surface Elevation (m)	Elevation of Well Depth (m)	Groundwater Elevation (m)	Aquifer	County	Depth-to-Groundwater Control Point	Groundwater Surface Control Point	Source	Note
ST 00146	486307	3541896	1,119	983	NA	NA	Otero	Y	Y	NMOSE	*
C 02253	525756	3541810	1,508	1,489	1,502	NA	Eddy	Y	Y	NMOSE	*
C 02251	527971	3541795	1,465	1,378	1,396	NA	Eddy	Y	Y	NMOSE	*
ST 00146 S	486307	3541696	1,118	1,064	NA	NA	Otero	Y	Y	NMOSE	*
ST 00248 POD1	515736	3541312	1,872	1,506	NA	NA	Eddy	Y	N	NMOSE	*
C 01302	539942	3541186	1,265	1,257	1,262	NA	Eddy	Y	Y	NMOSE	*
C 01884	540752	3541185	1,259	1,229	1,256	NA	Eddy	Y	Y	NMOSE	*
ST 00188	488115	3541086	1,111	1,026	1,090	NA	Otero	Y	Y	NMOSE	*
C 02935	539640	3541084	1,261	1,220	1,254	NA	Eddy	Y	Y	NMOSE	*
ST 00061 S	489122	3541081	1,111	1,085	1,097	NA	Otero	Y	Y	NMOSE	*
C 02962	540864	3540881	1,240	1,225	1,234	NA	Eddy	Y	Y	NMOSE	*
T 01559 POD2	408667	3540858	1,646	1,555	1,587	NA	Otero	Y	Y	NMOSE	*
ST 00245 POD1	515724	3540530	1,895	1,784	1,798	NA	Eddy	Y	Y	NMOSE	*
4806201	471768	3540444	1,201	866	1,111	318BSVP	Hudspeth	Y	Y	TWDB	*
4807218	481398	3540422	1,137	619	1,093	318BSVP	Hudspeth	Y	Y	TWDB	*
4807314	487616	3540412	1,111	1,044	1,096	318BSVP	Hudspeth	Y	Y	TWDB	*
4807217	481817	3540390	1,135	NA	1,098	318BSVP	Hudspeth	Y	N	TWDB	
ST 00061	489761	3540319	1,109	1,018	1,089	NA	Otero	Y	Y	NMOSE	*
4807209	481004	3540269	1,138	NA	1,100	318BSVP	Hudspeth	Y	N	TWDB	*
4808101	489111	3540195	1,110	NA	1,101	318BSVP	Hudspeth	Y	N	TWDB	
ST 00219	514868	3539926	2,045	1,588	NA	NA	Eddy	Y	Y	NMOSE	
4807303	485962	3539922	1,119	1,075	1,101	318BSVP	Hudspeth	Y	N	TWDB	*
4703204	529309	3539893	1,421	1,400	1,409	110AVPS	Culberson	Y	Y	TWDB	
4703107	525583	3539883	1,517	1,387	1,458	310PRMN	Culberson	Y	Y	TWDB	*
4808201	494201	3539760	1,106	NA	1,098	318BSVP	Hudspeth	Y	Y	TWDB	*
4702103	515639	3539647	1,917	1,012	1,134	310PRMN	Culberson	Y	N	TWDB	*
4807203	481029	3539560	1,132	1,047	1,098	318BSVP	Hudspeth	Y	N	TWDB	*
4807208	481816	3539559	1,131	NA	1,104	318BSVP	Hudspeth	Y	N	TWDB	

Table A-3.26 continued.

POD Number/ Well ID/ State Well Number	Easting	Northing	Ground Surface Elevation (m)	Elevation of Well Depth (m)	Groundwater Elevation (m)	Aquifer	County	Depth-to-Groundwater Control Point	Groundwater Surface Control Point	Source	Note
4807219	482603	3539496	1,129	945	1,090	318BSVP	Hudspeth	Y	Y	TWDB	
4807206	481002	3539407	1,131	1,065	1,094	318BSVP	Hudspeth	Y	Y	TWDB	
4703302	532775	3539349	1,395	1,375	1,385	110AVPS	Culberson	Y	Y	TWDB	
4703205	527579	3539272	1,446	1,435	1,441	110AVPS	Culberson	Y	Y	TWDB	*
4704101	539099	3539248	1,275	1,244	1,253	312CSTL	Culberson	Y	Y	TWDB	*
4703108	524588	3538926	1,543	1,470	1,520	310PRMN	Culberson	Y	Y	TWDB	*
4807313	485961	3538875	1,124	1,043	1,089	318BSVP	Hudspeth	Y	Y	TWDB	*
4807305	487010	3538781	1,112	1,036	1,103	318BSVP	Hudspeth	Y	N	TWDB	*
4808102	488165	3538688	1,111	992	1,095	318BSVP	Hudspeth	Y	Y	TWDB	
4807318	487325	3538658	1,112	NA	1,096	318BSVP	Hudspeth	Y	Y	TWDB	*
4702302	520732	3538609	1,586	1,578	1,580	110AVPS	Culberson	Y	Y	TWDB	
4806301	474466	3538497	1,179	889	1,095	318BSVP	Hudspeth	Y	Y	TWDB	*
4807213	482706	3538418	1,124	852	1,095	318BSVP	Hudspeth	Y	Y	TWDB	*
4704201	541072	3538147	1,251	1,196	1,228	312CSTL	Culberson	Y	Y	TWDB	*
4806303	475173	3538033	1,172	NA	1,096	318BSVP	Hudspeth	Y	Y	TWDB	
4807107	477456	3537967	1,160	798	1,089	318BSVP	Hudspeth	Y	Y	TWDB	*
4702305	523436	3537907	1,528	1,505	1,510	110AVPS	Culberson	Y	N	TWDB	*
4807302	487560	3537888	1,111	NA	1,101	318BSVP	Hudspeth	Y	Y	TWDB	
4808103	489424	3537886	1,108	NA	1,098	318BSVP	Hudspeth	Y	Y	TWDB	*
4807307	487035	3537858	1,112	NA	1,087	318BSVP	Hudspeth	Y	Y	TWDB	*
4807108	477823	3537750	1,155	798	1,088	318BSVP	Hudspeth	Y	Y	TWDB	*
4703203	529840	3537708	1,426	1,385	1,395	310PRMN	Culberson	Y	Y	TWDB	*
4807106	477692	3537658	1,155	790	1,089	318BSVP	Hudspeth	Y	Y	TWDB	
4703101	524304	3537293	1,506	1,464	1,473	310PRMN	Culberson	Y	Y	TWDB	
4807207	480998	3537159	1,131	914	1,095	318BSVP	Hudspeth	Y	Y	TWDB	
4807109	480210	3537130	1,136	1,016	1,093	318BSVP	Hudspeth	Y	Y	TWDB	*
4807220	482126	3537095	1,125	744	1,097	318BSVP	Hudspeth	Y	Y	TWDB	
4807204	482704	3537063	1,122	1,023	1,094	318BSVP	Hudspeth	Y	Y	TWDB	

Table A-3.26 continued.

POD Number/ Well ID/ State Well Number	Easting	Northing	Ground Surface Elevation (m)	Elevation of Well Depth (m)	Groundwater Elevation (m)	Aquifer	County	Depth-to-Groundwater Control Point	Groundwater Surface Control Point	Source	Note
4807101	476877	3537044	1,160	841	1,102	318BSVP	Hudspeth	Y	Y	TWDB	*
4807315	485722	3537028	1,114	846	1,092	318BSVP	Hudspeth	Y	Y	TWDB	*
4807308	485984	3537028	1,113	1,022	1,095	318BSVP	Hudspeth	Y	N	TWDB	
4807110	480184	3536976	1,136	1,060	1,097	318BSVP	Hudspeth	Y	Y	TWDB	*
4807306	487638	3536964	1,111	1,061	1,104	318BSVP	Hudspeth	Y	N	TWDB	*
4806304	474357	3536958	1,176	NA	1,096	318BSVP	Hudspeth	Y	Y	TWDB	*
4703102	525853	3536835	1,477	1,431	1,437	110AVPS	Culberson	Y	Y	TWDB	
4807304	487533	3536656	1,111	1,050	1,095	318BSVP	Hudspeth	Y	Y	TWDB	*
4807309	487585	3536656	1,111	1,050	1,101	318BSVP	Hudspeth	Y	N	TWDB	*
4806305	476298	3536522	1,170	NA	1,104	318BSVP	Hudspeth	Y	N	TWDB	
4807214	482703	3536386	1,121	969	1,095	318BSVP	Hudspeth	Y	Y	TWDB	*
4806302	474434	3536373	1,175	810	1,092	318BSVP	Hudspeth	Y	Y	TWDB	
4702301	521681	3536364	1,687	1,640	NA	313CPTN	Culberson	Y	Y	TWDB	*
4807205	480996	3536266	1,131	1,053	1,103	318BSVP	Hudspeth	Y	N	TWDB	*
4703206	530055	3536015	1,427	1,305	1,391	310PRMN	Culberson	Y	Y	TWDB	
4807102	476875	3535967	1,157	836	1,094	318BSVP	Hudspeth	Y	Y	TWDB	
4807111	479368	3535930	1,142	1,023	1,105	318BSVP	Hudspeth	Y	N	TWDB	*
4807112	479447	3535930	1,141	1,065	1,105	318BSVP	Hudspeth	Y	N	TWDB	*
4704501	540373	3535651	1,246	1,185	1,214	110ALVM	Culberson	Y	Y	TWDB	
4807631	486008	3535334	1,113	NA	1,095	318BSVP	Hudspeth	Y	Y	TWDB	
4807633	487557	3535332	1,111	NA	1,096	318BSVP	Hudspeth	Y	Y	TWDB	
4806608	475193	3535324	1,171	NA	1,096	318BSVP	Hudspeth	Y	Y	TWDB	
4806606	474458	3535295	1,180	845	1,097	318BSVP	Hudspeth	Y	Y	TWDB	
4807606	484459	3535244	1,114	1,038	1,097	318BSVP	Hudspeth	Y	Y	TWDB	*
4807611	484381	3535213	1,114	1,038	1,102	318BSVP	Hudspeth	Y	N	TWDB	*
4807521	482700	3534847	1,121	NA	1,096	318BSVP	Hudspeth	Y	Y	TWDB	*
4807403	479733	3534790	1,138	1,078	1,100	318BSVP	Hudspeth	Y	N	TWDB	*
4807404	479812	3534790	1,138	NA	1,099	318BSVP	Hudspeth	Y	N	TWDB	*

Table A-3.26 continued.

POD Number/ Well ID/ State Well Number	Easting	Northing	Ground Surface Elevation (m)	Elevation of Well Depth (m)	Groundwater Elevation (m)	Aquifer	County	Depth-to-Groundwater Control Point	Groundwater Surface Control Point	Source	Note
4702604	522289	3534610	1,623	1,513	1,531	310PRMN	Culberson	Y	Y	TWDB	
4806602	476031	3534583	1,166	837	1,097	318BSVP	Hudspeth	Y	Y	TWDB	
4807603	486007	3534565	1,113	1,052	1,103	318BSVP	Hudspeth	Y	N	TWDB	*
4807507	480835	3534480	1,130	1,037	1,102	318BSVP	Hudspeth	Y	N	TWDB	
4806605	472986	3534467	1,197	837	1,097	318BSVP	Hudspeth	Y	Y	TWDB	
4807417	476871	3534458	1,161	763	1,099	318BSVP	Hudspeth	Y	N	TWDB	*
4806604	472592	3534438	1,198	839	1,096	318BSVP	Hudspeth	Y	Y	TWDB	
4808403	488449	3534407	1,109	1,034	1,100	318BSVP	Hudspeth	Y	Y	TWDB	
4703401	523838	3534398	1,537	1,529	1,536	110AVPS	Culberson	Y	Y	TWDB	
4702603	522709	3534395	1,588	1,466	1,538	110AVPS	Culberson	Y	Y	TWDB	
4807616	485797	3534349	1,117	1,041	1,109	318BSVP	Hudspeth	Y	N	TWDB	
4807527	481806	3534294	1,124	1,013	1,095	318BSVP	Hudspeth	Y	Y	TWDB	*
4701401	503150	3534217	1,135	1,127	1,127	110ALVM	Hudspeth	Y	Y	TWDB	
4807522	481019	3534203	1,128	889	1,086	318BSVP	Hudspeth	Y	Y	TWDB	*
4806603	472591	3534191	1,197	832	1,083	318BSVP	Hudspeth	Y	Y	TWDB	*
4806609	475216	3534185	1,174	NA	1,096	318BSVP	Hudspeth	Y	Y	TWDB	
4702304	522263	3534179	1,625	1,555	1,577	310PRMN	Culberson	Y	Y	TWDB	*
4807632	484326	3534074	1,114	NA	1,095	318BSVP	Hudspeth	Y	Y	TWDB	*
4703403	526989	3534005	1,437	1,410	1,419	110AVPS	Culberson	Y	Y	TWDB	
4806601	473641	3534004	1,190	731	1,093	318BSVP	Hudspeth	Y	Y	TWDB	
4703402	526517	3533973	1,436	1,329	1,424	310PRMN	Culberson	Y	Y	TWDB	*
4807408	477736	3533779	1,153	1,046	1,105	318BSVP	Hudspeth	Y	N	TWDB	*
4807418	476869	3533688	1,160	871	1,094	318BSVP	Hudspeth	Y	Y	TWDB	*
4807423	480151	3533681	1,134	1,058	1,103	318BSVP	Hudspeth	Y	N	TWDB	
4807405	478733	3533653	1,144	1,056	1,096	318BSVP	Hudspeth	Y	Y	TWDB	*
4807407	479206	3533622	1,141	1,065	1,108	318BSVP	Hudspeth	Y	N	TWDB	*
4807411	478628	3533592	1,145	1,073	1,103	318BSVP	Hudspeth	Y	Y	TWDB	
4807610	486846	3533578	1,112	1,076	1,106	110ALVM	Hudspeth	Y	N	TWDB	

Table A-3.26 continued.

POD Number/ Well ID/ State Well Number	Easting	Northing	Ground Surface Elevation (m)	Elevation of Well Depth (m)	Groundwater Elevation (m)	Aquifer	County	Depth-to-Groundwater Control Point	Groundwater Surface Control Point	Source	Note
4807626	487634	3533577	1,110	1,019	1,098	318BSVP	Hudspeth	Y	Y	TWDB	
4808401	488579	3533576	1,108	1,017	1,102	318BSVP	Hudspeth	Y	N	TWDB	
4807604	486058	3533518	1,112	1,021	1,105	318BSVP	Hudspeth	Y	N	TWDB	
4807504	481044	3533495	1,127	1,074	1,098	318BSVP	Hudspeth	Y	N	TWDB	
4808406	488421	3533453	1,109	986	1,101	318BSVP	Hudspeth	Y	Y	TWDB	*
4807619	486583	3533363	1,112	1,036	1,097	318BSVP	Hudspeth	Y	Y	TWDB	
4808402	490600	3533358	1,103	1,094	1,100	100ALVM	Hudspeth	Y	Y	TWDB	
4807412	477735	3533255	1,152	1,042	1,104	318BSVP	Hudspeth	Y	Y	TWDB	
4807502	482697	3533246	1,118	1,057	1,095	318BSVP	Hudspeth	Y	N	TWDB	
4807601	486583	3533209	1,112	1,033	1,101	318BSVP	Hudspeth	Y	N	TWDB	*
4807512	482697	3533153	1,118	1,061	1,101	318BSVP	Hudspeth	Y	Y	TWDB	*
4807526	483485	3533152	1,115	1,024	1,088	318BSVP	Hudspeth	Y	N	TWDB	
4807612	484693	3533119	1,113	1,052	1,105	318BSVP	Hudspeth	Y	N	TWDB	
4807508	481148	3532940	1,127	1,057	1,104	318BSVP	Hudspeth	Y	N	TWDB	
4908601	401582	3532934	1,384	1,253	1,268	112HCBL	El Paso	Y	Y	TWDB	*
4807511	482697	3532845	1,118	1,041	1,106	318BSVP	Hudspeth	Y	N	TWDB	
4908603	401660	3532779	1,385	1,253	1,277	112HCBL	El Paso	Y	Y	TWDB	*
4807420	476894	3532764	1,159	702	1,096	318BSVP	Hudspeth	Y	Y	TWDB	
4807623	487659	3532592	1,110	1,041	1,097	318BSVP	Hudspeth	Y	Y	TWDB	
4807624	485978	3532563	1,111	989	1,095	318BSVP	Hudspeth	Y	Y	TWDB	*
4807501	481383	3532386	1,125	1,058	1,097	318BSVP	Hudspeth	Y	Y	TWDB	*
4807505	481304	3532355	1,125	848	1,096	318BSVP	Hudspeth	Y	Y	TWDB	
4702602	522793	3532117	1,543	NA	1,535	110AVPS	Culberson	Y	Y	TWDB	
4807427	477680	3532085	1,151	NA	1,096	318BSVP	Hudspeth	Y	Y	TWDB	*
4806610	475185	3532060	1,170	NA	1,097	318BSVP	Hudspeth	Y	Y	TWDB	*
4808407	489365	3532005	1,107	732	1,096	318BSVP	Hudspeth	Y	Y	TWDB	*
4807414	476892	3531933	1,157	950	1,096	318BSVP	Hudspeth	Y	Y	TWDB	*
4807410	479360	3531928	1,138	NA	1,097	318BSVP	Hudspeth	Y	Y	TWDB	*

Table A-3.26 continued.

795

POD Number/ Well ID/ State Well Number	Easting	Northing	Ground Surface Elevation (m)	Elevation of Well Depth (m)	Groundwater Elevation (m)	Aquifer	County	Depth-to-Groundwater Control Point	Groundwater Surface Control Point	Source	Note
4807627	484875	3531918	1,112	1,013	1,092	318BSVP	Hudspeth	Y	Y	TWDB	
4807607	485951	3531917	1,110	NA	1,095	318BSVP	Hudspeth	Y	Y	TWDB	
4808408	490363	3531911	1,103	NA	1,102	UNKNOWN	Hudspeth	Y	Y	TWDB	*
4908502	400443	3531898	1,360	NA	1,230	112HCBL	El Paso	Y	Y	TWDB	*
4807409	480227	3531895	1,131	NA	1,103	318BSVP	Hudspeth	Y	Y	TWDB	
4807628	484769	3531888	1,112	1,005	1,095	318BSVP	Hudspeth	Y	N	TWDB	*
4807503	481907	3531861	1,120	1,048	1,102	318BSVP	Hudspeth	Y	N	TWDB	*
4807510	482695	3531798	1,116	816	1,095	318BSVP	Hudspeth	Y	Y	TWDB	*
4807509	481933	3531769	1,120	1,048	1,104	318BSVP	Hudspeth	Y	N	TWDB	*
4807513	483693	3531704	1,113	NA	1,104	318BSVP	Hudspeth	Y	Y	TWDB	
4808405	490415	3531696	1,103	1,099	1,102	100ALVM	Hudspeth	Y	Y	TWDB	
4807402	478020	3531530	1,146	1,063	1,099	318BSVP	Hudspeth	Y	N	TWDB	*
4807615	486056	3531332	1,110	1,064	1,103	318BSVP	Hudspeth	Y	N	TWDB	
4807614	486029	3531301	1,110	1,065	1,104	318BSVP	Hudspeth	Y	N	TWDB	*
4807613	486003	3531239	1,111	1,020	1,103	318BSVP	Hudspeth	Y	N	TWDB	
4701701	502495	3531138	1,121	1,102	1,106	100ALVM	Hudspeth	Y	Y	TWDB	*
4807901	487657	3531083	1,109	1,018	1,094	318BSVP	Hudspeth	Y	Y	TWDB	
4807702	479358	3531004	1,136	NA	1,097	318BSVP	Hudspeth	Y	Y	TWDB	*
4702801	518751	3531001	1,734	1,532	1,664	313CRCX	Culberson	Y	Y	TWDB	
4807801	482667	3530906	1,115	1,054	1,094	318BSVP	Hudspeth	Y	Y	TWDB	*
4701901	509822	3530865	1,633	-394	1,196	UNKNOWN	Culberson	Y	Y	TWDB	*
4807802	482693	3530813	1,115	1,055	1,103	318BSVP	Hudspeth	Y	N	TWDB	*
4807809	481852	3530661	1,119	849	1,094	318BSVP	Hudspeth	Y	Y	TWDB	*
4807709	476652	3530579	1,154	925	1,098	318BSVP	Hudspeth	Y	N	TWDB	
4807810	482693	3530413	1,116	948	1,090	318BSVP	Hudspeth	Y	Y	TWDB	
4807914	485713	3530254	1,111	653	1,095	318BSVP	Hudspeth	Y	Y	TWDB	*
4806901	476074	3530242	1,158	776	1,095	318BSVP	Hudspeth	Y	Y	TWDB	*
4807806	482298	3530167	1,117	1,035	1,105	318BSVP	Hudspeth	Y	N	TWDB	

Table A-3.26 continued.

POD Number/ Well ID/ State Well Number	Easting	Northing	Ground Surface Elevation (m)	Elevation of Well Depth (m)	Groundwater Elevation (m)	Aquifer	County	Depth-to-Groundwater Control Point	Groundwater Surface Control Point	Source	Note
4807804	481300	3530108	1,123	1,032	1,105	318BSVP	Hudspeth	Y	N	TWDB	
4807714	477596	3529992	1,150	982	1,098	318BSVP	Hudspeth	Y	N	TWDB	
4807813	483795	3529949	1,115	955	1,083	318BSVP	Hudspeth	Y	Y	TWDB	*
4907802	386467	3529272	1,238	1,113	1,128	112HCBL	El Paso	Y	Y	TWDB	
4907801	386493	3529272	1,238	1,052	1,127	112HCBL	El Paso	Y	Y	TWDB	
4702804	516286	3528964	1,777	993	1,110	318BSPG	Culberson	Y	N	TWDB	
4807910	486367	3528960	1,109	731	1,093	318BSVP	Hudspeth	Y	Y	TWDB	
4807706	480194	3528878	1,131	876	1,096	318BSVP	Hudspeth	Y	Y	TWDB	*
4807908	485553	3528807	1,111	1,081	1,102	318BSVP	Hudspeth	Y	N	TWDB	
4702807	517468	3528597	1,716	1,671	1,677	310PRMN	Culberson	Y	Y	TWDB	*
4807902	485947	3528499	1,110	1,055	1,101	318BSVP	Hudspeth	Y	N	TWDB	
4807905	484475	3528470	1,115	1,014	1,102	318BSVP	Hudspeth	Y	N	TWDB	*
4807903	486052	3528468	1,110	1,052	1,101	318BSVP	Hudspeth	Y	N	TWDB	*
4907804	386562	3528347	1,238	1,025	1,126	112HCBL	El Paso	Y	Y	TWDB	*
4807904	484501	3528286	1,115	737	1,097	318BSVP	Hudspeth	Y	Y	TWDB	*
4907806	386480	3528101	1,238	1,042	1,122	112HCBL	El Paso	Y	Y	TWDB	
4807803	481060	3528014	1,125	973	1,097	318BSVP	Hudspeth	Y	Y	TWDB	
4807805	481007	3527984	1,126	1,041	1,103	318BSVP	Hudspeth	Y	N	TWDB	
4807815	481848	3527921	1,120	859	1,075	318BSVP	Hudspeth	Y	Y	TWDB	
4807916	486944	3527851	1,108	NA	1,101	318BSVP	Hudspeth	Y	N	TWDB	*
4807814	482241	3527704	1,118	966	1,096	318BSVP	Hudspeth	Y	Y	TWDB	*
4807703	477749	3527559	1,147	1,056	1,098	318BSVP	Hudspeth	Y	N	TWDB	*
4807716	480192	3527400	1,138	862	1,098	318BSVP	Hudspeth	Y	N	TWDB	
4807705	477722	3527220	1,153	1,001	1,104	318BSVP	Hudspeth	Y	N	TWDB	
4807712	476775	3526915	1,158	766	1,095	318BSVP	Hudspeth	Y	Y	TWDB	
4807811	481846	3526874	1,122	994	1,084	318BSVP	Hudspeth	Y	Y	TWDB	*
4807708	480191	3526846	1,135	653	1,092	318BSVP	Hudspeth	Y	Y	TWDB	*
4807812	481898	3526812	1,122	861	1,078	318BSVP	Hudspeth	Y	Y	TWDB	

Table A-3.26 continued.

797

POD Number/ Well ID/ State Well Number	Easting	Northing	Ground Surface Elevation (m)	Elevation of Well Depth (m)	Groundwater Elevation (m)	Aquifer	County	Depth-to-Groundwater Control Point	Groundwater Surface Control Point	Source	Note
4808903	498765	3526796	1,109	1,105	1,106	110ALVM	Hudspeth	Y	Y	TWDB	
4808902	498056	3526765	1,106	1,091	1,099	110ALVM	Hudspeth	Y	Y	TWDB	
4807713	476591	3526700	1,163	806	1,096	318BSVP	Hudspeth	Y	Y	TWDB	
4709208	504545	3526520	1,167	1,083	1,095	310PRMN	Hudspeth	Y	N	TWDB	
4815105	478481	3526018	1,149	NA	1,092	318BSVP	Hudspeth	Y	Y	TWDB	
4815204	482685	3525702	1,120	NA	1,104	318BSVP	Hudspeth	Y	N	TWDB	*
4815303	484340	3525546	1,113	795	1,096	318BSVP	Hudspeth	Y	Y	TWDB	*
4815203	481054	3525120	1,132	1,033	1,097	318BSVP	Hudspeth	Y	Y	TWDB	*
4815201	483761	3525023	1,114	1,023	1,096	318BSVP	Hudspeth	Y	Y	TWDB	*
4815202	481002	3524997	1,135	1,046	1,107	318BSVP	Hudspeth	Y	N	TWDB	
4815101	477506	3524881	1,179	-283	1,097	318BSVP	Hudspeth	Y	Y	TWDB	*
4815305	485180	3524867	1,111	1,026	1,101	318BSVP	Hudspeth	Y	N	TWDB	*
4815302	487676	3524833	1,109	916	1,096	318BSVP	Hudspeth	Y	Y	TWDB	
4815307	484365	3524745	1,113	921	1,095	318BSVP	Hudspeth	Y	Y	TWDB	
4815104	480134	3524691	1,142	711	1,095	318BSVP	Hudspeth	Y	Y	TWDB	*
4709201	505440	3524365	1,155	1,081	1,097	313CRCX	Hudspeth	Y	N	TWDB	
4709202	505440	3524334	1,155	1,083	1,093	313CRCX	Hudspeth	Y	N	TWDB	*
4815103	480159	3524260	1,145	686	1,095	318BSVP	Hudspeth	Y	Y	TWDB	*
4815102	480133	3524137	1,146	784	1,096	318BSVP	Hudspeth	Y	Y	TWDB	*
4916201	398291	3524128	1,336	NA	1,130	112HCBL	El Paso	Y	Y	TWDB	
4709203	504047	3523810	1,127	1,081	1,099	112SLBL	Hudspeth	Y	Y	TWDB	
4815301	484389	3523606	1,114	1,016	1,097	318BSVP	Hudspeth	Y	Y	TWDB	*
4709205	503916	3523472	1,121	1,075	1,099	112SLBL	Hudspeth	Y	Y	TWDB	
4710201	516032	3523391	1,447	1,069	1,103	310PRMN	Culberson	Y	Y	TWDB	*
4709206	504468	3523379	1,129	1,083	1,098	112SLBL	Hudspeth	Y	Y	TWDB	*
4709207	504258	3523287	1,123	746	1,093	313CRCX	Hudspeth	Y	N	TWDB	
4709204	504153	3523133	1,121	1,075	1,098	112SLBL	Hudspeth	Y	Y	TWDB	
4712101	535534	3523101	1,296	-1,624	1,140	NA	Culberson	Y	Y	TWDB	

Table A-3.26 continued.

POD Number/ Well ID/ State Well Number	Easting	Northing	Ground Surface Elevation (m)	Elevation of Well Depth (m)	Groundwater Elevation (m)	Aquifer	County	Depth-to-Groundwater Control Point	Groundwater Surface Control Point	Source	Note
4709101	503732	3522733	1,112	1,105	1,106	110ALVM	Hudspeth	Y	Y	TWDB	
4812401	442513	3521907	1,376	579	1,029	300PLZC	Hudspeth	Y	Y	TWDB	*
4710501	516904	3520621	1,386	1,051	1,142	318BSPG	Culberson	Y	Y	TWDB	
4709502	505731	3520270	1,125	1,082	1,095	112SBCRC	Hudspeth	Y	Y	TWDB	*
4812502	447994	3519292	1,354	1,077	1,110	318BSVP	Hudspeth	Y	Y	TWDB	
4815601	487091	3519230	1,118	430	1,095	318BSVP	Hudspeth	Y	Y	TWDB	
4816402	491218	3519103	1,114	1,071	1,100	318BSVP	Hudspeth	Y	Y	TWDB	
4710401	514330	3518401	1,282	1,033	1,114	313CRCX	Culberson	Y	Y	TWDB	
4709503	504970	3518084	1,110	16	1,090	313CRCX	Hudspeth	Y	Y	TWDB	
4816501	492716	3517962	1,113	1,092	1,101	318BSVP	Hudspeth	Y	Y	TWDB	*
4816403	491139	3517902	1,116	NA	1,098	318BSVP	Hudspeth	Y	Y	TWDB	*
4916501	400281	3517858	1,298	824	1,115	112HCBL	El Paso	Y	Y	TWDB	
4916701	395062	3516801	1,242	1,140	1,141	112HCBL	El Paso	Y	Y	TWDB	*
4709806	505733	3516145	1,126	897	1,095	313CRCX	Hudspeth	Y	Y	TWDB	*
4709805	505707	3516114	1,126	969	1,090	313CRCX	Hudspeth	Y	Y	TWDB	*
4709801	505681	3516114	1,126	1,000	1,098	313CRCX	Hudspeth	Y	N	TWDB	
4709804	505681	3516083	1,127	1,000	1,081	313CRCX	Hudspeth	Y	Y	TWDB	*
4815801	480695	3515884	1,206	1,069	1,093	318BSVP	Hudspeth	Y	Y	TWDB	*
4816702	491321	3515654	1,118	1,067	1,096	318BSVP	Hudspeth	Y	Y	TWDB	*
4709908	508680	3515161	1,178	1,060	1,098	310PRMN	Culberson	Y	Y	TWDB	*
4916901	402780	3515155	1,320	1,092	1,100	112HCBL	El Paso	Y	Y	TWDB	*
4709910	508890	3515100	1,179	1,011	1,102	310PRMN	Culberson	Y	Y	TWDB	*
4812901	451261	3515088	1,317	NA	1,112	318BSVP	Hudspeth	Y	Y	TWDB	
4709904	508890	3515069	1,179	1,062	1,097	112SBCRC	Culberson	Y	Y	TWDB	*
4812701	441475	3514955	1,379	1,028	1,150	318BSVP	Hudspeth	Y	Y	TWDB	
4709807	505787	3514944	1,135	NA	1,093	313CRCX	Hudspeth	Y	Y	TWDB	*
4709905	509522	3514885	1,181	1,003	1,093	313CRCX	Culberson	Y	N	TWDB	*
4816703	491320	3514453	1,120	1,029	1,090	318BSVP	Hudspeth	Y	Y	TWDB	*

Table A-3.26 continued.

POD Number/ Well ID/ State Well Number	Easting	Northing	Ground Surface Elevation (m)	Elevation of Well Depth (m)	Groundwater Elevation (m)	Aquifer	County	Depth-to-Groundwater Control Point	Groundwater Surface Control Point	Source	Note
4709903	507918	3514391	1,159	961	1,093	313CRCX	Culberson	Y	Y	TWDB	*
4709901	507918	3514330	1,160	980	1,098	112SBCRC	Culberson	Y	Y	TWDB	*
4814801	471459	3513997	1,230	NA	1,075	318BSVP	Hudspeth	Y	Y	TWDB	*
4814702	465119	3513955	1,270	1,042	1,101	318BSVP	Hudspeth	Y	Y	TWDB	
4709802	507813	3513899	1,159	1,083	1,099	313CRCX	Hudspeth	Y	Y	TWDB	
4709902	508234	3513868	1,169	1,071	1,109	313CRCX	Culberson	Y	Y	TWDB	
4709907	508997	3513776	1,169	986	1,090	313CRCX	Culberson	Y	Y	TWDB	
4709803	507840	3513344	1,156	NA	1,094	313CRCX	Hudspeth	Y	Y	TWDB	
4709808	506656	3513220	1,142	898	1,088	313CRCX	Hudspeth	Y	Y	TWDB	
4816705	488556	3513194	1,139	NA	1,090	318BSVP	Hudspeth	Y	N	TWDB	
4709702	503446	3513188	1,113	1,092	1,098	112SLBL	Hudspeth	Y	Y	TWDB	*
4816805	495501	3513096	1,106	NA	1,099	110ALVM	Hudspeth	Y	Y	TWDB	
4815902	488056	3513071	1,138	1,062	1,092	318BSVP	Hudspeth	Y	Y	TWDB	*
4709906	508997	3512883	1,165	1,055	1,094	313CRCX	Culberson	Y	Y	TWDB	
4815903	487661	3512733	1,141	1,065	1,090	318BSVP	Hudspeth	Y	Y	TWDB	*
4823202	481031	3512528	1,220	1,068	1,097	318BSVP	Hudspeth	Y	Y	TWDB	*
4717220	507814	3512451	1,150	967	1,090	313CRCX	Hudspeth	Y	Y	TWDB	*
4717324	510366	3512392	1,172	1,003	1,092	313CRCX	Culberson	Y	N	TWDB	*
4823201	480847	3512312	1,222	1,039	1,091	318BSVP	Hudspeth	Y	Y	TWDB	
4717315	508314	3512298	1,152	1,067	1,097	313CRCX	Culberson	Y	Y	TWDB	
4717216	506472	3512297	1,138	NA	1,096	112SLBL	Hudspeth	Y	Y	TWDB	*
4824203	492134	3512267	1,130	967	1,091	318BSVP	Hudspeth	Y	Y	TWDB	
4824101	491370	3512083	1,136	NA	1,103	318BSVP	Hudspeth	Y	Y	TWDB	
4717312	510919	3512023	1,178	1,031	1,107	313CRCX	Culberson	Y	Y	TWDB	
4717317	507919	3512020	1,147	964	1,095	313CRCX	Culberson	Y	Y	TWDB	*
4717201	507656	3511866	1,145	1,023	1,098	313CRCX	Hudspeth	Y	Y	TWDB	
4717209	507025	3511866	1,140	1,038	1,095	313CRCX	Hudspeth	Y	Y	TWDB	
4717212	507104	3511835	1,140	NA	1,091	313CRCX	Hudspeth	Y	Y	TWDB	

Table A-3.26 continued.

POD Number/ Well ID/ State Well Number	Easting	Northing	Ground Surface Elevation (m)	Elevation of Well Depth (m)	Groundwater Elevation (m)	Aquifer	County	Depth-to-Groundwater Control Point	Groundwater Surface Control Point	Source	Note
4717319	509419	3511714	1,159	NA	1,099	313CPTN	Culberson	Y	Y	TWDB	
4717211	506209	3511712	1,132	1,016	1,096	313CRCX	Hudspeth	Y	Y	TWDB	
4717323	509472	3511652	1,160	985	1,090	313CRCX	Culberson	Y	N	TWDB	
4717304	509393	3511560	1,159	1,026	1,097	313CRCX	Culberson	Y	N	TWDB	
4824201	495738	3511310	1,106	1,094	1,100	110ALVM	Hudspeth	Y	Y	TWDB	
4717214	505973	3511219	1,129	1,050	1,097	112SLBL	Hudspeth	Y	N	TWDB	
4717208	505999	3511188	1,129	615	1,095	313CRCX	Hudspeth	Y	Y	TWDB	*
4717206	507604	3511127	1,141	912	1,109	313CRCX	Hudspeth	Y	Y	TWDB	
4717307	509341	3511036	1,155	1,027	1,096	313CRCX	Culberson	Y	N	TWDB	
4717318	508868	3511036	1,151	926	1,097	313CRCX	Culberson	Y	N	TWDB	*
4717204	506210	3510911	1,128	854	1,093	313CRCX	Hudspeth	Y	Y	TWDB	
4717313	509815	3510698	1,161	1,015	1,102	313DLRM	Culberson	Y	N	TWDB	*
4717217	504210	3510694	1,109	1,095	1,099	110ALVM	Hudspeth	Y	Y	TWDB	*
4717203	507842	3510235	1,138	986	1,098	313CRCX	Hudspeth	Y	Y	TWDB	
4717205	506131	3510234	1,123	1,029	1,097	313CRCX	Hudspeth	Y	Y	TWDB	*
4717202	505421	3510233	1,117	1,041	1,095	112SBCRC	Hudspeth	Y	Y	TWDB	
4717320	511263	3510115	1,180	824	1,098	313CRDM	Culberson	Y	N	TWDB	
4717321	511000	3510114	1,178	836	1,096	313CRDM	Culberson	Y	Y	TWDB	*
4824202	494105	3510110	1,119	NA	1,096	318BSVP	Hudspeth	Y	Y	TWDB	
4717301	509316	3510020	1,146	1,029	1,098	313CRCX	Culberson	Y	Y	TWDB	*
4717207	506158	3510018	1,123	940	1,099	313CRCX	Hudspeth	Y	Y	TWDB	
4717302	509316	3509990	1,146	1,031	1,096	313CRCX	Culberson	Y	N	TWDB	
4717219	507868	3509988	1,136	771	1,092	313CRCX	Hudspeth	Y	N	TWDB	*
4717314	509684	3509959	1,152	1,042	1,101	313CRDM	Culberson	Y	N	TWDB	*
4717325	509421	3509959	1,149	966	1,092	313CRCX	Culberson	Y	Y	TWDB	
4717322	511264	3509314	1,173	990	1,096	313DLRM	Culberson	Y	N	TWDB	
4717215	506264	3508571	1,116	NA	1,100	112SLBL	Hudspeth	Y	Y	TWDB	
4718101	513239	3508424	1,206	1,069	1,130	313DLRM	Culberson	Y	Y	TWDB	

Table A-3.26 continued.

POD Number/ Well ID/ State Well Number	Easting	Northing	Ground Surface Elevation (m)	Elevation of Well Depth (m)	Groundwater Elevation (m)	Aquifer	County	Depth-to-Groundwater Control Point	Groundwater Surface Control Point	Source	Note
4823101	479813	3508250	1,185	NA	1,106	318BSVP	Hudspeth	Y	Y	TWDB	
4717218	506975	3508202	1,118	1,011	1,100	112SBCRC	Hudspeth	Y	Y	TWDB	*
4718402	513450	3508085	1,205	839	1,095	313DLRM	Culberson	Y	N	TWDB	*
4717606	509212	3507834	1,127	1,081	1,094	313CPTN	Culberson	Y	N	TWDB	
4717607	511713	3507806	1,184	650	1,090	313DMBS	Culberson	Y	N	TWDB	
4824501	495762	3507677	1,109	1,097	1,098	110ALVM	Hudspeth	Y	N	TWDB	
4824401	488366	3507621	1,169	1,058	1,097	318BSVP	Hudspeth	Y	Y	TWDB	*
4924415	395282	3507406	1,230	1,049	1,111	112HCBL	El Paso	Y	Y	TWDB	
4824502	495788	3507031	1,112	1,027	1,092	318BSVP	Hudspeth	Y	Y	TWDB	
4924418	395251	3506852	1,226	1,028	1,109	112HCBL	El Paso	Y	Y	TWDB	
4820601	452194	3506555	1,323	NA	1,088	318BSVP	Hudspeth	Y	Y	TWDB	
4924420	395035	3506362	1,226	1,034	1,106	112HCBL	El Paso	Y	Y	TWDB	*
4821401	454403	3505991	1,312	919	1,106	318BSVP	Hudspeth	Y	Y	TWDB	
4924401	395397	3505712	1,225	1,085	1,115	112HCBL	El Paso	Y	Y	TWDB	*
4821502	460062	3505598	1,282	NA	1,104	318BSVP	Hudspeth	Y	Y	TWDB	*
4717605	507872	3505124	1,110	1,095	1,099	112SLBL	Hudspeth	Y	Y	TWDB	*
4717601	509610	3505095	1,136	1,075	1,101	112SBDM	Culberson	Y	Y	TWDB	*
4717604	509610	3505064	1,135	1,087	1,095	112SBDM	Culberson	Y	N	TWDB	*
4717602	509189	3504694	1,130	1,069	1,096	112SBDM	Culberson	Y	Y	TWDB	*
4824601	497051	3504536	1,107	NA	1,097	318BSVP	Hudspeth	Y	Y	TWDB	
4718404	513008	3503713	1,165	984	1,097	112SBDM	Culberson	Y	N	TWDB	
4718707	512350	3503466	1,154	843	1,098	112SBDM	Culberson	Y	Y	TWDB	
4718705	511902	3503435	1,148	965	1,097	112SBDM	Culberson	Y	Y	TWDB	
4717904	511534	3503434	1,142	1,020	1,098	112SBDM	Culberson	Y	N	TWDB	*
4718802	515905	3503286	1,219	1,065	1,119	120BLSN	Culberson	Y	Y	TWDB	*
4718706	512324	3503004	1,151	988	1,100	112SBDM	Culberson	Y	Y	TWDB	*
4718901	520172	3502832	1,306	1,056	1,093	313DLRM	Culberson	Y	N	TWDB	*
4717903	511455	3502664	1,139	1,002	1,099	112SBDM	Culberson	Y	Y	TWDB	

Table A-3.26 continued.

POD Number/ Well ID/ State Well Number	Easting	Northing	Ground Surface Elevation (m)	Elevation of Well Depth (m)	Groundwater Elevation (m)	Aquifer	County	Depth-to-Groundwater Control Point	Groundwater Surface Control Point	Source	Note
4824901	499421	3501488	1,104	1,092	1,099	110ALVM	Hudspeth	Y	N	TWDB	*
4718801	515960	3501439	1,195	1,116	1,095	120BLSN	Culberson	Y	Y	TWDB	*
4824904	498025	3500503	1,114	NA	1,090	318BSVP	Hudspeth	Y	Y	TWDB	*
4924801	397452	3500487	1,238	1,086	1,101	112HCBL	El Paso	Y	Y	TWDB	*
4924802	398057	3500450	1,236	1,065	1,110	112HCBL	El Paso	Y	Y	TWDB	*
4824903	496497	3499457	1,141	1,037	1,051	318BSVP	Hudspeth	Y	Y	TWDB	
4823701	477319	3499450	1,243	NA	1,102	318BSVP	Hudspeth	Y	Y	TWDB	
4726101	512593	3498170	1,109	1,085	1,095	112SBDM	Culberson	Y	Y	TWDB	
4726102	514913	3497188	1,122	1,087	1,097	112SBDM	Culberson	Y	Y	TWDB	
4832301	498867	3496962	1,109	1,035	1,097	100ALVM	Hudspeth	Y	Y	TWDB	*
4829301	461266	3496603	1,305	1,097	1,103	318BSVP	Hudspeth	Y	Y	TWDB	
4829101	455179	3496536	1,331	1,297	1,309	210CRCS	Hudspeth	Y	Y	TWDB	
4829102	455205	3496536	1,330	1,300	1,309	210CRCS	Hudspeth	Y	Y	TWDB	
4829103	455231	3496535	1,330	1,296	1,308	210CRCS	Hudspeth	Y	Y	TWDB	
4829104	455205	3496505	1,330	1,302	1,309	210CRCS	Hudspeth	Y	Y	TWDB	
4828301	452300	3495255	1,351	NA	1,332	210CRCS	Hudspeth	Y	Y	TWDB	
4832601	499157	3493945	1,107	1,085	1,097	100ALVM	Hudspeth	Y	Y	TWDB	*
4832602	497760	3493576	1,132	1,068	1,095	318BSVP	Hudspeth	Y	Y	TWDB	
4726501	517081	3492912	1,107	1,073	1,094	112SLBL	Culberson	Y	Y	TWDB	*
4831401	477540	3491814	1,299	963	1,085	318BSVP	Hudspeth	Y	Y	TWDB	*
4830401	466018	3491476	1,305	970	1,118	318BSVP	Hudspeth	Y	Y	TWDB	*
4725401	502426	3490097	1,114	1,092	1,099	112SLBL	Hudspeth	Y	Y	TWDB	
4727401	525497	3489728	1,215	1,080	1,100	313DLRM	Culberson	Y	Y	TWDB	
4725802	505538	3488897	1,145	1,095	1,101	112SLBL	Hudspeth	Y	Y	TWDB	*
4827801	433360	3488370	1,543	1,323	1,427	210CRCS	Hudspeth	Y	Y	TWDB	*
4726702	515638	3488199	1,107	1,077	1,095	112SLBL	Culberson	Y	Y	TWDB	
4726701	511841	3488164	1,120	1,088	1,094	112SLBL	Culberson	Y	Y	TWDB	*
4725801	504483	3487973	1,202	1,063	1,096	318BSVP	Hudspeth	Y	Y	TWDB	*

Table A-3.26 continued.

POD Number/ Well ID/ State Well Number	Easting	Northing	Ground Surface Elevation (m)	Elevation of Well Depth (m)	Groundwater Elevation (m)	Aquifer	County	Depth- to- Groundwater Control Point	Groundwater Surface Control Point	Source	Note
4705201	522100	3487534	1,144	1,133	1,139	312CSTL	Culberson	Y	Y	TWDB	
4704301	522100	3487534	1,168	1,126	1,133	312CSTL	Culberson	Y	Y	TWDB	*
4705301	522100	3487534	1,164	1,151	1,158	312CSTL	Culberson	Y	Y	TWDB	*
4704302	522100	3487534	1,189	1,171	1,185	312CSTL	Culberson	Y	N	TWDB	*
4704305	522100	3487534	1,185	1,164	1,177	312CSTL	Culberson	Y	N	TWDB	*
4705602	522100	3487534	1,117	1,103	1,107	312CSTL	Culberson	Y	Y	TWDB	*
4706602	522100	3487534	1,029	NA	1,027	312CSTL	Culberson	Y	Y	TWDB	*
4706601	522100	3487534	1,029	NA	1,008	312CSTL	Culberson	Y	Y	TWDB	*
4704601	522100	3487534	1,175	1,125	1,163	312CSTL	Culberson	Y	N	TWDB	
4705401	522100	3487534	1,157	1,133	1,147	312CSTL	Culberson	Y	Y	TWDB	*
4705402	522100	3487534	1,157	1,096	1,147	310PRMN	Culberson	Y	Y	TWDB	
4705502	522100	3487534	1,116	1,092	1,111	312CSTL	Culberson	Y	Y	TWDB	*
4705501	522100	3487534	1,116	NA	1,110	312CSTL	Culberson	Y	N	TWDB	*
4704604	522100	3487534	1,164	NA	1,150	312CSTL	Culberson	Y	Y	TWDB	*
4705404	522100	3487534	1,145	1,133	1,142	312CSTL	Culberson	Y	Y	TWDB	
4705901	522100	3487534	1,086	NA	1,072	310PRMN	Culberson	Y	Y	TWDB	*
4706701	522100	3487534	1,057	NA	1,051	312CSTL	Culberson	Y	Y	TWDB	
4713102	522100	3487534	1,132	1,121	1,128	110ALVM	Culberson	Y	Y	TWDB	*
4726902	522100	3487534	1,155	1,068	NA	112SLBL	Culberson	Y	Y	TWDB	*
4725902	522100	3487534	1,229	1,227	1,094	300PLZC	Culberson	Y	Y	TWDB	*
4725901	522100	3487534	1,231	1,221	1,096	300PLZC	Culberson	Y	Y	TWDB	*
4725903	522100	3487534	1,237	1,064	1,090	300PLZC	Culberson	Y	Y	TWDB	*
4733301	522100	3487534	1,172	1,085	1,097	300PLZC	Culberson	Y	Y	TWDB	*
4734201	522100	3487534	1,110	1,096	1,096	112SLBL	Culberson	Y	Y	TWDB	*
4734106	522100	3487534	1,101	1,096	NA	112SLBL	Culberson	Y	Y	TWDB	*
4734102	522100	3487534	1,108	1,093	1,093	110ALVM	Culberson	Y	Y	TWDB	*
4734101	522100	3487534	1,096	NA	1,091	112SLBL	Culberson	Y	Y	TWDB	*
4735101	522100	3487534	1,156	1,063	1,083	112SLBL	Culberson	Y	Y	TWDB	

Table A-3.26 continued.

POD Number/ Well ID/ State Well Number	Easting	Northing	Ground Surface Elevation (m)	Elevation of Well Depth (m)	Groundwater Elevation (m)	Aquifer	County	Depth-to-Groundwater Control Point	Groundwater Surface Control Point	Source	Note
4734103	522100	3487534	1,114	1,086	1,091	112SLBL	Culberson	Y	Y	TWDB	*
4734104	522100	3487534	1,115	1,083	1,091	112SLBL	Culberson	Y	Y	TWDB	*
4734105	522100	3487534	1,117	1,053	1,086	112SLBL	Culberson	Y	Y	TWDB	*
4734301	522100	3487534	1,134	NA	1,088	112SLBL	Culberson	Y	Y	TWDB	
4734603	522100	3487534	1,122	831	1,085	313CRCX	Culberson	Y	Y	TWDB	
4734602	522100	3487534	1,123	1,031	1,092	112SLBL	Culberson	Y	Y	TWDB	*
4734401	522100	3487534	1,123	1,067	1,091	112SLBL	Culberson	Y	Y	TWDB	
4734902	522100	3487534	1,127	870	1,088	313CRCX	Culberson	Y	Y	TWDB	
4734903	522100	3487534	1,127	1,072	1,088	112SLBL	Culberson	Y	Y	TWDB	
4734901	522100	3487534	1,127	1,088	1,097	112SLBL	Culberson	Y	Y	TWDB	*
4734702	522100	3487534	1,132	NA	1,088	112SLBL	Culberson	Y	Y	TWDB	
4734701	522100	3487534	1,133	1,085	1,088	112SLBL	Culberson	Y	Y	TWDB	
4734703	522100	3487534	1,089	1,086	1,087	110ALVM	Culberson	Y	Y	TWDB	
4735701	522100	3487534	1,127	1,084	1,096	112SLBL	Culberson	Y	Y	TWDB	*
4737802	522100	3487534	1,316	1,298	1,304	312CSTL	Culberson	Y	Y	TWDB	
4743204	522100	3487534	1,199	1,033	NA	112SLBL	Culberson	Y	Y	TWDB	
4742101	522100	3487534	1,140	NA	1,089	112SLBL	Culberson	Y	Y	TWDB	*
4745104	522100	3487534	1,386	1,374	1,382	310PRMN	Culberson	Y	Y	TWDB	
4746101	522100	3487534	1,267	1,145	1,227	312RSLR	Culberson	Y	Y	TWDB	*
4743201	522100	3487534	1,165	NA	1,084	112SBDM	Culberson	Y	Y	TWDB	
4742201	522100	3487534	1,095	1,086	1,088	112SLBL	Culberson	Y	Y	TWDB	
4742203	522100	3487534	1,143	NA	1,084	112SLBL	Culberson	Y	Y	TWDB	
4742202	522100	3487534	1,142	1,095	NA	112SLBL	Culberson	Y	Y	TWDB	*
4743101	522100	3487534	1,122	1,082	1,101	112SLBL	Culberson	Y	N	TWDB	*
4745101	522100	3487534	1,355	1,336	1,339	310PRMN	Culberson	Y	Y	TWDB	*
4743202	522100	3487534	1,154	986	1,079	112SBDM	Culberson	Y	Y	TWDB	
4743203	522100	3487534	1,146	1,055	1,082	112SBDM	Culberson	Y	Y	TWDB	*
4743504	522100	3487534	1,149	NA	1,078	112SLBL	Culberson	Y	Y	TWDB	

Table A-3.26 continued.

POD Number/ Well ID/ State Well Number	Easting	Northing	Ground Surface Elevation (m)	Elevation of Well Depth (m)	Groundwater Elevation (m)	Aquifer	County	Depth-to-Groundwater Control Point	Groundwater Surface Control Point	Source	Note
4743505	522100	3487534	1,146	NA	1,090	112SLBL	Culberson	Y	Y	TWDB	
4743503	522100	3487534	1,156	980	1,077	313DLRM	Culberson	Y	Y	TWDB	*
4742401	522100	3487534	1,127	1,082	1,087	310PRMN	Culberson	Y	Y	TWDB	
4745504	522100	3487534	1,310	1,292	1,300	313CRCX	Culberson	Y	Y	TWDB	*
4745501	522100	3487534	1,305	1,301	1,302	313CRCX	Culberson	Y	Y	TWDB	*
4743502	522100	3487534	1,135	1,077	1,087	112SLBL	Culberson	Y	Y	TWDB	
4742403	522100	3487534	1,270	1,144	1,154	318BSPG	Culberson	Y	Y	TWDB	*
4745603	522100	3487534	1,273	1,254	1,261	313CRCX	Culberson	Y	Y	TWDB	*
4743601	522100	3487534	1,169	1,062	1,079	313CRCX	Culberson	Y	Y	TWDB	*
4744702	522100	3487534	1,219	1,052	1,066	313CRCX	Culberson	Y	Y	TWDB	
4742701	522100	3487534	1,161	NA	1,087	318BSPG	Culberson	Y	Y	TWDB	*
4743702	522100	3487534	1,117	1,069	1,081	112SLBL	Culberson	Y	Y	TWDB	*
4743802	522100	3487534	1,126	NA	1,081	112SLBL	Culberson	Y	Y	TWDB	*
4742901	522100	3487534	1,183	1,037	1,083	318BSPG	Culberson	Y	Y	TWDB	
4745802	522100	3487534	1,260	-347	1,073	367ELBG	Culberson	Y	Y	TWDB	*
4745803	522100	3487534	1,260	NA	1,073	UNKNOWN	Culberson	Y	Y	TWDB	
4743801	522100	3487534	1,127	1,068	1,084	112SLBL	Culberson	Y	Y	TWDB	*
4743701	522100	3487534	1,125	1,073	1,082	112SLBL	Culberson	Y	Y	TWDB	
4744701	522100	3487534	1,186	1,075	1,079	313CRCX	Culberson	Y	Y	TWDB	*
4751301	522100	3487534	1,120	1,074	1,096	112SLBL	Culberson	Y	Y	TWDB	*
4752101	522100	3487534	1,162	1,055	1,074	313CRCX	Culberson	Y	Y	TWDB	*
4752201	522100	3487534	1,286	1,051	1,081	313CRCX	Culberson	Y	Y	TWDB	
4752301	522100	3487534	1,388	866	1,079	313CRCX	Culberson	Y	Y	TWDB	
4752601	522100	3487534	1,396	963	1,076	313CRCX	Culberson	Y	Y	TWDB	
4752602	522100	3487534	1,402	929	1,078	313CRCX	Culberson	Y	Y	TWDB	
4753401	522100	3487534	1,543	933	1,072	313CRCX	Culberson	Y	Y	TWDB	
4726901	522074	3487503	1,155	1,091	1,093	112SLBL	Culberson	Y	Y	TWDB	
4728901	546770	3485276	1,376	NA	1,362	110ALVM	Culberson	Y	Y	TWDB	

Table A-3.26 continued.

POD Number/ Well ID/ State Well Number	Easting	Northing	Ground Surface Elevation (m)	Elevation of Well Depth (m)	Groundwater Elevation (m)	Aquifer	County	Depth-to-Groundwater Control Point	Groundwater Surface Control Point	Source	Note
4727701	526853	3485267	1,222	1,067	1,085	112SLBL	Culberson	Y	Y	TWDB	*
4836101	441569	3484996	1,548	NA	1,426	210CRCS	Hudspeth	Y	Y	TWDB	
4838101	465152	3484613	1,324	NA	1,275	210CRCS	Hudspeth	Y	Y	TWDB	*
4836301	450425	3483318	1,447	NA	1,323	210CRCS	Hudspeth	Y	N	TWDB	*
4836201	446803	3481950	1,488	NA	1,366	210CRCS	Hudspeth	Y	Y	TWDB	
4839101	478917	3481898	1,331	NA	1,043	210CRCS	Hudspeth	Y	Y	TWDB	*
4837302	463558	3481540	1,345	1,267	1,281	210CRCS	Hudspeth	Y	Y	TWDB	
4837301	460600	3480719	1,358	1,324	1,336	210CRCS	Hudspeth	Y	Y	TWDB	
4836601	451895	3475984	1,454	1,289	1,347	210CRCS	Hudspeth	Y	Y	TWDB	
4835702	431327	3475975	1,289	1,070	1,109	210CRCS	Hudspeth	Y	Y	TWDB	
4836801	444895	3475403	1,569	1,359	1,378	210CRCS	Hudspeth	Y	Y	TWDB	
4835701	430974	3474592	1,275	1,113	1,129	112HCBL	Hudspeth	Y	Y	TWDB	*
4834802	422048	3474532	1,180	NA	1,137	112HCBL	Hudspeth	Y	Y	TWDB	
4834903	427775	3474121	1,250	1,024	1,135	112HCBL	Hudspeth	Y	Y	TWDB	
4834902	427775	3474090	1,250	1,064	1,140	112HCBL	Hudspeth	Y	Y	TWDB	*
4835801	435295	3472994	1,313	1,089	1,119	210CRCS	Hudspeth	Y	Y	TWDB	
4833901	415486	3472982	1,183	1,071	1,083	210CRCS	Hudspeth	Y	Y	TWDB	*
4838703	467251	3472568	1,376	1,091	1,104	210CRCS	Hudspeth	Y	Y	TWDB	
4835901	437956	3471901	1,316	1,256	1,293	210CRCS	Hudspeth	Y	Y	TWDB	*
4842101	419379	3470919	1,184	1,047	1,082	112HCBL	Hudspeth	Y	Y	TWDB	*
4843101	431268	3467016	1,233	1,104	1,136	210CRCS	Hudspeth	Y	Y	TWDB	*
4846301	472730	3466888	1,466	1,101	1,106	210CRCS	Hudspeth	Y	Y	TWDB	*
4842501	422168	3465910	1,149	1,058	1,088	112HCBL	Hudspeth	Y	Y	TWDB	*
4846401	467122	3465241	1,424	1,091	1,107	210CRCS	Hudspeth	Y	Y	TWDB	
4843501	433052	3465065	1,222	NA	1,133	210CRCS	Hudspeth	Y	Y	TWDB	
4842404	418354	3464861	1,100	1,019	1,073	112HCBL	Hudspeth	Y	Y	TWDB	
4845601	461488	3463937	1,402	1,091	1,114	210CRCS	Hudspeth	Y	Y	TWDB	
4845602	461275	3463507	1,392	1,039	1,109	210CRCS	Hudspeth	Y	Y	TWDB	

Table A-3.26 continued.

POD Number/ Well ID/ State Well Number	Easting	Northing	Ground Surface Elevation (m)	Elevation of Well Depth (m)	Groundwater Elevation (m)	Aquifer	County	Depth-to-Groundwater Control Point	Groundwater Surface Control Point	Source	Note
4845603	462171	3462826	1,398	1,063	1,106	210CRCS	Hudspeth	Y	Y	TWDB	*
4845604	461271	3462460	1,405	1,097	1,107	210CRCS	Hudspeth	Y	Y	TWDB	*
4845901	463009	3460545	1,444	1,100	1,105	210CRCS	Hudspeth	Y	Y	TWDB	*
4844901	449971	3460137	1,278	1,096	1,206	210CRCS	Hudspeth	Y	Y	TWDB	
4846701	466735	3459917	1,408	1,061	1,067	210CRCS	Hudspeth	Y	Y	TWDB	*
4854201	469980	3457259	1,377	1,088	1,108	210CRCS	Hudspeth	Y	Y	TWDB	*
4850202	424507	3456656	1,089	1,058	1,070	111RGRD	Hudspeth	Y	Y	TWDB	
4850304	424586	3456594	1,088	1,058	1,075	111RGRD	Hudspeth	Y	Y	TWDB	*
4854202	470267	3455904	1,372	1,096	1,097	210CRCS	Hudspeth	Y	Y	TWDB	
4853101	453434	3453779	1,385	1,109	1,239	210CRCS	Hudspeth	Y	Y	TWDB	*
4853104	452424	3452952	1,402	1,299	1,334	110AVTV	Hudspeth	Y	Y	TWDB	
4853503	458561	3452341	1,433	1,236	1,295	210CRCS	Hudspeth	Y	Y	TWDB	*
4752402	539007	3451655	1,158	946	1,081	313CPTN	Culberson	Y	Y	TWDB	*
4853504	459562	3451168	1,415	1,266	1,273	210CRCS	Hudspeth	Y	Y	TWDB	
4853501	459376	3450891	1,419	1,081	1,307	210CRCS	Hudspeth	Y	Y	TWDB	*
4853502	459455	3450891	1,418	1,256	1,313	210CRCS	Hudspeth	Y	N	TWDB	*
4854401	466255	3450405	1,399	1,063	1,105	210CRCS	Hudspeth	Y	Y	TWDB	*
4853403	452995	3450333	1,462	1,401	1,437	120IVIG	Hudspeth	Y	Y	TWDB	*
4853402	453048	3450333	1,461	1,433	1,445	120IVIG	Hudspeth	Y	Y	TWDB	*
4751401	523979	3450101	1,147	1,077	1,082	112SLBL	Culberson	Y	Y	TWDB	
4854410	465089	3449793	1,382	1,008	1,117	210CRCS	Hudspeth	Y	Y	TWDB	*
4854502	471070	3449436	1,344	1,054	1,106	210CRCS	Hudspeth	Y	Y	TWDB	*
4854402	465616	3449114	1,382	1,092	1,101	210CRCS	Hudspeth	Y	Y	TWDB	*
4851601	437052	3448877	1,100	1,077	1,091	112HCBL	Hudspeth	Y	Y	TWDB	*
4854406	466780	3448864	1,368	1,033	1,109	210CRCS	Hudspeth	Y	Y	TWDB	*
4854404	467070	3448525	1,365	1,073	1,118	210CRCS	Hudspeth	Y	Y	TWDB	*
4854405	467070	3448494	1,365	1,073	1,119	210CRCS	Hudspeth	Y	Y	TWDB	*
4854503	468896	3448211	1,356	945	1,108	210CRCS	Hudspeth	Y	Y	TWDB	*

Table A-3.26 continued.

POD Number/ Well ID/ State Well Number	Easting	Northing	Ground Surface Elevation (m)	Elevation of Well Depth (m)	Groundwater Elevation (m)	Aquifer	County	Depth-to-Groundwater Control Point	Groundwater Surface Control Point	Source	Note
4856501	493938	3448198	1,455	1,418	1,435	400PCMB	Hudspeth	Y	Y	TWDB	
4855902	487823	3448049	1,418	1,360	1,372	400PCMB	Hudspeth	Y	Y	TWDB	*
4856804	494229	3447951	1,461	1,433	1,435	400PCMB	Hudspeth	Y	Y	TWDB	*
4751714	524117	3447762	1,156	NA	1,098	112SLBL	Culberson	Y	N	TWDB	*
4855901	487743	3447526	1,415	1,294	1,352	400PCMB	Hudspeth	Y	Y	TWDB	*
4853804	458142	3446802	1,419	1,124	1,308	210CRCS	Hudspeth	Y	N	TWDB	*
4856803	494890	3446781	1,451	1,411	1,428	400PCMB	Hudspeth	Y	Y	TWDB	
4854901	473868	3446505	1,336	985	1,096	210CRCS	Hudspeth	Y	Y	TWDB	*
4853803	457901	3446064	1,428	1,319	1,364	210CRCS	Hudspeth	Y	Y	TWDB	
4853902	460733	3445930	1,415	1,335	1,350	210CRCS	Hudspeth	Y	Y	TWDB	*
4854902	475005	3445701	1,334	1,080	1,106	210CRCS	Hudspeth	Y	Y	TWDB	
4853802	457926	3445602	1,431	1,344	1,374	210CRCS	Hudspeth	Y	Y	TWDB	
4853805	457925	3445571	1,432	1,341	1,364	210CRCS	Hudspeth	Y	Y	TWDB	
4853801	457898	3445417	1,438	1,383	1,387	210CRCS	Hudspeth	Y	Y	TWDB	*
4856802	493089	3445397	1,418	1,362	1,398	400PCMB	Hudspeth	Y	Y	TWDB	*
4856805	493116	3445397	1,418	NA	1,401	400PCMB	Hudspeth	Y	Y	TWDB	
4751717	524387	3445361	1,148	689	1,075	112SBCR	Culberson	Y	Y	TWDB	
4854904	475771	3445115	1,329	1,049	1,106	210CRCS	Hudspeth	Y	Y	TWDB	*
4854903	472831	3444722	1,327	1,077	1,106	210CRCS	Hudspeth	Y	Y	TWDB	
4854701	468038	3444673	1,368	1,087	1,092	210CRCS	Hudspeth	Y	Y	TWDB	*
4750901	523463	3444436	1,154	707	1,074	112SBCR	Culberson	Y	Y	TWDB	
4863303	485249	3443435	1,442	1,378	1,393	400PCMB	Hudspeth	Y	Y	TWDB	*
4861101	453997	3443401	1,535	1,400	1,453	120IVIG	Hudspeth	Y	Y	TWDB	*
4758203	518406	3443317	1,243	1,054	1,078	UNKNOWN	Culberson	Y	Y	TWDB	*
4758305	522803	3443264	1,158	737	1,076	112SBCR	Culberson	Y	Y	TWDB	
4861104	453334	3443127	1,589	1,436	1,442	120IVIG	Hudspeth	Y	Y	TWDB	*
4861103	453439	3442911	1,574	1,445	1,448	120IVIG	Hudspeth	Y	Y	TWDB	*
4859305	439242	3442891	1,062	902	1,055	111RGRD	Hudspeth	Y	Y	TWDB	

Table A-3.26 continued.

809

POD Number/ Well ID/ State Well Number	Easting	Northing	Ground Surface Elevation (m)	Elevation of Well Depth (m)	Groundwater Elevation (m)	Aquifer	County	Depth-to-Groundwater Control Point	Groundwater Surface Control Point	Source	Note
4863302	487022	3442478	1,374	1,191	1,266	400PCMB	Hudspeth	Y	Y	TWDB	*
4859303	438444	3442403	1,058	1,034	1,056	111RGRD	Hudspeth	Y	Y	TWDB	
4759105	525957	3442256	1,149	962	1,082	112SLBL	Culberson	Y	Y	TWDB	
4862301	474520	3442193	1,316	1,015	1,113	210CRCS	Hudspeth	Y	Y	TWDB	
4758306	520634	3442121	1,177	727	1,076	112SBCR	Culberson	Y	Y	TWDB	
4758204	517217	3442022	1,253	1,044	1,051	UNKNOWN	Culberson	Y	Y	TWDB	*
4759110	525164	3441638	1,153	787	1,071	112SLBL	Culberson	Y	Y	TWDB	
4758202	518410	3441563	1,222	874	1,075	112SBCR	Culberson	Y	Y	TWDB	*
4759104	526171	3441548	1,151	950	1,078	112SLBL	Culberson	Y	Y	TWDB	
4864301	499550	3441547	1,426	1,365	1,379	400PCMB	Hudspeth	Y	Y	TWDB	
4758301	521933	3441385	1,169	893	1,081	112SLBL	Culberson	Y	Y	TWDB	
4864302	496451	3441209	1,390	1,331	1,342	400PCMB	Hudspeth	Y	Y	TWDB	*
4759116	524132	3441020	1,158	783	1,073	112SBCR	Culberson	Y	Y	TWDB	
4758310	522808	3440955	1,166	735	1,076	112SBCR	Culberson	Y	Y	TWDB	
4758304	520980	3440829	1,180	960	1,080	112SLBL	Culberson	Y	Y	TWDB	*
4863101	478808	3440706	1,303	1,041	1,105	210CRCS	Hudspeth	Y	Y	TWDB	*
4864201	494728	3440593	1,373	1,304	1,329	400PCMB	Hudspeth	Y	Y	TWDB	*
4862101	468131	3440579	1,394	1,013	1,137	210CRCS	Hudspeth	Y	Y	TWDB	
4759102	527208	3440104	1,155	989	1,078	112SBCR	Culberson	Y	Y	TWDB	*
4759111	526757	3440103	1,155	989	1,077	112SLBL	Culberson	Y	Y	TWDB	*
4758303	521008	3440090	1,183	958	1,080	112SLBL	Culberson	Y	Y	TWDB	
4861201	459439	3439900	1,333	1,123	1,169	210CRCS	Hudspeth	Y	Y	TWDB	*
4759118	526096	3439855	1,156	815	1,074	112SBCR	Culberson	Y	Y	TWDB	
4759117	524824	3439852	1,159	842	1,073	112SBCR	Culberson	Y	Y	TWDB	
4860101	441661	3439645	1,055	1,029	1,052	111RGRD	Hudspeth	Y	Y	TWDB	
4758302	521010	3439259	1,189	969	1,081	112SLBL	Culberson	Y	Y	TWDB	*
4758201	518281	3439253	1,215	1,011	1,078	112SBCR	Culberson	Y	Y	TWDB	*
4759103	527713	3439120	1,156	866	1,084	112SBCR	Culberson	Y	Y	TWDB	

Table A-3.26 continued.

POD Number/ Well ID/ State Well Number	Easting	Northing	Ground Surface Elevation (m)	Elevation of Well Depth (m)	Groundwater Elevation (m)	Aquifer	County	Depth-to-Groundwater Control Point	Groundwater Surface Control Point	Source	Note
4861302	463013	3438933	1,305	1,079	1,176	112RLBL	Hudspeth	Y	Y	TWDB	*
4759403	524085	3438772	1,167	746	1,075	112SBCR	Culberson	Y	Y	TWDB	
4758606	522760	3438739	1,175	744	1,076	112SBCR	Culberson	Y	Y	TWDB	
4759404	525409	3438714	1,161	893	1,073	112SBCR	Culberson	Y	Y	TWDB	
4758605	521488	3438705	1,186	764	1,077	112SBCR	Culberson	Y	Y	TWDB	
4864601	497933	3438622	1,376	1,322	1,323	400PCMB	Hudspeth	Y	Y	TWDB	*
4863601	487097	3438568	1,339	1,068	1,126	210CRCS	Hudspeth	Y	Y	TWDB	*
4758601	521065	3438427	1,191	970	1,080	112SLBL	Culberson	Y	Y	TWDB	
4864605	499762	3438345	1,388	1,317	1,336	400PCMB	Hudspeth	Y	Y	TWDB	*
4864604	497774	3438099	1,369	1,302	1,319	112EFBL	Hudspeth	Y	Y	TWDB	*
4864603	497801	3438068	1,370	1,302	1,319	112EFBL	Hudspeth	Y	Y	TWDB	*
4864602	499497	3438068	1,384	1,311	1,326	400PCMB	Hudspeth	Y	Y	TWDB	
4759405	526842	3437917	1,160	NA	1,075	112SBCR	Culberson	Y	Y	TWDB	
4860401	443002	3437759	1,053	1,032	1,050	111RGRD	Hudspeth	Y	Y	TWDB	
4757401	500663	3437298	1,380	1,302	1,348	110ALVM	Hudspeth	Y	Y	TWDB	*
4757403	500689	3437267	1,380	1,346	1,348	110ALVM	Hudspeth	Y	Y	TWDB	*
4864501	494700	3436930	1,338	1,193	1,268	112EFBL	Hudspeth	Y	Y	TWDB	*
4864502	492077	3436901	1,330	995	1,118	112EFBL	Hudspeth	Y	Y	TWDB	*
4758608	519849	3436855	1,206	898	1,084	112SLBL	Culberson	Y	Y	TWDB	*
4759402	525070	3436435	1,168	1,025	1,078	112SBCR	Culberson	Y	Y	TWDB	*
4758607	519850	3436085	1,206	901	1,077	112SLBL	Culberson	Y	Y	TWDB	*
4757502	504320	3435514	1,404	1,380	1,398	110ALVM	Hudspeth	Y	Y	TWDB	*
4759401	526638	3434838	1,190	1,068	1,081	210CRCS	Culberson	Y	Y	TWDB	
4757501	506043	3434837	1,380	1,258	1,348	400PCMB	Hudspeth	Y	Y	TWDB	*
4758602	520621	3434732	1,196	998	1,078	112SLBL	Culberson	Y	Y	TWDB	
4758504	515983	3434694	1,238	1,059	1,086	112SLBL	Culberson	Y	Y	TWDB	
4758506	515983	3434694	1,238	992	1,085	112SLBL	Culberson	N	Y	TWDB	*
4759503	528838	3434690	1,187	979	1,076	318VCPK	Culberson	Y	Y	TWDB	

Table A-3.26 continued.

POD Number/ Well ID/ State Well Number	Easting	Northing	Ground Surface Elevation (m)	Elevation of Well Depth (m)	Groundwater Elevation (m)	Aquifer	County	Depth-to-Groundwater Control Point	Groundwater Surface Control Point	Source	Note
4758503	515983	3434447	1,236	1,053	1,084	112SLBL	Culberson	Y	Y	TWDB	
4758502	516646	3434356	1,232	1,048	1,086	112SLBL	Culberson	Y	Y	TWDB	*
4758501	516461	3434356	1,233	1,052	1,089	112SLBL	Culberson	Y	Y	TWDB	
4758505	516885	3434295	1,228	992	1,083	112SLBL	Culberson	Y	Y	TWDB	
4862807	468271	3434206	1,248	1,097	1,115	112RLBL	Hudspeth	Y	Y	TWDB	*
4757904	510417	3434194	1,300	1,273	1,288	400PCMB	Culberson	Y	Y	TWDB	
4757903	509490	3434070	1,321	1,297	1,300	400PCMB	Culberson	Y	Y	TWDB	
4862701	467263	3433932	1,254	1,094	1,118	112RLBL	Hudspeth	Y	Y	TWDB	*
4861901	463446	3433913	1,335	1,247	1,277	210CRCS	Hudspeth	Y	Y	TWDB	*
4757702	500689	3433881	1,364	1,339	1,350	110ALVM	Hudspeth	Y	Y	TWDB	*
4757701	500663	3433850	1,364	NA	1,349	110ALVM	Hudspeth	Y	Y	TWDB	*
4757704	500636	3433850	1,363	1,315	1,350	100ALVM	Hudspeth	Y	N	TWDB	*
4757703	502174	3433450	1,394	1,339	1,379	400PCMB	Hudspeth	Y	Y	TWDB	*
4758901	521711	3433257	1,183	1,083	1,141	112SLBL	Culberson	Y	Y	TWDB	
4757802	505090	3433082	1,428	1,426	1,428	400PCMB	Hudspeth	Y	Y	TWDB	*
4757902	508510	3433053	1,335	1,274	1,322	400PCMB	Hudspeth	Y	Y	TWDB	*
4757801	504242	3432989	1,397	1,348	1,388	400PCMB	Hudspeth	Y	Y	TWDB	*
4758902	521156	3432486	1,183	1,051	1,077	112SLBL	Culberson	Y	Y	TWDB	
4758703	512779	3431672	1,255	1,035	1,084	112SLBL	Culberson	Y	Y	TWDB	
4862801	470754	3431151	1,223	1,041	1,125	112RLBL	Hudspeth	Y	Y	TWDB	*
4862806	469959	3431091	1,230	1,099	1,113	210CRCS	Hudspeth	Y	Y	TWDB	*
4863902	487220	3430964	1,450	1,377	1,381	112EFBL	Hudspeth	Y	Y	TWDB	*
4862802	471019	3430873	1,221	1,056	1,110	112RLBL	Hudspeth	Y	Y	TWDB	
4862803	470912	3430750	1,222	1,058	1,111	112RLBL	Hudspeth	Y	Y	TWDB	*
4862804	471310	3430657	1,220	1,055	1,112	112RLBL	Hudspeth	Y	Y	TWDB	*
4757803	507716	3430621	1,342	1,239	1,326	400PCMB	Hudspeth	Y	Y	TWDB	*
4864901	498330	3430526	1,302	997	1,116	112EFBL	Hudspeth	Y	Y	TWDB	*
4864903	498356	3430526	1,302	NA	1,113	112EFBL	Hudspeth	Y	Y	TWDB	*

Table A-3.26 continued.

POD Number/ Well ID/ State Well Number	Easting	Northing	Ground Surface Elevation (m)	Elevation of Well Depth (m)	Groundwater Elevation (m)	Aquifer	County	Depth-to-Groundwater Control Point	Groundwater Surface Control Point	Source	Note
4864902	498356	3430495	1,302	997	1,116	112EFBL	Hudspeth	Y	Y	TWDB	*
4758702	514744	3430012	1,222	1,039	1,084	112SLBL	Culberson	Y	Y	TWDB	
4758701	515036	3429890	1,219	1,045	1,090	112SLBL	Culberson	Y	Y	TWDB	
4863802	481332	3429865	1,314	1,276	1,277	210CRCS	Hudspeth	Y	Y	TWDB	*
4863803	483983	3429676	1,382	1,317	1,375	210CRCS	Hudspeth	Y	Y	TWDB	*

Table A-3.26 continued.

Aquifer Key: 100ALVM = Alluvium, 110ALVM = Quaternary Alluvium, 110AVPS = Alluvium and Permian System, 110AVTV = Alluvium and Tertiary Volcanics, 111RGRD = Rio Grande Alluvium, 112EFBL = Eagle Flat Bolson, 112HCBL = Hueco Bolson, 112RLBL = Red Light Draw Bolson, 112SBCR = Salt Bolson and Cretaceous Rocks, 112SBCRC = Salt Bolson and Capitan Reef Complex, 112SBDM = Salt Bolson and Delaware Mountain Group, 112SLBL = Salt Bolson, 120BLSN = Bolson Deposits, 120IVIG = Intrusive Rocks, 210CRCS = Cretaceous System, 300PLZC = Paleozoic Erathem, 310PRMN = Permian System, 312CSTL = Castile Gypsum, 312RSLR = Rustler Formation, 313CPTN = Capitan Limestone, 313CRCX = Capitan Reef Complex and Associated Limestones, 313CRDM = Capitan Reef Complex - Delaware Mountain Group, 313DLRM = Delaware Mountain Formation or Group, 313DMBS = Delaware Mountain Group - Bone Spring Limestone, 318BSPG = Bone Spring Limestone, 318BSVP = Bone Spring and Victorio Peak Limestones, 318VCPK = Victorio Peak Limestone, 367ELBG = Ellenburger Group, 400PCMB = Precambrian Erathem, NA = Not applicable, UNKOWN = Unknown.
Depth-to-Groundwater Control Point Key: Y = Yes, N = No.
Groundwater Surface Control Point Key: Y = Yes, N = No.
Source Key: NMOSE = New Mexico Office of the State Engineer's New Mexico Water Rights Reporting System online database, SMHS = New Mexico Bureau of Geology & Mineral Resources' Sacramento Mountains Hydrogeology Study, TWDB = Texas Water Development Board groundwater database.
Note Key: * = One water level measurement.

Groundwater Well ID/ State Well Number	Location	State	Min. K (m/day)	Max. K (m/day)	Average K (m/day)	Median K (m/day)	Aquifer	Method	Source
NA	NA	NA	NA	NA	One to two orders of magnitude higher than Permian basin facies strata.	NA	Capitan Reef Complex	NA	Hiss (1980)
NA	Mescalero Apache Indian Reservation	NM	2.2E-03	1.1E-02	6.0E-03	NA	Yeso Fm. (unfractured siltstone and gypsum)	AT	Wasiolek (1991)
NA	Mescalero Apache Indian Reservation	NM	1.8E-01	4.6E-01	NA	NA	Yeso Fm. (fractured limestone)	AT	Wasiolek (1991)

Table A-3.27: Published values of hydraulic conductivity [K] for the Salt Basin region.

Method Key: AT = Aquifer test.

Groundwater Well ID/ State Well Number	Location	State	Min. T (m^2/day)	Max. T (m^2/day)	Average T (m^2/day)	Median T (m^2/day)	Aquifer	Method	Source
NA	Beacon Hill area	TX	NA	NA	5.0E+02	NA	Capitan Limestone	CSC	Gates et al. (1980)
NA	Beacon Hill area	TX	NA	NA	1.5E+03	NA	Capitan Limestone	AT	Gates et al. (1980)
NA	Mescalero Apache Indian Reservation	NM	3.3E-01	1.7E+00	NA	NA	Yeso Fm. (unfractured siltstone and gypsum)	AT	Wasiolek (1991)
NA	Mescalero Apache Indian Reservation	NM	4.2E+01	8.6E+01	NA	NA	Yeso Fm. (fractured limestone)	AT	Wasiolek (1991)
4 data points	Northeast Diablo Plateau, according to George et al. (2005)	TX	2.97E-02	2.13E+01	NA	1.07E+01	Permian Rocks on the Diablo Plateau	AT	Mayer (1995), referenced from Kreitler et al. (1987)
2 data points	Otero Mesa/ Diablo Plateau	TX	4.44E+03	4.83E+03	NA	4.64E+03	Otero Mesa/ Diablo Plateau aquifer	AT	Mayer (1995), referenced from Logan (1984)
4709207	Salt Flat	TX	NA	NA	7.4E+03	NA	Capitan Reef Complex and Associated Limestones	CSC	Angle (2001)
4717218	Salt Flat	TX	NA	NA	2.3E+02	NA	Salt Bolson	CSC	Angle (2001)
4717317	Salt Flat	TX	NA	NA	1.0E+03	NA	Capitan Reef Complex and Associated Limestones	AT	Angle (2001)
4717321	Salt Flat	TX	NA	NA	4.2E+03	NA	Salt Bolson and Capitan Reef Complex	CSC	Angle (2001)
4717903	Salt Flat	TX	NA	NA	1.3E+02	NA	Capitan Limestone	AT	Angle (2001)
4718402	Salt Flat	TX	NA	NA	3.7E+01	NA	Delaware Mountain Group	AT	Angle (2001)
4718404	Salt Flat	TX	NA	NA	4.6E+01	NA	Salt Bolson and Delaware Mountain Group	CSC	Angle (2001)

Table A-3.28: Published values of transmissivity [T] for the Salt Basin region. Key at bottom of table.

Groundwater Well ID/ State Well Number	Location	State	Min. T (m²/day)	Max. T (m²/day)	Average T (m²/day)	Median T (m²/day)	Aquifer	Method	Source
4718707	Salt Flat	TX	NA	NA	4.0E+02	NA	Salt Bolson and Delaware Mountain Group	CSC	Angle (2001)
4734902	Wild Horse Flat	TX	NA	NA	9.3E+02	NA	Capitan Reef Complex and Associated Limestones	AT	Angle (2001)
4743503	Wild Horse Flat	TX	NA	NA	1.0E+02	NA	Delaware Mountain Group	CSC	Angle (2001)
4751403	Wild Horse Flat	TX	NA	NA	1.8E+03	NA	Salt Bolson and Permian Rocks	AT	Angle (2001)
4751807	Wild Horse Flat	TX	NA	NA	3.8E+02	NA	Salt Bolson	CSC	Angle (2001)
4752301	Wild Horse Flat	TX	NA	NA	4.6E+01	NA	Capitan Reef Complex and Associated Limestones	CSC	Angle (2001)
4752601	Wild Horse Flat	TX	NA	NA	1.0E+03	NA	Capitan Reef Complex and Associated Limestones	CSC	Angle (2001)
4752602	Wild Horse Flat	TX	NA	NA	1.9E+02	NA	Capitan Reef Complex and Associated Limestones	AT	Angle (2001)
4758502	Wild Horse Flat	TX	NA	NA	8.4E+01	NA	Salt Bolson	CSC	Angle (2001)
4758505	Wild Horse Flat	TX	NA	NA	1.5E+02	NA	Salt Bolson	CSC	Angle (2001)
4758602	Wild Horse Flat	TX	NA	NA	4.6E+02	NA	Salt Bolson	AT	Angle (2001)
4758602	Wild Horse Flat	TX	NA	NA	5.9E+02	NA	Salt Bolson	AT	Angle (2001)
4759102	Wild Horse Flat	TX	NA	NA	5.6E+02	NA	Salt Bolson and Cretaceous Rocks	AT	Angle (2001)
4759209	Wild Horse Flat	TX	NA	NA	2.4E+02	NA	Cretaceous System	AT	Angle (2001)
4759307	Michigan Flat	TX	NA	NA	1.8E+02	NA	Salt Bolson and Cretaceous Rocks	AT	Angle (2001)
4759603	Michigan Flat	TX	NA	NA	1.9E+02	NA	Cretaceous System	CSC	Angle (2001)

Table A-3.28 continued.

Groundwater Well ID/ State Well Number	Location	State	Min. T (m²/day)	Max. T (m²/day)	Average T (m²/day)	Median T (m²/day)	Aquifer	Method	Source
4760404	Michigan Flat	TX	NA	NA	9.3E+01	NA	Salt Bolson	CSC	Angle (2001)
4760601	Michigan Flat	TX	NA	NA	2.8E+00	NA	Permian System	CSC	Angle (2001)
5102906	Lobo Flat	TX	NA	NA	8.0E+02	NA	Salt Bolson	CSC	Angle (2001)
5102918	Lobo Flat	TX	NA	NA	1.0E+02	NA	Salt Bolson	CSC	Angle (2001)
5102923	Lobo Flat	TX	NA	NA	4.6E+02	NA	Salt Bolson	CSC	Angle (2001)
5102926	Lobo Flat	TX	NA	NA	2.3E+02	NA	Salt Bolson	AT	Angle (2001)
5103702	Lobo Flat	TX	NA	NA	5.9E+02	NA	Salt Bolson	CSC	Angle (2001)
5103703	Lobo Flat	TX	NA	NA	4.6E+01	NA	Salt Bolson	CSC	Angle (2001)
5110306	Lobo Flat	TX	NA	NA	1.4E+02	NA	Salt Bolson	CSC	Angle (2001)
5110309	Lobo Flat	TX	NA	NA	5.4E+02	NA	Alluvium and Tertiary Volcanics	CSC	Angle (2001)
5110316	Lobo Flat	TX	NA	NA	4.7E+02	NA	Salt Bolson	CSC	Angle (2001)
5110317	Lobo Flat	TX	NA	NA	2.2E+02	NA	Alluvium and Tertiary Volcanics	CSC	Angle (2001)
5110321	Lobo Flat	TX	NA	NA	6.4E+02	NA	Salt Bolson	CSC	Angle (2001)
5110322	Lobo Flat	TX	NA	NA	1.9E+02	NA	Salt Bolson	CSC	Angle (2001)
5110328	Lobo Flat	TX	NA	NA	4.5E+02	NA	Salt Bolson	CSC	Angle (2001)
5110331	Lobo Flat	TX	NA	NA	3.9E+02	NA	Alluvium and Tertiary Volcanics	CSC	Angle (2001)
5110332	Lobo Flat	TX	NA	NA	4.4E+02	NA	Salt Bolson	CSC	Angle (2001)
5110603	Lobo Flat	TX	NA	NA	2.8E+02	NA	Salt Bolson	AT	Angle (2001)
5110603	Lobo Flat	TX	NA	NA	2.2E+02	NA	Salt Bolson	CSC	Angle (2001)
5110624	Lobo Flat	TX	NA	NA	3.5E+01	NA	Salt Bolson	CSC	Angle (2001)
5111105	Lobo Flat	TX	NA	NA	3.2E+02	NA	Salt Bolson	CSC	Angle (2001)
5111106	Lobo Flat	TX	NA	NA	1.5E+02	NA	Salt Bolson	CSC	Angle (2001)
5114501	Lobo Flat	TX	NA	NA	6.5E+00	NA	Volcanics	CSC	Angle (2001)
5119104	Lobo Flat	TX	NA	NA	2.8E+02	NA	Salt Bolson	CSC	Angle (2001)
5119301	Lobo Flat	TX	NA	NA	4.8E+02	NA	Salt Bolson	CSC	Angle (2001)
5120403	Lobo Flat	TX	NA	NA	7.4E+01	NA	Salt Bolson	CSC	Angle (2001)
5120404	Lobo Flat	TX	NA	NA	1.6E+02	NA	Salt Bolson	CSC	Angle (2001)
5127302	Ryan Flat	TX	NA	NA	8.5E+01	NA	Volcanics	CSC	Angle (2001)
5128303	Ryan Flat	TX	NA	NA	1.8E+02	NA	Salt Bolson	CSC	Angle (2001)
5128606	Ryan Flat	TX	NA	NA	1.1E+02	NA	Salt Bolson	CSC	Angle (2001)
5129104	Ryan Flat	TX	NA	NA	2.8E+00	NA	Salt Bolson	CSC	Angle (2001)
5129105	Ryan Flat	TX	NA	NA	2.1E+01	NA	Salt Bolson	CSC	Angle (2001)

Table A-3.28 continued.

817

Groundwater Well ID/ State Well Number	Location	State	Min. T (m²/day)	Max. T (m²/day)	Average T (m²/day)	Median T (m²/day)	Aquifer	Method	Source
5129403	Ryan Flat	TX	NA	NA	1.9E+02	NA	Salt Bolson	CSC	Angle (2001)
5128404	Ryan Flat	TX	NA	NA	5.1E+02	NA	Salt Bolson	CSC	Angle (2001)
5128406	Ryan Flat	TX	NA	NA	2.8E+02	NA	Salt Bolson	CSC	Angle (2001)
5128702	Ryan Flat	TX	NA	NA	8.5E+02	NA	Salt Bolson	CSC	Angle (2001)
5129704	Ryan Flat	TX	NA	NA	1.8E+02	NA	Salt Bolson	CSC	Angle (2001)
5129705	Ryan Flat	TX	NA	NA	4.6E+02	NA	Salt Bolson	CSC	Angle (2001)
5128701	Ryan Flat	TX	NA	NA	9.3E-01	NA	Salt Bolson	AT	Angle (2001)
5136601	Ryan Flat	TX	NA	NA	9.2E+02	NA	Salt Bolson	AT	Angle (2001)
NA	Dell City area	TX	1.1E+02	1.4E+03	NA	NA	Bone Spring-Victorio Peak	CSC data presented in Peckham (1963)	Mullican and Mace (2001)
NA	NA	TX	NA	1.50E+03	NA	NA	Permian Reef Facies	NA	Uliana (2001), referenced from Reed (1965)
4717202	Salt Flat	TX	NA	NA	1.43E+03	NA	Permian Shelf Facies	CSC, according to Nielson and Sharp (1985)	Uliana (2001), referenced from Davis and Leggat (1965)
4717204	Salt Flat	TX	NA	NA	2.00E+02	NA	Permian Shelf Facies	CSC, according to Nielson and Sharp (1985)	Uliana (2001), referenced from Davis and Leggat (1965)
4717602	Salt Flat	TX	NA	NA	4.02E+02	NA	Permian Shelf Facies	CSC, according to Nielson and Sharp (1985)	Uliana (2001), referenced from Davis and Leggat (1965)
4807203	Dell City area	TX	NA	NA	5.12E+02	NA	Permian Shelf Facies	CSC, according to Nielson and Sharp (1985)	Uliana (2001), referenced from Davis and Leggat (1965)
4807206	Dell City area	TX	NA	NA	1.65E+03	NA	Permian Shelf Facies	CSC, according to Nielson and Sharp (1985)	Uliana (2001), referenced from Davis and Leggat (1965)
4807207	Dell City area	TX	NA	NA	9.59E+02	NA	Permian Shelf Facies	CSC, according to Nielson and Sharp (1985)	Uliana (2001), referenced from Davis and Leggat (1965)
4807302	Dell City area	TX	NA	NA	3.34E+02	NA	Permian Shelf Facies	CSC, according to Nielson and Sharp (1985)	Uliana (2001), referenced from Davis and Leggat (1965)

Table A-3.28 continued.

Groundwater Well ID/ State Well Number	Location	State	Min. T (m²/day)	Max. T (m²/day)	Average T (m²/day)	Median T (m²/day)	Aquifer	Method	Source
4807601	Dell City area	TX	NA	NA	1.12E+03	NA	Permian Shelf Facies	CSC, according to Nielson and Sharp (1985)	Uliana (2001), referenced from Davis and Leggat (1965)
4807605	NA	TX	NA	NA	1.53E+03	NA	Permian Shelf Facies	CSC, according to Nielson and Sharp (1985)	Uliana (2001), referenced from Davis and Leggat (1965)
4807701	NA	TX	NA	NA	1.95E+03	NA	Permian Shelf Facies	CSC, according to Nielson and Sharp (1985)	Uliana (2001), referenced from Davis and Leggat (1965)
4807901	Dell City area	TX	NA	NA	1.31E+03	NA	Permian Shelf Facies	CSC, according to Nielson and Sharp (1985)	Uliana (2001), referenced from Davis and Leggat (1965)
4815201	Dell City area	TX	NA	NA	8.81E+02	NA	Permian Shelf Facies	CSC, according to Nielson and Sharp (1985)	Uliana (2001), referenced from Davis and Leggat (1965)
4816501	Salt Flat	TX	NA	NA	1.30E+03	NA	Permian Shelf Facies	CSC, according to Nielson and Sharp (1985)	Uliana (2001), referenced from Davis and Leggat (1965)
4816701	NA	TX	NA	NA	1.60E+02	NA	Permian Shelf Facies	CSC, according to Nielson and Sharp (1985)	Uliana (2001), referenced from Davis and Leggat (1965)
NA	Dell City area	TX	NA	NA	3.11E+03	NA	Permian Shelf Facies	CSC, according to Nielson and Sharp (1985)	Uliana (2001), referenced from Scalapino (1950)
NA	Southwest Diablo Plateau	TX	4.6E+02	6.2E+02	NA	NA	Cretaceous aquifer on the Diablo Plateau	NA	George et al. (2005), referenced from Kreitler et al. (1987)
10	Dell City area	TX	1.4E+03	3.7E+03	2.5E+03	NA	Bone Spring-Victorio Peak	CSC data presented in Scalapino (1950)	Hutchison (2006)
17	Dell City area	TX	1.2E+03	3.2E+03	2.2E+03	NA	Bone Spring-Victorio Peak	CSC data presented in Scalapino (1950)	Hutchison (2006)
21	Dell City area	TX	7.2E+02	1.9E+03	1.3E+03	NA	Bone Spring-Victorio Peak	CSC data presented in Scalapino (1950)	Hutchison (2006)
24	Dell City area	TX	1.6E+03	4.5E+03	3.0E+03	NA	Bone Spring-Victorio Peak	CSC data presented in Scalapino (1950)	Hutchison (2006)

Table A-3.28 continued.

Groundwater Well ID/ State Well Number	Location	State	Min. T (m^2/day)	Max. T (m^2/day)	Average T (m^2/day)	Median T (m^2/day)	Aquifer	Method	Source
29	Dell City area	TX	4.1E+02	1.0E+03	7.2E+02	NA	Bone Spring-Victorio Peak	CSC data presented in Scalapino (1950)	Hutchison (2006)
30	Dell City area	TX	2.2E+02	5.4E+02	3.8E+02	NA	Bone Spring-Victorio Peak	CSC data presented in Scalapino (1950)	Hutchison (2006)
34	Dell City area	TX	7.9E+02	2.0E+03	1.4E+03	NA	Bone Spring-Victorio Peak	CSC data presented in Scalapino (1950)	Hutchison (2006)
41	Dell City area	TX	1.1E+03	2.9E+03	1.9E+03	NA	Bone Spring-Victorio Peak	CSC data presented in Scalapino (1950)	Hutchison (2006)
42	Dell City area	TX	3.9E+03	1.2E+04	7.9E+03	NA	Bone Spring-Victorio Peak	CSC data presented in Scalapino (1950)	Hutchison (2006)
66	Dell City area	TX	2.3E+02	5.8E+02	4.1E+02	NA	Bone Spring-Victorio Peak	CSC data presented in Scalapino (1950)	Hutchison (2006)
67	Dell City area	TX	1.9E+02	4.6E+02	3.3E+02	NA	Bone Spring-Victorio Peak	CSC data presented in Scalapino (1950)	Hutchison (2006)
81	Dell City area	TX	1.2E+03	3.3E+03	2.2E+03	NA	Bone Spring-Victorio Peak	CSC data presented in Scalapino (1950)	Hutchison (2006)
111	Dell City area	TX	3.3E+03	9.6E+03	6.2E+03	NA	Bone Spring-Victorio Peak	CSC data presented in Scalapino (1950)	Hutchison (2006)
24.19.18.144	Crow Flats area	NM	1.0E+04	4.2E+04	2.6E+04	NA	Permian Shelf Facies	CSC data presented in Bjorklund (1957)	Hutchison (2006)
26.18.28.113	Crow Flats area	NM	4.0E+03	1.2E+04	7.9E+03	NA	Permian Shelf Facies	CSC data presented in Bjorklund (1957)	Hutchison (2006)
26.18.29.113	Crow Flats area	NM	5.5E+03	1.9E+04	1.2E+04	NA	Permian Shelf Facies	CSC data presented in Bjorklund (1957)	Hutchison (2006)
26.18.29.113a	Crow Flats area	NM	6.4E+03	2.3E+04	1.4E+04	NA	Permian Shelf Facies	CSC data presented in Bjorklund (1957)	Hutchison (2006)
26.18.30.122	Crow Flats area	NM	2.9E+03	8.4E+03	5.4E+03	NA	Permian Shelf Facies	CSC data presented in Bjorklund (1957)	Hutchison (2006)

Table A-3.28 continued.

Groundwater Well ID/ State Well Number	Location	State	Min. T (m^2/day)	Max. T (m^2/day)	Average T (m^2/day)	Median T (m^2/day)	Aquifer	Method	Source
26.18.32.122	Crow Flats area	NM	8.1E+02	2.1E+03	1.4E+03	NA	Permian Shelf Facies	CSC data presented in Bjorklund (1957)	Hutchison (2006)
26.18.33.111	Crow Flats area	NM	1.0E+02	2.5E+02	1.7E+02	NA	Permian Shelf Facies	CSC data presented in Bjorklund (1957)	Hutchison (2006)
26.18.33.133	Crow Flats area	NM	1.7E+02	4.1E+02	2.9E+02	NA	Permian Shelf Facies	CSC data presented in Bjorklund (1957)	Hutchison (2006)
4709207	Salt Flat	TX	1.6E+03	4.4E+03	2.9E+03	NA	Capitan Reef Complex and Associated Limestones	CSC data presented in White et al. (1980)	Hutchison (2006)
4709207	Salt Flat	TX	4.1E+03	1.3E+04	8.2E+03	NA	Capitan Reef Complex and Associated Limestones	CSC data presented in White et al. (1980)	Hutchison (2006)
4709801	Salt Flat	TX	3.1E+02	7.6E+02	5.3E+02	NA	Capitan Reef Complex and Associated Limestones	CSC data presented in White et al. (1980)	Hutchison (2006)
4717202	Salt Flat	TX	5.3E+02	1.3E+03	9.3E+02	NA	Salt Bolson and Capitan Reef Complex	CSC data presented in White et al. (1980)	Hutchison (2006)
4717203	Salt Flat	TX	4.7E+02	1.2E+03	8.2E+02	NA	Capitan Reef Complex and Associated Limestones	CSC data presented in White et al. (1980)	Hutchison (2006)
4717204	Salt Flat	TX	8.2E+01	2.0E+02	1.4E+02	NA	Capitan Reef Complex and Associated Limestones	CSC data presented in White et al. (1980)	Hutchison (2006)
4717206	Salt Flat	TX	9.7E+01	2.4E+02	1.7E+02	NA	Capitan Reef Complex and Associated Limestones	CSC data presented in White et al. (1980)	Hutchison (2006)
4717208	Salt Flat	TX	1.5E+02	3.7E+02	2.6E+02	NA	Capitan Reef Complex and Associated Limestones	CSC data presented in White et al. (1980)	Hutchison (2006)
4717218	Salt Flat	TX	2.0E+02	4.9E+02	3.5E+02	NA	Salt Bolson	CSC data presented in White et al. (1980)	Hutchison (2006)

Table A-3.28 continued.

Groundwater Well ID/ State Well Number	Location	State	Min. T (m^2/day)	Max. T (m^2/day)	Average T (m^2/day)	Median T (m^2/day)	Aquifer	Method	Source
4717317	Salt Flat	TX	7.0E+02	1.8E+03	1.3E+03	NA	Capitan Reef Complex and Associated Limestones	CSC data presented in White et al. (1980)	Hutchison (2006)
4717321	Salt Flat	TX	2.4E+03	6.6E+03	4.3E+03	NA	Salt Bolson and Capitan Reef Complex	CSC data presented in White et al. (1980)	Hutchison (2006)
4717602	Salt Flat	TX	1.1E+02	2.6E+02	1.8E+02	NA	Salt Bolson and Delaware Mountain Group	CSC data presented in White et al. (1980)	Hutchison (2006)
4717904	Salt Flat	TX	2.0E+02	4.9E+02	3.5E+02	NA	Salt Bolson and Delaware Mountain Group	CSC data presented in White et al. (1980)	Hutchison (2006)
4718706	Salt Flat	TX	2.0E+02	4.9E+02	3.5E+02	NA	Salt Bolson and Delaware Mountain Group	CSC data presented in White et al. (1980)	Hutchison (2006)

Table A-3.28 continued:

Method Key: CSC = Calculated from specific capacity, AT = Aquifer test.

Groundwater Well ID	Source	Distance Along Cross Section (m)	^{14}C Activity from Exponential Trend [A] (pmC)	[HCO_3^-] from Linear Trend (mmoles/L)	[Mg^{2+}] from Linear Trend (mmoles/L)	^{14}C Activity Calculated Using Dedolomitization Model [A_0] (pmC)	^{14}C Age (yr)
SM-0085	SMHS	537	84.4	6.4	0.3	NA	
SM-0044	SMHS	20,294	64.1	6.0	0.8	82.3	2,067
Doll Day	A&S	56,137	39.0	5.1	1.7	70.6	4,916
Uña	A&S	66,705	33.6	4.8	2.0	69.9	6,049
Runyan	A&S	71,399	31.5	4.7	2.1	69.8	6,572
Cauhape	A&S	77,842	28.8	4.6	2.3	69.5	7,280
Harvey Lewis Well	A&S	97,882	21.8	4.1	2.8	65.4	9,077
Evrage House	A&S	118,245	16.4	3.6	3.3	59.9	10,694

Table A-3.29: Continuous parameters used in stoichiometric dedolomitization model, and resultant ^{14}C activities and groundwater ages.

Source Key: SMHS = New Mexico Bureau of Geology & Mineral Resources' Sacramento Mountains Hydrogeology Study, A&S = This study.

Geologic Unit	Sample Depth (m)	n (%)	k (mD)	K (m/day)
Yeso	405	1.7	NA	NA
Yeso	430	18.3	NA	NA
Yeso	456	0	0.01	7.E-06
Yeso	470	12	NA	NA
Yeso	482	5.1	0.01	7.E-06
Yeso	488	9.9	0	0
Yeso	519	9.5	0.15	1.1E-04
Yeso	546	8.8	0.43	3.2E-04
Yeso	564	0	0	0
Yeso	581	0	0.01	7.E-06
Yeso	588	0.2	NA	NA
Abo	596	0	0	0
Abo	629	NA	1.75	1.30E-03
Abo	639	0.1	NA	NA
Abo	641	0	0	0
Abo	648	0.1	0.01	7.E-06
El Paso/Ellenburger	691	No visible porosity.	NA	NA
El Paso/Ellenburger	693	Minor porosity.	NA	NA
El Paso/Ellenburger	710	0.3	0.000342	2.54E-07
Bliss	823	2.5	NA	NA
Precambrian	833	0	0	0
Precambrian	841	0	0	0
Precambrian	849	0	0	0
Precambrian	858	0	0	0

Table A-3.30: Wellsite core analysis porosity [n] and permeability [k], and calculated hydraulic conductivity [K] data from the Yates Petroleum Corporation, One Tree Unit #2 (YPCOTU2) well along cross-section A - A'.

Cross Section Interval	K with n = 6.95% (m/day)	K with n = 0.1% (m/day)	K with n = 18.3% (m/day)
SM-0085 to SM-0044	6.38E-02	9.18E-04	1.68E-01
SM-0044 to Doll Day	1.51E-01	2.18E-03	3.98E-01
Doll Day to Uña	3.38E-01	4.86E-03	8.90E-01
Uña to Runyan	4.78E-02	6.88E-04	1.26E-01
Runyan to Cauhape	1.66E-01	2.39E-03	4.37E-01
Cauhape to Harvey Lewis Well	4.46E+00	6.42E-02	1.17E+01
Harvey Lewis Well to Evrage House	1.44E+00	2.08E-02	3.80E+00

Table A-3.31: Range of hydraulic conductivity [K] values calculated from stoichiometric dedolomitization model groundwater ages along cross-section A - A'.

Cross Section Interval	Average Saturated Aquifer Thickness Over Each Interval (m)	T with n = 6.95% (m^2/day)	T with n = 0.1% (m^2/day)	T with n = 18.3% (m^2/day)
SM-0085 to SM-0044	763	4.87E+01	7.00E-01	1.28E+02
SM-0044 to Doll Day	564	8.53E+01	1.23E+00	2.25E+02
Doll Day to Uña	142	4.78E+01	6.88E-01	1.26E+02
Uña to Runyan	152	7.26E+00	1.04E-01	1.91E+01
Runyan to Cauhape	160	2.66E+01	3.82E-01	6.99E+01
Cauhape to Harvey Lewis Well	438	1.95E+03	2.81E+01	5.14E+03
Harvey Lewis Well to Evrage House	840	1.21E+03	1.74E+01	3.19E+03

Table A-3.32: Range of transmissivity [T] values calculated from stoichiometric dedolomitization model groundwater ages along cross-section A - A'.

Groundwater Well ID/ State Well Number	Maximum Groundwater Level Change 2003 (m)	Minimum Groundwater Level Change 2003 (m)	Maximum Groundwater Level Change 2004 (m)	Average Amplitude of Water Level Fluctuation 2003 $[s_0]$ for 4807516 and $[s_T]$ for H&C 1, 2, and 3 (m)	S/T (day/m^2)
4807516	5.43E-01	-7.78E+00	-1.80E-01	3.98E+00	NA
H&C 1	9.34E-02	-3.33E+00	-4.72E-01	1.57E+00	4.52E-06
H&C 2	4.08E-01	-1.14E+00	-2.28E-01	6.16E-01	1.26E-06
H&C 3	2.56E-01	-5.03E-01	7.58E-02	3.35E-01	1.40E-06
H&C 4	NA	NA	1.03E-02	NA	NA

Table A-3.33: Maximum and minimum groundwater level change, average amplitude of water level fluctuation, and S/T values for 2003.

Groundwater Well ID/ State Well Number	Maximum Groundwater Level Change 2004 (m)	Minimum Groundwater Level Change 2004 (m)	Maximum Groundwater Level Change 2005 (m)	Average Amplitude of Water Level Fluctuation 2004 $[s_0]$ for 4807516 and $[s_T]$ for H&C 1, 2, 3, and 4 (m)	S/T (day/m^2)
4807516	-1.80E-01	-5.87E+00	5.73E-01	3.03E+00	NA
H&C 1	-4.72E-01	-2.98E+00	-7.36E-02	1.35E+00	3.88E-06
H&C 2	-2.28E-01	-1.42E+00	-4.99E-01	5.30E-01	1.14E-06
H&C 3	7.58E-02	-5.62E-01	1.70E-01	3.42E-01	1.15E-06
H&C 4	1.03E-02	-3.71E-02	6.18E-02	3.66E-02	3.63E-06

Table A-3.34: Maximum and minimum groundwater level change, average amplitude of water level fluctuation, and S/T values for 2004.

Groundwater Well ID/ State Well Number	Maximum Groundwater Level Change 2005 (m)	Minimum Groundwater Level Change 2005 (m)	Maximum Groundwater Level Change 2006 (m)	Average Amplitude of Water Level Fluctuation 2005 $[s_0]$ for 4807516 and $[s_T]$ for H&C 1, 2, 3, and 4 (m)	S/T (day/m^2)
4807516	5.73E-01	-6.46E+00	-6.10E-03	3.37E+00	NA
H&C 1	-7.36E-02	-3.12E+00	-5.07E-01	1.42E+00	4.18E-06
H&C 2	-4.99E-01	-1.99E+00	-1.19E+00	5.73E-01	1.17E-06
H&C 3	1.70E-01	-6.40E-01	-8.10E-02	3.42E-01	1.24E-06
H&C 4	6.18E-02	-2.90E-02	1.80E-02	3.45E-02	3.87E-06

Table A-3.35: Maximum and minimum groundwater level change, average amplitude of water level fluctuation, and S/T values for 2005.

Groundwater Well ID/ State Well Number	Distance from Dell City (m)	s_T/s_0 2003	S/T 2003 (day/m^2)	s_T/s_0 2004	S/T 2004 (day/m^2)	s_T/s_0 2005	S/T 2005 (day/m^2)
4807516	NA	NA	NA	NA	NA	NA	NA
H&C 1	8,224	3.95E-01	NA	4.45E-01	NA	4.20E-01	NA
H&C 2	24,591	1.55E-01	NA	1.75E-01	NA	1.70E-01	NA
H&C 3	28,920	8.40E-02	NA	1.13E-01	NA	1.01E-01	NA
H&C 4	47,476	NA	NA	1.20E-02	NA	1.02E-02	NA
			5.68E-07		1.00E-06		1.07E-06

Table A-3.36: Values of s_T/s_0 for each year, and values of S/T calculated from exponential trends of s_T/s_0 versus distance for each year.

Groundwater Well ID	Distance from H&C 1 (m)	Average Annual Phase Lag between H&C 1 and Indicated Well [t_L] 2003 (days)	S/T 2003 (day/m^2)	Average Annual Phase Lag between H&C 1 and Indicated Well [t_L] 2004 (days)	S/T 2004 (day/m^2)	Average Annual Phase Lag between H&C 1 and Indicated Well [t_L] 2005 (days)	S/T 2005 (day/m^2)
H&C 2	16,367	8	NA	19	NA	21	NA
H&C 3	20,696	17	NA	32	NA	34	NA
H&C 4	39,252	NA	NA	81	NA	104	NA
			1.30E-07		2.52E-07		4.65E-07

Table A-3.37: Average annual phase lag [t_L] between each well pair for each year, and values of S/T calculated from linear trends of t_L versus distance for each year.

Year	S/T from the Attenuation of the Amplitude of the Periodic Water Level Fluctuations (day/m^2)	Median T from ^{14}C Groundwater Ages Along Cross Section A to A' (m^2/day)	S Using Median T	Minimum T from ^{14}C Groundwater Ages Along Cross Section A to A' (m^2/day)	S Using Minimum T	Maximum T from ^{14}C Groundwater Ages Along Cross Section A to A' (m^2/day)	S Using Maximum T
2003	5.68E-07	4.78E+01	2.72E-05	1.04E-01	5.93E-08	5.14E+03	2.92E-03
2004	1.00E-06	4.78E+01	4.79E-05	1.04E-01	1.05E-07	5.14E+03	5.15E-03
2005	1.07E-06	4.78E+01	5.10E-05	1.04E-01	1.11E-07	5.14E+03	5.48E-03

Table A-3.38: Values of S calculated using S/T values estimated from the attenuation of the amplitude of the periodic water level fluctuations.

Year	S/T from the Phase Lag of the Periodic Water Level Fluctuations (day/m^2)	Median T from ^{14}C Groundwater Ages Along Cross Section A to A' (m^2/day)	S Using Median T	Minimum T from ^{14}C Groundwater Ages Along Cross Section A to A' (m^2/day)	S Using Minimum T	Maximum T from ^{14}C Groundwater Ages Along Cross Section A to A' (m^2/day)	S Using Maximum T
2003	1.30E-07	4.78E+01	6.23E-06	1.04E-01	1.36E-08	5.14E+03	6.69E-04
2004	2.52E-07	4.78E+01	1.21E-05	1.04E-01	2.64E-08	5.14E+03	1.30E-03
2005	4.65E-07	4.78E+01	2.22E-05	1.04E-01	4.85E-08	5.14E+03	2.39E-03

Table A-3.39: Values of S calculated using S/T values estimated from the phase lag of the periodic water level fluctuations.

Minimum S	Maximum S	Average S	Aquifer	Source
		8.5E-04	Yeso Fm. (unfractured siltstone and gypsum)	Wasiolek (1991)
1.0E-05	1.0E-03	NA	Confined	Schwartz and Zhang (2003)
3.5E-04	2.E-03	NA	Madison aquifer system	Greene (1993)
1.E-05	1.E-04	NA	Confined portion of Edwards-Trinity aquifer system	Ryder (1996)

Table A-3.40: Range of S values reported in the scientific literature for confined and/or predominantly carbonate aquifers.

TABLES – CHAPTER 4

Salt Basin Sub-basins Delineated by JSAI (2010)	Minimum Recharge Rate (cm/year)	Average Recharge Rate (cm/year)	Maximum Recharge Rate (cm/year)	Minimum Recharge (m^3/day)	Average Recharge (m^3/day)	Maximum Recharge (m^3/day)	Minimum Recharge (acre-feet/year)	Average Recharge (acre-feet/year)	Maximum Recharge (acre-feet/year)
Peñasco Basin	1.3	1.9	2.4	19,842	28,523	37,204	5,875	8,446	11,016
Upper Sacramento River and Upper Piñon Creek	0.5	1.0	1.2	9,637	19,275	22,166	2,854	5,707	6,564
Lower Piñon Creek	0.5	1.5	2.5	1,342	4,025	6,708	397	1,192	1,986
Collins Hills	1.0	2.5	5.0	3,970	9,925	19,850	1,176	2,939	5,878
Rim of the Guadalupes	2.0	2.8	4.0	8,542	11,746	17,085	2,529	3,478	5,059
Guadalupe Mountains	2.0	2.8	4.0	16,482	22,663	32,964	4,880	6,711	9,761
Upper Cornucopia Draw	1.0	2.5	3.5	3,888	9,720	13,607	1,151	2,878	4,029
limestone highlands	2.5	3.0	5.0	8,282	9,939	16,564	2,452	2,943	4,905
Lower Sacramento River and Otero Mesa	0.1	0.3	0.3	2,988	5,976	6,573	885	1,769	1,946
Lower Cornucopia Draw	2.5	3.0	5.0	28,064	33,676	56,127	8,310	9,972	16,620
Crow Flats	0.1	0.2	0.2	2,015	4,030	3,023	597	1,193	895
Shiloh Draw	0.1	0.2	0.2	1,655	4,413	4,965	490	1,307	1,470
Coffelt Draw	2.0	2.5	2.8	13,909	17,386	19,124	4,118	5,148	5,663
Big Dog Canyon	1.0	2.0	2.0	9,254	18,508	18,508	2,740	5,480	5,480
Long Canyon	2.0	3.0	3.3	3,559	5,339	5,784	1,054	1,581	1,713
Lewis Canyon	2.0	3.0	3.3	8,268	12,403	13,436	2,448	3,673	3,979
Brokeoff Mountains	0.8	1.5	1.5	5,709	11,417	11,417	1,690	3,381	3,381
Fourmile Draw	0.1	1.0	1.0	145	2,902	2,902	43	859	859
Cornudas Draw	0.5	1.5	1.8	6,817	20,452	23,861	2,019	6,056	7,065
Washburn Draw	0.1	0.1	0.1	348	695	695	103	206	206
Diablo Plateau	0.1	0.1	0.1	4,325	8,649	10,811	1,281	2,561	3,201
Delaware Mountains	0.8	1.5	1.5	5,647	11,294	11,294	1,672	3,344	3,344
Salt Flats	0.0	0.0	0.0	0	0	0	0	0	0
Sum all sub-basins				**164,688**	**272,956**	**354,670**	**48,765**	**80,824**	**105,020**

Table A-4.1: Water-balance based minimum, average, and maximum recharge rates and areal recharge applied to the Salt Basin sub-basins within the 3-D MODFLOW groundwater flow model domain.

Minimum Sacramento Mountains Recharge Factor (%)	Average Sacramento Mountains Recharge Factor (%)	Maximum Sacramento Mountains Recharge Factor (%)
4	22	44

Table A-4.2: Sacramento Mountains recharge factors from Newton et al. (2011).

Location	Minimum Recharge Rate (cm/year)	Average Recharge Rate (cm/year)	Maximum Recharge Rate (cm/year)
Creek beds and depressions	0.028	0.242	0.457
Outside creek beds	0.005	0.0125	0.020

Table A-4.3: Kreitler et al. (1987) recharge rates for Diablo Plateau from Mayer (1995).

Range of Average Annual Precipitation in Figure 1.11 Polygons (cm/year)	Median Average Annual Precipitation in Figure 1.11 Polygons (cm/year)	Minimum Recharge Factor (%)	Average Recharge Factor (%)	Maximum Recharge Factor (%)	Minimum Recharge Rate (cm/year)	Average Recharge Rate (cm/year)	Maximum Recharge Rate (cm/year)	Minimum Recharge (m^3/day)	Average Recharge (m^3/day)	Maximum Recharge (m^3/day)	Minimum Recharge (acre-feet/year)	Average Recharge (acre-feet/year)	Maximum Recharge (acre-feet/year)
61 to 66	64	4	22	44	2.5	14.0	27.9						
66 to 71	69	4	22	44	2.7	15.1	30.2						
71 to 76	74	4	22	44	2.9	16.2	32.4						
76 to 81	79	4	22	44	3.1	17.3	34.6						
Sum Sacramento Mountains recharge zone								7,366	40,513	81,026	2,181	11,996	23,992
61 to 66	64	4	22	44	2.5	14.0	27.9						
66 to 71	69	4	22	44	2.7	15.1	30.2						
71 to 76	74	4	22	44	2.9	16.2	32.4						
Sum Guadalupe Mountains recharge zone								1,572	8,644	17,288	465	2,560	5,119

Table A-4.4: Elevation-dependent minimum, average, and maximum recharge rates and areal recharge applied to the recharge zones within the 3-D MODFLOW groundwater flow model domain in the Sacramento and Guadalupe Mountains.

Location	Minimum Recharge Rate (cm/year)	Average Recharge Rate (cm/year)	Maximum Recharge Rate (cm/year)	Minimum Recharge (m^3/day)	Average Recharge (m^3/day)	Maximum Recharge (m^3/day)	Minimum Recharge (acre-feet/year)	Average Recharge (acre-feet/year)	Maximum Recharge (acre-feet/year)
Creek beds and depressions	0.028	0.242	0.457						
Outside creek beds	0.005	0.0125	0.020						
Sum Cornudas Mountains recharge zone				60	202	344	18	60	102
Creek beds and depressions	0.028	0.242	0.457						
Outside creek beds	0.005	0.0125	0.020						
Sum Diablo Plateau recharge zone				80	380	679	24	112	201

Table A-4.5: Elevation-dependent minimum, average, and maximum recharge rates and areal recharge applied to the recharge zones within the 3-D MODFLOW groundwater flow model domain in around the Cornudas Mountains and on the Diablo Plateau.

Groundwater Well ID/ State Well Number	Location	State	Length of Screened Interval (m)	Min K (m/day)	Max K (m/day)	Average K (m/day)	Median K (m/day)	Aquifer	Screened Interval Note	Transmissivity Source
4709207	Salt Flat	TX	71	NA	NA	1.0E+02	NA	Capitan Reef Complex and Associated Limestones	SI	Angle (2001)
4717218	Salt Flat	TX	82	NA	NA	2.8E+00	NA	Salt Bolson	SI	Angle (2001)
4717317	Salt Flat	TX	30	NA	NA	3.4E+01	NA	Capitan Reef Complex and Associated Limestones	SI	Angle (2001)
4717321	Salt Flat	TX	172	NA	NA	2.4E+01	NA	Salt Bolson and Capitan Reef Complex	SI	Angle (2001)
4717903	Salt Flat	TX	97	NA	NA	1.3E+00	NA	Capitan Limestone	MWL & WD	Angle (2001)
4718402	Salt Flat	TX	256	NA	NA	1.5E-01	NA	Delaware Mountain Group	MWL & WD	Angle (2001)
4718404	Salt Flat	TX	125	NA	NA	3.7E-01	NA	Salt Bolson and Delaware Mountain Group	SI	Angle (2001)
4718707	Salt Flat	TX	262	NA	NA	1.5E+00	NA	Salt Bolson and Delaware Mountain Group	SI	Angle (2001)
4734902	Wild Horse Flat	TX	19	NA	NA	5.0E+01	NA	Capitan Reef Complex and Associated Limestones	SI	Angle (2001)
4743503	Wild Horse Flat	TX	98	NA	NA	1.0E+00	NA	Delaware Mountain Group	SI	Angle (2001)

Table A-4.6: Hydraulic conductivity [K] values estimated from transmissivity [T]. Key at bottom of table.

Groundwater Well ID/ State Well Number	Location	State	Length of Screened Interval (m)	Min K (m/day)	Max K (m/day)	Average K (m/day)	Median K (m/day)	Aquifer	Screened Interval Note	Transmissivity Source
4751403	Wild Horse Flat	TX	160	NA	NA	1.1E+01	NA	Salt Bolson and Permian Rocks	SI	Angle (2001)
4751807	Wild Horse Flat	TX	75	NA	NA	5.1E+00	NA	Salt Bolson	SI	Angle (2001)
4752301	Wild Horse Flat	TX	168	NA	NA	2.8E-01	NA	Capitan Reef Complex and Associated Limestones	SI	Angle (2001)
4752601	Wild Horse Flat	TX	47	NA	NA	2.2E+01	NA	Capitan Reef Complex and Associated Limestones	SI	Angle (2001)
4752602	Wild Horse Flat	TX	94	NA	NA	2.0E+00	NA	Capitan Reef Complex and Associated Limestones	SI	Angle (2001)
4758502	Wild Horse Flat	TX	30	NA	NA	2.7E+00	NA	Salt Bolson	SI	Angle (2001)
4758505	Wild Horse Flat	TX	76	NA	NA	2.0E+00	NA	Salt Bolson	SI	Angle (2001)
4758602	Wild Horse Flat	TX	80	NA	NA	5.8E+00	NA	Salt Bolson	SI	Angle (2001)
4758602	Wild Horse Flat	TX	80	NA	NA	7.3E+00	NA	Salt Bolson	SI	Angle (2001)
4759102	Wild Horse Flat	TX	92	NA	NA	6.1E+00	NA	Salt Bolson and Cretaceous Rocks	SI	Angle (2001)
4759209	Wild Horse Flat	TX	61	NA	NA	4.0E+00	NA	Cretaceous System	SI	Angle (2001)
4759307	Michigan Flat	TX	74	NA	NA	2.4E+00	NA	Salt Bolson and Cretaceous Rocks	MWL & WD	Angle (2001)
4759603	Michigan Flat	TX	12	NA	NA	1.6E+01	NA	Cretaceous System	SI	Angle (2001)
4760404	Michigan Flat	TX	82	NA	NA	1.1E+00	NA	Salt Bolson	SI	Angle (2001)
4760601	Michigan Flat	TX	29	NA	NA	9.6E-02	NA	Permian System	SI	Angle (2001)
5102906	Lobo Flat	TX	50	NA	NA	1.6E+01	NA	Salt Bolson	SI	Angle (2001)
5102918	Lobo Flat	TX	79	NA	NA	1.3E+00	NA	Salt Bolson	SI	Angle (2001)
5102923	Lobo Flat	TX	84	NA	NA	5.4E+00	NA	Salt Bolson	SI	Angle (2001)
5102926	Lobo Flat	TX	37	NA	NA	6.2E+00	NA	Salt Bolson	SI	Angle (2001)

Table A-4.6 continued.

Groundwater Well ID/ State Well Number	Location	State	Length of Screened Interval (m)	Min K (m/day)	Max K (m/day)	Average K (m/day)	Median K (m/day)	Aquifer	Screened Interval Note	Transmissivity Source
5103702	Lobo Flat	TX	143	NA	NA	4.2E+00	NA	Salt Bolson	SI	Angle (2001)
5103703	Lobo Flat	TX	137	NA	NA	3.4E-01	NA	Salt Bolson	SI	Angle (2001)
5110306	Lobo Flat	TX	62	NA	NA	2.2E+00	NA	Salt Bolson	SI	Angle (2001)
5110309	Lobo Flat	TX	43	NA	NA	1.2E+01	NA	Alluvium and Tertiary Volcanics	MWL & WD	Angle (2001)
5110316	Lobo Flat	TX	60	NA	NA	7.9E+00	NA	Salt Bolson	MWL & WD	Angle (2001)
5110317	Lobo Flat	TX	66	NA	NA	3.4E+00	NA	Alluvium and Tertiary Volcanics	SI	Angle (2001)
5110321	Lobo Flat	TX	80	NA	NA	8.0E+00	NA	Salt Bolson	MWL & WD	Angle (2001)
5110322	Lobo Flat	TX	83	NA	NA	2.2E+00	NA	Salt Bolson	MWL & WD	Angle (2001)
5110328	Lobo Flat	TX	73	NA	NA	6.1E+00	NA	Salt Bolson	SI	Angle (2001)
5110331	Lobo Flat	TX	76	NA	NA	5.2E+00	NA	Alluvium and Tertiary Volcanics	MWL & WD	Angle (2001)
5110332	Lobo Flat	TX	32	NA	NA	1.4E+01	NA	Salt Bolson	SI	Angle (2001)
5110603	Lobo Flat	TX	30	NA	NA	9.3E+00	NA	Salt Bolson	MWL	Angle (2001)
5110603	Lobo Flat	TX	30	NA	NA	7.4E+00	NA	Salt Bolson	MWL	Angle (2001)
5110624	Lobo Flat	TX	52	NA	NA	6.8E-01	NA	Salt Bolson	SI	Angle (2001)
5111105	Lobo Flat	TX	167	NA	NA	1.9E+00	NA	Salt Bolson	SI	Angle (2001)
5111106	Lobo Flat	TX	141	NA	NA	1.1E+00	NA	Salt Bolson	SI	Angle (2001)
5114501	Lobo Flat	TX	12	NA	NA	5.3E-01	NA	Volcanics	SI	Angle (2001)
5119104	Lobo Flat	TX	58	NA	NA	4.8E+00	NA	Salt Bolson	SI	Angle (2001)
5119301	Lobo Flat	TX	106	NA	NA	4.5E+00	NA	Salt Bolson	MWL & WD	Angle (2001)
5120403	Lobo Flat	TX	119	NA	NA	6.2E-01	NA	Salt Bolson	SI	Angle (2001)
5120404	Lobo Flat	TX	169	NA	NA	9.3E-01	NA	Salt Bolson	SI	Angle (2001)
5127302	Ryan Flat	TX	69	NA	NA	1.2E+00	NA	Volcanics	SI	Angle (2001)
5128303	Ryan Flat	TX	791	NA	NA	2.2E-01	NA	Salt Bolson	SI	Angle (2001)
5128606	Ryan Flat	TX	769	NA	NA	1.4E-01	NA	Salt Bolson	SI	Angle (2001)
5129104	Ryan Flat	TX	175	NA	NA	1.6E-02	NA	Salt Bolson	MWL & WD	Angle (2001)
5129105	Ryan Flat	TX	162	NA	NA	1.3E-01	NA	Salt Bolson	SI	Angle (2001)
5129403	Ryan Flat	TX	205	NA	NA	9.1E-01	NA	Salt Bolson	SI	Angle (2001)
5129704	Ryan Flat	TX	390	NA	NA	4.5E-01	NA	Salt Bolson	SI	Angle (2001)

Table A-4.6 continued.

Groundwater Well ID/ State Well Number	Location	State	Length of Screened Interval (m)	Min K (m/day)	Max K (m/day)	Average K (m/day)	Median K (m/day)	Aquifer	Screened Interval Note	Transmissivity Source
5129705	Ryan Flat	TX	255	NA	NA	1.8E+00	NA	Salt Bolson	SI	Angle (2001)
5128701	Ryan Flat	TX	188	NA	NA	4.9E-03	NA	Salt Bolson	SI	Angle (2001)
5136601	Ryan Flat	TX	91	NA	NA	1.0E+01	NA	Salt Bolson	SI	Angle (2001)
4807203	Delly City area	TX	51	NA	NA	9.99E+00	NA	Permian Shelf Facies	MWL & WD	Uliana (2001), referenced from Davis and Leggat (1965)
4807206	Delly City area	TX	29	NA	NA	5.76E+01	NA	Permian Shelf Facies	MWL & WD	Uliana (2001), referenced from Davis and Leggat (1965)
4807207	Delly City area	TX	181	NA	NA	5.29E+00	NA	Permian Shelf Facies	MWL & WD	Uliana (2001), referenced from Davis and Leggat (1965)
4807302	Delly City area	TX	30	NA	NA	1.11E+01	NA	Permian Shelf Facies	MWL	Uliana (2001), referenced from Davis and Leggat (1965)
4807601	Delly City area	TX	35	NA	NA	3.20E+01	NA	Permian Shelf Facies	SI	Uliana (2001), referenced from Davis and Leggat (1965)
4807605	NA	TX	30	NA	NA	5.10E+01	NA	Permian Shelf Facies	WD	Uliana (2001), referenced from Davis and Leggat (1965)
4807701	NA	TX	30	NA	NA	6.51E+01	NA	Permian Shelf Facies	WD	Uliana (2001), referenced from Davis and Leggat (1965)
4807901	Delly City area	TX	76	NA	NA	1.73E+01	NA	Permian Shelf Facies	MWL & WD	Uliana (2001), referenced from Davis and Leggat (1965)
4815201	Delly City area	TX	82	NA	NA	1.07E+01	NA	Permian Shelf Facies	SI	Uliana (2001), referenced from Davis and Leggat (1965)

Table A-4.6 continued.

Groundwater Well ID/ State Well Number	Location	State	Length of Screened Interval (m)	Min K (m/day)	Max K (m/day)	Average K (m/day)	Median K (m/day)	Aquifer	Screened Interval Note	Transmissivity Source
4816501	Salt Flat	TX	9	NA	NA	1.44E+02	NA	Permian Shelf Facies	MWL & WD	Uliana (2001), referenced from Davis and Leggat (1965)
4816701	NA	TX	30	NA	NA	5.33E+00	NA	Permian Shelf Facies	WD	Uliana (2001), referenced from Davis and Leggat (1965)
10	Dell City area	TX	31	4.4E+01	1.2E+02	7.9E+01	NA	Bone Spring-Victorio Peak	MWL & WD	Hutchison (2006)
17	Dell City area	TX	67	1.8E+01	4.8E+01	3.2E+01	NA	Bone Spring-Victorio Peak	MWL & WD	Hutchison (2006)
21	Dell City area	TX	48	1.5E+01	3.9E+01	2.7E+01	NA	Bone Spring-Victorio Peak	MWL & WD	Hutchison (2006)
24	Dell City area	TX	28	6.0E+01	1.6E+02	1.1E+02	NA	Bone Spring-Victorio Peak	MWL & WD	Hutchison (2006)
29	Dell City area	TX	61	6.7E+00	1.7E+01	1.2E+01	NA	Bone Spring-Victorio Peak	MWL & WD	Hutchison (2006)
30	Dell City area	TX	59	3.7E+00	9.2E+00	6.5E+00	NA	Bone Spring-Victorio Peak	MWL & WD	Hutchison (2006)
34	Dell City area	TX	51	1.5E+01	4.0E+01	2.8E+01	NA	Bone Spring-Victorio Peak	MWL & WD	Hutchison (2006)
41	Dell City area	TX	30	3.6E+01	9.5E+01	6.5E+01	NA	Bone Spring-Victorio Peak	WD	Hutchison (2006)
42	Dell City area	TX	48	8.2E+01	2.6E+02	1.6E+02	NA	Bone Spring-Victorio Peak	MWL & WD	Hutchison (2006)
66	Dell City area	TX	67	3.5E+00	8.6E+00	6.1E+00	NA	Bone Spring-Victorio Peak	MWL & WD	Hutchison (2006)
67	Dell City area	TX	68	2.8E+00	6.8E+00	4.8E+00	NA	Bone Spring-Victorio Peak	MWL & WD	Hutchison (2006)
81	Dell City area	TX	33	3.8E+01	1.0E+02	6.8E+01	NA	Bone Spring-Victorio Peak	MWL & WD	Hutchison (2006)

Table A-4.6 continued.

Groundwater Well ID/ State Well Number	Location	State	Length of Screened Interval (m)	Min K (m/day)	Max K (m/day)	Average K (m/day)	Median K (m/day)	Aquifer	Screened Interval Note	Transmissivity Source
111	Dell City area	TX	65	5.0E+01	1.5E+02	9.6E+01	NA	Bone Spring-Victorio Peak	MWL & WD	Hutchison (2006)
24.19.18.144	Crow Flats area	NM	103	9.9E+01	4.1E+02	2.5E+02	NA	Permian Shelf Facies	MWL & WD	Hutchison (2006)
26.18.28.113	Crow Flats area	NM	110	3.6E+01	1.1E+02	7.2E+01	NA	Permian Shelf Facies	MWL & WD	Hutchison (2006)
26.18.29.113	Crow Flats area	NM	85	6.5E+01	2.2E+02	1.4E+02	NA	Permian Shelf Facies	MWL & WD	Hutchison (2006)
26.18.29.113a	Crow Flats area	NM	75	8.5E+01	3.1E+02	1.9E+02	NA	Permian Shelf Facies	MWL & WD	Hutchison (2006)
26.18.30.122	Crow Flats area	NM	90	3.2E+01	9.3E+01	6.0E+01	NA	Permian Shelf Facies	MWL & WD	Hutchison (2006)
26.18.32.122	Crow Flats area	NM	82	9.9E+00	2.6E+01	1.8E+01	NA	Permian Shelf Facies	MWL & WD	Hutchison (2006)
26.18.33.111	Crow Flats area	NM	122	8.3E-01	2.0E+00	1.4E+00	NA	Permian Shelf Facies	MWL & WD	Hutchison (2006)
26.18.33.133	Crow Flats area	NM	124	1.3E+00	3.3E+00	2.3E+00	NA	Permian Shelf Facies	MWL & WD	Hutchison (2006)
4709207	Salt Flat	TX	71	2.3E+01	6.2E+01	4.1E+01	NA	Capitan Reef Complex and Associated Limestones	SI	Hutchison (2006)

Table A-4.6 continued.

Groundwater Well ID/ State Well Number	Location	State	Length of Screened Interval (m)	Min K (m/day)	Max K (m/day)	Average K (m/day)	Median K (m/day)	Aquifer	Screened Interval Note	Transmissivity Source
4709207	Salt Flat	TX	71	5.7E+01	1.8E+02	1.2E+02	NA	Capitan Reef Complex and Associated Limestones	SI	Hutchison (2006)
4709801	Salt Flat	TX	43	7.1E+00	1.8E+01	1.2E+01	NA	Capitan Reef Complex and Associated Limestones	SI	Hutchison (2006)
4717202	Salt Flat	TX	55	9.6E+00	2.4E+01	1.7E+01	NA	Salt Bolson and Capitan Reef Complex	MWL & WD	Hutchison (2006)
4717203	Salt Flat	TX	112	4.1E+00	1.0E+01	7.3E+00	NA	Capitan Reef Complex and Associated Limestones	MWL & WD	Hutchison (2006)
4717204	Salt Flat	TX	253	3.3E-01	7.9E-01	5.6E-01	NA	Capitan Reef Complex and Associated Limestones	SI	Hutchison (2006)
4717206	Salt Flat	TX	191	5.1E-01	1.2E+00	8.8E-01	NA	Capitan Reef Complex and Associated Limestones	SI	Hutchison (2006)
4717208	Salt Flat	TX	469	3.2E-01	7.8E-01	5.5E-01	NA	Capitan Reef Complex and Associated Limestones	SI	Hutchison (2006)
4717218	Salt Flat	TX	82	2.4E+00	6.0E+00	4.2E+00	NA	Salt Bolson	SI	Hutchison (2006)
4717317	Salt Flat	TX	30	2.3E+01	5.9E+01	4.1E+01	NA	Capitan Reef Complex and Associated Limestones	SI	Hutchison (2006)
4717321	Salt Flat	TX	172	1.4E+01	3.9E+01	2.5E+01	NA	Salt Bolson and Capitan Reef Complex	SI	Hutchison (2006)

Table A-4.6 continued.

Groundwater Well ID/ State Well Number	Location	State	Length of Screened Interval (m)	Min K (m/day)	Max K (m/day)	Average K (m/day)	Median K (m/day)	Aquifer	Screened Interval Note	Transmissivity Source
4717602	Salt Flat	TX	27	3.9E+00	9.6E+00	6.8E+00	NA	Salt Bolson and Delaware Mountain Group	MWL & WD	Hutchison (2006)
4717904	Salt Flat	TX	78	2.6E+00	6.3E+00	4.5E+00	NA	Salt Bolson and Delaware Mountain Group	MWL & WD	Hutchison (2006)
4718706	Salt Flat	TX	112	1.8E+00	4.4E+00	3.1E+00	NA	Salt Bolson and Delaware Mountain Group	MWL & WD	Hutchison (2006)

Table A-4.6 continued.

Screened Interval Note Key: SI = total length of screened/open interval used for aquifer thickness, MWL & WD = distance from mean groundwater level to total well depth used for aquifer thickness, MWL = only mean groundwater level available; assumed 30 meters (98 feet) aquifer thickness, WD = only total well depth available; assumed 30 meters (98 feet) aquifer thickness.

Hydrogeologic Unit	Model Layers	Initial Horizontal K (m/day)	Vertical Anisotropy	Calibrated Water-balance Based Minimum Recharge Scenario Horizontal K (m/day)	Calibrated Water-balance Based Average Recharge Scenario Horizontal K (m/day)	Calibrated Water-balance Based Maximum Recharge Scenario Horizontal K (m/day)
Cenozoic alluvium	1, 2, and 3	1	100	10	10	10
Cenozoic intrusions	1, 2, 3, 4, and 5	0.0001	1,000	0.00001 to 0.0001	0.00001 to 0.001	0.00001 to 0.001
Cretaceous	1	0.01	100	0.005	0.0075	0.0075
Low permeability confining unit beneath Cretaceous	2	0.000001	1,000	0.00000001	0.00000001	0.00000001
Unfractured Permian	1, 2, 3, 4, and 5	0.01 to 0.1	100	0.005 to 0.5	0.0075 to 1	0.01 to 2.5
Fractured Permian	1, 2, 3, 4, and 5	1 to 10	10	0.025 to 25	0.025 to 250	0.025 to 250
Paleozoic (Cambrian through Pennslyvanian)	2, 3, 4, 5, and 6	0.001	1,000	0.00005 to 0.5	0.00005 to 0.5	0.00005 to 0.5
Precambrian	1, 2, 3, 4, 5, and 6	0.001	1,000	0.00001 to 0.01	0.00001 to 0.01	0.00001 to 0.01

Table A-4.7: Initial horizontal hydraulic conductivity [K], vertical anisotropy, and final horizontal K assigned to each hydrogeologic unit for the calibrated water-balance based minimum, average, and maximum recharge scenario models.

Hydrogeologic Unit	Model Layers	Initial Horizontal K (m/day)	Vertical Anisotropy	Calibrated Elevation-dependent Minimum Recharge Scenario Horizontal K (m/day)	Calibrated Elevation-dependent Average Recharge Scenario Horizontal K (m/day)	Calibrated Elevation-dependent Maximum Recharge Scenario Horizontal K (m/day)
Cenozoic alluvium	1, 2, and 3	1	100	0.005 to 10	0.0075 to 10	0.01 to 10
Cenozoic intrusions	1, 2, 3, 4, and 5	0.0001	1,000	0.00001 to 0.1	0.00001 to 0.1	0.00001 to 0.1
Cretaceous	1	0.01	100	0.0005	0.0025	0.005
Low permeability confining unit beneath Cretaceous	2	0.000001	1,000	0.00000001	0.00001	0.0001
Unfractured Permian	1, 2, 3, 4, and 5	0.01 to 0.1	100	0.005 to 0.5	0.005 to 5	0.005 to 5
Fractured Permian	1, 2, 3, 4, and 5	1 to 10	10	0.0075 to 5	0.075 to 25	0.25 to 25
Paleozoic (Cambrian through Pennslyvanian)	2, 3, 4, 5, and 6	0.001	1,000	0.00005 to 0.1	0.00005 to 0.1	0.00005 to 0.1
Precambrian	1, 2, 3, 4, 5, and 6	0.001	1,000	0.00001 to 0.01	0.00001 to 0.01	0.00001 to 0.01

Table A-4.8: Initial horizontal hydraulic conductivity [K], vertical anisotropy, and final horizontal K assigned to each hydrogeologic unit for the calibrated elevation-dependent minimum, average, and maximum recharge scenario models.

POD Number/ Well ID/ State Well Number	Easting	Northing	Model Row	Model Column	Model Layer or Layers Intersected by Screened Interval	Elevation of Top of Screen (m)	Elevation of Bottom of Screen (m)	Observed Groundwater Elevation (m)	Source	Note
PN 00308	442967	3628994	108	23	1	2,231	2,213	2,231	NMOSE	*
PN 00119	453798	3628887	97	23	1	2,043	1,919	2,043	NMOSE	*
PN 00966	455641	3628866	96	23	1	1,988	1,932	1,988	NMOSE	*
PN 00561	445394	3628678	106	23	1	2,233	2,207	2,233	NMOSE	*
PN 00949	446088	3628596	103	23	1	2,207	2,189	2,207	NMOSE	*
PN 00417	446288	3628596	105	23	1	2,219	2,199	2,219	NMOSE	*
SM-0075	447829	3628594	105	23	1	2,180	2,153	2,180	SMHS	*
PN 00750	445692	3628385	106	23	1	2,245	2,240	2,245	NMOSE	*
PN 00196 POD2	442050	3628215	109	23	1	2,298	2,237	2,298	NMOSE	*
PN 00196	442155	3628153	109	23	1	2,292	2,286	2,292	NMOSE	*
PN 00708	441748	3628136	109	23	1	2,334	2,321	2,334	NMOSE	*
PN 00594	442054	3628052	109	24	1	2,295	2,288	2,295	NMOSE	*
PN 00526	442254	3628052	109	24	1	2,294	2,263	2,294	NMOSE	*
PN 00357	458020	3627889	93	24	1	1,938	1,915	1,938	NMOSE	*
PN 00202	442148	3627748	109	24	1	2,274	2,270	2,274	NMOSE	*
PN 00174	441744	3627731	109	24	1	2,311	2,294	2,311	NMOSE	*
PN 00073	451331	3627670	100	24	1	2,085	2,062	2,085	NMOSE	*
PN 00004	447404	3627541	104	24	1	2,191	2,183	2,191	NMOSE	*
PN 00552	450369	3627370	101	24	1	2,075	2,054	2,075	NMOSE	*
PN 00016	451191	3627359	100	24	1	2,102	2,077	2,102	NMOSE	*
PN 00587	441735	3627325	109	24	1	2,276	2,224	2,276	NMOSE	*
PN 00799	439811	3627141	111	24	1	2,418	2,396	2,418	NMOSE	*
PN 00929	441727	3626918	109	25	1	2,312	2,282	2,312	NMOSE	*
PN 00383	454601	3626841	97	25	1	1,990	1,984	1,990	NMOSE	*
PN 00700	451138	3626824	100	25	1	2,060	2,022	2,060	NMOSE	*
PN 00677	452954	3626641	95	25	1	2,038	2,012	2,038	NMOSE	*
PN 00810	453553	3626641	98	25	1	2,029	2,011	2,029	NMOSE	*
PN 00616	456041	3626639	98	25	1	1,992	1,971	1,992	NMOSE	*
PN 01027 POD1	450938	3626624	100	25	1	2,056	1,995	2,056	NMOSE	*

Table A-4.9: Calibration targets for the steady-state 3-D MODFLOW groundwater flow model. Key at bottom of table.

POD Number/ Well ID/ State Well Number	Easting	Northing	Model Row	Model Column	Model Layer or Layers Intersected by Screened Interval	Elevation of Top of Screen (m)	Elevation of Bottom of Screen (m)	Observed Groundwater Elevation (m)	Source	Note
PN 00152	441442	3626588	96	25	1	2,354	2,348	2,354	NMOSE	*
PN 00166	455330	3626534	110	25	1	1,980	1,962	1,980	NMOSE	*
PN 00236	451289	3626498	100	25	1	2,065	1,961	2,065	NMOSE	*
PN 00182	441562	3626354	100	25	1	2,326	2,313	2,326	NMOSE	*
PN 00669	451477	3626306	110	25	1	2,062	1,998	2,062	NMOSE	*
PN 00426	453238	3626121	98	25	1	2,053	1,992	2,053	NMOSE	*
PN 00211	456449	3626025	95	26	1	1,959	1,942	1,959	NMOSE	*
PN 00704	452352	3626017	99	26	1	2,059	1,958	2,059	NMOSE	*
PN 00841	452352	3625817	99	26	1	2,067	2,048	2,067	NMOSE	*
PN 00871	452147	3625610	99	26	1	2,061	2,017	2,061	NMOSE	*
PN 00738	452248	3625511	99	26	1	2,056	2,030	2,056	NMOSE	*
PN 00729	455646	3625420	96	26	1	2,010	1,964	2,010	NMOSE	*
PN 00758	452347	3625410	99	26	1	2,057	1,999	2,057	NMOSE	*
PN 00382	435462	3625068	116	27	1	2,610	2,587	2,610	NMOSE	*
PN 00942	459827	3621825	91	30	1	1,888	1,846	1,888	NMOSE	*
PN 00511	453047	3621586	98	30	1	1,979	1,959	1,979	NMOSE	*
PN 00787	449823	3619557	101	32	1	2,032	1,936	2,032	NMOSE	*
ST 00115 S-10	446461	3615401	105	36	1	2,041	1,961	2,041	NMOSE	*
ST 00111	434903	3612163	70	40	1	2,096	1,980	2,096	NMOSE	*
ST 00005	481574	3612051	81	40	1	1,519	1,474	1,519	NMOSE	*
ST 00008	469786	3612015	116	39	1	1,492	1,480	1,492	NMOSE	*
ST 00009	467376	3611968	84	40	1	1,466	1,448	1,466	NMOSE	*
ST 00111 S-4	434269	3610961	117	41	1	1,989	1,946	1,989	NMOSE	*
ST 00165	457467	3610375	94	41	1	1,658	1,553	1,658	NMOSE	*
ST 00166	461985	3609637	89	42	1	1,515	1,448	1,515	NMOSE	*
ST 00006	483181	3608828	68	43	1	1,505	1,425	1,505	NMOSE	*
ST 00221	463074	3608381	88	43	1	1,446	1,332	1,446	NMOSE	*
ST 00020	453685	3607880	98	44	1	1,797	1,666	1,797	NMOSE	*
SM-0046	442173	3607555	109	44	1	1,776	1,715	1,776	SMHS	*

Table A-4.9 continued.

845

POD Number/ Well ID/ State Well Number	Easting	Northing	Model Row	Model Column	Model Layer or Layers Intersected by Screened Interval	Elevation of Top of Screen (m)	Elevation of Bottom of Screen (m)	Observed Groundwater Elevation (m)	Source	Note
ST 00003	478550	3606619	73	45	1	1,312	1,287	1,312	NMOSE	*
ST 00007	485591	3603997	66	48	1	1,459	1,421	1,459	NMOSE	*
ST 00021	465694	3603733	86	48	1	1,408	1,399	1,408	NMOSE	*
ST 00236 POD1	481499	3602715	70	49	1	1,316	1,244	1,316	NMOSE	*
ST 00080	451407	3598958	100	53	1	1,487	1,481	1,487	NMOSE	*
ST 00194 S	484877	3598063	66	54	1	1,194	1,178	1,194	NMOSE	*
ST 00018	473476	3596830	78	55	1	1,392	1,353	1,392	NMOSE	*
ST 00194	484918	3594393	66	57	1	1,349	1,319	1,349	NMOSE	*, +
ST 00068	485622	3592884	66	59	1	1,334	1,326	1,334	NMOSE	*
ST 00022	471858	3592609	79	59	1, 2, and 3	1,225	825	1,225	NMOSE	*
ST 00200	483909	3588157	65	63	1	1,101	1,094	1,101	NMOSE	*
ST 00196	486119	3588154	67	63	1	1,116	1,108	1,116	NMOSE	*
ST 00019	476365	3588074	75	64	1	1,157	1,131	1,157	NMOSE	*
ST 00081	454291	3584921	97	67	1	1,171	1,167	1,171	NMOSE	*
ST 00075	487572	3583723	64	68	1	1,124	1,093	1,124	NMOSE	*
ST 00055	444554	3582645	107	69	1	1,136	1,106	1,136	NMOSE	*
ST 00195	484099	3581318	67	70	1	1,098	1,095	1,098	NMOSE	*
ST 00132	444847	3580934	106	71	1	1,168	1,153	1,168	NMOSE	*
ST 00056	447353	3580223	104	71	1	1,165	1,127	1,165	NMOSE	*
ST 00133	452054	3579701	99	72	1	1,196	1,158	1,196	NMOSE	*
ST 00198	485704	3579307	66	72	1	1,102	1,096	1,102	NMOSE	*
ST 00254 POD1	478461	3578608	73	73	1 and 2	1,119	1,053	1,119	NMOSE	*
ST 00052	494206	3578272	57	73	1	1,104	1,089	1,104	NMOSE	*
ST 00072	493805	3578067	57	74	1	1,118	1,057	1,118	NMOSE	*
ST 00078	489782	3575872	61	76	1	1,106	1,084	1,106	NMOSE	*
ST 00069	499785	3575849	51	76	1	1,112	1,099	1,112	NMOSE	*
ST 00071	490990	3574863	60	77	1 and 2	1,100	986	1,100	NMOSE	*
ST 00102	434576	3573550	78	78	1	1,336	1,317	1,336	NMOSE	*
ST 00199	473613	3573502	50	78	1	1,154	1,146	1,154	NMOSE	*

Table A-4.9 continued.

POD Number/ Well ID/ State Well Number	Easting	Northing	Model Row	Model Column	Model Layer or Layers Intersected by Screened Interval	Elevation of Top of Screen (m)	Elevation of Bottom of Screen (m)	Observed Groundwater Elevation (m)	Source	Note
ST 00070	500796	3573438	117	78	1	1,096	1,088	1,096	NMOSE	*
ST 00035	465493	3573243	86	78	1	1,163	1,148	1,163	NMOSE	*
ST 00053	492193	3572648	59	79	1	1,103	1,058	1,103	NMOSE	*
ST 00103	439978	3568708	111	83	1	1,294	1,272	1,294	NMOSE	*
ST 00048	495206	3567420	56	84	1	1,138	1,133	1,138	NMOSE	*
ST 00036	467360	3566280	84	85	1	1,127	1,105	1,127	NMOSE	*
ST 00086	492587	3565618	59	86	1	1,110	1,089	1,110	NMOSE	*
ST 00015	492488	3565519	59	86	1	1,113	1,089	1,113	NMOSE	*
ST 00037	500007	3565208	51	86	1	1,138	1,079	1,138	NMOSE	*
ST 00074	496386	3564607	55	87	1 and 2	1,108	1,016	1,108	NMOSE	*
ST 00077	508213	3564589	43	87	1	1,082	1,037	1,082	NMOSE	*
ST 00161	477637	3564446	74	87	1	1,124	1,029	1,124	NMOSE	*
ST 00088	487550	3563011	64	89	1	1,098	1,025	1,098	NMOSE	*
ST 00162	481454	3561014	70	91	1	1,090	1,075	1,090	NMOSE	*
ST 00087	487547	3561001	63	91	1	1,103	1,076	1,103	NMOSE	*
ST 00084	487747	3561001	64	91	1	1,102	1,064	1,102	NMOSE	*
ST 00089	487950	3561000	63	91	1	1,100	1,004	1,100	NMOSE	*
ST 00092	444365	3560630	107	91	1	1,227	1,166	1,227	NMOSE	*
ST 00097	440344	3560061	111	92	1	1,403	1,278	1,403	NMOSE	*
ST 00180 S	488148	3559592	63	92	1, 2, and 3	1,109	947	1,109	NMOSE	*
ST 00049	494596	3559387	57	92	1	1,106	1,104	1,106	NMOSE	*
ST 00038	458735	3558565	92	93	1 and 2	1,154	1,032	1,154	NMOSE	*
ST 00042	463561	3557747	88	94	1	1,152	1,121	1,152	NMOSE	*
ST 00163	479239	3557196	72	94	1	1,093	1,076	1,093	NMOSE	*
ST 00164	488754	3556577	62	95	1	1,106	1,088	1,106	NMOSE	*
ST 00192	493185	3555562	58	96	1	1,102	1,030	1,102	NMOSE	*
ST 00191	494594	3555559	57	96	1	1,112	1,039	1,112	NMOSE	*
ST 00028	445541	3554322	106	97	1	1,426	1,421	1,426	NMOSE	*
ST 00054	489965	3553359	61	98	1	1,106	1,037	1,106	NMOSE	*

Table A-4.9 continued.

847

POD Number/ Well ID/ State Well Number	Easting	Northing	Model Row	Model Column	Model Layer or Layers Intersected by Screened Interval	Elevation of Top of Screen (m)	Elevation of Bottom of Screen (m)	Observed Groundwater Elevation (m)	Source	Note
ST 00033	492178	3552346	59	99	1	1,104	1,025	1,104	NMOSE	*
ST 00182	492380	3552344	59	99	1	1,101	1,070	1,101	NMOSE	*
ST 00026	438231	3552247	113	99	1	1,441	1,426	1,441	NMOSE	*
ST 00110	491775	3551945	59	100	1 and 2	1,103	965	1,103	NMOSE	*
ST 00027	441810	3551427	109	100	1	1,389	1,371	1,389	NMOSE	*
ST 00107	428705	3550603	86	101	1	1,443	1,412	1,443	NMOSE	*
ST 00043	465163	3550511	123	101	1	1,105	1,044	1,105	NMOSE	*
ST 00040	469119	3549792	82	102	1	1,117	1,086	1,117	NMOSE	*
ST 00041	450338	3548063	101	104	1	1,413	1,398	1,413	NMOSE	*
ST 00051	451746	3547855	99	104	1	1,406	1,389	1,406	NMOSE	*
ST 00187 S	481046	3547755	70	104	1	1,105	1,084	1,105	NMOSE	*
C 02318	519164	3547455	32	104	1	1,793	1,776	1,793	NMOSE	*
ST 00024	438171	3547423	113	104	1	1,383	1,375	1,383	NMOSE	*
ST 00039	448727	3547265	102	104	1	1,447	1,425	1,447	NMOSE	*
ST 00106	437663	3546802	114	105	1	1,416	1,370	1,416	NMOSE	*
ST 00044	466258	3546182	85	105	1 and 2	1,119	1,024	1,119	NMOSE	*
ST 00032	453546	3545833	98	106	1	1,397	1,359	1,397	NMOSE	*
ST 00101	442084	3545493	109	106	1	1,423	1,365	1,423	NMOSE	*
ST 00046	474148	3545352	77	106	1	1,100	1,077	1,100	NMOSE	*
ST 00099	447914	3545254	103	106	1	1,550	1,535	1,550	NMOSE	*
ST 00108	432019	3545238	119	106	1	1,417	1,396	1,417	NMOSE	*
ST 00090	417884	3544898	85	107	1 and 2	1,558	1,545	1,558	NMOSE	*
ST 00045	465851	3544774	40	107	1 and 2	1,157	1,002	1,157	NMOSE	*
ST 00160	511665	3544666	133	107	1	1,101	988	1,101	NMOSE	*
ST 00186 S	487526	3544312	64	107	1	1,080	1,055	1,080	NMOSE	*
ST 00253 POD1	489252	3544154	62	107	1	1,091	1,060	1,091	NMOSE	*
ST 00186	487526	3544112	64	108	1	1,096	1,053	1,096	NMOSE	*
ST 00123	489740	3544106	61	108	1	1,095	1,045	1,095	NMOSE	*
ST 00057	490345	3544103	61	108	1	1,090	1,066	1,090	NMOSE	*

Table A-4.9 continued.

POD Number/ Well ID/ State Well Number	Easting	Northing	Model Row	Model Column	Model Layer or Layers Intersected by Screened Interval	Elevation of Top of Screen (m)	Elevation of Bottom of Screen (m)	Observed Groundwater Elevation (m)	Source	Note
ST 00091	416873	3544102	62	108	1 and 2	1,387	1,329	1,387	NMOSE	*
ST 00059	489135	3543905	134	108	1	1,092	986	1,092	NMOSE	*
ST 00116 B	487724	3543709	63	108	1	1,091	1,048	1,091	NMOSE	*
ST 00058	489939	3543499	61	108	1 and 2	1,092	983	1,092	NMOSE	*
ST 00187	479815	3543323	71	108	1	1,100	1,077	1,100	NMOSE	*
ST 00116	487320	3543307	64	108	1	1,090	1,069	1,090	NMOSE	*
ST 00034	449111	3543234	102	108	1	1,429	1,414	1,429	NMOSE	*
ST 00116 S	486716	3542904	65	109	1	1,091	1,088	1,091	NMOSE	*
ST 00059 S-3	489332	3542899	62	109	1, 2, and 3	1,092	806	1,092	NMOSE	*
ST 00031	455145	3542811	96	109	1	1,372	1,362	1,372	NMOSE	*
ST 00029	459818	3542789	91	109	1	1,127	1,117	1,127	NMOSE	*
ST 00047	468499	3542756	83	109	1	1,115	1,106	1,115	NMOSE	*
ST 00060 S-2	487519	3542699	64	109	1 and 2	1,092	950	1,092	NMOSE	*
ST 00125	488927	3542696	62	109	1	1,068	1,038	1,068	NMOSE	*, +
ST 00060	487519	3542499	64	109	1 and 2	1,091	958	1,091	NMOSE	*
ST 00187 S-2	483837	3542303	67	109	1	1,095	1,049	1,095	NMOSE	*
ST 00120	486712	3542298	65	109	1	1,092	1,043	1,092	NMOSE	*
ST 00059 S	489128	3542292	62	109	1 and 2	1,088	982	1,088	NMOSE	*
ST 00030	452522	3542012	99	110	1	1,399	1,394	1,399	NMOSE	*
ST 00188	488115	3541086	63	111	1	1,090	1,026	1,090	NMOSE	*
ST 00061 S	489122	3541081	62	111	1	1,097	1,085	1,097	NMOSE	*
ST 00245 POD1	515724	3540530	35	111	1	1,798	1,784	1,798	NMOSE	*
4806201	471768	3540444	64	111	1	1,111	866	1,111	TWDB	
4807218	481398	3540422	70	111	1, 2, 3, and 4	1,093	619	1,093	TWDB	*
4807314	487616	3540412	79	111	1, 2, and 3	1,081	1,044	1,096	TWDB	*
ST 00061	489761	3540319	61	111	1	1,089	1,018	1,089	NMOSE	*
4808201	494201	3539760	57	112	1	1,098	1,068	1,098	TWDB	*, +
4807219	482603	3539496	69	112	1, 2, and 3	1,032	945	1,090	TWDB	
4807206	481002	3539407	70	112	1	1,094	1,065	1,094	TWDB	

Table A-4.9 continued.

849

POD Number/ Well ID/ State Well Number	Easting	Northing	Model Row	Model Column	Model Layer or Layers Intersected by Screened Interval	Elevation of Top of Screen (m)	Elevation of Bottom of Screen (m)	Observed Groundwater Elevation (m)	Source	Note
4807313	485961	3538875	65	113	1	1,089	1,043	1,089	TWDB	*
4808102	488165	3538688	63	113	1 and 2	1,095	992	1,095	TWDB	
4807318	487325	3538658	64	113	1	1,096	1,066	1,096	TWDB	*, +
4806301	474466	3538497	77	113	1, 2, and 3	1,169	889	1,095	TWDB	*
4807213	482706	3538418	69	113	1, 2, and 3	1,095	852	1,095	TWDB	
4806303	475173	3538033	76	114	1	1,096	1,066	1,096	TWDB	*, +
4807107	477456	3537967	74	114	1, 2, and 3	1,143	798	1,089	TWDB	
4808103	489424	3537886	62	114	1	1,098	1,068	1,098	TWDB	*, +
4807307	487035	3537858	64	114	1	1,087	1,057	1,087	TWDB	*, +
4807108	477823	3537750	73	114	1, 2, and 3	1,139	789	1,088	TWDB	
4807106	477692	3537658	74	114	1, 2, and 3	1,138	790	1,089	TWDB	
4807207	480998	3537159	70	114	1, 2, and 3	1,095	914	1,095	TWDB	
4807109	480210	3537130	71	114	1	1,050	1,016	1,093	TWDB	
4807220	482126	3537095	69	115	1, 2, and 3	1,097	744	1,097	TWDB	*
4807204	482704	3537063	69	115	1	1,104	1,023	1,094	TWDB	*
4807315	485722	3537028	65	115	1	1,092	846	1,092	TWDB	*
4807308	485984	3537028	66	115	1, 2, and 3	1,104	1,022	1,095	TWDB	*
4807110	480184	3536976	71	115	1	1,097	1,060	1,097	TWDB	*
4806304	474357	3536958	77	115	1	1,096	1,066	1,096	TWDB	*, +
4807304	487533	3536656	64	115	1	1,095	1,050	1,095	TWDB	
4807214	482703	3536386	69	115	1 and 2	1,095	969	1,095	TWDB	
4806302	474434	3536373	77	115	1, 2, and 3	1,092	810	1,092	TWDB	
4807102	476875	3535967	74	116	1, 2, and 3	1,094	836	1,094	TWDB	
4807631	486008	3535334	64	116	1	1,095	1,065	1,095	TWDB	*, +
4807633	487557	3535332	65	116	1	1,096	1,066	1,096	TWDB	*, +
4806608	475193	3535324	76	116	1	1,096	1,066	1,096	TWDB	*, +
4806606	474458	3535295	77	116	1, 2, and 3	1,166	845	1,097	TWDB	*
4807606	484459	3535244	67	116	1	1,093	1,038	1,097	TWDB	

Table A-4.9 continued.

850

POD Number/ Well ID/ State Well Number	Easting	Northing	Model Row	Model Column	Model Layer or Layers Intersected by Screened Interval	Elevation of Top of Screen (m)	Elevation of Bottom of Screen (m)	Observed Groundwater Elevation (m)	Source	Note
4807521	482700	3534847	69	117	1	1,096	1,066	1,096	TWDB	*, +
4806602	476031	3534583	75	117	1, 2, and 3	1,155	837	1,097	TWDB	
4806605	472986	3534467	78	117	1, 2, and 3	1,181	837	1,097	TWDB	
4806604	472592	3534438	63	117	1	1,181	839	1,096	TWDB	*
4808403	488449	3534407	79	117	1, 2, and 3	1,100	1,034	1,100	TWDB	
4807527	481806	3534294	69	117	1	1,087	1,013	1,095	TWDB	*
4701401	503150	3534217	48	117	1	1,127	1,127	1,127	TWDB	*
4807522	481019	3534203	70	117	1, 2, and 3	1,086	889	1,086	TWDB	
4806603	472591	3534191	76	117	1	1,184	832	1,083	TWDB	
4806609	475216	3534185	79	117	1, 2, and 3	1,096	1,066	1,096	TWDB	*, +
4807632	484326	3534074	67	118	1	1,095	1,065	1,095	TWDB	*, +
4806601	473641	3534004	78	118	1, 2, and 3	1,162	731	1,093	TWDB	
4807418	476869	3533688	74	118	1, 2, and 3	1,094	871	1,094	TWDB	
4807405	478733	3533653	72	118	1	1,126	1,056	1,096	TWDB	
4807626	487634	3533577	63	118	1	1,098	1,019	1,098	TWDB	*
4808401	488579	3533576	64	118	1	1,102	1,017	1,102	TWDB	
4808406	488421	3533453	63	118	1 and 2	1,100	986	1,101	TWDB	*
4807619	486583	3533363	61	118	1	1,069	1,036	1,097	TWDB	*
4808402	490600	3533358	65	118	1	1,100	1,094	1,100	TWDB	
4807502	482697	3533246	69	118	1	1,095	1,057	1,095	TWDB	
4807526	483485	3533152	68	118	1	1,054	1,024	1,088	TWDB	*
4807420	476894	3532764	74	119	1, 2, and 3	1,116	702	1,096	TWDB	*
4807623	487659	3532592	64	119	1	1,097	1,041	1,097	TWDB	*
4807624	485978	3532563	65	119	1 and 2	1,078	989	1,095	TWDB	*
4807501	481383	3532386	70	119	1	1,088	1,058	1,097	TWDB	
4807505	481304	3532355	70	119	1, 2, and 3	1,096	848	1,096	TWDB	
4807427	477680	3532085	74	120	1	1,096	1,066	1,096	TWDB	*, +
4806610	475185	3532060	76	120	1	1,097	1,067	1,097	TWDB	*, +

Table A-4.9 continued.

POD Number/ Well ID/ State Well Number	Easting	Northing	Model Row	Model Column	Model Layer or Layers Intersected by Screened Interval	Elevation of Top of Screen (m)	Elevation of Bottom of Screen (m)	Observed Groundwater Elevation (m)	Source	Note
4808407	489365	3532005	62	120	1 and 2	971	732	1,096	TWDB	*
4807414	476892	3531933	61	120	1	1,096	950	1,096	TWDB	
4807410	479360	3531928	65	120	1	1,097	1,067	1,097	TWDB	+
4807627	484875	3531918	66	120	1	1,092	1,013	1,092	TWDB	*
4807607	485951	3531917	72	120	1	1,095	1,065	1,095	TWDB	+
4808408	490363	3531911	74	120	1 and 2	1,102	1,072	1,102	TWDB	*, +
4807628	484769	3531888	66	120	1	1,095	1,005	1,095	TWDB	*
4807510	482695	3531798	69	120	1 and 2	994	816	1,095	TWDB	*
4808405	490415	3531696	61	120	1	1,102	1,099	1,102	TWDB	*
4701701	502495	3531138	49	120	1	1,106	1,102	1,106	TWDB	*
4807901	487657	3531083	64	121	1	1,094	1,018	1,094	TWDB	
4807702	479358	3531004	72	121	1	1,097	1,067	1,097	TWDB	+
4807801	482667	3530906	69	121	1	1,094	1,054	1,094	TWDB	
4701901	509822	3530865	41	121	1, 2, 3, 4, and 5	1,196	-394	1,196	TWDB	*
4807809	481852	3530661	69	121	1, 2, and 3	1,114	849	1,094	TWDB	*
4807810	482693	3530413	69	121	1	980	948	1,090	TWDB	*
4807914	485713	3530254	66	121	1, 2, 3, and 4	1,095	653	1,095	TWDB	*
4806901	476074	3530242	75	121	1, 2, and 3	1,149	776	1,095	TWDB	*
4807813	483795	3529949	67	122	1 and 2	1,083	955	1,083	TWDB	
4807910	486367	3528960	65	123	1	926	731	1,093	TWDB	*
4807706	480194	3528878	71	123	1, 2, and 3	1,113	876	1,096	TWDB	
4807904	484501	3528286	67	123	1, 2, and 3	1,111	737	1,097	TWDB	
4807803	481060	3528014	70	124	1 and 2	1,097	973	1,097	TWDB	
4807815	481848	3527921	69	124	1, 2, and 3	1,075	859	1,075	TWDB	*
4807814	482241	3527704	69	124	1 and 2	1,096	966	1,096	TWDB	*
4807712	476775	3526915	74	125	1, 2, and 3	1,144	766	1,095	TWDB	
4807811	481846	3526874	69	125	1 and 2	1,102	994	1,084	TWDB	*
4807708	480191	3526846	71	125	1, 2, 3, and 4	1,092	653	1,092	TWDB	

Table A-4.9 continued.

POD Number/ Well ID/ State Well Number	Easting	Northing	Model Row	Model Column	Model Layer or Layers Intersected by Screened Interval	Elevation of Top of Screen (m)	Elevation of Bottom of Screen (m)	Observed Groundwater Elevation (m)	Source	Note
4807812	481898	3526812	52	125	1	1,078	861	1,078	TWDB	*
4808903	498765	3526796	69	125	1, 2, and 3	1,106	1,105	1,106	TWDB	*
4808902	498056	3526765	53	125	1	1,099	1,091	1,099	TWDB	*
4807713	476591	3526700	75	125	1, 2, and 3	1,149	806	1,096	TWDB	
4815105	478481	3526018	73	126	1	1,092	1,062	1,092	TWDB	*, +
4815303	484340	3525546	67	126	1, 2, and 3	1,033	795	1,096	TWDB	*
4815203	481054	3525120	70	126	1	1,107	1,033	1,097	TWDB	
4815201	483761	3525023	67	127	1	1,105	1,023	1,096	TWDB	
4815101	477506	3524881	74	127	1, 2, 3, and 4	973	-283	1,097	TWDB	
4815302	487676	3524833	64	127	1, 2, and 3	1,007	916	1,096	TWDB	
4815307	484365	3524745	67	127	1, 2, and 3	1,095	921	1,095	TWDB	*
4815104	480134	3524691	71	127	1, 2, and 3	1,094	711	1,095	TWDB	
4815103	480159	3524260	71	127	1, 2, 3, and 4	1,099	686	1,095	TWDB	
4815102	480133	3524137	71	127	1, 2, and 3	1,096	778	1,096	TWDB	
4709203	504047	3523810	47	128	1	1,099	1,081	1,099	TWDB	*
4815301	484389	3523606	67	128	1	1,097	1,016	1,097	TWDB	
4709205	503916	3523472	47	128	1	1,099	1,075	1,099	TWDB	*
4710201	516032	3523391	35	128	1	1,103	1,069	1,103	TWDB	*
4709206	504468	3523379	47	128	1	1,098	1,083	1,098	TWDB	*
4709204	504153	3523133	47	128	1	1,098	1,075	1,098	TWDB	*
4709101	503732	3522733	47	129	1	1,106	1,105	1,106	TWDB	*
4812401	442513	3521907	109	130	1, 2, 3, and 4	1,029	579	1,029	TWDB	*
4710501	516904	3520621	34	131	1	1,142	1,051	1,142	TWDB	*
4709502	505731	3520270	45	131	1	1,095	1,082	1,095	TWDB	*
4812502	447994	3519292	64	132	1, 2, 3, and 4	1,348	1,077	1,110	TWDB	*
4815601	487091	3519230	103	132	1	1,095	430	1,095	TWDB	
4816402	491218	3519103	60	133	1	1,078	1,071	1,100	TWDB	
4710401	514330	3518401	37	133	1	1,277	1,033	1,114	TWDB	*

Table A-4.9 continued.

POD Number/ Well ID/ State Well Number	Easting	Northing	Model Row	Model Column	Model Layer or Layers Intersected by Screened Interval	Elevation of Top of Screen (m)	Elevation of Bottom of Screen (m)	Observed Groundwater Elevation (m)	Source	Note
4709503	504970	3518084	46	134	1, 2, and 3	808	16	1,090	TWDB	*
4816501	492716	3517962	59	134	1	1,101	1,092	1,101	TWDB	*
4816403	491139	3517902	60	134	1	1,098	1,068	1,098	TWDB	*, +
4709806	505733	3516145	45	135	1, 2, and 3	1,028	897	1,095	TWDB	
4709805	505707	3516114	46	136	1 and 2	1,096	969	1,090	TWDB	
4709804	505681	3516083	46	136	1	1,035	1,000	1,081	TWDB	
4815801	480695	3515884	71	136	1	1,093	1,069	1,093	TWDB	
4816702	491321	3515654	60	136	1	1,106	1,067	1,096	TWDB	
4709908	508680	3515161	43	136	1	1,098	1,060	1,098	TWDB	
4709910	508890	3515100	42	137	1	1,102	1,011	1,102	TWDB	*
4812901	451261	3515088	42	137	1	1,112	1,082	1,112	TWDB	*, +
4709904	508890	3515069	100	137	1	1,097	1,062	1,097	TWDB	
4812701	441475	3514955	45	137	1	1,324	1,028	1,150	TWDB	*
4709807	505787	3514944	110	137	1 and 2	1,093	1,063	1,093	TWDB	+
4816703	491320	3514453	60	137	1	1,090	1,029	1,090	TWDB	*
4709903	507918	3514391	43	137	1 and 2	1,076	961	1,093	TWDB	
4709901	507918	3514330	43	137	1 and 2	1,105	980	1,098	TWDB	
4814801	471459	3513997	80	138	1	1,075	1,045	1,075	TWDB	*, +
4814702	465119	3513955	43	138	1	1,101	1,042	1,101	TWDB	
4709802	507813	3513899	86	138	1	1,099	1,083	1,099	TWDB	
4709902	508234	3513868	43	138	1	1,109	1,071	1,109	TWDB	
4709907	508997	3513776	42	138	1 and 2	1,090	986	1,090	TWDB	*
4709803	507840	3513344	43	138	1	1,094	1,064	1,094	TWDB	+
4709808	506656	3513220	45	138	1 and 2	974	898	1,088	TWDB	
4816705	488556	3513194	63	138	1	1,090	1,060	1,090	TWDB	+
4816805	495501	3513096	56	139	1	1,099	1,069	1,099	TWDB	+
4815902	488056	3513071	63	139	1	1,101	1,062	1,092	TWDB	
4709906	508997	3512883	42	139	1	1,094	1,055	1,094	TWDB	

Table A-4.9 continued.

POD Number/ Well ID/ State Well Number	Easting	Northing	Model Row	Model Column	Model Layer or Layers Intersected by Screened Interval	Elevation of Top of Screen (m)	Elevation of Bottom of Screen (m)	Observed Groundwater Elevation (m)	Source	Note
4815903	487661	3512733	64	139	1	1,090	1,065	1,090	TWDB	
4823202	481031	3512528	70	139	1	1,097	1,068	1,097	TWDB	
4717220	507814	3512451	43	139	1 and 2	1,090	967	1,090	TWDB	*
4823201	480847	3512312	43	139	1	1,091	1,039	1,091	TWDB	
4717315	508314	3512298	45	139	1	1,097	1,067	1,097	TWDB	
4717216	506472	3512297	70	139	1	1,096	1,066	1,096	TWDB	*, +
4824203	492134	3512267	59	139	1 and 2	1,091	967	1,091	TWDB	*
4824101	491370	3512083	60	140	1	1,103	1,073	1,103	TWDB	*, +
4717312	510919	3512023	40	140	1	1,107	1,031	1,107	TWDB	*
4717317	507919	3512020	43	140	1	995	964	1,095	TWDB	
4717201	507656	3511866	44	140	1	1,072	1,023	1,098	TWDB	
4717209	507025	3511866	44	140	1	1,079	1,038	1,095	TWDB	
4717212	507104	3511835	44	140	1	1,091	1,061	1,091	TWDB	*, +
4717319	509419	3511714	42	140	1	1,099	1,069	1,099	TWDB	*, +
4717211	506209	3511712	45	140	1	1,096	1,016	1,096	TWDB	
4824201	495738	3511310	55	140	1	1,100	1,094	1,100	TWDB	*
4717208	505999	3511188	45	140	1, 2, 3, and 4	1,084	615	1,095	TWDB	
4717206	507604	3511127	44	140	1, 2, and 3	1,104	912	1,109	TWDB	
4717204	506210	3510911	45	141	1, 2, and 3	1,107	854	1,093	TWDB	
4717313	509815	3510698	41	141	1	1,102	1,015	1,102	TWDB	*
4717203	507842	3510235	43	141	1 and 2	1,098	986	1,098	TWDB	
4717205	506131	3510234	45	141	1	1,084	1,029	1,097	TWDB	
4717202	505421	3510233	46	141	1	1,095	1,041	1,095	TWDB	
4717320	511263	3510115	40	142	1, 2, and 3	1,003	824	1,098	TWDB	
4824202	494105	3510110	57	142	1	1,096	1,066	1,096	TWDB	*, +
4717301	509316	3510020	42	142	1	1,099	1,029	1,098	TWDB	
4717207	506158	3510018	45	142	1, 2, and 3	1,037	940	1,099	TWDB	
4717314	509684	3509959	42	142	1	1,101	1,042	1,101	TWDB	*

Table A-4.9 continued.

POD Number/ Well ID/ State Well Number	Easting	Northing	Model Row	Model Column	Model Layer or Layers Intersected by Screened Interval	Elevation of Top of Screen (m)	Elevation of Bottom of Screen (m)	Observed Groundwater Elevation (m)	Source	Note
4717215	506264	3508571	45	143	1	1,100	1,070	1,100	TWDB	*, +
4718101	513239	3508424	38	143	1	1,130	1,069	1,130	TWDB	*
4823101	479813	3508250	71	143	1	1,106	1,076	1,106	TWDB	*, +
4717218	506975	3508202	44	143	1	1,103	1,020	1,100	TWDB	
4824401	488366	3507621	63	144	1	1,097	1,058	1,097	TWDB	*
4824502	495788	3507031	55	145	1	1,087	1,028	1,092	TWDB	*
4820601	452194	3506555	99	145	1	1,088	1,058	1,088	TWDB	+
4821401	454403	3505991	97	146	1, 2, and 3	1,106	919	1,106	TWDB	*
4821502	460062	3505598	91	146	1	1,104	1,074	1,104	TWDB	*, +
4717605	507872	3505124	43	146	1	1,099	1,095	1,099	TWDB	
4717601	509610	3505095	42	147	1	1,104	1,075	1,101	TWDB	
4717602	509189	3504694	42	147	1	1,096	1,069	1,096	TWDB	
4824601	497051	3504536	54	147	1	1,097	1,067	1,097	TWDB	*, +
4718707	512350	3503466	39	148	1, 2, and 3	1,105	843	1,098	TWDB	
4717904	511534	3503434	40	148	1	1,098	1,020	1,098	TWDB	
4718802	515905	3503286	35	148	1	1,104	1,065	1,119	TWDB	
4718706	512324	3503004	39	149	1 and 2	1,100	988	1,100	TWDB	
4717903	511455	3502664	40	149	1	1,099	1,002	1,099	TWDB	
4718801	515960	3501439	35	150	1	1,095	1,065	1,095	TWDB	*, +
4824904	498025	3500503	53	151	1	1,090	1,060	1,090	TWDB	*, +
4824903	496497	3499457	55	152	1	1,051	1,037	1,051	TWDB	*
4823701	477319	3499450	74	152	1	1,102	1,072	1,102	TWDB	*, +
4726101	512593	3498170	39	153	1	1,095	1,085	1,095	TWDB	
4726102	514913	3497188	36	154	1	1,097	1,087	1,097	TWDB	*
4832301	498867	3496962	52	155	1	1,097	1,035	1,097	TWDB	*
4829301	461266	3496603	90	155	1	1,256	1,097	1,103	TWDB	
4829101	455179	3496536	96	155	1	1,322	1,297	1,309	TWDB	*
4829102	455205	3496536	96	155	1	1,323	1,300	1,309	TWDB	*

Table A-4.9 continued.

POD Number/ Well ID/ State Well Number	Easting	Northing	Model Row	Model Column	Model Layer or Layers Intersected by Screened Interval	Elevation of Top of Screen (m)	Elevation of Bottom of Screen (m)	Observed Groundwater Elevation (m)	Source	Note
4829103	455231	3496535	96	155	1	1,324	1,296	1,308	TWDB	*
4829104	455205	3496505	96	155	1	1,323	1,302	1,309	TWDB	*
4828301	452300	3495255	99	156	1	1,332	1,302	1,332	TWDB	*, +
4832601	499157	3493945	52	158	1	1,097	1,085	1,097	TWDB	*
4832602	497760	3493576	53	158	1	1,095	1,068	1,095	TWDB	*
4726501	517081	3492912	34	159	1	1,081	1,073	1,094	TWDB	
4830401	466018	3491476	85	160	1, 2, and 3	1,118	970	1,118	TWDB	
4836101	441569	3484996	110	167	1	1,426	1,396	1,426	TWDB	*, +

Table A-4.9 continued.

Source Key: NMOSE = New Mexico Office of the State Engineer's New Mexico Water Rights Reporting System online database, SMHS = New Mexico Bureau of Geology & Mineral Resources' Sacramento Mountains Hydrogeology Study, TWDB = Texas Water Development Board groundwater database.

Note Key: * = One water level measurement, Assumed 30 meter (98 feet) screened interval length.

Hydrogeologic Unit	Minimum Porosity (%)	Averge Porosity (%)	Maximum Porosity (%)
Cenozoic alluvium	5	12.5	20
Cenozoic intrusions	0.1	0.5	1
Cretaceous	5	12.5	20
Low permeability confining unit beneath Cretaceous	5	12.5	20
Unfractured Permian	5	12.5	20
Fractured Permian	5	12.5	20
Paleozoic (Cambrian through Pennslyvanian)	1	5.5	10
Precambrian	0.1	0.5	1

Table A-4.10: Minimum, average, and maximum porosity values used for MODPATH solution.

Groundwater Age Well ID	POD Number	Easting	Northing	Model Row	Model Column	Model Layer	Ground Surface Elevation (m)	Well Depth (m)	Elevation of Well Depth (m)	Note
Doll Day	ST 00241 POD1	472590	3607544	79	44	1	1,718	475	1,243	Well depth from well owner
Piñon Well	ST 00003	478550	3606619	73	45	1	1,623	335	1,287	Well depth from NMOSE
Webb House	NA	465825	3606007	85	46	1	1,815	457	1,358	Well depth unkown; estimated
Uña	ST 00018	473476	3596830	78	55	1	1,743	390	1,353	Well depth from NMOSE
Cauhape	ST 00019	476365	3588074	75	64	1	1,447	315	1,131	Well depth from NMOSE
Jeffer's Well	NA	467327	3585742	84	66	1	1,481	305	1,177	Well depth from well owner
Ellett Lower	NA	469670	3578554	82	73	1	1,397	160	1,237	Well depth from well owner
Harvey Lewis Well	ST 00014	487565	3571656	64	80	1	1,181	91	1,090	Well depth from NMOSE
Collins	NA	499579	3568454	52	83	1	1,238	183	1,055	Well depth from well owner
Evrage House	ST 00050	496187	3563804	55	88	1	1,147	61	1,086	Well depth from NMOSE
Lewis	ST 00163	479239	3557196	72	94	1	1,230	154	1,076	Well depth from NMOSE
Butterfield Well	ST 00044	466258	3546182	85	105	2	1,268	244	1,024	Well depth from NMOSE
Hunt 8	ST 00057	490345	3544103	61	108	1	1,114	48	1,066	Well depth from NMOSE

Table A-4.11: Groundwater age wells incorporated into MODPATH particle tracking exercise.

POD Number Key: NA = Not applicable.

Groundwater Age Well ID	Elevation of Well Depth (m)	Water-balance Based Minimum Recharge Scenario			Water-balance Based Average Recharge Scenario			Water-balance Based Maximum Recharge Scenario		
		Elevation of Computed Groundwater Surface (m)	Elevation of Midpoint (m)	Elevation of Bottom of Cell (m)	Elevation of Computed Groundwater Surface (m)	Elevation of Midpoint (m)	Elevation of Bottom of Cell (m)	Elevation of Computed Groundwater Surface (m)	Elevation of Midpoint (m)	Elevation of Bottom of Cell (m)
Doll Day	1,243	1,401	1,297	1,192	1,398	1,295	1,192	1,412	1,302	1,192
Pinon Well	1,287	1,359	1,256	1,154	1,349	1,251	1,154	1,368	1,261	1,154
Webb House	1,358	1,429	1,328	1,227	1,428	1,328	1,227	1,445	1,336	1,227
Una	1,353	1,334	1,227	1,120	1,323	1,222	1,120	1,338	1,229	1,120
Cauhape	1,131	1,276	1,167	1,058	1,254	1,156	1,058	1,267	1,163	1,058
Jeffer's Well	1,177	1,301	1,201	1,101	1,272	1,186	1,101	1,276	1,189	1,101
Ellett Lower	1,237	1,269	1,173	1,077	1,231	1,154	1,077	1,230	1,154	1,077
Harvey Lewis Well	1,090	1,157	1,087	1,018	1,143	1,080	1,018	1,154	1,086	1,018
Collins	1,055	1,169	1,093	1,018	1,152	1,085	1,018	1,164	1,091	1,018
Evrage House	1,086	1,146	1,093	1,040	1,135	1,088	1,040	1,144	1,092	1,040
Lewis	1,076	1,155	1,076	997	1,139	1,068	997	1,139	1,068	997
Butterfield Well	1,024	1,031	1,006	981	1,031	1,006	981	1,031	1,006	981
Hunt 8	1,066	1,110	1,054	997	1,109	1,053	997	1,111	1,054	997

Table A-4.12: Elevations at which MODPATH particles were generated for the calibrated water-balance based minimum, average, and maximum recharge scenario models.

Orange highlighted rectangles indicate the vertical position of generated MODPATH particles chosen to represent the potential pathlines and residence times of groundwater sampled at each well.

Groundwater Age Well ID	Elevation of Well Depth (m)	Elevation-dependent Minimum Recharge Scenario			Elevation-dependent Average Recharge Scenario			Elevation-dependent Maximum Recharge Scenario		
		Elevation of Computed Groundwater Surface (m)	Elevation of Midpoint (m)	Elevation of Bottom of Cell (m)	Elevation of Computed Groundwater Surface (m)	Elevation of Midpoint (m)	Elevation of Bottom of Cell (m)	Elevation of Computed Groundwater Surface (m)	Elevation of Midpoint (m)	Elevation of Bottom of Cell (m)
Doll Day	1,243	1,462	1,327	1,192	1,464	1,328	1,192	1,454	1,323	1,192
Pinon Well	1,287	1,399	1,276	1,154	1,396	1,275	1,154	1,390	1,272	1,154
Webb House	1,358	1,491	1,359	1,227	1,495	1,361	1,227	1,483	1,355	1,227
Una	1,353	1,338	1,229	1,120	1,334	1,227	1,120	1,332	1,226	1,120
Cauhape	1,131	1,248	1,153	1,058	1,231	1,145	1,058	1,240	1,149	1,058
Jeffer's Well	1,177	1,274	1,188	1,101	1,267	1,184	1,101	1,284	1,193	1,101
Ellett Lower	1,237	1,243	1,160	1,077	1,226	1,152	1,077	1,251	1,164	1,077
Harvey Lewis Well	1,090	1,143	1,081	1,018	1,123	1,071	1,018	1,125	1,071	1,018
Collins	1,055	1,140	1,079	1,018	1,125	1,072	1,018	1,123	1,071	1,018
Evrage House	1,086	1,136	1,088	1,040	1,122	1,081	1,040	1,121	1,081	1,040
Lewis	1,076	1,149	1,073	997	1,135	1,066	997	1,142	1,070	997
Butterfield Well	1,024	1,031	1,006	981	1,031	1,006	981	1,031	1,006	981
Hunt 8	1,066	1,113	1,055	997	1,114	1,056	997	1,110	1,054	997

Table A-4.13: Elevations at which MODPATH particles were generated for the calibrated elevation-dependent minimum, average, and maximum recharge scenario models.

Orange highlighted rectangles indicate the vertical position of generated MODPATH particles chosen to represent the potential pathlines and residence times of groundwater sampled at each well.

Water-balance Based Minimum Recharge Scenario					
Boundary Condition	Inflow (m^3/day)	Inflow (acre-feet/year)	Outflow (m^3/day)	Outflow (acre-feet/year)	Percent Difference
Recharge	164,688	48,765			
Wells (Discharge at Salt Flats)	0	0	164,688	48,765	
Total	164,688	48,765	164,688	48,765	0
Water-balance Based Average Recharge Scenario					
Boundary Condition	Inflow (m^3/day)	Inflow (acre-feet/year)	Outflow (m^3/day)	Outflow (acre-feet/year)	Percent Difference
Recharge	272,956	80,824			
Wells (Discharge at Salt Flats)	0	0	272,956	80,824	
Total	272,956	80,824	272,956	80,824	0
Water-balance Based Maximum Recharge Scenario					
Boundary Condition	Inflow (m^3/day)	Inflow (acre-feet/year)	Outflow (m^3/day)	Outflow (acre-feet/year)	Percent Difference
Recharge	354,670	105,020			
Wells (Discharge at Salt Flats)	0	0	354,670	105,020	
Total	354,670	105,020	354,670	105,020	0

Table A-4.14: Mass balances for the calibrated water-balance based minimum, average, and maximum recharge scenario models.

Elevation-dependent Minimum Recharge Scenario					
Boundary Condition	Inflow (m³/day)	Inflow (acre-feet/year)	Outflow (m³/day)	Outflow (acre-feet/year)	Percent Difference
Recharge	9,078	2,688			
Wells (Discharge at Salt Flats)	0	0	9,078	2,688	
Total	9,078	2,688	9,078	2,688	0
Elevation-dependent Average Recharge Scenario					
Boundary Condition	Inflow (m³/day)	Inflow (acre-feet/year)	Outflow (m³/day)	Outflow (acre-feet/year)	Percent Difference
Recharge	49,738	14,728			
Wells (Discharge at Salt Flats)	0	0	49,738	14,728	
Total	49,738	14,728	49,738	14,728	0
Elevation-dependent Maximum Recharge Scenario					
Boundary Condition	Inflow (m³/day)	Inflow (acre-feet/year)	Outflow (m³/day)	Outflow (acre-feet/year)	Percent Difference
Recharge	99,337	29,414			
Wells (Discharge at Salt Flats)	0	0	99,337	29,414	
Total	99,337	29,414	99,337	29,414	0

Table A-4.15: Mass balances for the calibrated elevation-dependent minimum, average, and maximum recharge scenario models.

Water-balance Based Minimum Recharge Scenario	
Sum Residuals (m)	44
Sum Absolute Residuals (m)	11,780
Sum Squared Residuals (m^2)	1,400,350
RMS Error (m)	61
Residual Mean (m)	0.1
Absolute Residual Mean (m)	16
Residual Standard Deviation (m)	61
Minimum Observed Hydraulic Head (m)	1,029
Maximum Observed Hydraulic Head (m)	2,610
Residual Standard Deviation/Range	0.039
Residual Mean/Range	0.00007
Water-balance Based Average Recharge Scenario	
Sum Residuals (m)	-649
Sum Absolute Residuals (m)	10,793
Sum Squared Residuals (m^2)	1,379,233
RMS Error (m)	60
Residual Mean (m)	-2
Absolute Residual Mean (m)	13
Residual Standard Deviation (m)	60
Minimum Observed Hydraulic Head (m)	1,029
Maximum Observed Hydraulic Head (m)	2,610
Residual Standard Deviation/Range	0.038
Residual Mean/Range	-0.001
Water-balance Based Maximum Recharge Scenario	
Sum Residuals (m)	236
Sum Absolute Residuals (m)	10,568
Sum Squared Residuals (m^2)	1,318,998
RMS Error (m)	59
Residual Mean (m)	0.6
Absolute Residual Mean (m)	14
Residual Standard Deviation (m)	59
Minimum Observed Hydraulic Head (m)	1,029
Maximum Observed Hydraulic Head (m)	2,610
Residual Standard Deviation/Range	0.037
Residual Mean/Range	0.0004

Table A-4.16: Residual hydraulic head statistics for the calibrated water-balance based minimum, average, and maximum recharge scenario models.

Elevation-dependent Minimum Recharge Scenario	
Sum Residuals (m)	1,364
Sum Absolute Residuals (m)	15,478
Sum Squared Residuals (m^2)	2,208,280
RMS Error (m)	76
Residual Mean (m)	4
Absolute Residual Mean (m)	22
Residual Standard Deviation (m)	76
Minimum Observed Hydraulic Head (m)	1,029
Maximum Observed Hydraulic Head (m)	2,610
Residual Standard Deviation/Range	0.048
Residual Mean/Range	0.002

Elevation-dependent Average Recharge Scenario	
Sum Residuals (m)	1,621
Sum Absolute Residuals (m)	16,612
Sum Squared Residuals (m^2)	2,291,432
RMS Error (m)	78
Residual Mean (m)	4
Absolute Residual Mean (m)	24
Residual Standard Deviation (m)	78
Minimum Observed Hydraulic Head (m)	1,029
Maximum Observed Hydraulic Head (m)	2,610
Residual Standard Deviation/Range	0.049
Residual Mean/Range	0.003

Elevation-dependent Maximum Recharge Scenario	
Sum Residuals (m)	951
Sum Absolute Residuals (m)	14,836
Sum Squared Residuals (m^2)	2,018,583
RMS Error (m)	73
Residual Mean (m)	3
Absolute Residual Mean (m)	21
Residual Standard Deviation (m)	73
Minimum Observed Hydraulic Head (m)	1,029
Maximum Observed Hydraulic Head (m)	2,610
Residual Standard Deviation/Range	0.046
Residual Mean/Range	0.002

Table A-4.17: Residual hydraulic head statistics for the calibrated elevation-dependent minimum, average, and maximum recharge scenario models.

Recharge Scenario	Minimum T (m^2/day)	Maximum T (m^2/day)
Water-balance Based Minimum	0.53	23,000
Water-balance Based Average	0.80	230,000
Water-balance Based Maximum	0.68	230,000

Table A-4.18: Range of transmissivity [T] values derived from the calibrated water-balance based minimum, average, and maximum recharge scenario models.

Recharge Scenario	Minimum T (m^2/day)	Maximum T (m^2/day)
Elevation-dependent Minimum	0.083	4,500
Elevation-dependent Average	0.31	23,000
Elevation-dependent Maximum	0.33	23,000

Table A-4.19: Range of transmissivity [T] values derived from the calibrated elevation-dependent minimum, average, and maximum recharge scenario models.

Water-balance Based Minimum Recharge Scenario										
Groundwater Age Well ID	NETPATH Age (years)	Minimum Porosity			Average Porosity			Maximum Porosity		
		MODPATH Age on Computed Groundwater Surface (years)	MODPATH Age on Midpoint (years)	MODPATH Age on Bottom of Cell (years)	MODPATH Age on Computed Groundwater Surface (years)	MODPATH Age on Midpoint (years)	MODPATH Age on Bottom of Cell (years)	MODPATH Age on Computed Groundwater Surface (years)	MODPATH Age on Midpoint (years)	MODPATH Age on Bottom of Cell (years)
Doll Day	2,900	NA	1,211	5,051	NA	3,027	12,627	NA	4,844	20,203
Pinon Well	4,200	2	639	NA	5	1,599	NA	8	2,558	NA
Webb House	1,000	2	2,163	NA	5	5,409	NA	8	8,654	NA
Una	7,100	1	NA	NA	3	NA	NA	4	NA	NA
Cauhape	8,000	NA	290	6,541	NA	726	16,351	NA	1,161	26,162
Jeffer's Well	8,200	NA	223	462	NA	558	1,155	NA	893	1,848
Ellett Lower	13,800	0	214	NA	1	535	NA	2	856	NA
Harvey Lewis Well	12,000	7	301	NA	17	753	NA	28	1,204	NA
Collins	9,700	NA	447	1,087	NA	1,116	2,719	NA	1,786	4,350
Evrage House	12,800	NA	409	543	NA	1,023	1,358	NA	1,636	2,174
Lewis	11,000	NA	231	609	NA	577	1,523	NA	924	2,437
Butterfield Well	16,100	1,758	1,870	NA	4,396	4,675	NA	7,033	7,480	NA
Hunt 8	14,100	6	1,585	NA	14	3,961	NA	23	6,338	NA

Table A-4.20: NETPATH ages from Sigstedt (2010) and MODPATH ages from the calibrated water-balance based minimum recharge scenario MODFLOW solution using minimum, average, and maximum porosities.

Orange highlighted rectangles indicate the MODPATH ages chosen to bound the residence time of groundwater sampled at each well.

		Water-balance Based Average Recharge Scenario								
		Minimum Porosity			Average Porosity			Maximum Porosity		
Groundwater Age Well ID	NETPATH Age (years)	MODPATH Age on Computed Groundwater Surface (years)	MODPATH Age on Midpoint (years)	MODPATH Age on Bottom of Cell (years)	MODPATH Age on Computed Groundwater Surface (years)	MODPATH Age on Midpoint (years)	MODPATH Age on Bottom of Cell (years)	MODPATH Age on Computed Groundwater Surface (years)	MODPATH Age on Midpoint (years)	MODPATH Age on Bottom of Cell (years)
Doll Day	2,900	NA	772	3,631	NA	1,930	9,078	NA	3,087	14,525
Pinon Well	4,200	1	395	NA	2	989	NA	3	1,582	NA
Webb House	1,000	1	1,035	NA	3	2,588	NA	4	4,141	NA
Una	7,100	0	NA	NA	1	NA	NA	2	NA	NA
Cauhape	8,000	NA	222	3,886	NA	554	9,716	NA	886	15,546
Jeffer's Well	8,200	NA	151	277	NA	377	692	NA	603	1,108
Ellett Lower	13,800	0	NA	NA	1	NA	NA	1	NA	NA
Harvey Lewis Well	12,000	3	159	NA	8	397	NA	12	636	NA
Collins	9,700	NA	189	421	NA	472	1,052	NA	756	1,683
Evrage House	12,800	NA	365	368	NA	912	919	NA	1,459	1,471
Lewis	11,000	0	142	NA	1	356	NA	1	569	NA
Butterfield Well	16,100	1,483	2,462	NA	3,706	6,157	NA	5,930	9,850	NA
Hunt 8	14,100	3	1,254	NA	7	3,136	NA	11	5,017	NA

Table A-4.21: NETPATH ages from Sigstedt (2010) and MODPATH ages from the calibrated water-balance based average recharge scenario MODFLOW solution using minimum, average, and maximum porosities.

Orange highlighted rectangles indicate the MODPATH ages chosen to bound the residence time of groundwater sampled at each well.

		Water-balance Based Maximum Recharge Scenario								
		Minimum Porosity			Average Porosity			Maximum Porosity		
Groundwater Age Well ID	NETPATH Age (years)	MODPATH Age on Computed Groundwater Surface (years)	MODPATH Age on Midpoint (years)	MODPATH Age on Bottom of Cell (years)	MODPATH Age on Computed Groundwater Surface (years)	MODPATH Age on Midpoint (years)	MODPATH Age on Bottom of Cell (years)	MODPATH Age on Computed Groundwater Surface (years)	MODPATH Age on Midpoint (years)	MODPATH Age on Bottom of Cell (years)
Doll Day	2,900	NA	686	2,776	NA	1,715	6,939	NA	2,744	11,103
Pinon Well	4,200	0	339	NA	1	848	NA	2	1,357	NA
Webb House	1,000	1	1,053	NA	2	2,633	NA	4	4,212	NA
Una	7,100	0	NA	NA	1	NA	NA	1	NA	NA
Cauhape	8,000	NA	137	2,499	NA	342	6,248	NA	547	9,997
Jeffer's Well	8,200	NA	85	159	NA	213	397	NA	341	634
Ellett Lower	13,800	0	NA	NA	0	NA	NA	1	NA	NA
Harvey Lewis Well	12,000	5	119	NA	11	297	NA	18	476	NA
Collins	9,700	NA	210	445	NA	524	1,112	NA	838	1,779
Evrage House	12,800	NA	254	296	NA	635	739	NA	1,016	1,182
Lewis	11,000	0	134	NA	1	334	NA	1	534	NA
Butterfield Well	16,100	801	906	NA	2,002	2,265	NA	3,203	3,624	NA
Hunt 8	14,100	4	943	NA	10	2,359	NA	15	3,774	NA

Table A-4.22: NETPATH ages from Sigstedt (2010) and MODPATH ages from the calibrated water-balance based maximum recharge scenario MODFLOW solution using minimum, average, and maximum porosities.

Orange highlighted rectangles indicate the MODPATH ages chosen to bound the residence time of groundwater sampled at each well.

Elevation-dependent Minimum Recharge Scenario									
		Minimum Porosity			Average Porosity			Maximum Porosity		
Groundwater Age Well ID	NETPATH Age (years)	MODPATH Age on Computed Groundwater Surface (years)	MODPATH Age on Midpoint (years)	MODPATH Age on Bottom of Cell (years)	MODPATH Age on Computed Groundwater Surface (years)	MODPATH Age on Midpoint (years)	MODPATH Age on Bottom of Cell (years)	MODPATH Age on Computed Groundwater Surface (years)	MODPATH Age on Midpoint (years)	MODPATH Age on Bottom of Cell (years)
Doll Day	2,900	NA	29,209	31,326	NA	73,024	78,315	NA	116,838	125,304
Pinon Well	4,200	39,254	39,614	NA	98,136	99,034	NA	157,017	158,455	NA
Webb House	1,000	NA	25,841	28,442	NA	64,603	71,104	NA	103,365	113,767
Una	7,100	30,123	NA	NA	75,308	NA	NA	120,492	NA	NA
Cauhape	8,000	NA	37,965	65,573	NA	94,912	174,911	NA	151,860	284,339
Jeffer's Well	8,200	NA	37,819	38,024	NA	94,548	95,061	NA	151,277	152,097
Ellett Lower	13,800	47,809	47,940	NA	119,524	119,850	NA	191,238	191,761	NA
Harvey Lewis Well	12,000	43,494	43,553	NA	108,736	108,882	NA	173,978	174,210	NA
Collins	9,700	NA	619,774	611,088	NA	1,552,414	1,530,378	NA	2,485,056	2,450,553
Evrage House	12,800	NA	64,322	62,917	NA	160,806	157,294	NA	257,290	251,670
Lewis	11,000	77,238	81,206	NA	193,095	203,015	NA	308,953	324,823	NA
Butterfield Well	16,100	27,025	27,276	NA	67,562	68,191	NA	108,100	109,106	NA
Hunt 8	14,100	91,061	92,916	NA	227,653	248,452	NA	364,245	406,894	NA

Table A-4.23: NETPATH ages from Sigstedt (2010) and MODPATH ages from the calibrated elevation-dependent minimum recharge scenario MODFLOW solution using minimum, average, and maximum porosities.

Orange highlighted rectangles indicate the MODPATH ages chosen to bound the residence time of groundwater sampled at each well.

Elevation-dependent Average Recharge Scenario									
		Minimum Porosity			Average Porosity			Maximum Porosity		
Groundwater Age Well ID	NETPATH Age (years)	MODPATH Age on Computed Groundwater Surface (years)	MODPATH Age on Midpoint (years)	MODPATH Age on Bottom of Cell (years)	MODPATH Age on Computed Groundwater Surface (years)	MODPATH Age on Midpoint (years)	MODPATH Age on Bottom of Cell (years)	MODPATH Age on Computed Groundwater Surface (years)	MODPATH Age on Midpoint (years)	MODPATH Age on Bottom of Cell (years)
Doll Day	2,900	NA	5,057	8,541	NA	12,642	21,352	NA	20,227	34,163
Pinon Well	4,200	4,558	4,688	NA	11,396	11,721	NA	18,233	18,753	NA
Webb House	1,000	NA	4,131	5,751	NA	10,328	14,376	NA	16,525	23,002
Una	7,100	4,973	NA	NA	12,434	NA	NA	19,894	NA	NA
Cauhape	8,000	NA	6,352	8,984	NA	15,880	22,459	NA	25,408	35,935
Jeffer's Well	8,200	NA	5,721	5,776	NA	14,303	14,439	NA	22,885	23,103
Ellett Lower	13,800	7,474	NA	NA	18,685	NA	NA	29,896	NA	NA
Harvey Lewis Well	12,000	6,924	7,281	NA	17,311	18,203	NA	27,697	29,125	NA
Collins	9,700	NA	401,260	406,635	NA	1,003,149	1,016,589	NA	1,605,040	1,626,542
Evrage House	12,800	387,340	7,445	NA	968,351	18,612	NA	1,549,362	29,780	NA
Lewis	11,000	21,646	22,039	NA	54,115	55,098	NA	86,585	88,157	NA
Butterfield Well	16,100	5,094	5,217	NA	12,736	13,043	NA	20,377	20,869	NA
Hunt 8	14,100	24,184	33,523	NA	60,459	83,808	NA	96,734	134,093	NA

Table A-4.24: NETPATH ages from Sigstedt (2010) and MODPATH ages from the calibrated elevation-dependent average recharge scenario MODFLOW solution using minimum, average, and maximum porosities.

Orange highlighted rectangles indicate the MODPATH ages chosen to bound the residence time of groundwater sampled at each well.

| Elevation-dependent Maximum Recharge Scenario | | | | | | | | | |
| Groundwater Age Well ID | NETPATH Age (years) | Minimum Porosity | | | Average Porosity | | | Maximum Porosity | | |
		MODPATH Age on Computed Groundwater Surface (years)	MODPATH Age on Midpoint (years)	MODPATH Age on Bottom of Cell (years)	MODPATH Age on Computed Groundwater Surface (years)	MODPATH Age on Midpoint (years)	MODPATH Age on Bottom of Cell (years)	MODPATH Age on Computed Groundwater Surface (years)	MODPATH Age on Midpoint (years)	MODPATH Age on Bottom of Cell (years)
Doll Day	2,900	NA	2,446	4,669	NA	6,116	11,672	NA	9,785	18,675
Pinon Well	4,200	2,353	2,408	NA	5,882	6,020	NA	9,411	9,632	NA
Webb House	1,000	2,001	2,174	NA	5,002	5,435	NA	8,004	8,696	NA
Una	7,100	2,515	NA	NA	6,287	NA	NA	10,060	NA	NA
Cauhape	8,000	NA	3,216	5,989	NA	8,039	14,971	NA	12,863	23,954
Jeffer's Well	8,200	NA	3,256	3,279	NA	8,140	8,197	NA	13,024	13,115
Ellett Lower	13,800	3,929	3,948	NA	9,824	9,871	NA	15,718	15,794	NA
Harvey Lewis Well	12,000	3,540	3,580	NA	8,851	8,950	NA	14,161	14,321	NA
Collins	9,700	NA	836,078	676,253	NA	2,734,009	2,107,019	NA	4,638,479	3,543,782
Evrage House	12,800	39,353	3,748	NA	98,381	9,370	NA	157,410	14,992	NA
Lewis	11,000	6,904	7,009	NA	17,259	17,522	NA	27,615	28,035	NA
Butterfield Well	16,100	2,512	2,520	NA	6,279	6,301	NA	10,046	10,081	NA
Hunt 8	14,100	7,254	7,517	NA	18,136	18,792	NA	29,017	30,067	NA

Table A-4.25: NETPATH ages from Sigstedt (2010) and MODPATH ages from the calibrated elevation-dependent maximum recharge scenario MODFLOW solution using minimum, average, and maximum porosities.

Orange highlighted rectangles indicate the MODPATH ages chosen to bound the residence time of groundwater sampled at each well.

Water-balance Based Minimum Recharge Scenario								
	Minimum Porosity			Average Porosity			Maximum Porosity		
Groundwater Age Well ID	Standard Deviation of MODPATH Ages on Computed Groundwater Surface (years)	Standard Deviation of MODPATH Ages on Midpoint (years)	Standard Deviation of MODPATH Ages on Bottom of Cell (years)	Standard Deviation of MODPATH Ages on Computed Groundwater Surface (years)	Standard Deviation of MODPATH Ages on Midpoint (years)	Standard Deviation of MODPATH Ages on Bottom of Cell (years)	Standard Deviation of MODPATH Ages on Computed Groundwater Surface (years)	Standard Deviation of MODPATH Ages on Midpoint (years)	Standard Deviation of MODPATH Ages on Bottom of Cell (years)
Doll Day	NA	108	315	NA	269	788	NA	430	1,260
Pinon Well	0	12	NA	0	29	NA	0	46	NA
Webb House	0	39	NA	0	97	NA	0	156	NA
Una	0	NA	NA	0	NA	NA	0	NA	NA
Cauhape	NA	0	253	NA	1	632	NA	1	1,011
Jeffer's Well	NA	0	7	NA	1	18	NA	2	29
Ellett Lower	0	2	NA	0	6	NA	0	10	NA
Harvey Lewis Well	1	5	NA	4	13	NA	6	21	NA
Collins	NA	3	24	NA	8	61	NA	12	98
Evrage House	NA	55	141	NA	137	352	NA	219	562
Lewis	NA	6	75	NA	15	188	NA	23	301
Butterfield Well	37	49	NA	92	124	NA	148	198	NA
Hunt 8	0	297	NA	0	742	NA	0	1,188	NA

Table A-4.26: Standard deviation of MODPATH ages from the calibrated water-balance based minimum recharge scenario MODFLOW solution using minimum, average, and maximum porosities.

Orange highlighted rectangles indicate the vertical position of generated MODPATH particles chosen to represent the potential pathlines and residence times of groundwater sampled at each well.

	Water-balance Based Average Recharge Scenario								
	Minimum Porosity			Average Porosity			Maximum Porosity		
Groundwater Age Well ID	Standard Deviation of MODPATH Ages on Computed Groundwater Surface (years)	Standard Deviation of MODPATH Ages on Midpoint (years)	Standard Deviation of MODPATH Ages on Bottom of Cell (years)	Standard Deviation of MODPATH Ages on Computed Groundwater Surface (years)	Standard Deviation of MODPATH Ages on Midpoint (years)	Standard Deviation of MODPATH Ages on Bottom of Cell (years)	Standard Deviation of MODPATH Ages on Computed Groundwater Surface (years)	Standard Deviation of MODPATH Ages on Midpoint (years)	Standard Deviation of MODPATH Ages on Bottom of Cell (years)
Doll Day	NA	40	265	NA	99	661	NA	159	1,058
Pinon Well	0	20	NA	0	51	NA	0	82	NA
Webb House	0	20	NA	0	50	NA	0	79	NA
Una	0	NA	NA	0	NA	NA	0	NA	NA
Cauhape	NA	0	58	NA	1	145	NA	1	231
Jeffer's Well	NA	2	12	NA	5	31	NA	7	49
Ellett Lower	0	NA	NA	0	NA	NA	0	NA	NA
Harvey Lewis Well	0	6	NA	1	16	NA	2	26	NA
Collins	NA	5	9	NA	12	22	NA	19	35
Evrage House	NA	71	67	NA	178	169	NA	285	270
Lewis	0	1	NA	0	4	NA	0	6	NA
Butterfield Well	114	2,260	NA	286	6,384	NA	457	10,497	NA
Hunt 8	0	465	NA	0	1,164	NA	0	1,862	NA

Table A-4.27: Standard deviation of MODPATH ages from the calibrated water-balance based average recharge scenario MODFLOW solution using minimum, average, and maximum porosities.

Orange highlighted rectangles indicate the vertical position of generated MODPATH particles chosen to represent the potential pathlines and residence times of groundwater sampled at each well.

	Water-balance Based Maximum Recharge Scenario								
	Minimum Porosity			Average Porosity			Maximum Porosity		
Groundwater Age Well ID	Standard Deviation of MODPATH Ages on Computed Groundwater Surface (years)	Standard Deviation of MODPATH Ages on Midpoint (years)	Standard Deviation of MODPATH Ages on Bottom of Cell (years)	Standard Deviation of MODPATH Ages on Computed Groundwater Surface (years)	Standard Deviation of MODPATH Ages on Midpoint (years)	Standard Deviation of MODPATH Ages on Bottom of Cell (years)	Standard Deviation of MODPATH Ages on Computed Groundwater Surface (years)	Standard Deviation of MODPATH Ages on Midpoint (years)	Standard Deviation of MODPATH Ages on Bottom of Cell (years)
Doll Day	NA	38	188	NA	95	471	NA	151	753
Pinon Well	0	8	NA	0	21	NA	0	34	NA
Webb House	0	22	NA	0	54	NA	0	86	NA
Una	0	NA	NA	0	NA	NA	0	NA	NA
Cauhape	NA	0	34	NA	1	86	NA	1	137
Jeffer's Well	NA	1	6	NA	4	15	NA	6	23
Ellett Lower	0	NA	NA	0	NA	NA	0	NA	NA
Harvey Lewis Well	1	3	NA	2	7	NA	4	12	NA
Collins	NA	3	6	NA	9	14	NA	14	22
Evrage House	NA	43	57	NA	108	142	NA	173	228
Lewis	0	0	NA	0	1	NA	0	1	NA
Butterfield Well	18	35	NA	46	88	NA	73	141	NA
Hunt 8	0	289	NA	0	722	NA	0	1,156	NA

Table A-4.28: Standard deviation of MODPATH ages from the calibrated water-balance based maximum recharge scenario MODFLOW solution using minimum, average, and maximum porosities.

Orange highlighted rectangles indicate the vertical position of generated MODPATH particles chosen to represent the potential pathlines and residence times of groundwater sampled at each well.

	Elevation-dependent Minimum Recharge Scenario								
	Minimum Porosity			Average Porosity			Maximum Porosity		
Groundwater Age Well ID	Standard Deviation of MODPATH Ages on Computed Groundwater Surface (years)	Standard Deviation of MODPATH Ages on Midpoint (years)	Standard Deviation of MODPATH Ages on Bottom of Cell (years)	Standard Deviation of MODPATH Ages on Computed Groundwater Surface (years)	Standard Deviation of MODPATH Ages on Midpoint (years)	Standard Deviation of MODPATH Ages on Bottom of Cell (years)	Standard Deviation of MODPATH Ages on Computed Groundwater Surface (years)	Standard Deviation of MODPATH Ages on Midpoint (years)	Standard Deviation of MODPATH Ages on Bottom of Cell (years)
Doll Day	NA	329	493	NA	822	1,232	NA	1,315	1,971
Pinon Well	996	635	NA	2,490	1,588	NA	3,984	2,541	NA
Webb House	NA	172	588	NA	429	1,471	NA	687	2,353
Una	171	NA	NA	428	NA	NA	685	NA	NA
Cauhape	NA	158	3,889	NA	396	21,983	NA	633	40,224
Jeffer's Well	NA	253	456	NA	633	1,140	NA	1,012	1,825
Ellett Lower	1,205	623	NA	3,013	1,557	NA	4,821	2,491	NA
Harvey Lewis Well	839	543	NA	2,099	1,358	NA	3,358	2,174	NA
Collins	NA	9,922	21,980	NA	24,816	50,286	NA	39,712	78,658
Evrage House	NA	1,524	6,899	NA	3,809	17,248	NA	6,094	27,597
Lewis	495	289	NA	1,238	722	NA	1,981	1,155	NA
Butterfield Well	524	204	NA	1,309	509	NA	2,095	815	NA
Hunt 8	3,478	10,600	NA	8,695	44,605	NA	13,911	78,891	NA

Table A-4.29: Standard deviation of MODPATH ages from the calibrated elevation-dependent minimum recharge scenario MODFLOW solution using minimum, average, and maximum porosities.

Orange highlighted rectangles indicate the vertical position of generated MODPATH particles chosen to represent the potential pathlines and residence times of groundwater sampled at each well.

Groundwater Age Well ID	Elevation-dependent Average Recharge Scenario								
	Minimum Porosity			Average Porosity			Maximum Porosity		
	Standard Deviation of MODPATH Ages on Computed Groundwater Surface (years)	Standard Deviation of MODPATH Ages on Midpoint (years)	Standard Deviation of MODPATH Ages on Bottom of Cell (years)	Standard Deviation of MODPATH Ages on Computed Groundwater Surface (years)	Standard Deviation of MODPATH Ages on Midpoint (years)	Standard Deviation of MODPATH Ages on Bottom of Cell (years)	Standard Deviation of MODPATH Ages on Computed Groundwater Surface (years)	Standard Deviation of MODPATH Ages on Midpoint (years)	Standard Deviation of MODPATH Ages on Bottom of Cell (years)
Doll Day	NA	27	733	NA	67	1,832	NA	106	2,931
Pinon Well	32	35	NA	79	87	NA	127	139	NA
Webb House	NA	46	314	NA	114	784	NA	183	1,255
Una	30	NA	NA	75	NA	NA	121	NA	NA
Cauhape	NA	226	44	NA	566	110	NA	905	176
Jeffer's Well	NA	42	77	NA	104	193	NA	167	309
Ellett Lower	90	NA	NA	224	NA	NA	359	NA	NA
Harvey Lewis Well	46	57	NA	114	142	NA	182	227	NA
Collins	NA	7,929	17,309	NA	19,821	43,273	NA	31,714	69,238
Evrage House	189,368	394	NA	473,424	984	NA	757,472	1,574	NA
Lewis	325	187	NA	812	468	NA	1,300	748	NA
Butterfield Well	129	318	NA	322	796	NA	514	1,274	NA
Hunt 8	162	23,465	NA	406	89,419	NA	650	157,061	NA

Table A-4.30: Standard deviation of MODPATH ages from the calibrated elevation-dependent average recharge scenario MODFLOW solution using minimum, average, and maximum porosities.

Orange highlighted rectangles indicate the vertical position of generated MODPATH particles chosen to represent the potential pathlines and residence times of groundwater sampled at each well.

Elevation-dependent Maximum Recharge Scenario								
Groundwater Age Well ID	Minimum Porosity			Average Porosity			Maximum Porosity		
	Standard Deviation of MODPATH Ages on Computed Groundwater Surface (years)	Standard Deviation of MODPATH Ages on Midpoint (years)	Standard Deviation of MODPATH Ages on Bottom of Cell (years)	Standard Deviation of MODPATH Ages on Computed Groundwater Surface (years)	Standard Deviation of MODPATH Ages on Midpoint (years)	Standard Deviation of MODPATH Ages on Bottom of Cell (years)	Standard Deviation of MODPATH Ages on Computed Groundwater Surface (years)	Standard Deviation of MODPATH Ages on Midpoint (years)	Standard Deviation of MODPATH Ages on Bottom of Cell (years)
Doll Day	NA	29	716	NA	74	1,793	NA	118	2,872
Pinon Well	20	12	NA	50	30	NA	80	49	NA
Webb House	19	28	NA	48	71	NA	77	113	NA
Una	14	NA	NA	34	NA	NA	54	NA	NA
Cauhape	NA	14	99	NA	34	247	NA	55	395
Jeffer's Well	NA	49	64	NA	123	159	NA	196	254
Ellett Lower	53	29	NA	132	73	NA	211	118	NA
Harvey Lewis Well	78	40	NA	194	100	NA	310	160	NA
Collins	NA	17,863	60,125	NA	71,110	145,820	NA	130,618	231,676
Evrage House	12,212	93	NA	30,531	232	NA	48,850	370	NA
Lewis	57	35	NA	143	88	NA	229	141	NA
Butterfield Well	77	54	NA	194	134	NA	310	215	NA
Hunt 8	304	500	NA	760	1,250	NA	1,216	2,000	NA

Table A-4.31: Standard deviation of MODPATH ages from the calibrated elevation-dependent maximum recharge scenario MODFLOW solution using minimum, average, and maximum porosities.

Orange highlighted rectangles indicate the vertical position of generated MODPATH particles chosen to represent the potential pathlines and residence times of groundwater sampled at each well.

| Water-balance Based Minimum Recharge Scenario | | | | | | | | | |
| Groundwater Age Well ID | Minimum Porosity | | | Average Porosity | | | Maximum Porosity | | |
	Residual Age on Computed Groundwater Surface (years)	Residual Age on Midpoint (years)	Residual Age on Bottom of Cell (years)	Residual Age on Computed Groundwater Surface (years)	Residual Age on Midpoint (years)	Residual Age on Bottom of Cell (years)	Residual Age on Computed Groundwater Surface (years)	Residual Age on Midpoint (years)	Residual Age on Bottom of Cell (years)
Doll Day	NA	-1,689	2,151	NA	127	9,727	NA	1,944	17,303
Pinon Well	-4,198	-3,561	NA	-4,195	-2,601	NA	-4,192	-1,642	NA
Webb House	-998	1,163	NA	-995	4,409	NA	-992	7,654	NA
Una	-7,099	NA	NA	-7,097	NA	NA	-7,096	NA	NA
Cauhape	NA	-7,710	-1,459	NA	-7,274	8,351	NA	-6,839	18,162
Jeffer's Well	NA	-7,977	-7,738	NA	-7,642	-7,045	NA	-7,307	-6,352
Ellett Lower	-13,800	-13,586	NA	-13,799	-13,265	NA	-13,798	-12,944	NA
Harvey Lewis Well	-11,993	-11,699	NA	-11,983	-11,247	NA	-11,972	-10,796	NA
Collins	NA	-9,253	-8,613	NA	-8,584	-6,981	NA	-7,914	-5,350
Evrage House	NA	-12,391	-12,257	NA	-11,777	-11,442	NA	-11,164	-10,626
Lewis	NA	-10,769	-10,391	NA	-10,423	-9,477	NA	-10,076	-8,563
Butterfield Well	-14,342	-14,230	NA	-11,704	-11,425	NA	-9,067	-8,620	NA
Hunt 8	-14,094	-12,515	NA	-14,086	-10,139	NA	-14,077	-7,762	NA

Table A-4.32: Residual ages (i.e. MODPATH ages minus NETPATH ages) from the calibrated water-balance based minimum recharge scenario MODFLOW solution using minimum, average, and maximum porosities.

Orange highlighted rectangles indicate the vertical position of generated MODPATH particles chosen to represent the potential pathlines and residence times of groundwater sampled at each well.

Groundwater Age Well ID	Minimum Porosity			Average Porosity			Maximum Porosity		
	Residual Age on Computed Groundwater Surface (years)	Residual Age on Midpoint (years)	Residual Age on Bottom of Cell (years)	Residual Age on Computed Groundwater Surface (years)	Residual Age on Midpoint (years)	Residual Age on Bottom of Cell (years)	Residual Age on Computed Groundwater Surface (years)	Residual Age on Midpoint (years)	Residual Age on Bottom of Cell (years)
Doll Day	NA	-2,128	731	NA	-970	6,178	NA	187	11,625
Pinon Well	-4,199	-3,805	NA	-4,198	-3,211	NA	-4,197	-2,618	NA
Webb House	-999	35	NA	-997	1,588	NA	-996	3,141	NA
Una	-7,100	NA	NA	-7,099	NA	NA	-7,098	NA	NA
Cauhape	NA	-7,778	-4,114	NA	-7,446	1,716	NA	-7,114	7,546
Jeffer's Well	NA	-8,049	-7,923	NA	-7,823	-7,508	NA	-7,597	-7,092
Ellett Lower	-13,800	NA	NA	-13,799	NA	NA	-13,799	NA	NA
Harvey Lewis Well	-11,997	-11,841	NA	-11,992	-11,603	NA	-11,988	-11,364	NA
Collins	NA	-9,511	-9,279	NA	-9,228	-8,648	NA	-8,944	-8,017
Evrage House	NA	-12,435	-12,432	NA	-11,888	-11,881	NA	-11,341	-11,329
Lewis	-11,000	-10,858	NA	-10,999	-10,644	NA	-10,999	-10,431	NA
Butterfield Well	-14,617	-13,638	NA	-12,394	-9,943	NA	-10,170	-6,250	NA
Hunt 8	-14,097	-12,846	NA	-14,093	-10,964	NA	-14,089	-9,083	NA

Table A-4.33: Residual ages (i.e. MODPATH ages minus NETPATH ages) from the calibrated water-balance based average recharge scenario MODFLOW solution using minimum, average, and maximum porosities.

Orange highlighted rectangles indicate the vertical position of generated MODPATH particles chosen to represent the potential pathlines and residence times of groundwater sampled at each well.

Water-balance Based Maximum Recharge Scenario									
	Minimum Porosity			Average Porosity			Maximum Porosity		
Groundwater Age Well ID	Residual Age on Computed Groundwater Surface (years)	Residual Age on Midpoint (years)	Residual Age on Bottom of Cell (years)	Residual Age on Computed Groundwater Surface (years)	Residual Age on Midpoint (years)	Residual Age on Bottom of Cell (years)	Residual Age on Computed Groundwater Surface (years)	Residual Age on Midpoint (years)	Residual Age on Bottom of Cell (years)
Doll Day	NA	-2,214	-124	NA	-1,185	4,039	NA	-156	8,203
Pinon Well	-4,200	-3,861	NA	-4,199	-3,352	NA	-4,198	-2,843	NA
Webb House	-999	53	NA	-998	1,633	NA	-996	3,212	NA
Una	-7,100	NA	NA	-7,099	NA	NA	-7,099	NA	NA
Cauhape	NA	-7,863	-5,501	NA	-7,658	-1,752	NA	-7,453	1,997
Jeffer's Well	NA	-8,115	-8,041	NA	-7,987	-7,803	NA	-7,859	-7,566
Ellett Lower	-13,800	NA	NA	-13,800	NA	NA	-13,799	NA	NA
Harvey Lewis Well	-11,995	-11,881	NA	-11,989	-11,703	NA	-11,982	-11,524	NA
Collins	NA	-9,490	-9,255	NA	-9,176	-8,588	NA	-8,862	-7,921
Evrage House	NA	-12,546	-12,504	NA	-12,165	-12,061	NA	-11,784	-11,618
Lewis	-11,000	-10,866	NA	-10,999	-10,666	NA	-10,999	-10,466	NA
Butterfield Well	-15,299	-15,194	NA	-14,098	-13,835	NA	-12,897	-12,476	NA
Hunt 8	-14,096	-13,157	NA	-14,090	-11,741	NA	-14,085	-10,326	NA

Table A-4.34: Residual ages (i.e. MODPATH ages minus NETPATH ages) from the calibrated water-balance based maximum recharge scenario MODFLOW solution using minimum, average, and maximum porosities.

Orange highlighted rectangles indicate the vertical position of generated MODPATH particles chosen to represent the potential pathlines and residence times of groundwater sampled at each well.

	Elevation-dependent Minimum Recharge Scenario								
	Minimum Porosity			Average Porosity			Maximum Porosity		
Groundwater Age Well ID	Residual Age on Computed Groundwater Surface (years)	Residual Age on Midpoint (years)	Residual Age on Bottom of Cell (years)	Residual Age on Computed Groundwater Surface (years)	Residual Age on Midpoint (years)	Residual Age on Bottom of Cell (years)	Residual Age on Computed Groundwater Surface (years)	Residual Age on Midpoint (years)	Residual Age on Bottom of Cell (years)
Doll Day	NA	26,309	28,426	NA	70,124	75,415	NA	113,938	122,404
Pinon Well	35,054	35,414	NA	93,936	94,834	NA	152,817	154,255	NA
Webb House	NA	24,841	27,442	NA	63,603	70,104	NA	102,365	112,767
Una	23,023	NA	NA	68,208	NA	NA	113,392	NA	NA
Cauhape	NA	29,965	57,573	NA	86,912	166,911	NA	143,860	276,339
Jeffer's Well	NA	29,619	29,824	NA	86,348	86,861	NA	143,077	143,897
Ellett Lower	34,009	34,140	NA	105,724	106,050	NA	177,438	177,961	NA
Harvey Lewis Well	31,494	31,553	NA	96,736	96,882	NA	161,978	162,210	NA
Collins	NA	610,074	601,388	NA	1,542,714	1,520,678	NA	2,475,356	2,440,853
Evrage House	NA	51,522	50,117	NA	148,006	144,494	NA	244,490	238,870
Lewis	66,238	70,206	NA	182,095	192,015	NA	297,953	313,823	NA
Butterfield Well	10,925	11,176	NA	51,462	52,091	NA	92,000	93,006	NA
Hunt 8	76,961	78,816	NA	213,553	234,352	NA	350,145	392,794	NA

Table A-4.35: Residual ages (i.e. MODPATH ages minus NETPATH ages) from the calibrated elevation-dependent minimum recharge scenario MODFLOW solution using minimum, average, and maximum porosities.

Orange highlighted rectangles indicate the vertical position of generated MODPATH particles chosen to represent the potential pathlines and residence times of groundwater sampled at each well.

Groundwater Age Well ID	Elevation-dependent Average Recharge Scenario								
	Minimum Porosity			Average Porosity			Maximum Porosity		
	Residual Age on Computed Groundwater Surface (years)	Residual Age on Midpoint (years)	Residual Age on Bottom of Cell (years)	Residual Age on Computed Groundwater Surface (years)	Residual Age on Midpoint (years)	Residual Age on Bottom of Cell (years)	Residual Age on Computed Groundwater Surface (years)	Residual Age on Midpoint (years)	Residual Age on Bottom of Cell (years)
Doll Day	NA	2,157	5,641	NA	9,742	18,452	NA	17,327	31,263
Pinon Well	358	488	NA	7,196	7,521	NA	14,033	14,553	NA
Webb House	NA	3,131	4,751	NA	9,328	13,376	NA	15,525	22,002
Una	-2,127	NA	NA	5,334	NA	NA	12,794	NA	NA
Cauhape	NA	-1,648	984	NA	7,880	14,459	NA	17,408	27,935
Jeffer's Well	NA	-2,479	-2,424	NA	6,103	6,239	NA	14,685	14,903
Ellett Lower	-6,326	NA	NA	4,885	NA	NA	16,096	NA	NA
Harvey Lewis Well	-5,076	-4,719	NA	5,311	6,203	NA	15,697	17,125	NA
Collins	NA	391,560	396,935	NA	993,449	1,006,889	NA	1,595,340	1,616,842
Evrage House	374,540	-5,355	NA	955,551	5,812	NA	1,536,562	16,980	NA
Lewis	10,646	11,039	NA	43,115	44,098	NA	75,585	77,157	NA
Butterfield Well	-11,006	-10,883	NA	-3,364	-3,057	NA	4,277	4,769	NA
Hunt 8	10,084	19,423	NA	46,359	69,708	NA	82,634	119,993	NA

Table A-4.36: Residual ages (i.e. MODPATH ages minus NETPATH ages) from the calibrated elevation-dependent average recharge scenario MODFLOW solution using minimum, average, and maximum porosities.

Orange highlighted rectangles indicate the vertical position of generated MODPATH particles chosen to represent the potential pathlines and residence times of groundwater sampled at each well.

Groundwater Age Well ID	Minimum Porosity			Average Porosity			Maximum Porosity		
	Residual Age on Computed Groundwater Surface (years)	Residual Age on Midpoint (years)	Residual Age on Bottom of Cell (years)	Residual Age on Computed Groundwater Surface (years)	Residual Age on Midpoint (years)	Residual Age on Bottom of Cell (years)	Residual Age on Computed Groundwater Surface (years)	Residual Age on Midpoint (years)	Residual Age on Bottom of Cell (years)
Doll Day	NA	-454	1,769	NA	3,216	8,772	NA	6,885	15,775
Pinon Well	-1,847	-1,792	NA	1,682	1,820	NA	5,211	5,432	NA
Webb House	1,001	1,174	NA	4,002	4,435	NA	7,004	7,696	NA
Una	-4,585	NA	NA	-813	NA	NA	2,960	NA	NA
Cauhape	NA	-4,784	-2,011	NA	39	6,971	NA	4,863	15,954
Jeffer's Well	NA	-4,944	-4,921	NA	-60	-3	NA	4,824	4,915
Ellett Lower	-9,871	-9,852	NA	-3,976	-3,929	NA	1,918	1,994	NA
Harvey Lewis Well	-8,460	-8,420	NA	-3,149	-3,050	NA	2,161	2,321	NA
Collins	NA	826,378	666,553	NA	2,724,309	2,097,319	NA	4,628,779	3,534,082
Evrage House	26,553	-9,052	NA	85,581	-3,430	NA	144,610	2,192	NA
Lewis	-4,096	-3,991	NA	6,259	6,522	NA	16,615	17,035	NA
Butterfield Well	-13,588	-13,580	NA	-9,821	-9,799	NA	-6,054	-6,019	NA
Hunt 8	-6,846	-6,583	NA	4,036	4,692	NA	14,917	15,967	NA

Table A-4.37: Residual ages (i.e. MODPATH ages minus NETPATH ages) from the calibrated elevation-dependent maximum recharge scenario MODFLOW solution using minimum, average, and maximum porosities.

Orange highlighted rectangles indicate the vertical position of generated MODPATH particles chosen to represent the potential pathlines and residence times of groundwater sampled at each well.

Water-balance Based Minimum Recharge Scenario			
Statistic	Minimum Porosity	Average Porosity	Maximum Porosity
Sum Residuals (years)	-209,047	-170,567	-132,087
Sum Absolute Residuals (years)	215,675	215,796	222,213
Sum Squared Residuals (years^2)	2,382,279,439	2,216,152,581	2,440,163,800
RMS Error (years)	9,762	9,415	9,880

Water-balance Based Average Recharge Scenario			
Statistic	Minimum Porosity	Average Porosity	Maximum Porosity
Sum Residuals (years)	-203,679	-177,848	-152,017
Sum Absolute Residuals (years)	205,212	196,812	197,014
Sum Squared Residuals (years^2)	2,256,174,267	2,013,764,816	1,954,184,998
RMS Error (years)	9,696	9,160	9,024

Water-balance Based Maximum Recharge Scenario			
Statistic	Minimum Porosity	Average Porosity	Maximum Porosity
Sum Residuals (years)	-209,049	-191,273	-173,496
Sum Absolute Residuals (years)	209,155	202,616	200,321
Sum Squared Residuals (years^2)	2,352,235,737	2,170,874,905	2,072,649,619
RMS Error (years)	9,900	9,511	9,293

Table A-4.38: Residual age statistics for the calibrated water-balance based minimum, average, and maximum recharge scenario MODFLOW solutions using minimum, average, and maximum porosities.

Elevation-dependent Minimum Recharge Scenario			
Statistic	Minimum Porosity	Average Porosity	Maximum Porosity
Sum Residuals (years)	894,651	2,586,717	4,281,779
Sum Absolute Residuals (years)	894,651	2,586,717	4,281,779
Sum Squared Residuals (years^2)	43,034,332,815	352,316,919,807	963,202,659,626
RMS Error (years)	176,283	449,210	722,450
RMS Error with outliers removed (years)	43,256	123,766	204,642

Elevation-dependent Average Recharge Scenario			
Statistic	Minimum Porosity	Average Porosity	Maximum Porosity
Sum Residuals (years)	16,661	324,702	632,743
Sum Absolute Residuals (years)	120,743	337,545	632,743
Sum Squared Residuals (years^2)	1,159,868,251	12,142,411,637	38,117,422,665
RMS Error (years)	140,235	356,675	573,260
RMS Error with outliers removed (years)	7,615	24,640	43,656

Elevation-dependent Maximum Recharge Scenario			
Statistic	Minimum Porosity	Average Porosity	Maximum Porosity
Sum Residuals (years)	-115,734	14,416	144,565
Sum Absolute Residuals (years)	123,621	90,478	168,711
Sum Squared Residuals (years^2)	1,019,805,143	553,112,221	1,934,670,863
RMS Error (years)	212,501	687,851	1,165,130
RMS Error with outliers removed (years)	6,808	5,014	9,378

Table A-4.39: Residual age statistics for the calibrated elevation-dependent minimum, average, and maximum recharge scenario MODFLOW solutions using minimum, average, and maximum porosities.